Technical Report
TR-22-06
September 2022

Large scale gas injection test (Lasgit) performed at the Äspö Hard Rock Laboratory

Final report

Robert J Cuss
Jon F Harrington
Elena Tamayo-Mas
David J Noy
David J Birchall
Patrik Sellin
Matti Nord

SVENSK KÄRNBRÄNSLEHANTERING AB

SWEDISH NUCLEAR FUEL
AND WASTE MANAGEMENT CO

Box 3091, SE-169 03 Solna
Phone +46 8 459 84 00
skb.se

SVENSK KÄRNBRÄNSLEHANTERING

ISSN 1404-0344
SKB TR-22-06
ID 1977136
September 2022

Large scale gas injection test (Lasgit) performed at the Äspö Hard Rock Laboratory

Final report

Robert J Cuss, Jon F Harrington, Elena Tamayo-Mas,
David J Noy, David J Birchall

British Geological Survey

Patrik Sellin, Matti Nord
Svensk Kärnbränslehantering AB

Keywords: Lasgit, Gas injection, Bentonite, Modelling, Hydration, Hydraulic, Storage, Gas entry pressure.

This report is published on www.skb.se

Foreword

This report is the published product of a study by the British Geological Survey (BGS) undertaken on behalf of SKB working closely with Patrik Sellin (SKB). The authors would like to thank Keith Bateman for his review of this report. The research leading to these results has received funding from the European Union's Sixth Framework Euratom Programme (2002–2006) under grant number 516514 as part of the NF-Pro: Understanding and Physical and Numerical Modelling of the Key Processes in the Near-Field and their Coupling for Different Host Rocks and Repository Strategies project; the European Union's Seventh Framework Euratom Programme (2007–2013) under grant agreement number 230357 as part of the Fate of Repository Gases (FORGE) project; and the European Union's Horizon 2020 research and innovation programme under grant agreement number 847593 as part of the EURAD GAS: Mechanistic understanding of gas transport in clay materials project.

Acknowledgements

This study was undertaken by staff from the British Geological Survey (Radioactive Waste Team). Funding for the study was provided by SKB (Stockholm), the British Geological Survey, and the European Commission through the NF-PRO, FORGE, and EURAD GAS projects.

The BGS authors (Cuss, Harrington) would like to thank Patrik Sellin for his support of the research area and for many stimulating discussions over the years. There are many SKB and subcontractor staff at Äspö that without whom Lasgit would not have been possible. For managing the project on the ground, we greatly appreciate and acknowledge the help of Rikard Bäck, Anders Wikman, Mats Lundqvist, and Matti Nord. We greatly benefitted from the expert skills of Stefan Grandin Svärdh throughout the Lasgit project from set-up to decommissioning. In the final year of operation, we gratefully acknowledge the assistance of Thomas Andolfsson, Lars Hjalmarsson, and Terese Bladström, the latter of whom made all of the geotechnical measurements. We would also like to thank the project administrators and Sicada team including Anna Blomqvist, Annelie Borg, Maria Eriksson, Titti Falk, Siren Bortelid Moen, Karin Nilsson, and David Zander. Without the dedicated and skilled staff at Äspö, the set-up, maintenance and operation of the Lasgit experiment would not have been possible. BGS would also like to thank our colleagues at Clay Technology AB, including Torbjörn Sandén, who were responsible for the original installation of the Geokon instrumentation and buffer clay. We would like to thank Thomas Nowak and co-workers at BGR for their work on defining the permeability of the wall rock within the deposition hole and Carl-Johan Hardenby of SwedPower AB for his mapping of the deposition hole and the TBM assembly hall. There are many people that we have forgotten to mention and this does not reflect a lack of gratitude, more that we have forgotten everybody's name.

We would also like to thank many of our BGS colleagues for assistance and hard work over the years. Dave Birchall and Ben Charlton were instrumental in the setup and construction of the Lasgit laboratory. Humphrey Wallis and the staff of the Engineering Workshops for manufacturing the canister filters; Simon Holyoake for visiting Äspö and replacing the National Instruments logger; Dave Noy for performing the scoping calculations and early modelling calculations; Marcus Sen for the derivation of flow equations; Caroline Graham for the compilation of bentonite data; and Elena Tamayo-Mas for the modelling work carried out at the end of the experiment.

The authors would also like to acknowledge the important contribution made by Dr Steve Horseman during the earlier stages of the project before his untimely death in 2004. Steve pioneered work on the movement of gas in clays and mudrocks and remains a much-respected scientist whose encyclopaedic knowledge, enthusiasm and energy for his science continues to be greatly missed by all those who knew and worked with him.

Abstract

Lasgit was a full-scale demonstration experiment conducted at a depth of 420 m at the Äspö Hard Rock Laboratory. The experiment started following the closure of the deposition hole on 1st February 2005 and logged data for a total of 5 782 days, finally being decommissioned by mid-February 2021.

The main objectives for the Lasgit experiment were fully achieved during this 17-year project, allowing the upscaling of laboratory-derived process understanding to the field scale. The findings provide fundamental information that addresses key questions relating to the treatment of gas in safety assessment and the resulting implications for the evolution of the buffer in the event of a deposition hole containing a defective canister. The main conclusions were: 1) In all tests, regardless of initial gas volume, the movement of gas occurred at a pressure very close to the local total stress; 2) No signs of localised consolidation of the bentonite were observed; 3) The measured peak gas pressures should not lead to any mechanical damage to the buffer or to other barrier components in the repository; 4) Peak gas pressure is linked to the hydraulic permeability of the buffer and the ease at which gas can exit a deposition hole; 5) Gas is transported through a limited number of dilatant pathways. The pathways are expected to be small, in relation to the total volume of the buffer, and temporally variable; 6) No desaturation of the bentonite buffer as a result of gas transport was observed; 7) Over the time-scale of the project, pathway closure was only partially successful; 8) The gas pathways are expected to slowly close at a finite "shut-in" pressure; 9) Gas migration through a bentonite will notis highly unlikely to alter the favourable hydromechanical properties of the barrier; 10) The impact of emplaced and long-lived persistent heterogeneities within the bentonite on gas pressure remains unclear.

The results from GT1 through GT6 and the FCT show gas transport processes are scale invariant when compared with laboratory experiments and insensitive to the initial upstream gas volume. This may have been expected but had never been tested, beyond laboratory scales, prior to Lasgit. The role of water and the maturity (i.e. state of pore-pressure, hydraulic conductivity, and stress homogenisation of the buffer in the time-frame of the experiment) have been shown to strongly impact gas flow in the buffer. Given the similarities in behaviour between individual tests and those performed in the laboratory, it is reasonable to assume that while peak gas pressures would increase as the buffer continued to mature and reach a state of hydraulic equilibrium, any change would be relatively small, linked to increases in swelling and porewater pressure. The absence of high peak gas pressures such as those sometimes observed during laboratory testing is an important outcome from Lasgit. While gas-induced consolidation may not have been directly observed, the similarities in gas migration behaviour at both scales indicate that it can be further investigated in the laboratory.

Sammanfattning

Lasgit var ett fullskaligt demonstrationsexperiment som genomfördes på 420 meters djup i Äspölaboratoriet. Experimentet startade efter förslutningen av deponeringshålet den 1 februari 2005 och data loggades under totalt 5 782 dagar. Experimentet avvecklades slutligen i mitten av februari 2021.

Huvudmålen för Lasgit-experimentet uppnåddes till fullo under detta 17-åriga projekt. Detta möjliggjorde uppskalning av processförståelse från laboratorietester till fältskala. Resultaten ger grundläggande information angående nyckelfrågor som rör hanteringen av gas i säkerhetsutvärderingar och de resulterande konsekvenserna för buffertens utveckling i händelse av ett deponeringshål med en defekt kapsel. Huvudslutsatserna var: 1) I alla tester, oavsett initial gasvolym, skedde gasgenomströmingen först vid ett tryck som ligger mycket nära det lokala totaltrycket; 2) Inga tecken på lokaliserad konsolidering av bentoniten observerades; 3) De uppmätta maximala gastrycken bör inte leda till någon mekanisk skada på bufferten eller på andra barriärkomponenter i förvaret; 4) Det maximala gastrycket är relaterat till buffertens hydrauliska permeabilitet och hur lätt gas kan lämna ett deponeringshål; 5) Gas transporteras genom ett begränsat antal dilatanta vägar. Vägarna förväntas vara små, i förhållande till buffertens totala volym, och varierar med tiden; 6) Ingen uttorkning av bentonitbufferten som följd av gastransport observerades; 7) I projektets tidsskala stängdes transportvägarna endast delvis; 8) Transportvägarna förväntas långsamt stängas vid ett givet ”stängningstryck”; 9) Gastransport genom bentonit kommer sannolikt inte att förändra barriärens fördelaktiga hydromekaniska egenskaper; 10) Effekten av installerade och kvarvarande heterogeniteter inom bentoniten på gastrycket är fortfarande oklart.

Resultaten från GT1 till GT6 och FCT visar att gastransportprocesserna är oberoende av skala jämfört med laboratorieexperiment och okänsliga för den initiala uppströms gasvolymen. Detta hade förväntats men hade aldrig testats, i annat än laboratorieskala, före Lasgit. Vattnets roll och bentonitbuffertens mognad (dvs tillståndet på portryck, hydraulisk konduktivitet och tryckhomogenisering hos bufferten under experimentets tidsram) har visat sig att starkt påverka gasflödet i bufferten. Med tanke på likheterna i beteende mellan individuella testerna i Lasgit och de som har utförs i laboratoriet är det rimligt att anta att även om maximala gastrycken skulle öka när bufferten fortsatte att mogna och nå ett tillstånd av hydraulisk jämvikt, skulle varje förändring vara relativt liten, kopplat till ökningar av svällning och porvattentryck. Frånvaron av de höga maximala gastryck som ibland observeras under laboratorietester är ett viktigt resultat från Lasgit. Även om gasinducerad konsolidering kanske inte har observerats direkt, indikerar likheterna i gastransportbeteende i det båda skalorna att processen kan undersökas i laboratorier i framtiden.

Contents

1 Introduction

In the Swedish KBS-3 repository concept for spent nuclear fuel, copper/steel canisters containing spent fuel will be placed in large diameter (~1.8 m) boreholes drilled into the floor of the repository tunnels. The space around each canister will be filled with pre-compacted bentonite blocks, which over time, will draw in the surrounding groundwater and swell, closing up any remaining construction gaps. While the copper/steel canisters are expected to have a very substantial life, from a performance assessment perspective, it is important to consider the possible impact of groundwater penetrating a canister. Under certain conditions corrosion of the steel insert of each canister will lead to the formation of hydrogen. Radioactive decay of the waste and the radiolysis of water will produce some additional gas. Depending on the gas production rate and the rate of diffusion of gas molecules in the pores of the bentonite, it is possible that gas will accumulate in the void-space of each canister.

The state of knowledge pertaining to the movement of gas in initially saturated buffer bentonite prior to Lasgit was based on small-scale laboratory studies (Donohew et al. 2000, Harrington and Horseman 1999, Horseman et al. 1997, 1999, Hume 1999, Pusch et al. 1985, 1987, Tanai et al. 1997). Laboratory tests have demonstrated the importance of the boundary condition on gas migration (Harrington and Horseman 2003, Horseman et al. 2004). Gas penetration and subsequent flow is accompanied by local dilation of the buffer clay. Porewater pressure and total stress acting within the clay are strongly affected by the passage of gas. The maximum gas pressure attainable during a discharge event, in part, relates to the geometry and spatial distribution of both the gas pathways within the buffer and the characteristics of the fractures distributed along the walls of the emplacement borehole. The transmissivity and hydrostatic pressure of these features will affect the maximum gas pressure that can be generated within the buffer.

While significant improvements in our understanding of the gas-buffer system had taken place prior to Lasgit (Harrington and Horseman 2003), laboratory work had highlighted a number of uncertainties, notably the sensitivity of the gas migration process to experimental boundary conditions and possible scale-dependency of the measured responses. These issues were best addressed by undertaking a **LA**rge-**S**cale **G**as **I**njection **T**est or "**Lasgit**".

Lasgit was a full-scale demonstration experiment operated by SKB at the Äspö Hard Rock Laboratory at a depth of 420 m. The objective of Lasgit was to provide quantitative data to improve process understanding and to validate modelling approaches used in performance assessment. The full-scale experiment aimed to observe gas movement on the component scale to confirm observations made at the laboratory scale. At the component scale, Lasgit included an engineered gap between the bentonite blocks and the canister, as well as a zone of pellets of lower density; these had been absent from laboratory experiments.

Lasgit started following the closure of the deposition hole on 1st February 2005, although the experiment began before this date with the construction of the Lasgit laboratory, manufacture of bentonite blocks, characterisation of the deposition hole, and emplacement of the experimental infrastructure. The experiment logged data for a total of 5 782 days (15.8 years) and was finally decommissioned by mid-February 2021.

This report is the third in a series published on the status of the Lasgit experiment. Harrington et al. (2007) covered the initial stage of artificial hydration and the first stage of gas testing. Cuss et al. (2008) covered the activities of 2008 (artificial hydration), but also re-examined all data to date with particular emphasis placed on the impact of annual variations on experimental parameters and the evolution of the system over the first 3.7 years of testing. In addition, an update was given on activities as part of the EU FORGE project (Cuss et al. 2012). In the current report, the complete test history is reported, which includes large sections of the previous reports in order to make this final report the definitive account of the activities in Lasgit.

To date, five peer reviewed papers have been published on Lasgit (Cuss et al. 2011, 2014, Bennett et al. 2012, 2014, 2015). Findings from Lasgit have been presented externally on 18 occasions. As part of the Lasgit project, a PhD was conducted by Danothy Bennett at the University of Cardiff, co-supervised by BGS and SKB (Bennett 2014, Bennett et al. 2012, 2014, 2015).

After Lasgit was decommissioned a selection of copper components from the Lasgit canister was examined. The purpose of performing the corrosion analyses was to gather more information about the corrosion mechanisms that can occur in repository-type conditions. In addition to the analysis of the canister components, a sample of corrosion products from the Lasgit canister mantle area was characterised. Also, iron corrosion products on the canister insert – resulting from an initially opened valve in the canister base – were analysed for presence of microorganisms able to conduct microbially influenced corrosion (MIC). These studies are presented in a separate report (Wendel et al. 2022).

1.1 Structure of the report

This report has been organised into 18 chapters following this Introduction, arranged into four sections:

Section A covers the description of the experimental setup. In Chapter 2 the characterisation of the deposition hole and the tunnel surrounding Lasgit are introduced. In Chapter 3 the experimental setup and processing are outlined. Chapter 4 is an introduction to the experimental chapters. It defines several considerations and definitions that the reader should consider when reading the experimental chapters.

Section B covers the technical detail of each of the experimental stages of the experiment. This can be considered as a Technical Report on the experiment. Chapters 5 to 14 introduce each experimental phase of the Lasgit experiment. This includes Hydration Stage 1 (Chapter 5), Gas Injection Test 1 (Chapter 6), Hydration Stage 2 (Chapter 7), Gas injection test 2 (Chapter 8), Gas Injection Test 3 (Chapter 9), Gas Injection Test 4 (Chapter 10), Natural Hydration Stage 3 (Chapter 11), Gas Injection Test 5 (Chapter 12), Gas Injection Test 6 (Chapter 13), and the Full Canister Test (Chapter 14).

Section C covers the decommissioning of the experiment and the analysis of the buffer. This can also be considered as a technical report. The final experimental chapter covers the decommissioning of the experiment and all the post-mortem analysis of the bentonite buffer.

Section D brings together the observations of Section B and Section C to reach conclusions on the performance and learnings of the Lasgit experiment. Chapter 16 brings together all observations of the boundary conditions for the full test history and relates to the state of the buffer. Chapter 17 brings together all observations of the gas injection tests and compares and contrasts results from the three gas injection points. The next chapter relates the observations of Lasgit to Safety Assessment, with the final chapter summarising all the observations made during Lasgit.

Section E summarises all the major findings of the Lasgit experiment

Section A – Description of the experimental setup

2 Characterisation of the deposition hole

This section is a review of a number of SKB International Progress Reports (IPR). These include Hardenby and Lundin (2003) on the geological mapping of the assembly hall and deposition hole, Hardenby (2004) on the hydrogeology of the Lasgit hole DA3147G01, and Nowak et al. (2007) on the hydraulic tests conducted in the Lasgit deposition hole. Additional information is also introduced that was presented at various Lasgit project meetings.

The Lasgit experiment was commissioned in deposition hole number DA3147G01, which was the first emplacement borehole to be drilled at the Äspö Hard Rock Laboratory (HRL). The experiment was located within the Tunnel Boring Machine (TBM) assembly hall on the 420 m-level of the tunnel system. The tunnel system at Äspö is comprised of an underground access ramp approximately 3 600 m long. It is initially straight but between sections 1 600 – 3 100 m turns into a spiral.

The deposition hole had a length of 8.5 m and a diameter of around 1.75 m. A full scale KBS-3 canister was modified for the Lasgit experiment with twelve circular filters of varying dimensions located on its surface to provide point sources for gas injection, mimicking potential canister defects (Section 3.2.3). These filters were used to inject water during the hydration stage and gas during gas testing.

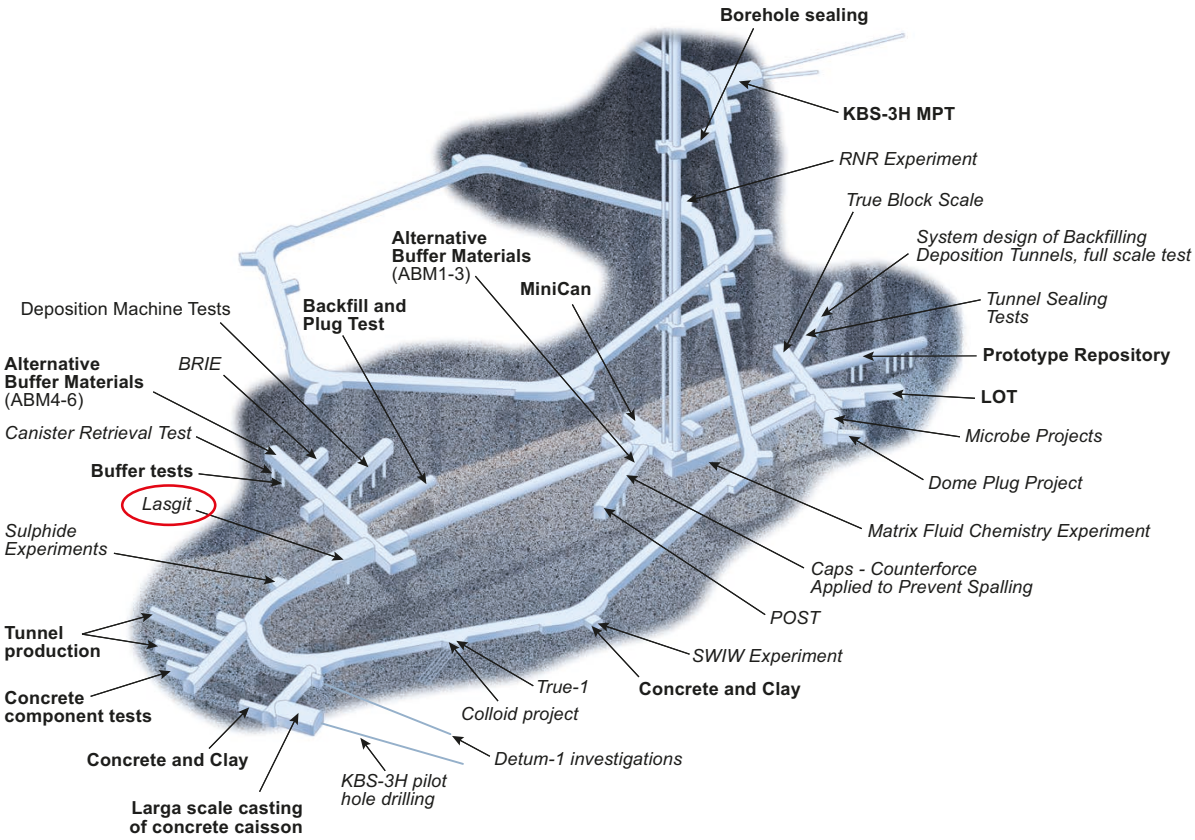

Figure 2-1. *Location of Lasgit at 420 m depth in the Äspö Hard Lock Laboratory.*

2.1 Geological mapping (IPR-03-28)

The area around the Lasgit experiment was comprehensively mapped by Hardenby and Lundin (2003). These studies can be divided into 1) the TBM assembly hall and trial pit, and 2) the deposition hole DA3147G01.

2.1.1 Geological mapping of the TBM assembly hall

The assembly hall constitutes an enlarged section of the TASA main tunnel. It is higher and wider than the connecting tunnels for about 30 m of its length. It was excavated using conventional drilling and blasting techniques in 1994 and was created for the assembly of the tunnel boring machine that was used, later in 1994, to bore the final part of the HRL tunnel (408.5 m, section 3191.2 – 3599.7).

As a part of the general geological characterization of the tunnels at Äspö HRL the geological mapping of the walls and roof of the TBM assembly hall was completed shortly after the excavation was completed in 1994. The majority of the exposed surface of the walls and roof in the assembly hall were covered with shotcrete and the floor paved.

The TBM assembly hall was previously used for the SKB-project "Demonstration of the Deposition Technology". The purpose of that project was to develop and test methodology and equipment for deposition of canisters for spent fuel in full-scale and in a realistic environment. The assembly hall was intended to serve as a reloading station for canisters. During the reloading process a temporary deposition hole for a canister was required. However, the reloading station was never constructed.

As a part of the characterisation work in 1998 a pit was excavated to expose the rock in the TBM assembly hall floor in an area suitable for the reloading station. The pit floor was mapped and the results were used to decide where to drill two short bore holes, KA3147G01 and KA3153G01. The results from all of these studies were used to decide where DA3147G01 was to be completed. Basic information for these boreholes is given in Table 2-1.

Table 2-1. Co-ordinates of the pilot and the deposition holes in the TBM assembly hall. Notes: The co-ordinate system is the reference Äspö coordinates. Negative dip indicates downwards; # = centre of the top of the hole, top of tunnel concrete floor at the time of the drilling; * = centre of the top of the hole, natural tunnel rock floor; @ = centre of the hole bottom.

Borehole category	ID – Codes	X co-ordinate	Y co-ordinate	Z co-ordinate	Dip°	Length (m)
Deposition hole	DA3147G01	7312.491	2313.562	−418.450#	−90	8.83@
Pilot hole	KA3147G01	7312.490	2313.554	−419.561*	−90	8.00
Pilot hole	KA3153G01	7311.511	2308.194	−419.053*	−90	8.00

The results of the various geological mappings of the TBM assembly hall are shown in Figure 2-2. There are basically four rock types present (Table 2-2 summarises the relative proportions of the three main rock types):

- Grey, medium-grained Äspö diorite (with or without feldspar megacrysts). This is the dominant rock type.
- Reddish or sometimes grey, fine to medium-grained "fine-grained granite." Occurs in minor amounts as veins, dykes or irregular bodies.
- A dark-blackish green, fine- to medium-grained greenstone. Less common than the reddish fine-grained granite and occurs mainly as xenoliths within the Äspö diorite.
- Pinkish to reddish pegmatite. This is the least common rock type in the TBM assembly hall. Fine-grained granite sometimes forms hybrids with Äspö diorite.

The rock can be regarded as "fresh" (i.e. no alteration aside from some minor oxidation of the rock normally in connection with fractures). The contacts between the rock types were mostly tight and sharp. More diffuse contacts were commonly found where a distinct rock type grades into a hybrid one.

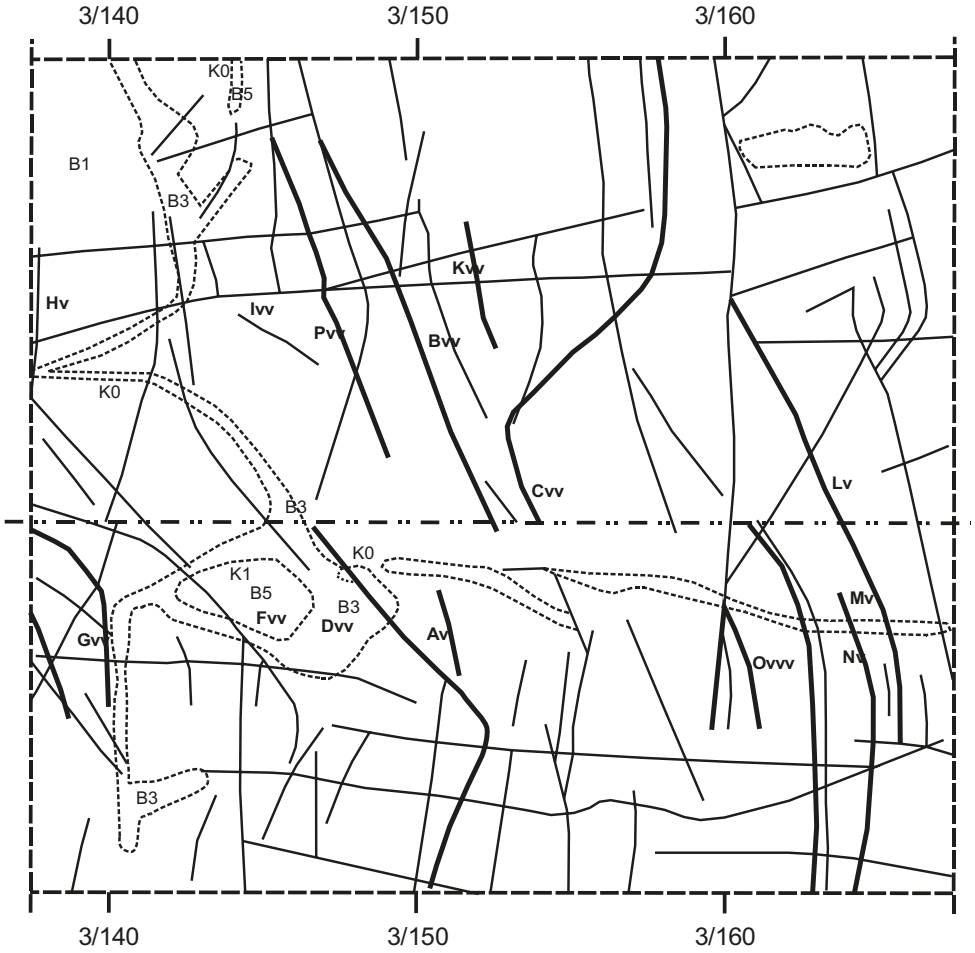

Figure 2-2. *Geological mapping of the TBM assembly hall, roof and side walls. Legend: Rock types: B1 = Äspö diorite, greyish and medium-grained with feldspar megacrysts. B3 = fine-grained granite, reddish brown. B5 = Greenstone, dark and fine-grained. Contacts: K0 – K1 and dashed line. K0 = contact between B1 and B3. K1 = contact between B3 and B5. Fractures: 01–81 and continuous line (thick lines represent water bearing fractures). Water: A-I and K-P and v = damp-minor seepage, occasional drops, vv = wet-seepage, drops or minor flow or vvv = flow.*

Table 2-2. Rock type distribution for the TBM assembly hall, walls and roof.

Rock type	Area m^2	Percentage of mapped area (side walls, and roof, 809 m^2)
Äspö diorite	752	93
Fine-grained granite	40.5	5
Greenstone	16.2	2
Total	**809**	**100**

All recorded fracture orientations have been plotted in Schmidt net and joint rosette diagrams, as shown in Figure 2-3. Three major fracture sets have been distinguished having the following mean orientations: 120°/80°, 180°/15° and 20°/80° (strike/dip right hand rule). The 120°/80° fracture set is the most prominent. However, Hardenby and Lundin (2003) showed that in certain locations the major fracture sets may be divided into two sets with mean orientations of 120°/80° and 140°/90°.

Only a few fractures showed evidence of displacements along the fracture surfaces. The apparent dislocations varied between 0.05 – 0.2 m. All fractures except one were steeply dipping. Three of them strike WNW–NW or ESE–SE and two of them, found in the deposition hole, lack record of strike. Lineations on the fracture planes have not been recorded, neither on dislocated planes or non-dislocated ones.

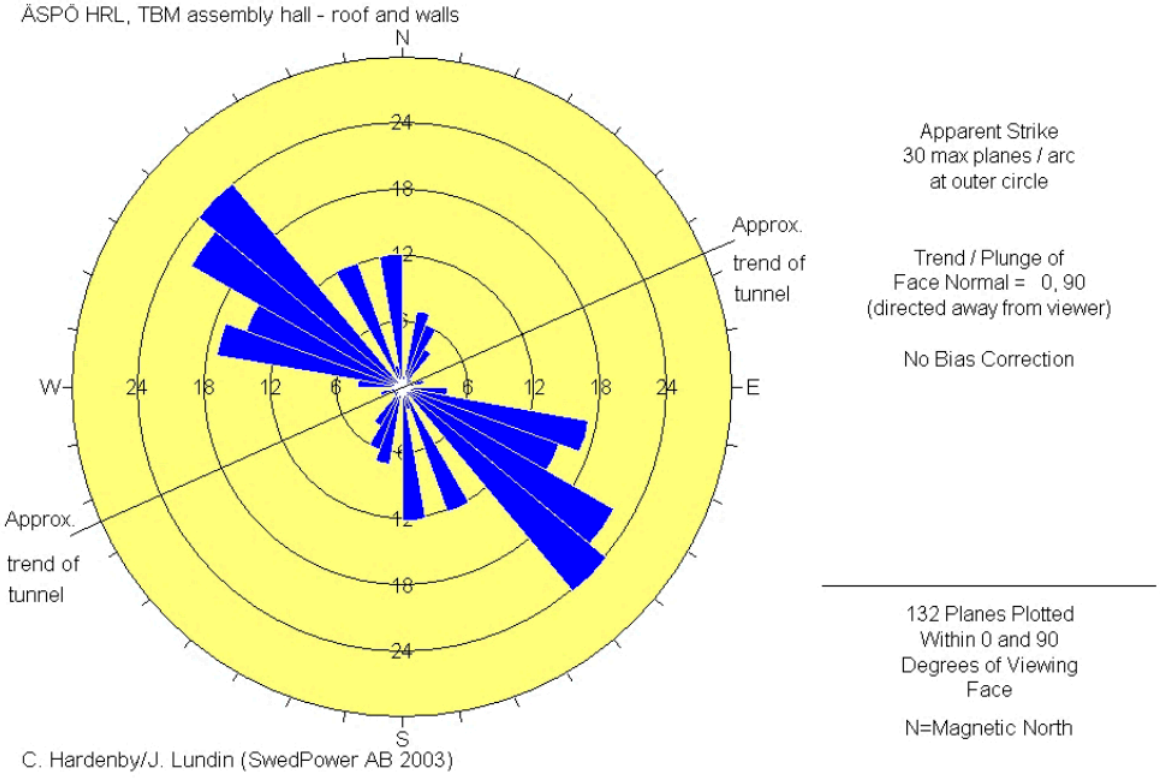

Figure 2-3. *Fracture orientations from the roof and side walls of the TBM assembly hall presented in Schmidt net and joint rosette diagrams.*

Most fractures contained more than one type of filling. Chlorite was by far the most common fracture filling and was found in 60–80 % of all fractures, see Table 2-3. Calcite, epidote and oxidation rims along fractures also appear frequently. Quartz, fine-grained granite and pegmatite appear in a few of the fractures. The latter two fillings were veins that are too thin to be recorded as rock types. Clay and grout were observed in a few fractures in the walls of the TBM assembly hall. Fe-precipitation/gel was found in a few fractures in the deposition hole.

Table 2-3. Distribution of fracture fillings in the TBM assemble hall, walls, and roof.

Filling	No of observations	% of all observations (total 132 fractures)
Chlorite	104	79
Calcite	47	36
Oxidation rim	38	29
Epidote	4	3
Clay	8	6
Grout	9	7
Fine-grained granite	1	1
Pegmatite	1	1
No filling or not observed	2	2

The fracture surfaces were mostly planar and rough. Planar and smooth fracture surfaces were rather common too in the walls, roof and pit floor of the TBM assembly hall. A few fractures were undulating or arched; they may be smooth or rough. Since healed and tight fractures were commonly considered to be rough, this “roughness-class” is believed to be over-represented. It is often impossible to judge how rough fracture planes of tight, healed fractures were.

When the mapping of the walls and roof of the TBM assembly hall was undertaken, all fractures were regarded as tight and healed. If all the water bearing fractures in the walls and roof are considered as open they would constitute 13 % of the fractures recorded there, which was similar to the deposition hole (Section 2.1.2).

With a few exceptions, the fracture widths were not recorded while the geological mapping of the TBM assembly hall took place. Most fractures were, however, rather narrow, < 1–2 mm. The standard mapping of the assembly hall (walls and roof) and the pit-floor, using a cut-off of about 1 m, showed that only 7 % and about 45 % respectively of the fractures were shorter than 2 m. With the same cut-off, about 70 % of the fractures measured in the deposition hole were less than 2 m in length. The longest fracture observed in the deposition hole was just under 6 m, in the pit-floor 7 m and in the walls and roof of the assembly hall 20–25 m.

The Rock Mass Rating (RMR)-values (approximately 70–75) indicate that the rock mass of the TBM assembly hall and the deposition hole can be classified as being of good quality.

2.1.2 Mapping of deposition hole DA3147G01

Deposition hole DA3147G01 was constructed in 1999 using a specially made vertically drilling Robbins TBM. Soon after completion the hole was geologically mapped in detail from a cage hooked up to a lift. The result of the detailed mapping of the deposition hole is shown in Figure 2-4.

Similar to the geological mapping of the TBM assembly hall, four major rock types have been distinguished in the deposition hole; Äspö diorite, greenstone, fine-grained granite, and pegmatite. Besides some specific features (listed below) the rock types resemble those that have been described for the walls and roof of the assembly hall:

- **Äspö diorite.** In the deposition hole the Äspö diorite was mainly of the feldspar megacryst bearing type. The colour was grey-dark grey sometimes slightly reddish grey. It constituted about 85 % of the hole-surfaces (wall and bottom) and was spread throughout the hole.
- **Greenstone.** The “greenstone” that was found in the deposition hole was fine-grained and black. It occurred as xenoliths scattered in the Äspö diorite. The patches of “greenstone” (7 % of the hole-surfaces) may sometimes include minor amounts of the Äspö diorite itself and pegmatite.
- **Fine-grained granite.** Two greyish red to pinkish red rock varieties assembled under the generic name fine-grained granite constituted 5 % of the hole-surfaces. They appeared in approximately equal amounts mainly in the lower part of the hole. One type was medium grained and may be regarded as a hybrid between fine-grained granite and Äspö diorite and occurred often as small “lenses” in the Äspö diorite proper. The other, fine- to medium-grained type and a more typical representative of the fine-grained grained granite formed 0.05 – 0.1 m wide veins. It occurred also as fracture filling.
- **Pegmatite.** It constituted only 3 % of the mapped surfaces. It appeared as a light red approximately 0.1 m wide vein in the lower part of the hole.

Table 2-4 summarises the occurrence of the rock types. It is shown as the estimated area of rock type exposure and in percentage of total mapped area. About 50 % of the contacts were tight and sharp. These are the ones between Äspö diorite and pegmatite, Äspö diorite and the fine-grained granite (in its “pure” state) and Äspö diorite and greenstone xenoliths (without any admixture of Äspö diorite or pegmatite). The boundaries between Äspö diorite and the impure greenstone xenolites, the Äspö diorite and the hybrid variety of fine-grained granite as well as the boundaries between the latter and the “pure” variety were on the other hand diffuse.

The distribution of fractures on the deposition hole wall and bottom are shown in Figure 2-4. The fracture orientations are presented in Schmidt net and joint rosette diagrams in Figure 2-5, which shows two major fracture sets. One of them is rather steeply dipping and has a mean orientation of approximately 120°/75° (strike/dip right). The other is gently dipping with a mean orientation of 195°/20°.

Most of the fractures (57 %) in the deposition hole were found to be natural, most probably previously healed and tight fractures, that were re-opened due to the drilling of the hole, 29 % were healed, tight fractures and 14 % were truly open natural fractures.

Table 2-4. Rock type distribution in deposition hole DA3147G01.

Rock type	Area (m²)	% of mapped area (hole wall and bottom 48 m²)
Äspö diorite	40.8	85
Greenstone	3.36	7
Fine grained granite	2.40	5
Pegmatite	1.44	3
Total	**48.0**	**100**

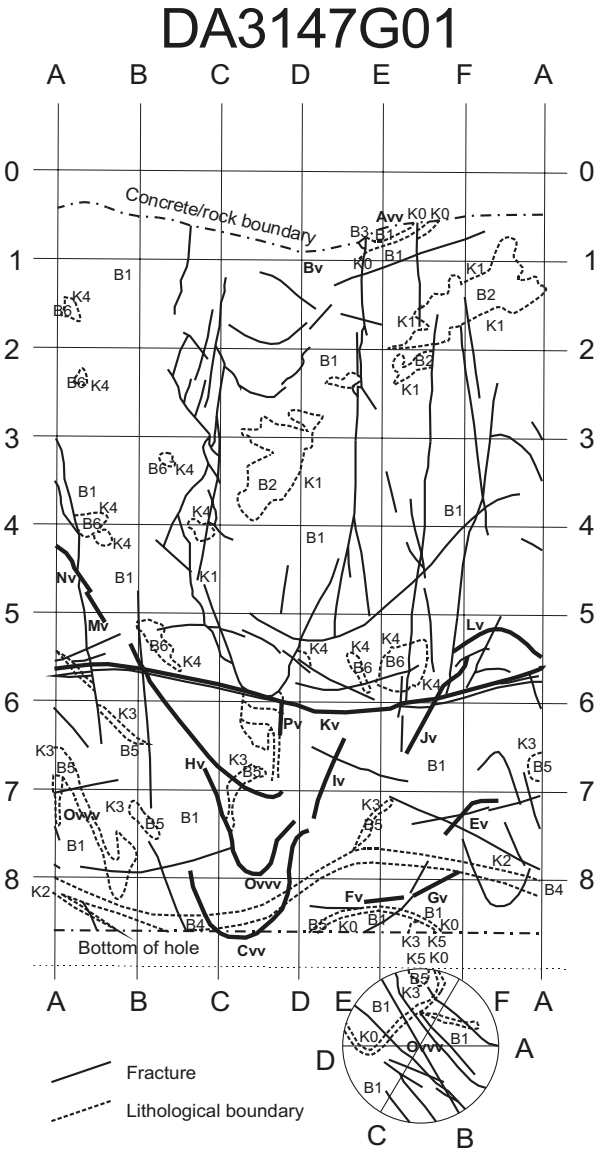

Figure 2-4. *Geological mapping of the deposition hole DA3147G01. Legend:* ***Rock types:*** *B1 = Äspö diorite, greyish and medium-grained with feldspar megacrysts; B2 = greenstone xenolith, black and fine-grained, includes some B1 and B4; B3 = "fine-grained" granite, greyish red and medium-grained; B4 = pegmatite, red and coarse-grained; B5 = "fine-grained" granite – hybrid of B1 and B3, greyish red and medium grained; B6 = greenstone xenolith, black and fine-grained.* ***Contacts:*** *K0–K5 and dashed line; K0 = contact between B1 and B3; K1 = contact between B1 and B2; K2 = contact between B1 and B4; K3 = contact between B1 and B5; K4 = contact between B1 and B6; K5 = contact between B5 and B3.* ***Fractures:*** *01–90 and continuous line (thick lines represent water bearing fractures).* ***Water:*** *A–Q and v = damp-minor seepage, occasional drops; vv = wet-seepage, drops or minor flow; vvv = flow.* ***Note:*** *direction A occurs at reference direction of 0°, depth (Y-axis) is a datum used for mapping and increases down the hole, compared with the refence coordinate system that increases from the base of the hole.*

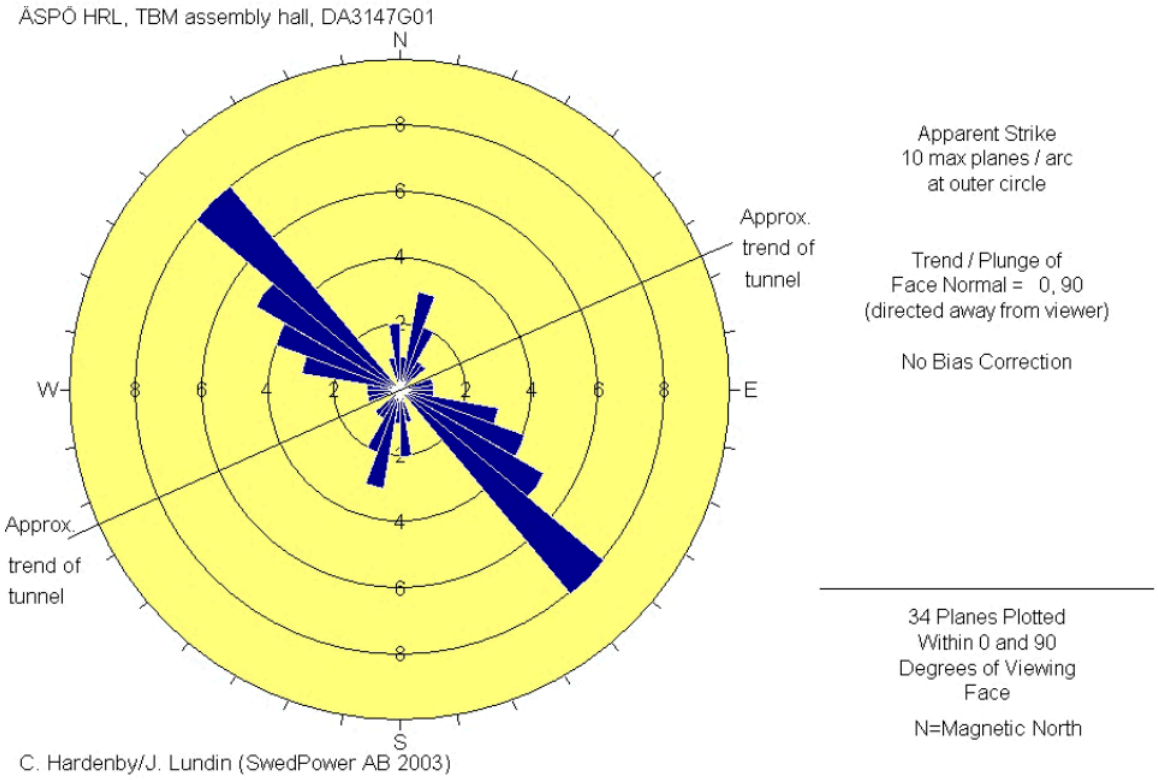

Figure 2-5. *Fracture orientations (partly compass readings and partly graphical interpretation) from DA3147G01 presented in Schmidt net and joint rosette diagrams.*

Six types of fracture filling material (oxidation included) were observed (Table 2-5). The most common material was chlorite that was found in 72 % of the 92 recorded fractures. Epidote and calcite were noted in 13 % and 12 % respectively of the observations. Fine-grained granite and quartz were found in 5 % and 2 % respectively of the fractures. Reddish oxidation of the rock was found along some of the fractures proper or occasionally as separate thin reddish streaks, recorded as fractures. Oxidation was observed in 28 % of the fractures. Some Fe-precipitate, often as a gel, was found along a few (8 %) of the fractures of which about half were water bearing.

Table 2-5. Distribution of fracture fillings in deposition hole DA3147G01.

Filling	No of observations	% of all observations (total 92 fractures)
Chlorite	66	72
Oxidation rim/streak	26	28
Epidote	12	13
Calcite	11	12
Fine-grained granite	5	5
Quartz	2	2
Fe-precipitate/gel	7	8
No filling or not observed	6	7

All mapped fractures had a rough surface, mostly planar (80 % of all fractures) but also undulating (19 %) and arched (1 %), see Table 2-6. Since many fractures were tight and healed it was often difficult to determine the surface roughness. For these cases, the surface structure term “undefined” was introduced by Hardenby and Lundin (2003). When all fractures that were tight and healed were considered having surface roughness “undefined” and those that were open are “rough” as originally indicated in the database, then the distribution will be as “alternative 2” in Table 2-6.

Table 2-6. Distribution of fracture surface categories in deposition hole DA3147G01.

Surface category	No of fractures (alternative 1)	% of all fractures (total 92)	No of fractures (alternative 2)	% of all fractures (total 92)
Planar and rough	74	80	49	54
Planar and undefined			25	27
Undulating and rough	17	19	14	15
Undulating and undefined			3	3
Arched and rough	1	1	1	1
Total	**92**	**100**	**92**	**100**

The size of the canister deposition hole limited the fracture trace lengths. In Table 2-7 the fracture lengths have been grouped into intervals of 1 m. The table shows that 45 % of the fractures were shorter than 1 m while 38 % were found within the interval 1–2 m. Therefore, most of the fractures (about 85 %) in the deposition hole were shorter than 2 m. Only 2 % of the fractures exceed 4.0 m in length. The table also shows what the distribution of fracture lengths would be if a cut off of 1 m is used instead of 0.5 m. When making a comparison with the fracture length distribution obtained from mapping of the walls, roof and floor of the assembly hall it has to be remembered that fracture length cut off was about 1 m when that mapping took place.

Table 2-7. Distribution of fracture lengths in deposition hole DA3147G01.

Length interval in meters	Detailed mapping of canister deposition hole			
	Cut off of 0.5 m			Cut off of 1 m
	No of fractures		% of all the 92 fractures	% of all the 51 fractures
< 1	41	(-)	45	-
1–2	35	(35)	38	68
2–3	9	(9)	10	18
3–4	5	(5)	5	10
4–5	1	(1)	1	2
5–6	1	(1)	1	2
Total	**92**	**(51)**	**100**	**100**

2.2 Hydrogeology (IPR-04-52)

Several observations of water occurrence were made during the geological mapping. Additionally, as a part of the Lasgit project some hydrogeological tests were performed in the large deposition hole DA3147G01. These included pressure build up and pressure drop tests and gas leakage tests.

2.2.1 Water observations in the TBM assembly hall

Leakage of water was recorded at a number of locations of which some were patches on the rock surface and some were fractures. In the Äspö tunnel system as a whole the water-bearing fractures commonly were steeply dipping, striking NW or SE.

Where the quantity of the water leakage, originating from micro-cracks in the rock mass or from distinct fractures in the walls and roof of the assembly hall, were measured it was normally < 0.3 l min^{-1}. However, three fractures discharged as much as 2–4 l min^{-1}. Observations of water leakage are lacking from the pit-floor due to constant inflow from the side-walls of the pit.

The measured inflow of water in the two pilot holes KA3147G01 and KA3153G01 was about 1.15 and 0.1 l min^{-1} respectively during the pressure build up test with water pressures about 9 and 13 bar.

The TBM assembly hall was no wetter than the rest of the Äspö tunnel system. However, the walls and roof both discharge some water, though this was mainly from discrete locations which were unevenly distributed.

2.2.2 Water observations in the large deposition hole DA3147G01

The water-bearing fractures in the deposition hole were, apart from a few sub-horizontal-gently dipping ones, rather steeply dipping towards SW whereas those in the walls and roof of the assembly hall were steeply dipping towards the SW or NE. Occurrences of water are summarised in Table 2-8.

The leakage of water in the deposition hole was of minor seepage or occasional drops. It was, however, not measured. Leakage between concrete and rock at the top of the hole and a drill hole ending close to the bottom of the deposition hole gave each about 0.5 litres of water per minute.

Table 2-8. Occurrences of water in deposition hole DA3147G01.

Origin of water	Number of observations	Character of water leakage	Flow (l m^{-1})	Remarks
Rock	1	(1) Damp, minor seepage or occasional drops	"0"	The whole hole wall is damp to wet
Rock	2	(3) Wet – Flow	0.1–0.5	Quantity estimated from leakage between concrete and rock. The whole bottom is very wet due to leakage above
Fracture	11	(1) Damp, minor seepage or occasional drops	"0"	Quantity has not been estimated or measured
Fracture	1	(2) Wet, seepage, minor flow or drops	"0"	Quantity has not been estimated or measured
Fracture	1	(3) Wet – Flow	"0"	Quantity has not been estimated or measured. Most leakage from lower part of fracture
Drill hole	1	(3) Wet – Flow	0.5	

2.2.3 Hydrogeological tests in the deposition hole

The inflow of water into the Lasgit hole was measured using the setup shown in Figure 2-6. Water originating from the surrounding tunnel floor (termed "external water") was prevented from entering the deposition hole and was measured separately. Ingress of water to the Lasgit hole, entering through the fractures and the rock mass of the hole wall and bottom ("internal water"), was measured by using a level indicator to study the rise of the water level over time.

Figure 2-6. *Deposition hole DA3147G01 with the circular drain and small plastic container (greyish) used to collect inflowing water.*

During the period the measurements took place, the inflow of "external water" varied between 10–20 litres per day (0.007–0.013 l min^{-1}), as shown in Figure 2-7.

The inflow of "internal water" was about 240 litres per day (0.17 l min^{-1}) if the theoretical evaporation was not considered and 266 litres per day (0.2 l min^{-1}) if it was, as summarised in Table 2-9.

To get an estimate of the evaporation in the TBM assembly hall an *in situ* test was performed in March 2004. It showed that the evaporation from a 1 metre square free water surface was 0.67 litres/day. This meant that the evaporation from the free, circular water surface down in the deposition hole was 1.6 litres/day (possible evaporation from the hole wall not included). This corresponds to 0.7 % of the "internal" inflow, which is much less than the accuracy of the method used to measure the inflow (± 2.5 – 3 %). Thus, the evaporation from the free water surface down in the hole may be neglected.

Table 2-9. Inflow of internal water into deposition hole DA3147G01 in December 2003 (water level refers to recorded level relative to a reference level at the upper part of the hole at the end date of an interval).

Start	End	Interval (h)	Water level (m)	Change in water level (m)	Quantity of water (litres)	Inflow rate		
Day/Time	Day/Time					(litres/day)	(litres/hr)	(litres/min)
	12/13:50		8.203					
12/13:50	15/16:07	74.3	7.915	0.315	757.7	244.8	10.2	0.17
15/16:07	17/10:30	42.4	7.745	0.170	408.9	231.5	9.6	0.16
Total		116.7		0.485	1 166.6			
Mean						239.9	10.0	0.17

At the time when the measurements of "internal water" inflow took place the theoretical evaporation from the hole wall could have been as much as about 24 litres/day. This assumed that the entire hole wall acted as a free water surface, which is not the case since large parts of the wall were dry-damp. As such the evaporation from the hole wall was of minor importance for this study and the measured inflow of "internal water" can be regarded as the real inflow.

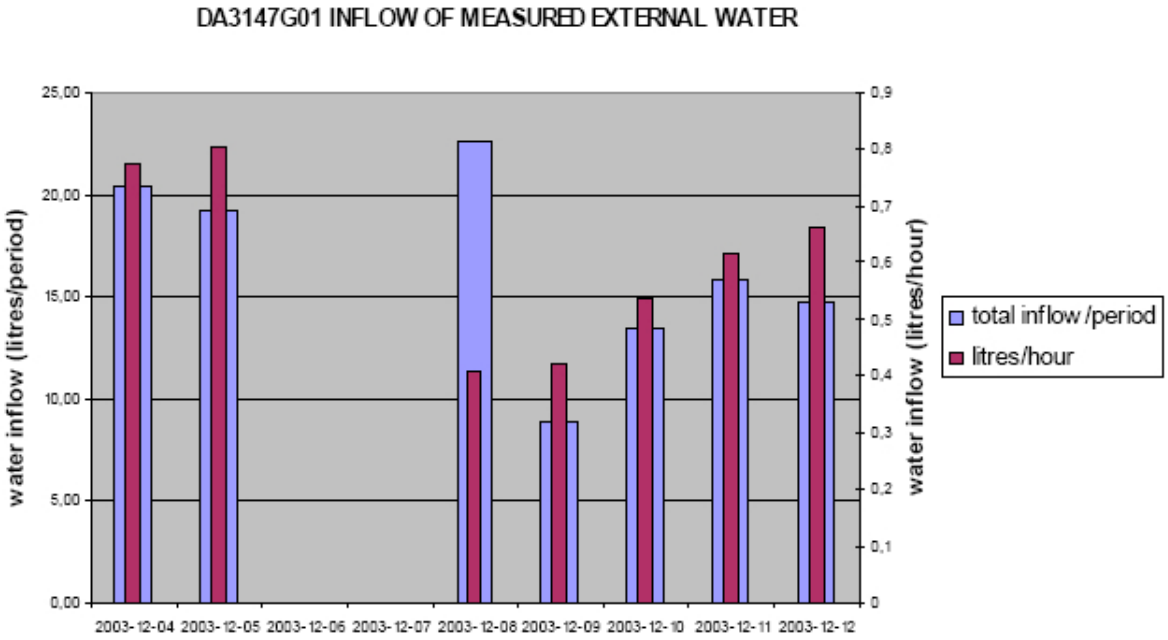

Figure 2-7. *Inflow of measured external water, total inflow and inflow rate (l h^{-1}) per measuring interval in deposition hole DA3147G01.*

2.2.4 Pressure build up and pressure drop tests

Pressure build up tests were made not only in the anchor holes but also in pilot holes drilled in the planned centres of all the large deposition holes on the 420 m level prior to the drilling of the Lasgit deposition hole. These tests showed a water pressure varying between 3–20 bar in the anchor holes and 0–27 bar in the pilot holes.

The pressure drop tests or pulse tests performed in the anchor holes gave varying results too. While none of the curves reach a well defined asymptote, the pressure decays were sufficiently well defined to provide an estimate of the hydraulic properties. The calculated hydraulic conductivities and transmissivities varied between $1 \times 10^{-12} – 7 \times 10^{-10}$ m s^{-1} and $9 \times 10^{-12} – 3 \times 10^{-9}$ m^2 s^{-1} respectively. Figure 2-8 shows an example of a pressure drop test.

2.2.5 Gas leakage test

A gas leakage test was performed in six of the ten anchor holes in order to investigate whether there were any connections between the anchor holes and the water filled Lasgit hole. Anchor holes were incrementally pressurised. Gas leakage was seen as bubbles on the water surface in the Lasgit hole, as shown in Figure 2-9, and in the neighbouring anchor holes. With the help of a video camera the gas leakage was located on the wall of the Lasgit hole and registered on drawings; one example is shown in Figure 2-10. Results from these tests clearly demonstrated that a number of fractures intersected both the neighbouring anchor holes and the Lasgit deposition hole. Table 2-10 summarises the observations during the gas leakage tests.

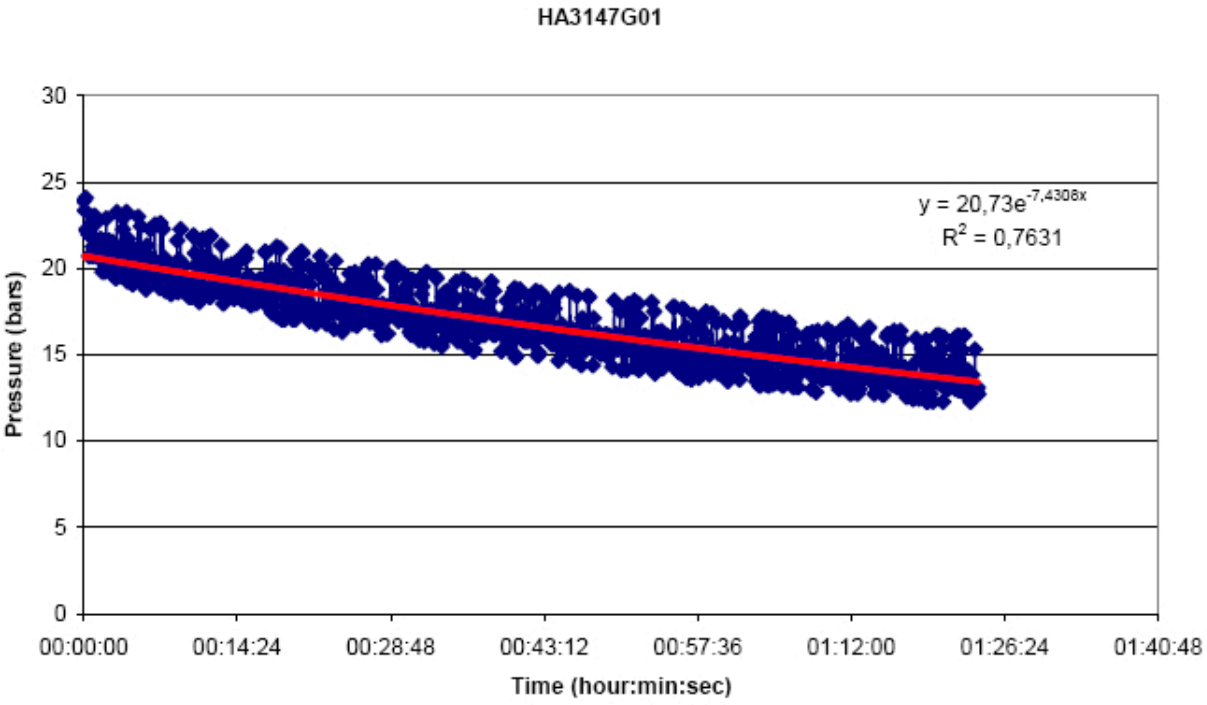

Figure 2-8. *Pressure drop test in HA3147G01 (individual readings and trend line).*

Figure 2-9. *Gas bubbles on the water surface in the Lasgit hole.*

Table 2-10. Notes from the gas leakage test in the Lasgit hole DA3147G01 and some of the anchor holes.

Pressurized Anchor Hole No	Start April 2004 Day/time (d/h:m)	Max pressure		End April 2004 Day/time (d/h:m)	End pressure (bar)	Notes G01–G10 refer to the anchor holes.
		Time (h:m)	Pressure (bar)			
HA3147G01	21/13:37	13:41	20	21/15:26	16.5	G01: some bubbles observed above the packer, G10: bubbles, G02 and G09: a few bubbles.
HA3147G02	20/13:22	13:32	20	20/15:24	16	G02: lots of bubbles observed above the packer, G03: lots of bubbles, G01 and G10: bubbles and G05: a few bubbles
HA3147G04	20/10:26	10:35	20	20/11:45	16	G04: bubbles observed above the packer and G05: bubbles
HA3147G06	--/10:39	10:55	20	--/11:21	20	G06: some bubbles above the packer
HA3147G08	21/10:59	11:11	20	21/12:11	19.5	G08: a few bubbles above the packer
HA3147G10	21/08:48	09:00	20	21/09:40	19	G10: a few bubbles above the packer, G01 and G09: a few bubbles

It can also be seen that pressurising the rock anchors on one side of the deposition hole often resulted in gas leakage on the opposite side of the hole. This shows that the fracture network is complex and that gas does not always flow to the nearest fracture in the deposition hole, but follows a path of least resistance. The varying results of the respective pressure tests are likely to be because of variations in fracture geometry and transmissivity as well as the geospatial distribution of boreholes along the various features. Leakage between packer and hole walls is, however, another possibility and cannot be ruled out.

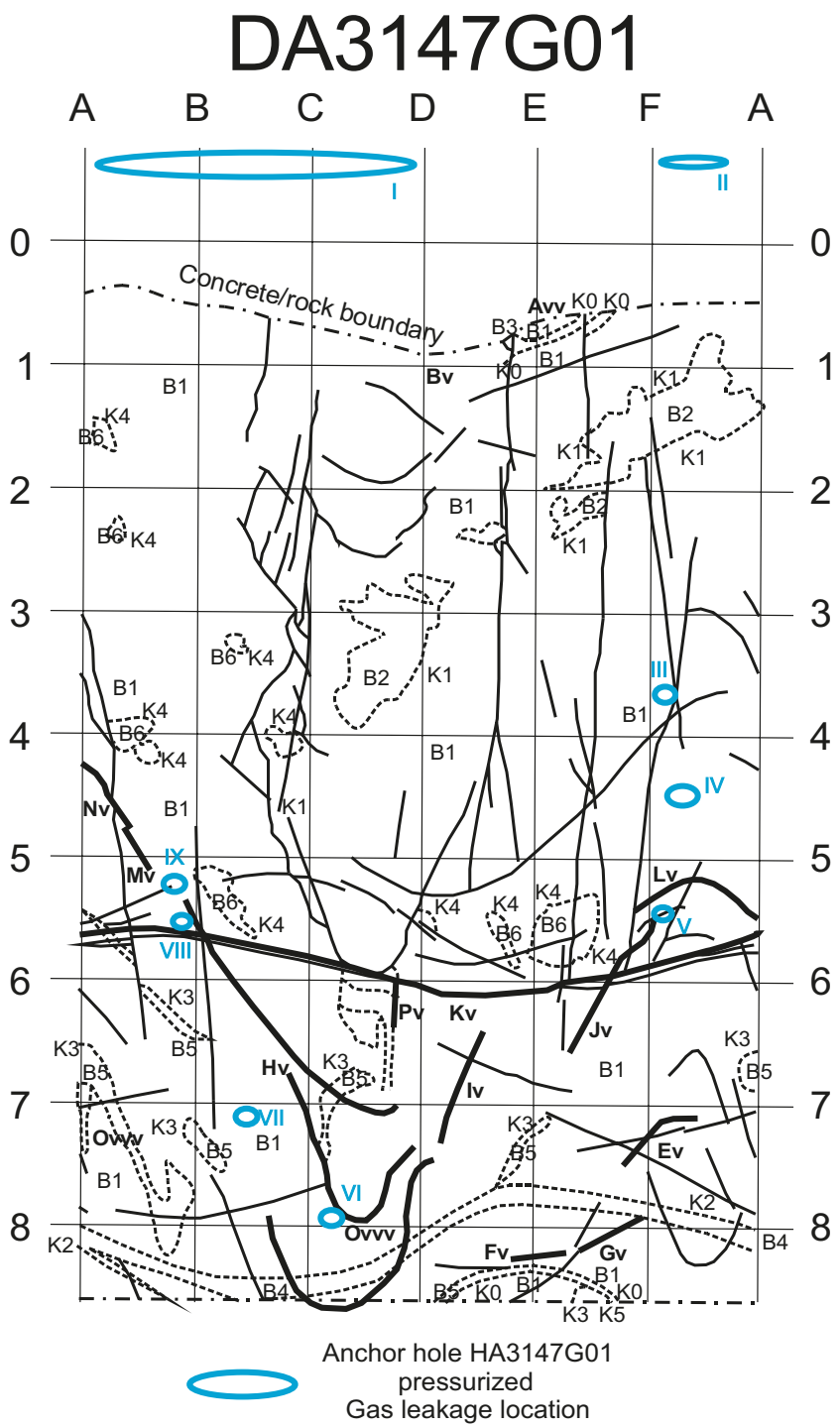

Figure 2-10. *Gas leakage locations in DA3147G01 when anchor hole HA3147G01 was pressurized. Legend: I. Bubbles on the surface; II. Some bubbles on the surface; III–V. Bubbles from one spot; VI. Bubbles; VII. Some bubbles, one spot; VIII. Bubbles, one spot, top of slot; IX. Bubbles from three spots in a row.* ***Note:*** *direction A occurs at reference direction of 0°, depth (Y-axis) is a datum used for mapping and increases down the hole, compared with the refence coordinate system that increases from the base of the hole.*

2.2.6 EDZ in the deposition hole (IPR-07-14)

An Excavation Disturbed/Damaged Zone (EDZ) is formed around openings (boreholes, tunnels etc) when they are constructed. During construction, supporting rock material is removed. However, the stress in the system is not reduced, so the rock around the perimeter of a tunnel has to support the load that was previously carried by the removed mass from within the tunnel. This leads to stress concentrations round the circumference of the tunnel wall and boreholes.

The geological mapping of the deposition hole did not describe any of the "classic" features observed around tunnels with significant EDZ's. However, the damage can often be microscopic and not visible to the naked eye, so the lack of spalling material is not symptomatic of an absent EDZ and further tests were performed in order to establish (or not) the existence of an EDZ.

Bundesanstalt für Geowissenschaften und Rohstoffe (BGR) developed a surface packer system designed to test for the presence of an EDZ at the Äspö site. This type of packer is fixed directly on the gallery wall and is therefore able to characterize the surface area most damaged during excavation of the deposition hole. This surface packer system was used at a number of locations in the HRL at Äspö including galleries (excavated by drill and blast), the TBM and deposition holes; including DA3147G01 **(**the Lasgit deposition hole).

A photograph of the surface packer system is shown in Figure 2-11 and as a schematic in Figure 2-12. The packer comprised a circular metal unit sealed to the rock surface using bentonite which was held in place by fixing bolts attached within the rock. Water or gas was introduced and pressure decay was monitored. For the measurements within the Lasgit deposition hole only local water was used as an injection fluid.

Tests were planned at two positions with water-bearing fractures in the deposition hole and on one position without visible fractures. The tests on the fractured positions failed. Instead of swelling, the bentonite was washed out of the furrow during the hydration stage by the inflowing water from the fracture. A similar response was noted during the initial hydration stage of the main Lasgit experiment (Chapter 5). The asperities on the wall of the deposition hole on these positions turned out to be too rough.

Figure 2-11. *The surface packer system of BGR shown* ***in situ*** *ready for the start of a test.*

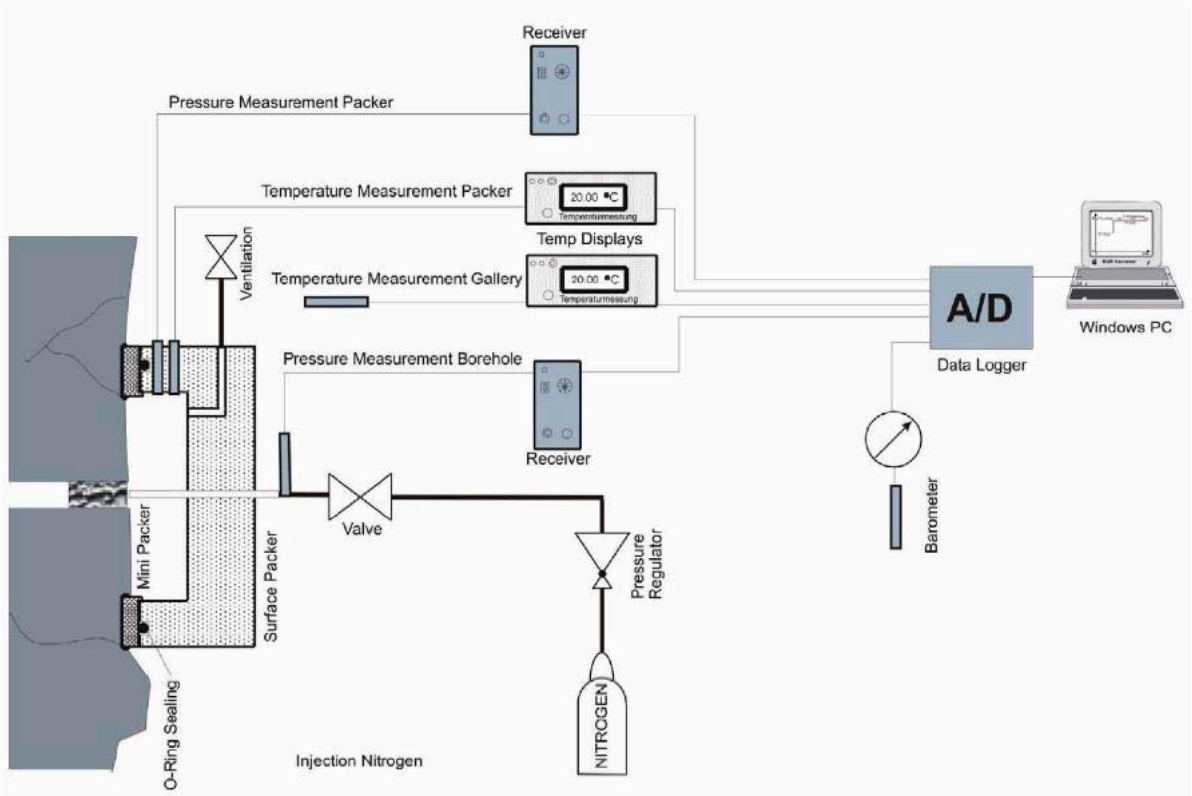

Figure 2-12. *The surface packer and mini packer system shown as a schematic.*

On the position without visible fractures a test sequence of two pulses (160 kPa and 220 kPa) was conducted. An axially symmetric model was used for the test analysis. Figure 2-13 shows a comparison of the measured pressure evolution in the surface packer (grey line) and calculated pressure evolutions for several permeability values. The calculated pressure evolution for a permeability of the rock of 10^{-19} m² agrees well with the measured data. However, one limitation of this method is the potential for water leakage through the bentonite packer assembly rather than within the diorite rock mass. Assuming this effect is negligible, Nowak et al. (2007) concluded there was no evidence of an EDZ in the Lasgit deposition hole and as such quote a permeability value for the "intact" granite of 10^{-19} m^2.

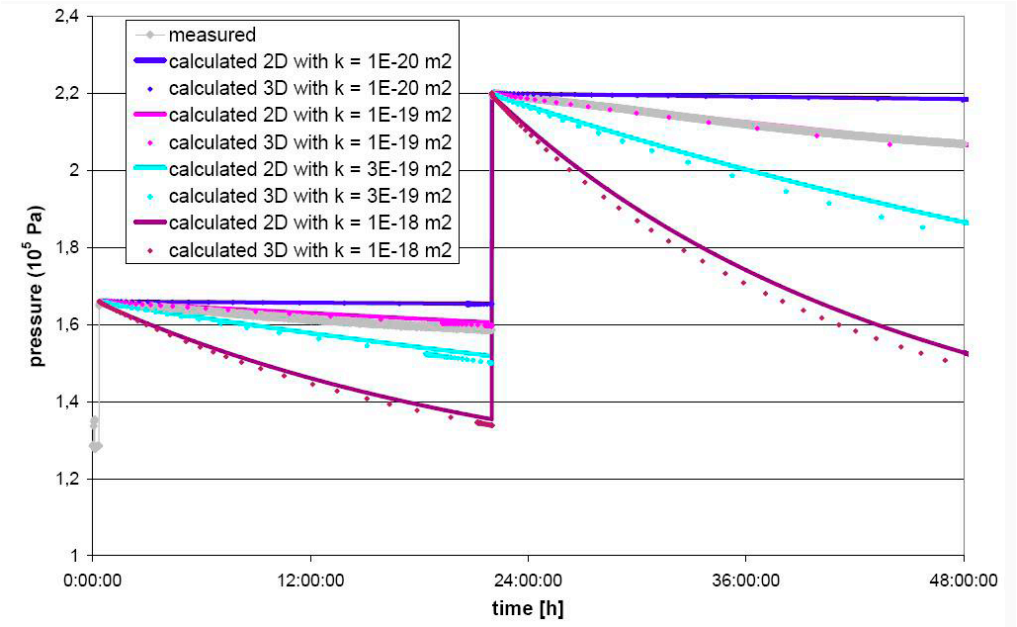

Figure 2-13. *Result from surface packer test in deposition hole DA3147G01 (Lasgit).*

3 Experimental geometry and data reduction

The Lasgit experiment was commissioned in deposition hole No. DA3147G01; the first emplacement borehole to be drilled at the Äspö HRL. The deposition hole had a length of 8.5 m and a diameter of around 1.75 m. A full scale KBS-3 canister was modified for the Lasgit experiment with twelve circular filters of varying dimensions located on its surface to provide point sources for gas injection, mimicking potential canister defects. These filters could also be used to inject water during the hydration stage.

Figure 3-1 shows the location of the deposition hole DA3147G01 within the Äspö Hard Rock Laboratory and Figure 3-2 shows a photograph of the test site following the installation stage. Lasgit was situated within the TBM assembly Hall at the 420 m depth as highlighted in Figure 3-1a. Within the assembly hall, the position of DA3147G01 is shown. The orientation of the reference direction is taken from the local coordinate system, with 0° parallel with the direction of the tunnel system (Figure 3-1b). For mapping purposes, this was deemed direction A. Figure 3-1c shows the deposition hole coordinate system with the position of all sensors defined as a height z above the bottom of the deposition hole, at a distance r from the centre of the deposition hole, at an angle of α to the Lasgit reference direction.

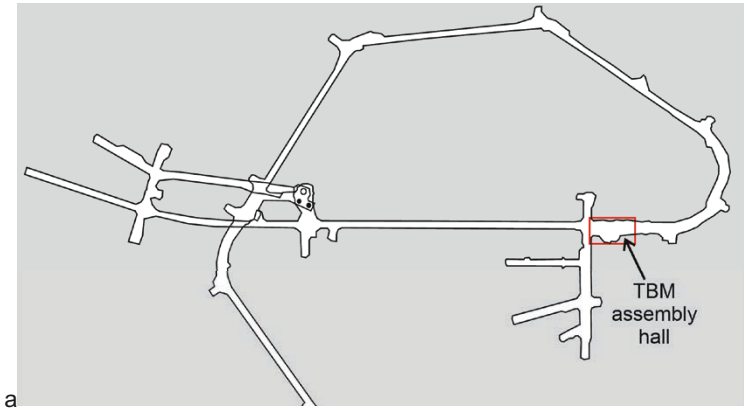

a

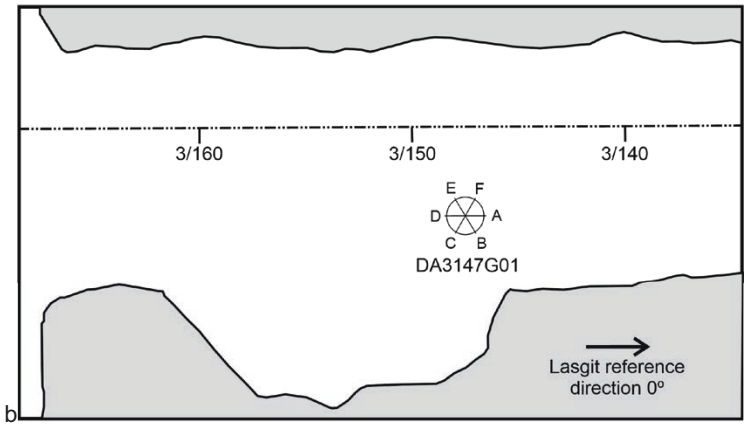

b

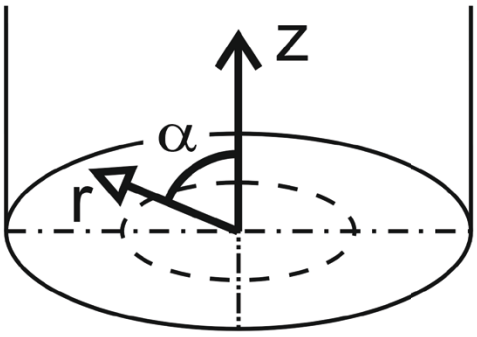

c

Figure 3-1. *Location and reference direction of the Lasgit experiment in the Äspö Hard Rock Laboratory.*

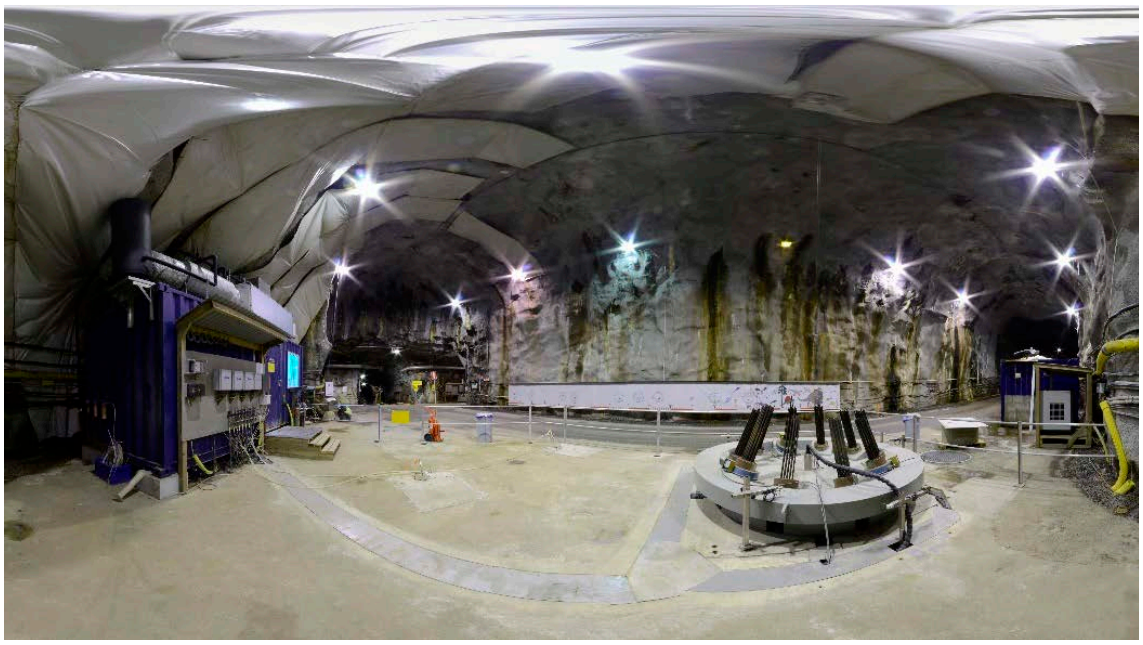

Figure 3-2. *A panoramic view of the Large-scale gas injection test (Lasgit) 420 m below ground at the Äspö Hard Rock Laboratory in Sweden.*

The deposition hole, buffer and canister were equipped with instrumentation to measure the total stress, porewater pressure, and relative humidity in 32, 26 and 7 positions respectively. Additional instrumentation continually monitored variations in temperature, relative displacement of the lid, and the restraining forces on the rock anchors. The emplacement hole was capped by a conical concrete plug retained by a reinforced steel lid capable of withstanding over 5 000 tonnes of force.

The state-of-the-art experimental monitoring and control systems for Lasgit were housed in the "Gas Laboratory" which was a self-contained unit designed and assembled by BGS within a modified shipping container. A customised graphical interface based on National Instruments LabVIEW™ software enabled remote control and monitoring to be undertaken by project staff from any internet connected PC around the world.

3.1 Gas laboratory

The Gas Laboratory was housed in a fully insulated pre-fabricated shipping container. This facility housed all experimental circuits (hydration, hydraulic, and gas injection) as well as data acquisition and telemetry systems.

The shipping container housing the Gas Laboratory was partitioned into two sections. The first comprised the office area and contained the workstation plus general office furniture, telemetry system, and main electrical consumer unit. The second area contained all of the experimental apparatus, test circuits, and data acquisition systems. Figure 3-3 shows a full 360° panorama inside the gas laboratory.

Temperature in both the office and laboratory sections was controlled by two independent air conditioning systems. The temperature set point in the Laboratory section was 14 °C, similar to the ambient conditions within the Lasgit deposition hole; the air-conditioning achieved a mean temperature of 15.8 °C. To prevent overloading of the air-conditioning system the temperature in the office compartment was reduced after Day 750 and although temperature oscillated on an annual basis the mean temperature reduced to 15.0 °C. To maintain a flow-through of air and help to minimise condensation, the air was continuously replaced, and its humidity controlled to prevent damage to test systems. Temperature sensors located in both compartments of the Gas Laboratory were continuously monitored by the data acquisition software and by the Alpha Alarm system at Äspö, the latter providing 24 hr support in the event of a system failure.

Figure 3-3. *A panoramic view of the Lasgit gas laboratory.*

3.2 Apparatus and instrumentation

The experimental set-up was highly instrumented with 20 pore pressure sensors on the deposition hole wall, 6 pore pressure sensors within the bentonite buffer, 20 radial stress sensors on the deposition hole wall, 9 total stress sensors within the bentonite buffer, 3 stress sensors on the canister surface, and 7 psychrometer sensors within the bentonite buffer. Figure 3-4 shows the distribution of all sensors within the deposition hole in plan view at a number of sections at different height. Figure 3-5 shows a map of the deposition hole wall and the distribution of the sensors. Table 3-1 summarises the name of each sensor at each level within the depoisiton hole. The following sections describe the key components of the Lasgit system.

Table 3-1. Summary of all sensors at 17 intervals in the deposition deposition hole.

	Filters	Pore pressure in bentonite UB	Stress in bentonite PB	Pore pressure on rock wall UR	Stress on rock wall PR	Stress on canister PC	Relative humidity WB
Section 17			PB927 PB928 PB929				
Section 16		UB925 UB926					WB907
Section 15	FM904						
Section 14		UB923 UB924					WB905 WB906
Section 13	FR902		PB923 PB924 PB925 PB926				
Section 12	FM903						
Section 11							WB903 WB904
Section 10				UR919 UR920 UR921 UR922	PR919 PR920 PR921 PR922		
Section 9	UFA1 UFA2 UFA3 UFA4			UR915 UR916 UR917 UR918	PR915 PR916 PR917 PR918		
Section 8						PC903	
Section 7	MPFA1 MPFA2 MPFA3 MPFA4			UR911 UR912 UR913 UR914	PR911 PR912 PR913 PR914		
Section 6						PC902	
Section 5	LFA1 LFA2 LFA3 LFA4			UR907 UR908 UR909 UR910	PR907 PR908 PR909 PR910		
Section 4				UR903 UR904 UR905 UR906	PR903 PR904 PR905 PR906		
Section 3						PC901	
Section 2	FR901	UB902					WB901 WB902
Section 1		UB901	PB901 PB902				

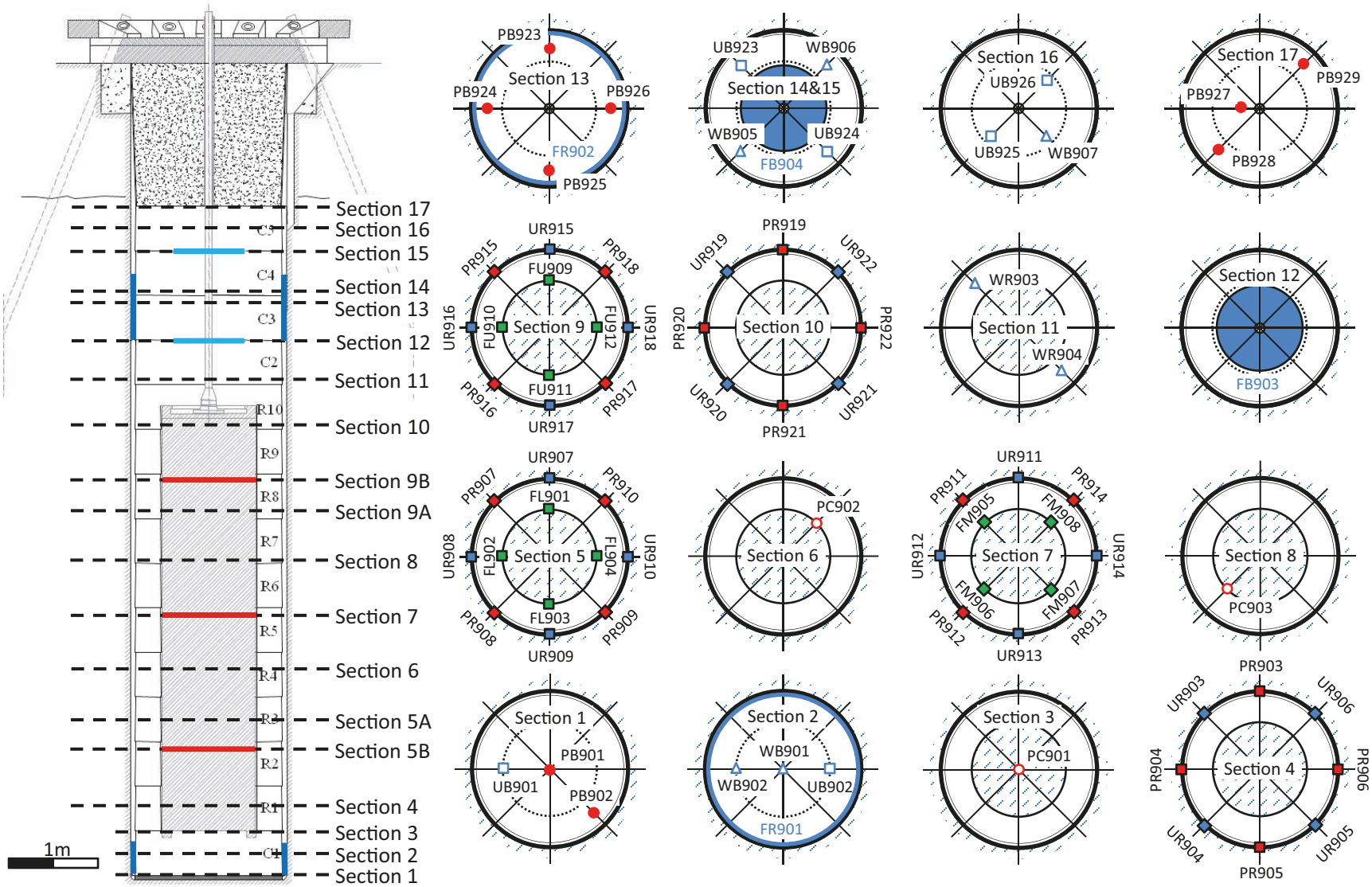

Figure 3-4. *Plan view of the location of all sensors at 17 intervals in the deposition deposition hole.*

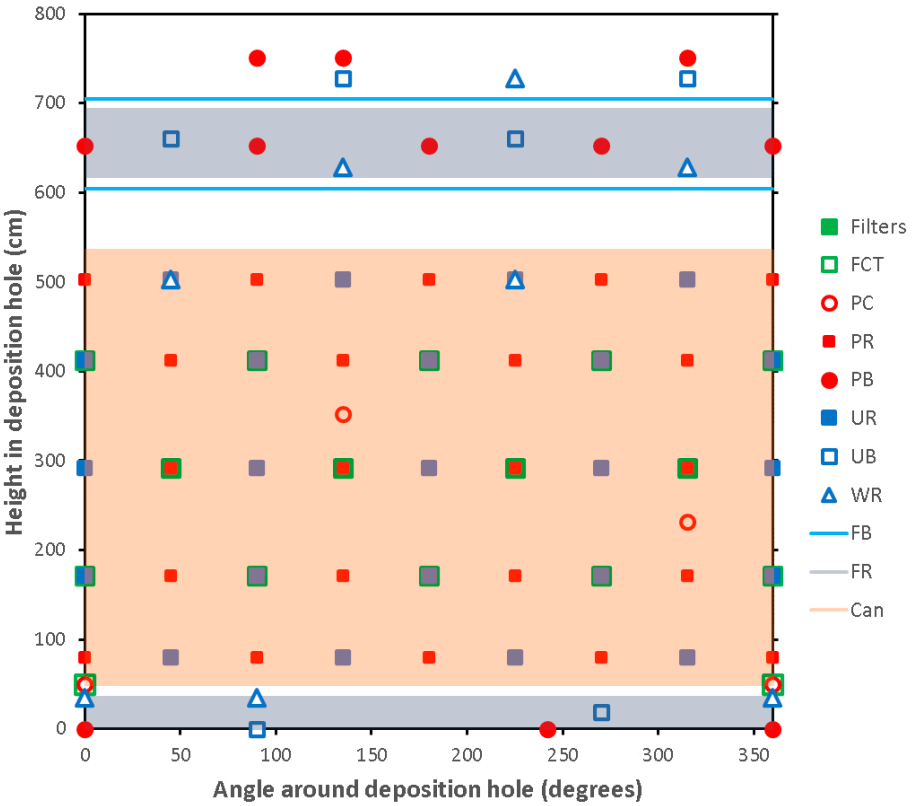

Figure 3-5. *Map of the deposition hole wall showing the location of all sensors. Each sensor type is introduced in the following sections.*

3.2.1 The lid and retaining setup

The pressure that would be exerted by the backfill as the tunnel gallery was closed was generated using a heavy 2 600 mm diameter SS2172 carbon steel lid; this also prevented an uncontrolled expansion of the bentonite. At the top of the buffer, a waterproof and sealed rubber mat was placed, upon which a conical shaped concrete plug was poured using K 40 quality concrete to close the deposition hole, the top of which was level with the TBM assemble floor. On top of this plug, the steel lid was anchored to the rock by 10 anchor cables. The lid and rock anchors can be seen in Figure 3-2.

The retaining system (i.e. concrete plug, steel lid and anchoring cables) was designed for a maximum operating pressure of 20 000 kPa. The rationale in using a conically shaped concrete plug was to (a) ensure that the plug could move upwards when subject to high axial pressures and (b) could be readily dismantled at the end of testing.

The anchor system comprised cables of type VSL 19-15, which were secured using a low-pH cementitious injection grout within ten holes of 162 mm diameter, 11 000 mm length, and angled at 21.8° from the deposition hole. Each cable was grouted for 8 m length of the cable to ensure the anchors could accommodate the forces which would be generated during testing. The retaining system was also designed to allow small vertical deformations of the concrete plug and steel lid when subjected to high axial forces.

The anchor cables holding the lid were pre-tensioned to 1 300 kN using two hydraulic jacks in parallel. Three of the anchors included Glötzl (GLÖTZL Gesellschaft für Baumesstechnik mbH, Germany) load cells of type kN 5000 A160 M/DKV6, with a maximum load of 5 500 kN. These were used to log load on the rock anchors, and thus the load exerted by the buffer, during the operation of the test. **Note:** The Glötzl load cells were not temperature compensated.

3.2.2 Bentonite buffer

Figure 3-6 shows a sketch cross-section through the deposition hole, giving dimensions of the individual elements of the KBS-3V concept. The space around the canister was filled with pre-compacted bentonite blocks, which, once hydrated, act as a low permeability diffusional barrier. The unique physicochemical properties of the bentonite depend on its colloidal behaviour and enormous specific surface. These include high sorption capacity, very high plasticity and excellent fracture self-sealing characteristics, severely limiting the migration of any radionuclides released from a canister after closure of the repository.

The bentonite used was MX-80 with a water content of 22 % (for the ring-shaped blocks) and 26 % (for the cylindrical blocks). The natural water content of MX-80 is 10 %, therefore water had to be added to the starting bentonite powder to achieve the desired water content and a saturation of > 95 %.

Blocks were manufactured from bentonite powder that was pre-checked to meet the required specification. The quality-control included tests of natural water content, free swelling, liquid limit, and grain size distribution for each of the delivered Big-Bags. Variable water content is common and varies between 8 and 13 %, although the water content of each delivery tends to be very small. The grain size distribution test uses a sieve to determine the size of the granules of clay particles. This test was performed to avoid deliveries with very fine powder, which might be hard to both mix and compact.

To achieve a high degree of saturation, water of a specific quantity was mixed with the powdered bentonite using an Eirich mixer at Hackman-Rörstrand AB. Once mixed, the water content of the mix was determined by drying a sample at 105 °C for 24 hours, with the rest of the bentonite placed in plastic bags to avoid desiccation during transportation and storage. The mixed bentonite was transported to Hydroweld AB in Ystad for pre-compaction. The mixture was poured into a rigid mould for either a complete block or a ring and was compacted vertically using a 30 000-ton press. Limited clearance in the press meant that the sample was compressed in three stages, adding more pistons as the sample compressed. Throughout the compaction the mould was connected to a vacuum pump to de-air the powder/block. Full compression took ~ 10 minutes to reach 50 MPa (10 734 ton for segments and 6 159 ton for rings), with maximum load held for 60 minutes. Unloading took a further 10 minutes with the blocks then removed from the mould and checked for dimension and weight and that the desired density had been achieved. Up to three blocks were manufactured a day.

Table 3-2 shows the dimensions and starting physical properties of the pre-compacted bentonite rings and blocks. As shown, a high degree of saturation (between 95.1 % and 99.7 %) was achieved, with bulk densities ranging between 2 018 kg.m^{-3} and 2 061 kg.m^{-3}. Table 3-3 shows the expected density and swelling pressure after saturation at different sections of the deposition hole. This predicts a swelling pressure of between 3 970 kPa and 4 368 kPa within the Lasgit depositional hole, with greater pressure achieved above and below the canister.

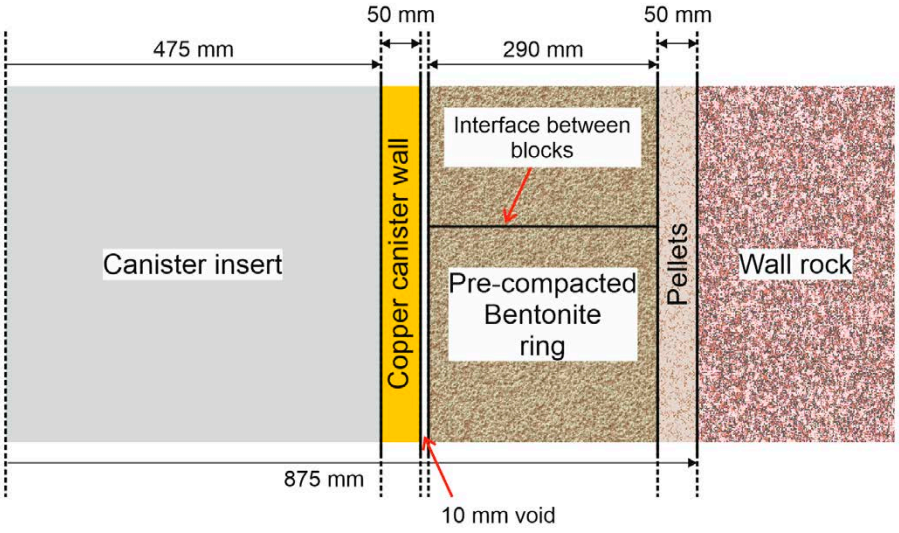

Figure 3-6. *Cross-section sketch through the Lasgit deposition hole showing the canister, enginnered void, pre-compacted bentonite ring, pellets, and wall rock.*

Table 3-2. Properties and dimensions of the bentonite buffer. Diameter D1 and D2 are measured widths of the blocks measured orthogonal to one another, D3 is the inner diameter of the annular rings.

Block No	Date at comp	Block No in deposition hole	Moisture content	Bulk density (kg/m^3)	Degree of saturation	Void ratio	Dry density (kg/m^3)	Dens at sat (kg/m^3)	Weight (kg)	Height (mm)	Diam D1 (mm)	Diam D2 (mm)	Diam D3 (mm)
LASC1	16/09/2003	Extra block	0.265	2018.1	0.993	0.743	1594.9	2021.2	2140.0	507.4	1623.3	1639.3	0
LASC2	17/09/2003	C1	0.264	2015.2	0.986	0.743	1594.8	2021.2	2112.0	501.4	1623.5	1639.35	0
LASC3	17/09/2003	C2	0.262	2020.4	0.989	0.736	1601.2	2025.2	2116.0	501.0	1623.45	1639.4	0
LASC4	18/09/2003	C3	0.261	2017.4	0.984	0.738	1599.9	2024.4	2096.0	496.9	1623.75	1639.45	0
LASC5	18/09/2003	C4	0.268	2017.9	0.997	0.746	1592.0	2019.3	2116.0	501.6	1623.7	1639.45	0
LASC6	19/09/2003	C5	0.260	2020.9	0.986	0.733	1604.0	2027.0	2114.0	500.5	1623.45	1639.3	0
LASR1	23/09/2003	Extra block	0.225	2055.5	0.951	0.656	1678.6	2074.8	1268.0	516.7	1625.25	1639.65	1070
LASR2	25/09/2003	R1	0.230	2050.2	0.958	0.668	1666.6	2067.1	1248.0	509.4	1625.6	1639.65	1069.6
LASR3	25/09/2003	R2	0.226	2054.1	0.953	0.659	1675.2	2072.6	1236.0	504.3	1624.8	1639.7	1070
LASR4	25/09/2003	R3	0.227	2059.6	0.962	0.656	1678.6	2074.8	1234.0	501.9	1624.75	1639.65	1069.7
LASR5	26/09/2003	R4	0.232	2057.0	0.970	0.665	1669.8	2069.2	1234.0	502.5	1624.95	1639.4	1069.5
LASR6	26/09/2003	R5	0.228	2059.7	0.964	0.657	1677.6	2074.2	1236.0	502.6	1624.9	1639.6	1069.6
LASR7	29/09/2003	R6	0.233	2058.4	0.974	0.665	1669.3	2068.9	1236.0	502.6	1625	1639.5	1069.2
LASR8	29/09/2003	R7	0.228	2050.8	0.953	0.664	1670.3	2069.5	1224.0	499.8	1625	1639.6	1069.5
LASR9	29/09/2003	Extra block	0.224	2060.6	0.956	0.651	1683.4	2077.9	1246.0	506.1	1624.75	1639.6	1069
LASR10	30/09/2003	R8	0.228	2054.1	0.957	0.661	1673.4	2071.4	1228.0	500.3	1624.85	1639.7	1069
LASR11	30/09/2003	R9	0.227	2061.4	0.964	0.655	1679.9	2075.6	1238.0	502.7	1625.25	1639.45	1069.3
LASR12	30/09/2003	R10	0.227	2061.1	0.964	0.655	1679.5	2075.3	1236.0	502.3	1625	1639.5	1069.2
Average LASC			0.263	2018.3					2115.7	501.4	1623.5	1639.4	0.0
Average LASR			0.228	2056.9					1238.7	504.3	1625.0	1639.6	1069.5

Table 3-3. Expected density and swelling pressure after saturation at different sections of the deposition hole. Calculation does not take into account the engineered gap or pellet region and represent the maximum possible swelling pressure.

Section	Density at saturation ($kg.m^{-3}$)	Void ratio	Dry density ($kg.m^{-3}$)	Expected swelling pressure (kPa)
C – above and below canister	1 972	0.831	1 518	4 368
R – at canister	1 964	0.846	1 506	3 970

The four upper most segments required a centre hole to be drilled using a seam drill to accomate the Monel pipe. The bottom (C1) block was machined to accommodate the bottom of the canister with a track of 1 070 mm outer diameter and 830 mm inner diameter to a depth of 85 mm. This was done using a drilling device for hole-drilling in concrete. Certain blocks were also prepared for mounting transducers. This was done using ordinary drills and grinding machines.

The space between the bentonite rings and wall-rock was in-filled using bentonite pellets, manufactured by Saut-Conreursin in France. Each pellet was pressed from bentonite and had dimensions of 16.3 × 16.3 × 8.3 mm, a water content of about 17 % and an expected density of a single pellet of about 2 050 $kg.m^{-3}$. The expected bulk density of the fillings was approximately 1 230 $kg.m^{-3}$.

3.2.3 The canister and filter array

The canister used in Lasgit was a standard KBS-3 design, with additional filters. This design consisted of a 50 mm thick outer copper skin, which acts as a corrosion barrier in the oxygen-poor groundwater of the crystalline rock selected for disposal, and a nodular iron insert to provide strength and rigidity (see Figure 3-7a). Each canister weighs up to 27 tonnes (including the fuel rod assemblies), is 4 835 mm long and has a diameter of 1 050 mm.

A series of filters were added to the canister surface in order to simulate a point defect perforation of the canister. A filter was also added to the bottom of the canister to look at the impact of the energy stored within a large volume of gas and its impact on the mechanisms of gas entry and movement. The design of the filter assemblies (Figure 3-7b) had to accommodate a number of engineering and experimental considerations. To help maintain structural integrity and strength of the canister, the diameters of the filter assemblies were minimised, in order to retain as much of the original canister material as possible (Figure 3-7c). The rigidity of the canister was enhanced by securing each filter assembly with 8 Monel cap-screws, tensioned uniformly to apply an even load.

To minimise leakage of test fluids around each filter assembly into the main body of the canister, a dual O-ring sealing mechanism was developed. All pressure connections were made using standard 1/8” BSP stainless steel male connectors. An advantage of using this type of fitting was that it ensured engaged thread lengths were constant for each pressure connection, allowing each fitting to be tightened to a similar torque, reducing the chance of leakage and accidental shearing of the copper threads.

Each filter array had been designed with dual ports to facilitate the removal of test permeants and “sweeping” of the sintered filter. The size of the filter discs installed in each housing were varied to examine the effect of gas pressure gradient on the gas entry pressure (Table 3-4). The filter housings were also profiled with respect to the major axis of the cylinder to help reduce the potential for voids or “bridging”, caused by the flat face of the housing protruding from the curved surface of the canister.

The maximum fluid pressure generated within each filter assembly was continuously monitored and controlled by reciprocating ISCO syringe pumps (Section 3.2.4). Alarm functions embedded in each pump controller provided a facility for controlling the maximum fluid pressure generated by the pump system. Force gauges, mounted on a number of the rock anchors holding the lid in position, continually monitored the pressure applied to the lid by the bentonite so that pumping could be stopped if the force exceeded a pre-determined value.

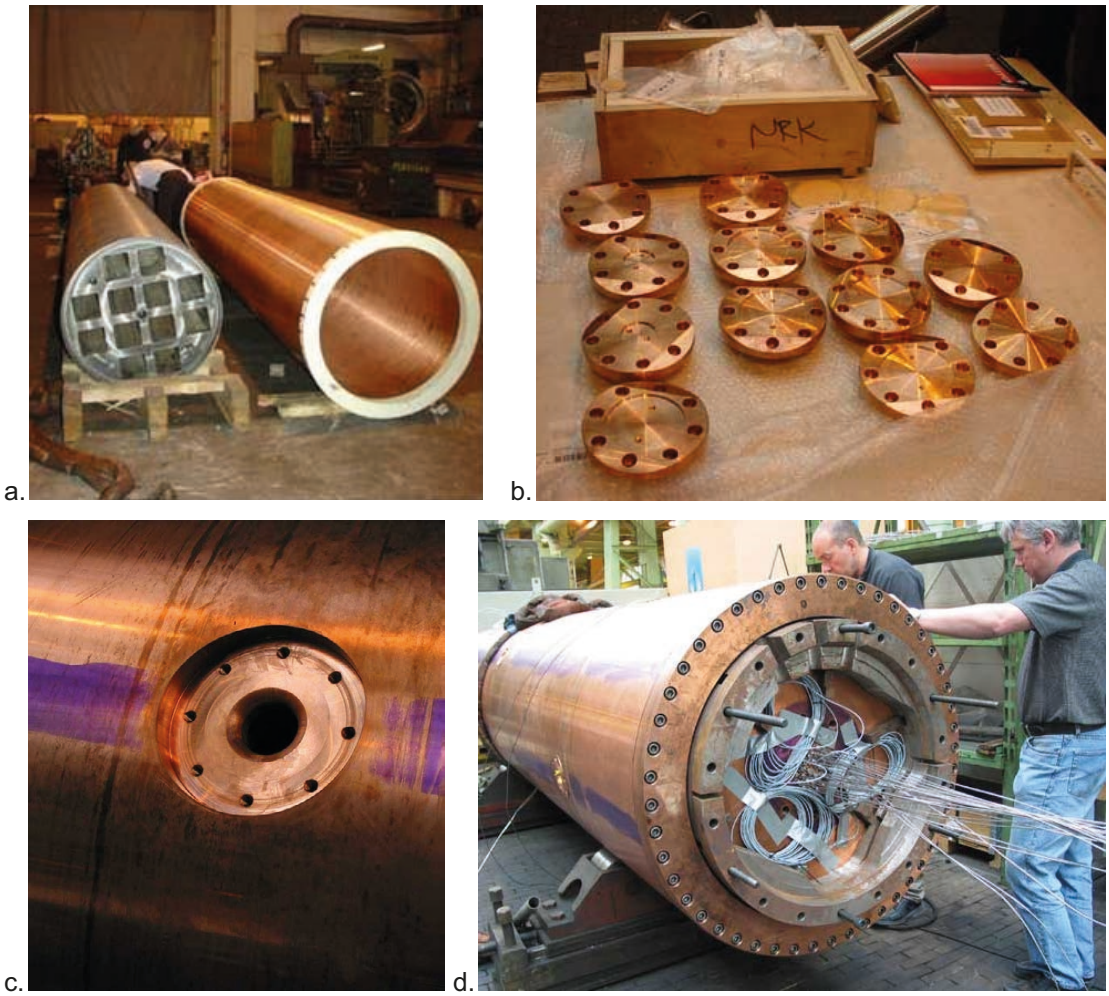

Figure 3-7. *The canister as used in the Lasgit test. The canister comprised a standard KBS-3 canister, made up of a copper canister and cast-iron insert (a). Twelve filters (b) were placed at three levels along the length of the canister in recesses (c). The complete Lasgit canister is shown in (d) with the filters in place and the associated pipework coming through the canister lid.*

To minimise corrosion and galvanic responses between the porous filter and the main body of the filter assembly (manufactured from C103 copper), a number of alternative sinter materials were examined. After consultation with SKB, it was decided to use sintered bronze as the filter material. This copper-alloy is mechanically robust, can be readily machined, and because of its copper content, should exhibit low corrosion and galvanic responses when in communication with the canister infrastructure and test permeants. To prevent intrusion of bentonite during the testing, a relatively small mean pore size distribution for the sintered bronze discs was selected (i.e. 4 to 8 µm). This range in pore size equates to an air entry pressure of between 20 and 40 kPa, assuming circular pores and an interfacial tension coefficient between the gas and porewater of 7.275×10^{-2} Nm^{-1} at 20 °C. This air-entry value was well below the expected gas entry pressure for saturated buffer bentonite.

Table 3-4. Dimensions of hydration mats and canister filters.

Device name	Location	Unit	Description	Dimensions (mm)			Filter position		
				Height	Width	Radius	α (°)	r (mm)	z (mm)
AXG0FR901	Rock wall	kPa	Pressure in filter mat 1	350	5500		-	875	351
AXG0FR902	Rock wall	kPa	Pressure in filter mat 2	750	5500		-	875	6778
AXG0FB903	Bentonite	kPa	Pressure in filter mat 3	-	-	400	-	-	6043
AXG0FB904	Bentonite	kPa	Pressure in filter mat 4	-	-	400	-	-	7048
PXG0FL901	Canister	kPa	Pressure in injection filter	-	-	50	0	525	1709
PXG0FL902	Canister	kPa	Pressure in injection filter	-	-	5	90	525	1709
PXG0FL903	Canister	kPa	Pressure in injection filter	-	-	50	180	525	1709
PXG0FL904	Canister	kPa	Pressure in injection filter	-	-	25	270	525	1709
PXG0FM905	Canister	kPa	Pressure in injection filter	-	-	50	45	525	2916
PXG0FM906	Canister	kPa	Pressure in injection filter	-	-	50	135	525	2916
PXG0FM907	Canister	kPa	Pressure in injection filter	-	-	50	225	525	2916
PXG0FM908	Canister	kPa	Pressure in injection filter	-	-	50	315	525	2916
PXG0FU909	Canister	kPa	Pressure in injection filter	-	-	50	0	525	4124
PXG0FU910	Canister	kPa	Pressure in injection filter	-	-	25	90	525	4124
PXG0FU911	Canister	kPa	Pressure in injection filter	-	-	50	180	525	4124
PXG0FU912	Canister	kPa	Pressure in injection filter	-	-	5	270	525	4124
PXG0FC901	Canister	kPa	Pressure in injection filter	-	-	-	0	175	501

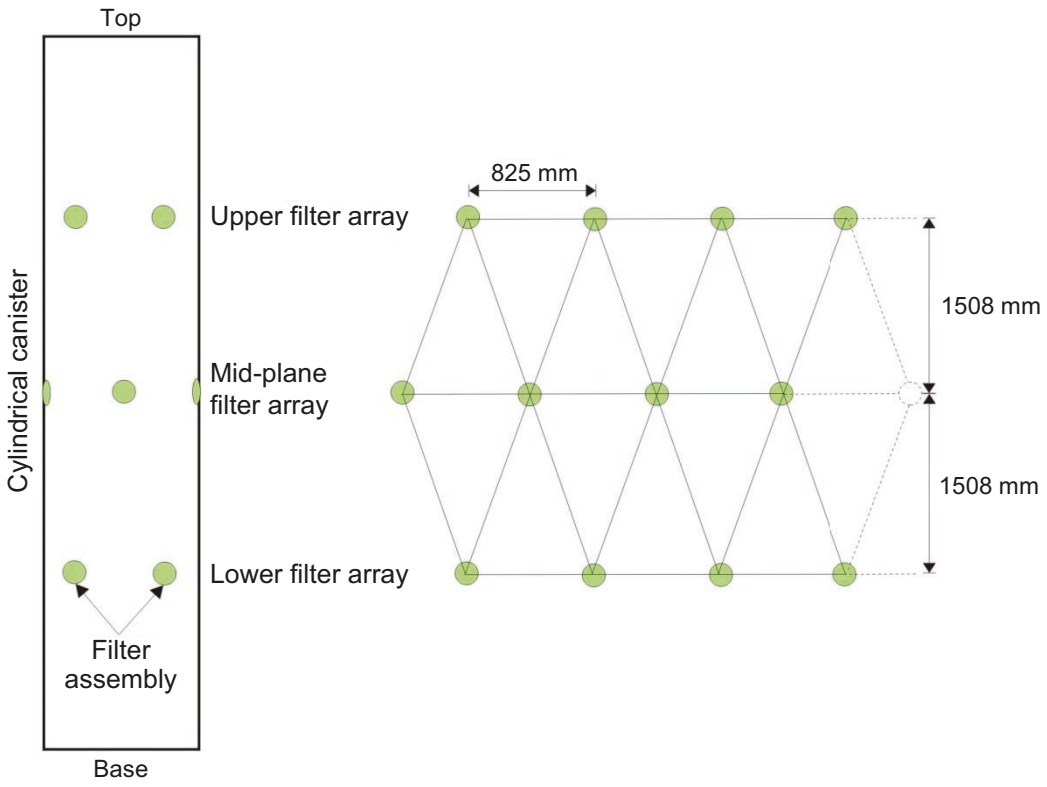

Figure 3-8. *Schematic side view of canister and visible filters (shown in green). The second graphic is a 2D representation showing the relative positions of the 12 radial injection filters.*

Given the relatively low cost of manufacture it was decided to place 13 filter assemblies at specific locations on the canister surface. In order to provide adequate contingency and provide additional points of porewater pressure measurement, a decision was made to place four filter assemblies at 90° intervals around the circumference of the canister at each selected elevation (Figure 3-8). To improve the spatial coverage of porewater pressure measurements, the upper and lower filter arrays were rotated 45° with respect to the mid-plane array. This resulted in a triangular mesh of porewater pressure measurements. An additional filter assembly was also placed in the base of the canister (Figure 3-9) in communication through a gas-actuated valve with the internal void space of the canister. Figure 3-10 summarises the location of the filters within the deposition hole.

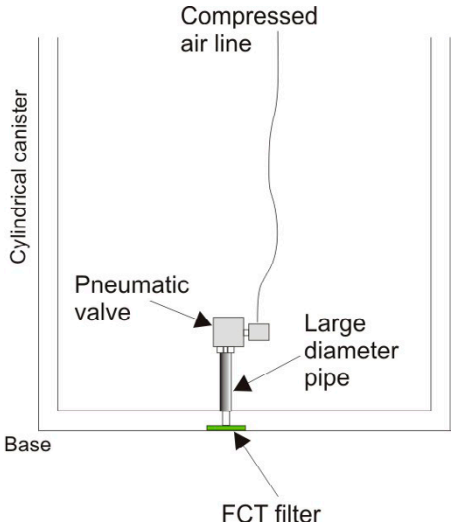

Figure 3-9. *Schematic showing the filter assembly located in the base of the canister.*

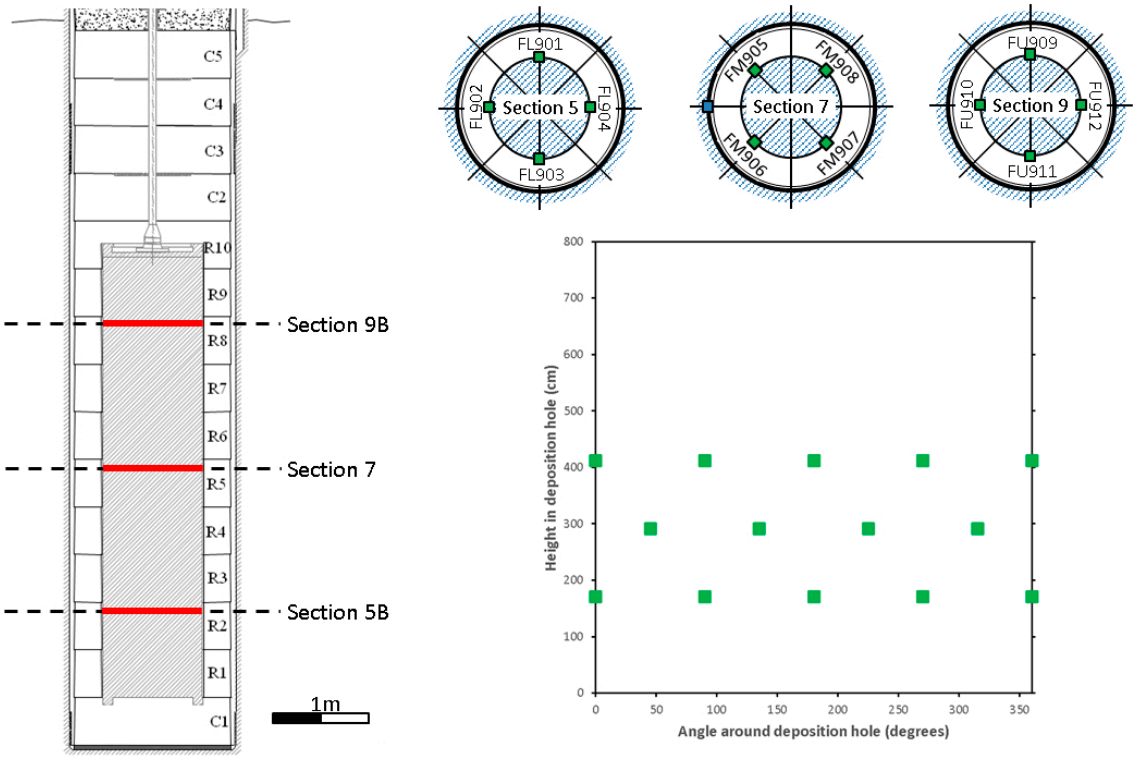

Figure 3-10. *Plan view of the location of the canister filters.*

3.2.4 Reciprocating syringe pumps

Volumetric flow rates or pressure were controlled or monitored using four ISCO™ 500D series syringe pumps operated from two digital control units. The position of each pump piston was determined by an optically encoded disc graduated in segments equivalent to a change in volume of 31.71 nl. Movement of the pump piston is controlled by a micro-processor, which continuously monitors and adjusts the rate of rotation of the encoded disc using a DC-motor connected to the piston assembly via a geared worm drive. This allowed each pump to operate in either constant pressure or constant flow modes. A programme written in LabVIEW™ elicited data from the pump at pre-set time intervals. The pumps were situated within the temperature-controlled laboratory as the pumps are sensitive to changes in temperature. Table 3-5 gives a list of the parameters logged from both ISCO™ pump controllers.

Table 3-5. List of logged parameters from the ISCO 500 Series D syringe pumps.

Device	Location	Unit	Description
PXG0PP901	Gas Laboratory	kPa	Pressure in pump A1
PXG0PP902	Gas Laboratory	kPa	Pressure in Pump A2
PXG0PP903	Gas Laboratory	kPa	Pressure in pump B1
PXG0PP904	Gas Laboratory	kPa	Pressure in pump B2
PXG0QP901	Gas Laboratory	µl h^{-1}	Flowrate of pump A1
PXG0QP902	Gas Laboratory	µl h^{-1}	Flowrate of pump A2
PXG0QP903	Gas Laboratory	µl h^{-1}	Flowrate of pump B1
PXG0QP904	Gas Laboratory	µl h^{-1}	Flowrate of pump B2
PXG0VP901	Gas Laboratory	ml	Volume in pump A1
PXG0VP902	Gas Laboratory	ml	Volume in pump A2
PXG0VP903	Gas Laboratory	ml	Volume in pump B1
PXG0VP904	Gas Laboratory	ml	Volume in pump B2
PXG0VD901	Gas Laboratory	l	Total cumulative volume pumped by pumps A1 and A2
PXG0VD902	Gas Laboratory	l	Total cumulative volume pumped by pumps B1 and B2

3.2.5 Pressure transducers

Individual pressure transducers connected to each canister filter and hydration mat (Figure 3-11) provided a continuous measure of up-hole pressure (relative pressure) for each system component (Table 3-6). Each transducer was rated to 25 000 kPa and was accurate to 0.25 % full scale. Output signals from the pressure transducers (4–20 mA) were logged by the data acquisition system. Prior to the commencement of testing each transducer was calibrated on site to a known pressure standard (Section 3.4), with repeat calibrations occurring at regular intervals.

Table 3-6. List of pressure transducers attached to the canister filters and large hydration mats showing sensor name, location, unit of measurement and a description of the monitored parameter.

Device	Location	Unit	Description
AXG0FR901	Rock wall	kPa	Pressure in filter mat 1
AXG0FR902	Rock wall	kPa	Pressure in filter mat 2
AXG0FB903	Bentonite	kPa	Pressure in filter mat 3
AXG0FB904	Bentonite	kPa	Pressure in filter mat 4
PXG0FL901	Canister	kPa	Pressure in injection filter
PXG0FL902	Canister	kPa	Pressure in injection filter
PXG0FL903	Canister	kPa	Pressure in injection filter
PXG0FL904	Canister	kPa	Pressure in injection filter
PXG0FM905	Canister	kPa	Pressure in injection filter
PXG0FM906	Canister	kPa	Pressure in injection filter
PXG0FM907	Canister	kPa	Pressure in injection filter
PXG0FM908	Canister	kPa	Pressure in injection filter
PXG0FU909	Canister	kPa	Pressure in injection filter
PXG0FU910	Canister	kPa	Pressure in injection filter
PXG0FU911	Canister	kPa	Pressure in injection filter
PXG0FU912	Canister	kPa	Pressure in injection filter
PXG0FC901	Canister	kPa	Pressure in injection filter

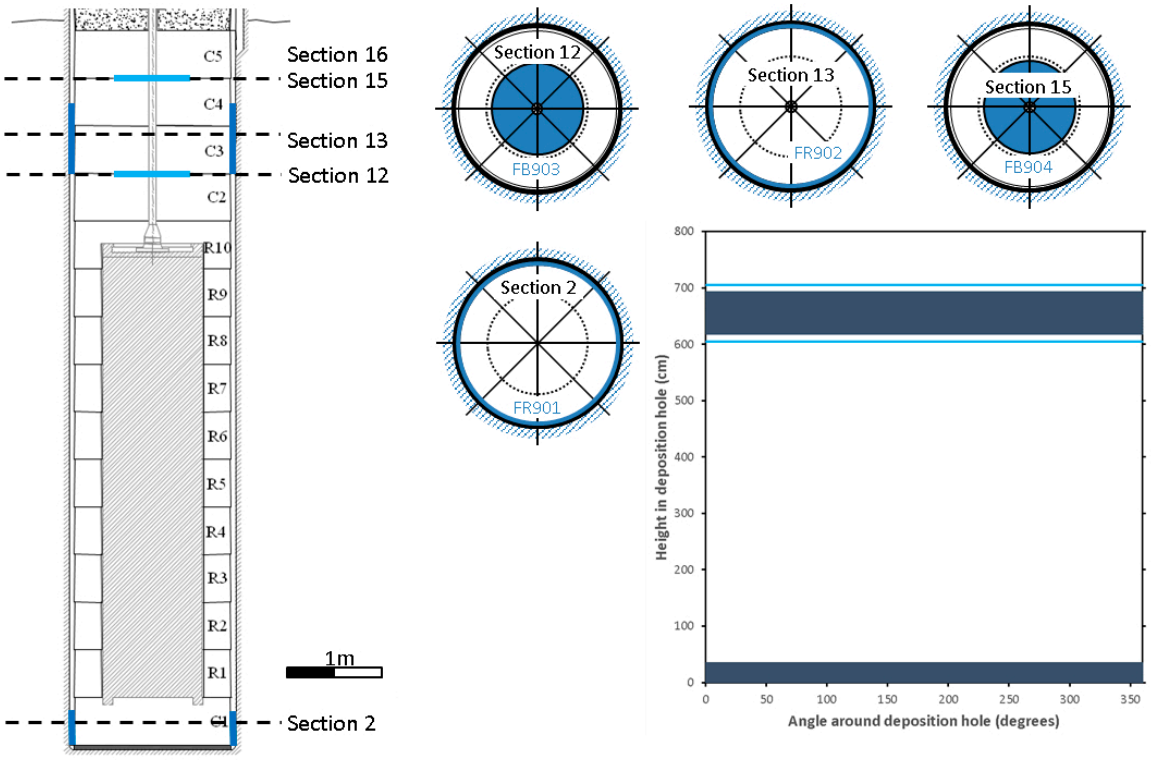

Figure 3-11. *Location of the filter mats within the deposition hole.*

3.2.6 Total stress sensors

Total stress in the Lasgit deposition hole was monitored at 32 separate locations (Table 3-7). Of these devices, 20 Geokon® sensors were mounted on the rock wall (Figure 3-12), 9 Geokon® sensors were located within the buffer material itself, and 3 Sensotec™ sensors were positioned at specific locations on the canister surface. Each Geokon® sensor incorporated an integrated thermocouple which was used to correct the output signal from each device for fluctuations in background temperature. Factory calibrations were used to process the Geokon® data into a stress value. An additional offset was then applied to the data to compensate for "drift" during the installation process. Each device outputted a resistance measurement which was collected by a custom built multilogger and then relayed to the data acquisition and control system (DAQ) within the laboratory.

Figure 3-12. *Sensors on the rock wall. The photograph on the left-hand side shows a view looking into the Lasgit deposition hole showing tube work containing the electrical connections from total stress and porewater pressure sensors mounted on the rock face. The photographs on the upper and lower right-hand show a total stress and a porewater pressure sensor respectively.*

Table 3-7. List of total stress sensors showing name, location, unit of measurement and a description of the monitored parameter.

Device/name	Location	Unit	Description	Filter position		
				α (°)	r (mm)	z (mm)
PXG0PC901	Canister	kPa	Pressure on outside of canister	0	0	501
PXG0PC902	Canister	kPa	Pressure on outside of canister	315	525	2312
PXG0PC903	Canister	kPa	Pressure on outside of canister	135	525	3520
PXG0PB901	Bentonite	kPa	Pressure in bentonite	0	0	0
PXG0PB902	Bentonite	kPa	Pressure in bentonite	242	675	0
PXG0PR903	Rock wall	kPa	Pressure at bentonite/rock interface	0	875	803
PXG0PR904	Rock wall	kPa	Pressure at bentonite/rock interface	90	875	803
PXG0PR905	Rock wall	kPa	Pressure at bentonite/rock interface	180	875	803
PXG0PR906	Rock wall	kPa	Pressure at bentonite/rock interface	270	875	803
PXG0PR907	Rock wall	kPa	Pressure at bentonite/rock interface	45	875	1709
PXG0PR908	Rock wall	kPa	Pressure at bentonite/rock interface	135	875	1709
PXG0PR909	Rock wall	kPa	Pressure at bentonite/rock interface	225	875	1709
PXG0PR910	Rock wall	kPa	Pressure at bentonite/rock interface	315	875	1709
PXG0PR911	Rock wall	kPa	Pressure at bentonite/rock interface	45	875	2916
PXG0PR912	Rock wall	kPa	Pressure at bentonite/rock interface	135	875	2916
PXG0PR913	Rock wall	kPa	Pressure at bentonite/rock interface	225	875	2916
PXG0PR914	Rock wall	kPa	Pressure at bentonite/rock interface	315	875	2916
PXG0PR915	Rock wall	kPa	Pressure at bentonite/rock interface	45	875	4124
PXG0PR916	Rock wall	kPa	Pressure at bentonite/rock interface	135	875	4124
PXG0PR917	Rock wall	kPa	Pressure at bentonite/rock interface	225	875	4124
PXG0PR918	Rock wall	kPa	Pressure at bentonite/rock interface	315	875	4124
PXG0PR919	Rock wall	kPa	Pressure at bentonite/rock interface	0	875	5029
PXG0PR920	Rock wall	kPa	Pressure at bentonite/rock interface	90	875	5029
PXG0PR921	Rock wall	kPa	Pressure at bentonite/rock interface	180	875	5029
PXG0PR922	Rock wall	kPa	Pressure at bentonite/rock interface	270	875	5029
PXG0PB923	Bentonite	kPa	Pressure in bentonite	0	675	6529
PXG0PB924	Bentonite	kPa	Pressure in bentonite	90	675	6529
PXG0PB925	Bentonite	kPa	Pressure in bentonite	180	675	6529
PXG0PB926	Bentonite	kPa	Pressure in bentonite	270	675	6529
PXG0PB927	Bentonite	kPa	Pressure in bentonite	90	250	7512
PXG0PB928	Bentonite	kPa	Pressure in bentonite	135	675	7512
PXG0PB929	Bentonite	kPa	Pressure in bentonite	315	675	7512

The three stress sensors located on the canister outputted a current directly into the data acquisition system. These devices were calibrated prior to installation. Figure 3-13 shows the location and distribution of the radial stress sensors located on the deposition hole wall, Figure 3-14 shows the location of the total stress sensors within the bentonite buffer, and Figure 3-15 shows the location of the total stress sensors on the canister surface.

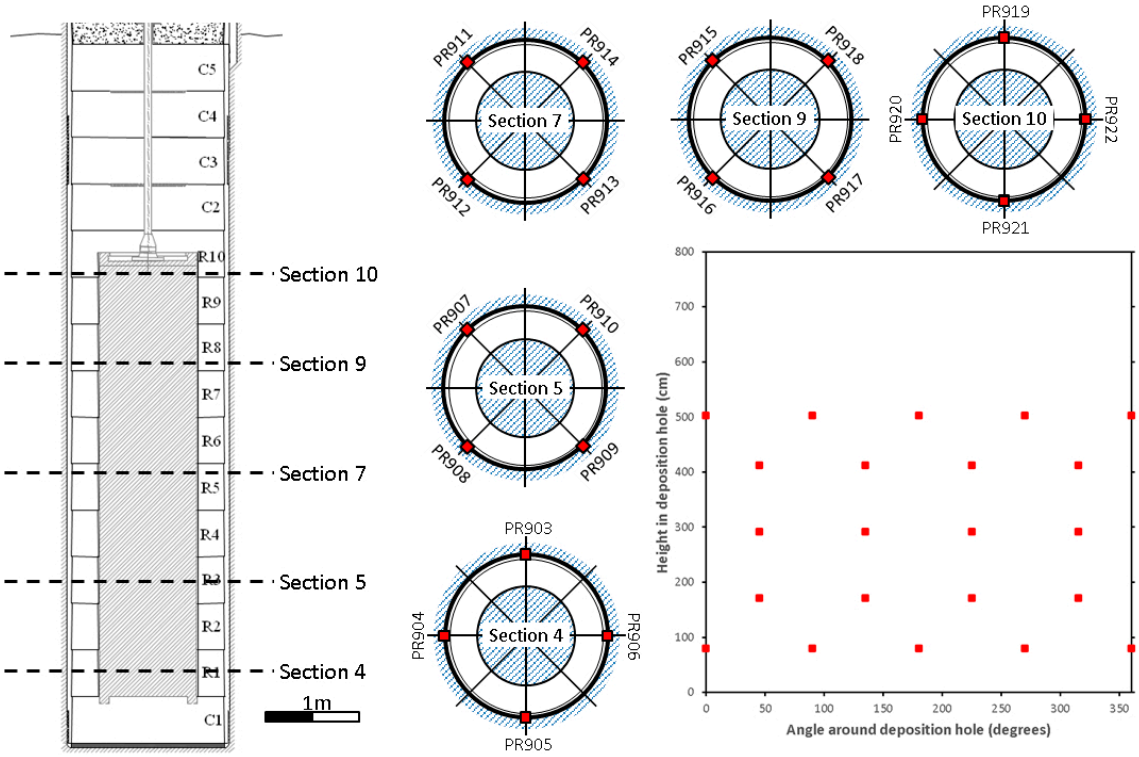

Figure 3-13. *Location of the radial stress sensors (PXG0PR9xx) on the deposition hole wall.*

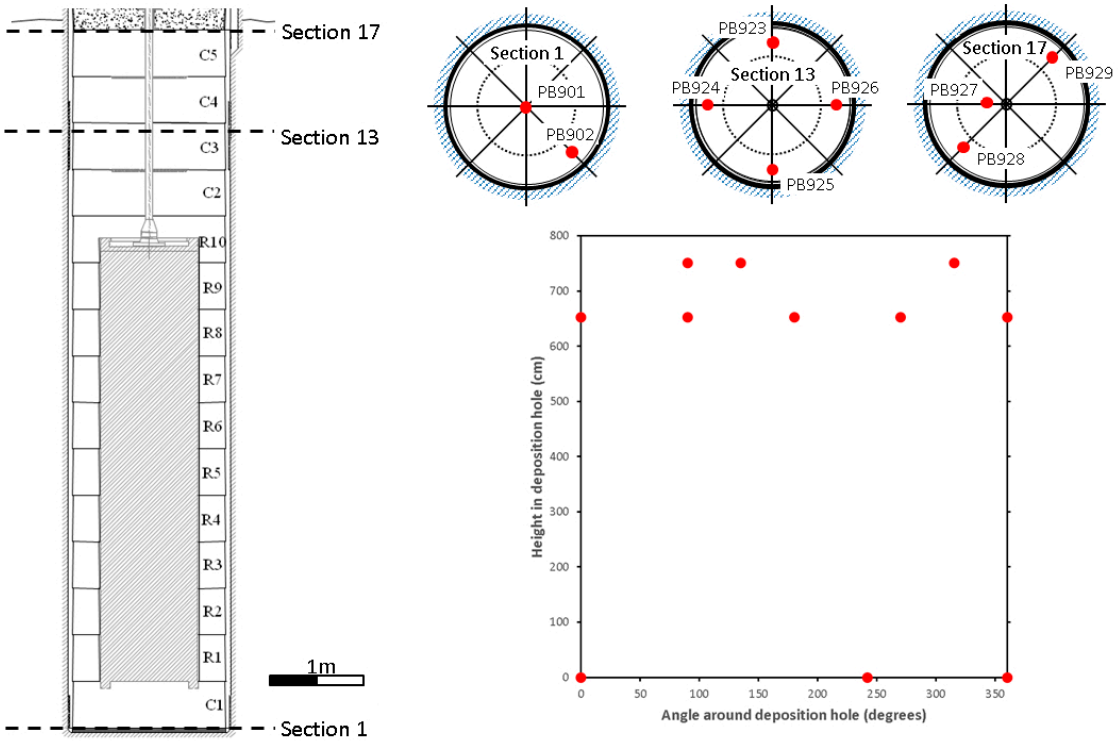

Figure 3-14. *Location of the total stress sensors (PXG0PB9xx) within the bentonite buffer.*

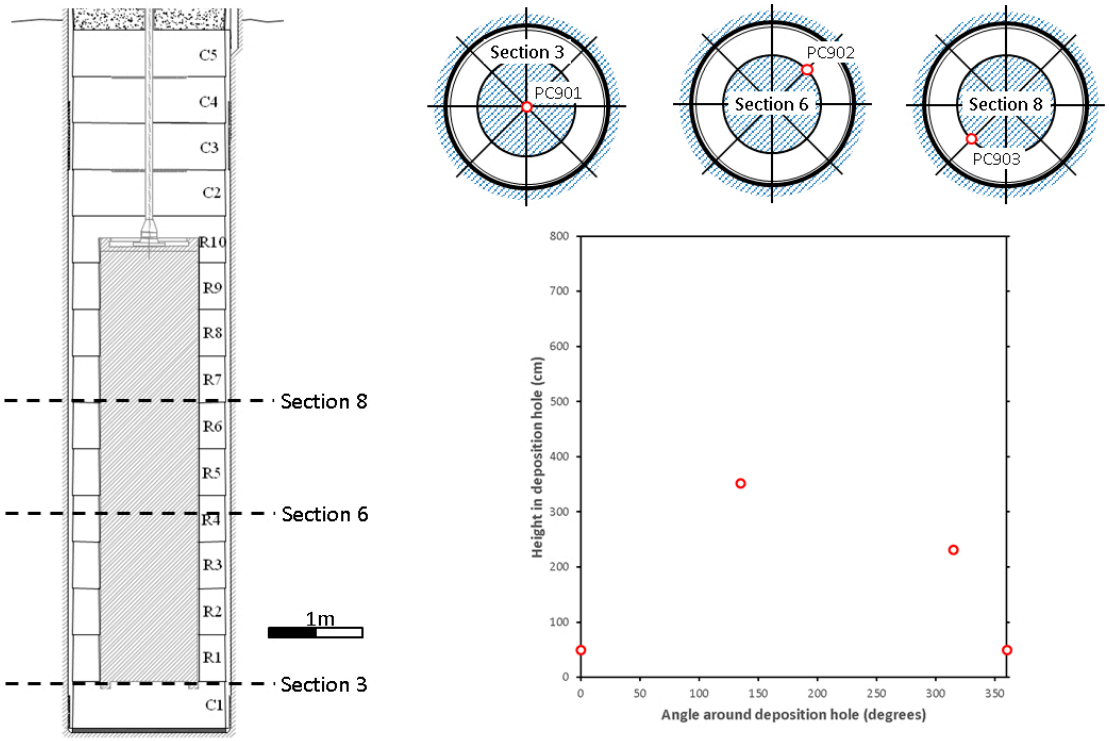

Figure 3-15. *Location of the total stress sensors (PXG0PC90x) on the canister surface.*

3.2.7 Porewater pressure sensors

The Lasgit experiment also used Geokon® porewater pressure sensors to monitor water pressure (relative pressure) inside the buffer material and at the bentonite/diorite interface (Figure 3-12). A total of 26 sensors were used in the Lasgit hole, of which 20 were located on the rock face at the bentonite/diorite interface and 6 were positioned inside the buffer mass (Table 3-8). As with the total stress instruments described in Section 3.2.6, each device used an integrated thermocouple to correct the output signal for thermal fluctuations in background temperature. This data was logged through the multilogger, which in turn passed on the raw outputs to the Lasgit DAQ system for scaling into calibrated figures. Figure 3-16 shows the location and distribution of the pore pressure sensors located on the deposition hole wall, while Figure 3-17 shows the location of the pore pressure sensors within the bentonite buffer.

Table 3-8. List of porewater pressure sensors showing name, unit of measurement, a description of the monitored parameter, and location.

Device	Unit	Description	Filter position		
			α (°)	r (mm)	z (mm)
PXG0UB901	kPa	Porewater pressure in bentonite	90	300	0
PXG0UB902	kPa	Porewater pressure in bentonite	270	437.5	182
PXG0UR903	kPa	Porewater pressure at bentonite/rock interface	45	875	803
PXG0UR904	kPa	Porewater pressure at bentonite/rock interface	135	875	803
PXG0UR905	kPa	Porewater pressure at bentonite/rock interface	225	875	803
PXG0UR906	kPa	Porewater pressure at bentonite/rock interface	315	875	803
PXG0UR907	kPa	Porewater pressure at bentonite/rock interface	0	875	1709
PXG0UR908	kPa	Porewater pressure at bentonite/rock interface	90	875	1709
PXG0UR909	kPa	Porewater pressure at bentonite/rock interface	180	875	1709
PXG0UR910	kPa	Porewater pressure at bentonite/rock interface	270	875	1709
PXG0UR911	kPa	Porewater pressure at bentonite/rock interface	0	875	2916
PXG0UR912	kPa	Porewater pressure at bentonite/rock interface	90	875	2916
PXG0UR913	kPa	Porewater pressure at bentonite/rock interface	180	875	2916
PXG0UR914	kPa	Porewater pressure at bentonite/rock interface	270	875	2916
PXG0UR915	kPa	Porewater pressure at bentonite/rock interface	0	875	4124
PXG0UR916	kPa	Porewater pressure at bentonite/rock interface	90	875	4124
PXG0UR917	kPa	Porewater pressure at bentonite/rock interface	180	875	4124
PXG0UR918	kPa	Porewater pressure at bentonite/rock interface	270	875	4124
PXG0UR919	kPa	Porewater pressure at bentonite/rock interface	45	875	5029
PXG0UR920	kPa	Porewater pressure at bentonite/rock interface	135	875	5029
PXG0UR921	kPa	Porewater pressure at bentonite/rock interface	225	875	5029
PXG0UR922	kPa	Porewater pressure at bentonite/rock interface	315	875	5029
PXG0UB923	kPa	Porewater pressure in bentonite	45	675	6602
PXG0UB924	kPa	Porewater pressure in bentonite	225	675	6602
PXG0UB925	kPa	Porewater pressure in bentonite	135	440	7280
PXG0UB926	kPa	Porewater pressure in bentonite	315	440	7280

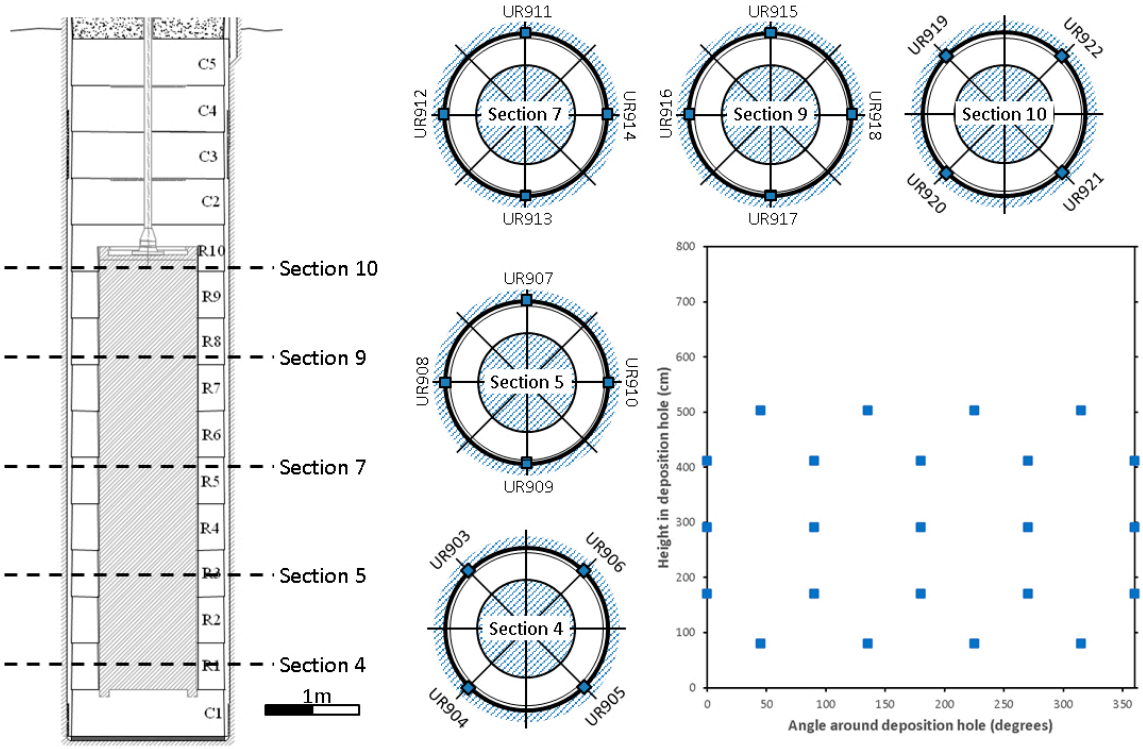

Figure 3-16. Location of the pore pressure sensors (PXG0UR9xx) on the deposition hole wall.

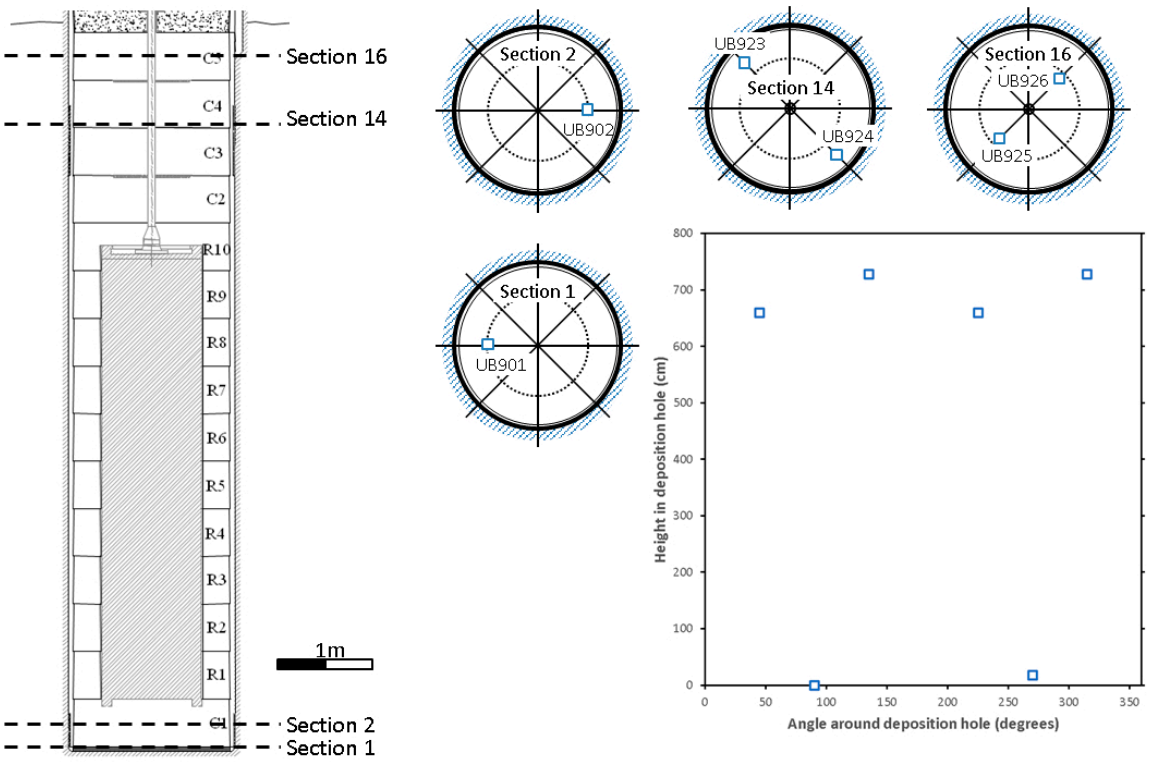

Figure 3-17. *Location of the pore pressure sensors (PXG0UB9xx) within the bentonite buffer.*

3.2.8 Psychrometers

To monitor the state of suction within the bentonite seven Wescor® psychometric microvolt meters were installed at various locations within the buffer mass (Table 3-9). These devices gave an output between 10 and 300 µV and were factory calibrated with an effective operating range of 95 to 100 % relative humidity. The outputs from these devices were recorded by a Campbell multilogger and downloaded to a separate standalone PC attached to another experiment. Figure 3-18 shows the location of the psychrometer sensors within the bentonite buffer.

Table 3-9. List of psychrometers sensors showing name, unit of measurement, a description of the monitored parameter, and location.

Device	Unit	Description	Filter position		
			α (°)	r (mm)	z (mm)
WB901	%	RH in section 2	0	0	351
WB902	%	RH in section 2	90	525	351
WB903	%	RH in section 11	45	675	5029
WB904	%	RH in section 11	225	675	5029
WB905	%	RH in section 14	135	675	6279
WB906	%	RH in section 14	315	675	6279
WB907	%	RH in section 16	225	440	7280

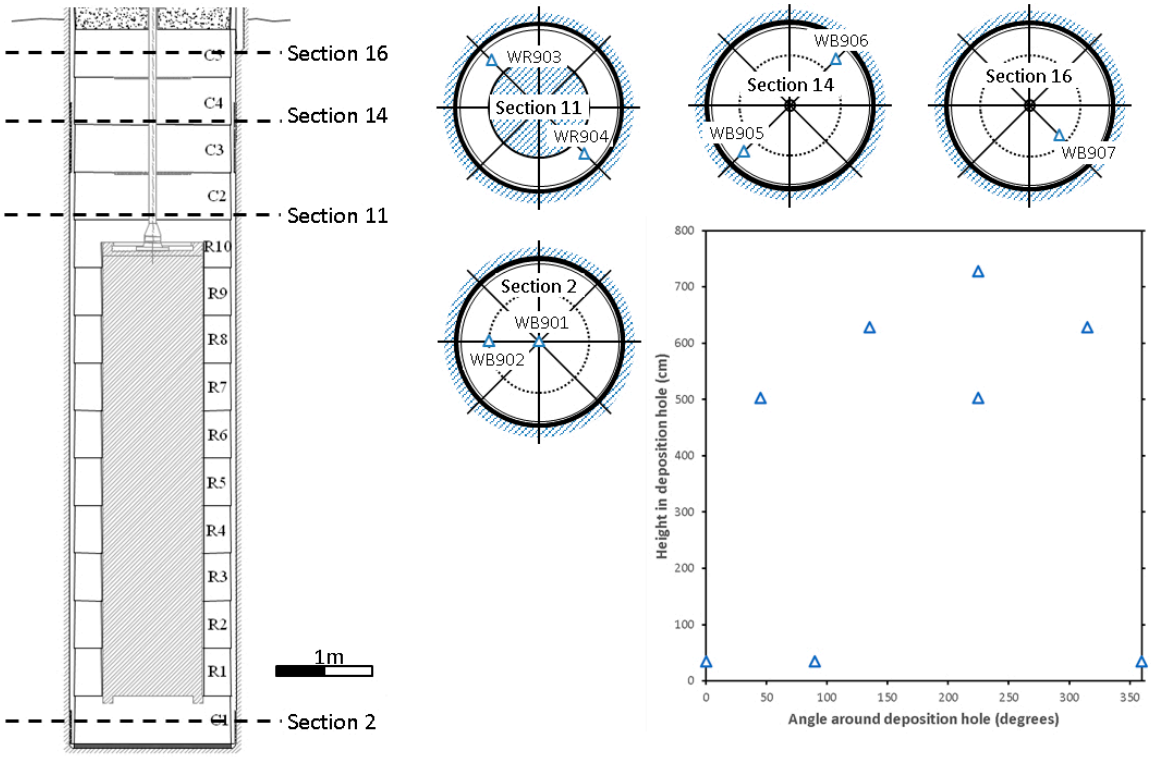

Figure 3-18. *Location of the psychrometer sensors (WB9xx) within the bentonite buffer.*

3.2.9 Linear displacement sensors

Four linear displacement sensors (LDS) were used to continuously monitor the movement of the lid in relation to both the gallery floor and ceiling (Table 3-10). A fifth sensor was used to monitor the movement of the canister in relation to the lid. Each LDS was fixed into position by a retaining clamp bolted to either the gallery floor, lid, or Monel pipe (connected to the canister), with the measuring armature resting against the lid providing a continuous measure of linear displacement.

To monitor the movement of the lid with respect to the gallery ceiling, an invar wire ran from the roof to an LDS mounted on the lid. This provided a mechanism for monitoring the true vertical displacement of the steel retaining lid. The output from each device (−3.6 to +3.6 mm) was logged directly by the DAQ system.

In late 2008, two additional LDS were installed to monitor the lateral movement of the lid to give a full three-dimensional description of the position of the lid. These two sensors were separated by 90° around the lid. During the installation of the new LDS, the three existing LDS were replaced with higher precision instruments.

Table 3-10. List of linear displacement sensors showing name, location, unit of measurement and a description of the monitored parameter.

Device	Location	Unit	Description	Orientation α (°)
PXG0DP901	Monel to Lid	mm	Movement of Monel pipe to lid	-
PXG0DP902	Lid to Floor	mm	Movement of lid to gallery floor	0
PXG0DP903	Lid to Floor	mm	Movement of lid to gallery floor	240
PXG0DP904	Lid to Floor	mm	Movement of lid to gallery floor	120
PXG0DP905	Lid to Ceiling	mm	Movement of lid to gallery ceiling	-
PXG0DP906	Lateral lid	mm	Lateral movement of the lid	0
PXG0DP907	Lateral lid	mm	Lateral movement of the lid	270

3.2.10 Load sensors

Axial movement of the lid was limited by 10 rock anchors equally spaced around the circumference of the hole; initially pre-tensioned to 1 300 kN. Glötzl load cells (Figure 3-19) were located on three of the anchor cables at approximately 120° to each other (Table 3-11). These devices provided a continuous measure of the force acting on the lid. Output signals (0–10 volts) from these devices were logged by the DAQ system. To prevent possible damage to either the rock anchors or the retaining systems during gas testing, the output from each device was alarmed (Section 3.5).

Table 3-11. List of Glötzl load cells showing name, location, unit of measurement, a description of the monitored parameter, and orientation.

Device	Location	Unit	Description	Orientation α (°)
PXG0LP901	Lid	kN	Force on anchor cables	90
PXG0LP902	Lid	kN	Force on anchor cables	198
PXG0LP903	Lid	kN	Force on anchor cables	306

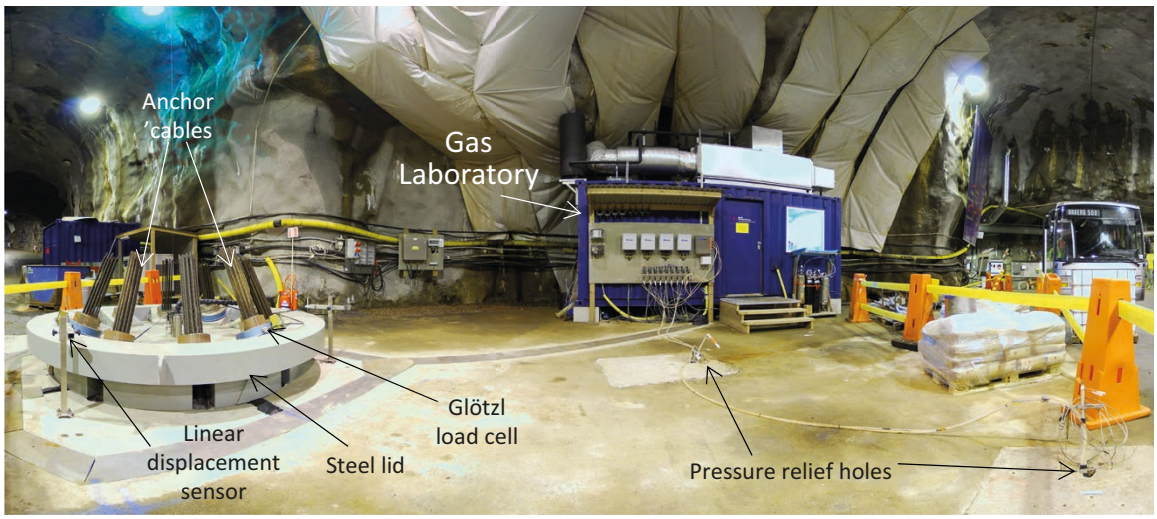

Figure 3-19. *Photograph showing the lid (coloured grey), the anchor cables, and linear displacement sensors. The Gas Laboratory (coloured blue) with its air-conditioning system mounted on the roof can be seen in the background.*

3.2.11 Pressure relief holes

Following closure of the deposition hole on 1st February 2005 porewater pressure increased rapidly within the hole resulting in the extrusion of bentonite through the instrumentation ducts. In order to reduce the hydraulic gradients around the hole, and therefore the inflow rates, two pressure relief holes (PRH1 and PRH2) were drilled. Submersible pumps were initially placed in each borehole to further reduce the local porewater pressure. Once the bentonite had swelled sufficiently to close these flow pathways, packers were installed into each borehole (Day 413) and sections within them closed off over the following 106 days (until Day 519). The position of the packers was determined from the geological mapping of the two boreholes in order to isolate key fracture zones. Figure 3-20 and Table 3-12 shows the names and position of the packered intervals for each pressure relief hole.

Table 3-12. List of pressure sensors within the two pressure relief holes.

Device		Location	Unit	Description
PRH1-1	PXG0U923	PRH hole 1	kPa	Pressure relief hole
PRH1-2	PXG0U924	PRH hole 1	kPa	Pressure relief hole
PRH1-3	PXG0U925	PRH hole 1	kPa	Pressure relief hole
PRH1-4	PXG0U926	PRH hole 1	kPa	Pressure relief hole
PRH1-5	PXG0U927	PRH hole 1	kPa	Pressure relief hole
PRH2-1	PXG0U928	PRH hole 2	kPa	Pressure relief hole
PRH2-2	PXG0U929	PRH hole 2	kPa	Pressure relief hole
PRH2-3	PXG0U930	PRH hole 2	kPa	Pressure relief hole
PRH2-4	PXG0U931	PRH hole 2	kPa	Pressure relief hole

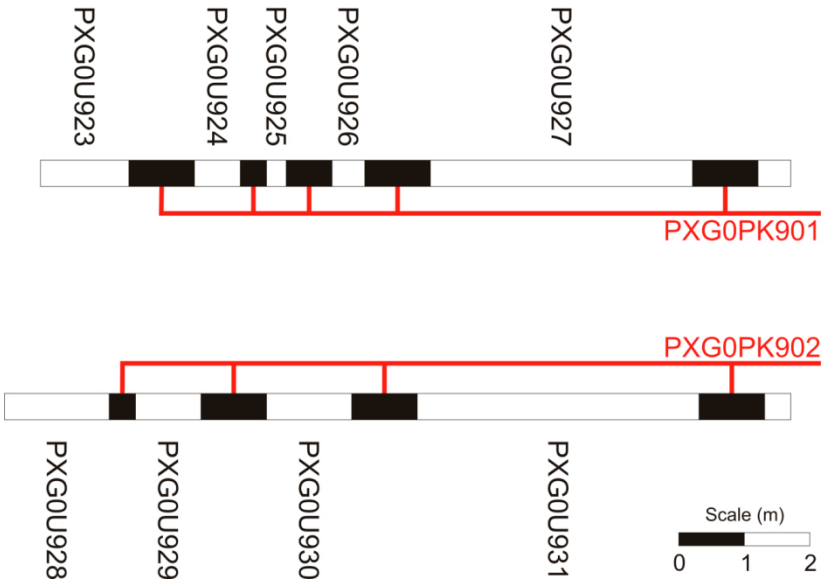

Figure 3-20. *Schematic showing the position and sizes of the packered intervals in the two pressure relief holes.*

3.2.12 Ancillary systems

A number of ancillary systems were monitored by the DAQ (Table 3-13). These include water pressure from a nearby borehole piped into the Gas Laboratory; gas pressure in the supply lines running around the laboratory section; compressed air pressure in the receiver (used to actuate servo-controlled valve-work), and Geokon battery voltage (used to initiate the logging sequence).

Table 3-13. List of ancillary systems contained in or connected to the Gas Laboratory.

Device	Location	Unit	Description
PXG0TC901	Canister	°C	Temperature inside the canister
PXG0TL902	Lab	°C	Temperature near the ceiling in the lab
PXG0TL903	Lab	°C	Temperature near the floor in the lab
PXG0TO904	Office	°C	Temperature in the office
PXG0TA905	HRL	°C	Temperature outside the lab
PXG0FC901	Canister	kPa	Pressure in injection filter
PXG0RW901	Lab	kPa	Pressure of water used to refill pumps A1, A2, B1, B2
PXG0RH902	Lab	kPa	Pressure of Helium Gas inside lab
PXG0RA903	Lab	kPa	Pressure of Compressed air in lab
PXG0VG901	Geokon	Volts	Geokon Battery level

3.3 Data acquisition and control system (DAQ)

In total, over 150 instrument outputs were monitored and recorded by a customised data acquisition (DAQ) graphical interface based on National Instruments LabVIEW™ software. The data acquisition system, located in the office area of the Gas Laboratory, operated on a PC that was connected to the SKB local area network (LAN) providing real-time data acquisition and control. Key experimental circuits and down-hole instrumentation were represented by a schematic display spread across a number of screens (Figure 3-21, Figure 3-22) located in the office section of the Gas Laboratory.

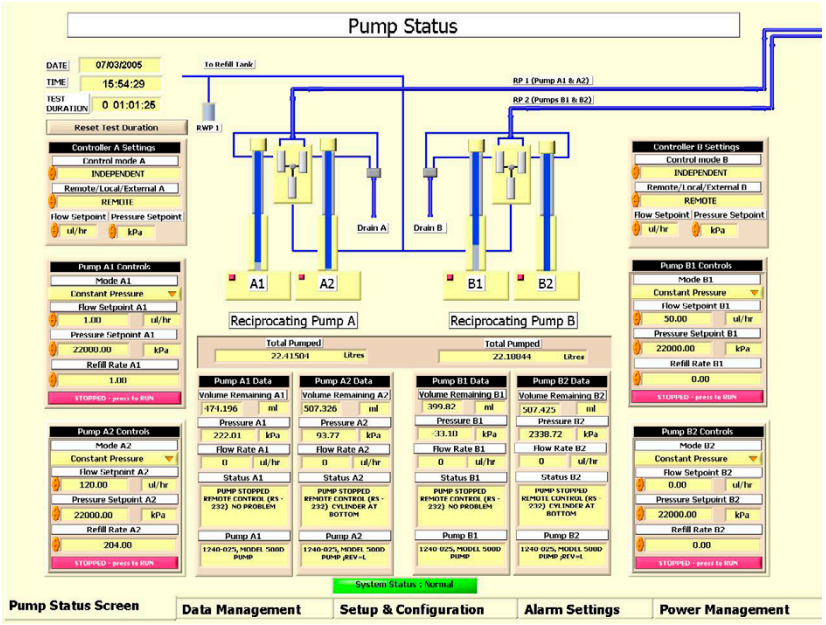

Figure 3-21. *Screen shots taken from the data acquisition software (screen 1).*

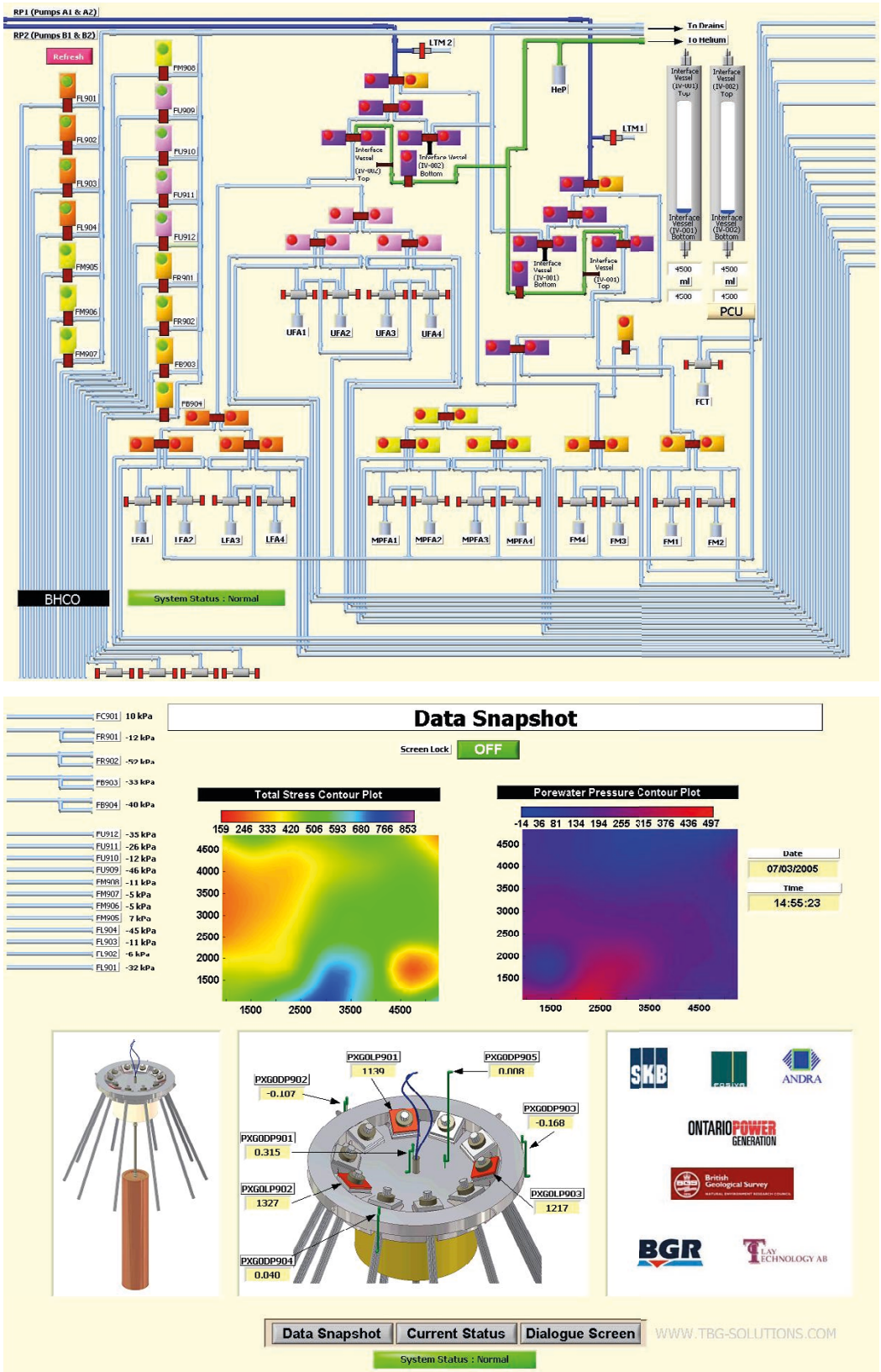

Figure 3-22. *Screen shots taken from the data acquisition software (screen 2 and 3).*

The LabVIEW software performed two primary functions. The first was to log all device outputs from both the depositional hole and the experimental apparatus (excluding the RH sensors which were monitored by existing equipment attached to another experiment at the HRL). Data was written to a hierarchical file structure that could be accessed through a secure user interface. Project participants could download experimental data from a private website. The second function of the system was to provide remote control of key experimental systems such as the ISCO syringe pumps and automated servo-controlled valve work. Proximity sensors mounted on each valve provided continuous feedback to the control system identifying the current status of a particular valve. This facility enabled staff at BGS Headquarters in Keyworth, UK, to change pump settings and/or open/close any of the 68 actuated valves housed within the gas laboratory, remotely in real-time in order to initiate test sequences.

Automated alarm systems embedded in the Lasgit software (Section 3.5) were configured to provide both e-mail notification and, under certain circumstances shutdown the ISCO pump systems if required.

Following the failure of the lab PC on 2nd October 2017 (Day 4626.03) the computer was replaced. The National Instruments logging hardware was also upgraded from Compact Fieldpoint to Compact RIO (cRIO) as support for the former was no longer available and further failure of the hardware could not be fixed. The existing software shown in Figure 3-22 was not compatible with cRIO, which necessitated the re-writing of the logging software. To save development time, the software used at the Transport Properties Research Laboratory at BGS was modified to operate Lasgit. This only required an additional utility to be written to control the air-actuated valve system. As a result, the graphical user interface was lost and meant that greater care had to be used when opening and closing valves. In operation, the loss of the graphical interface did not result in any accidental opening or closing of a valve because of the experience of the experimental operators.

3.4 Calibration

The complete Lasgit setup can be divided into two sets of sensors; those that are accessible and those that are buried within the deposition hole and therefore inaccessible. These two sets of sensors were calibrated in different ways.

For the inaccessible sensors, the factory calibrations were used. These were calibrated against known standards to ensure accurate and comparable outputs during the course of the experimental programme. The inaccessible sensors were of Geokon or Glötzl instruments. Some sensors were retrieved during decommissioning and re-calibrated to compensate for sensor drift over time. Where necessary, a linear drift was assumed.

The majority of the accessible transducers measured pressure, with additional sensors measuring lid displacement and temperature. These were re-calibrated at regular intervals, aimed at every 6 months, but in practice the interval was more like annual. Calibrations were conducted at Days 0, 393, 481, 854, 1000, 1109, 1180, 1288, 1444, 1577, 1967, 2206, 2458, 2969, 3283, 3640, 4242, 4529, 4900, 5061, 5264, and 5748. During each calibration, the sensors were isolated from downhole. A Fluke pressure calibrator was attached to the system, itself having annual calibration during an annual service. For canister and filter mat transducers an ISCO syringe pump was used to pressurise the calibration line of the apparatus at 0 (atmospheric), 2.5, 5, 7.5, 10, 7.5, 5, 2.5, and 0 kPa stages. At each stage the pressure reading of the calibrator was noted along with the voltage of all sensors. The four syringe pumps were calibrated in a similar manner. The pressure sensors of the pressure relief holes were of lower rating and therefore the calibration steps were 0, 0.8, 1.6, 2.4, 3.2, 4, 3.2, 2.4, 1.6, 0.8, and 0 kPa. The final regular calibration was that of temperature. Here a heated bath was used with a calibrated temperature probe, measuring digital readings of temperature at 10, 20, and 30 °C. For temperature it was not deemed necessary to perform calibration steps both up and down the scale.

For all calibration data the slope, intercept, and R^2 was calculated, the latter being used to ascertain whether the calibration had been of sufficient quality, with R^2 expected to be close to unity. As well as R^2, graphs of the calibration were also inspected. Where necessary, calibration was repeated if R^2 was not acceptable.

As well as determining whether individual calibration steps had been successful, it was necessary to quality control the complete calibration dataset. A problem was noted for the pressure within the canister (PXGOFC901), as shown in Figure 3-23. Throughout the history of the experiment, the canister was vented to atmosphere, therefore the calibrated result for this sensor should read atmospheric. Yet, as seen, between the calibrations at Day 3640 and 4242 the pressure was recorded as reaching nearly −200 kPa. This could not be possible as the sensors used were not designed to record a vacuum and indicated a calibration error. The negative feature seen around Day 100 has been attributed to an electrical issue with the sensor. Figure 3-24 shows the calibration data for PXGOFC901 and clearly identifies the calibration at Day 4242 as erroneous. Re-examination of the calibration data at this time showed a good R^2 value, indicating that the calibration had been performed as expected. The reason for the error was likely to be an issue with the Fluke pressure transducer at the time. Careful consideration was given to the correction of the calibration data, with regression used to "smooth" the calibration data, or to just remove the single problematic data point. It was decided to discount the calibration at Day 4242 and to assume linear drift between the calibrations at Day 3640 and 4529. As shown in Appendix 2, this was done for all canister and filter mat pressure sensors. Appendix 2 summarises the quality control of the calibration data. During data processing, a linear drift was assumed for all sensors between calibration times. Even after calibration, Figure 3-23 shows negative pressure in the first 100 days of the experiment, which could not have been measured by the sensor. This shows that the sensor used was prone to error at low pressure because of its high pressure rating.

Data reduction during gas testing also requires an accurate determination of the total system volume during any particular test stage. Where possible the total volume of each test circuit from the syringe pump to injection filter was measured prior to the start of testing.

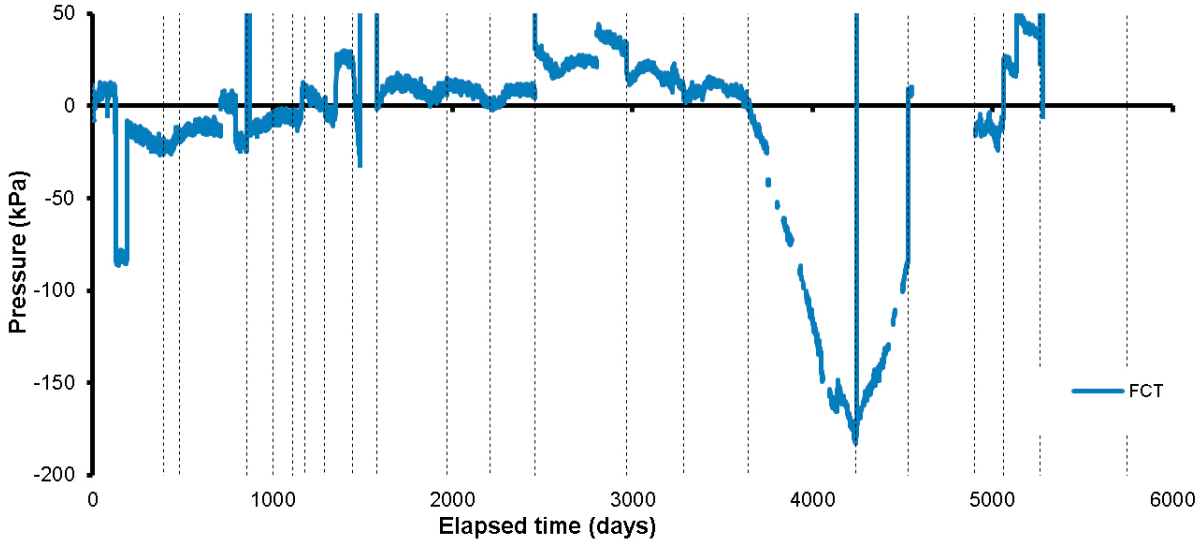

Figure 3-23. *Data for canister pressure (PXGOFC901).* ***Note:*** *pre-corrected data.*

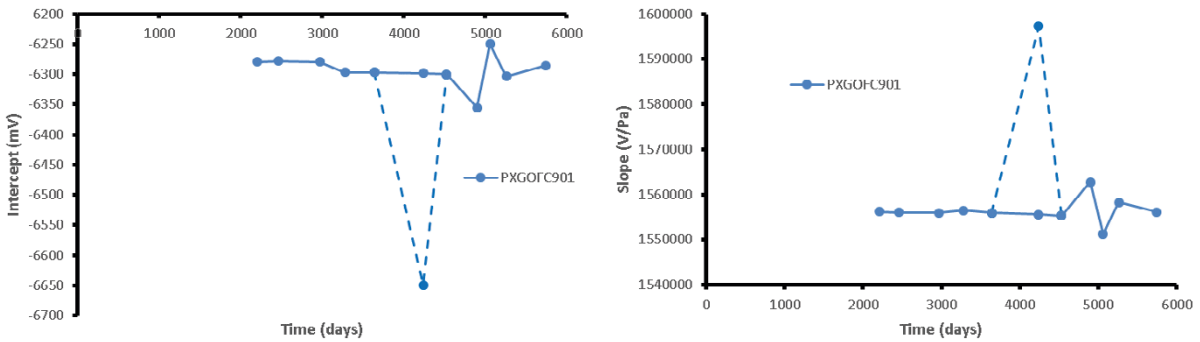

Figure 3-24. *Calibration data for canister pressure (PXGOFC901).*

To minimise possible errors introduced into the data from instrumentation drift caused by the extended test duration of the Lasgit experiment, recalibration of laboratory pressure transducers and thermocouples was performed every 6–12 months, the exact date of which, was based on convenience to the test programme. As such, Lasgit data were processed in six monthly blocks as described in Section 3.6.

3.5 Alarm systems

Instrumentation outputs were monitored by an alarm system incorporated into the data acquisition software. This allowed the end-user to pre-set minimum and maximum values for each device output. If any instrument over or under ranged then an e-mail message was sent to a predefined list of project staff alerting them to the problem. When safety critical instruments such as the Glötzl cells or pumps over-ranged, the alarm system also automatically stopped all of the ISCO pumps, preventing any risk of over pressurising the experiment or downhole infrastructure.

3.6 Error checking of Lasgit data

The Lasgit experiment lasted 5 782 days, resulting in 432 314 data records of 175 channels; a total of 75 654 950 data points. However, taking in account of data "drop-outs" and following full QC of the data, a total of 69 752 457 data were accepted.

Data were generally transferred three times a week from Äspö Hard Rock Laboratory to BGS Keyworth using the remote Citrix server link (later replaced by a TeamViewer link). Once the data had been transferred to the UK, it was visually checked in a text editor program to ensure that the data were not corrupt. A check was made that data were not missing by comparing the time stamp of the new data with that from the previous data transfer. Once these initial checks had been conducted the data was imported to an Excel spreadsheet that contained all of the unprocessed (raw) data.

All data were processed in a second spreadsheet, which was linked to the raw data sheet. Here, data were converted from raw to scaled units ready for graphing and interpretation. Graphs of all parameters of interest were available for viewing and allowed on-going quality control (QC) of the data.

During 2008, the daily QC procedure was modified with every sensor being checked in individual graphs displaying the last 10 days' worth of data. This improved method allowed events that created only subtle changes in values to be observed. Events could be identified by their elapsed time and were plotted on all other graphs, this allowed cross-correlations of sensors to be identified much easier and offered new insight into the hydro-mechanical response of the Lasgit system. At this time, the processing procedure was also improved. Initially, data were logged on an hourly basis, but this was changed at first to 30-minute intervals, and then 15-minute intervals. The latter being the fastest the Geokon logger could achieve. With 15-minute intervals it was possible to filter the data over 3 or 5 records and to automatically highlight erroneous data. Therefore, from 2008 onwards all "raw" data have a minor amount of time-averaged smoothing.

3.6.1 Data processing and traceability

There are a number of issues that arise in the recorded data. These include data synchronisation, erroneous values, loss of data during servicing or interruptions to logging system and transducer drift. However, a number of QC methodologies were routinely employed to ensure both the quality and traceability of the collected Lasgit data. On a six-monthly basis, all data were thoroughly QC checked. This was performed using a series of conditional formatted Excel spreadsheets. Data were thoroughly checked for erroneous values or "outliers", with every anomaly examined and a n informed decision made whether to remove, edit, or retain the data point in question. To ensure a coherent and traceable process a log was made of each change to the data sheet. No changes were made to the raw data files. The QC procedures were also repeated at the end of the experiment on the complete dataset in order to achieve the definitive dataset. All identified anomalies with the dataset were investigated.

For such a long-term experiment it is necessary to re-calibrate certain devices on a regular basis; for Lasgit this occurred approximately annually. The change in calibration sometimes altered data values in the Excel spreadsheet, which manifested themselves as an instantaneous step in value. In order to minimise this, a time dependent correction was applied to the calibration coefficients. Linear drift of each instrument was assumed between the two calibrations, resulting in a steady variation over a 6-month to 1-year period; this provides a clean, smooth data set.

3.7 Summary of experimental geometry and data reduction

Lasgit was well instrumented to answer the questions set for the experiment. A robust procedure for processing, calibration, and QC of the data was established meaning that problems were quickly identified and remedied. This resulted in a high-quality dataset with high levels of confidence in the results achieved.

4 Test history and points of note

Figure 4-1 summarises the full test history of the Lasgit experiment. The experiment started at 09:30 on 1st February 2005 and ran until 12:30 on 1st December 2020, a total of 5 782.12 days. It should be noted that two total drop-outs of data occurred between 27/7/06 and 8/8/06 (Day 541.52 to Day 552.94) and 2/10/17 to 9/7/18 (Day 4626.02 to 4906.03); these were related to issues with the logging computer.

Following an initial period of natural hydration only, the filter mats were used to artificially hydrate the system, as shown in Figure 4-1 in blue. This continued until Day 3745.87 when problems were encountered, with a final filter mat hydration occurring between Days 4262.24 and 4340.12. From Day 4340.12 the system was only naturally hydrated, except for localised hydration at the individual filter mats on the canister.

Figure 4-1 shows the periods where gas testing was conducted. A total of four gas injection tests were conducted in canister filter FL903 (red), with two further tests conducted in FU910 (green). For most of these gas injection tests, the periods of testing included hydraulic tests before and after the gas injection test. Note Figure 4-1 does not show the periods of lock-in following gas injection. The final gas injection test was the Full Canister Test (FCT, black). This aimed at investigating the behaviour of gas when the volume of gas in the system was significant.

Figure 4-1 concluded with decommissioning (orange). Where possible, the system continued to log the output of all working sensors during the exhumation of the bentonite buffer. This aimed to learn as much as possible of the hydromechanical behaviour of the buffer.

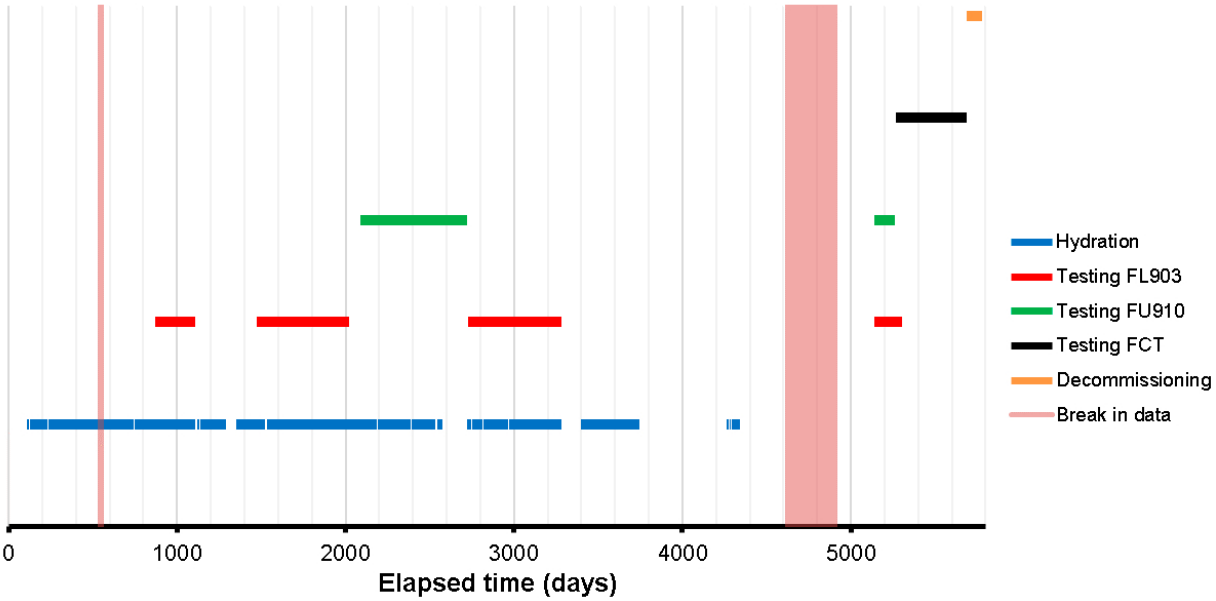

Figure 4-1. *Summary test history of the Lasgit experiment.*

Chapter 5 of this report covers the natural and artificial hydration of the system. The first gas test in filter FL903 is described in Chapter 6 (Gas Test 1). Following this stage, a period of artificial and natural hydration was conducted, as described in Chapter 7. The following three chapters describe the back-to-back gas tests; Chapter 8 describes Gas Test 2 in filter FL903, Chapter 9 described the gas injection test in filter FU910 (Gas Test 3), Chapter 10 describes the third gas injection test conducted in filter FL903 (Gas Test 4). Chapter 11 describes the lengthy period of time between gas injection tests and covers the transition from artificial hydration to natural hydration only. Chapter 12 describes the fourth gas test conducted in filter FL903 (Gas Test 5), with Chapter 13 documenting the second gas injection test in filter FU910 (Gas Test 6). Chapter 14 outlines the full canister test, with a detailed description of the mechanical loading of the canister. Finally, Chapter 15 describes the behaviour of the system during decommissioning and exhumation of the bentonite buffer.

The final chapters of the report bring together all of the observations of the test stages. Chapter 16 discusses the data from the full test and makes observations of the hydration of the buffer. Chapter 17 compares and contrasts the gas injection tests conducted in filters FL903, FU910, and the Full Canister Test. This reports the learning of the Lasgit experiment and what is known about advective gas transfer in a KBS-3V arrangement. Chapter 18 presents the test findings in the context of Safety Assessment.

4.1 Points of note

Each chapter outlining a different stage of the Lasgit history is ordered as follows. Firstly, the boundary conditions are introduced. This outlines how water pressure in the filter mats; pore-water pressure in the bentonite; pressure of the canister filters; pore-water pressure at the deposition hole wall; total stress at the deposition hole wall; stresses on the canister; stress within the bentonite; force on the canister lid; movement of the canister lid; pore pressure in the pressure-relief holes; temperature; total pore fluid pumped during the stage; and averages for all parameters. Establishing the boundary conditions means that changes as a result of gas injection can be determined and external influences identified and not considered as part of gas movement. Secondly, hydraulic testing as part of gas injection is introduced. Thirdly, a detailed description of gas injection is given.

As experimentalists it is important to separate out features that are a consequence of the operation of Lasgit, external factors that are either natural or man-made, and observations of gas injection. As will be discussed in the following chapters, artificial hydration played a role on the observations of gas transport properties. Routine artificial hydration of filter mats and non-testing canister filters was stopped around Day 3746. Therefore, the final three gas tests (5, 6, and FCT) occurred under periods of natural hydration only, whilst the other gas tests occurred when natural and artificial hydration was active. For various reason, there were also equipment failures in the laboratory that resulted in hydration being paused and this may have influenced gas behaviour. Therefore, artificial hydration is an important consideration. All graphs of system data when introducing boundary conditions have white backgrounds for periods of artificial hydration and grey backgrounds for when hydration is natural. This highlights the coupling of artificial hydration with certain boundary conditions. However, graphs related to gas injection testing have not been treated this way as features are highlighted with grey dashed event lines instead.

Data for pore pressure and total stress at the rock wall are presented as contoured plots. There are two important points to be considered with this data. Firstly, the convention for the orientation of features of the Lasgit experiment are anti-clockwise. Therefore, a sensor orientated at 90° is to the “left” of the reference direction (0°). This means that the contoured plots appear as wraps of the borehole wall as if the viewer is outside of the deposition hole looking in, and not what would be seen if within the deposition hole looking at the wall. All orientations are consistent in the report and this only becomes an issue if data are considered geographically. Secondly, data interpolation can be confusing and bias interpretation. For pore pressure (UR9xx sensors) and total stress (PR9xx sensors) minimum curvature interpolation was used in the Surfer v22 (Golden Software, USA) data analysis software package to produce the plots. If a single sensor changes, this can appear as a much broader change in the gridded data. Data for the geotechnics of the buffer material in plan view was gridded in Surfer v22 using the Radial Bias Function. Data in this instance are arranged in a much more varied manner than for UR9xx/PR9xx sensors and so care also needs to be given when interpreting results away from where data coverage is high.

Subtle changes in pore pressure or stress were observed during gas injection tests at the point of gas entry. Plotting of data full-scale misses this subtlety and can appear as if little is seen in the data. Therefore, key data channels are presented to best show the coupling between gas entry and pressure, stress/force, and displacement. In order to elicit the most detail from the test results, parameters have been transposed about the y-axis. This way, the change of amplitude has been retained, but the ultimate magnitude of the parameters has been lost. Other than removing a baseline from each parameter, no other changes have been applied. The exception has been when a multiplier less than one has been applied to a channel in order to observe subtle signals in other channels. This has been clearly stated on the appropriate graphs and has been rarely applied in this report.

Time is reported in two main ways. For discrete events that can be clearly identified, time is reported as Day D.dd. For events that a definitive start is difficult to determine or are non-discrete, such as an increasing value, time is reported as D (as an integer). Therefore, if time is reported with decimal places there is a significance of the exact timing of that event, whereas time reported without decimal places do not require such precision and/or are events that are difficult to accurately determine. Note that the decimal component of the reported time does not relate to the time of day, which in Lasgit is largely irrelevant. The time reported is the elapsed time since the start of the experiment, which happened to be 09:00.

Each parameter type is shown with an "average" for that sensor type. This is calculated as a mean of each parameter type. For certain sensor types this is questionable, however, it offers insight into general variation of that sensor type and highlights features that are seen in limited numbers of sensors, or features that are limited in duration. The progression of sensor average is of greatest value when assessing the progression of stress and pore pressure over the whole duration of the experiment. Care should be taken when interpreting the average during each experimental stage.

In the interpretation of gas injection tests, we introduce the concepts of "sinks." At the start of the experiment there was a 10 mm engineered gap between the canister and the pre-compacted bentonite rings. This was closed following the swelling of the bentonite early in the test. However, void space could have prevailed in areas that did not get sufficient hydration. This is an unlikely scenario and was not seen during decommissioning. However, limited open porosity may have formed in this area. It is also feasilble that the join between bentonite blocks was not perfect and that open porosity may have formed here as well. Finally, the pellet zone may have had open porosity formed as a result of erosion of bentonite pellets early in the test. However, this open porosity would see gas entering the wall rock rather than filling with gas. Therefore, open porosity zones may have formed that could fill with gas and act as a "sink." We use the term to refer to any open void/porosity within the set-up.

We also introduce the concept of buffer maturity. The scenario under investigation during Lasgit would occur after the thermal stage of deposition many thousands of years after canister emplacement. The buffer would have had time to reach full saturation, to equilibrate stresses, and to reach hydraulic equilibrium, a buffer state of full maturity. However, Lasgit was designed to perform experiments within a 5 – 15 year timeframe. This was insufficient to reach full maturity of the buffer and the experiment was therefore conducted under partial maturity with incomplete hydraulic and stress equilibrium. Laboratory experiments have shown that while pore pressure and stress equilibrium can be achieved relatively quickly, small samples can still show hydraulic disequilibrium. The maturity of the buffer, i.e., the completeness of pore pressure, stress, and hydraulic equilibrium, have to be considered when interpreting results from Lasgit and assessing whether observations of gas movement would occur if the buffer had thousands of years to develop.

Section B – Individual test stages

5 Hydration Stage 1 (Day 0 – Day 849)

The first stage of hydration (Day 106 – 849) of the bentonite buffer was comprehensively reported in Harrington et al. (2007) and is reproduced here for completeness. No changes have been made to the data or observations since that time. The stage history is summarised in Figure 5-1.

Note: The grey areas displayed in the graphs in this chapter show periods when artificial hydration was not occurring.

The aim of this phase of testing was to hydrate the bentonite blocks through natural and artificial means, thereby raising the saturation state in the bulk of the buffer to a value close to unity. The time period for hydration depended on a number of factors, including:

- The initial geotechnical properties of the bentonite blocks (dry density, saturation, moisture content);
- The buffer dimensions, suction gradient and permeability to water;
- The availability of water, which depended on the number, location, and discharge rates of the hydration sources;
- The volume of gas voids and the capacity of the buffer to expel trapped air;
- The amount of unfilled void space, including construction gaps that must be filled by clay swelling.

Hydration of the bentonite was undertaken in a series of stages with hydraulic pressure artificially increased at a number of locations within the system in an attempt to reduce hydration times. *In situ* porewater collected from a nearby sealed borehole was used as the injection permeant at this time. During artificial hydration, porewater was actively injected through all of the filters located on the canister surface (excluding the FCT) and the large filter mats sandwiched between blocks C2–C3 and C4–C5. It should be noted that hydrating from the canister filters may lead to a heterogeneous buffer saturation that could lead to preferential flow paths. However, it was more desirable to achieve full saturation at the point of gas injection to be representative of the condition of the buffer at the time gas movement might occur.

The deposition hole was closed on the 1st February 2005 signifying the start of the hydration phase. In order to allow *in situ* porewater pressure to equilibrate and provide the bentonite with time to swell and begin closure of the engineering voids, the start of artificial hydration was deferred. During this time, groundwater was flushed through the system in an attempt to remove the bulk of the residual air trapped in the engineering voids. Localised groundwater inflow through a number of highly-conductive discrete fractures quickly resulted in elevated porewater pressures (> 870 kPa) throughout large sections of the borehole. This led to the formation of conductive channels (piping) and bypass flow, leading to the extrusion of bentonite from the hole and the discharge of groundwater to the gallery floor.

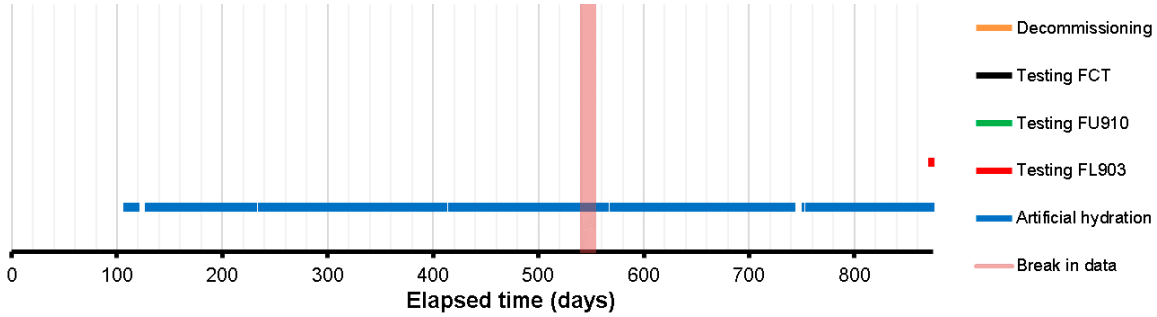

Figure 5-1. *Test stages of the Lasgit experiment showing what was conducted during Hydration Stage 1.*

To address this issue, two pressure relief holes (PRH1 and PRH2) were drilled in the surrounding rock mass in an attempt to lower the porewater pressure in the vicinity of the deposition hole. With the insertion of submersible pumps into the pressure relief holes, piping and bypass flow stopped and water pressure within the deposition hole was stabilised. Packer assemblies were inserted into the pressure relief holes on Day 413 and the packers inflated on Day 415. Individual sections were then closed off over the period from Day 476 to Day 519. Artificial hydration began on the 18th May 2005 after 106 days of testing. Table 5-1 shows a summary of key events through November 2007.

Table 5-1. Log of dates and events in the Lasgit test history to June 2007 (Day 870).

Date	Day	Description of event
1/02/2005	0	Deposition hole closed and water flushed through system in an attempt to remove air trapped in engineering voids
2/02/2005	1	Extrusion of bentonite plus water into the instrumentation slot around the top of the deposition hole
	1	Canister filters and injection mats connected to the Gas Laboratory (GL)
4/02/2005	3	De-airing of tubework from GL to canister filters and hydration mats
13/02/2005	12	Increased discharge to instrumentation slot.
14/02/2005	13	Pressure lines from filter mats to the Gas lab disconnected to improve drainage from hole in an attempt to moderate the increase in porewater pressure
13/03/2005	40	Interruption in Geokon data acquisition due to corrupted library file
4/04/2005	62	Pressure relief hole 1 drilled in the surrounding rock mass
7/04/2005	65	Submersible pump placed in pressure relief hole 1
12/04/2005	70	Pressure relief hole 2 drilled in the surrounding rock mass
19/04/2005	77	Submersible pump placed in pressure relief hole 2
25/04/2005	83	Air-conditioning unit failed resulting in an increase in laboratory and office temperatures. Test unaffected.
27/04/2205	85	Air-conditioning unit repaired
3/05/2005	91	Submersible pumps switched off
10/05/2005	98	Submersible pumps removed from and packers installed in both pressure relief holes. Packered intervals open to atmospheric pressure and free to drain. Discharge rates monitored on a regular basis from this date onwards.
18/05/2005	106	Start of artificial hydration. Pump pressure in RP2 initially set to 100 kPa (uncalibrated value) to stabilise pressures in all canister filters (except the FCT) and filter mats FB903 and FB904.
	106	RP2 pressure then increased to 150 kPa (uncalibrated value).
23/05/2005	111	Filter mat FR902 opened to pumpset RP2 set at 150 kPa (uncalibrated value).
24/05/2005	112	Error checking of the software required isolation of individual test circuits from the pump system. The momentary reduction in pressure of filter mat FR902 occurred during this process.
27/05/2005	115	Pressure increased in RP2 to 250 kPa (calibrated value) in all canister filters (except the FCT) and filter mats FR902, FB903 and FB904.
2/06/2005	121	Software revision installed. FCT valve opened by accident resulting in a drop in all filter pressures and the discharge of groundwater into the canister void.
7/06/2005	126	FCT valve closed and system pressures restored.
9/06/2005	128	Pressure increased in RP2 to 500 kPa (calibrated value) in all canister filters (except the FCT) and filter mats FB903 and FB904. FR902 left closed so that inflow to other circuits could be measured.
11/06/2005	129	Power supply to acquisition system (Field-Point module) failed leading to a loss of fluid pressure in the system.
13/06/2005	132	Power supply to acquisition system (Field-Point module) replaced, system reset and pressures raised to 500 kPa (calibrated value).
16/06/2005	135	Multi-logger software “crashed” resulting in the loss of Geokon data
21/06/2005	140	Attempted to raise pressure to 1 000 kPa (calibrated value). After pumping > 800 ml of fluid into FM906 process suspended and pressure reset in all previous open filters to 500 kPa. During this time an additional ~ 8 litres of fluid were injected into FM906.
22/06/2005	141	Pressure increased in RP2 to 750 kPa (calibrated value) in all canister filters (except the FCT) and filter mats FR902, FB903 and FB904.
	141	Once stable pressure obtained, then increased in RP2 to 1 000 kPa (calibrated value) in all canister filters (except the FCT) and filter mats FR902, FB903 and FB904.
4/07/2005	153	Interruption in LabVIEW control software led to the momentary closure of all automated valves resulting in a number of clearly defined negative pressure transients
7/07/2005	156	Multi-logger software revision installed resulting in a loss of data and a short-term reduction in system pressure
13/07/2005	162	Repair and leak-testing of pumpset RP1 complete. Pressure set to 1 000 kPa (calibrated) and thereafter used to control pressure in filter mats FR902, FB903 and FB904 as well as canister filters FM905 to FM908. All other filters pressures (except FR901) remain controlled by RP2.

Table 5-1. Continued.

Date	Day	Description of event
14/02/05	163	Software fault on RP1 resulted in a temporary loss of pressure to filter mats FR902, FB903 and FB904 as well as canister filters FM905 to FM908.
18/07/2005	167	Pressure increased in RP2 to 2 000 kPa (calibrated value). When the pressure in filter FL903 reached ~1 800 kPa increases in pressure were observed in FR901 as well as multiple total stress and porewater pressure sensors located within the clay and on the surface of the borehole, indicating the formation of highly conductive channels ("piping"). Pressure in RP2 was immediately lowered to 1 200 kPa.
	167	Further attempts were made to substantially increase water pressure in both RP1 and RP2 systems without success. Pressure in both pump systems were then set to 1 250 kPa.
19/07/2005	168	Another attempt was undertaken to incrementally raise water pressure to 2 000 kPa. When water pressure reached ~1 750 kPa in FU910 piping occurred resulting in a rapid increase in monitored porewater pressure and total stress. Pressure in both pump systems was finally set to 1 350 kPa resulting in a massive reduction of flow into the system.
20/07/2005	169	Pressure increased in both RP1 and RP2 to 1 500 kPa. No piping observed.
9/08/2005	189	New system for monitoring the relative movement of the steel lid to gallery roof was successfully installed (DP905).
10/08/2005	190	Gas pressure inside the canister was gently raised to expel the groundwater which had been accidentally pumped into the void (2/06/2005). This resulted in a temporary increase in FCT pressure and noise in the signal from the canister thermocouple.
23/08/2005	203	Another attempt was undertaken to incrementally raise water pressure to 2 000 kPa. When water pressure was raised in FM906 piping reoccurred resulting in a rapid increase in monitored porewater pressures and total stresses coupled with an increase flow rate from both pump systems (> 60 ml.min^{-1}). Pressure in both pump systems was finally set to 1 500 kPa.
22/09/2005	233	Both pump systems taken off-line for < 1 day while software upgrades installed. During this period the pressure in the circuits controlled by RP1 and RP2 dropped to ~1 200 kPa and ~1 100 kPa respectively.
23/09/2005	234	System re-pressurised to 1 500 kPa.
11/10/2005	252	Interruption in data acquisition caused by the "crashing" of the laboratory PC.
13/10/2005	254	PC rebooted and software restarted. When communication with the control systems were re-established the pressure in the FL and FU circuits had increased slightly to ~1 600 kPa.
18/01/2006	351	The code was temporary stopped to disable contour plots. Temporary spike in pressures were observed when the acquisition software was restarted.
6/03/2006	397	Logging system stopped while new acquisition cards were installed to log the new transducers.
7/03/2006	399	Logging system stopped momentarily to back-up sources code. Valve to FB904 failed to automatically open when code restarted. Resulted in a slight drop in pressure – valve reopened < 4 hours later.
18/03/2006	410	Revised code uploaded to Lasgit PC.
21/03/2006	413	Logging software stopped while new transducers added to data acquisition system.
	413	System restarted but both pumpsets failed to initialise leading to a reduction in filter pressures overnight.
	413	Packer assemblies installed in PRH1 and PRH2.
22/03/2006	414	Packers inflated – drain valves left open.
23/03/2006	415	Top packer interval on PRH1 ruptured (Day 414.73) resulting in the deflation of all packered intervals in PRH1. PRH2 remained inflated.
	415	Ruptured packer replaced and re-inflated at Day 415.08. Failed again on pressurisation.
	415	At 415.09 the drain valves to sections PRH2-1 to PRH2-4 closed and pressures monitored to define flowing intervals.
	415	At 415.12 days, the drain valves to PRH2-1 to PRH2-3 were opened momentarily while pressure relief valves installed. PRH2-4 left closed as no significant flux observed.
	415	At 415.15 days drain valve to PRH2-2 opened and pressure relief valve removed and attached to PRH1-1.
	415	Packer interval moved to prevent a third failure and re-inflated at Day 415.21.
	415	At 415.26 days the drain valve to PRH1-1 was closed. Data subsequently deleted due to problems with the transducer.
	415	Drain valve to PRH1-1 opened as pressure had increased to around 2 200 kPa.
24/03/2006	415	New calibration values applied to data.
	416	Data corrupted. Code stopped, revised and uploaded less than 2 hours later. Resulted in a small drop in pressure in most of the filter systems.
23/05/2006	476	PRH1-1 online.
	476	PRH2-4 closed.
31/05/2006	484	PRH2-2 closed.
08/06/2006	492	PRH1-5 closed.
14/06/2006	498	PRH1-4 closed.
16/06/2006	499	Pressurisation system for PRH1 packers began to leak.
20/06/2006	504	PRH1-3 closed.

Table 5-1. Continued.

Date	Day	Description of event
21/06/2006	504	All PRH pressures (in both holes) in packered intervals begin to decrease as the packers in PRH1 continue to deflate (Day 504.82).
22/06/2006	506	Pressure from PRH1-3 bleeds into PRH1-4 and 1-5 as gas bottle pressure not sufficient to create seal between PRH1-3 and rockface.
26/06/2006	510	Leak fixed in the pressurisation system for PRH1 packers (510.02).
29/06/2006	513	PRH1-2 closed.
05/07/2006	519	PRH1-1 closed.
27/07/2006	541	Computer crashes – was restarted 12 days later when Äspö staff returned from leave.
22/08/2006	567	Pumps taken offline for maintenance. Drops in pressure to all canister filters, FM2,3,4 and Refill water line.
22/08/2006	567	Total pump volumes inaccurate due to leak whilst maintaining pressure (caused by deposits on barrels). Leakages from the standby pump are therefore included in the total pumped. (Pumps taken for servicing at this point A1/A2).
19/09/2006	595	Calibration of transducers for ~2 days.
05/10/2006	611	Lab temp increased due to compressor overworking. Caused by faulty Isonic valve.
20/11/2006	657	Pressures in all filters (except FR901) raised to 2350 kPa (calibrated) using RP2. Connectivity between UFA4 and UFA1 observed when UFA1 pressure raised. FB903 and FB904 also took largest volumes of fluid to pressurise. Total fluid volume used ~44 ml.
09/01/2007	707	Inlet water supply switched to fresh water.
11/01/2007	709	Air con system failed until ~710 days.
17/01/2007	715	Maintenance of air conditioning system.
31/01/2007	729	Reconfigured air conditioning system in lab area to redistribute air flow over Isonic values. It took around 2 days for the system to equilibrate resulting in an offset between lab high and low temperatures.
13/02/2007	742	A2 recalibrated. Values not input into sheet as the difference in calibrated value at 2300 kPa was only around 3 kPa and A2 was moved to A1 position on 5/3/07 invalidating the calibration.
14/02/2007	743	Hydration system moved across to pump A2.
15/02/2007	744	Pressure in all hydration circuits dropped as the A2 pump ran out of water. For the next ~6 days the pressure in the hydration system dropped.
16/02/2007	745	B1 and B2 removed for servicing.
16/02/2007	745	Office temperature lowered by 3 °C.
21/02/2007	750	Pump A2 refilled and hydration pressures restored.
22/02/2007	751	Lab and office temperatures lowered by a further 1 degree to ~13.5 C to bring them in line with canister.
23/02/2007	752	A2 alarm tripped and stopped pump for no obvious reason. Pressure in hydration system fell.
23/02/2007	752	A2 alarm tripped and stopped pump for no obvious reason. Pressure in hydration system fell to around 2000 kPa.
24/02/2007	753	A2 restarted and alarm disabled.
05/03/2007	762	A1 removed and pump A2 connected to controller to act as A1. A2 not recalibrated – but opened to atmospheric and pressure zeroed. Calibration now invalid. Pressure in hydration system dropped by around 60 kPa. Raw data filed edited to move pump A2 data to its correct column.
07/03/2007	764	Increased pump A2 by 65 kPa to 2387 kPa (to account for the fact that the pump was now out of calibration having been moved to the A1 position) to raise pressure in hydration system to match previous values.
30/03/2007–11/04/2007	787 to 799	Air-con temperature increased resulting in a drop in pressure. Temperatures fluctuated for a few days before settling down.
10/04/2007	798	TBG logged on to system and pump over pressured circuits to 4000 kPa momentarily. Hydration data deleted from sheet. A small offset noted in the lid displacement data but since it didn't return to the original value when the system was depressurised the offset was left in.
10/04/2007	798	B1 and B2 reinstated. A2 used to control hydration system.
2/05/2007	820	System isolated whilst pumps leak-tested. All hydration circuits dropped in pressure.
3/05/2007	821	Hydration circuits re-pressurised using B1.
17/05/2007	835	B1 ran out whilst hydrating. Refilled it whilst connected to downhole as no-one onsite at Äspö. Pressures downhole dropped momentarily and then recovered.
25/05/2007	843	All lower filters isolated for start of hydraulic pressure decay test.
5/06/2007	854	PRH transducers calibrated.
8/06/2007	857	Canister filters, filter mats, A1, A2, B1 and B2 transducers calibrated.
	857	FC901 transducer only left in communication with the calibration manifold pressurised by pump B1. Valve to canister closed at all times.
	857	Pump B1 raised by approx 100 kPa to lift the hydration filter pressures to approx the same value as before following calibration of the system.
21/06/2007	870	Jump in hydration circuits caused by switching from pump B1 to RP1 (A1 and A2).

5.1 Evolution of porewater pressure

The following sections describe the temporal evolution of porewater pressure in the Lasgit system, reflecting the complex interaction between artificial and natural sources and their cumulative role in the hydration of the buffer clay. Table 5-2 summarises key hydration events occurring during this stage of testing. Table 5-3 provides details of the sequence of events during installation of packers into the pressure relief boreholes.

5.1.1 Canister filters FL901 to FU912.

Data from the canister filters are shown in Figure 5-2. Artificial hydration began at Day 106 at a pressure of 150 kPa. During this initial stage of the test, the pressure in all of the canister filters (excluding the FCT) and the filter mats FB903 and FB904 were controlled using reciprocating pump-set RP2. At Day 111, filter mat FR902 was added to the RP2 circuit and its pressure raised to 150 kPa (the temporary reduction in pressure at Day 112 occurred during error checking of the data acquisition software). Three days later (Day 115) the pressure in the RP2 circuit was raised to 250 kPa. For each increase in pressure, the flowrate and injection pressure was monitored to ensure that the inflow was not sufficient to result in buffer erosion.

The drop in pressure to near atmospheric conditions observed at Day 121 was caused by the accidental opening of the FCT valve while upgrading the data acquisition software. System pressures were restored a few days later and the pressure subsequently raised to around 500 kPa at Day 128. The failure of a power unit at Day 129 (early on a Saturday morning) resulted in the temporary loss of data and a small reduction in system pressures until the transformer was replaced the following Monday (Day 131).

Table 5-2. Timeline of key hydration events.

Date	Day	Activity
1/02/2005	0	Closure of deposition hole
13/02/2005	12	High water pressures around the bentonite resulted in by-pass flow. Initial corrective measures proved unsuccessful
04/04/2005	62–70	Pressure relief holes drilled in surrounding rock mass
10/05/2005	98	Submersible pumps removed and pressure relief holes packered
18/05/2005	106	Start of artificial hydration (water pressure 150 kPa)
27/05/2005	115	Artificial porewater pressure increased to 250 kPa
09/06/2005	128	Artificial porewater pressure increased to 500 kPa
21/06/2005	140	Attempted to raise artificial porewater pressure to 1000 kPa (failed)
22/06/2005	141	Artificial porewater pressure increased to 1000 kPa
18/07/2005	167–168	Attempted to raise artificial porewater pressure to 2000 kPa (failed)
20/07/2005	169	Artificial porewater pressure increased to 1500 kPa
23/08/2005	203	Attempted to raise artificial porewater pressure to 2000 kPa (failed)
		Artificial porewater pressure reset to 1500 kPa
21/03/2006	413	Packer assemblies installed into pressure relief holes
23/03/2006	415	Packers in pressure relief holes inflated
23/05/2006	476–519	Packered sections in pressure relief holes isolated
20/11/2006	657	Pressures in all filters (except FR901) raised to 2350 kPa
25/05/2007	843	Lower canister filters isolated for the start of the first hydraulic test

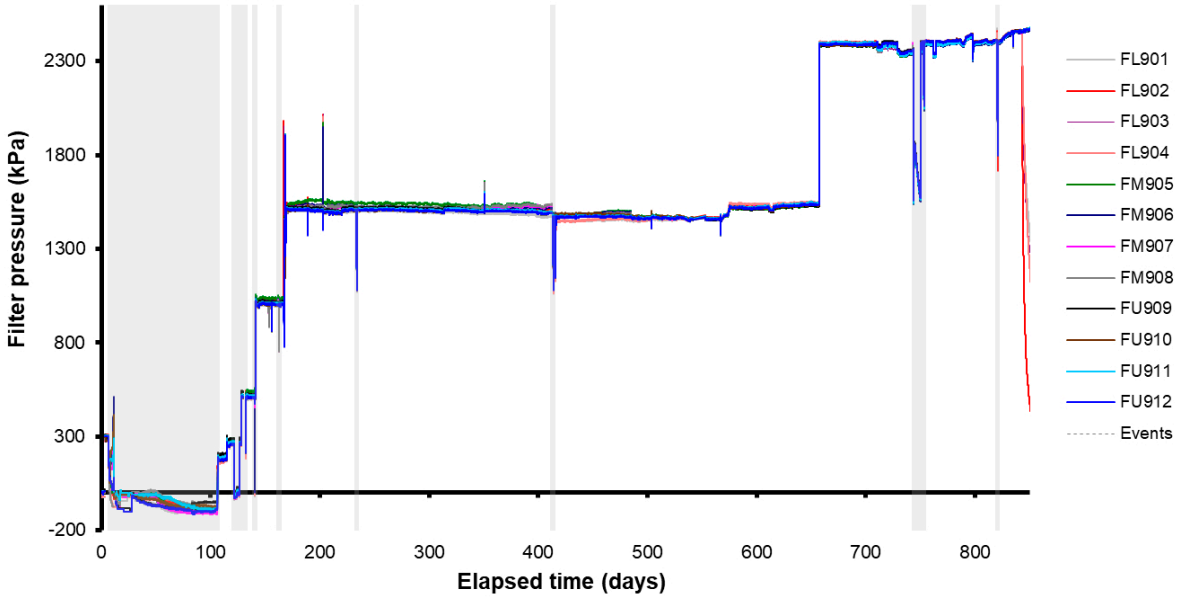

Figure 5-2. *Evolution of water pressure within the canister filters.*

Table 5-3. Sequence of events during the installation of packers into the pressure relief boreholes PRH1 and PRH2.

Date	Day	Activity
23/03/2006	415	Valves to sections PRH2-1 and PRH2-3 closed. Valve to section PRH1-1 temporarily closed (few hours) but reopened as pressure increased rapidly
23/05/2006	476	Valve to section PRH2-4 closed
31/05/2006	484	Valve to section PRH2-2 closed
08/06/2006	492	Valve to section PRH1-5 closed
14/06/2006	498	Valve to section PRH1-4 closed
20/06/2006	504	Valve to section PRH1-3 closed
21/06/2006	505	All PRH pressures (in both holes) begin to decrease as the packers in PRH1 deflate
26/06/2006	510	Pressurisation system for PRH1 packers repaired
29/06/2006	513	Valve to section PRH1-2 closed
05/07/2006	519	Valve to section PRH1-1 closed

At Day 141, the pressure within the RP2 circuit was successfully increased to around 750 kPa and then 1 000 kPa using the following methodology. In an attempt to minimise the time taken to hydrate the bentonite, a decision was made at the start of the project to actively hydrate the clay through the canister filters and the large hydration mats installed at key locations within the system. Water pressure, controlled by the reciprocating syringe pumps, was simultaneously applied to all of the filter arrays except FR901, which was in hydraulic communication with the fracture system of the host rock. Before an increase in porewater pressure was applied to the system, all canister filters and filter mats were isolated from each other using the automated valve-work situated within the Gas Laboratory. The pressure in each filter was continuously monitored during this time by the appropriate transducer. A note was then made for each pump-set (RP1 and RP2) recording the total volume of fluid pumped into the system. Pressure was then increased to the desired value. The total volumes were recorded again and the isolating valve to the first canister filter then opened. Each filter was pressurised in turn when the volumetric flow rate into the system dropped below 1 ml min^{-1}, starting at the base of the canister with FL901 and then proceeding vertically upwards until the pressure in FU912 reached the target value. The total volumes pumped into the system by each pump-set were recorded before each new valve was opened. In this way, the pressures in all 12 canister filters was increased to the target value and are thereafter in direct communication with their respective pump-sets.

A short interruption to update the control software (~5.5 h) resulted in the adoption of a "fail safe" mode of operation, whereby all system valves automatically defaulted to the closed position, isolating individual test circuits. During this time a number of transducers exhibited clearly defined negative pressure transients. A similar affect was observed at Day 156 when an update to the multi-logger (Geokon) software was applied. At Day 162, control of the pressure in canister filters FM905 to FM909 and filter mats FR902, FB903, and FB904 was migrated to pump-set RP1. During this transition a temporary reduction in pressure occurred.

Between Days 167 and 168 several attempts were made to incrementally raise water pressure in the canister filters to a target value of 2 000 kPa. When water pressure in filter FL903 reached ~1 950 kPa, an increase in pressure was observed in FR901 as well as multiple total stress and porewater pressure sensors located within the clay and on the surface of the borehole; indicating the formation of highly conductive channels ("piping") exploiting interfaces between the canister and buffer, as well as interfaces between the bentonite rings. The pressure in RP2 was immediately lowered to ~1 200 kPa to prevent the possible extrusion of bentonite slurry and the formation of long-term pathways. After a short period of time the pressure in each pump system was incrementally raised to around 1 250 kPa without any obvious signs of pathway flow. At this point in the test history it was decided to increase the pressure in each pump system to approximately 1 300 kPa without isolating individual test circuits. This proved successful, so the pressure in the artificial hydration system was increased in 50 kPa steps. When the pressure reached 1 450 kPa both reciprocating pump-sets began to rapidly inject water into the system, indicating that one or more conductive pathways had formed. The pressure in each pump system was reduced to around 1 250 kPa and the system allowed to stabilise.

The next day (Day 168), pressure in each of the canister filters and hydration mats was incrementally raised to approximately 1 500 kPa without any signs of pathway flow. Another attempt was made to incrementally raise water pressure in the artificial hydration system to 1 750 kPa. This was successful up to the inclusion of FM905, at which point pathway flow re-occurred. The pressure was immediately reduced to around 1 500 kPa. However, when an attempt was made to restore the water pressure in FU910, which had declined slightly while isolated from the pumps, pathway flow again occurred. At this point, FU910 was isolated from the rest of the hydration system and the pressure allowed to equilibrate. Shortly afterwards, both pump sets began to rapidly inject water into the system indicating the sudden formation of one or more conductive features. To stabilise the system the pressure in both pump sets was reduced to 1 350 kPa. The following day at an elapsed time of Day 169 water pressures were incrementally raised to around 1 500 kPa in each system without any obvious signs of pathway flow.

These pressure dependent features appear to be relatively short lived with the channels closing when the water pressure was reduced. Figure 5-3 shows a series of contour plots showing the propagation of a high-pressure water zone around the periphery of the borehole during the piping event described above.

At 203 days another attempt was undertaken to incrementally raise porewater pressure in the artificial hydration system to 2 000 kPa. As the pressure was increased, piping occurred when the tube work to filter FM906 was opened. This resulted in a rapid inflow of water and an increase in monitored porewater pressure and total stress. Pressure in both pump systems was immediately reset to 1 500 kPa and the system allowed to re-stabilise at the lower pressure.

At Day 233 both pump sets were taken off-line for ~24 h while software upgrades were applied to the system. During this time each test circuit exhibited a small decrease in water pressure. However, when a similar activity occurred 21 days later the pressure in the lower and upper filter arrays actually increased to around 1 600 kPa.

At 657 days, after the pressure relief holes had been closed for about 140 days, the pressures on the canister filters and filter mats FR902, FB903, and FB904 were all raised to around 2 350 kPa. A six day drop in pressure occurred at Day 744 when pump A2 ran out of water. A further drop in pressure occurred at Day 821 when the injection pumps were leak tested. Phase 1 of hydration was completed 849 days after the start of the testing.

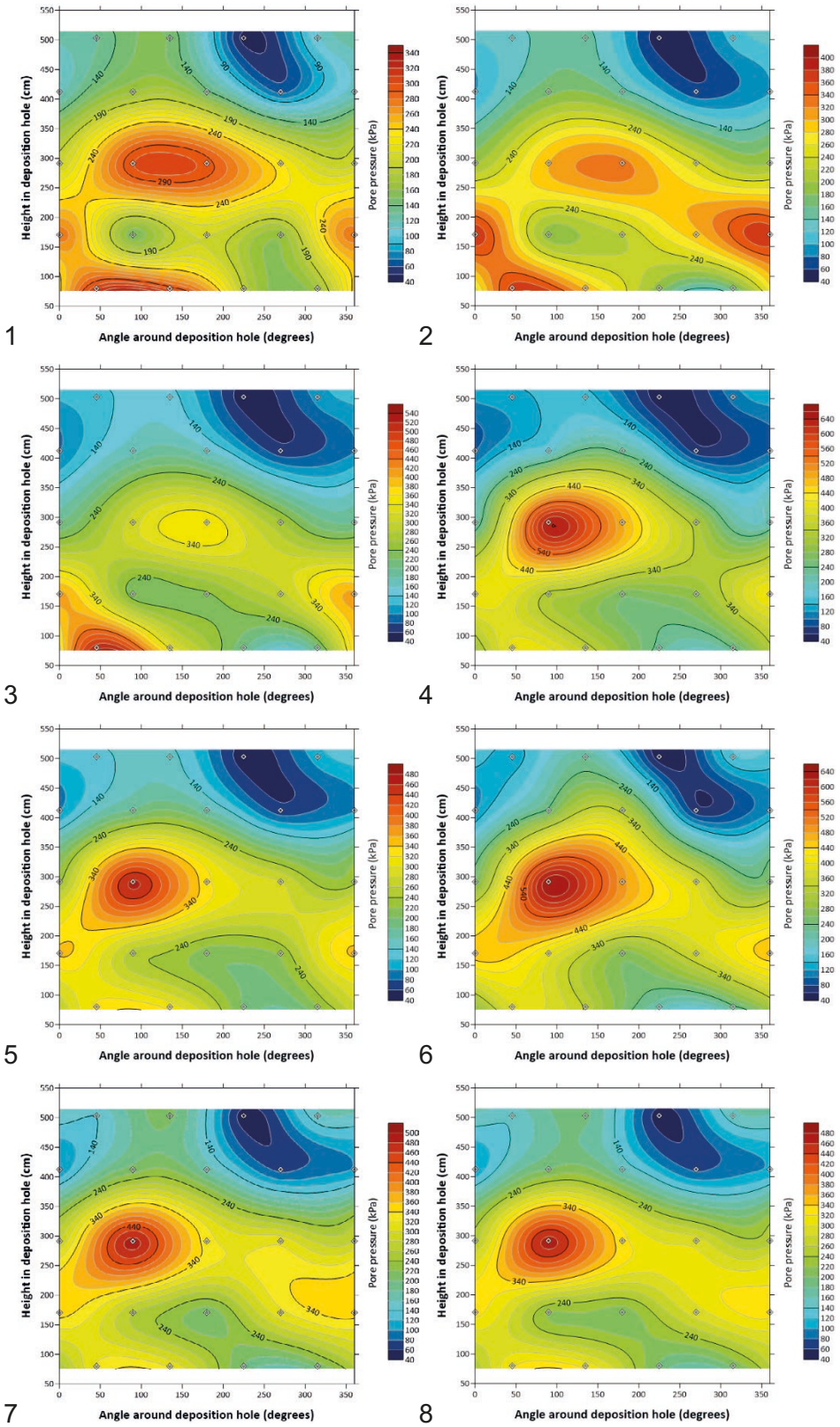

Figure 5-3. *Evolution of water pressure at the borehole wall due to hydraulically induced piping during artificial hydration activities. The series of images start at Day 167 and finish at Day 172 (Days 167.00, 167.20, 167.22, 167.35, 168.22, 168.47, 169.97, 172.02).*

5.1.2 Filter mats FR901, FR902, FB903 and FB904

Data from the filter mat sensors are shown in Figure 5-4. The erratic output from the transducers during the first 14 days of testing was primarily due to de-airing of the tube work (post-closure of the deposition hole) and the depressurisation of system components in an early attempt to moderate the rapid build-up of porewater pressure which occurred during the early stages of the hydration test. Towards the end of this period the pressure lines from each filter mat were disconnected from the Gas Laboratory where they emerged from the deposition hole, in an attempt to improve discharge rates out of the arrays. As a mechanism for moderating pore pressure build-up, this was unsuccessful and the problem was only solved by drilling the two pressure relief holes.

The water pressure in the upper filter mat (FR902) located on the rock face and the two filter mats (FB903 and FB904) sandwiched between bentonite blocks C2–C3 and C4–C5 respectively, were subject to the same artificial pressure history as the canister filters described in Section 5.1.1. The water pressure in the base filter mat FR901 (Figure 5-4) was in direct hydraulic communication with the drain holes and as such was left to evolve independently from the rest of the system. The rise in pressure of FR901 at Day 167 was caused by the "piping" event through the bentonite discussed in Section 5.1.1.

Close inspection of the data from FR901 shows a small but progressive increase in porewater pressure between Day 200 and 400. While the cause of this response was unclear it may indicate some form of time dependent (temporal) evolution in the hydraulic characteristics of the surrounding rock mass. Clogging and associated permeability reduction of fracture pathways may explain this response. It is also interesting to note that the hydrogeological regime in the Assembly Hall area of the HRL appears to have changed during the operation of Lasgit, with fresh discharges observed from previously dormant fractures.

The pressure at FR901 increased abruptly at Day 415 when the packers were installed in the pressure relief holes and in a series of further steps as the various packered sections were isolated, reaching a peak of about 2 450 kPa at Day 520. After that there was a steady decline in pressure. The cause of this behaviour remains unclear but may relate to a regional decline caused by engineering works elsewhere at the Äspö site.

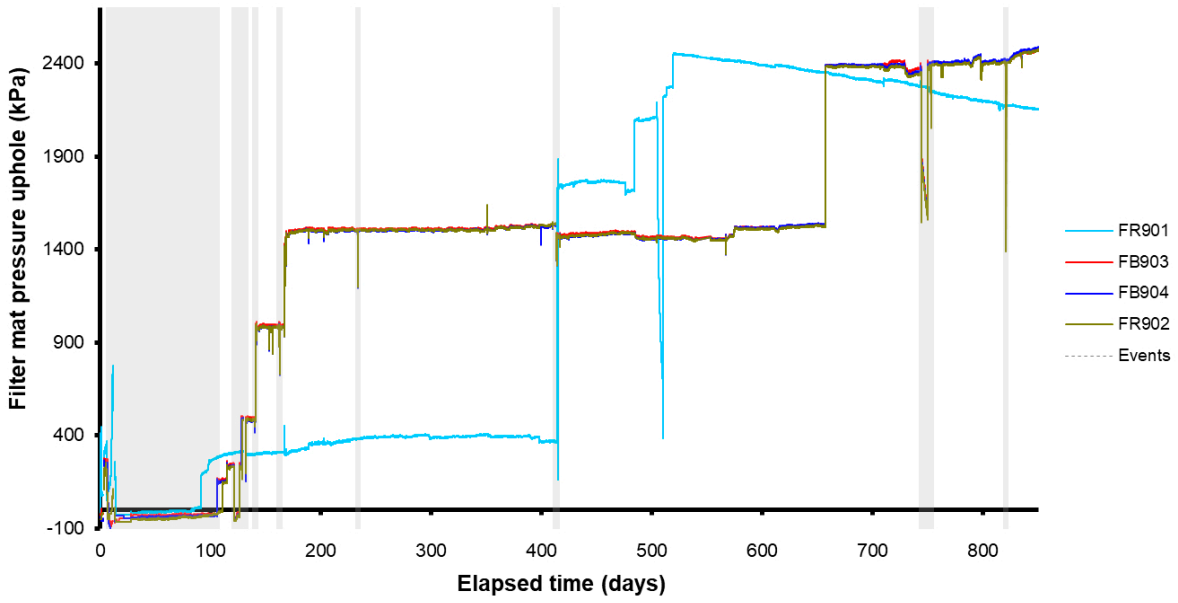

Figure 5-4. *Evolution of water pressure in the filter mats located on the borehole wall and within the bentonite blocks. Filter mat FR901 is in direct communication with the drain holes and was therefore allowed to evolve independently from the other filter mats.*

5.1.3 Porewater pressure within the bentonite

Porewater pressure within the bentonite was measured at 6 discrete locations. Figure 5-5 shows spikes in porewater pressure at Day 128 (UB923), Day 140 (UB924) and Day 167 (UB902). These features were caused by localised channelling through the clay as porewater pressure was increased in the canister filters. It is interesting to note that channelling occurred at multiple locations at different times within the clay rather than being consistently focused in one specific location. The small increase in pressure at Day 203 in UB902 corresponds with another attempt to raise water pressure in the artificial hydration system.

Pressures in UB901 and UB902 show a clear effect from the installation of packers in the pressure relief holes with pressures rising steadily from that point on, although UB901 appears to have levelled off after 770 days at about 300 kPa. Pressures in UB923 and UB924 rose steadily from Day 200 onwards with little apparent effect from the changes to the pressure relief holes, though UB923 exhibited a small increase in pressure at around Day 485 probably cause by the closure of the packered interval PRH2-2. At about Day 600 pressure in UB923 levelled off at about 200 kPa, but pressure in UB924 continued to rise steadily through to Day 840. Pressures in UB925 and UB926 remained largely unchanged until the introduction of packers in the pressure relief holes, which resulted in a small but noticeable increase in the rate of change of pressure in UB925. In contrast, UB926 exhibited little additional pressure sensitivity until around Day 489, when the rate of pressure increase rose, steepening markedly after about Day 720 and again at Day 760. The latter date roughly corresponds to the observed levelling seen in UB901 and may indicate a readjustment of the ingress of water in the buffer clay.

While all porewater pressure sensors were fully operational, the integrated thermocouple within UB924 was not functioning. However, this does not affect the functionality of the test which was performed under isothermal conditions. Thermocouple values from the neighbouring device (UB923) was used to correct outputs from the affected sensor.

It is clear from the data presented in Figure 5-5 that porewater pressures within the clay remained very low when compared to the *in situ* boundary condition, and that the bentonite remained in a state of hydraulic disequilibrium. This is an important observation when interpreting the subsequent hydraulic and gas test phases.

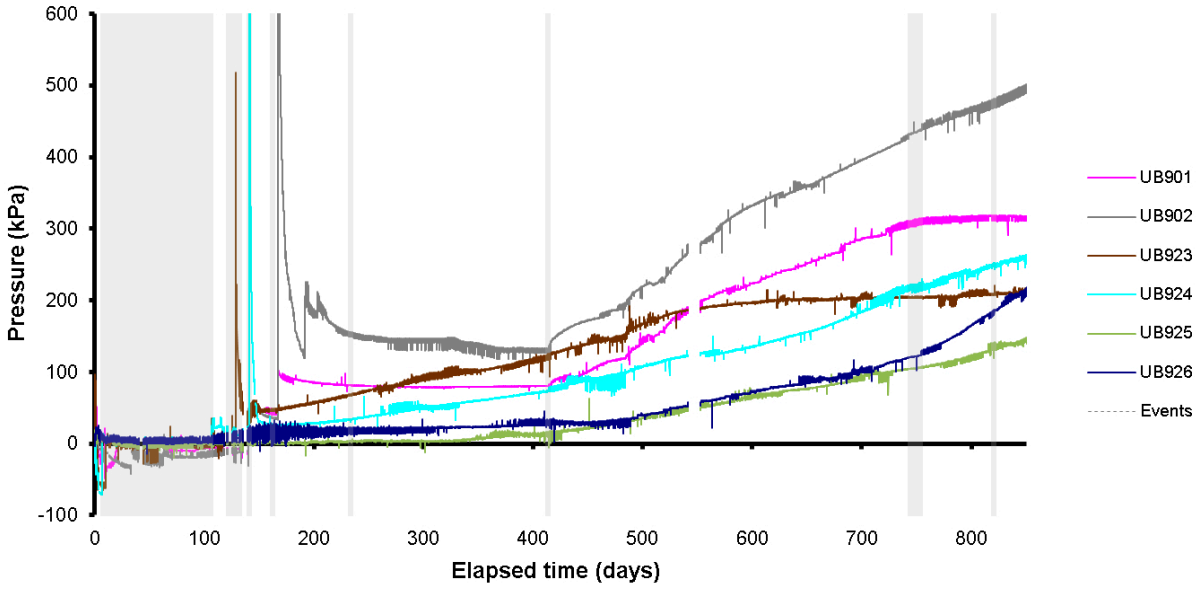

Figure 5-5. *Variation in porewater within the bentonite at the 6 monitoring points. The large spikes in the data correspond with attempts to increase porewater pressure within the artificial hydration system early in the test history.*

5.1.4 Porewater pressure measured at the rock wall (UR903 to UR922)

Porewater pressure was measured at 20 separate locations on the borehole surface and the data are shown in Figure 5-6. Once the pressure relief holes were drilled in the surrounding rock mass, the pressure in the deposition hole stabilised and local increases in porewater pressure at Days 141, 167, 168, and 203 were caused by the movement of water along temporary channels when water pressure in the filter assemblies was increased (Figure 5-2). These pathways appear to be ephemeral features which sealed when the water pressure was allowed to decay. Therefore, the small pulse-like events are attributed to sudden porewater pressure changes, whereas the general increasing trend reflects the total stress changes due to swelling processes. It is interesting to note that many of the sensors actually exhibit a similar progressive increase in value with time as that observed by FR901.

Close inspection of the data in Figure 5-6 indicates a reduction in the rate of pressure decay in a number of porewater pressure sensors at around Day 775. Indeed, a number of sensors (UR907, 910, 911, 912, 913, 914, 915, 917, 919, 920, 921 and 922) appear to plateau at around Day 818. However, porewater pressures in the lower sections of the deposition hole continue to exhibit a general trend of reducing porewater pressure. As stated for FR901, the cause for this behaviour remains unclear.

The contour plots (Figure 5-7) show the spatial and temporal evolution in porewater pressure measured at the interface between the rock wall and the bentonite from Days 130 to 272. The contour plots give explanation of the distribution of pressure, whereas the magnitude may be more clearly identified in Figure 5-6. Examination of the initial data, images [1] and [2], clearly shows a zone of elevated porewater pressure extending from the base of the plot diagonally upwards from left to right. The "pulses" in high water pressure, images [3] and [5], stem from a number of attempts to raise porewater pressure in the artificial hydration system resulting in piping of water through the buffer. The pressure in these regions quickly decayed with time, images [4] and [6] respectively, indicating that these pressure-induced pathways were no longer conductive.

As hydration progressed, a small increase in porewater pressure can be observed left of centre in plots [7] and [8]. The origin for this expanding zone of porewater pressure is unclear but may relate to the suggested evolution in the near-field hydrogeological behaviour discussed earlier.

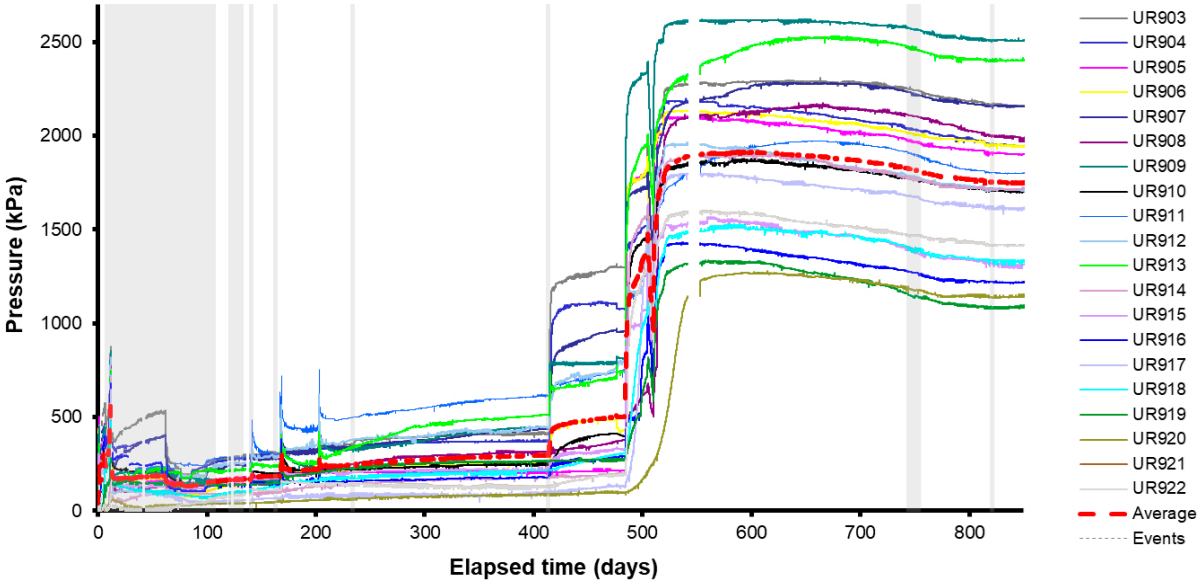

Figure 5-6. *Variation in porewater pressure with time measured at the rock face. The spikes in the data from Days 141 to 203 correlate with attempts to increase porewater pressure in the artificial hydration system. The rapid increase in pressure from around Day 415 relate to changes in the boundary condition during the installation of packers in PRH1 and 2 and their subsequent closure.*

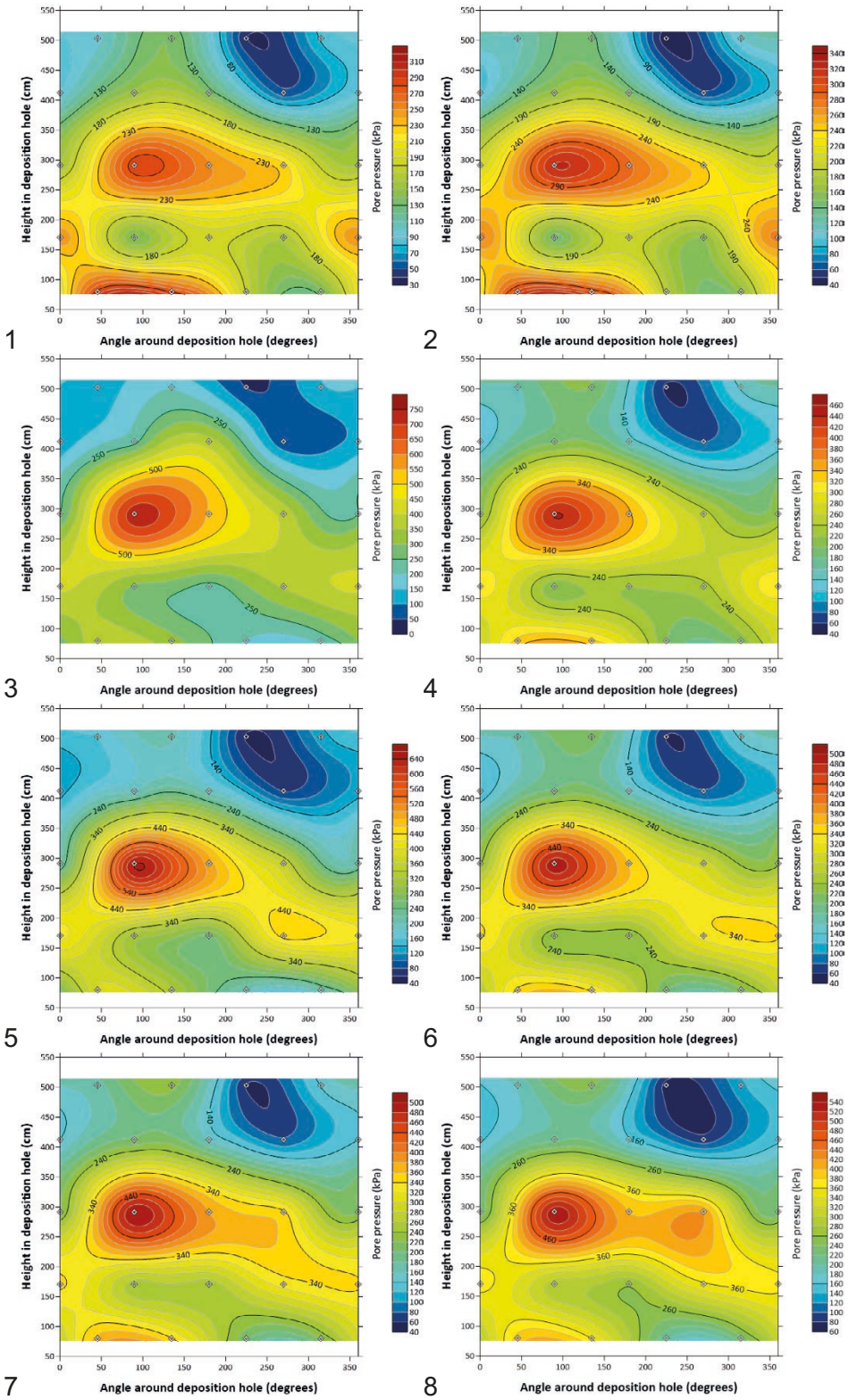

Figure 5-7. *Evolution in porewater pressure measured at the interface between the rock wall and the bentonite from Day 132 to 275. The series of images show a general increase in porewater pressure. The high-pressure zones in images (3) and (5) relate to piping events during artificial hydration activities (Days 132.16, 150.09, 168.35, 197.02, 203.20, 212.09, 235.02, 275.35).*

In the contour plots of Figure 5-8 the changes of pore pressure during the closure of the pressure relief hole packers can be traced. Comparing images [1] and [2] shows that the introduction of the packers raised pressures at the base of the hole sharply. Then, as the packer sections were closed the zone of highest pressures migrated to an area around 270° and 2 m up from the base of the hole (note the changes in the colour scale between [2] and [3]). Following the completion of the changes in the pressure relief holes there has been a gradual reduction in the overall levels of the pore pressures, which is also seen in Figure 5-6, with little change in the pattern of pressure variations.

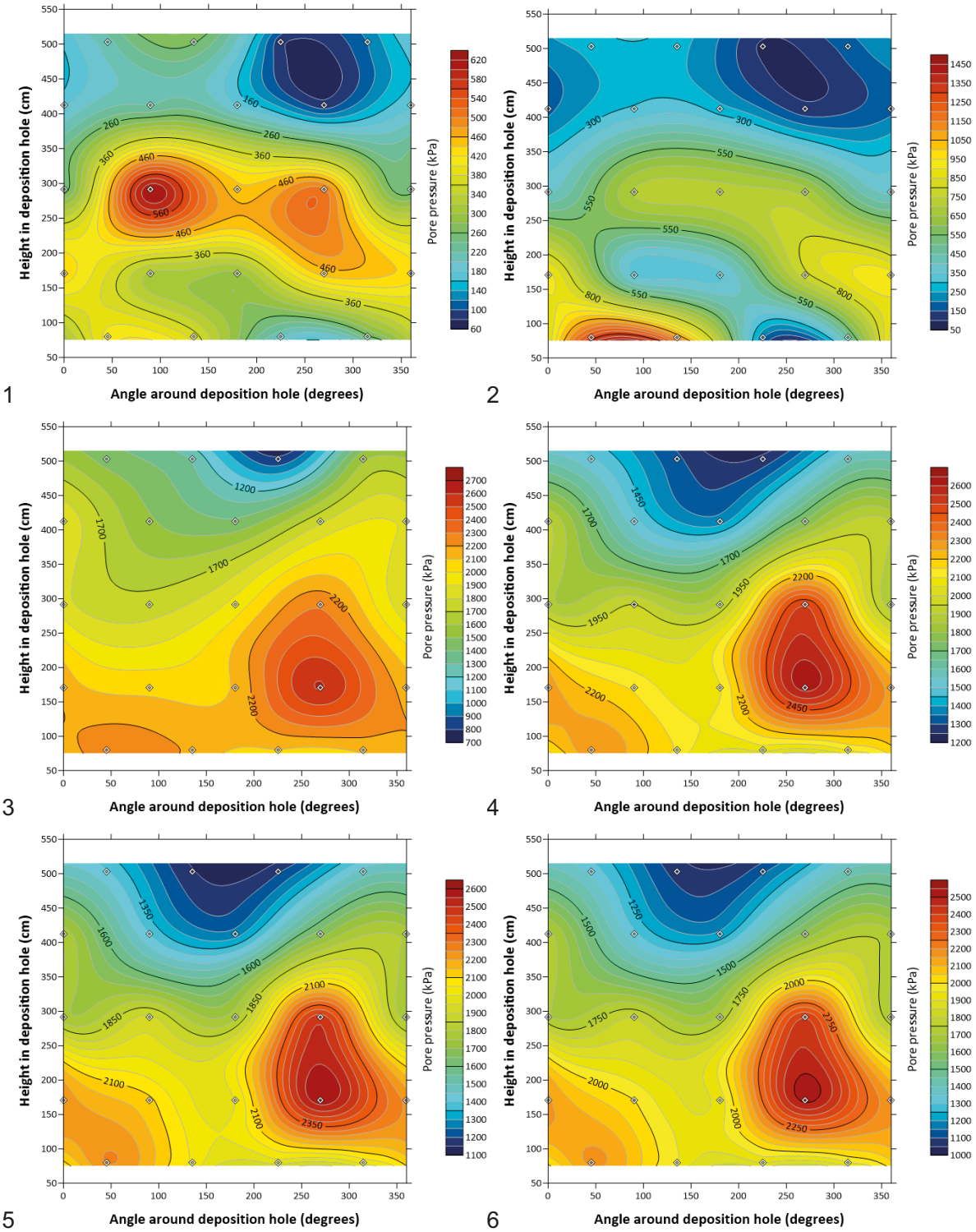

Figure 5-8. *Evolution of pore pressure at the deposition hole wall from Day 400 to 840 (Days 400.27, 449.98, 529.86, 618.4, 743.07, 833.66).*

5.1.5 Porewater pressure in the pressure relief holes

Pressure data from the individual packered sections of the two pressure relief boreholes are shown in Figure 5-9. After the packers had been inflated and the sections isolated the pressures form a pattern that is maintained through the rest of the test, but with the overall magnitude of the pressures declining gradually with time. Section PRH1-1 had the highest pressure at 2 540 kPa on Day 525 and declining to 2 230 kPa. Section PRH2-1 was next highest with a pressure of 2 360 kPa on Day 525, declining to 2 130 kPa. The five sections PRH1-2, PRH1-3, PRH2-2, PRH2-3, and PRH2-4 all plot together with pressures of about 2 070 kPa on Day 525, declining to about 1 830 kPa. Section PRH1-4 reached a pressure of 1 550 kPa on Day 525 and declined to 1 300 kPa. The lowest pressures were found in section PRH1-5 which reached about 1 255 kPa on Day 525, increased slightly to about 1 290 kPa on Day 590 and then declined to about 1 050 kPa.

Close inspection of the PRH transducer outputs exhibited qualitatively similar responses for most devices to those observed by the porewater pressure sensors mounted on the rock wall (UR) at around Days 775 and 816. This indicates that the hydraulic boundary conditions around the Lasgit borehole had evolved during the test. This behaviour could be related to periodic construction work related to the commissioning and decommissioning of new tests at the Äspö HRL. While no such activities could be identified for the event at Day 775, the change in porewater pressures observed at Day 816 correlates with over-coring activities of the LTDE project which was located in a niche just above the Lasgit test site.

A cross-plot of the porewater pressure against depth to base of each packered interval for both PRH's (Figure 5-10), indicates a fairly linear trend with pressure decreasing towards the gallery floor. The data clearly demonstrates the decreasing trend in local porewater pressure with time, strongly indicating some form of temporal evolution in the local hydrogeological boundary condition.

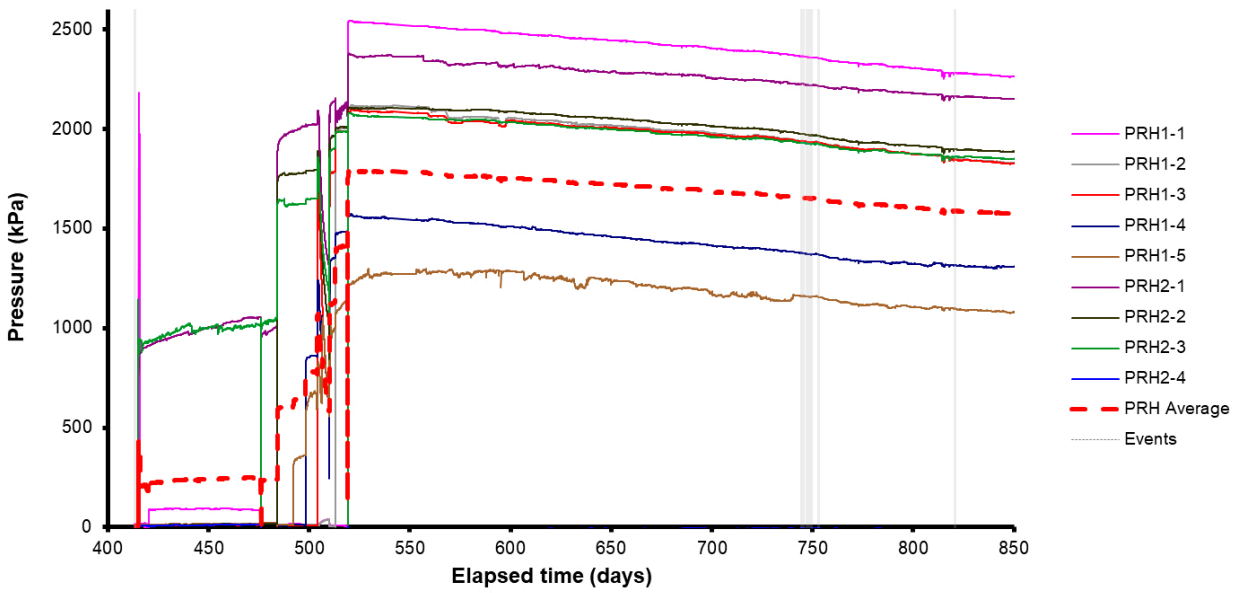

Figure 5-9. *Porewater pressures measured in the packered sections of the pressure relief boreholes.*

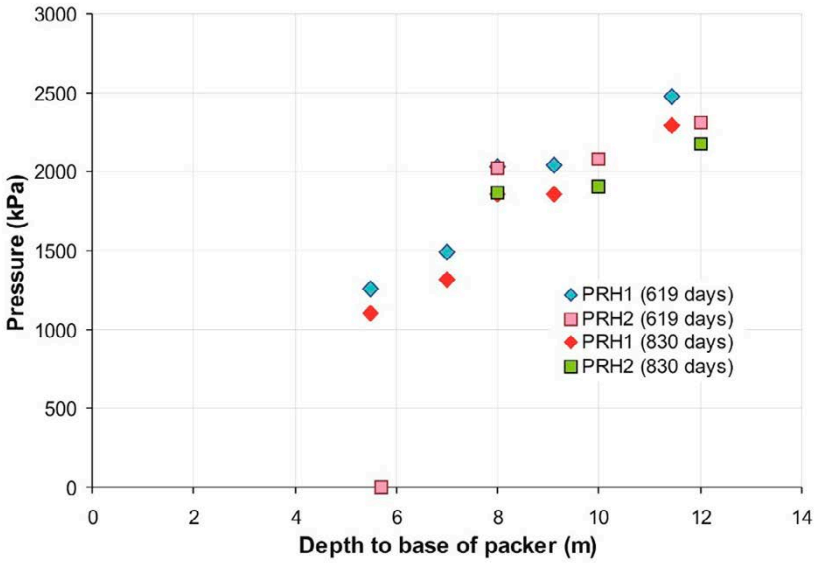

Figure 5-10. *Evolution of pressure in packered intervals within PRH1 and PRH2.*

5.2 Evolution of total stress

Total stress within the Lasgit system was measured at 32 locations within the borehole. Sensors mounted on the canister, rock wall, and within the clay were used to determine both the axial and radial components of stress and the distribution of values throughout the borehole.

5.2.1 Radial stress measured at the rock wall (PR903 to PR922)

Data from total pressure sensors PR903 to PR922 are plotted in Figure 5-11. As in previous sections, the small increases in radial stress at Days 141, 167, 168, and 203 were all caused by localised piping events when water pressure in the canister filters and hydration mats were increased, resulting in hydraulic flow through/across the bentonite. These events were generally short-lived with the radial stress traces returning to their predicted trend-lines within a few days. The absence of any lasting effects supports the results presented in Harrington and Horseman (2003) examining the validity of the effective stress law. In the absence of piping events the rate at which radial stress increased within the deposition hole was insensitive to the absolute value of porewater pressure applied to the filter assemblies.

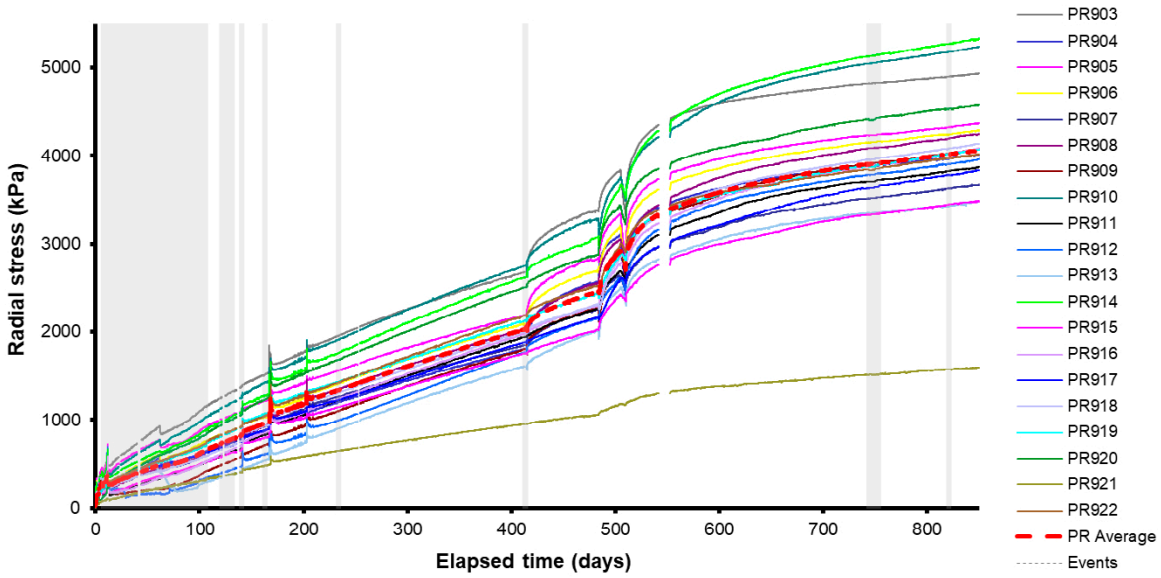

Figure 5-11. *Variation in radial stress with time. In the absence of preferential flow (piping), the rate at which total stress increased was insensitive to the absolute value of porewater pressure applied to the filters.*

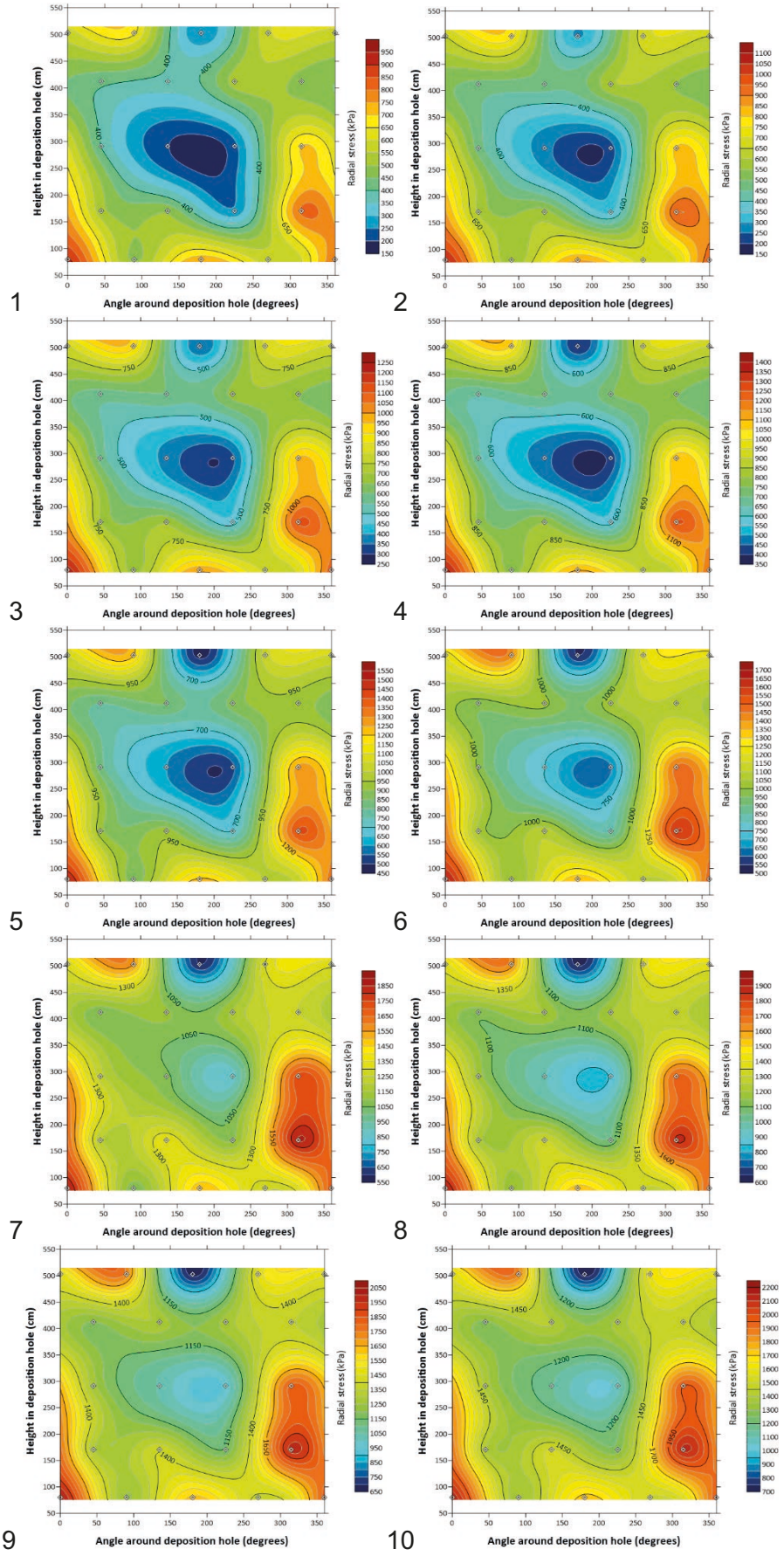

Figure 5-12. *Evolution in radial stress around the deposition hole wall from Days 75 to 272. From image [5] onwards a narrow zone of high pressure can be seen propagating upwards (Days 75.00, 96.39, 117.14, 139.02, 160.13, 180.00, 203.20, 223.09, 245.48, 272.27).*

The contour plots (Figure 5-12) show the spatial and temporal evolution in radial stress measured around the canister between the rock wall and the bentonite from Days 75 to 272.

Inspection of the data clearly shows a narrow zone of elevated stress propagating vertically upwards to around 3.5 m by Day 270. This zone seemed to be expanding as the test progressed. At this stage of the hydration history, the remaining buffer exhibited a fairly uniform distribution in stress with the exception of the upper zone, at around 5 m, which had somewhat larger variations in stress. This could be explained by the close proximity of the large filter mat located between blocks C2 and C3 causing preferential swelling of the clay.

Comparison of the images in Figure 5-7 [8] and Figure 5-12 [10] shows a poor correlation between pore pressure and radial stress at a similar point in time. Given the quasi-static nature of the boundary condition, it is unclear what mechanism was directly responsible for the preferential swelling of the clay observed propagating upwards from the base of the borehole.

The contour plots in Figure 5-13 show that the pattern of stress around the deposition hole wall did not change greatly through the installation of packers into the pressure relief holes except for a general rise in stress levels, which is also apparent in Figure 5-11. It is also apparent from Figure 5-11 and the contour plots of Figure 5-13 that the readings from sensor PR921 were anomalously low compared to those from all other sensors.

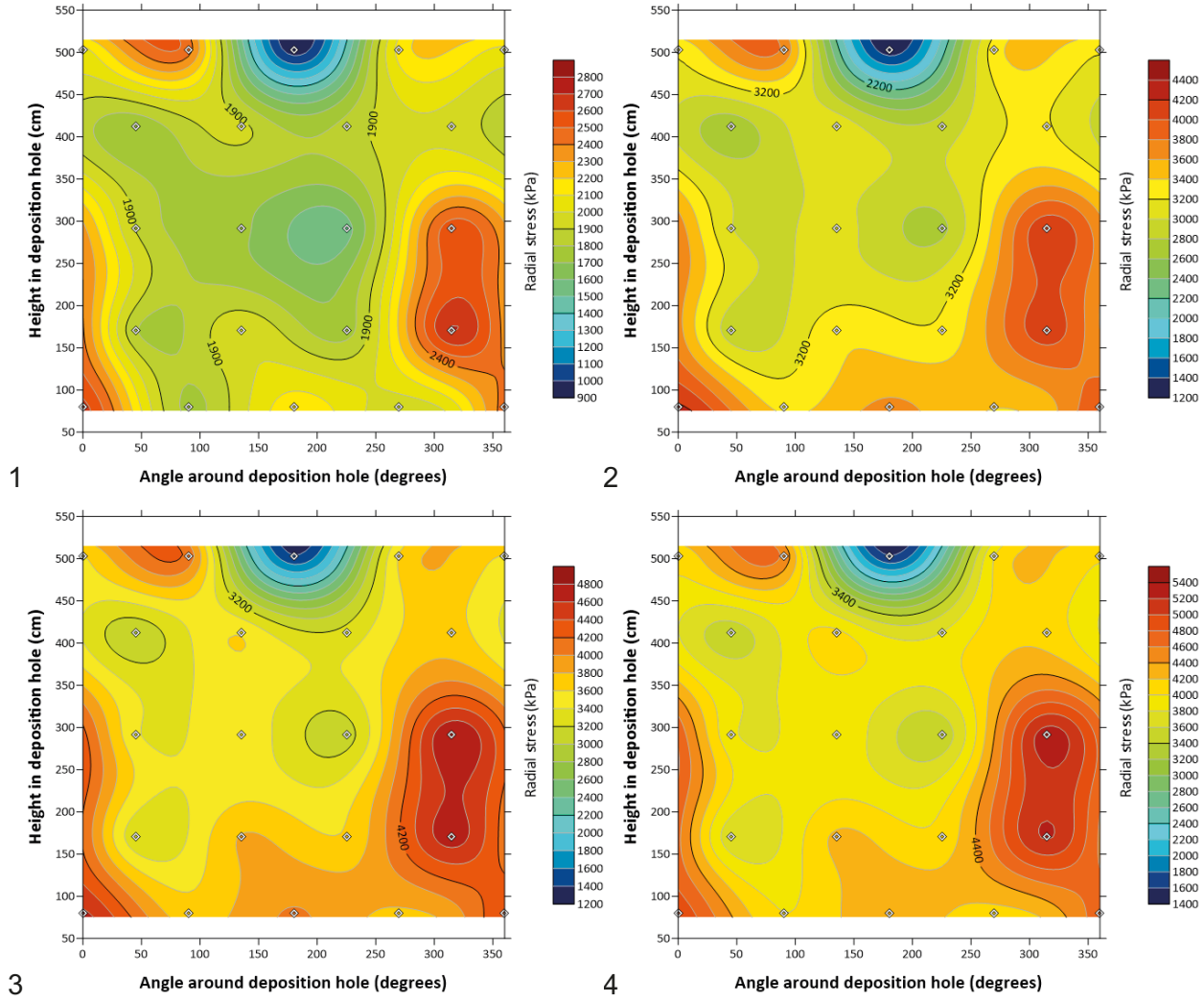

Figure 5-13. *Evolution of radial stress around the deposition hole wall from Day 400 to 840 (Days 400.23, 529.86, 618.40, 841.66).*

5.2.2 Radial and axial stress on the canister (PC901 to PC903)

Axial and radial stress around the canister had increased steadily during the course of the hydration history (Figure 5-14). At Day 878 radial stress on the canister surface ranged from 4 620 kPa to 4 810 kPa. The radial stress monitored by PC903 increased at Day 167 and 203 (due to piping) attaining a value close to that of the artificially applied porewater pressure. This indicates that device PC903 was in good calibration and operating correctly. Spontaneous increases in pressure for all sensors correlate with the experimental activities discussed in Section 5.1.1.

At Day 878 axial stress acting on the base of the canister (monitored by PC901) was 3 810 kPa. This value was relatively low when compared to the equivalent outputs from axial stress sensors located within the bentonite above the canister (Section 5.2.3) and the Glötzl cells (Section 5.4) located on three of the rock anchors. This suggests that a poor contact probably existed between the face of the stress sensor and the clay, indicating that the clay in this region of the system was poorly hydrated.

In the absence of pathway flow the rate at which stress around the canister increased was insensitive to the absolute value of porewater pressure applied to the filter assemblies. A similar result was observed for the development of radial stress at the rock wall (Section 5.2.1).

Analysis of the stress data in Figure 5-14 also indicated a small inflection at around Day 775, when the rate of stress increase rising marginally after this time. This observation correlates with the previous responses noted.

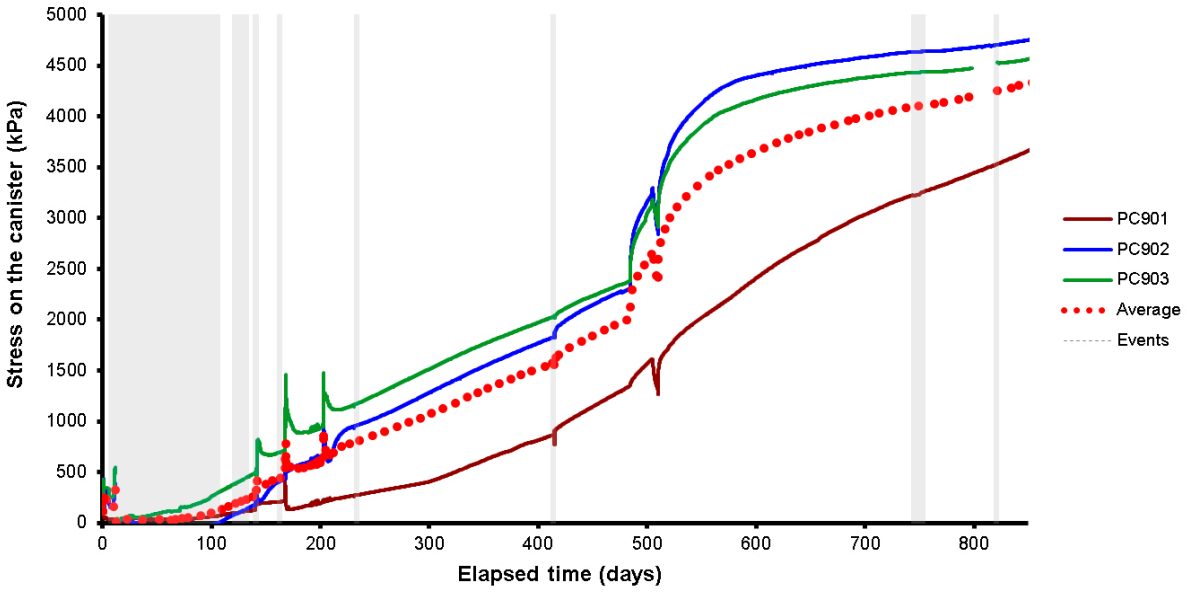

Figure 5-14. *Development of axial and radial pressure on the side and base of canister. Sensor PC901 measures axial stress, while PC902 and PC903 measure radial stress.* ***Note:*** *no events are highlighted.*

5.2.3 Axial stress within the bentonite (PB901, PB902, and PB923 to PB929)

Data from the axial stress sensors is shown in Figure 5-15. The variability in axial stress within the bentonite was considerable during the first 200 days, but significantly reduced during the next 200 days, with all sensors (except PB901 which was located directly under the canister) ranging from 2 770 to 3 560 kPa by Day 400. However, following installation of the packers in the pressure relief holes, the variability increased again with values ranging from 4 740 to 5 910 kPa at Day 841.

Outputs from these devices generally demonstrated only a minor sensitivity to changes in porewater pressure. These events often correlated with other experimental activities such as changes in artificial hydration pressure or drilling and abstraction of groundwater from the pressure relief holes. In general, the rate at which axial stress increased within the clay was insensitive to the absolute value of water pressure applied to the canister and hydration filters.

The contour plots shown in Figure 5-16 have been constructed using the axial stress data from all sensors, except PB901. The plot clearly shows the development of non-uniform axial stresses across the major axis of the emplacement hole, which may help to explain the minor differences in lid displacement observed in Section 5.5. After the completion of packer installation in the pressure relief holes the general distribution of axial stress was relatively stable (images [3] to [6]) with just a gradual extension of the high-pressure zone near PB928 towards the centre of the section.

Both stress sensors located in the base of the deposition hole (PB901 and PB902) exhibited a small but noticeable increase in the rate of pressure rise at around Day 775. This affect was most pronounced in PB901 located directly beneath the canister. This observation correlates with previous data from the porewater pressure sensors mounted on the rock wall and would suggest that the hydrogeological boundary condition changed at this time, with the effect most pronounced in the base of the deposition hole.

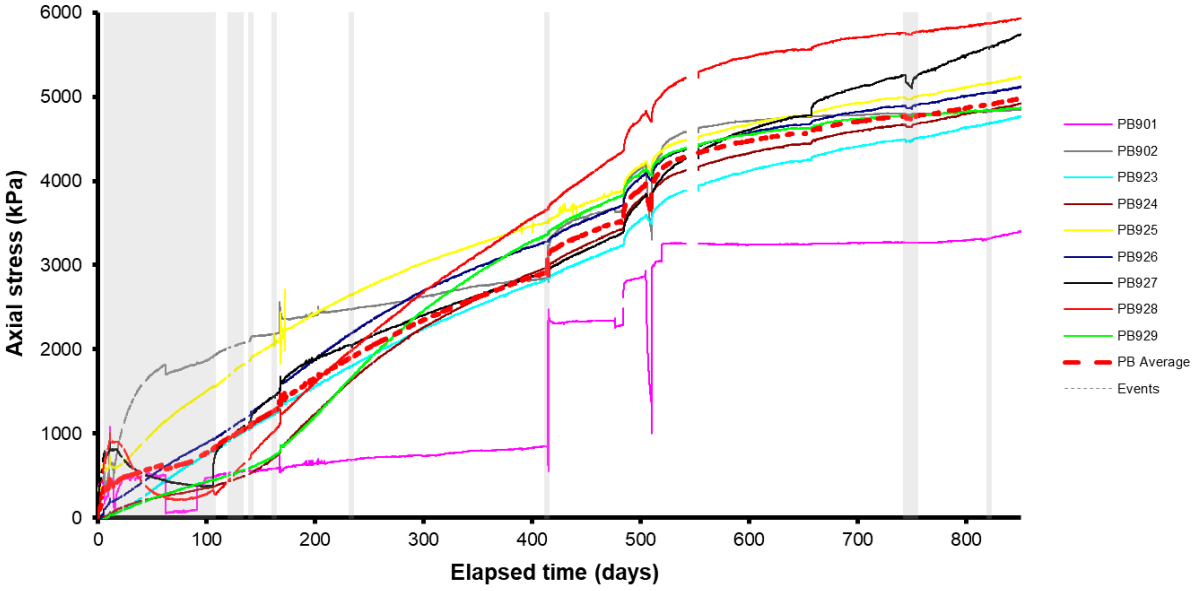

Figure 5-15. *Development of axial stress measured at 12 locations within the buffer.*

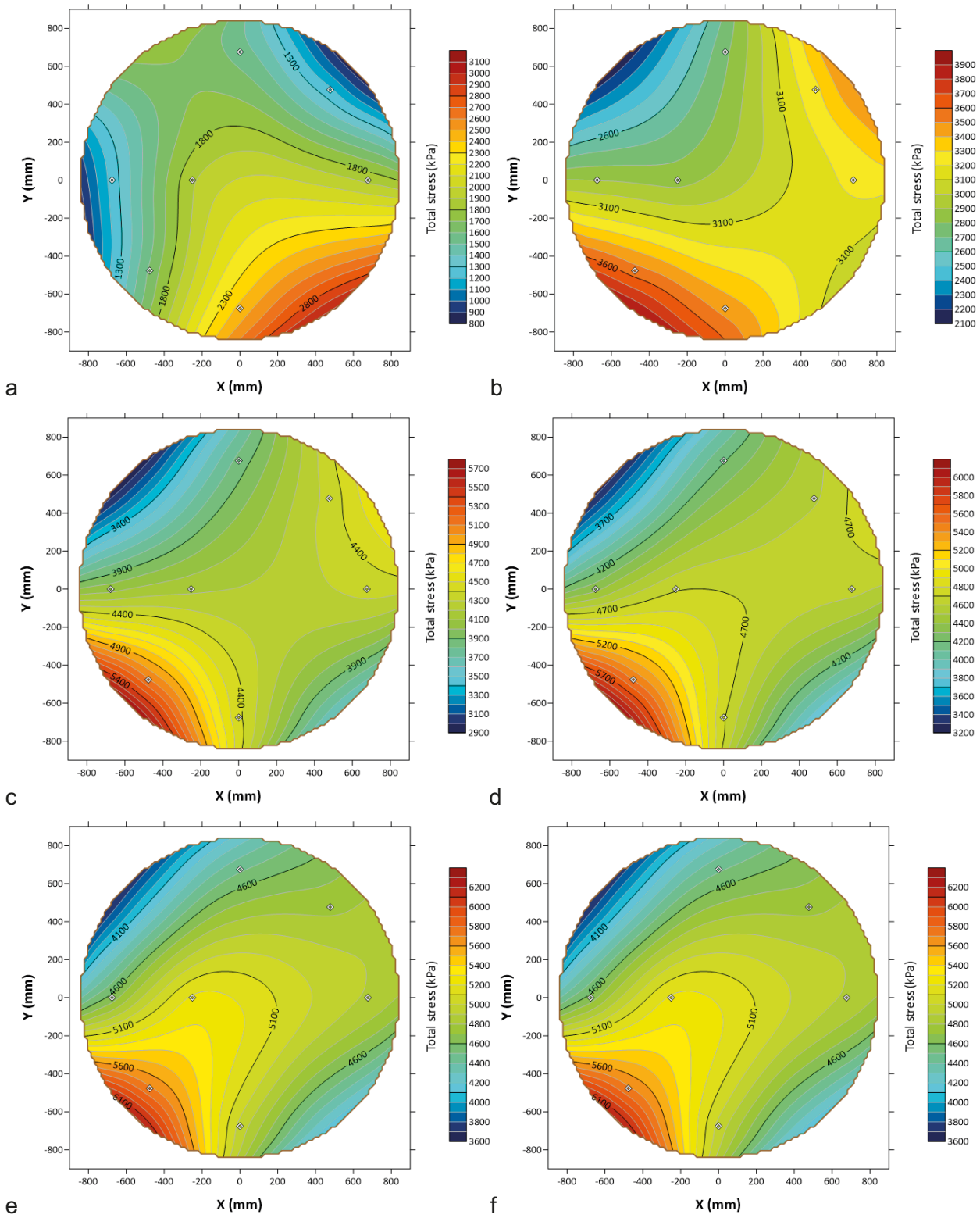

Figure 5-16. *Contour plots showing the distribution of axial stress across the borehole from Day 200 to 847. The range of colour variations has been adjusted to the range of stress values in each plot to highlight the variation over the section. a) Day 200.11; b) Day 400.46; c) Day 530.63; d) Day 620.22; e) Day 730.01; f) Day 841.66.*

5.3 Evolution of water content in the bentonite buffer

Figure 5-17 shows the suction pressures recorded at the seven psychrometers WB901 to WB907 embedded at locations within the bentonite buffer. It can be seen that suction at each location was declining, confirming that resaturation was progressing, although the rate of hydration did appear to be slowing. Greatest progress was made near to the filter mats above the canister whilst the least progress occurred just below the canister. There is no data available from WB903. While a number of psychrometers appeared to be levelling (e.g. WB902), close inspection of the data revealed a steady downward trend.

It was anticipated that when the buffer bentonite was in hydraulic equilibrium, psychrometer values would plateau at a finite (positive) suction, caused by the natural salinity of the Äspö groundwater. However, the data in Figure 5-17 clearly shows that most, if not all of the clay, remained in a state of suction. It is important to remember that clay can be in suction even when fully saturated. Ideally, in relation to subsequent testing, the clay should be in a state of hydraulic equilibrium, otherwise, the suction would introduce an unknown variable in the interpretation of the results.

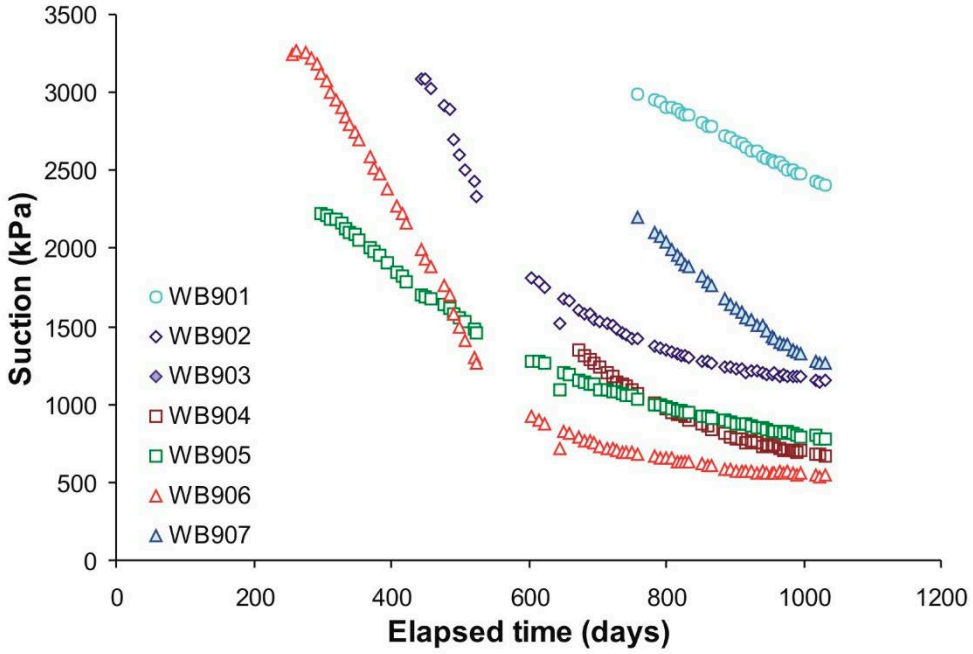

Figure 5-17. *Suction pressures recorded at sensors WB901 to WB907 for the entire test.*

5.4 Axial force acting on the steel lid

Figure 5-18 shows a plot of the axial force (measured by the Glötzl cells) applied by the lid to the concrete plug and bentonite column. The initial reduction in the axial force can be explained by a time dependent relaxation of forces due to compression of the bentonite blocks and the engineering void space. Differences in sensor output can be explained by minor errors in the factory calibration of each device (i.e. < 0.4 % FSR).

From around Day 40 (LP902) and Day 80 (LP901/903) the load cells began to exhibit a positive gradient, suggesting that the continuum axial swelling pressure within the bentonite was greater than the initial pre-stress applied by the lid. From approximately Day 220 onwards, all three load cells showed a small but progressive reduction in force. This can be explained by convex deformation of the steel lid in response to the large axial forces developed in the system as the bentonite continued to swell. This hypothesis is supported by the strain data presented in Section 5.5.

Following packer installation, the forces on sensors LP901 and LP902 started to increase steadily, with a slight steepening of gradient at about Day 755. The force on sensor LP902 also increased initially but then levelled off at about Day 600 until Day 755 when the force began to rise again. This would suggest uneven loading of the lid which is in line with the axial stress data. From Day 755 onwards the forces at LP901 and LP903 were equal whilst LP902 had maintained an excess of 170 kN over them.

The data in Figure 5-18 clearly shows that axial forces within the deposition hole continued to evolve with time. By the end of the period, there was no sign based on the output from the Glötzl load cells that any of the sensors would imminently asymptote at a finite value in the near future.

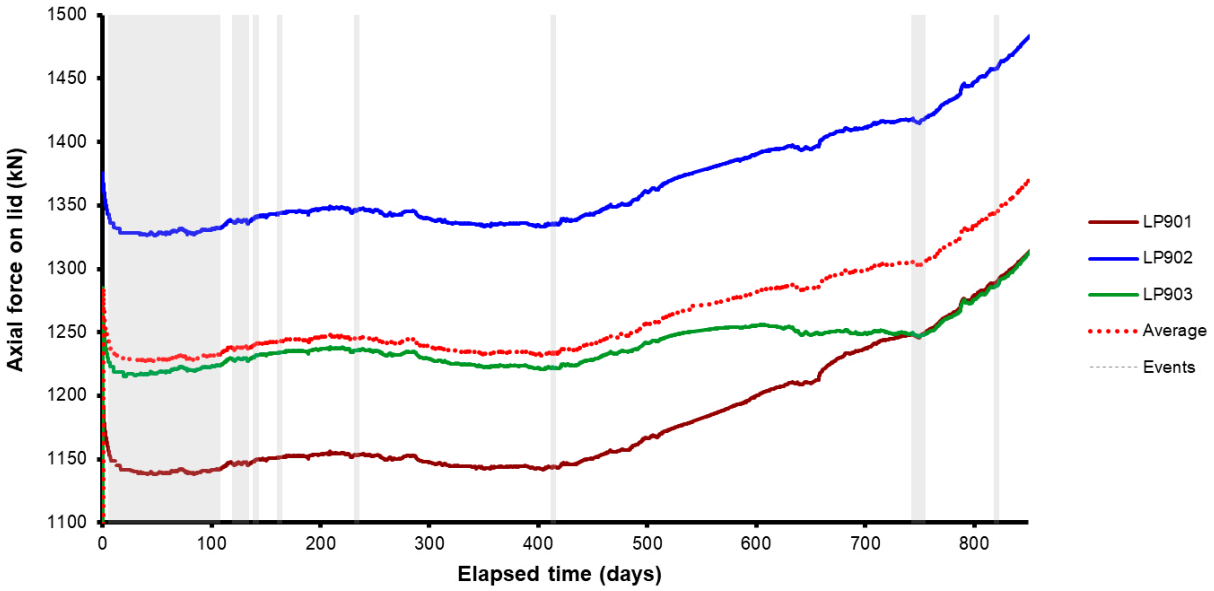

Figure 5-18. *Axial force acting on steel lid measured by 3 load cells attached to separate rock anchors.*

5.5 Displacement of lid and canister

Data from sensors DP901 to DP905 are plotted in Figure 5-19. Sensors DP902-905 continuously monitored movement of the steel lid relative to both the gallery floor and ceiling whilst DP901, attached between the Monel pipe and lid, detected relative changes in canister position. Post closure of the deposition hole, sensors DP902 to DP904 exhibited a negative transient signifying a fairly uniform drop in lid height with respect to the gallery floor. This can be explained by the relaxation in the initial pre-stressing applied to the lid. Comparison of the data from Figure 5-19 with that in Figure 5-2, suggests movements of the lid were insensitive to changes in the porewater pressure applied to the filter arrays. In contrast, displacement of the canister appears highly sensitive to changes in porewater pressure. Examination of the data clearly shows that after the first 16 days of testing where porewater pressures varied considerably, the canister moved progressively upwards associated with preferential hydration of bentonite around the base of the deposition hole. This trend continued until the first pressure relief hole was drilled at Day 62, at which point the canister reversed direction and moved slightly downwards away from the lid. This was probably because of the reduction in porewater pressure within the Lasgit borehole. A second upward trend was then observed at around Day 91 corresponding to the removal of the submersible pumps from both pressure relief holes.

In general, once artificial hydration began at Day 106, the canister reversed direction moving away from the lid as hydration preferentially occurred above the canister through the large filter mats FB903/4. At an elapsed time of 415 days, at the initial installation of packers into the pressure relief holes, the canister resumed an upward movement which continued, with minor interruption around Day 500 during packer inflation, until about Day 660 when the direction of motion was reversed again. By Day 880 the canister displacement was −1.58 mm.

Analysis of the lid displacement data shows a general progressive drop in lid height, relative to the gallery floor, ranging from −0.12 to −0.17 mm at Day 400. The data from DP902 to DP904 would seem to suggest a slight distortion of the lid may have occurred as it deformed to accommodate the uneven distribution in axial stress shown in Figure 5-15.

At Day 189, the original DP905 sensor was replaced with a new measurement system which included a high-resolution displacement transducer. The device clearly showed a small but progressive uplift of the steel lid relative to the gallery roof, supporting the hypothesis of convex deformation. This type of deformation could also help to explain the minor drop in axial force observed by LP901 to LP903 from around Day 220 onwards (Figure 5-18).

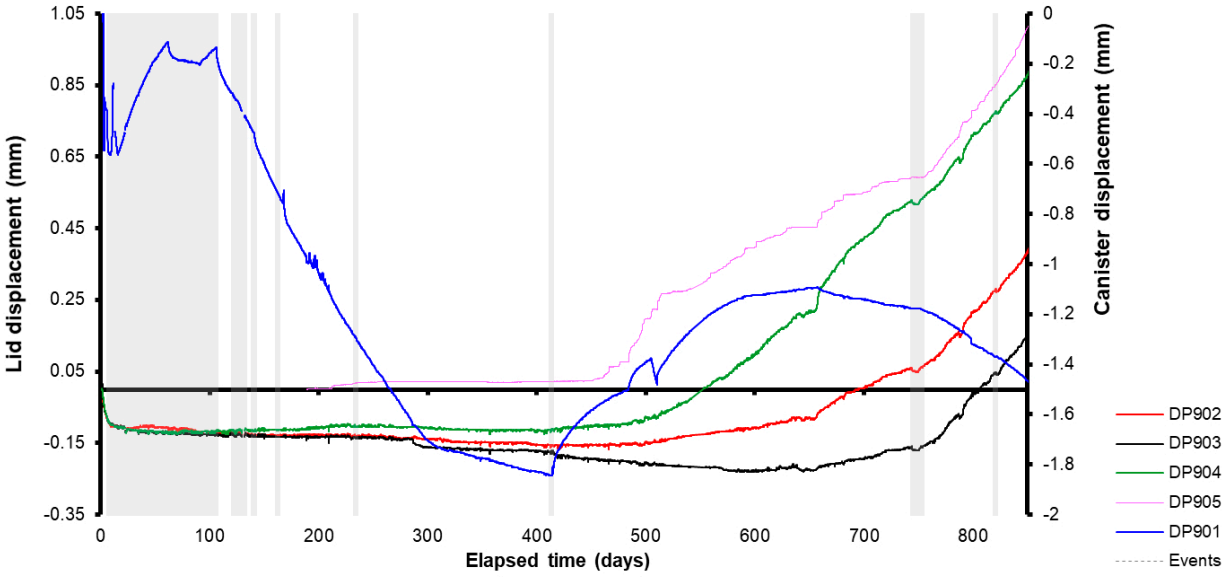

Figure 5-19. *Linear displacement of the steel lid and copper canister. Movements of the lid are measured relative to both the gallery floor and ceiling. Movements of the canister are measured relative to the steel lid.*

Following the initial installation of packers into the pressure relief holes at Day 415 the displacements measured at DP902 to DP904 started to diverge with DP904 rising, DP903 falling, and DP902 remaining steady until about Day 480. DP905 showed no response until about Day 460 when it started to rise sharply. Gradually, displacements at DP902 to DP904 changed to a progressively steeper upward gradient until from about Day 760 all sensors DP902 to DP905 were moving upwards at similar rates. By Day 842 displacements ranged from +0.12 mm at DP903 to +0.96 mm at DP905.

Inspection of the data in Figure 5-19 clearly confirms the observations from previous sections that the forces and strains within the Lasgit test remained in a state of disequilibrium.

5.6 Discharge rates from Lasgit deposition hole

Discharge rates from the Lasgit deposition hole are shown in Figure 5-20. As flux from the canister filters reduced with time (negligible flow after 15 days), the discharge rate to the slot and tube work AR901–904 all increased. At Day 30, flux to the instrumentation slot was stopped by collecting fluid directly from one of the neighbouring rock anchor holes. During this early stage of the test the total volumetric flow rate out of the system remained fairly constant at around 240 l day^{-1}.

When the first pressure relief hole (PRH1) was completed on the 5th April 2005 (Day 63) the discharge rate from AR901–904 tube work immediately reduced to a negligible amount, while at the same time flux to the anchor hole also declined by nearly 30 % to around 105 l day^{-1}. However, when a submersible pump was installed in PRH1 (at around Day 64), it had no significant effect on the monitored discharge rates.

The second pressure relief hole (PRH2) was completed on 12th April 2005 (Day 70). While this had the desired effect of reducing flux to a negligible quantity to the anchor hole, it had no observed effect on the discharge rate from PRH1. Even when a submersible pump was installed 5 days later and the discharge rate from PRH2 increased by 300 %, there was no observed change in volumetric flow rate from PRH1. While the data is somewhat contradictory it would seem to suggest that the Lasgit borehole was bisected by at least two non-communicating fracture zones.

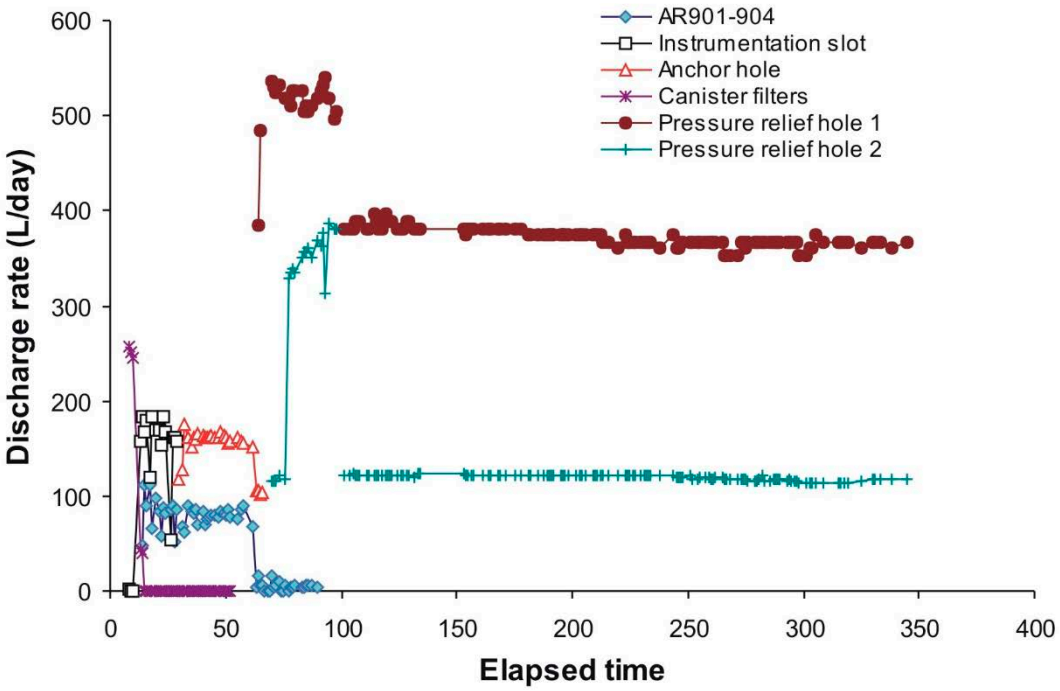

Figure 5-20. *Discharge rates from the Lasgit deposition hole.*

Close inspection of the data from PRH2 from Days 100 to 300 shows a small progressive reduction in discharge rate, suggesting a temporal reduction in the transmissivity of the fracture systems. A similar response was observed from PRH1 until around Day 225 when discharge rates levelled at around 365 litre per day. Data from the PRH holes supported the general hypothesis regarding the temporal evolution of permeability within the rock mass surrounding the Lasgit hole. This affect may have also been caused by a regional decline in ground water pressure.

5.7 Volumetric flow rate into artificial hydration system

Artificial hydration began on the 18th May 2005 at an elapsed time of 106 days. The pressure in each hydration filter was initially controlled using pump-set RP2. During the course of the hydration procedure, porewater pressure was increased in a series of steps as outlined in Table 5-2. The volumetric flow rate into the hydration system is shown in Figure 5-21. Inspection of the data clearly shows that flow rate into the system spontaneously increased as the pressure was raised. This was then followed by a well-defined negative transient leading to a slow and extremely protracted reduction in volumetric flow. Analysis of the data shows that the rate of flux into the system was not particularly sensitive to the modest pressures applied to the filters.

Table 5-4. Volumetric flow rate into the canister filters and artificial hydration systems (flux values in the table have been rounded to 2 decimal places and have been time averaged approximately 0.25 days either side of the quoted time).

Time	Volumetric flow rate (ml h^{-1})			Flux through canister filters (%)	Flux through hydration mats (%)
	Canister filters	Hydration mats	Total flux		
200	0.39	3.92	4.32	9	91
250	0.33	3.07	3.40	10	90
300	0.35	2.59	2.93	12	88
350	0.29	2.34	2.63	11	89
400	0.29	2.09	2.38	12	88
450	0.21	1.72	1.93	11	89

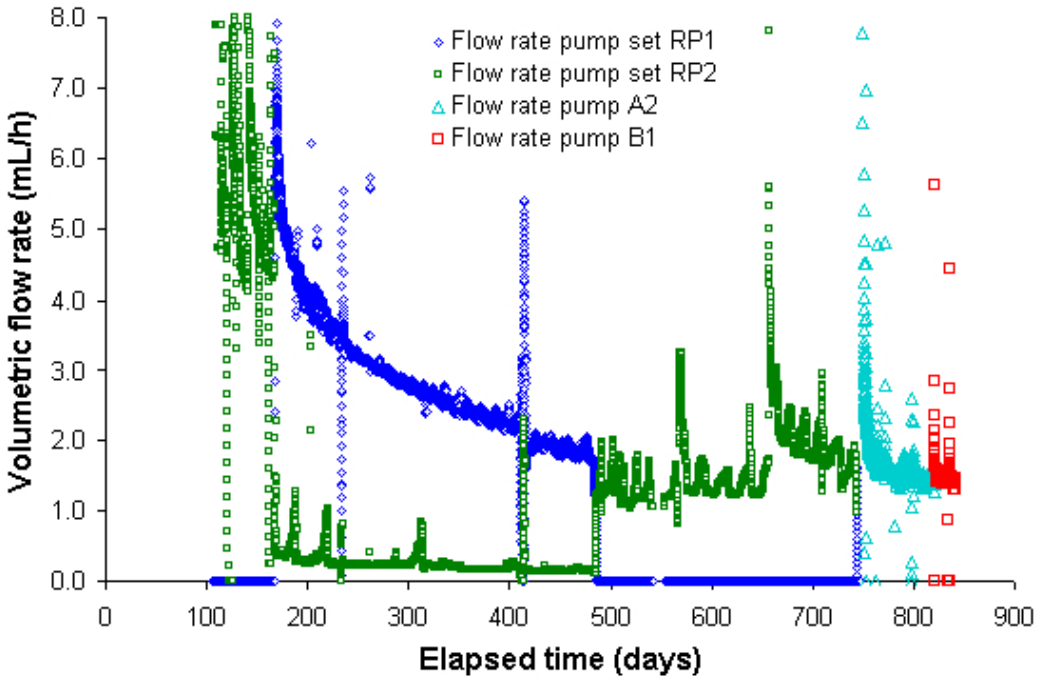

Figure 5-21. *Volumetric flow rate into the artificial hydration systems. From Day 485 onwards, control of the separate hydration systems alternated between individual pumps or pump-sets while repairs (due to corrosion and scoring of the barrels) were made to affected systems.*

A second set of reciprocating syringe pumps (RP1) were commissioned 162 days into the test. From this point onwards, pump-set RP1 controlled porewater pressure in the filters located at the mid-plane of the canister (FM905 to FM908) and the large hydration mats FR902, FB903, and FB904. This arrangement of pumps provided a mechanism to estimate the distribution of flow into the system between the canister filters and the large hydration mats (Table 5-4). Volumetric flow rate through the mid-plane filters was estimated by determining the flux through the upper and lower filter arrays and then applying a ratio factor based on the surface area open to flow.

Examination of the data in Table 5-4 shows that around 89 % of the total flux pumped into the Lasgit system had been through the large hydration filters. This is somewhat lower than expected from a purely hydraulic perspective, as the large filter arrays constituted over 98 % of the total surface area open to flow. This would seem to suggest that the zone around the canister had a higher permeability than the rest of the clay buffer. Volumetric flow rate into the filter mats exhibited a small but progressive decrease in volumetric flow. This observation can be explained by preferential swelling of the clay in the vicinity of the mats, resulting in a reduction in the permeability of the clay. This effect may also be compounded by compaction of the filter mats which were subject to high compressive forces.

A similar general trend of decreasing flow rate with time was observed for the ingress of water through the canister filters. It is clear from the data that the general proportion of flux into the clay from the various hydration sources remained fairly constant with time, suggesting that a reduction in clay permeability was the primary cause for the apparent reduction in volumetric flow rate observed in Table 5-4.

5.8 Laboratory utilities

5.8.1 Temperature

Temperature in the Gas Laboratory, canister and Assembly Hall area were continuously monitored by a series of thermocouples (Figure 5-22). Apart from minor failures of the air-conditioning system (Day 83 and Day 710), the laboratory and office temperatures remained constant (approximately ± 0.5 °C) until an adjustment to the office temperature was made at Day 745. An upward drift of about 2 °C was experienced between Days 750 and 870. The HRL air temperature showed a clear annual variation, cycling between ~11–16 °C. The canister also showed an annual variation, but with a much smaller range of 13.0–13.8 °C, and with a phase offset of about 90 days from the HRL.

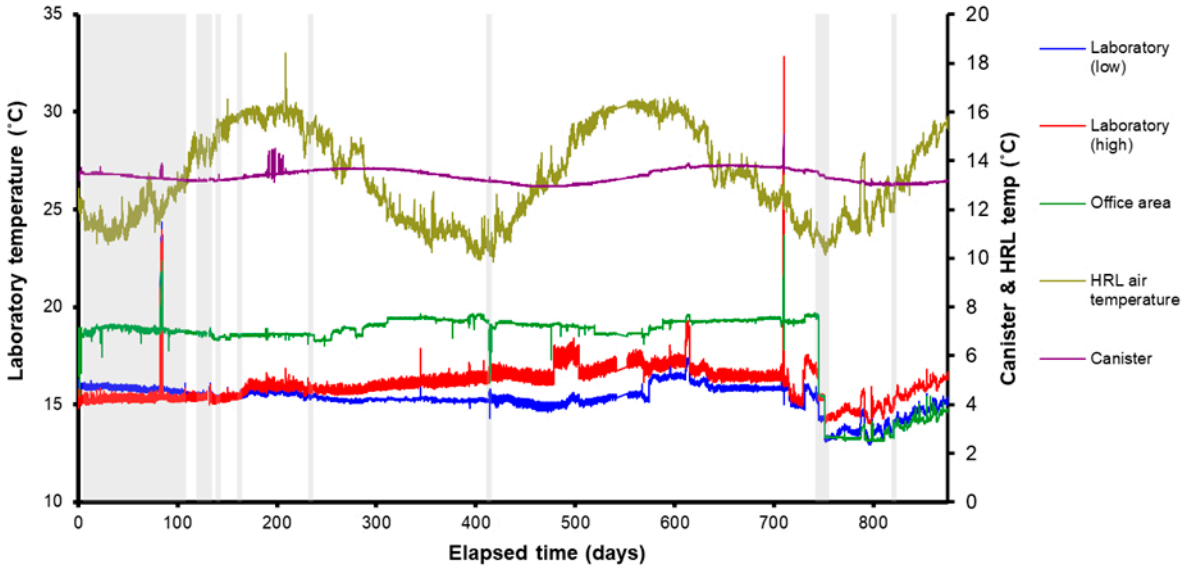

Figure 5-22. *Temperatures recorded in the Gas Laboratory, office, canister, and HRL.*

5.8.2 Compressed air and water pressure

Figure 5-23 shows a plot of the pressure history for the compressed air and hydraulic feeds to the Gas Laboratory. The apparent noise in the compressed air pressure response (green line) can be simply explained by the frequency with which the system re-pressurised in order to maintain the required air pressure. The sudden drops in water pressure (red line) during the early stage of history were caused when the reservoir tanks for the TBT experiment were refilled. To minimise this effect the feed pipe to the Gas Laboratory was upgraded by installing a dedicated large diameter pipe at around Day 90.

The hydraulic pressure in the supply borehole remained fairly constant for the first part of the test history at around 600 kPa. However, from approximately Day 220 a slow progressive reduction in borehole pressure was observed. The cause for this response is unclear but would seem to support the general hypothesis that the hydrogeological properties of the rock mass in the vicinity of the Lasgit borehole were temporally evolving. This could be caused by a number of reasons from clogging and permeability reduction along conductive fractures near the Lasgit deposition hole, to operational activities (e.g. driving new tunnel headings; sinking of new borehole and deposition holes; block sampling; setup of new experiments etc.) performed at other locations within the HRL. Pressure rose again between Days 550 and 650, but then dropped down once more, with a step of about 50 kPa at about Day 707 when the inlet supply was switched to fresh water, to address the problem of pump damage caused by scoring and corrosion of the barrels. Pressure had remained close to 500 kPa since Day 707 up to the end of the period.

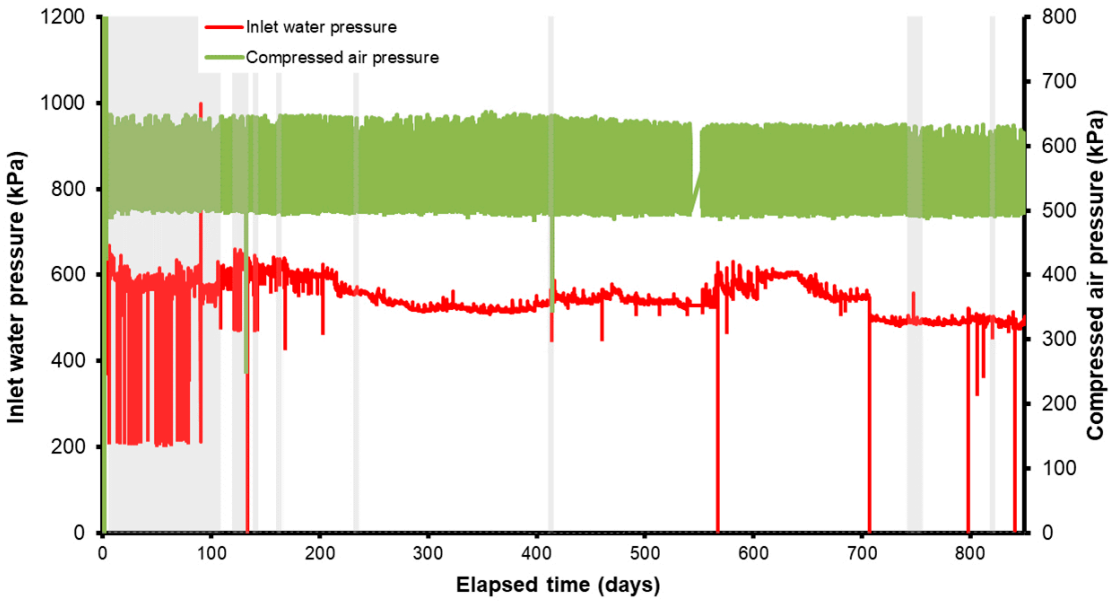

Figure 5-23. Plot showing the variation in pressure for both the compressed air lines and the water inlet feed from a near-by borehole. From Day 707 onwards, the water inlet feed was switched to a fresh water supply.

5.9 Average parameters

Figure 5-24 shows how the averages (mean) of each sensor-type progressed during the first 849 days of the Lasgit experiment. It shows how stresses started to rise and increase to high (> 3 500 kPa) values by the end of the period. The exception was the force on the lid, which because of pre-stressing did not vary much throughout the stage. Pore pressures took time to increase because of the piping issues previously outlined. Pore pressure can be seen to only marginally increase within the bentonite. Overall, stress was influenced by pore pressure, but as pore pressure decayed the stress in the system continued to increase.

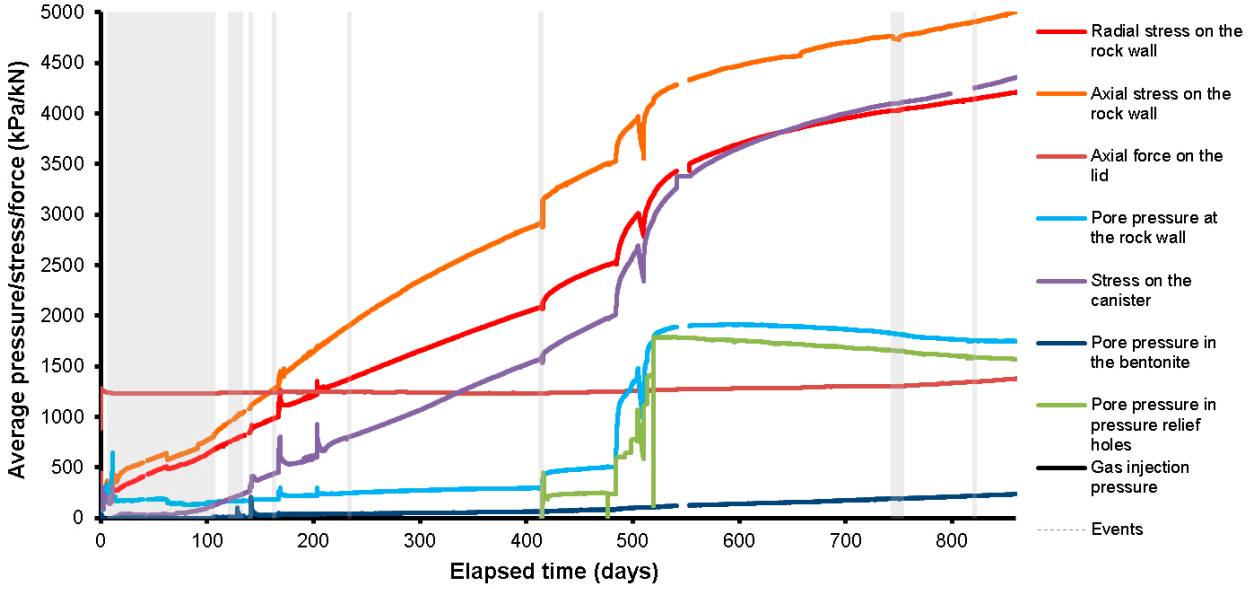

Figure 5-24. *Plot showing the variation in average stress and pressure readings.*

5.10 Conclusions of initial hydration

The main conclusions from the initial hydration stage (Day 0 – 849) were:

- Artificial hydration began on Day 106 of testing (18th May 2005). Initial attempts to raise porewater pressure in the artificial hydration arrays often resulted in the formation of preferential pathways. These pressure dependent features were not focused in one location but occurred at multiple sites at different times in the test history. These pathways appeared to be relatively short lived, closing when water pressure was reduced. These formed, most likely, along the interface between the canister and buffer and between bentonite blocks as the stress generated in the buffer was not sufficient to close the engineered gaps sufficiently. The hydration mats on the rock wall may also have resulted in piping within the pellets at the outside of the buffer as this low-density zone would have taken time to close fully.
- It was determined that both pressure relief holes should remain open until the bentonite had generated sufficient swelling pressure in order to withstand the high water pressures within the deposition hole. Packers were installed into the pressure relief holes on Day 415 (23rd March 2006) and sections in them closed off over the period to Day 519 (5th July 2006). There was no repeat of the formation of piping through discrete channels so, on Day 657 (20th November 2006); pressures to the artificial hydration filters within the deposition hole were increased to 2 350 kPa.
- Pressure data from a number of sensors including FR901, RW901 and most of the porewater pressure sensors mounted on the borehole surface, seemed to suggest some form of time dependent (temporal) evolution in the hydraulic characteristics of the rock mass adjacent to the Lasgit deposition hole that probably relate to the radial stresses acting on the rock wall as swelling pressure developed. It may also relate to clogging of the fractures in the rock wall by the powdered bentonite used in the pellet zone. Prior to closure of the packers, monitored discharge rates from the pressure relief holes showed a slow progressive reduction in value with time.
- Monitored porewater pressures within the bentonite remained low by the end of the first hydration stage, ranging from 230 kPa to 635 kPa. This was in contrast to the water pressure measured on the wall of the deposition hole which ranged from 1 055 kPa to 2 510 kPa. Suction pressures recorded at psychrometers embedded within the bentonite showed that suction was declining, confirming that resaturation was progressing, although the rate of hydration appeared to be slowing.
- Throughout this stage, monitored radial stresses around the clay continued to increase steadily ranging in value from 1 685 kPa to 5 515 kPa, with an average value of 4 230 kPa. In the absence of hydraulic piping the rate at which radial stress increased appeared insensitive to the absolute value of porewater pressure applied to the filter assemblies, confirming earlier BGS modelling work (Harrington et al. 2007). Analysis of the distribution in radial stress showed a narrow expanding zone of elevated stress propagating vertically upwards to around 3.5 m. It should be noted that hydration of the buffer also occurs from the outside of the deposition hole and this is not controlled for pressure or have a measured water supply.
- Stress measurements on the canister surface indicated radial stresses in the range 4 800 kPa and 5 030 kPa, which was comparable with the average value of radial stress monitored on the rock face. Axial stress was significantly lower at 4 380 kPa.
- Axial stress within the clay ranged from 4 910 kPa to 6 230 kPa (excluding sensor PB901 which was ~3 350 kPa by the end of the stage). Axial stress was non-uniformly distributed across the major axis of the emplacement hole and during this stage of the test generally exhibited only minor sensitivity to changes in porewater pressure. It should be noted that PB sensors were internal to the buffer and some were far from areas of natural and/or artificial hydration, while four of the sensors were close to artificial hydration sites.
- The axial force acting on the steel lid initially reduced after the deposition hole was closed but then increased following the closure of the pressure relief holes. By the end of the stage, the continuum axial swelling pressure within the bentonite was greater than the initial pre-stress applied by the lid. The slight reduction in force prior to the closure of the pressure relief hole packers can be explained by convex deformation of the steel lid in response to the uneven distribution in axial stress.

- Displacement sensors indicated a fairly uniform drop in lid height relative to the gallery floor during the early part of the test history, mirroring the relaxation in the initial pre-stressing applied to the lid. Analysis of the subsequent displacement data suggests a slight distortion of the lid may have occurred as it deformed to accommodate the uneven distribution in axial stress. Since the installation and closure of packers into the pressure relief holes the lid had moved significantly upwards with an increasing disparity in displacements at different locations, indicating an increased distortion, again probably linked to the uneven distribution of the axial force across the deposition hole.
- Analysis of the volumetric flow rate data indicated a disproportionably large flux into the bentonite from the canister filters, suggesting a higher permeability zone in this region of the system. Volumetric flow rate through the artificial hydration filters was not particularly sensitive to the modest pressures applied to the hydration filters.
- The effectiveness of the seal between canister and bentonite appears to be a critical parameter in determining the overall time taken to re-saturate the facility.

6 Gas Injection Test 1 (Day 843 – Day 1110)

At the request of project stakeholders, a preliminary gas injection history was undertaken in 2007 with a view to verifying the operation and data reduction methodologies outlined in the original concept report and to provide qualitative data on hydraulic and gas transport parameters for a bentonite buffer during the hydration process. It was decided that preliminary mass transport measurements would be undertaken in FL903, one of the 100 mm filters positioned in the lower canister array. Figure 6-1 summarises the test history during the current stage of experimentation, with Figure 6-2 showing the stages of the gas injection test.

Note: The grey areas displayed in the graphs in this chapter show periods when artificial hydration was not occurring.

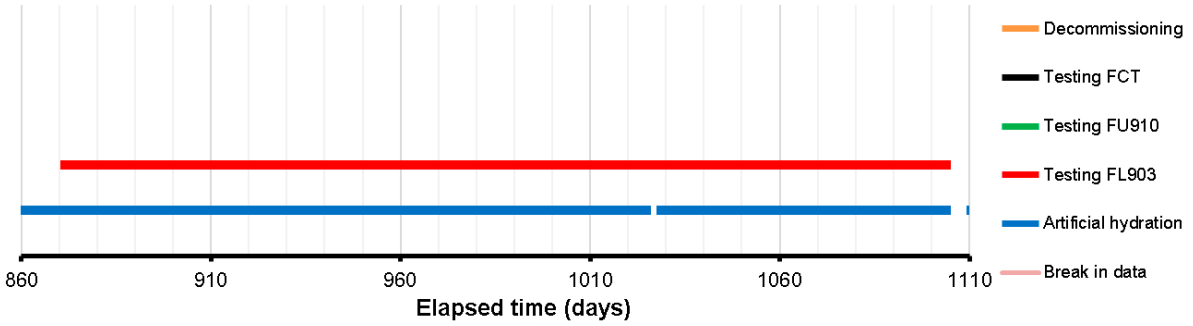

Figure 6-1. *Test stages of the Lasgit experiment showing what was conducted during gas injection test 1.*

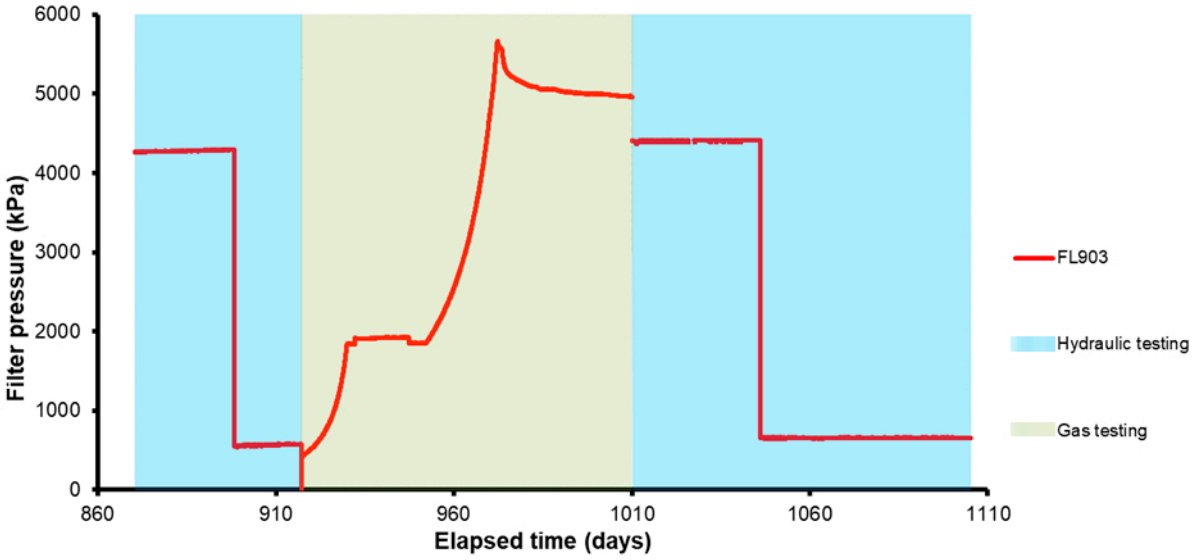

Figure 6-2. *The filter pressure of FL903 during Gas Injection Test 1. Two two-stage hydraulic tests were conducted either side of two stage gas injection test.* ***Note:*** *blue shading shows periods of hydraulic testing, green shows gas testing.*

On Day 843 (25th May 2007) the lower filter arrays (FL901 to FL904) were isolated from all neighbouring test circuits by closing the appropriate valves and the pressures allowed to decay to provide information on the spatial distribution of local porewater pressures in the vicinity of each filter. Then on Day 870 (21st June) a constant head test was started in FL903, with the pressure on that filter raised to 4 300 kPa. During this hydraulic test the remaining filters in the lower level remained isolated from the artificial hydration system and their pressure was allowed to evolve in order to provide temporal data on local porewater pressures within the buffer clay. At the same time, artificial hydration continued through all remaining canister filters and hydration mats. Pressure on FL903 was maintained at 4 300 kPa until Day 898 (19th July 2007), when it was reduced to 560 kPa and was then held constant until Day 917 (7th August 2007). During this period flow rates into and out of FL903 were monitored with time.

On Day 917 (7th August 2007) gas injection into FL903 began. Starting with an estimated gas volume of 1.26×10^{-3} m^3, the gas was pressurised by introducing water into the gas reservoir at a steady rate until Day 930 (20th August 2007) when the test was temporarily stopped, and the pressure held constant. This continued until Day 952 (11th September 2007) when the gas volume was re-charged to 1.337×10^{-3} m^3 and pressurisation resumed, until Day 974 (3rd October 2007) when gas injection was stopped. The pressure decay in FL903 was then monitored through to Day 1010. To examine the evolution of hydraulic properties following a gas injection event, a repeat hydraulic test was performed immediately after the cessation of gas injection. This had the additional benefit of flushing gas from the system and aiding the hydration of the clay.

6.1 Basline hydraulic test results (day 843 – day 917)

The pressure responses at filters FL901 to FL904 during the course of the hydraulic test (Day 843 to Day 917) are shown in Figure 6-3 and the flow rates at FL903 during the two steps of the constant head test (Day 870 to Day 917) are shown in Figure 6-4. For comparison, the porewater pressures on the deposition hole wall at sensors UR907 to UR910 are shown in Figure 6-5. These sensors are located at the same elevation as the injection filters FL901 to FL904. It can be seen that the pressures in all the injection filters rapidly dropped well below the pressures present at the deposition hole wall, strongly suggesting that a significant volume of the bentonite buffer near the canister remained in a partially saturated state. This explanation (rather than simple hydraulic disequilibrium) seems probable as it would require a much lower bentonite permeability to yield such low pressures (measured at FL901, FL902, and FL904) after extended periods of hydration. If such permeabilities were the case, then the response to the shut-ins would take much longer than observed in Figure 6-3.

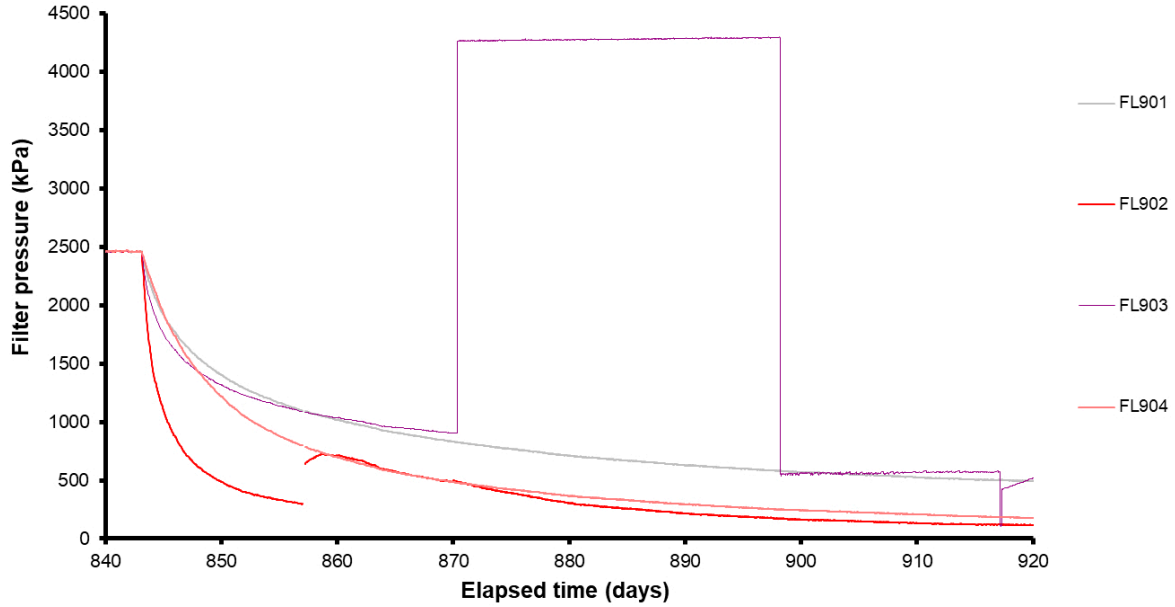

Figure 6-3. *Pressures observed at the lower canister filters FL901 to FL904 during the hydraulic test.*

It can also be seen that the pressures at the various injection filters declined at different rates. These rates seem to reflect the sizes of the filters, with the smallest filter, FL902, falling most rapidly to about 300 kPa within 15 days of the start of the shut-in. The cause of the pressure discontinuity at Day 857 in this sensor is not known. The two largest filters, FL901 and FL903, remain at the highest pressure at Day 870, at 820 and 900 kPa respectively, and the intermediate sized filter, FL904, falls to about 480 kPa by Day 870. These observations were consistent with the suggestion that the volume of bentonite around each filter that had been re-saturated in proportion to the size of the filter. However, the fact that the pressure at FL903 initially decreased more rapidly than either FL901 or FL904 shows that additional factors may well have been involved. One will be the differences in the porewater pressures at the deposition hole wall opposite each of the injection filters (Figure 6-5), which may have caused local variations in the degree of resaturation. Another may have been some degree of heterogeneity within the buffer as it swelled, which may also be affected by any eccentricity in the position of the canister with respect to the bentonite blocks.

The flow rate data in Figure 6-4 show that there was a transient of about 10 days after each of the two pressure changes in FL903 before the flows settled to a fairly steady level, although the data following the second pressure change at Day 898 exhibited considerably more noise.

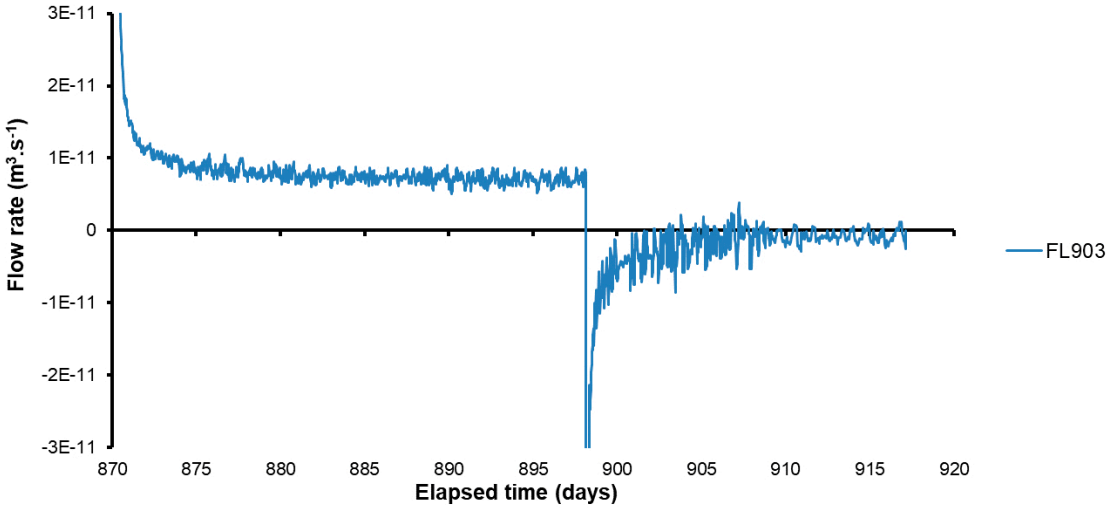

Figure 6-4. *Flow rate observed at lower canister filter FL903 during the constant pressure stages of the hydraulic test.*

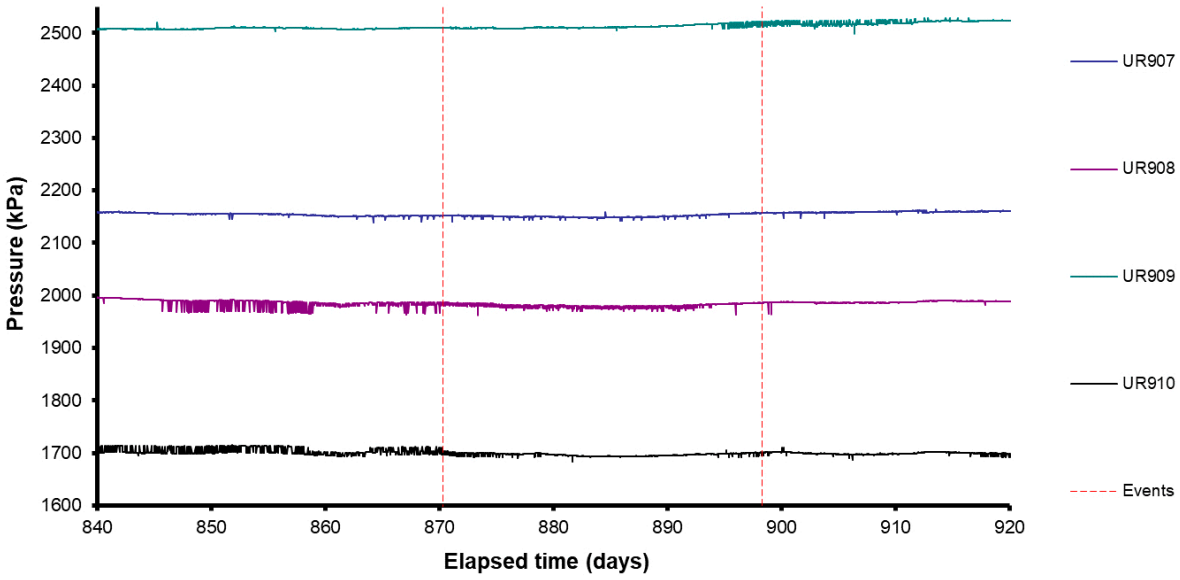

Figure 6-5. *Porewater pressures observed at deposition hole wall sensors UR907 to UR910 during the hydraulic test. Red dashed line shows start points of constant head stages.*

6.1.1 Hydraulic test modelling

In order to obtain estimates of the hydraulic conductivity and specific storage of the bentonite from these data it was necessary to develop a model of the flow processes occurring within the clay. As noted above, the data strongly suggest that a significant volume of partially saturated material remained around the canister at this time, and that the extent of this partially saturated zone varied with location around the canister. This meant that the initial state of saturation of the system could not be specified *a-priori*. Instead, it was necessary to model the whole of the hydration stage of the Lasgit test in order to arrive at a suitable spatial definition of the initial saturation state for the hydraulic test. Running such a detailed simulation with a full multi-phase model such as TOUGH2 (Xu et al. 2004) would take too long for this preliminary assessment, so a finite element porous media flow model parameterised in terms of hydraulic conductivity and specific storage with a variable saturation capability was used for these calculations.

Attempting to model variably saturated flow in the full bentonite buffer in 3D with sufficient grid refinement to accurately resolve flow processes around filters as small as 10 mm in diameter was not feasible with the available resources. However, a preliminary model of one quarter of a cylinder centred on one filter and extending just 0.7 m vertically up and down the canister from the filter was constructed, in order to test the possibility of using such a model to interpret the test data (the initial void space around the canister was represented in the model). The mesh created contained 86 000 nodes on 507 000 tetrahedral elements and took about 5.5 hours to run a single simulation of the hydration and hydraulic test stages of the experiment. The results of a simulation of the hydration stage that assumed a hydraulic conductivity of 1.3×10^{-13} m s^{-1} and a specific storage of 1.5×10^{-4} m^{-1} is shown in Figure 6-6.

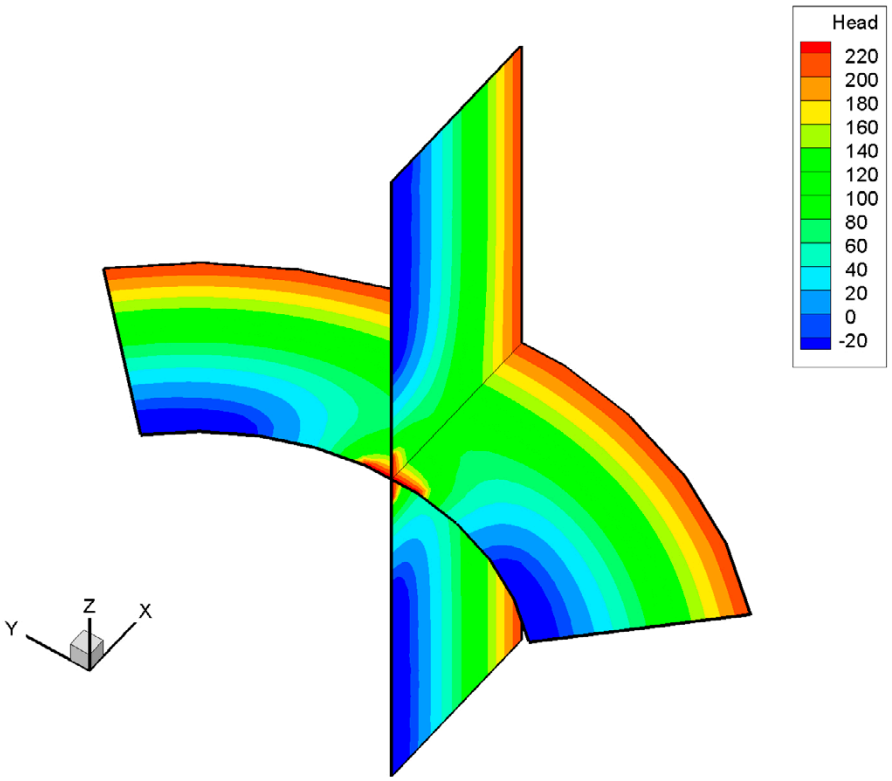

Figure 6-6. *Pressure heads in a finite element model of single phase variably saturated flow around filter FL901 after 840 days of hydration. Dark blue bands indicate remaining zones of partially saturated material.*

Table 6-1. Hydraulic parameters obtained from fits to shut-in pressure curves for injection filters FL901 to FL904.

	K (m s^{-1})	S_s (m^{-1})
FL901	1.10×10^{-13}	1.20×10^{-4}
FL902	0.90×10^{-13}	5.50×10^{-4}
FL903	1.24×10^{-13}	0.55×10^{-4}
FL904	1.58×10^{-13}	4.00×10^{-4}

While this model gave a useful general picture of the likely saturation state of the bentonite around an injection filter at the end of the initial hydration stage, detailed examination of the solution suggested that the mesh was not sufficiently refined to give accurate results close to the filters. In addition, run times were such that the model would be very difficult to use for data interpretation so a slightly simplified and more efficient approach was sought. After some experimentation, a 2D axially symmetric model was chosen, centred on an injection filter, with the axis of symmetry projecting perpendicular to the canister towards the deposition hole wall. Using a mesh of about 2 000 nodes on about 4 000 triangular elements a single simulation could be run in around 40 seconds. This makes it possible to obtain fits to data for each of the filters in a reasonable timescale. Figure 6-7 shows the fits obtained to the shut-in pressure data, using separate parameter values for each filter, with the parameter values given in Table 6-1 for each model. It can be seen that relatively similar values for hydraulic conductivity have been obtained but that there is quite a wide range of specific storage values.

The same model was also used to interpret the constant head steps applied to FL903, but in this case comparing the flow rate data to the model simulation. However, using parameters from the shut-in stage gave a poor fit to the flow rate data, as shown in Figure 6-8. A revised model provided a much-improved fit with $K = 0.75 \times 10^{-13}$ m s^{-1} and $S_s = 0.25 \times 10^{-4}$ m^{-1}.

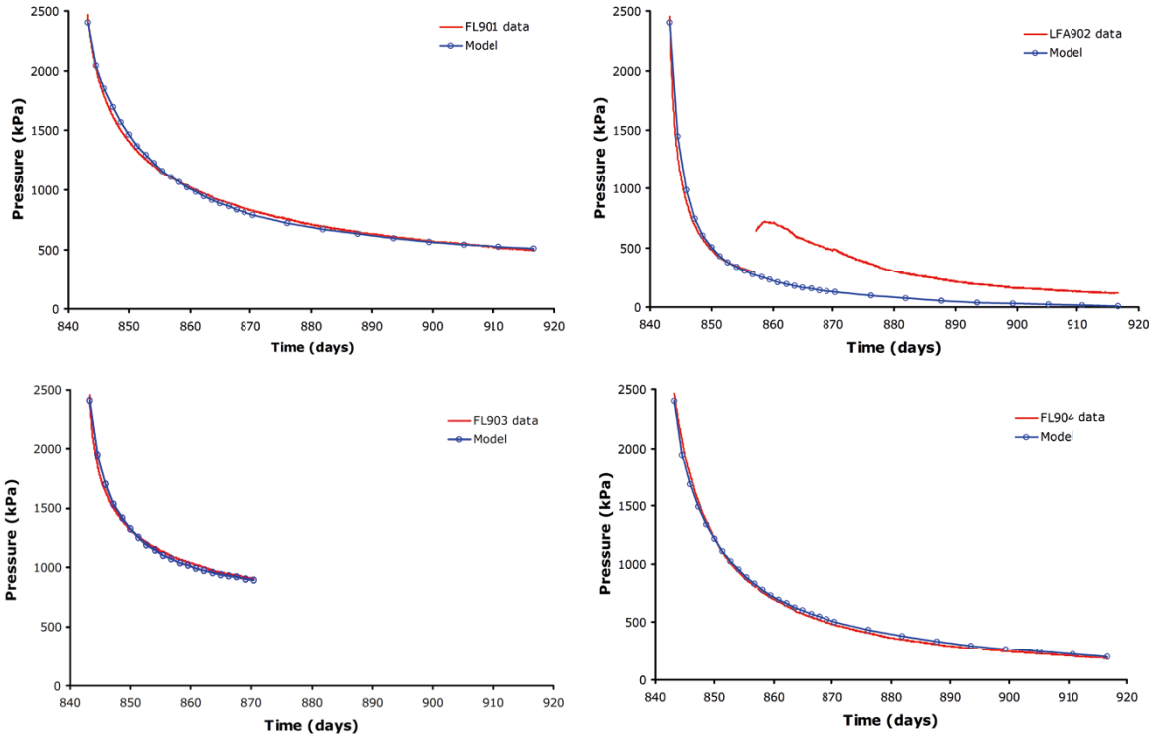

Figure 6-7. Comparison of model simulations to shut-in pressure data for the injection filters FL901 to FL904 during the hydraulic test.

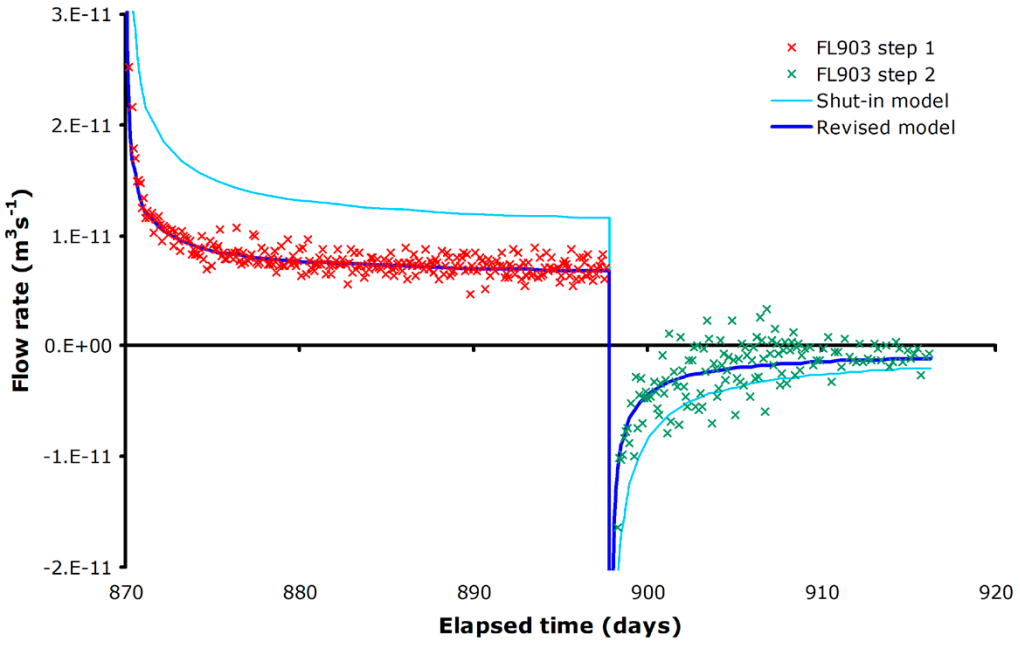

Figure 6-8. *Comparison of model simulations with flow rates at FL903 during the constant pressure test steps.*

These models were used to derive the initial conditions for the filter shut-in calculations also give an indication of the progress of the resaturation of the bentonite in this part of the borehole. Figure 6-9 shows the simulated pressures, plotted as hydraulic heads, at each filter at Day 840, close to the end of the hydration stage, the parameters for the individual fits from Table 6-1 being used in each case. In these plots the two darkest blue bands show the extent of unsaturated conditions. It can be seen that the unsaturated zone was much more extensive near the smallest filter, FL902, than near the larger filters FL901 and FL903.

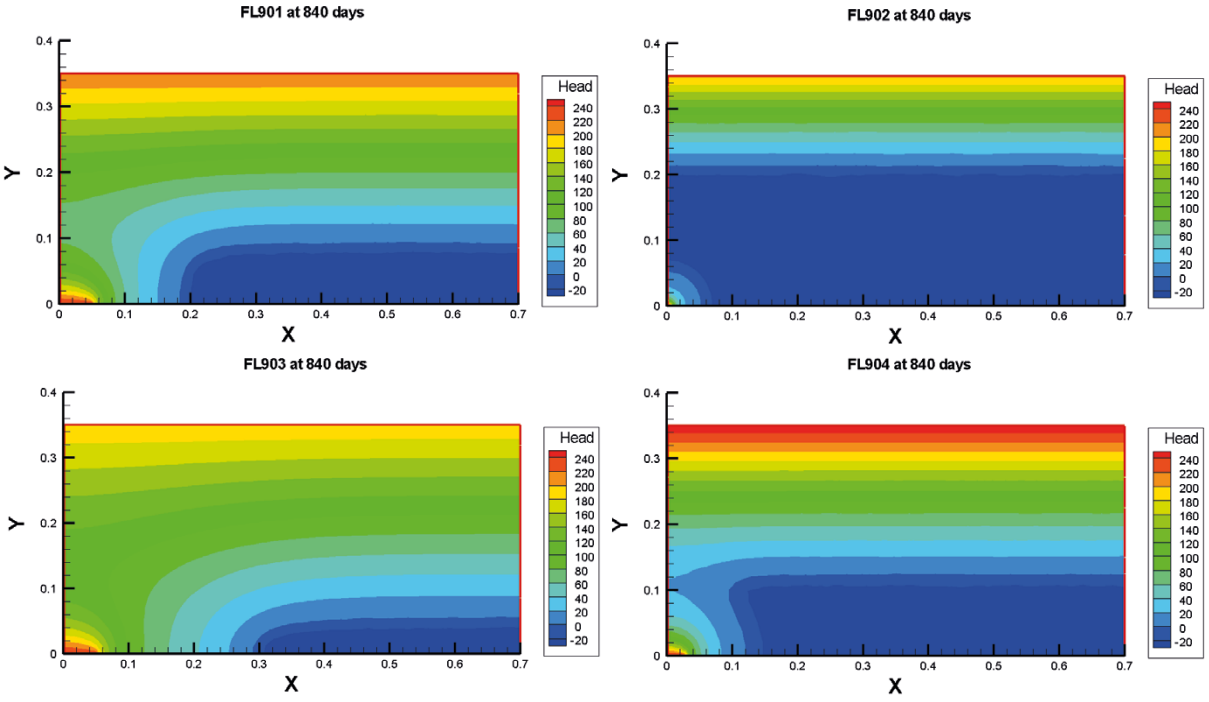

Figure 6-9. *Simulated pressure heads around each filter at Day 840, the end of the hydration stage.*

6.2 Gas injection test results (day 917 – day 1010)

Gas injection testing began on Day 917 through canister filter FL903. Gas with an initial volume of 1.26×10^{-3} m^3 (1 260 ml) was introduced to the interface vessel and then pressurised by pumping water into the cylinder. On 20th August (Day 930) the pressure in FL903 was held constant until Day 952 when the gas was re-charged to a volume of 1.337×10^{-3} m^3 (1 337 ml) and pressurisation restarted. This second stage of pressurisation continued until Day 974 when the filter was again isolated by means of closing a valve and gas pressure allowed to decay. The observed gas pressure at the filter is shown in Figure 6-10, which also shows the predicted pressure for a confined ideal gas undergoing constant flow operation of the confining system. **Note:** both predicted gas pressure and the derived volumetric flow rate of gas into the deposition hole are strongly dependent on the start volume of gas.

During the first stage of gas pressurisation (Day 917 – 930) the observed pressure started to depart from the pressure predicted for an ideal gas[1] at about Day 924. As gas pressure increased the departure in predicted gas pressure cannot be explained by gas moving into solution and must be symptomatic of gas penetration of the buffer. Figure 6-11 shows this period in more detail together with the estimated rate of flow of gas into the clay. These data suggest that gas starts to flow into the buffer at a pressure of about 650 kPa, which is much lower than the expected gas entry pressure for saturated intact bentonite. It therefore seems likely that gas is flowing between the bentonite and the canister and possibly between bentonite blocks (the interface between bentonite rings 2 and 3 lies just 50 mm above the injection filter).

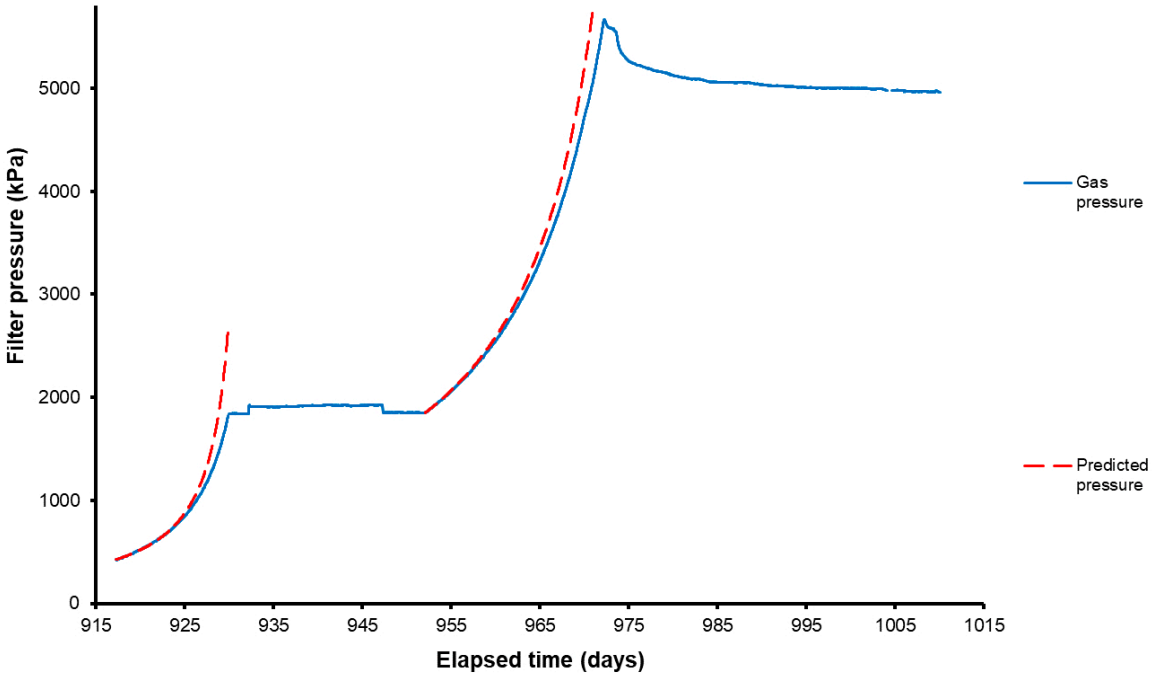

Figure 6-10. *Comparison of predicted and observed gas pressures at FL903 during the gas injection test.*

[1] The initial start volume of gas was estimated by fitting the early predicted pressure response to that of the measured values from FL903. The start gas volume for the second test phase was estimated at the end of the test by displacing the remaining gas with water through the FL903 drain vent.

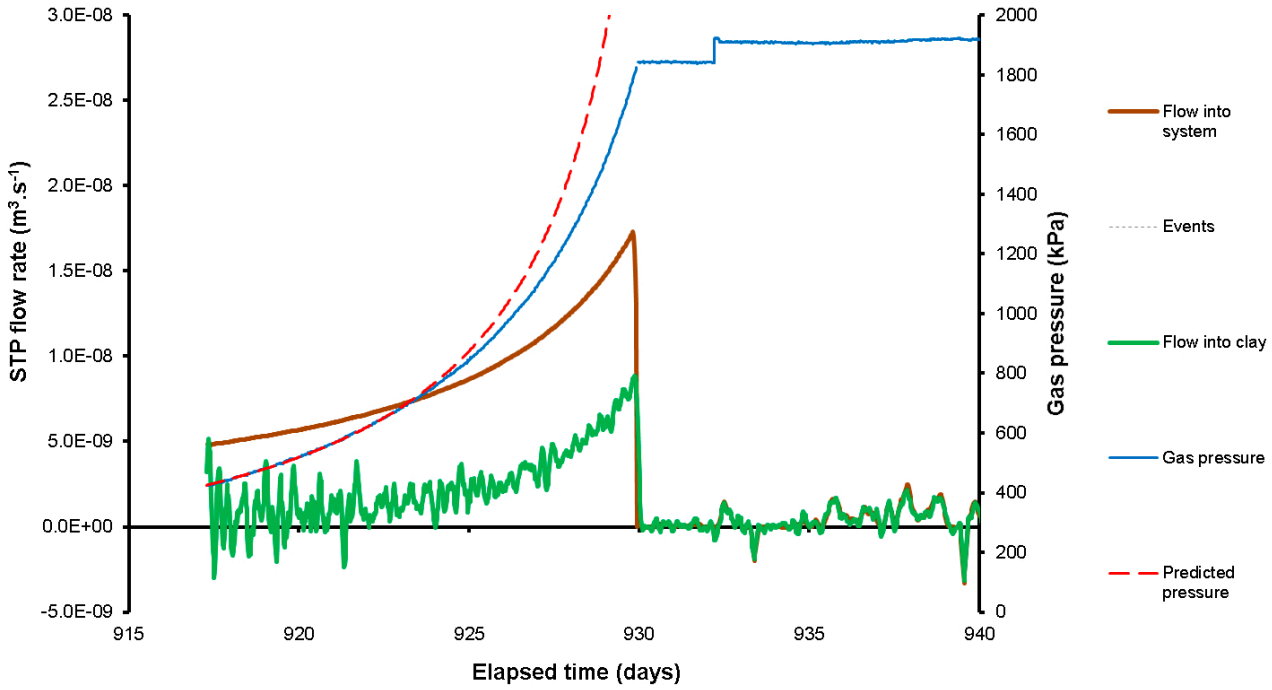

Figure 6-11. *Estimated rate of gas flow into the system and the clay compared to the predicted and observed gas pressures during the first stage of the gas injection test. Flow into the clay was calculated using a combination of weighted moving average and time moving average (mean).*

When gas pressurisation stopped at Day 930 and the pressure was held constant, flow into the clay dramatically reduced by around 98.5 %, indicating that propagation of the main gas pathway(s) practically ceased when the pressure stopped rising. In its most basic form, this can be viewed as the expansion of gas pathway(s), which is conceptually little different to that of inflating a balloon, where the walls of the balloon represent the pathway surfaces within the clay. The small continuous flux observed following this event may have resulted from the movement of gas along small-scale pre-existing features which were only present because the bentonite remained in suction and was not in hydraulic equilibrium. If correct, these fluxes should reduce in magnitude during later tests as hydration of the buffer progressed. Given the sudden reduction in flow, it seems clear from the data that gas was not flowing within the original porosity of the clay and that the initial network of gas pathways failed to locate an adequate sink capable of accommodating the previous in-flow of gas.

Following the onset of the second stage of gas pressurisation (Day 952) the observed pressure started to deviate from the predicted ideal gas compression curve almost immediately (see Figure 6-12), indicating that the pathway continued to extend without any delay. Gas flow into the clay during this second stage increased gradually with time until about Day 970 at which point it increased much more sharply until gas pressurisation was stopped again at Day 974. The sharp rise in flow rate occurred when the gas pressure was marginally greater (approximately 200 kPa) than the local total stress measured on the rock wall but was around 250 kPa lower than the radial stress monitored on the canister surface at PC903. Axial stress measured at PB902 was also marginally higher than the gas pressure (around 300 kPa). Gas pressure continued to increase reaching a peak pressure of 5 660 kPa at Day 972.3. This was followed by a small spontaneous negative transient leading to a quasi-steady state illustrated in detail in Figure 6-13 at a gas pressure of around 5 500 kPa. This behaviour is qualitatively similar to results from laboratory scale tests reported by Horseman et al. (1999) and Harrington and Horseman (2003).

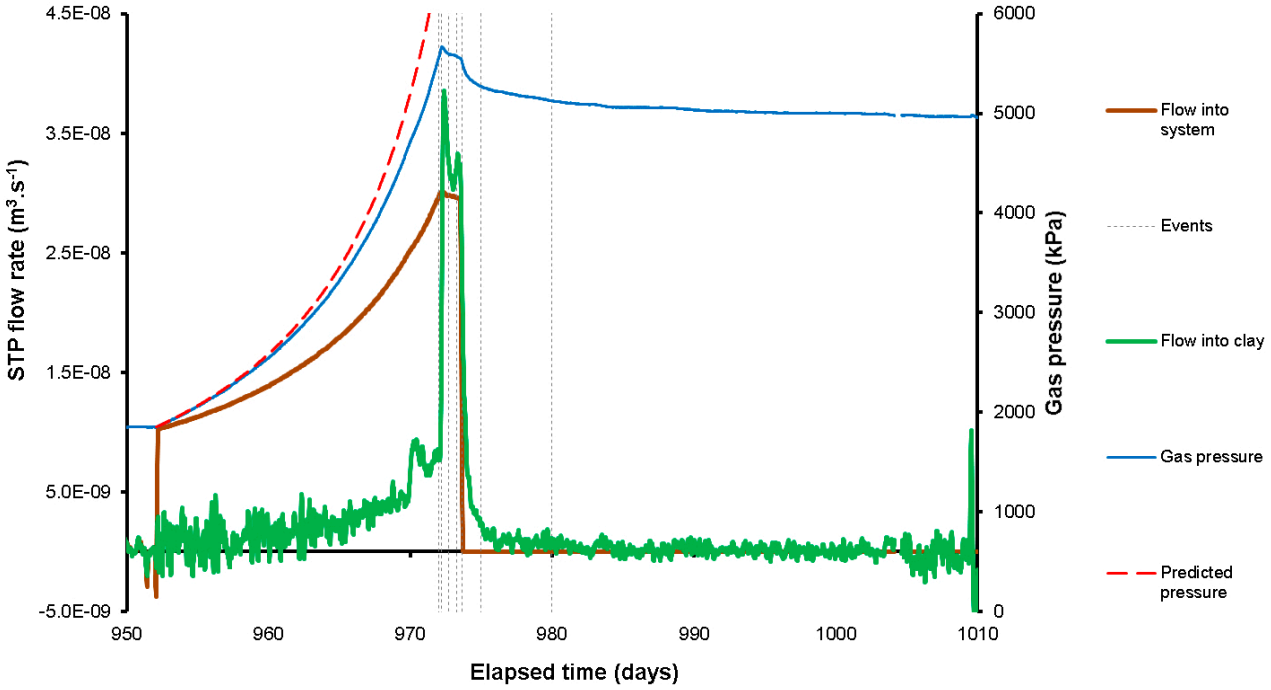

Figure 6-12. *Estimated rate of gas flow into the clay compared to the predicted and observed gas pressures during the second stage of the gas injection test.*

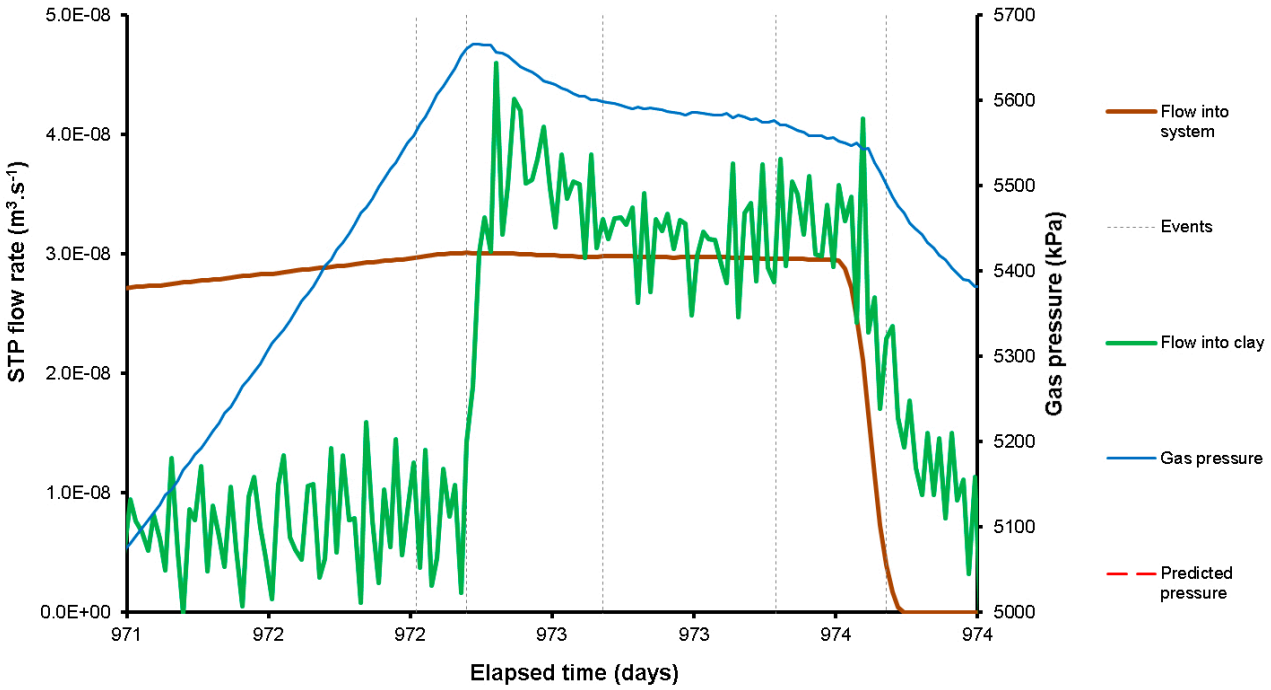

Figure 6-13. *Unsmoothed flow rate and pressure responses around peak gas pressure. Gas flow into the clay rapidly increases following the peak which is followed by a small spontaneous negative transient.*

The injection pump was stopped at Day 974 and the gas pressure allowed to decay to provide an estimate for the apparent capillary threshold pressure. It can be seen in Figure 6-12 and Figure 6-13 that just before injection was stopped, the post peak gas flux exhibited dynamic behaviour (over and undershooting flux into the system) suggestive of unstable gas flow. Following the cessation of injection, the flux declined rapidly at first but then entered an extended period of very small flows. These fluxes were significantly smaller than that observed during the earlier constant pressure phase, which may have been previously related to flux along small-scale pre-existing features. This was reflected in the pressure response which dropped rapidly initially but then decayed very slowly towards an asymptotic capillary threshold pressure, Figure 6-14, which is tentatively estimated to be around 4 900 kPa. This is very similar to the average radial stress measured on the canister, which is also close to the axial stress measured at PB902. This result, if correct, suggests a strong correlation between gas transport and total stress and supports the observations reported by Harrington and Horseman (2003) based on laboratory scale tests. The breaks in slope in the pressure decay curve (Figure 6-14) are indicative of the sealing and temporary formation of highly unstable gas pathways.

However, this observation raises a simple question: why does the gas pressure appear to asymptote at a value far in excess of that required to initiate gas flow? To help answer this question we must return to the conceptual model of the "expanding balloon" mentioned earlier. Initial results (with gas pressure below total stress) demonstrate that in the absence of a sink, continued gas penetration of the buffer and or canister interface, required an increasing gas pressure to drive major pathway propagation. The small continuous flux noted from the initial constant pressure gas test was probably along pre-existing small-scale features, which may have been present because the bentonite remained in suction and was not in hydraulic equilibrium during this phase of testing. Analysis of the data indicates that only a relatively small amount of gas was injected into the clay during the test. The fact that the subsequent gas pressure reached asymptote at a value close to that of the local total stress suggests that the majority of the gas remained resident in the buffer/deposition hole. As the pressure within the pathways declined, the effective gas permeability of the clay significantly reduced.

Figure 6-15 and Figure 6-16 show details of the radial stress and pore pressure responses to the sharp increase of gas flow, prior to and just after the peak gas pressure of the second gas injection stage, in a selection of sensors close to the injection filter FL903. It is notable that the most pronounced responses are seen in the sensors from section 4, which were 600 mm below the injection point, rather than the section 5A sensors, which were 300 mm above it. Examination of the data indicates changes in stress and porewater pressure began at the peak in gas pressure.

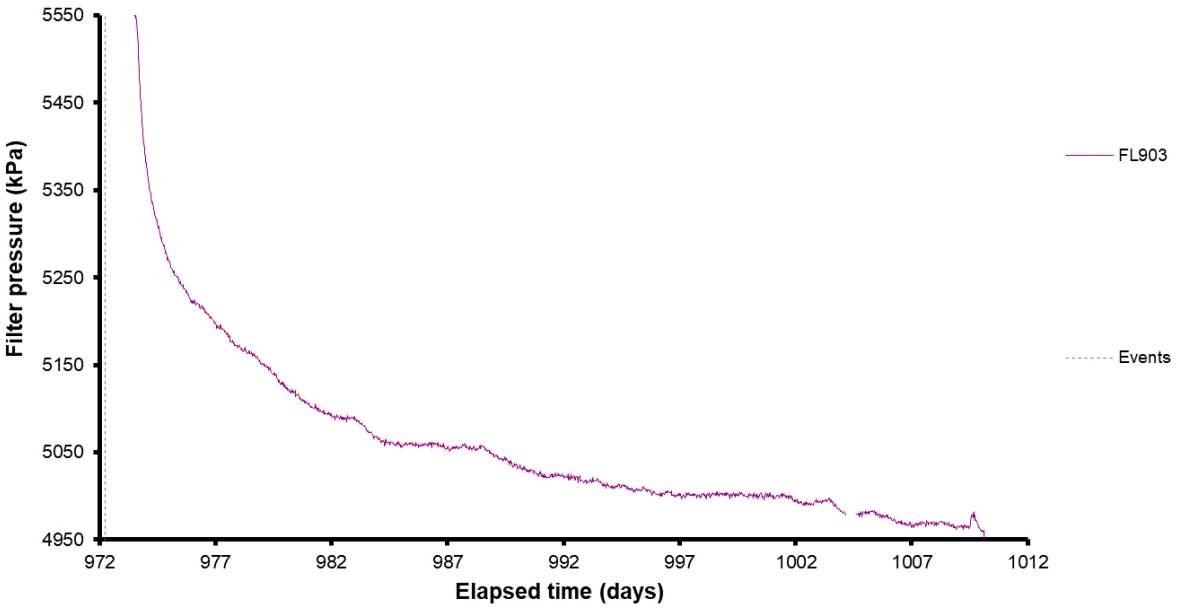

Figure 6-14. *Shut-in response for filter FL903. The inflections in the pressure decay response are suggestive of dynamic gas flow and pathway closure.*

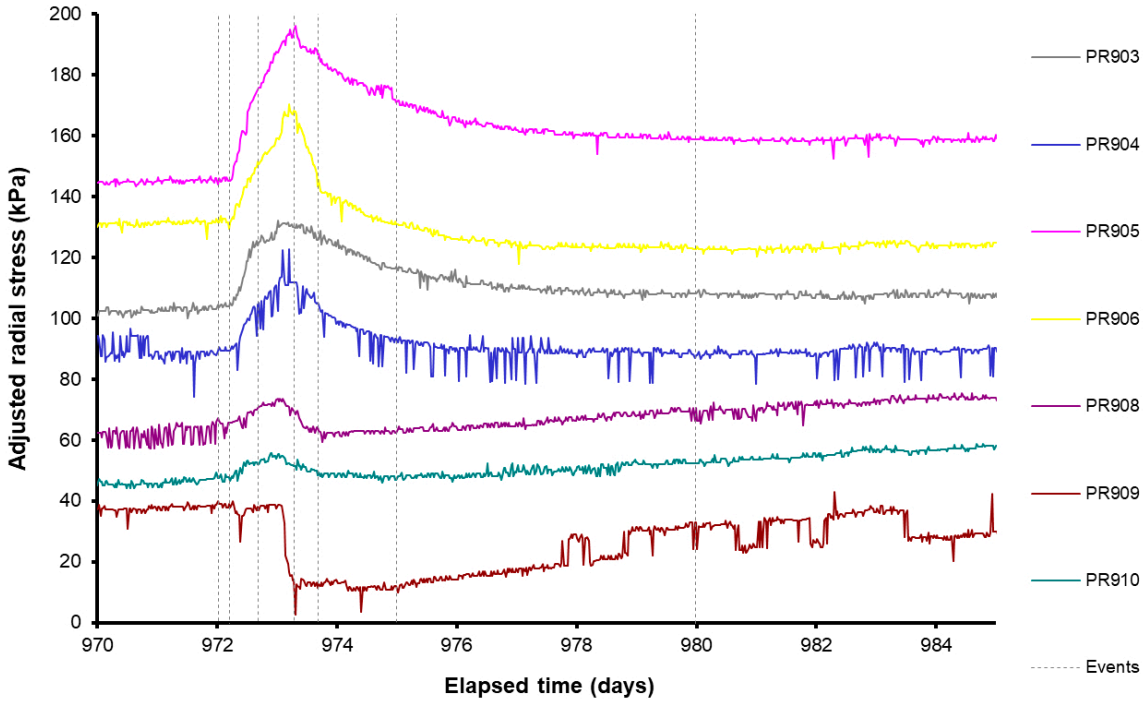

Figure 6-15. *Radial stresses observed in a selection of sensors close to FL903 at the end of the second gas pressurisation stage.*

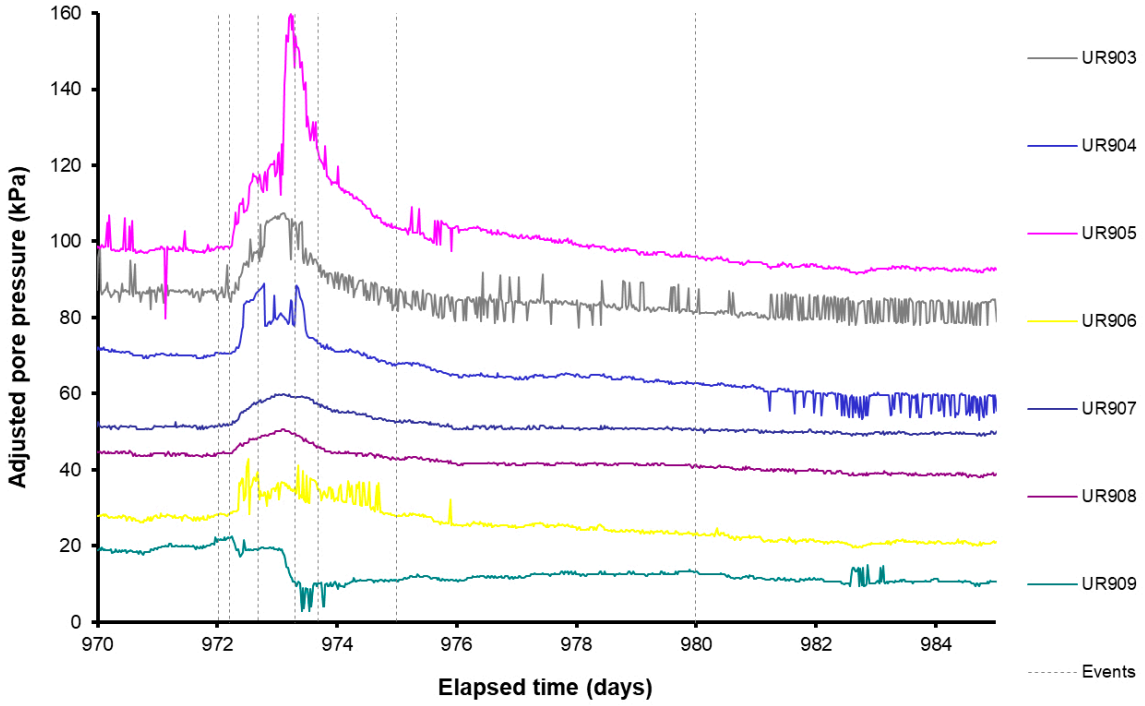

Figure 6-16. *Pore pressures observed in a selection of sensors close to FL903 at the end of the second gas pressurisation stage.*

Figure 6-17 and Figure 6-18 show the temporal evolution in radial stress and porewater pressure during this time (normalised to zero at Day 972.02). Figure 6-17 shows a well pronounced increase in radial stress around the entire base of the deposition hole, with the highest increase noted in the vertical plane below the point of injection. This indicates the gas preferentially moved downwards, probably along

the interface between the canister and buffer. It is notable that the radial stress immediately adjacent to FL903 actually decreased during this time. A similar observation is also seen in the porewater pressure trace (Figure 6-18). The cause of this behaviour remains unclear.

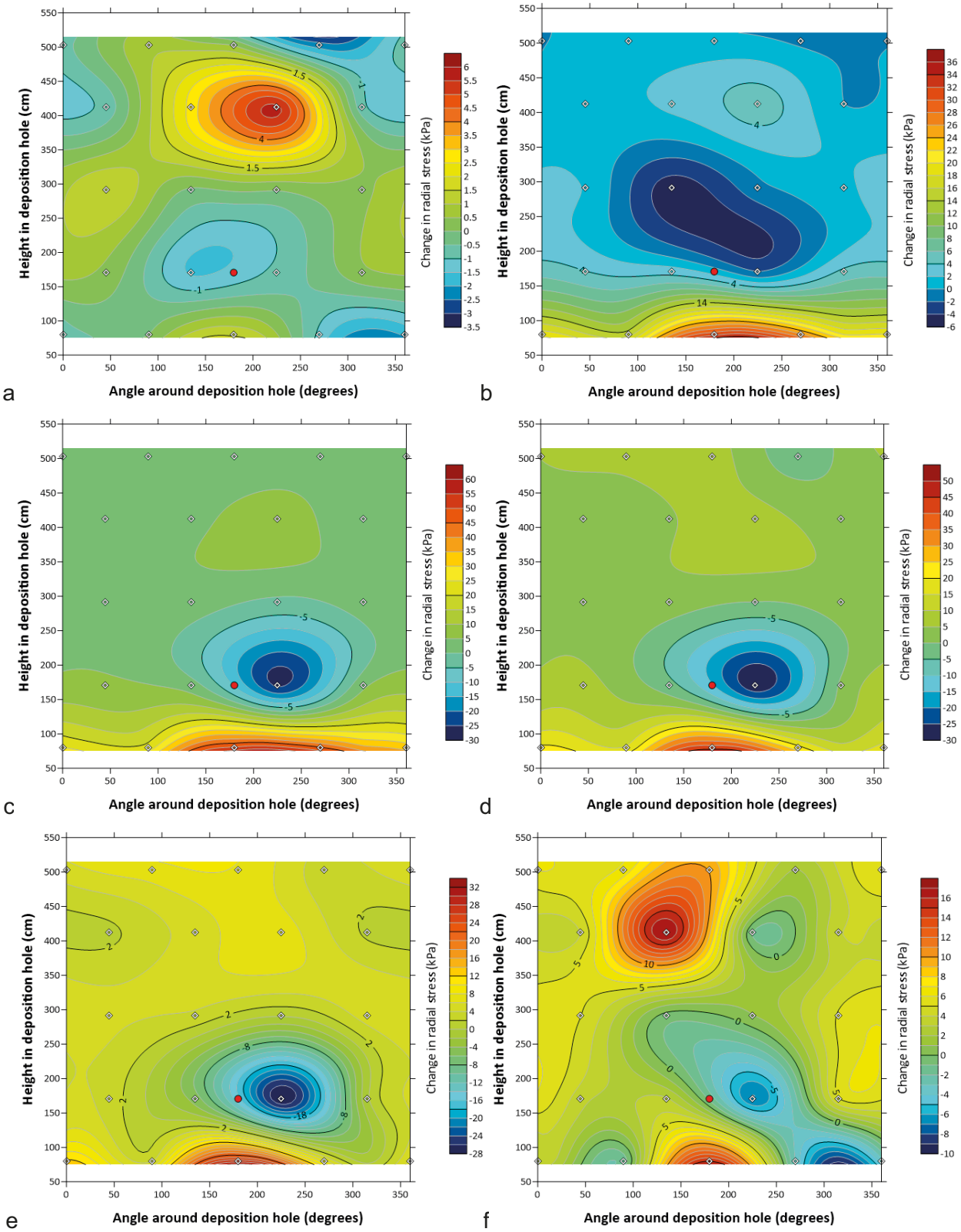

Figure 6-17. *Evolution in normalised radial stress around the deposition hole wall prior to and after the peak in gas pressure (Day 972.20 to 979.99). The contour plots indicate a general increase in radial stress around the base of the deposition hole. Adjacent to the filter radial stresses appear to decline momentarily (Day 972.20, 972.68, 973.41, 973.68, 974.99, 979.99 – all normalised with respect to Day 972.02).*

Detailed inspection of the porewater pressure contour plots (Figure 6-18) generally confirms the above observations, though initial results suggest that the pulse in porewater pressure dissipated at a faster rate than that of the radial stress. The rise in porewater pressure can be interpreted as a hydrodynamic response caused by the local increase in stress (Figure 6-15) around the gas pathways.

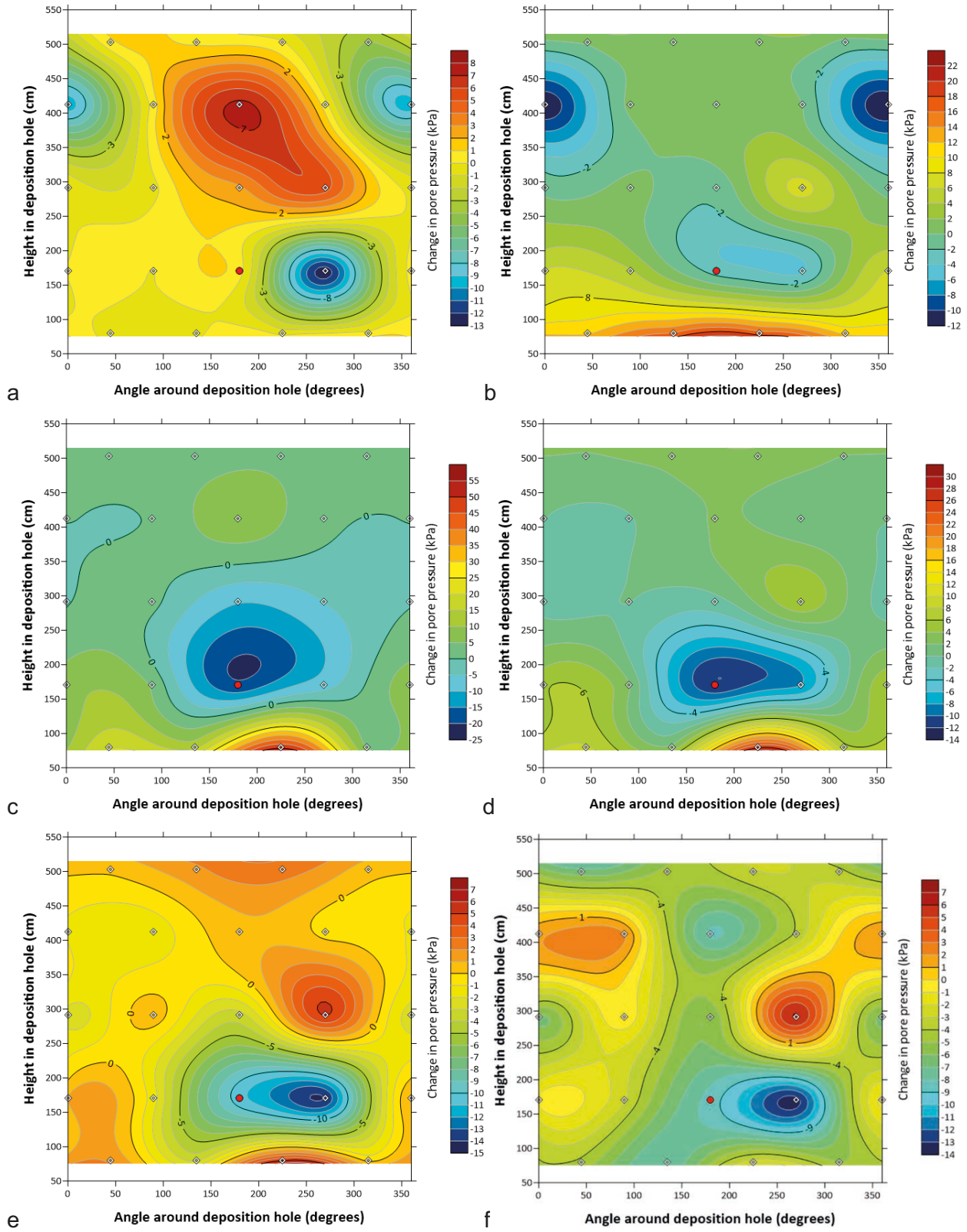

Figure 6-18. *Evolution in normalised porewater pressure around the deposition hole wall prior to and after the peak in gas pressure (Day 972.20 to 979.99). The contour plots indicate a general increase in porewater pressure around the base of the deposition hole focussed in the vertical plane of the source filter (FL903). Adjacent to the filter porewater pressure appear to decline momentarily (Days 972.20, 972.68, 973.41, 973.68, 974.99, 979.99 – all normalised with respect to Day 972.02).*

Analysis of the porewater pressure sensors located within the buffer show no obvious sensitivity to the injection of gas. In contrast, axial stress sensors located beneath and above the canister appear to have registered the passage of gas, probably detecting reflected stresses normal to the gas flow path (Figure 6-19). Indeed, the slow and then rapid increase in PB902 immediately following the peak gas pressure is strongly indicative of the time dependent propagation of gas pathways.

A small deflection (reduction) in the rate of increase in axial stress at the base of the canister (PB901) occurred around 0.85 days (20 h) after the peak in gas pressure. A reduction in stress can only be caused by the removal of load. This would suggest some form of displacement had occurred within the system as a result of gas injection.

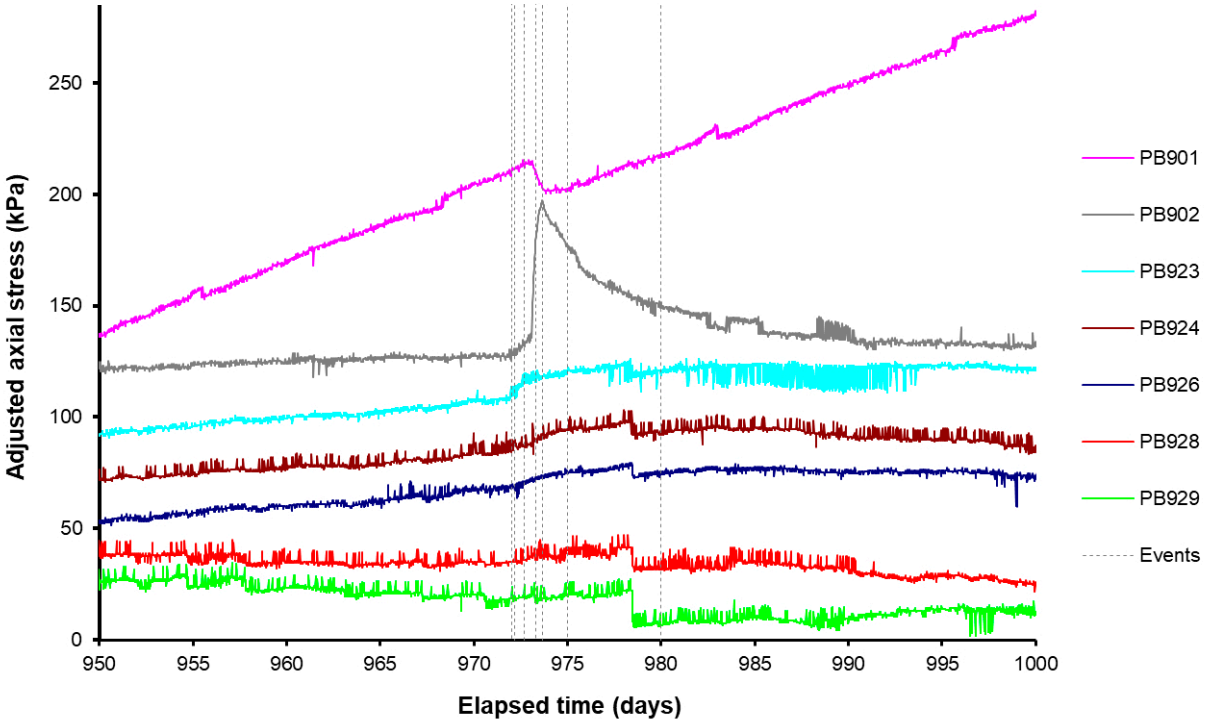

Figure 6-19. *Selected axial stress data during the second stage of gas injection. The strongest response is observed by PB902, which, located below the canister, exhibits signs of time dependant pathway flow.*

While it is difficult with the available data to make definitive statements regarding the exact direction and number of gas flow paths, it seems highly probable that the gas moved generally downwards away from the filter and then along the interface between blocks C1 and R1 and/or R1 and R2 (Figure 6-20). The fact that the gas pressure reached asymptote at a value close to the local total stress, may suggest that the small amount of gas injected during the test remained resident in the buffer/deposition hole. This observation compliments the findings of the predictive modelling work described in Harrington et al. (2007), which identified the effectiveness of the seal between canister and bentonite as a critical parameter in determining the overall time taken to re-saturate the facility. This is also logical as there is a clear axial stress gradient running from high to low from the top of the deposition hole (PB928 ~6 000 kPa) to the lowest stress sensor (PB902 ~4 900 kPa). Under most conditions gas would be expected to propagate along such a stress vector.

However, the observed general coupling between gas, stress, and porewater pressure at the repository scale is extremely important and is strongly indicative of pathway dilatancy as a gas transport mechanism. These observations are qualitatively similar to those reported by Horseman et al. (2004).

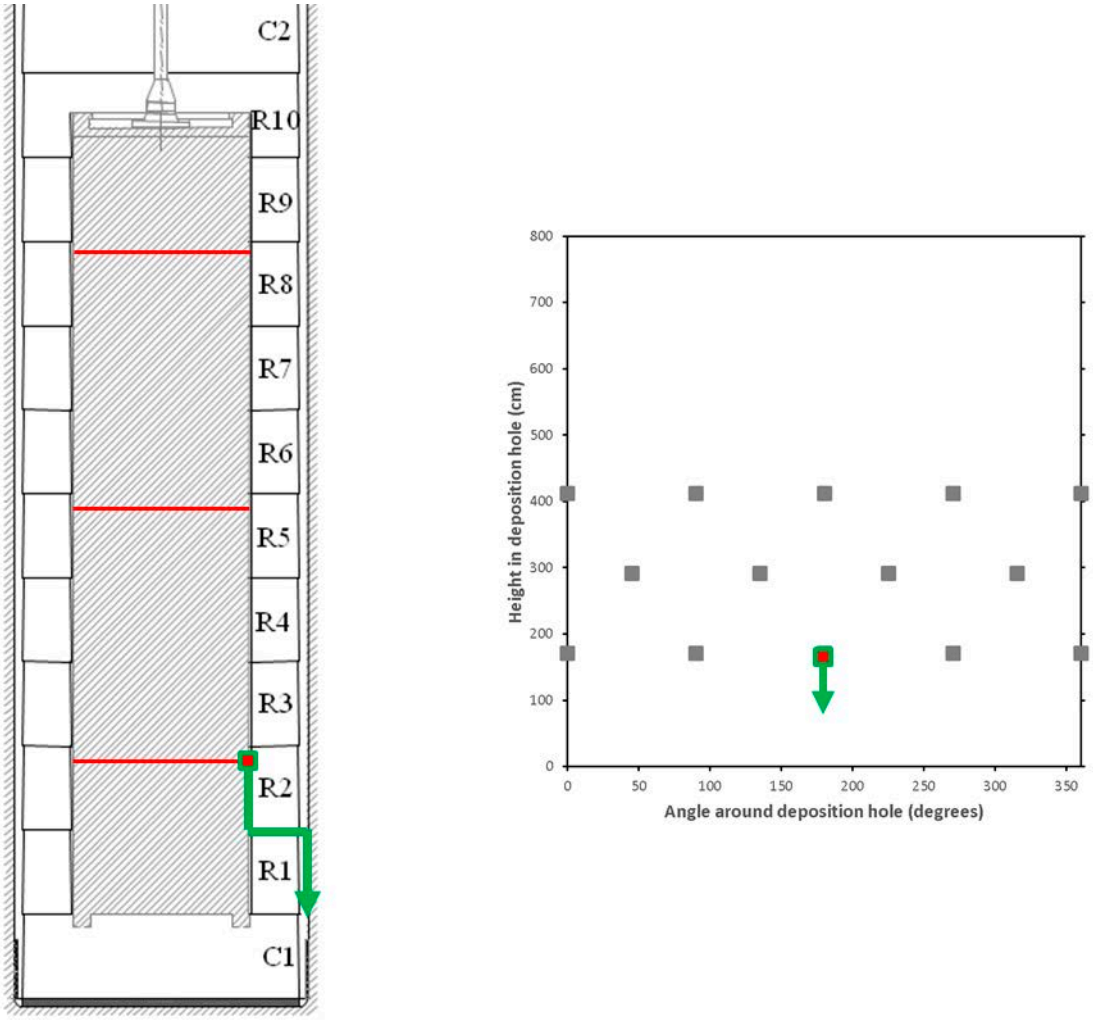

Figure 6-20. *Schematic of the direction of gas flow during Gas Test 1 in lower filter FL903.*

6.3 Hydraulic test post gas injection (day 1010 – day 1110)

To examine the affect, if any, on the hydraulic properties of the buffer following gas injection, a second hydraulic test was performed. Prior to the start of this test, the drain valve to FL903 was opened to atmospheric pressure and the gas in the test system vented. Water was then injected in order to help sweep any residual gas from the injection system. Once a steady stream of water was discharged from the drain valve, it was closed and the hydraulic pressure in the test system raised to 4 400 kPa (very close to the original test pressure in Section 6.1). Once steady-state conditions were established, the hydraulic pressure was again reduced to 480 kPa and the recovery stage monitored. Figure 6-21 shows the evolution in flow rate from both hydraulic tests (pre- and post-gas injection) plotted against the duration of each test.

A visual inspection of Figure 6-21 clearly indicates that little, if any, significant change in permeability had occurred because of the injection of gas. The slight offset in the red line is indicative of a small change in hydraulic storage. Based on the data available, the nascent gas pathways would appear to have no significant effect on the hydraulic performance of the buffer. This was expected given the limited duration of the gas tests and the quantities of helium injected.

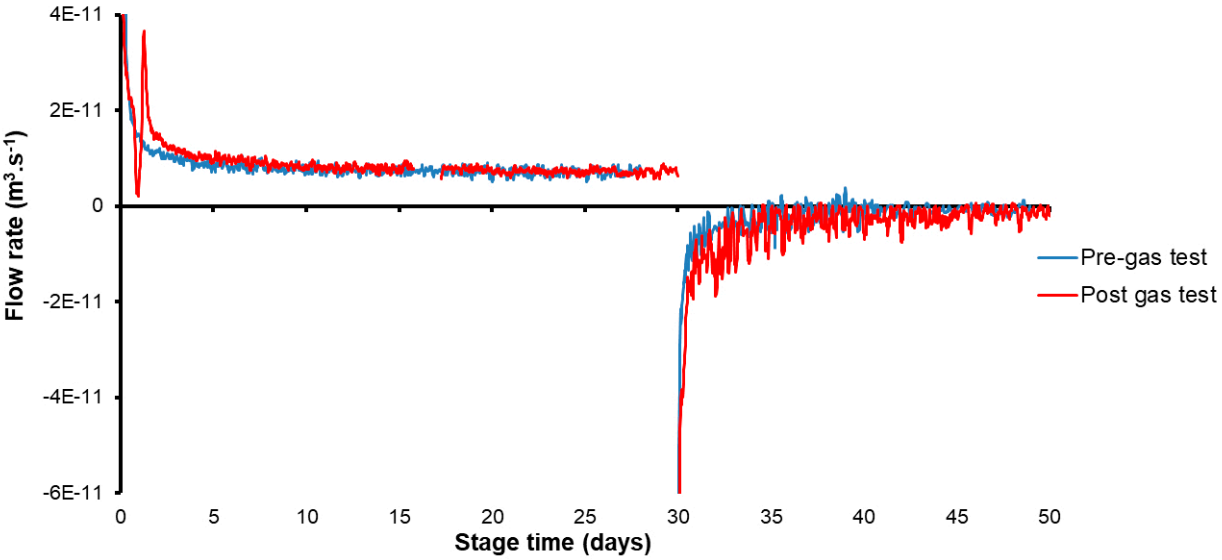

Figure 6-21. *Evolution in flow rate for hydraulic tests performed before and after gas injection.*

6.4 1-D Modelling of hydraulic tests

The two-stage constant head hydraulic tests were modelled using a simplified one-dimensional approach. This approach was adopted as the model used early in the test history was no longer available. Figure 6-22 shows the construct of this model. One-dimensional flow was assumed along a cylinder of length equal to the thickness of the bentonite at the injection filter, l = 0.35 m. The diameter of the cylinder was assumed equal to the diameter of the injection filter. The pressure at the injection end of the cylinder was the hydraulic pressure imposed in the hydraulic test, with the pore-pressure at the other end of the cylinder equal to the pore pressure recorded at the corresponding UR sensor on the deposition hole wall. This simplified model was in-reality unrealistic as flow will also occur in three-dimensions, including along the interface between the bentonite and the canister. However, it enabled comparisons over time and space to be made.

Data from the hydraulic tests have been interpreted using a one-dimensional model that has been analytically solved by means of the Laplace transform technique. This model allows the analysis of the flow movement through a finite bar of length L (L = 0.35 m) when a constant pressure p_0 (and thus, a constant hydraulic head $h(0, t) - h_0$) is prescribed at the end $x = 0$ and a constant pressure p_L (and thus, a constant hydraulic head $h(L, t) - h_L$) is prescribed at the end $x = L$. Affine initial conditions $h(x, 0) = \frac{h_{IL}-h_{I0}}{L}\, x + h_{I0}$ have also been assumed and the water flux per unit area of the sample at any point along its length is assumed to be described by the Darcy's law.

Applying first the Laplace transform to the Darcy's law and evaluating at $x = 0$ and $x = L$, the analytical expressions for the Laplace transform of the flux per unit area

$$Q(0,s) = K\lambda \frac{h_L - h_{IL} - (h_0 - h_{I0})\cosh(\lambda L)}{s\sinh(\lambda L)} + K\frac{\mu}{s} \tag{6-1}$$

$$Q(L,s) = K\lambda \frac{\cosh(\lambda L)(-h_L + h_{IL}) + (h_0 - h_{I0})}{s\sinh(\lambda L)} - K\frac{\mu}{s} \tag{6-2}$$

are obtained, where K is the hydraulic conductivity (m/s), $\lambda = \sqrt{\frac{s \cdot S_s}{K}}$ is an adimensional parameter (with S_s being the specific storage (m^{-1}) and s being the Laplace parameter) and $\mu = \frac{h_{IL}-h_{I0}}{L}$. Second, and after using the standard Talbot method to derive their inverse Laplace transform, and applying a least-squares algorithm, best estimates of S_s and K are obtained.

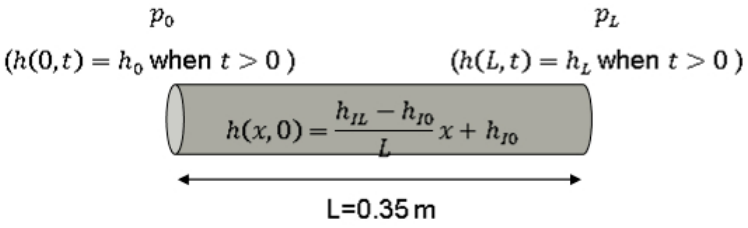

Figure 6-22. *One-dimensional boundary value problem.*

Figure 6-23 shows the results of the two-stage hydraulic tests, which have been adjusted so that the tests conducted before and after the gas injection test can be compared. Figure 6-23a shows the pore pressure imposed during the test. There was a slight difference in pressure for the two tests, which could result in differences in the results, but this should be corrected in the model. Figure 6-23b, c and Figure 6-24a show that the high-pressure stage resulted in an initially high flow into the buffer in excess of 4×10^{-11} m^3 s^{-1}, which quickly reduced to an asymptote of 7.07×10^{-12} m^3 s^{-1} for the test before the gas test and 7.19×10^{-12} m^3 s^{-1} for the repeat test after gas injection. The repeat test had an unexplained anomaly in the first couple of days of the test. Figure 6-23b, c and Figure 6-24b show that the low-pressure stage resulted in an initially high outflow in excess of 6×10^{-11} m^3 s^{-1}, which quickly reduced to an asymptote of 7.44×10^{-13} m^3 s^{-1} for the test before the gas test and 1.35×10^{-12} m^3 s^{-1} for the repeat test after gas injection. The low-pressure stage resulted in a much noisier result, but it is clear that the outflow during this stage was considerably lower than the inflow during the high-pressure stage.

Figure 6-25 shows the modelled results for the two hydraulic tests. The fit of the data can be seen to be good, although it hasn't perfectly modelled the data. Table 6-2 summarises the calculated values for hydraulic conductivity and specific storage for the two tests.

Figure 6-23c shows that the two tests resulted in asymptote at a similar flow rate for both before- and after-gas injection testing. What varied between the tests was the rate of decay, with the test before the gas injection test reducing to an asymptote quicker than the test conducted afterwards. This would be related to the gas that remained in the buffer near to the injection filter. The asymptote of the data related to the flow properties of the bentonite, while the curvature of the flow related to the storage in the system. After gas injection, there was apparently more storage, but no change in hydraulic flow. This is confirmed in the modelled data, which show comparable results for hydraulic conductivity and specific storage. Therefore, the injection of gas had not resulted in a change in the flow properties of the buffer.

Table 6-2. Modelling results for the two-stage constant head hydraulic tests conducted during Gas Injection Test 1.

Filter	Radius of the filter (mm)	Step	Fitted hydraulic conductivity (m s^{-1})	Fitted specific storage (m^{-1})	Boundary conditions		Initial conditions	
					p_0 (MPa)	p_L (MPa)	p_{I0} (MPa)	p_{IL} (MPa)
FL903	50	1	1.62×10^{-12}	9.65×10^{-6}	4.28	1.91	0.98	1.91
		2	1.06×10^{-12}	6.68×10^{-6}	0.56	1.91	4.28	1.91
		Average	**1.34×10^{-12}**	**8.16×10^{-6}**				
FL903	50	1	1.41×10^{-12}	4.35×10^{-5}	4.41	1.87	0.98	1.91
		2	1.56×10^{-12}	3.51×10^{-6}	0.65	1.83	4.28	1.91
		Average	**1.49×10^{-12}**	**1.97×10^{-5}**				

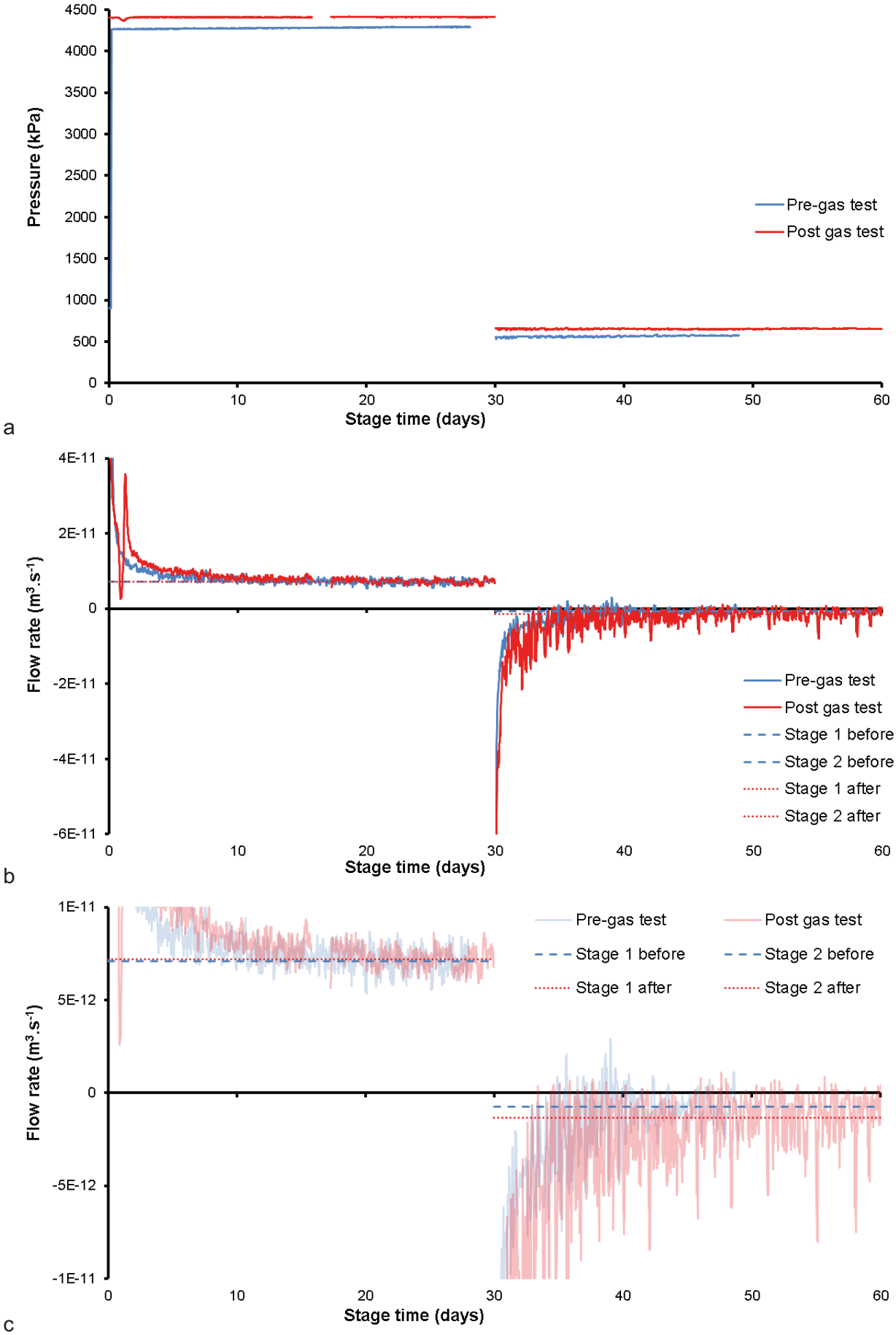

Figure 6-23. *Two-stage constant head hydraulic tests conducted during Gas Injection Test 1. a) Pressure of the injection fluid; b) Flow response; c) Detail of flow response.*

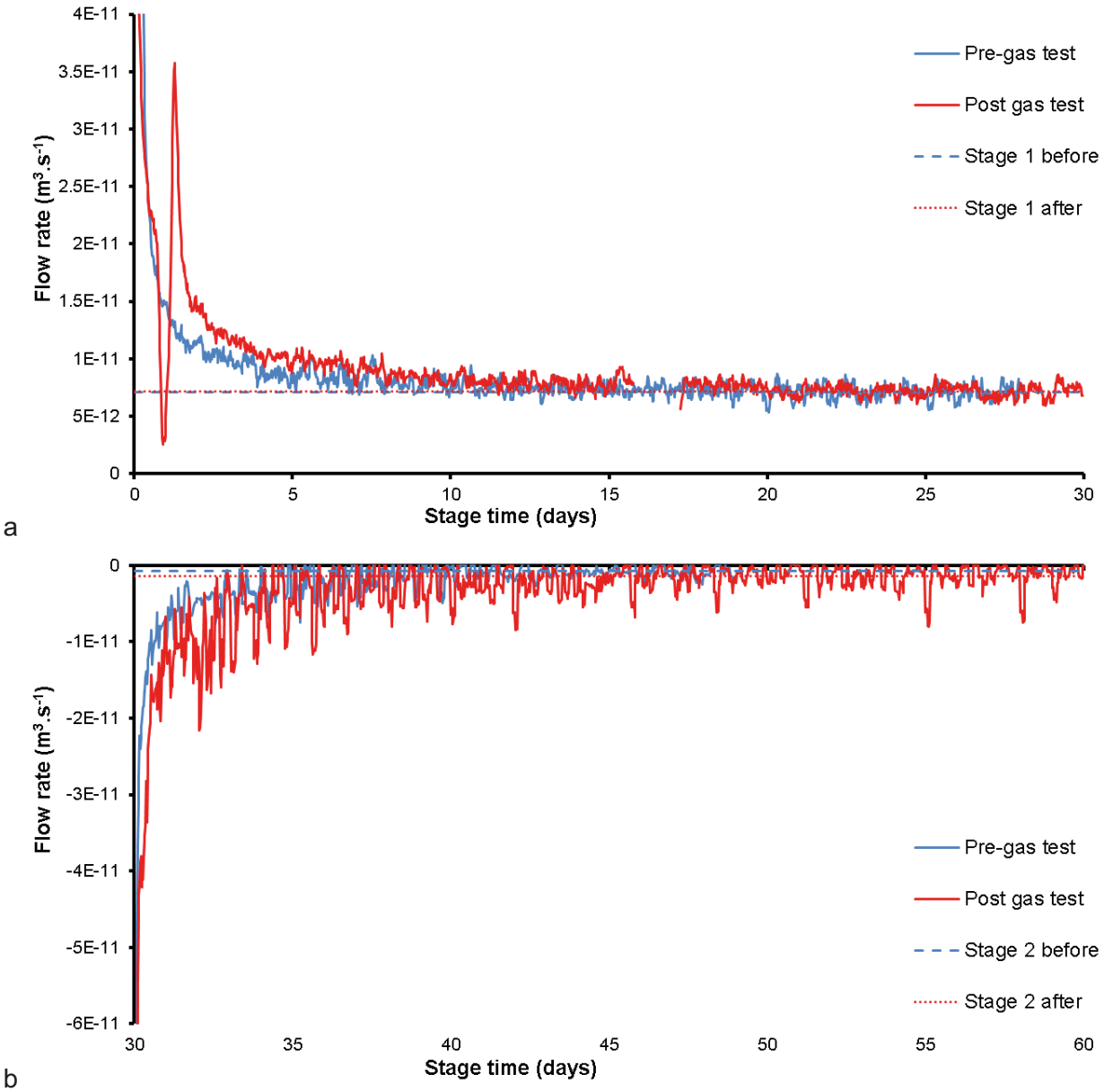

Figure 6-24. *Detail of the flow into the clay during the two-stage constant head hydraulic tests conducted during Gas Injection Test 1. a) High-pressure stage; b) Low pressure stage.*

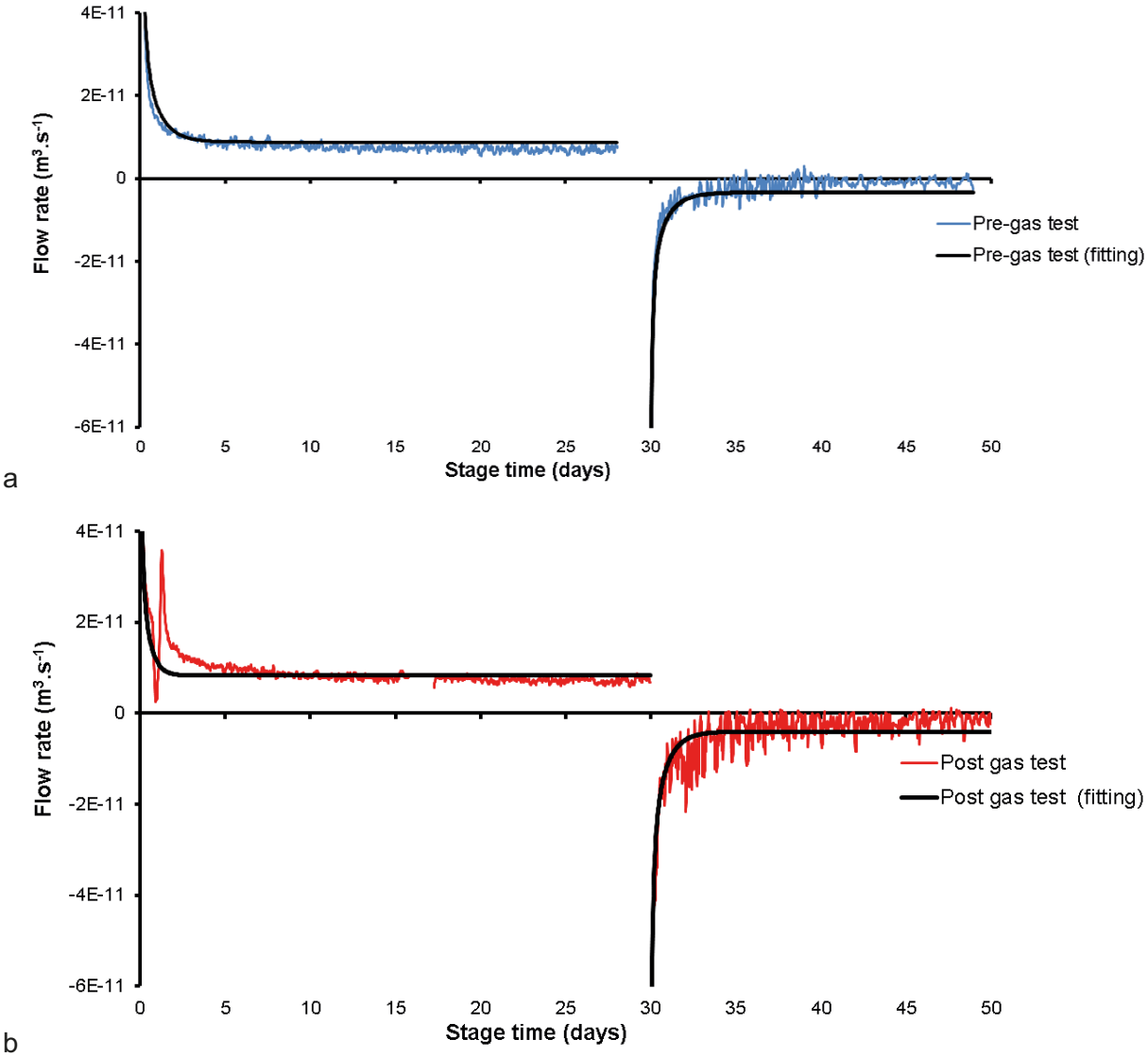

Figure 6-25. *Modelled results for the two-stage constant head hydraulic tests conducted during Gas Injection Test 1. a) Pre-gas test; b) Post-gas test.*

6.5 Summary of gas injection test 1

A preliminary set of baseline hydraulic measurements were started on the Day 843 (25th May 2007) with the isolation of the lower canister filters FL901 to FL904 while artificial hydration continued through all other canister filters and filter mats. After a period of 27 days a constant head test was initiated in filter FL903, raising its pressure to 4 300 kPa for 28 days and then reducing it to 560 kPa for a further 19 days. Preliminary modelling of the initial hydraulic test has been carried out using a 2D axisymmetric variably saturated finite element porewater flow model. The initial saturation conditions for the hydraulic test cannot be determined *a-priori*, so it was necessary to try to model the whole hydration stage in order to set these initial conditions. Using this approach, fits were obtained to the initial pressure decay data for the four filters that were isolated using values for hydraulic conductivity ranging from 9×10^{-14} to 1.6×10^{-13} m s^{-1} and specific storage values ranging from 5.5×10^{-5} to 4.4×10^{-4} m^{-1}. The constant pressure test in filter FL903 was modelled with a hydraulic conductivity of 7.5×10^{-14} m s^{-1} and a specific storage of 2.5×10^{-5} m^{-1}. The design specifications of the KBS-3V concept states that hydraulic conductivity should not exceed 10^{-12} m s^{-1} (SKB 2009) and Harrington and Horseman (2003) have previously reported the hydraulic conductivity of MX-80 as between 3.9×10^{-15} and 9.28×10^{-14} m s^{-1}.

Gas injection to FL903 was begun on Day 917 with an initial volume of gas being compressed at a steady rate for 13 days, a period of 22 days with gas pressure held constant and then a further period of 22 days during which pressures were raised again. Compression of the gas was then halted, and the pressure monitored as it decayed for a further 4 weeks. Analysis of the data suggest that gas started to flow into the buffer at a pressure of ~ 775 kPa, which is much lower than the expected gas entry pressure for intact bentonite. It therefore seems likely that gas was flowing between the bentonite and the canister and possibly between bentonite blocks. When initial gas pressurisation stopped and the pressure was held constant at ~ 1 850 kPa, flow into the clay suddenly reduced, indicating that propagation of the gas pathway(s) practically ceased when the pressure stopped increasing.

Upon restarting gas injection, the observed pressure began to deviate from the predicted value, indicating pathway propagation continued at the onset of testing. Gas flux into the clay gradually increased as the pressure in the system increased. At a gas pressure marginally greater than the local total stress measured on the rock wall (but a little smaller than the radial and axial stresses measured on and near the canister surface respectively which were between 1 049 and 2 149 mm from the gas injection point, flux into the clay rapidly increased. Gas pressure continued to rise reaching a peak pressure of 5 670 kPa, which was marginally greater than the axial stress measured at PB902. This was followed by a small spontaneous negative transient leading to a quasi-steady state as pathways grew. The post peak gas flux exhibited dynamic behaviour (over and undershooting flux into the system) suggestive of unstable gas pathways, which were linked to a strong couple between pore pressure and gas flow as indicated by changes in porewater pressure during and after gas breakthrough. This general behaviour is reminiscent of the responses observed in laboratory scale tests reported by Horseman et al. (1999) and Harrington and Horseman (2003).

Following the cessation of pumping, the injection flux through the bentonite declined rapidly at first but then entered an extended period of very low flows. This was reflected in the pressure response which dropped rapidly initially but then decayed very slowly towards an asymptotic capillary threshold pressure, which was estimated to be about 4 900 kPa, equating to the average radial stress (PC902 and PC903) measured on the canister surface.

Following peak gas pressure, a well pronounced increase in radial stress occurred around the entire base of the deposition hole, with the highest increase noted in the vertical plane below the point of injection. This indicates the gas preferentially moved downwards, probably along the interface between the canister and buffer. It is notable that the radial stress immediately adjacent to FL903 actually decreased during this time.

Porewater pressure data from the deposition hole wall exhibited similar behaviour to that of radial stress, though initial results suggested that the pulse in porewater pressure dissipated at a faster rate than that of the radial stress.

Analysis of the porewater pressure sensors located within the buffer showed no obvious sensitivity to the injection of gas. In contrast, axial stress sensors located beneath and above the canister appeared to register the passage of gas. Indeed, the slow and then rapid increase in PB902 immediately following the peak gas pressure is strongly indicative of the time dependent propagation of gas pathways.

A small inflection in the rate of increase in axial stress at the base of the canister occurred shortly after the peak in gas pressure. Such a reduction in stress could only be caused by the removal of load, suggesting some form of displacement had occurred as a result of gas injection.

While it is difficult to make definitive statements regarding the exact direction and number of gas flow paths, it seems highly probably that the gas moved generally downwards away from the injection filter and then along the interface between blocks C1 and R1 and/or R1 and R2. This is logical as there is a clear axial stress gradient running from high to low from the top of the deposition hole to the lowest stress sensor. Under most conditions, gas flow would be expected to propagate along such a stress vector.

The observed general coupling between gas, stress, and porewater pressure at the repository scale is extremely important and can be readily explained through concepts of pathway dilatancy. These observations are qualitatively similar to those reported by Horseman et al. (2004).

7 Hydration Stage 2 (Day 1110 – Day 1472)

The third significant stage of the Lasgit experiment started on Day 1105.12 (11th February 2008) and was completed at Day 1472.27 (12th February 2009); a total stage time of 367.15 days, or 1.01 years. Hydration stage 2 was initiated after the system had been recalibrated fully on day 1110. The lower canister filters (FL901–904) were re-pressurised in line with the other hydration filters and the second stage of hydration begun. Figure 7-1 summarises the test history during the current stage of experimentation.

Note: The grey areas displayed in the graphs in this chapter show periods when artificial hydration was not occurring.

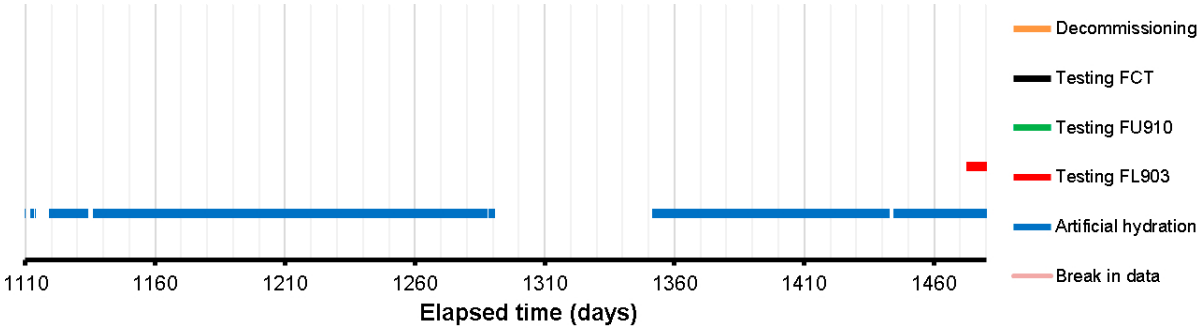

Figure 7-1. *Test stages of the Lasgit experiment showing what was conducted during Hydration Stage 2.*

Below is a summary of noteworthy events that occurred during hydration stage 2, some of which are discussed in more detail later. It should be noted that discrete date events are quoted to 2 decimal places, whereas non-discrete events such as calibration, are quoted on the day the event occurred.

- **Day 1084:** Calibration was first attempted once the second hydraulic test had completed. At this time there was significant blasting activity within the HRL which prevented calibration.
- **Day 1105:** A second attempt was made to calibrate the system. This was again made problematic by blasting activity and battery issues with the calibration Fluke.
- **Day 1109:** Calibration was successfully achieved.
- **Day 1110.00:** Following calibration, the system was re-configured so that all filters participated in the artificial hydration of the clay. The observed slow reaction of FL903 to the increase in pressure suggested that the air actuated valve had failed. On inspection this was not seen to be the case.
- **Day 1122:** Pressure sensor FM906 began to drift. This appears to have lasted for ~8 days. After this time the pressure response of FM906 matched that of the other filter mat transducers. The decision to replace the transducer at the earliest opportunity was taken.
- **Day 1126.70:** Following biannual QC checking of the data, it became apparent that problems existed between the transfer of Geokon data to the LabVIEW logging computer system. This meant that any issues with the Geokon data may not become apparent until after each biannual QC check. Measures were put in place and the problem was resolved.
- **Days 1134.92 – 1135.69:** The first of two planned power cuts to the entire Äspö laboratory occurred. During this period the lab PC failed to log, unlike the Geokon system which remained active.
- **Days 1135.96 – 1136.63:** The second of the two planned power cuts occurred.
- **Day 1157.17:** The configuration of the artificial hydration system was changed.
- **Day 1211.92:** The FM906 pressure transducer was replaced during a site visit, with calibration occurring of the old and new FM906 pressure transducers. Calibration was complete, with FM906 left with a high shut-in pressure of over 18 000 kPa (isolated from down-hole) in order to leak test the new pressure sensor. This elevated pressure remained until Day 1262, when the sensor was reconnected to the hydration system; no leaks were noted. During the site visit it was also confirmed that there were no issues with the air actuated valve controlling FL903. All air actuated valves were checked and were found to be operating satisfactorily.
- **Day 1289:** Calibration of the complete system was conducted during a site visit.
- **Day 1289:** During the site visit two additional LVDT instruments were wired into the data acquisition system. The supports for the LVDTs were not complete, so the actual installation date was Day 1332. These two high precision instruments have been placed in order to observe lateral movements of the lid. The two new transducers were identified as LDS5 and LDS6.
- **Day 1291.70:** The compressor failed. This was initially observed as all air actuated valves were designed to close when air pressure in the receiver was depleted. This effectively shut off the down-hole filter arrays from the laboratory and meant that no artificial hydration occurred.
- **Day 1347:** The two new horizontal lid transducers (LDS5 and LDS6) were calibrated against LDVT calibration wedges.
- **Day 1351.88:** The new compressor was connected to the Lasgit system.
- **Day 1373.72:** The lab PC crashed during external connection from BGS. The PC was successfully brought back online.

7.1 Failure of the compressor (day 1289)

On Day 1289, the Spiralair KS1/T compressor failed. This was initially observed as a reduction in system pressures caused by the closure of the air actuated valves once the compressed air in the receiver had been depleted. This effectively shut-off the down-hole filters from the laboratory preventing continued artificial hydration of the clay.

During the site visit of an engineer it was deemed necessary to replace the existing compressor. This resulted in a considerable time delay to the restart of the artificial hydration activities while the new compressor was ordered, delivered, and commissioned. Whilst this situation was not ideal, it allowed the pressure decay in all filters to be observed, giving an opportunity to observe the state of hydration of the bentonite buffer.

As can be seen in Figure 7-2, the compressed air reduced and was off-line between Days 1291.7 and 1351.88; a total of just over 60 days (marked as a grey band in all appropriate figures). The re-start of artificial hydration was initiated once all pressures in the filters had achieved asymptote. The compressed air data after Day 1351 showed that the new compressor behaved in a similar manner to the old unit. As the compressor was simply the means of operating the air actuated valves it was concluded that the change in compressor had no effect on the test results.

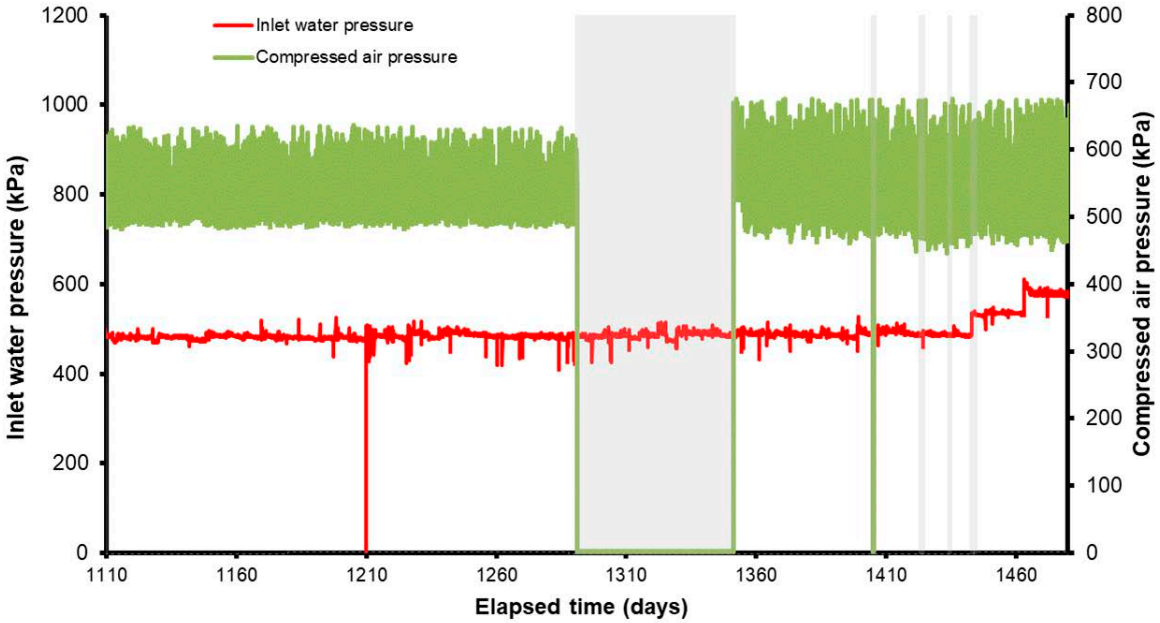

Figure 7-2. *Plot of inlet water pressure and compressed air pressure during hydration stage 2 (the grey band delineates the failure of the compressor).*

7.2 Pressure sensor drift and replacement

Soon after calibration had been completed, pressure sensor FM906 started to behave differently from the other pressure transducers, as seen in Figure 7-3 from Day 1122. At this time, examination of the data and experimental setup did not show anything of concern and the decision was taken to observe the seemingly erroneous result. Over the following 8 days the pressure transducer continued to drift in a linear manner, but by about Day 1130 the behaviour levelled, giving a similar response to all other filter mat pressure transducers. **Note:** all filters were being artificially hydrated and should have registered the same pressure.

The result for FM906 was carefully monitored to ensure that the drift was not a precursor to a more significant failure of the sensor or a true system response. No additional drift was observed and the transducer continued to mirror the behaviour of the other transducers, all be it with an offset in pressure. It was therefore concluded that the pressure transducer was only affected for an 8-day period and the decision was taken to replace the FM906 transducer to prevent any future drifts during more important experimental stages. This was done during a site visit on Day 1211.

The pressure transducer was calibrated before being changed. This data suggests that the transducer was behaving normally. The decision was taken to remove the drift from the FM906 dataset as there appeared to be no reason for the erroneous behaviour. A linear function was applied between Day 1122 and Day 1130 and a correction for the apparent drift of the transducer applied. This gave the result shown in Figure 7-4. The correction is not perfect as FM906 then appeared to have a slightly lower pressure than the other filter pressures. However, it represents a best estimate for the parameter during this time.

The new pressure transducer for FM906 was attached and calibrated on Day 1211. FM906 was left with a high shut-in pressure of approximately 18 500 kPa (isolated from down-hole) in order to leak test the new pressure sensor on Day 1212. The raised pressure was allowed to decay and remained at an elevated pressure until Day 1263, when the sensor was reconnected to the hydration system. No leaks were found following installation of the new pressure transducer.

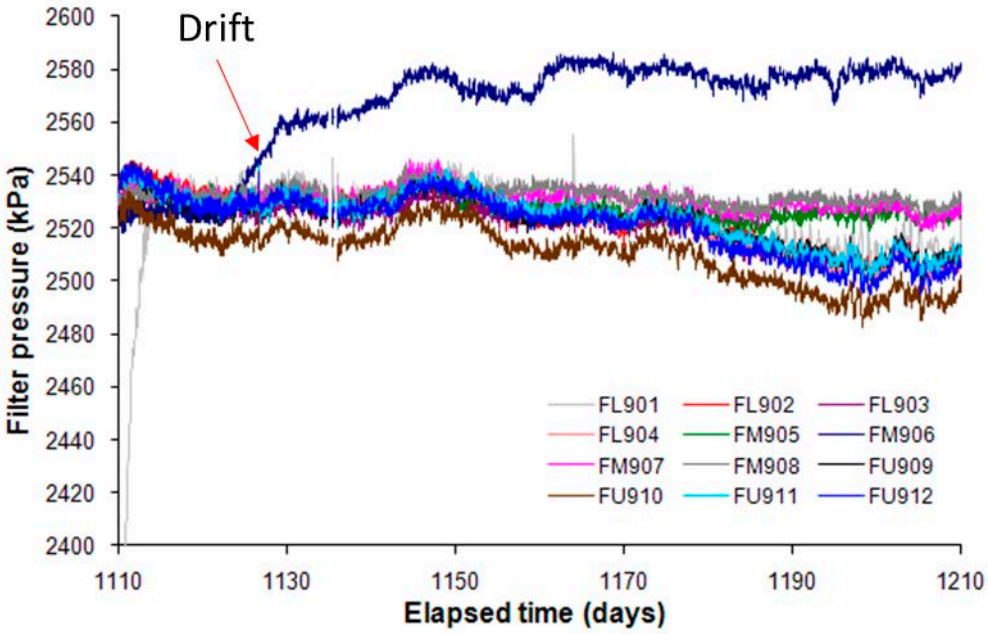

Figure 7-3. *Plot of canister filter pressures to illustrate the drift seen in FM906. This drift was interpreted as a linear drift from Day 1122.19 to Day 1129.33, whereby the intercept of calibration coefficient had drifted. Compare this with the result in Figure 7-4 which shows FM906 after the data had been corrected. The removal of the 6-day drift brought FM906 in line with the other pressure transducers.*

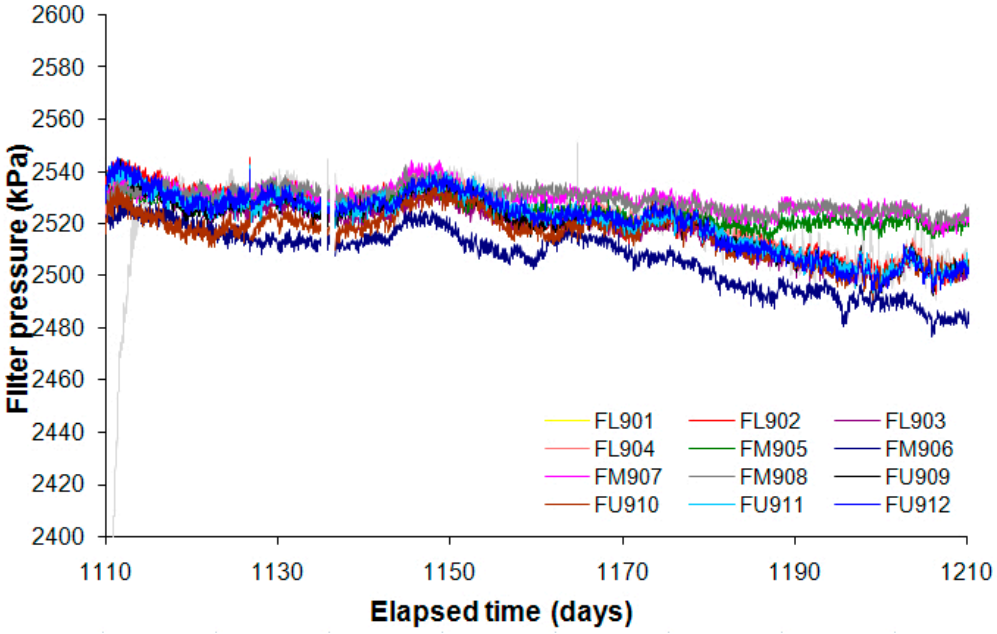

Figure 7-4. *Plot of canister filter pressures after FM906 had been corrected.*

7.3 Blasting activity

Between Day 1048 and Day 1118 considerable blasting activity occurred within the Äspö Hard Rock Laboratory. This activity generally occurred at a depth of 450 m, several hundred metres from the Lasgit experiment. Vibration logs showed that blasting or related activity occurred on Days 1043, 1048–1051, 1105–1107, 1110, 1112, 1114, and 1118. During these times data were thoroughly analysed to ensure that no detrimental effects were observed in the Lasgit experiment.

As will be outlined later (Section 16.3), there are many temporal effects of pore pressure oscillation that correlate with temperature. This makes it difficult to identify any changes in pore pressure as a result of the construction of the new tunnel at 450 m depth. As discussed in detail later (Section 7.7), it was deemed necessary to ensure that the measurements of canister lid displacement were also not influenced by blasting. An underpinning assumption of Lasgit is that the assembly hall roof is static; the roof to lid distance was accurately monitored. Stick-slip movement of the lid was observed during the period of blasting. These movements were fairly regular and some corresponded with blasting activity. However, a large number of blast events did not correlate with any observed displacement of the lid. As discussed later (Section 7.7), it can be shown that the gallery roof was indeed static and the observed movements in the Lasgit lid were unlikely to be due to blasting.

In light of the available information, it can be concluded that the blasting activity within the HRL did not have a detrimental effect on the Lasgit experiment. Whilst pore pressure may have altered as a result of the construction of the new gallery, the long-term data indicated that several boreholes in the 420–450 m depth range exhibited a long-term background decay in pore pressure.

7.4 Evolution of porewater pressure

The following sections describe the temporal evolution of porewater pressure in the Lasgit system, reflecting the complex interaction between artificial and natural sources and their cumulative role in the hydration of the buffer clay.

7.4.1 Canister filters FL901 to FU912

Data from the canister filters are shown in Figure 7-5. Artificial hydration continued in all filters after the lower filter array was brought back on-line at Day 1110 to a pressure of 2 500 kPa. Pressure in the filters quickly increased to the new pressure level with the exception of FL901 which exhibited a much more gradual increase in pressure compared to the other filters. This has been attributed to the non-operation of the air actuated valve that controls the water pumped into this filter. However, the valve was inspected during a site visit and appeared to be in working order. The slow build up in pressure therefore suggests that the valve was open, but flow may have been restricted by debris in the system.

As can be seen in Figure 7-5, the pore pressure results are dominated by the pressure decay seen in all sensors as the compressor failed at Day 1289. This is shown in more detail in Figure 7-6.

Figure 7-6 shows that considerable reductions in pressure were observed during the 60-day period of cessation of artificial hydration as a result of the failure of the compressor. These are presented in Table 7-1. The greatest pressure drop was seen in one of the smallest filters, the 5 mm radius FL902 which recorded a decrease in pressure of over 85 % from 2 235 to 380 kPa. However, the linear trend shown in Figure 7-7, which can be considered as the average pressure drop observed for each sized filter, exhibits the expected trend with a greater reduction in pressure recorded for filters with a smaller surface area. It should also be noted that these results would have been affected by local variations in saturation of the clay, which may help to explain the anomalously large decreases in pressure for certain filters. This general observation agrees with previous pressure decay tests (Section 6.1.1), which also showed rapid declines in pressure associated with the smallest filters.

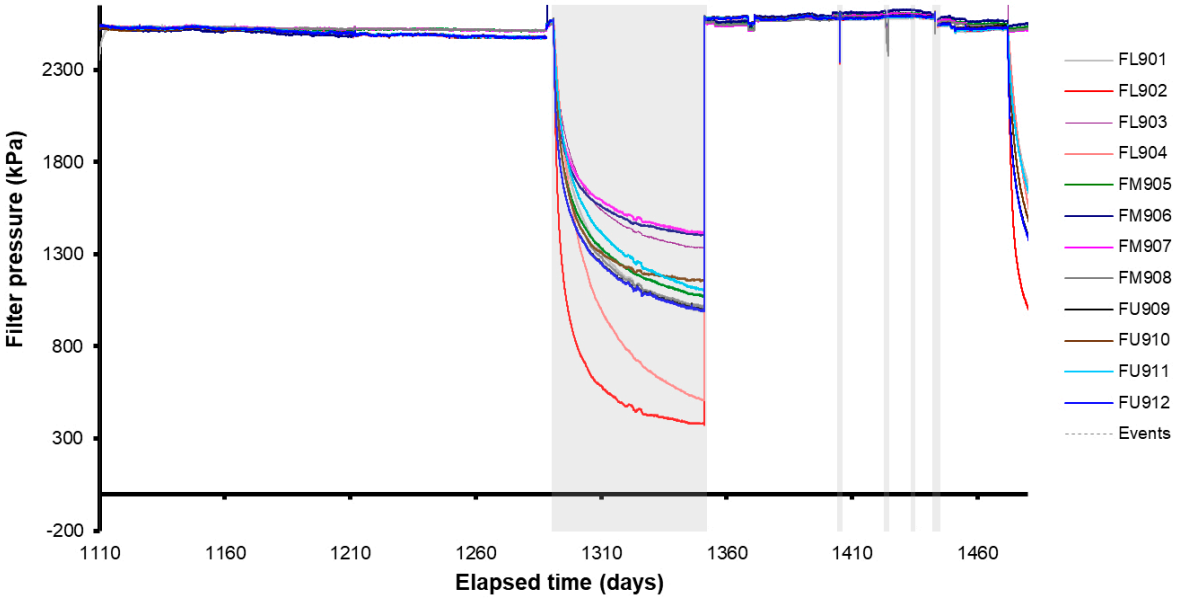

Figure 7-5. *Evolution of water pressure within the canister filters. Large grey shaded area shows the failure of the compressor.*

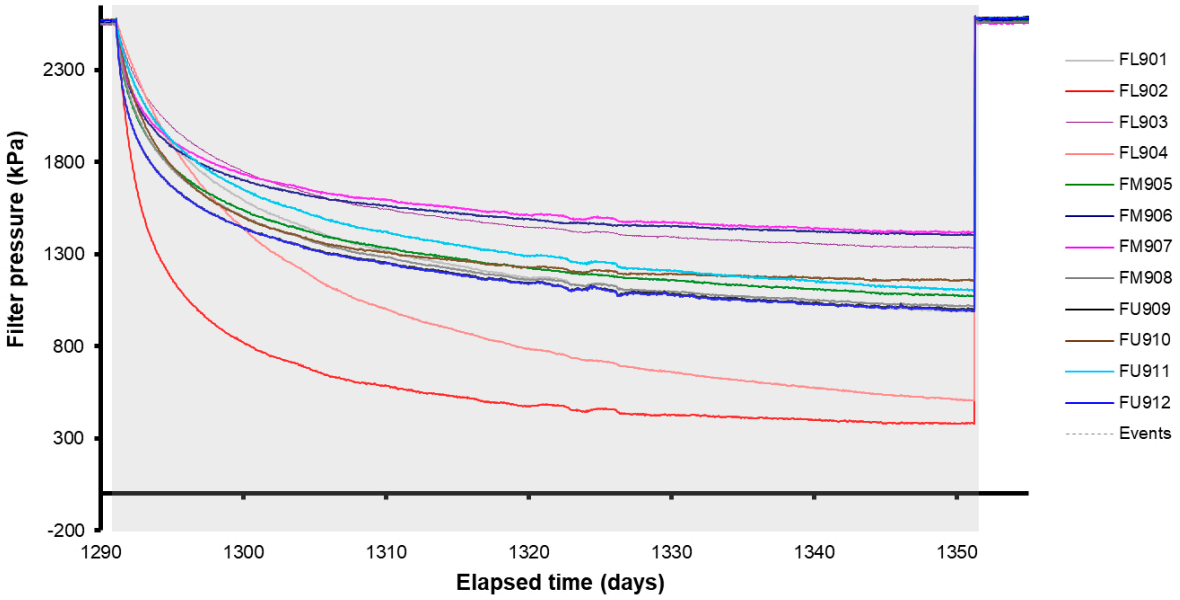

Figure 7-6. Detail of the pressure decline seen in the canister filters during the period when artificial hydration had ceased.

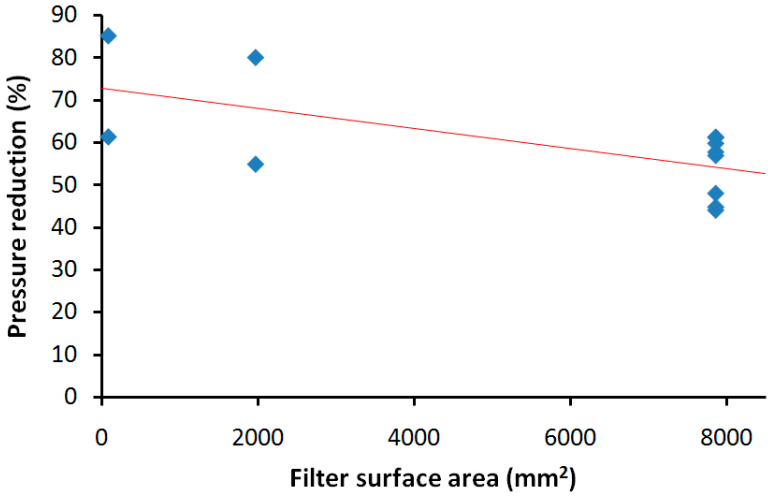

Figure 7-7. Pressure reduction seen in each filter plotted against their surface area. As seen, the higher the surface area of the filter the greater degree of pressure reduction.

Table 7-1. Reduction in pressure seen in the filters and their corresponding dimensions.

Filter	Starting pressure (kPa)	End pressure (kPa)	Pressure reduction (%)	Filter radius (mm)	Filter area (mm²)
FU909	2238.8	996.2	61.3	50	7854
FU910	2397.7	1158.7	54.9	25	1963
FU911	2426.7	1105.8	57.0	50	7854
FU912	2238.3	991.7	61.4	5	79
FM905	2314.2	1076.5	57.8	50	7854
FM906	2350.3	1410.6	44.8	50	7854
FM907	2353.6	1425.7	44.1	50	7854
FM908	2334.2	1024.5	59.9	50	7854
FL901	2432.7	989.2	61.3	50	7854
FL902	2234.8	377.9	85.3	5	79
FL903	2449.8	1331.1	48.0	50	7854
FL904	2482.7	509.2	80.2	25	1963

7.4.2 Modelling canister filters FL901 to FU912 during compressor failure

Data from the canister filters during the 'compressor failure' event have been interpreted using the same 2D, axially symmetric, finite element model of variably saturated porewater flow presented in Section 6.1.1. The axis of the model was centred on each filter and extended out to the perimeter of the emplacement borehole. The curvature of the canister was ignored to make possible the application of cylindrical symmetry and the model radius was set to one eighth of the canister circumference. The model bentonite was initially set to 95 % saturation and the porewater pressures at the filter and outer boundaries were applied as linear segment approximations to the respective measured pressures. The bentonite saturated permeability and specific storage were adjusted to attempt to reproduce the pressure decline at the filter during the compressor failure event. Table 7-2 gives the estimated parameter values and the plots in Figure 7-8 to Figure 7-10 show the fits obtained. Data from FL903 were not considered since this filter was used for gas testing and the model used for interpretation was not able to simulate that event, being only a single-phase flow model.

Table 7-2. Parameter values obtained from model fits to data from each canister filter during the compressor failure event.

Filter id#	Permeability ($\times 10^{-21}$ m^2)	Specific storage ($\times 10^{-5}$ m^{-1})
FL901	8.0	9.0
FL902	7.2	5.0
FL904	13.5	45.0
FM905	7.0	3.0
FM906	8.1	3.5
FM907	6.7	3.0
FM908	5.8	3.0
FU909	9.0	7.5
FU910	50.0	33.0
FU911	23.0	17.0
FU912	33.0	30.0

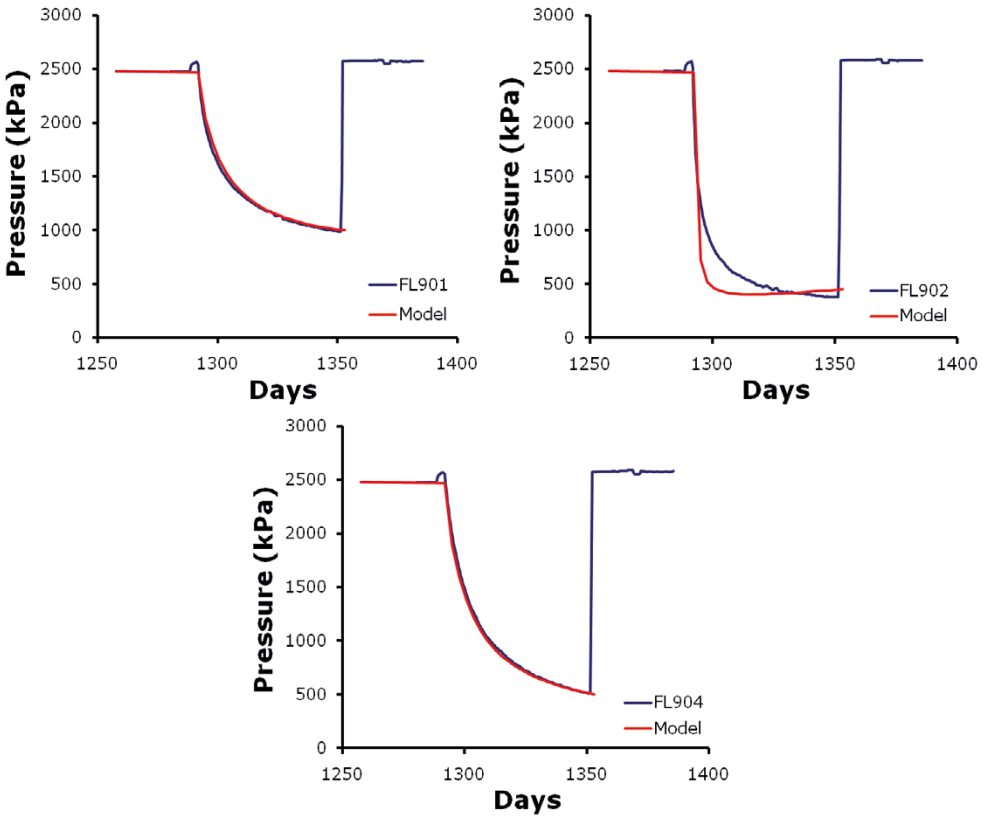

Figure 7-8. Comparison of models to data for the lower canister filters, FL901, FL902, and FL904.

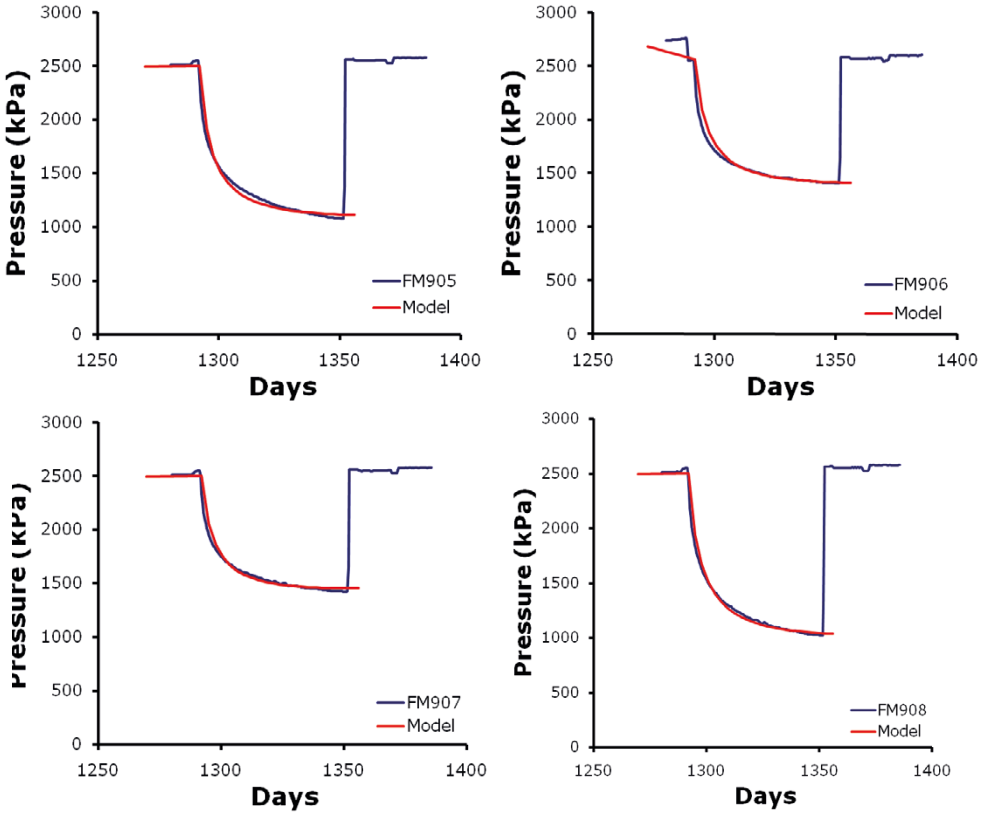

Figure 7-9. Comparison of models to data for the middle canister filters, FM905 to FM908.

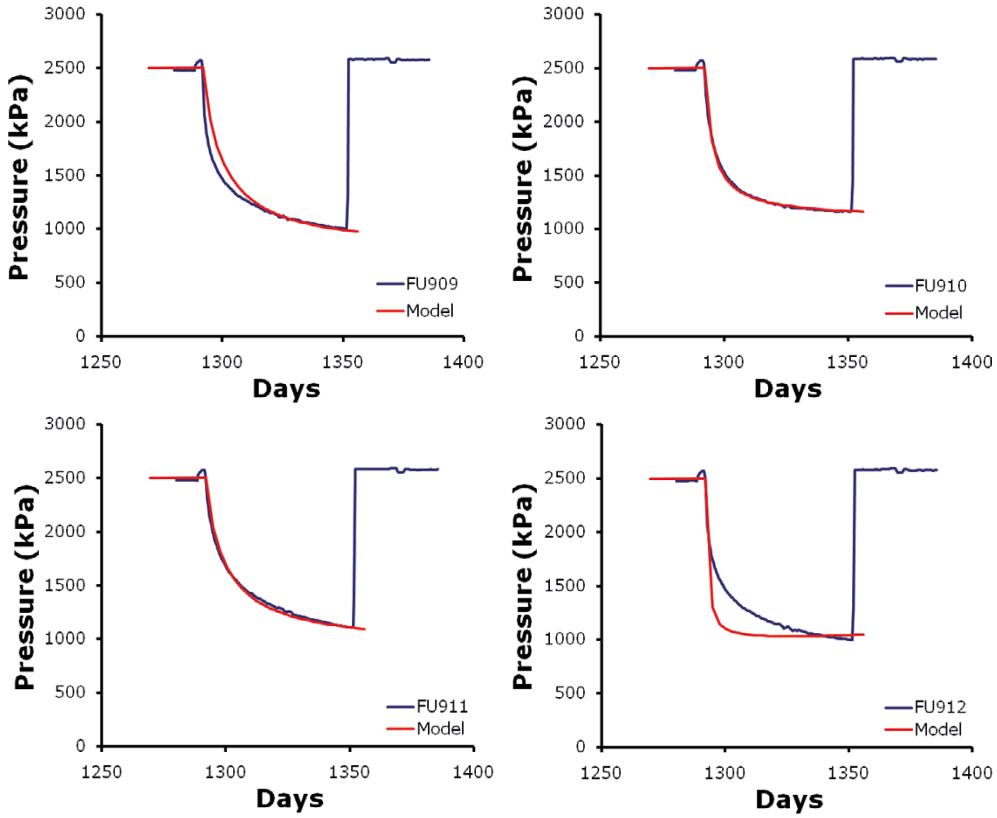

Figure 7-10. Comparison of models to data for the upper canister filters, FU909 to FU912.

Care had to be taken in modelling FM906 as the pressure data included the pressure shut-in used during leak testing of the replacement transducer. During this time there was no pressure data for FM906. It may be noted that the fits for filters FL902 and FU912 were rather poor. These were the two small 5 mm radius filters and it would seem that the approximations made by the model are particularly poor for these data.

It would appear from the results in Table 7-2 that the upper filters (FU909 to FU912) were indicating generally higher values for permeability and specific storage than elsewhere, which suggests the clay in this region was less hydrated, with flow along the suction gradient increasing the rate of pressure decay compared to sections of the clay with a higher saturation. This is consistent with the observations from Hardenby (2004, see also Section 2.2.2) which indicated a lower density of conductive fractures on the depositional hole wall at this section of the borehole. However, it is also possible that the approximations of the model had a different effect on the outcome at these locations. The parameter values obtained for filters FL901 and FL904 are quite similar to those obtained from the hydraulic test earlier.

7.4.3 Filter mats FR901, FR902, FB903 and FB904

Data from the filter mats generally showed a steady pressure throughout this period of experimentation, with an occasional change in pressure due to the resetting of the control pumps, as shown in Figure 7-11. However, as with the results from the canister filters, the filter mats showed a distinct drop in pressure when artificial hydration stopped.

As can be seen the two circular filter mats (FB903 and FB904), which were sandwiched between bentonite blocks C2–C3 and C4–C5, behaved in a similar fashion (Figure 7-12), with a reduction in filter pressure from approximately 2 500 to 1 500 kPa. Differences can be seen in the two filter mats that were emplaced along the wall of the hole (FR901 and FR902). The higher of these (FR902) dropped very rapidly from 2 500 kPa to an eventual asymptote of almost 400 kPa (a decrease of ~84 %). This suggests that this filter was well connected to some form of sink and that water injected at this point quickly drained. The eventual filter pressure of 400 kPa was close to the pore pressure observed naturally in this location of the hole. Filter mat FR902 occurred at a height of 6 030 mm from the base of the deposition hole. Extrapolated pore pressures recorded in the pressure relief holes at this depth (Figure 7-13) indicate a pressure of between 400 and 500 kPa. It can be seen in Figure 7-12 that the two filter mats within the bentonite buffer had not reached an asymptote by the time the new compressor was commissioned and that pore pressure was continuing to slowly decay.

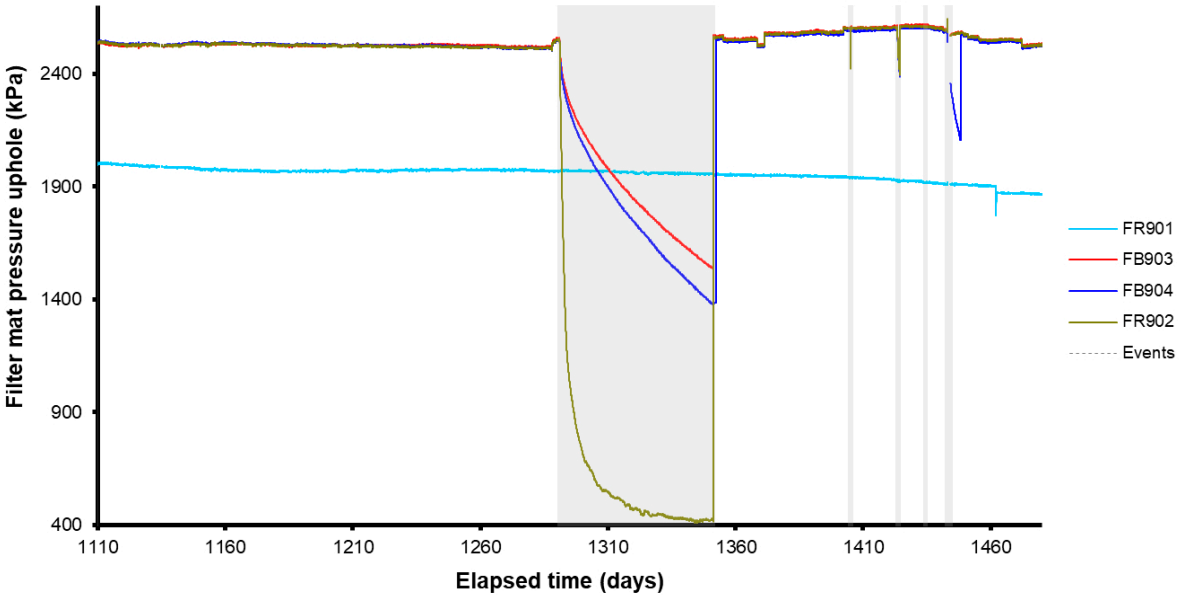

Figure 7-11. *Evolution of water pressure in the filter mats located on the deposition hole wall and sandwiched between the bentonite blocks. Filter mat FR901 (which was in direct communication with a number of packered intervals within the drain holes) was unaffected by the loss in artificial hydration pressure.*

The history of filter FR901 had evolved differently from those of the other filter mats. This filter mat (located towards the bottom of the hole) was isolated from the hydration system due to the increase in pore pressure experienced early in the experiment (section 5). No change in fluid pressure was seen during the period of cessation of artificial hydration. Therefore, it can be deduced that no communication occurred between FR901 and any other filter array.

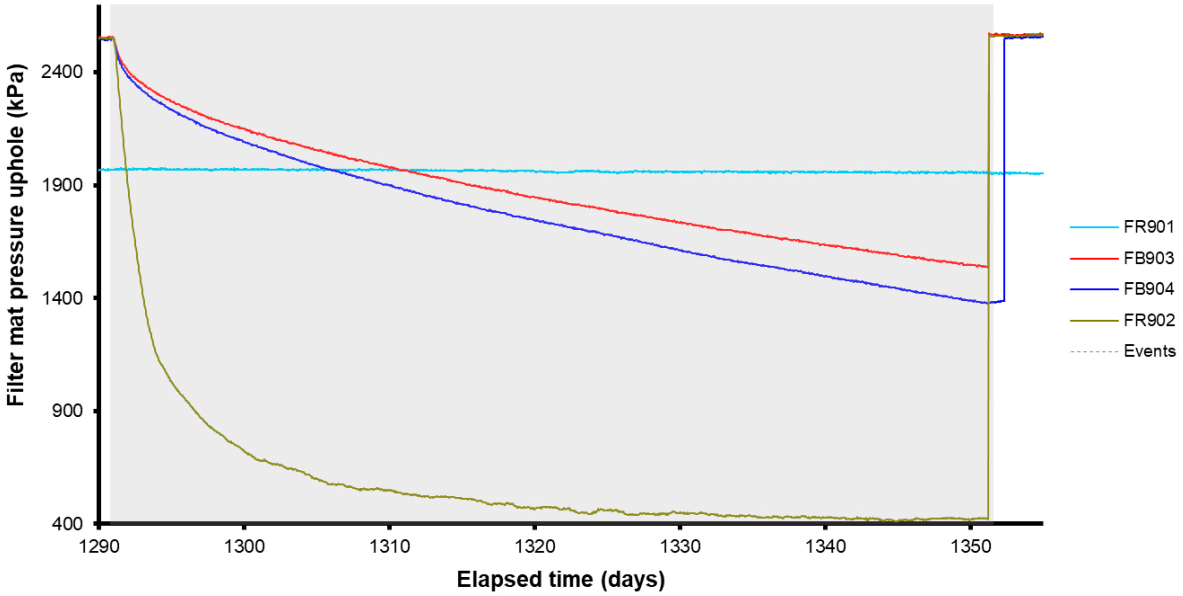

Figure 7-12. *Detail of the pressure decay seen in the filter mats during the period of cessation of artificial hydration. The two filter mats within the bentonite buffer had not reached asymptote.*

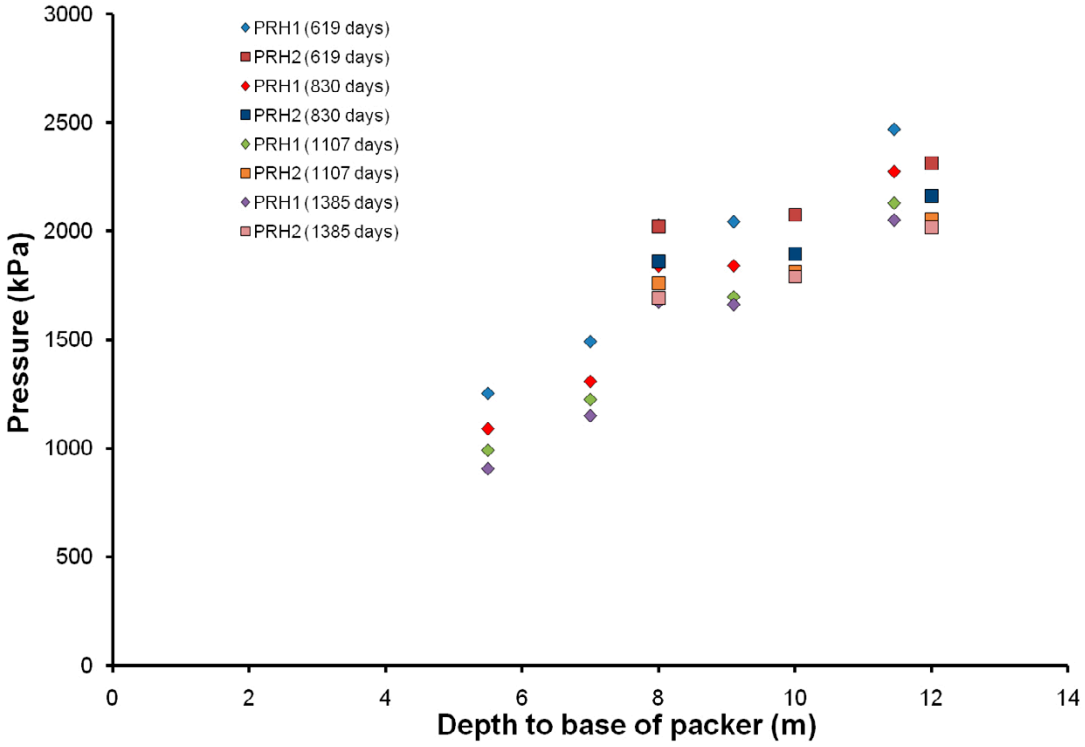

Figure 7-13. *Evolution of pressure in packered intervals within PRH1 and PRH2.*

7.4.4 Porewater pressure within the bentonite

Porewater pressure within the bentonite was measured at 6 discrete locations. As shown in Figure 7-14, three of the locations (UB901, UB923 and UB924) showed a general slow increase in pore pressure during this period of experimentation. In contrast, the remaining three locations (UB901, UB902 and UB926) all showed a noticeable reduction in pore pressure. In each of these locations it can be seen that the reduction initiated between Day 1240 and Day 1280; which was prior to the compressor failure and the cessation of artificial hydration (Day 1292). Thus, the reduction in pore pressure at these times was not related to the compressor failure and must therefore have been caused by a different event.

7.4.5 Porewater pressure measured at the rock wall (UR903 to UR922)

Porewater pressure was measured at 20 separate locations on the borehole surface and the data are shown in Figure 7-15. For 17 of the 20 sensors (excluding UR903, UR907, and UR910) it can be seen that this period of experimentation exhibited relatively stable porewater pressures, with possible underlying annual variation (discussed later in Section 16.3). The annual variation is best observed in UR914 in Figure 7-15.

Four unexpected events occurred during this period in pore pressure (see Figure 7-16):

- An almost instantaneous pressure rise of approximately 700 kPa occurred in UR907 at Day 1112, followed by a long decay of pressure.
- An almost instantaneous pressure rise of 300 kPa occurred in UR910 at Day 1135, followed by a long decay. A second event in UR910 occurred 109 days later at approximately day 1244, when, over a 5-day period, the pore pressure slowly rose by 50 kPa to a new level.
- A pressure drop in UR903 of approximately 100 kPa occurred at Day 1368.

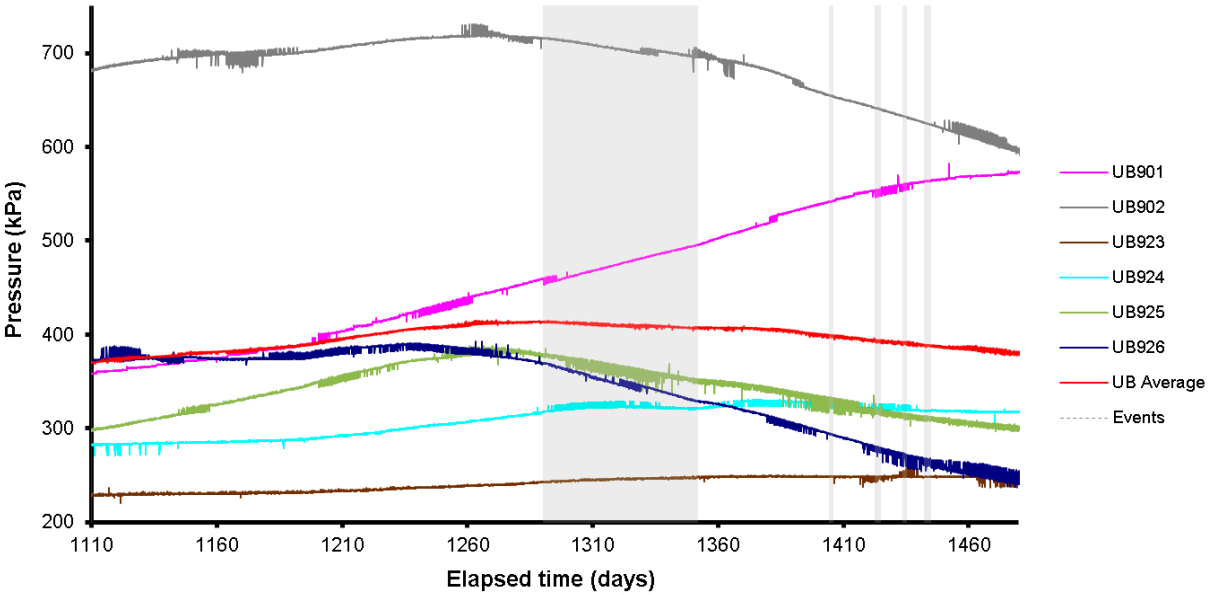

Figure 7-14. *Variation in porewater within the bentonite at the 6 monitoring points.*

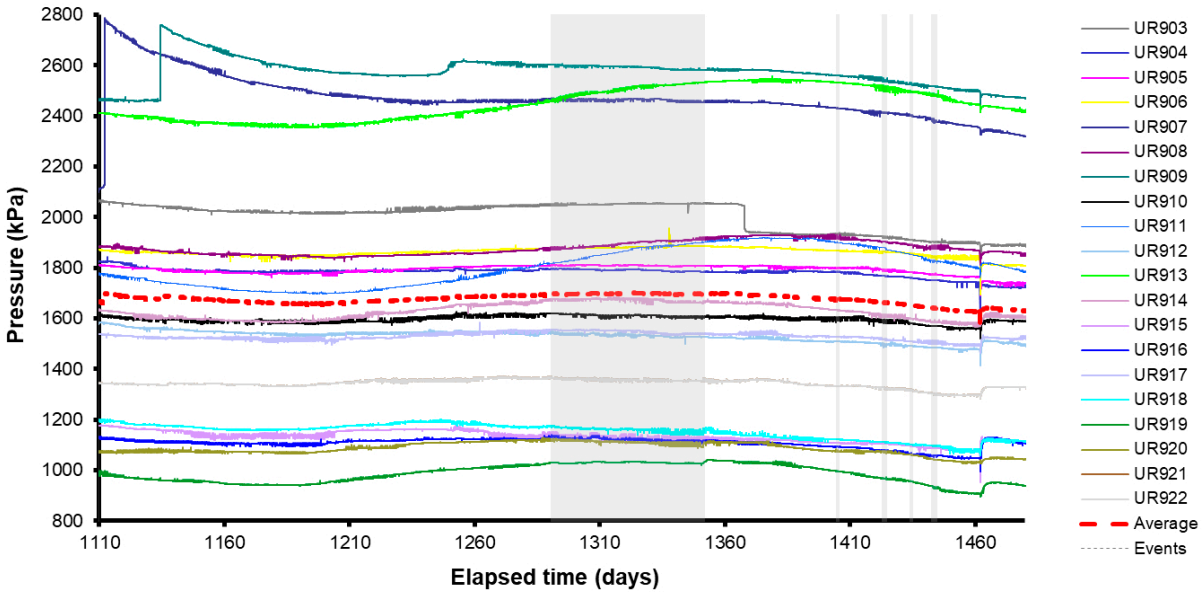

Figure 7-15. *Variation in porewater pressure with time measured at the rock face.*

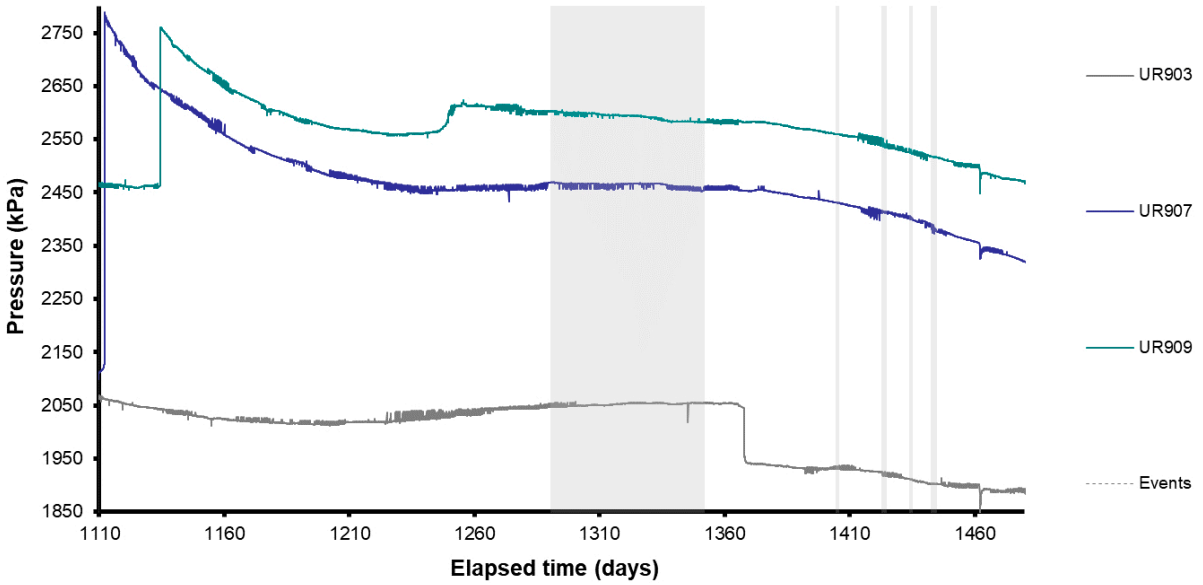

Figure 7-16. *Pressure changes observed in pore pressure sensors UR903, UR907 and UR910.*

The first pore pressure "break-through" was observed at Day 1112.79 with a pressure jump from 2 140 to 2 790 kPa in UR907, as shown in Figure 7-17. After the event had been identified, close examination of the data showed that a precursor to the break-through occurred over the previous three days, as pressure built from approximately 2 100 to 2 140 kPa; although this may be the response as hydration restarted after calibration. The main feature was "instantaneous" with the 650 kPa jump observed between successive data points (logged hourly). Pressure decayed over the following 270 days to asymptote at a new pore pressure level of approximately 2 460 kPa, which was approximately 350 kPa higher than before the break-through.

This event resulted in a change to the daily data QC routine. Whereas previously all groups of data (i.e. UR or PR sensors) were plotted together, the procedure changed so that every channel was displayed in a separate graph of limited range. The purpose of this was to help identify subsequent pre-cursor events. Data was then checked by viewing the previous 10 days only, allowing short term and low amplitude variations to be monitored.

The new QC arrangement also allowed significant events to be marked and shown on all data channels, providing a powerful tool for observing correlations between different sensors. In the case of this event, it allowed careful scrutiny of the data, leading to the conclusion that the pressure rise must have occurred in response to a 'real' event and not by an error associated with the experimental setup or measurement system. Examination of the fracture map (Figure 2-4) showed that sensor UR907 was located very close to a fracture. It seems highly probable that the pressure build-up stems from external events outside of the Lasgit deposition hole, possibly related to the blasting events in the HRL (blasting was active at this time).

The second pore-pressure event was observed at Day 1134.43 in UR910, as seen in Figure 7-18. At this time, pressure jumped from 2 465 to 2 750 kPa, i.e. approximately 300 kPa. On this occasion, a precursor event was not observed prior to the increase in porewater pressure. In addition, pore pressure continued to rise and peak at a value of 2 760 kPa over the next few hours, before starting a pressure decay curve similar in form to that of UR907.

It should be noted that the total pressure observed during these events were very similar; 2 790 kPa for UR907 and 2 760 kPa for UR910. This is significant for two reasons; 1) the pore pressure peak is considerably (200 kPa) higher than that imposed by the artificial hydration system, 2) pore pressure prior to the break-through event was much higher for UR910, at approximately 2 450 kPa, compared with approximately 2 150 kPa for UR907. It is also interesting to note that the decay curve for both sensors was of a similar form following the initial break-through (Figure 7-16). This suggests similar storage and permeability coefficients of the bentonite, which was not surprising as both sensors were situated on the same level, separated by 90 degrees.

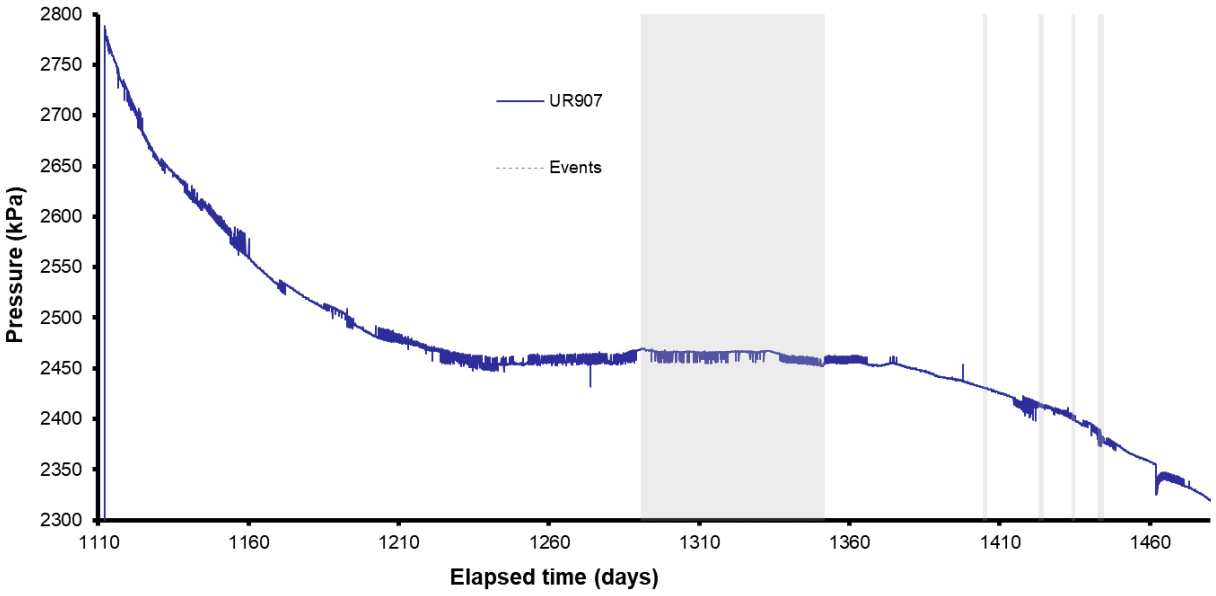

Figure 7-17. *Detail of pressure changes observed in pore pressure sensor UR907.*

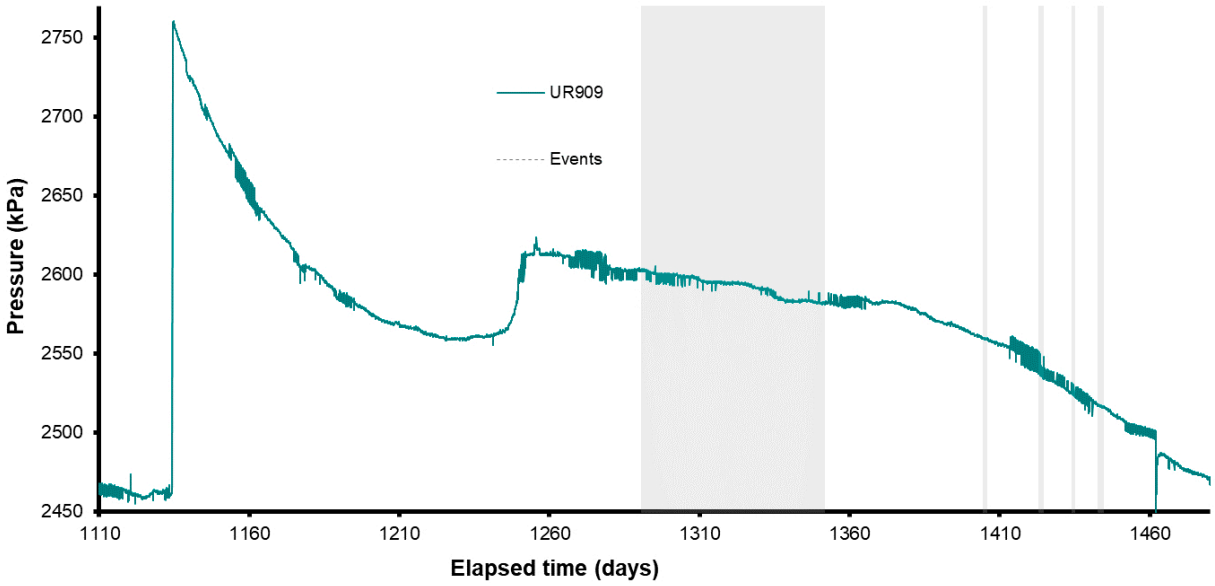

Figure 7-18. *Detail of pressure changes observed in pore pressure sensor UR910.*

The location of UR910 was not near a mapped fracture. However, the continuation of an existing nearby fracture would intercept the sensor very closely. It is possible that the full extent of this fracture had not been identified.

Whilst everything described for UR910 is similar to that seen in UR907, differences started to occur around Day 1240, when pressure slowly increased over a ten-day period by approximately 45 kPa, from ~2 560 to 2 605 kPa. Pressure over the remaining 135 days decayed in a similar manner to UR910. The cause of this event remains unknown.

The final significant pore pressure event occurred in UR903 and was observed on Day 1368, as shown in Figure 7-19. Over the previous ~1 day, pore pressure decayed from 2 050 to 2 045 kPa and then dropped spontaneously a further 85 kPa in one hour before levelling over the next few hours to 1 945 kPa. All previously described events were pressure increases followed by subsequent pressure decays, this was different in that pressure only decayed. The nature of this feature would suggest that it was a real pressure event and not a spurious sensor reading.

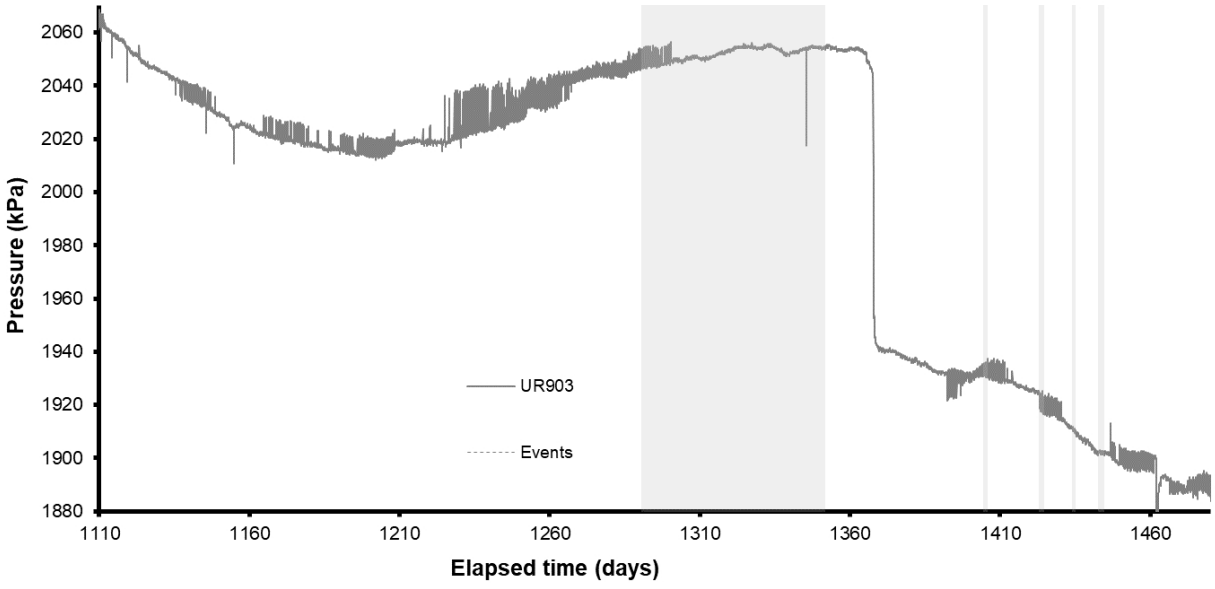

Figure 7-19. *Detail of pressure changes observed in pore pressure sensor UR903.*

As shown in Figure 7-15, pore pressure variation on the rock wall was minimal during the second stage of hydration; apart from the four pressure events described above. Figure 7-20 shows a series of contour plots for Day 1110, Day 1250 and Day 1385. These show little variation in the spatial distribution of pore pressure during this time. While porewater pressure did increase, the spatial distribution of pressure remained similar to that prior to gas testing (section 5).

The presence of mapped or extrapolated fractures close to the three pore pressure sensors that displayed break-throughs (i.e. UR903, UR907 and UR910) suggest these features played a significant role in the observed behaviour. Mechanistically, it is hard to conceive of an event within the deposition hole that could result in the generation of porewater pressures that are significantly in excess of those imposed through the artificial hydration system. It seems more probable that events outside of the Lasgit deposition hole were in some way responsible for the behaviour noted above. Whist a definitive correlation to external events such as blasting could not be made, it is reassuring to note that the measurement system within the deposition hole was sufficiently accurate to register these occurrences.

The observations described above, are symptomatic of a highly dynamic and temporally evolving complex fracture network surrounding the deposition hole. This had remained unaffected by gas testing exemplified by the fact that the geospatial distribution of pore pressure had remained largely unchanged.

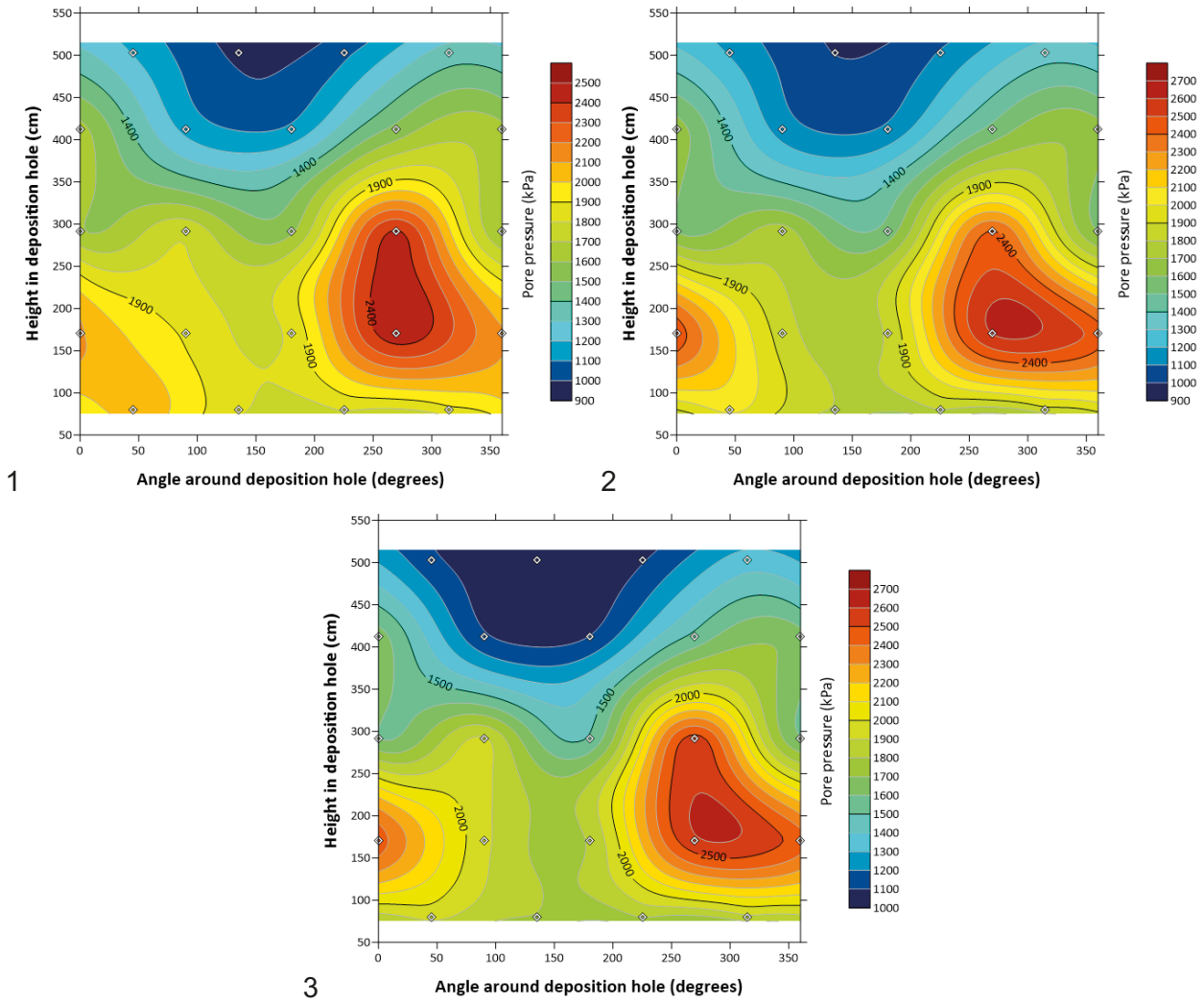

Figure 7-20. *Evolution of pore pressure at the deposition hole wall at Day (1) 1110.24, (2) 1249.94, (3) 1384.85.*

7.4.6 Porewater pressure in the pressure relief holes

Pressure data from the individual packered sections of the two pressure relief boreholes are shown in Figure 7-21. All pressure readings showed a general decline during this period of experimentation, with no individual decrease greater than 100 kPa. The data suggest that intervals PRH2-1 and PRH2-2 were in equilibrium, with only minor decreases in pressure noted in PRH2-3, PRH1-2 and PRH1-3. It is possible that part of the observed change in pressure related to annual variations as discussed later in Chapter 16. However, it is also likely that this may reflect the general decline of porewater pressure seen in the HRL (Section 16.3).

The data show that there was great variation within the packered sections, with PRH1-1 exhibiting the highest pressure ~2 100 kPa and PRH1-5 having the lowest pressure of ~900 kPa. This was consistent with drawdown around the tunnel opening.

While interesting, the short-term fluctuations seen in certain packered sections (such as PRH1-3) are not mirrored in the deposition hole. Further inspection of the data showed that small-scale features with a periodicity of approximately one day were observed towards the end of this stage of experimentation. The cause of these events is unknown but may relate to diurnal variations in HRL temperature.

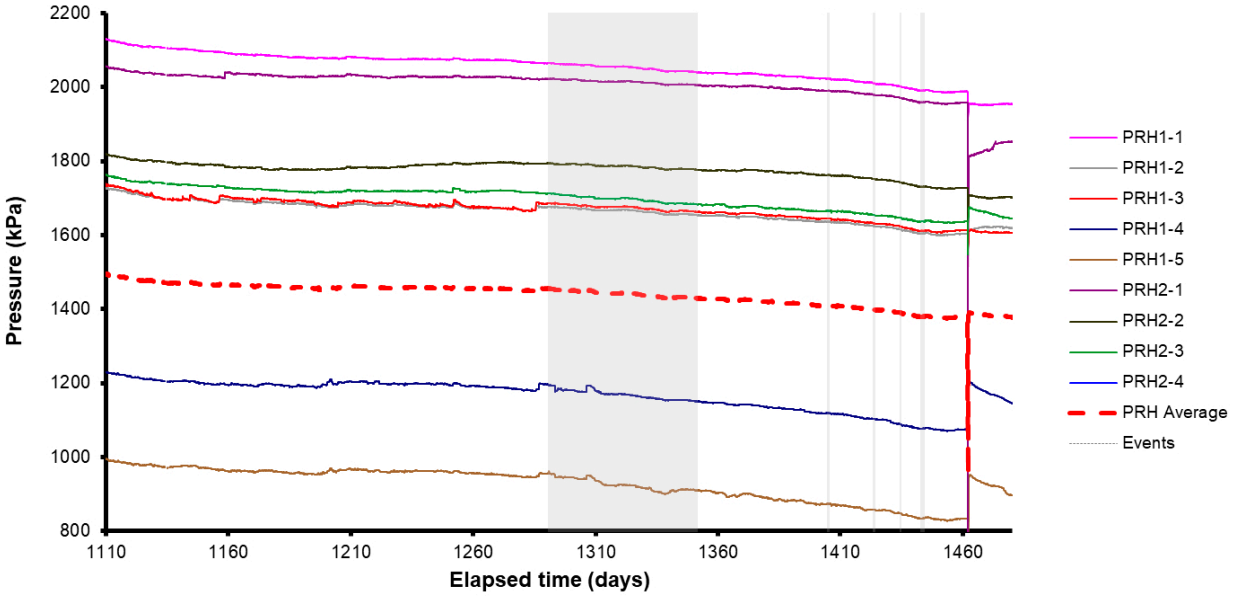

Figure 7-21. *Porewater pressures measured in the packered sections of the pressure relief boreholes.*

7.5 Evolution of total stress

Total stress within the Lasgit system was measured at 32 locations within the deposition hole. Sensors mounted on the canister (PC90x), rock wall (PR9xx) and within the clay (PB9xx) were used to determine both the axial and radial components of stress and the distribution of values throughout the borehole.

7.5.1 Radial stress measured at the rock wall (PR903 to PR922)

Data from the 20 total pressure sensors PR903 to PR922 are plotted in Figure 7-22. As can be seen, all radial stress sensors showed a slow increase in total stress of no more than 100 kPa during this stage of the experiment. Long-term variations were noted, but as will be discussed later these can be attributed to annual variations in radial stress (see Section 16.4). The three contour plots in Figure 7-23 show the spatial and temporal evolution in radial stress measured at the rock wall from Day 1110 to Day 1385. No significant variation in radial stress was observed, as all the radial stress sensors increased at a similar rate.

Figure 7-23 shows the variation of effective stress on the deposition hole wall for Day 1110, Day 1250 and day 1385. These have been produced by subtracting the interpolated results of pore pressure from total stress. The spatial distribution of effective stress remained fairly constant through this time with only small variations noted, primarily caused by the spontaneous increases in porewater pressure described in Section 7.4.5. The data indicate effective stress generally changed around the circumference of the depositional hole and did not exhibit any significant correlation to depth. The data suggest that the development of effective stress was related to the distribution and frequency of fractures.

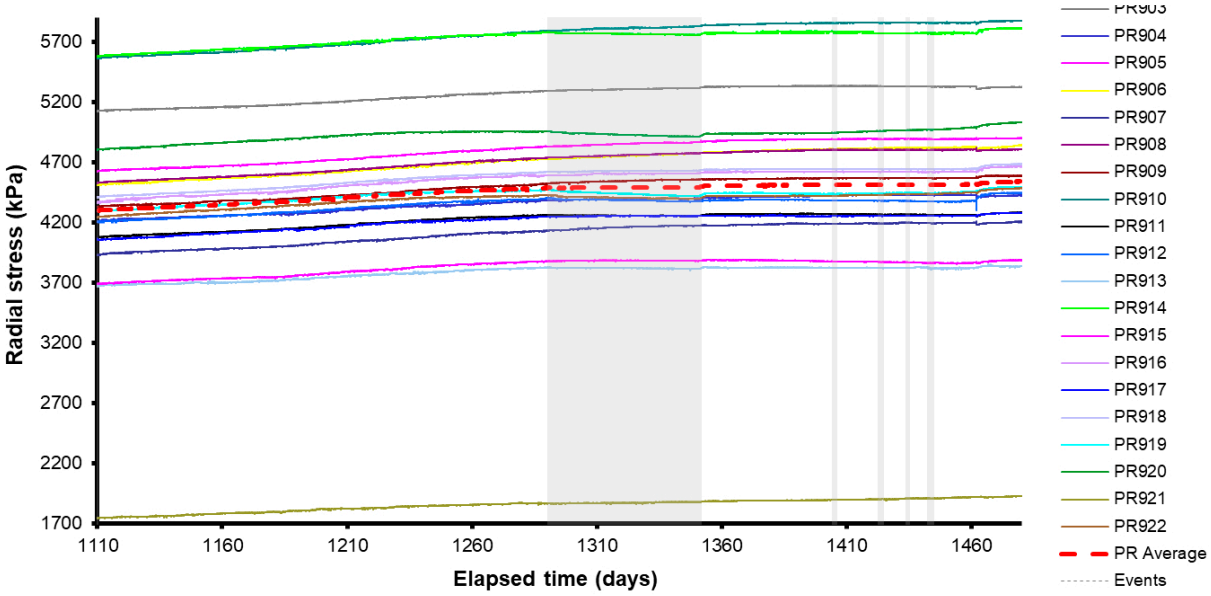

Figure 7-22. *Variation in radial stress with time. In the absence of preferential flow (piping), the rate at which total stress increased was insensitive to the absolute value of porewater pressure applied to the filters.*

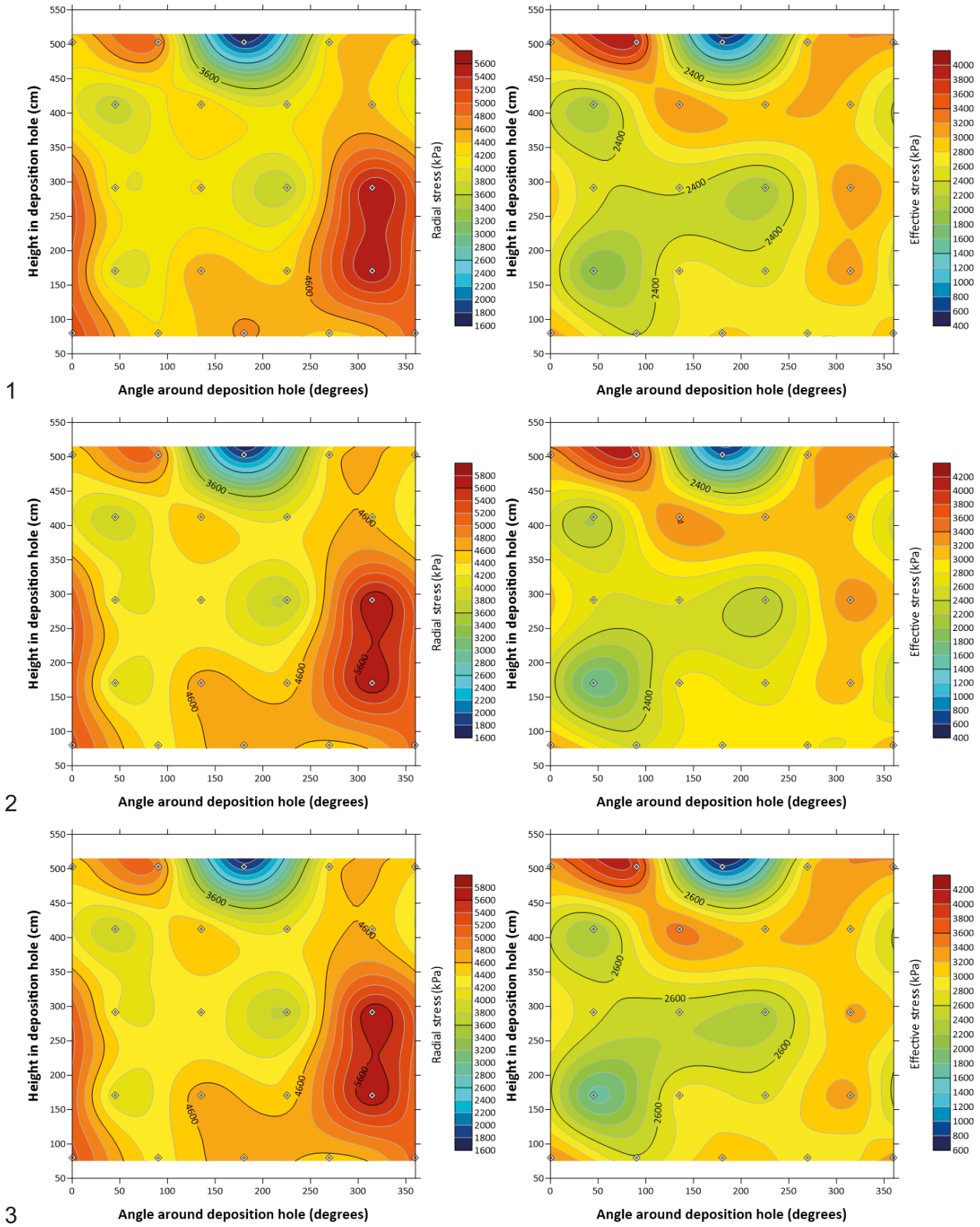

Figure 7-23. *Evolution in radial stress (left) and effective stress (right) around the deposition hole wall for Day (1) 1110.24, (2) 1249.94, (3) 1384.85.*

7.5.2 Radial and axial stress on the canister (PC901 to PC903)

Axial and radial stress around the canister increased steadily during the course of the hydration stage (Figure 7-24). At the start of this experimental period stress ranged from 4 540 to 5 070 kPa, which then increased to between 5 000 and 5 380 kPa. The increase in radial stresses mirror one another, whereas axial stress had increased at a much greater rate, such that it represented the intermediate principal stress acting on the canister by the end of the period. The change in slope in axial stress seen at approximately Day 1350 corresponds with the switch-on of the new compressor and the recommencement of artificial hydration. Detailed analysis of the stress gradient for axial stress showed a clear change in slope at the time when the compressor failed (Day 1291). However, PC902 and PC903 suggest only some sensitivity to the cessation of hydration on radial stresses. It should be noted that there is significant "noise" in the data and it is difficult to differentiate between annual and experimental variations at such low stress gradients. However, by the end of the stage PC902 and PC903 were reducing in magnitude, probably as a result of annual variation.

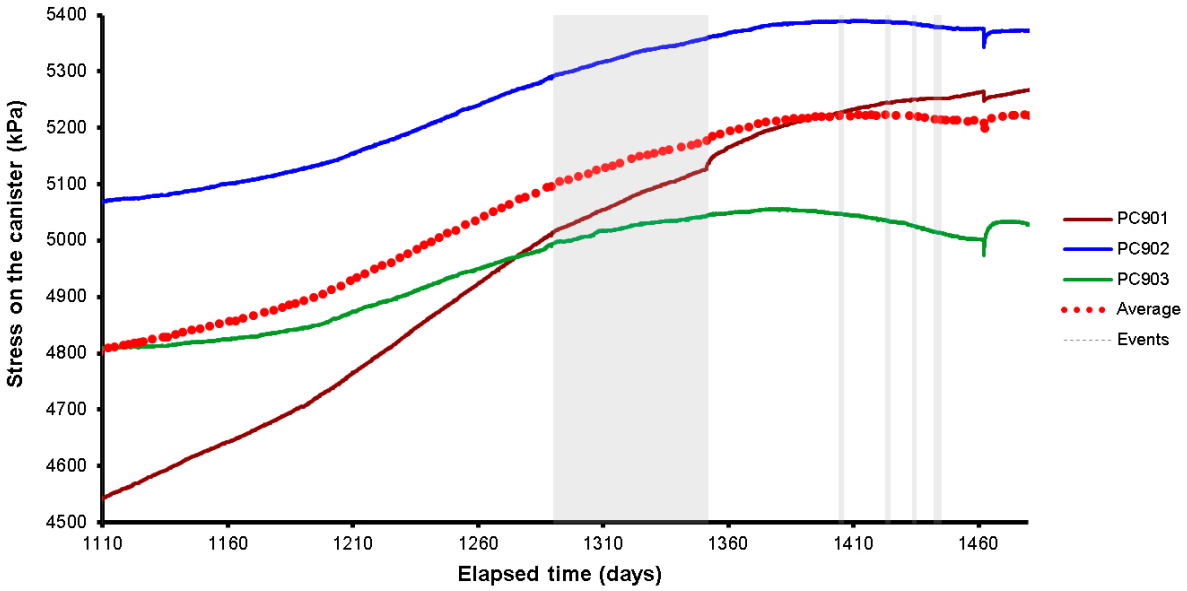

Figure 7-24. *Development of axial (PC901) and radial (PC902, PC903) pressure on the side and base of canister.*

7.5.3 Axial stress within the bentonite (PB901, PB902, and PB923 to PB929)

Data from the axial stress sensors within the bentonite are shown in Figure 7-25. At the start of this stage of experimentation axial stress ranged from 4 190 kPa to 6 300 kPa. In six of the nine sensors stress increased, while in three (PB928, PB902 and PB929) it remained approximately equal. The increase in axial stress continued until artificial hydration was stopped when the compressor failure at Day 1289. At this point total stress ranged from 4 650 to 6 565 kPa.

During this period, it can be seen that two of the stress sensors (PB902 and PB929) remained stable, whilst all other sensors exhibited either a decrease in total stress or a reduction in the rate of stress increase. The most prominent stress change occurred in PB927, which decreased from 6 560 to 6 215 kPa; a reduction of nearly 350 kPa. All other sensors observed a smaller reduction in axial stress. Sensor PB927 was located at the top of the bentonite buffer at the interface with the concrete plug. Also situated at this level were PB928 and PB929, which as shown in Figure 7-25 showed very small pressure drops. This suggests that the stress build up at the top of the bentonite buffer had become very heterogeneous. As pore pressure within the filter mat FB904 (located directly below PB927) dropped, the total stress decreased in response to the change in pore pressure. Similar decreases in stress were not observed in PB928 and PB929, which were situated outside of the footprint of the mat, which therefore had less of an impact on the development of stress at these points within the bentonite.

After re-starting the artificial hydration at Day 1351, axial stress rapidly increased. However, Figure 7-25 indicates that by the end of the reporting period, most of the stress sensors had reached a plateau. This is contrary to expectation, as perceived wisdom would suggest stress sensors would exhibit similar stress gradients to those before and after the cessation and restart of hydration. For some locations, in particular PB927, the end stress level was less than that at Day 1289 when the compressor failed.

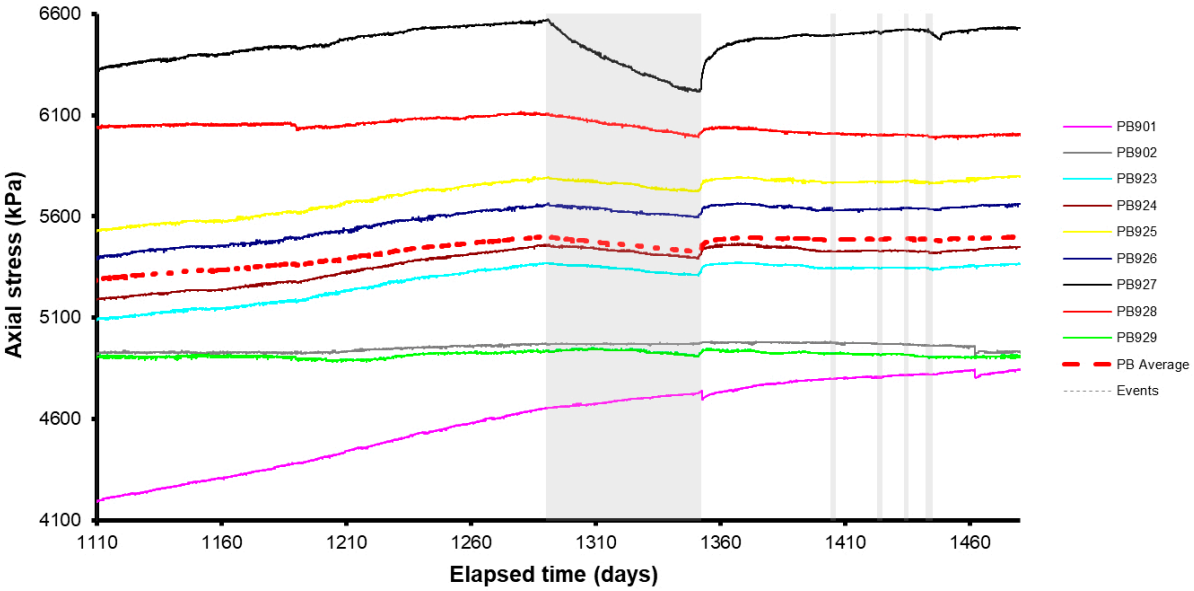

Figure 7-25. *Development of axial stress measured at 12 locations within the buffer. The effect on total stress caused by the compressor failure was variable depending on a number of factors in particular the location of the sensor in relation to sources of artificial hydration.*

The contour plots shown in Figure 7-26 have been constructed using the axial stress data from all sensors, except PB901. The plot clearly shows that axial stresses remained non-uniformly distributed across the major axis of the emplacement hole, as originally reported in Harrington et al. (2007). The increase in stress at PB927 provided an explanation for the minor differences in lid displacement observed in Section 7.7. It is interesting to note that the interruption in artificial hydration has not had a major effect on the distribution and direction of stress, but has had an effect on the magnitude of stress.

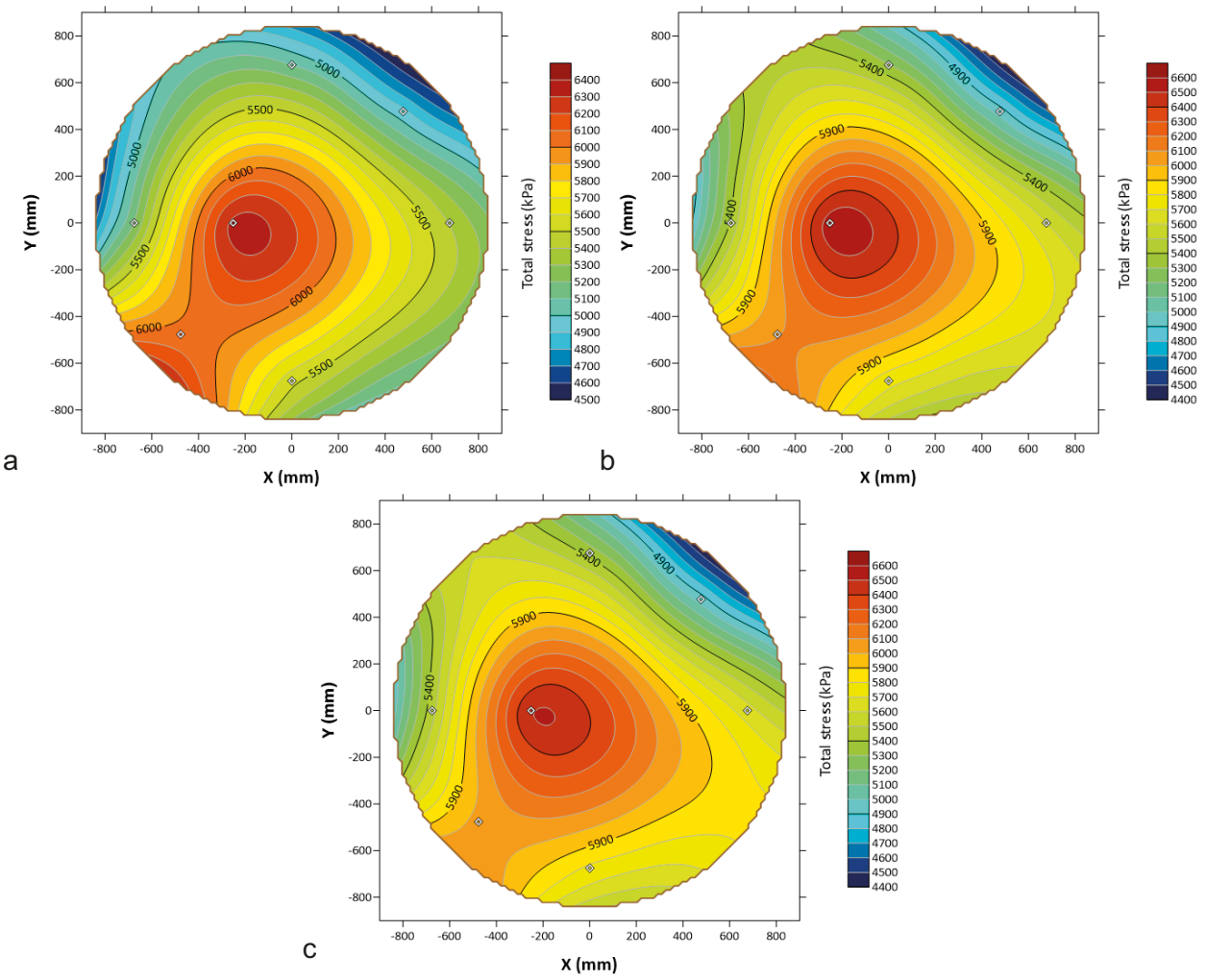

Figure 7-26. *Contour plots showing the distribution of axial stress across the borehole from Day 1110 to Day 1385. a) Day 1110.35; b) Day 1249.89; c) Day 1384.85.*

7.6 Axial force acting on the steel lid

Figure 7-27 shows a plot of the axial force (measured by the Glötzl cells) acting on the lid. As can be seen, at the start of the reporting period the forces were 1 280 kN, 1 390 kN and 1 555 kN in LP903, LP901 and LP902 respectively. Therefore, forces on the canister lid were heterogeneous.

Two very significant events occurred at Day 1190 and Day 1200 with force drops observed in LP901 and LP902 respectively. The first of these occurred in LP901 which for one day showed an increase in axial force, followed by an almost instantaneous decrease in force from 1 425 to 1 405 kN, a drop of ~20 kN. Close examination of all canister lid data shows that this force decrease was observed in all three Glötzl cells and had a corresponding movement in all displacement sensors. One possible explanation for the decrease in axial force is the movement of the Glötzl cell laterally, which could relieve force on one set of tie-rods, or from the failure of a tie-rod. As movement was observed instantaneously in all the lid data it strongly suggests that this stress drop occurred as a result of an event within the hole and not as a result of failure of the lid. Force drops were also observed in the PB sensors within the bentonite.

The second force change event occurred some 10 days later at Day 1200 with an instantaneous decrease in force on LP902 from 1 595 to 1 575 kN; again, a decrease of ~20 kN. Unlike in the earlier event, no changes in force were seen in the other LP sensors, only two of the four lid displacement sensors showed any movement and these were not as significant displacements as observed in the earlier event. This can be explained by possible stick slip movement of the conical concrete plug, which may also help to explain some of the variations in axial stress recorded in the upper PB sensors. The hypothesis of stick slip is further supported by the analysis of the gradient of the axial force pre- and post-force drop (dotted lines in Figure 7-27), observed as a recovery in force over a 30–40-day period.

As shown in Figure 7-27, axial stress continued to build at a rate of almost 0.5 kN per day up until the point of compressor failure at Day 1289. During the period of no artificial hydration the axial force on the lid decayed in a linear manner at a rate of ~0.1 kN a day. Once hydration was restarted at Day 1351 the axial force began to rise, but soon peaked and fell to a new level and remained at this new force level. It wasn't for some time (50–100 days) that force started to increase once more around Day 1440.

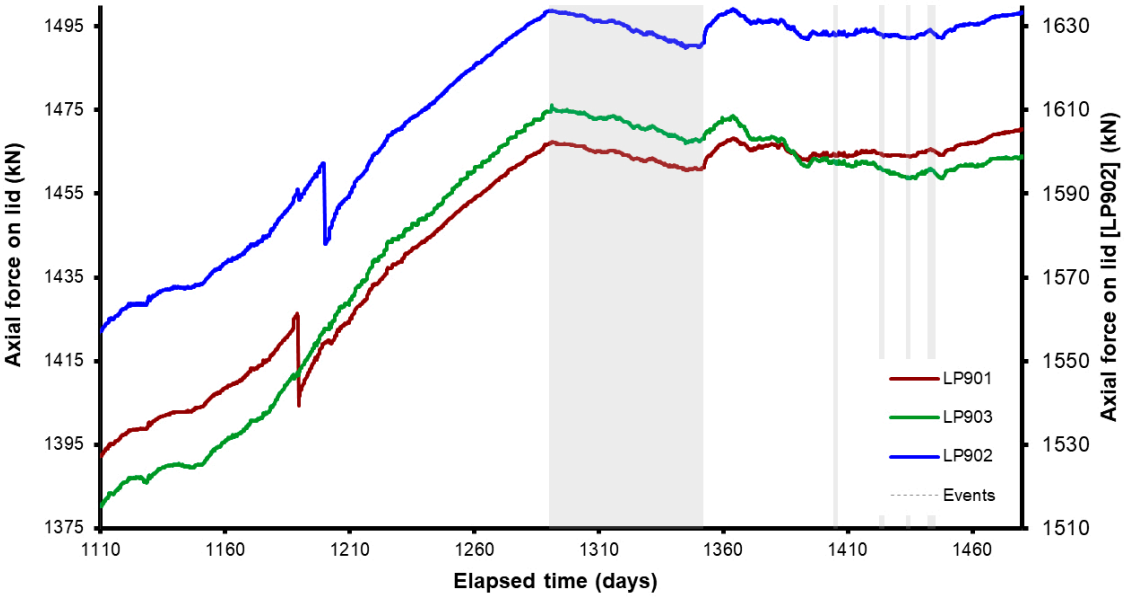

Figure 7-27. *Axial force acting on the steel lid measured by 3 Glötzl load cells attached to separate rock anchors.*

Careful observations have been made of axial force once the compressor was replaced on Day 1351. The improved daily quality control check of the data allowed all parameters to be cross checked easily. As shown in Figure 7-28 it was noted that the changes in axial force closely correlated with the temperature observed within the HRL. This can be explained by either the temperature dependency of the Glötzl cells or the thermal expansion of other system components (e.g. steel lid, tie rods). However, it is highly probable that the observed effect relates to the Glötzl cells, which operated by measuring the pressure of a reservoir of fluid within the device. While the transducers were thermally compensated, there was no allowance for the thermal expansion/contraction of the fluid.

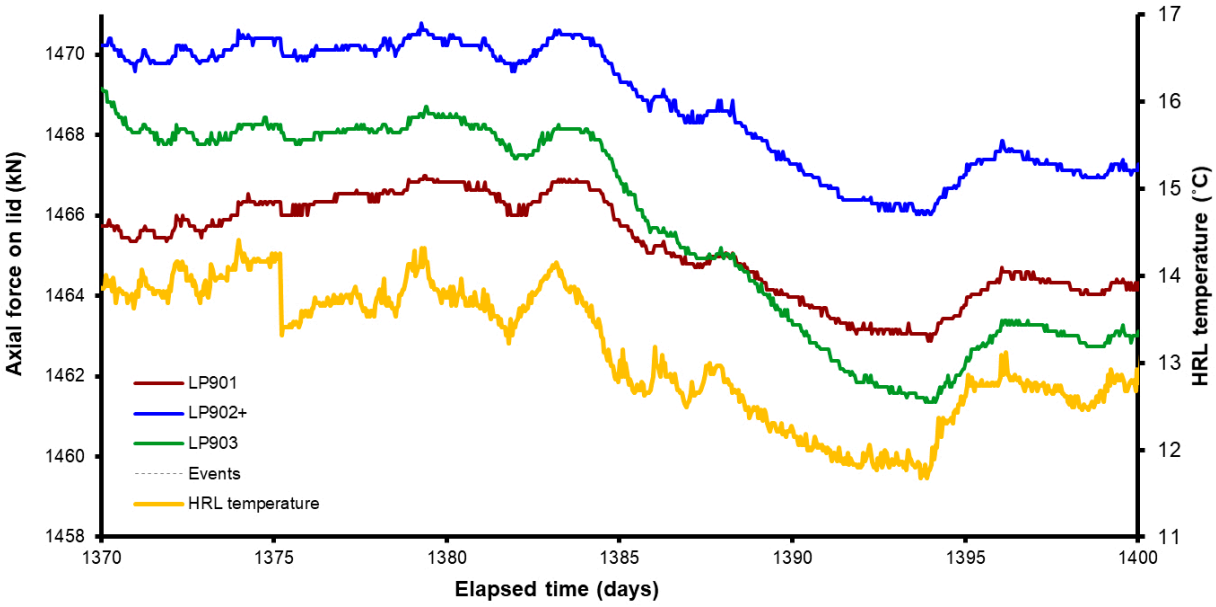

Figure 7-28. *Axial force acting on the steel lid plotted with temperature of the HRL.*

7.7 Displacement of lid and canister

Data from sensors DP901 to DP905 are plotted in Figure 7-29a, while lateral movement is shown in Figure 7-29b. Sensors DP902–905 continuously monitored movement of the steel lid relative to both the gallery floor and ceiling whilst DP901, attached to the Monel pipe and lid, gave relative changes in canister position. As shown, sensors DP902–DP905 showed similar results, in general mirroring one another up to the point when artificial hydration stopped at Day 1289[2]. This shows that the lid movement was homogeneous, indicating the even movement of the lid as the bentonite swelled within the hole. Whilst this observation may appear counterintuitive given the non-uniform distribution of axial stress within the hole, it can be explained as non-uniform stresses acting on the base of the rigid concrete plug which then behaved as a piston resulting in uniform displacement of the lid.

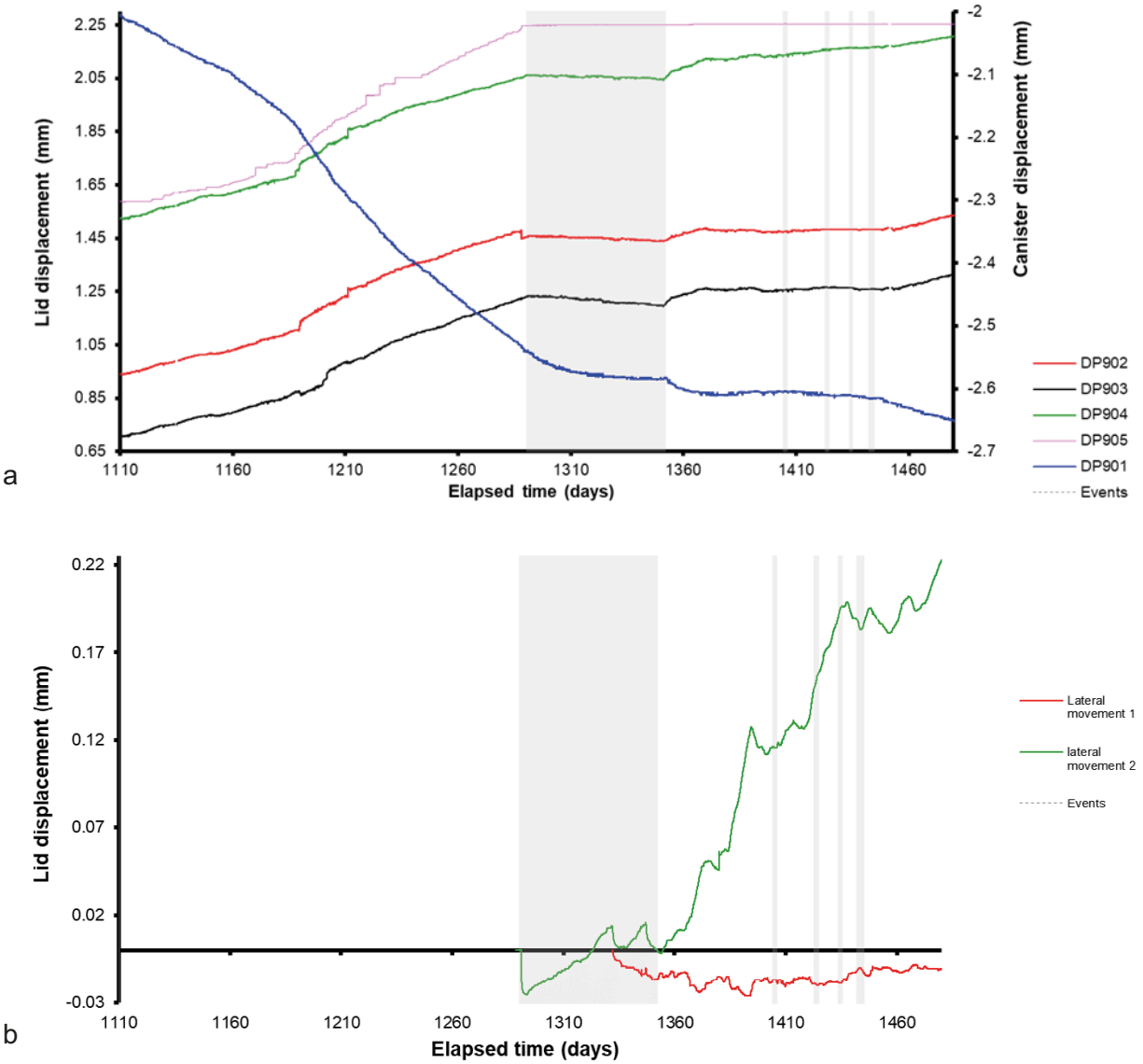

Figure 7-29. *Linear displacement of the steel lid and copper canister. a) Movements of the lid were measured relative to both the gallery floor and ceiling. Movements of the canister were measured relative to the steel lid. b) lateral movement of the lid.*

[2] The exception to this occurs at Day 1192 in DP903, when it showed a reduction in displacement in contrast to all other sensors that exhibit an increase in value. This could be explained by tilting of the lid.

As shown in Figure 7-30, data for DP905[3] showed stick-slip movement of the lid throughout this period of testing. These small displacements were not always accompanied by movement recorded by the three displacement transducers at the edge of the lid (DP902 – DP904). This suggests that the lid was buckling with the central portion bowing upwards. The data could also be explained by movement of the gallery roof, which was initially assumed to be static. However, with blasting occurring during this stage of experimentation it is possible that movement of the gallery roof had indeed taken place (Day 1105 – 1107, 1113). Since stick-slip movements occurred with regular frequency it was possible to correlate some with the blasting events. However, the vast majority of movements occurred when no blasting took place. This scenario (i.e. movement of the roof) was discounted by examination of data accrued during the compressor failure and the accompanying cessation in artificial hydration. During this period the lid remained relatively stationary, with a small decline in height, for a prolonged period of time, strongly suggesting that the vast majority of observed deformations were as a direct result of lid movement and not the roof.

It can be seen that the three displacement transducers around the edge of the canister lid all showed a slight reduction in lid height during the cessation of artificial hydration. During the same period, the high-resolution lid to gallery roof transducer (DP905), showed no reduction in height and remained constant, with the exception of one slip event.

Considerable effort has been afforded to studying the movement of the lid. To aide this process, it was decided to add lateral displacement sensors in order to be able to describe fully in 3-D the movement of the lid (Figure 7-29b). While movement of the lid may be viewed as a secondary issue (i.e. merely offering confining pressure to the experiment), it is in fact a vital component, dictating the boundary condition to the test. Changes to this boundary will impact on both the results of gas injection and the subsequent modelling of the data.

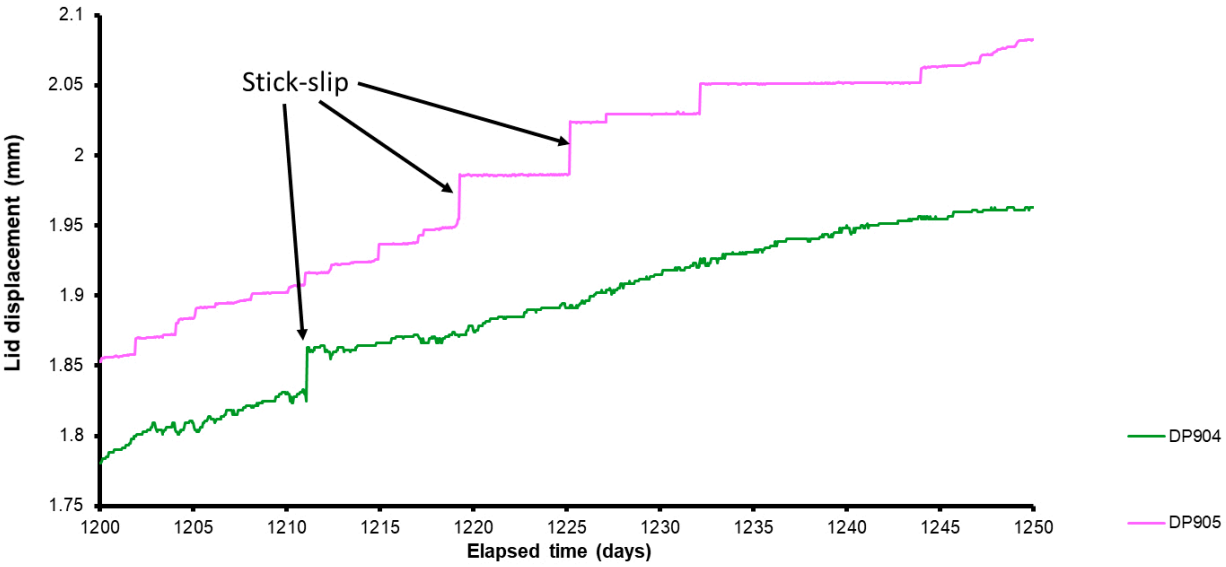

Figure 7-30. *Illustration of stick-slip movement of the canister lid from sensors DP904 and DP905.*

[3] DP905 is the sensor measuring the gallery roof to the centre of the lid and had the highest resolution of the displacement sensors.

It can be seen that when the compressor failed at Day 1289 the lid slowly settled as the stresses within the hole changed. Once the compressor was re-started at Day 1351 the lid quickly began to move at a similar gradient of that observed prior to compressor failure, but within 20 days reached a plateau which continued to Day 1440, when sensors started to increase or decrease once more. This suggests that the system exhibited considerable hysteresis with all of the sensors showing increasing displacement by the end of the stage. This type of behaviour had previously been reported by Harrington and Horseman (2003).

During the current period, the canister continued to drop relative to the lid, with over 0.6 mm of movement observed. This strongly indicated that preferential swelling of the clay had occurred above the canister. Intuitively this was to be expected given the availability of water from the artificial hydration system located in the upper section of the deposition hole.

7.8 Laboratory utilities

Temperature in the Gas Laboratory, canister, and Assembly Hall area were continuously monitored by a series of thermocouples (Figure 7-31). Apart from minor failures of the air-conditioning system at elapsed times of Day 1317 and Day 1324, temperature within the laboratory was continuously controlled. However, the air conditioning unit had not performed consistently during this reporting period. It can be seen that the temperature in the office area was very stable between Days 1110 – 1186 and Days 1331 – 1380. Between Day 1186 and Day 1331 temperature varied by over a degree. Temperature within the laboratory had been variable throughout the period and correlates with the temperature within the HRL, which shows a clear annual variation, cycling between ~ 10 °C and 16 °C. The canister also showed an annual variation, but with a much smaller range of 12.8 °C to 13.6 °C, and with a phase offset of about 90 days from the HRL temperature data.

Analysis of step changes in laboratory temperature (e.g. Day 745.0) show that these events had no significant effect on any of the sensor outputs recorded within the lab. Almost all recorded devices were either thermally compensated (pressure transducers) or use an internal thermocouple located with the device (e.g. all Geokon equipment) to correct for minor changes in temperature. However, when temperature was "noisy" the flow data from the ISCO syringe pumps also increased in noise.

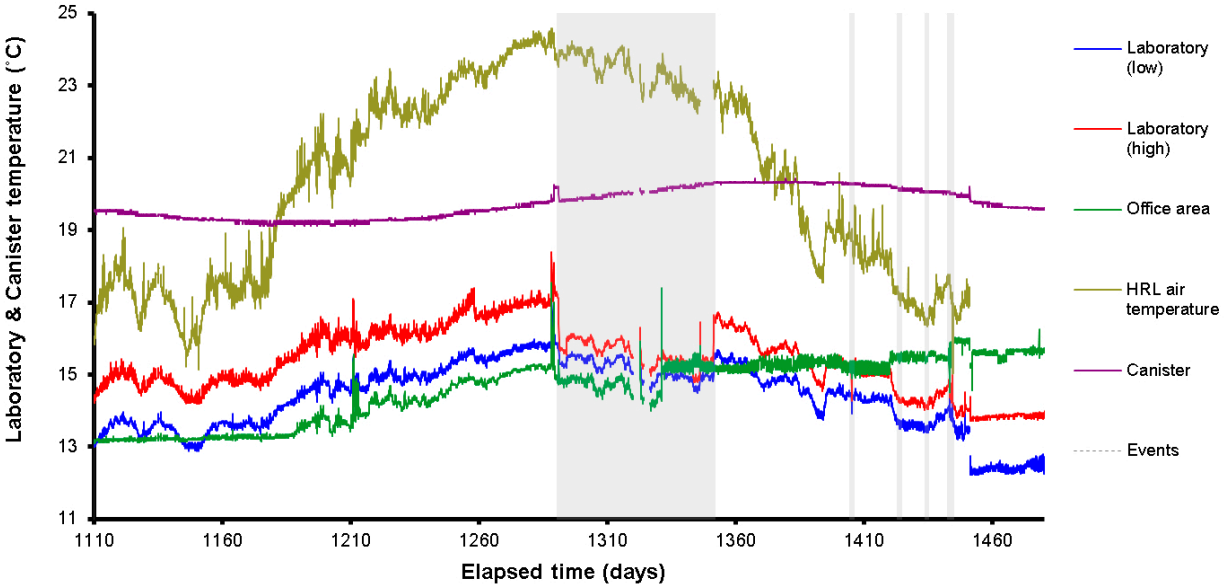

Figure 7-31. *Temperatures recorded in the Gas Laboratory, office, canister, and HRL.*

Figure 7-32a shows the total volume of water pumped into the Lasgit system during artificial hydration. As shown, a total of 7.048 litres was pumped in during the current period. Figure 7-32b shows the flowrate into the system during artificial hydration. As can be seen, when hydration was restarted after the compressor failure the flow rate into the system was much greater than before the failure and remained higher all through the rest of the stage, although it was reducing towards a similar flow of that seen before the failure.

Averages can be calculated for each set of parameters (Figure 7-33). Apart from the variation caused by the compressor failure and the pause of artificial hydration, all parameters remained relatively static throughout the current stage. Some annual variation can be seen in individual channels, such as stress on the canister. Pore water pressure at the rock-wall and within the pressure relief holes continued to decline, while pore water pressure within the bentonite remained low. Considerable heterogeneity persisted within the deposition hole.

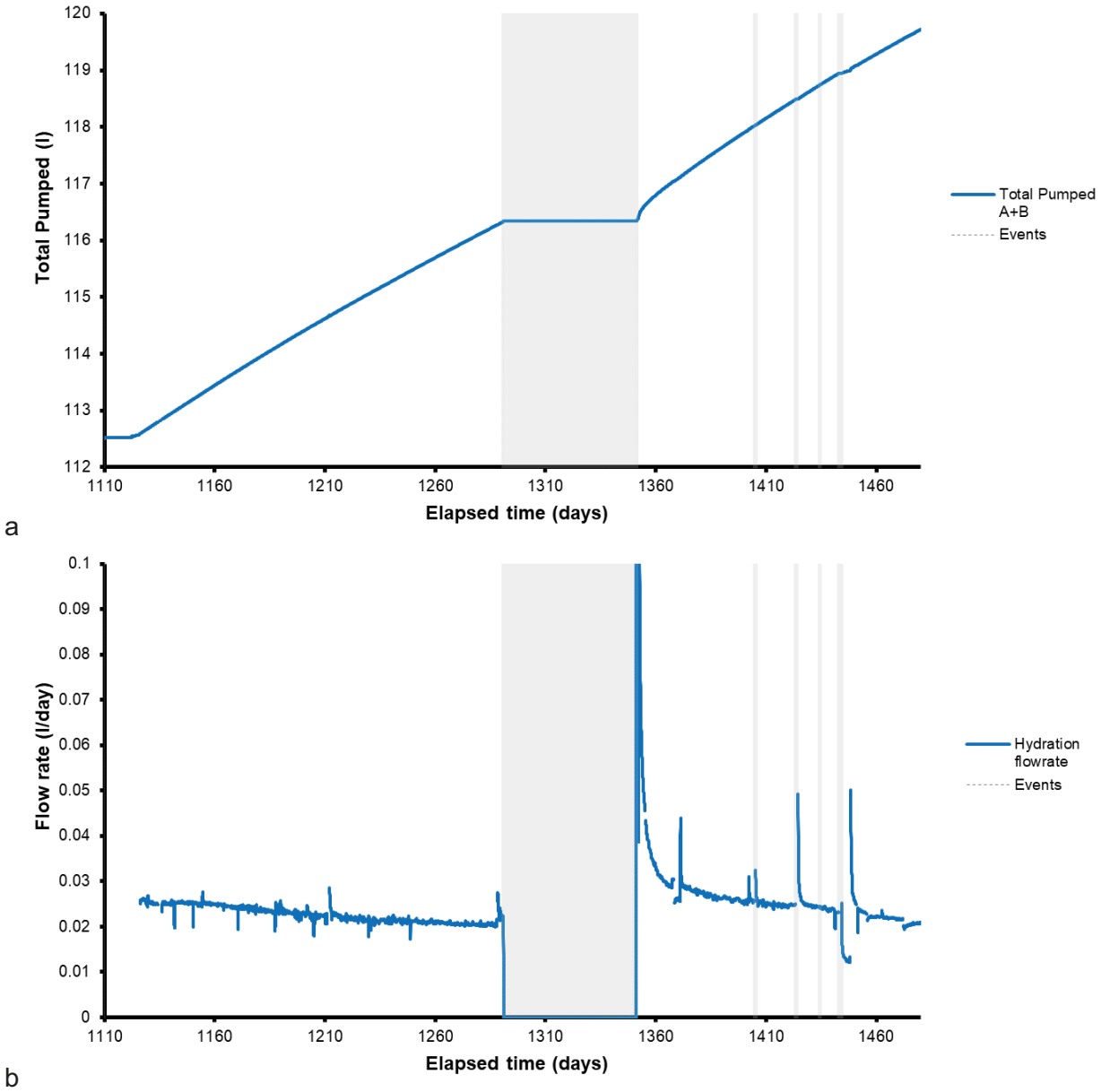

Figure 7-32. *Total volume of water pumped into the system during hydration stage 2 (a). b) hydration flow rate.*

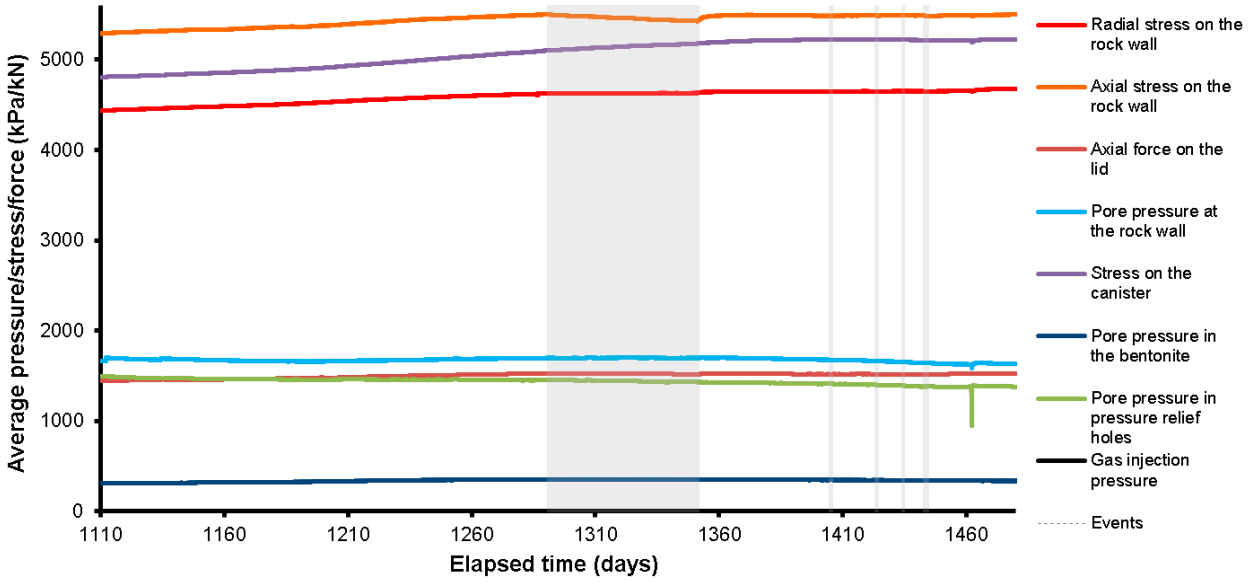

Figure 7-33. *Plot showing the variation in average stress and pressure readings.*

7.9 Summary of hydration stage 2

The second stage of artificial hydration began on Day 1110. This was interrupted by the failure of the Spiralair KS1/T compressor on Day 1289, which caused all air actuated valves to close and effectively shut-off the down-hole filter mats from the laboratory, preventing continued artificial hydration of the clay. Whilst this situation was not ideal, it allowed the pressure decay in all filters to be observed, giving an unplanned observation of the state of hydration of the bentonite buffer.

During this time, considerable decreases in pressure were observed with one of the smallest filters, the 5 mm radius FL902, recording a reduction of pressure of over 85 % from 2 235 to 380 kPa. The pressure at the two circular filter mats reduced from approximately 2 500 to 1 500 kPa. Filter mat FR902 decreased very rapidly from 2 500 kPa to an eventual asymptote of ~400 kPa; this was a decrease of almost 84 % and was equal to the pore pressure at the corresponding depth in the pressure relief holes. Filter mat FR901 showed no influence of the compressor failure as it was isolated from artificial hydration. It should be noted that pressure changes would be affected by local variations in the saturation state of the clay, which may help to explain anomalously large decrease in pressure for certain filters.

Data from the canister filters during the compressor failure event were also interpreted using the same 2D finite element model. Good model fits were achieved for most of the filters, which suggested that the transient behaviour could be captured in terms of a single hydraulic transport coefficient and a single hydraulic storage coefficient. The upper filters generally indicated higher values for permeability and specific storage than elsewhere in the system, ranging from 9×10^{-21} to 50×10^{-21} m^2. The parameter values obtained for filters FL901 and FL904 (8×10^{-21} and 13.5×10^{-21} m^2 respectively) were quite similar to those from the hydraulic test earlier, indicating that little change had occurred since this time.

Monitored porewater pressures within the bentonite had significantly increased during the test but remained relatively low ranging from 250 to 685 kPa. This was in contrast to the water pressure measured at the face of the deposition hole which ranged from 1 025 to 2 555 kPa. However, three sensors in the clay showed a slow decrease in pressure initiated at approximately Day 1240, a time before the compressor failed.

Suction had decreased throughout the experiment confirming the ongoing hydration of the clay, though the rate of hydration appeared to be slowing. Greatest progress had been made near to the large filter mats above the canister, whilst the least progress had occurred just below the canister. While some of psychrometers appeared to be levelling (e.g. WB906), close inspection of the data revealed a general continuous downward trend, indicating that most of the clay remained in a state of suction.

Pore pressure at the rock wall greatly increased in response to the commissioning of the packers. Since this time, pore pressure had slowly decayed, ranging between 1 025 and 2 555 kPa. During hydration stage 2, four pressure "break-throughs" were observed in three of the sensors. The events in UR907 and UR910 resulted in similar total pressures, both of which were significantly higher than the pressure imposed by the artificial hydration system. The third event, which also occurred in UR910, caused a less pronounced change, resulting in a small progressive increase in pressure over a ten-day period. This was followed by pressure decay similar in manner to UR907. The final event occurred in UR903 on Day 1368 when a pressure drop of approximately 100 kPa occurred. Close examination of all available data shows that these four events were real and not symptomatic of sensor failure.

The presence of mapped or extrapolated fractures close to the three pore pressure sensors that displayed break-through (UR903, UR907, and UR910) suggested that these fractures played a significant role in the observed behaviour. Mechanistically, it is hard to conceive of an event within the deposition hole that could result in the generation of porewater pressures that were significantly in excess of those imposed through the artificial hydration system. It seems more probable that events outside of the Lasgit deposition hole were in some way responsible for the behaviour seen. While a direct correlation to external events such as blasting could not be made, it is reassuring to note that the measurement system within the deposition hole was sufficiently sensitive to register these events.

The total pressure sensors mounted on the rock wall showed a slow increase in total stress during the experiment to range between 1 890 and 5 850 kPa. The spatial and temporal evolution in radial stress measured at the rock wall showed no significant variation in radial stress during the current stage. The spatial distribution of effective stress remained fairly constant with only small variations noted, primarily caused by the spontaneous increases in porewater pressure. Effective stress generally changed around the circumference of the depositional hole and did not exhibit any significant correlation to depth.

Axial stress monitored within the clay had also increased steadily to range from 4 770 to 6 480 kPa. The data clearly shows a non-uniform distribution of axial stress across the major axis of the emplacement hole. The effect of the compressor failure was complex with two sensors having no change, whilst other sensors exhibited either an absolute decrease in total stress or a reduction in the rate of stress increase. The most prominent stress drop occurred at the interface between the bentonite buffer and the concrete plug (PB927), with a near 350 kPa reduction from 6 565 to 6 215 kPa. However, sensors PB928 and PB929 showed very small pressure drops suggesting that stress at the top of the bentonite had become very heterogeneous, but this may be due to the foot-print of FB904. Axial stress was quick to recover after artificial hydration was re-started at Day 1351. By the end of the stage, most of the stress sensors had reached a plateau, albeit at a magnitude below that in the corresponding sensors at the time of the compressor failure.

Stress measurements on the canister surface indicate that radial and axial stress varied between 5 055 and 5 385 kPa, which was comparable with the average value of radial stress monitored on the rock face. The increases in radial stresses mirrored one another, while axial stress had increased at a much greater rate, such that it represented the intermediate principal stress acting on the canister.

The axial force acting on the steel lid was now greater than the initial pre-stressing value applied during the installation phase and ranged between 1 465 and 1 630 kPa. Since the installation and closure of packers into the pressure relief holes there had been a marked rise in the axial force acting on the lid. There is also strong evidence in later data for the stick slip movement of the conical concrete plug.

8 Gas Injection Test 2 (Day 1472 – 2084)

The second significant stage of the Lasgit experiment started on Day 1472.27 (12th February, 2009) and was completed at Day 2086.23 (18th October, 2010); a total stage time of 613.96 days.

Following a year of continued natural and artificial hydration, it was decided to repeat the gas test in filter FL903, which was located towards the bottom of the canister. One question arising from Gas Injection Test 1 was whether the gas "escaped from" the deposition hole. In order to address this in Gas Injection Test 2, neon was selected as the test permeant, to facilitate tracking of the gas through the host rock by gas sampling of the packered intervals in the two pressure relief holes; neon is absent in the natural pore waters of the Äspö Hard Rock Laboratory. This repeat test of FL903 would also investigate whether gas properties of the bentonite had changed with time. Figure 8-1 shows the plan of the test period. Throughout the stage, artificial and natural hydration was occurring. Between Day 1472.27 and Day 2019.02 (~547 d) the second gas injection test was conducted. The remainder of the stage (67 d) could be described as recovery before the next stage of testing commenced.

Gas Injection Test 2 comprised of four stages (Figure 8-2); 1) a two-stage hydraulic test to determine the hydraulic properties of the bentonite at filter FL903; 2) four-stage gas injection ramp to achieve gas entry at filter FL903; 3) continued gas injection for a prolonged time period in order to observe the movement of gas within the deposition hole; 4) a repeat two-stage hydraulic test to determine the hydraulic properties of the bentonite at filter FL903.

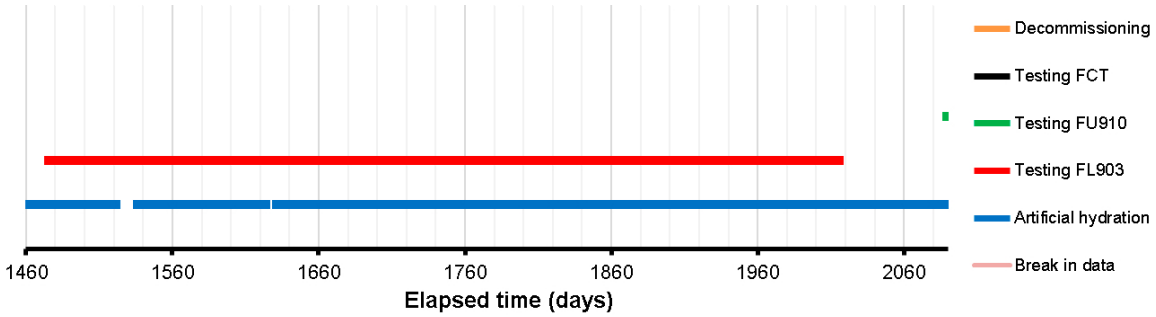

Figure 8-1. *Test stages of the Lasgit experiment during Gas Injection Test 2.*

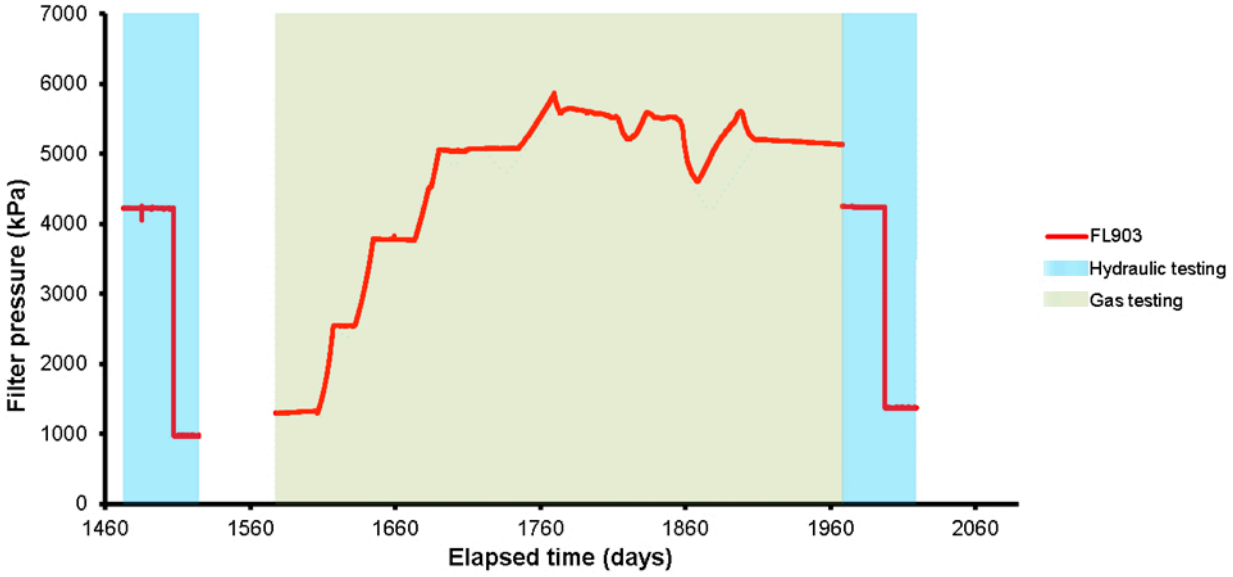

Figure 8-2. *The filter pressure of FL903 during Gas Injection Test 2. Two two-stage hydraulic tests were conducted either side of four stage gas injection test.* ***Note:*** *blue shading shows periods of hydraulic testing, green shows gas testing.*

8.1 Description of the field parameters during the period

Before describing the gas injection test, the field parameters will be described (boundary conditions). **Note:** The grey areas displayed in the graphs shows periods when artificial hydration was not occurring.

Figure 8-3 shows the pore fluid pressure of the filter mats. As with previous stages, filter FR901 was not artificially hydrated and recorded local pore pressure. As seen, FR901 slowly decayed during the period, indicative of drawdown of the pore pressure as a result of proximity to the drained tunnels. The remaining filters were all artificially hydrated at a nominal pore pressure of 2 500 kPa. At Day 1524.60 the logging computer failed and the pneumatic valves operating the filters closed. When the computer was re-started at Day 1533.04 it was noted that filter FR902 had lost over 1 500 kPa of pressure in just 9 days. It was decided to reinitiate hydration in just this filter and to observe the pressure decay in filters FB903 and FB904. As can be seen, these continued to decay, with hydration restarted at Day 1543.02 and Day 1554.04 for filters FB903 and FB904 respectively. Compressed air was lost to the pneumatic valves at Day 1572.02, resulting in a short term (less than 2 hour) loss of hydration and a quick reduction in filter pressure. The final event of note occurred at the start of the second hydraulic test of the stage at Day 1967.27. Artificial hydration of filter FB904 was stopped and the pressure within the filter allowed to equilibrate. This led to a rapid reduction in pressure to a steady 590 kPa. Hydration of this filter mat was resumed at Day 2067.06.

Figure 8-4 shows the pore pressure within the bentonite buffer, recorded at six locations. Figure 8-4a shows the results are dominated by pressurisation of filter UB902 during the gas injection stage of this test; this is described in Section 8.3. Figure 8-4b shows that initially, UB902, UB925, and UB926 were all reducing, while UB901, UB923, and UB924 were either steady or increasing. Sensor UB901 increased from a starting 570 kPa, to reach a peak of around 750 kPa at approximately Day 2020. Filter UB924 showed two peaks in pore pressure. The first occurred around Day 1715 at 460 kPa, with second reaching 570 kPa at Day 2070. These two peaks are approximately 357 days apart and may suggest an annual cyclicity. Similar, but lower magnitude, increases in pore pressure were observed in sensor UB923. Throughout the stage, the pore pressure at UB925 continued to reduce, from a starting 300 kPa to an end of 285 kPa. Sensor UB926 displayed a similar rate of pressure reduction. However, around Day 2060 the pore pressure at this locality increased, peaking at 305 kPa at Day 2078.

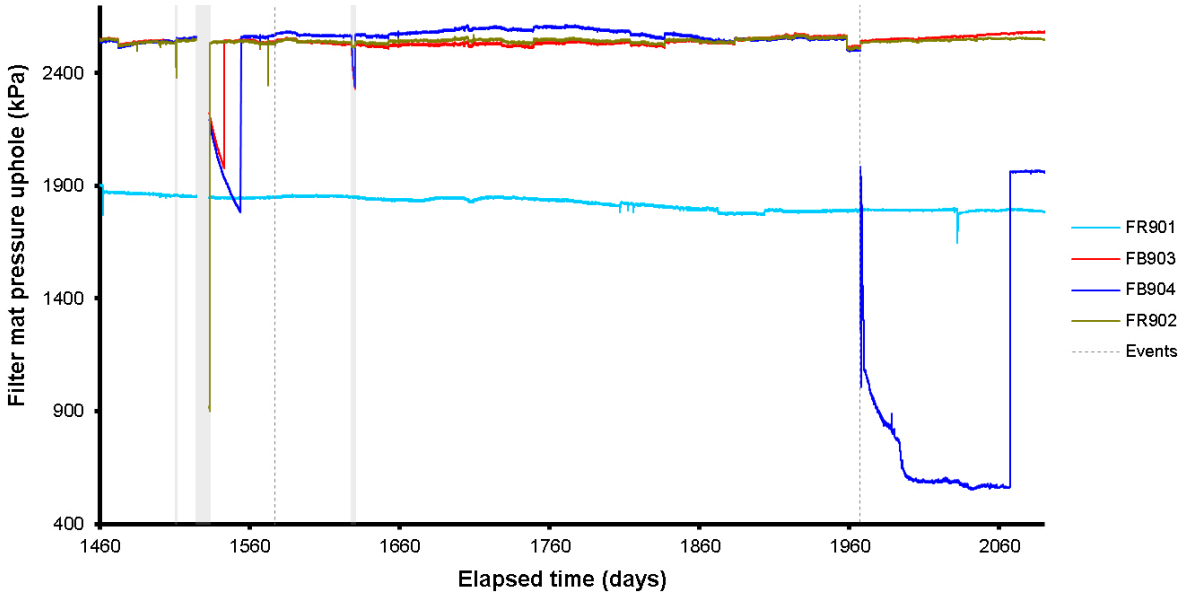

Figure 8-3. *Evolution of water pressure in the filter mats located on the borehole wall and within the bentonite blocks.*

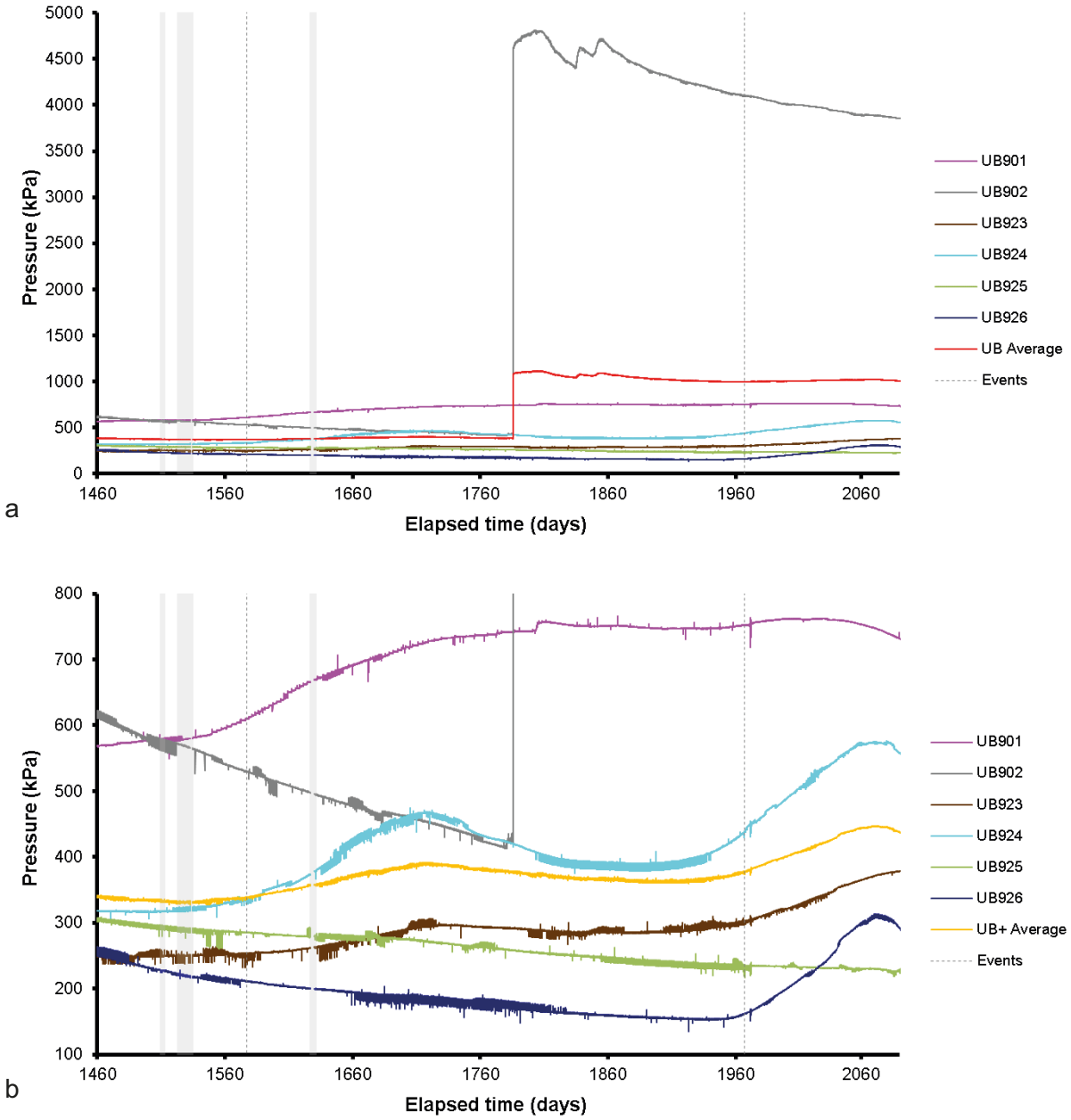

Figure 8-4. *Variation in porewater pressure within the bentonite at the 6 monitoring points: a) all six sensors; b) detail of five sensors.*

Pore pressure within the bentonite (UB) shows clear coupling, as seen by the similarities in pore pressure increases, i.e. similarity in UB924 and UB923, and shows clear differences. This includes a considerable spread in pore pressure within the deposition hole, and sensor UB925 not showing the peaks in pore pressure seen at the other sensor locations.

Pore pressure is also recorded at the canister filters when these are not used for artificial hydration of the system. Figure 8-5a shows that the data during this period is dominated by the operation of filter FL903 for the hydraulic and gas injection testing, along with the pressurisation of filter FL901; this will be discussed in Section 8.3. Figure 8-5b shows that mid-plane filters were artificially hydrated, while the upper and lower array of filters were shut-in. The upper array of filters rapidly decayed from the nominal hydration pressure of 2 500 kPa to around 1 000 kPa, with annual variation seen. The lower array of filters showed distinctly different behaviour. Filters FL901, FL902, and FL904 all decayed in a similar manner to the mid-plane filters but with considerable heterogeneity on the same level. Filters FL902 and FL904 both decayed to around 500 kPa. However, filter FL902 recovered to 1 100 kPa by Day 2067 when artificial hydration was re-started. It should be noted that the pressure increase in FL902 was not smooth and showed noise, in contrast to all other filters. Filter FL901 only decayed to 1 000 kPa, showing a difference in pore pressure of 405 kPa at the lower array at Day 1171.00 when filter FL901 was pressurised by gas (discussed later). This compares with a difference of only 175 kPa in the upper array of filters, all of which in contrast to the lower array of filters mirror one another. It should be noted that filters FL902 and FL904 were re-pressurised to the nominal artificial hydration pressure of 2 500 kPa at Day 1485.04 before the pressure decay was complete.

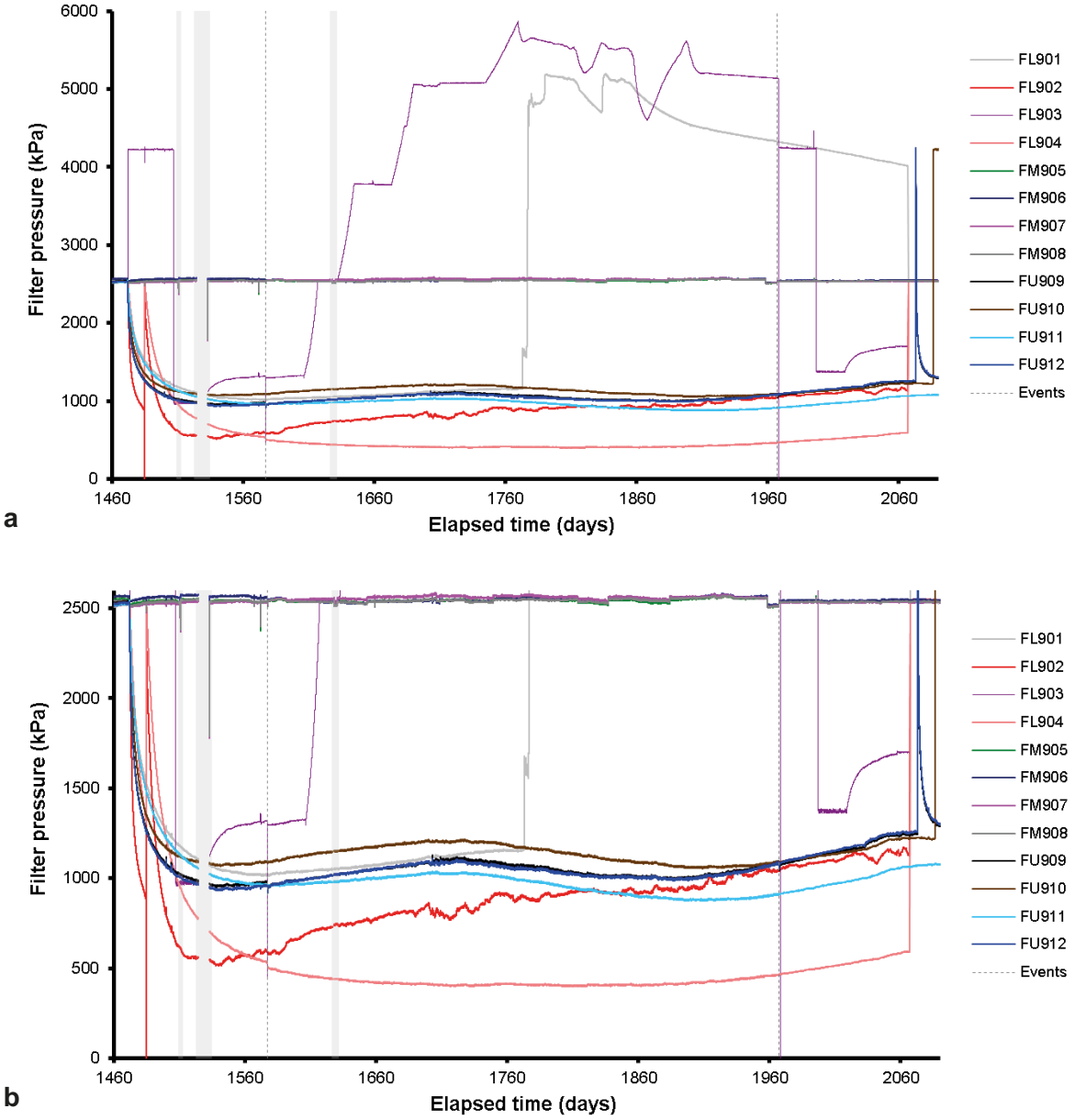

Figure 8-5. *Filter pressures on the canister surface. a) complete range of filter pressures dominated by the activities in filter FL903; b) detail of the pore pressures in the canister filters.*

Figure 8-6 shows the variation of pore water pressure at the rock wall. As can be seen, pressure is heterogeneous within the deposition hole, with around 1 500 kPa variation. The data is dominated by two features; increases in pore fluid pressure for UR907 & UR909, and annual cyclicity differences throughout the deposition hole.

Two increases in pore fluid pressure were seen (Figure 8-6). The first occurred at UR907, when pore pressure increased nearly 500 kPa from 2 245 to 2 735 kPa around Day 1770. In detail, a small increase (~35 kPa) in pore pressure was first seen at UR905 at Day 1770.70. This started the pore pressure in UR907 to increase, with an almost instantaneous increase of 450 kPa occurring at Day 1771.05. At this time, a small increase also occurred in UR905 and it is just apparent that small increases or decreases occurred at other localities, most notably a variation at UR909. Following this large instantaneous increase in pore fluid pressure, UR905 and UR907 decayed. The second pore pressure increase was more instantaneous and occurred in UR909. Pore pressure increased by nearly 600 kPa at Day 1832.82. Following this rise in pore pressure, UB909 slowly decayed. Again, it is just apparent that small increases or decreases occurred at other localities within the sensor array.

Considerable heterogeneity is seen in the distribution of pore fluid pressure within the deposition hole (see Figure 8-6). Generally, pore pressure was greatest at the base of the deposition hole, decreasing with height up the deposition hole. This holds for all levels, except for the bottom UR level within bentonite ring 4 (R4), which was lower in pressure than the level in ring 5 (R5) and similar to that of ring 7 (R7). It is also noted that the pore pressure cyclicity, with a period of a year, was greatest in the middle of the array of sensors, located at the canisters middle. Here, the variation in pore pressure within the level was also greatest, with around 1 000 kPa variation. Pore pressure variation was least at the base of the deposition hole, where the wall rock had a greater numbers of fractures. Also of note is sensor UR910 (black line in Figure 8-6) where the "noise" of the sensor changed from Day 1970 onwards.

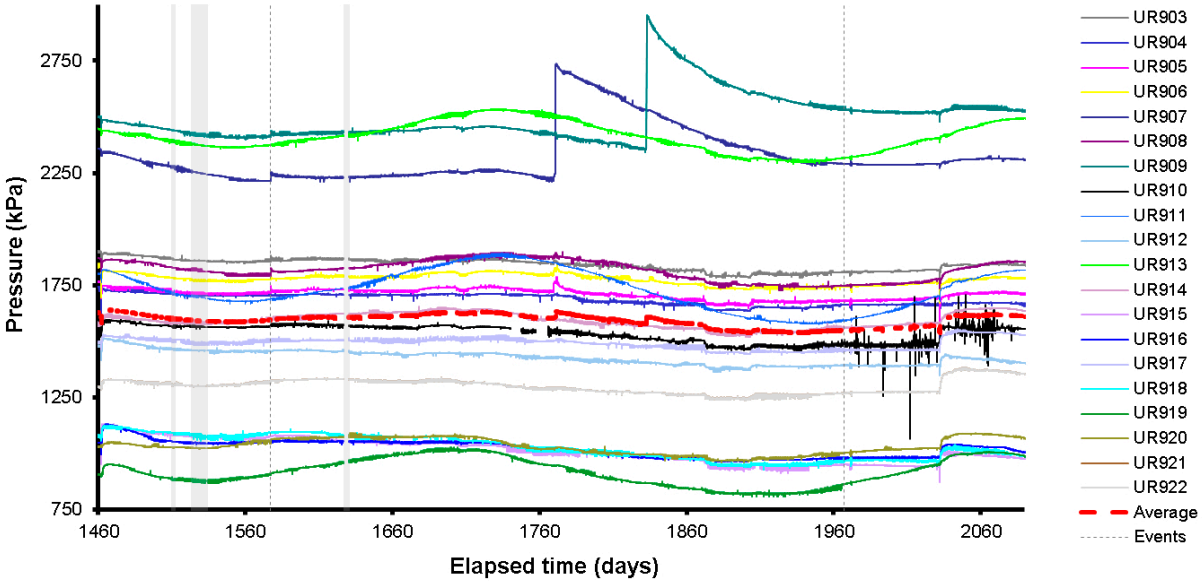

Figure 8-6. *Variation in porewater pressure with time measured at the rock face.*

Radial stress measured at the rock wall is shown in Figure 8-7a for all locations and Figure 8-7b in detail for all sensors excluding PR921. As seen, radial stress increased over the period, with a annual variation seen superimposed. The radial stress within the bottom of the deposition hole was greatest in bentonite rings 4 and 5 (R4–5), with the lowest stress seen in the top of the deposition hole within bentonite ring 10 (R10). There was additional heterogeneity within the deposition hole, with the greatest range seen within R10 with a 3 000 kPa variation, although it should be noted this level included the low stress value seen in PR921. The next greatest variation of nearly 2 000 kPa was seen centrally within the deposition hole at bentonite ring 7 (R7). The lowest variation at a height basis was seen at the bottom of the hole at R4 and towards the top of the hole at ring R9.

On a shorter time consideration, there are a couple of stress variations seen. The event highlighted at Day 1577 signifies the start of the gas injection test when the canister filter was flushed of water using gas in order to ensure that the filter lines were only filled with gas. During this process, it was necessary to lower the fluid pressure in the filter FL903. This resulted in small increases in radial stress during this operation. The second increase in radial stress occurred at Day 1770.70 with small increases in most locations. This corresponds with the first instance of pore pressure increase in pore pressure at the rock wall (UR905). The final variation occurred at Day 2033 when stress changes occurred at most locations. This does not appear to correspond to any operational change of the system.

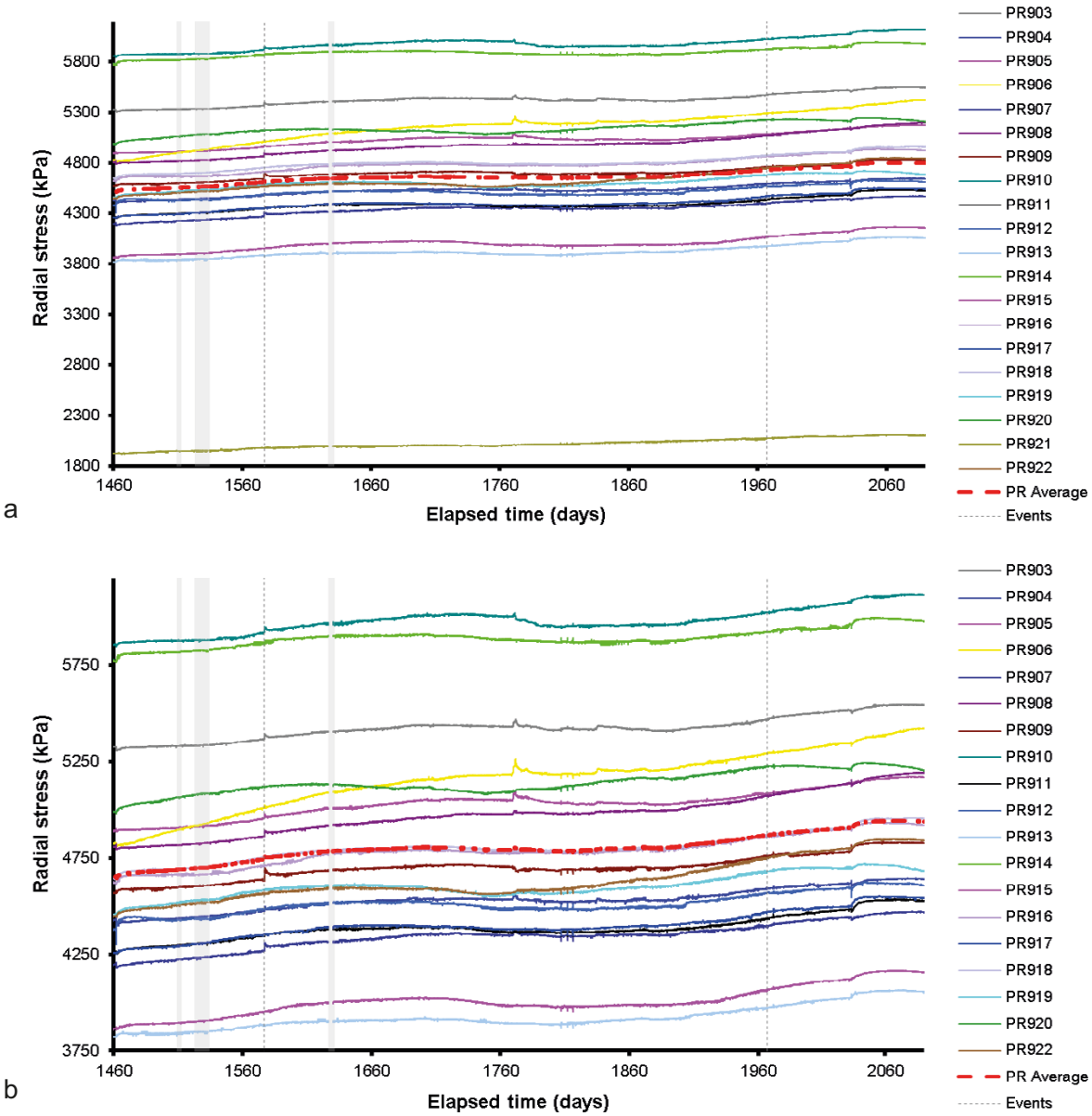

Figure 8-7. *Variation in radial stress at the rock wall with time. a) radial stress for all locations; b) radial stress for all locations excluding PR921.*

The stress acting on the canister was measured at three locations, as shown in Figure 8-8. Over the period the average stress increased around 400 kPa, with annual variation superimposed. Sensors PC902 and PC903 mirror one another well, with the greatest increase seen in PC901. The increase in stress noted above for the radial stresses on the rock wall at Day 2033 was also seen in all three canister stresses, showing that the variation was seen throughout the bentonite buffer.

Axial stress within the bentonite is shown in Figure 8-9. This shows considerable spread of approximately 1 600 kPa within the deposition hole. All locations showed a degree of annual cyclicity, expect for PB927 and PB902, both of which were relatively static throughout the period. Generally, axial stress was lowest at the base of the deposition hole within the bottom segment of the bentonite buffer. Stress within the upper most section of the hole within segment 5 (C5) was generally constant throughout the period and averaged around 5 800 kPa, whereas stress increased within segments 1 and 3 (C1, C3).

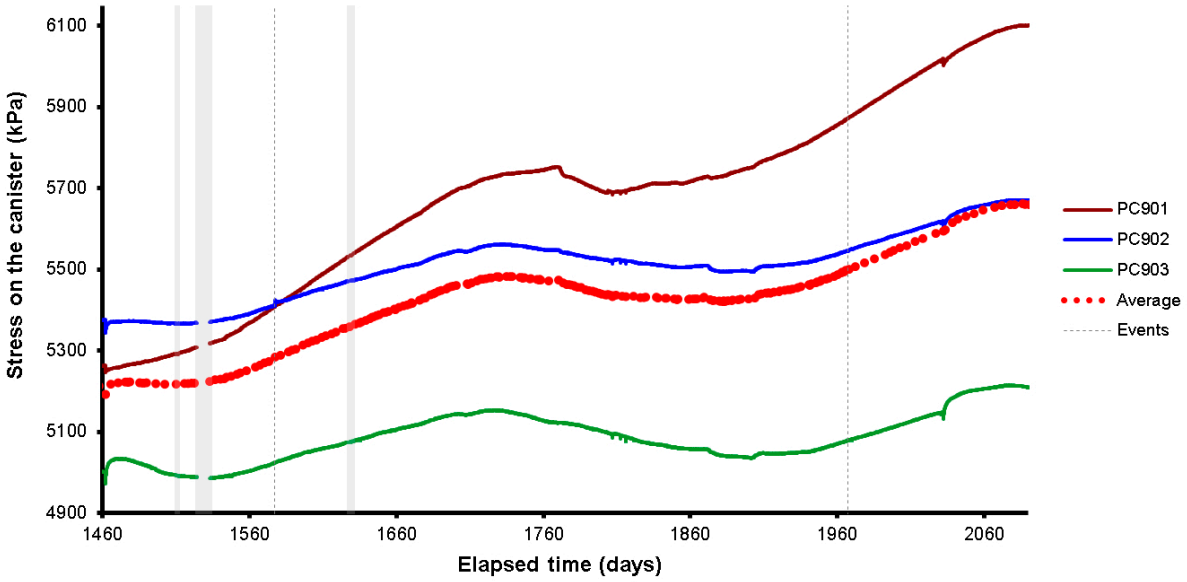

Figure 8-8. *Development of axial and radial pressure on the side and base of canister.*

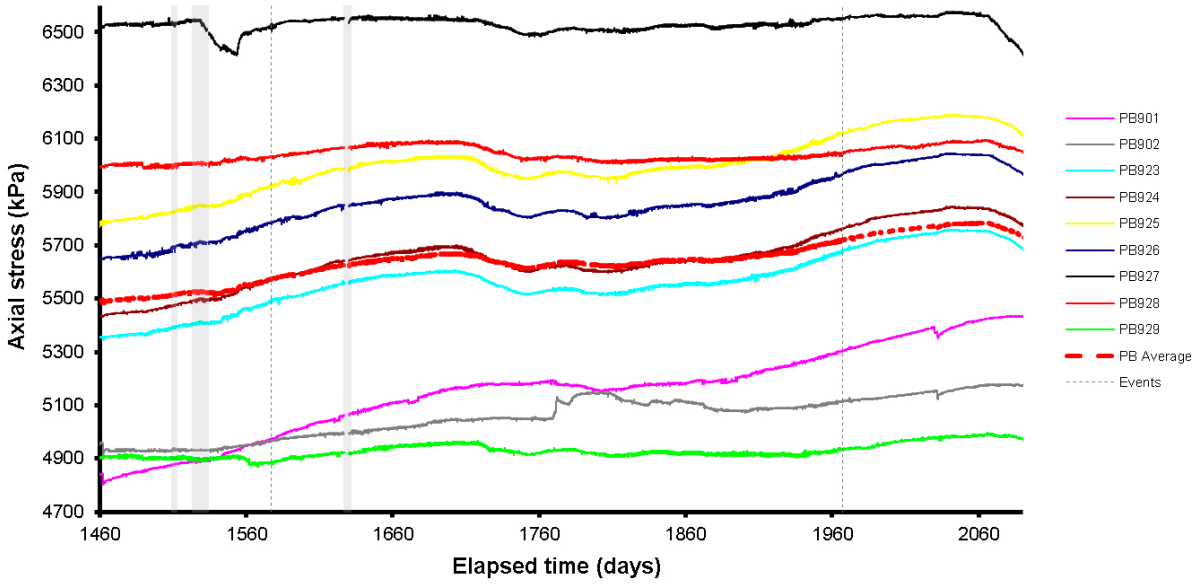

Figure 8-9. *Development of axial stress measured at 9 locations within the buffer.*

The increase of stress within the bentonite was mirrored in the axial force measured on the lid, as shown in Figure 8-10. Annual variation is again observed, with a general increase of approximately 100 kPa. A similar trend was seen within the sensors measuring the displacement, as shown in Figure 8-11a. During the period approximately 1.5 mm displacement was observed vertically. The canister was seen to move downwards by 0.8 mm, driven by artificial hydration within the bentonite segments at the top of the deposition hole. Lateral movement of the lid (Figure 8-11b) only showed small movements of less than a quarter of a millimetre. Lateral movement sensor No. 2 shows distinctive annual variation, whereas Lateral movement sensor No. 1 does not. The latter shows significantly less movement than the former. Lateral movement sensor No. 1 shows a small instantaneous movement at Day 1967.33. This occurred during calibration and as Lateral movement sensor No. 1 does not show any movement is likely to be the sensor being accidentally disturbed during the site visit.

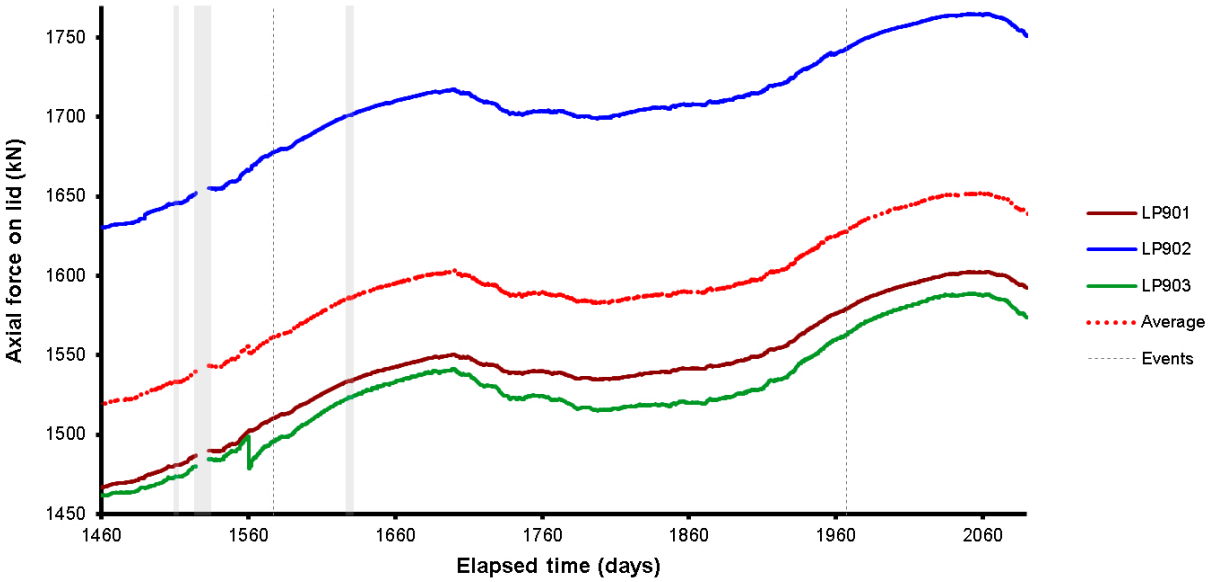

Figure 8-10. *Axial force acting on the steel lid measured by 3 Glötzl load cells attached to separate rock anchors.*

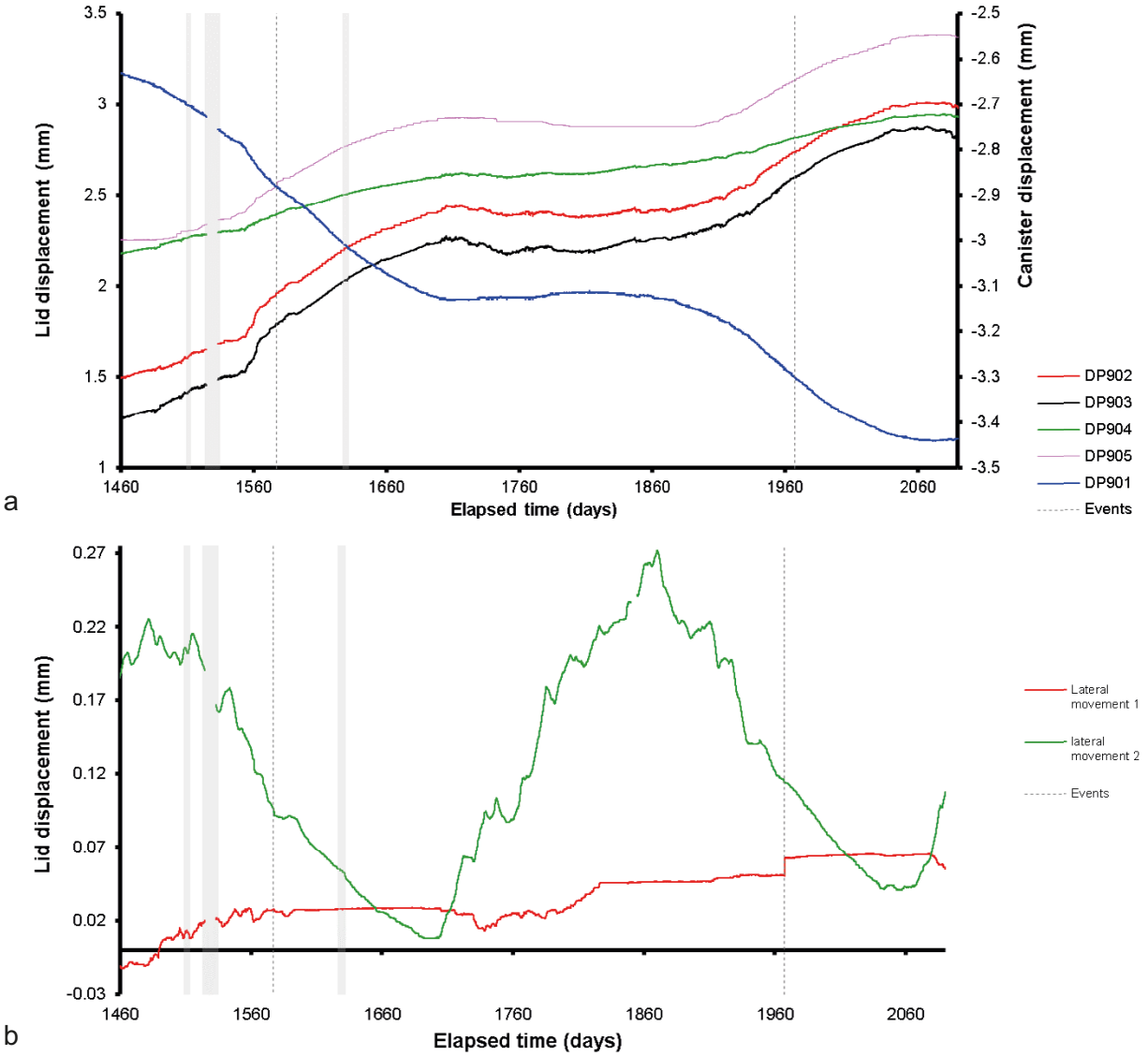

Figure 8-11. *Linear displacement of the steel lid and copper canister (a) and lateral movement of the lid (b). Movements of the lid are measured relative to both the gallery floor and ceiling. Movements of the canister are measured relative to the steel lid.*

Pore pressure away from the deposition hole within the pressure relief hole is shown in Figure 8-12. A small reduction in pressure over the period was seen, most pronounced in PRH1-5. This interval was closest to the gallery and illustrated that this feature was caused by drawdown, created by the continued pumping of the Äspö HRL galleries, see Section 16.3. As seen, interval PRH2-4 was affectively at atmospheric pressure, again this interval was closest to the gallery.

Temperature was monitored within the Lasgit laboratory, the HRL, and the canister. Figure 8-13 shows that the air conditioning unit within the laboratory was problematic at the beginning of the time period. The air conditioning unit should have delivered stable temperature, as seen between Days 1719 and 1967. However, between Day 1480 and 1719 the temperature within the laboratory was variable, with the air conditioning unit failing on Day 1700. The variation seen had not adversely affected any of the systems within the laboratory, with small offsets considered when analysing the data. The temperature within the HRL tunnel showed distinctive annual variation as the HRL was not kept to the same close limits as the Lasgit laboratory and office. The variation of the temperature between Days 1719 and 1967 reduced when the system was calibrated at Day 1967. Following this time, a small variation in temperature was observed.

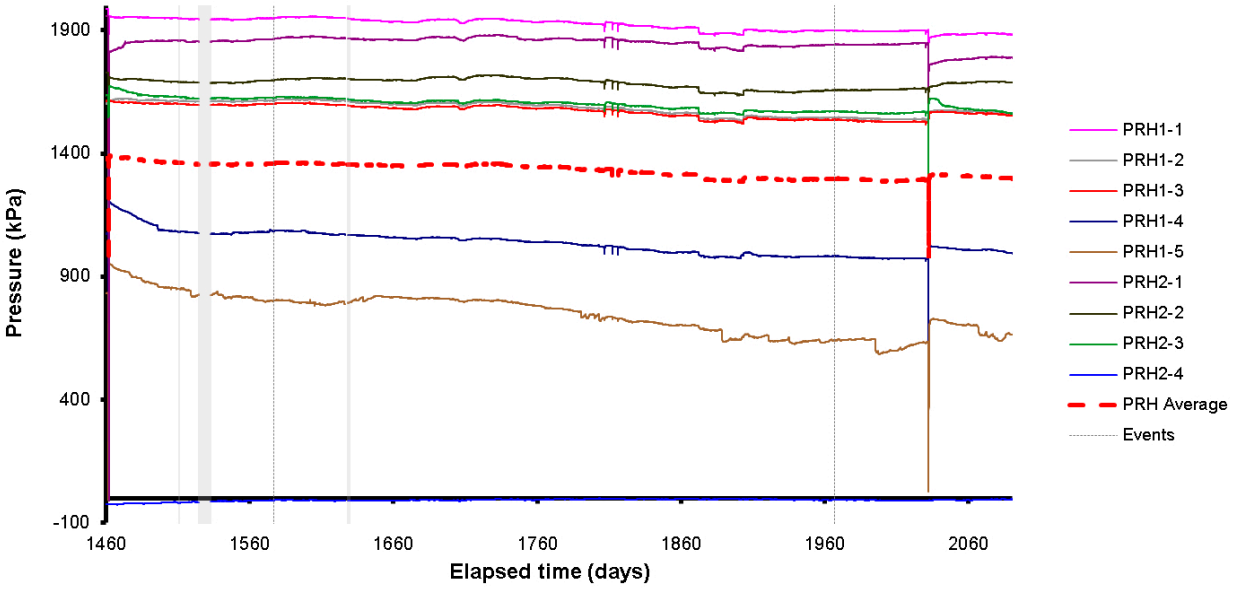

Figure 8-12. *Porewater pressures measured in the packered sections of the pressure relief boreholes.*

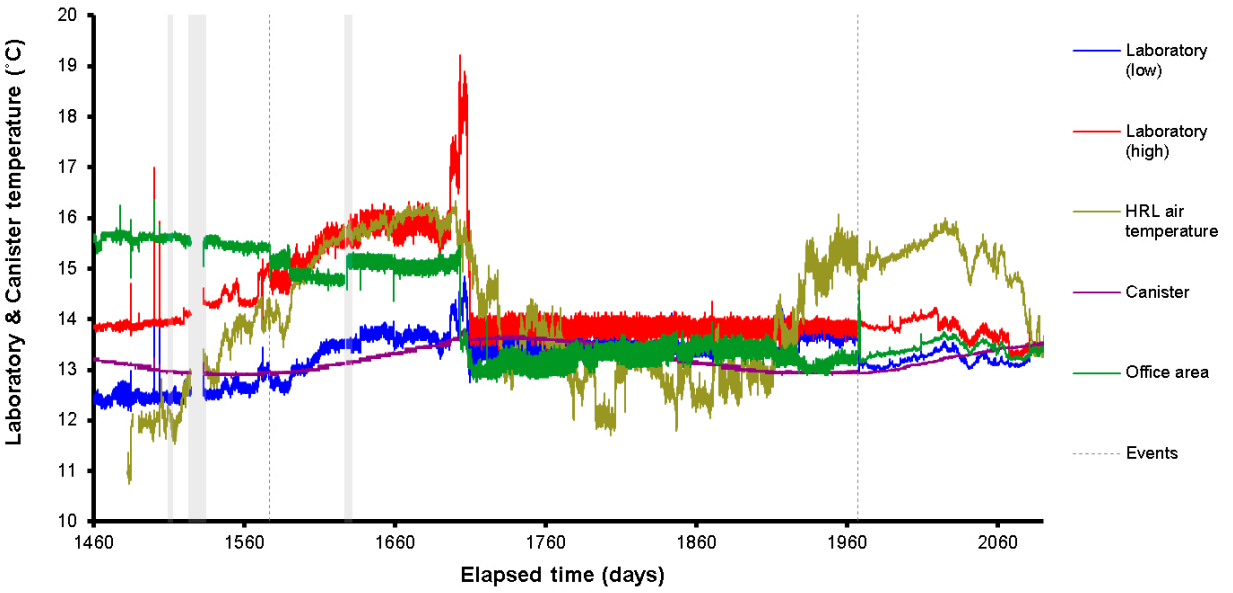

Figure 8-13. *Temperatures recorded in the Gas Laboratory, office, canister, and HRL.*

Figure 8-14 shows the total volume of water pumped into the system during this reporting period. A small pause in artificial hydration occurred between Days 1524.42 and 1533.17 following a power failure to the Lasgit laboratory. On recommissioning on Day 1533, the valve to filter mat 3 was not reopened in error, with reduced hydration occurring until Day 1542. Almost 10 litres of water were pumped into the buffer during the period. A slow gradual reduction in in-flow can be observed.

Figure 8-15 shows average stresses, pore pressure, and forces observed during the current reporting period. What can be noted is that radial stresses; axial stress on the rock wall; axial force on the lid; stress on the canister and pore pressure within the bentonite all increased marginally during the period. Many of these datasets show an annual variation associated with temperature fluctuations. In contrast, pore pressure at the rock wall and pore pressure within the pressure relief holes marginally decreased during the period as a result of drawdown and extraction of fluid within the gallery. The pore pressure within the bentonite increased while the other pore pressures decreased as this was dominated by artificial hydration and uptake of water by the bentonite buffer.

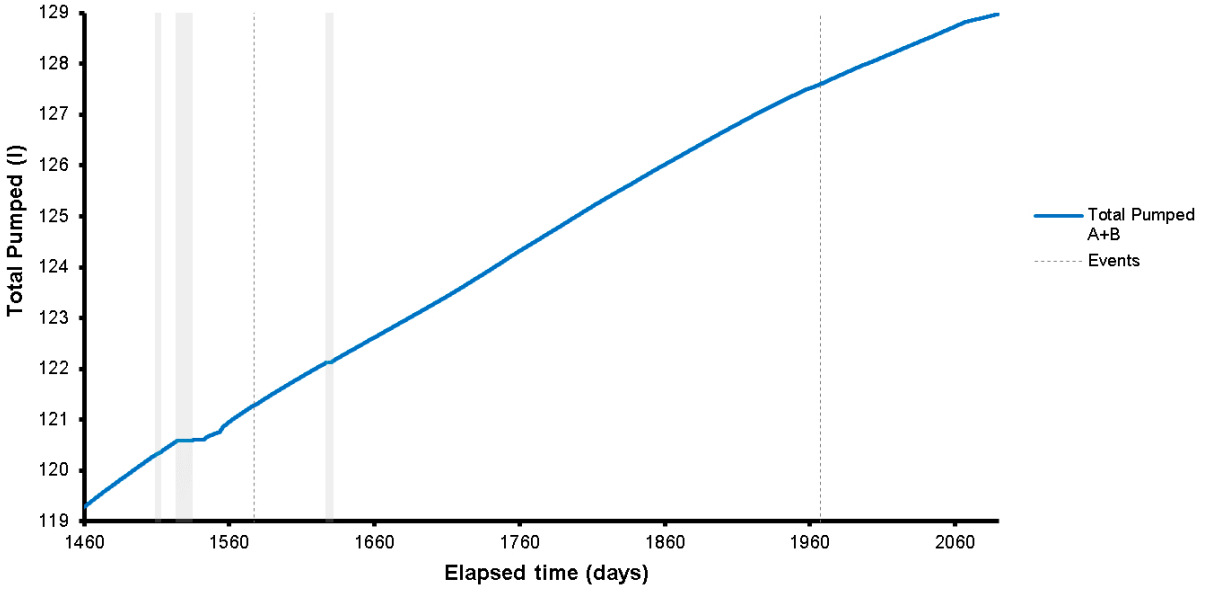

Figure 8-14. *Total pumped during artificial hydration and hydraulic testing.*

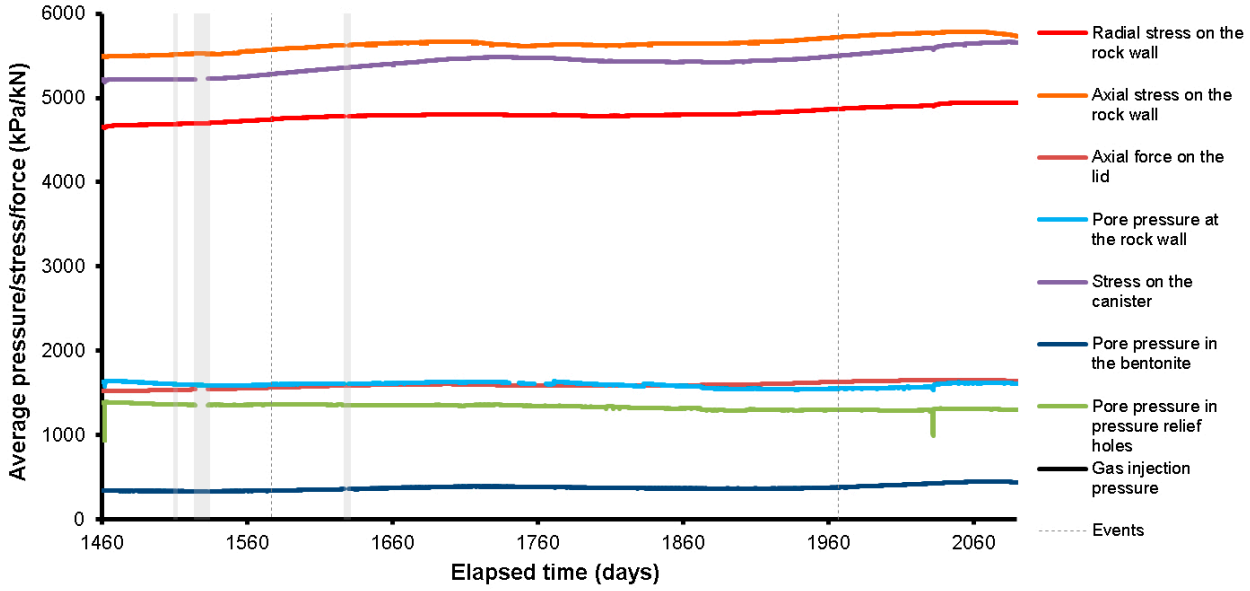

Figure 8-15. *Average pressures, stress, and force observed during the reporting period.*

8.2 Hydraulic test prior and after the gas injection test 2

Figure 8-16 shows the results of the two-stage hydraulic tests, which have been adjusted so that the tests conducted before and after the gas injection test can be compared. a shows the pore pressure imposed during the test. There was a slight difference in pressure for the low-pressure stage of the two tests, which could result in differences in the results, but this should be corrected in the model. Figure 8-16b, c and Figure 8-17a show that the high-pressure stage resulted in an initially high flow into the buffer in excess of 4×10^{-11} m^3 s^{-1}, which quickly reduced to an asymptote of 5.04×10^{-12} m^3 s^{-1} for the test before the gas test and 4.82×10^{-12} m^3 s^{-1} for the repeat test after gas injection. Figure 8-16b, c and Figure 8-17b show that the low-pressure stage resulted in an initially high outflow in excess of 6×10^{-11} m^3 s^{-1}, which quickly reduced to an asymptote of 1.11×10^{-12} m^3 s^{-1} for the test before the gas test and 9.51×10^{-13} m^3 s^{-1} for the repeat test after gas injection. The low-pressure stage resulted in a much noisier result, but it is clear that the outflow during this stage was considerably lower than the inflow during the high-pressure stage.

The two-stage hydraulic head tests were modelled using the 1-D modelled described in Section 6.4, Figure 8-18 shows the modelled results for the two hydraulic tests. The fit of the data can be seen to be good, although it hasn't perfectly modelled the data. Table 8-1 summarises the calculated values for hydraulic conductivity and specific storage for the two tests.

Figure 8-16c shows that the two tests resulted in asymptote at a similar flow rate for both before- and after-gas injection testing. What varied between the tests was the rate of decay, with the test before the gas injection test reducing to an asymptote quicker than the test conducted afterwards. This would be related to the gas that remained in the buffer near to the injection filter. The asymptote of the data related to the flow properties of the bentonite, while the curvature of the flow related to the storage in the system. After gas injection, there was apparently more storage, but no change in hydraulic flow. This is confirmed in the modelled data, which show comparable results for hydraulic conductivity and specific storage. Therefore, the injection of gas had not resulted in a change in the flow properties of the buffer.

Table 8-1. Modelling results for the two-stage constant head hydraulic tests conducted during Gas Injection Test 2.

Filter	Radius of the filter (mm)	Step	Fitted hydraulic conductivity (m s^{-1})	Fitted specific storage (m^{-1})	Boundary conditions		Initial conditions	
					p_0 (MPa)	p_L (MPa)	p_{I0} (MPa)	p_{IL} (MPa)
FL903	50	1	1.00×10^{-12}	6.00×10^{-6}	4.20	1.74	2.52	1.74
		2	1.49×10^{-12}	6.34×10^{-6}	0.98	1.74	4.20	1.74
		Average	**1.24×10^{-12}**	**6.17×10^{-6}**				
FL903	50	1	9.44×10^{-13}	4.87×10^{-6}	4.24	1.69	1.7	1.69
		2	2.44×10^{-13}	1.60×10^{-5}	1.37	1.69	4.24	1.69
		Average	**5.94×10^{-13}**	**1.04×10^{-5}**				

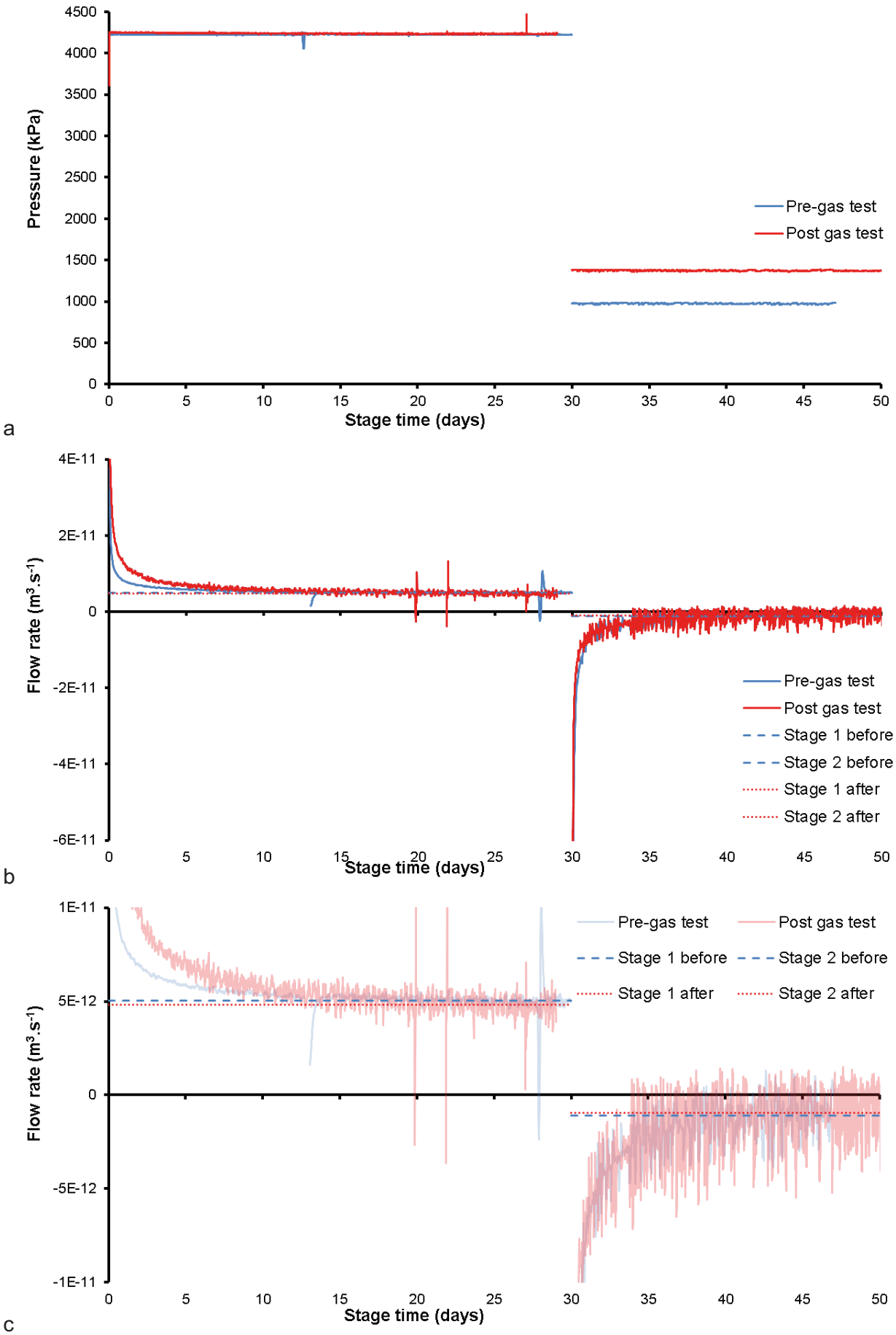

Figure 8-16. *Two-stage constant head hydraulic tests conducted during Gas Injection Test 2. a) Pressure of the injection fluid; b) Flow response; c) Detail of flow response.*

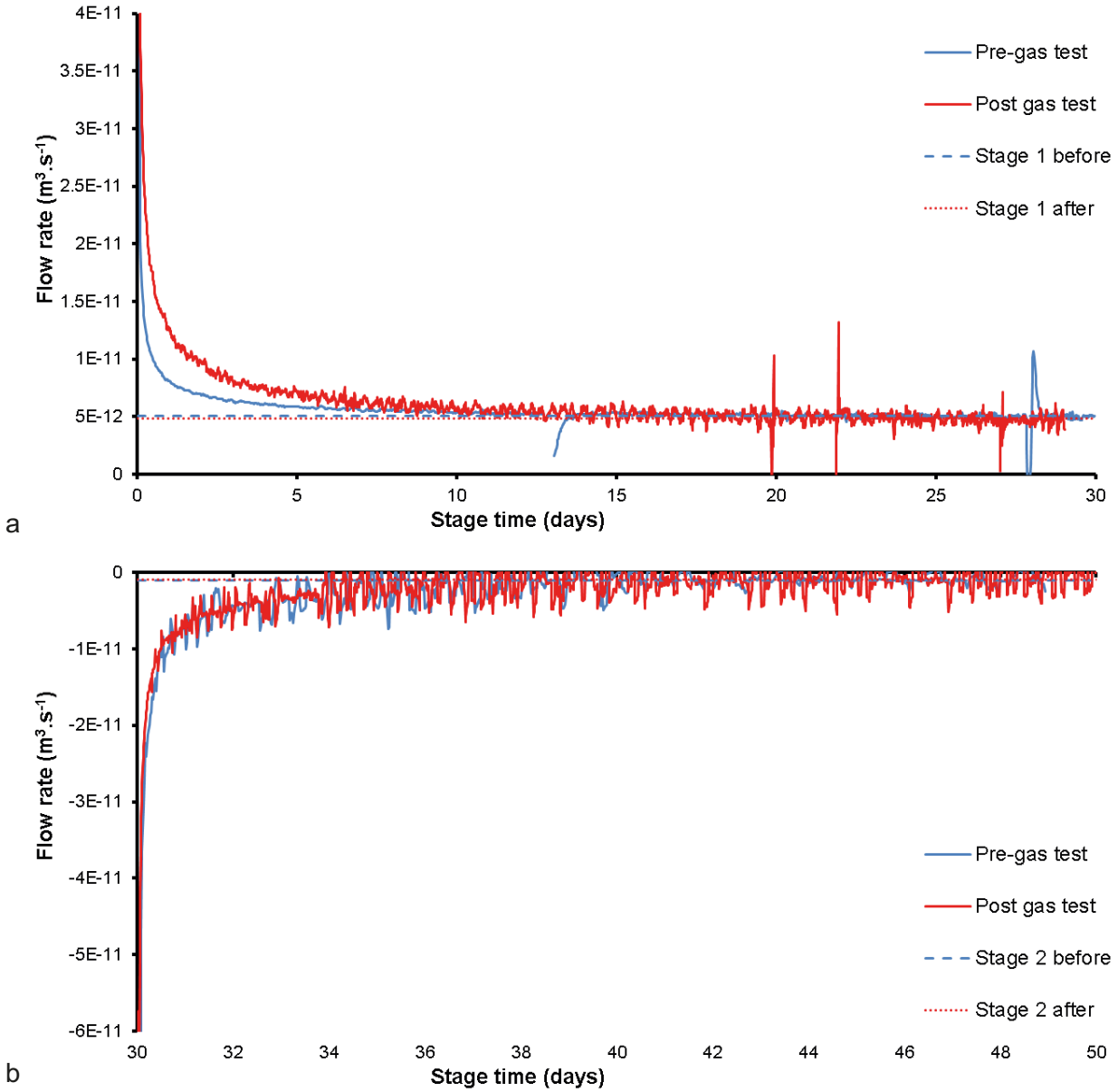

Figure 8-17. *Detail of the flow into the clay during the two-stage constant head hydraulic tests conducted during Gas Injection Test 2. a) High-pressure stage; b) Low pressure stage.*

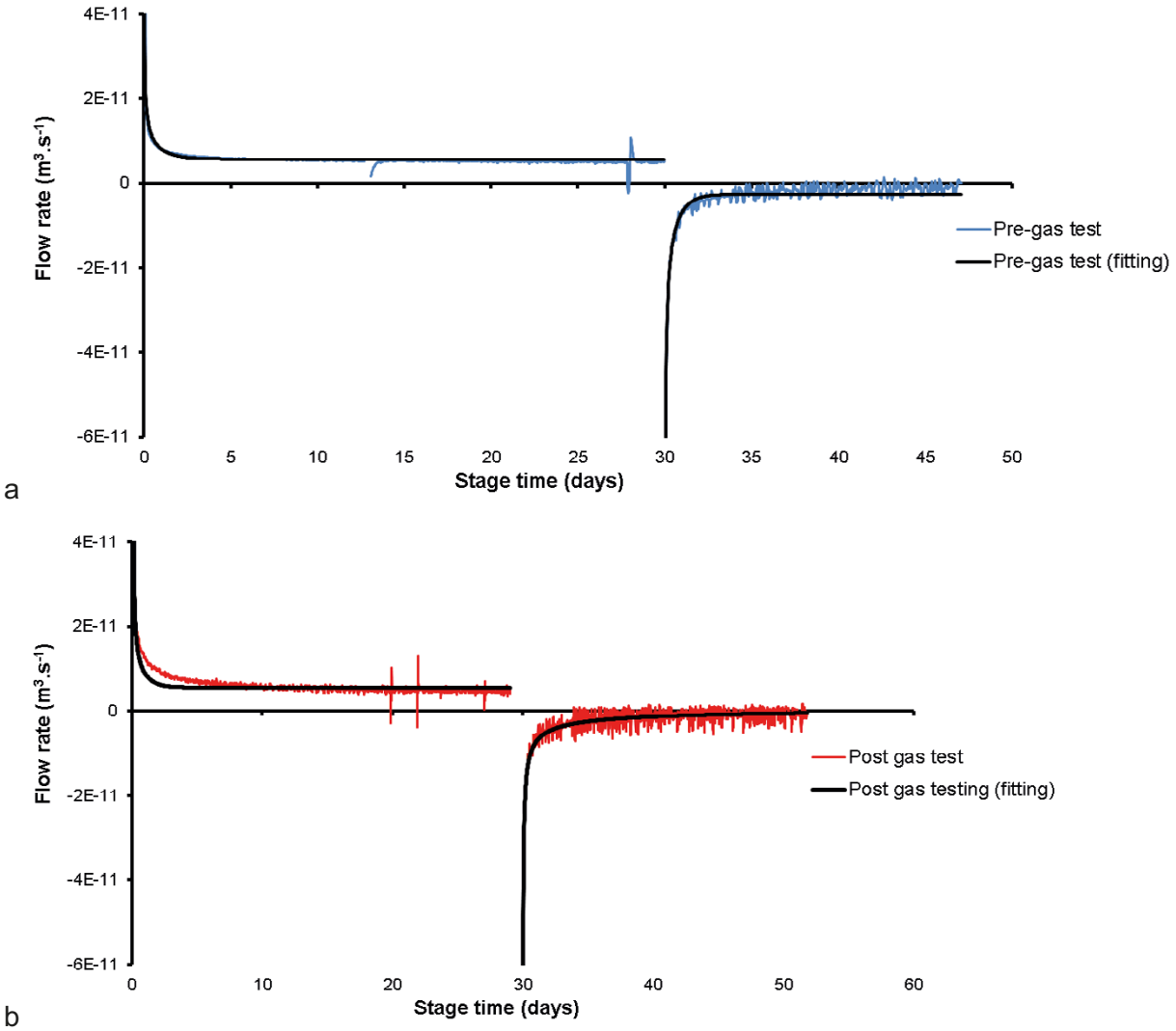

Figure 8-18. *Modelled results for the two-stage constant head hydraulic tests conducted during Gas Injection Test 2. a) Pre-gas test; b) Post-gas test.*

8.3 Gas injection test 2

Gas Injection Test 2 was conducted in filter FL903 on the lower array of filters on the canister surface. It was the second such test using FL903 and started 596 days after the end of the first test. As with the previous tests in FL903, gas pressure was raised from background levels up to gas peak pressure using four distinct pressure ramps, being held at constant pressure in between. Following gas peak pressure, gas flow was continued for a period of 191 days. The aim of the test was to see if gas injection behaviour had changed since the first test and the response of the system to a much longer injection post-gas entry. The injection gas was also changed to neon, which is absent from the pore waters at the Äspö Hard Rock Laboratory and therefore could act as a tracer.

Approximately 2 065 ml of neon was added to the interface vessel at a starting pressure of 1 299 kPa. The injection filter was thoroughly flushed of water using pressurised gas and the drain from filter FL903. Once flushed, it is common for flow to take a few days to stabilise as gas goes into solution and any remaining water within the filter is expelled into the bentonite. The first pressure ramp was started at Day 1606.25 (15:40 26th June 2009) by the injection of water into the base of the interface vessel by the syringe pump at a rate of 4.0 ml h^{-1}. This raised the pressure from 1 299 to 2 545 kPa in 10.9 days, as shown in Figure 8-19, after which pressure was held constant from Day 1617.13 for 14.9 days. The second pressure ramp was started at Day 1632.06 (11:10 22nd July 2009) by the injection of water into the base of the interface vessel at a rate of 1.25 ml h^{-1}. This raised the pressure from 2 546 to 3 783 kPa in 12.6 days, after which the pressure was held constant from Day 1644.69 for 28.6 days. During this period the interface vessel was re-charged with approximately 2 800 ml of neon at a pressure of 3 771 kPa. The third pressure ramp was started at Day 1673.29 (16:41 1st September 2009) by the injection of water into the base of the interface vessel at a rate of 2.0 ml h^{-1}. This raised the pressure from 3 771 to 5 059 kPa in 16.7 days, when pressure was held constant from Day 1689.98 for 55.1 days. The fourth, and final, pressure ramp was started at Day 1745.11 (12:14 12th November 2009) by the injection of water into the base of the interface vessel at a rate of 0.5 ml h^{-1}. This raised the gas pressure from 5 089 kPa to a peak pressure of 5 868 kPa at Day 1769.65, 24.5 days after the start of the fourth pressure ramp. The injection of water into the base of the interface vessel continued at 0.5 ml h^{-1}, until Day 1910.10 (12:03 26th April 2010). This meant that gas injection continued 140.5 days after gas peak pressure. In total, 4 295 ml of water was injected into the base of the interface vessel during Gas Injection Test 2.

The prediction of gas pressure shown in Figure 8-19 derives from the ideal gas law. A close approximation can be seen. Although a slow process, care was taken to determine the starting volume of gas during the filling of gas in the interface vessel and showed an estimated volume of 2 100 ml. A secondary measure of the starting volume was made by changing the volume of the gas by injecting water into the interface vessel and observing the change in pressure; this gave an estimate of 1 075 ml. It was assumed that the estimate from known volume change was the estimate that was wrong and that the pressure response observed would better define the volume. Figure 8-20 shows the difference between the predicted and observed gas pressures. This gave a volume of 2 065 ml. This latter estimate has been used for calculations, with the starting volume of gas determined for each pressure ramp. Without an adjustment it would suggest that gas was always moving into the buffer. Gas volume can be lost through diffusion and in solution at the gas/water contact within the interface vessel, but this is likely to be a small effect as flow into the clay is minor during the pressure hold periods.

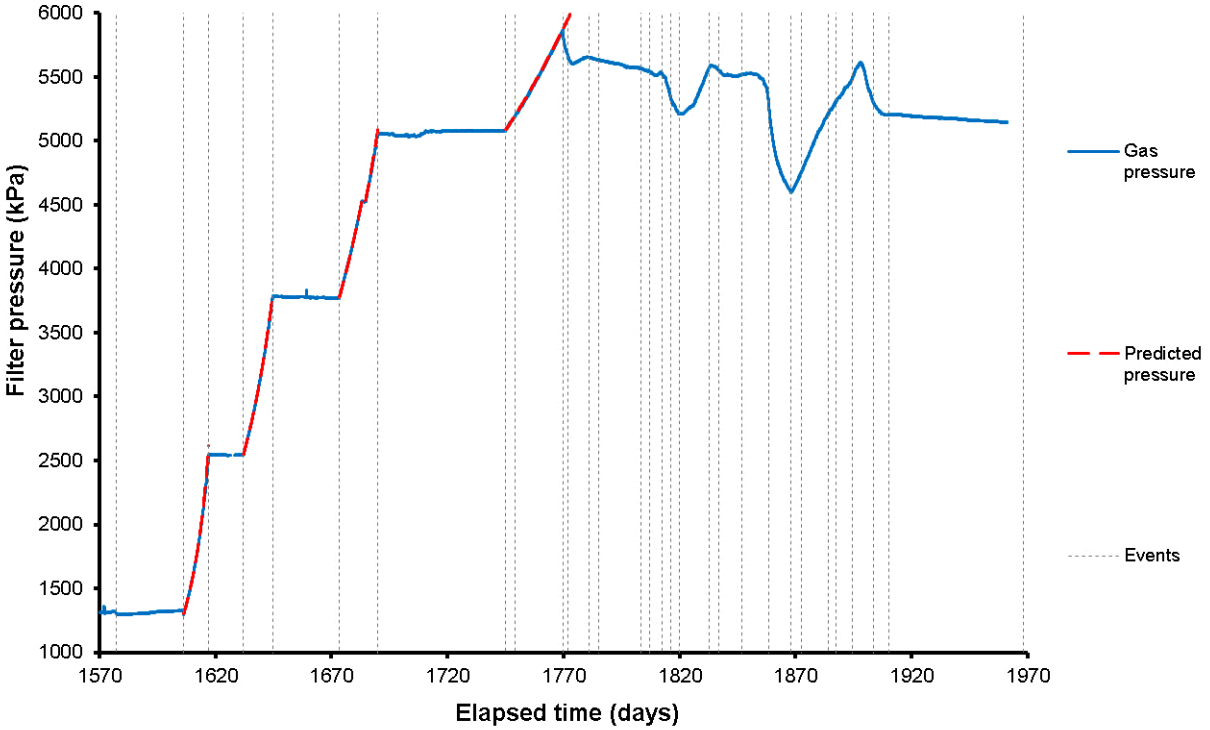

Figure 8-19. *Recorded and predicted gas pressure during Gas Injection Test 2.*

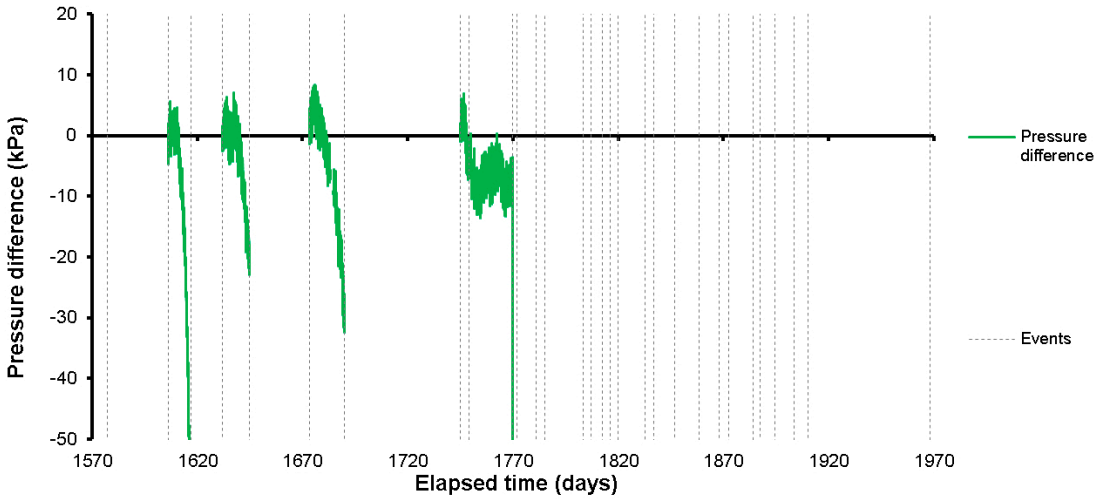

Figure 8-20. *Difference between recorded and predicted pressure during Gas Injection Test 2. This was used to estimate the volume of gas during a constant flow gas compression stage.*

Figure 8-21 shows the flow of gas into the system and into the clay at STP[4]. This clearly shows that the rate of gas entry reduced between each successive gas ramp. Flow into the clay is seen in each ramp, with little flow observed during periods of constant pressure. Each injection ramp will be introduced in detail in the following paragraphs.

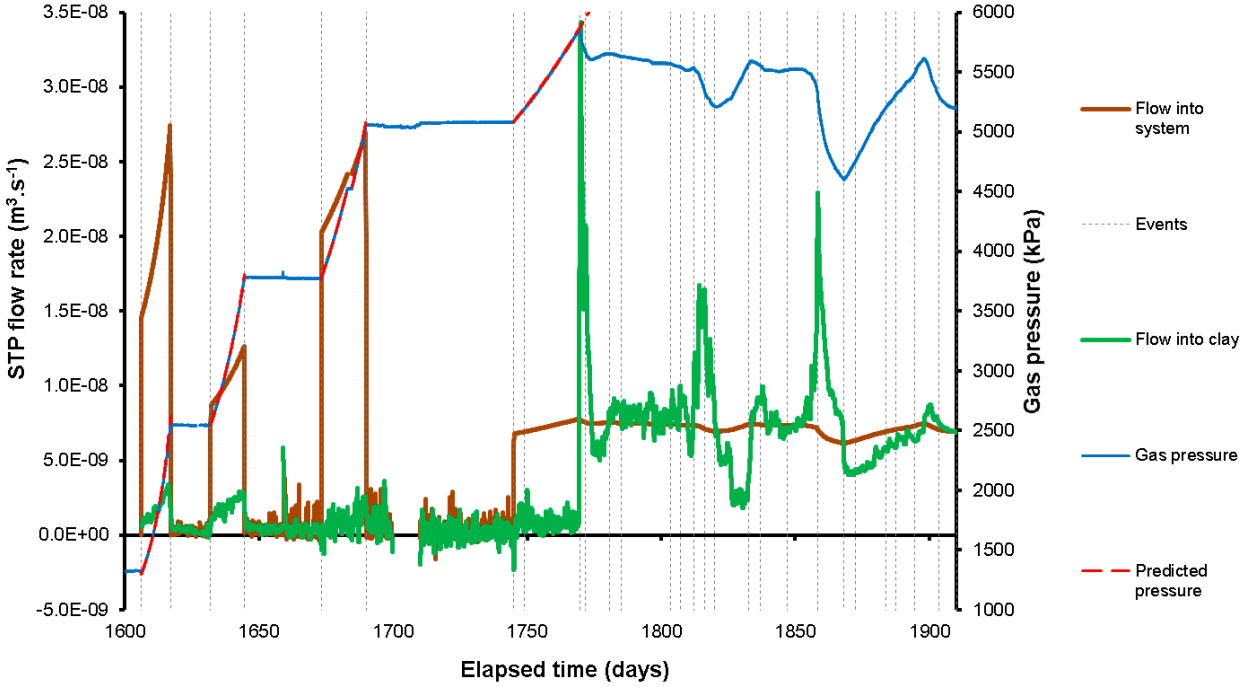

Figure 8-21. *Flow of gas into the system and the clay during Gas Injection Test 2.*

[4] STP – Standard temperature and pressure – a temperature of 273.15 K (0 °C) and an absolute pressure of 10^5 Pa

Figure 8-22 shows the detail of the first gas ramp conducted in Gas Injection Test 2. The predicted pressure seen in Figure 8-22a was derived from the revised estimate of the starting volume of gas of 2 065 ml, which as shown in Figure 8-22b gave a very good estimate with negligible difference between the predicted and observed gas pressure at the start of pressurisation. Throughout the period, the STP flow into the clay ranged from 5.89×10^{-10} to 3.42×10^{-9} $m^3 s^{-1}$. This resulted in a small flow into the clay, with ~0.07 mol entering the clay (Figure 8-22c). This may have occurred through diffusion and/or solution and was not interpreted as representing advective movement of gas. Observed pressure can be seen to diverge from predicted pressure at around Day 1611.14, when gas pressure was 1 679 kPa. This is not interpreted as advective gas flow into the buffer. When the gas pressure was held constant at around 2 545 kPa a small background flux of around 2.5×10^{-10} $m^3 s^{-1}$ was seen. This was around 95 % lower than that observed prior to the switch to constant pressure. During the holding stage a flow rate of 46.8 µl h^{-1} was observed between Day 1617.13 and 1632.06, representing 1 214 µmol d^{-1}.

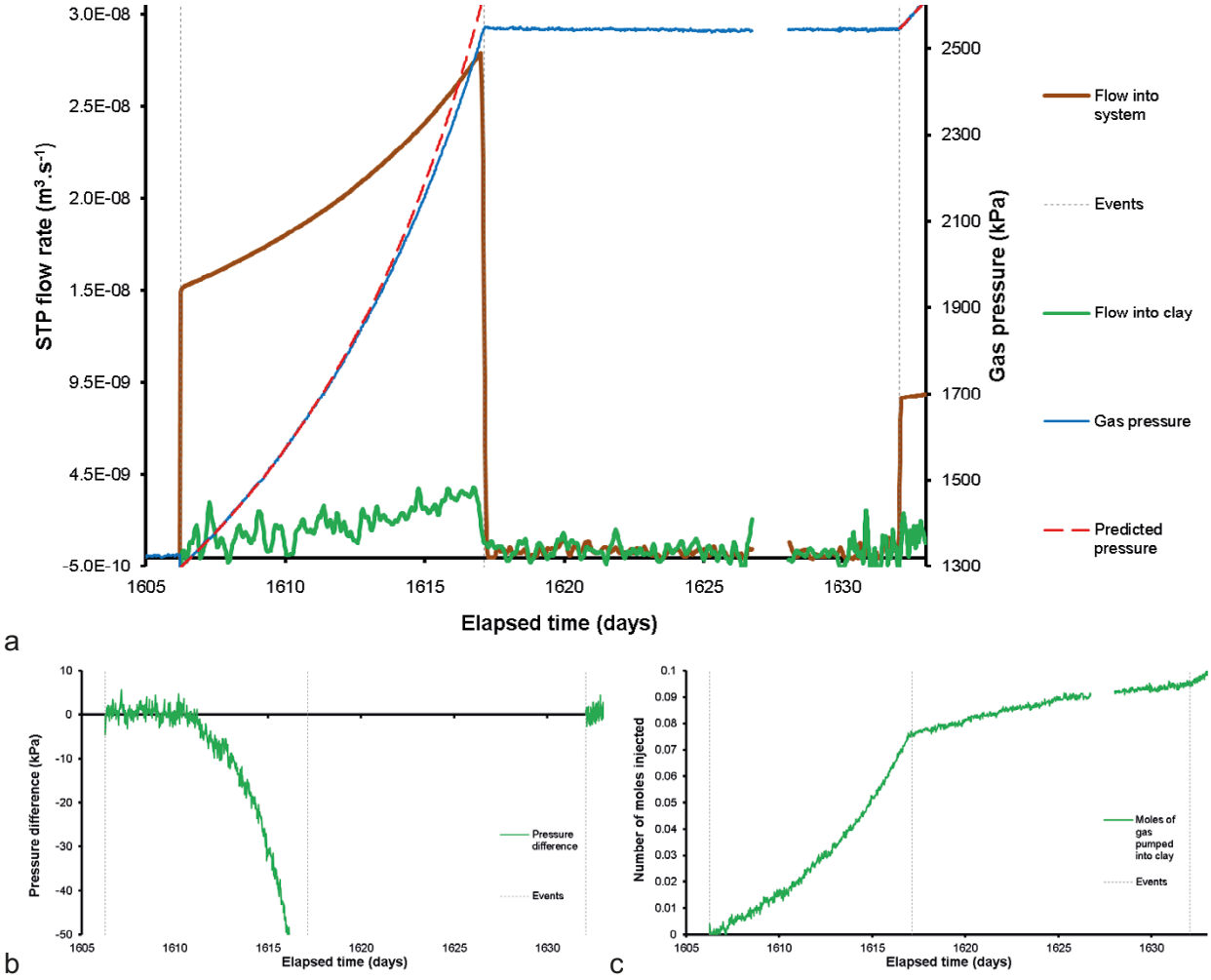

Figure 8-22. *Detail of gas ramp 1 of Gas Injection Test 2. a) Flow of gas into the system and the clay, b) Difference between recorded and predicted pressure, c) Moles pumped into the clay.*

Figure 8-23 shows the detail of the second gas ramp conducted in Gas Test 2. The predicted pressure seen in Figure 8-23a was derived from a revised estimate of the starting volume of gas of 1 145 ml, which as shown in Figure 8-23b gave a very good estimate with negligible difference between the predicted and observed gas pressure. The predicted and observed pressures started to diverge around Day 1639, when gas pressure was 3 110 kPa. This did not result in a significant increase in flow into the clay. Throughout the period, the STP flow into the clay ranged from 1.76×10^{-9} to 2.83×10^{-9} $m^3 s^{-1}$. This resulted in a small flow into the clay, with 0.10 mol entering the clay (Figure 8-23c). When gas pressure was held constant at ~3 780 kPa, a total of 0.044 mol entered the clay, with an average flow rate of 36.2 µl h^{-1}, representing 1 533 µmol d^{-1}. Prior to the interface vessel being refilled, a small background flux of around 4.57×10^{-10} $m^3 s^{-1}$ was seen.

Figure 8-24 shows the detail of the third gas ramp conducted in Gas Injection Test 2. As seen in Figure 8-24a, there was a break in flow between Days 1683.12 and 1684.70. This was caused by a problem with the injection pump. Figure 8-24b shows some agreement between the predicted and observed gas pressures until approximately Day 1681 when gas pressure was 4 340 kPa. Throughout the period, the STP flow into the clay ranged from 2.58×10^{-11} to 2.61×10^{-9} $m^3 s^{-1}$. This resulted in a small flow into the clay, with 0.06 mol entering the clay (Figure 8-24c). When gas pressure was held constant at around 5 060 kPa a flow rate of 18.5 µl h^{-1} was observed, representing 661 µmol d^{-1}. This represented a small background flux of around 3.05×10^{-10} $m^3 s^{-1}$. Figure 8-25 shows the variation of gas flow into the clay at STP for the three constant pressure stages. The relationship of flow with gas pressure is uncertain.

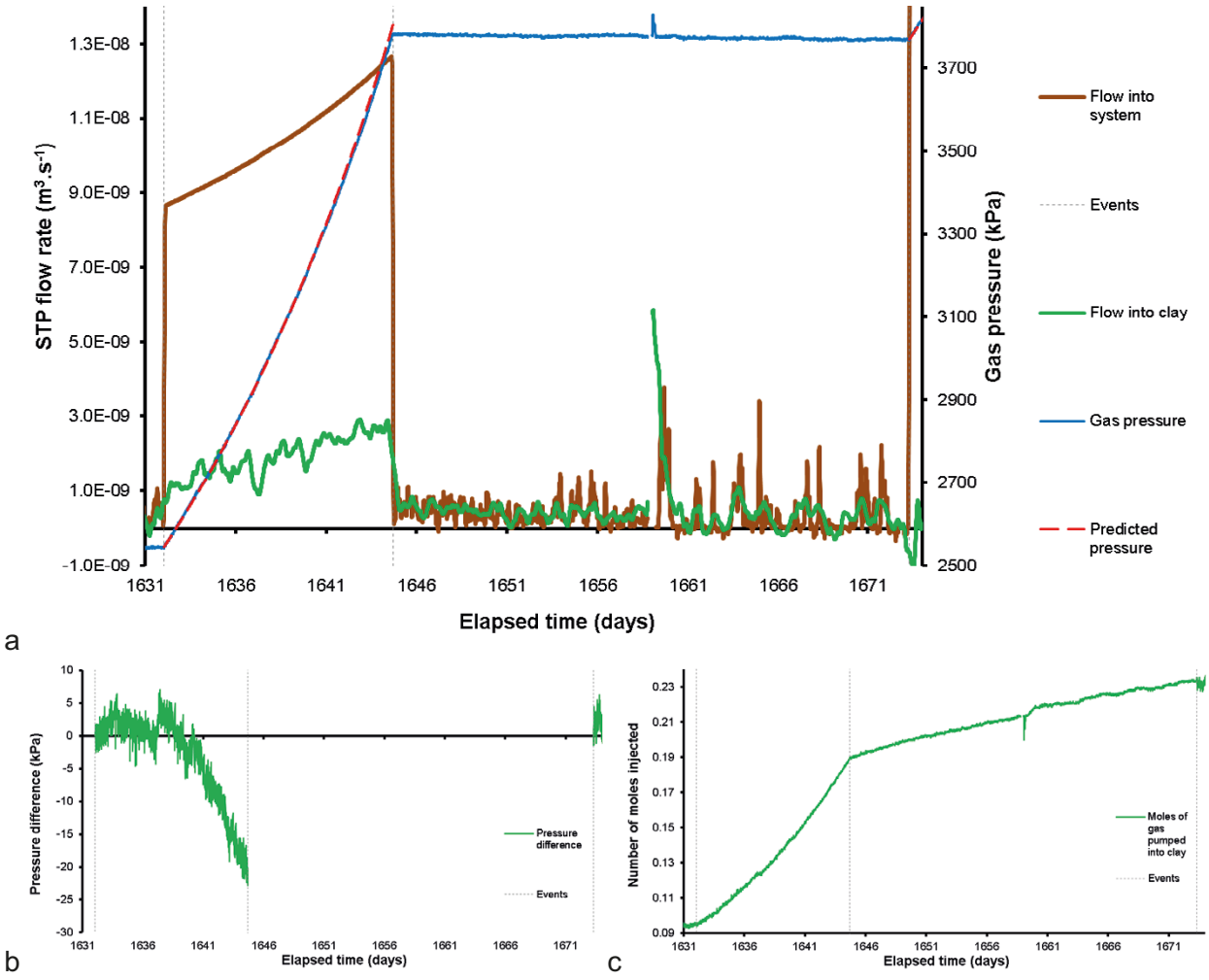

Figure 8-23. *Detail of gas ramp 2 of Gas Injection Test 2. a) Flow of gas into the system and the clay, b) Difference between recorded and predicted pressure, c) Mole pumped into the clay.*

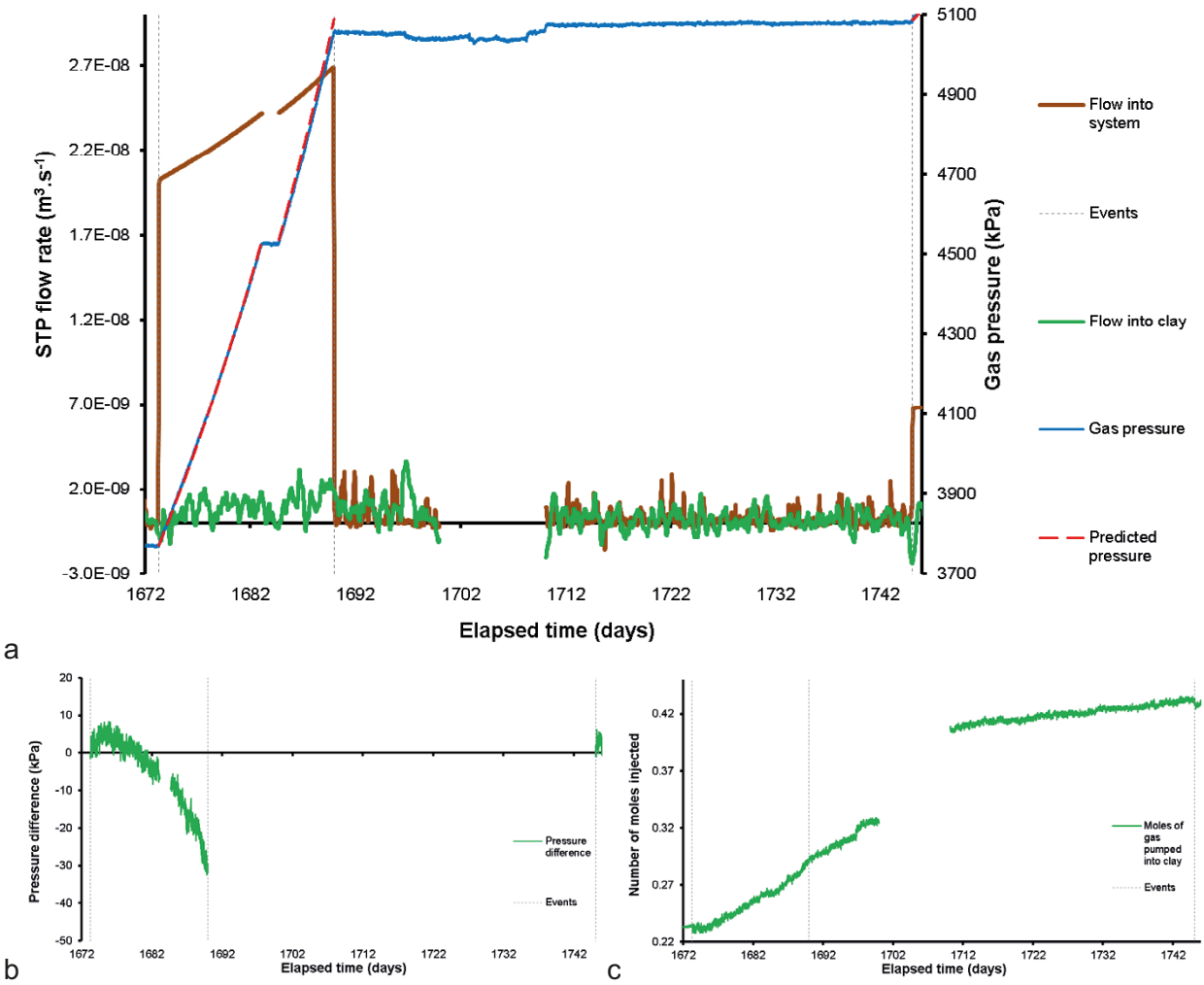

Figure 8-24. *Detail of gas ramp 3 of Gas Injection Test 2. a) Flow of gas into the system and the clay, b) Difference between recorded and predicted pressure, c) Mol pumped into the clay.*

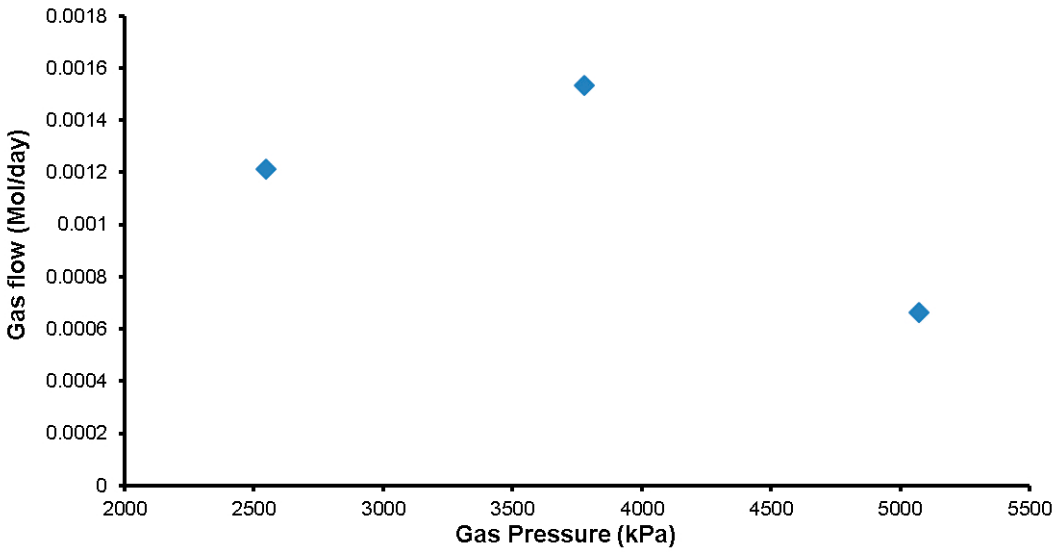

Figure 8-25. *Gas flow rate into the clay at STP at the three constant pressure steps of Gas Injection Test 2.*

Figure 8-26 shows the detail of the fourth gas ramp conducted in Gas Injection Test 2 up until the time of accelerated flow into the gas at Day 1769.65. As seen in Figure 8-26a, despite a good correlation between the predicted and observed gas pressures, flow was seen into the clay at a nominal rate of around 8.77×10^{-10} $m^3 s^{-1}$. Figure 8-26b shows good agreement between the predicted and observed gas pressures until Day 1769.65 when gas pressure was 5 868 kPa. A small flow was seen into the clay, with 0.08 mol entering the clay (Figure 8-26c). Significant gas entry was seen to begin at Day 1769.65, as seen by an increase in flow rate into the clay (Figure 8-26a), deviation between the predicted and observed gas pressure (Figure 8-26b), and the volume of gas pumped into the clay (Figure 8-26c).

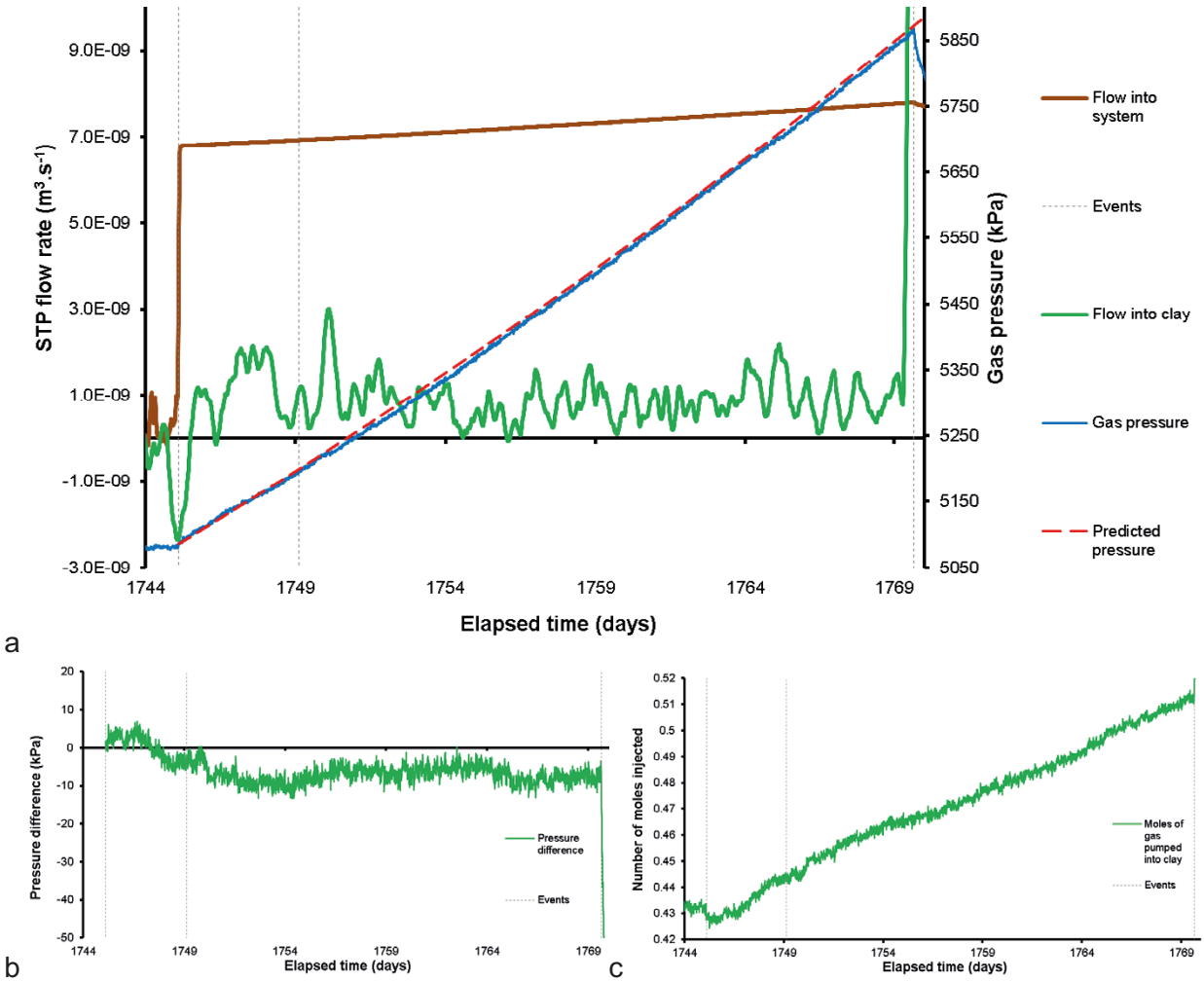

Figure 8-26. *Detail of gas ramp 4 of Gas Injection Test 2 up until the time of clear gas entry. a) Flow of gas into the system and the clay, b) Difference between recorded and predicted pressure, c) Mol pumped into the clay.*

The fourth gas ramp took the test through to peak gas pressure and post-entry, Figure 8-27 shows the flow result. As described above, a small flow was seen into the clay until Day 1769.95 with an average of 8.77×10^{-10} m^3 s^{-1}, when flow into the clay began to accelerate. This resulted in a peak in flow of 6.82×10^{-8} m^3 s^{-1} at Day 1769.70 (note: data shown in Figure 8-27 is time averaged). The peak in flow was short-lived with flow into the clay reducing to be less than flow into the system within 5 days. Gas pressure started to recover from around Day 1774.4 when flow into the clay was less than flow into the system, and reached a secondary, smooth, peak around Day 1780.40 at a pressure of 5 650 kPa. For the following 20 days the flow into the clay was marginally higher than the flow into the system as the gas pressure decreased at a constant rate. This was disturbed by a number of flow features starting at Day 1810. This ultimately resulted in a secondary increase in flow and a reduction in pressure of approximately 300 kPa by Day 1821, before recovering over the following 22 days by 375 kPa. Between Day 1834 and 1855 the rate of decay of pressure was similar to that seen between Days 1780 and 1810, with flow into the clay marginally greater than flow into the system. A second pressure decrease started around Day 1856, with a reduction in gas pressure of approximately 850 kPa over 12 days. This event will be discussed in more detail later. Over the following 30 days (Day 1868 to 1898), pressure recovered by over 1 000 kPa to a peak of 5 607 kPa at Day 1898.33. For the remainder of the injection stage, pressure decreased to around 5 200 kPa as flow into the clay reduced to match flow into the system, resulting in steady flow. Therefore, during gas ramp 4 there were 5 peaks in flow into the clay, resulting in 5 events of reducing pressure. The general behaviour seen shows under- and over-shooting of flow into the clay around the flow into the system, probably as new pathways formed. Figure 8-28 shows the number of moles pumped into the clay; 0.51 mol entered the clay up until peak gas pressure. Following gas entry, a total of 4.23 mol entered the clay.

Highlighted in Figure 8-27 in red is a period that requires particular consideration. On Day 1868 the injection pump required re-filling, which was a standard procedure. Following this, gas pressure started to increase once pumping had been re-started. As this behaviour was instantaneous, it has been deduced that one of the air-actuated valves on the control board had partially been opened and that the pump had therefore been slowly leaking between Day 1860 and 1868. This was not immediately remediated as the behaviour was similar to that seen at Day 1813. As pressure had "leaked" from the pumping system it was decided to continue injection of the remaining volume of neon and to observe behaviour once gas flow had been re-established.

Figure 8-27. *Flow of gas into the system and the clay during the fourth ramp of Gas Injection Test 2.*

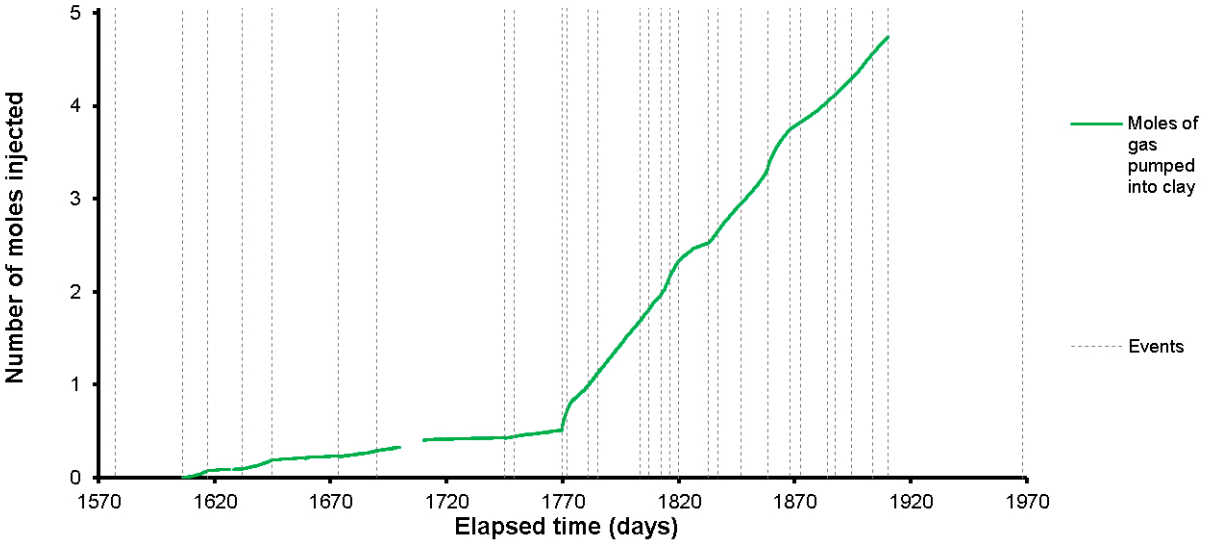

Figure 8-28. *Number of moles pumped into the clay during Gas Injection Test 2.*

The detail of gas entry is shown in Figure 8-29. The complexity seen at gas entry is shown in Figure 8-29a. Whilst the general appearance of the peak in flow into the clay appears to be a single peak, it includes as least three peaks in flow; the first at Day 1769.66, second at 1770.36, and third at 1771.64. The latter of these events was a prolonged period of increased flow. These individual events may represent the formation of new pathways and as a result the increased volume occupied by the gas reduced gas pressure. Figure 8-29b shows the second gas entry event, starting at around Day 1812. This time, a series of five peaks in gas flow (Days 1812.28, 1814.27, 1815.44, 1816.13, and 1818.14) contribute to the reducing gas pressure, again suggesting the opening of new pathways. The new pathway network became unstable and stopped growing, resulting in the increase in gas pressure from around Day 1821.

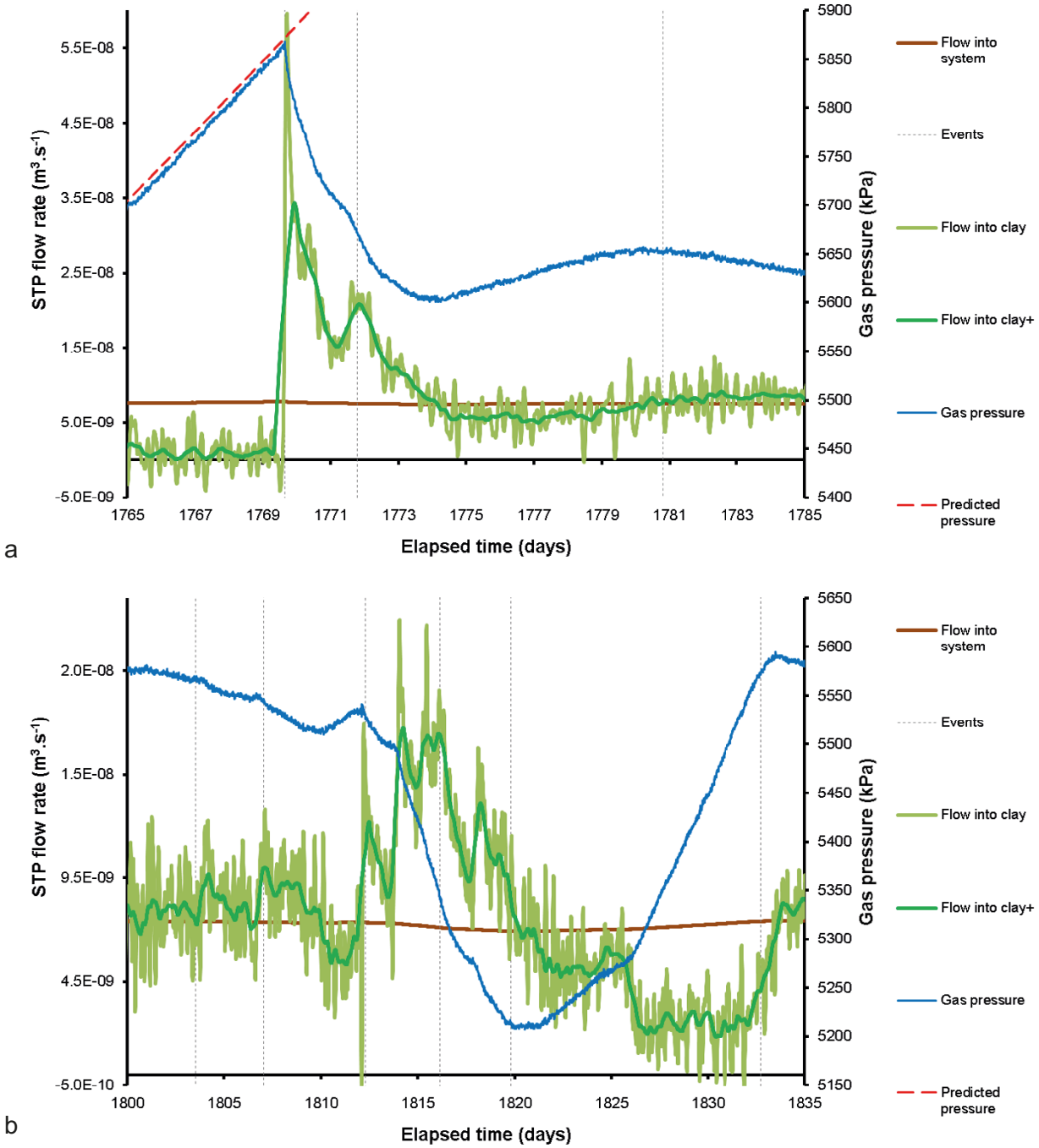

Figure 8-29. *Detail of the flow of gas into the clay and the system around the time of gas entry during Gas Injection Test 2.*

Porewater pressure at the rock wall showed limited coupling with gas entry, and more coupling during gas movement (Figure 8-30a, Figure 8-31a). At the time of accelerating flow into the clay at Day 1769.66 and gas peak pressure, a stepped response was seen in UR905 and UR904 with increases of 30 and 5 kPa respectively. At this time, pore pressure at UR908 started to increase, as did pressure at UR907. The next event line highlighted corresponds with the second peak in flow during the reduction in gas pressure. This corresponds with a further short-lived increase in pressure at UR905 of 26 kPa and a peak in pressure at UR907, which increased rapidly by 490 kPa. This latter observation is a large change in pressure, much greater than any previously described UR sensor response. At this time a short-lived reducing pressure response was seen in UR909 of around 10 kPa.

The next event of note was at Day 1780.82 with a small peak feature in UR905 and a distinct reduction in pressure at UR909. Around the time of gas entry, the final event of note was at Day 1785.18 when pressure reduced by about 20 kPa in UR904. Following this event all UR sensors showed a relatively stable decrease in pressure until Day 1807.03. This time represents the first of three similar events at Days 1807.03, 1812.28, and 1816.13 when pressure in many UR sensors deceased and quickly recovered. This was the time when gas flow into the clay was increasing and gas pressure was reducing as a consequence.

At Day 1832.75 an event line shows the start of pressure increase in several UR sensors (Figure 8-30a) and the instantaneous increase in pore pressure at UR910 by 580 kPa (Figure 8-31a). This time corresponds with the increase in flow into the clay. Of note is what occurred at the interpreted leakage event between Days 1858 and 1868 correspond with a very "quiet" period in the pore pressure data. This suggests that the pressure reduction seen at this time was not associated with gas movement. The final two events of note in pore pressure occurred at Days 1872.41 and 1903.42. The first of these caused a reduction in pore pressure in almost all UR sensors, with changes of between 30 and 5 kPa. The second saw an instantaneous increase, often of similar magnitude.

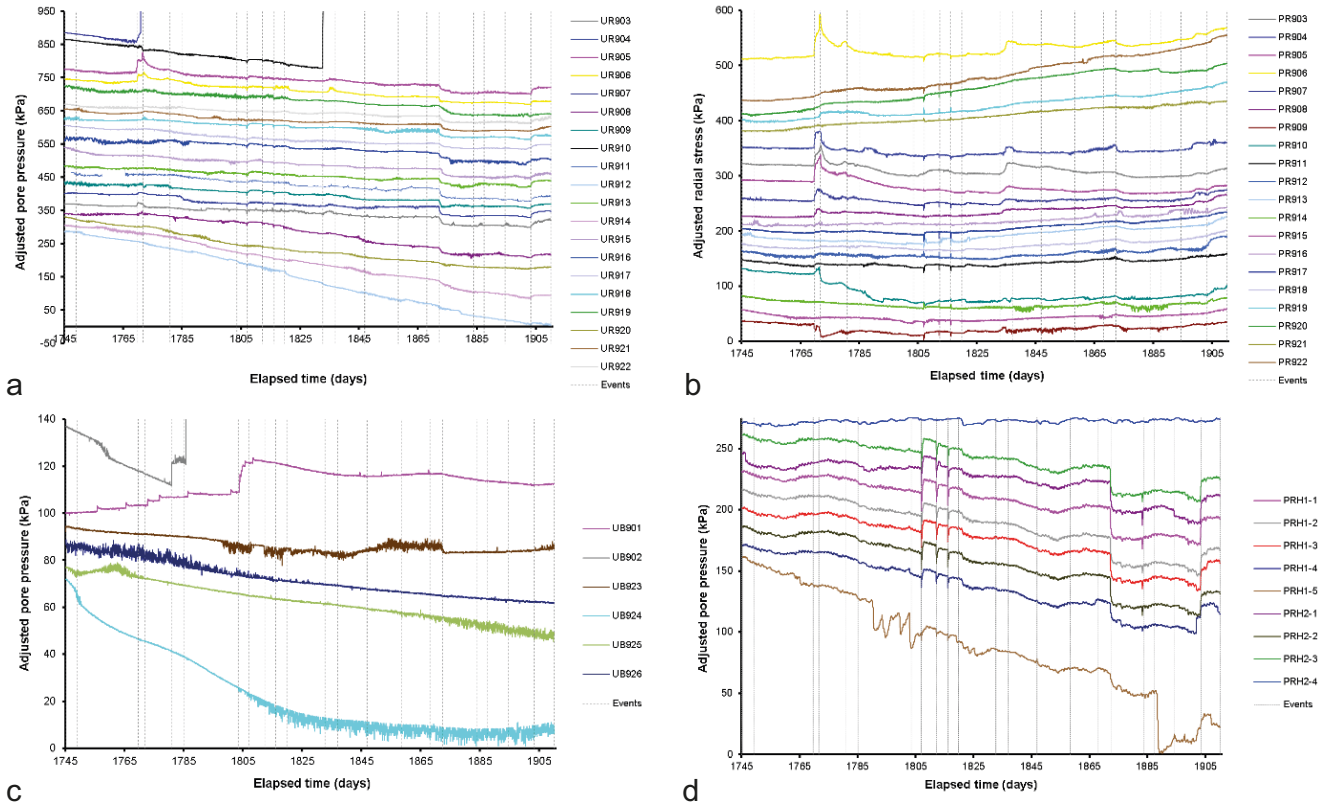

Figure 8-30. *Example of sensor response around the time of gas entry during Gas Injection Test 2. All parameters have been transposed about the y-axis to emphasise the detail observed. a) Pore pressure at the deposition wall; b) Radial stress on the deposition wall; c) pore pressure within the bentonite; d) pore pressure at the pressure relief holes.*

Radial stress at the rock wall also showed complex behaviour with many events (Figure 8-30b, Figure 8-31b). At the time of accelerating flow into the clay at Day 1769.66 and gas peak pressure, a stepped response was seen in most PR sensors, especially those highlighted in Figure 8-31b. Location PR906 showed the greatest increase of 75 kPa, whilst PR905, PR904, PR903, and PR908 increased by 48, 29, 35, and 12 kPa respectively. A different behaviour was seen at PR909, which saw a decrease in stress of approximately 20 kPa, reaching a minimum at the same time while the other sensors saw a maximum. This was at Day 1771.79, when the second peak in gas entry occurred. This event relieved stress in the system, with most PR sensors reducing rapidly after this time, many reaching a stress lower than before gas entry. The sequence of three events seen in UR sensors at Days 1807.03, 1812.28, and 1816.13 was also seen in many PR sensors. This was seen as a spike in stress, in some sensors in a positive sense (e.g. PR905), while in other these were negative (e.g. PR909). Radial stress showed another feature between the events lines at Days 1832.75 and 1836.98, with less defined peaks than the initial gas entry. This corresponds with the second peak in gas pressure. The final two events of note in radial stress occurred at Days 1872.41 and 1898.06. The first of these caused a reduction in stress of many of the PR sensors, with changes of between 15 and 2 kPa. The second saw an instantaneous increase, often of similar magnitude. It should be noted that similar was seen in UR, except the time of the second event was earlier for the PR sensors.

Figure 8-30c shows the pore pressure within the bentonite. This shows many features that were coincident with the events described for PR and UR sensors. This shows two features of note in UB901 and UB902. For UB901, from Day 1756 until 1809, the pore pressure increased in a series of steps, this behaviour was unusual and started pre-gas entry. At the start of each step a peak was seen that quickly decayed to a new pore pressure greater than before the step. The steps accelerated at Day 1803.53. This behaviour may be indicative of bubble propagation to UB901 of gas and may suggest that gas was mobile at a pressure lower than previously described. However, closer examination of the data shows that the first of the stepped responses happened on Day 1549.71, and gas injection did not begin until Day 1606.25. In fact, filter FL903 was not flushed and opened to gas pressure until Day 1577.40, some 27.7 days later. Therefore, the features seen were not associated with gas testing. However, the acceleration in the steps at Day 1803.53 may be associated with gas testing. The second feature of note was in UB902. At the time of gas entry, pressure in UB902 increased by approximately 10 kPa, before increasing rapidly by more than 4250 kPa at Day 1785.53. This indicates that gas had directly reached the sensor.

The final dataset highlighted in Figure 8-30d is the pore pressure recorded within the packered intervals of the two pressure relief holes (PRH). The PRH data gave an independent measure of pore pressure outside of the deposition hole and can give an indication of when outside features were acting upon the deposition hole. It can also indicate when major features were occurring in the deposition hole that affected the surrounding rock mass. There are two features of note. The first is the series of features seen in 7 of the 9 intervals at Days 1807.03, 1812.28, and 1816.13, as highlighted in UR and PR data. These have a similar form to that seen in the UR data and suggests a wider variation in pore pressure than simply just within the deposition hole. The second feature of note is the stepped decrease and stepped increase in pore pressure seen at Days 1872.41 and 1903.42. This is similar to that previously described for the UR and PR sensors. For both of these events, it either suggests that they occurred outside of the Lasgit experiment, or that pore pressure/stress changes as a result of gas entry had resulted in either gas entering the rock mass or subtle movements along the fracture network as a result of elevated stresses that caused pore pressure to change.

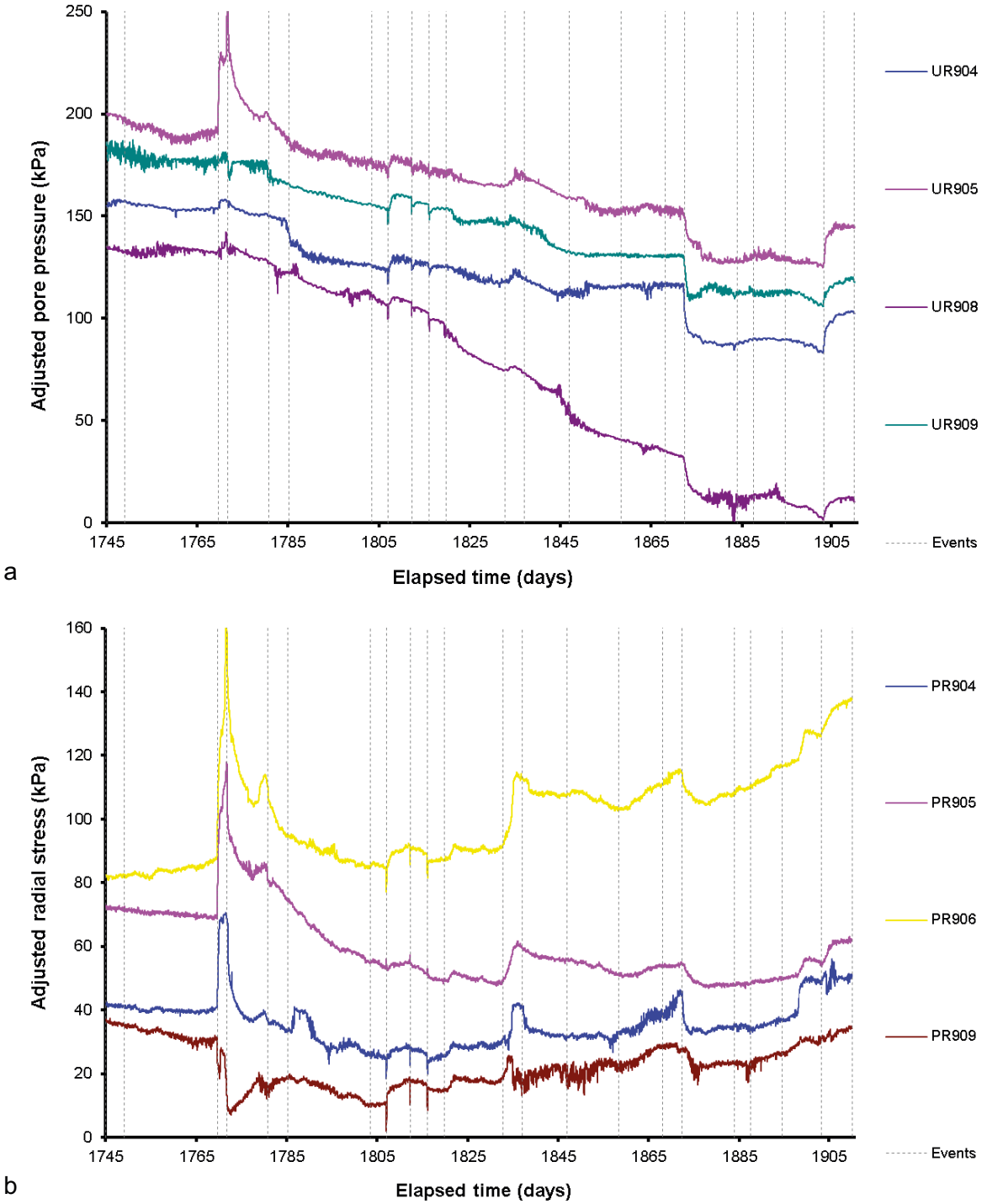

Figure 8-31. *Detail of radial stress and pore fluid pressure at the rock wall around the time of gas entry. a) Pore pressure at the deposition wall; b) Radial stress on the deposition wall.*

Figure 8-32 shows the pore pressure distribution at the deposition hole wall and how this varied during Gas Injection Test 2. Figure 8-32a shows pore pressure distribution just prior to peak gas pressure at Day 1768.00. This shows that the gas injection filter, highlighted in red, was 90° anti-clockwise of a region of high pore pressure. Generally, pore pressure increased from the top of the deposition downwards, with also higher pressure seen at around 270°. Figure 8-32b shows the variation in pore pressure at Day 1770.26. Pore pressure increased below the injector at an orientation of 225°, while the pressure in the high-pressure region reduced marginally. It is worth noting that the sensor directly opposite FL903 (FU909) did not register a change at gas entry. Figure 8-32c shows the change in pore pressure soon after gas entry at Day 1771.63. By this time, UR907 had increased by nearly 500 kPa and dominates the results, the centre of the high-pressure zone was 180° from the injector. The final image (Figure 8-32d) shows the change in pore water pressure more than 100 days after initial gas entry. It shows that the high-pressure region had broadened as UR910 had also increased by more than 500 kPa. Even though the high-pressure region dominated the results, a low-pressure region can be seen to have formed above the injector. In general, pore pressure had increased on the level of the injection filter and below, whilst it had reduced above the injector.

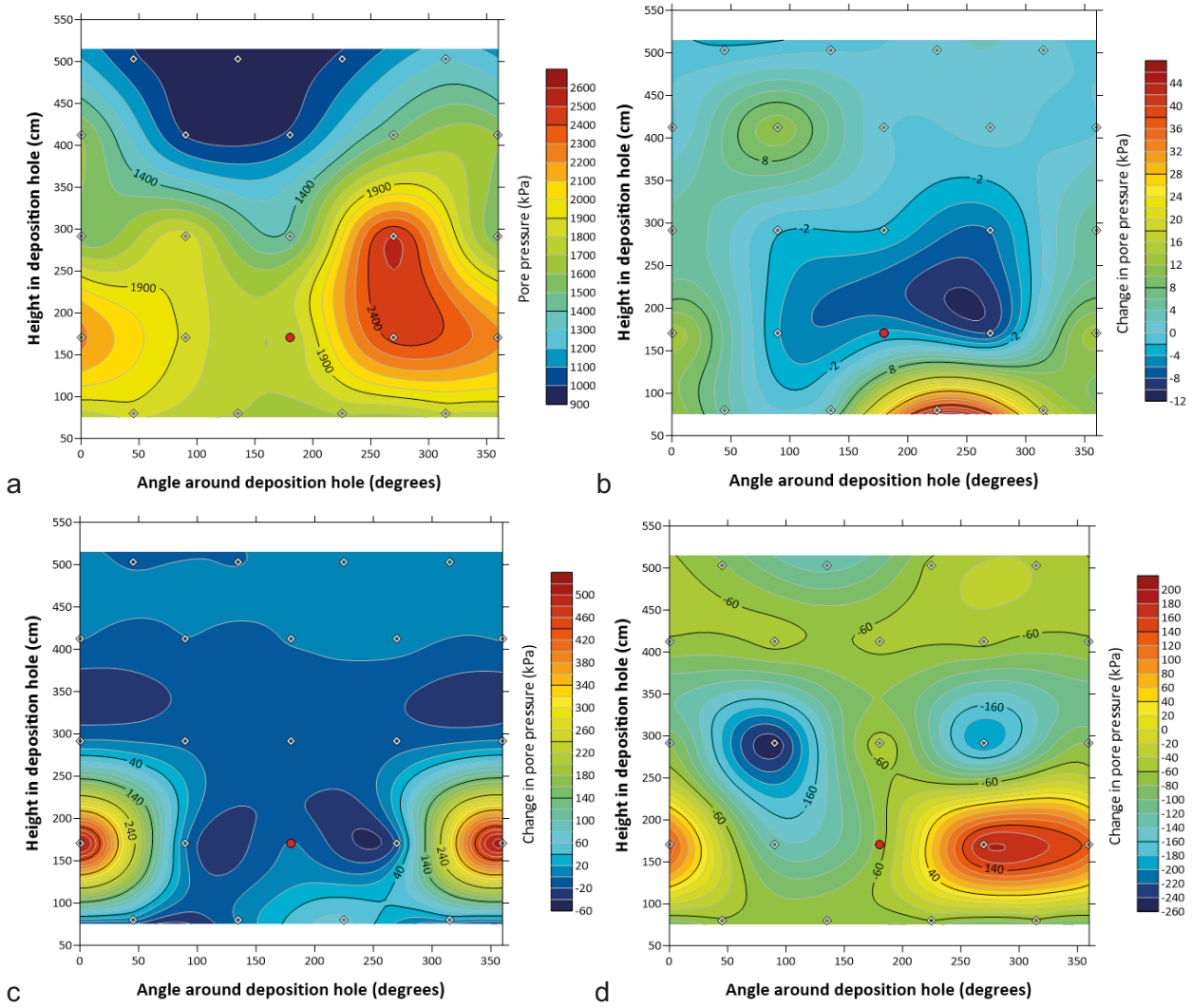

Figure 8-32. *Pore pressure distribution at the deposition hole wall around the time of gas entry during Gas Injection Test 2. a) Day 1768.00 (total pore pressure); b) Day 1770.26 (change in pore pressure); c) Day 1771.63 (change in pore pressure); d) Day 1903.42 (change in pore pressure).* ***Note:*** *the location of the injection filter is shown as a red circle.*

The distribution of radial stress on the deposition hole wall is shown in Figure 8-33. Stress prior to peak gas pressure is shown in Figure 8-33a at Day 1768.00. Generally, the stress level at the height of the injection filter was greater than higher in the deposition hole. A region of high stress existed along the length of the deposition hole at an orientation of 315°. The change in stress soon after gas entry is shown in Figure 8-33b at Day 1770.26. Stress increased in the base of the deposition hole below the injection filter. A low stress region formed at an orientation of about 240°, some 60° around the canister from FL903. Figure 8-33c shows the stress soon after at Day 1771.63. By this time, pore pressure at UR907 had greatly increased (orientation of 0°). However, no change was seen in radial stress, although stress was increasing in the base of the sensor array and the low stress region had increased in magnitude. By Day 1779.00 (Figure 8-33d) the changes in the stress sensors appeared to have finished, but the general pattern of stress persisted. Generally, stress was little changed within the deposition hole, with a raised stress at the base of the sensor array and a low stress region at 240°. Stress had also started to increase at the top of the sensor array as well. This increased region of stress became more pronounced by Day 1803.54 (Figure 8-33e), with a newly developed region of increased stress from near the injector up to the top of the sensor array at an orientation of approximately 135°. The low stress region persisted. By Day 1903.42 towards the end of gas injection, the ridge of elevated stress from the injector towards the top of the sensor array had subsided, but the region of raised stress at the top of the array persisted. The region of elevated stress in the base of the filter array had almost completely diminished, with the low stress region still evident. The plots in Figure 8-33 suggest a temporally evolving stress field as a result of gas movement. It suggests that gas at first migrated towards the base of the deposition hole, but in time it migrated upwards towards the top of the sensor array.

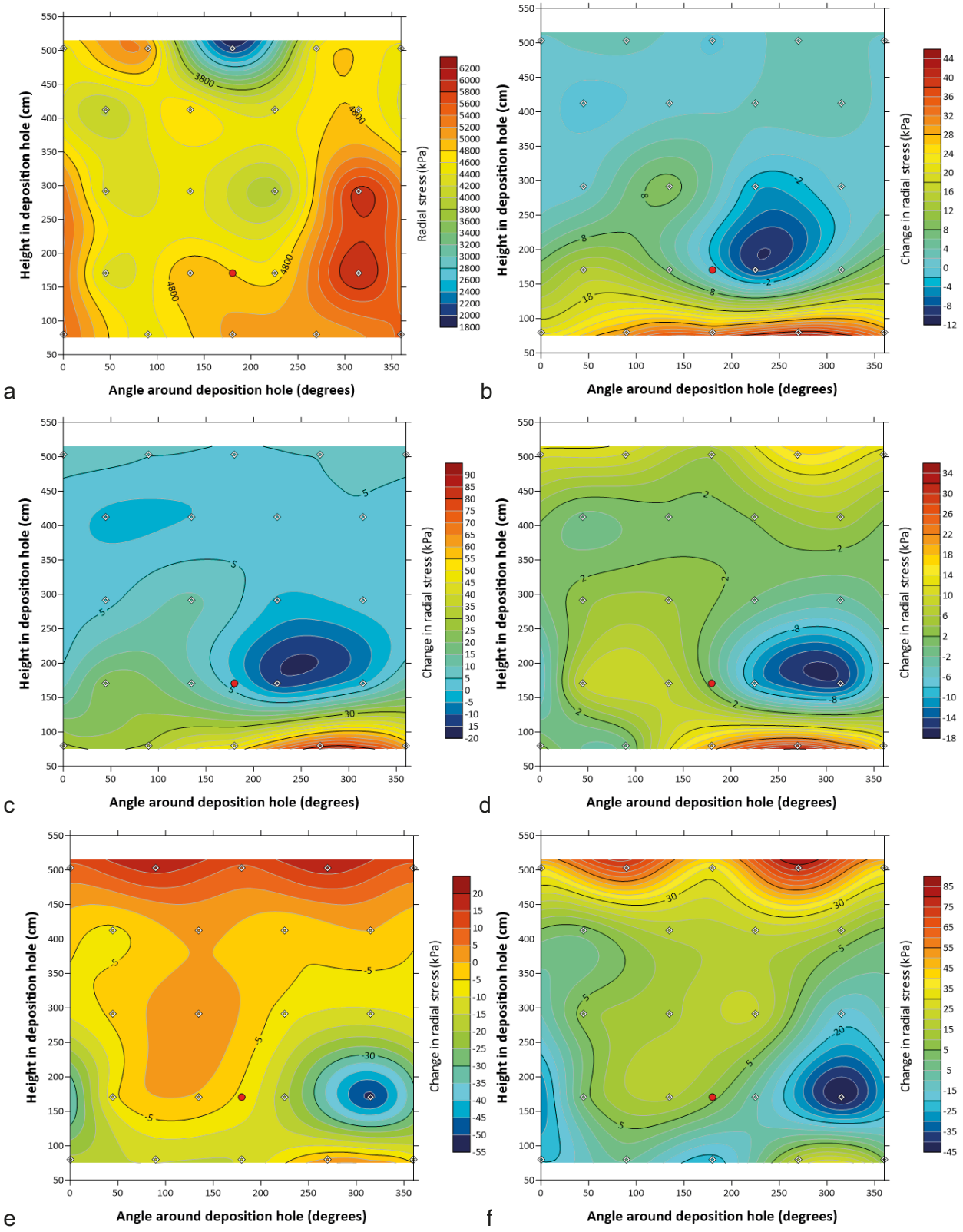

Figure 8-33. *Radial stress distribution at the deposition hole wall at times around gas entry during Gas Injection Test 2. a) Day 1768.00 (total stress); b) Day 1770.26 (change in stress); c) Day 1771.63 (change in stress); d) Day 1779.00 (change in stress); e) Day 1803.54 (change in stress); f) Day 1883.91 (change in stress).* ***Note:*** *the location of the injection filter is shown as a red circle.*

Comparing the observations of pore pressure and radial stress during the gas injection time shows many similarities and several differences (Figure 8-34). On Day 1769.66 (Figure 8-34a) there was correspondence in the changes in pore pressure and radial stress. A low pressure/stress region formed at an orientation of approximately 270° at a similar height as the injection filter, with a high pressure/stress region formed at the base of the sensor array. Considerable difference were then seen by Day 1780.82 (Figure 8-34b), although these results may have been masked by the pressure breakout at UR907. At this time a high water-pressure zone existed coincident with a low stress region at approximately 300–360° at a height similar, or just above the level of the injection filter. Towards the end of gas injection at Day 1903.42 (Figure 8-34c) there was considerable difference between the distribution of stress and pore pressure. The coincident high pressure/low stress feature persisted. A secondary low pore pressure region had formed at an orientation of 90° and a height of ~300 cm. This feature did not correspond with anything significant in radial stress. Both pore pressure and radial stress have a ridge feature orientated almost vertically at ~180°, starting from the injection filter and upwards towards the top of the sensor array. In radial stress, this led to a region of high stress at the top of the sensor array but there was no similar feature in the pore pressure data.

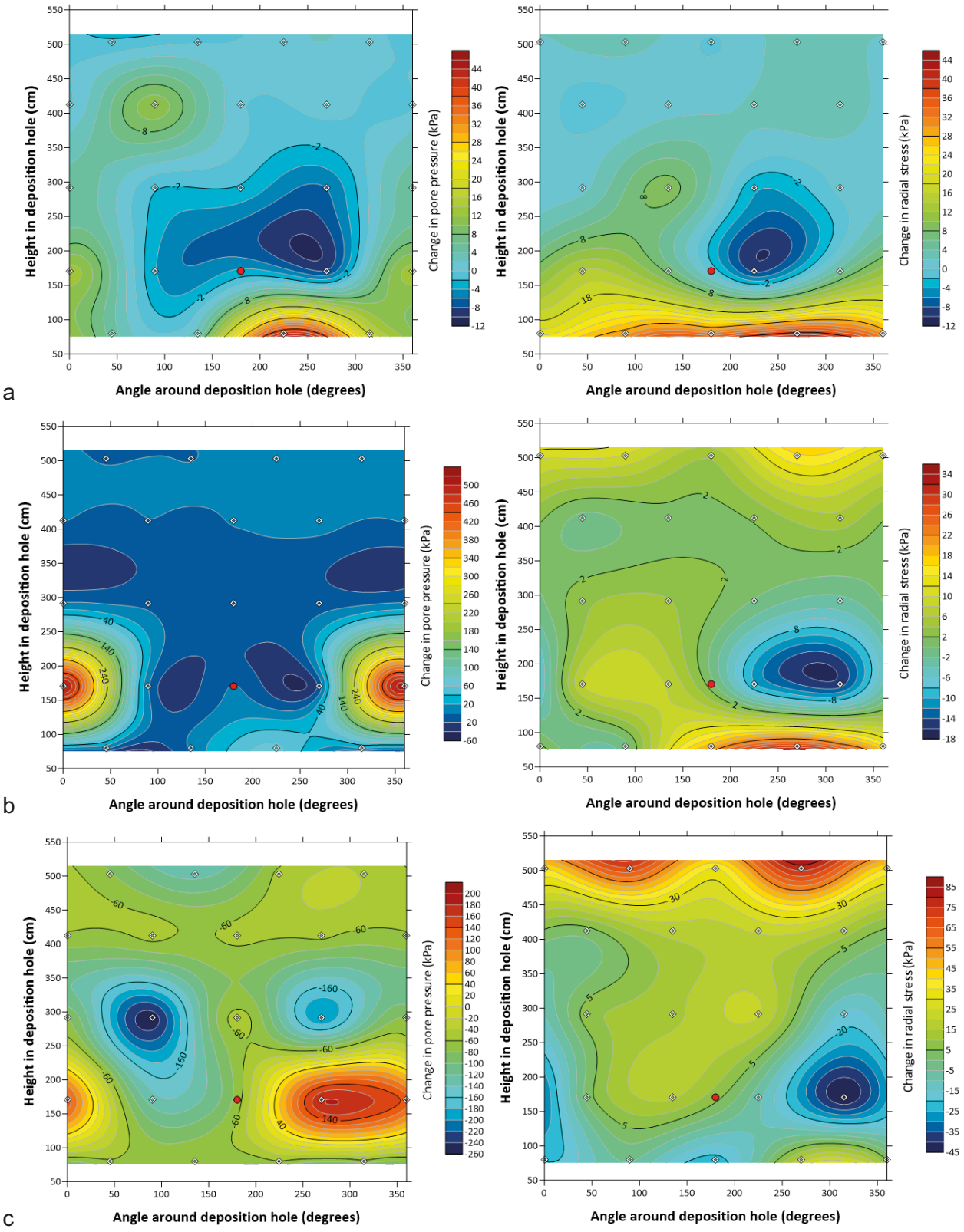

Figure 8-34. *Comparison of changes in pore pressure and radial stress at the deposition hole wall at times around gas entry during Gas Injection Test 2. a) Day 1769.66; b) Day 1780.82; c) Day 1903.42.* ***Note:*** *the location of the injection filter is shown as a red circle.*

Figure 8-35 shows sensor locations that show direct movement of gas. Peak gas pressure occurred at Day 1769.66. After 3.5 days, pressure at canister filter FL901 increased rapidly by 515 kPa and then started to decay (Figure 8-35b). A second pressure increase occurred on Day 1774.09 but this time only an increase of 95 kPa. Pressure slowly decayed until Day 1776.36, when pressure started to increase. This event was not instantaneous and took around a day to increase by around 3 290 kPa, up to 4 845 kPa. Pressure generally remained about this level until around Day 1790.03, when after a slow pressure increase, pressure increased to 5 185 kPa. Therefore, it took 17.57 days between the first entry of gas at FL903 and complete connection with filter FL903. Figure 8-36a shows a schematic of the initial gas flow, showing gas reaching filter FL901 without intercepting either FL902 or FL904.

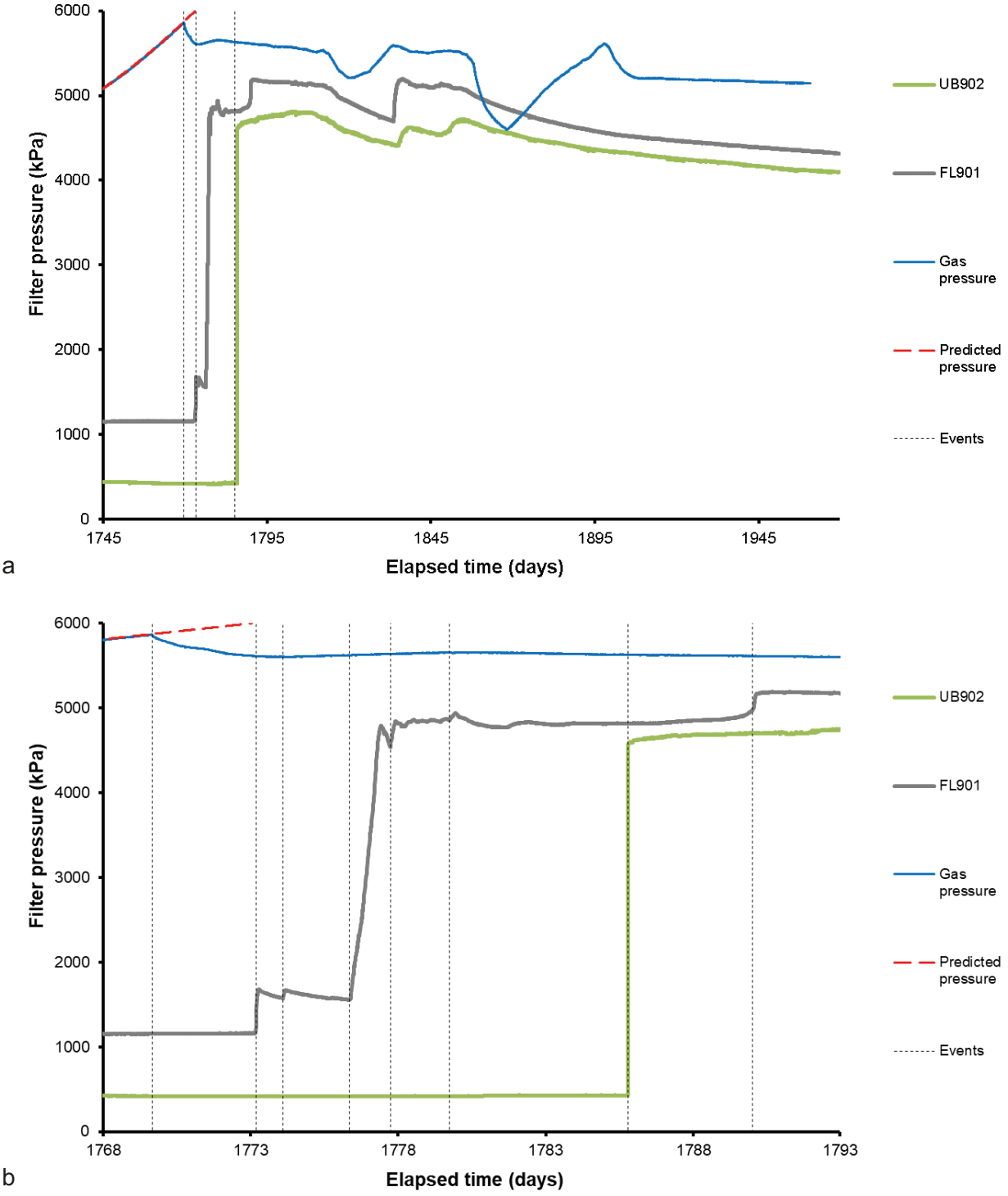

Figure 8-35. *Detail of sensors that show evidence of gas pressurisation during Gas Injection Test 2. a) Full injection stage, b) Detail around the time of gas injection.*

The second sensor highlighted in Figure 8-35 is UB902, a pore pressure sensor buried within the bentonite below the canister. This was at a constant pressure ~425 kPa and then increased almost instantaneously by 4 150 kPa at Day 1785.80 and continued to increase to a new level of 4 690 kPa. This was interpreted to be in direct communication with the injection filter. Figure 8-35a shows that UB902 continued to slowly increase until around Day 1812, when the gas injection pressure started to decay. In response, FL901 and UB902 also started to decay, but at a slower rate. The injection filter started to increase again at Day 1821 but FL901 and UB902 continued to decay. This shows that the reduction in gas pressure had closed the pathways communicating the injector with FL901 and UB902. Injection pressure peaked around Day 1833.5, when pressure in FL901 started to increase. This shows that the peak was caused by the re-opening of the pathway to FL901. This sensor nearly reached peak when pressure in UB902 started to increase at Day 1835. Again, this was likely to be because of the re-opening of the pathway to the sensor. It took a second pressure increase around Day 1850 for UB902 to be fully re-connected with the injector. As stated above, a suspected leak from an air activated valve resulted in the reduction in gas injection pressure between Days 1857.90 and 1868.09. Refilling the injection pump and re-establishing gas injection at Day 1868.09 caused the gas injection pressure to increase. Yet it can be seen that FL901 and UB902 continued to decay. The "leakage" event had severed the connection between the injection filter and FL901 and UB902, and this connection was not re-established for the remainder of the injection period. Gas pressure peaked once more at Day 1899 and injection pressure started to decay. There was no sign of this in FL901 and UB902 suggesting that this peak was caused by the establishment of a new pathway. Figure 8-36b shows a schematic of the continued gas flow, showing gas reaching UB902 towards the bottom of the deposition hole.

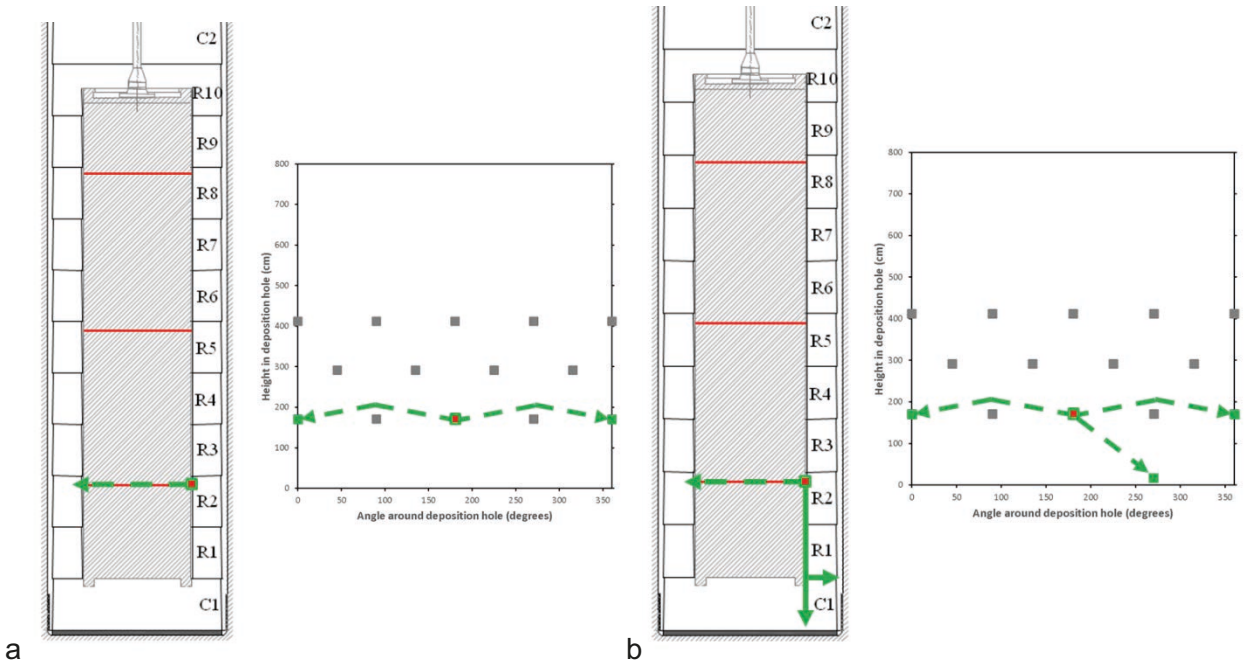

Figure 8-36. *Schematic of the direction of gas flow during Gas Test 2 in lower filter FL903. a) Gas movement to FL901; b) Gas movement to UB902.*

8.4 Gas sampling

One of the objectives of Gas Test 2 was to determine if gas had exited from the deposition hole. Gas migration was interpreted as propagating along the outside of the canister downwards. It is probable that gas exited the deposition hole along the interface between blocks R1 and R2. Neon was used as the gas permeant for Gas Test 2 as it was absent from the pore water at Äspö and its detection at the pressure relief holes would confirm that gas had exited the deposition hole. Gas sampling in the pressure relief holes after the completion of the gas-injection phase clearly showed a trace of neon of 117 ppm in interval PRH1–2. All other PRH intervals showed undetectable (< 50 ppm) amounts of neon both before and after Gas Injection Test 2. Therefore, gas had exited the buffer and transported to one of the PRH intervals through the fracture network.

8.5 Summary of Gas Test 2

Gas Injection Test 2 was conducted in filter FL903 on the lower array of filters on the canister surface. It was the second test using FL903 starting 596 days after the first test in this filter, with a much longer injection after gas entry of 191 days, with neon as the injection gas. Gas pressure was raised from background levels up to gas peak pressure using four distinct pressure ramps, being held at constant pressure in between.

1) The first pressure ramp started at Day 1606.25 using a constant injection rate of 4.0 ml h^{-1} with an initial volume of 2 065 ml of gas. This raised pressure from 1 299 to 2 545 kPa in 10.9 days when pressure was held constant from Day 1617.13 for 14.9 days. Throughout the period, the STP flow into the clay ranged from 5.89×10^{-10} to 3.42×10^{-9} m^3 s^{-1}. This resulted in a small flow into the clay, with 0.07 mol entering the clay. As gas pressure was held constant at around 2 545 kPa, a small amount of gas entered the clay, following which a flow rate of 2.5×10^{-10} m^3 s^{-1} (1 282 µmol d^{-1}) was observed.

2) The second pressure ramp was started at Day 1632.06 using a constant injection rate of 1.2 ml h^{-1}. This raised pressure from 2 546 to 3 783 kPa in 12.6 days, when pressure was held constant from Day 1644.70 for 28.6 days. During this period the interface vessel was re-charged with ~2 800 ml of neon at a pressure of 3 771 kPa. STP flow into the clay ranged from 1.76×10^{-9} to 2.83×10^{-9} m^3 s^{-1}, resulting in a small flow into the buffer, with 0.1 mol entering the clay. When gas pressure was held constant at around 3 780 kPa, a total of 0.044 mol entered the clay, with an average flow rate of 4.57×10^{-10} m^3 s^{-1} (1 533 µmol d^{-1}).

3) The third pressure ramp was started at Day 1673.29 using a constant injection rate of 2.0 ml h^{-1}. This raised pressure from 3 771 to 5 059 kPa in 16.7 days, when pressure was held constant from Day 1689.98 for 55.1 days. STP flow into the clay ranged from 2.58×10^{-11} to 2.61×10^{-9} m^3 s^{-1}, resulting in a small flow into the clay, with 0.06 mol entering the clay. As gas pressure was held constant at around 5 060 kPa with an average flow rate of 3.05×10^{-10} m^3 s^{-1} (661 µmol d^{-1}).

4) The fourth, and final, pressure ramp was started at Day 1745.11 using a constant injection rate 0.5 ml h^{-1}. This raised pressure from 5 089 to a gas peak pressure of 5 868 kPa at Day 1769.65 in 24.5 days, following which injection continued for a further 191 days. Up until gas entry, flow was seen into the clay at a nominal rate of around 8.77×10^{-10} m^3 s^{-1}, resulting in a small flow into the clay, with 0.08 mol of gas entering the clay.

Major gas entry and peak pressure occurred during gas ramp 4.

1) Day 1769.95: The first clear evidence of gas entry occurred, when flow into the clay began to accelerate. This resulted in a peak in gas flow of 6.82×10^{-8} m^3 s^{-1} at Day 1769.7. This peak was short-lived with flow into the clay reducing to less than the flow into the system within 5 days. At Day 1769.95 a stepped response was seen in UR905 and UR904 with increases of 30 and 5 kPa respectively, while PR906, PR505, PR904, PR903, and PR908 showed increases of 75, 48, 29, 35, and 12 kPa respectively. At this time, pore pressure at UR908 and UR907 started to increase, while PR909 saw a decrease in stress of approximately 20 kPa. Pore pressure increased below the injector at an orientation of 225°, while the sensor directly opposite FL903 (FU909) did not register a change at gas entry. Stress increased in the base of the deposition hole below the injection filter with a low stress region forming at an orientation of about 240°, some 60° around the canister from FL903.

2) Day 1771.64: A second significant peak in gas flow occurred. Around this time a further short-lived increase in pressure at UR905 of 26 kPa occurred, together with an increase in pressure of 490 kPa at UR907, and a short-lived reduction in UR909 of around 10 kPa was seen. No corresponding change in radial stress was observed near to UR907. Radial stress at the base of the sensor array was increasing, but most PR sensors started to reduce rapidly after this time, many reaching a stress lower than before gas entry.

3) Day 1773.19: the pressure at filter FL901 increased rapidly by 515 kPa and then started to decay. This was the start of a series of pressure increases that took 17.57 days to establish full connectivity between FL901 and FL903, which was located 180° around the canister from the injector, with pressure reaching 5 185 kPa, only 420 kPa less than the gas injection pressure.

4) Day 1780.40: Gas pressure started to recover from around Day 1774.40 and reached a smooth secondary peak around Day 1780.40 at a pressure of 5 650 kPa.

5) Day 1780.82: A small peak feature in UR905 and a distinct reduction in pressure at UR909 occurred. By this time the distribution of stress was little changed within the deposition hole, with a raised stress at the base of the sensor array and a low stress region at 240°. Stress had also started to increase at the top of the sensor array as well. The pattern of pore pressure distribution was dominated by UR907, but a high-pressure region existed coincident with a low stress region at approximately 300–360° at a height similar to the injection filter.

6) Day 1785.18: pressure reduced by about 20 kPa in UR904, soon after (Day 1785.53), UB902 increased by more than 4 250 kPa. This indicated that gas had directly reached this point.

7) Day 1803.53: Sensor UB901 had been showing unusual behaviour in a stepped increase in pressure from before Gas Injection Test 2 had started. However, at Day 1803.53, the steps accelerated, probably as a response to gas pressure. By this time, the stress distribution in the deposition hole showed a newly developed region of increased stress from near the injector up to the top of the sensor array at an orientation of approximately 135°.

8) Days 1807.03, 1812.28, and 1816.13: A series of three similar events occurred when pressure in many UR sensors decreased and quickly recovered. Spikes were seen in stress, in some sensors the response was positive (e.g. PR905), whilst in others it was negative (e.g. PR909). This triplet of events was also seen in 7 of the 9 intervals in the pressure relief holes, indicating that a wider variation in pore pressure was occurring and not just simply within the deposition hole.

9) Day 1812: A secondary gas entry event started. A series of five peaks in gas flow (Days 1812.28, 1814.27, 1815.44, 1816.13, and 1818.14) contributed to a reduction of gas pressure by approximately 300 kPa by Day 1821, before recovering over the following 22 days by 375 kPa.

10) Day 1832.75: A second peak in gas pressure occurred, with a less defined peak than at initial gas entry. This was seen in the radial stress, as a pressure increase in several UR sensors and the instantaneous increase in pore pressure at UR910 by 580 kPa.

11) Day 1856: A second pressure decrease started, with a reduction in gas pressure of approximately 850 kPa over 12 days. On Day 1868 the injection pump required re-filling, which was a standard procedure. Following this, gas pressure started to increase once pumping had been re-initiated. As this behaviour was instantaneous, it has been deduced that one of the air-actuated valves on the control board had partially been opened and that the pump had therefore been slowly leaking between Days 1860 and 1868. The re-establishment of gas injection and the increase in gas pressure was not seen in the directly connected sensors at UB902 or FL901, showing that the connection had been lost by the reduction in gas pressure.

12) Days 1872.41 and 1903.42: The final two events of note. The first of these caused a reduction in pore pressure of almost all UR sensors, with changes of between 5 and 30 kPa and a reduction in stress of many of the PR sensors, with changes of between 2 and 15 kPa. The second saw an instantaneous increase, often of similar magnitude. It should be noted that similar was seen in UR, except the time of the second event was earlier for the PR sensors. Both features were seen in the pressure relief holes, suggesting that they occurred outside of the Lasgit experiment, or that pore pressure/stress changes as a result of gas entry has resulted in either gas entering the rock mass or subtle movements along the fracture network as a result of elevated stresses caused pore pressure to change.

By the end of gas injection, a total of 4.23 mol of neon had entered the buffer. The ridge of elevated stress from the injector towards the top of the sensor array had subsided, but the region of raised stress at the top of the array persisted. The region of elevated stress in the base of the filter array had almost completely diminished, with the low stress region still evident. In general, pore pressure had increased at the level of the injection filter and below, whilst it had reduced above the injector. The distribution of pore pressure and stress suggests a temporally evolving stress field as a result of gas movement. It suggests that gas at first migrated 180° around the canister to filter FL901 and from there propagated downwards towards the bottom of the deposition hole. However, in time it migrated up the deposition hole towards the top of the sensor array. Gas sampling in the pressure relief holes showed a trace of neon of 117 ppm in interval PRH1–2, all other intervals were undetectable (< 50 ppm). This demonstrated that trace neon had exitted the deposition hole. The use of neon did not alter the characteristics of the system during gas injection and showed that the different molecular weight of neon compared to helium did not alter the underlying physics of gas migration. Given the greater molecular size of neon compared to helium then helium would have migrated in greater amounts.

9 Gas Injection Test 3 (Day 2086 – 2722)

The third significant stage of the Lasgit experiment started on Day 2086.23 (19th October 2009) and was completed at Day 2722.15 (16th July 2012); a total stage time of 635.92 days. The repeat test in FL903 conducted as Gas Injection Test 2 was deemed a success and did not need repeating immediately after Gas Injection Test 2. The filter array on the canister was designed with filters of differing size. Two questions arose from the first two gas injection tests that were addressed during a third gas injection test;

1) Does gas behave the same at a location where local stress is markedly different from FL903?

2) What role does the filter dimension play on gas injection properties?

Laboratory experiments had shown that gas entry occurred at a pressure close to the local stress (Harrington and Horseman 2003), therefore performing a test within an upper array filter would allow observation of the gas flow properties under lower stress conditions. Filter FL903, as used in Gas Injection Test 1 and 2, had a filter radius of 50 mm. In contrast, filter FU910, as used in this gas injection test, had a radius of 25 mm. It had been hoped to use filter FU912 with a diameter of 5 mm. However, this was found to be problematic and could not hold hydraulic pressure without a high flow-rate. Filter FU910 therefore had an area ¼ of that of filter FL903. Figure 9-1 shows the plan of the test period. Throughout the stage, artificial and natural hydration was occurring, apart from at times when problems were encountered with the hydration system. Gas Injection Test 3 was conducted between Day 2257.23 and 2614.42 (Figure 9-2).

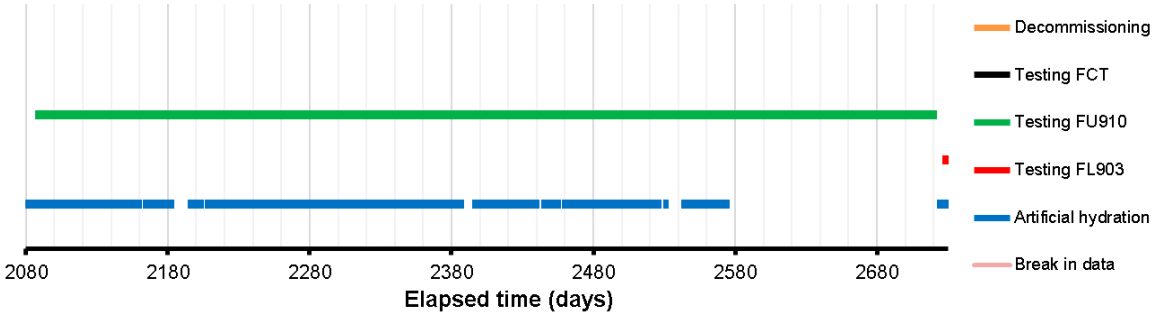

Figure 9-1. *Test stages of the Lasgit experiment showing what was conducted during Gas Injection Test 3.*

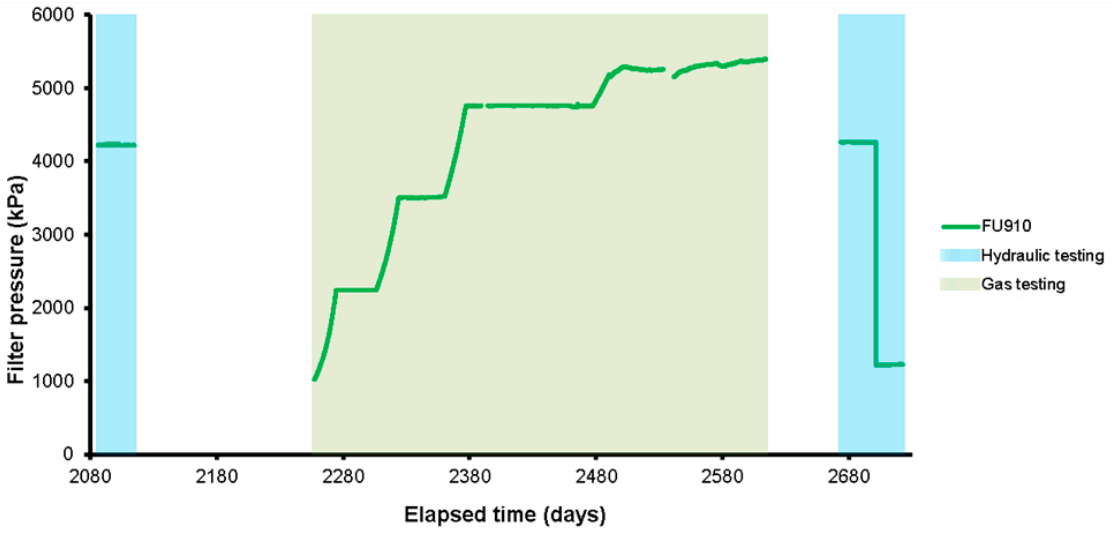

Figure 9-2. *The filter pressure of FU910 during Gas Injection Test 3. Two two-stage hydraulic tests were conducted either side of four stage gas injection test.* ***Note:*** *blue shading shows periods of hydraulic testing, green shows gas testing.*

Gas Injection Test 3 comprised of four stages (Figure 9-2); 1) a two-stage hydraulic test to determine the hydraulic properties of the bentonite at filter FU910; 2) four-stage gas injection ramp to achieve gas entry at filter FU910; 3) continued gas injection for a prolonged time period in order to observe the movement of gas within the deposition hole; 4) a repeat two-stage hydraulic test to determine the hydraulic properties of the bentonite at filter FU910.

9.1 Description of the field parameters during the period

Before describing the gas injection test, the field parameters will be described (boundary conditions). **Note:** The grey areas displayed in the graphs below show periods when artificial hydration did not occur.

Figure 9-3 shows the pore fluid pressure in the filter mats. As with previous stages, filter FR901 was not artificially hydrated and recorded local pore pressure. As seen, FR901 slowly decayed during the period, indicative of drawdown of the pore pressure as a result of proximity to the drained tunnels. However, it can be noted that filter FB904 showed a lower pressure since the previous calibration at Day 1967. In error, FB904 had been isolated from downhole and was measuring the pressure in the calibration line in the laboratory and not the filter mat pressure. During the calibration visit at Day 1967 it was decided to replace the transducer for FB903 as the calibration data suggested this could be a damaged pressure transducer. Once the data was calibrated it can be seen that FB903 had drifted until Day 1967 and this was assumed to be transducer drift since it was unlikely that the pressure in the filter mat was greater than the hydration pressure in the syringe pump. From Day 1967 onwards filters FR902, FB903, and FB903 all recorded the same pressure; that of the hydration pump. The laboratory PC failed at Day 2389 and was fixed by Day 2394. During this 45-day period the system would have been shut-in. On re-establishing the PC all systems returned to the hydration pressure. However, filter FB904 was accidentally isolated from the system and underwent pressure decay. This was remedied within 24 hours, but is seen as a small reduction in filter pressure. The logging computer also failed between Days 2533 and 2541, losing only National Instruments logged parameters and causing a short pause in artificial hydration.

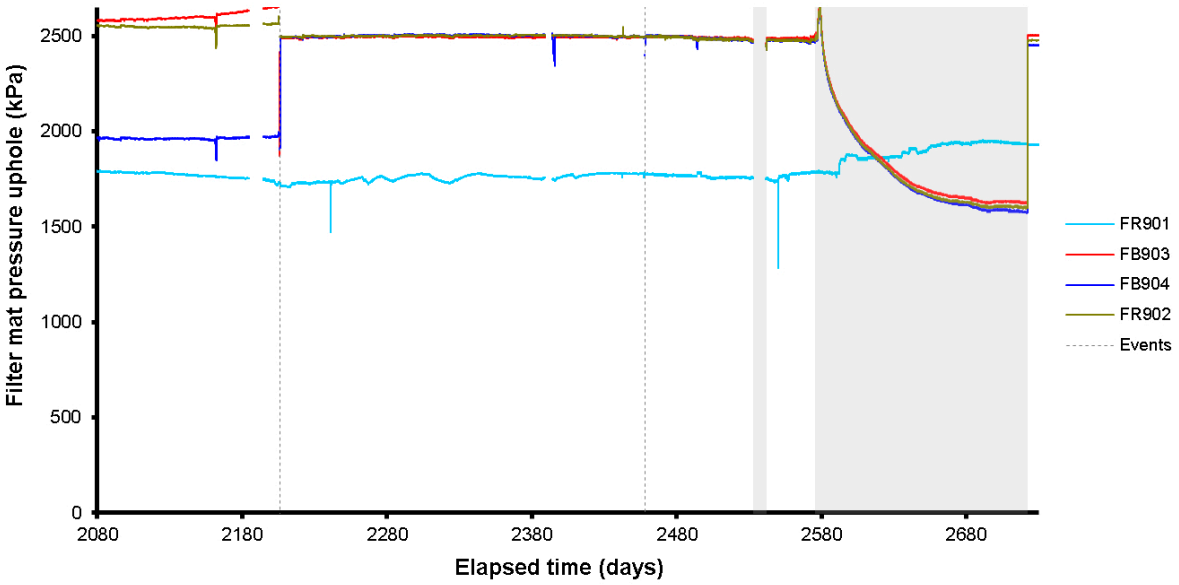

Figure 9-3. *Evolution of water pressure in the filter mats located on the borehole wall and within the bentonite blocks.*

On Day 2576 (22nd February 2012) it was noted that pressure in all of the upper canister filters had been decreasing for 24 hours, while the lower and mid-array filters showed a 20 kPa change. This was seen as indicative that gas had reached one of the canister filters. It was decided to stop artificial hydration in all filters, including the filter mats. This would identify if gas migration had reached any of these points. Therefore, the filter mats were shut-in between Days 2575.89 and 2722.22. It can be seen in Figure 9-3 that the pressure in the filters mats decayed to approximately 1 600 kPa for filter mats FR902, FB903, and FB904. This is substantially lower than the nominal hydration pressure of 2 500 kPa.

Figure 9-4 shows the pore pressure within the bentonite buffer, recorded at six locations. Figure 9-4a shows the results were dominated by pressurisation of filter UB902 during the previous gas injection test. Filter UB902 saw a steady decrease. However, in contrast with previous observations, pressure started to increase around the time of filter shut-in at Day 2575.89. By this time UB902 had reduced by 600 kPa. The correlation between the stopping of artificial hydration and the increase may have been co-incidental. At this time, as seen in Figure 9-4b, UB926 also started to increase markedly, all other filters within the bentonite also showed an increase in pressure. However, their increase was delayed by up to 75 days. All filter locations showed a annual variation, with UB924 being the most prominent. At this location an annual fluctuation of 200–250 kPa was seen. Filter UB926 showed the greatest variation, with 450 kPa seen around Day 2 280 and 300 kPa seen starting around Day 2580. All filters showed pore pressure in the bentonite was increasing.

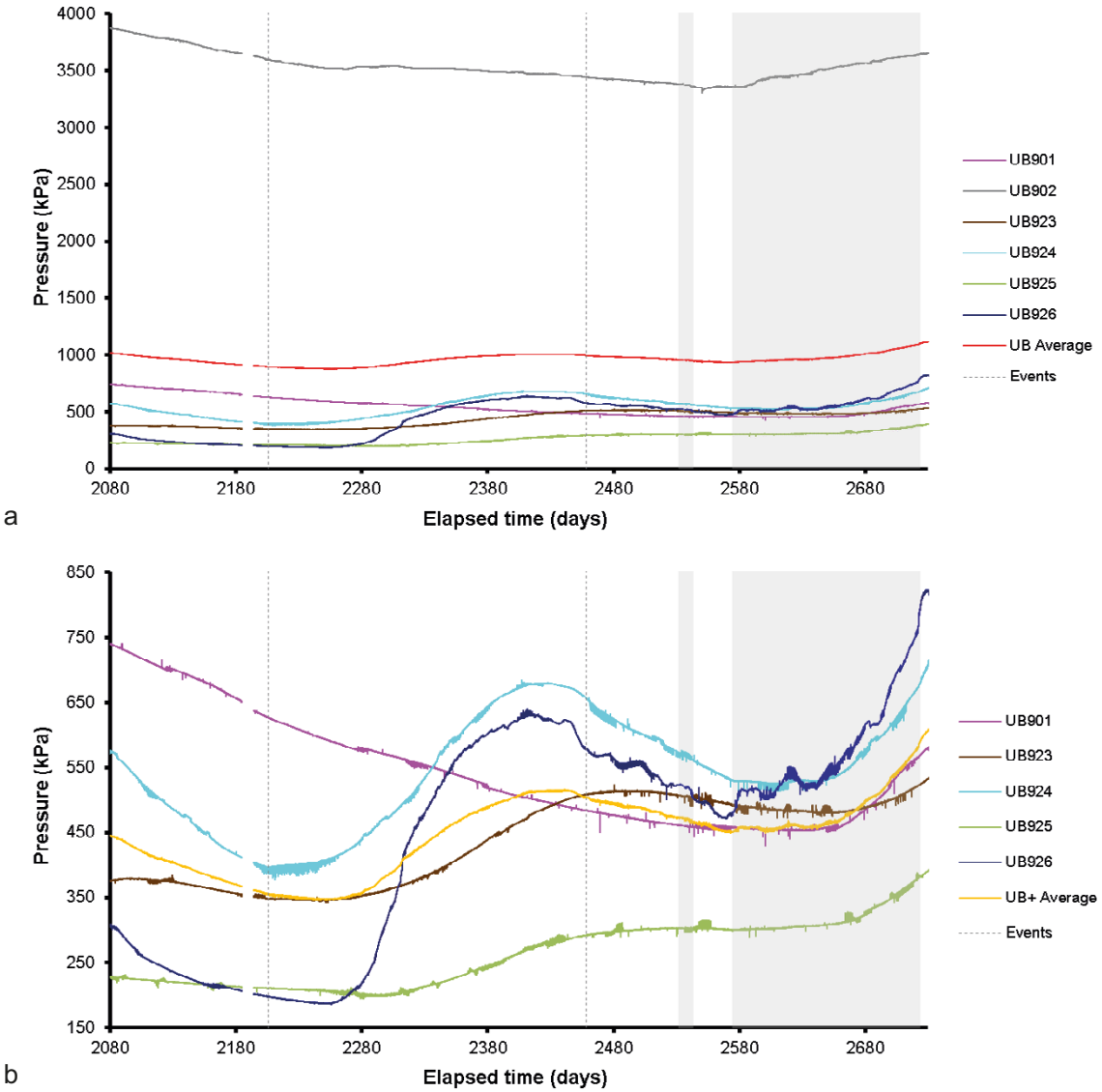

Figure 9-4. *Variation in porewater pressure within the bentonite at the 6 monitoring points: a) all six sensors; b) detail of five sensors.*

When not used for artificial hydration of the system pore pressure was also recorded in the canister filters. Figure 9-5a shows that the data during this period was dominated by the operation of filter FU910 for the hydraulic and gas injection testing. Only the upper array of filters was isolated during the reporting period. Filters FU909 and FU912 mirrored one another. This was later found to be because of a plumbing error within the Lasgit laboratory, with FU912 connected to the drain of FU909. This was remedied at the calibration visit on Day 2968 (19th March 2013). The upper filters generally showed an annual variability, Figure 9-5b. However, they were dominated by pressurisation events seen in FU911 and FU912. These related to the gas injection test and are described in more detail in Section 9.3. The pumps attached to the upper- and lower-array filters reacted at Day 2575, suggested that one, or more, of these filters was being pressurised as a result of the gas test. Artificial hydration in all canister filters was therefore halted, creating the distinctive decay in pressure, as seen in Figure 9-5b. Most filters reached a minimum and then started to increase, with only FM905 reaching a steady asymptote.

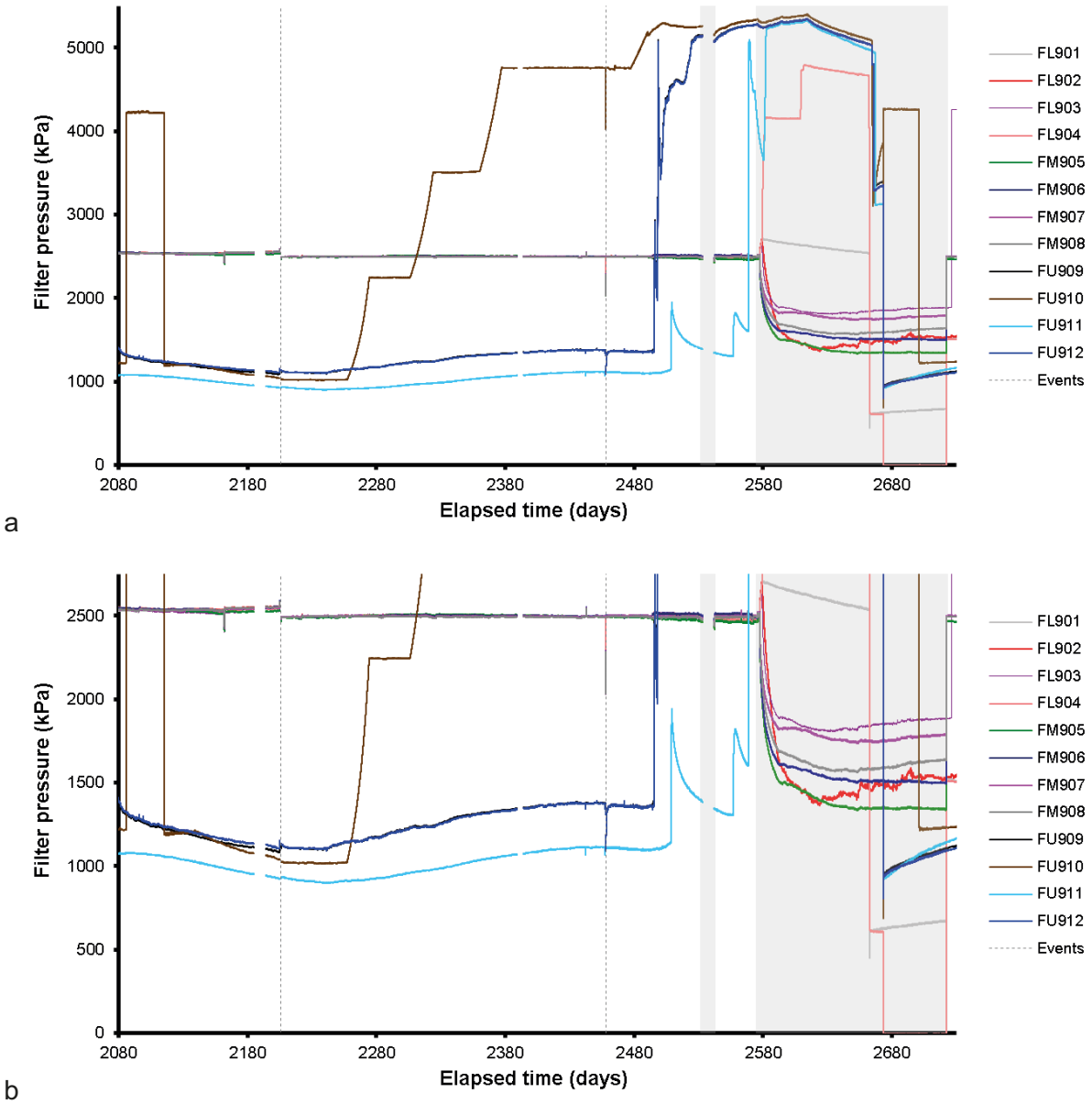

Figure 9-5. *Filter pressures on the canister surface. a) complete range of filter pressures dominated by the activities in filter FU910; b) detail of the pore pressures in the canister filters.*

Figure 9-6 shows the variation of pore water pressure at the rock wall. As can be seen, pressure was heterogeneous within the deposition hole, with around 2 000 kPa variation. The data were dominated by two features; increase in pore fluid pressure for UR909 and annual cyclicity differences throughout the deposition hole.

During Gas Injection Test 2 two increases in pore fluid pressure were seen in UR907 and UR909. During Gas Injection Test 3 (Figure 9-6), two further pressurisation events were seen in UR909. The first occurred at Day 2241.10, initially as a reduction in pressure of approximately 100 kPa, then progressing to a rapid increase in pressure of 550 kPa starting at Day 2241.22. Pore pressure at this location peaked at 2 818 kPa and then slowly decayed to a new asymptote of around 2 600 kPa. The event at the increase in pressure can be seen in almost all UR sensors.

The second event also occurred with a small decrease in pore pressure, followed by a sharp increase in pressure. The initial decrease was ~50 kPa and occurred at Day 2550.20. Pressure then increased rapidly, beginning at Day 2550.32, peaking at 2 930 kPa some 450 kPa above the minimum of the initial pressure response. This event was more pronounced in all of the UR sensors. After reaching a peak in pressure, pressure then decreased, with a small secondary event at Day 2592.35. Similarly, this could be seen as a small disturbance in most UR sensors. Pressure in UR909 decayed to a new asymptote of 2 830 kPa, some 100 kPa below the peak in pressure.

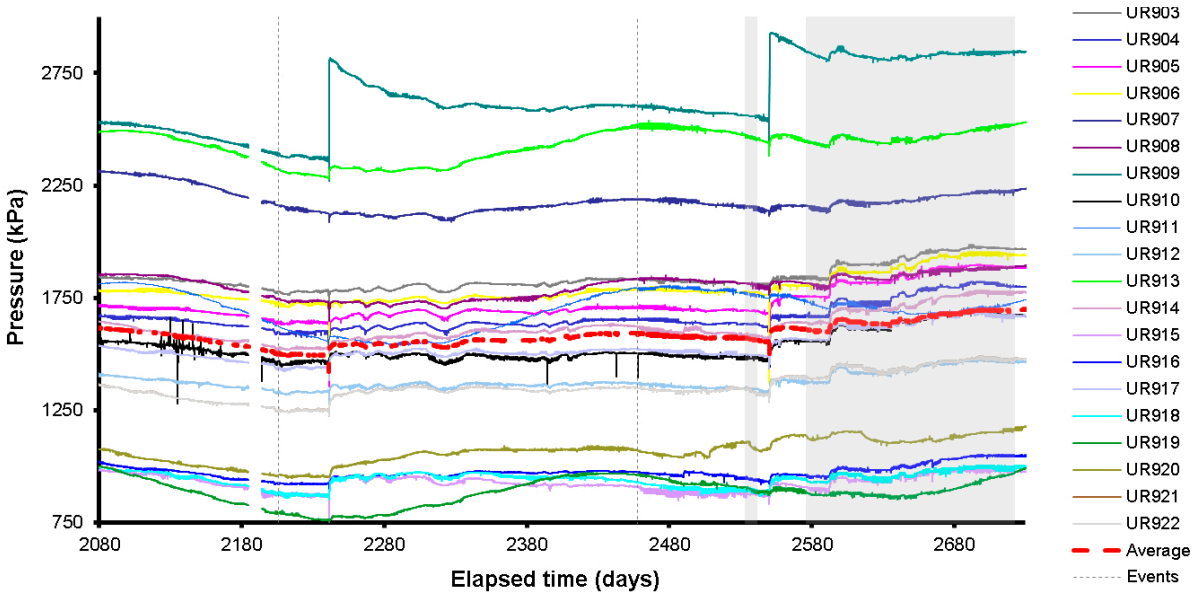

Figure 9-6. *Variation in porewater pressure with time measured at the rock face.*

Figure 9-7 compares the three pore pressure events seen in FU909. This shows that each successive event was lower in magnitude than the previous and that the settling of pressure after the peak also reduced with subsequent events. Therefore, each event was increasing pore pressure by increasing amounts with each event.

As noted for Gas Injection Test 2, considerable heterogeneity was seen in the distribution of pore fluid pressure within the deposition hole (see Figure 9-6). Generally, pore pressure was greatest at the base of the deposition hole, decreasing with height. This holds for all levels, except for the bottom UR level within bentonite ring 4 (R4), which was lower in pressure than the level in ring 5 (R5) and similar to that of ring 7 (R7). It was also noted that the pore pressure cyclicity, with a period of a year, was greatest in the middle of the array of sensors, located at the canisters middle. Here, the variation in pore pressure within the level was also greatest, with around 1 000 kPa variation. Pore pressure variation was least at the base of the deposition hole, where the wall rock had greater numbers of fractures. The heterogeneity seen in the pore pressure at the rock wall is described in greater detail in Section 16.3.4.

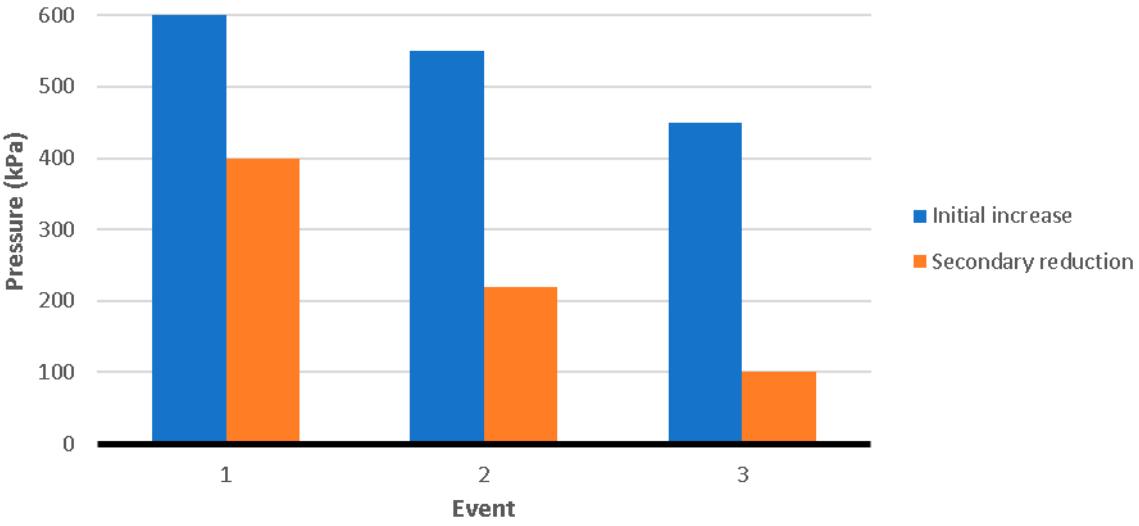

Figure 9-7. *Pore pressure events in FU909.*

Radial stress measured at the rock wall is shown in Figure 9-8a for all locations and Figure 9-8b in detail for all sensors excluding PR921. As seen, the radial stress had increased over the period, with annual variation seen. The radial stress within the bottom of the deposition hole was greatest in bentonite rings R4 and R5, with the lowest stress seen in the top of the deposition hole within bentonite ring R10. There was additional heterogeneity within the deposition hole, with the greatest range seen within R10. The next greatest variation of nearly 2 000 kPa was seen centrally within the deposition hole at bentonite ring R7. The lowest variation at a height basis was seen at the bottom of the hole at bentonite ring R4 and towards the top of the hole at ring R9. The range was consistent for the period, except for the sensors at the level of ring R7; where the range had slowly decreased during Gas Injection Test 3.

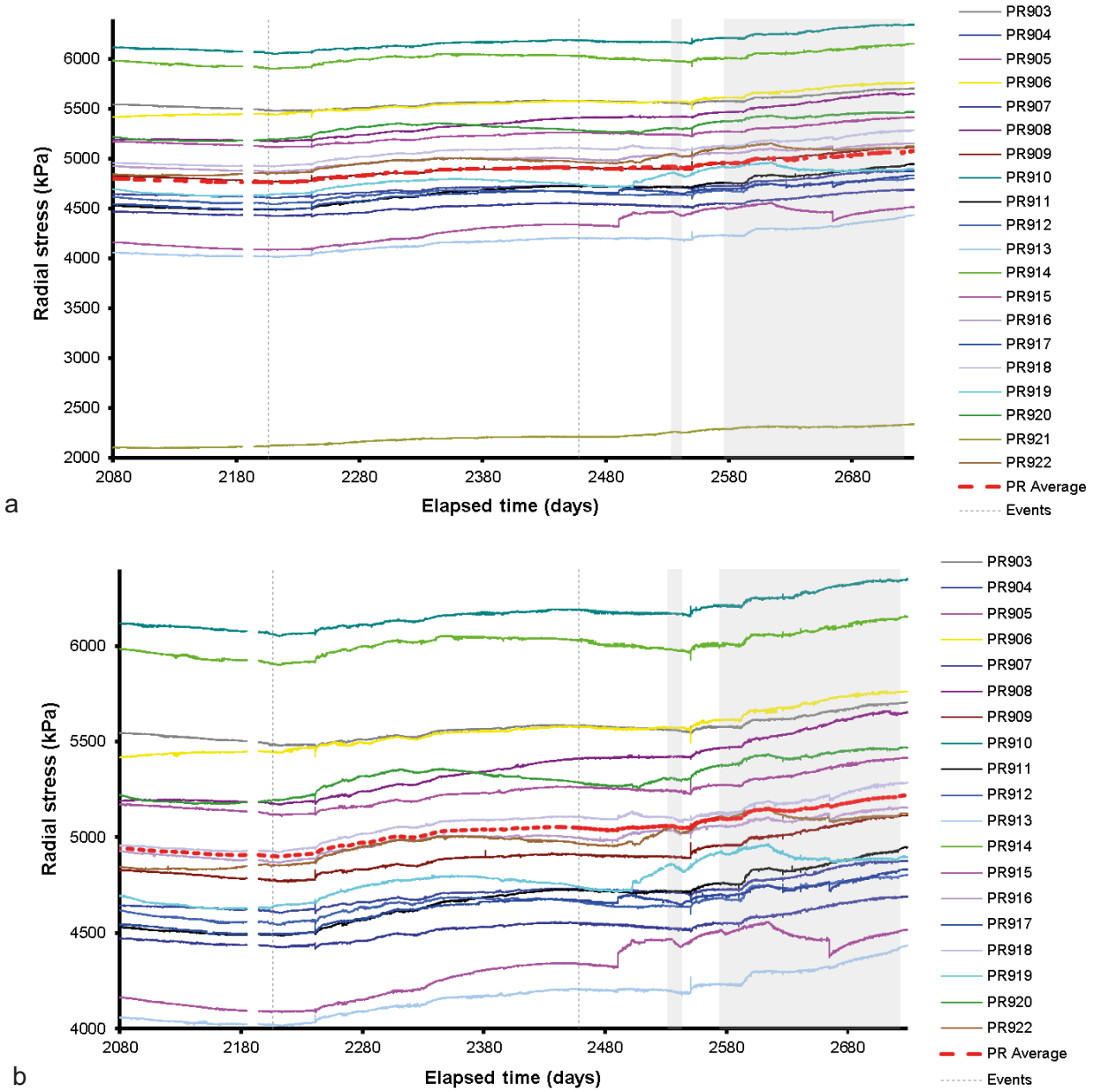

Figure 9-8. *Variation in radial stress at the rock wall with time. a) radial stress for all locations; b) radial stress for all locations excluding PR921.*

On a shorter time frame, there are a couple of stress variations seen. The pore pressure events at Day 2241 and Day 2550 show in all radial stress sensors. This demonstrates the close coupling of pore pressure and stress at the rock wall. The most significant radial stress variations were seen between Day 2490 and Day 2665. These were seen predominantly in the sensors at the level of ring R9, with lesser disturbance in all other levels. This is described in greater detail in Section 16.4.1.

The stress acting on the canister was measured at three locations, as shown in Figure 9-9. During the current stage the average stress increased around 300 kPa, with annual variation superimposed. Compared with the previous chapters, there was less correlation between the three sensors. All three sensors showed similar features up until Day 2518, when PC903 had considerably different response to PC901 and PC902. This change in PC903 may have been associated with gas flow and is described in greater detail in Section 9.3. Generally, it can be noted that PC901 increased in magnitude much more than the other two sensors, with PC903 showing little increase over the time period, albeit with a complicated response that may be associated with gas flow. All three sensors showed events that may correlate with gas testing.

Axial stress within the bentonite is shown in Figure 9-10. This shows considerable spread of ~1 500 kPa within the deposition hole. All locations showed a degree of annual cyclicity. Generally, axial stress was lowest at the base of the deposition hole within the bottom segment of the bentonite buffer (C1). Stress within the upper most section of the hole within segment C5 was generally constant throughout the period, whereas stress increased within segments C1 and C3. Axial stress during the period was dominated by two features. The first occurred between Day 2080 and calibration at Day 2206. As stated earlier, the valve arrangement to filter FB904 meant that the filter was not being hydrated and that the pressure monitored was that of the calibration line within the laboratory. Therefore, FB904 was undergoing shut-in and natural pressure decay. This resulted in the slow gradual loss of axial stress, most notably in PB927 which lost around 400 kPa in magnitude during the current chapter. Re-establishing the connection to FB904 saw stresses recover. Initially, there was a sharp increase in pressure, but for PB927 it took around 100 days to fully recover stress. This influence was restricted to the top of the deposition hole, with PB901 and PB902 being unaffected.

The second dominant feature occurred between Day 2575.89 and Day 2722.22. This is when artificial hydration was paused as gas had reached one of the filters. This second pause in hydration of FB904 did not have such a significant influence on the stress in PB927 with only a reduction of 175 kPa, which had reached a minimum, whereas in the first hydration pause a plateau did not occur. In this second pause of hydration, all filter mats were shut-in. As the reduction in stress was less than previously observed it is suggested that FB903 did not contribute greatly to the axial stress within the bentonite. In contrast to the first shut-in, all axial stress sensors showed an increase during the shut-in period, with even PB927 showing increase after an initial loss of stress. This may be associated with annual variations as the two events occurred at different times during the calendar year.

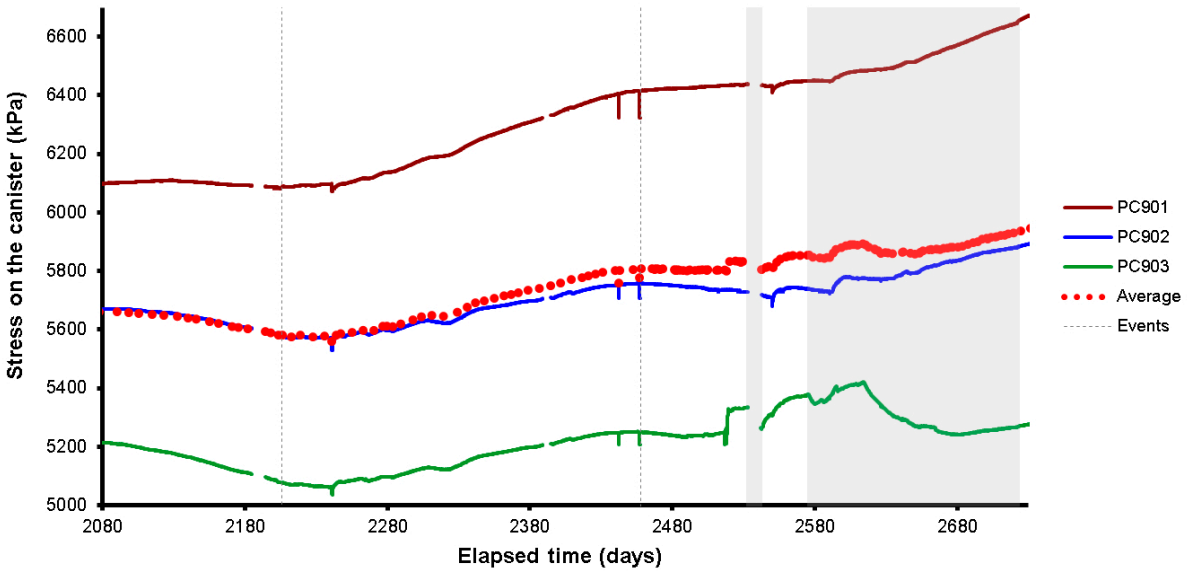

Figure 9-9. *Development of axial and radial pressure on the side and base of canister.*

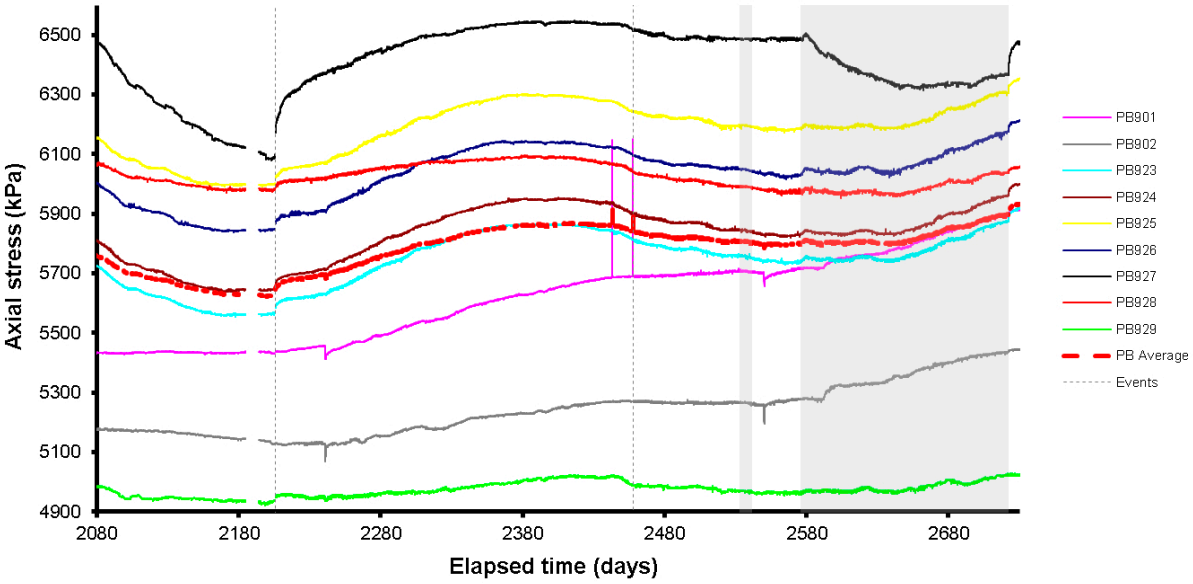

Figure 9-10. *Development of axial stress measured at 9 locations within the buffer.*

The axial force measured on the lid is shown in Figure 9-11. Annual variation was again observed, with a general increase of approximately 50 kPa. A similar trend was seen within the sensors measuring the displacement (Figure 9-12a). During this chapter ~0.5 mm vertical displacement of the lid was observed. The canister was seen to move downwards by 0.4 mm, driven by artificial hydration within the bentonite segments at the top of the deposition hole. Lateral movement of the lid (Figure 9-12b) showed movements of ~0.25 mm. Both lateral movement devices showed annual variation, although it was more pronounced in Lateral movement sensor 2, which also showed considerably more movement.

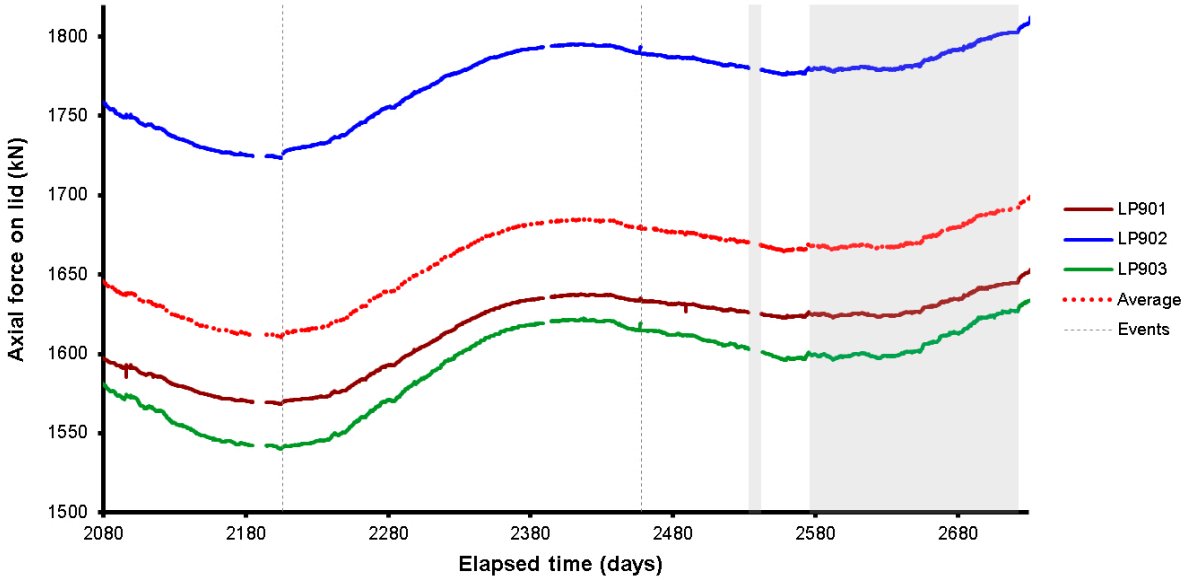

Figure 9-11. *Axial force acting on the steel lid measured by 3 Glötzl load cells attached to separate rock anchors.*

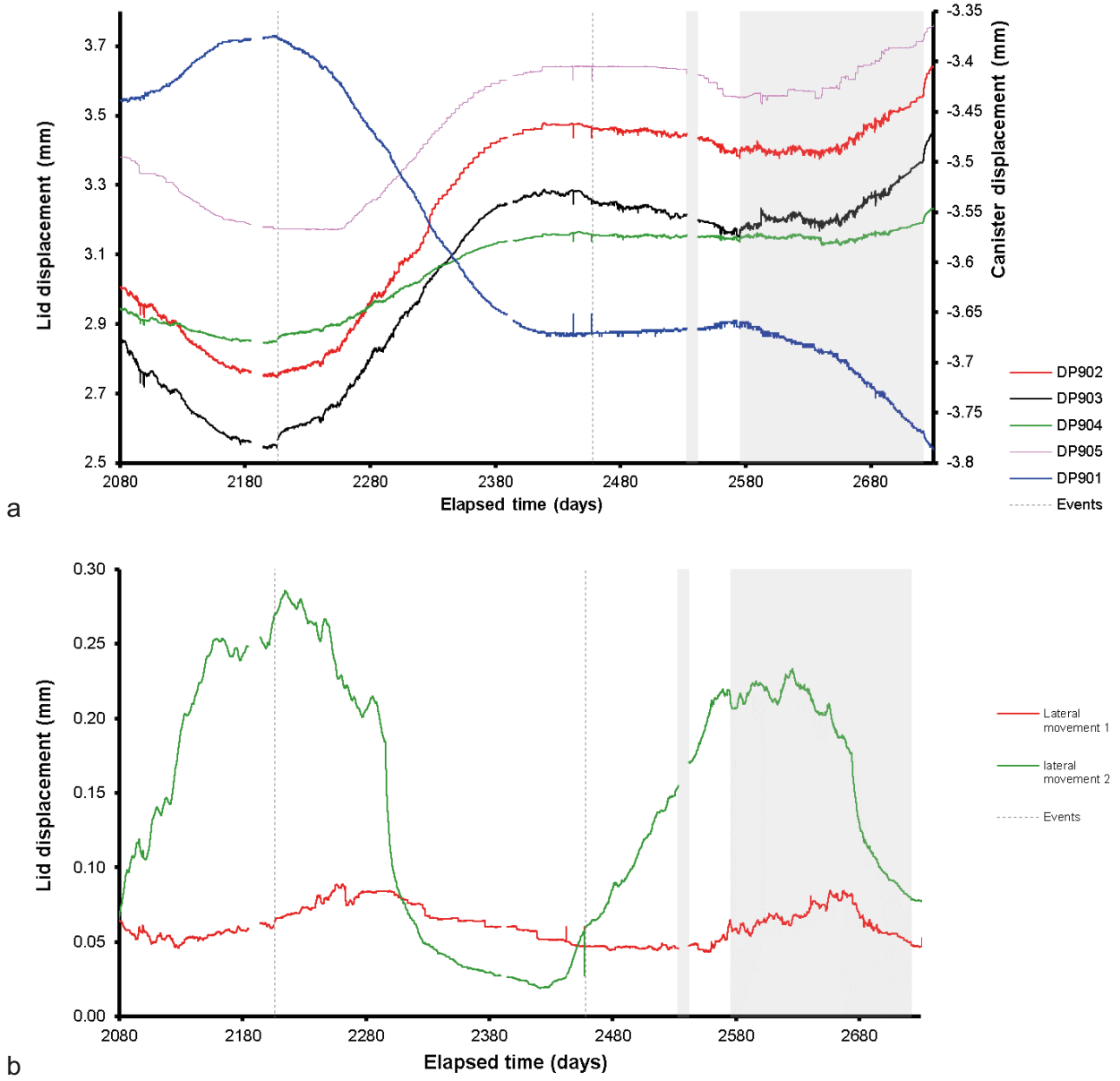

Figure 9-12. *Linear displacement of the steel lid and copper canister (a) and lateral movement of the lid (b). Movements of the lid are measured relative to both the gallery floor and ceiling. Movements of the canister are measured relative to the steel lid.*

Pore pressure away from the deposition hole within the pressure relief hole is shown in Figure 9-13. A small reduction in pressure over the period was seen up until Day 2550, following which the pressure started to rise in all intervals. The largest pressure drop was seen in PRH1–5, which also saw the least pressure increase following Day 2550. This interval was closest to the gallery and showed that this feature was caused by drawdown, created by the continued pumping of the Äspö HRL galleries. As seen, interval PRH2–4 was affectively at atmospheric pressure, again this interval was closest to the gallery. Two events can be seen at Day 2241 and Day 2550 with reduction of pressure in all intervals, followed by pressure recovery. Both of these correspond with the large pressure increase seen in pore pressure sensor UR909 on the rock wall. This shows that whilst the pore pressure at the rock wall was increasing, the pore pressure further from the deposition hole was decreasing. This is suggestive of movement of the wall rock creating enhanced pressure ahead of the fracture movement and creating porosity along the fracture that resulted in a reduction in pressure.

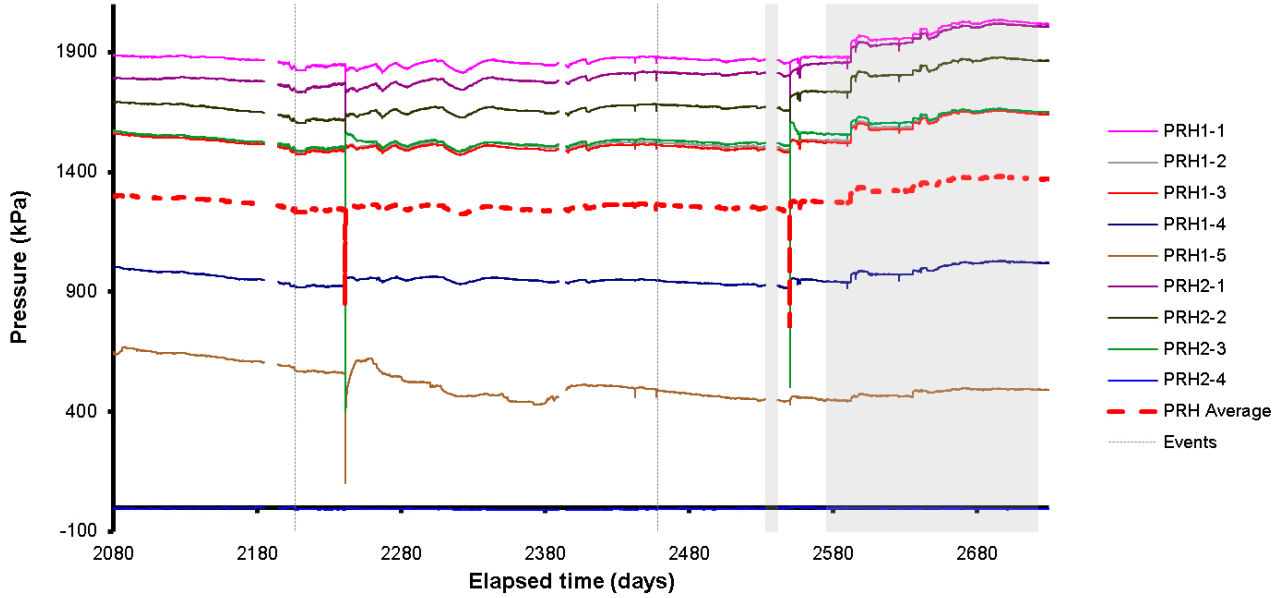

Figure 9-13. *Porewater pressures measured in the packered sections of the pressure relief boreholes.*

Temperature was monitored within the Lasgit laboratory, the HRL, and the canister. Figure 9-14 shows that the air conditioning unit within the laboratory was generally stable during this chapter, although it did show drift and small amplitude variations. It was not expected that these small amplitude features would have had an impact on the pump data. The temperature within the HRL tunnel showed distinctive annual variation as the HRL was not kept to the same close limits as the Lasgit laboratory and office.

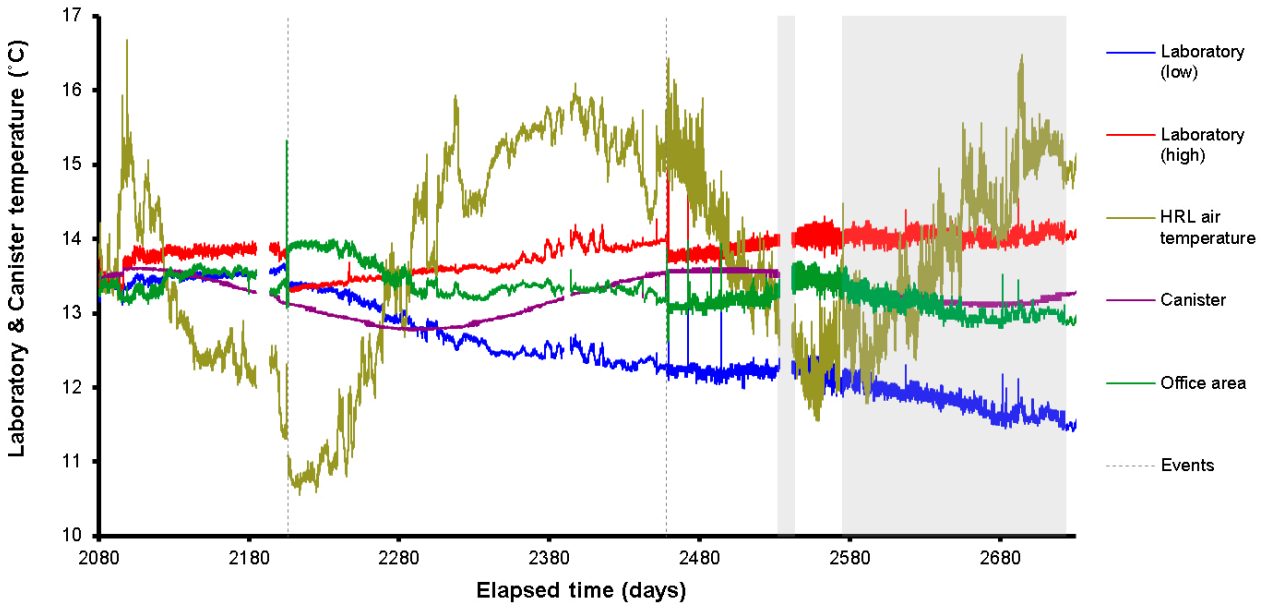

Figure 9-14. *Temperatures recorded in the Gas Laboratory, office, canister, and HRL.*

Figure 9-15 shows the total volume of water pumped into the system during this reporting period. A small pause in artificial hydration occurred between Day 2533 and Day 2541 and a longer pause between Day 2575 and Day 2722. This was related to the aforementioned closing of the hydraulic system, with the later event being related to the possible passage of gas to one of the filters. Approximately 4.5 litres of water were pumped into the system.

Figure 9-16 shows average stresses, pore pressure, and forces observed during the current reporting period. What can be noted is that radial stresses, axial stress on the rock wall, axial force on the lid, stress on the canister and pore pressure within the bentonite all increased marginally during the period. Many of these datasets showed an annual variation associated with temperature fluctuations. In contrast, pore pressure at the rock wall and pore pressure within the pressure relief holes generally remained unchanged during the period. The pore pressure within the bentonite increased during the period as the hydration state of the bentonite buffer increased.

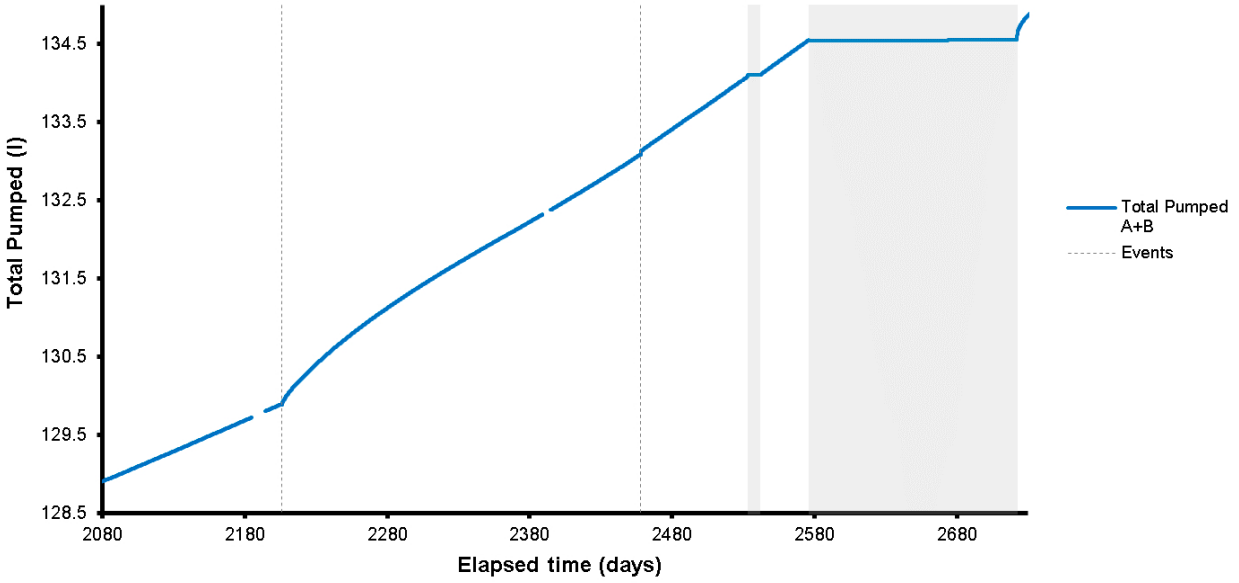

Figure 9-15. *Total pumped during artificial hydration and hydraulic testing.*

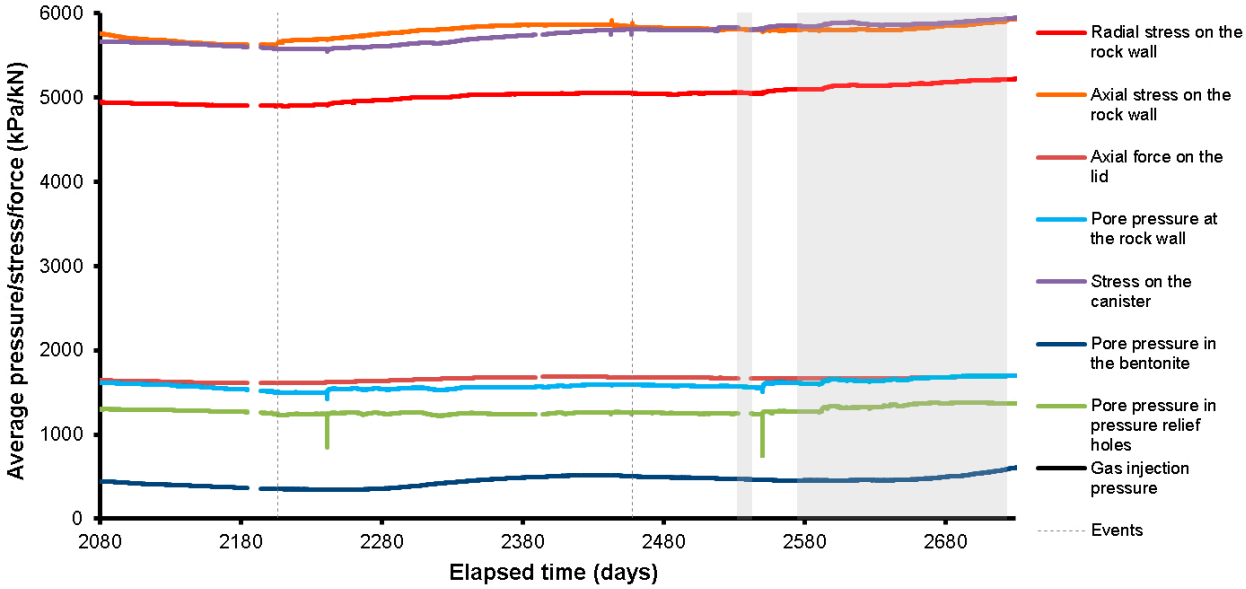

Figure 9-16. *Average pressures, stress, and force observed during the reporting period.*

9.2 Hydraulic test prior and after the gas injection test 3

Figure 9-17 shows the results of the two-stage hydraulic tests, which have been adjusted so that the tests conducted before and after the gas injection test can be compared. Figure 9-17a shows the pore pressure imposed during the test. Note that the test pre-gas injection only had a high-pressure stage. Figure 9-17b, c and Figure 9-18a show that the high-pressure stage resulted in an initially high flow into the buffer in close to 4×10^{-11} m^3 s^{-1}, which quickly reduced to an asymptote of 3.06×10^{-12} m^3 s^{-1} for the test before the gas test and 3.11×10^{-12} m^3 s^{-1} for the repeat test after gas injection. Figure 9-17b, c and Figure 9-18b show that the low-pressure stage resulted in an initially high outflow in excess of 6×10^{-11} m^3 s^{-1}, which quickly reduced to an asymptote of 1.14×10^{-13} m^3 s^{-1} for the repeat test after gas injection. The low-pressure stage resulted in a much noisier result, but it is clear that the outflow during this stage was considerably lower than the inflow during the high-pressure stage.

The two-stage hydraulic head tests were modelled using the 1-D modelled described in Section 6.4, Figure 9-19 shows the modelled results for the two hydraulic tests. The fit of the data can be seen to be good, although it hasn't perfectly modelled the data. Table 9-1 summarises the calculated values for hydraulic conductivity and specific storage for the two tests.

Figure 9-17c shows that the two tests resulted in asymptote at a similar flow rate for both before- and after-gas injection testing. What varied between the tests was the rate of decay, with the test before the gas injection test reducing to an asymptote quicker than the test conducted afterwards. This would be related to the gas that remained in the buffer near to the injection filter. The asymptote of the data related to the flow properties of the bentonite, while the curvature of the flow related to the storage in the system. After gas injection, there was apparently more storage, but no change in hydraulic flow. This is confirmed in the modelled data, which show comparable results for hydraulic conductivity and specific storage. Therefore, the injection of gas had not resulted in a change in the flow properties of the buffer.

Table 9-1. Modelling results for the two-stage constant head hydraulic tests conducted during Gas Injection Test 3.

Filter	Radius of the filter (mm)	Step	Fitted hydraulic conductivity (m/s)	Fitted specific storage (m^{-1})	Boundary conditions		Initial conditions	
					p_0 (MPa)	p_L (MPa)	p_{I0} (MPa)	p_{IL} (MPa)
FU910	25	1	1.71×10^{-12}	2.13×10^{-6}	4.22	0.98	1.22	0.98
		Average	**1.71×10^{-12}**	**2.13×10^{-6}**				
FU910	25	1	1.32×10^{-12}	6.64×10^{-4}	4.26	0.98	3.83	0.98
		2	2.70×10^{-12}	2.20×10^{-5}	1.23	0.98	4.26	0.98
		Average	**2.01×10^{-12}**	**3.43×10^{-4}**				

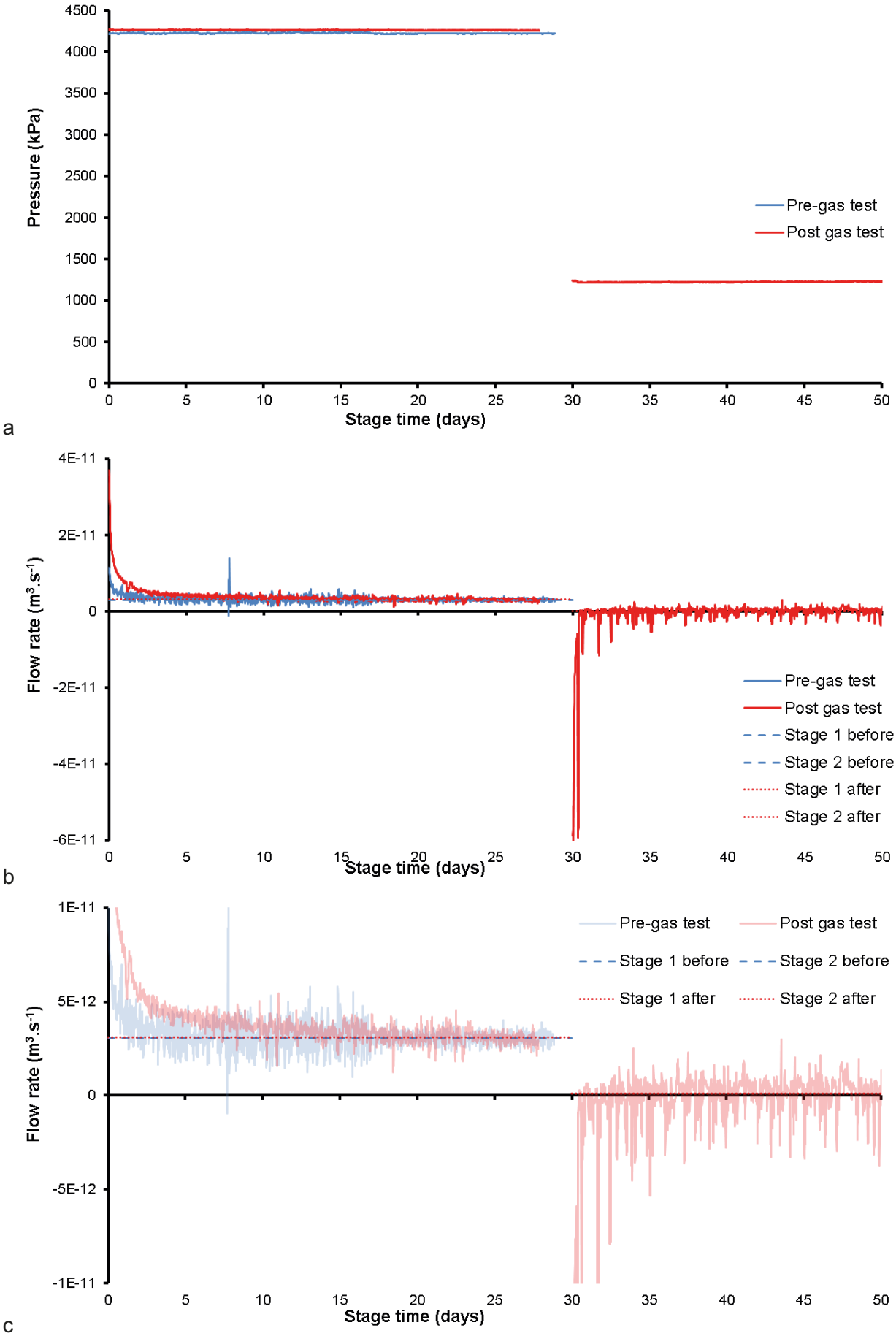

Figure 9-17. *Two-stage constant head hydraulic tests conducted during Gas Injection Test 3. a) Pressure of the injection fluid; b) Flow response; c) Detail of flow response.*

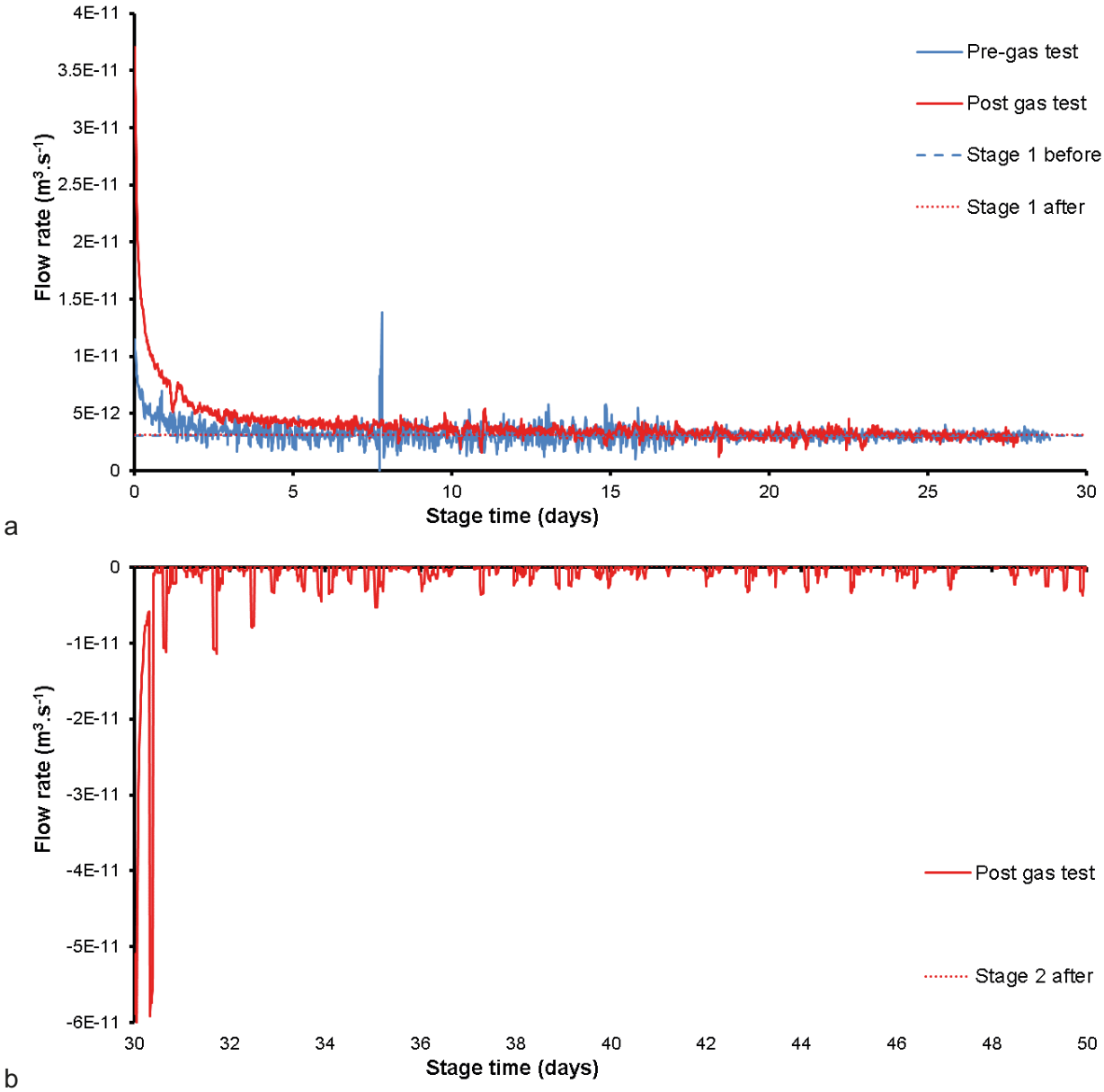

Figure 9-18. *Detail of the flow into the clay during the two-stage constant head hydraulic tests conducted during Gas Injection Test 3. a) High-pressure stage; b) Low pressure stage.*

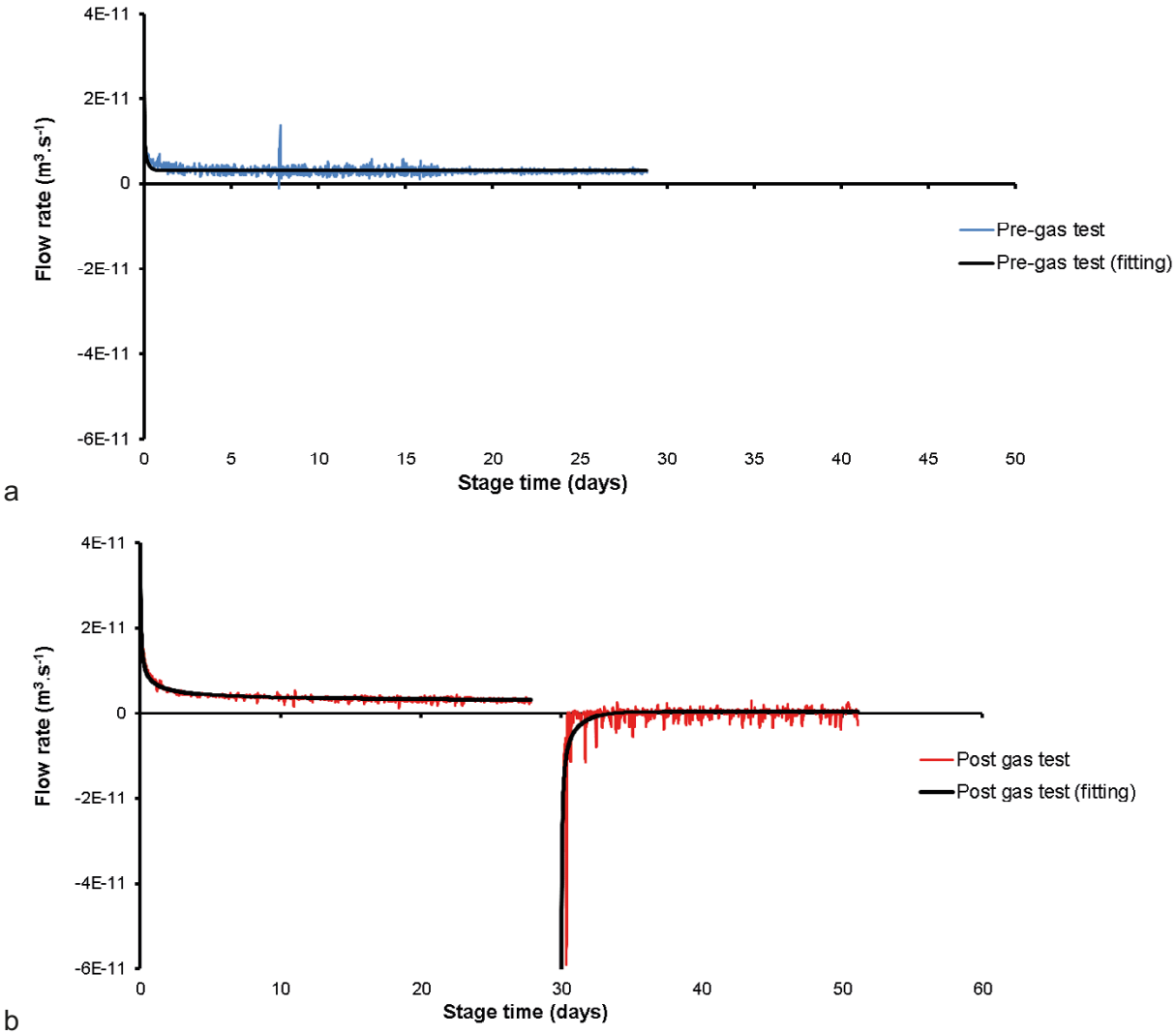

Figure 9-19. *Modelled results for the two-stage constant head hydraulic tests conducted during Gas Injection Test 3. a) Pre-gas test; b) Post-gas test.*

9.3 Gas injection test 3

Gas Injection Test 3 was conducted in filter FU910 on the upper array of filters on the canister surface. The previous two gas injection tests were conducted in filter FL903 on the lower array. It was decided to investigate gas injection in one of the other filters to see if the system behaviour was the same at a location where stress was different. It also gave the opportunity to investigate if filter diameter influenced gas flow. Filter FU910 was selected as this was an area of lower stress as there was a general stress gradient within the deposition hole with higher stress towards the bottom of the canister. Filter FU910 had a diameter of 25 mm, compared with 50 mm for FL903. This would result in differing states of hydration around the different diameter filters. As with the previous tests, gas pressure was raised from background levels up to gas peak pressure using four distinct pressure ramps, being held at constant pressure in between. Following gas peak pressure, gas flow was continued for a limited period of 124 days. The gas test lasted a total of 357 days.

Approximately 4 700 ml of helium was added to the interface vessel at a starting pressure of 1 026 kPa. The injection filter was thoroughly flushed of water using helium and the drain from filter FU910. Once flushed, it was common for flow to take a few days to stabilise as gas went into solution and any remaining water within the filter was expelled into the buffer. A short test was conducted to determine the volume of the gas by changing the volume by a known amount and monitoring pressure. Changing the starting volume of the isolated interface vessel by 87 ml resulted in a change of pressure of 23.4 kPa, giving an estimated starting volume of 3 885 ml. Increasing the volume of the system by 100.8 ml resulted in a pressure decrease of 33.1 kPa, giving a starting volume estimate of 3 086 ml; considerably lower than the first volume estimate. Therefore, it was decided to use the higher volume calculation to set the required pump flow rate and to refine the volume estimate from the observed gas pressure response assuming the ideal gas law.

The first pressure ramp was started at Day 2257.23 (8th April 2011) by the injection of water into the base of the interface vessel by the syringe pump at a rate of 6.5 ml h^{-1}. This raised pressure from 1 026 to 2 245 kPa in 17.2 days, as shown in Figure 9-20, after which pressure was held constant from Day 2306.22 for 31.8 days. The second pressure ramp was started at Day 2306.22 (27th May 2011) by the injection of water into the base of the interface vessel by the syringe pump at a rate of 2.0 ml h^{-1}. This raised pressure from 2 249 to 3 502 kPa in 17.7 days, after which pressure was held constant from Day 2323.90 for 36.3 days. The third pressure ramp was started at Day 2360.23 (20th July 2011) by the injection of water into the base of the interface vessel by the syringe pump at a rate of 1.0 ml h^{-1}. This raised pressure from 3 519 to 4 762 kPa in 16.8 days, when pressure was held constant from Day 2377.02 for 100.25 days. At Day 2457.89 (26th October 2011) the interface vessel was recharged with gas, ~2 830 ml of helium at 4 761.5 kPa. The fourth, and final, pressure ramp was started at Day 2477.27 (14th November 2011) by the injection of water into the base of the interface vessel at a rate of 0.75 ml h^{-1}. This raised pressure from 4 756 kPa to a gas peak pressure of 5 192 kPa at Day 2490.37, 13.1 days after the start of the fourth pressure ramp. Injection was stopped at Day 2614.46 (30th March 2012).

The prediction of gas pressure shown in Figure 9-20 was derived from the ideal gas law. As stated above, the estimate of starting gas volume proved problematic. The first estimate gave a range of 3 086 to 3 885 ml, whilst the recharged estimate gave an estimate of 2 302 ml. Figure 9-21 shows the difference between the predicted and observed gas pressures. This was used to refine the estimate of the starting volume, which in this case gave a volume of 4 700 ml. This latter estimate has been used for calculations, with the starting volume of gas determined for each pressure ramp. Without an adjustment it would suggest that gas was always moving into the buffer. Gas volume can be lost through diffusion and in solution at the gas/water contact within the interface vessel.

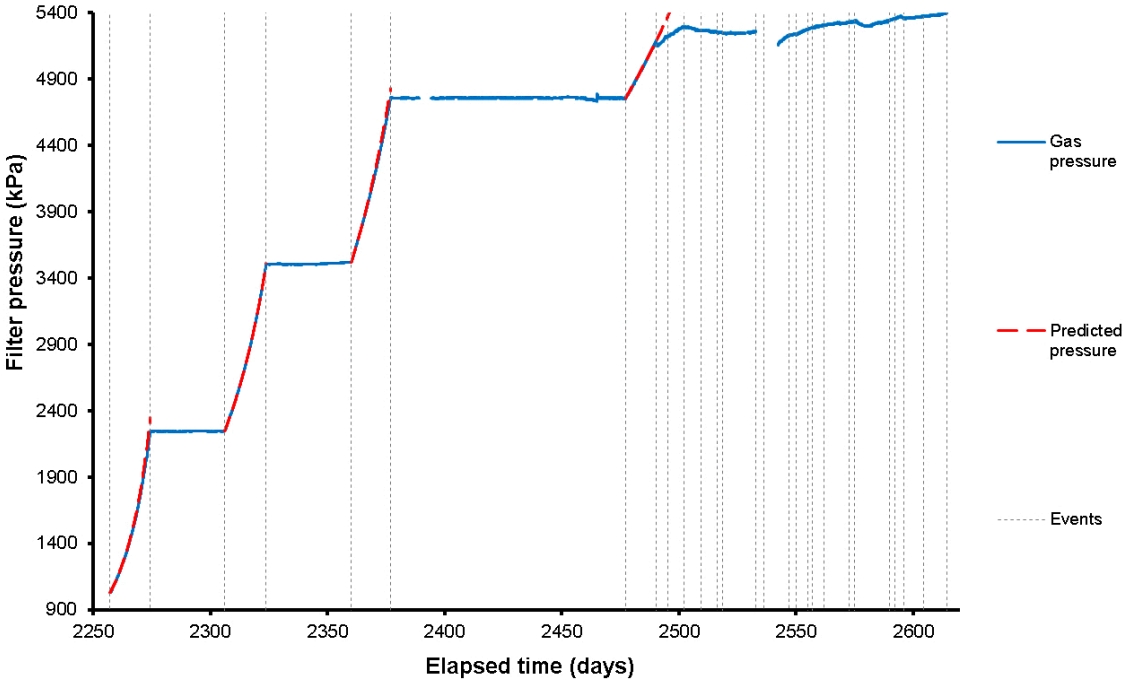

Figure 9-20. *Recorded and predicted gas pressure during Gas Injection Test 3.*

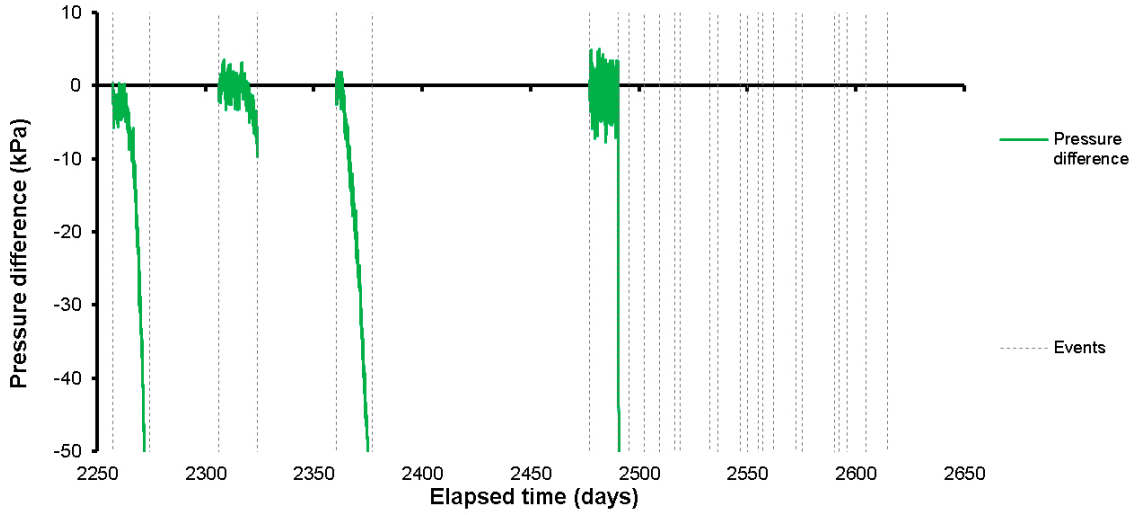

Figure 9-21. *Difference between recorded and predicted pressure during Gas Injection Test 3. This was used to estimate the volume of gas during a constant flow gas compression stage.*

Figure 9-22 shows the flow of gas into the system and into the clay at STP. This clearly shows that the rate of gas entry reduced between each successive gas ramp. Flow into the clay was seen during each ramp, with little flow observed during periods of constant pressure. Each injection ramp will be discussed in detail in the following paragraphs.

Figure 9-23 shows the detail of the first gas ramp conducted in Gas Injection Test 3. The STP flow into the clay ranged from 1.92×10^{-8} to 3.97×10^{-8} $m^3 s^{-1}$. This resulted in a small flow into the clay, with 0.2 mol entering the clay (Figure 9-23c). This may have occurred through diffusion and/or solution and was not interpreted as representing advective movement of gas. When the gas pressure was held constant at around 2 247 kPa, a flow rate of 24.7 µl h^{-1} was observed between Day 2274 and 2306, representing 473 µmol d^{-1}.

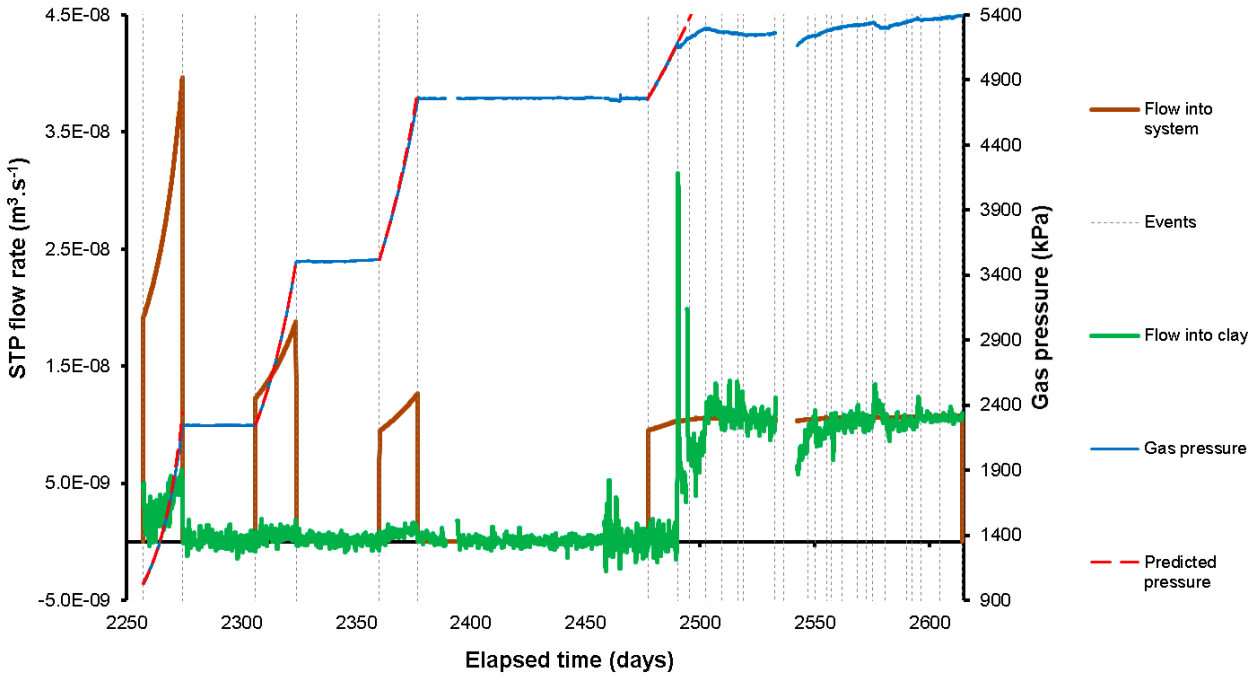

Figure 9-22. *Flow of gas into the system and the clay during Gas Injection Test 3.*

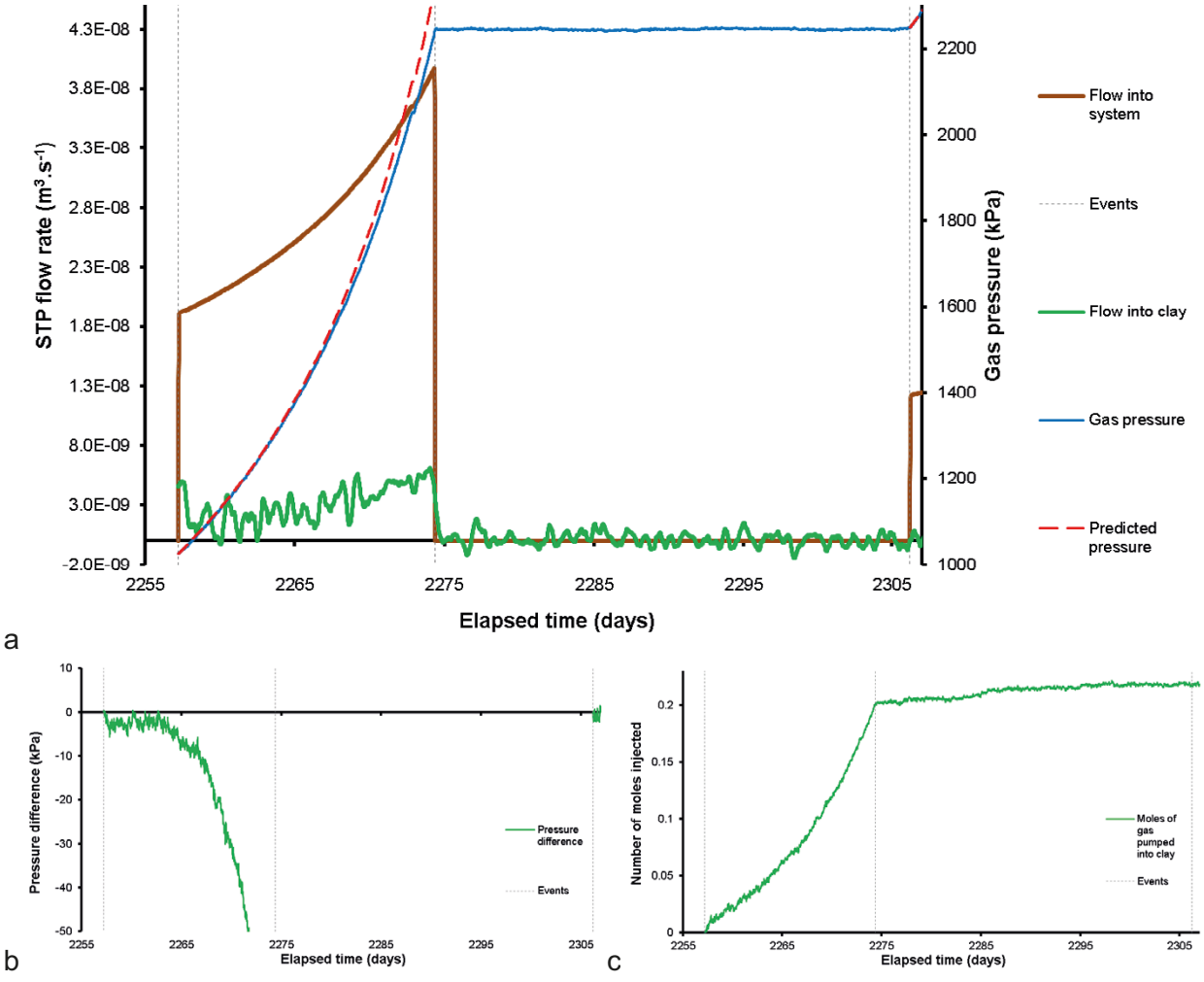

Figure 9-23. *Detail of gas ramp 1 of Gas Injection Test 3. a) Flow of gas into the system and the clay, b) Difference between recorded and predicted pressure, c) Mole pumped into the clay.*

Figure 9-24 shows the detail of the second gas ramp conducted in Gas Injection Test 3. The predicted pressure seen in Figure 9-24a was derived from a revised estimate of the starting volume of gas of 2 360 ml, which as shown in Figure 9-24b gave a very good estimate with negligible difference between the predicted and observed gas pressure. The predicted and observed pressures started to diverge around Day 2316.76, when gas pressure was 2 865 kPa. This did not result in a significant increase in flow into the clay. The STP flow into the clay ranged from 1.3×10^{-10} to 2.1×10^{-9} $m^3 s^{-1}$. This resulted in a small flow into the clay, with 0.2 mol entering the clay (Figure 9-24c). When the gas pressure was held constant at around 3 510 kPa, a total of 0.018 mol entered the clay, with an average flow rate of 20.8 µl h^{-1}, representing 452 µmol d^{-1}.

Figure 9-25 shows the detail of the third gas ramp conducted in Gas Injection Test 3. As seen in Figure 9-25a, despite a good correlation between the predicted and observed gas pressures, flow was seen into the clay at a nominal rate of around 3×10^{-9} $m^3 s^{-1}$. Figure 9-25b shows good agreement between the predicted and observed gas pressures until ~Day 2362.90 when gas pressure was 3 683 kPa. The STP flow into the clay ranged from 3.15×10^{-10} to 1.99×10^{-9} $m^3 s^{-1}$. This resulted in a small flow into the clay, with 0.05 mol entering the clay (Figure 9-25c). As gas pressure was held constant at around 4 761 kPa a flow rate of 8.3 µl h^{-1} was observed, representing 427 µmol d^{-1}. However, this only included flow up to the time of refilling of the interface vessel, after which the data shows enhanced flow for a short period as gas went into solution.

Figure 9-26 shows the variation of gas flow into the clay at STP for the three constant pressure stages with a linear fit. It should be noted that a fourth constant pressure step existed for a limited time prior at the start of the first gas ramp. However, as this was of limited duration after the charging of the interface vessel with gas, the data results were dominated by the transfer of gas into solution within the interface vessel and so have been omitted.

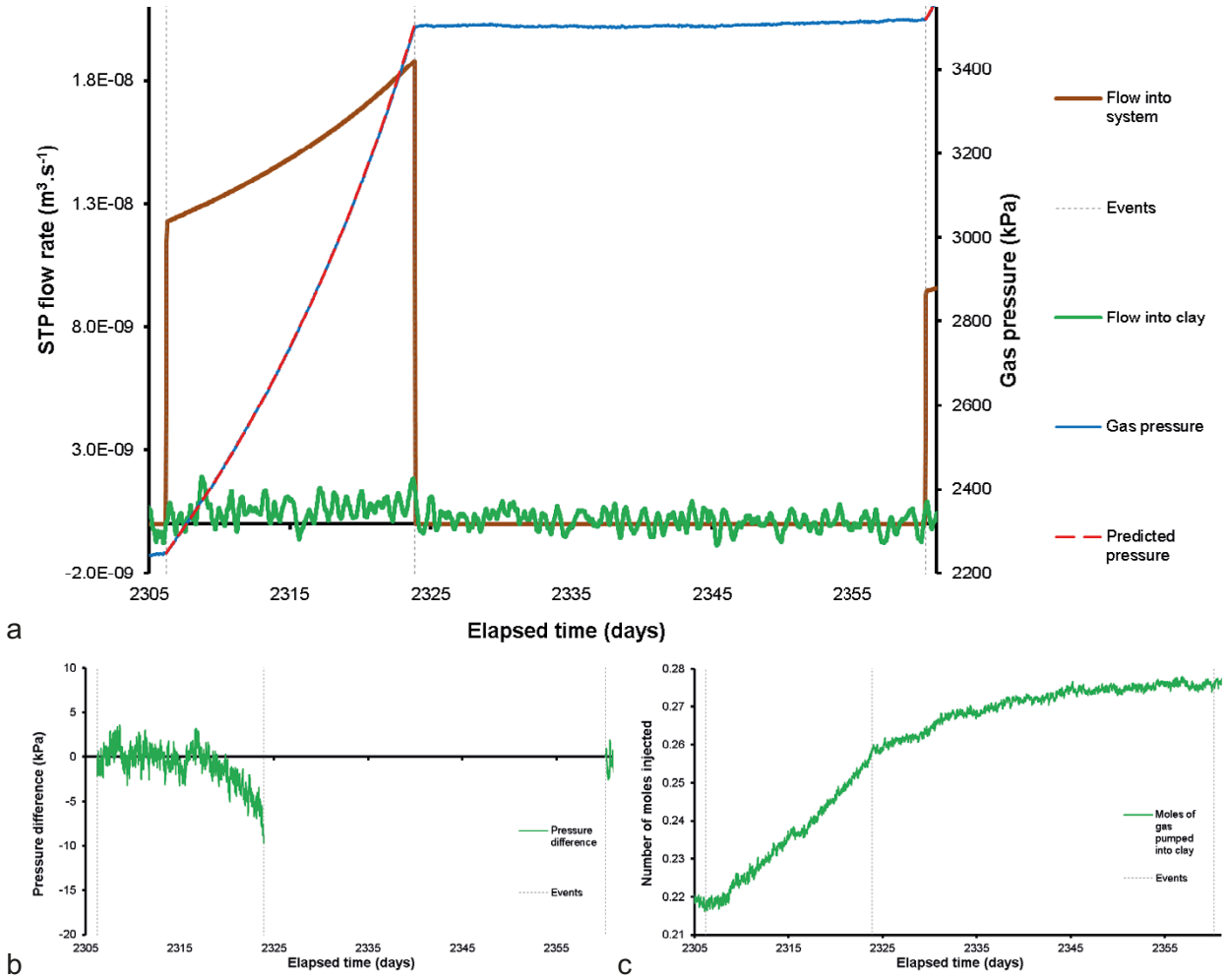

Figure 9-24. *Detail of gas ramp 2 of Gas Injection Test 3. a) Flow of gas into the system and the clay, b) Difference between recorded and predicted pressure, c) Mol pumped into the clay.*

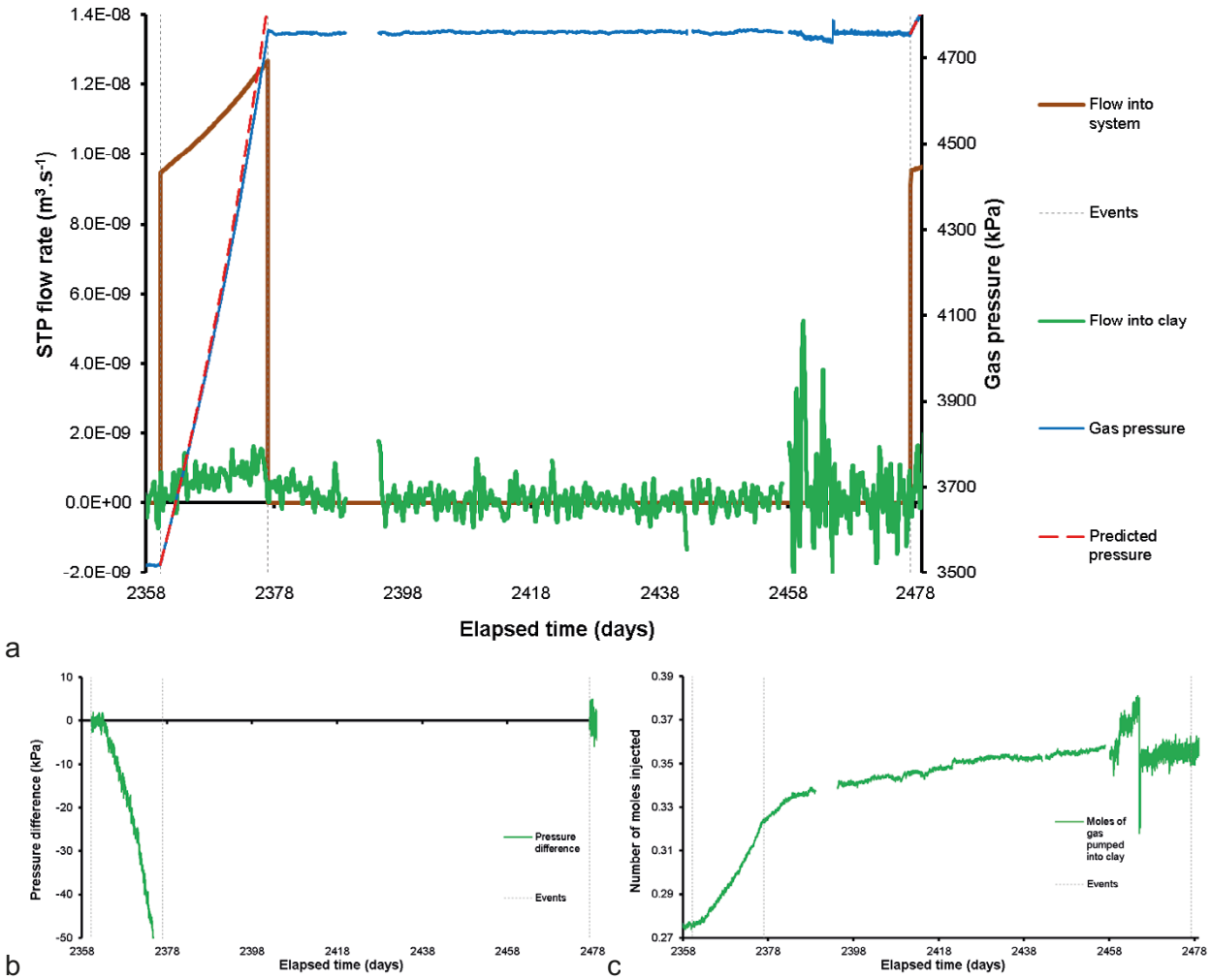

Figure 9-25. *Detail of gas ramp 3 of Gas Injection Test 3. a) Flow of gas into the system and the clay, b) Difference between recorded and predicted pressure, c) Mol pumped into the clay.*

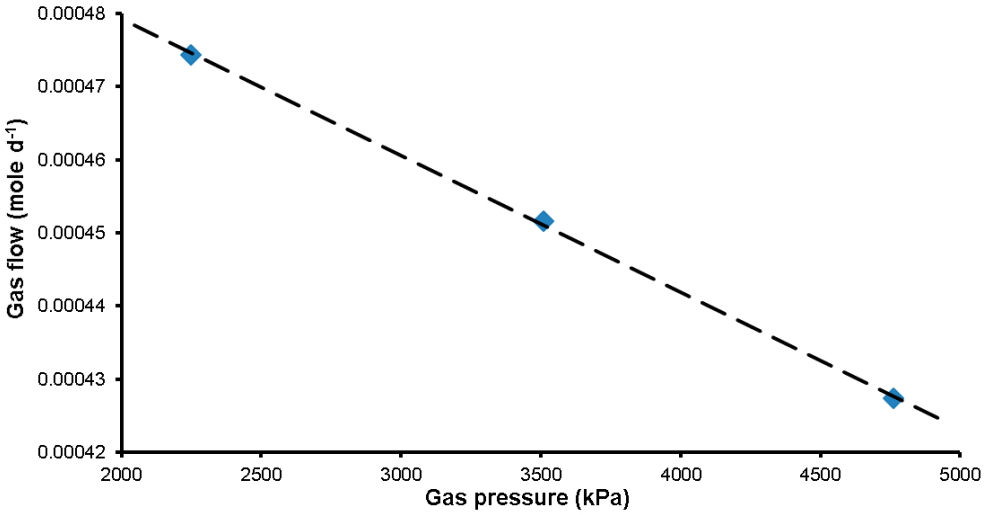

Figure 9-26. *Gas flow rate into the clay at STP at the three constant pressure steps of Gas Injection Test 3.*

Figure 9-27 shows the detail of the fourth gas ramp conducted in Gas Injection Test 3 up until the time of accelerated flow into the gas at Day 2490.37. As seen in Figure 9-27a, despite a good correlation between the predicted and observed gas pressures, flow was seen into the clay at a nominal rate of $\sim 1.98 \times 10^{-10}$ m^3 s^{-1}. Figure 9-27b shows good agreement between the predicted and observed gas pressures until ~Day 2490.37 when gas pressure was 5 192 kPa. Throughout the period, the STP flow into the clay was relatively constant, with only a nominal flow into the clay. This resulted in a small flow into the clay, with 0.01 mol entering the clay (Figure 9-27c). Significant gas entry was seen to begin at Day 2490, as seen by an increase in flow rate into the clay (Figure 9-27a), as well as a deviation between the predicted and observed gas pressure (Figure 9-27b), and the volume of gas pumped into the clay (Figure 9-27c).

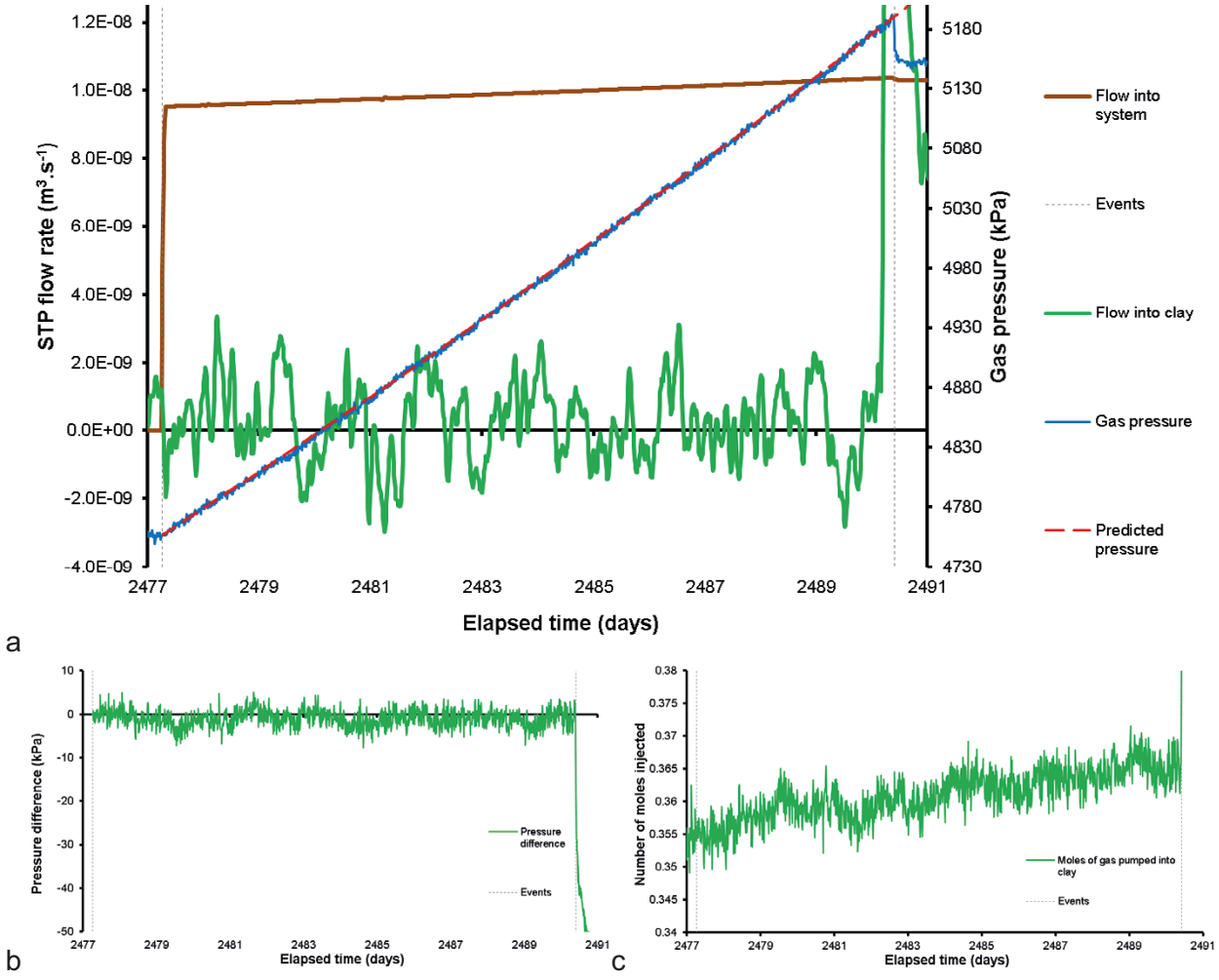

Figure 9-27. *Detail of gas ramp 4 of Gas Injection Test 3 up until the time of clear gas entry. a) Flow of gas into the system and the clay, b) Difference between recorded and predicted pressure, c) Mol pumped into the clay.*

The fourth gas ramp took the test through to peak gas pressure and post-entry. Figure 9-28 shows the flow result. As described above, a small flow was seen into the clay until Day 2490.37 with an average of 1.98×10^{-10} m^3 s^{-1}, after which flow into the clay began to accelerate rapidly. This resulted in a single peak in flow of 4.70×10^{-7} m^3 s^{-1} at Day 2490.41 (note: data shown in Figure 9-28 is time averaged). The peak in flow was short-lived with flow into the clay matching flow into the system within 10 hours. The peak in flow resulted in the gas pressure decreasing rapidly from a maximum of 5 192 kPa to a minimum of 5 147 kPa, some 45 kPa lower than the peak. Following this was a prolonged period where the flow into the system was greater than the flow into the clay, resulting in gas pressure increasing. The flow data shows a second peak at Day 2494.39. However, this was created by a system failure that lasted for 8 hours that resulted in the closure of the air actuated valves to the injection filter. Therefore, this peak represented the reopening of that valve and enhanced flow into the now open injection filter. Pressure continued to increase, until it reached a second peak in gas pressure of 5 298 kPa at Day 2502.01. This second peak was 106 kPa above the first peak, suggesting that continued propagation of flow pathways required higher gas pressure. At this time, flow into the clay was greater than into the system and so the gas pressure slowly reduced to reach a low of 5 239 kPa at Day 2520, following which the pressure slowly increased again.

From Day 2527.06 onwards the control PC had issues that resulted in the cessation of gas injection three time (Figure 9-28). The fail-safe operation of the logging computer meant that all air-actuated valves within the Lasgit laboratory close, and on the third failure at Day 2533.04 the system remained isolated for 9.2 days until the computer was repaired. As seen in Figure 9-28, gas pressure had reduced whilst the system was isolated, and no flow had occurred into the system. Gas pressure recovered with the re-establishment of gas flow and for the rest of the test generally increased, reaching a maximum of 5 401 kPa before gas injection was stopped. Although gas pressure showed a general increase, two distinct peaks were seen in gas flow into the clay, both of which led to a reduction in the gas pressure. The first of these occurred at Day 2575.10 with a peak in flow of 9.38×10^{-8} m^3 s^{-1}. The reduction in pressure was not instantaneous and instead resulted in a slow reduction in gas pressure of approximately 45 kPa before the gas pressure recovered. A second peak in flow into the clay occurred at Day 2596.14 of 7.51×10^{-8} m^3 s^{-1}, resulting in a ~25 kPa reduction in gas pressure. These peaks in flow suggest gas pathways continued to form over time, with new pathways resulting in a reduction of pressure. Figure 9-29 shows the volume of gas pumped into the clay in mol. It shows that 0.37 mol entered the clay up until peak gas pressure. Following gas entry, a total of 4.99 mol entered the clay.

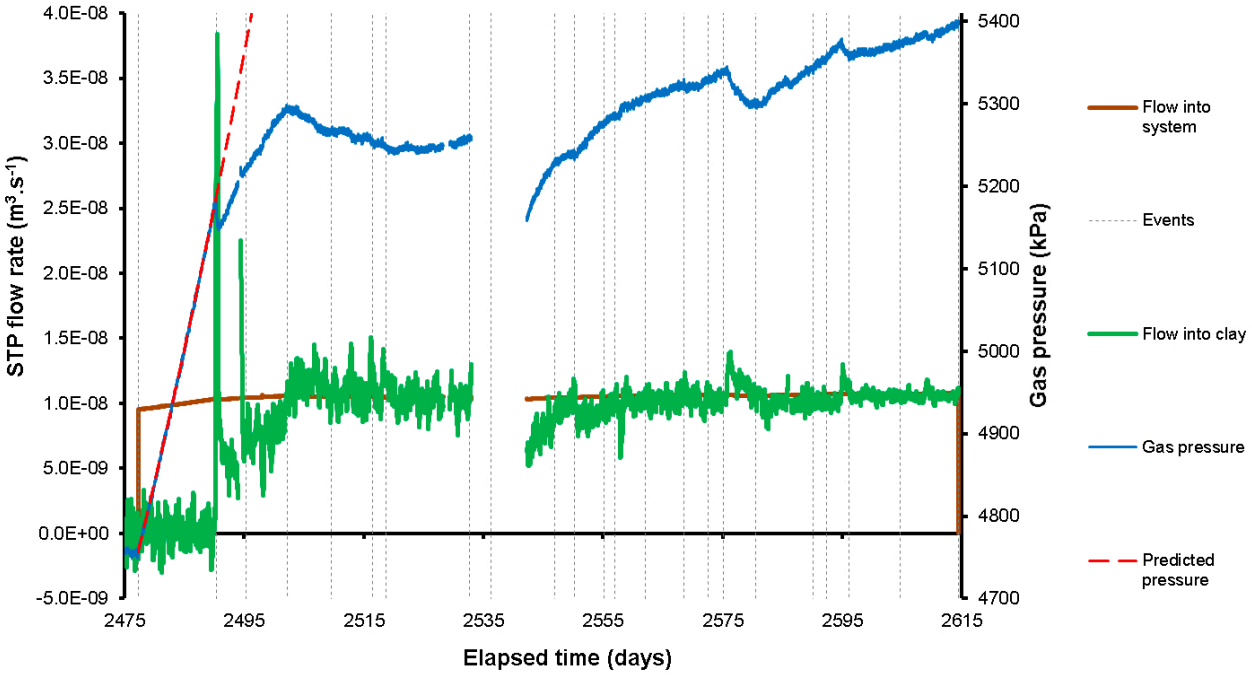

Figure 9-28. *Flow of gas into the system and the clay during the fourth ramp of Gas Injection Test 3.*

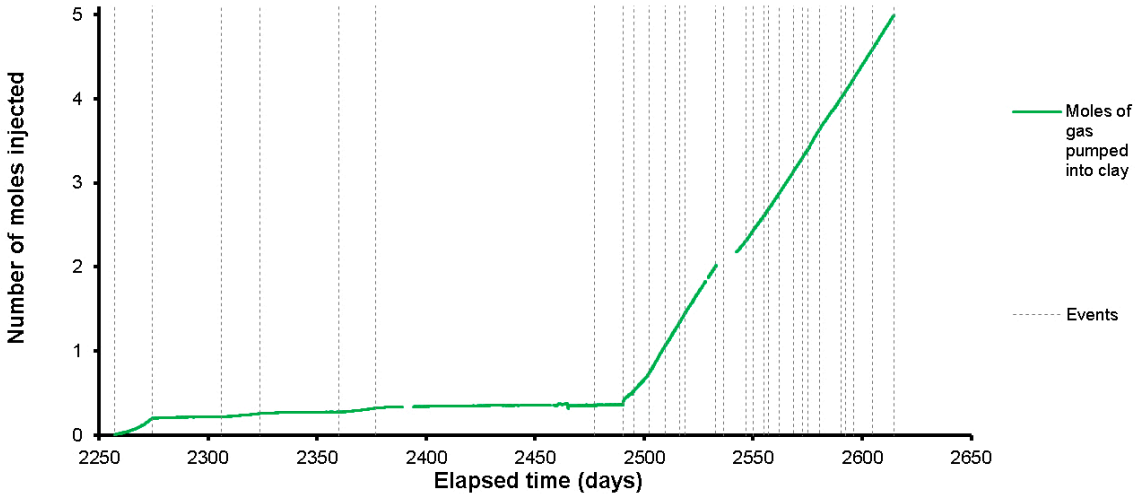

Figure 9-29. *Mol of gas pumped into the clay during Gas Injection Test 3.*

Figure 9-30 shows the flow data in more detail around the time of peak pressure and subsequent gas movement within the buffer at a constant rate of injection. Flow into the clay shows similar behaviour to previous tests. Following the initial peak in flow, the response reduced to be lower than the flow into the system, before recovering.

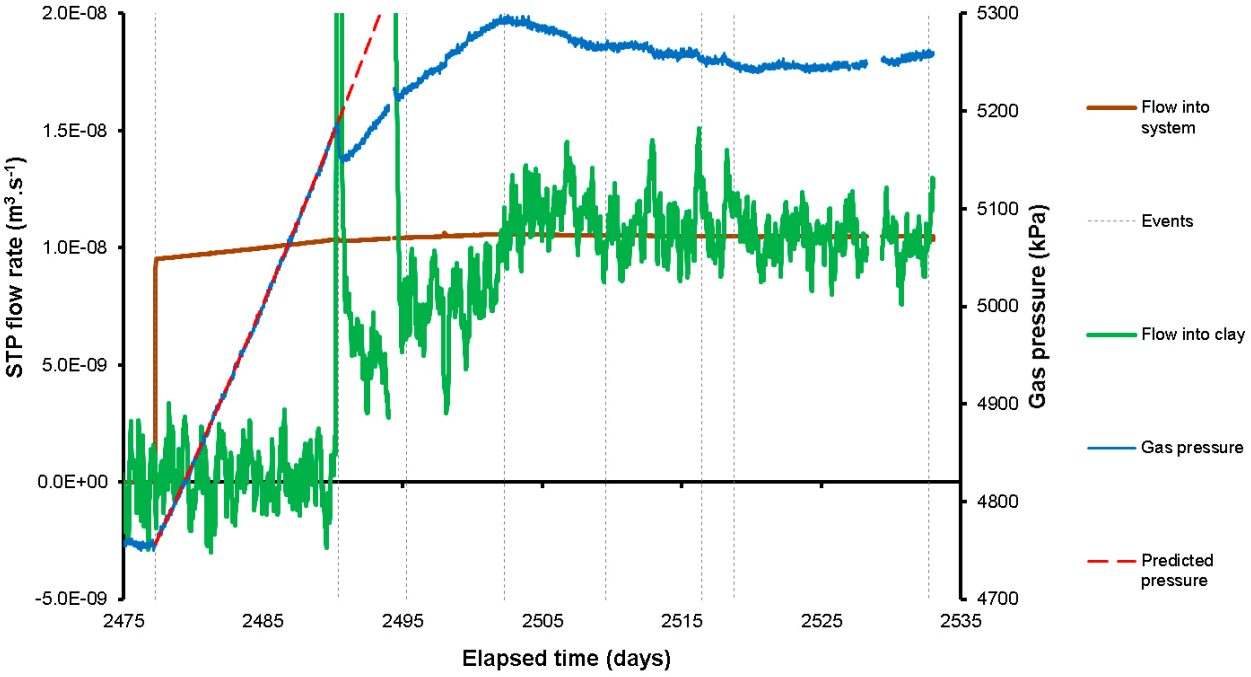

Figure 9-30. *Detail of the flow of gas into the clay and the system around the time of gas entry during Gas Injection Test 3.*

Pore water pressure at the rock wall showed considerable coupling with gas entry (Figure 9-31a, Figure 9-32a). Around the time of accelerating flow into the clay and gas peak pressure at Day 2490.37, a response was seen in UR921 and UR915 with abrupt increases in pore pressure of 18.6 and 17.1 kPa respectively. Pore pressure at these sites remained raised until the second peak of gas pressure at Day 2502.28, when they both reduced to near their previous magnitudes. Sensor UR921 increased a second time at Day 2509.53 by ~30 kPa. It remained raised until the system was locked in during the failure of the logging PC at Day 2533. In addition to the two sensors mentioned, UR916 also showed a feature at the time of the initial gas peak at Day 2490.37, although this was subtle. The second significant event seen in the pore pressure data occurred at Day 2550.23. Pore pressure disturbance can be seen in all UR sensors. The most significant change occurred in UR910. Pore pressure dropped initially by 52 kPa, before rapidly increasing by 435 kPa. Many sensors showed the characteristic reduction in pore pressure followed by a greater pressure increase. Several sensors showed increases of the order of 50 kPa or more, including UR915, UR916, and UR921 (Figure 9-32a). Following the increase in pore pressure at UR910, some locations showed a decrease in pressure, whilst others remained at the elevated pressure level. At UR921, the general trend of increasing pore pressure initiated at peak gas pressure continued. A third event was seen around Day 2557 when almost all UR sensors showed a short-lived reduction of pore pressure of the order of 5–20 kPa. A fourth significant pore pressure event occurred at Day 2592.36, with the majority of sensor locations registering an abrupt pressure increase. Only a small increase in pore pressure occurred at UR910, suggesting that the source of the pore pressure increase had moved between events 2 and 4. Pore pressure increased by 61 kPa in UR915 in a series of events and 54 kPa in UR916.

Radial stress at the rock wall also showed complex behaviour with many events (Figure 9-31b, Figure 9-32b). The start of enhanced gas flow and peak pressure at Day 2490.37 was clearly seen to correlate with abrupt increases in PR915 and PR917, which increased by 79 and 26 kPa respectively. Sensors PR913, PR916, PR918, and PR922 also showed small magnitude increases in stress. The second significant radial stress event occurred at Day 2502.28 at the time of the second peak in gas pressure. This time a more complex response was seen. At PR919, stress increased by 37 kPa, with smaller stress increases seen at PR915 and PR914. However, stress decreases were seen in PR918, PR920, and PR922.

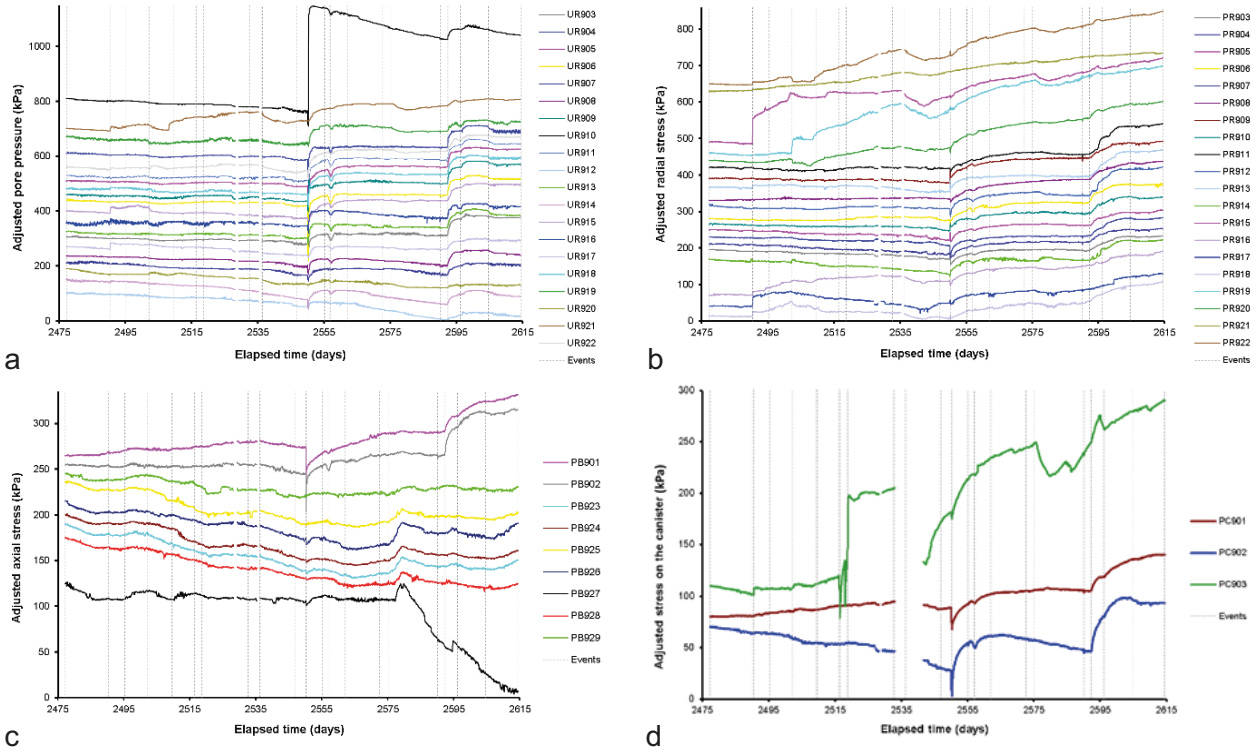

Figure 9-31. *Example of sensor response around the time of gas entry during Gas Injection Test 3. All parameters have been transposed about the y-axis to emphasise the detail observed. a) Pore pressure at the deposition wall; b) Radial stress on the deposition wall; c) stress within the bentonite; d) stress on the canister surface.*

The third event of note affected most sensors and was caused by the failure of the logging PC. Radial stress can be seen to start to decrease at Day 2535.29 until Day 2541.63 when the issues with the PC were corrected and the air-actuated valves re-opened and gas injection was resumed. This reduction was most clear in PR915 and PR919 (Figure 9-32b) and shows that the increased stress was a direct consequence of gas pressure. The fourth event occurred at Day 2550.23, coincident with the events described in pore pressure above. Stress was perturbed at most locations at this time, but only by small amounts. The fifth event of note occurred at Day 2575.10 when gas pressure peaked for a third time, resulting in increased flow into the clay and the reduction of stress at PR915, PR917, PR919 and PR922. This suggests stress was relieved as gas moved within the system. The sixth and final event of note occurred around Day 2595, with another complex series of features. At this time gas pressure peaked once more with enhanced flow into the system. At PR915 and PR919 a short-lived peak was seen. Stress began to rise in many sensors, as shown in Figure 9-32b for PR911, with a series of increases resulting in radial stress increasing by 75 kPa. The final increase seen in PR911 corresponded with an abrupt increase in stress at PR917. This shows that the sixth event was a series of events over a period of about 10 days and may indicate the formation of multiple pathways.

Figure 9-31c shows the stress within the bentonite. This shows three events of note. The first occurred at Day 2550.23 with a reduction in stress at PB901 and PB902. At PB902, stress quickly recovered in a few days, whereas at PB901 it took ~10 days. Disturbances in stress were seen for all PB sensors, with the exception of PB925. The second event of note started at Day 2575.10 with gradual increases seen in the stress sensors above the canister (PB923–PB929). The rate of change of stress increased with time, until a peak was reached at Day 2580.20. At PB927, the increase in stress was more instantaneous and was delayed compared to the other sensors. Following the peak in stress, a gradual decrease in stress was seen to recover to previous levels within 30 days. The exception was PB927, which continued to decrease until the termination of gas injection. The peak in stress seen within the bentonite did not correspond with the stress changes seen at the rock wall, which suggested a response from a localised feature. The third event of note occurred at Day 2592.36, with increases seen in stress below the canister at PB901 and PB902. Stress was seen to increase by around 50 kPa over a 22-day period.

The final dataset, highlighted in Figure 9-31d, is the radial and axial stress sensors on the canister surface. Four events are worth noting. The first was a pair of responses at Day 2516.41 and 2518.77 seen in PC903. In the first of these, stress decreased by around 30 kPa and quickly recovered. At the latter time, stress again initially decreased by ~30 kPa, and then quickly increased by ~120 kPa. These events were interpreted to be because of the arrival of gas at PC903. The formation of a pathway near the sensor firstly relieved the stress, until the direct communication of gas with the filter resulted in the sensor becoming pressurised. The second event of note occurred at Day 2550.23. At PC902 stress decreased by 25 kPa and then quickly recovered, resulting in enhanced stress. At PC901 stress decreased by 20 kPa and had a much slower recovery, only reaching a stress marginally higher than before the event after around 20 days. The third event of note was seen in PC903 at Day 2575.10 when stress began to decrease. This corresponds with the reduction in gas pressure and demonstrates the direct connection of the injection filter and PC901. The fourth and final event was seen at Day 2592.36 and shows a gradual increase in stress at PC901 and PC902, the latter changing by 48 kPa over a period of 8.9 days.

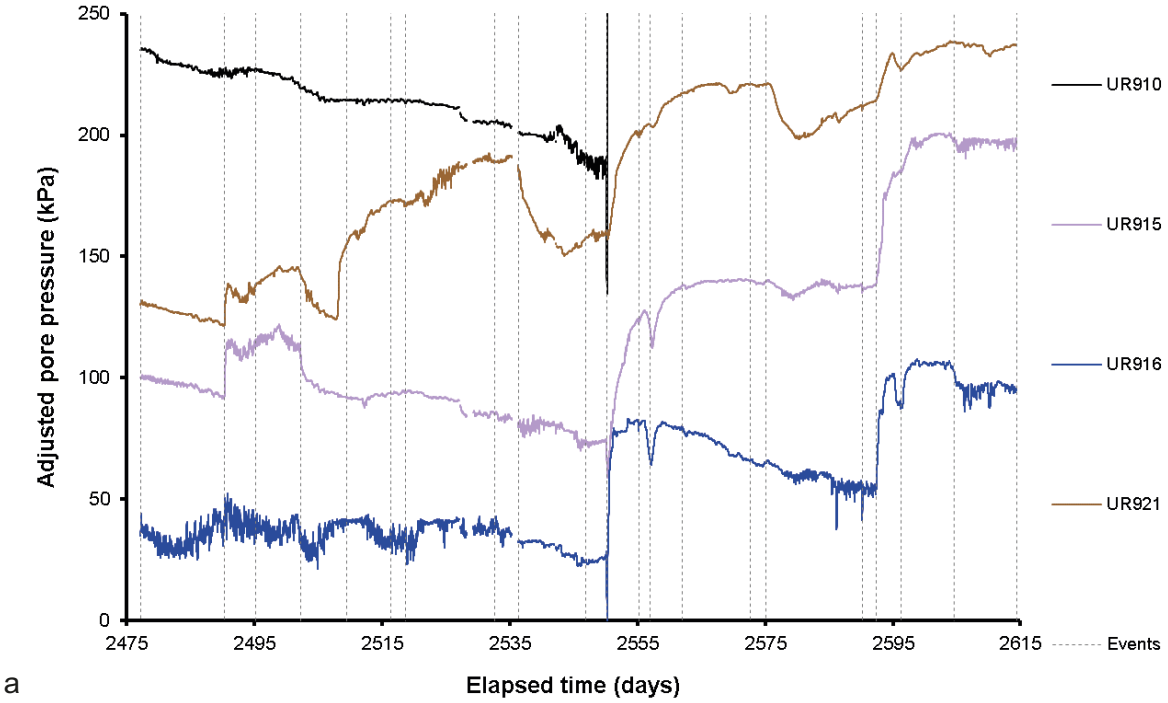

a

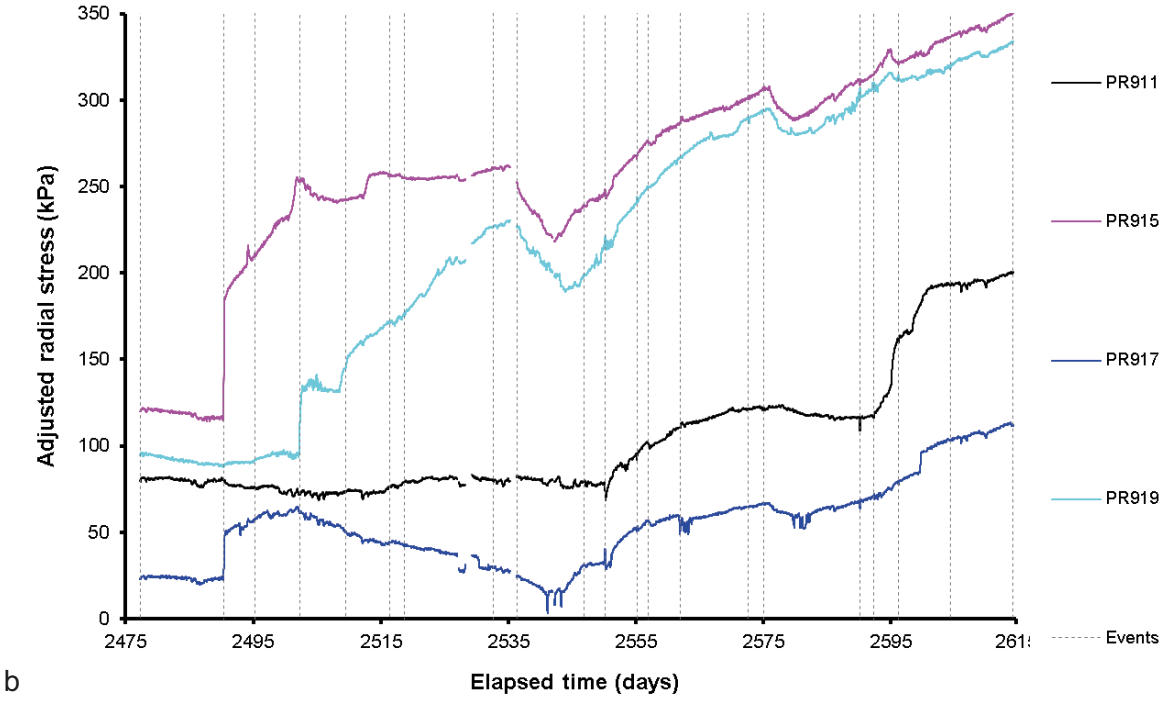

b

Figure 9-32. *Detail of radial stress and pore fluid pressure at the rock wall around the time of gas entry during Gas Injection Test 3. a) Pore pressure at the deposition wall; b) Radial stress on the deposition wall.*

Figure 9-33 shows the distribution of pore pressure at the deposition hole wall and how this varied during Gas Injection Test 3. Figure 9-33a shows the pore pressure just prior to peak gas pressure at Day 2487.24. This shows that the gas injection filter, highlighted in red, was situated in a region of low pore pressure. An area of high pore pressure existed between the mid-plane and lower canister filters at an angle of 270°. Generally, pore pressure increased from the top of the deposition downwards.

Figure 9-33b shows the variation in pore pressure at Day 2491.26. This shows that pore pressure at the same elevation as the injection filter had increased, with little change opposite the filter, but with increases 90° from the injection filter at 0° and 180° orientations. As a consequence, pore pressure on the level of the lower filter array generally decreased, with a low-pressure region forming at an orientation of 0°. By Day 2503.23 (Figure 9-33c) the higher-pressure region at the level of the injection filter had broadened and now showed a change opposite the injection filter and an increase in pressure on a level above the injector, but 180° around the canister. The high-pressure region opposite the injection filter was relatively short-lived and had subsided by Day 2546.90 (Figure 9-33d). Low pore pressure regions had formed with a band from the mid-plane at 270° to the lower filter array at 0° to the midplane at 90°. The high-pressure region at the top of the deposition hole at 270° was still persisting. By Day 2554.25 (Figure 9-33e), pore pressure in general had returned to that seen before gas entry. The low-pressure regions were still apparent, but a new high-pressure region had formed at the level of the lower canister filters at 270°, opposite filter FL904. At the end of injection, at Day 2600.31 (Figure 9-33f), The pore pressure at the deposition hole can be seen to have changed considerably as a result of gas injection. A strong high had formed, as had low pressure regions. The pore pressure data shows that gas moved considerable distances within the deposition hole during the Gas Injection Test 3.

The distribution of radial stress on the deposition hole wall is shown in Figure 9-34. The plot of stress prior to peak gas pressure is shown in Figure 9-34a at Day 2487.24. It shows a high in radial stress at an angle of 300° from the top to the bottom of the sensor array. Generally, a band of high stress also exists at the height of the lower canister filters (170.9 cm height). Gas entry made a significant change to the stress field at Day 2491.29 (Figure 9-34b). A high stress region formed at the level of the injector (412.4 cm), with a peak at the 90° direction near to the injection filter. This suggests that the first movement of gas was from the injector to an orientation of 90°. By Day 2503.23 (Figure 9-34c), the high-pressure region at 90° had increased in magnitude. This region started to move by Day 2546.90 (Figure 9-34d), spreading upwards and anti-clockwise, with a new high forming at 0° at the top of the sensor array. This region of high stress persisted and increased in magnitude, as seen at Day 2554.25 (Figure 9-34e). Also developing by this time was a band of mildly increased stress from the injector to the bottom of the sensor array at 270°. By the end of injection at Day 2600.31 (Figure 9-34f), clear persistent regions of both increased and decreased stress had formed. Anti-clockwise and above the level of the injector a region of increased stress had formed and remained. This may continue to the base of the filter array at 270°, which as a result formed a low stress region 180° from the region of increased stress (i.e. from the level of the injector at 270° to the base of the filter array at 45°).

Comparing the observations of pore pressure and radial stress during the gas injection time shows many similarities and several differences (Figure 9-35). At Day 2491.29 (Figure 9-35a) there is a relative correspondence in the changes in pore pressure and radial stress. In both, pressure/stress increased all around the deposition hole at the level of the injector, with both showing increases more anti-clockwise of the injector than directly opposite. The formation of elevated pore pressure resulted in the formation of a low-pressure region at the level of the lower array of filters (170.9 cm) at 0°. However, this change was not seen in radial stress. By Day 2546.90 (Figure 9-35b) stress had started to migrate up from the injector, whilst remaining at a high level, whereas pore pressure had generally subsided. However, the high pore pressure at the top of the sensor array at 502.9 cm, 225°, had increased in magnitude. Both observations may suggest gas movement upwards. By the end of the injection test at Day 2600.31 (Figure 9-35c) considerable differences were seen between radial stress and pore pressure. The high in pore pressure at the top of the filter array had subsided and a new high had formed at the level of the lower filter array (170.9 cm, 270°). This does correspond with a linear region of increased stress that ran from the injector to the base of the filter array at 270°. This suggests that gas movement may have followed this trajectory. The region of high stress at the level of the injector and above had prevailed, unlike in pore pressure.

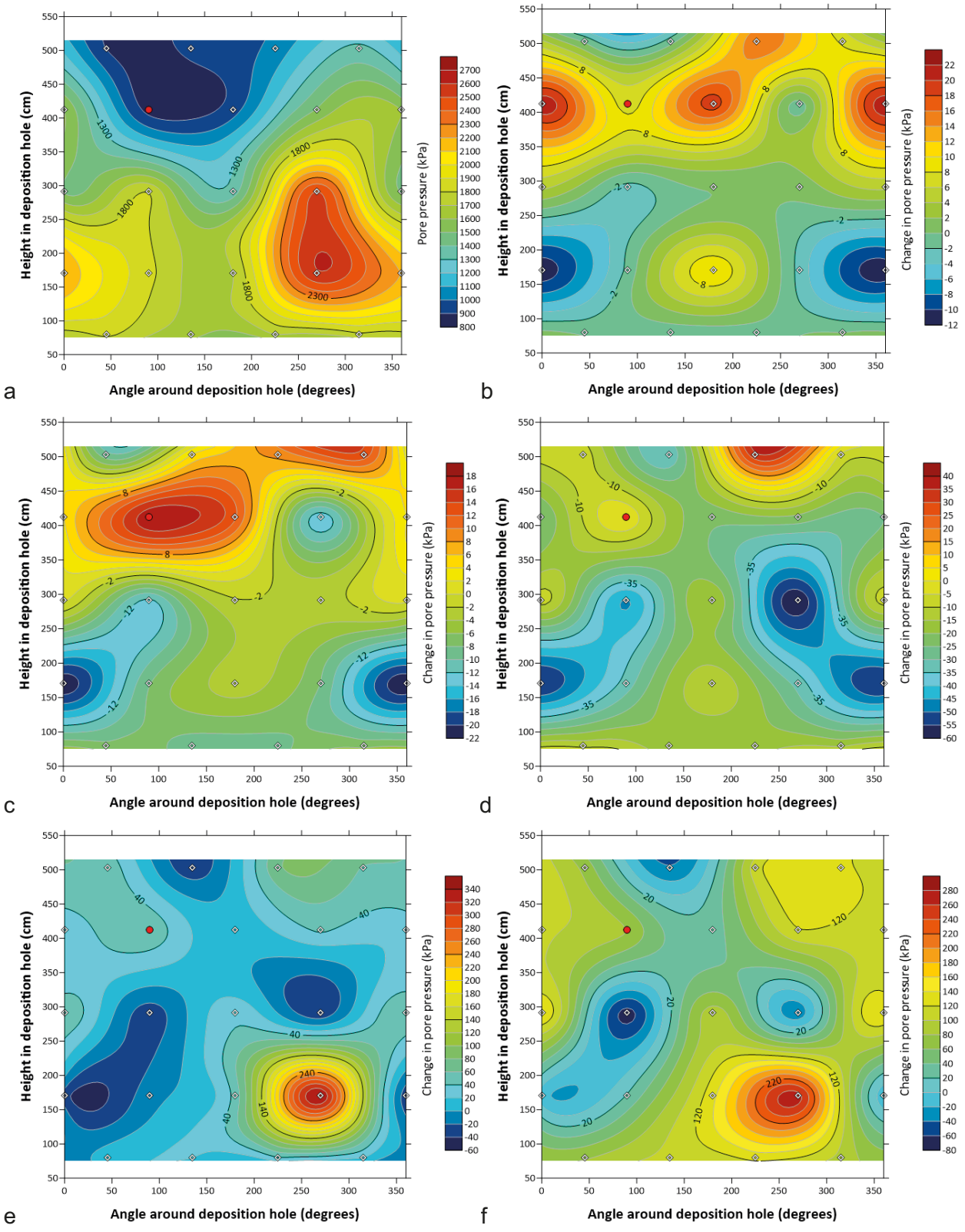

Figure 9-33. *Distribution of pore pressure at the deposition hole wall at times around gas entry during Gas Injection Test 3. a) Day 2487.24 (total pore pressure); b) Day 2491.29 (change in pore pressure); c) Day 2503.23 (change in pore pressure); d) Day 2546.90 (change in pore pressure); e) Day 2554.25 (change in pore pressure); f) Day 2600.31 (change in pore pressure).* ***Note:*** *the location of the injection filter is shown as a red circle.*

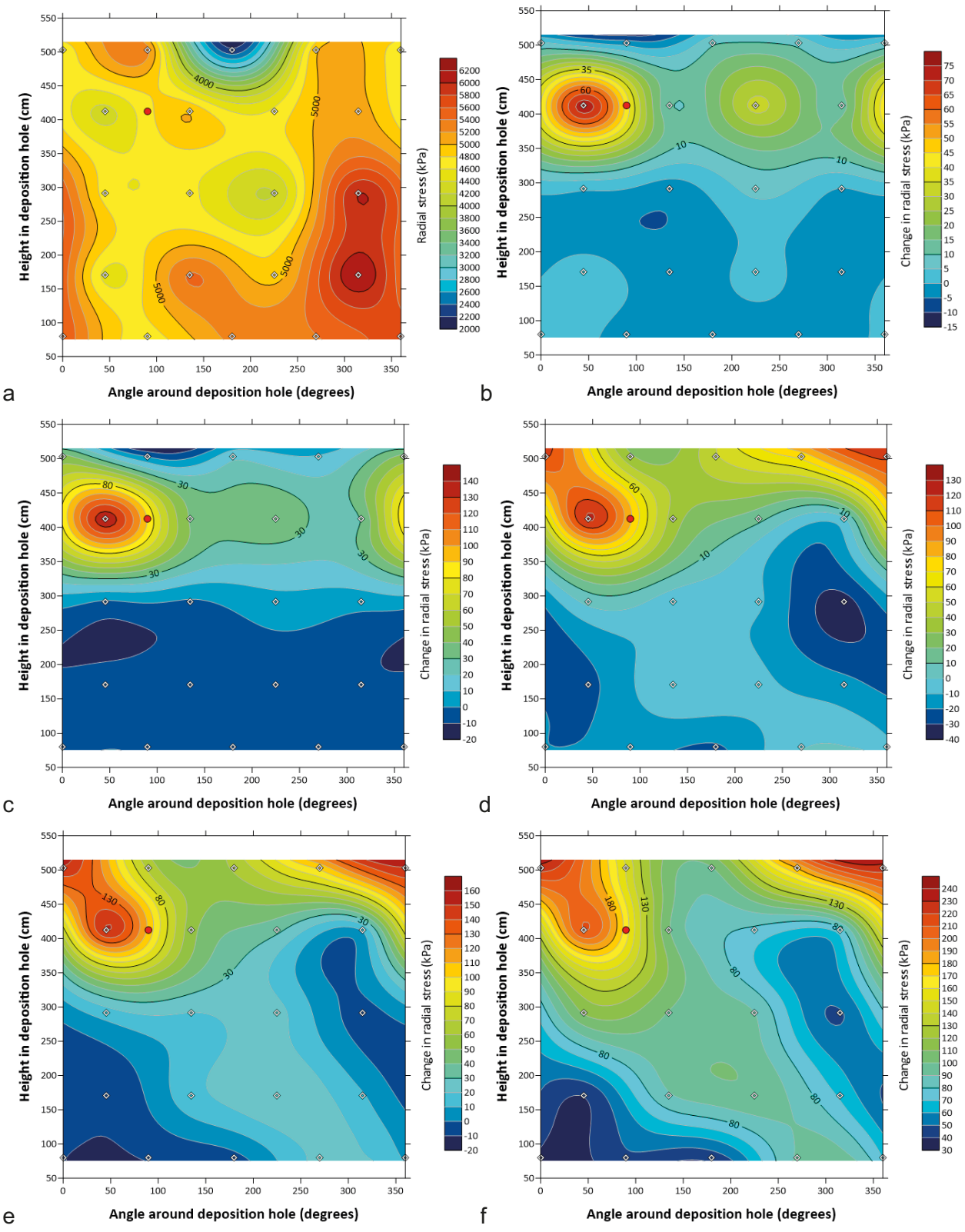

Figure 9-34. *Map of radial stress at the deposition hole wall at times around gas entry during Gas Injection Test 3. a) Day 2487.24 (total stress); b) Day 2491.29 (change in stress); c) Day 2503.23 (change in stress); d) Day 2546.90 (change in stress); e) Day 2554.25 (change in stress); f) Day 2600.31 (change in stress).* ***Note:*** *the location of the injection filter is shown as a red circle.*

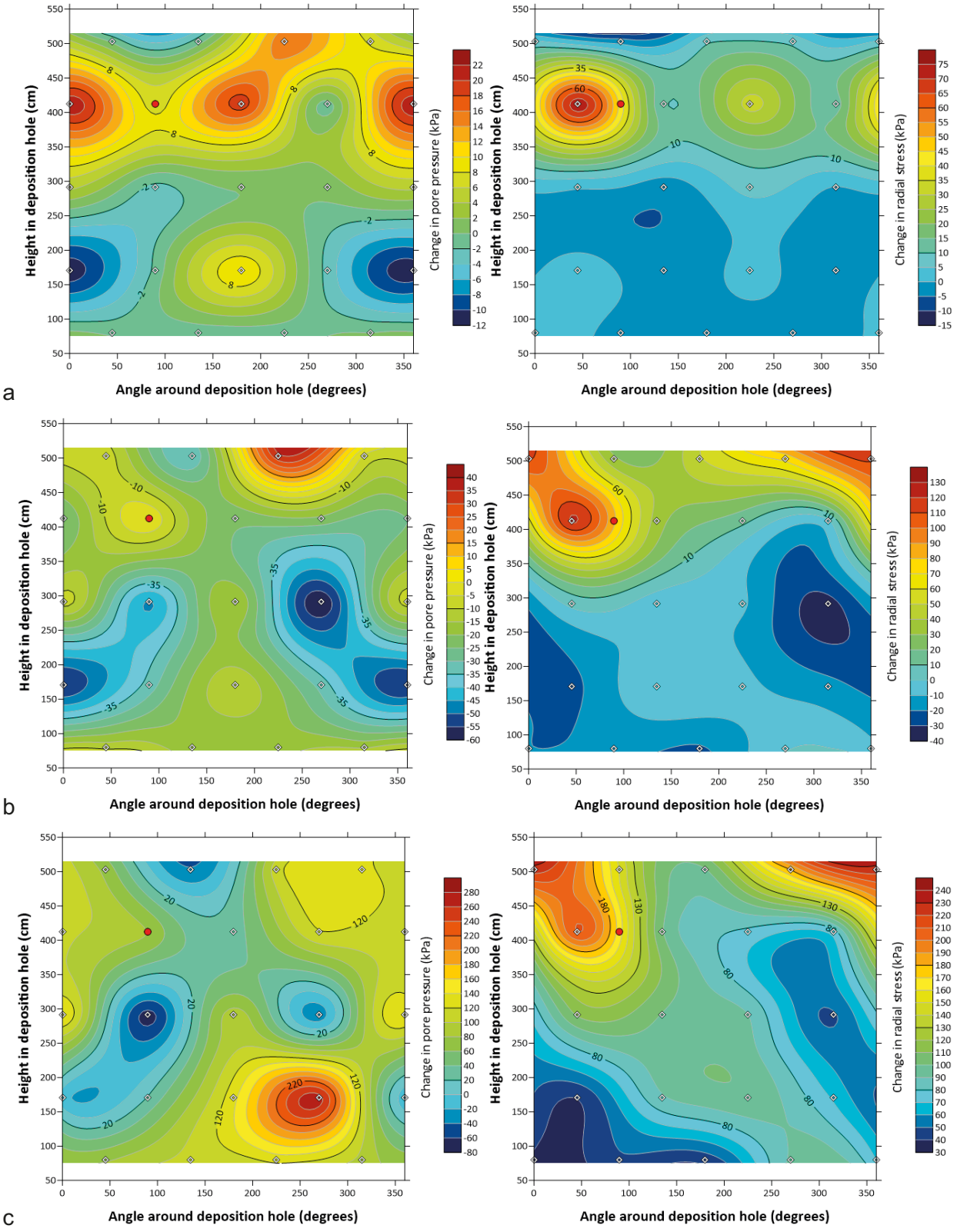

Figure 9-35. *Comparison of changes in pore pressure and radial stress at the deposition hole wall at times around gas entry during Gas Test 3. a) Day 2491.29; b) Day 2546.90; c) Day 2600.31.* ***Note:*** *the location of the injection filter is shown as a red circle.*

Figure 9-36a shows sensor locations that showed direct movement of gas. The first event line shows gas peak pressure at Day 2490.41. Some 4.89 days later at Day 2495.30 a second event line is highlighted (Figure 9-36a). This shows the first increase in pressure at filter FU909 and FU910. This event highlighted an issue with the plumbing of the system. Each injection filter had a stainless steel tube connection from the laboratory to the filter and a second tube back to allow for drainage. Following investigation, filters FU909 and FU912 were found to be incorrectly attached, which meant that the two filters were in direct communication. Therefore, given the data presented above, it is more probable that gas had reached FU909 90° around the canister as opposed to FU912 180° around the canisters surface. Only the first increase in gas pressure is highlighted. This increased gas pressure to 2 347 kPa before quickly reducing. This was followed at Day 2495.77, 2547.28, and 2496.29 by abrupt pressure increases followed by pressure decay, each taking pressure in FU912 to 2 450 kPa, 2 914 kPa, and 2 613 kPa. The next pressure increase occurred at Day 2497.97 taking pressure to 3 153 kPa over a series of pressure events. The final gas peak started at Day 2498.33 and after three pressure increase events reached a peak in pressure of 5 036 kPa at Day 2498.72 close to the gas injection pressure. Gas pressure decayed over a period of two days, before increasing in a more gradual manner up to a pressure close to the gas injection pressure. This response suggests that gas reached FU909 through a number of burst events, similar to the propagation of bubbles, before a stable, open pathway formed allowing gas pressure to increase to near injection values.

The Third event heighted in Figure 9-36a occurred at Day 2508.46, when gas had reached FU911. This showed similar behaviour to FU909 with three peaks in gas pressure seen, each followed by subsequent decay. However, these were distributed over a greater timescale than seen in FU912. The first peak resulted in a pressure of 1 920 kPa. The second feature occurred at Day 2556.84, some 48 days after the first indication of gas reaching FU911. This second event had a much smoother peak with a pressure of 1 814 kPa. The third feature started at Day 2568.36, with a rapid increase in pressure up to 5 050 kPa in a series of pressure events. The final feature in FU911 began at Day 2580.63 with pressure increasing to close to the gas injection pressure over a period of 1 day. As with the interpretation of FU912, gas appears to have migrated to FU911 through a series of "bubbles" until stable pathways formed. The large feature starting at Day 2568.36 appears to almost reach stable conditions, before the pathway closed and pressure dissipated. It took considerable time for a direct, open pathway to form. The fourth event highlighted in Figure 9-36a occurred at Day 2518.77 and shows gas reaching canister stress sensor PC903. The fifth and final event highlighted in Figure 9-36a occurred at Day 2577.20 when pressure started to increase in filter FL904. This initially increased pressure to 4 157 kPa, before increasing again at Day 2609.16 up to 4 783 kPa. The behaviour of FL904 differs from that seen at FU909 and FU911 with stable pathways reaching FL904 suggesting that pressure decay did not follow the increases in pressure.

Figure 9-36b shows the location of the sensors highlighted in Figure 9-36a. This shows that the migration of gas followed the observations of the plots of pore-pressure and radial stress distribution at the deposition hole wall. This suggests gas migrated first at the level of the injection filters, before migrating downwards towards 270° at the base of the canister. It should also be noted that the behaviour in pressure/stress shown in Figure 9-36a after the restart of gas injection at Day 2541.64 showed that each of these sensors was in direct communication with the injection filter. This is further highlighted in Figure 9-37 with every change in gas injection pressure mirrored in the other sensors once they were pressurised.

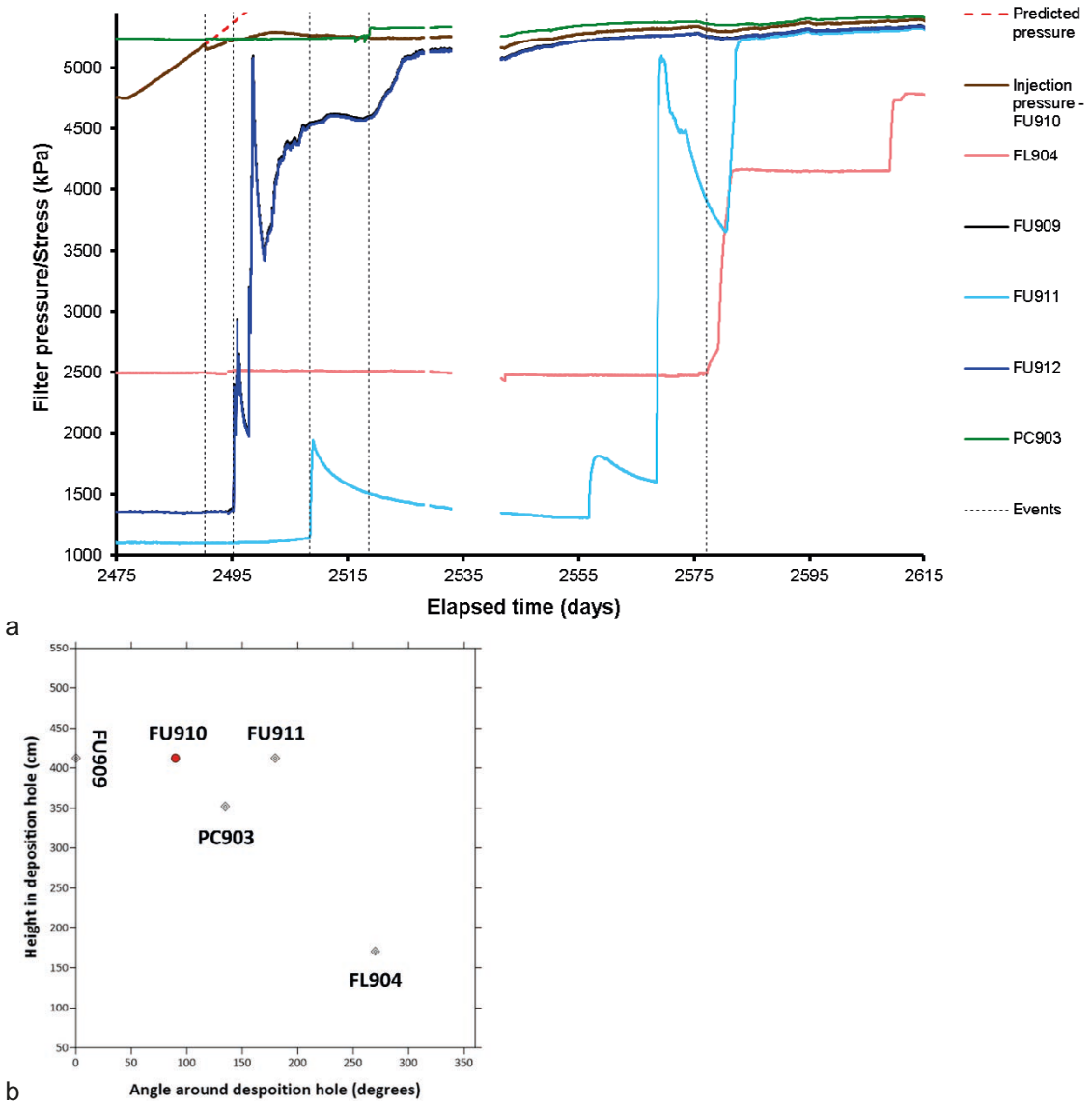

Figure 9-36. *Detail of sensors that show evidence of gas pressurisation during Gas Injection Test 3. a) Pressure/stress data; b) location of sensors highlighted in (a).*

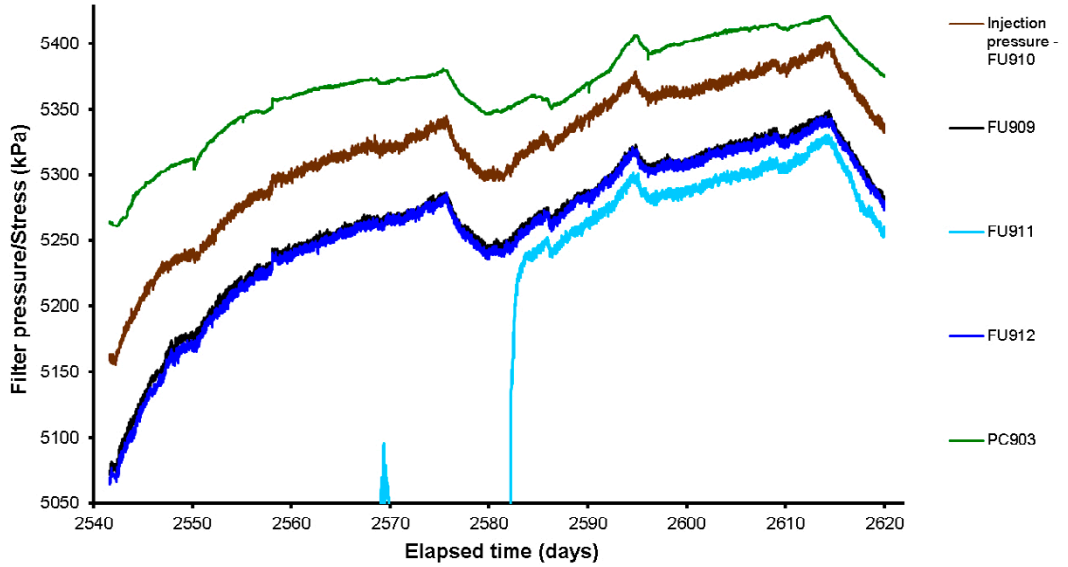

Figure 9-37. *Direct connection between sensors during Gas Injection Test 3.*

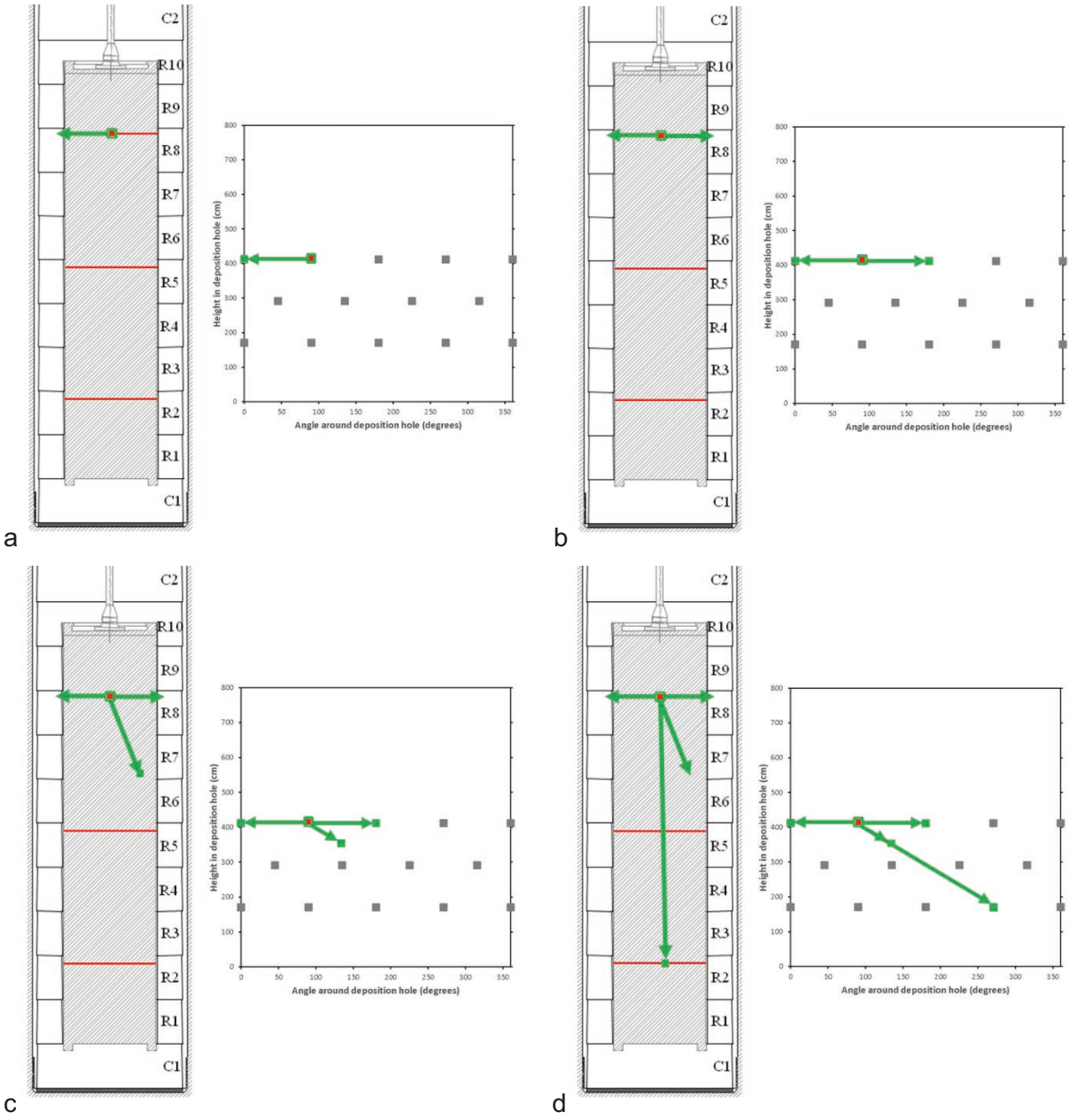

Figure 9-38. *Schematic of the direction of gas flow during Gas Test 3 in upper filter FU910. a) Gas reaching filter FU909; b) Gas reaching filter FU911; c) Gas reaching canister stress sensor PC903; d) Gas reaching filter FL904.*

9.4 Summary of Gas Injection Test 3

Gas Injection Test 3 was conducted in filter FU910 on the upper array of filters on the canister surface, the first test to be conducted in this filter. The aim of the gas test was to examine differences in gas testing at a site that was under a lower stress state and the influence of injection filter size on the hydration state surrounding the filter. Gas pressure was raised from background levels up to gas peak pressure using four distinct pressure ramps, being held at constant pressure in between.

1) The first pressure ramp started at Day 2257.23 using a constant injection rate of 6.5 ml h^{-1} into the interface vessel containing 4 700 ml of helium. This raised pressure from 1 026 to 2 245 kPa in 17.2 days when pressure was held constant from Day 2274.23 for 31.8 days. Throughout the period, the STP flow into the clay ranged from 1.92×10^{-8} to 3.97×10^{-8} m^3 s^{-1}. This resulted in a small flow into the clay, with 0.2 mol entering the clay. As gas pressure was held constant at around 2 247 kPa, a small amount of gas entered the clay, following which a flow rate of 473 µmol d^{-1} was observed.

2) The second pressure ramp started at Day 2306.22 using a constant injection rate of 2.0 ml h^{-1}. This raised pressure from 2 249 to 3 502 kPa in 17.7 days when pressure was held constant from Day 2 323.9 for 36.3 days. Throughout the period, the STP flow into the clay ranged from 1.3×10^{-10} to 2.1×10^{-9} m^3 s^{-1}. This resulted in a small flow into the clay, with 0.2 mol entering the clay. As gas pressure was held constant at around 3 510 kPa, a small amount of gas (0.018 mol) entered the clay with an average flow rate of 452 µmol d^{-1}.

3) The third pressure ramp started at Day 2360.23 using a constant injection rate of 1.0 ml h^{-1}. This raised pressure from 3 519 to 4 762 kPa in 16.8 days when pressure was held constant from Day 2377.02 for 100.2 days, during which time the gas volume was re-filled to 2 830 ml. Throughout the period, the STP flow into the clay was a nominal 3.0×10^{-9} m^3 s^{-1}. This resulted in a small flow into the clay, with 0.2 mol entering the clay. As gas pressure was held constant at around 3 510 kPa, a small amount of gas entered the clay (0.05 mol) with an average flow rate of 427 µmol d^{-1}.

4) The fourth pressure ramp started at Day 2477.27 using a constant injection rate of 0.75 ml h^{-1}. This raised pressure from 4 756 to a gas peak pressure of 5 192 kPa in 13.1 days, following which gas injection was continued at a constant rate for a further 124.1 days. Up until the time of peak pressure, the STP flow into the clay was constant at a nominal 1.98×10^{-10} m^3 s^{-1}. This resulted in a small flow into the clay, with 0.01 mol entering the clay.

Major gas entry and peak pressure occurred during gas ramp 4.

1) Day 2490.37: The first evidence of gas entry occurred around the time of gas peak pressure. This resulted in a single peak in flow of 4.70×10^{-7} m^3 s^{-1} that only lasted around 10 hours and reduced gas pressure by 45 kPa. Responses were seen in PR913, PR915–PR918, PR922 UR915, UR916, and UR921. Pore pressure/stress increased all around the deposition hole at the level of the injector, with both showing increases more anti-clockwise of the injector than directly opposite it. This suggests that the first movement of gas was from the injector to an orientation of 90°.

2) Day 2495.30: Gas arrived at filter FU909, with a series of pressure increases followed by leak-off. The response of the filter suggests that gas reached FU909 through a number of burst events, similar to the propagation of bubbles, before a stable, open pathway formed allowing gas pressure to increase to near injection values after 33 days.

3) Day 2502.28: Following gas peak and the initial pressure drop, pressure recovered and started to rise. A second, more gradual, peak in gas pressure of 5 298 kPa was seen around Day 2502.28, some 106 kPa greater than the first peak. This suggests that continued propagation of flow pathways required higher gas pressure. At this time, pore pressure in UR915 and UR921 reduced, whilst a complex response was seen in the radial stress sensors. At PR914, PR915, and PR919 stress increased, while it reduced at PR918, PR920, and PR922. The plot of radial stress showed the increasing magnitude of the formed high stress region, with pore pressure increasing on a level above the injector, but 180° around the canister.

4) Day 2508.46: Gas had reached FU911. Similar behaviour to FU909 was seen with 3 peaks in gas pressure seen, although much more distributed in time. It took 75 days for a direct, open pathway to form with pressure at FU911 mirroring the gas injection pressure. The third peak in pressure seen appears to almost reach stable conditions, before the pathway closed and pressure dissipated.

5) Day 2518.77: Gas was seen to propagate as far as PC903 by a pair of responses at Day 2516.41 and Day 2518.77, the latter being the time gas actually reached the sensor. The formation of a pathway near the sensor firstly relieved stress, until the direct communication of gas with the filter resulted in the sensor becoming pressurised.

6) Day 2533.04: Issues with the controller PC started on Day 2527.06, resulting in the closure of all air-actuated valves at Day 2533.04, therefore isolating the pump from the injection filter for 9.2 days. Radial stress at most sensors started to reduce. The air-actuated vales resumed operation once the logging PC was fixed, which initiated the recovery of the PR sensors. This shows that the increased stress was a direct consequence of gas pressure.

7) Day 2550.23: A significant disturbance in most sensors was seen. Pore pressure at UR910 following an initial drop of 52 kPa increased by 400 kPa. This event was seen in all pore pressure sensors and most of the radial stresses, both at the deposition hole wall and within the bentonite. For some of the pore pressure sensors pressure slowly decayed following the increase, whilst some remained at an elevated level. Stress on the canister surface was perturbed by this event, initially decreasing, followed by a recovery. By this time, a new high-pore-pressure region had formed at the level of the lower canister filters at 270°, opposite filter FL904. The distribution of radial stress suggests the formation of a region of elevated stress between the injection filter and FL904.

8) Day 2557.10: Gas had directly reached filter FU911 for a second time, resulting in a short-lived reduction in almost all pore pressure sensors.

9) Day 2575.74: A third peak in gas pressure of 5 346 kPa was seen. Flow into the clay started to increase, reaching a peak of 9.38×10^{-8} m^3 s^{-1}, reducing gas injection pressure slowly by approximately 45 kPa before gas pressure recovered. The increased flow corresponds with the start of pressure increase at filter FL904, which initially increased to a steady 4 157 kPa. At this time, radial stress decreased at PR915, PR917, PR919 and PR922 at the rock wall, and gradually increased within the bentonite above the canister. This suggests that the arrival of gas at FL904 resulted in the lowering of gas pressure and the relief of stress within the system. Stress began to reduce on the canister surface at PC903, mirroring gas injection pressure, demonstrating the direct connection of the injection filter and PC901.

10) Day 2596.14: A series of interlinked events started at Day 2596.14, when flow into the clay peaked once more at 7.51×10^{-8} m^3 s^{-1}, resulting in a reduction in gas pressure of around 25 kPa. Around this time, the majority of pore pressure sensors on the deposition hole wall registered an abrupt pressure increase. Radial stress at PR915 and PR919 showed a short-lived peak, while stress began to rise in many sensors. Stress within the bentonite below the canister at PB901 and PB902 started to increase, as did stress on the canister surface at PC901 and PC902.

11) Day 2600: the distribution of stress and pore pressure around the deposition hole wall had greatly modified. Radial stress changes suggest gas migrated first at the level of the injection filters, before migrating downwards towards 270° at the base of the canister, i.e. towards FL904. The response of the pressurised sensors shows that direct, open, pathways connected the injection filter with FU909, FU911, and PC903.

Following gas entry, a total of 4.99 mol entered the clay over a 124-day period, with an average flow rate of 40 mmol d^{-1}. The gas injection test lasted a total of 357 days.

10 Gas Injection Test 4 (Day 2726 – 3283)

The sixth significant stage of the Lasgit experiment started on Day 2726.08 (20th July 2012) and was completed at Day 3283.06 (26th January 2014); a total stage time of 556.98 days.

The first test in filter FU910, conducted as Gas Injection Test 3, gave results that have similarities to the two previous tests in filter FL903. However, differences were noted. Following the conclusion of the third test it was decided to repeat the gas test in filter FL903. The test was designed to examine whether gas entry pressure would continue to rise in response to a rising local stress field. This repeat test also investigated if the gas transport properties of the bentonite had changed with time and whether gas migration was the same as previously observed. Figure 10-1 shows the plan for the test period. Throughout the stage, artificial and natural hydration was occurring.

Gas Injection Test 4 comprised of two stages (Figure 10-2); 1) a two-stage hydraulic test to determine the hydraulic properties of the bentonite at filter FL903; 2) four-stage gas injection ramp to achieve gas entry at filter FL903. A repeat two-stage hydraulic test was not conducted as the filter was shut-in for a prolonged period of time after gas injection had stopped.

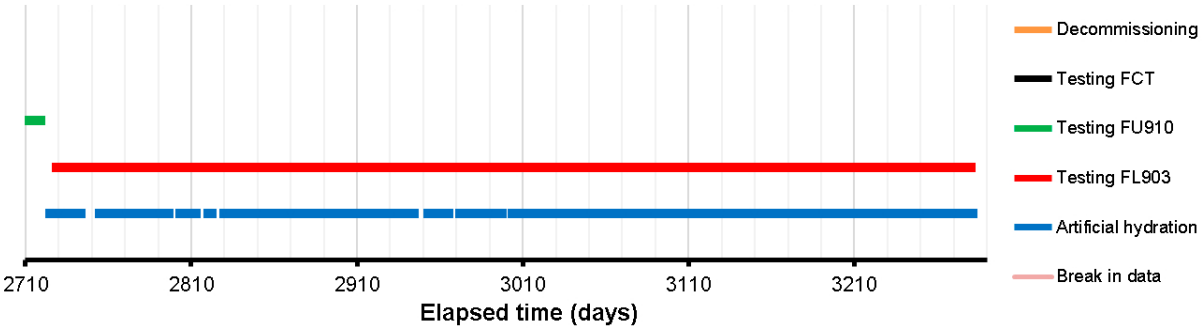

Figure 10-1. *Test stages of the Lasgit experiment showing what was conducted during Gas Injection Test 4.*

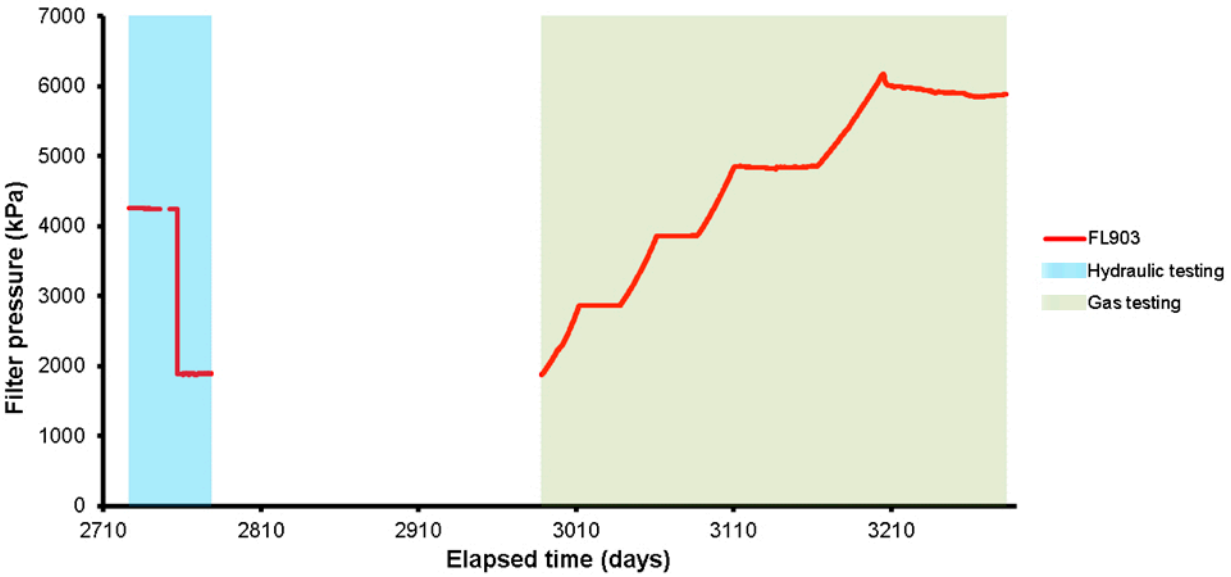

Figure 10-2. *The filter pressure of FL903 during Gas Injection Test 4. A two-stage hydraulic tests was conducted prior to a four stage gas injection test.* ***Note:*** *blue shading shows periods of hydraulic testing, green shows gas testing.*

10.1 Description of the field parameters during the period

Before describing the gas injection test, the field parameters will be described (boundary conditions). **Note:** The grey areas displayed in the graphs show periods when artificial hydration was not occurring.

Figure 10-3 shows the pore fluid pressure of the filter mats. As with previous stages, filter FR901 was not artificially hydrated and recorded local pore pressure. As seen, FR901 slowly decayed by approximately 100 kPa during the experimental stage, indicative of drawdown of the pore pressure as a result of the proximity to the drained tunnels. The remaining filters were all artificially hydrated at a nominal pore pressure of 2 500 kPa from the start of the experimental stage, following pressure decay at the end of the previous reporting period. The data in the first half of the period for sensors FB902–4 show variation of around 50 kPa. This was remedied at the calibration visit at Day 2969 when all of the pressure transducers were re-calibrated. Issues were found with several air-actuated valves not opening properly. It is expected that the variation seen was related to either this problem or could simply be down to calibration values, although the calibration data do not support the latter.

The first half of the experimental stage was dominated by problems with the compressor in maintaining sufficient air to keep the air-actuated valves open. This resulted in pressure drops at Day 2824.82–2827.08 and 2947.49–2950.12. The second half of the experimental stage shows stable pressure within the filter mats.

Figure 10-4 shows the pore pressure within the bentonite buffer (UB), recorded at six locations. Figure 10-4a shows that the results were dominated by the pressurisation of filter UB902 during the previous gas injection test. Figure 10-4b shows that all sensors showed considerable annual variation. This was most pronounced in filter UB926 towards the top of the deposition hole. Taking annual variation into account, pore pressure within the bentonite increased during the period. The peak of the initial pressure high in UB926 at Day 2279 was 965 kPa, compared with 1 335 kPa at Day 3163 for the second pressure peak. Increases were seen in all UB sensors. This suggests that the saturation state of the system was increasing but was dominated by annual influences.

Pore pressure within the bentonite (UB) showed clear coupling, as seen by the similarities in pore pressure increases, i.e. similarity in UB924 and UB926, and shows clear differences. This includes a considerable spread in pore pressure within the deposition hole, and sensor UB901 within the base of the deposition hole did not show much annual variation, suggesting that this feature was created by the ventilation of the gallery.

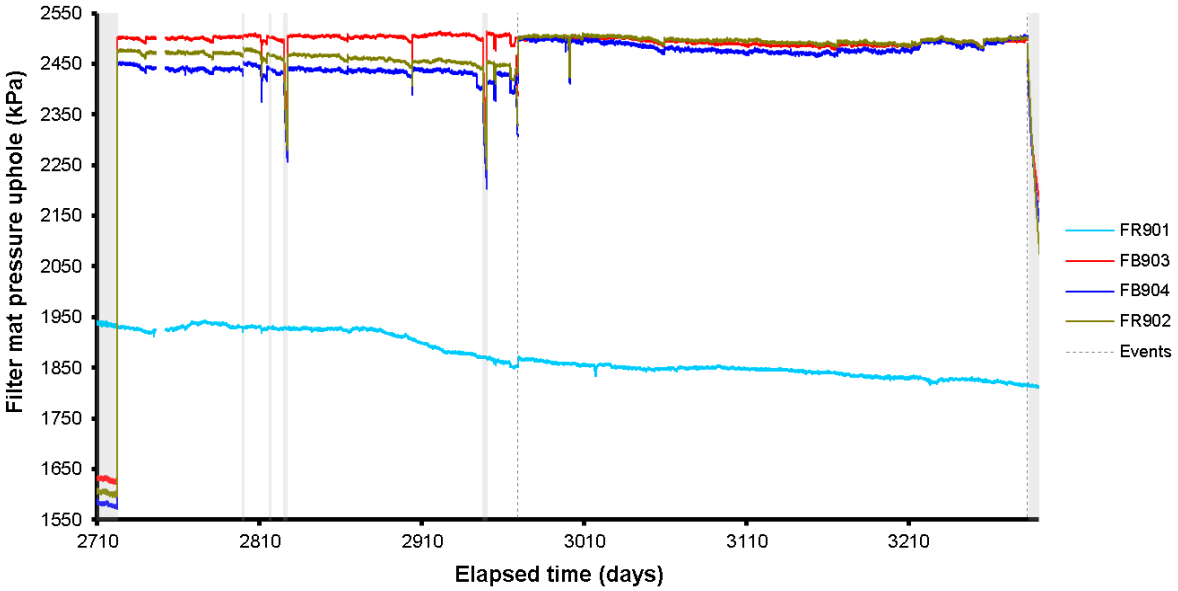

Figure 10-3. *Evolution of water pressure in the filter mats located on the borehole wall and within the bentonite blocks.*

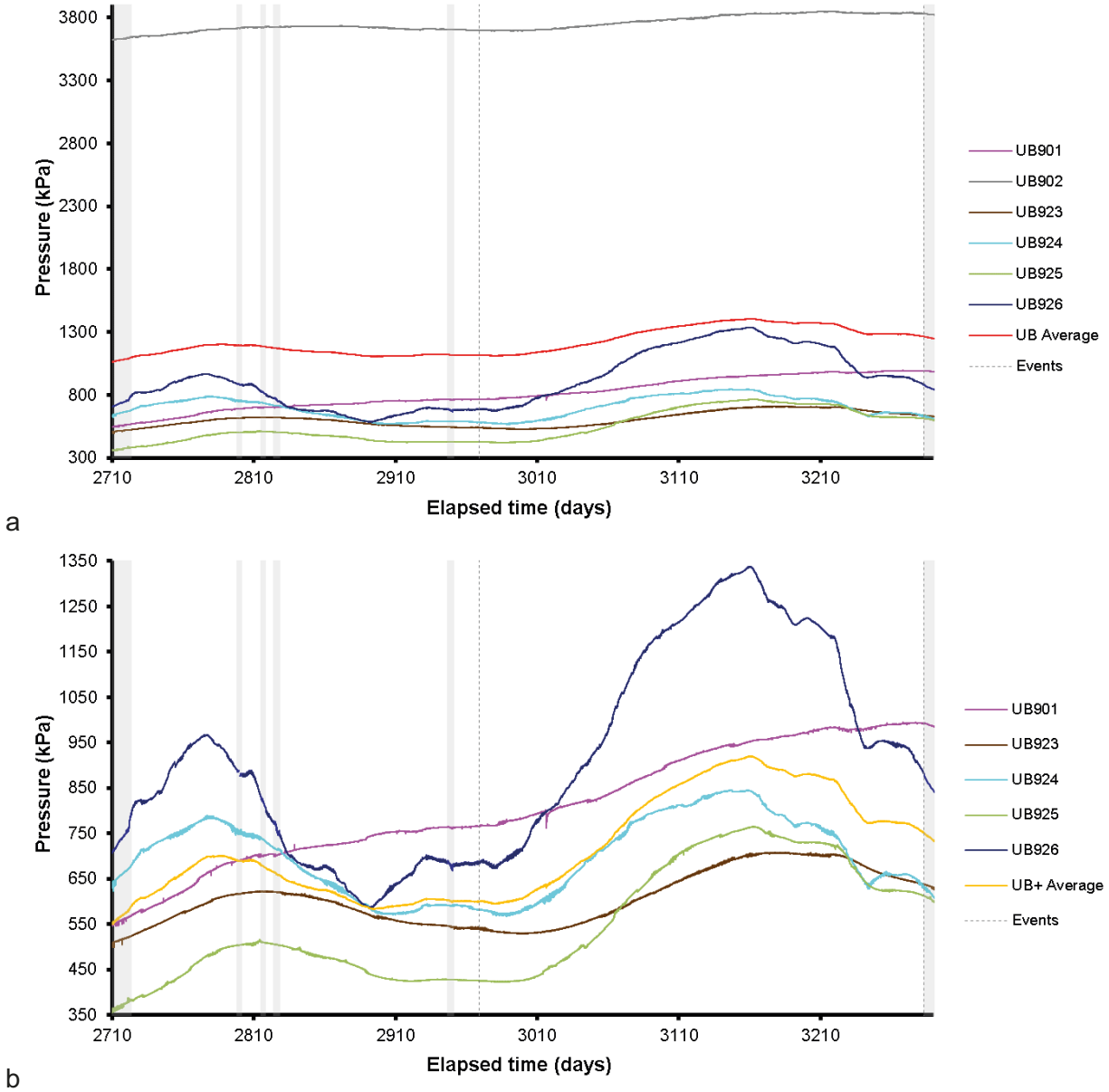

Figure 10-4. *Variation in porewater pressure within the bentonite at the 6 monitoring points: a) all six sensors; b) detail of five sensors.*

Pore pressure is also noted at the filter canisters when these were not used for artificial hydration of the system. Figure 10-5a shows that the data during this period was dominated by the operation of filter FL903 for the hydraulic and gas injection testing. Figure 10-5b shows that the pressure history of the canister filters was complex. The behaviour of the midplane filters (FM905–FM908) were the simplest, with all undergoing artificial hydration at the nominal pressure of 2 500 kPa. As with the filter mats, pressure decreases were observed when the compressor failed (Day 2824.82–2827.08 and 2947.49–2950.12). The upper array of filters (FU909–FU912) was shut-in for the first half of the period following the previous gas injection test. Therefore, these were recording natural pore pressure at this location and ranged between 1 050 and 1 360 kPa. During the calibration visit to site at Day 2969 the upper array of filters had pressure raised to the nominal artificial hydration pressure of 2 500 kPa. Therefore, for the second half of the experimental stage, when the gas injection test was conducted, both the mid- and upper-plane filters were artificially hydrated. The lower array of filters was more complicated. Filter FL903 was used for the gas injection test and therefore shows artificial boundary conditions dominated by the two-stage hydraulic constant head test and the gas injection test. Filter FL904 was raised to the nominal hydration pressure at the start of the stage, but was shut-off, giving a small and gradual decrease in pressure during the first half of the period. At the calibration visit to

site, it was discovered that the drains for filters FL901 and FL904 had been swapped over and this was corrected. As a result, FL904 was pressurised to a raised 2 250 kPa and shut-off to observe pressure decay. FL901 showed natural pressure throughout the stage of approximately 1 500 kPa, with a slight increase during the period. The most complicated result was seen in FL902. This was also showing a pressure of around 1 500 kPa. However, the signal was not stable and quite noisy. This was suspected to be a sign of gas migration and so gas was drained from this filter at Day 2975. As seen, pressure at FL902 then showed a saw-tooth effect, suggesting episodic flow at this filter.

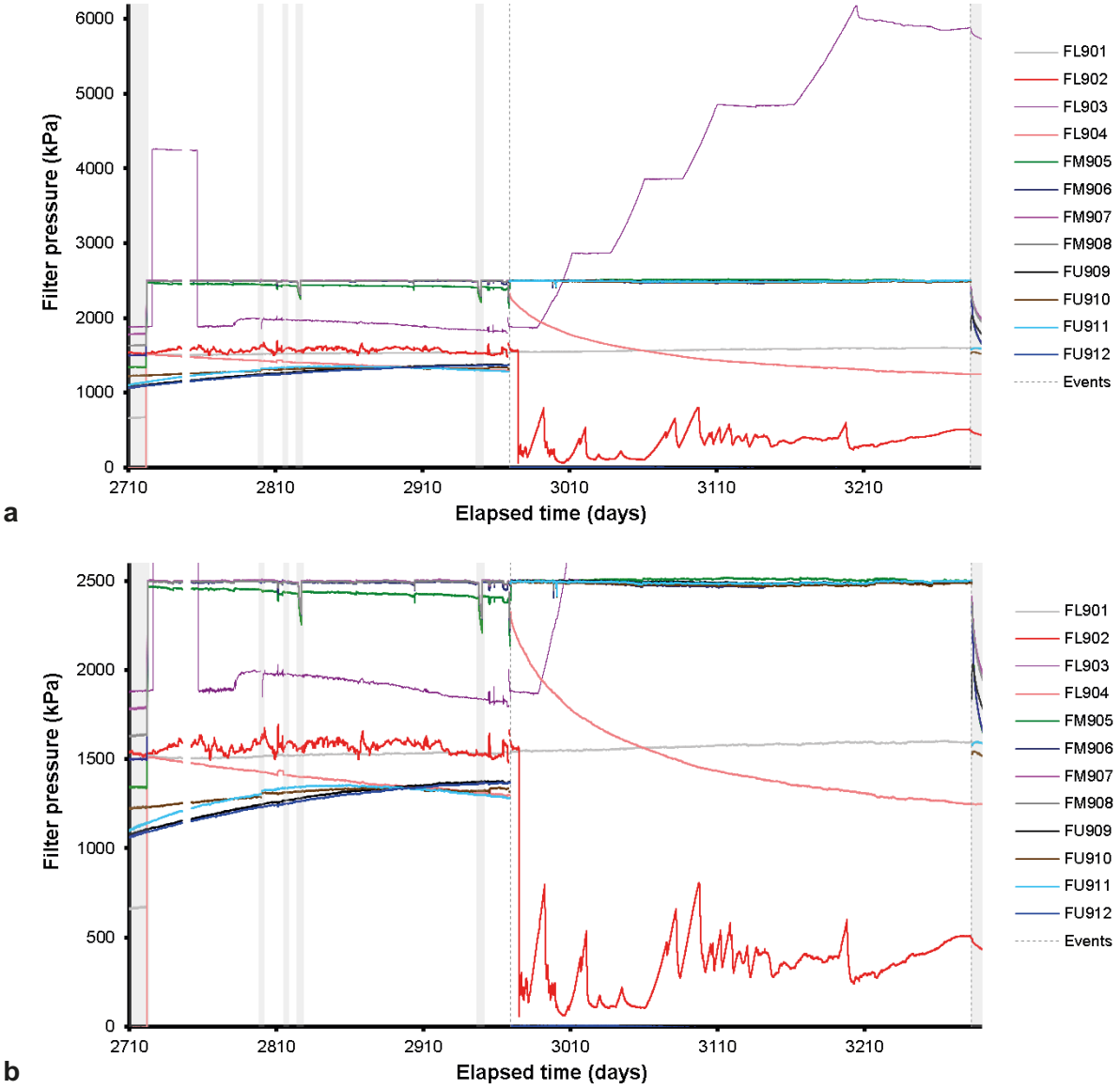

Figure 10-5. *Filter pressures on the canister surface. a) complete range of filter pressures dominated by the activities in filter FL903; b) detail of the pore pressures in the canister filters.*

Figure 10-6 shows the variation of pore water pressure at the rock wall. As can be seen, pressure was heterogeneous within the deposition hole, with around 2 000 kPa variation. The data is dominated by annual cyclicity differences throughout the deposition hole. Generally, pore pressure was greatest at the base of the deposition hole, decreasing with height. This was the same for all levels, except for the bottom UR level within bentonite ring R4, which was lower in pressure than the level in ring R5 and similar to that of ring R7. However, it should be noted that the variation in pore water pressure at ring R4 was only 200 kPa, compared with ~850 kPa in ring R5. This suggests a much better-connected network of fractures at the level of R4. It is also noted that the pore pressure cyclicity, with a period of a year, was greatest in the middle of the array of sensors, located at the canisters middle. Here, the variation in pore pressure within the level was also greatest, ~1 100 kPa variation. The heterogeneity seen in the pore pressure at the rock wall is described in greater detail in Section 16.3.4.

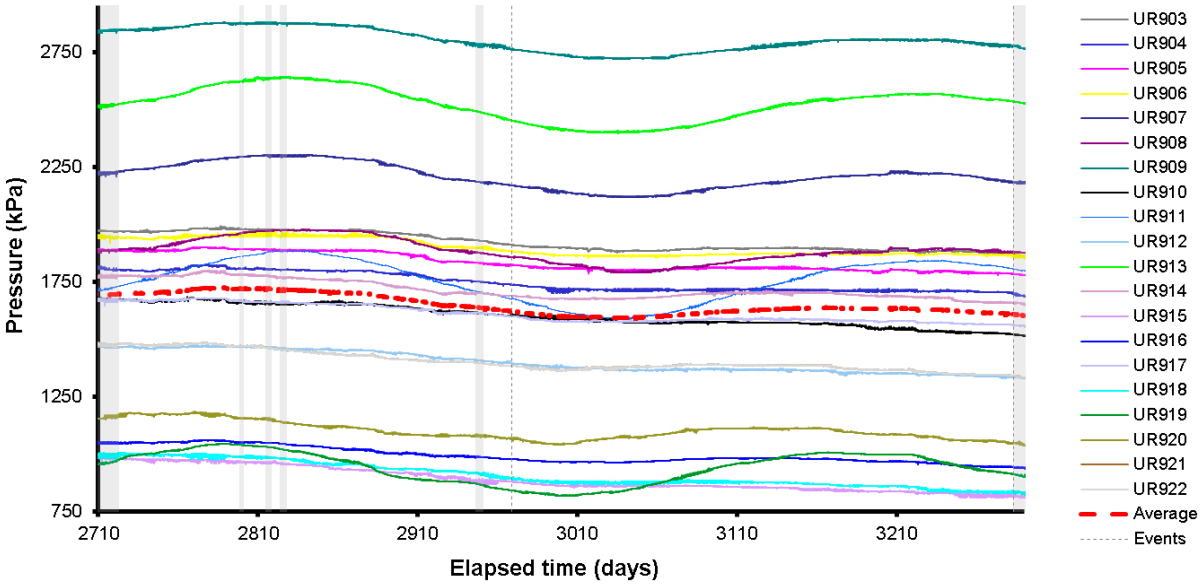

Figure 10-6. *Variation in porewater pressure with time measured at the rock face.*

Radial stress measured at the rock wall is shown in Figure 10-7a for all locations and in Figure 10-7b in detail for all sensors excluding PR921. As seen, the radial stress history was complicated during the reporting period. Some sensors exhibited very little change, while others showed either small increases or decreases. All sensors showed a clear annual variation. The radial stress within the bottom of the deposition hole was greatest in bentonite rings R4 and R5, with a lower stress seen further up the deposition hole. However, the upper most section of radial stress sensors at ring R10 showed a high stress. Therefore, it appears stress generally increased from the centre of the canister in both an upward and downward direction. The variation was not always apparent because of the differences in stress observed at each interval. It should be noted that the interval with the lowest stress also included PR921, which recorded a stress considerably lower than all other PR sensors. No significant radial stress events were noted during the reporting period, with annual variation dominating. However, it should be noted that the peaks and troughs of the annual signal varied with depth and even within depth sections, suggesting a complex and sometimes localised response.

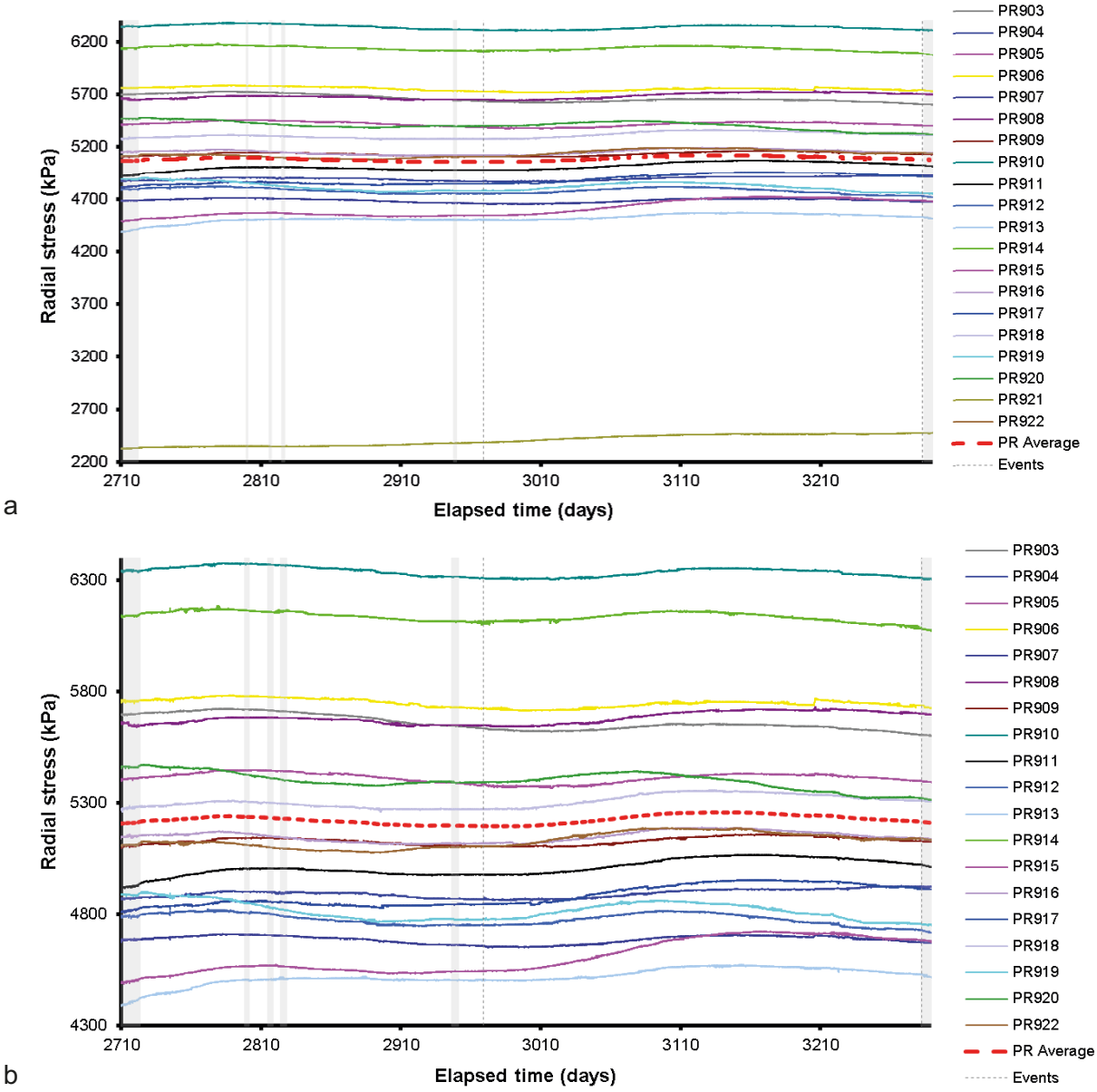

Figure 10-7. *Variation in radial stress at the rock wall with time. a) radial stress for all locations; b) radial stress for all locations excluding PR921.*

The stress acting on the canister was measured at three locations, as shown in Figure 10-8. During Gas Injection Test 4 the average stress only marginally increased, with annual variation superimposed. Sensors PC902 and PC903 mirrored one another well with little change over the whole experimental stage, with a stress increase seen in PC901.

Axial stress within the bentonite is shown in Figure 10-9 and was complex. Within the deposition hole there was considerable spread of ~1 500 kPa within the deposition hole. All locations showed a degree of annual cyclicity. Generally, axial stress was lowest at the base of the deposition hole within the bottom segment of the bentonite buffer (C1); the exception was PB929, which recorded the lowest axial stress of approximately 5 000 kPa. The two sensors within the base of the deposition hole also showed less annual variation than the sensors at the top of the hole; again, PB929 was the exception to this, showing little annual variation. The most significant observation was the "uneven" signal noted in the sensors towards the top of the hole. Superimposed upon the long-period (annual) annual variation was a much higher frequency variation of ~50 days. This signal was absent from the base of the deposition hole and does not correspond with the periods when artificial hydration was paused. As these were seen in all sensors of PB92x notation it must be a real feature occurring relating to the current gas injection testing. At the start of the reporting period an increase in axial stress was seen that did correspond with the re-establishment of artificial hydration in the filter mats.

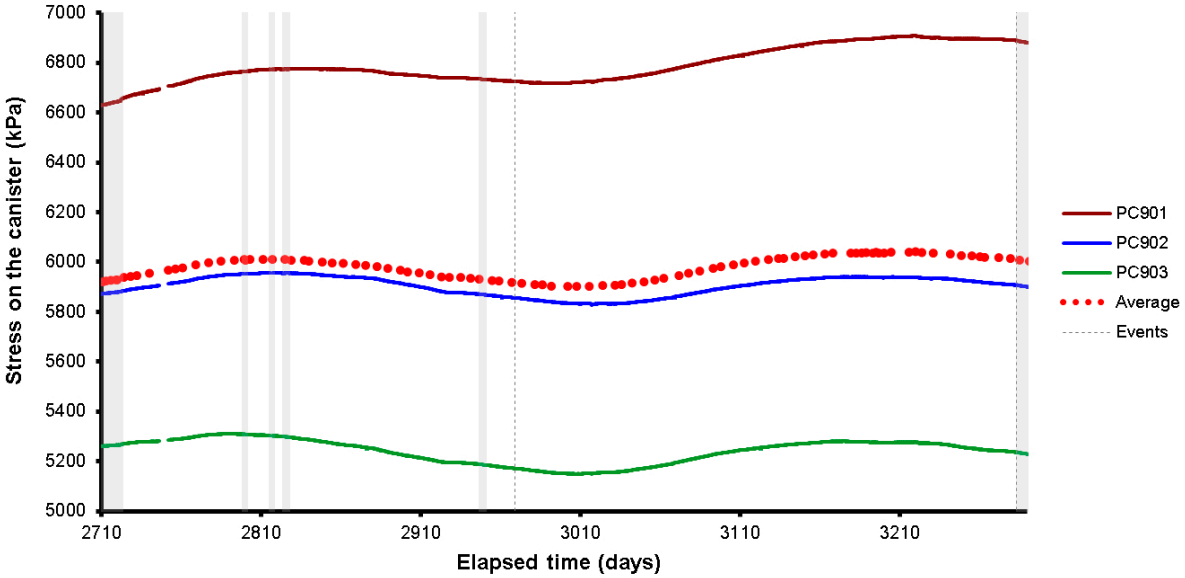

Figure 10-8. *Development of axial and radial pressure on the side and base of canister.*

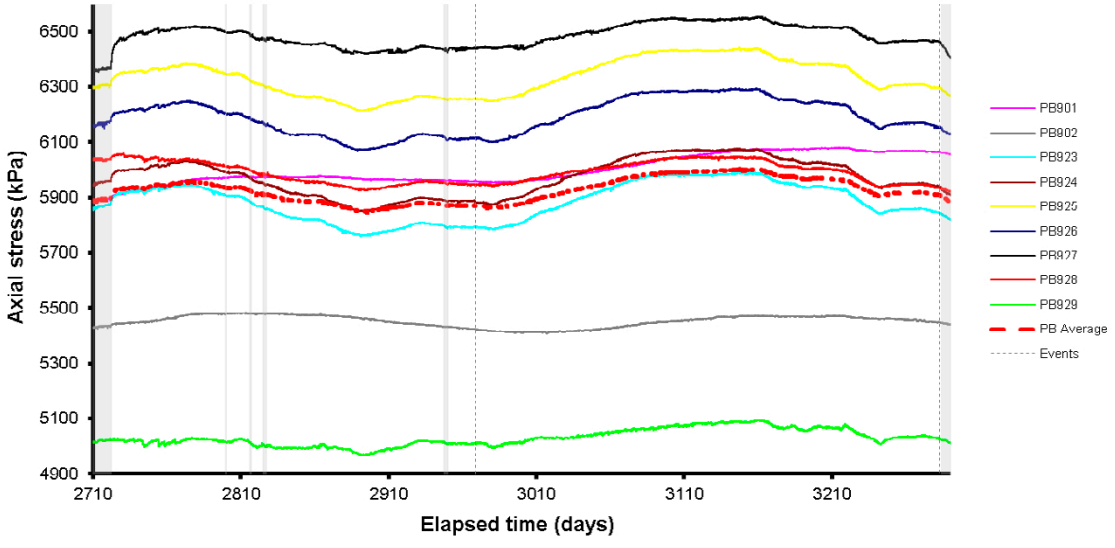

Figure 10-9. *Development of axial stress measured at 9 locations within the buffer.*

The increase of stress within the bentonite was mirrored in the axial force measured on the lid, as shown in Figure 10-10. An annual variation was again observed, with a small increase over the experimental stage. As with the axial stress sensors, a higher frequency variation was superimposed upon the season variation. This suggests that the behaviour seen in axial stress was a real response.

A similar trend was seen within the sensors measuring the displacement of the lid (Figure 10-11a). During the experimental stage ~0.2 mm displacement was observed vertically. The canister was seen to move downwards by 0.25 mm, driven by artificial hydration within the bentonite segments at the top of the deposition hole. As described for LP and PB sensors, the lid movement showed a higher frequency variation component superimposed upon year-long seasonal variation. Lateral movement of the lid (Figure 10-11b) only showed small movements of < 0.1 mm. Lateral movement sensor 2 showed a distinct annual variation, whereas Lateral movement sensor 1 did not. The lateral movement was complex, probably enhanced by the small movements noted above.

Pore pressure away from the deposition hole within the pressure relief hole is shown in Figure 10-12. A small reduction in pressure over the period was seen of ~50–100 kPa. Interval PRH2–4 was affectively at atmospheric pressure, this interval was closest to the gallery. A few short interval events were observed.

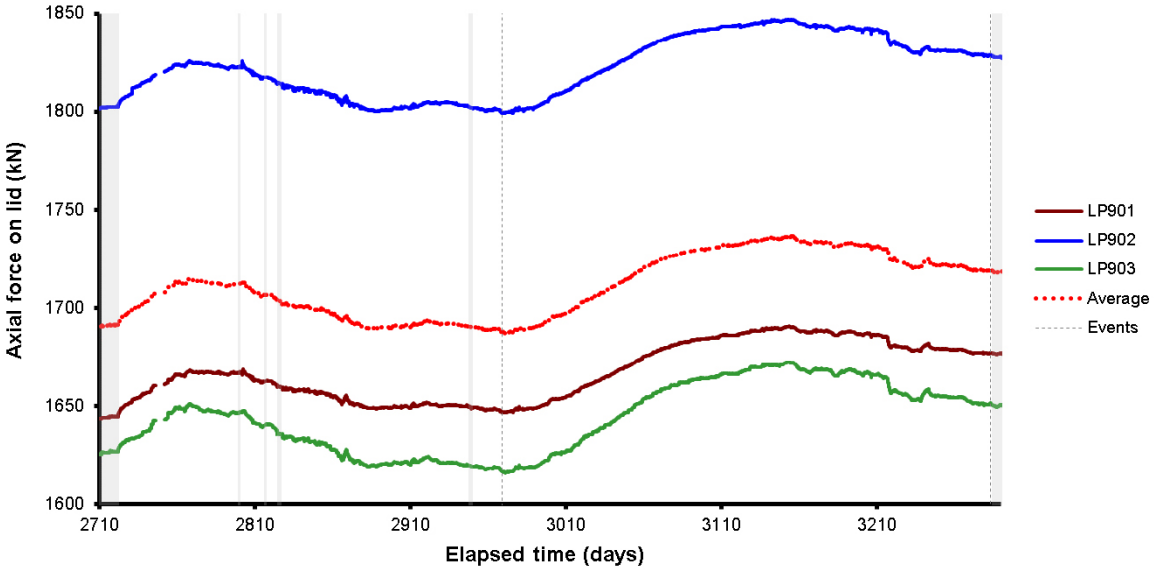

Figure 10-10. *Axial force acting on the steel lid measured by 3 Glötzl load cells attached to separate rock anchors.*

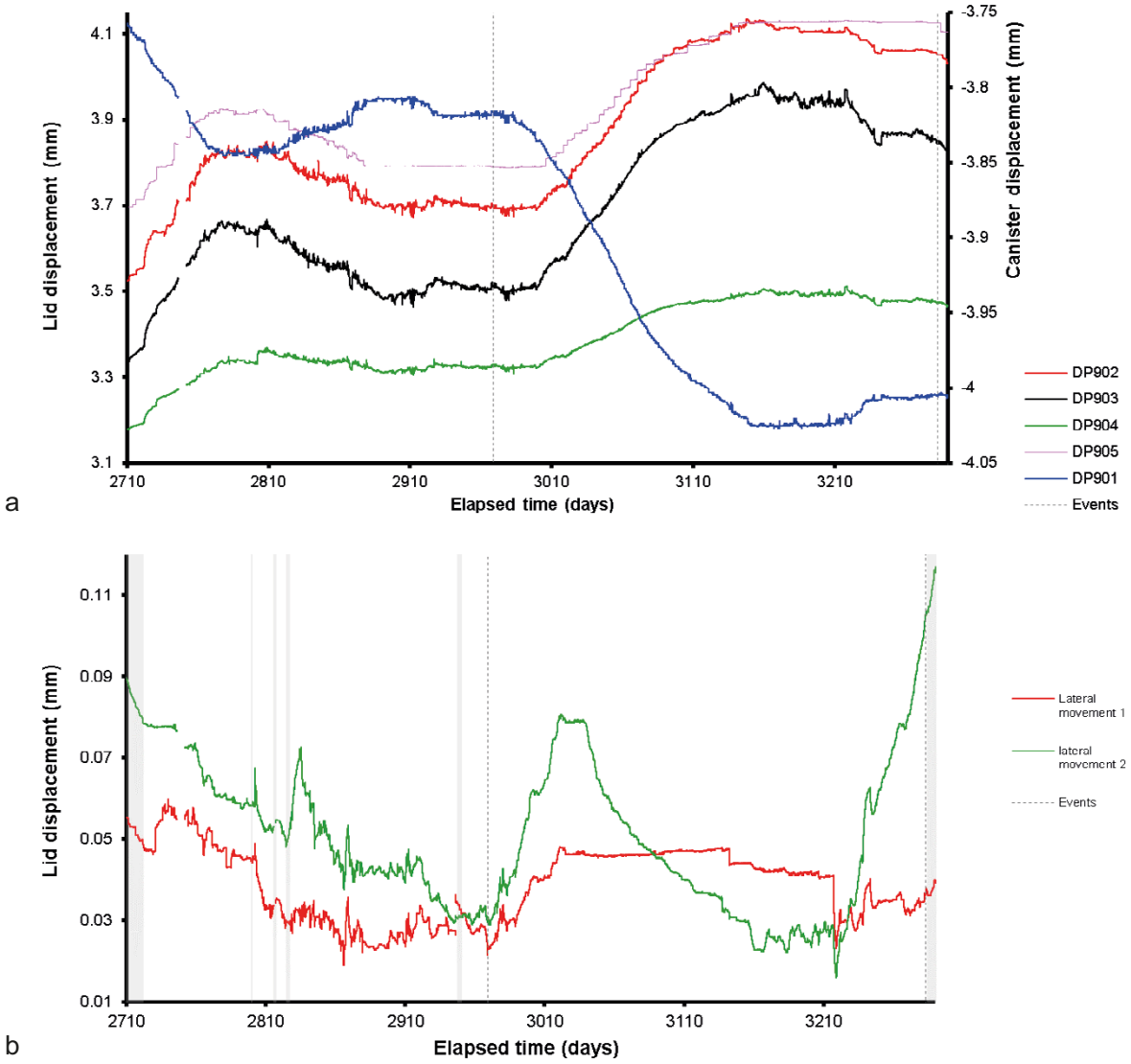

Figure 10-11. *Linear displacement of the steel lid and copper canister (a) and lateral movement of the lid (b). Movements of the lid are measured relative to both the gallery floor and ceiling. Movements of the canister are measured relative to the steel lid.*

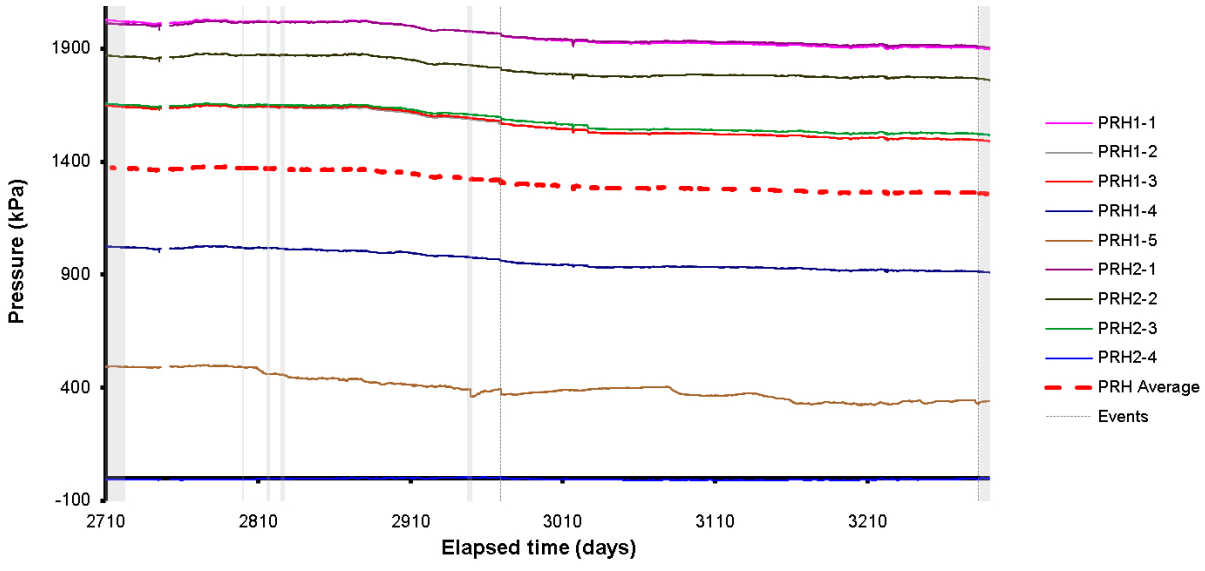

Figure 10-12. *Porewater pressures measured in the packered sections of the pressure relief boreholes.*

Temperature was monitored within the Lasgit laboratory & office, the HRL, and the canister. Figure 10-13 shows that the air conditioning unit within the laboratory was problematic at the start of the test. The air conditioning unit should have been able to maintain a stable temperature, as seen between Days 2820 and 2950. However, at Day 2967 the temperature in the lab increased ~3 °C. The air-conditioning unit was examined and fixed at Day 2969. However, following this time the unit failed to maintain a steady temperature, giving rise to both an annual variation and a short-term variation. The temperature within the Lasgit laboratory closely matched the temperature in the HRL gallery. This needs consideration when examining data from the ISCO syringe pumps.

Figure 10-14 shows the total volume of water pumped into the system during this experimental stage. At the start of the stage artificial hydration was resumed. Following this time, a generally steady flowrate into the buffer was seen. Approximately 6 litres of water were pumped into the buffer during the experimental stage.

Figure 10-15 shows average stresses, pore pressure, and forces observed during the current reporting period. What can be noted was that radial stresses, axial stress on the rock wall, axial force on the lid, stress on the canister all increased marginally or remained constant during the experimental stage. Pore pressure within the bentonite showed a clear increase during the period. In contrast, pore pressure at the rock wall and pore pressure within the pressure relief holes reduced marginally.

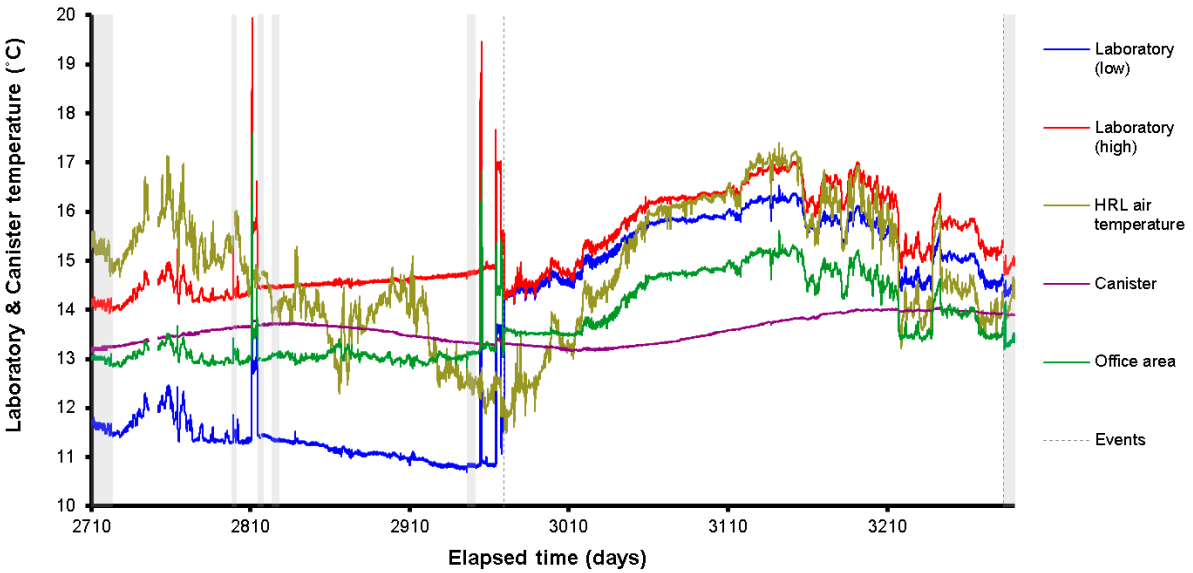

Figure 10-13. *Temperatures recorded in the Gas Laboratory, office, canister, and HRL.*

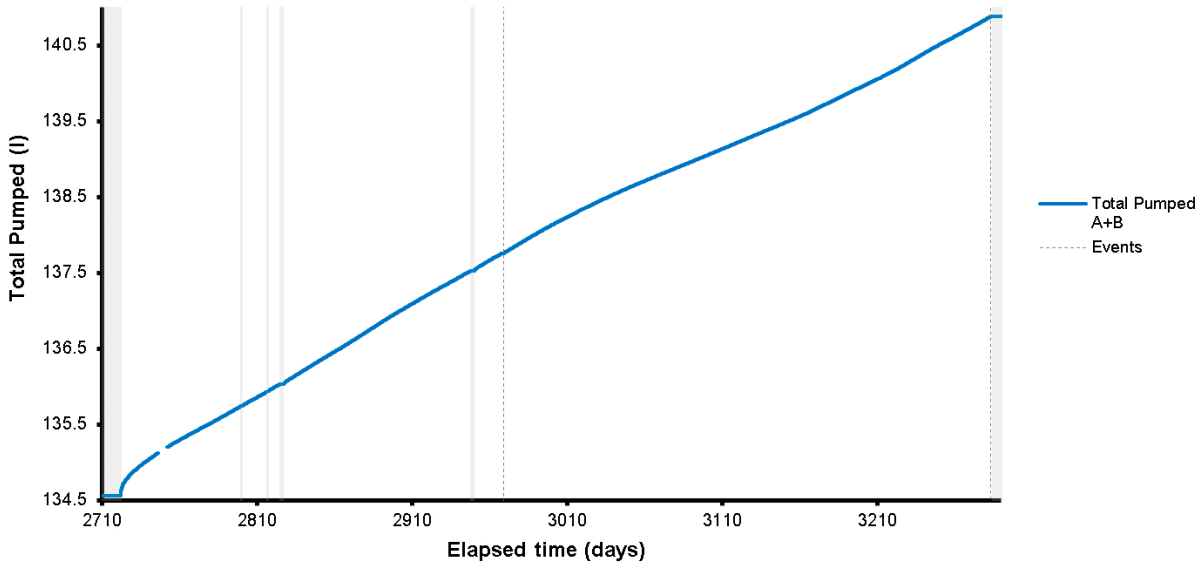

Figure 10-14. *Total pumped during artificial hydration and hydraulic testing.*

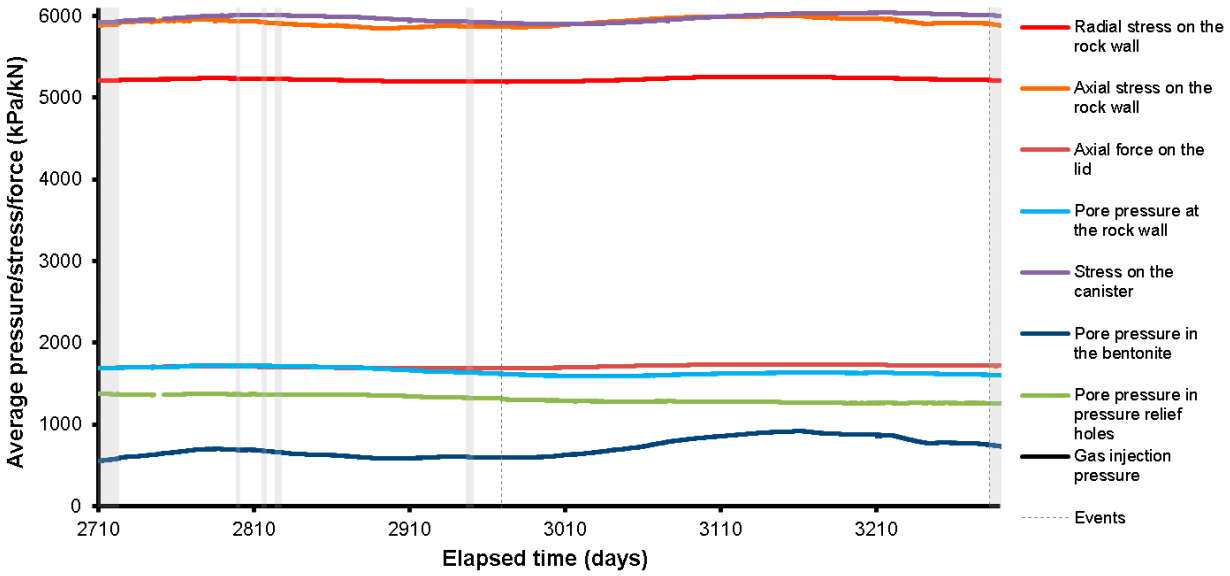

Figure 10-15. *Average pressures, stress, and force observed during Gas Injection Test 4.*

10.2 Hydraulic test prior to the gas injection test

Figure 10-16 shows the results of the two-stage hydraulic test conducted before the gas injection test. The injection filter was "shut-in" after the gas injection test to see how the gas pressure evolved. This meant there wasn't a hydraulic test after gas injection. Figure 10-16a shows the pore pressure imposed during the test. Note there was a data drop-out 20 days into the high-pressure stage. Figure 10-16b, c and Figure 10-17a show that the high-pressure stage resulted in an initially high flow into the buffer in excess of 4×10^{-11} m^3 s^{-1}, which quickly reduced to an asymptote of 3.70×10^{-12} m^3 s^{-1}. Figure 10-16b, c and Figure 10-17b show that the low-pressure stage resulted in an initially high outflow in excess of 6×10^{-11} m^3 s^{-1}, which quickly reduced to an asymptote of 3.31×10^{-13} m^3 s^{-1}. The low-pressure stage resulted in a much noisier result, but it is clear that the outflow during this stage was considerably lower than the inflow during the high-pressure stage.

The two-stage hydraulic head test was modelled using the 1-D modelled described in Section 6.4, Figure 10-18 shows the modelled result. The fit of the data can be seen to be good, although it hasn't perfectly modelled the data. Table 10-1 summarises the calculated values for hydraulic conductivity and specific storage.

Table 10-1. Modelling results for the two-stage constant head hydraulic tests conducted during Gas Injection Test 4.

Filter	Radius of the filter (mm)	Step	Fitted hydraulic conductivity (m/s)	Fitted specific storage (m^{-1})	Boundary conditions		Initial conditions	
					p_0 (MPa)	p_L (MPa)	p_{I0} (MPa)	p_{IL} (MPa)
FL903	50	1	7.75×10^{-13}	6.45×10^{-6}	4.25	1.89	1.88	1.89
		2	3.73×10^{-12}	1.34×10^{-5}	1.93	1.89	4.25	1.89
		Average	**2.25×10^{-12}**	**9.94×10^{-6}**				

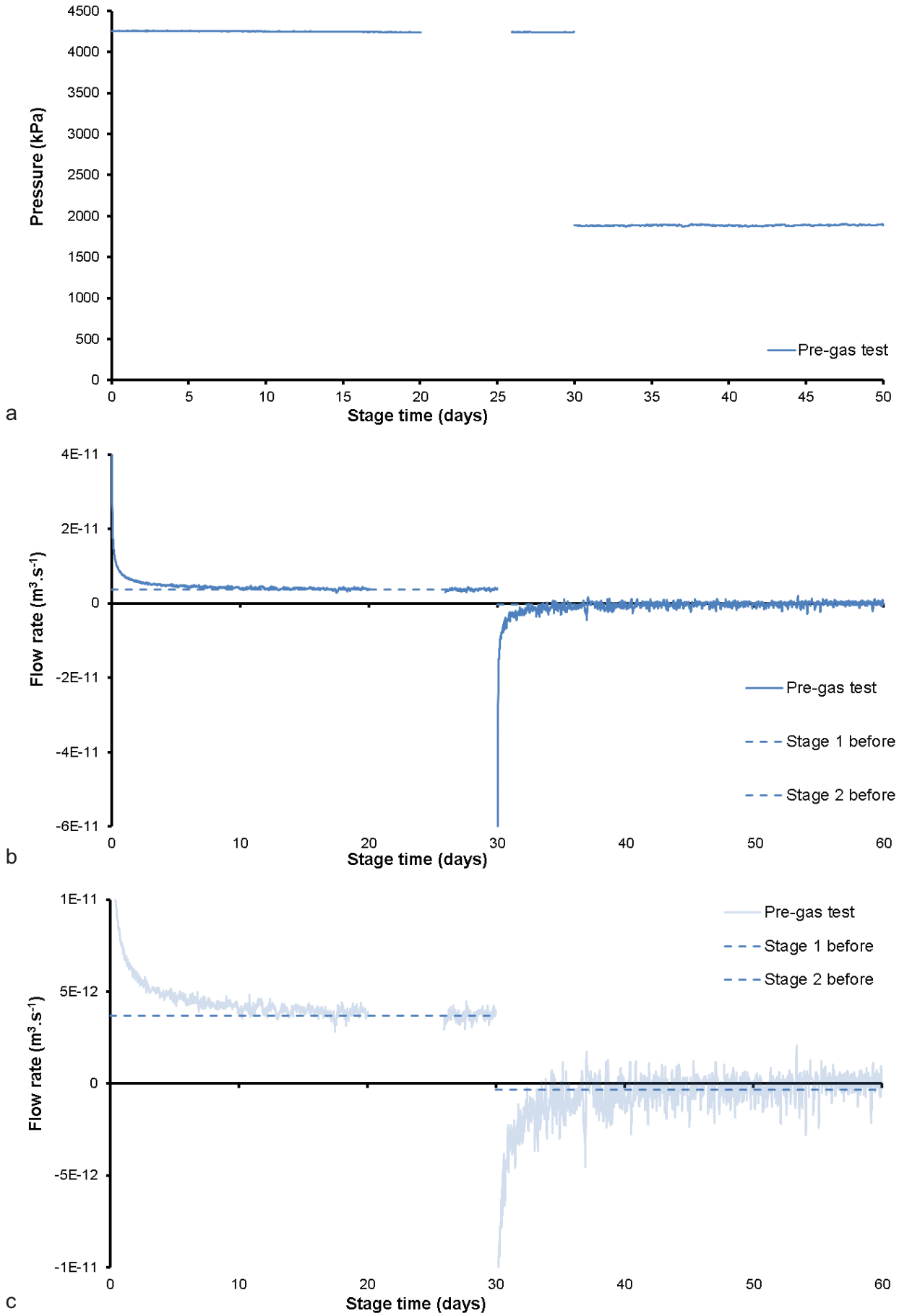

Figure 10-16. *Two-stage constant head hydraulic tests conducted during Gas Injection Test 4. a) Pressure of the injection fluid; b) Flow response; c) Detail of flow response.*

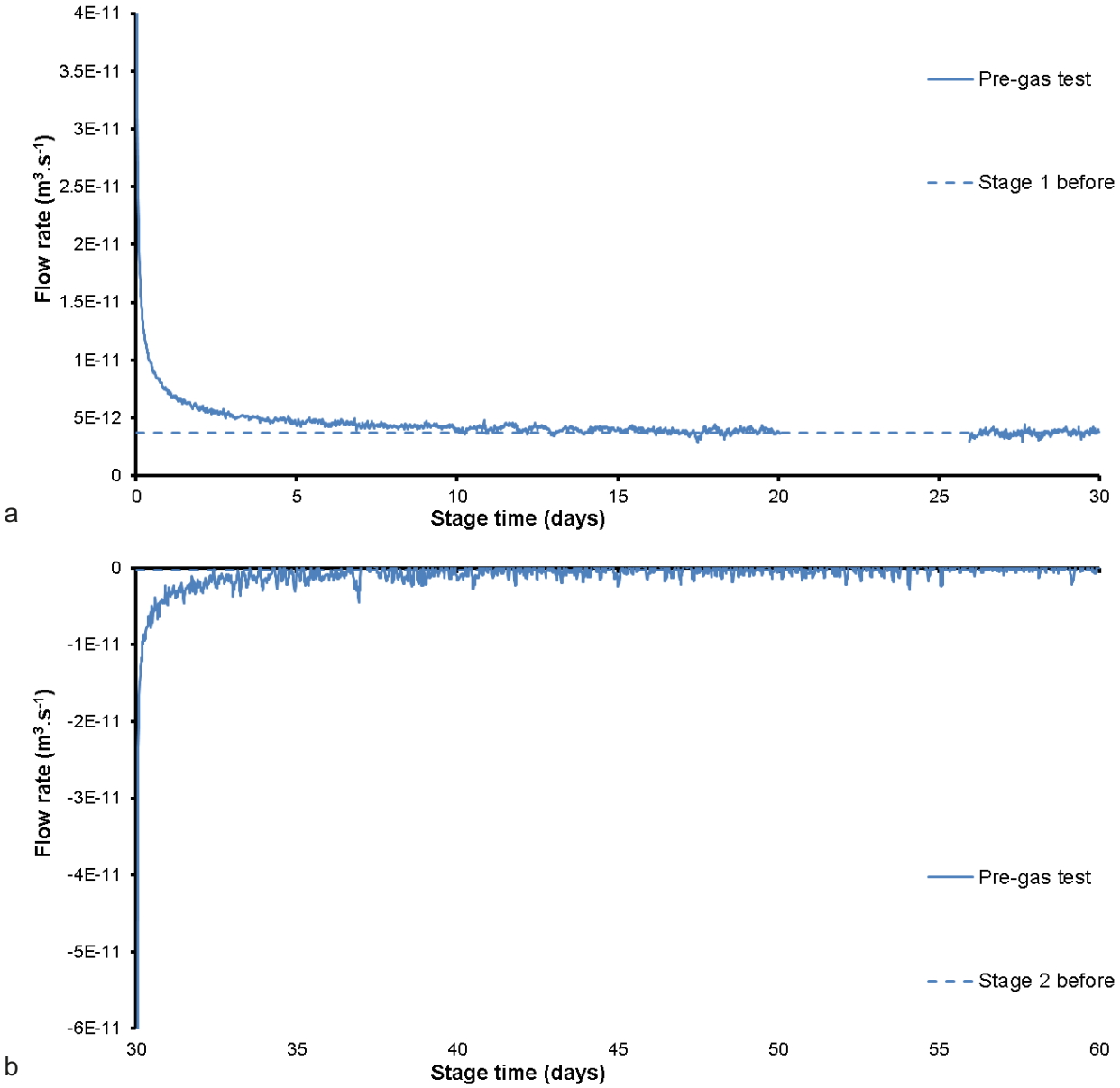

Figure 10-17. *Detail of the flow into the clay during the two-stage constant head hydraulic tests conducted during Gas Injection Test 4. a) High-pressure stage; b) Low pressure stage.*

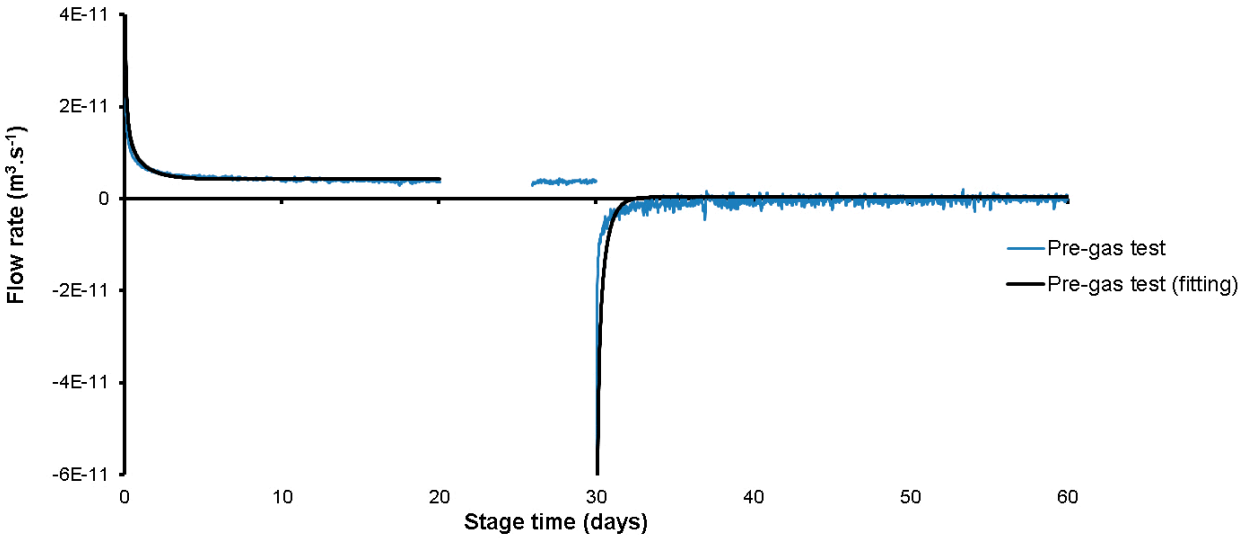

Figure 10-18. *Modelled results for the two-stage constant head hydraulic tests conducted during Gas Injection Test 4. a) Pre-gas test; b) Post-gas test.*

10.3 Gas injection test 4

Gas Injection Test 4 was conducted in filter FL903 on the lower array of filters on the canister surface. It was the third such test using FL903 and started 1 020 days after the end of the previous test (GT2), and 1 978 days after the first test in FL903 (GT1). As with the previous tests in FL903, gas pressure was raised from background levels up to gas peak pressure using four distinct pressure ramps, being held at constant pressure in between. Following gas peak pressure, gas flow was continued for a limited period of 78 days. During this prolonged period of injection, the injection rate into the system was varied to determine how the buffer reacted.

Approximately 3 750 ml of helium was added to the interface vessel at a starting pressure of 1 868 kPa. The injection filter was thoroughly flushed of water using pressurised helium and the drain from filter FL903. Once flushed, it was common for flow to take a few days to stabilise as gas went into solution and any remaining water within the filter was expelled into the bentonite. The first pressure ramp was started at Day 2988.07 (8th April 2013) by the injection of water into the base of the interface vessel at a rate of 2.45 ml h^{-1}. This raised pressure from 1 868 to 2 867 kPa in 23.9 days, as shown in Figure 10-19, when pressure was held constant from Day 3011.99 for 26.0 days. The second pressure ramp was started at Day 3038.04 on (28th May 2013) by the injection of water into the base of the interface vessel at a rate of 1.2 ml h^{-1}. This raised pressure from 2 868 to 3 856 kPa in 23.1 days, after which pressure was held constant from Day 3061.17 for 26.1 days. The third pressure ramp was started at Day 3087.24 (16th July 2013) by the injection of water into the base of the interface vessel at a rate of 0.725 ml h^{-1}. This raised pressure from 3 867 to 4 852 kPa in 23.2 days, after which pressure was held constant from Day 3110.48 for 52.6 days. The fourth, and final, pressure ramp was started at Day 3163.04 (30th September 2013) by the injection of water into the base of the interface vessel at a rate of 0.35 ml h^{-1}. This raised pressure from 4 854.01 to a gas peak pressure of 6 174 kPa at Day 3205.31, 42 days after the start of the fourth pressure ramp. The injection of water into the base of the interface vessel continued at 0.35 ml h^{-1}, until Day 3235.13 when flow was reduced to 0.175 ml h^{-1}, and Day 3256.19 when it was reduced further to 0.088 ml h^{-1}. Injection was stopped at Day 3283.02 (10:10 28th January 2014). In total, 2 910.5 ml of water was injected into the base of the interface vessel during Gas Injection Test 4.

The prediction of gas pressure shown in Figure 10-19 derives from the ideal gas law. A close agreement can be seen with the experimental data. Although a slow process, care was taken to determine the starting volume of gas during the filling of gas and showed an estimated starting volume of 3 515 ml. A secondary measure of starting volume was estimated by changing the volume of the gas and observing the change in pressure; this gave an estimate of starting volume of 3 471 ml. Figure 10-20 shows the difference between the predicted and observed gas pressures. This was used to refine the estimate of the starting volume, which in this case gave a volume of 3 750 ml. This latter estimate was used for calculations, with the starting volume of gas determined for each pressure ramp. Without an adjustment it would suggest that gas was always moving into the buffer. Gas volume can be lost through diffusion and in solution at the gas/water contact within the interface vessel.

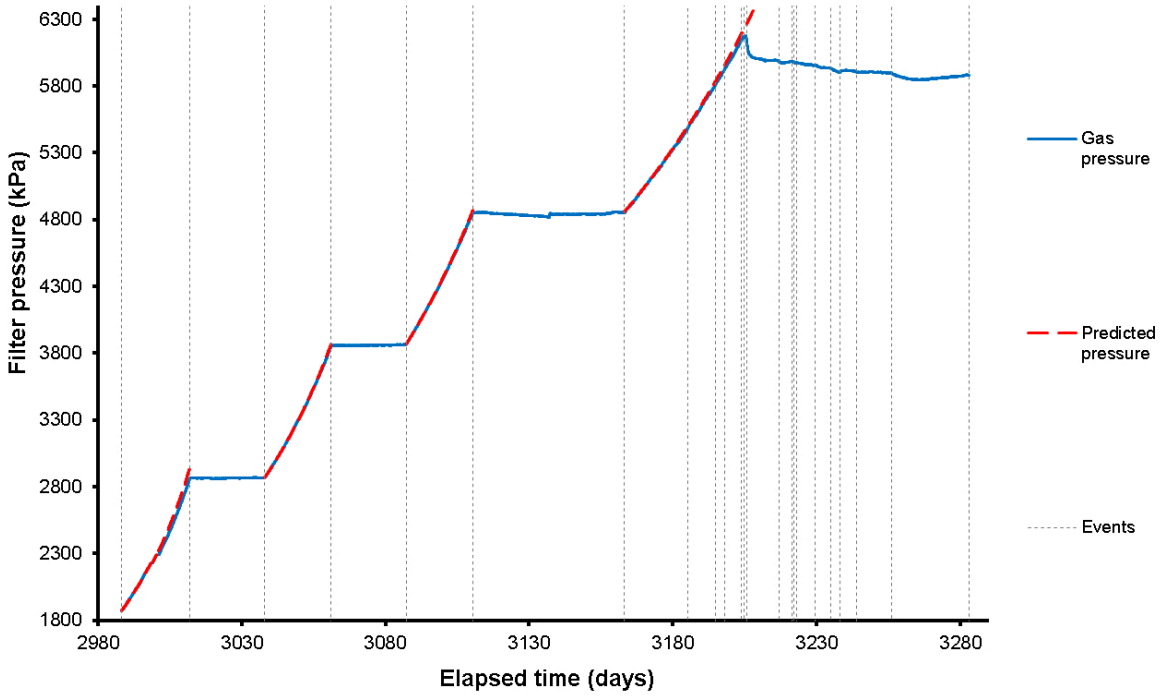

Figure 10-19. *Recorded and predicted gas pressure during Gas Test 4.*

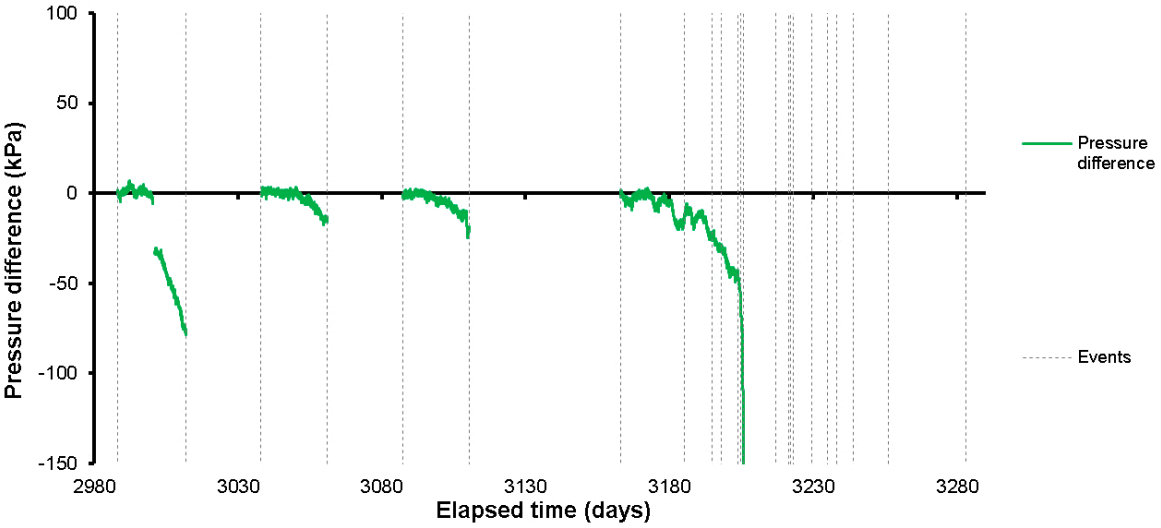

Figure 10-20. *Difference between recorded and predicted pressure during Gas Test 4. This is used to estimate the volume of gas during a constant flow gas compression stage.*

Figure 10-21 shows the flow of gas into the system and into the clay at STP. This clearly shows that the rate of gas entry reduced between each successive gas ramp. Flow into the clay was seen in each ramp, with little flow observed during periods of constant pressure. Each injection ramp will be introduced in detail in the following paragraphs.

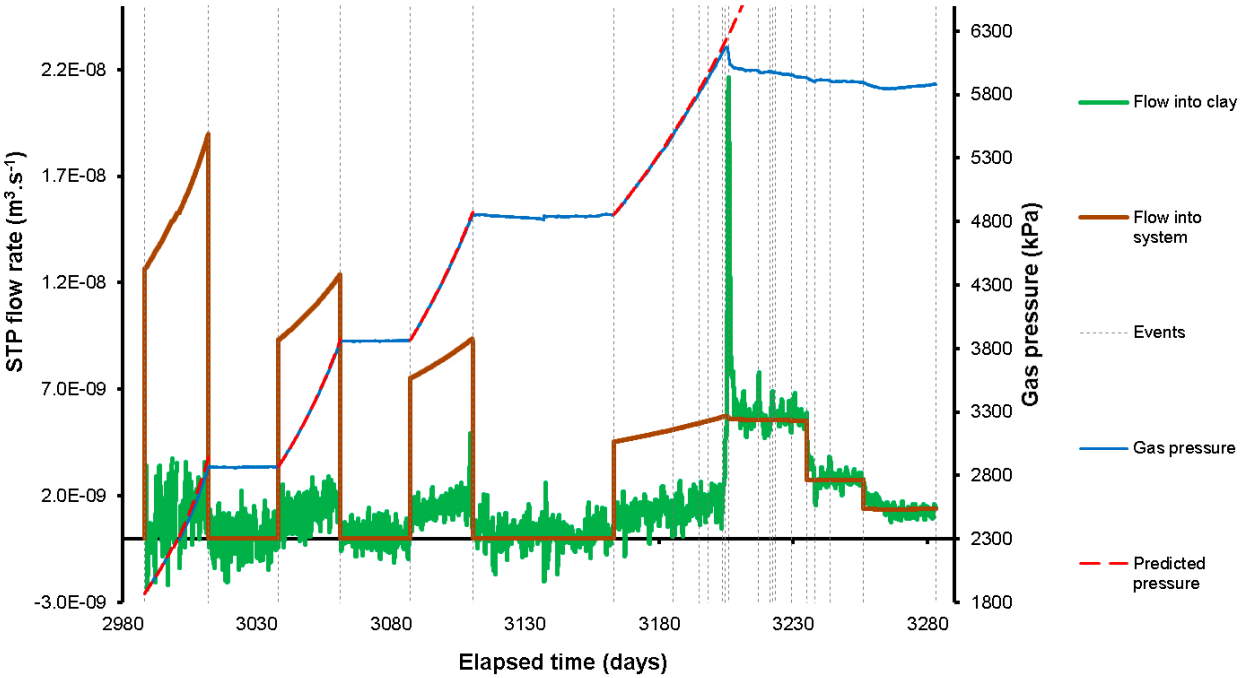

Figure 10-21. *Flow of gas into the system and the clay during Gas Test 4.*

Figure 10-22 shows the detail of the first gas ramp conducted in Gas Injection Test 4. As seen in Figure 10-22a, there were two breaks during the pressure ramp, with the second resulting in a shift in the difference between observed and predicted pressure (Figure 10-22b). The cause of this is not known and may indicate that the pump was isolated from the interface vessel for a limited time and that the volume change registered by the pump was not pumped into the interface vessel. At this stage in the test it was not a significant issue and was not representative of gas flow into the clay. Throughout the period, the STP flow into the clay ranged from 1.25×10^{-8} to 1.48×10^{-8} $m^3 s^{-1}$. This resulted in a small flow into the clay, with 0.1 mol entering the clay (Figure 10-22c). This may have occurred through diffusion and/or solution and was not interpreted as representing advective movement of gas. As gas pressure was held constant at around 2 867 kPa, a small amount of gas was seen to leave the buffer, as shown by a reducing cumulative volume of gas in Figure 10-22c. Following this initial reduction, a flow rate of 17.8 µl h^{-1} was observed between Day 3021 and 3037, representing 282 µmol d^{-1}.

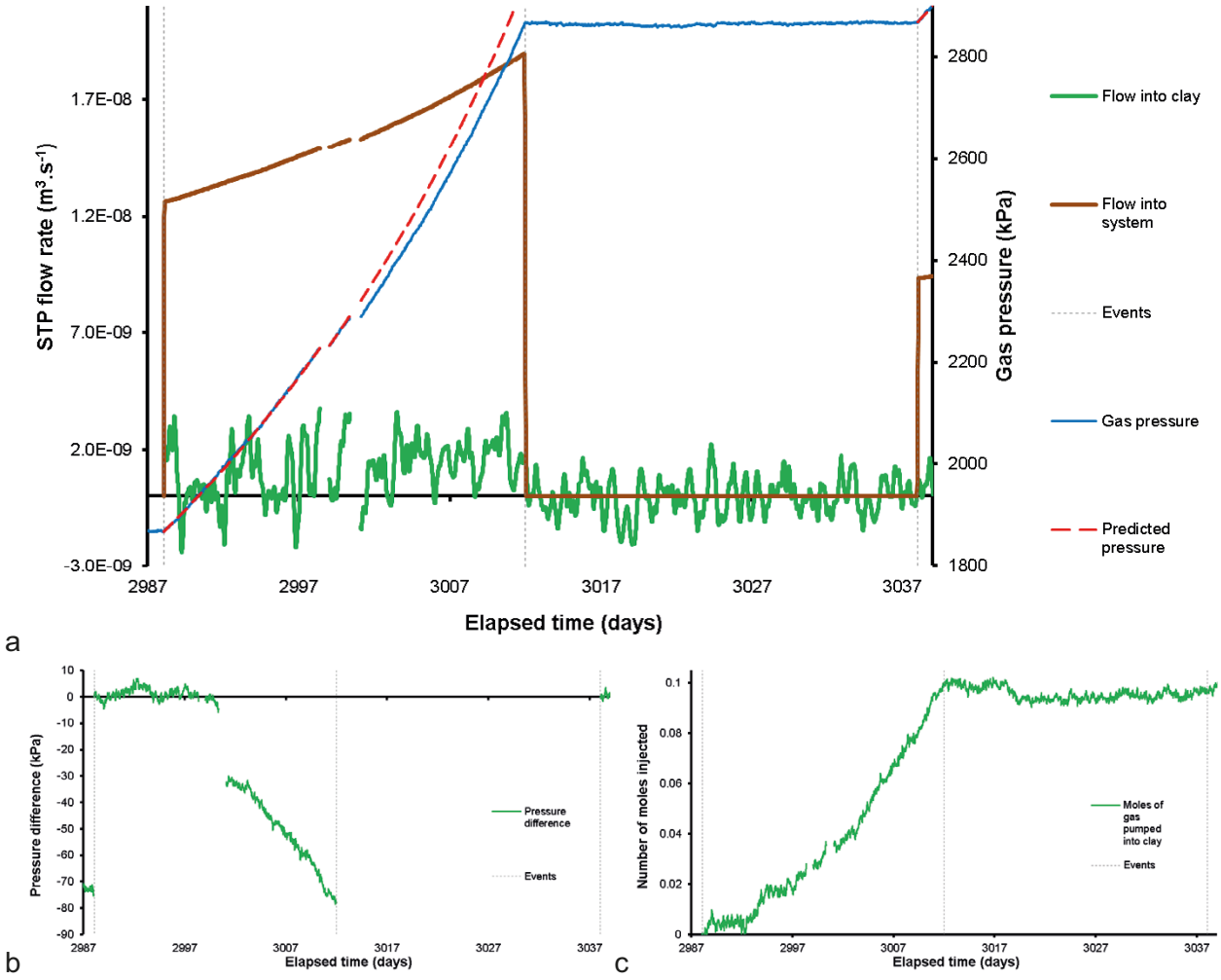

Figure 10-22. *Detail of gas ramp 1 of Gas Injection Test 4. a) Flow of gas into the system and the clay, b) Difference between recorded and predicted pressure, c) Mol pumped into the clay.*

Figure 10-23 shows the detail of the second gas ramp conducted in Gas Injection Test 4. The predicted pressure seen in Figure 10-23a was derived from a revised estimate of the starting volume of gas of 2 570 ml, which as shown in Figure 10-23b gave a very good estimate with negligible difference between the predicted and observed gas pressure. The predicted and observed pressures started to diverge around Day 3051.20, when gas pressure was 3 364 kPa. This had not resulted in a significant increase in flow into the clay. Throughout the period, the STP flow into the clay ranged from 9.3×10^{-9} to 1.24×10^{-8} $m^3 s^{-1}$. This resulted in a small flow into the clay, with 0.12 mol entering the clay (Figure 10-23c). As gas pressure was held constant at around 3 860 kPa, a total of 0.014 mol entered the clay, with an average flow rate of 21.3 µl h^{-1}, representing 538 µmol d^{-1}.

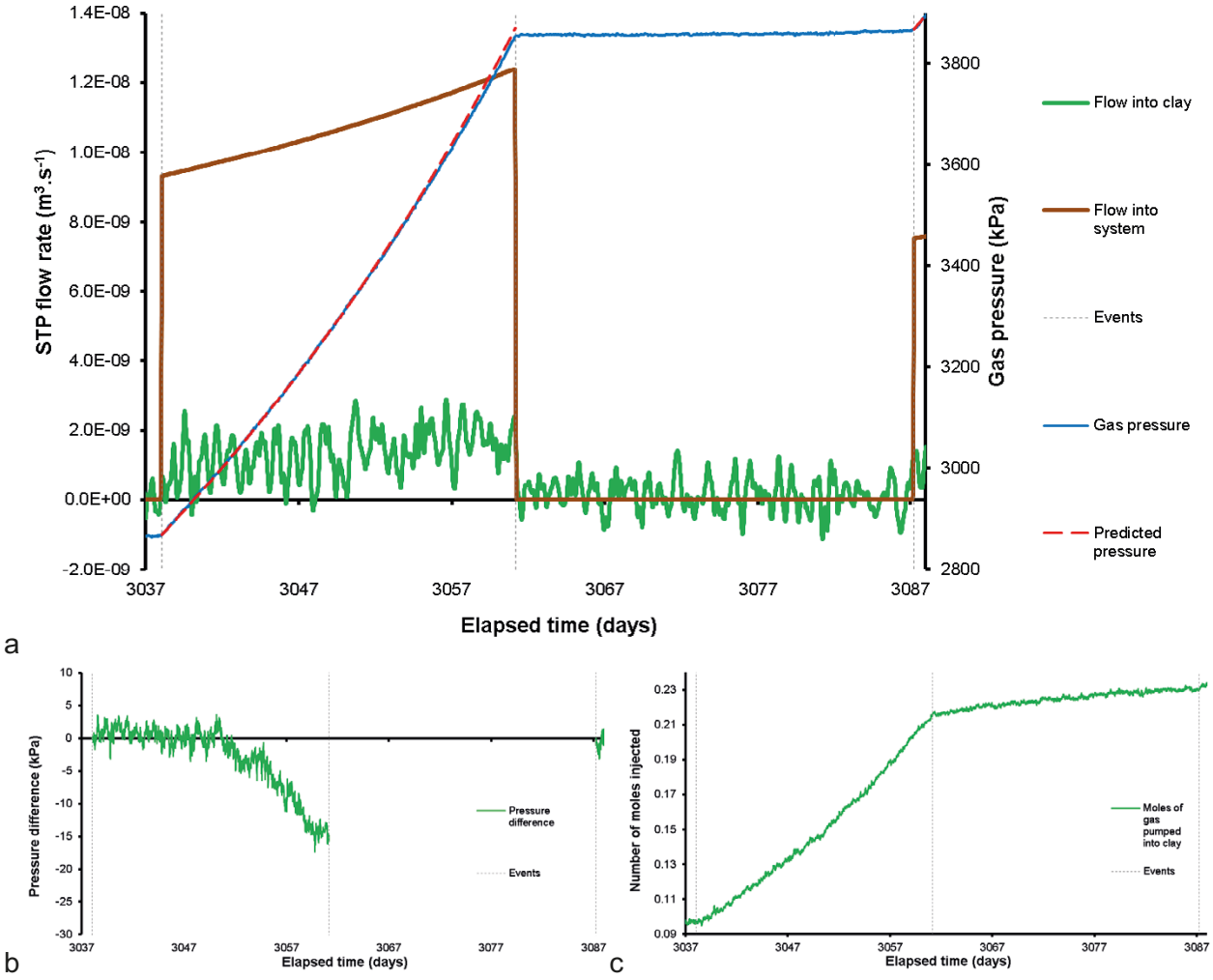

Figure 10-23. *Detail of gas ramp 2 of Gas Injection Test 4. a) Flow of gas into the system and the clay, b) Difference between recorded and predicted pressure, c) Mol pumped into the clay.*

Figure 10-24 shows the detail of the third gas ramp conducted in Gas Injection Test 4. As seen in Figure 10-24a, despite a good correlation between the predicted and observed gas pressures, flow was seen into the clay at a nominal rate of around 1×10^{-9} m^3 s^{-1}. Figure 10-24b shows good agreement between the predicted and observed gas pressures until approximately Day 3095.20 when gas pressure was 4 160 kPa. Throughout the period, the STP flow into the clay ranged from 7.51×10^{-9} to 9.41×10^{-9} m^3 s^{-1}. This resulted in a small flow into the clay, with 0.13 mol entering the clay (Figure 10-24c). As gas pressure was held constant at around 4 853 kPa a flow rate of 13.5 µl h^{-1} was observed, representing 651 µmol d^{-1}. However, it should be noted that pressure was not held perfectly constant and was adjusted at Day 3137.1, with the pump stopped and re-started.

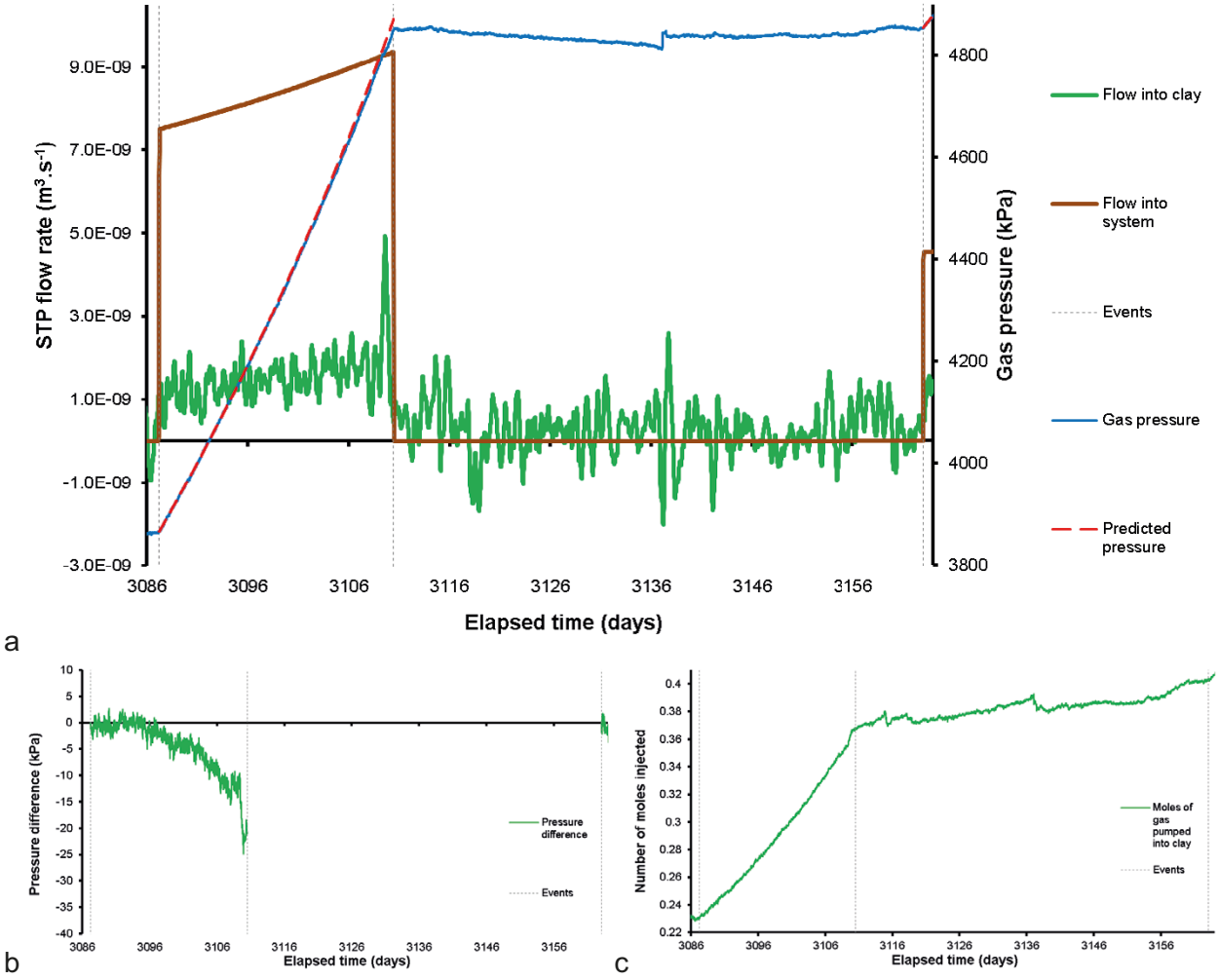

Figure 10-24. *Detail of gas ramp 3 of Gas Injection Test 4. a) Flow of gas into the system and the clay, b) Difference between recorded and predicted pressure, c) Mol pumped into the clay.*

Figure 10-25 shows the variation of gas flow into the clay at STP for the three constant pressure stages. It should be noted that a fourth constant pressure step existed for a limited time prior to the start of the first gas ramp. However, as this was of limited duration after the charging of the interface vessel with gas, the data results were dominated by the transfer of gas into solution within the interface vessel. This gave high apparent flow rates at these times i.e. a flow of 609 µmol per d^{-1} and has not been included.

Figure 10-26 shows the detail of the fourth gas ramp conducted in Gas Injection Test 4 up until the time of accelerated flow into the gas at Day 3203.73. As seen in Figure 10-26a, despite a good correlation between the predicted and observed gas pressures, flow was seen into the clay at a nominal rate of around 1.3×10^{-9} $m^3 s^{-1}$. Figure 10-26b shows good agreement between the predicted and observed gas pressures until approximately Day 3185 when gas pressure was 5 482 kPa. Throughout the period, the STP flow into the clay ranged from 4.52×10^{-9} to 5.71×10^{-9} $m^3 s^{-1}$. This resulted in a small flow into the clay, with 0.21 mol entering the clay (Figure 10-26c). Significant gas entry was seen to begin at Day 3203.73, as seen by an increase in flow rate into the clay (Figure 10-26a), deviation between the predicted and observed gas pressure (Figure 10-26b), and the volume of gas pumped into the clay (Figure 10-26c).

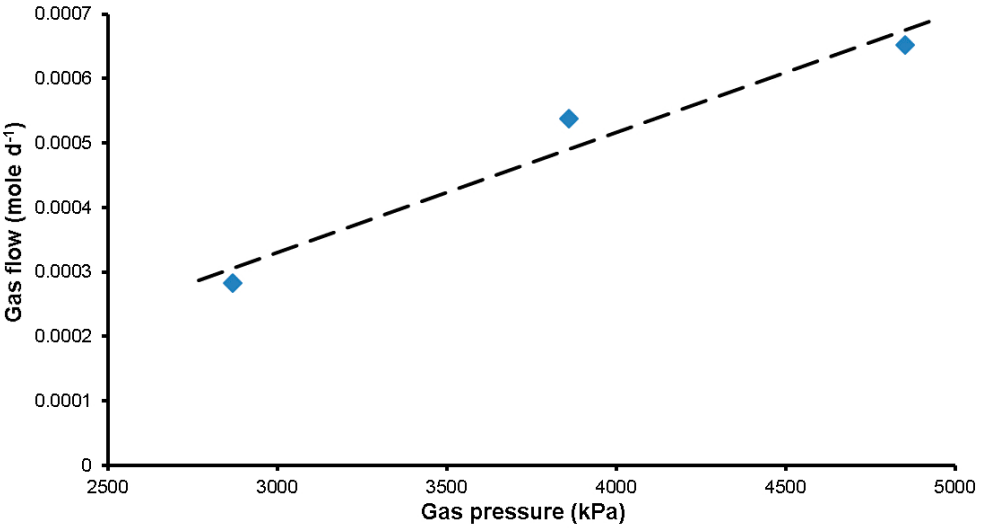

Figure 10-25. *Gas flow rate into the clay at STP at the three constant pressure steps of Gas Injection Test 4.*

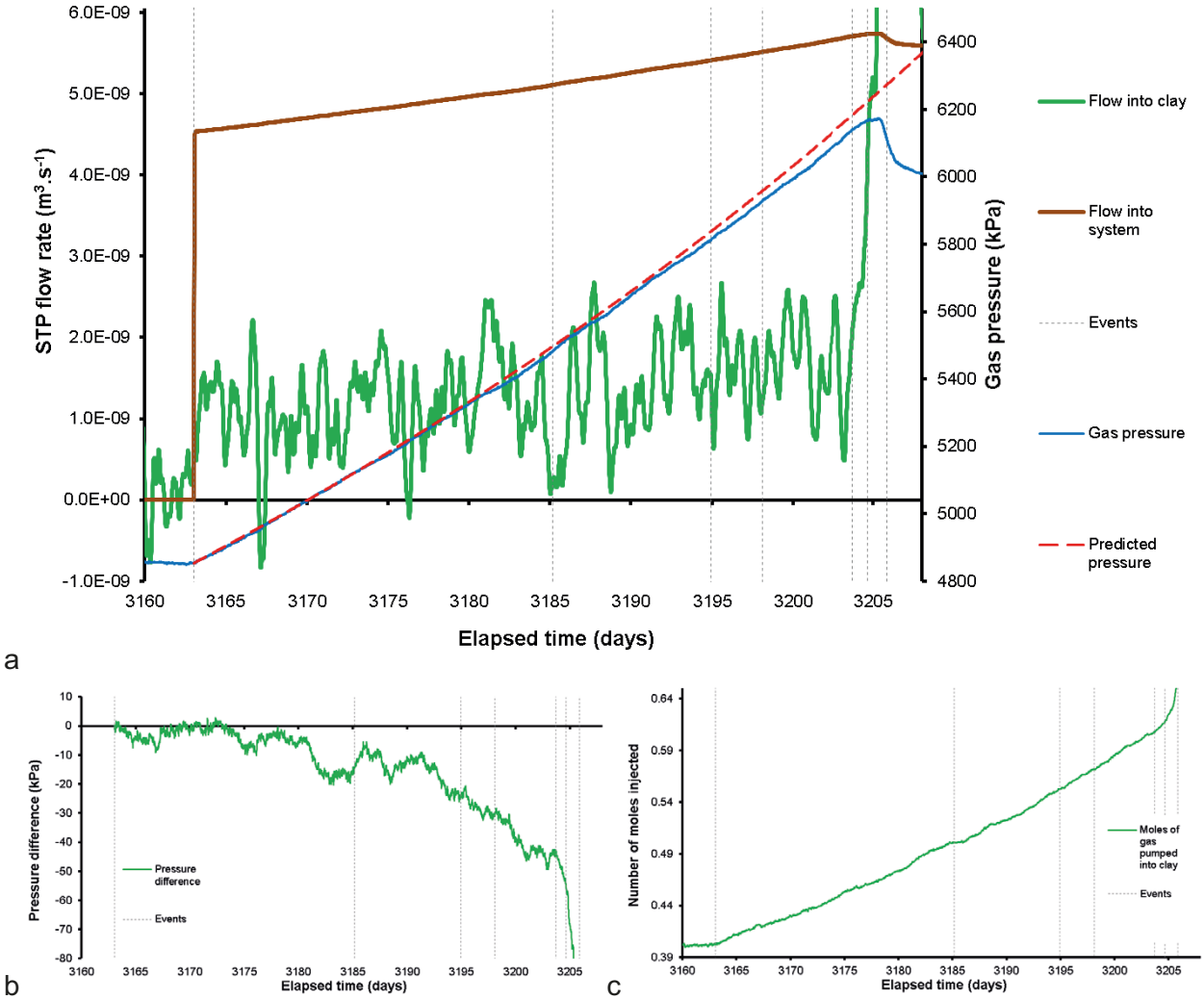

Figure 10-26. *Detail of gas ramp 4 of Gas Injection Test 4 up until the time of clear gas entry. a) Flow of gas into the system and the clay, b) Difference between recorded and predicted pressure, c) Mol pumped into the clay.*

The fourth gas ramp took the test through to peak gas pressure and continued gas injection. Figure 10-27 shows the flow result. As described above, a small flow was seen into the clay until Day 3203.73 with an average of 5.07×10^{-9} m^3 s^{-1}, when flow into the clay began to accelerate. This resulted in a single peak in flow of 3.27×10^{-8} m^3 s^{-1} at Day 3205.72 (note: data shown in Figure 10-27 is time averaged). The peak in flow was short-lived with flow into the clay matching flow into the system within four days. From then afterwards the flow into the clay was slightly greater than the flow into the system, giving a slow reduction in gas pressure. As gas reduction appeared steady, the flow rate of the injection pump was lowered in two steps, approximately halving flow at each step. As before, flow into the clay approximated flow into the system, with slightly higher flow into the clay resulting in the continued reduction in gas pressure. However, in the final stage the flow into the clay reduced, resulting in an increase in gas pressure. Figure 10-28 shows the volume of gas pumped into the clay in mole. It shows that 0.21 mol entered the clay up until peak gas pressure. Following gas entry, a total of 1.13 mol entered the clay.

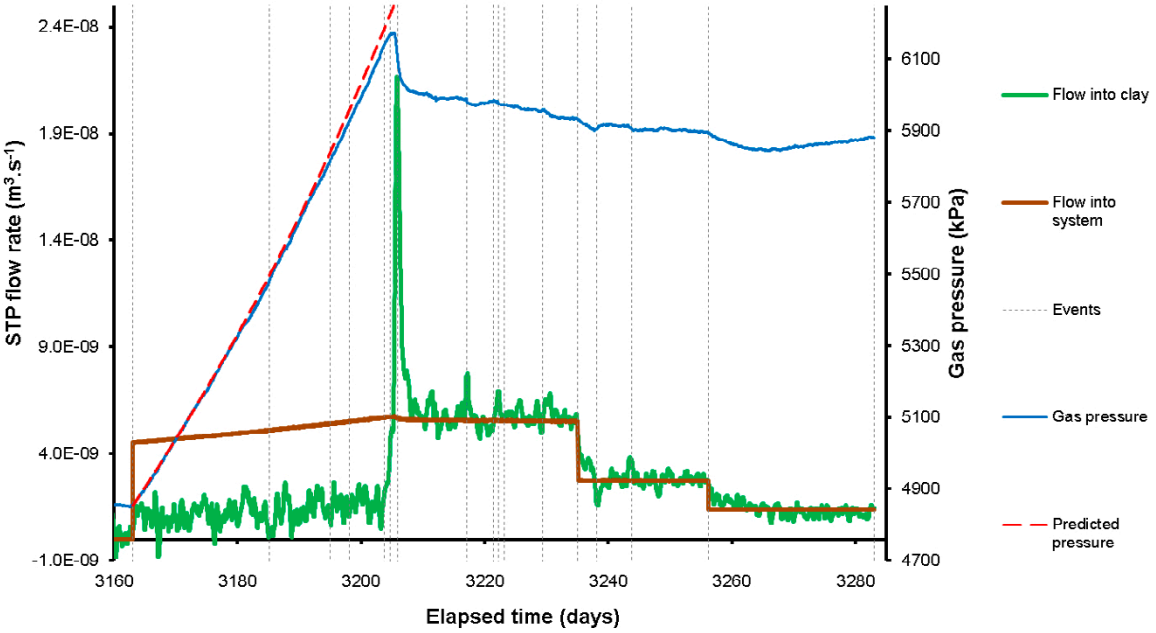

Figure 10-27. *Flow of gas into the system and the clay during the fourth ramp of Gas Injection Test 4.*

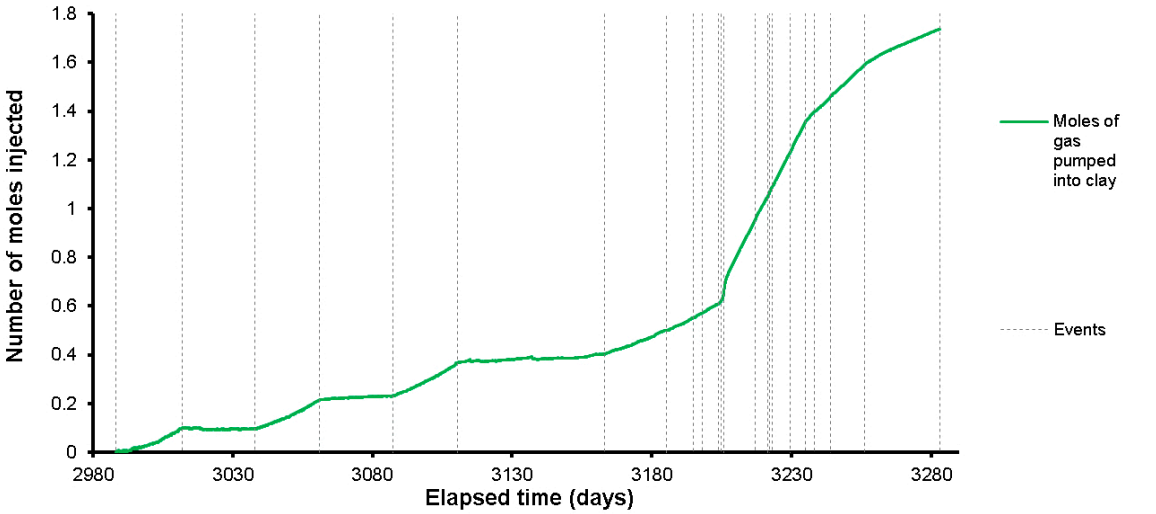

Figure 10-28. *Volume of gas pumped into the clay during Gas Injection Test 4.*

Figure 10-29 shows the flow data in more detail around the time of peak pressure and subsequent gas movement within the buffer at a constant rate of injection. Flow into the clay showed similar behaviour to previous tests. Following the initial peak in flow, the response reduced to approximate the flow into the system. Previous tests had seen a reduction in flow to be lower than the flow into the system, before recovering. This was not seen in this test, with flow into the clay remaining slightly greater than flow into the system, resulting in a reduction in gas pressure. Small variations in flow were seen, suggesting the flow paths forming were complex, with some opening and some closing. However, generally flow was stable and allowed gas pressure to reduce.

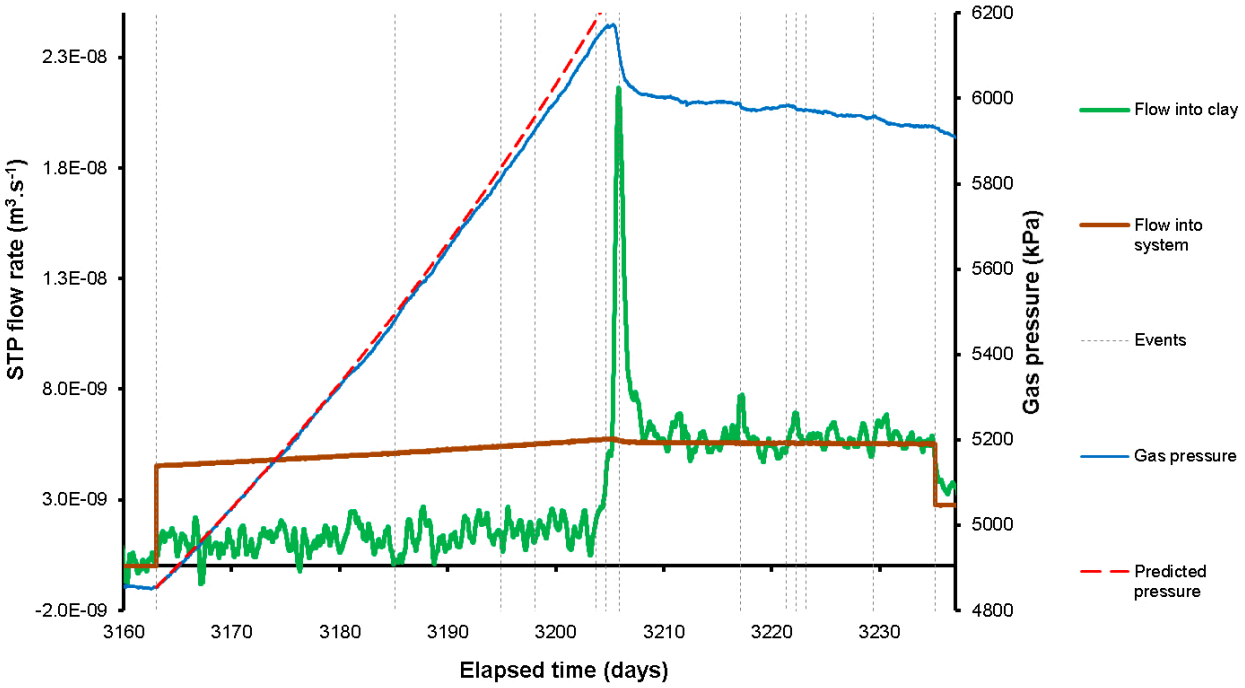

Figure 10-29. *Detail of the flow of gas into the clay and the system around the time of gas entry during Gas Injection Test 4.*

Pore water pressure at the rock wall showed considerable coupling with gas entry (Figure 10-30a, Figure 10-31a). At the time of accelerating flow into the clay at Day 3203.73, a response was seen in UR905 and the start of increase of UR908. The latter locality then increased by around 12 kPa at Day 3204.66. This event corresponded with enhanced flow into the clay. Sensor UR908 later started to increase, with both UR905 and UR908 peaking soon after gas peak pressure at Day 3205.88. Similar response was also seen in UR907. Pore pressure then remained relatively static, until Day 3217.11, when UR908 dropped by ~10 kPa. Of note was a series of three events seen most clearly in UR916 at Days 3221.39, 3222.30, and 3223.20, each ~24 hours apart. These showed small, short lived, reductions in pore pressure of ~4 to 10 kPa. These features were seen in all four sensors shown in Figure 10-31a. This may suggest that gas flow was pulsed. The final event of note in Figure 10-31a showed a decrease in UR919 and disturbances to UR905, UR908, and UR916 at Day 3235.11. Figure 10-30a shows that many sensors showed a number of events for the rest of the stage. UR908 had a second drop in pressure of 10 kPa again at Day 3238.16. Following this the pore pressure at this location was unstable and almost "saw-tooth" in nature.

Radial stress at the rock wall also showed complex behaviour with many events (Figure 10-30b, Figure 10-31b). At Day 3204.67 several sensors started to show an increase, most notably PR907 and PR908. Around Day 3205.88, PR905, PR906, and PR907 increased by 8.6, 28.6, 9.6 kPa respectively, while PR909 reduced by 7.1 kPa. The behaviour of PR908 was more complex. Stress at this point increased from Day 3204.66 onwards and coincident with the changes seen in the other sensors reduced by around 5 kPa, before quickly recovering and a peak in stress seen around 15 kPa higher than the starting magnitude. Sensor PR908 continued to show a series of features that may suggest pulsed gas flow. At Day 3217.11 stress increased in PR908 and PR905 by 6 kPa and 3 kPa respectively. It could be suggested that prior to Day 3217.11 pulsed flow was seen in PR908 and this transferred to PR905 at this time. A second stepped decrease of around 3 kPa occurred at this time in PR909. As seen in the pore pressure data, three events were seen at Days 3221.39, 3222.30, and 3223.20, most clearly seen in PR909. Further events were seen in PR917, PR909, and PR906, but these are not discussed in detail.

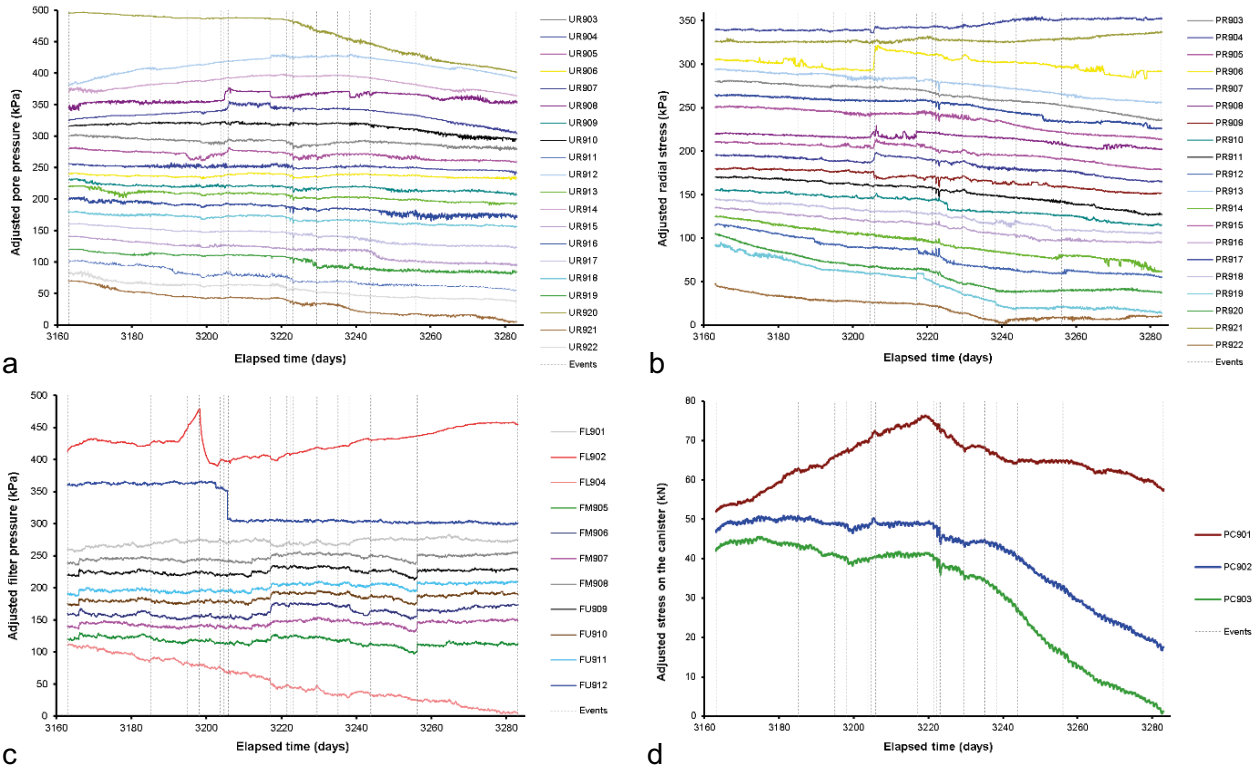

Figure 10-30. *Example of sensor response around the time of gas entry during Gas Injection Test 4. All parameters have been transposed about the y-axis to emphasise the detail observed. a) Pore pressure at the deposition wall; b) Radial stress on the deposition wall; c) canister filter pressure; d) stress on the canister surface.*

Figure 10-30c shows the canister filter pressures around the time of gas entry. Filter FL902, which was 90° around the canister surface from the injector, showed a complex behaviour. Around the time of gas entry, filter FU912 showed a small decrease in pressure, with a larger 49 kPa drop occurring at Day 3205.88. Of note are a number of events that show disturbance in most of the filters, even though these changes were small. These include Days 3217.11, 3238.15, and 3256.19. The latter corresponds with the second reduction in flow rate of the test.

The final dataset highlighted in Figure 10-30d is the radial and axial stress sensors on the canister surface. These showed an increase in PC901 and PC902 at the time of peak gas pressure and the same three events noted above at Days 3221.39, 3222.30, and 3223.20. Stress at PC901 was seen to increase until around Day 3220, when it began to decrease. Soon after, PC902 and PC903 also started to decrease. This suggests that PC901 indicated when gas exitted from the deposition hole.

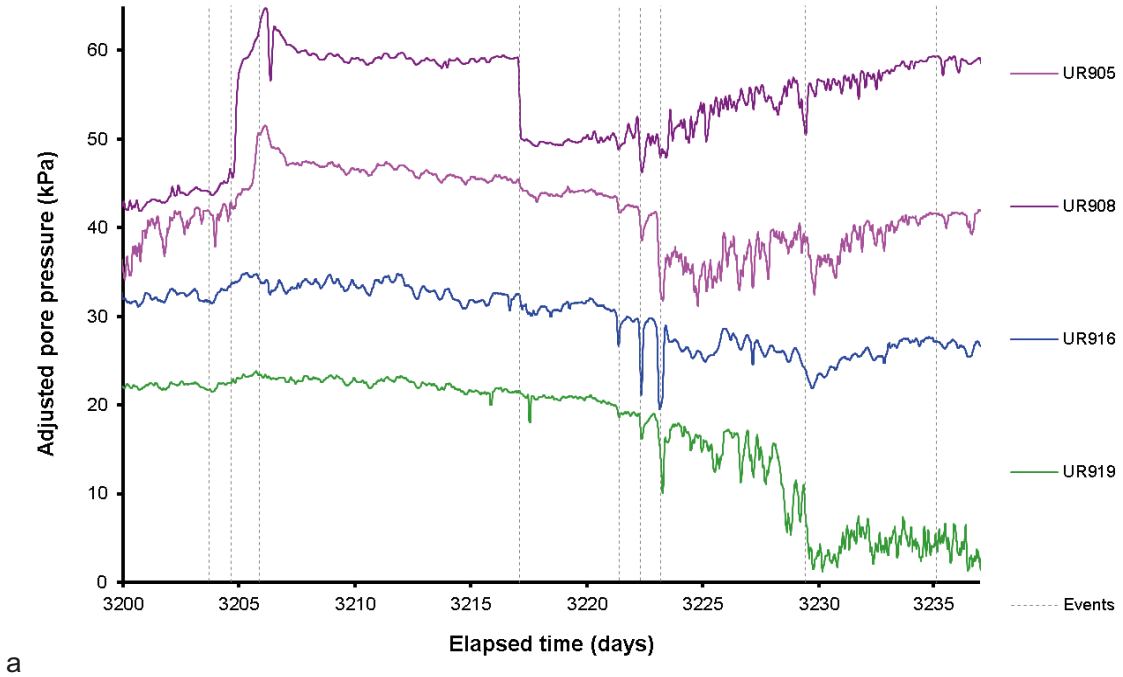

a

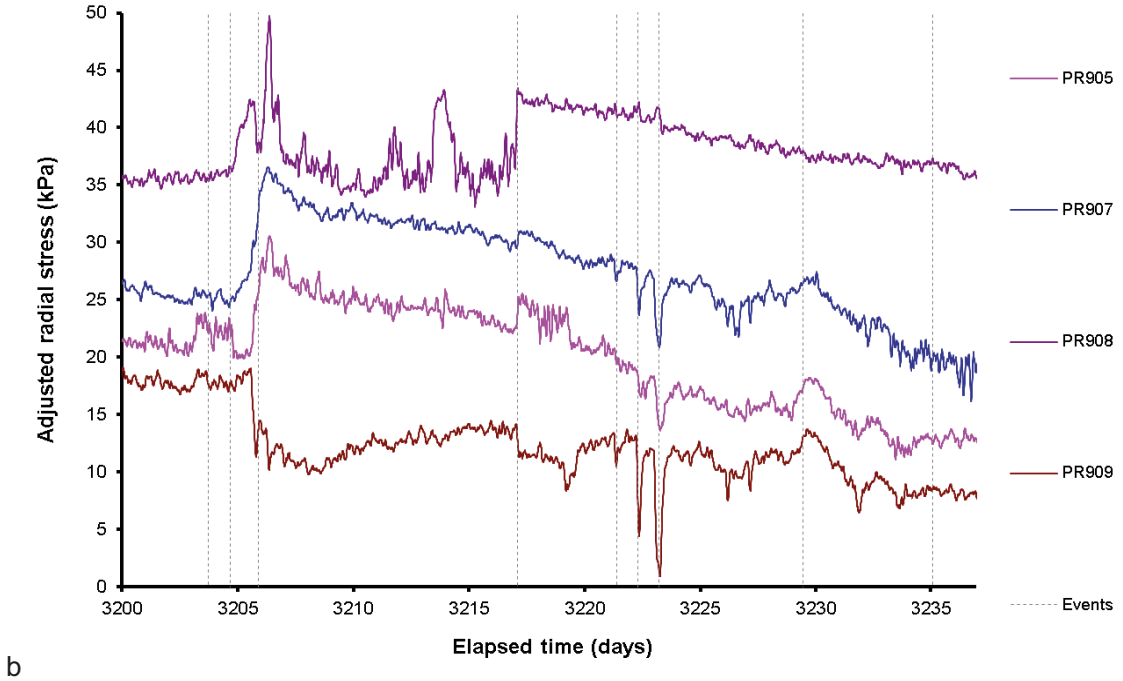

b

Figure 10-31. *Detail of radial stress and pore fluid pressure at the rock wall around the time of gas entry. a) Pore pressure at the deposition wall; b) Radial stress on the deposition wall.*

Figure 10-32 shows the pore pressure at the deposition hole wall and how this varied during Gas Injection Test 4. Figure 10-32a illustrates the distribution of pore pressure at the deposition hole wall just prior to peak gas pressure at Day 3204.67. This shows that the gas injection filter, highlighted in red, was 90° from a region of high pore pressure at 270°. Generally, pore pressure increased from the top of the deposition downwards, with also higher pressure seen at around 270°. Figure 10-32b shows the variation in pore pressure at Day 3206.07. The noted high in pore pressure at 270° decreased, while a new high formed at 90°; both features 90 ° around the canister from the injection filter. By Day 3206.40 (Figure 10-32c) the high in pore pressure had slightly decayed but shows evidence of migrating up the deposition hole. By Day 3216.44 (Figure 10-32d) as well as the high-pressure region, a low-pressure region started to develop higher in the deposition hole at around 350 cm height. This developed further by Day 3217.94 and migrated upwards, as did the high-pressure region. The final plot of pore pressure is shown at Day 3236 at a time after gas peak pressure. Pore pressure increased from the midplane downwards, with pressure above this level being reduced. The high-pressure region at an orientation of 90° had now established. This feature showed a transient form over the timeframe shown and appeared to migrate.

The distribution of radial stress on the deposition hole wall is shown in Figure 10-33. The distribution of stress prior to peak gas pressure is shown in Figure 10-33a at Day 3204.67. This shows that near the gas injection filter radial stress was generally higher than average, with the lower array of filters within a horizontal zone of elevated stress. A second zone of elevated stress was also seen at an orientation of around 310° along the full height of the sensor array. At Day 3206.07 (Figure 10-33b), soon after the first evidence of gas entry, a low stress region formed clockwise of FL903, with stress increasing below the level of the injector. A moderate increase in stress occurred anti-clockwise of FL903. By Day 3206.40 (Figure 10-33c), the two high and one low stress regions continued to develop, with little change above the mid-plane of the canister. Figure 10-33d shows that the distribution of stress had changed by Day 3216.44. The high stress region anti-clockwise of the injector had started to subside, while the stress opposite the injector had decreased. The low pression region clockwise of the injector had migrated further clockwise and up the deposition hole. By Day 3217.94 (Figure 10-33e) further regions of reduced stress formed. Figure 10-33f shows the change in stress at Day 3236 much after peak gas pressure. This shows that the stress at the deposition hole had reduced, while the stress in the base of the deposition hole had increased. Figure 10-33 shows that the changes in radial stress during the limited time period were complex and transient. It implies high and low stress zones had migrated during gas entry, with stress increasing in the base of the deposition hole, suggesting gas had moved downwards during Gas Injection Test 4.

Comparing the observations of pore pressure and radial stress during the time of gas entry shows many similarities and several differences (Figure 10-34). At Day 3206.40 (Figure 10-34a) there was correspondence in changes in pore pressure and radial stress. A low pressure/stress region formed at an orientation of approximately 270° at a similar height as the injection filter, with a high pressure/stress region forming at 65°. At the base of the sensor array, a high press/stress region formed at 290°, with a low at around 180°. This shows correlation soon after gas entry. Differences started to form by Day 3217.94 (Figure 10-34b). At an orientation of approximately 135°, the high stress region remained static, while the pore pressure high moved higher in the deposition hole. Above this high, a low pore-pressure region formed, corresponding with a high in radial stress. The low pressure/stress region at 270° remained static in pore pressure, but a high region formed above at a height of around 300 cm. In radial stress, the low stress region broadened and may include a second low region. At Day 3236.00 (Figure 10-34c) after the initial disturbance created by gas entry, pore pressure and radial stress show considerable differences. The region of raised pore pressure formed at 90° had broadened in height, with radial stress showing little variation. At this orientation, radial stress had increased at the bottom of the sensor array. In both pore pressure and stress, a low region formed at the top of the sensor array. Stress data showed an increase downwards in time from the injection filter, while pore pressure suggests an increase at 90°, with movement upwards from the level of the injection filter.

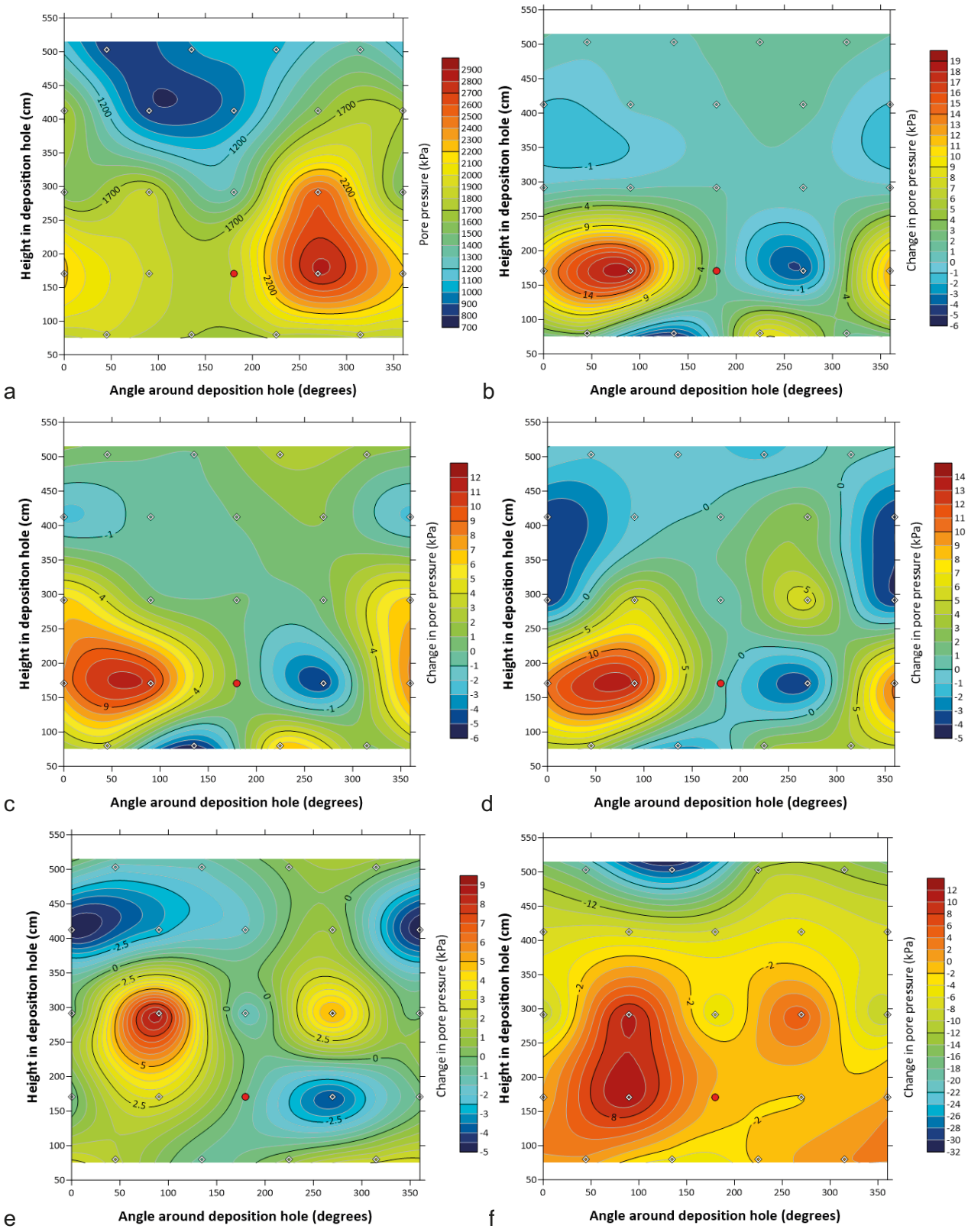

Figure 10-32. *Distribution of pore pressure at the deposition hole wall at times around gas entry during Gas Injection Test 4. a) Day 3204.67 (total pore pressure); b) Day 3206.07 (change in pore pressure); c) Day 3206.40 (change in pore pressure); d) Day 3216.44 (change in pore pressure); e) Day 3217.94 (change in pore pressure); f) Day 3236.00 (change in pore pressure).* ***Note:*** *the location of the injection filter is shown as a red circle.*

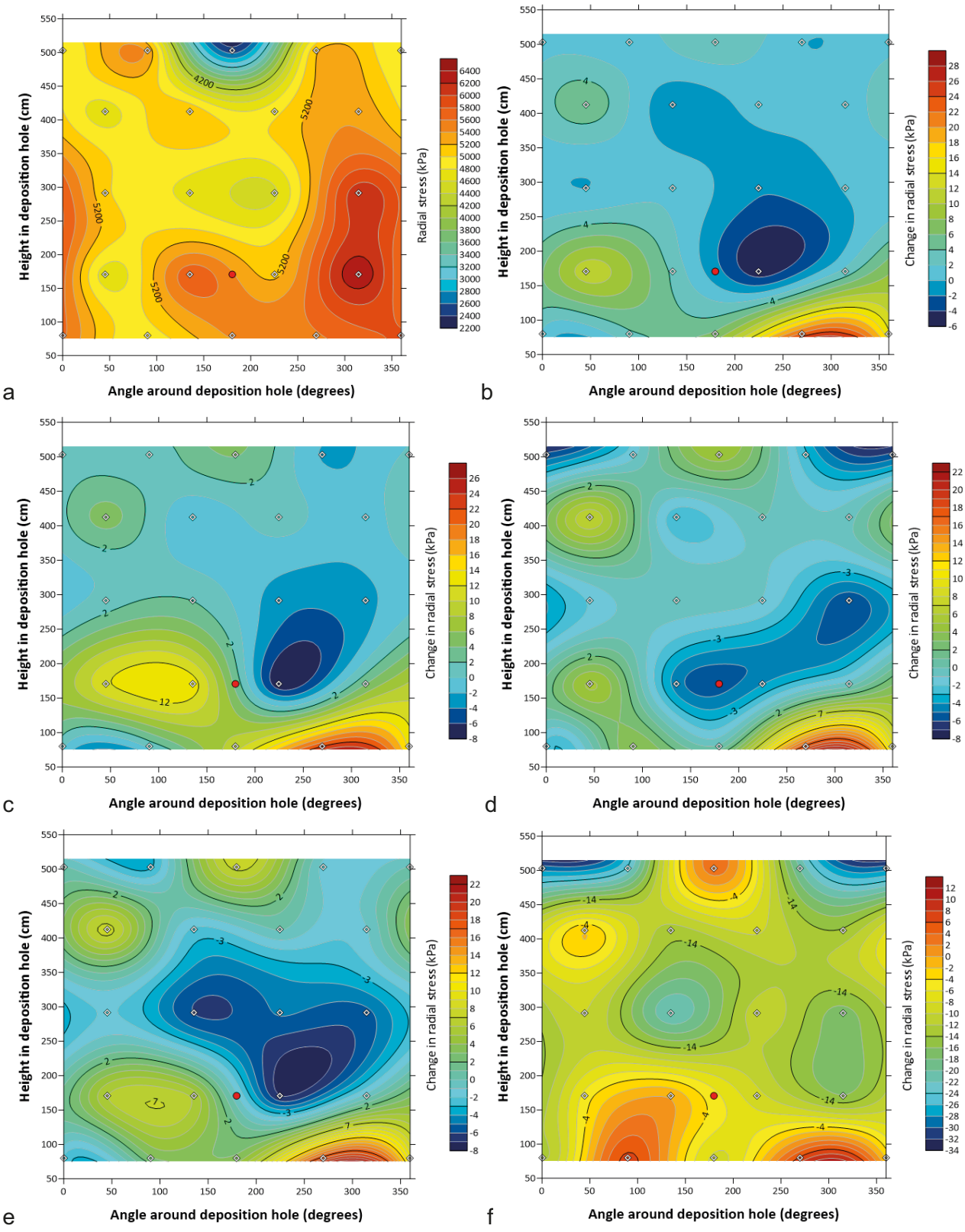

Figure 10-33. *Distribution of radial stress at the deposition hole wall at times around gas entry during Gas Injection Test 4. a) Day 3204.67 (total stress); b) Day 3206.07 (change in stress); c) Day 3206.40 (change in stress); d) Day 3216.44 (change in stress); e) Day 3217.94 (change in stress); f) Day 3236.00 (change in stress).* ***Note:*** *the location of the injection filter is shown as a red circle.*

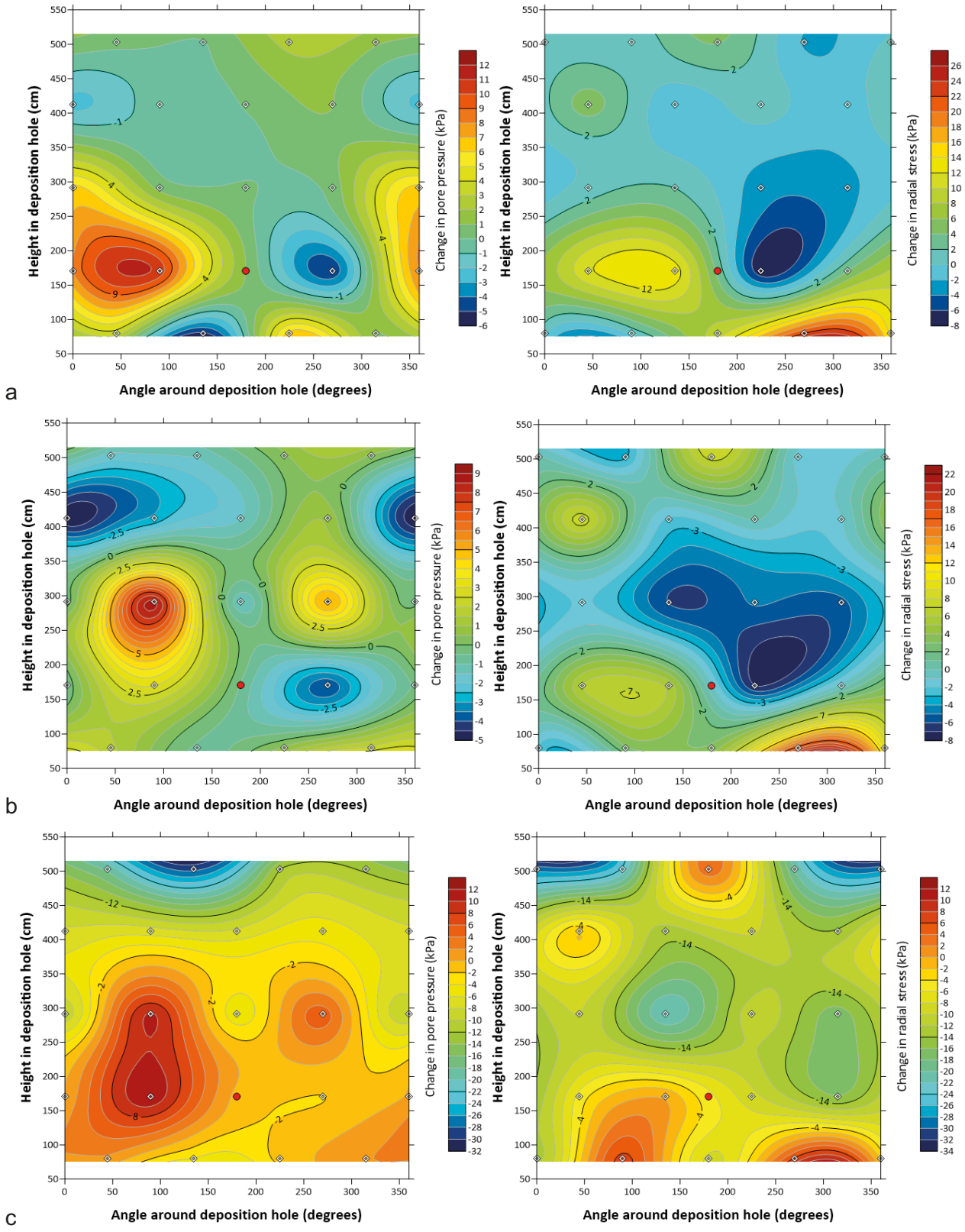

Figure 10-34. *Comparison of changes in pore pressure and radial stress at the deposition hole wall at times around gas entry during Gas Injection Test 4. a) Day 3206.40; b) Day 3217.94; c) Day 3236.00.* ***Note:*** *the location of the injection filter is shown as a red circle.*

Figure 10-35 shows sensor locations that may show direct movement of gas. The only locality identified was filter FL902, 90° around the canister from the injection filter. This showed a saw-tooth behaviour, with pressure increasing at a relatively constant rate until a threshold, which created a peak in pressure and then a sharp decrease in pressure. This has a form similar to fault-valve behaviour, which is used to explain the temporal transmission of fluid along a geological fault. As pressure increases it reaches a magnitude where the fluid on a fault becomes transmitted along the fault, lower pressure at the injector. Therefore, the pressure response seen in FL902 suggests episodic flow. However, the first peak seen began before the first gas ramp started but after gas was added to filter FL903. Examining the data prior to the gas test showed that the pressure in FL902 was reduced at the time of adding gas to the lower array of filters and FL901–904 were no longer artificially hydrated. Prior to this, FL902 showed similar behaviour but with much reduced amplitude, suggesting that the observed behaviour had been long established and was not associated with the gas test in filter FL903. The feature observed may be associated with continued gas movement from Gas Injection Test 3. Figure 10-36 shows a possible interpretation of the direction of gas movement during Gas Test 4 suggesting that a similar response to Gas Test 1 occurred.

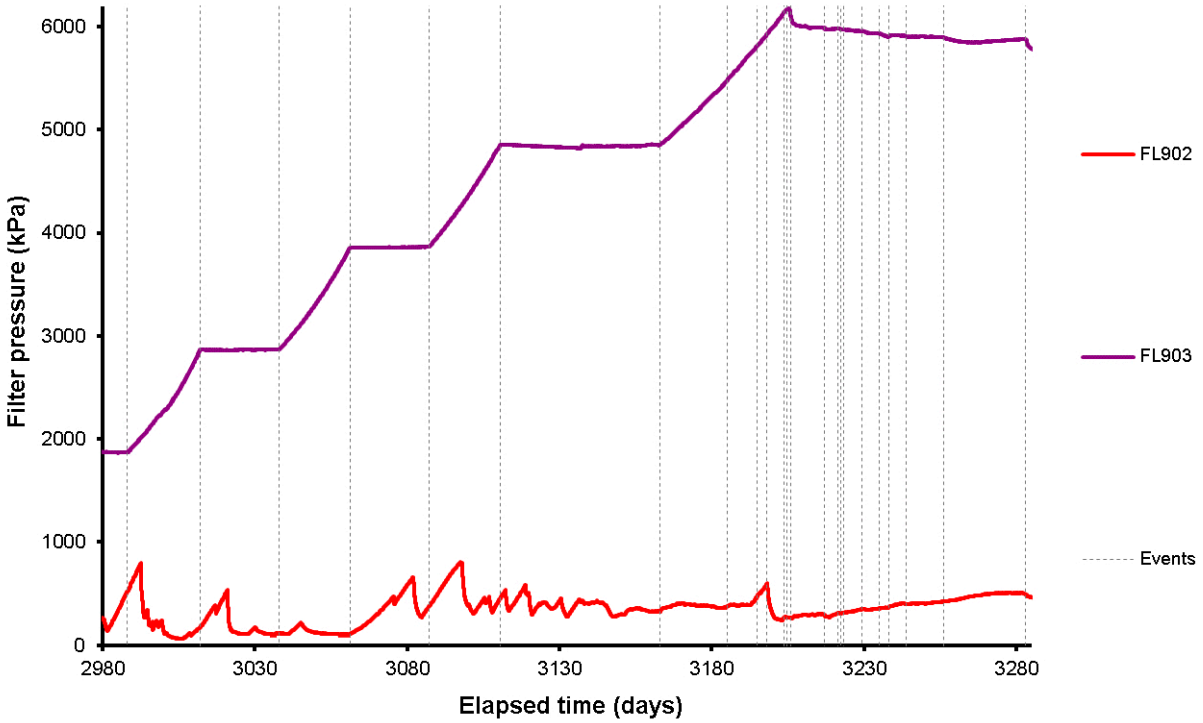

Figure 10-35. *Detail of sensors that show evidence of gas pressurisation during Gas Injection Test 4.*

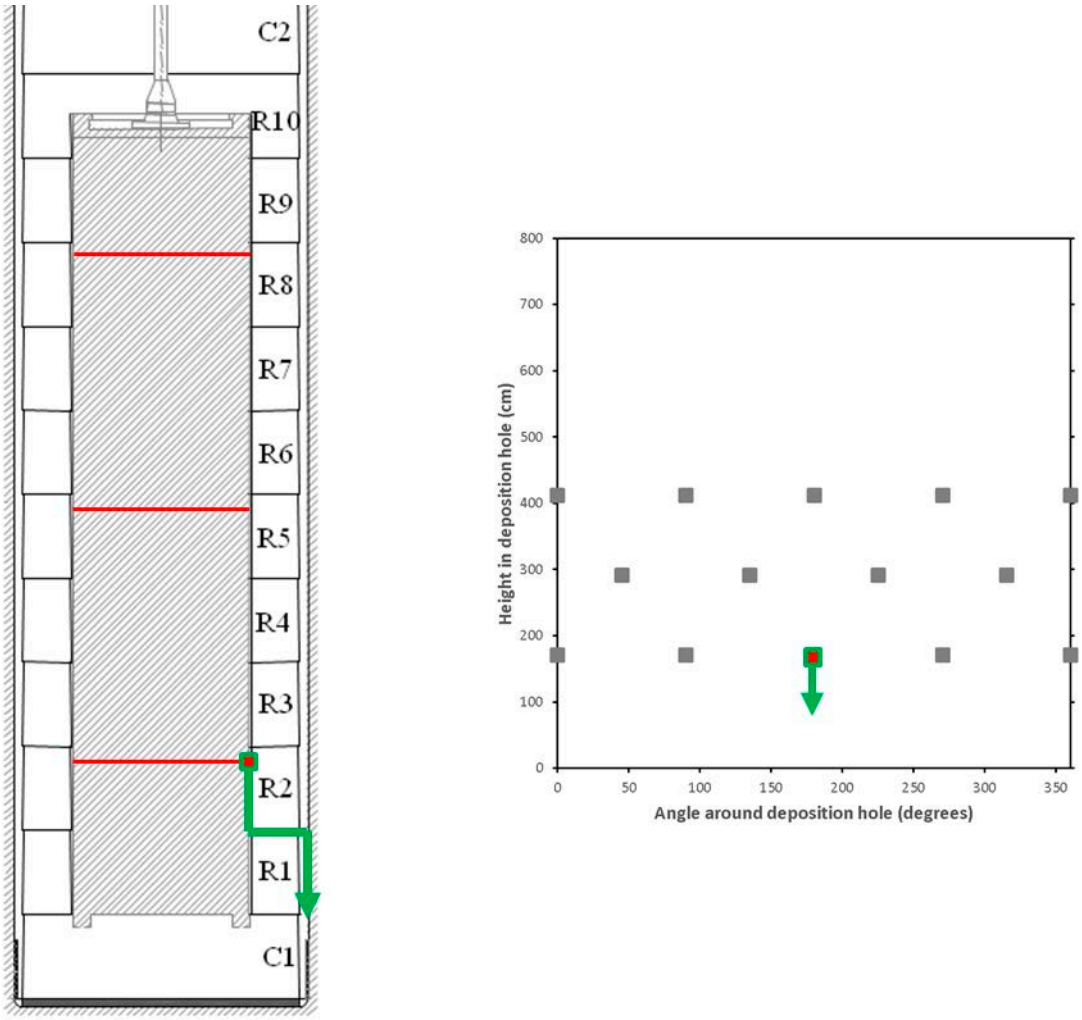

Figure 10-36. *Schematic of the direction of gas flow during Gas Test 4 in lower filter FL903.*

10.4 Summary of Gas Injection Test 4

Gas Injection Test 4 was conducted in filter FL903 on the lower array of filters on the canister surface. It was the third test using FL903. Gas pressure was raised from background levels up to gas peak pressure using four distinct pressure ramps, being held at constant pressure in between.

1) The first pressure ramp started at Day 2988.07 using a constant injection rate of 2.45 ml h^{-1}. This raised pressure from 1 868 to 2 867 kPa in 23.9 days when pressure was held constant from Day 3011.99 for 26.0 days. Throughout the period, the STP flow into the clay ranged from 1.25×10^{-8} to 1.48×10^{-8} m^3 s^{-1}. This resulted in a small flow into the clay, with 0.1 mol entering the clay. As gas pressure was held constant at around 2 867 kPa, a small amount of gas entered the clay, following which a flow rate of 282 µmol d^{-1} was observed.

2) The second pressure ramp was started at Day 3038.04 using a constant injection rate of 1.2 ml h^{-1}. This raised pressure from 2 868 to 3 856 kPa in 23.1 days, when pressure was held constant from Day 3061.17 for 26.1 days. STP flow into the clay ranged from 9.3×10^{-9} to 1.24×10^{-8} m^3 s^{-1}, resulting in a small flow into the buffer, with 0.12 mol entering the clay. As gas pressure was held constant at around 3 860 kPa, a total of 0.014 mol entered the clay, with an average flow rate of 538 µmol d^{-1}.

3) The third pressure ramp was started at Day 3087.24 using a constant injection rate of 0.725 ml h^{-1}. This raised pressure from 3 867 to 4 852 kPa in 23.2 days, when pressure was held constant from Day 3110.48 for 52.6 days. STP flow into the clay ranged from 7.51×10^{-9} to 9.41×10^{-9} m^3 s^{-1}, resulting in a small flow into the clay, with 0.13 mol entering the clay. As gas pressure was held constant at around 4 853 kPa a total of 0.034 mol entered the clay, with an average flow rate of 651 µmol d^{-1}.

4) The fourth, and final, pressure ramp was started at Day 3163.04 using a constant injection rate 0.35 ml h^{-1}. This raised pressure from 4 854.01 to a gas peak pressure of 6 174 kPa at Day 3205.31 in 42 days, following which injection continued for a further 78 days. Up until gas entry, STP flow into the clay ranged from 4.52×10^{-9} to 5.71×10^{-9} m^3 s^{-1}, resulting in a small flow into the clay, with 0.21 mol entering the clay.

Major gas entry and peak pressure occurred during gas ramp 4.

1) Day 3203.73: The first evidence of gas entry when flow into the clay began to increase, with a response seen in UR905 and the start of increase of UR908. This occurred at a gas pressure of 6 141 kPa.

2) Day 3204.66: Pore pressure at UR908 showed a stepped increase of around 12 kPa. Radial stress at PR907 and PR908 started to increase, as did flow into the clay.

3) Day 3205.31: Peak gas pressure occurred at a pressure of 6 174 kPa. At Day 3205.88, pore pressure at UR905, UR907, and UR908 peaked. The high region of pore pressure at an orientation of 270° decreased at this time, while a new high formed at 90°. By Day 3206.40 the high in pore pressure had slightly decayed, but shows evidence of migrating up the deposition hole. Radial stress at PR905, PR906, and PR907 increased by 8.6, 28.6, and 9.6 kPa respectively, while PR909 decreased by 7.1 kPa. Stress at PR908 increased from Day 3204.66 onwards and coincident with the changes seen in the other sensors reduced by ~5 kPa, before quickly recovering with a peak in stress ~15 kPa higher than the starting magnitude. The distribution of radial stress showed a low stress region formed clockwise of FL903, with stress increasing below the level of the injector. A moderate increase in stress occurred anti-clockwise of FL903. Canister filter FU912 on the upper array of filters showed a drop of 49 kPa at this event, while canister stress sensors PC901 and PC902 showed an increased. Gas peak pressure resulted in a single peak in flow of 3.27×10^{-8} m^3 s^{-1} at Day 3205.72. The peak in flow was short-lived with flow into the clay matching flow into the system within four days. From then onwards the flow into the clay was slightly greater than the flow into the system, giving a slow reduction in gas pressure.

4) Day 3216.44: A low-pore-pressure region started to develop higher in the deposition hole than the injection filter at around 350 cm height. Radial stress had also developed with the high stress region anti-clockwise of the injector subsiding, while the stress opposite the injector had decreased. The low pressure region clockwise of the injector had migrated further clockwise and up the deposition hole.

5) Day 3217.11: Pore pressure at UR908 reduced by nearly 10 kPa. Radial stress increased in PR908 and PR905 by 6 and 3 kPa respectively. It could be suggested that prior to Day 3217.11 pulsed flow was seen in PR908 and this transferred to PR905 at this time. A second stepped decrease of around 3 kPa occurred at this time in PR909.

6) Days 3221.39, 3222.3, and 3223.2: A mini-series of events occurred each approximately 24 hours apart. Small, short lived, reductions in pore pressure, radial stress and PC901 and PC902 were seen.

7) Day 3235.11: A decrease was seen in pore pressure at UR919, with disturbances in UR905, UR908, and UR916. The map of pore pressure change showed an increase from the midplane downwards, with pressure above reduced. The high-pressure region 90° had now established. Stress change within the deposition hole had generally reduced, while the stress in the base of the deposition hole had increased.

8) Day 3238.16: A10 kPa step reduction in UR908 followed by irregular pore pressure.

The flow rate of the injection pump was lowered in two steps, approximately halving flow at each step. Flow into the clay approximated flow into the system, with slightly higher flow into the clay resulting in the continued reduction in gas pressure. In the final stage the flow into the clay reduced, resulting in an increase in gas pressure. Prior to gas peak pressure, 0.21 mol entered the clay, with a total of 1.13 mol entered the clay following gas entry. It has been interpreted that the direction of gas movement during Gas Test 4 was similar response to that seen in Gas Test 1 with gas moving along the interface between the canister and the buffer before finding a way out of the deposition hole between bentonite blocks.

11 Hydration Stage 3 (Day 3283 – 5138)

The seventh significant stage of the Lasgit experiment started on Day 3283.06 (28th January 2014) and was completed at Day 5138.09 (26th February 2019); a total stage duration of 1 855.03 days (i.e. approximately five years).

Following Gas Injection Test 4, Lasgit entered a prolonged period of hiatus, from day 3283 onwards to Day 5138, and this represented the third hydration stage. During this period the system was monitored but did not include any gas injection. This allowed the system to recover from the previous gas testing, providing time for gas to dissipate. It also allowed stresses and pressures to continue to reach a plateau and thus establish different boundary conditions for any further gas injection testing. Figure 11-1 shows the outcome of the test period. At the start of the stage it was planned that artificial hydration would continue throughout the test period. However, issues were encountered with the compressor, the air actuated valve system, and the logging PC throughout. This meant that artificial hydration was abandoned at Day 3751.98, with a short resumption between Day 4262.33 and Day 4340.11. It should be noted that Day 4340.11 was the final time that any artificial hydration occurred through the filter mats within the bentonite and the rock wall.

It should be noted that the results for the period were dominated by two events, as shown in Figure 11-1. The first occurred between Day 3758.21 and Day 3922.37; a total of 164.16 days. This was caused by the failure of the Geokon logging equipment and affected the UB, UR, PR, and PB sensors. The second, more serious event, occurred between Day 4626.02 and Day 4906.03; a total of 280.01 days. This was caused by the total failure of the logging PC. The new PC hardware was not compatible with the previous National Instrument FieldPoint system, necessitating the upgrade of the data logger system to National Instruments cRio and the implementation of new bespoke logging software.

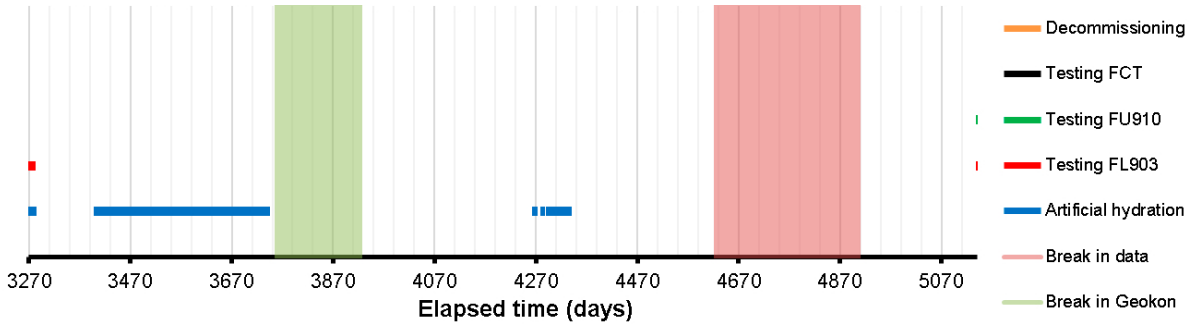

Figure 11-1. *Test stages of the Lasgit experiment showing what was conducted during Natural Hydration Stage 3.*

11.1 Description of the field parameters during the period

In this section the field parameters will be described (boundary conditions). **Note:** The grey areas displayed in the graphs show periods when artificial hydration was not occurring.

Figure 11-2 shows the pore fluid pressure of the filter mats. As with previous stages, filter FR901 was not artificially hydrated and recorded local pore pressure. As seen, FR901 slowly decayed during the period, indicative of drawdown of the pore pressure as a result of proximity to the drained tunnels of the Äspö Hard Rock Laboratory. The remaining filters were all artificially hydrated at various times during the Hydration Stage 3. The start of the stage showed shut-in of the filter mats up to Day 3360.18. As can be seen, FR902 showed the typical decay curve which did not reach a steady asymptote. It is likely that the filter would have decayed to almost atmospheric pressure. Filters FB903 and FB904 mirrored one another and showed a more unusual decay profile. Initially FR902, FB903, and FB904 mirrored one another, until around Day 3335 when FB903 and FB904 were close to reaching asymptote. Pressure then started to decrease again, but this time with a "convex" shape as opposed to the expected "concave" response. This response mirrored the annual variation seen in pore pressure at the rock wall (Figure 11-5) for the corresponding level and showed that the filter mats within the bentonite were sensitive to the boundary condition creating annual variation.

Artificial hydration within the filter mats was re-established on Day 3360, with a period of artificial hydration at the nominal pressure of 2 500 kPa. The pressure in the filter mats can be seen to deviate from constant pressure up until the calibration of the system on Day 3640, as highlighted as an event in Figure 11-2. The variation correlates with the temperature variation seen in the Lasgit laboratory (Figure 11-12). The temperature compensation of the ISCO syringe pumps was not perfect and tended to under-compensate for temperature changes. Following the calibration visit the pressure in the filter mats was more consistent.

Artificial hydration of the filter mats was terminated on Day 3745. The pressure within the three filter mats that had undergone artificial hydration was reduced. This was most marked in FR902 with pressure reduced to below 100 kPa and retained at this pressure. Pore pressure in FB903 and FB904 was reduced by 500 kPa and all three filter mats were left to equilibrate. Pressure in FR902 on the rock wall slowly increased over the next 500 days and almost doubled in pressure. Filter mats FB903 and FB904 reduced in a near linear manner for approximately 360 days until Day 4115. At this time pressure within these filter mats within the bentonite above the canister started to increase, peaking 200 kPa higher than at Day 4115. This increase corresponds with pore water pressure increases at the rock wall, in particular filter UR920. Therefore, this feature was related to annual variation and again showed that the FB filter mats are sensitive to the phenomena driving the annual signal.

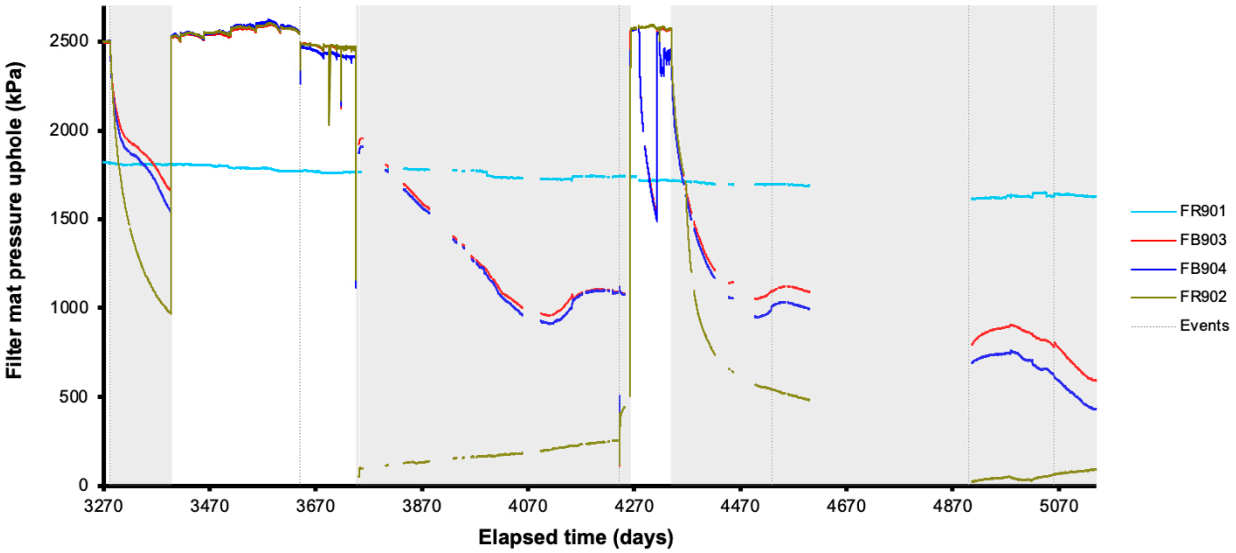

Figure 11-2. *Evolution of water pressure in the filter mats located on the borehole wall and within the bentonite blocks.*

Artificial hydration was re-established at Day 4262. However, issues were encountered. For the first 17 days filters FR902, FB903, and FB903 were artificially hydrated at a nominal pressure of 2 500 kPa. Issues were encountered with the air actuated valves within the laboratory that resulted in filters FB903 and FB904 not being hydrated and entering shut-in. This started at Day 4279.32, resulting in a loss of filter mat pressure. Hydration of these filter mats was re-established at Day 4313.12 some 34 days later. However, issues were still apparent in FB904, which did not achieve as high a pressure as FB903 and FR902. After five days, at Day 4318.03, FB904 entered shut-in again. The logging system crashed and when it came back online the air actuated valve operating FB904 did not actuate fully. For the following 22 days FB904 showed an erratic response as the valve was partially opening and closing depending on the pressure generated by the air compressor. On Day 4340 it was decided to abandon artificial hydration. The system had experienced several issues mainly related to the age of the infrastructure. The compressor had been replaced, the Isonic valves that actuated the pneumatic valves had started to fail and the reserve of spares was exhausted. In addition, the control PC had experienced several issues. As described above the artificial boundary conditions were being disturbed by equipment failures. Therefore, the decision was taken to suspend artificial hydration and to allow the system to reach equilibrium by natural hydration alone.

From Day 4340 onwards, the three artificially hydrated filter mats underwent shut-in. All three filters mirrored one another up until Day 4377.58 when the logging PC failed. It was brought back online at Day 4382.32, following which time filter mat FR902 had a much more rapid pressure decay. This suggests that one of the pneumatic valves had not operated properly and was now in operation. Up until the failure of the PC at Day 4626.02 filter mat FR902 underwent pressure decay to reach a near-steady 400 kPa. Filter mats FB903 and FB904 also showed pressure decay. However, as noted earlier, the response showed annual variation and it was not clear if the pressure response represented a steady pore pressure.

Following the replacement of the logging PC at Day 4906.03, filter mats FB903 and FB904 again showed annual variation. Although it was apparent that the pressure in the filter mats was still decreasing. During the change and upgrade of the system it is unfortunate that the pressure in FR902 was accidentally drained to near atmospheric pressure. As a result, the remainder of the reporting period saw an increase in pressure of this filter mat.

Figure 11-3 shows the pore pressure within the bentonite buffer, recorded at six locations. Figure 11-3a shows the results were dominated by pressurisation of filter UB902 during Gas Injection Test 2. What can be seen is that not only had UB902 reached a plateau it had increased during the reporting period. A degree of annual variation was apparent. The data were dominated by both artificial hydration and annual variation. However, the pressure variation was complex. In the bottom of the deposition hole at UB901 and UB902 both showed strong annual variation, and both showed an increase in pore pressure over the reporting period. UB901 had increased by around 400 kPa over the current timeframe. It was evident from the data that stopping and starting artificial hydration had little effect on the data. This is not unsurprising given that the filter mats were generally towards the top of the deposition hole. There was, however, one feature that did strongly correspond with artificial hydration, and this feature was apparent in all the UB sensors. During the resumption of artificial hydration between Day 4262 and Day 4340, the white band in Figure 11-3, a sinusoidal pressure response was seen superimposed upon the annual variation. This was related to the short-term resumption of pore pressure within filter mats FB903 and FB904. This was soon shut-in, and pressure later recovered. This had generated the complex almost sinusoidal response seen in all UB filters. This demonstrated that by this time the system was dominated by the pore pressure in the artificial filter mats.

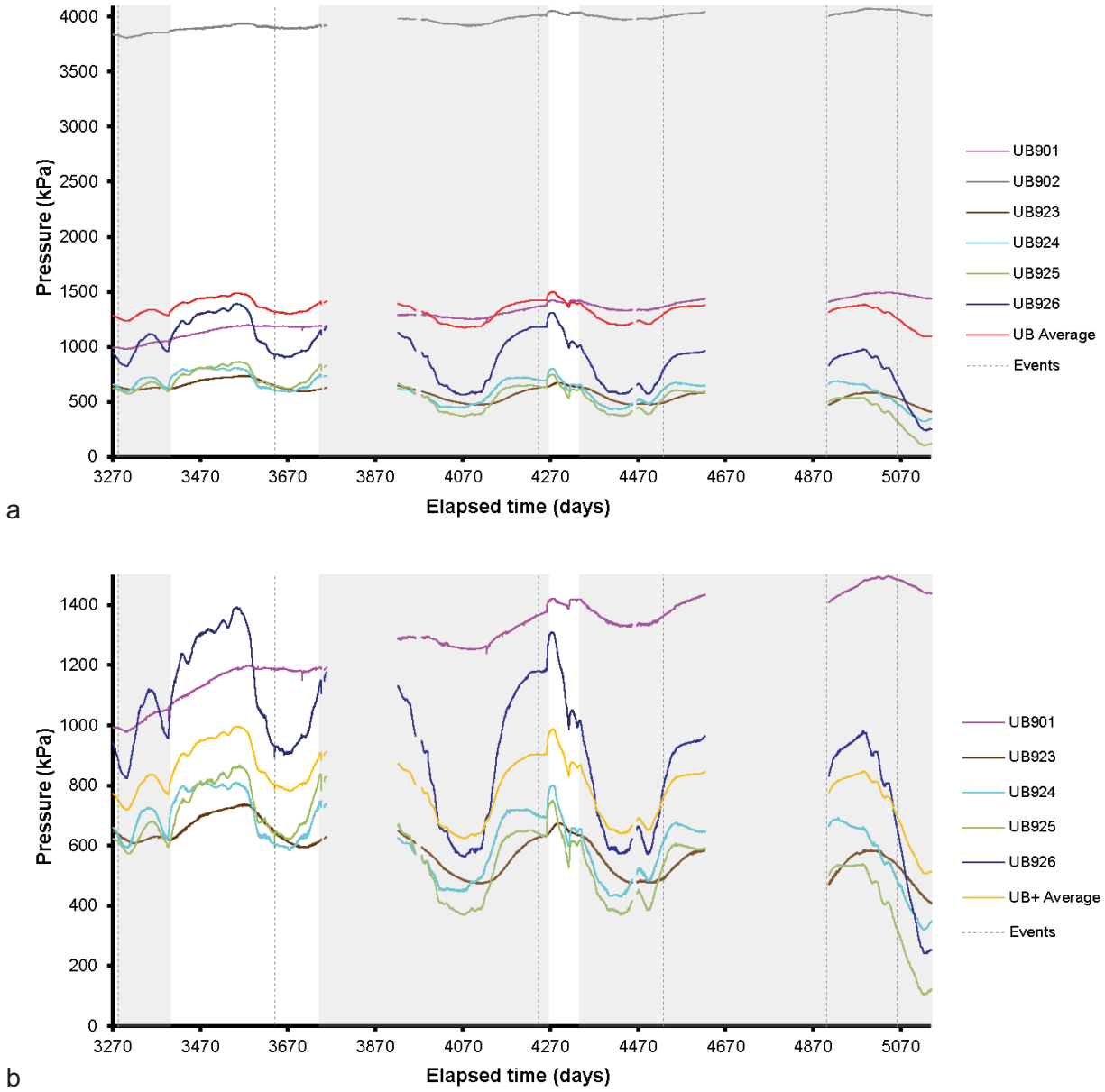

Figure 11-3. *Variation in porewater pressure within the bentonite at the 6 monitoring points: a) all six sensors; b) detail of five sensors.*

Pore pressure within the bentonite at UB923 showed a smooth sinusoidal signal with a slow decrease in pressure during the Hydration Stage 3, approximately 200 kPa pressure was lost. The three remaining pore pressure localities showed a much more complex response. This was most apparent in UB926 for the first 400 days of the stage. As well as a year-long seasonal variation, there was a much shorter-period oscillation of pore pressure. This can be seen to correlate well with the variation in temperature seen in both the HRL gallery and the Lasgit laboratory (see Figure 11-12). Sensors UB923 and UB924 were located at section 14 within the deposition hole, with UB925 and UB926 at section 16 within the upper-most bentonite segment. Therefore, it is likely that the complex behaviour seen in UB924, UB925, and UB926 was related to the temperature change within the HRL. It is surprising that UB924 initially showed complex behaviour, whereas UB923 on the same level did not. As UB923, UB902 and UB901 did not exhibit such a complex signal this suggests that the observed pore pressure variations were not caused by the poor temperature compensation of the ISCO syringe pumps. The clearest example of correlation between pore pressure and HRL temperature can be seen around Day 5000. At this time, the temperature in the HRL reduced by around 3 °C over a period of around 100 days. This was clearly seen as a reduction in pore pressure in UB924, UB925, and UB926. This reporting period clearly demonstrated a coupling of HRL temperature with observed pore pressure within the bentonite.

Pore pressure variation was also noted at the filter canisters when these were not used for artificial hydration of the system. Figure 11-4a shows that the data during this period were dominated by two effects: 1) the high shut-in pressure in filter FL903, and 2) the switching between artificial and natural hydration. The pressure in FL903 reduced from 5 869 kPa at the start of the period to 4 167 kPa at Day 4171, a decrease of 1 702 kPa over 888 days at an average rate of just less than 2 kPa d^{-1}. The gas in FL903 was vented to air at Day 4171, reducing the pressure to 17 kPa. For the remainder of the period the pressure in the filter increased to 820 kPa by Day 5102, an increase of around 800 kPa in 931 days, at a rate of almost 1 kPa d^{-1}.

At the start of Hydration Phase 3, all filters were shut-in and allowed to decay to a natural level in time. As seen in Figure 11-4b, the filters reached a plateau of between 1 180 and 1 770 kPa, excluding FL902 and FU912, which were at a level of 350 and −50 respectively. This showed that heterogeneity was still evident in the natural pressure of the filters. Once a steady pore pressure had been established, two-stage hydraulic constant head tests were conducted in FL901, FL902, FL904 to FU911. It should be noted that FL902 and FL904 were not performed as two stage hydraulic tests for operational reasons. All of the hydraulic tests are described in more detail in Section 11.2. At Day 3360 a period of artificial hydration was established in most of the canister filters at a nominal pressure of 4 200 kPa. Issues were experienced with the pneumatic valves of filters FU910 at Day 3640 and FL904 at Day 3690, which resulted in these filters being isolated and entering shut-in. On Day 3758 the logger system experienced problems and as a result the system entered the fail-safe default mode of shut in. All filters remained in this condition until Day 4270, when artificial hydration was re-started. It should be noted that during this period of shut-in some unusual behaviour was seen in the four mid-plane filters of an almost saw-tooth appearance. These were believed to have been caused by problems with the air-actuated valve system. In addition, FU909 and FU911 decreased in pressure and then recovered. Again, this was believed to have been caused by the air-actuated valve system.

Artificial hydration of the filters also occurred between Day 4264 and Day 4341, when the decision was taken to cease all artificial hydration of the system because of the problems that had been encountered with the compressor, the air-actuated valve system, the logging computer, and the water supply to the Lasgit laboratory. All filters were left to shut-in. By the end of the stage pore pressure ranged between approximately 800 and 1 600 kPa; still displaying heterogeneity in pore pressure distribution.

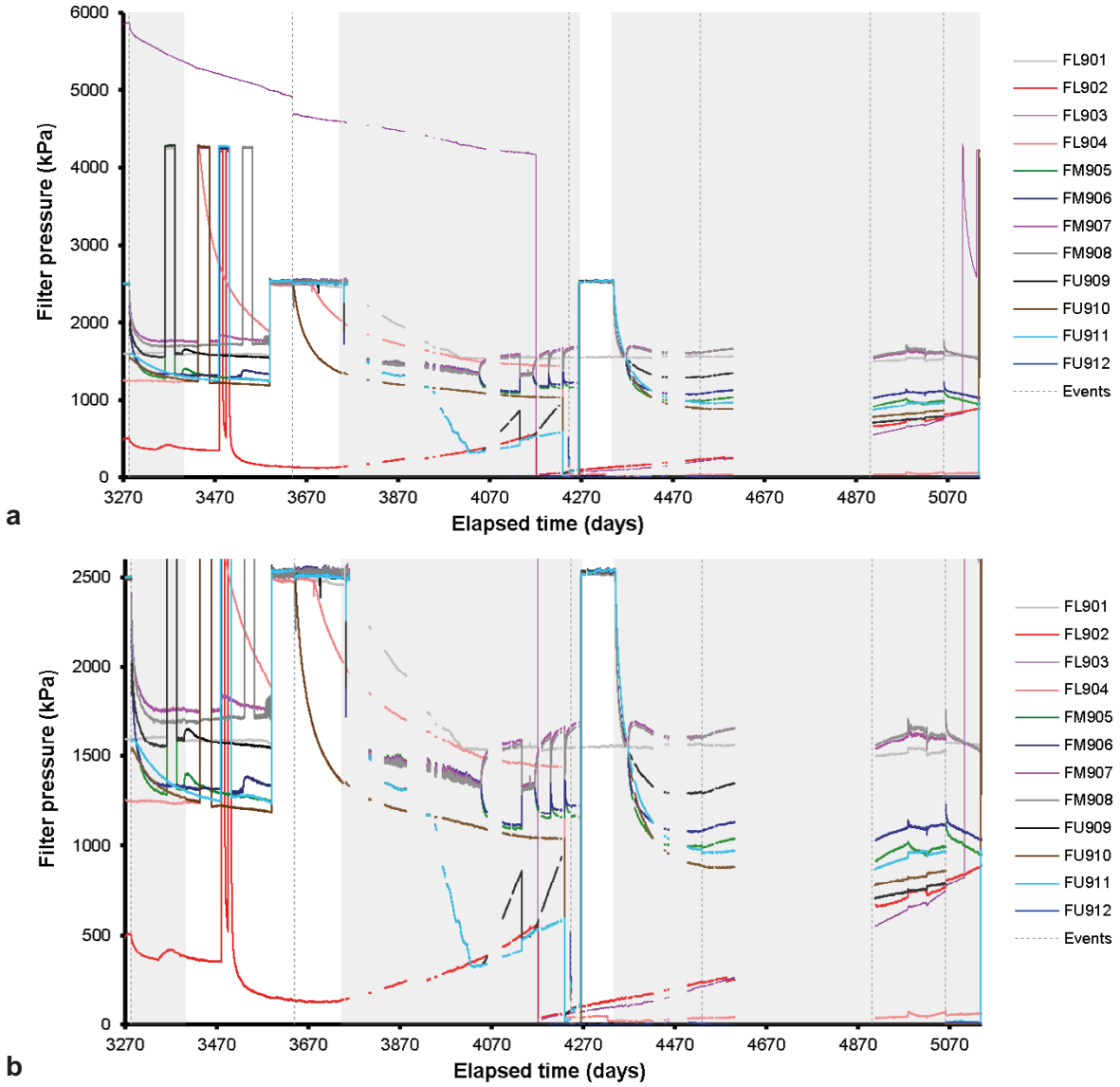

Figure 11-4. *Filter pressures on the canister surface. a) complete range of filter pressures dominated by the pressure in filter FL903; b) detail of the pore pressures in the canister filters.*

Figure 11-5 shows the variation of pore water pressure at the rock wall. At the start of Hydration Stage 3 the pore pressure ranged between 818 and 2 777 kPa (i.e., a range of 1 959 kPa). By the end of the stage pore pressure ranged between 637 and 2 277 kPa (i.e., a range of 1 640 kPa). Even considering annual variation, a clear decrease in pore pressure was seen during the reporting period. As reported in previous chapters, the greatest annual variation was seen at intervals closest to the centre of the canister. Other than annual variation, only a couple of features were worthy of note. Sensor UR919 started a slow decrease in pressure around Day 3593 that resembled a shut-in response. However, at Day 3697 the pore pressure at UR919 recovered rapidly to where the previous pore pressure before it then started to decay. The other feature of note occurred in sensor UR916, when at Day 3697 pore pressure started to increase, raising the general level of pore pressure by ~170 kPa. No other sensor showed such behaviour. There were other smaller-scale features noted, including a small increase at UR915 and UR918 between Day 3479 and Day 3613 and feature in UR916, UR920, and UR922 between Day 4261 and Day 4304. As the pore pressure sensors on the rock wall were generally free from the influence of artificial hydration, these were likely to be hydraulic features occurring in the rock wall.

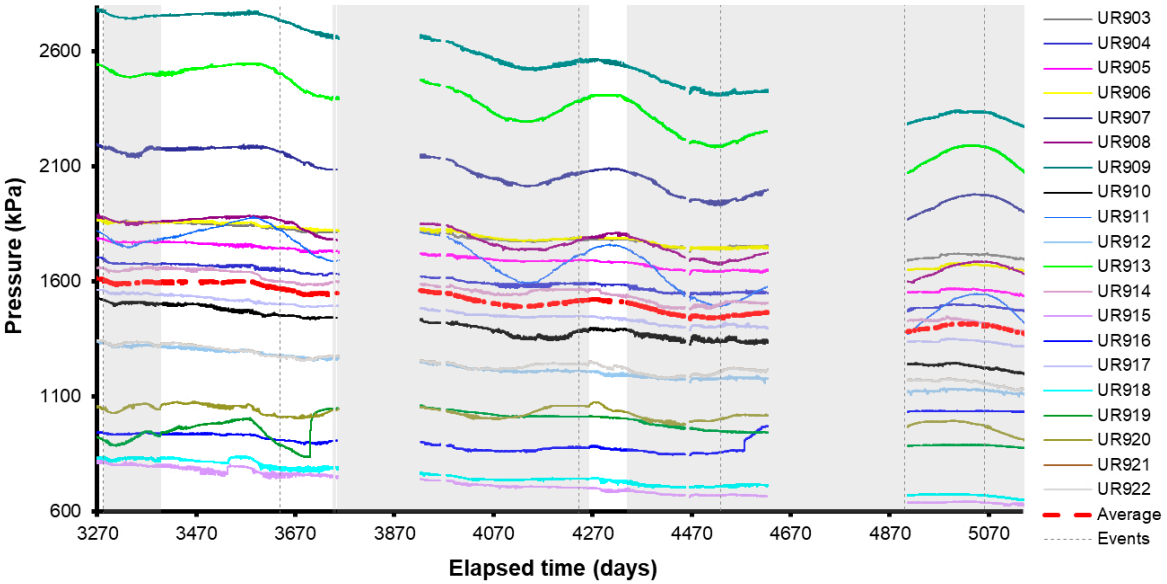

Figure 11-5. *Variation in porewater pressure with time measured at the rock face.*

Radial stress measured at the rock wall is shown in Figure 11-6a, for all locations and Figure 11-6b in detail for all sensors excluding PR921. As seen, the radial stress had generally reached plateau and remained constant during Hydration Stage 3. At the start of the stage the average radial stress was 5 079 kPa with a total range of 3 836 kPa. By the end of Hydraulic Stage 3 the average was 5 077 kPa with a spread of 3 640 kPa. Therefore, average stress remained constant with only a small reduction in the spread of stress, caused by a reduction in PR910. The most obvious feature of note was the annual variation seen in the data, this being strongest at the mid-height of the canister.

The data in Figure 11-6b shows that the stress evolution at the rock face was complicated. For example, PR903, PR905, and PR920 decreased by 310, 125, and 113 kPa respectively, while PR907, PR908, and PR915 increased by 410, 164, and 140 kPa respectively. This shows that the net stress in the system was constant (as shown by the constant average), but that the distribution of stress was changing. The radial stress within the bottom of the deposition hole was greatest in bentonite rings R4 and R5, with the lowest stress seen at the top of the deposition hole within bentonite ring R10. There was additional heterogeneity within the deposition hole, with the greatest range seen within bentonite ring R10 with a 2 600 kPa variation, although it should be noted this level included the low stress value seen in PR921. The next greatest variation of around 1 400 kPa was seen centrally within the deposition hole at bentonite ring R7. Generally, the spread at each level reduced with time and the system had become more homogenous at each level.

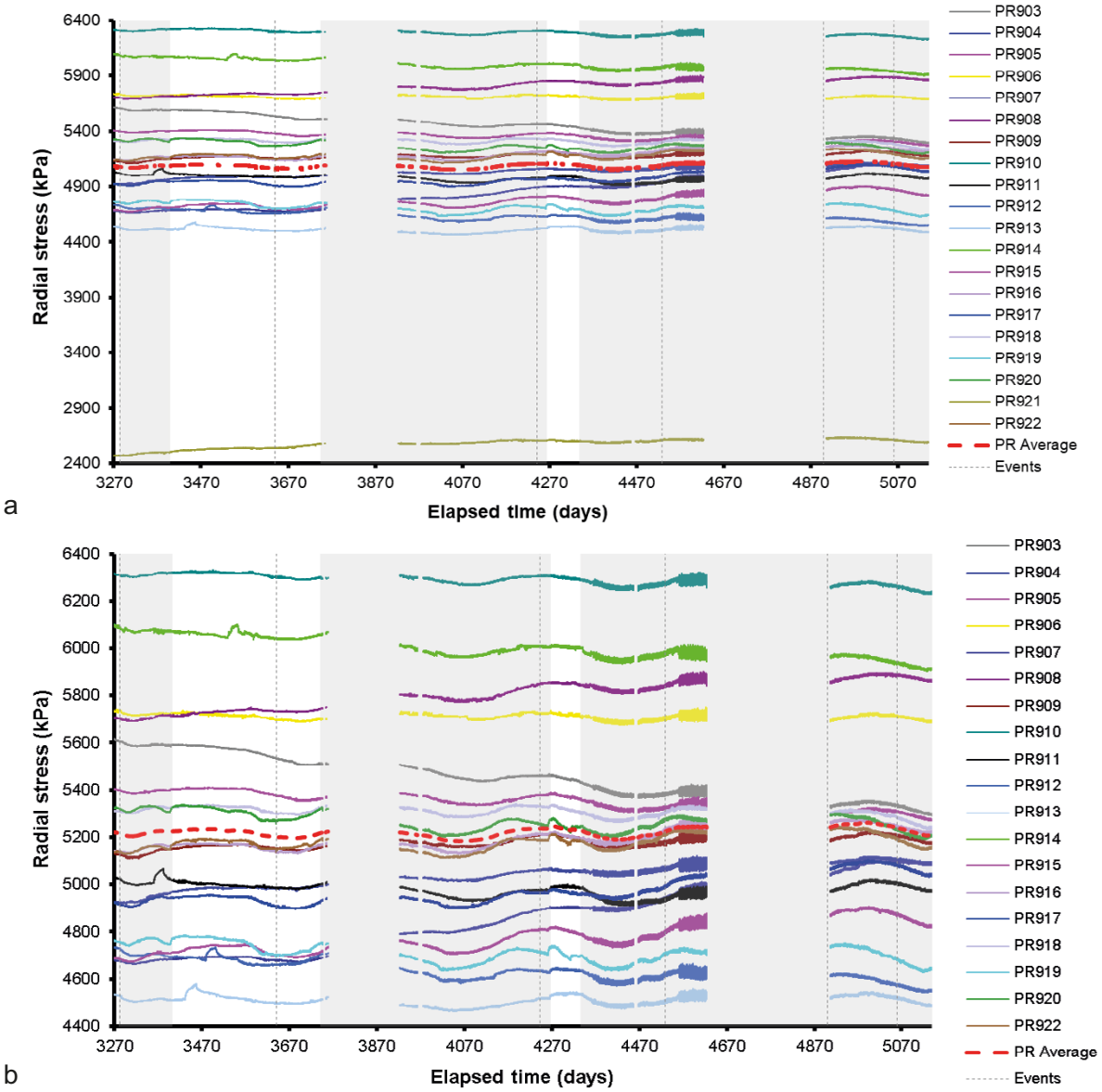

Figure 11-6. *Variation in radial stress at the rock wall with time. a) radial stress for all locations; b) radial stress for all locations excluding PR921.*

On a shorter time consideration, there were a few stress variations seen. The first was observed around Day 3360 in PR911, when stress started to increase eventually reaching a stress 55 kPa higher at Day 3377, after which, over the next 50 days the stress started to return to the original level. During this event, radial stress decayed and recovered in PR919, PR920, and PR922. This shows that the system was coupled between sections 7 and 10. This event does correspond with features seen in the pore pressure at the rock wall (UR sensors). Three similar events were seen in sensors PR913 at Day 3432, PR912 at Day 3478, and PR914 at Day 3529. All three of these events had a similar form (shape, magnitude, duration) as that described for PR911. However, there was no corresponding changes in other PR sensors. The event in PR914 corresponds with pore pressure changes in UR sensors. The final event of note occurred at Day 4262 in sensors PR911, PR912, PR913, PR917, PR919, PR920, and PR922 and lasted until Day 4320. The feature was near sinusoidal in some of the sensors and corresponded with the feature described in pore fluid pressure.

It is worth noting the system problems encountered in the PR sensors. The "noise" in the data can increased around Day 4262, with a further increase noted at Day 4562, when all PR sensors became very noisy. This was remedied when the computer and Geokon logger were replaced, and the system was restarted on Day 4906.

The stress acting on the canister was measured at three locations, as shown in Figure 11-7. During Hydration Stage 3 the average stress generally stayed constant at around 6 000 kPa, with PC901 increasing, while PC902 and PC903 decreased slightly. This shows that the stress in the system was constant, with the distribution of stress changing. Other than the annual variation seen in the data, the only feature of note was the stress variation seen in PC901 around the time that artificial hydration was re-established (~Day 4262). This corresponded with the change in PR and UR sensors previously described. It should also be noted that when the system was replaced on Day 4906 problems were initially encountered with the stress sensors and that logging of these was not restarted until Day 5141.

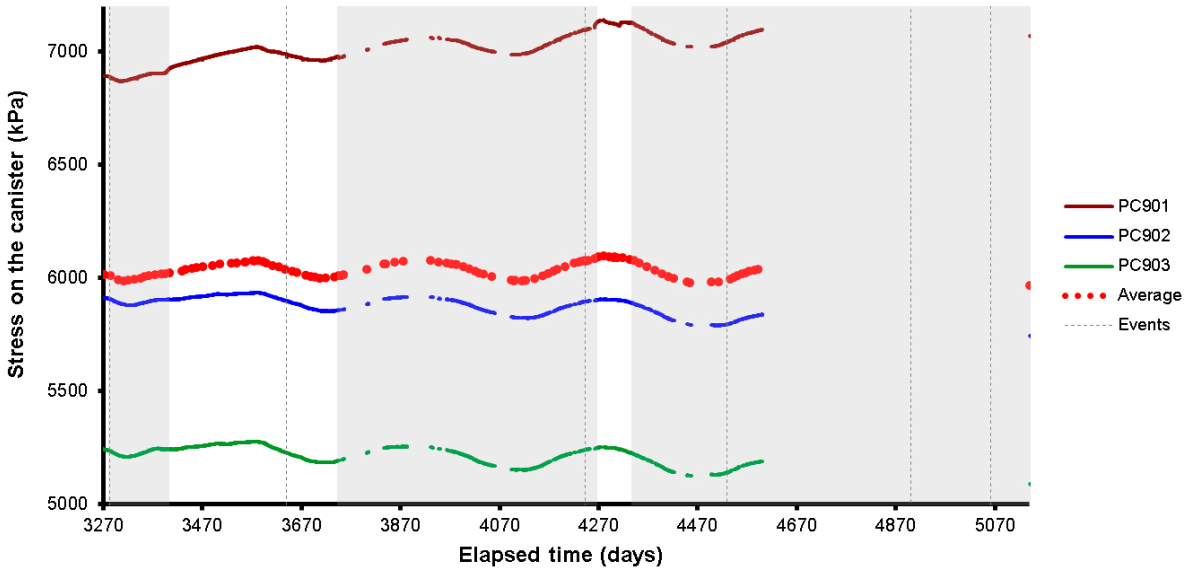

Figure 11-7. *Development of axial and radial pressure on the side and base of canister.*

Axial stress within the bentonite is shown in Figure 11-8. A clear correlation was seen between axial stress and if artificial hydration was occurring. At the start of Hydration Stage 3 the system was shut-in with no artificial hydration. This resulted in the loss of stress in PB927. Re-starting hydration at Day 3360 resulted in a stress response in all sensors, with most showing an increase of at least 100 kPa as a result. For the remainder of the time of artificial hydration until Day 3745 the data showed annual variation.

At Day 3745 the system was again shut-in and artificial hydration was paused once more. This resulted in the reduction of stress in most sensors (Figure 11-8), with the exclusion of the sensors in the base of the deposition hole (PB901 and PB902) and at the top of the deposition hole (PB929). The greatest reduction in stress occurred in PB927, which following shut-in reduced by ~500 kPa, before reaching a new stress value with annual variation. As described previously, hydration was re-established between Day 4262 and Day 4340. As a result, axial stress changed in all sensors, although the change in the base of the deposition hole was small. PB927 showed an increase in stress of around 250 kPa. However, the shut-in of filter FB904 during the hydration stage had resulted in an irregular stress response and it can be clearly seen when this filter mat was shut-in and when it was re-opened. This almost sinusoidal response was mirrored in the UR and PR sensors described above.

At Day 4340.12 hydration of the filter mats was stopped for the final time. The stresses slowly returned to the level they were prior to the 78-day long hydration albeit with annual variation, until the PC failed at Day 4626 (Figure 11-8). In the final part of Hydration Stage 3, axial stress reduced significantly in the sensors above the canister, while in the sensors below the canister there was no such change. Sensor PB927 slowly reduced by more than 200 kPa, significantly greater than had been previously observed during annual variation.

At the start of the reporting period the average axial stress was 5 906 kPa with a spread of 1 430 kPa (Figure 11-8). By the end of the period, it was an average of 5 694 kPa with a spread of 1 272 kPa. Therefore, a reduction in average axial stress of over 200 kPa and a reduced spread in values. These changes were all because of the cessation of artificial hydration and the resultant homogenisation of the system.

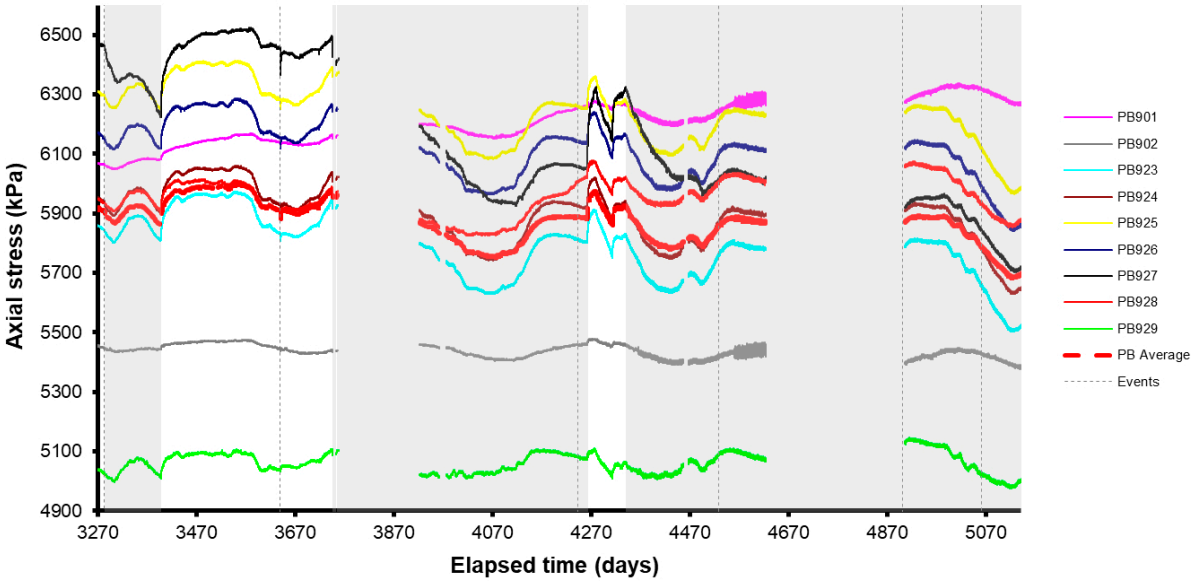

Figure 11-8. *Development of axial stress measured at 9 locations within the buffer.*

The chances in stress within the bentonite was mirrored in the axial force measured on the lid, as shown in Figure 11-9. Annual variation was again observed, with a general decrease of stress. At the start of Hydration Stage 3, the average force was 1 719 kN with a spread of 178 kN. By the end of the period the average force had reduced to 1 670 kN with a similar spread of 174 kN. The general form of the data and variations within, corresponded with periods of hydration, as described for the stress within the bentonite.

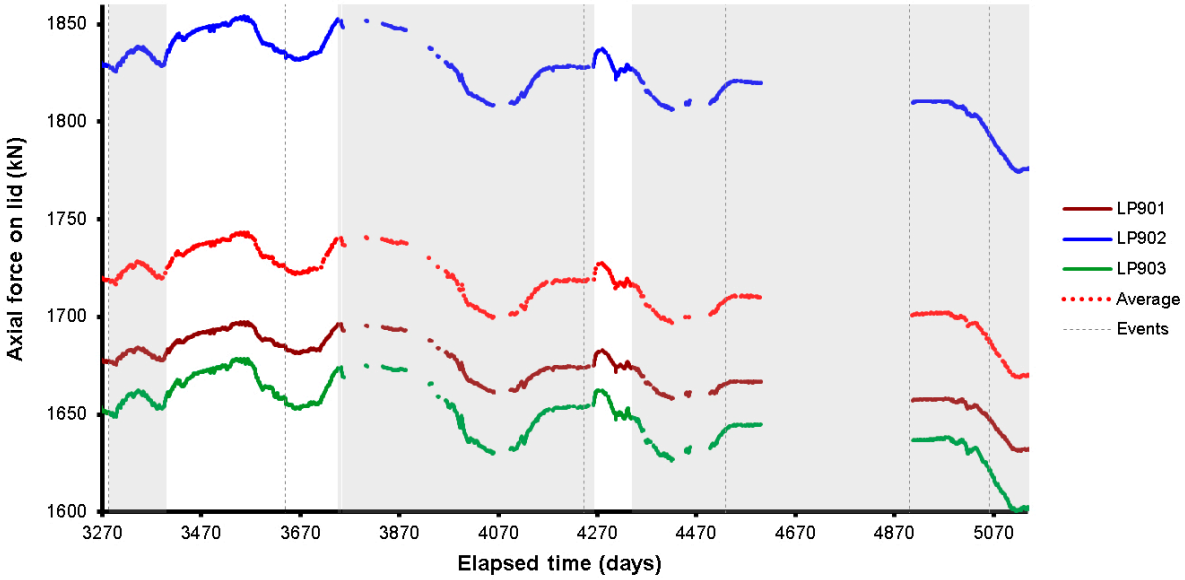

Figure 11-9. *Axial force acting on the steel lid measured by 3 Glötzl load cells attached to separate rock anchors.*

The displacement of the canister lid is shown in Figure 11-10, with vertical movement shown in Figure 11-10a and lateral movement in Figure 11-10b. Generally, the movement of the lid was controlled by the stress on the lid, which was dictated by the periods when the buffer was being artificially hydrated. The vertical displacement (DP902–DP904) was dominated by annual variation and artificial hydration. The position of the canister also showed correlation with the times of artificial hydration, with hydration resulting in negative movement, whilst periods of shut-in generally resulted in a positive movement. It should be noted that issues were experienced with the LVDTs measuring the vertical movements of the lid and that when the system was restarted at Day 4906 considerable noise was experienced in DP901–5 and that this data was removed during Quality Control of the full dataset. The lateral movement of the canister lid is shown in Figure 11-10b. This data shows relatively small displacements with the dataset dominated by annual variation.

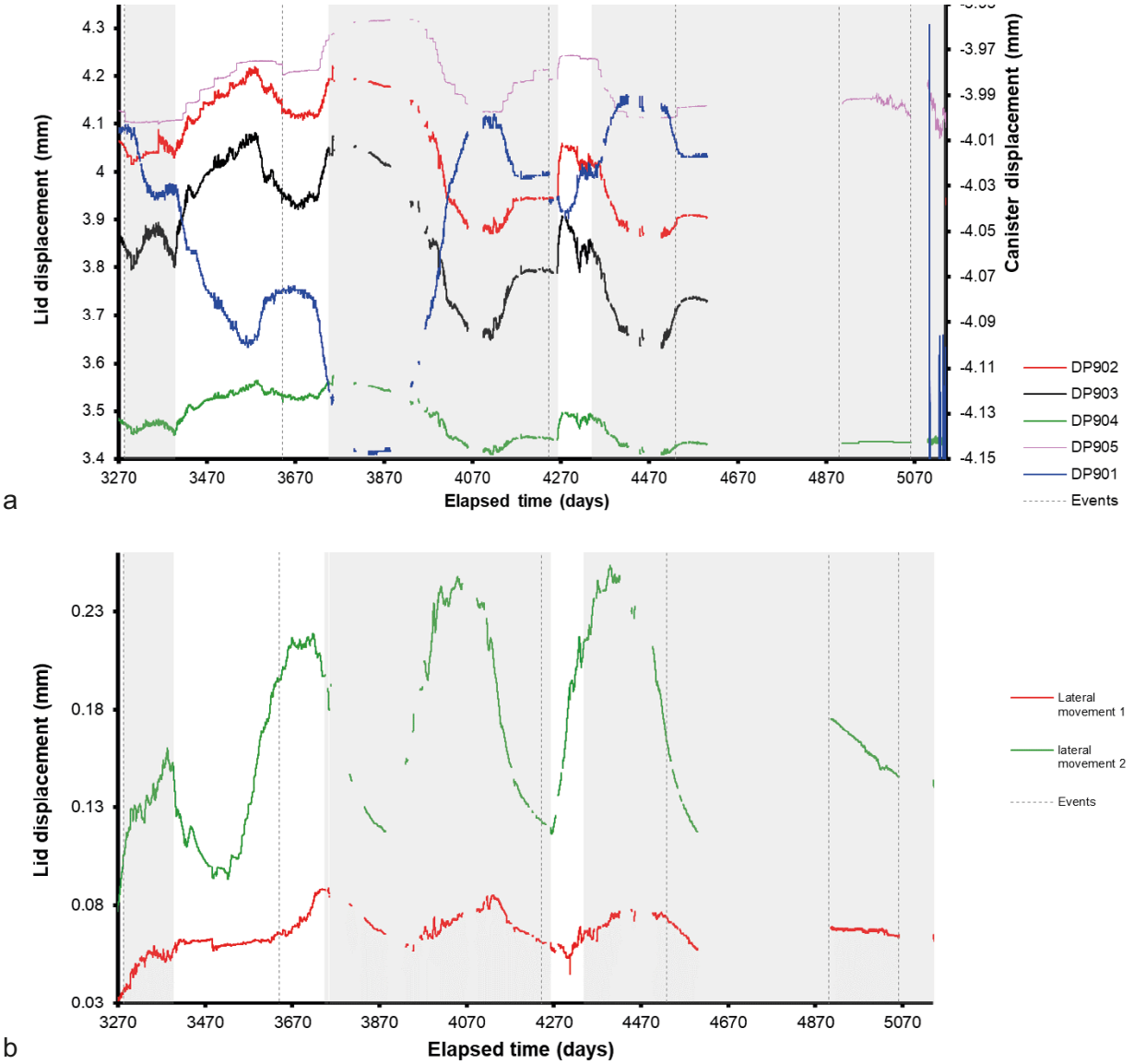

Figure 11-10. *Linear displacement of the steel lid and copper canister (a) and lateral movement of the lid (b). Movements of the lid are measured relative to both the gallery floor and ceiling. Movements of the canister are measured relative to the steel lid.*

Pore pressure within the pressure relief hole is shown in Figure 11-11. All intervals showed a reduction in pore pressure. At the start of the period the average pore pressure was 1 259 kPa, with a spread of 1 911 kPa. This reduced to an average of 1 119 kPa with a spread of 1 713 kPa by the end of the period. Pore pressure in interval PRH1–3 was seen to increase at the calibration visit at Day 5061. This was believed to be as a direct result of the calibration. It should be noted that PRH1–2 had a noisy response compared with the other intervals and that interval PRH2–4 was affectively at atmospheric pressure, this interval was closest to the gallery.

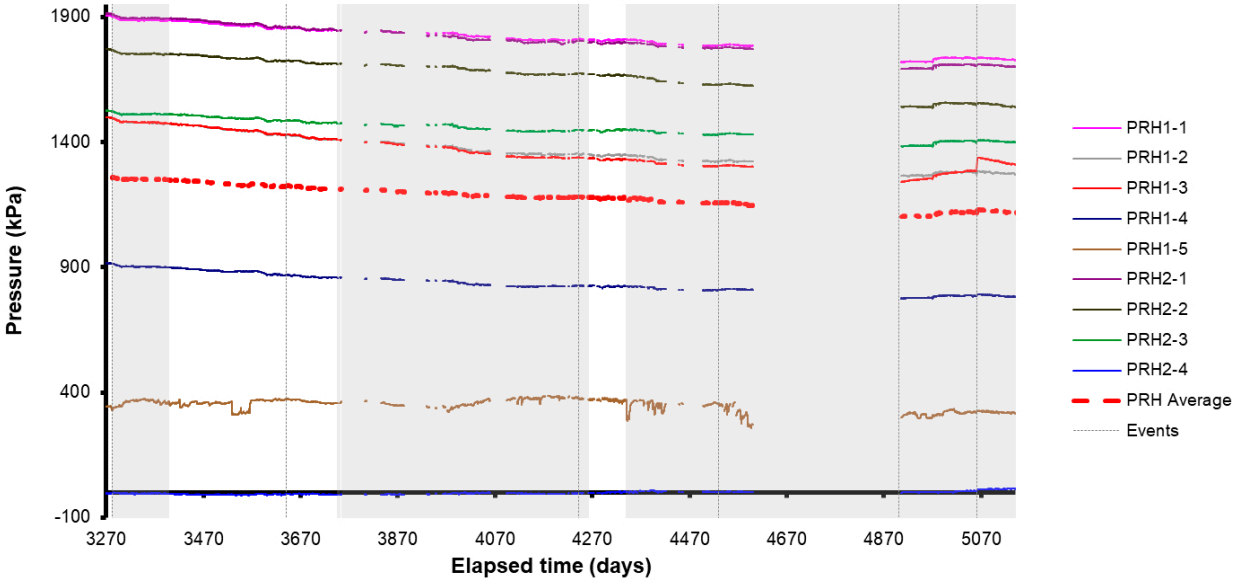

Figure 11-11. *Porewater pressures measured in the pressure relief boreholes.*

Temperature was monitored within the Lasgit laboratory, the HRL, and the canister. Figure 11-12 shows that the air conditioning unit within the laboratory was problematic at times during the 5-year hydration stage. At certain times the air-conditioning unit was delivering a constant temperature, whereas at others the temperature was seen to mirror the HRL air temperature, indicating that the air-conditioning unit was failing to deliver constant temperature. This was not deemed problematic as the system was in a state of hibernation and since no gas tests were being conducted it was not vital to have a steady temperature. Figure 11-12 shows that the air-conditioning unit failed at Day 4253.15 with the temperature within the laboratory rising to 22 °C. The air-conditioning unit was fixed and for a period operated at a relatively stable temperature. The temperature spike was not apparent in any data as this was a period of shut-in. The air-conditioning unit was later replaced around the time of the calibration visit at Day 4529. Temperature was steady following this, although temperature reduced by around 3 °C between Day 4980 and the calibration visit at Day 5061, when the air-conditioning unit was serviced.

Figure 11-13 shows the total volume of water pumped into the system during Hydration Stage 3 and clearly shows the two periods of artificial hydration. In the first period, a total of 6.25 litres was pumped into the system. In the second hydration stage a further 1.529 litres of water were pumped. This means that a total of 7.78 litres of water was pumped into the system during Hydration Stage 3 in two stages.

Figure 11-14 shows average stresses, pore pressure, and forces observed during Hydration Stage 3. Generally, it can be noted that all parameters appeared relatively constant over the five-year Hydration Stage. Axial stress on the rock wall showed a small decrease, as did the pore pressure at the rock wall and the pore pressure in the pressure relief holes. The pore pressure in the bentonite had stopped increasing and appeared to maintain a new level, although the end of Hydration Stage 3 it showed a reduction, as did the axial stress on the rock wall. All parameters showed annual variation to varying degrees, with the pore pressure in the bentonite showing the most variation. The data suggests that the system had reached, or was close to attaining, an equilibrium state of constant boundary conditions.

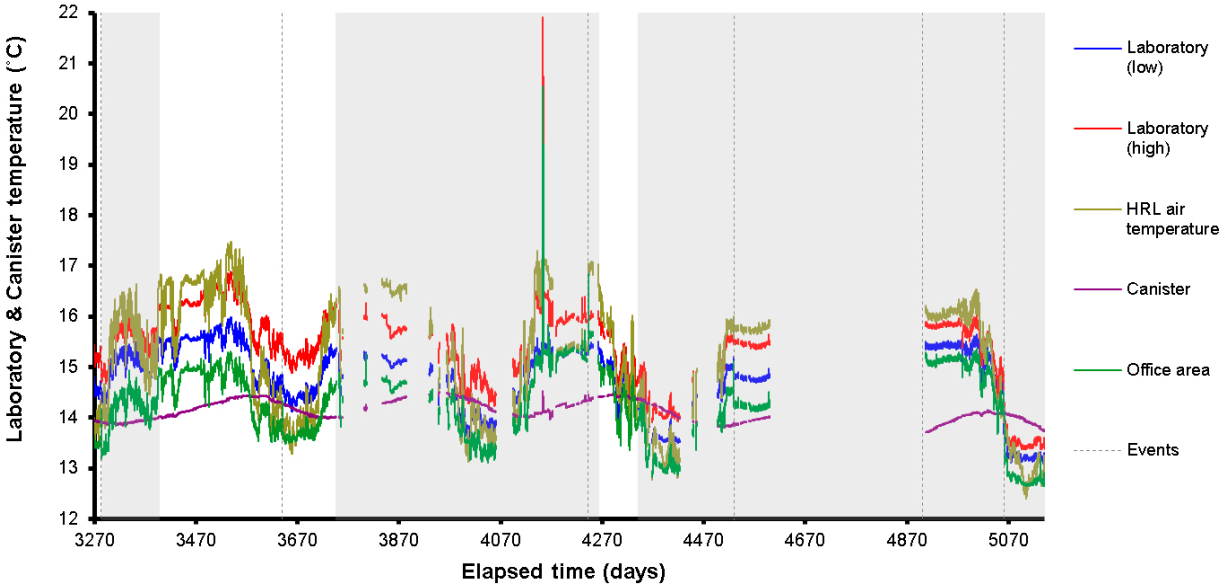

Figure 11-12. *Temperatures recorded in the Gas Laboratory, office, canister, and HRL.*

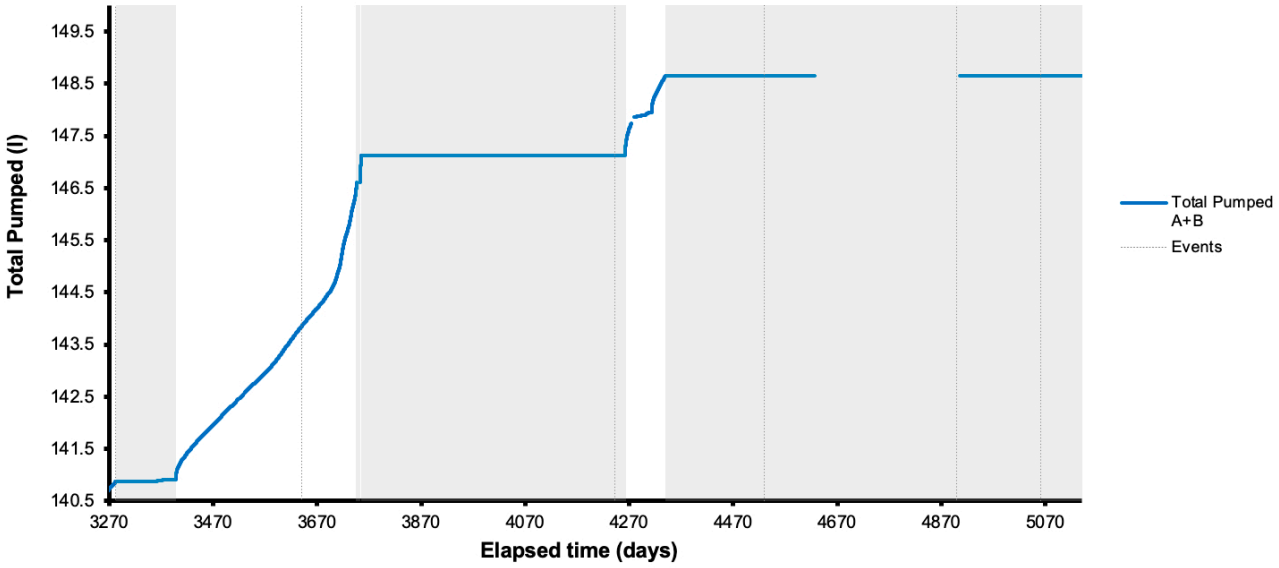

Figure 11-13. *Total pumped during artificial hydration and hydraulic testing.*

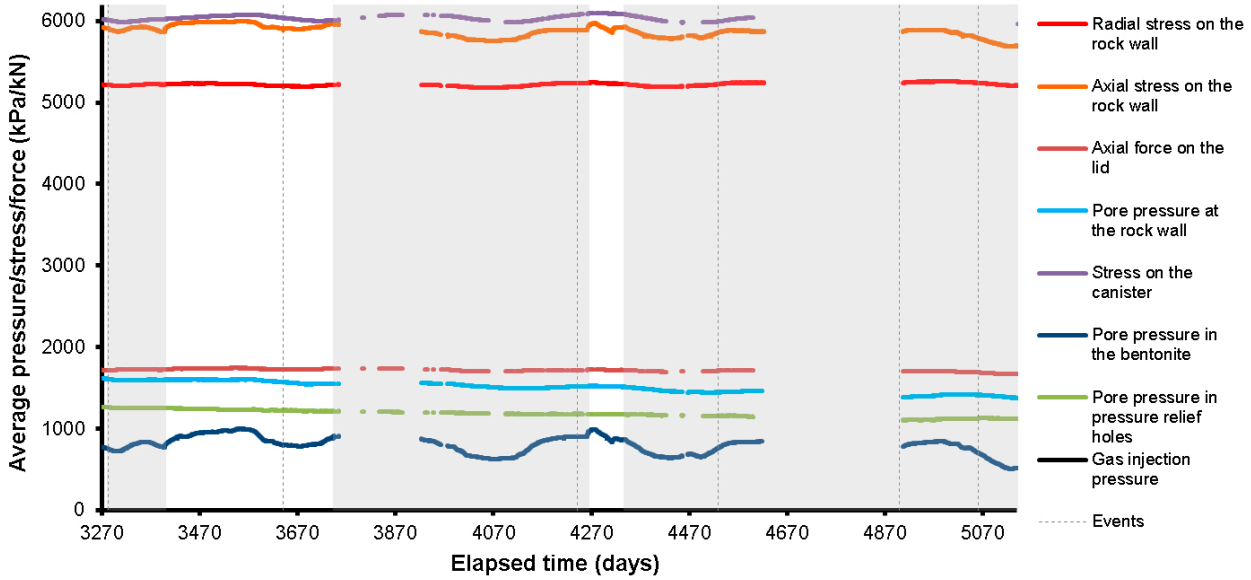

Figure 11-14. *Average pressures, stress, and force observed during Hydration Stage 3.*

11.2 Hydraulic two-stage constant head tests

Between Day 3360 and Day 3576 the canister filters were tested with a two-stage constant head hydraulic test. However, as filter FL903 had multiple tests already, this filter was not tested. Filters FL902 and FL904 were problematic and failed their respective tests and insufficient data was achieved to model hydraulic properties. Filter FU912 was also not tested as this filter had not seen any artificial hydration during the experiment as it had been wrongly plumbed and this location offered a snap-shot of what a naturally hydrated filter would look like. Therefore, eight successful tests were achieved. The two-stage hydraulic head tests were modelled using the 1-D modelled described in Section 6.4. The results of the tests are shown with their modelled fit in Figure 11-15 to Figure 11-17. Table 8-1 summarises the calculated values for hydraulic conductivity and specific storage for the two tests. These results are discussed in Section 16.8.

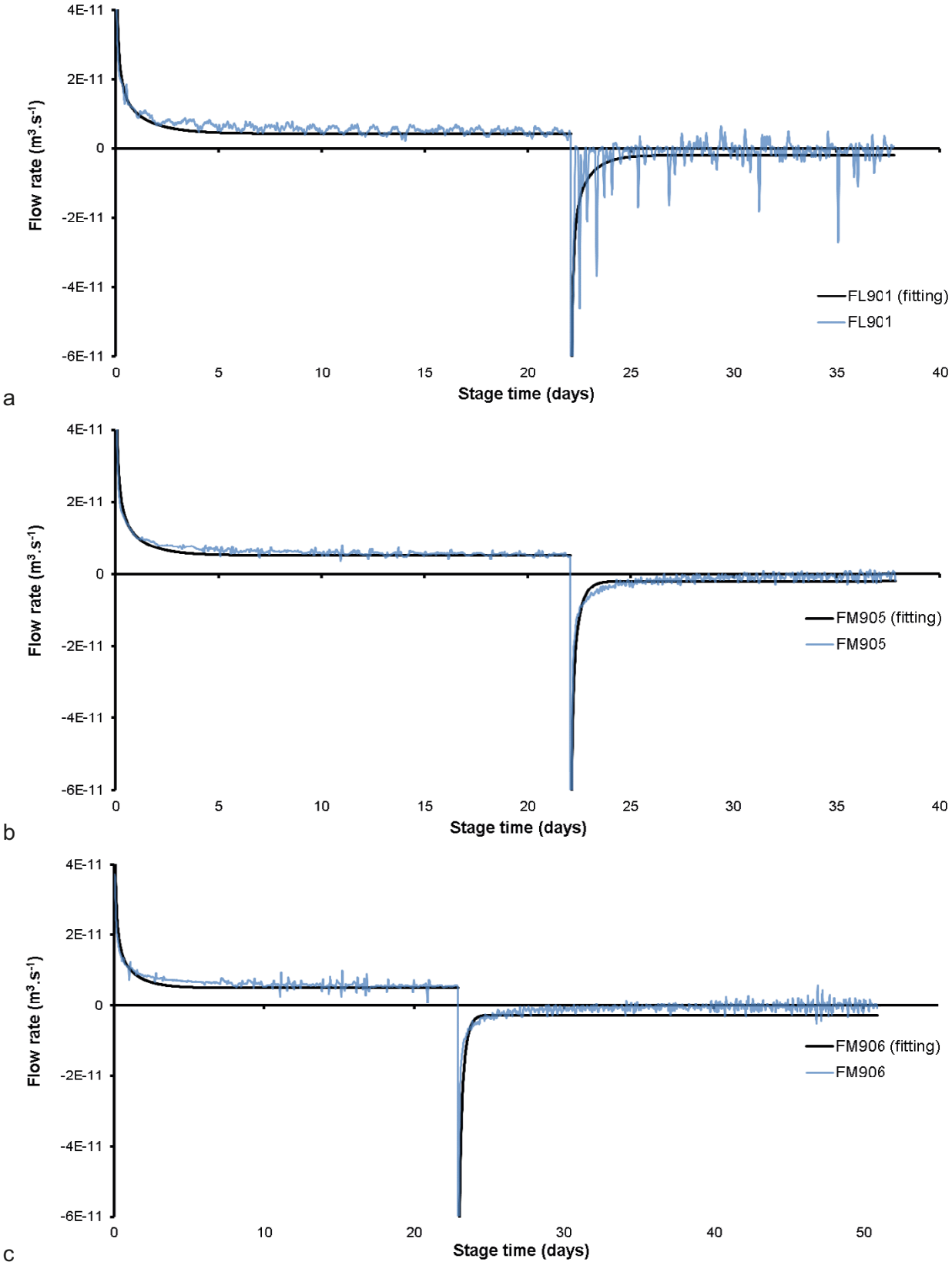

Figure 11-15. *Two-stage constant head tests and modelled fit. a) FL901; b) FM905; c) FM906.*

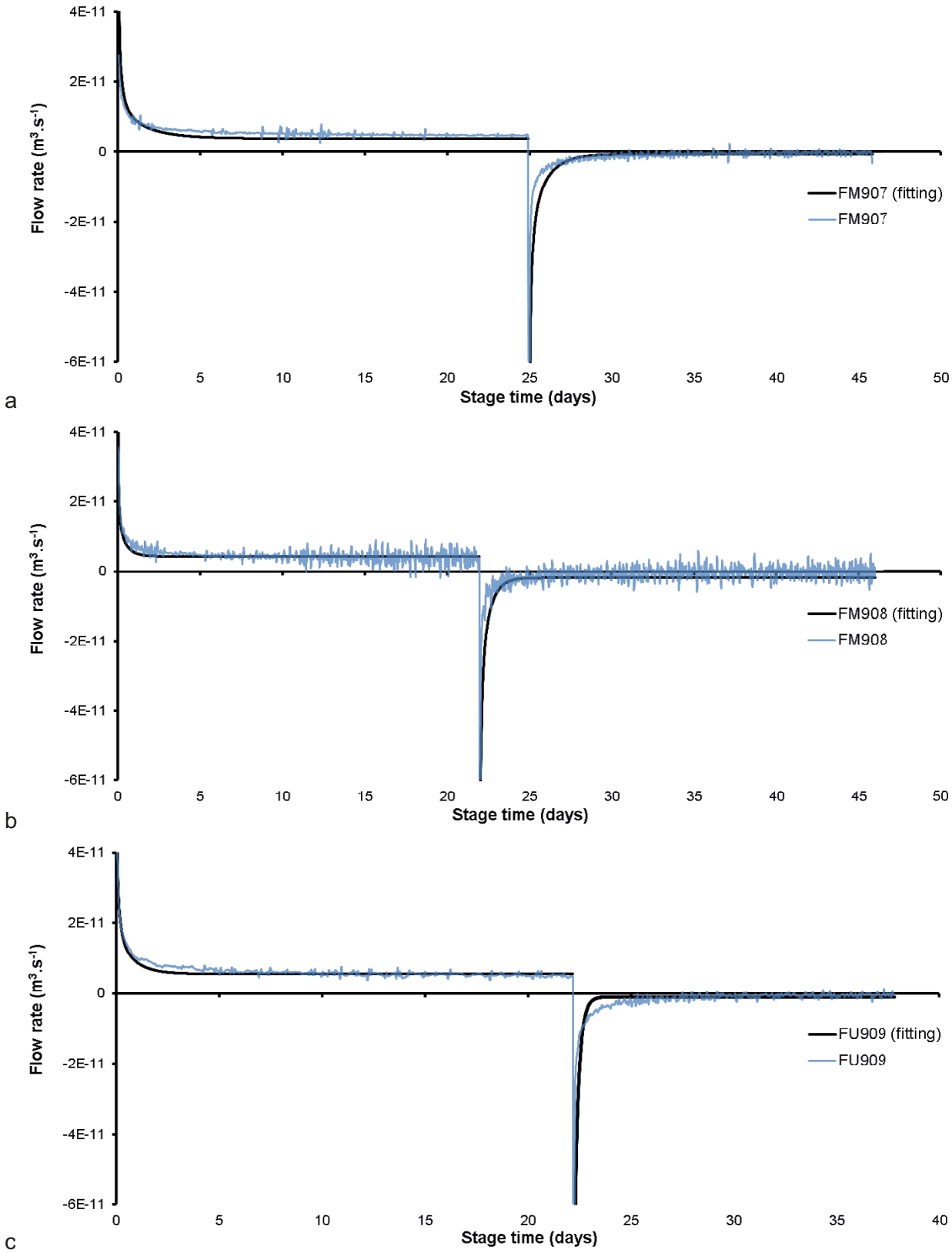

Figure 11-16. *Two-stage constant head tests and modelled fit. a) FM907; b) FM908; c) FM909.*

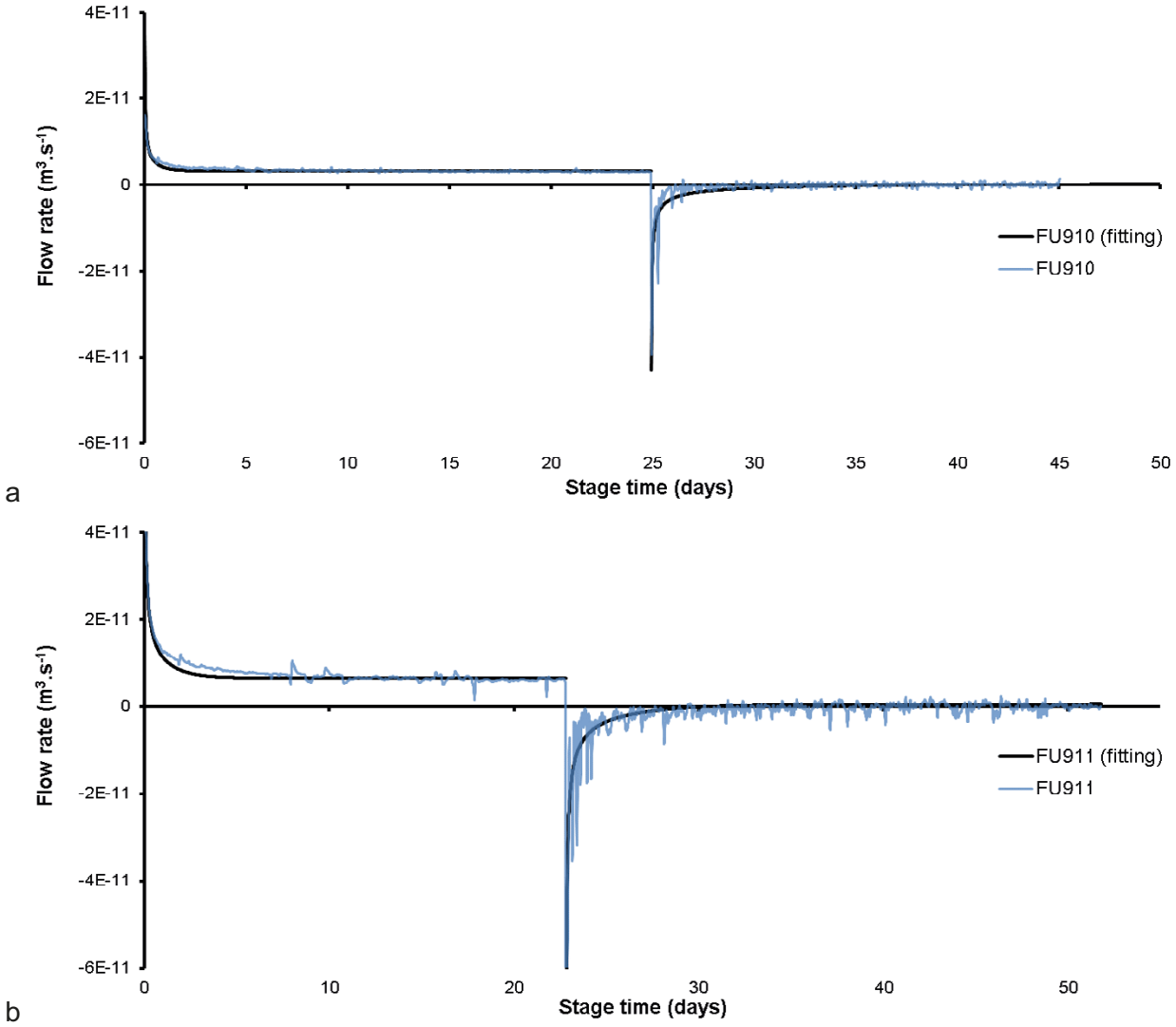

Figure 11-17. *Two-stage constant head tests and modelled fit. a) FU910; b) FU911.*

Table 11-1. Modelling results for the two-stage constant head hydraulic tests conducted between Day 3360 and Day 3576.

Filter	Radius of the filter (mm)	Step	Fitted hydraulic conductivity (m/s)	Fitted specific storage (m^{-1})	Boundary conditions		Initial conditions	
					p_0 (MPa)	p_L (MPa)	p_{I0} (MPa)	p_{IL} (MPa)
FL901	50	1	9.08×10^{-13}	8.81×10^{-6}	4.24	2.17	1.61	2.17
		2	1.47×10^{-12}	8.16×10^{-6}	1.59	2.17	4.24	2.17
		Average	**1.19×10^{-12}**	**8.48×10^{-6}**				
FM905	50	1	8.49×10^{-13}	7.02×10^{-6}	4.28	1.64	1.31	1.64
		2	2.66×10^{-12}	6.07×10^{-6}	1.32	1.64	4.28	1.64
		Average	**1.76×10^{-12}**	**6.55×10^{-6}**				
FM906	50	1	8.11×10^{-13}	7.31×10^{-6}	4.24	1.57	1.32	1.57
		2	4.42×10^{-12}	8.79×10^{-6}	1.30	1.57	4.24	1.57
		Average	**2.62×10^{-12}**	**8.05×10^{-6}**				
FM907	50	1	7.03×10^{-13}	8.66×10^{-6}	4.26	1.92	1.75	1.92
		2	1.85×10^{-12}	1.24×10^{-5}	1.75	1.92	4.26	1.92
		Average	**1.28×10^{-12}**	**1.05×10^{-5}**				
FM908	50	1	8.38×10^{-13}	2.72×10^{-6}	4.26	2.01	1.71	2.01
		2	2.80×10^{-12}	9.96×10^{-6}	1.72	2.01	4.26	2.01
		Average	**1.82×10^{-12}**	**6.34×10^{-6}**				
FU909	50	1	9.19×10^{-13}	5.07×10^{-6}	4.28	1.66	1.56	1.66
		2	7.45×10^{-12}	1.08×10^{-5}	1.60	1.66	4.28	1.66
		Average	**4.18×10^{-12}**	**7.94×10^{-6}**				
FU910	25	1	1.71×10^{-12}	2.13×10^{-6}	4.22	0.98	1.22	0.98
		Average	**1.71×10^{-12}**	**2.13×10^{-6}**				
FU911	50	1	8.45×10^{-13}	6.25×10^{-6}	4.27	0.94	1.26	0.94
		2	5.66×10^{-13}	1.11×10^{-5}	1.28	0.94	4.27	0.94
		Average	**7.06×10^{-13}**	**8.70×10^{-6}**				

12 Gas Injection Test 5 (Day 5133 – 5306)

The eighth significant stage of the Lasgit experiment started on Day 5138.09 (26th February 2019) and was completed at Day 5235.45 (3rd June, 2019); a total stage time of 97.37 days. **Note:** unlike in previous test stages, overlap existed between Gas Injection Test 5, Gas Injection Test 6, and the Full Canister Test stages.

Before the final Full Canister Test, it was decided to conduct one final test each in filters FL903 and FU910 to see if the properties of the bentonite had altered since the long elapsed time since the previous gas injection tests. With limited time to conduct the tests, there was an overlap in time of the Gas Injection Test 5 and Gas Injection Test 6. This overlap was mainly in the timing of the hydraulic tests before and after the gas injection stage. The first of the gas injection tests was conducted in filter FU910, 2 568 days or 7 years since the end of the previous gas injection test in that filter. Gas Injection Test 5 investigated whether gas properties of the bentonite had changed with time and if the gas migration behaviour was the same as previously observed. Figure 12-1 shows the plan for the test period and clearly shows the overlap in Gas Injection Tests 5 and 6. Limited hydration occurred during this stage during the hydraulic testing of the test filters.

Gas Injection Test 5 comprised of three distinct stages (Figure 12-2); 1) a two-stage hydraulic test to determine the hydraulic properties of the bentonite at filter FU910; 2) a single-stage gas injection ramp to achieve gas entry at filter FU910; and 3) a repeat hydraulic test, although this was of limited duration and only covered the high-pressure stage.

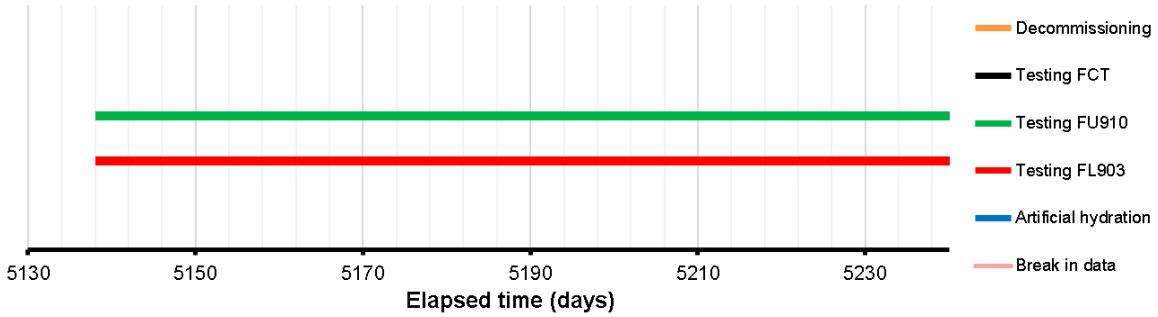

Figure 12-1. *Test stages of the Lasgit experiment showing what was conducted during Gas Injection Test 5.*

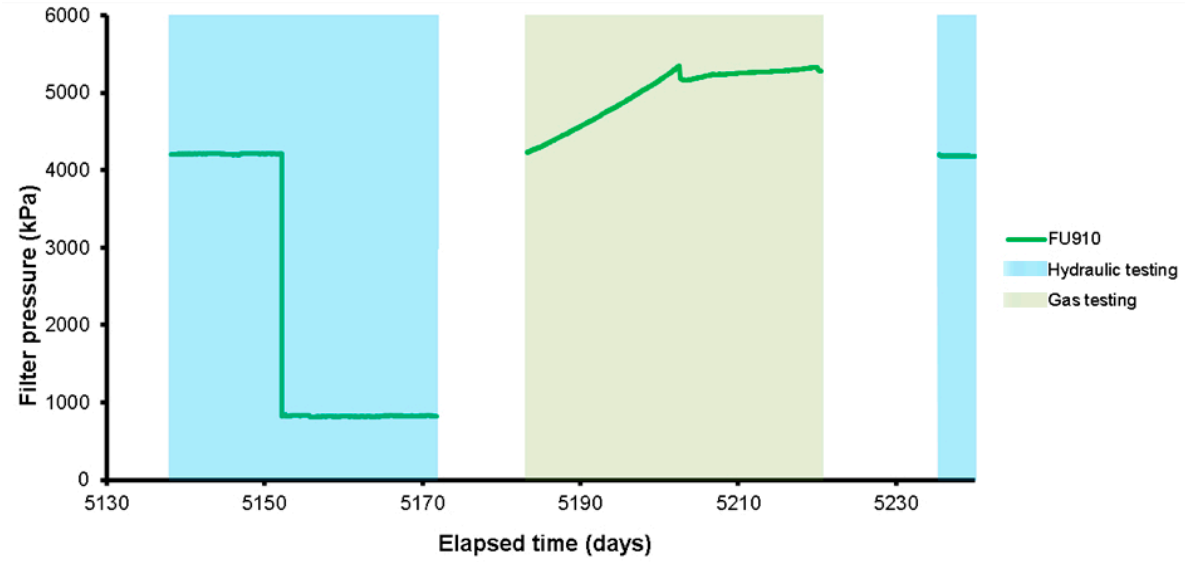

Figure 12-2. *The filter pressure of FU910 during Gas Injection Test 5. A two-stage hydraulic test was conducted prior to a single stage gas injection test.* ***Note:*** *blue shading shows periods of hydraulic testing, green shows gas testing.*

12.1 Description of the field parameters during the period

Before describing the gas injection test, the field parameters will be described (boundary conditions). **Note:** The grey areas displayed in the graphs show periods when artificial hydration was not occurring. As artificial hydration was abandoned in the previous stage, all graphs are shown with a full grey background.

Figure 12-3 shows the pore fluid pressure of the filter mats. Throughout Gas Injection Test 5 there was no artificial hydration of the filter mats and therefore the pressures recorded represent the equilibrated pore fluid pressure. Filter mat FR901 on the rock wall showed the highest pressure of approximately 1 600 kPa, this filter being at the bottom of the deposition hole. In contrast, filter mat FR901 on the rock wall showed the lowest pore pressure of only approximately 100 kPa. This filter was towards the top of the deposition hole. These differences show the heterogeneity of pore pressure and fracturing in the deposition hole wall. Over the 97-day period of the stage there was little variation in pore pressure within the filter mats at the rock wall.

Within the bentonite, the pore pressure at FB903 and FB904 was generally low and approximately 600 and 420 kPa respectively. A small variation was seen over the 97-day stage, although not significant enough to have influenced the gas injection test.

Figure 12-4 shows the pore pressure within the bentonite buffer (UB), recorded at six locations. Figure 12-4a shows the results were dominated by the pressurisation of filter UB902 during previous gas injection testing. Figure 12-4b shows that two of the sensors (UB925, UB926) showed an increasing pore pressure from around Day 5200, whilst UB924 increased throughout the test period. These locations were towards the top of the deposition hole. All locations showed a minor cyclicity of around 20 days. Generally, pore pressure within the bentonite was low, with most locations showing pressure < 500 kPa. The only exception was UB901 below the canister, where 1 400 kPa of pressure was established. This data shows considerable differences in the pore pressure above and below the canister.

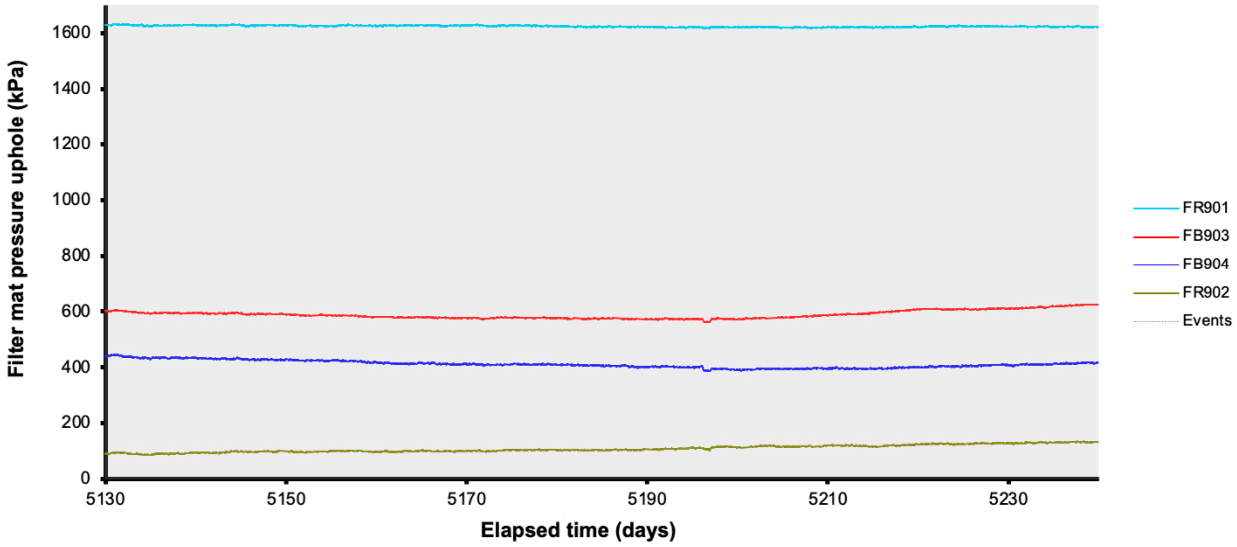

Figure 12-3. *Evolution of water pressure in the filter mats located on the borehole wall and within the bentonite blocks.*

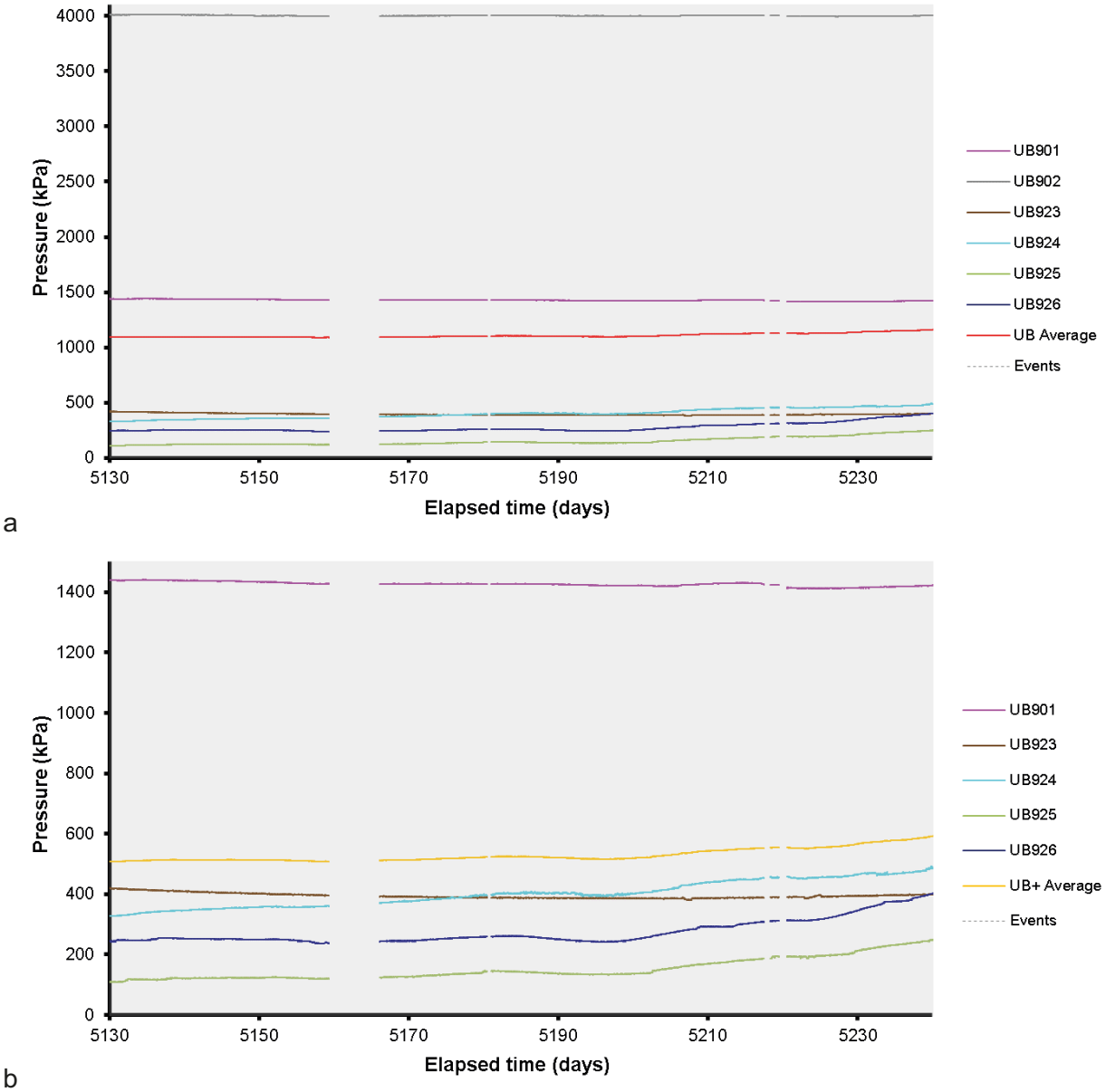

Figure 12-4. *Variation in porewater pressure within the bentonite at the 6 monitoring points: a) all six sensors; b) detail of five sensors.*

Changes in pore pressure were also noted at the canister filters when these were not used for hydraulic or gas testing of the system. Figure 12-5a shows that the data during this period was dominated by the operation of filters FL903 and FU910 for the hydraulic and gas injection testing. Figure 12-5b shows that the pressure history of the other canister filters in more detail. Filters FL901, FM907, and FM908 show the highest pore pressure, of approximately 1 525 kPa. Pore pressure at these locations was generally stable, although FM907 and FM908 showed pressure increases that correlated with events seen in filter FU910, this is discussed in more detail in Section 12.3. A second set of filters were seen to have a pressure of ~1 000 kPa, these being FL902, FM905, FM906, and FU911. In detail, FL902 showed an increase in pressure throughout Gas Injection Test 5. Filters FM905, FM906, and FU911 showed similar behaviour with a decrease in pressure until around Day 5200 when pressure started to plateau and then increase. Filters FM905 and FM906 showed stepped increase in pressure related to the gas test and this is discussed in more detail in Section 12.3. Filter FU909 was inadvertently pressurised when hydraulic testing started on filter FU910. This was caused by a seized air actuated valve and was closed as soon as it was possible for someone to visit the laboratory. The final two filters measured low pressure. Filter FU912 effectively registered a pore pressure of zero, while FL904 measured ~80 kPa. Filter FL904 showed an increasing pore pressure throughout the Gas Injection Test 5.

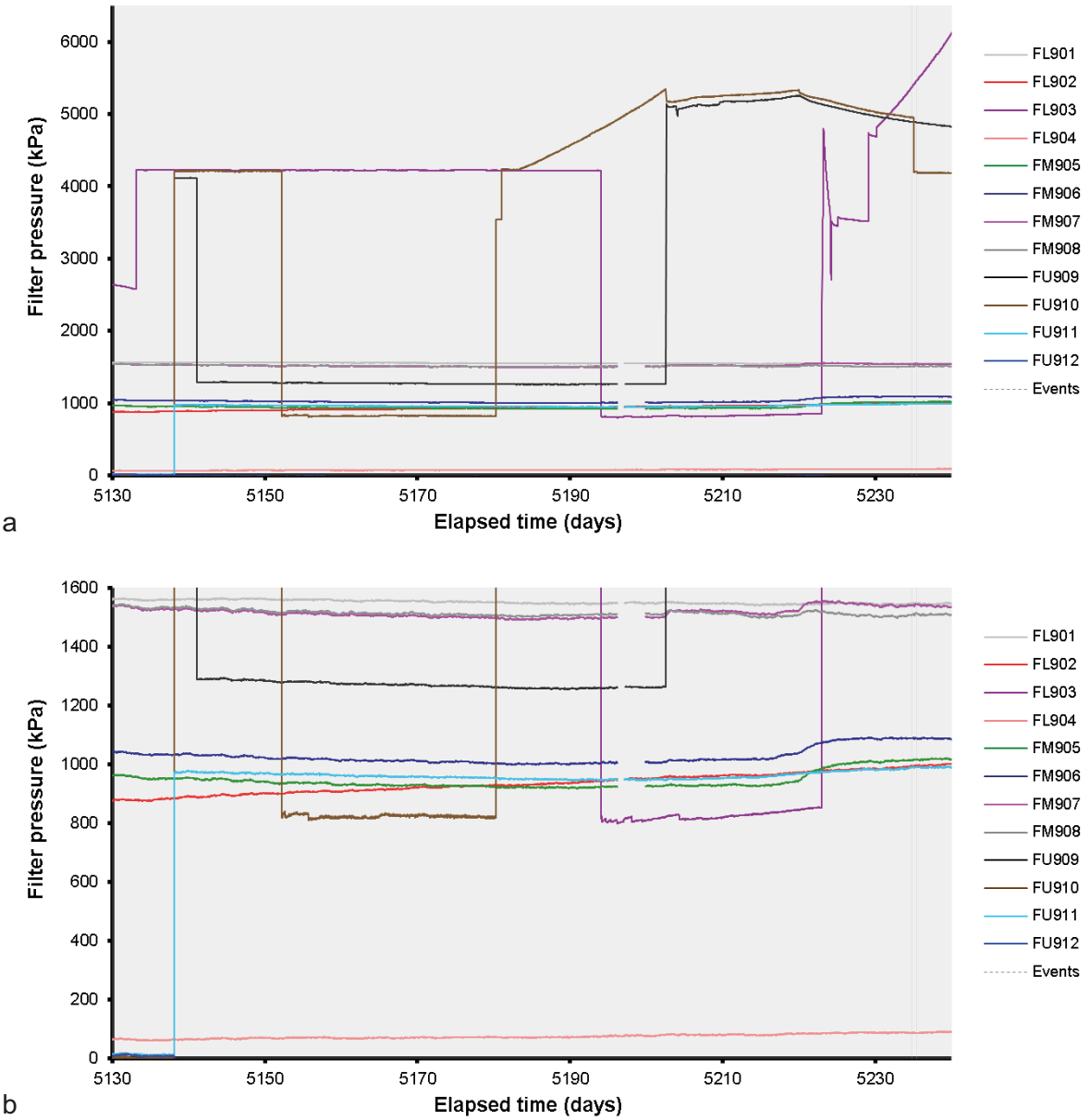

Figure 12-5. *Filter pressures on the canister surface. a) complete range of filter pressures dominated by the activities in filters FL903 and FU910; b) detail of the pore pressures in the canister filters.*

Figure 12-6 shows the variation of pore water pressure at the rock wall. As can be seen, pressure was heterogeneous within the deposition hole, with around 1 500 kPa variation. It has been reported in previous chapters that UR sensors were dominated by annual cyclicity. This is not immediately apparent in the current test stage as the data only represent 110 days, but in detail it can be seen that most sensors showed a decaying pore pressure related to annual variations in pore pressure. Nine of the UR sensors showed a response that corresponded with the gas injection experiment. This is most noticeable in stepped changes in UR913, UR914, UR917 and UR912, with longer term increases seen in UR920 and UR922. Sensors UR911 and UR910 showed a stepped response later than the other sensors, while UR911 showed a small decrease in pore fluid pressure. Figure 12-7 shows the distribution of pore pressure within the deposition hole at the start, mid-point, and end of the current period. This shows the usual distribution of pore fluid pressure with a general decrease in pore pressure down the deposition hole and a high in pore pressure at around 275°. Over the full test stage, the high-pressure region increased in magnitude.

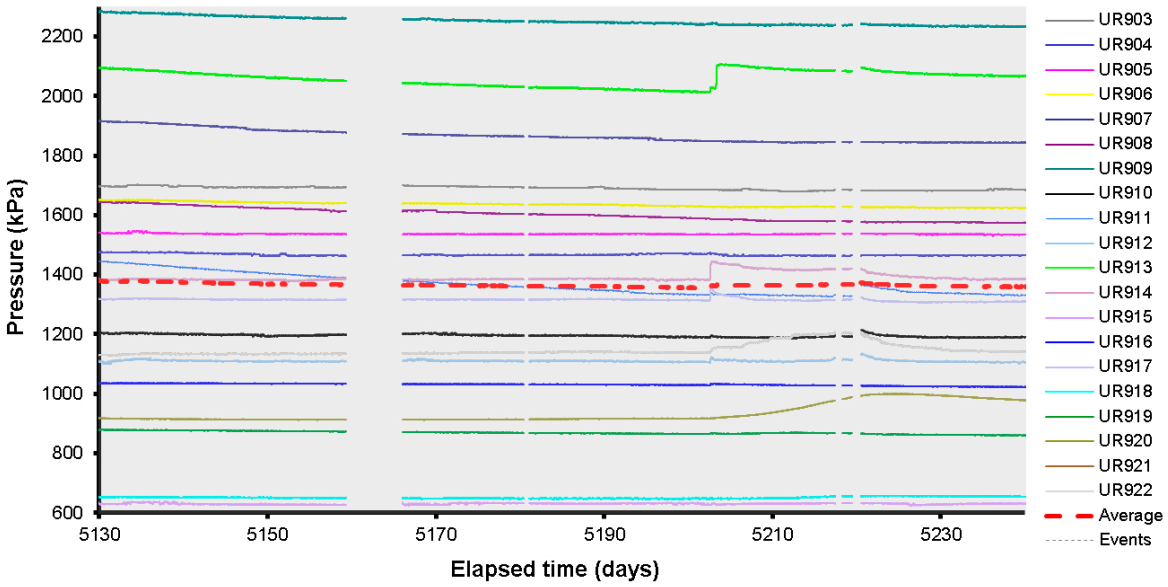

Figure 12-6. *Variation in porewater pressure with time measured at the rock face.*

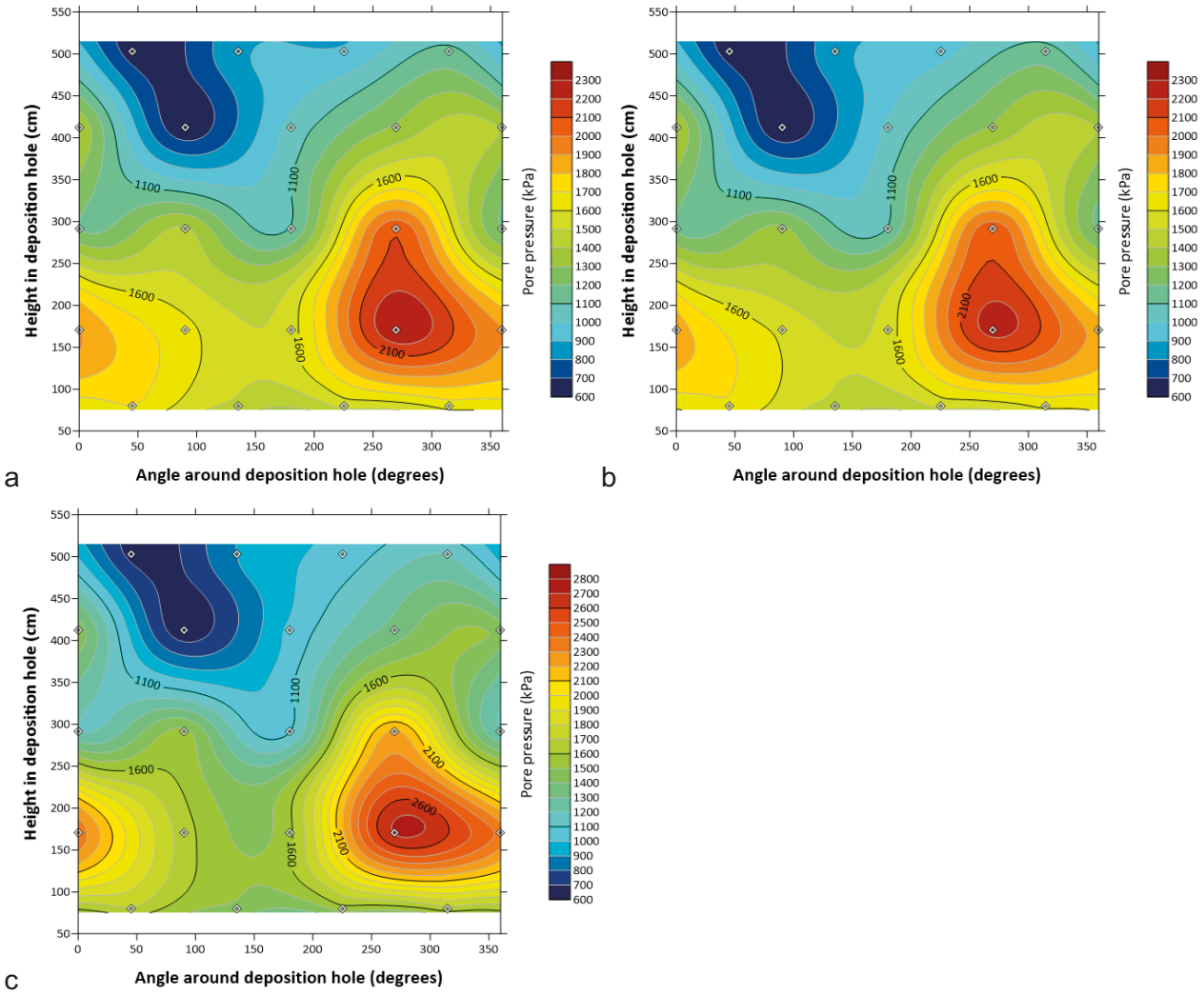

Figure 12-7. *Porewater pressure distribution at the rock face. a) Day 5140.00, b) Day 5250.00, c) Day 5300.00.*

Radial stress measured at the rock wall is shown in Figure 12-8a for all locations and Figure 12-8b in detail for all sensors excluding PR921. As Gas Injection Test 5 was relatively short, annual cyclicity was not seen. This allowed the gas response to be observed during a period of relatively stable boundary conditions. The radial stresses showed considerable heterogeneity with a range from 2 550 to 6 250 kPa; excluding PR921, radial stress ranged from 4 500 kPa to 6 250 kPa (i.e. a range of 1 750 kPa). The data were dominated by the stress responses caused by the gas injection test and this is discussed in more detail in Section 12.3. The radial stress at the bottom of the deposition hole was greatest in bentonite rings R4 and R5, with the lower stress seen further up the deposition hole. However, the upper most section of radial stress sensors at ring R10 showed a high stress. Therefore, it appears stress generally increased from the centre of the canister in both an upward and downward direction. Figure 12-9 shows the distribution of stress at the deposition hole wall. This clearly shows the general reduction of stress from the top to the bottom of the hole and that stress tended to be greatest at 315°. The radial stress distribution was complex with some localised response. The stress maps show that during Gas Injection Test 5 the majority of variation occurred at the level of the upper filter array (412.4 cm height).

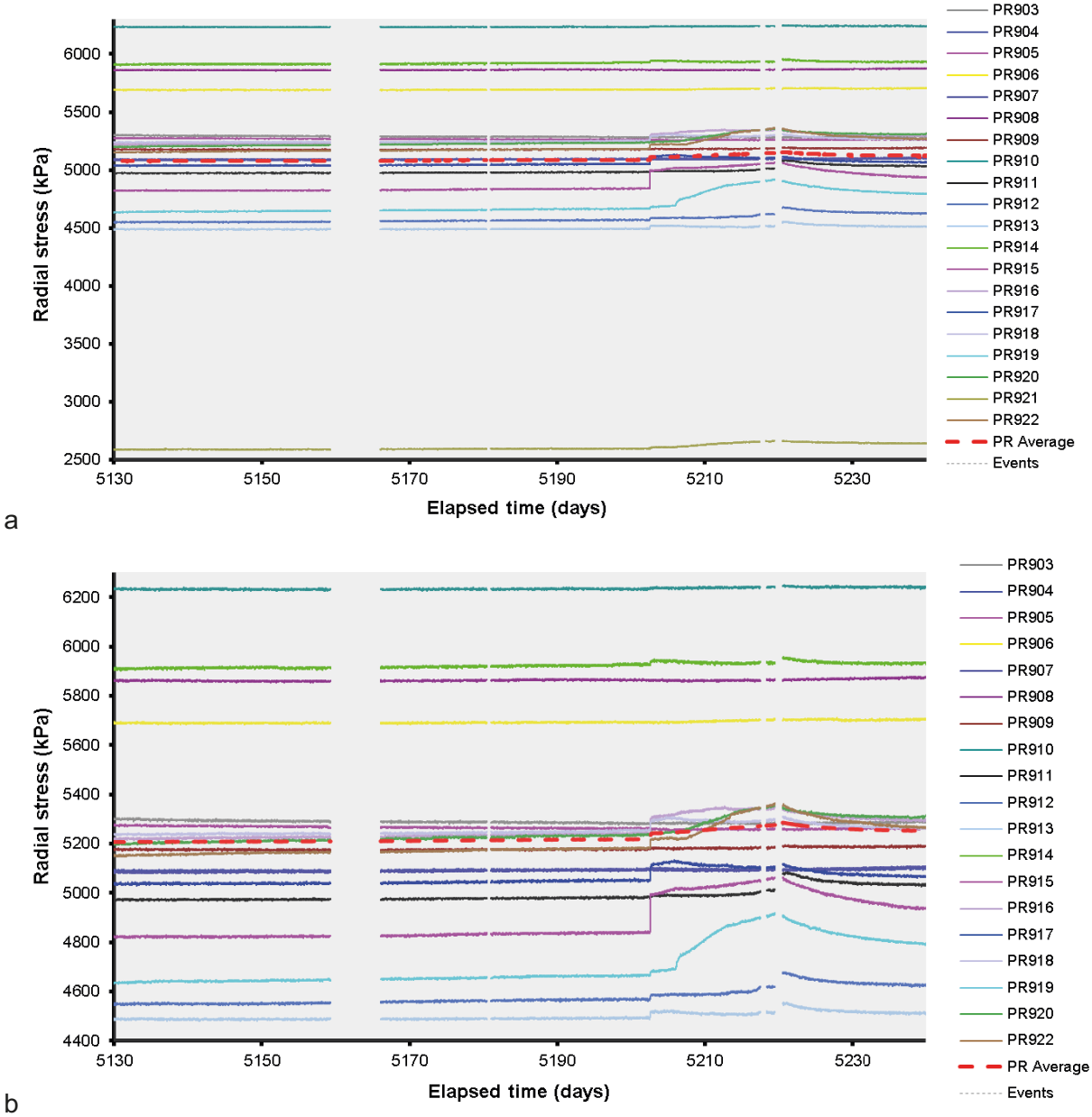

Figure 12-8. *Variation in radial stress at the rock wall with time. a) radial stress for all locations; b) radial stress for all locations excluding PR921.*

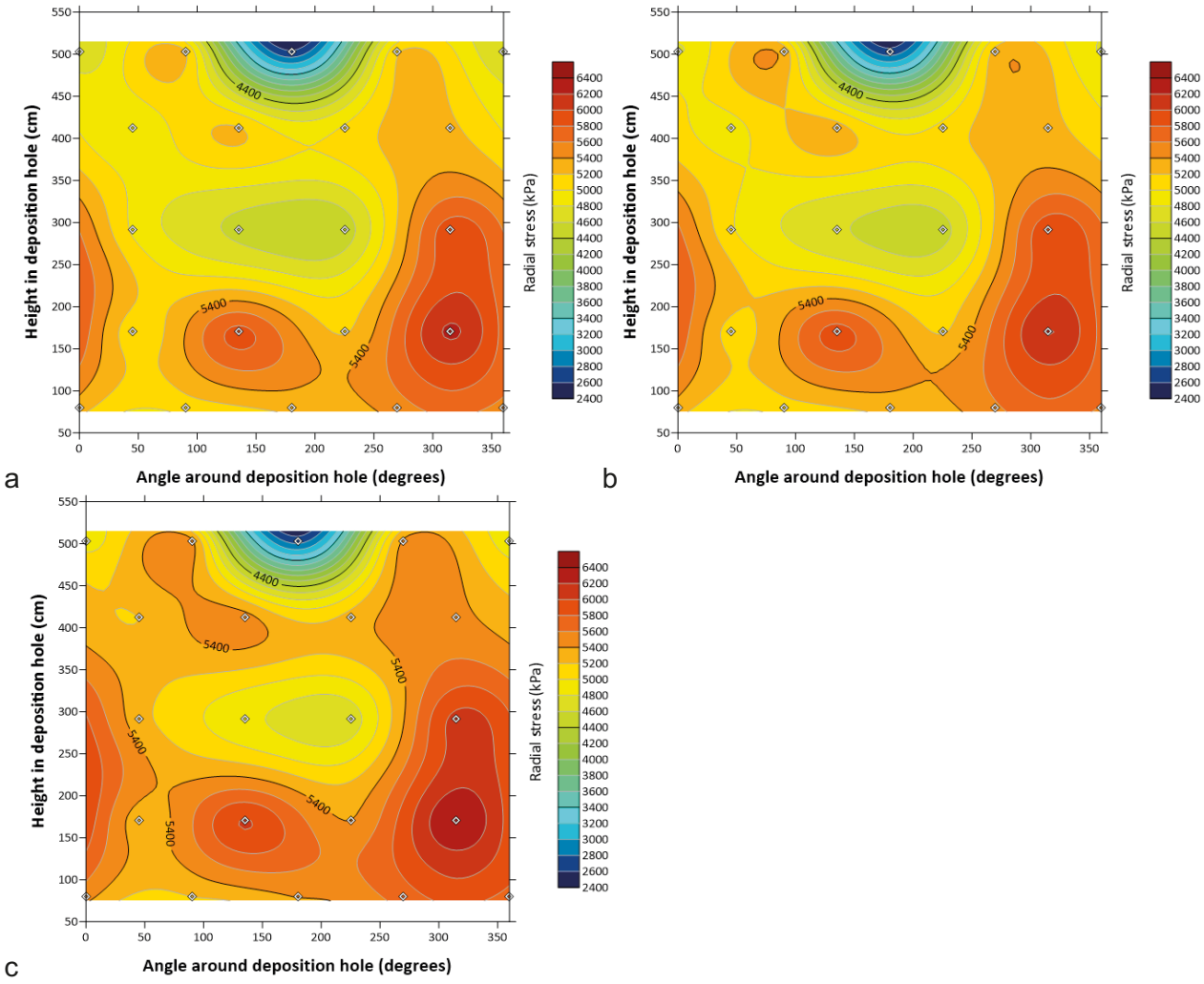

Figure 12-9. *Total stress distribution at the rock face. a) Day 5140.00, b) Day 5250.00, c) Day 5300.00.*

The stress acting on the canister was measured at three locations, as shown in Figure 12-10, and shows a total range of around 2 000 kPa. During Gas Injection Test 5 the average stress only marginally decreased because of annual variation. The data were dominated by the response of the gas injection test. Sensor PC903 showed evidence of gas migration to this location. This will be discussed more in Section 12.3.

Axial stress within the bentonite is shown in Figure 12-11 and was generally complex. Within the deposition hole there was considerable spread of approximately 1 400 kPa within the deposition hole. It should be noted that sensors PB901 and PB902 were below the canister, whereas all other sensors were above. Both above and below the canister there was considerable variation in stress. In contrast to the stresses on the canister, the axial stress within the bentonite above the canister generally increased during the period and showed a degree of cyclicity that was not annual. This feature, which had a cyclicity ~ 50 days, had been previously observed. Axial stress below the canister did not vary and showed less cyclicity. This suggests that the cause of the cyclicity may be an influence from the HRL and was attenuated with depth.

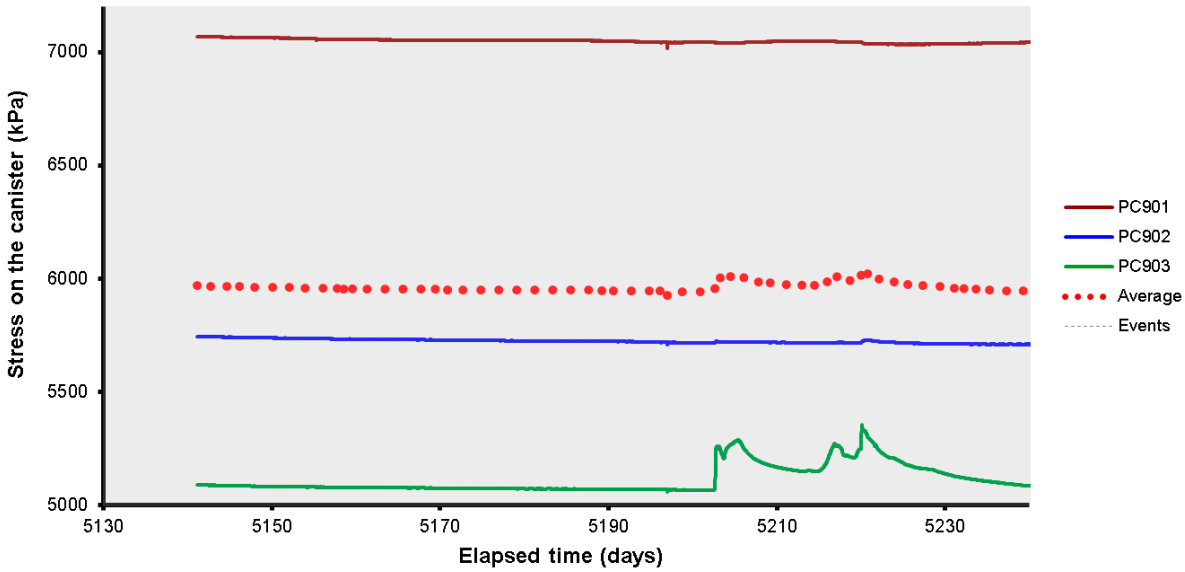

Figure 12-10. Development of axial and radial pressure on the side and base of canister.

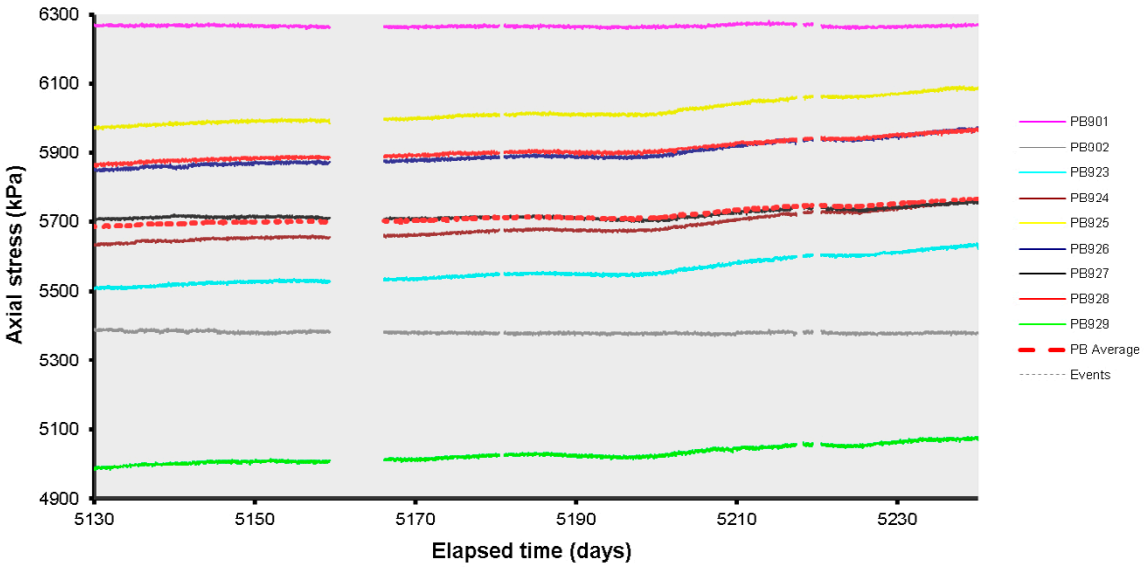

Figure 12-11. Development of axial stress measured at 9 locations within the buffer.

The increase of stress within the bentonite was mirrored in the axial force measured on the lid, as shown in Figure 12-12. During Gas Injection Test 5, axial force on the lid only marginally increased by around 5 kPa and within this variation a cyclicity of around 20–30 days was seen. This was of higher frequency than seen in the axial stress within the bentonite (Figure 12-11). This was likely to derive from temperature variations within the gallery.

A similar trend was seen within the sensors measuring the displacement of the lid, as shown in Figure 12-13a. During Gas Injection Test 5 little variation was seen in lid displacement, with a general small decrease of less than 0.05 mm. However, the canister was seen to vary by about 0.7 mm and showed a complex response that may mirror the gas injection pressure. As described for LP and PB sensors, lid movement showed a higher frequency variation component superimposed upon year-long seasonal variation. Lateral movement of the lid (Figure 12-13b) only showed small movements of approximately a hundredth of a millimetre. It is suspected that the two lateral LVDTs had failed and that the stepped response represents a faulty sensor. As shown, the sensors were not recorded from around Day 5200 onwards.

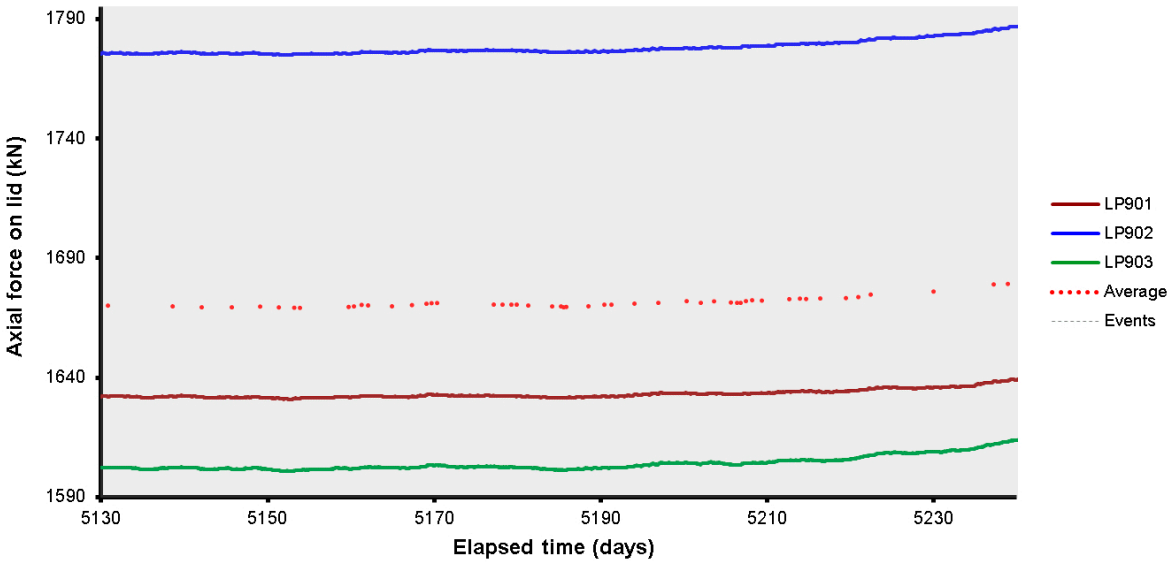

Figure 12-12. *Axial force acting on the steel lid measured by 3 Glötzl load cells attached to separate rock anchors.*

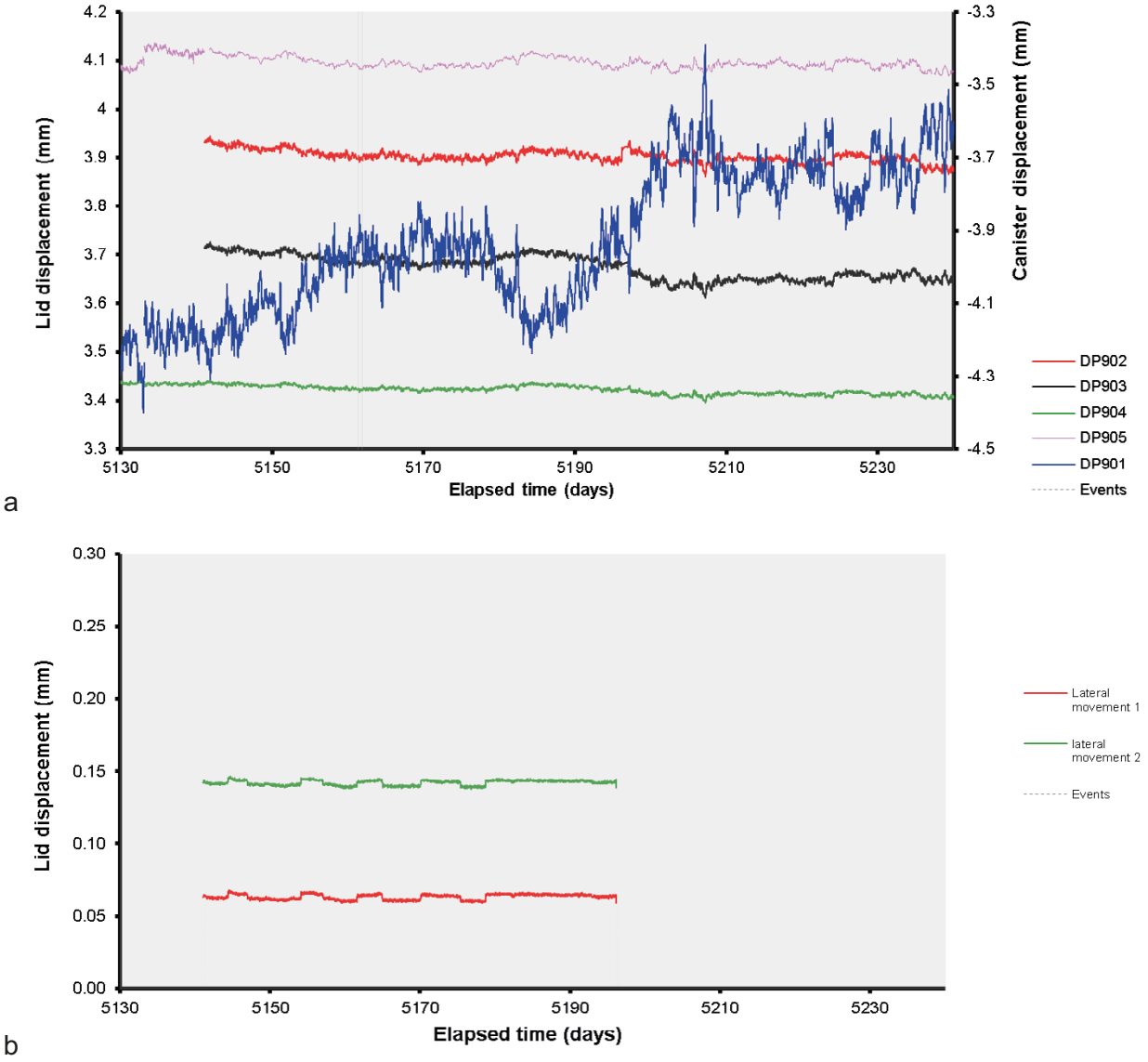

Figure 12-13. *Linear displacement of the steel lid and copper canister (a) and lateral movement of the lid (b). Movements of the lid are measured relative to both the gallery floor and ceiling. Movements of the canister were measured relative to the steel lid.*

Pore pressure away from the deposition hole within the pressure relief hole is shown in Figure 12-14. A small reduction in pressure during Gas Injection Test 5 was seen of between 5 – 15 kPa, with PRH1–3 showing the greatest reduction. The PRH data showed an observed cyclicity of around 40 days.

Temperature was monitored within the Lasgit laboratory & office, the HRL, and the canister. Figure 12-15 shows between Day 5135 and Day 5180 a stepped response was seen, as described for the lateral LVDTs on the canister lid. This suggested that the faulty LVDTs were interfering with the temperature sensors in the data logger, as this stepped behaviour stopped once the lateral LVDTs were removed from the system. It is unlikely that the temperature was stepped in such a way. However, the length of the steps was not coincident and HRL temperature sensors did not show the same behaviour. There was no correlation between the steps in temperature and flow rate of the gas injection pump, which suggests the laboratory temperature did not vary. Taking the steps into consideration, the temperature within the laboratory was generally constant throughout Gas Injection Test 5. The canister decreased in temperature during the stage as a result of annual variation. The only significant temperature variation was seen in the HRL temperature, which increased by 1.5 °C during the test. This may have influenced the observed boundary conditions. The noted 20–30 day and 40-day period of some sensors was not obvious within the HRL temperature sensors.

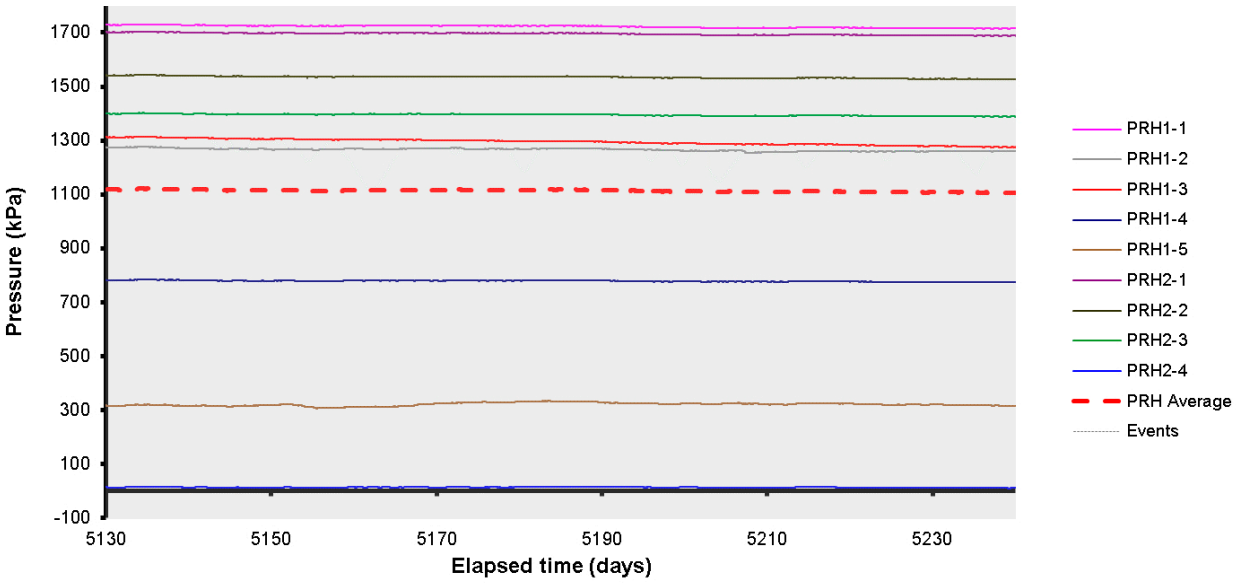

Figure 12-14. *Porewater pressures measured in the packered sections of the pressure relief boreholes.*

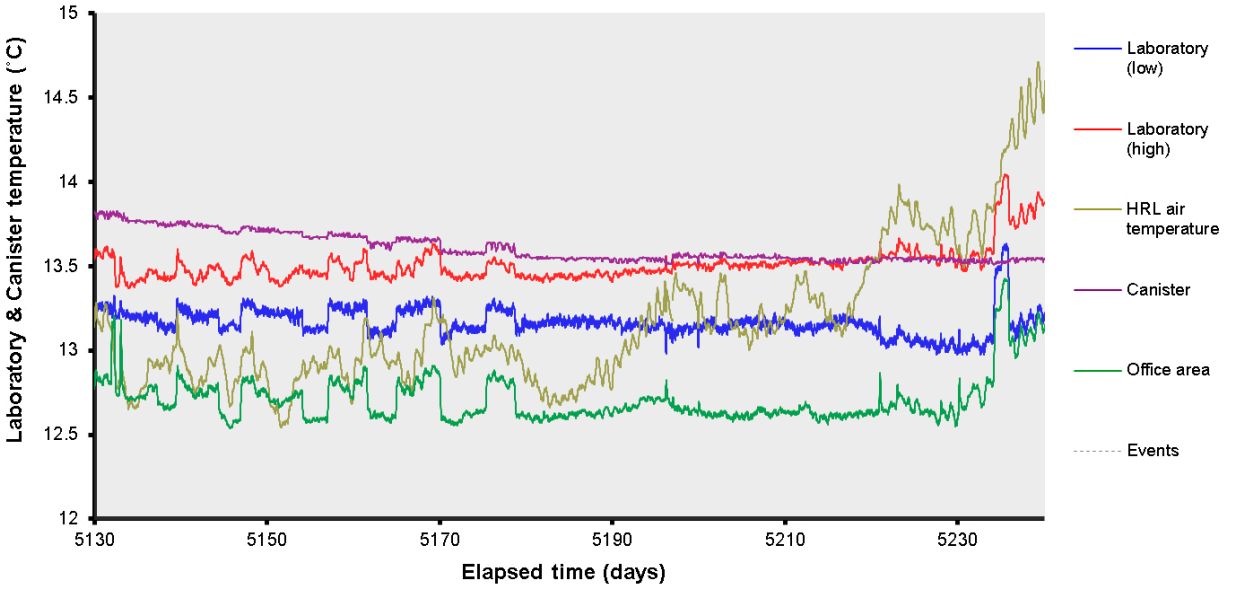

Figure 12-15. *Temperatures recorded in the Gas Laboratory, office, canister, and HRL.*

Figure 12-16 shows the total volume of water pumped into the system during Gas Injection Test 5. No artificial hydration of the filter mats or filters occurred during the test and the data merely shows the flow that occurred during the two-step hydraulic test. Less than 5 ml of water was pumped into the system during Gas Injection Test 5.

Figure 12-17 shows average stresses, pore pressure, and forces observed during Gs Injection Test 5. On the scale shown, all parameters appear constant. The detail of each average shows the following: pore pressure at the rock wall; pore pressure within the pressure relief holes and stress on the canister reduced by small amounts; whilst radial stress on the rock wall; stress within the bentonite; pore pressure in the bentonite; pressure within the canister filters; pressure within the filter mats; and force on the canister lid all showed an increase.

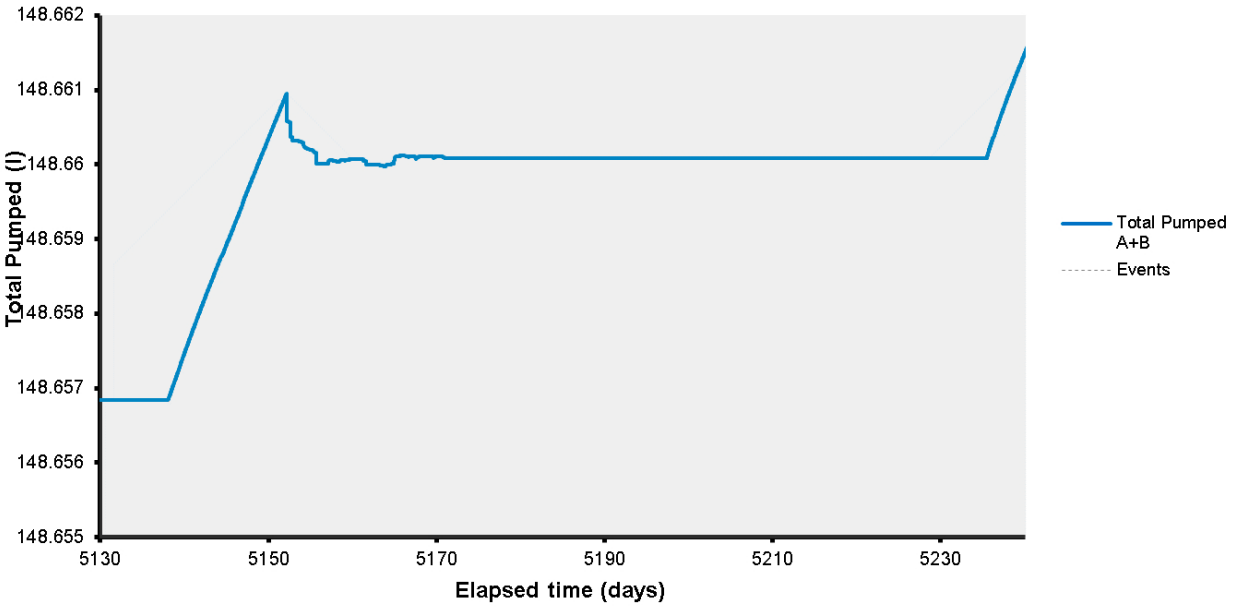

Figure 12-16. *Total pumped during artificial hydration and hydraulic testing.*

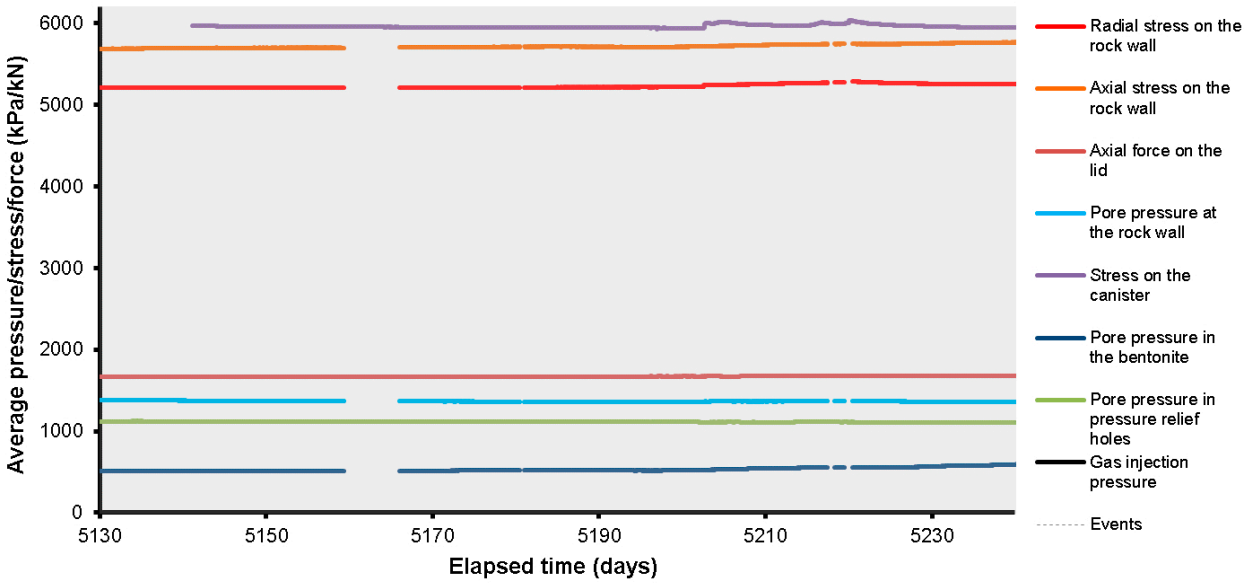

Figure 12-17. *Average pressures, stress, and force observed during the reporting period.*

12.2 Hydraulic test prior and after the gas injection test 5

Figure 12-18 shows the results of the two-stage hydraulic tests, which have been adjusted so that the tests conducted before and after the gas injection test can be compared. Figure 12-18a shows the pore pressure imposed during the test. Figure 12-18b, c and Figure 12-19a show that the high-pressure stage did not result in much flow compared with previous tests, with flow reducing to an asymptote of 3.23×10^{-12} m^3 s^{-1} for the test before the gas test and 2.99×10^{-12} m^3 s^{-1} for the repeat test after gas injection. Figure 12-18b, c and Figure 12-19b show that the low-pressure stage resulted in an initially high outflow in excess of 2×10^{-11} m^3 s^{-1}, which quickly reduced to an asymptote of 1.04×10^{-13} m^3 s^{-1} for the test before the gas test and 2.67×10^{-13} m^3 s^{-1} for the repeat test after gas injection. It should be noted that this flow is still an inflow and may represent an asymptote of zero flow. The low-pressure stage resulted in a much noisier result, but it is clear that the outflow during this stage was considerably lower than the inflow during the high-pressure stage.

The two-stage hydraulic head tests were modelled using the 1-D modelled described in Section 6.4, Figure 12-20 shows the modelled results for the two hydraulic tests. The fit of the data can be seen to be good, although it hasn't perfectly modelled the data. Table 12-1 summarises the calculated values for hydraulic conductivity and specific storage for the two tests.

Figure 12-18c shows that the two tests resulted in asymptote at a similar flow rate for both before- and after-gas injection testing. What varied between the tests was the rate of decay, with the test before the gas injection test reducing to an asymptote quicker than the test conducted afterwards. This would be related to the gas that remained in the buffer near to the injection filter. The asymptote of the data related to the flow properties of the bentonite, while the curvature of the flow related to the storage in the system. After gas injection, there was apparently more storage, but no change in hydraulic flow. This is confirmed in the hydraulic conductivity modelled data, but the specific storage shows that the initial test had higher specific storage. The injection of gas had not resulted in a change in the flow properties of the buffer, but the noise in the repeat test suggests gas was still present.

Table 12-1. Modelling results for the two-stage constant head hydraulic tests conducted during Gas Injection Test 5.

Filter	Radius of the filter (mm)	Step	Fitted hydraulic conductivity (m/s)	Fitted specific storage (m^{-1})	Boundary conditions		Initial conditions	
					p_0 (MPa)	p_L (MPa)	p_{I0} (MPa)	p_{IL} (MPa)
FU910	25	1	Not achieved	Not achieved	4.21	0.63	0.00	0.63
		2	1.63×10^{-12}	8.78×10^{-6}	0.82	0.63	4.21	0.63
		Average	**1.63×10^{-12}**	**8.78×10^{-6}**				
FU910	25	1	Not achieved	Not achieved	4.18	0.63	5.18	0.63
		2	7.80×10^{-13}	5.91×10^{-6}	0.86	0.63	4.18	0.63
		Average	**7.80×10^{-13}**	**5.91×10^{-6}**				

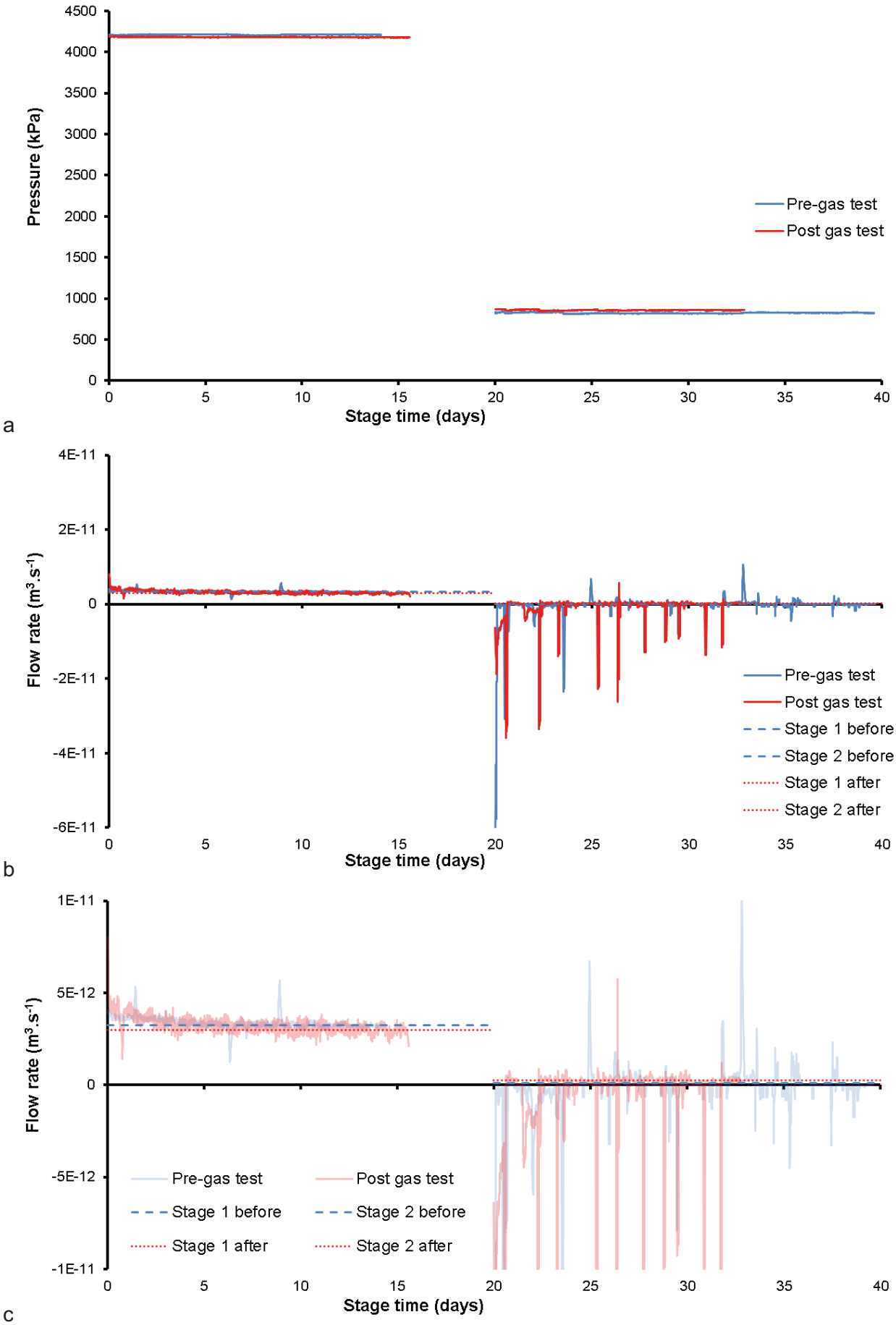

Figure 12-18. *Two-stage constant head hydraulic tests conducted during Gas Injection Test 5. a) Pressure of the injection fluid; b) Flow response; c) Detail of flow response.*

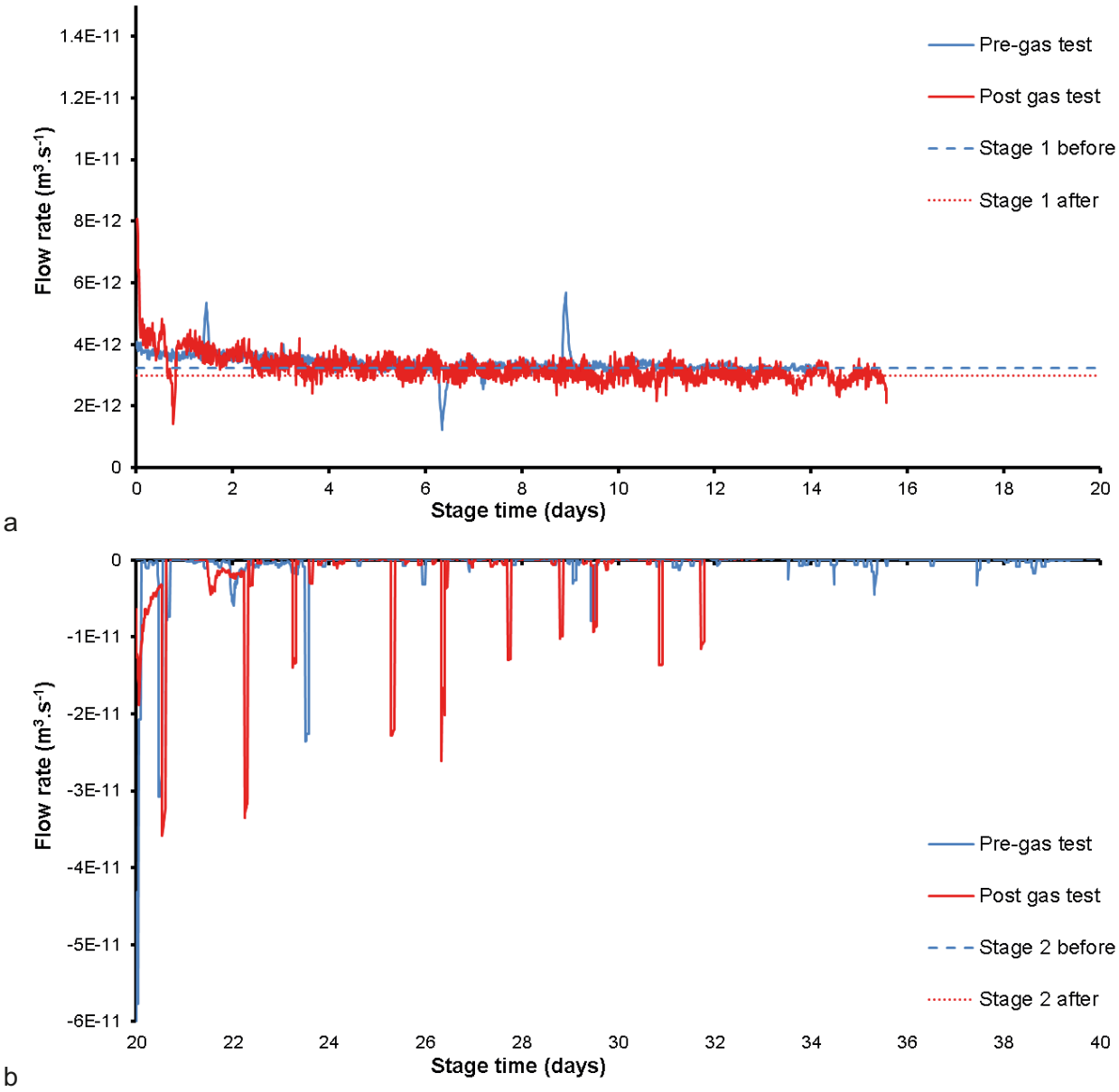

Figure 12-19. *Detail of the flow into the clay during the two-stage constant head hydraulic tests conducted during Gas Injection Test 5. a) High-pressure stage; b) Low pressure stage.*

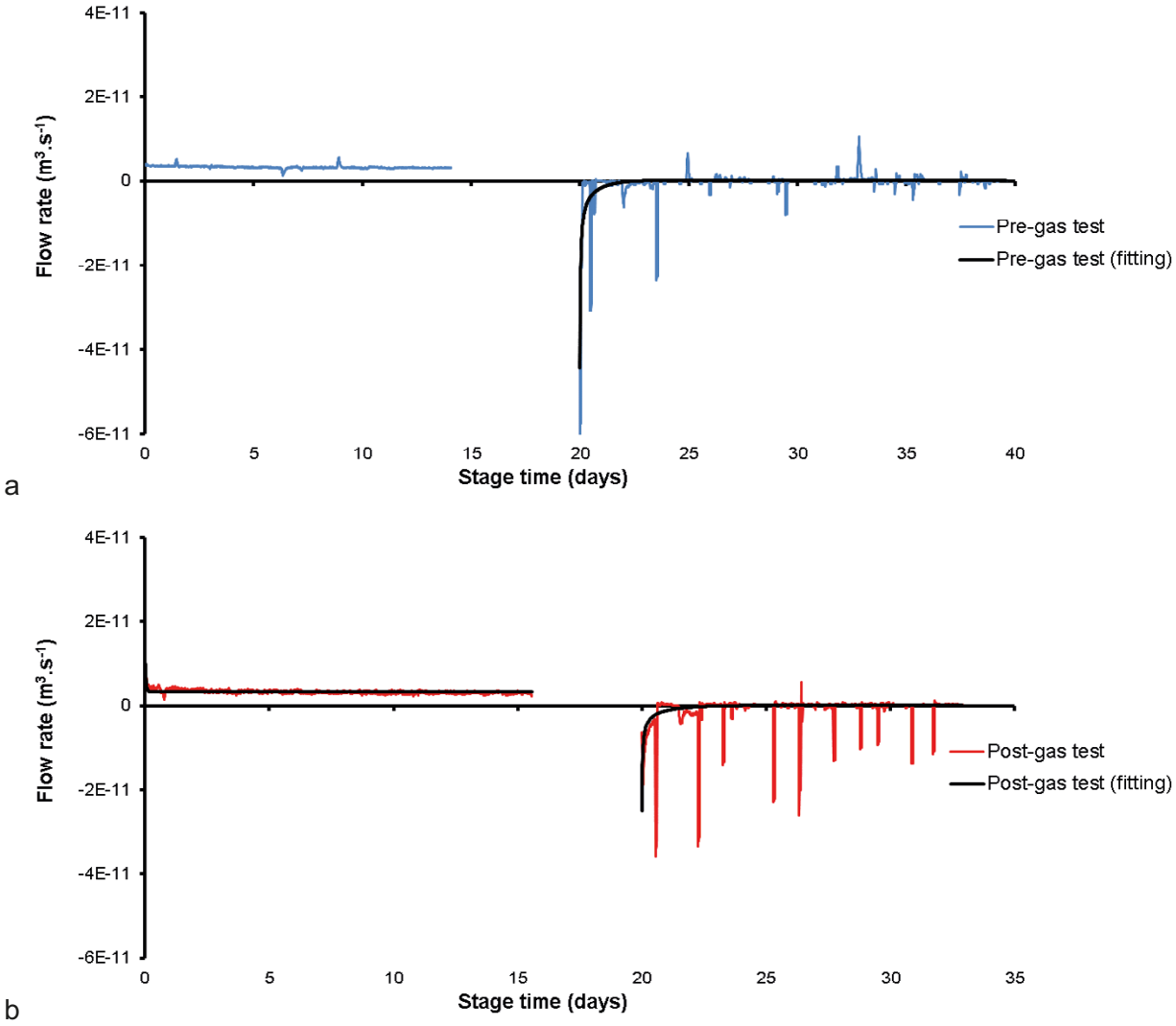

Figure 12-20. *Modelled results for the two-stage constant head hydraulic tests conducted during Gas Injection Test 5. a) Pre-gas test; b) Post-gas test.*

12.3 Gas injection test 5

A limited time period was available to perform the last two gas injection tests. This meant that Gas Injection Test 5 was conducted slightly different to the previous gas injection tests. Previously, gas pressure within the injection filter was raised from the natural pore fluid pressure at that locality to gas entry pressure in four constant-injection stages. In all previous tests, gas entry had occurred at a gas pressure approximately equal to the local stress conditions at the injection locality. It was therefore reasonable to start gas injection at a pressure close to the local stress. There was no reason to suspect that the gas entry pressure would reduce significantly from previous tests. Therefore, the single gas injection stage conducted in Gas Injection Test 5 was the same as would have been the fourth stage had time allowed.

Approximately 4200 ml of helium was added to the interface vessel at a starting pressure of 4230 kPa. The injection filter was thoroughly flushed of water using pressurised helium and the drain from filter FU910. Once flushed, it was common for flow to take a few days to stabilise as gas went into solution and any remaining water within the filter was expelled into the bentonite. The gas injection ramp was started at Day 5183.26 (24th April 2019) by the injection of water into the base of the interface vessel at a rate of 2.1 ml h^{-1}. Figure 12-21 shows the response of predicted and observed gas pressure. The prediction derives from the ideal gas law. A close approximation can be seen. Although a slow process, care was taken to determine the starting volume of gas during the filling of gas and showed an estimated volume of 4231.2 ml. Figure 12-22 shows the difference between the predicted and observed gas pressures. This can be used to refine the estimate of the starting volume, but in this case was not necessary as the estimated volume was good. This graph shows an unexpected response at Day 5192.65 when the gas pressure instantaneously increased, meaning that the difference went from being negative to positive. This suggests movement of the buffer and the closure of void-space. The pressure difference was seen to start increasing at Day 5196.20. This may represent the first evidence of localised gas entry and occurred at a gas pressure of 4920 kPa. Gas pressure continued to increase until Day 5202.57, when the difference between predicted and observed changed significantly. This occurred at a gas pressure of 5347 kPa. This shows that there was 6.4 days between the first evidence of gas entry and peak pressure, representing a difference in gas pressure of 427 kPa. At peak pressure, gas pressured reduced by about 185 kPa.

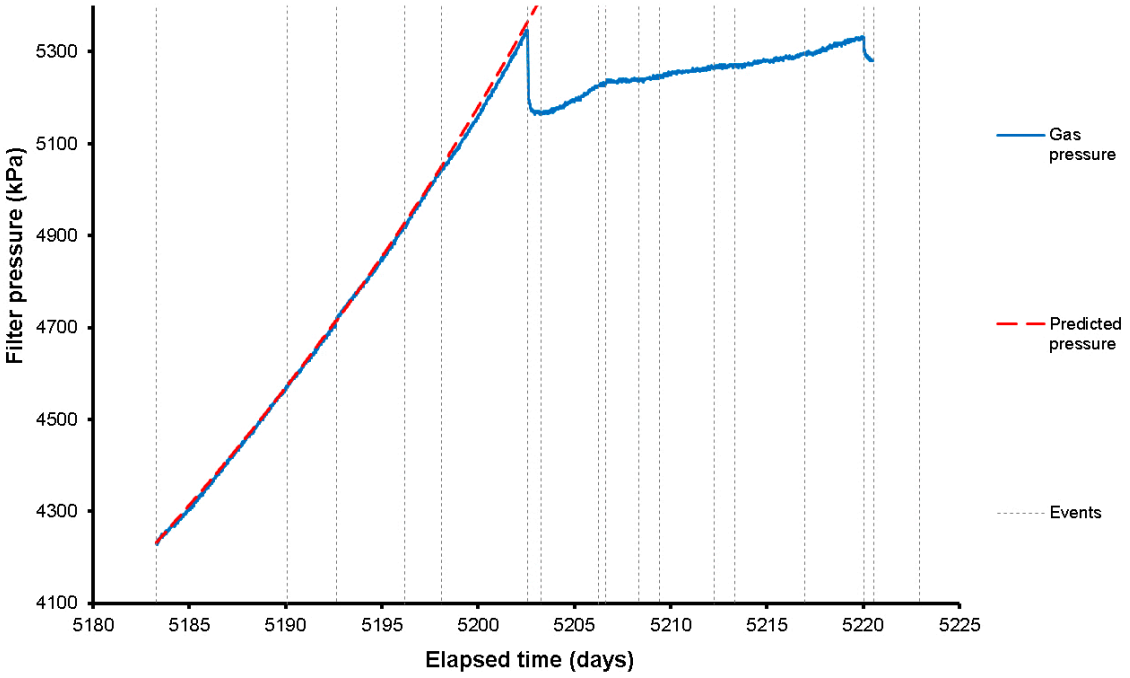

Figure 12-21. *Recorded and predicted gas pressure during Gas Injection Test 5.*

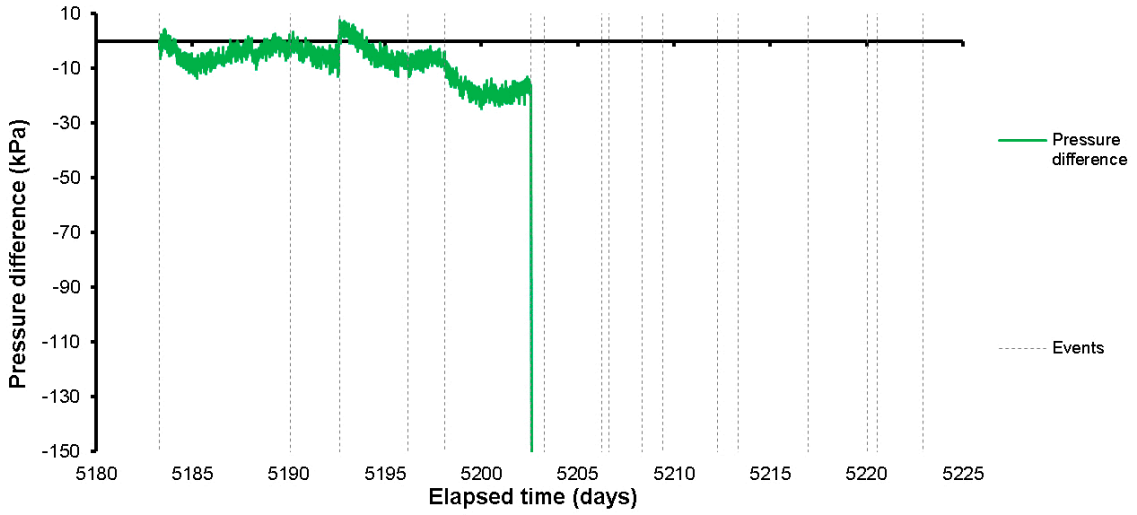

Figure 12-22. *Difference between recorded and predicted pressure during Gas Injection Test 5. This can be used to estimate the volume of gas during a constant flow gas compression stage.*

Figure 12-23 shows the flow of gas into the system and into the clay at STP. Up until the first evidence of gas entry, average flow into the clay was 2.06×10^{-9} m^3 s^{-1}. At peak gas pressure, flow greatly increased, giving a peak flowrate of 4.12×10^{-6} m^3 s^{-1} (note: data shown in Figure 12-23 is time averaged). The peak in flow was short-lived with flow into the clay reducing to equal the flow into the system within 0.4 days (9 hours). Figure 12-24 shows the volume of gas pumped into the clay. It shows that 0.24 mol entered the clay up until peak gas pressure. During the initial pressure drop following peak pressure, around 0.25 mol entered the buffer. In total, 2.19 mol entered the clay following peak pressure.

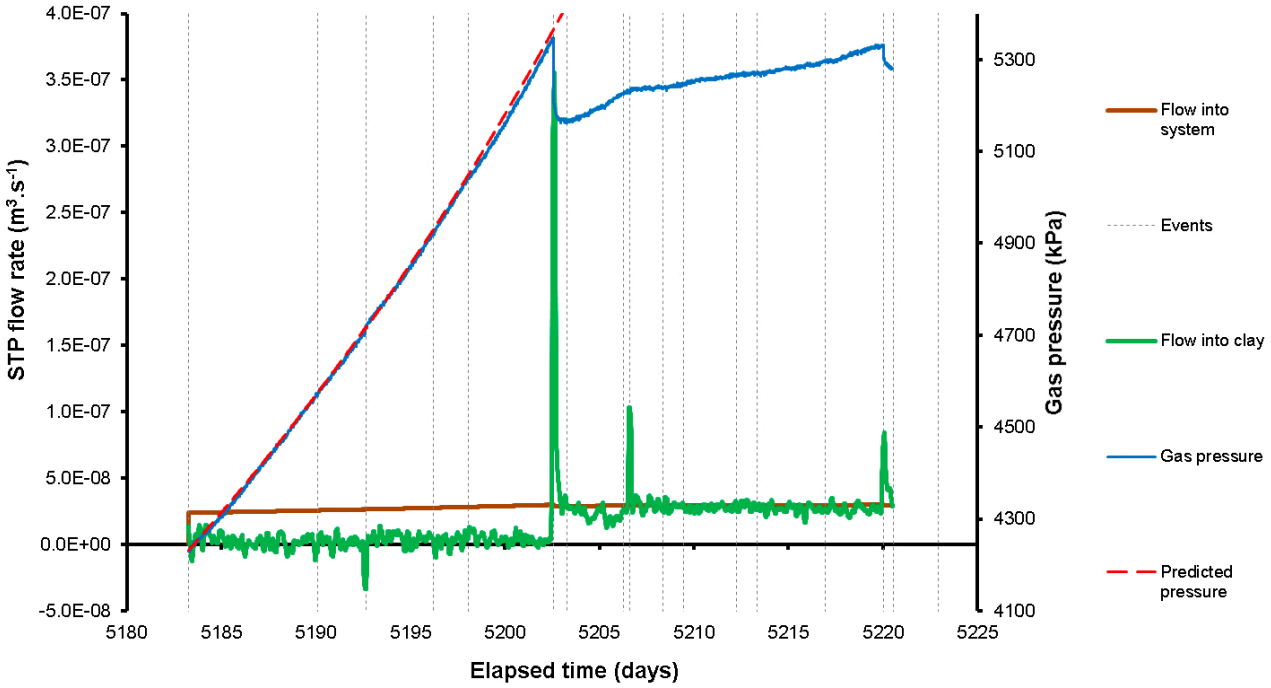

Figure 12-23. *Flow of gas into the system and the clay during Gas Injection Test 5.*

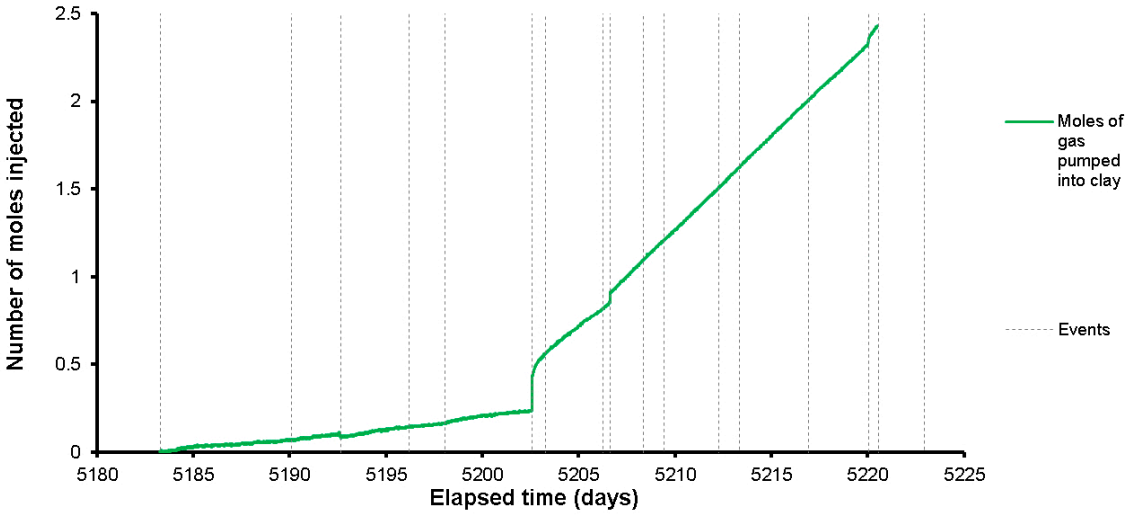

Figure 12-24. *Volume of gas pumped into the clay during Gas Injection Test 5.*

Figure 12-25 shows the flow data in more detail around the time of peak pressure and subsequent gas movement within the buffer. Flow into the clay showed similar behaviour to previous tests. Following the initial peak in flow, the response reduced to approximate the flow into the system. The detail shown in Figure 12-25 shows that the flow into the clay reduced to be lower than the flow into the system, before recovering. This had been seen in previous tests. When flow into the clay returned to equal flow into the system at approximately Day 5206.60 a second peak in flow was seen. This second flow peak resulted in a flow of 1.47×10^{-6} m^3 s^{-1}. In the pressure response this was seen as a change in slope, following which the pressure remained relatively constant. This suggests that stable pathway migration had occurred. During this time flow into the system approximately equalled flow into the clay. Figure 12-23 shows that a third peak in flow occurred at Day 5220.05 at 7.05×10^{-7} m^3 s^{-1}. Following this peak, the gas pressure decreased, suggesting considerable pathway growth or that gas had found a way out of the deposition hole. Figure 12-26 shows a plot of the peak gas flow for the three events noted in Gas Injection Test 5. This suggests a power law decrease in initial flow rate for each event, although the relationship would be clearer if more events had been observed.

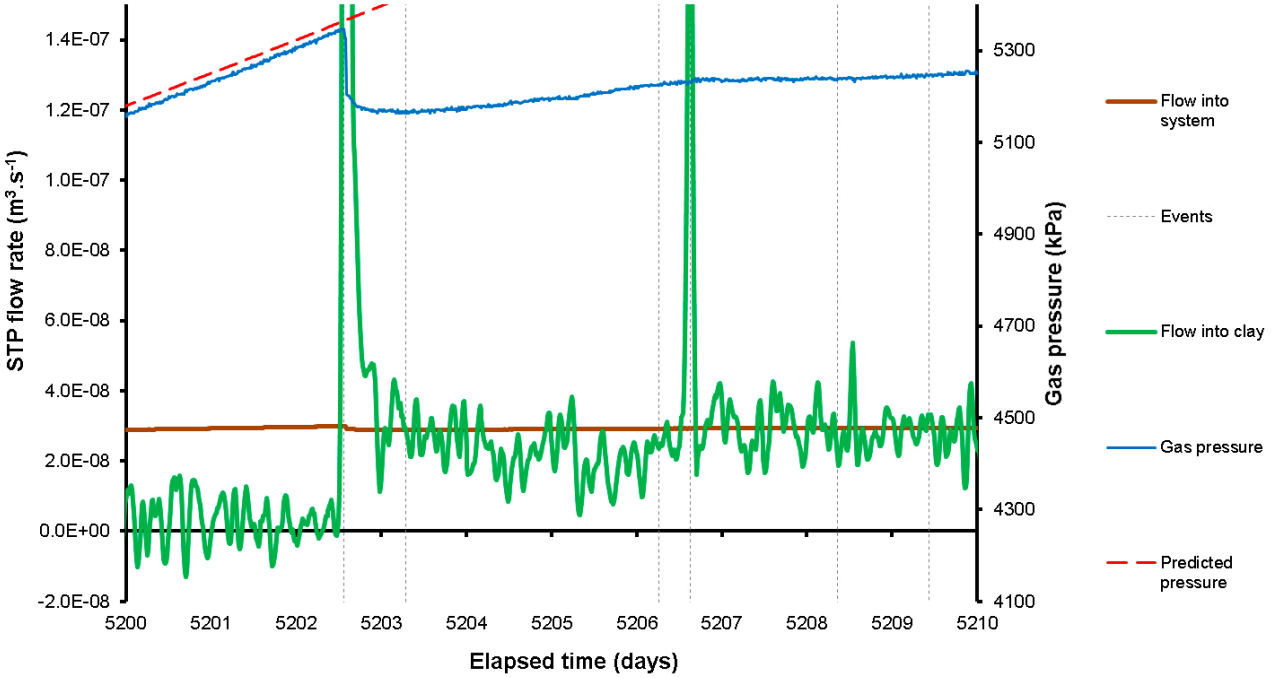

Figure 12-25. *Detail of the flow of gas into the clay and the system around the time of gas entry during Gas Injection Test 5.*

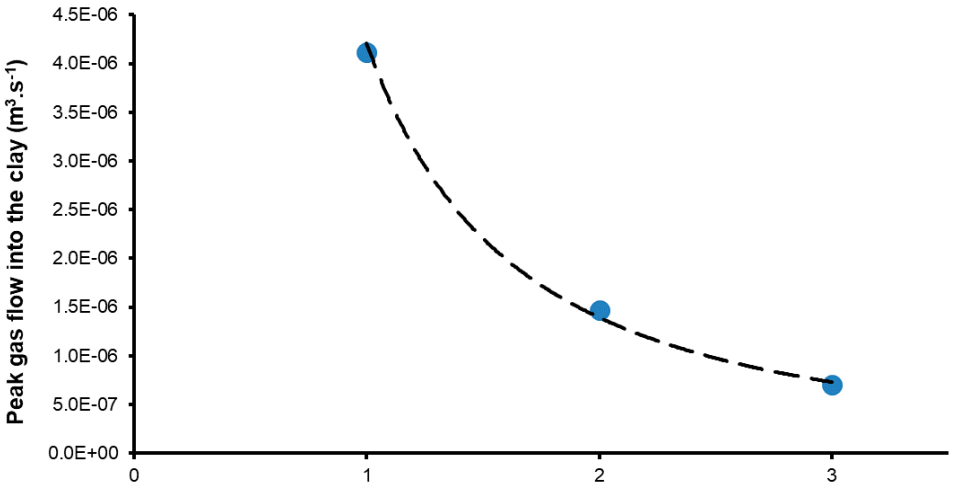

Figure 12-26. *Magnitude of the initial flow into the clay for the three events highlighted in Gas Injection Test 5.*

Figure 12-27a shows the response of pore fluid pressure at the deposition hole wall. Gas peak pressure occurred at Day 5202.57, which resulted in increases in pore pressure at UR914, UR922, UR915, UR918, and UR913 of 93, 66, 62, 45, and 15 kPa respectively. It should be noted that UR914 reached a peak following a small increase in pore pressure of ~15 kPa. Most of these locations experienced a steep increase in pressure, followed by a slow decay. The exception was UR922, which took 16.8 days to reach its peak in a series of 5 steps. Sensor UR921 also greatly increased in pressure by 82 kPa, but unlike the other locations this occurred slowly and gradually. All sensors showed a decay in pore pressure after a potential increase at a time when the Geokon logger was not working, as seen from Day 5220.50.

At the time of gas peak pressure at Day 5202.57, several of the radial stress sensors at the rock wall showed a variation (Figure 12-27b). The largest change was seen in PR915, with a 150 kPa increase. Notable changes were also seen in PR917, PR916, PR918, and PR922, with variations of 62, 61, 41, and 35 kPa respectively. Several other sensors showed a step too, but of lower amplitude. Following gas entry, PR915, PR917, PR916, and PR918 continued to increase, at least until Day 5206.26, when the secondary gas flow peak occurred. At this time, PR919 increased for a second time and over the subsequent 12 days increased by a further 200 kPa. As a result of the change in PR919, PR916 and PR917 started to decrease in magnitude. Unfortunately, the Geokon logger failed to record the time of the third gas peak at Day 5220.04. However, this event can be seen to cause all of the radial stress sensors shown in Figure 12-27b to slowly decrease. This suggests that gas had escaped the deposition hole, resulting in relief of stress within the system.

The radial and axial stresses measured on the canister surface showed direct and indirect evidence of gas movement (Figure 12-27c). At the time of peak gas pressure at Day 5202.57, the stress at PC903 increased by around 200 kPa. The magnitude of the stress at this time suggests that gas had migrated directly to the sensor. A much smaller response was seen in PC902, which was likely to be a hydrodynamic effect. A small decrease was seen at this time in PC901. The response in PC903 was complex. It shows periods of stress decrease and stress increase. The first peak corresponded with the gas peak pressure, the second occurred slightly before the second peak in gas flow into the clay. The third occurred at Day 5216.95, which corresponded with the start in increase in UR903 and PR912. The fourth peak in PC903 corresponded with the third peak in gas flow and the start of gas pressure reduction. At this time, PC902 started to increase and PC901 decrease.

Figure 12-27d shows the changes seen in pore pressure within the bentonite buffer. This was quite complex with many events of pore pressure increase and decrease that correspond with the events described above.

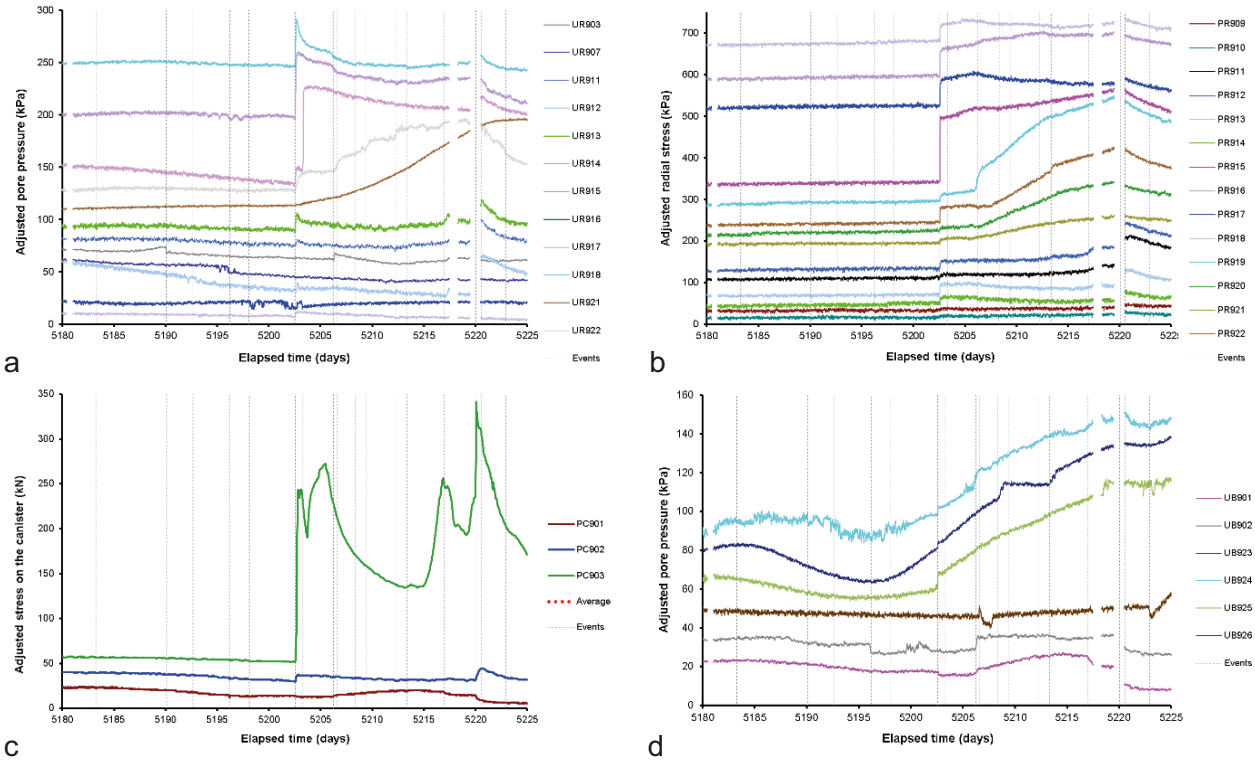

Figure 12-27. *Example of sensor response around the time of gas entry during Gas Injection Test 5. All parameters have been transposed about the y-axis to emphasise the detail observed. a) Pore pressure at the deposition wall; b) Radial stress on the deposition wall; c) stress on the canister surface; d) pore pressure within the bentonite.*

Figure 12-28 shows the pore pressure at the deposition hole wall and how this varied during Gas Injection Test 5. Figure 12-28a shows the pore pressure distribution just prior to peak gas pressure at Day 5201.20. This shows that opposite the gas injection filter, highlighted in red, the system had a low in pore pressure, with a high in pore pressure much lower in the deposition hole on the opposite side. Figure 12-28b shows how pore pressure changed between Day 5201.20 and Day 5202.67, i.e. the variation as a result of gas entry. This showed a little change opposite the point of injection, which generated a high in pore pressure not 180° around the deposition hole, but in the direction of 345° (injection filter was at 90°). At Day 5204.46 the pore pressure had changed considerably. The peak seen at 345° had subsided, but pore pressure at the midplane at 270 ° had increased. By Day 5220.54 a band of decreased pore pressure was seen towards the base of the canister at ~150 cm height all around the canister. The raised region of pore pressure still centred on 270° at 291.6 cm height, i.e. at UR914. The contour map of pore pressure at the deposition hole wall suggests that the increase in pore pressure was a response to gas movement first along the upper array and then to the midplane of the canister.

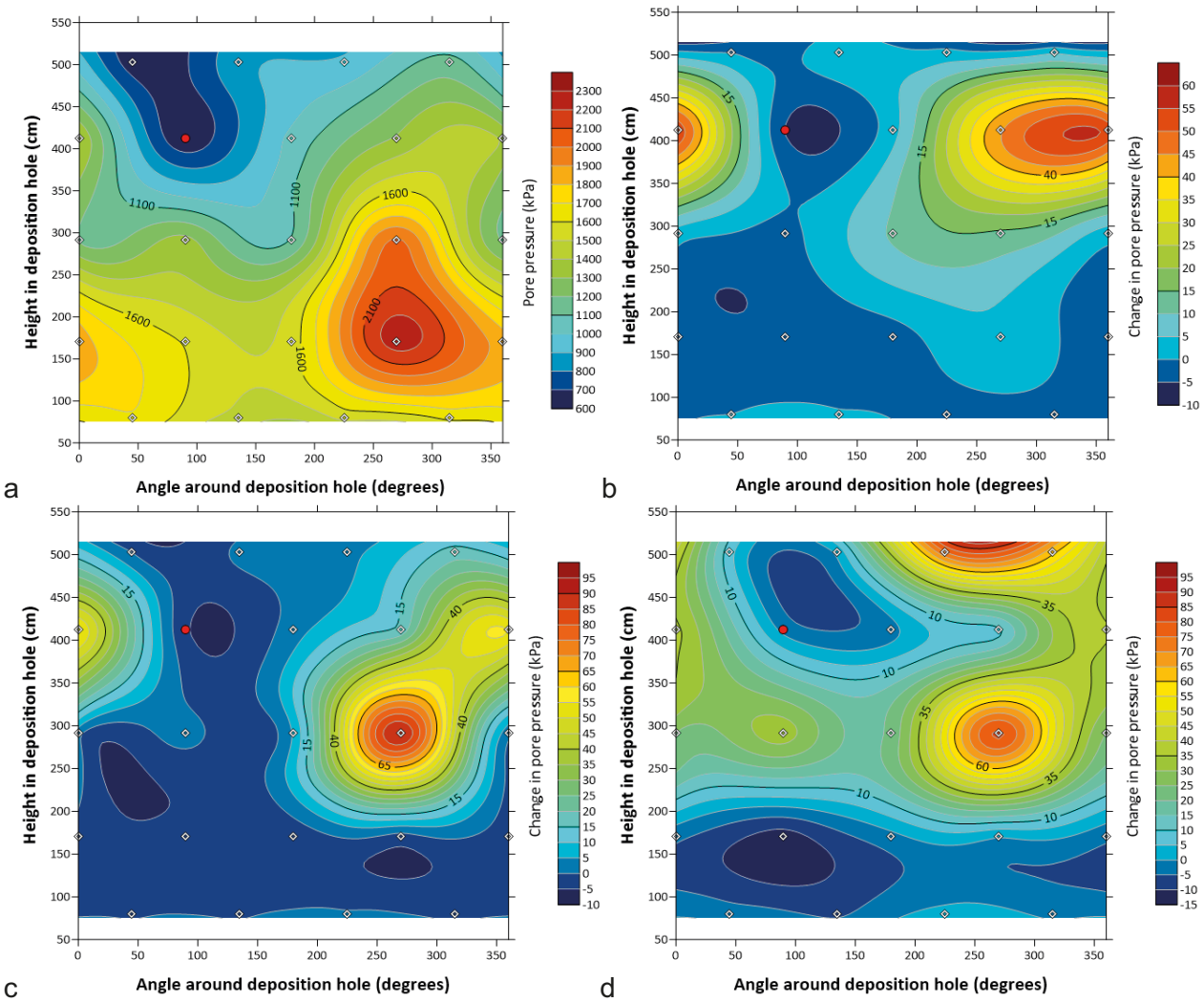

Figure 12-28. *Pore pressure distribution at the deposition hole wall at times around gas entry during Gas Injection Test 5. a) Day 5201.20 (total pore pressure); b) Day 5202.67 (change in pore pressure); c) Day 5204.46 (change in pore pressure); d) Day 5220.54 (change in pore pressure).* ***Note:*** *the location of the injection filter is shown as a red circle.*

The distribution of radial stress on the deposition hole wall is shown in Figure 12-29. The map of stress prior to peak gas pressure is shown in Figure 12-29a at Day 5201.20. This shows that near the gas injection filter radial stress was only moderate compared with the full area. Stress was greatest towards the bottom of the deposition hole in a band at around 150 cm height all around the canister. A band of high radial stress was also seen vertically, centred on 315°. A stress gradient was observed whereby the least stress was generally seen towards the top of the deposition hole, with stress increasing with depth. Figure 12-29b shows the change in radial stress from Day 5291.20 to Day 5202.67. Radial stress increased at the same level as the injection filter, with the greatest increase anticlockwise of the injection filter. Figure 12-29c shows that little variation in this response was seen at Day 5204.46, in contrast to the changes seen in pore fluid pressure described above at this time. By Day 5220.54 (Figure 12-29d) stress at the bottom of the deposition hole was generally unchanged. Stress had increased above the injection level, but still remained high at that level. This suggests that stresses increased above the injection interval.

Comparing the observations of pore pressure and radial stress during the gas injection time shows some differences. Radial stress remained relatively static with an increase above the injection interval, suggesting gas propagation in that direction. However, the pore pressure response suggests that the gas moved around the canister surface and then downwards.

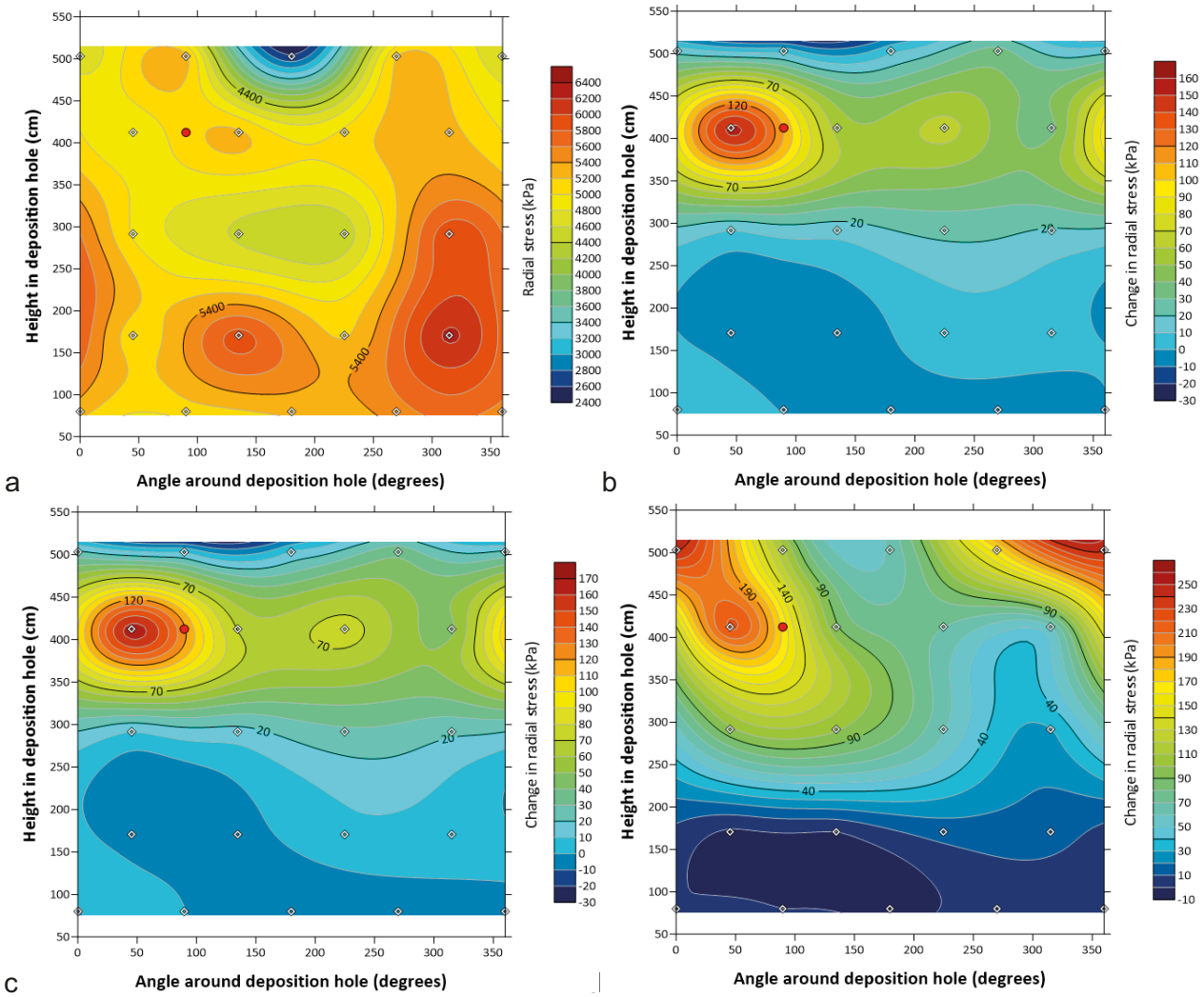

Figure 12-29. *Distribution of radial stress at the deposition hole wall at times around gas entry during Gas Test 5. a) Day 5201.20 (total stress); b) Day 5202.67 (change in stress); c) Day 5204.46 (change in stress); d) Day 5220.54 (change in stress).* ***Note:*** *the location of the injection filter is shown as a red circle.*

Figure 12-30 and Figure 12-31 shows sensor locations that show direct movement of gas. Gas pressure increased during gas injection at FU910 until peak pressure occurred at Day 5202.57. At this time, pressure at FU909 increased. There was no slow increase of pressure at FU909, it showed instantaneous increase. This suggests that the reduction in gas pressure occurred as gas migrated from FU910 to FU909, some 90° around the canister surface. At this time, PC903 also showed an increase that was interpreted to be direct gas flow to this location. However, the increase in stress at the location was slow which suggests an evolving pathway forming to reach this location. Stress sensor PC903 was on section 8, 60 cm below the injection filter and 45° around the canister. This shows that gas moved both clockwise around the canister to FU909 and anti-clockwise and downwards towards PC903.

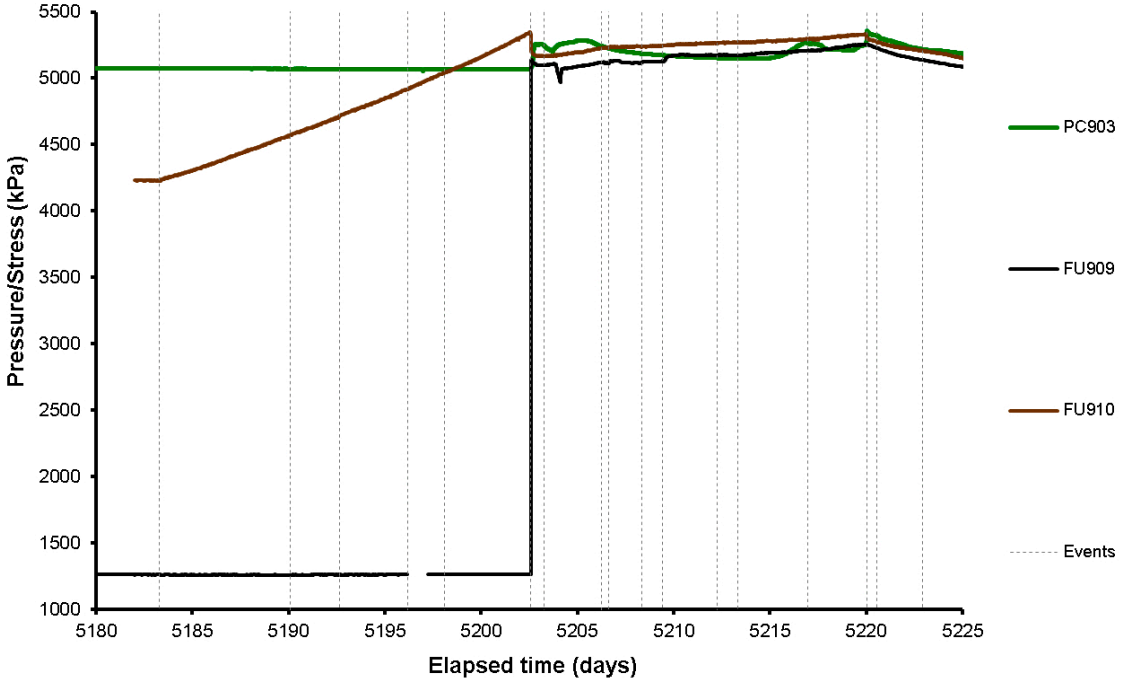

Figure 12-30. *Detail of sensors that show evidence of gas pressurisation during Gas Injection Test 5.*

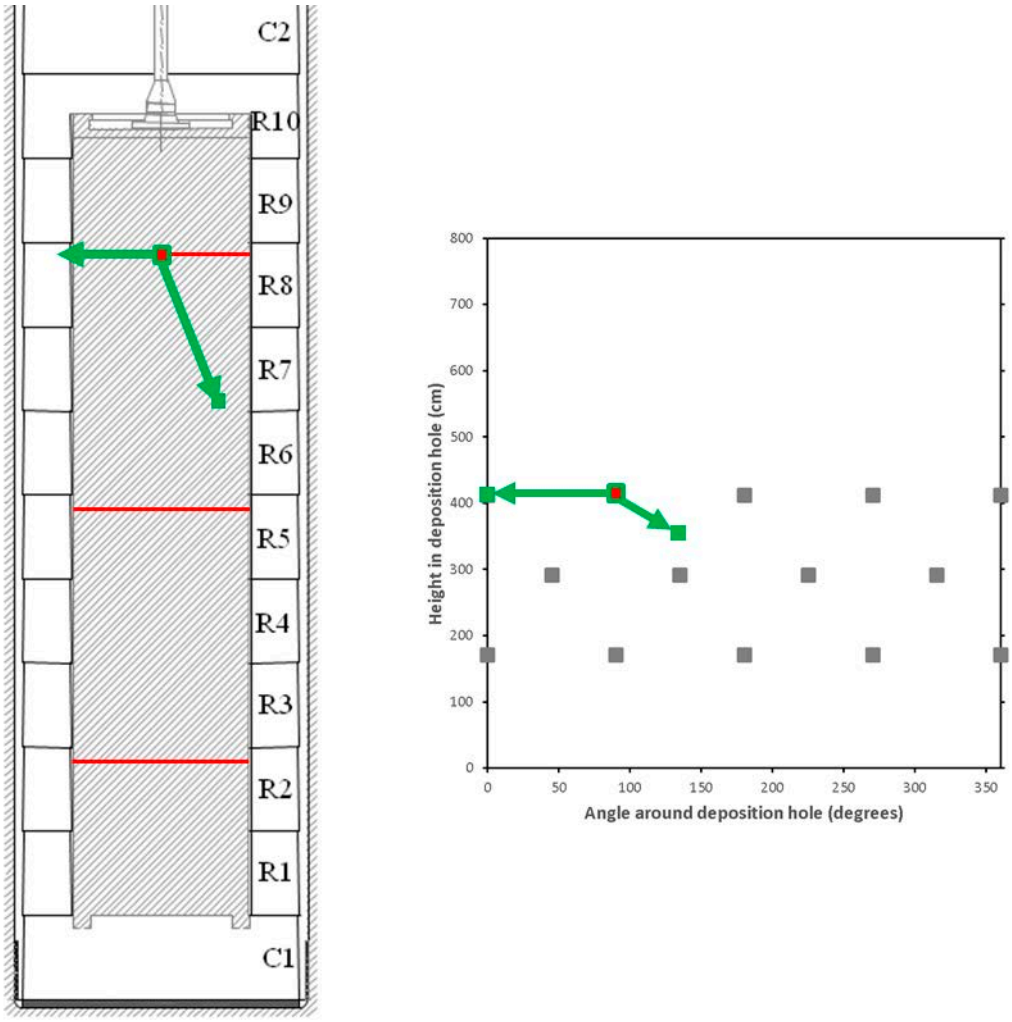

Figure 12-31. *Schematic of the direction of gas flow during Gas Test 5 in upper filter FU910.*

12.4 Summary of Gas Injection Test 5

Gas Injection Test 5 was a relatively short test and was the second test conducted using filter FU910.

1) Day 5196.20 :The first evidence of gas entering the clay at a gas pressure of 4 920 kPa.

2) Day 5202.57: Gas pressure continued to increased and reached a peak at a gas pressure of 5 347 kPa. Up until peak gas pressure, flow into the clay averaged 2.06×10^{-9} m^3 s^{-1}. A decrease in gas pressure of 185 kPa was observed as 0.25 mol He entered the clay at a peak flow rate of 4.12×10^{-6} m^3 s^{-1}. Gas directly travelled 90° clockwise around the canister to filter FU909 and slowly towards PC903, 60 cm below the injection filter and 45° anticlockwise around the canister. Gas entry resulted in an increase in radial stress near to the gas injection point and increased radial stress all around the canister at the level of the injection filter. In contrast, the pore pressure at the deposition hole wall showed very little variation at the injection filter and instead showed an increase opposite FU909. From here, pore pressure generally moved towards the mid-plane at 270°.

3) Day 5206.63: Gas flow into the clay showed a second peak when flow peaked at 1.47×10^{-6} m^3 s^{-1} and 0.061 mol He entered the clay. This event corresponds with a reduction in pressure seen at PC903 and a change in slope of the gas injection pressure to give relatively constant pressure, suggesting that a new pathway had formed.

4) Day 5220.94: A third flow event was seen, which resulted in the reduction of gas injection pressure, and both pore pressure and radial stress at the deposition hole wall. Flow into the clay peaked at 7.05×10^{-7} m^3 s^{-1}, with 0.027 mol He entering the clay. This is interpreted to be the break-through of gas from the buffer into the surrounding rock.

Each successive flow event saw a reduction in peak flow. Therefore, the three flow events are interpreted as:

1) gas entering the clay and migrating to filter FU909 and PC903;

2) movement of gas towards the mid-plane of the deposition hole;

3) the exit of gas from the deposition hole through an interface between blocks.

13 Gas Injection Test 6 (Day 5138 – 5264)

The ninth significant stage of the Lasgit experiment started on Day 5138.09 (26th February 2019) and was completed at Day 5305.91 (13th August 2019); a total stage time of 167.87 days. **Note:** unlike in previous tests, overlap existed between gas injection test 5, gas injection test 6, and the full canister test stages.

Before the Full Canister Test, it was decided to conduct one final test each in filters FL903 and FU910 to see if the properties of the bentonite had altered in the long-time gap since the previous gas injection tests. With limited time to conduct the tests, there was a clear overlap in time of the Gas Injection Test 5 and Gas Injection Test 6. This overlap was mainly in the timing of the hydraulic tests before and after the gas injection stage. The second of the gas injection tests prior to the Full Canister Test was conducted in filter FL903, 1 947 days or 5.3 years since the end of the previous gas injection test in that filter. Gas Injection Test 6 investigated whether gas properties of the bentonite changed with time and if gas migration was the same as previously observed. Figure 13-1 shows the plan for the test period and clearly shows the overlap in Gas Injection Tests 5 and 6. Limited hydration occurred during this stage during the hydraulic testing of the test filters.

Gas Injection Test 6 comprised of three stages (Figure 13-2); 1) a two-stage hydraulic test to determine the hydraulic properties of the bentonite at filter FL903; 2) a single-stage gas injection ramp to achieve gas entry at filter FL903; 3) a repeat hydraulic test.

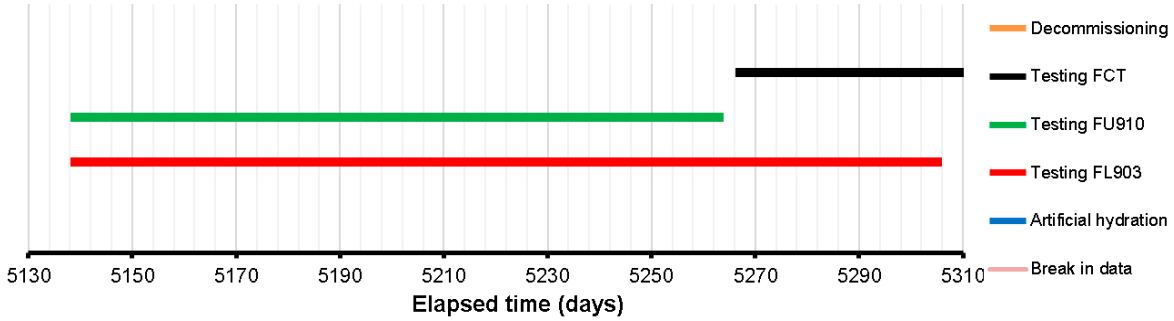

Figure 13-1. *Test stages of the Lasgit experiment showing what was conducted during Gas Injection Test 6.*

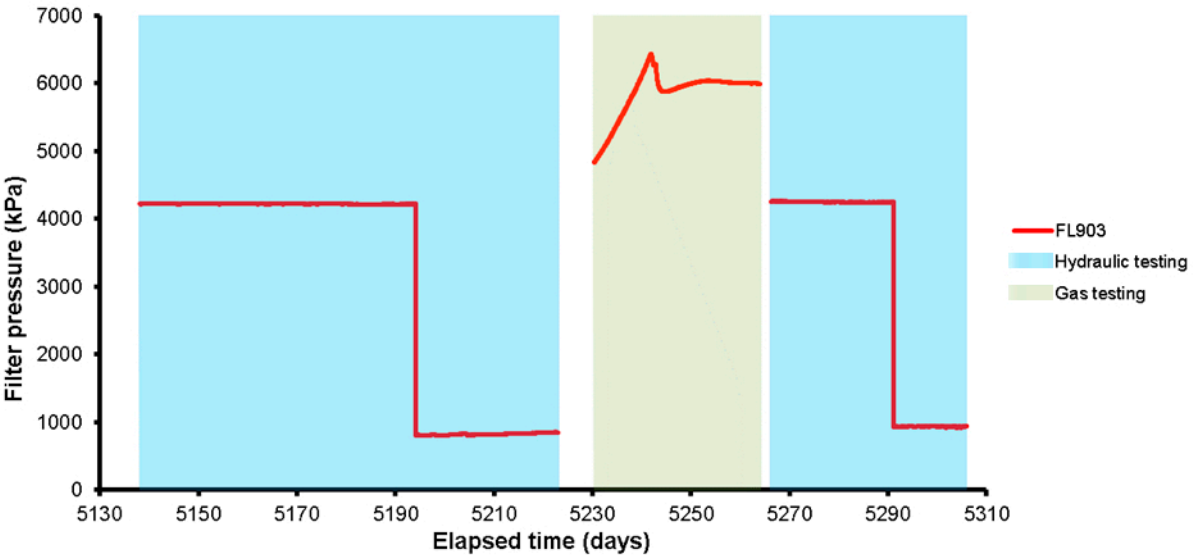

Figure 13-2. *The filter pressure of FL903 during Gas Injection Test 6. A two-stage hydraulic test was conducted prior to and following a single stage gas injection test.* ***Note:*** *blue shading shows periods of hydraulic testing, green shows gas testing.*

13.1 Description of the field parameters during the period

Before describing the gas injection test, the field parameters will be described (boundary conditions). Because of the overlap between Gas Injection Tests 5 and 6, the boundary conditions up to Day 5240 have already been described in Section 12.1, with the current section describing up to Day 5310. **Note:** The grey areas displayed in the graphs show periods when artificial hydration was not occurring. As artificial hydration was abandoned before the previous stage, all graphs are shown with a full grey background, signifying no artificial hydration.

Figure 13-3 shows the pore fluid pressure of the filter mats. Throughout Gas Injection Test 6 there was no artificial hydration of the filter mats and therefore the pressures recorded represent the equilibrated pore fluid pressure. Filter mat FR901 on the rock wall showed the highest pressure of approximately 1 600 kPa, this filter being at the bottom of the deposition hole. In contrast, filter mat FR902 on the rock wall showed the lowest pore pressure of only approximately 100 kPa. This filter was towards the top of the deposition hole. These differences show the heterogeneity of pore pressure and fracturing in the deposition hole wall. Over the 168-day Gas Injection Test 6 there was little variation in pore pressure at the rock wall, except in FB903. At Day 5263.95 filter mat FB903 was seen to drop by around 400 kPa. This happened during a site visit to set up the system for the Full Canister Test, with FB903 unintentionally drained during testing and modification of the valves in the Lasgit laboratory. While this will have created a localised change in boundary condition, it occurred following the end of the gas injection stage and will only have impacted the repeat hydraulic test. A small annual variation was seen over the 168-day period of Gas Injection Test 6, although not significant enough to have influence on the gas injection test.

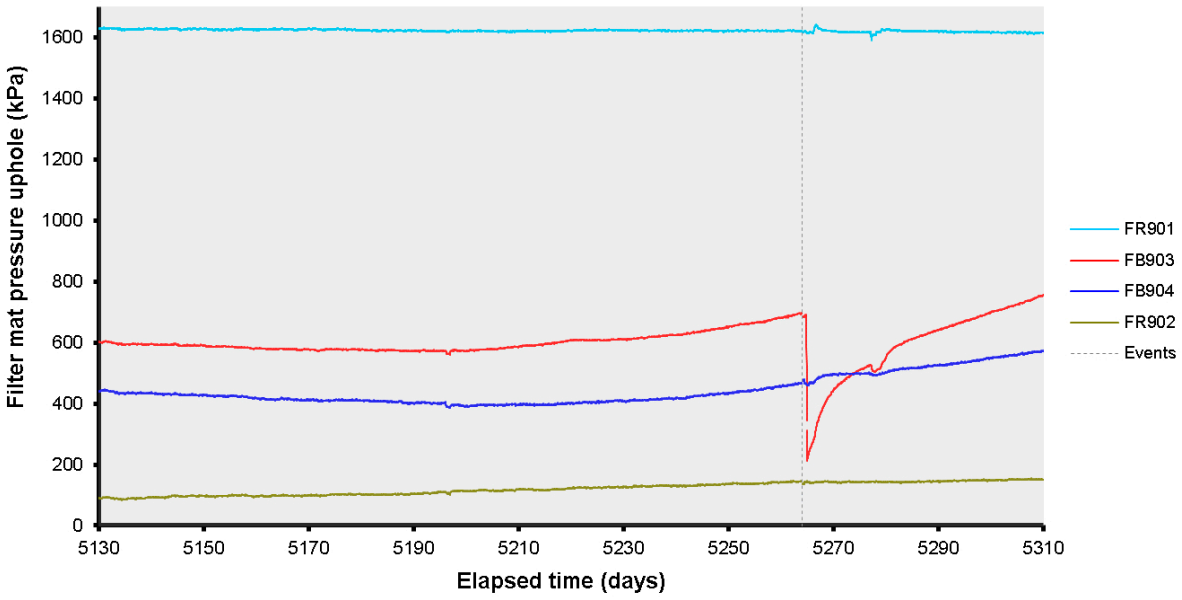

Figure 13-3. *Evolution of water pressure in the filter mats located on the borehole wall and within the bentonite blocks.*

Figure 13-4 shows the pore pressure within the bentonite buffer (UB), recorded at six locations. Figure 13-4a shows the results were dominated by pressurisation of filter UB902 during previous gas injection testing. Figure 13-4b shows that two of the sensors (UB925, UB926) showed an increasing pore pressure from around Day 5200, whilst UB924 increased throughout the test period. These locations were towards the top of the deposition hole. All locations showed a minor cyclicity of around 20 days. Generally, pore pressure within the bentonite was low, with most locations showing pressure of less than 500 kPa. The only exception was UB901 below the canister, where 1 400 kPa of pressure had established. This data showed considerable differences in the pore pressure above and below the canister. The data were dominated by the features seen after Day 5266. These are related to the pressurisation of the canister in readiness for the Full Canister Test. They occurred after the end of the gas injection phase and if they had an impact on the experiment would only have influenced the second hydraulic test. This event is described in detail in section 14.

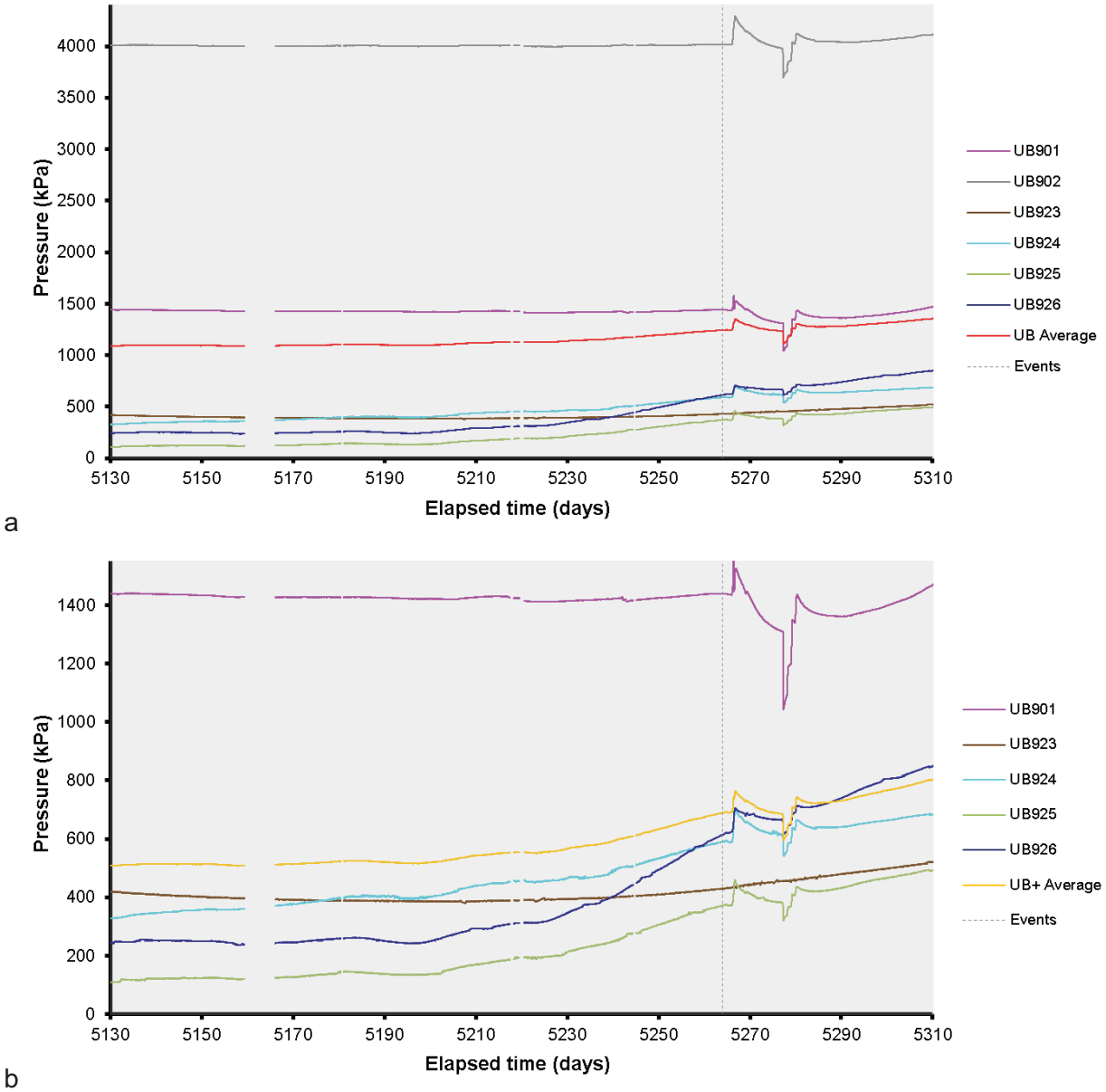

Figure 13-4. *Variation in porewater pressure within the bentonite at the 6 monitoring points: a) all six sensors; b) detail of five sensors.*

Pore pressure was also noted at the canister filters when these were not used for hydraulic or gas testing of the system. Figure 13-5a shows that the data during this period were dominated by the operation of filters FL903 and FU910 for the hydraulic and gas injection testing. Figure 13-5b shows that the pressure history of the other canister filters in more detail. Filters FL901, FM907, and FM908 show the highest pore pressure, of ~1 525 kPa. Pore pressure at these locations was generally stable, although FM907 and FM908 showed pressure increases that correlate with events seen in filter FU910. A second set of filters were seen to be ~1 000 kPa, these being FL902, FM905, FM906, and FU911. In detail, FL902 showed an increase in pressure throughout the stage. Filters FM905, FM906, and FU911 showed similar behaviour with a decrease in pressure until around Day 5200 when pressure started to plateau and then increase. Filters FM905 and FM906 showed a stepped increase in pressure related to Gas Injection Test 5. Filter FU909 was unintentionally pressurised when hydraulic tested started in filter FU910. This was caused by a seized air actuated valve and was remedied as soon as it was possible for someone to visit the laboratory. The final two filters recorded low pressures. Filter FU912 effectively registered a pore pressure of zero, while FL904 was ~80 kPa. Filter FL904 showed an increasing pore pressure throughout the test period. The data following Gas Injection Test 6, i.e. after Day 5266, are dominated by the pressurisation of the canister in preparation for the Full Canister Test. This created a complex pore pressure response, which only had an impact on the second hydraulic test of filter FL903. This event is described in detail in section 14.

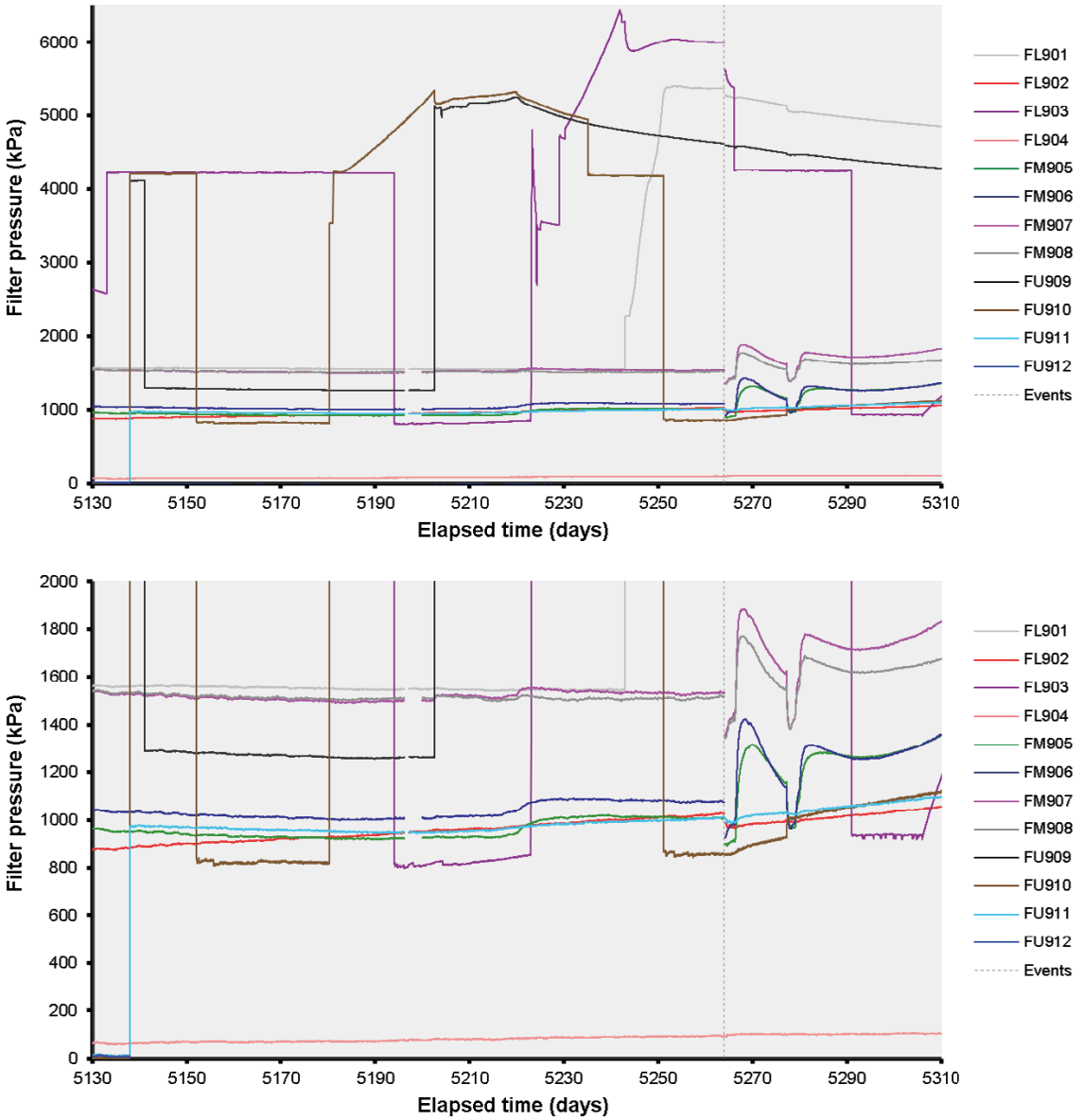

Figure 13-5. *Filter pressures on the canister surface. a) complete range of filter pressures dominated by the activities in filter FL903; b) detail of the pore pressures in the canister filters.*

Figure 13-6 shows the variation of pore water pressure at the rock wall. As can be seen, pressure was heterogeneous within the deposition hole, with ~1 500 kPa variation. It has been reported in previous chapters that UR sensors were dominated by annual cyclicity. This was not immediately apparent in the Gas Injection Test 6 as the data only represent 180 days, but in detail it can be seen that most sensors showed a decaying pore pressure related to annual variations in pore pressure. Many of the UR sensors showed a response that corresponded with both Gas Injection Tests 5 and 6. During the gas injection stage of Gas Injection Test 6, sensors UR903, UR905–UR907, and UR908–UR910 all showed changes that correlate with the injection of gas. These responses are discussed more in Section 13.3. Following the gas injection stage from Day 5266 onwards, the data were dominated by the pressurisation of the canister. This operation had greatly perturbed the porewater pressure and may have had an influence on the repeat hydraulic test flowing the gas injection test.

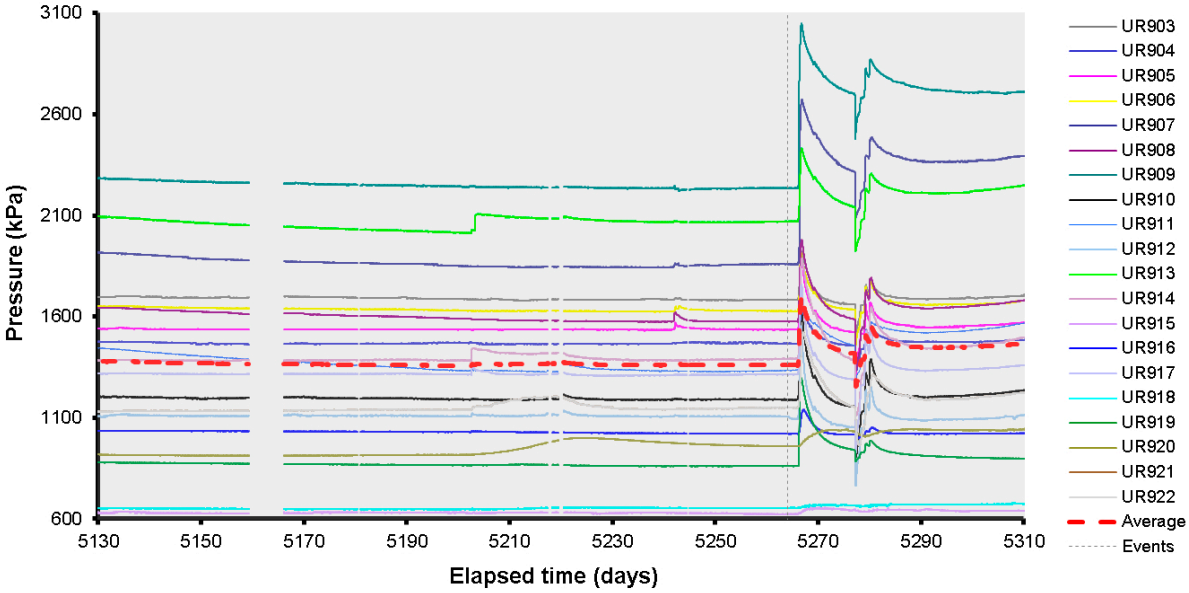

Figure 13-6. *Variation in porewater pressure with time measured at the rock face.*

Figure 13-7 shows the distribution of pore pressure within the deposition hole at the start, mid-point, and end of the current period. This shows the usual distribution of pore fluid pressure with a general decrease in pore pressure down the deposition hole and a high in pore pressure at around 275°. During Gas Injection Test 6 the high pressure region increased in magnitude. The pressurisation of the canister had not significantly changed the distribution of pore pressure (Figure 13-7c), but it had altered the magnitude of the pressures.

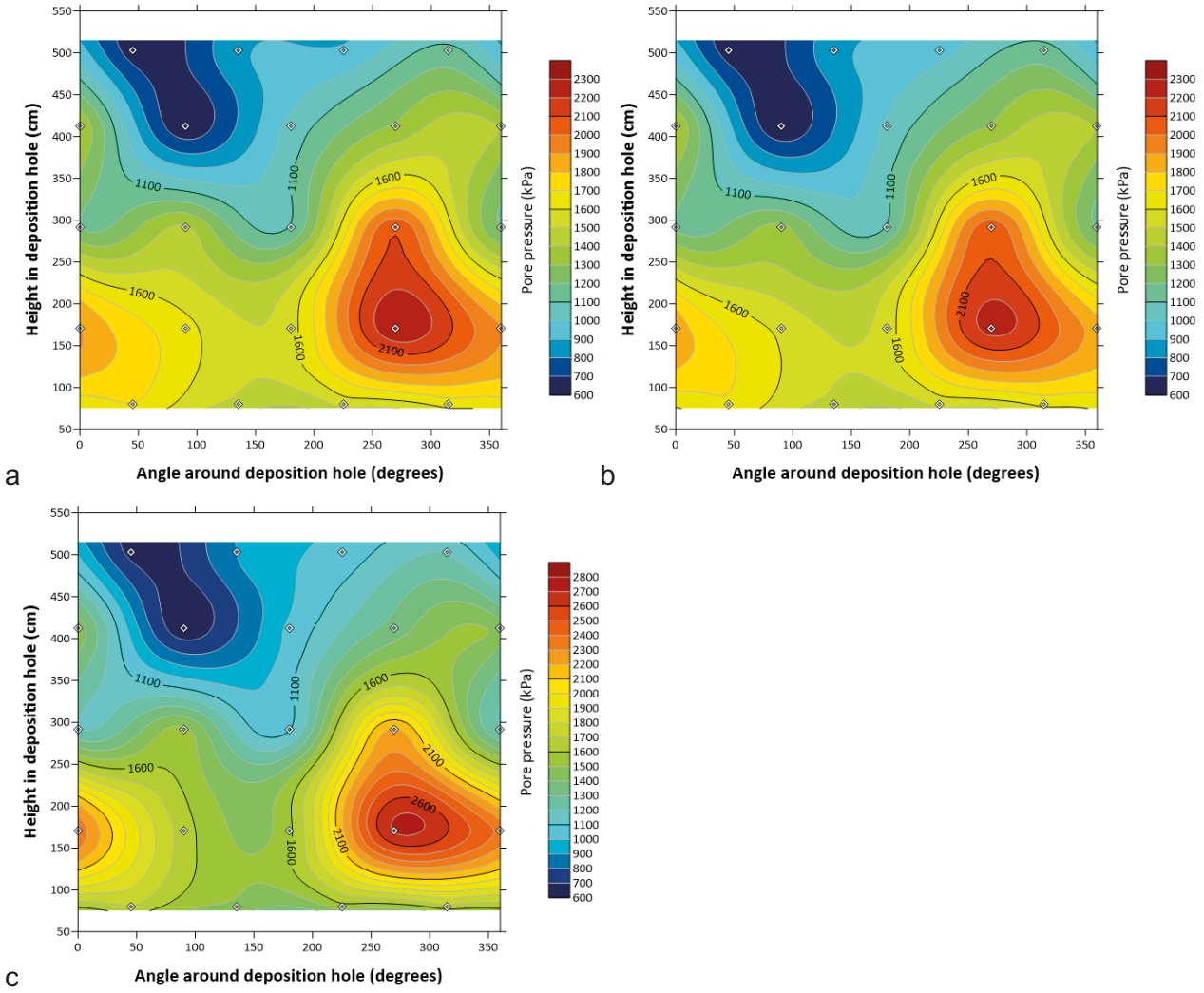

Figure 13-7. *Porewater pressure map at the rock face. a) Day 5140.00, b) Day 5250.00, c) Day 5300.00.*

Radial stress measured at the rock wall is shown in Figure 13-8a for all locations and Figure 13-8b in detail for all sensors excluding PR921. As Gas Injection Test 6 was relatively short, annual cyclicity was not seen. This allowed the gas response to be observed during a period of relatively stable boundary conditions. The radial stresses showed considerable heterogeneity with a range from 2 550 to 6 250 kPa (pre-Day 5266); excluding PR921, radial stress ranged from 4 500 to 6 250 kPa, a range of 1 750 kPa. The data were dominated by the stress responses caused by Gas Injection Test 5, with only minor features created during the current gas test; this is discussed in more detail in Section 13.3. It should be noted that the variation caused by Gas Injection Test 5 in filter FU910 had not fully subsided before Gas Injection Test 6 started gas injection. Radial stress within the bottom of the deposition hole was greatest in bentonite rings R4 and R5, with lower stress seen further up the deposition hole. However, the upper most section of radial stress sensors at ring R10 showed a high stress. Therefore, it appears stress generally increased from the centre of the canister in both upward and downward directions. After Day 5266, the data were dominated by the response of the system to the pressurisation of the canister. As stated previously, this may have influenced the repeat hydraulic test conducted after gas injection had finished.

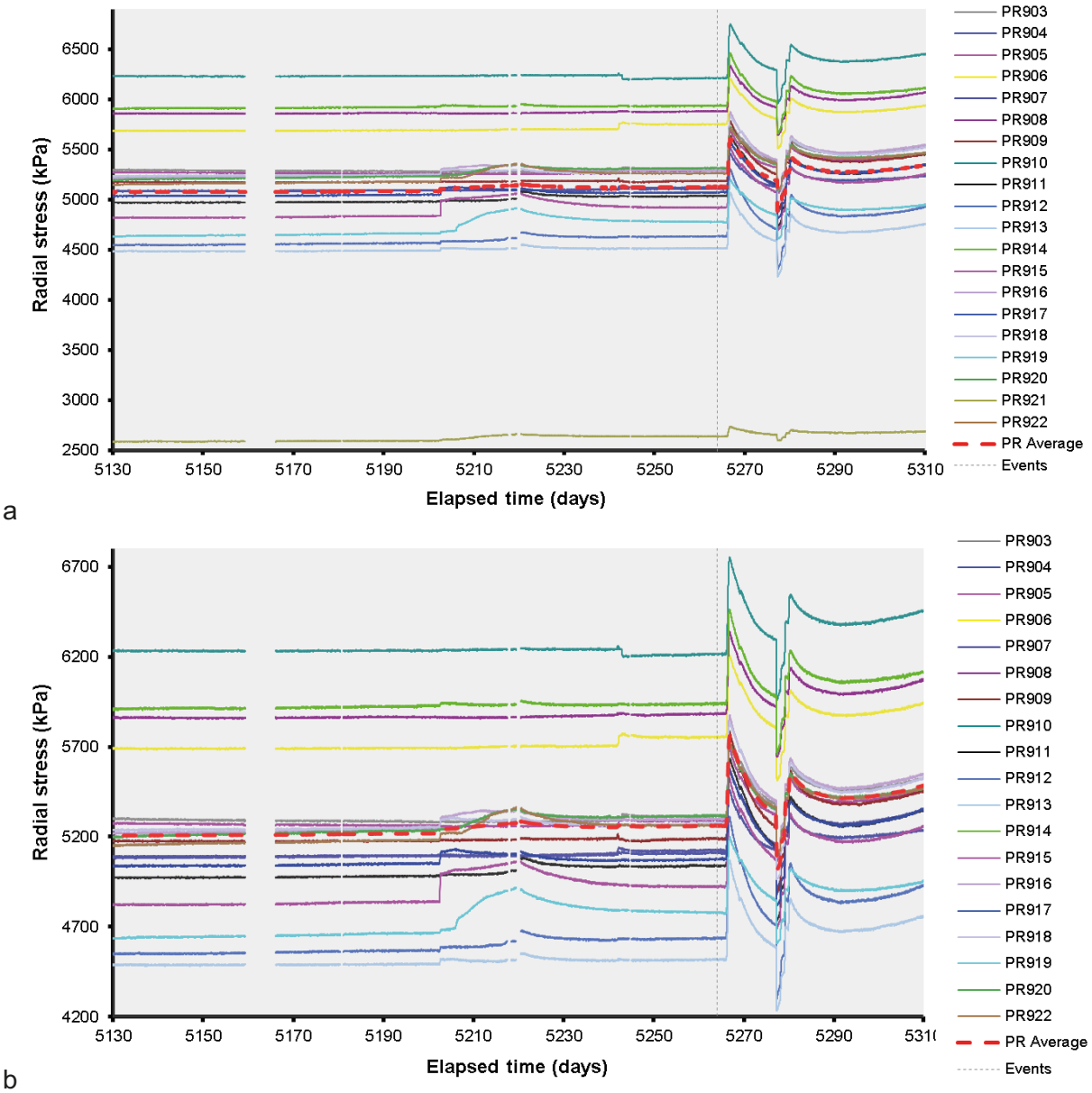

Figure 13-8. *Variation in radial stress at the rock wall with time. a) radial stress for all locations; b) radial stress for all locations excluding PR921.*

Figure 13-9 shows the distribution of stress at the deposition hole wall. This clearly shows the general reduction of stress from the top to the bottom of the hole and that stress tended to be greatest at 315°. The radial stress distribution was complex with some localised response. The pressurisation of the canister had not significantly altered the distribution of stress. However, it had increased radial stress more at 315° and at the level of the lower canister filters (170.9 cm).

The stress acting on the canister was measured at three locations, as shown in Figure 13-10, and showed a total range of ~2 000 kPa. The average stress only marginally decreased because of annual variation. The data were dominated by the response of Gas Injection Test 5. Sensor PC903 showed evidence of gas migration to this location. The response of the sensors to Gas Injection Test 6 will be discussed more in Section 13.3. Figure 13-10 shows that the canister sensors stopped recording at Day 5266.13. When pressurising the canister, it was apparent that the conduit carrying the cable from the canister to the surface was not gas tight. The only way to seal the canister was to sever the PC sensor cables and to seal the tube.

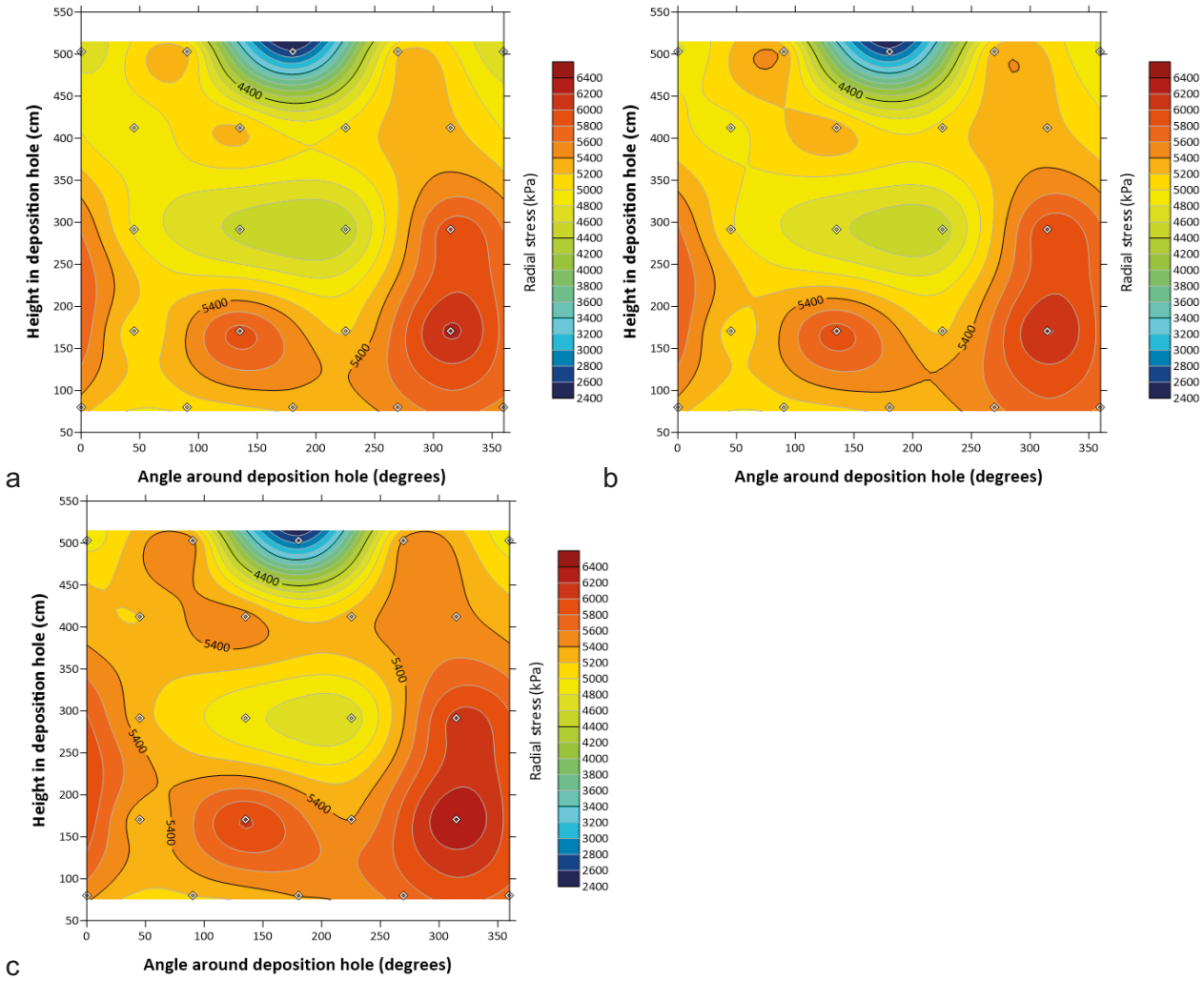

Figure 13-9. *Total stress at the rock face. a) Day 5140.00, b) Day 5250.00, c) Day 5300.00.*

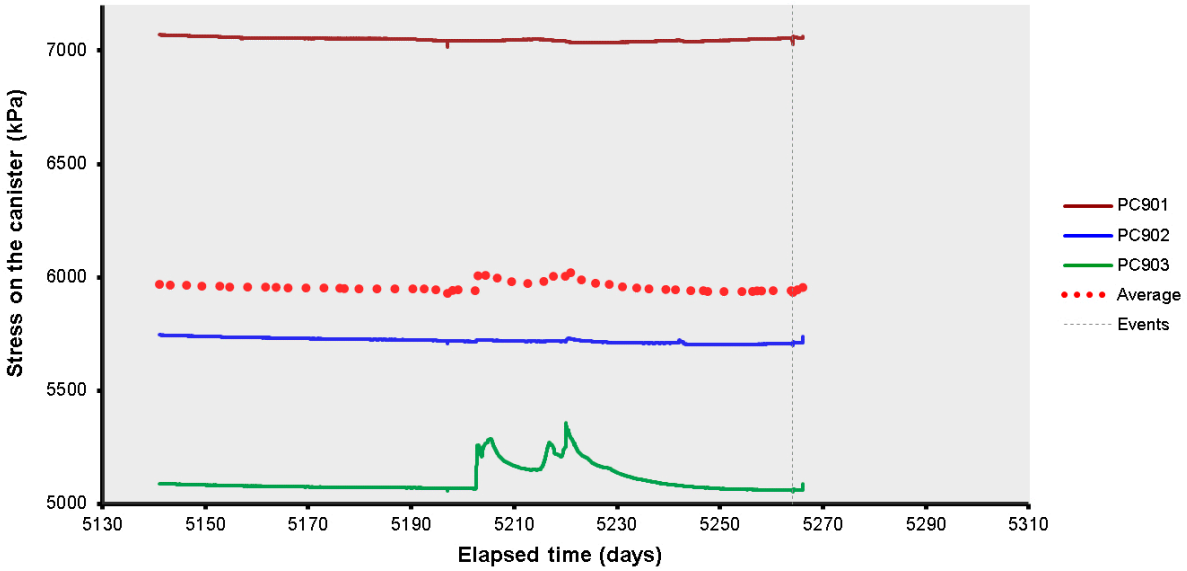

Figure 13-10. *Development of axial and radial pressure on the side and base of the canister.*

Axial stress within the bentonite is shown in Figure 13-11 and was complex. Within the deposition hole there was considerable spread of ~1 400 kPa. It should be noted that sensors PB901 and PB902 were below the canister, whereas all other sensors were above. Both above and below the canister there was considerable variation in stress. In contrast to the stresses on the canister, the axial stress within the bentonite above the canister generally increased during the period and showed a degree of cyclicity that was not annual. This feature, which had a cyclicity of ~50 days, had been previously observed. Axial stress below the canister did not vary and showed less cyclicity. This suggests that the cause of the cyclicity may have been influenced by the HRL and was attenuated with depth. The data after Day 5266 were dominated by the response of the system to the pressurisation of the canister. This feature had greatly perturbed pore pressure and may have had an influence on the repeat hydraulic test.

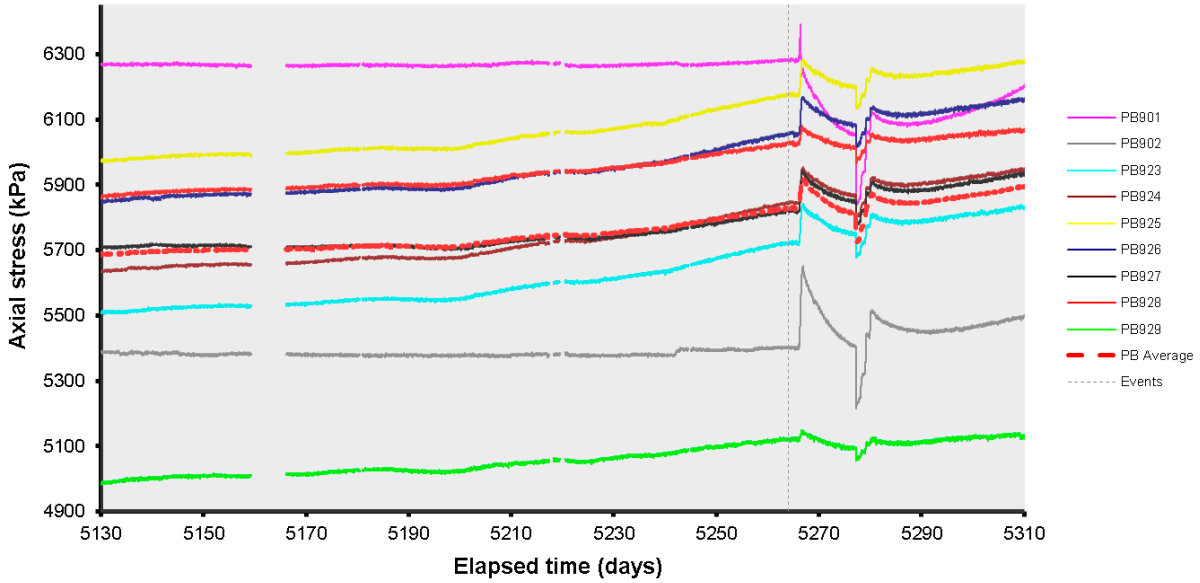

Figure 13-11. *Development of axial stress measured at 9 locations within the buffer.*

The increase of stress within the bentonite was mirrored in the axial force measured on the lid, as shown in Figure 13-12. Axial force on the lid only marginally increased by around 5–10 kPa and within this variation a cyclicity of around 20–30 days was seen. This was of higher frequency than seen in the axial stress within the bentonite (Figure 13-11). This is likely to have derived from temperature variations within the gallery. The data after Day 5266 was dominated by the response of the system to the canister being pressurized.

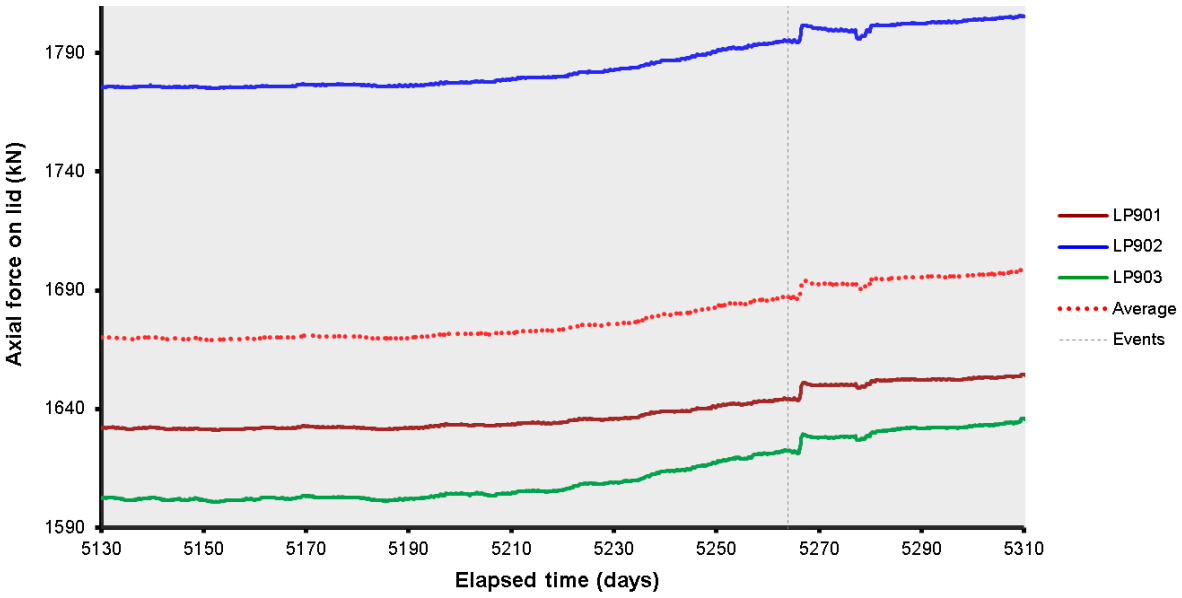

Figure 13-12. *Axial force acting on the steel lid measured by 3 Glötzl load cells attached to separate rock anchors.*

A similar trend was seen within the sensors measuring the displacement of the lid, as shown in Figure 13-13a. Little variation was seen in lid displacement, with a general small decrease of less than 0.05 mm. However, the canister was seen to vary by about 0.7 mm and showed a complex response that seemed to mirror the gas injection pressure. As described for LP and PB sensors, lid movement showed a higher frequency variation component superimposed upon year-long seasonal variation. Lateral movement of the lid (Figure 13-13b) only showed small movements of ~0.01 mm. It was suspected that the two lateral LVDTs had failed and that the stepped response represented a faulty sensor. All displacement sensors were replaced during a site visit on Day 5266. As can be seen, these then gave markedly different results, especially noticeable in DP901. It is suspected that the replacement LVDTs were also faulty or subject to electrical noise. Their inclusion in the data is therefore to identify events and not to determine absolute displacement.

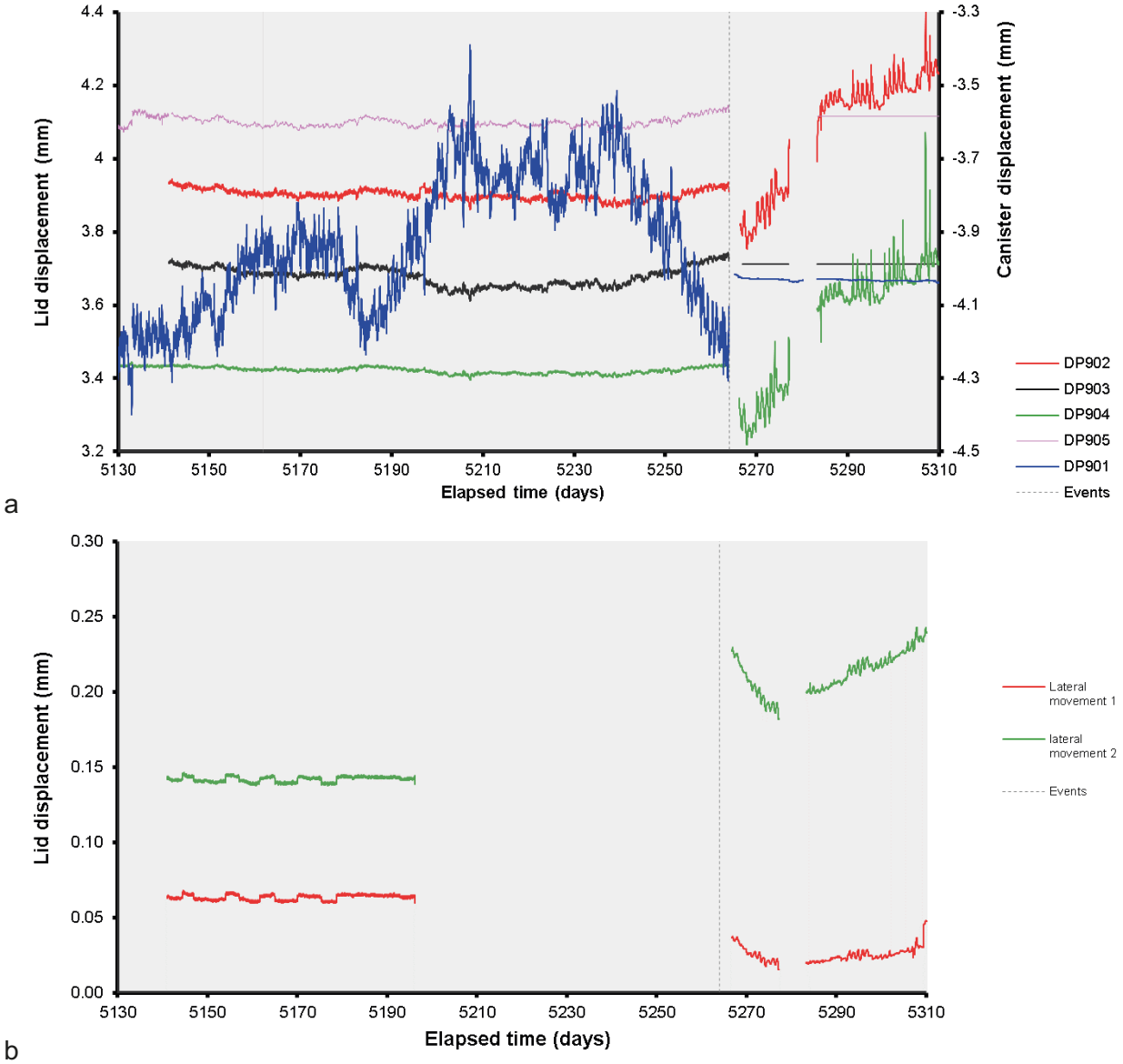

Figure 13-13. *Linear displacement of the steel lid and copper canister (a) and lateral movement of the lid (b). Movements of the lid were measured relative to both the gallery floor and ceiling. Movements of the canister were measured relative to the steel lid.*

Pore pressure away from the deposition hole within the pressure relief hole is shown in Figure 13-14. A small reduction in pressure over the period was seen of between 5 and 15 kPa, with PRH1-3 showing the greatest reduction. The PRH data showed an observed cyclicity of ~40 days. After Day 5266 the data were again dominated by the inflation of the canister, showing that the mechanical inflation of the canister had an influence greater than just within the buffer.

Temperature was monitored within the Lasgit laboratory & office, the HRL, and the canister. Figure 13-15 shows between Day 5135 and 5180 a stepped response was seen, as described for the lateral LVDTs on the canister lid. This may suggest that the faulty LVDTs were interfering with the temperature sensors in the data logger, as the stepped behaviour stopped once the lateral LVDTs were removed from the system. It is unlikely that the temperature was stepped in such a way. However, the length of the steps was not coincident and HRL temperature did not see the same behaviour. There is no correlation between the steps in temperature and flow rate of the gas injection pump, which suggests the laboratory temperature was not varying. Taking the steps into consideration, the temperature within the laboratory was generally constant throughout the period. The canister decreased in temperature during the period as a result of annual variation. The only significant temperature variation was seen in the HRL temperature, which increased by 1.5 °C during the period. This may have influenced the observed boundary conditions. The noted 20–30 day and 40-day period of some sensors was not observed within the HRL temperature records. The filling of the canister with gas around Day 5266 resulted in the temperature of the canister increasing as relatively warm gas was pumped into the cool canister. HRL temperature was lost at Day 5268.68 and may have been damaged. Canister temperature also was lost at Day 5277.17. During a laboratory visit to fix the leaking canister it was suspected that the canister thermocouple was the source of the leak and it was severed. However, it was found that the cables for the canister stress sensors was the cause of the leak and it were not possible to re-establish the canister thermocouple.

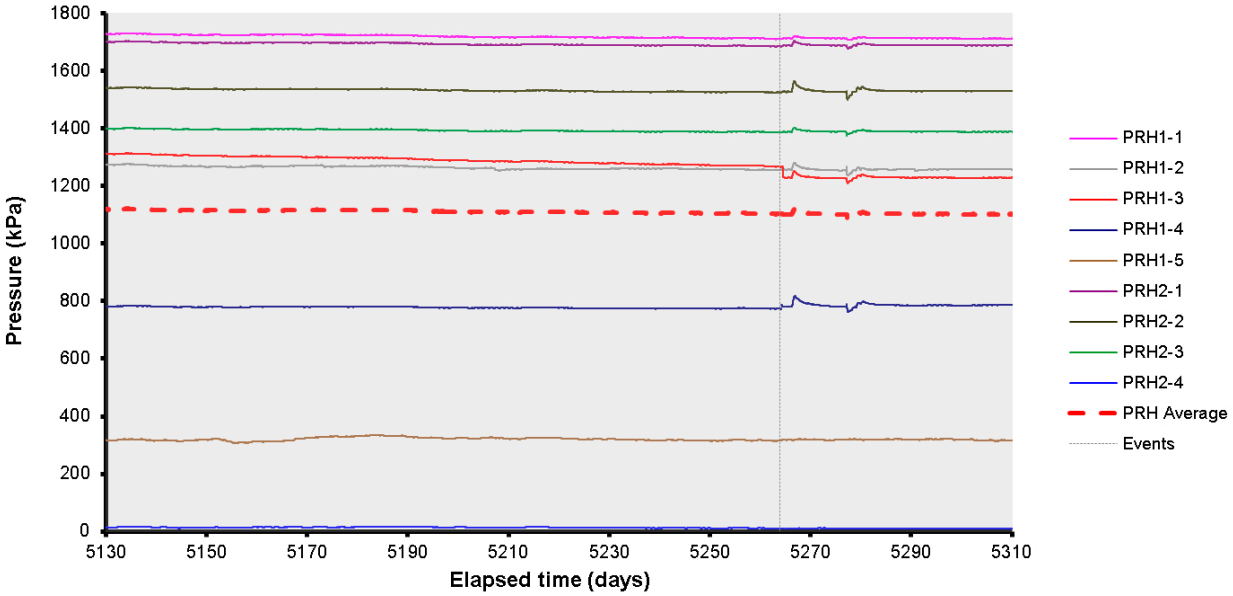

Figure 13-14. *Porewater pressures measured in the packered sections of the pressure relief boreholes.*

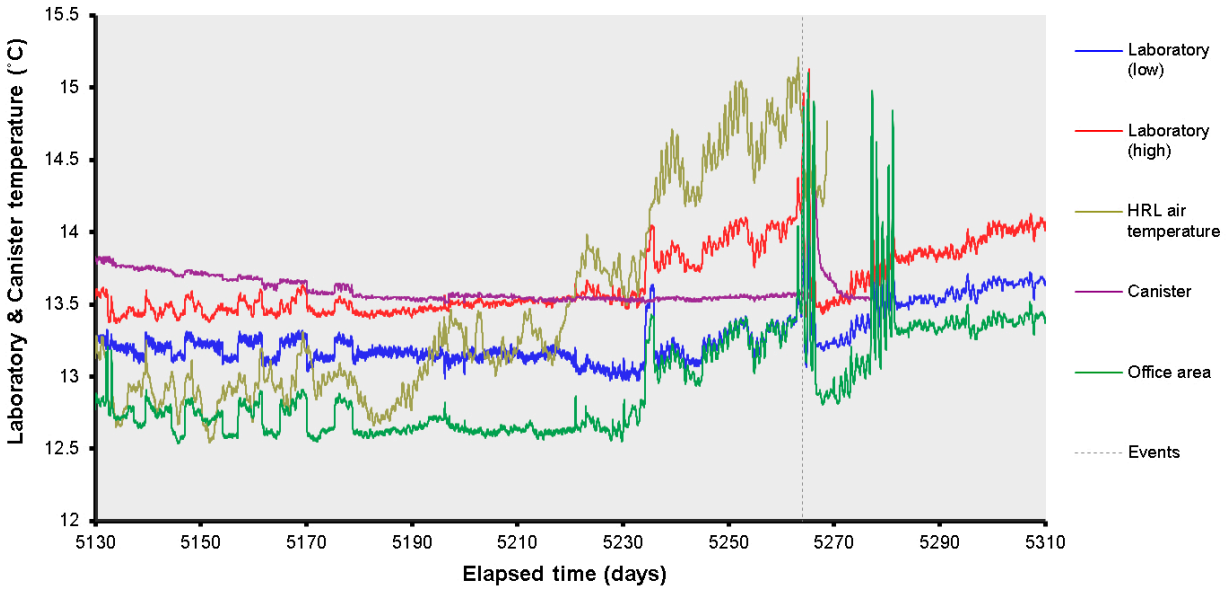

Figure 13-15. *Temperatures recorded in the Gas Laboratory, office, canister, and HRL.*

Figure 13-16 shows the total volume of water pumped into the system during this reporting period. No artificial hydration of the filter mats or filters occurred during the period and the data merely show the flow that occurred during the two-step hydraulic tests for both Gas Injection Tests 5 and 6. Less than 20 ml of water was pumped into the system during the period. Figure 13-17 shows the pressure of the canister. This is shown to highlight the mechanical loading as a result of inflation of the canister and the influence this had on many of the parameters in the deposition hole. This is discussed in more detail in section 14.

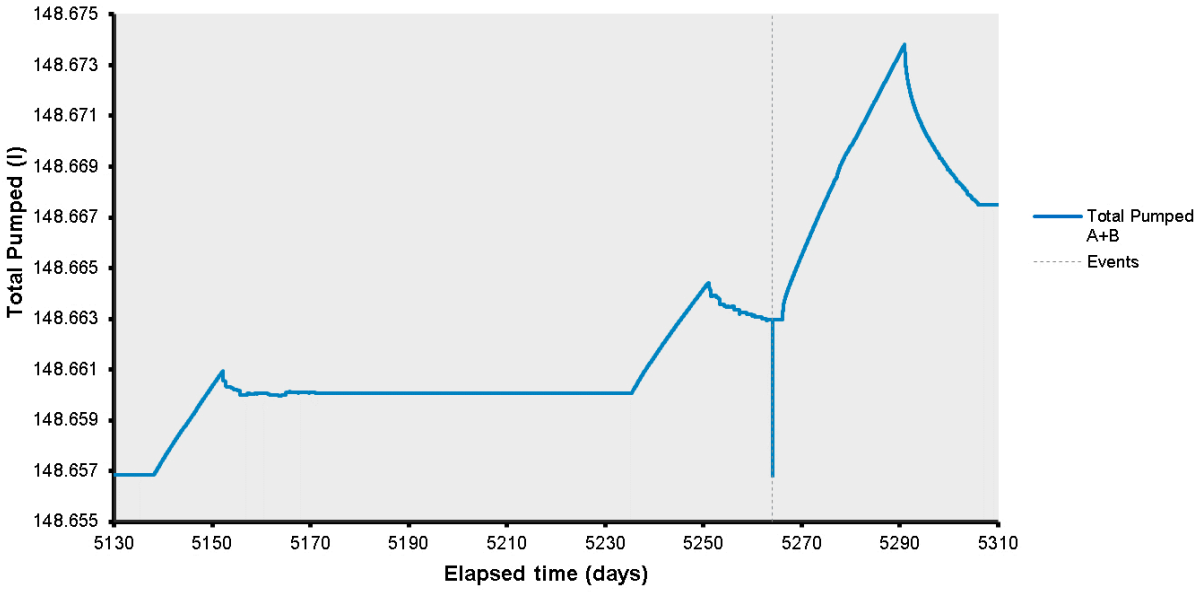

Figure 13-16. *Total pumped into the buffer during hydraulic testing.*

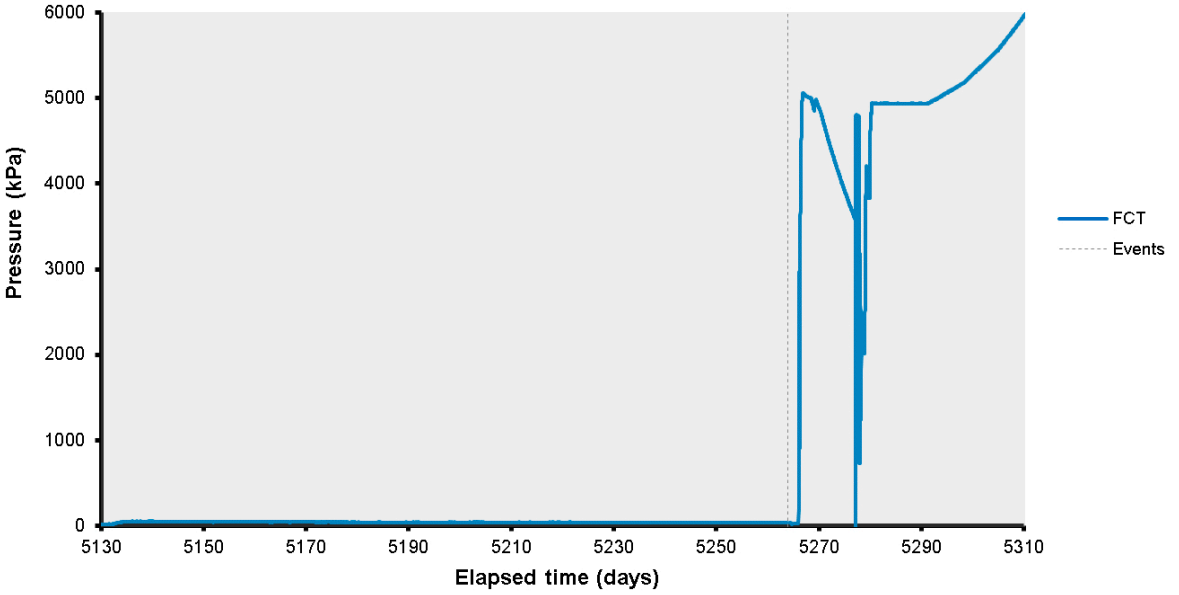

Figure 13-17. *Pressure within the canister.*

Figure 13-18 shows average stresses, pore pressure, and forces observed during Gas Injection Test 6. On the scale shown, all parameters appear constant. The detail of each sensor average shows the following: pore pressure at the rock wall; pore pressure within the pressure relief holes; and stress on the canister reduced by small amounts, whilst radial stress on the rock wall; stress within the bentonite; pore pressure in the bentonite; pressure within the canister filters; pressure within the filter mats; and force on the canister lid all showed an increase. The inflation of the canister after Day 5266 had an influence on all parameters to a lesser or greater extent.

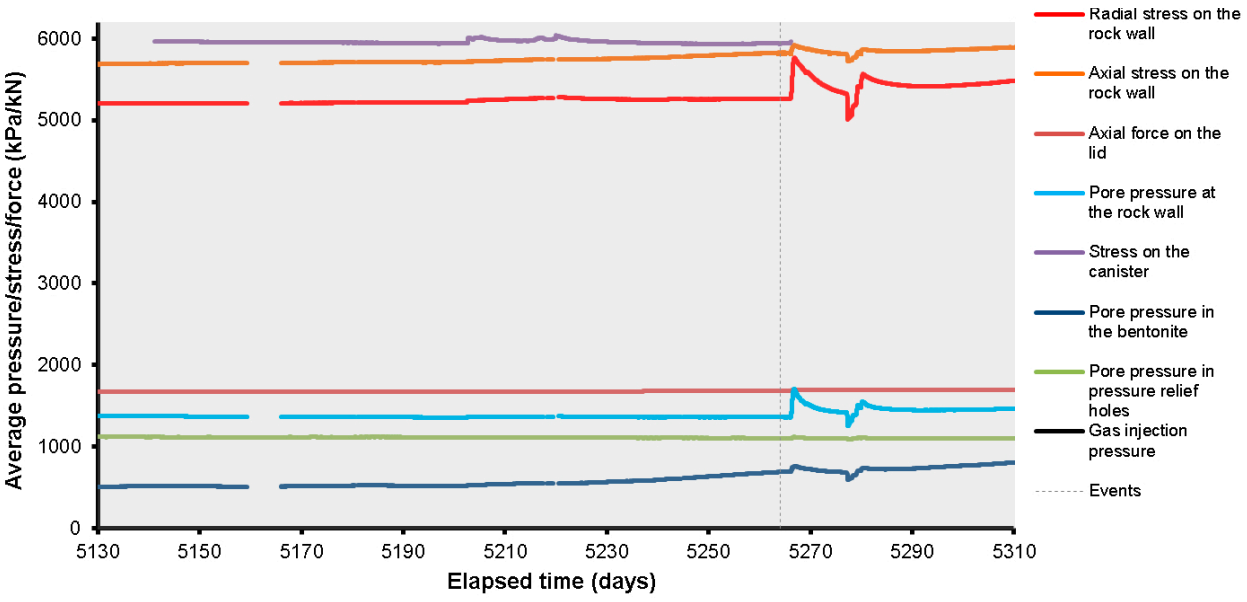

Figure 13-18. *Average pressures, stress, and force observed during the reporting period.*

13.2 Hydraulic test prior and after the gas injection test 6

Figure 13-19 shows the results of the two-stage hydraulic test. Note, the test conducted before the gas injection test was problematic as the pump was leaking, which was replaced for the gas injection test and the subsequent hydraulic test after the gas test. Figure 13-19a shows the pore pressure imposed during the test. Figure 13-19b, c and Figure 13-20a show that the high-pressure stage resulted in an initially high flow into the buffer in excess of 4×10^{-11} m^3 s^{-1}, which quickly reduced to an asymptote of 4.24×10^{-12} m^3 s^{-1}. Figure 13-19b, c and Figure 13-20b show that the low-pressure stage resulted in an initially high outflow in excess of 6×10^{-11} m^3 s^{-1}, which quickly reduced to an asymptote of 2.74×10^{-12} m^3 s^{-1}. The low-pressure stage resulted in a much noisier result, but it is clear that the outflow during this stage was considerably lower than the inflow during the high-pressure stage.

The two-stage hydraulic head test was modelled using the 1-D modelled described in Section 6.4, Figure 13-21 shows the modelled results, rhe fit of the data can be seen to be good, although it hasn't perfectly modelled the data. Table 13-1 summarises the calculated values for hydraulic conductivity and specific storage.

Table 13-1. Modelling results for the two-stage constant head hydraulic tests conducted during Gas Injection Test 6.

Filter	Radius of the filter (mm)	Step	Fitted hydraulic conductivity (m/s)	Fitted specific storage (m^{-1})	Boundary conditions		Initial conditions	
					p_0 (MPa)	p_L (MPa)	p_{I0} (MPa)	p_{IL} (MPa)
FL903	50	1	Not achieved	Not achieved	4.25	1.58	5.77	1.58
		2	1.69×10^{-13}	3.08×10^{-5}	0.94	1.58	4.25	1.58
		Average	**1.69×10^{-13}**	**3.08×10^{-5}**				

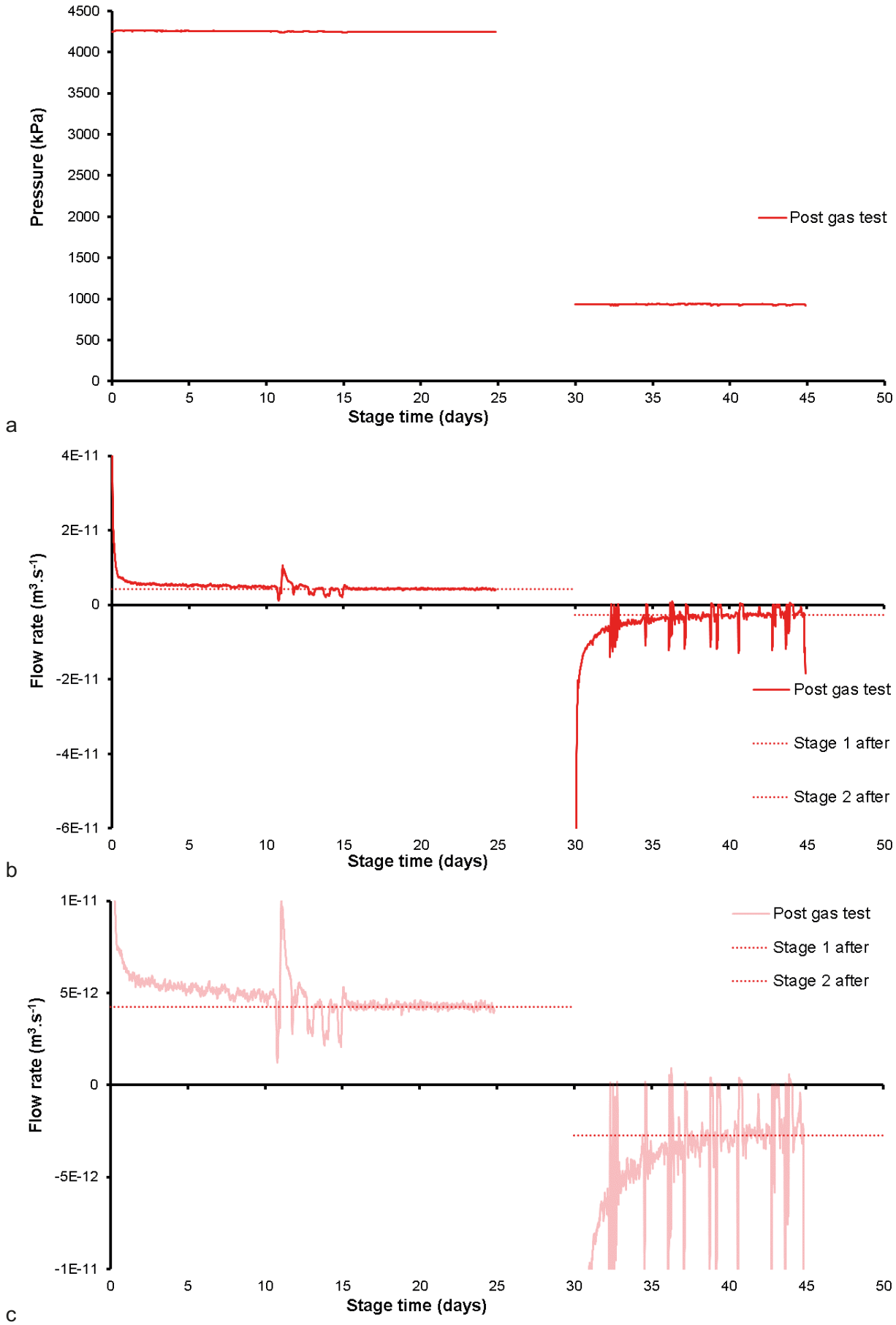

Figure 13-19. *Two-stage constant head hydraulic tests conducted during Gas Injection Test 6. a) Pressure of the injection fluid; b) Flow response; c) Detail of flow response.*

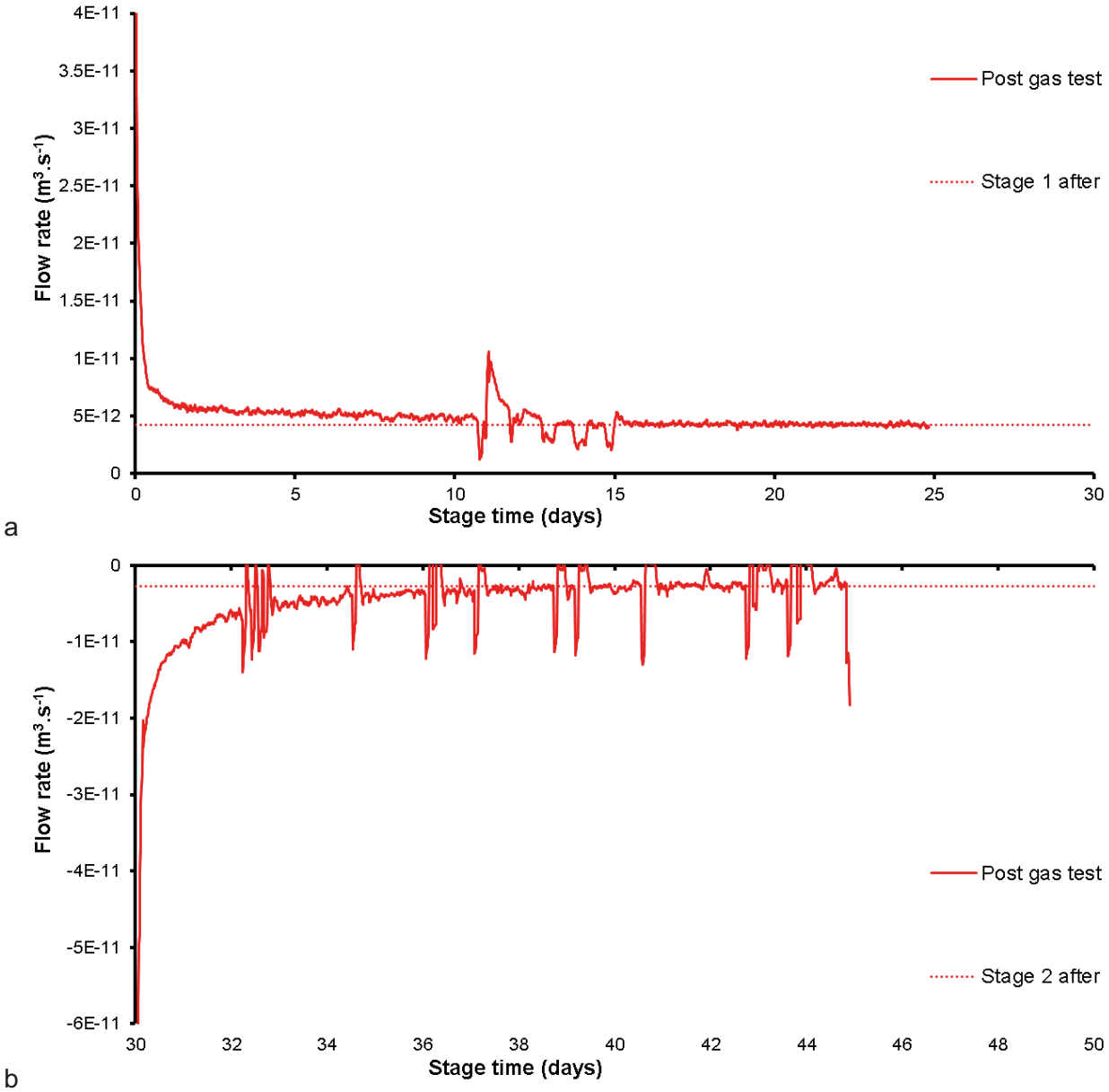

Figure 13-20. *Detail of the flow into the clay during the two-stage constant head hydraulic tests conducted during Gas Injection Test 6. a) High-pressure stage; b) Low pressure stage.*

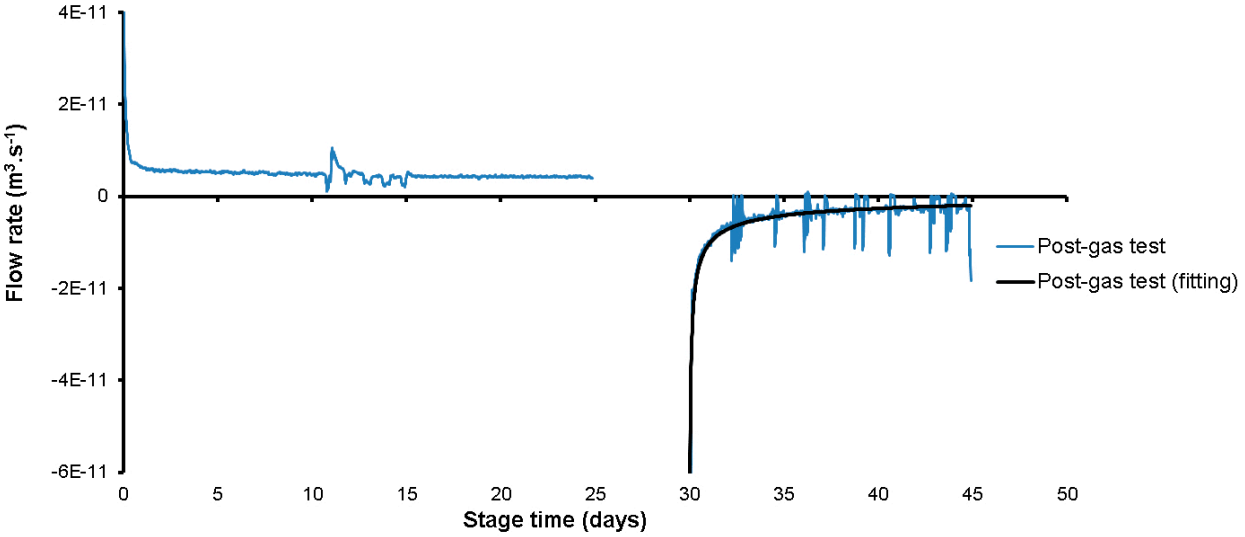

Figure 13-21. *Modelled results for the two-stage constant head hydraulic tests conducted during Gas Injection Test 6. a) Pre-gas test; b) Post-gas test.*

13.3 Gas injection test 6

A limited time period was available to perform the last two gas injection tests. This meant that Gas Injection Test 6 was conducted slightly different to previous gas injection tests that occurred in the same filter (FL903). Previously, gas pressure within the injection filter had been raised from the natural pore fluid pressure at that locality to gas entry pressure in four constant-injection stages. In all previous tests in FL903, gas entry had occurred at a gas pressure approximately equal to the local stress conditions at the injection locality. It was therefore reasonable to start gas injection at a pressure close to the local stress. There was no reason to suspect that the gas entry pressure would reduce significantly from previous tests. Therefore, the single gas injection stage conducted in Gas Injection Test 6 was the same as would have been the fourth stage had time allowed.

The interface vessel was not recharged between Gas Injection Test 5 and 6. The injection filter was thoroughly flushed of water using pressurised helium and the drain from filter FL903. This meant that the starting volume of gas was approximately 2 230 ml of helium at a pressure of 4 829 kPa. The gas injection ramp was started at Day 5230.28 (16:14 29th May 2019) by the injection of water into the base of the interface vessel at a rate of 2.1 ml h^{-1}. Figure 13-22 shows the response of predicted and observed gas pressure. The prediction derives from the ideal gas law, with a close correlation seen. Because of the use of the interface vessel to flush the filter of water, it was not possible to accurately know the starting volume of gas. Figure 13-23 shows the difference between the predicted and observed gas pressures. This was used to estimate the starting volume. The pressure difference was seen to start to diverge at Day 5235.96 when the gas pressure was 5 530 kPa, this may represent the first evidence of localised gas entry. Gas pressure continued to increase until Day 5238.13, when gas pressure remained constant for an hour. This resulted in the difference between predicted and recorded to increase by 20 kPa and was likely to be gas moving further into the buffer. At this time, the gas pressure was 5 827 kPa, i.e. 297 kPa above the first indication of gas movement.

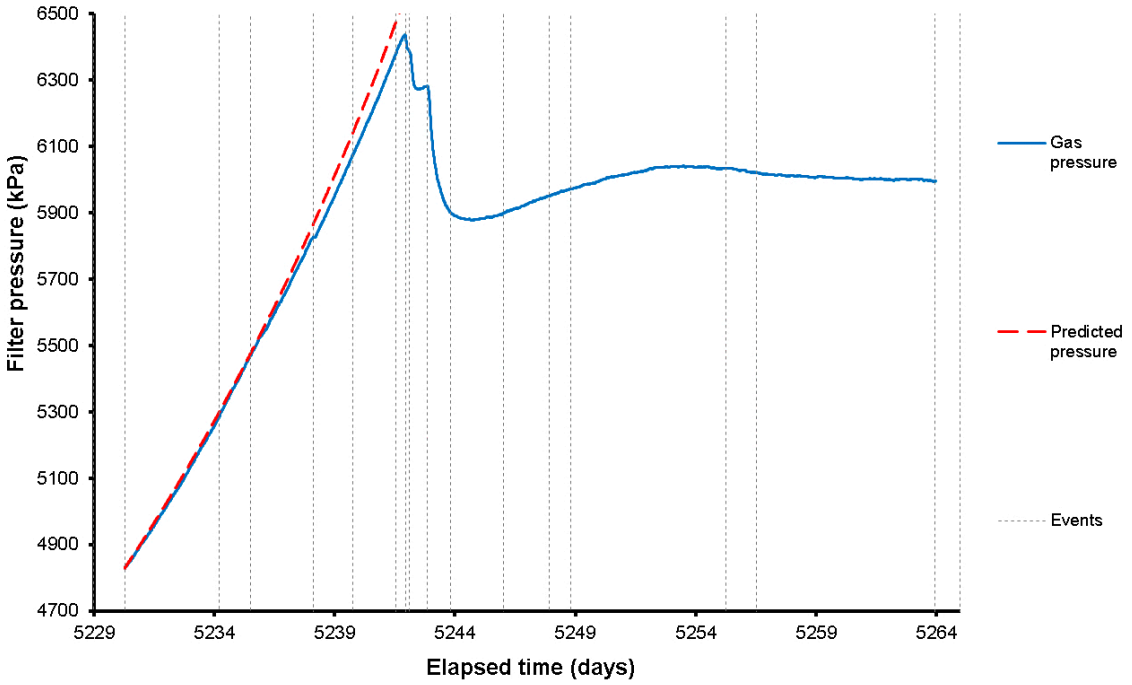

Figure 13-22. *Recorded and predicted gas pressure during Gas Injection Test 6.*

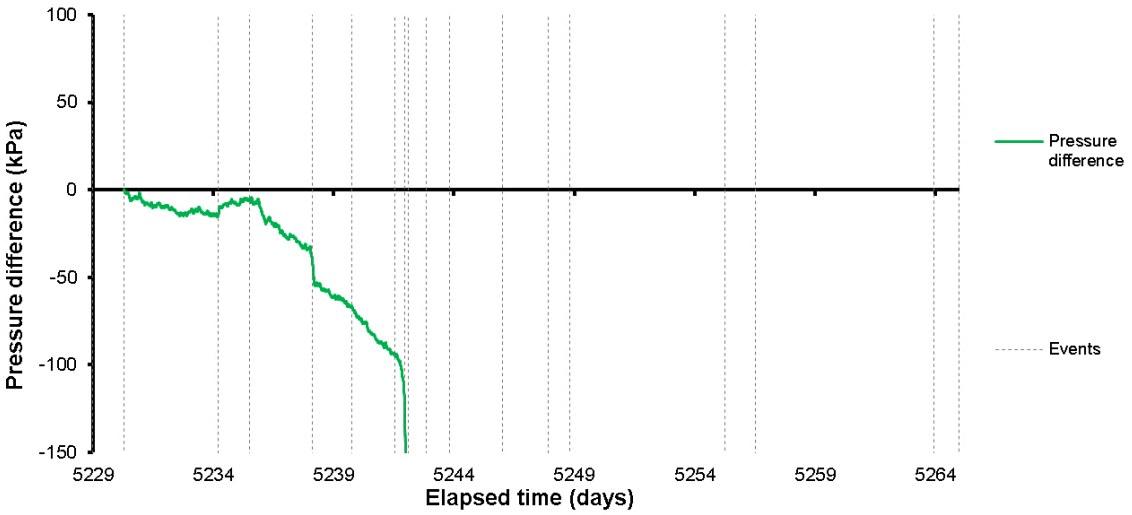

Figure 13-23. *Difference between recorded and predicted pressure during Gas Injection Test 6. This was used to estimate the volume of gas during the test.*

The difference between predicted and observed gas pressure continued to diverge at the same rate until Day 5241.55, when it started to accelerate. This event occurred at a gas pressure of 6 382 kPa, 850 kPa above the first evidence of gas movement and 555 kPa above the previous event. The current event was the beginning of significant gas movement into the buffer. Gas pressure still continued to increase, until a gas peak pressure of 6 437 kPa at Day 5241.92. This showed that gas pressure continued to rise, even after gas had started to migrate into the buffer. Initially, gas pressure reduced by ~45 kPa before stabilising, and was then followed by a further decrease of 120 kPa. This was followed by a period of gas pressure increase, which lasted 9 hours until pressure began to significantly decrease again. This time, a stable pressure decrease was seen, with gas pressure reaching a minimum of 5 878 kPa by Day 5244.68. This represented a total reduction in gas pressure of ~560 kPa. At least three distinct events were observed to reduce gas pressure, suggesting that gas pathways were migrating a distance before arresting, with higher gas pressures being required to form more pathways. As seen in previous tests, gas pressure then recovered and established a near stable value.

Figure 13-24 shows the flow of gas into the system and into the clay at STP. Up until the first evidence of gas entry, average flow into the clay was 1.41×10^{-9} m^3 s^{-1}. Four distinct peaks in flow into the clay were seen. The first occurred at Day 5238.13, with a peak flow of 4.52×10^{-8} m^3 s^{-1} (note: data shown in Figure 13-24 is time averaged). The second peak occurred at the time of gas peak pressure, with a peak in flow of 1.74×10^{-7} m^3 s^{-1}, around 90 minutes after peak pressure. The third peak in flow into the clay was seen at Day 5242.21 with a peak flow of 2.11×10^{-7} m^3 s^{-1}. This event corresponds with the second decrease in gas pressure described above. The final peak in gas flow into the clay reached a maximum of 2.42×10^{-7} m^3 s^{-1} at Day 5242.96. The peak in flow was short-lived with flow into the clay reducing to equal the flow in the system within 1 day. Figure 13-25 shows the volume of gas pumped into the clay. It shows that 0.1 mol He entered the clay up until peak gas pressure. During the initial pressure drop, which included two peaks in flow, around 0.25 mol He entered the buffer. In total, 3.15 mol He entered the clay following peak pressure.

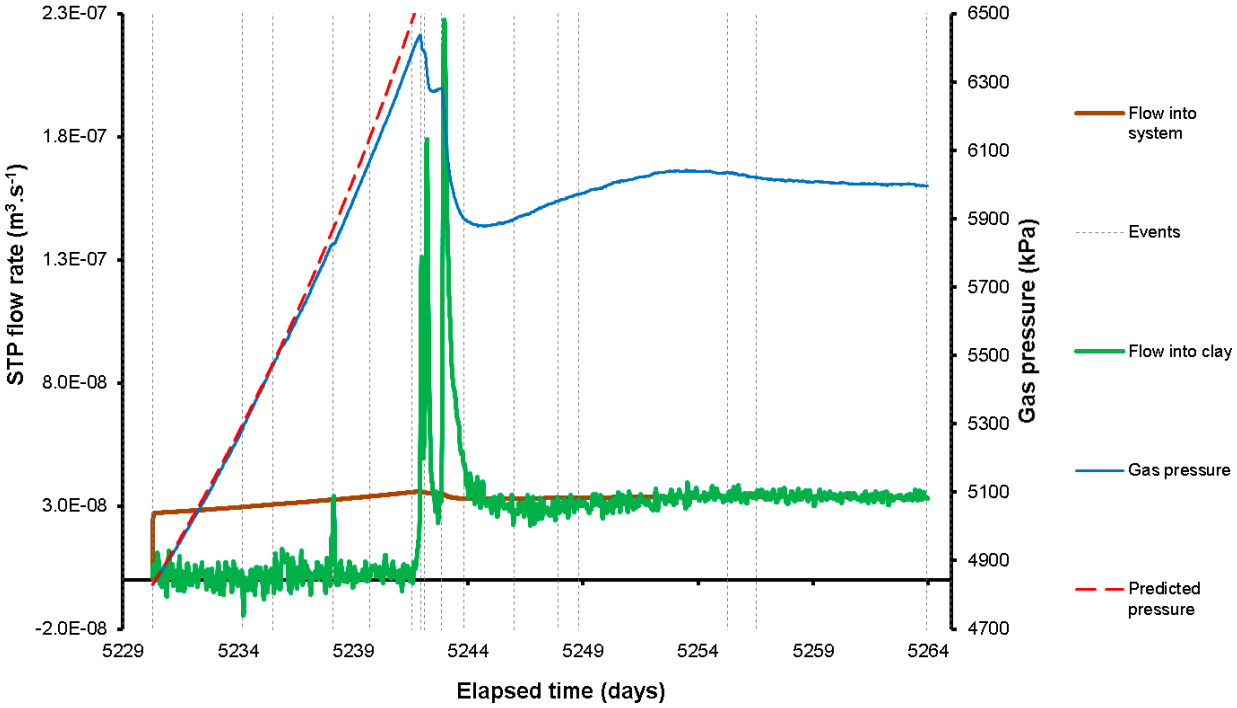

Figure 13-24. *Flow of gas into the system and the clay during Gas Injection Test 6.*

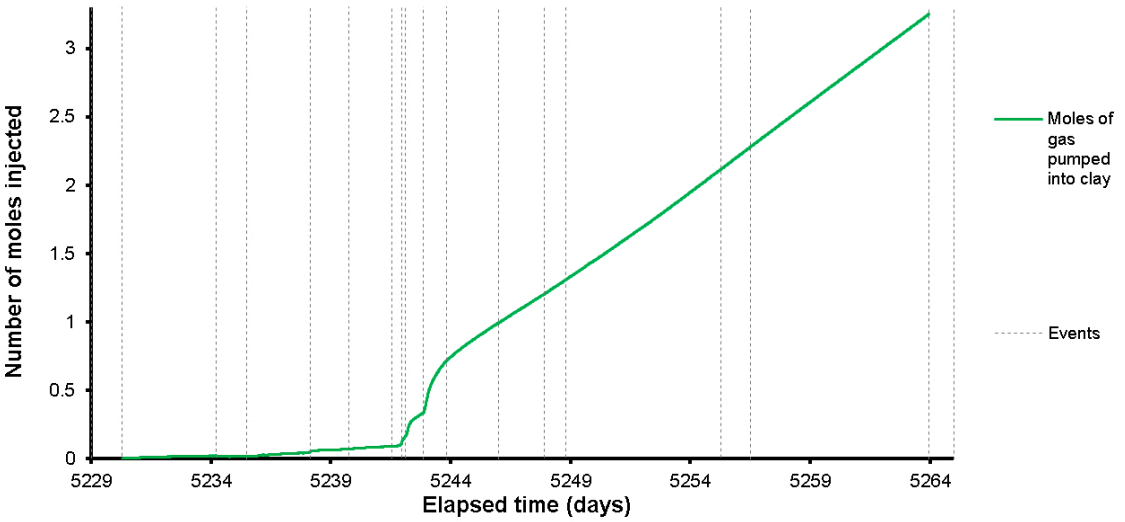

Figure 13-25. *Moles of gas pumped into the clay during Gas Injection Test 6.*

Figure 13-26 shows the flow data in more detail around the time of peak pressure and subsequent gas movement within the buffer. Flow into the clay showed similar behaviour to previous tests. Following the initial two peaks in flow, the response reduced to approximate the flow into the system. A third peak was also followed by the system quickly recovering with flow into the clay matching flow into the system. The detail shown in Figure 13-26 shows that the flow into the clay reduced to lower than the flow into the system, before recovering. This had been seen in previous gas tests. When flow into the clay returned to equal flow into the system at approximately Day 5253.40, gas pressure entered a period of being relatively constant, with only a small decrease in pressure. This suggests that stable pathway migration had occurred. Figure 13-27 shows a plot of the peak gas flow for the four events noted in Gas Injection Test 6. This suggests a logarithmic increase in peak flow rate for each event.

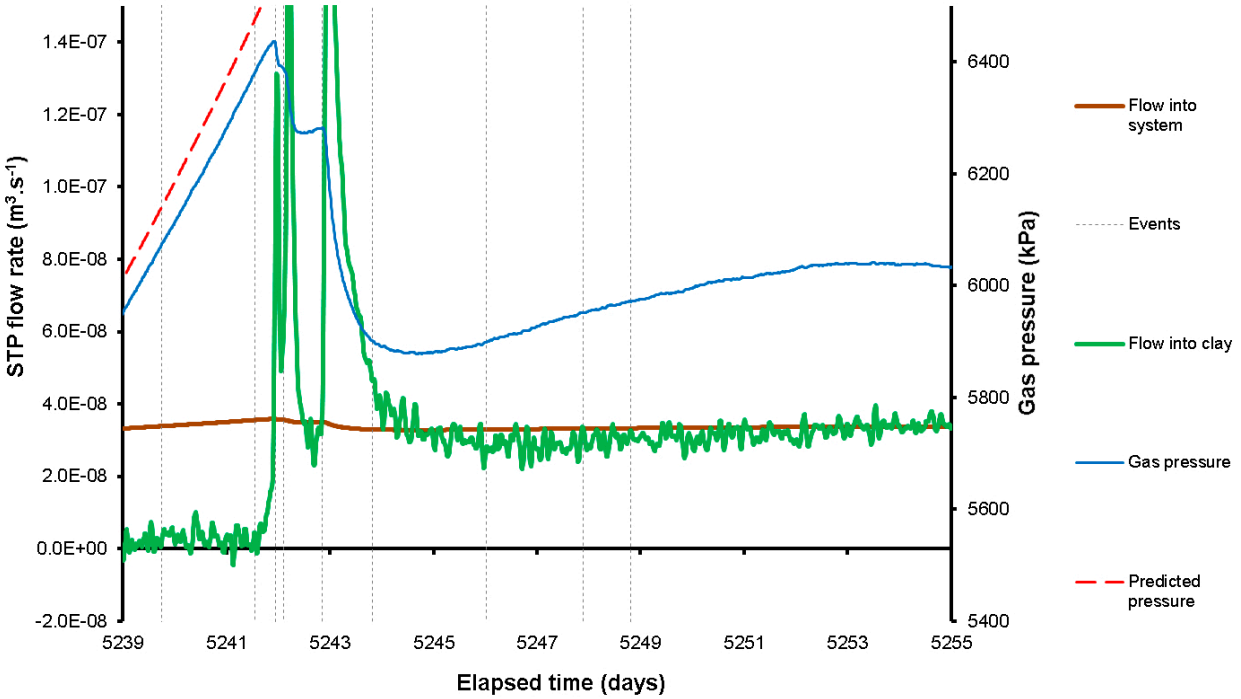

Figure 13-26. *Detail of the flow of gas into the clay and the system around the time of gas entry during Gas Injection Test 6.*

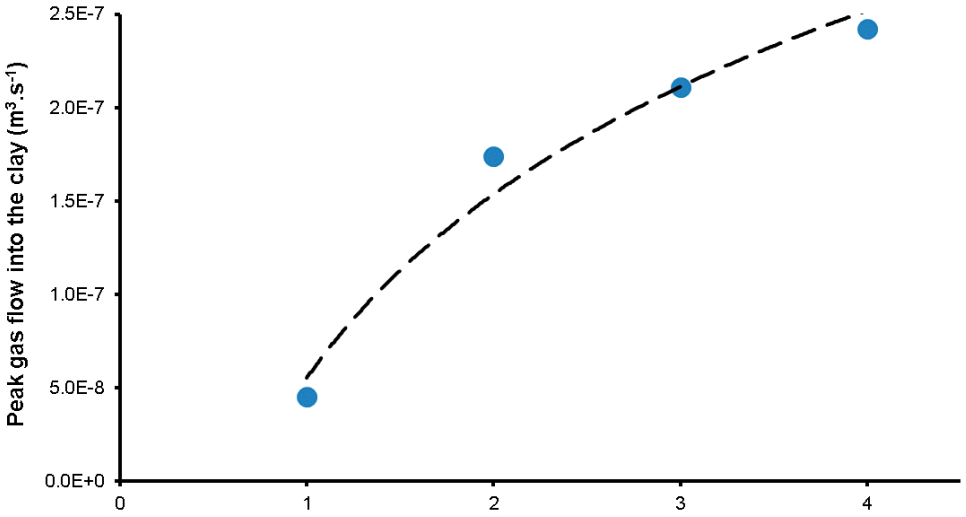

Figure 13-27. *Magnitude of the peak flows into the clay for the four events highlighted in Gas Injection Test 6.*

Figure 13-28a and Figure 13-29a show the pore water response at the deposition hole wall at the time of peak gas pressure. Location UR904 shows the first response at Day 5241.55 with a stepped increase in pressure. This was the time when flow into the clay was seen to start increasing. This was accompanied by increases in pressure at UR904–UR908. Several sensor locations showed a response at gas peak pressure at Day 5241.92. Sensor UR908 had the largest response of 45 kPa. Sensors UR907–UR910 showed a similar stepped increase, but of lower magnitude. At UR905 a small increase of ~10 kPa occurred at this time, followed by a larger increase of ~30 kPa at the time of the second pressure drop following peak gas pressure. Sensor UR906 showed a similar response of ~25 kPa increase, followed by a second pressure increase around Day 5242.85. This feature was accompanied by increases in UR903 and UR905, with negative responses at UR907 and UR910. The multiple events seen in the pore pressure data showed that the gas was moving within the deposition hole.

At the time of gas peak pressure at Day 5241.92, several of the radial stress sensors at the rock wall showed variations (Figure 13-28b, Figure 13-29b). The largest change was seen in PR906, with 67 kPa increase. Notable changes were also seen in PR903, PR905, and PR907, with variations of 39, 39, and 27 kPa respectively. Several other sensors showed a step too, but of lower amplitude. Of note was sensor PR910, which saw a reduction of 41 kPa. Not all of the increases occurred in single step events, with PR903, PR905, and PR906 having two-steps coincident with the two drops in gas pressure. Sensors PR907 and PR910 showed a single stepped change. Variation in radial stress corresponded with changes in gas injection pressure and flow into the clay, with no features of significance in the subsequent changes in flow or gas pressure.

The radial and axial stresses measured on the canister surface showed direct and indirect evidence of gas movement (Figure 13-28c). At the time of peak gas pressure at Day 5241.92, the stress at PC901 and PC902 increased by ~5 and ~10 kPa respectively. This represents a hydrodynamic response, unlike the direct migration of gas seen in Gas Injection Test 5. In both sensors, the increase in stress was accompanied with a larger decrease at Day 5242.85, which corresponded with pressure and stress changes seen at the rock wall. This suggests that stress was relieved at the canister as gas migrated further into the barrier system.

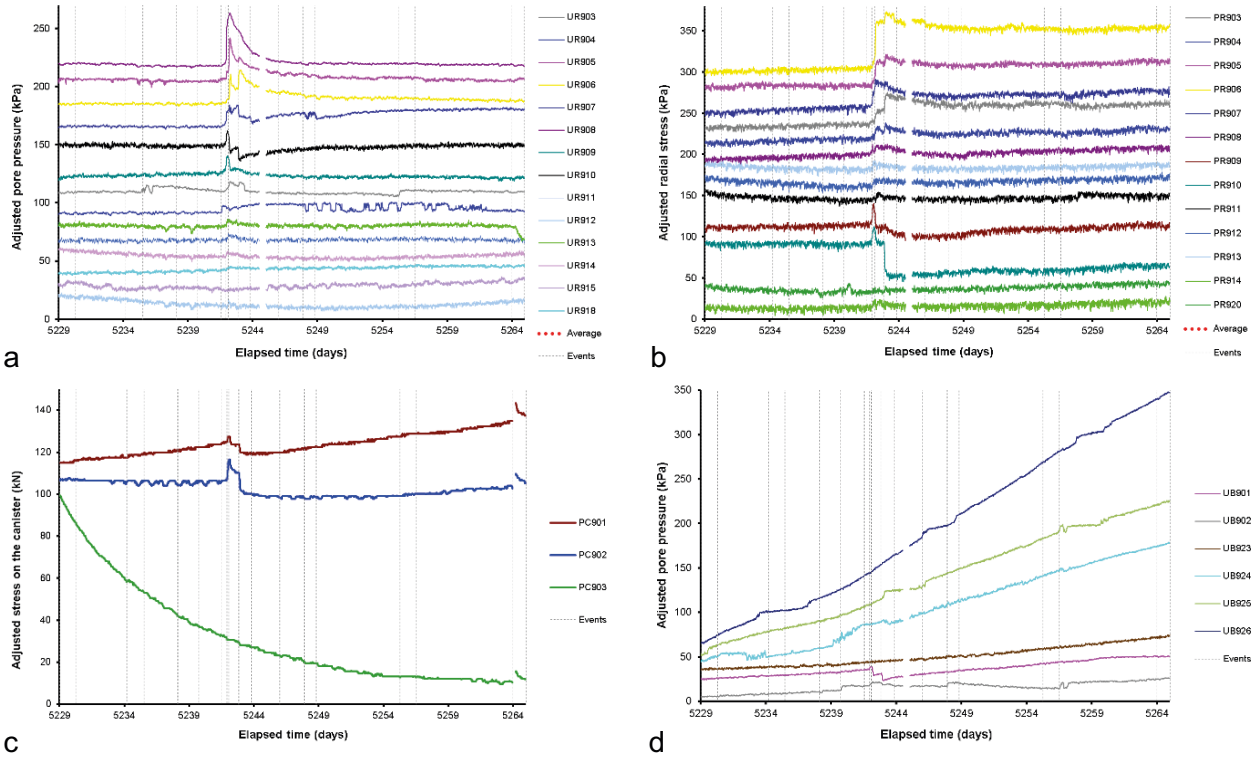

Figure 13-28. *Example of sensor response around the time of gas entry during Gas Injection Test 6. All parameters have been transposed about the y-axis to emphasise the detail observed. a) Pore pressure at the deposition wall; b) radial stress on the deposition wall; c) stress on the canister surface; d) pore pressure within the bentonite.*

Figure 13-28d shows the changes seen in pore pressure within the bentonite buffer. This was quite complex with many events of pore pressure increase and decrease that corresponded with the events described above. Of most note was the coupling of pressure seen at UB901 and UB902 with the previously described events. These sensors were situated below the canister. At UB902 pore pressure increased at Day 5239.74, which did not correspond with any other feature pre-gas peak pressure. Both UB901 and UB902 showed stepped variation at the time of peak pressure, and during the subsequent two drops in gas pressure.

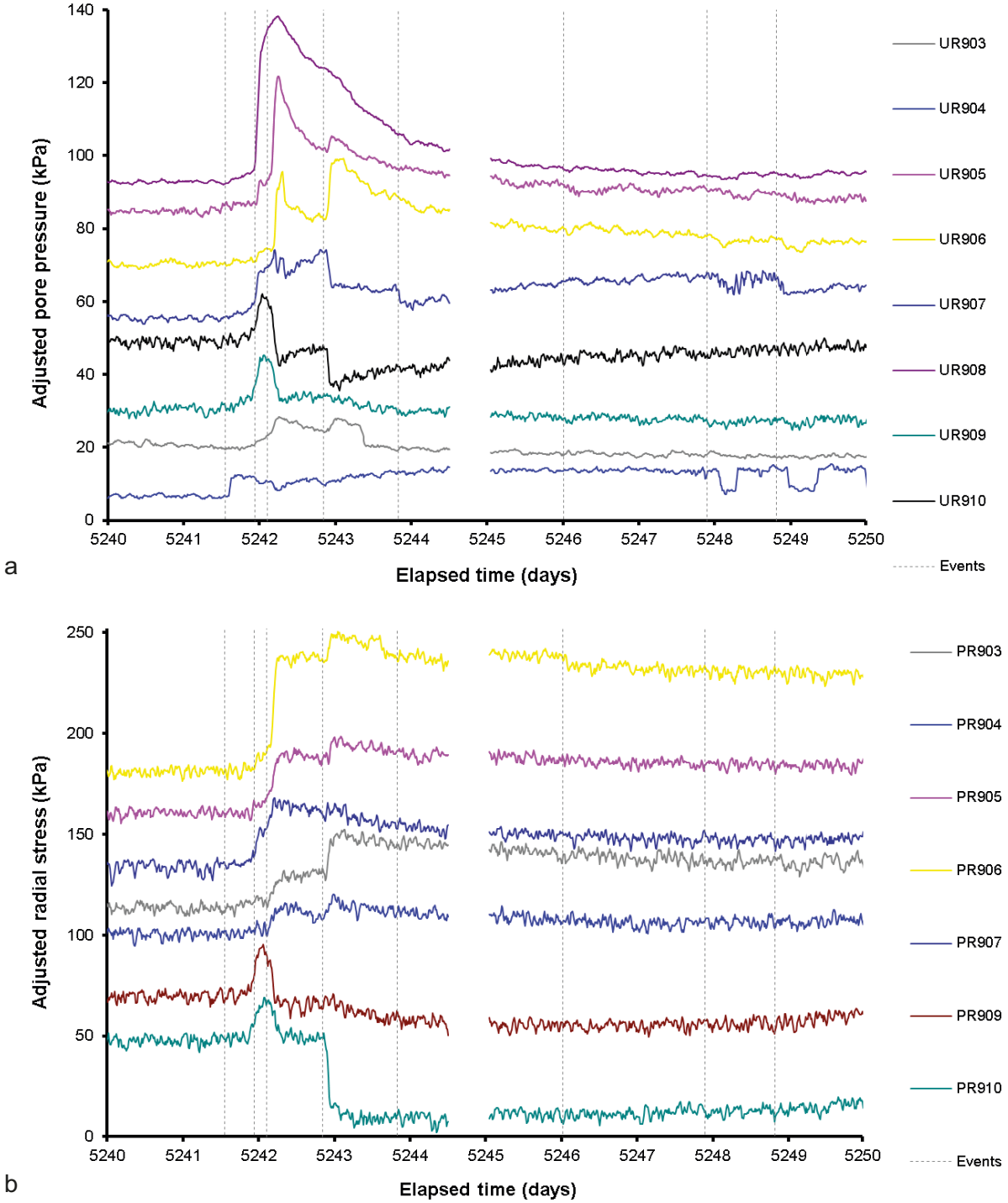

Figure 13-29. *Detail of radial stress and pore fluid pressure at the rock wall around the time of gas entry. a) Pore pressure at the deposition wall; b) Radial stress on the deposition wall.*

The distribution of radial stress and change in radial stress on the deposition hole wall is shown in Figure 13-30. Stress prior to peak gas pressure is shown in Figure 13-30a at Day 5241.55. This shows that near the gas injection filter radial stress was higher than the general stress level. Stress was greatest towards the bottom of the deposition hole in a band at around 150 cm height all around the canister. A band of high radial stress was also seen vertically, centred on 315°. A stress gradient was observed whereby the least stress was generally seen towards the top of the deposition hole, with stress increasing with depth.

Figure 13-30b shows the change in radial stress from Day 5241.55 to Day 5242.11. Radial stress increased at the same level as the injection filter, with the greatest increase clockwise of the injection filter. The increase in stress resulted in a lowering in stress higher in the deposition hole wall at around 420 cm height. Figure 13-30c shows that the raised stress at the level of the injector was short-lived and by Day 5242.85 stress had returned to near pre-peak gas pressure levels, with stress now increasing below the injector. By Day 5263.95 (Figure 13-30d) stress at the top of the deposition hole was generally unchanged. A stress reduction persisted clockwise of the injector, with stress below the injector still raised.

Figure 13-31 shows the pore pressure at the deposition hole wall and how this varied during Gas Injection Test 6. Figure 13-31a shows the pore pressure distribution just prior to peak gas pressure at Day 5241.55. This shows a general decrease in pore pressure down the deposition hole and a high in pore pressure at around 275°. The high in pressure was on the same level as the injection filter, 90° around the canister. The first pore pressure response at Day 5242.11 (Figure 13-31b) shows the creation of a high in pressure at 90°, with the only changes occurring at the level of the injector.

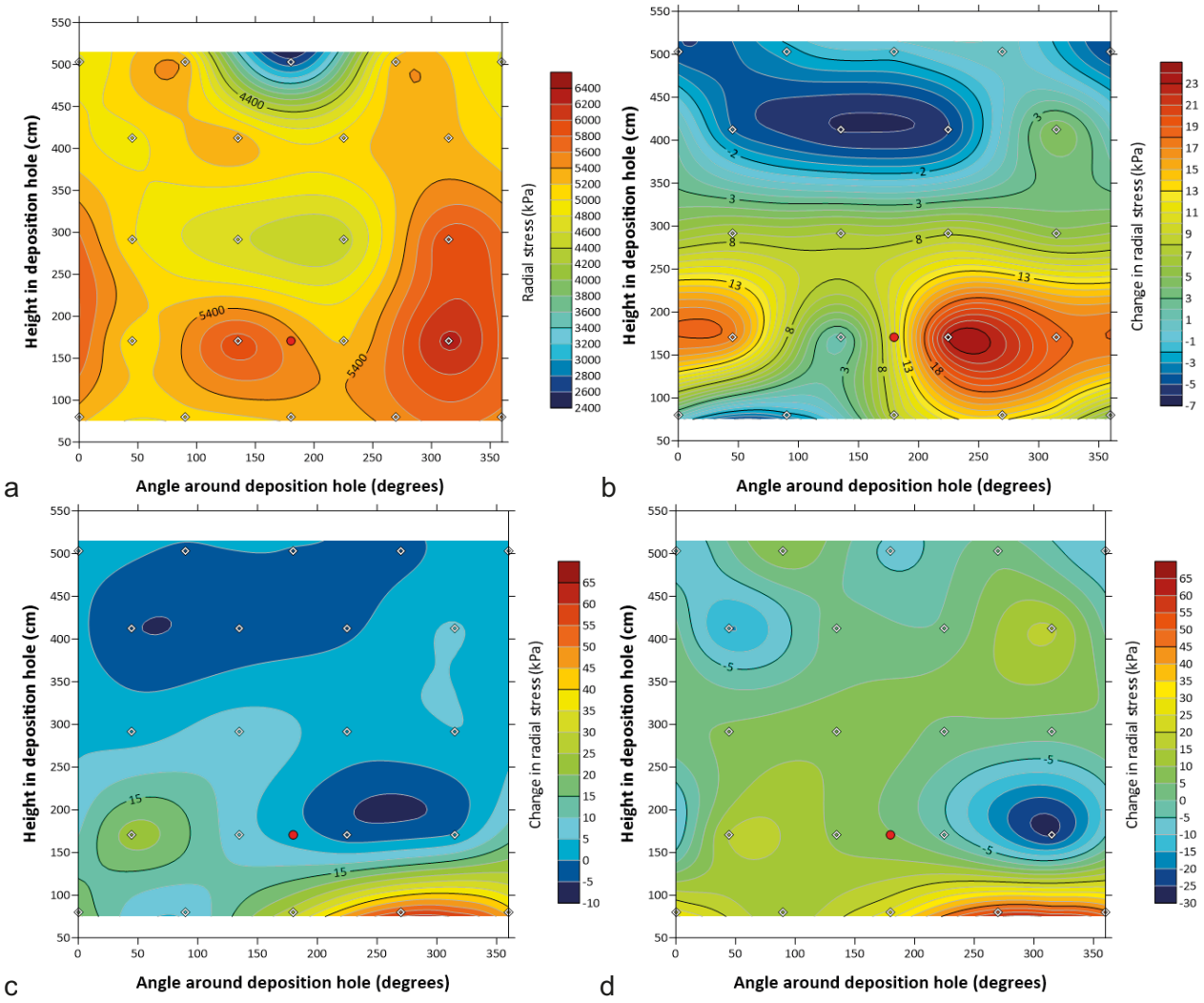

Figure 13-30. *Distribution of radial stress at the deposition hole wall at times around gas entry during Gas Injection Test 6. a) 5 241.55, b) 5 242.11, c) 5 242.85, d) 5 263.95.*

By Day 5242.26 (Figure 13-31c), a low pore pressure zone had formed 90° of FL903 at 270°, with pore pressure increasing below the level of the injection filter. Figure 13-31d and Figure 13-31e show that the minimum pore pressure seen at the injector level at 270° reduced and then increased in negative magnitude, with the pore pressure increase below the injector also varying. By Day 5263.95 (Figure 13-31f) the high-pressure zone had migrated further around the deposition hole to now be on the opposite side of the deposition hole to FL903 (i.e. at 0°. The negative pore pressure zone had dissipated, as had the elevated pore pressure zone below the injector. This result may indicate the movement of the gas front around the canister and in the buffer.

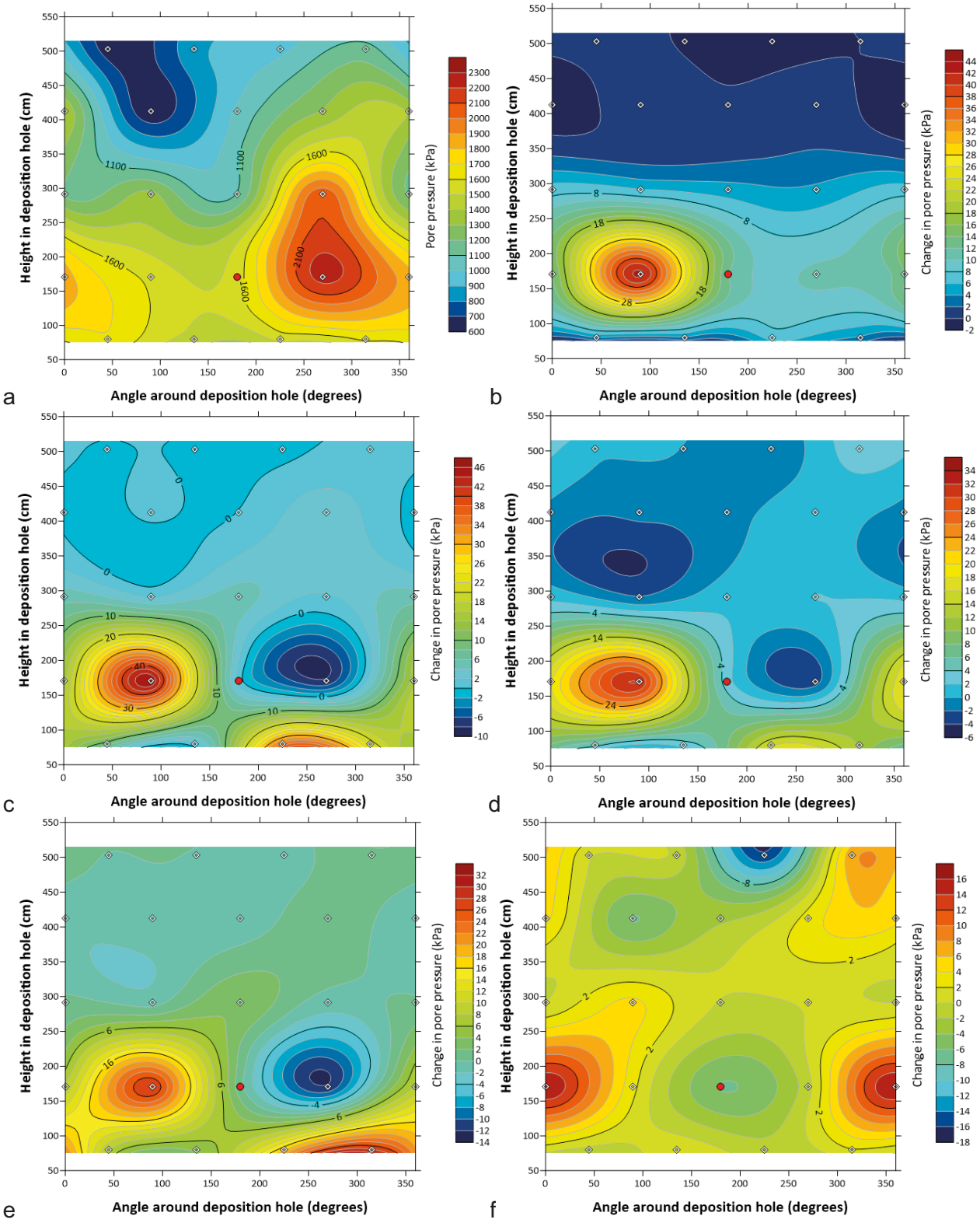

Figure 13-31. *Map of pore pressure at the deposition hole wall at times around gas entry during Gas Injection Test 6. a) 5 241.55, b) 5 242.11, c) 5 242.26, d) 5 242.85, e) 5 243.09, f) 5 263.95.*

Comparing the observations of pore pressure and radial stress during the gas injection time shows different observations. Initially, a localised pore pressure variation was seen, while radial stress showed a much more distributed change. The influence of elevated and/or reduced stress appeared to be temporary, with pore pressure increase appearing to move around the deposition hole.

Figure 13-32 shows sensor locations that show direct movement of gas. As described previously, following peak gas pressure two events of gas pressure drop were described. The second of these resulted in stable pressure decay and a peak in gas flow into the clay. This latter event corresponded with gas reaching canister filter FL901, some 180° around the canister. It should be noted that gas did not intercept FL902 or FL904. Over a period of ~8.5 days, the pressure in FL901 continued to increase until it reached a pressure of ~5 400 kPa, ~650 kPa below the gas injection pressure. No other sensors showed evidence of direct gas movement.

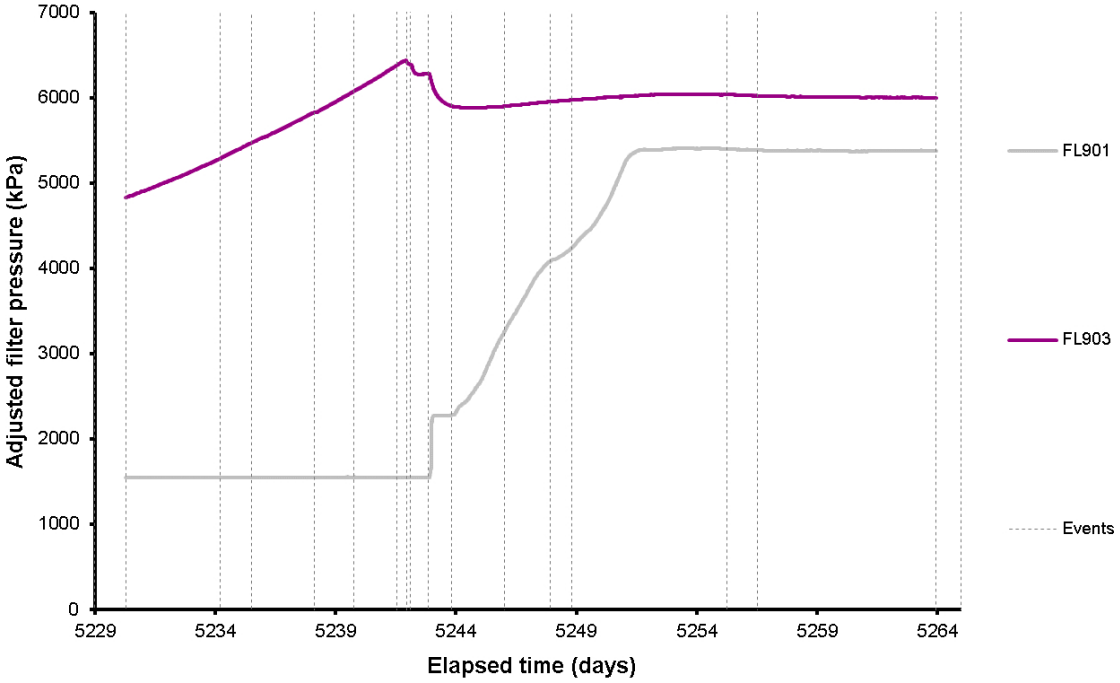

Figure 13-32. *Detail of sensors that show evidence of gas pressurisation during Gas Injection Test 6.*

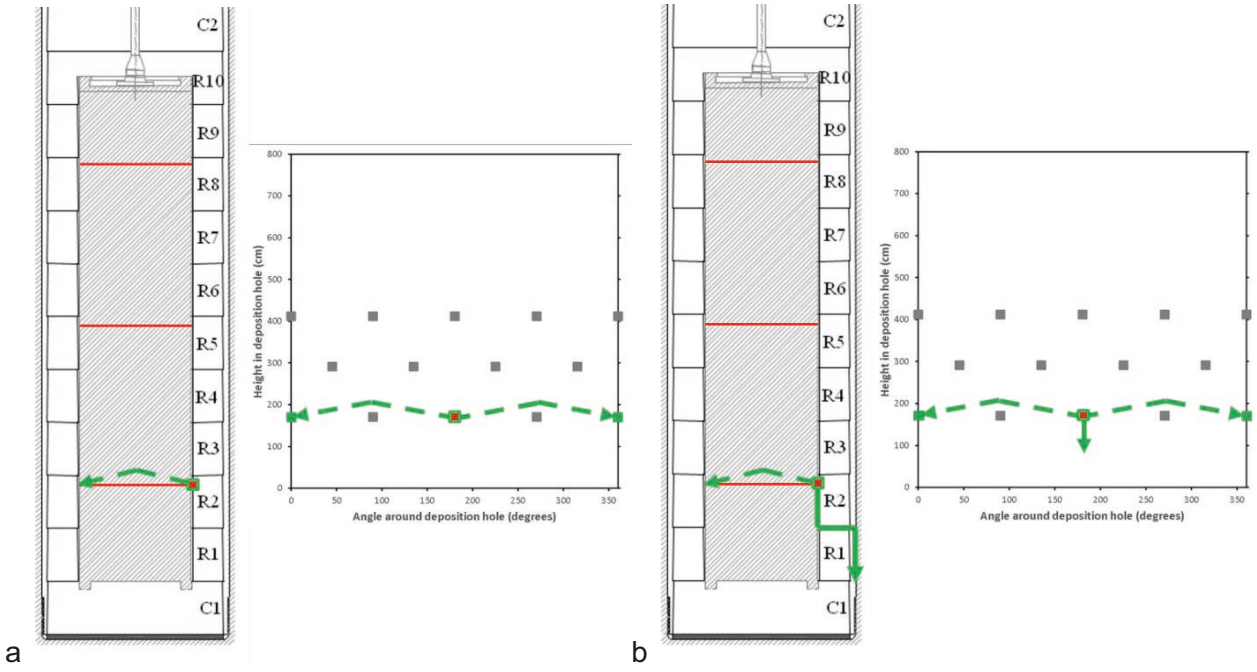

Figure 13-33. *Schematic of the direction of gas flow during Gas Test 6 in lower filter FL903. a) Gas reaching canister filter FL901; b) Gas moving downwards and out of the deposition hole.*

13.4 Summary of Gas Injection Test 6

Gas Injection Test 6 was a relatively short test and was the fourth test conducted using filter FL903.

1) Day 5235.96 : The first evidence of gas entering the clay occurred at a gas pressure of 5 530 kPa. Up until this time, average flow into the clay was 1.41×10^{-9} m^3 s^{-1}.

2) Day 5238.13: Gas pressure increased until an event at a pressure of 5 827 kPa, when a small amount of gas entered the clay, flow peaked at 4.52×10^{-8} m^3 s^{-1} with 0.015 mol He entering the clay. This event only correlated with a subtle change in PB925, a stress sensor within the bentonite above the canister.

3) Day 5241.56: Gas entering the clay began to accelerate when the gas pressure was 6 382 kPa. This event corresponded with a stepped change in pore pressure at the deposition hole wall at UR904 and the start of a more gradual change in many UR and PR sensors local to the injection filter.

4) Day 5241.92: Peak gas pressure was achieved at a gas pressure was 6 437 kPa. Gas pressure initially decreased by ~45 kPa, resulting in a peak in flow of 1.74×10^{-7} m^3 s^{-1}, around 90 minutes after peak pressure. Approximately 0.05 mol He entered at this time. Many of the rock wall sensors registered this event, with a high in radial stress forming 90° clockwise of the injection filter and a high in pore pressure forming 90° anticlockwise of FL903. This event also registered in a hydrodynamic effect seen at the stress sensors on the canister surface.

5) Day 5242.21: The third peak in flow into the clay occurred with a peak flow of 2.11×10^{-7} m^3 s^{-1}. Approximately 0.1 mol He was injected into the clay at this time. This event corresponded with peaks in the disturbance of many of the rock wall and bentonite sensors, both pore water pressure and radial stress. This event was followed by the flow into the clay reducing to become less than the flow into the system and as a result the gas pressure began to increase again.

6) Day 5242.85: The fourth, and final, peak in gas flow into the clay began when gas injection pressure started to decrease. This event resulted in a stable gradual decrease in gas pressure of 560 kPa, reaching a minimum of 5 878 kPa. Flow into the clay reached a maximum of 2.42×10^{-7} m^3 s^{-1} at Day 5242.96. The peak in flow was short-lived with flow into the clay reducing to equal the flow into the system within one day. Most significantly, this event corresponded with the direct movement of gas to filter FL901, 180° around the canister from the injector, with the two intermediate filters (FL902, FL904) not recording any gas flow. This showed that gas movement was not direct and was likely to be localised.

This event corresponded with both positive and negative responses in many sensors on the rock wall and within the bentonite, both pore pressure and stress. This resulted in the formation of a low radial stress and pore pressure region 90° clockwise from the injector and a raised stress region below the level of the injection filter. A raised pore pressure region was formed at 270°.

7) Filter FL901 took 8.5 days to reach a pressure of 5 400 kPa, ~ 650 kPa below the gas injection pressure. At this time, the gas pressure in FL903 reached a plateau and it was interpreted that gas was flowing steadily out of the deposition hole. In total, 3.15 mol He entered the clay following peak pressure.

The data suggests that gas flow occurred through a series of events, with pathways forming resulting in more gas entering the clay. This resulted in gas movement around the canister surface and towards the bottom of the canister, from where, the gas followed a pathway out of the deposition hole, most likely along the interface between bentonite rings R1 and R2, or R1 and C1 at the level of the bottom of the canister.

14 Full Canister Test (Day 5264 – 5689)

The Tenth significant stage of the Lasgit experiment started on Day 5266.20 (4th July 2019) and was completed at Day 5688.95 (30th August 2020); a total stage time of 422.75 days. **Note:** unlike in previous test stages, overlap existed between Gas Injection Test 5, Gas Injection Test 6, and the Full Canister Test stages.

All of the previous gas injection tests were conducted using a limited volume of gas. The Lasgit set-up included two interface vessels of 5 litre volume each in the laboratory. This limited the gas volume to 5 litres at the start of gas injection or whenever the interface vessel was re-charged as the two interface vessels were on separate parts of the injection system. The Full Canister Test aimed to investigate whether the volume of gas played a role in gas migration. In effect, the 5-litre interface vessel was replaced by the copper canister, with an internal volume initially estimated to be greater than one cubic metre (1 000 litre). The test would also be conducted differently, with new gas added (interface vessel) to a constant volume (canister) to increase gas pressure, as opposed to a fixed quantity of starting gas being compressed to increase pressure. During a normal test at gas entry, the limited volume of gas in the interface vessel was increased as pathways formed. This resulted in a reduction in gas pressure. Assuming that the FCT would result in the formation of dilatant pathways of similar volume to that seen in GT1 to GT6, there would be no noticeable reduction in gas pressure at peak conditions. In other words, in GT1 to GT6 the pathway volume was significant compared with the volume occupied by the gas in the interface vessel, whereas the pathway volume in the FCT is very small, and therefore insignificant, compared with the volume of gas in the canister. The Full Canister Test would examine whether this changed the dynamics of pathway propagation. Figure 14-1 shows the plan for the test period. No artificial hydration occurred during the period, with a small overlap between the Full Canister Test and the repeat hydraulic tests conducted in filters FL903 and FU910.

Because of the limitations of the set-up, the Full Canister test only had a gas injection stage; a two gas-ramp injection test (Figure 14-2). It was not possible to conduct a hydraulic test either before, or after the gas injection test. As will be described later, the raising of gas pressure within the canister did not result in gas entry and the pressure of the canister was maintained until gas movement was initiated.

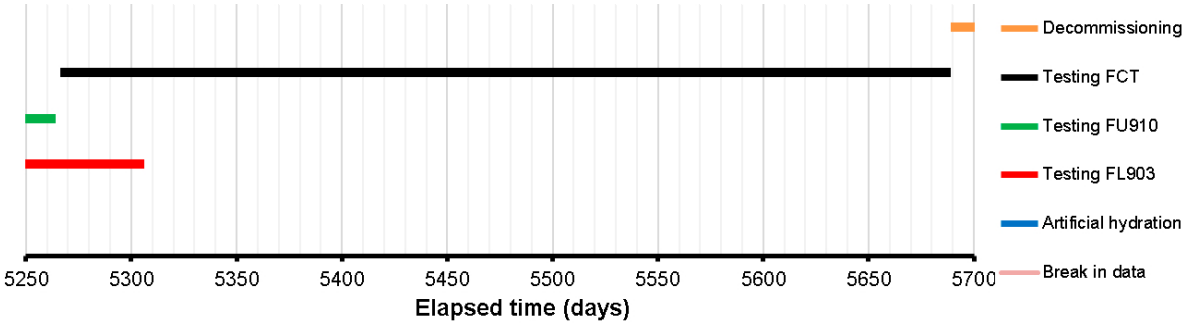

Figure 14-1. *Test stages of the Lasgit experiment showing what was conducted during the Full Canister Test.*

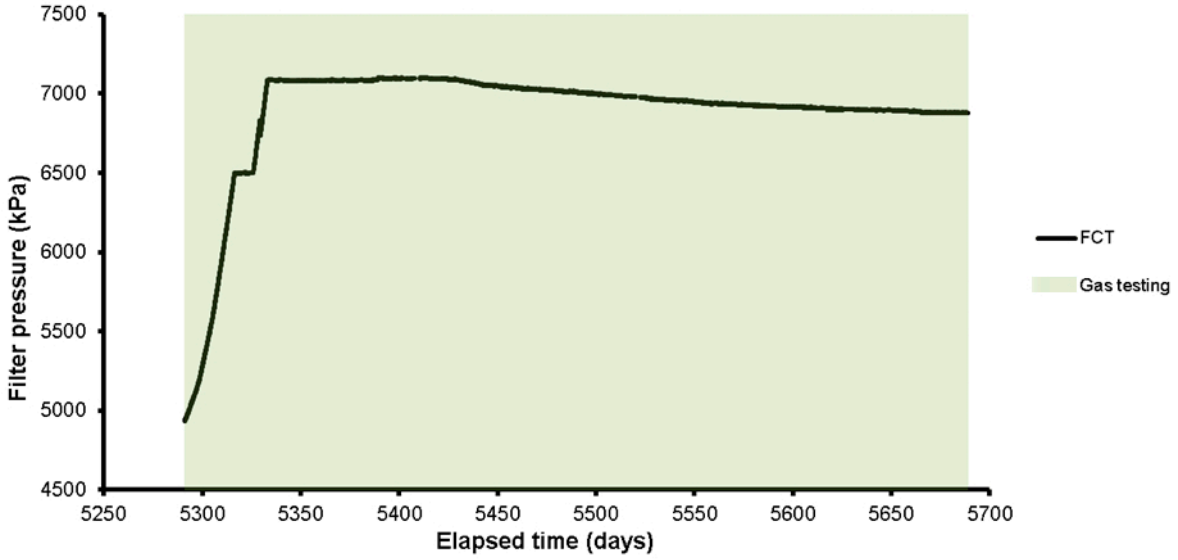

Figure 14-2. *The gas pressure of canister during the Full Canister Test.* ***Note:*** *green shading shows periods of gas testing.*

14.1 Modification of the test setup and gas injection procedure

In order to conduct the Full Canister Test a number of important modifications were needed to the existing Lasgit Laboratory. 1) A large supply of gas was needed and this was achieved by adding a pallet of 12 J-cylinders of Nitrogen to the system (see Figure 14-4). This was a sufficient volume of gas to raise the pressure in the canister up to the expected gas entry pressure. 2) A reliable supply of water was needed in order to use the existing interfaces vessels to get an accurate estimate of gas pumped into the canister. 3) An additional pressure sensor in the interface vessel circuit to measure the pressure of the interface vessels. 4) Re-plumbing of the system to facilitate the test. 5) The addition of two one-way valves to add safety in the Lasgit laboratory.

A schematic of the modified laboratory is shown in Figure 14-3. The following will outline the modifications and how the test was operated:

1) The first modification was to allow both interfaces to be used in series, meaning that 10 litres of pressurised gas could be added to the canister in one go and mean that the refilling of the interface vessels would occur less frequently. This gave 10 litres of volume per refill. A pore pressure sensor (labelled P) was added so that the pressure in the interface vessels was known.

2) The second modification was the addition of the gas pallet (as shown in Figure 14-4 and green square in Figure 14-3) to the end of the interface vessel circuit through valve V056.

3) The third modification was the addition of two one-way valves to the system to add safety to the ISCO pumps. If the ISCO pump was to leak, it could mean that the contents of the interface vessel could discharge through the pump/refill circuit. At certain times in the pressurisation procedure, it could mean the contents of the interface vessel or gas supply could leak through the pump. Therefore, two one-way valves were added near valves V002 and V016 (as shown by arrows in Figure 14-3) to prevent backflow.

4) The fourth modification was the addition of the water bowser (see Figure 14-3) to the water inlet of the syringe pumps.

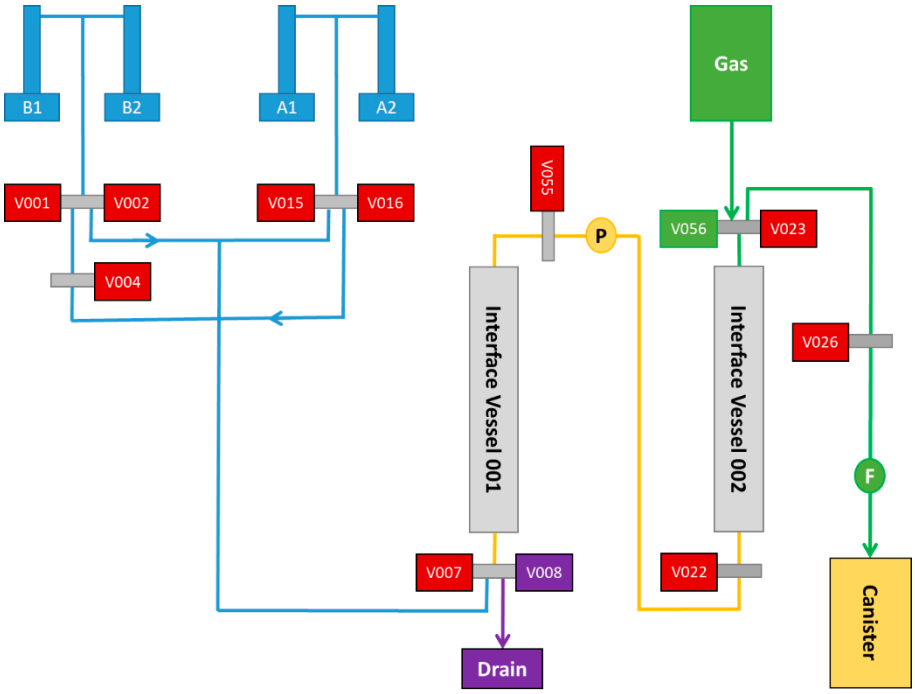

Figure 14-3. *Schematic of the modifications made to the Lasgit laboratory to allow the Full Canister Test to be conducted. Blue lines are water; green lines are gas; yellow lines are water or gas depending on refill state.*

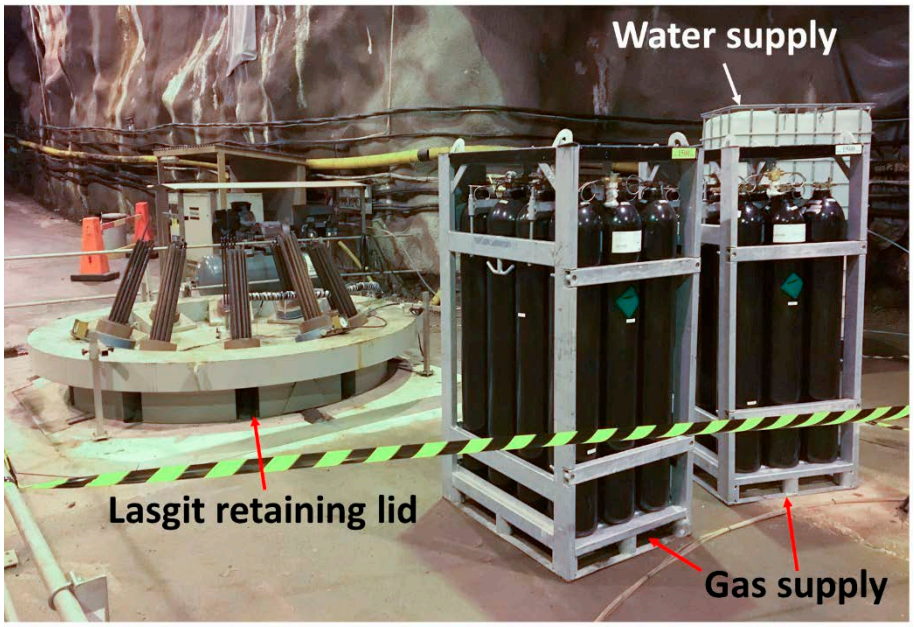

Figure 14-4. *The addition of a pallet of 12 J-cylinders of gas and a water bowser to the Lasgit experiment in order to perform the Full Canister Test.*

14.1.1 Operation of the Full Canister Test

The following bullet points will describe how the Full Canister Test was conducted:

1. The gas supply was used to directly fill the canister to a starting pressure of around 5 000 kPa, this took nearly 24 hours as filling was slow being limited by the small diameter of the pressure lines.
2. With valve V023 closed (canister isolated from system), and valve V007 closed (pump system isolated), valve V008 was opened to drain the interface vessel. Once this was fully drained, V008 was closed.
3. The interface vessel was filled by opening valve V056. The pressure of the interface vessel was monitored at P until the pressure was approximately equal to the pressure in the canister. Valve V056 was closed and the starting interface vessel pressure was noted once pressure was stable.
4. Valve V023 was opened, re-connecting the interface vessel with the canister. The pressure of the interface vessel and canister were noted.
5. Valve V007 was then opened and either pump-set A or B was started.
6. The pumps, operating in reciprocating mode, would then fill the interface vessel with water, adding gas to the canister. If would take 20 pump refills to fully empty the interface vessels of gas, as each pump's volume was only 0.5 l, so 19 full refills were aimed for.
7. Valve V007 was closed to isolate the pump and the pump was stopped and the volume of the pump noted. Valves V026 and V023 were closed to isolate the interface vessel from the canister. Valve V008 (drain) was opened and the pressure of the interface vessel was monitored. The small (~ 1 litre) remaining volume of gas pushed out the water from the interface vessels. The rate of pressure decay was relatively slow and when the water was expelled, the rate of change would increase as it was easier for gas to drain through the narrow pressure tube-work. Once the rate of change was detected, valve V008 was closed. It took around 20–25 minutes to drain the interface vessel, depending on the pressure and volume of the remaining gas.
8. The procedure was repeated by performing stages 3–7. For each re-fill procedure, the total volume of water pumped into the interface vessel was calculated.

The procedure was timed so that refilling occurred between 12 and 24 hours, with most occurring on a 12-hour interval. Throughout the pressure ramp, a total of 55 refills were performed.

At the end of the experiment it was necessary to reduce the pressure of the canister in a controlled and safe manner. This was done in a similar way to filling. Valve V026 was opened to fill the interface vessel with gas and closed when full, as indicated by a stable pressure. Valve V026 was then closed and V008 opened to drain the contents of the interface vessel. The pressure of the interface vessel was observed and indicated when it was empty. Valve V008 was then closed and the procedure repeated. It took 55 emptying cycles until the pressure was such that the remaining volume of gas could be directly vented. Each single cycle took between 15 and 50 minutes depending on the pressure of the canister.

14.2 Description of the field parameters during the period

Before describing the gas injection test, the field parameters will be described (boundary conditions). **Note:** The grey areas displayed in the graphs shows periods when artificial hydration was not occurring.

14.2.1 Initial pressurisation of the canister

As this section will highlight, the boundary conditions of the Full Canister Test were substantially modified by the pressurisation of the canister. This was compounded by a leak, which resulted in a second fill of the canister. Before describing the boundary conditions, it is necessary to detail how the canister was pressurised.

Figure 14-5 shows the initial pressurisation of the canister during the site visit on Day 5266. It should be noted that the pressure sensor of the canister was located on the gas supply side of the system. In effect, the setup comprised a gas supply connected to the canister by a single thin high-pressure line. Therefore, if pressure was raised on the gas supply side it took some time for gas to flow into the canister through the restriction of the pressure line. This meant that during initial filling, the pressure registered by the canister pressure sensor represented the pressure on the gas supply side and not necessarily the pressure within the canister itself. This resulted in the complex initial response shown in Figure 14-5. The fill of the canister directly from the pallet of gas cylinders was controlled by a regulator. As shown, it took around 5 hours before a stable fill was established and the system was left to fill overnight. It took nearly 24 h to bring the pressure in the canister up to the starting pressure of approximately 5 000 kPa. The system was left with the canister in direct communication of the gas supply and was left to equilibrate.

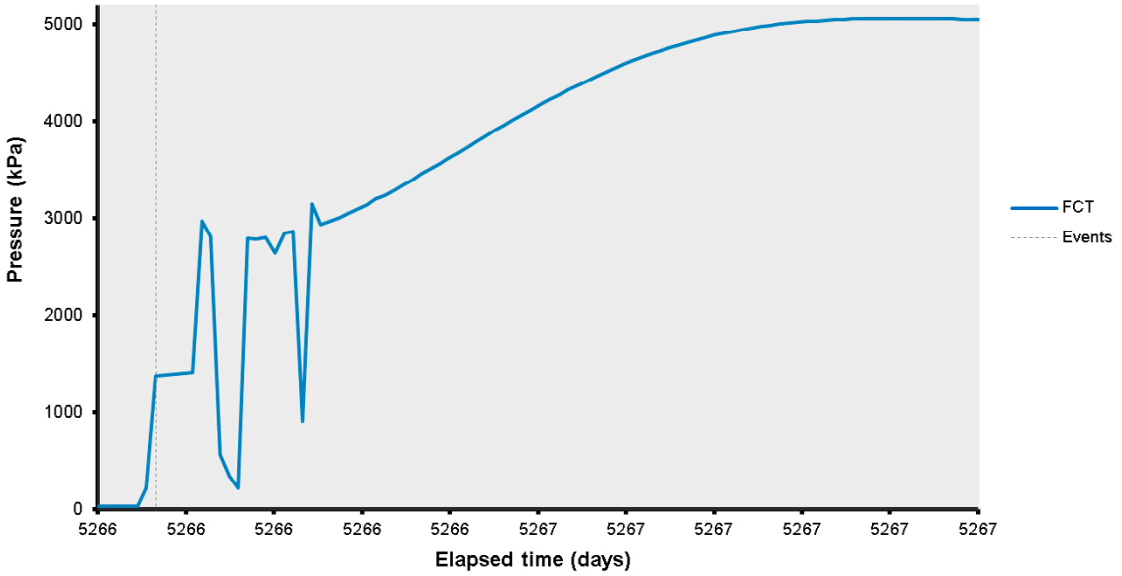

Figure 14-5. *Initial pressurisation of the canister.*

Figure 14-6 shows the pressure of the canister. Following the lab visit and filling of the canister, local staff of the Äspö HRL inspected the system on Day 5268. This showed that the cylinder side of the regulator on the cylinder pallet had significantly reduced in pressure over the weekend, i.e. the volume of gas in the pallet was significantly reduced. The canister was isolated at Day 5268.56 to observe pressure. It was expected that an initial loss of pressure would happen as gas cooled in the canister and gas went into solution. However, pressure was reducing at 10 kPa per hour, which was significant. The gas supply was re-established to the canister at Day 5269.14 to see if re-pressurisation would change the rate of pressure decay. The canister was isolated for a second time at Day 5269.44, this time giving a pressure reduction rate of around 7 kPa per hour. This was lower than previous but still a substantial rate, this confirming the presence of a leak in the system.

Staff at the Äspö HRL could not identify position of the leak. Therefore, an emergency site visit was necessary, with BGS staff arriving on Day 5277. It was quickly established that the leak was not occurring within the Lasgit laboratory, meaning that it was either occurring in the pressure line to the canister or from one or more of the connections to the canister. The hollow Monel pipe was filled with water to see if any bubbles were apparent. No such bubbles were seen, suggesting that the leak was not from the inaccessible pressure fittings on the lid of the canister. The bundle of cables and pressure lines running from the laboratory to the Monel pipe running through the retaining lid to the canister were carefully examined. It was at first believed that the thermocouple from the canister was the cause of the leak as this was not pressure sealed in any way. The thermocouple was severed and capped to make the line from the canister pressure tight. This made no difference to the rate of pressure decay. It was postulated that the compressed air line to the canister could have been a source of a leak, although a raised pressure was not detected. The valve operating the Full Canister Test valve was closed. Further examination of the bundle of cables and pressure lines leading to the canister found that the cable leading to the canister stress sensors were not pressure sealed and that one of these was a source of leaking gas, as detected by a leak solution with a slow but steady, release of gas. It was decided to sever all three stress sensor cables and to pressure seal the lines transporting the cables. Unfortunately, cutting the cables greatly increased the rate of gas flow with a high-pressure discharge of gas that was too high to cap in a safe manner. Therefore, gas was allowed to drain from the canister until it was safe to cap the lines. This resulted in a reduction in canister pressure to ~750 kPa before the lines were capped and sealed. It should be noted that the pressure in the canister was not measured between Day 5278.05 and Day 5277.96 as part of the system was isolated to ensure that the leak was not from the pressure transducer part of the system and the pressure sensor was shut-in; to determine if that the transducer was leaking.

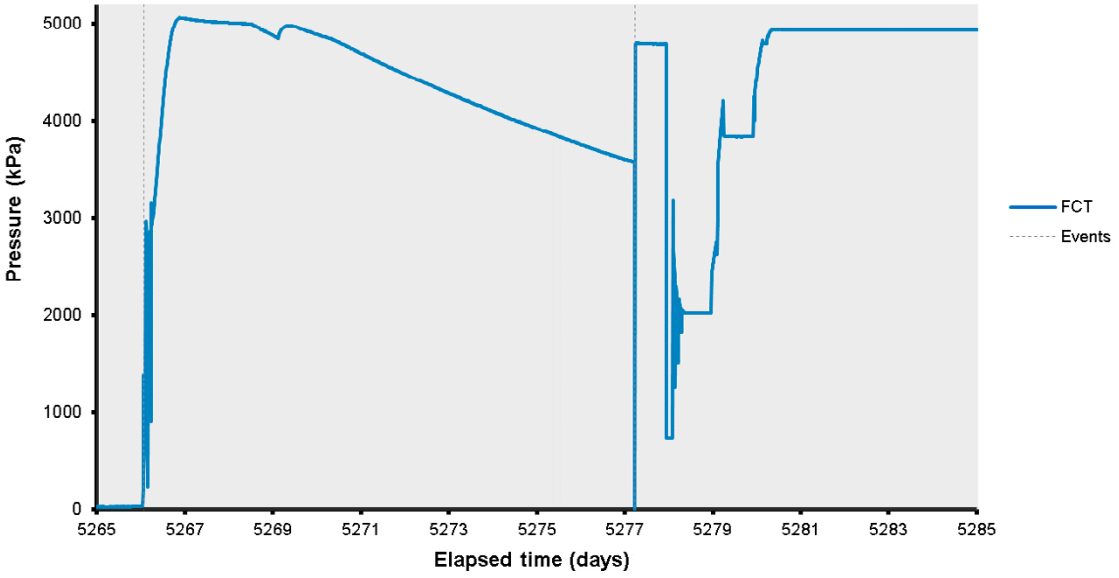

Figure 14-6. *Pressure of the canister during the initial pressurisation, showing the leak in pressure and the re-establishment of canister pressure.*

Pressure monitoring at Day 5277.96 showed that the canister pressure was no longer reducing and that the leak was sealed, assuming that it was not a pressure dependent feature. The amount of gas lost from the system was sufficient to mean that not enough gas was available in the gas pallet to enable a full gas ramp. Therefore, a second pallet was added.

The canister was re-filled from the cylinder pallet carefully to make sure the canister was leak tight. Initially, gas pressure was raised to ~2 000 kPa on Day 5278 in order to determine the leakage rate, which was found to be negligible. Pressure was increased in a number of steps up to 4 950 kPa, with no leaks detected. Therefore, the experiment could progress, and the system was setup to allow a gas ramp to occur.

In establishing a leak tight pressurised system, the canister was pressurised, slowly depressurised, rapidly depressurised, and then re-pressurised in steps. Figure 14-7 shows that this complex history had a profound impact on the entire Lasgit system. Radial stress is shown in Figure 14-7a, while the change in stress is shown in Figure 14-8a. As shown, the initial pressurisation of the canister resulted in an increase of all PR sensors. The change ranged between 344 and 675 kPa, with PR912 showing the greatest change and PR904 showing the least. Radial stress increased while the canister was being pressurised and once the canister had reached pressure the radial stresses started to decay. By the time of lowering the pressure in the canister at Day 5277.36, the increase in stress as a result of pressurisation had decayed to range between 21 and 145 kPa. Figure 14-10a shows the distribution of the change of radial stress distribution as a result of canister pressurisation. It shows that the greatest increase occurred at the mid-height of the canister, while the least change occurred at the top and the bottom of the sensor array. This was not unexpected as the greatest mechanical deformation of the canister will have occurred at its centre (barrelling). Figure 14-10c shows the change in stress when the canister was depressurised. This shows the inverse of pressurisation, with the centre decreasing the most and the top and bottom of the array showing only a minor reduction in stress compared with the starting condition.

Figure 14-7b shows the response of pore pressure at the deposition hole wall as a result of canister pressurisation, while Figure 14-8b shows the change in pore pressure. This shows that the pressurisation of the canister had a profound influence on all UR sensors. However, unlike in the PR sensors, there were differences in the general form of the change. Some sensors, such as UR910, reacted very quickly to the pressurisation, whilst others, such as UR921, took much more time to react, or reacted more gradually. At the end of initial pressurisation, the UR sensors changed between 6 and 814 kPa, with UR910 showing the greatest change and UR919 showing the least. Prior to the depressurisation of the canister, the change in pore pressure had decayed to range between −70 and 463 kPa. When the canister was de-pressurised change in pore pressure ranged between −375 and 291 kPa, with UR918 showing the lowest pressure and UR910 still showing positive pressure change. Figure 14-10b shows the distribution of the change of pore pressure at the end of initial pressurisation. This shows an increase in pore pressure towards the bottom of the canister and the least change towards the top of the sensor array. When the canister was depressurised (Figure 14-10d), the largest reduction occurred towards the top of the canister, with the high-pressure region that formed at the base of the canister still prevailing.

Figure 14-9 compares the average change in pore pressure and radial stress at the deposition hole wall. In general, the two compare well, with pore pressure showing a lower magnitude change. There were differences when the canister was re-pressurised in steps.

Figure 14-7c shows the change of radial stress within the bentonite. This highlights that the changes seen were not just at the deposition hole wall and were occurring throughout the bentonite buffer. Sensor PB902 showed the largest change of 250 kPa, while sensor PB901 showed the least change of −24 kPa. The form of all responses was similar, except for PB902, which showed a decrease before all other sensors peaked.

The sensors all showed considerable change when the pressure in the canister was reduced in order to fix the leaking canister. Figure 14-7 and Figure 14-8 shows that all sensors greatly decreased in reading at this time. For pore pressure, most UR sensors reduced considerably to be lower than when the canister was first pressurised. The only exceptions were UR907 and UR910, which after decreasing were still at an elevated level. All radial stress sensors decreased to be less than at the start of canister pressurisation. Re-pressurisation then increased pore pressure and stress, although not to the same values as during the first initial pressurisation.

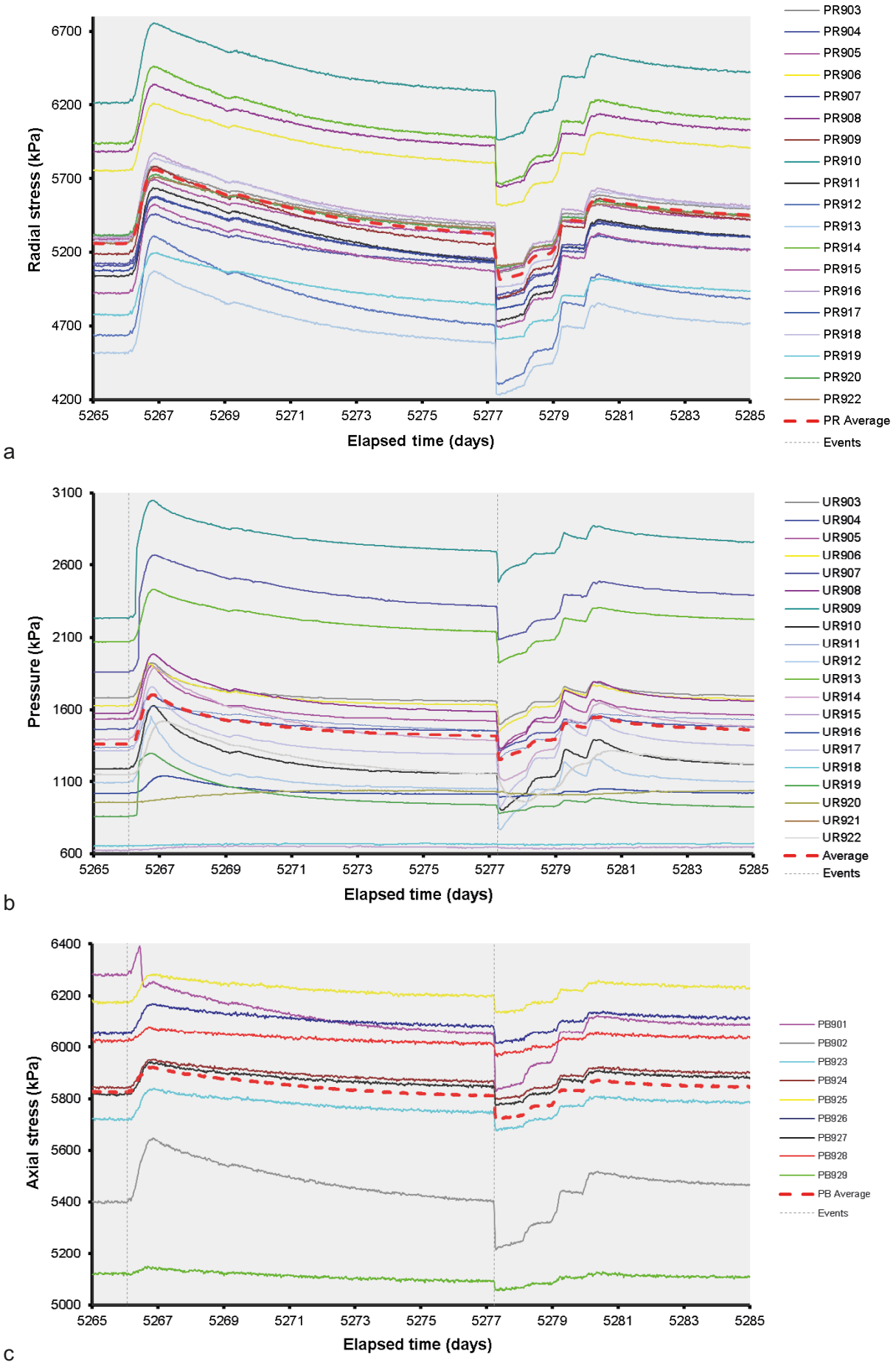

Figure 14-7. *Stress and pore pressure response of the canister being pressurised. a) Radial stress at the deposition hole wall; b) Pore pressure at the deposition hole wall; c) axial stress within the bentonite buffer.*

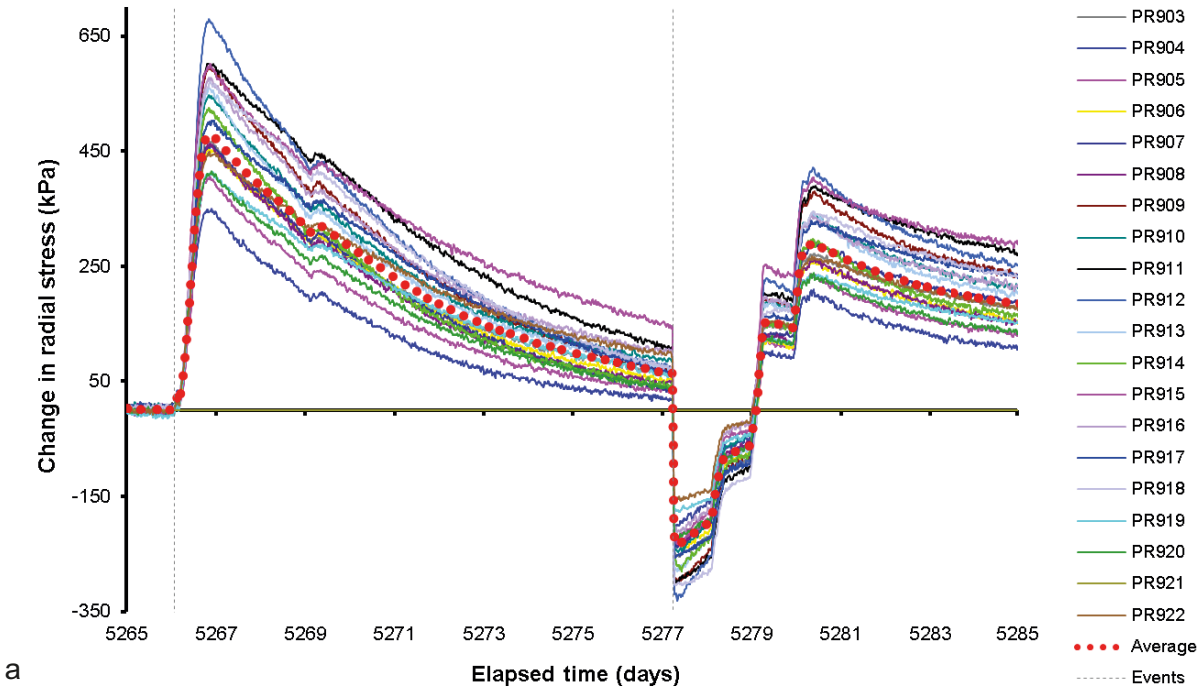

a

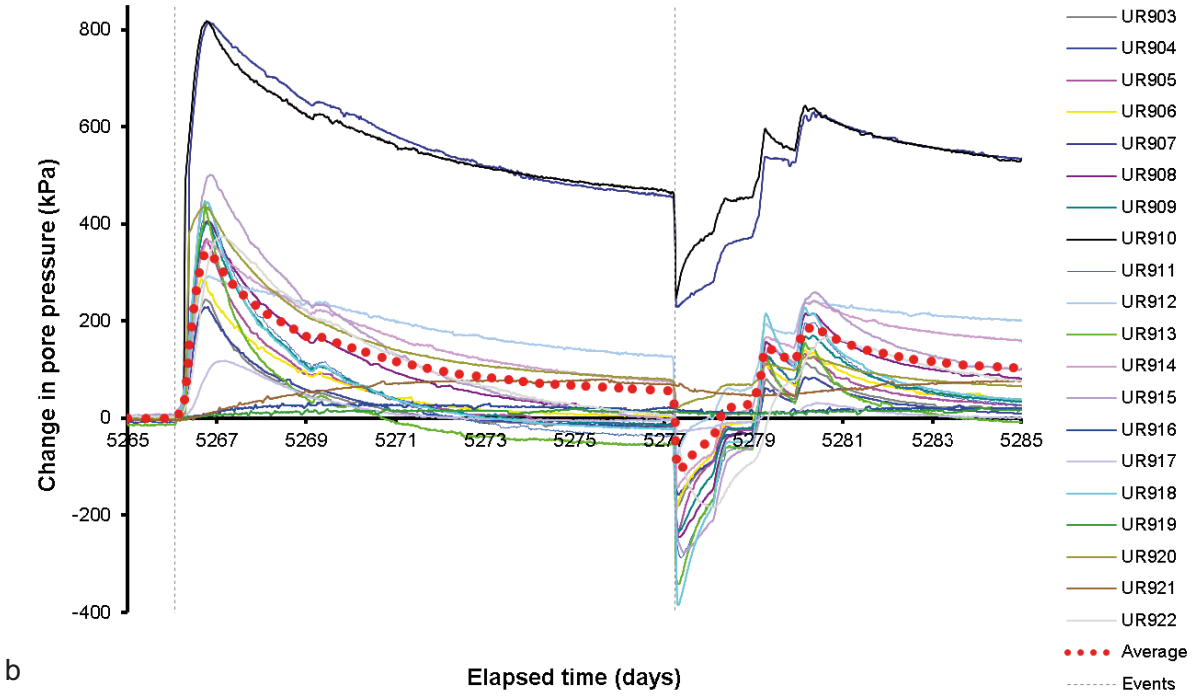

b

Figure 14-8. *Change in stress and pore pressure at the deposition hole normalised to Day 5266.00. a) Radial stress; b) Pore pressure.*

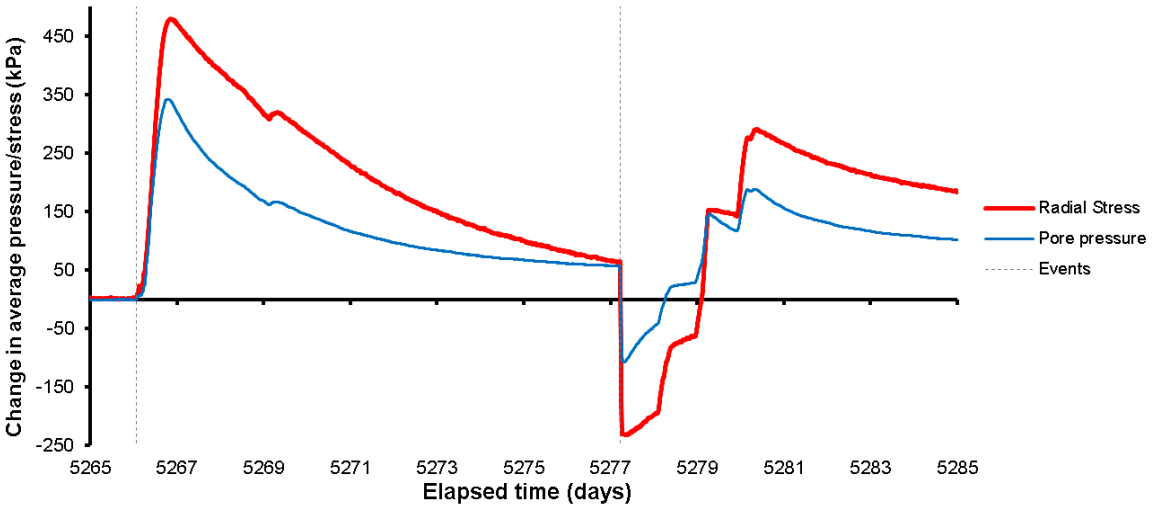

Figure 14-9. *Average change in radial stress and pore pressure at the deposition hole normalised to the Day 5266.00.*

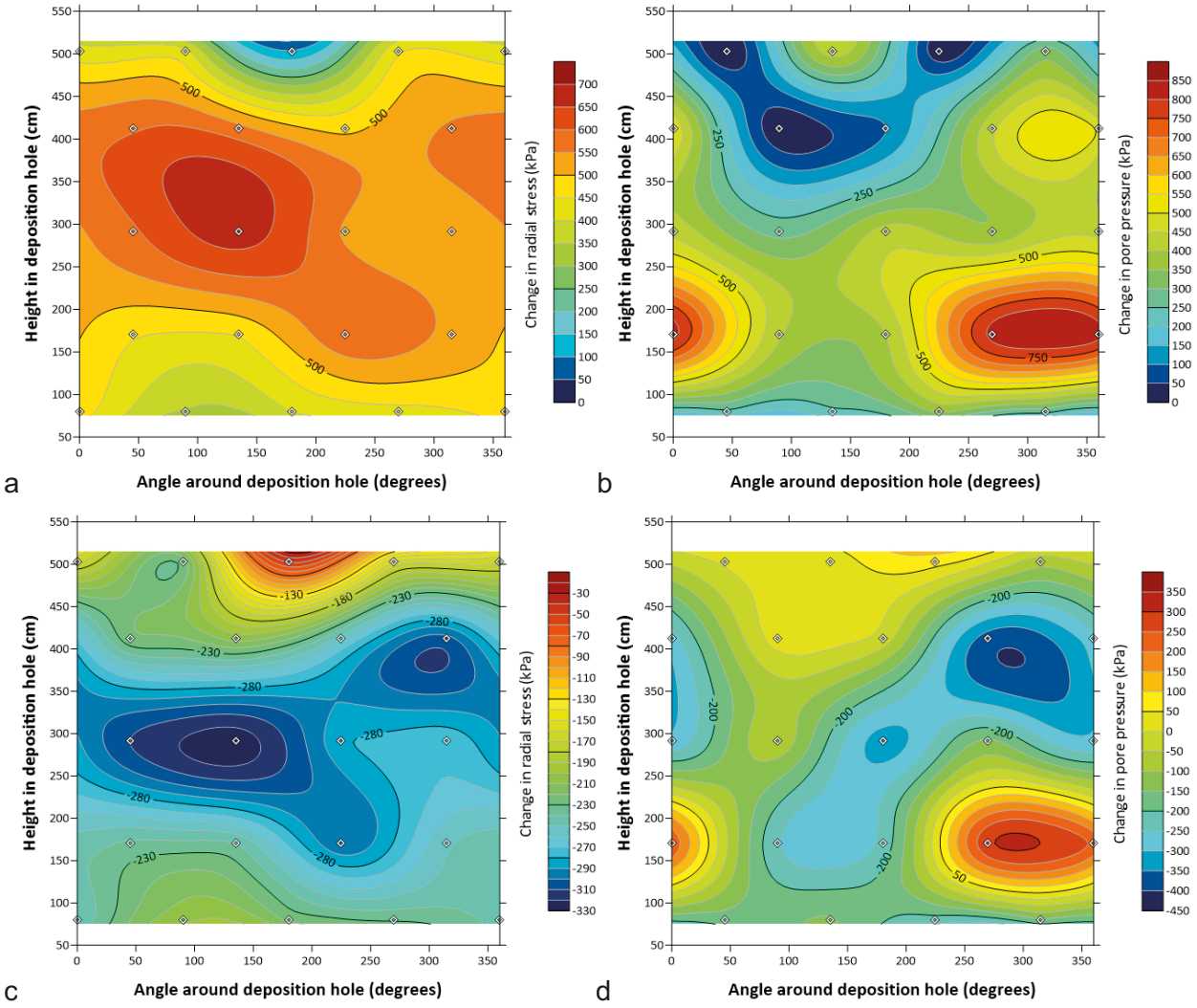

Figure 14-10. *Change in stress and pore pressure distribution as a result of initial canister pressurisation. a) Radial stress change during pressurisation (Day 5266.81); b) Pore pressure change during pressurisation (Day 5266.81); c) Radial stress change during de-pressurisation (Day 5277.36); d) Pore pressure change during de-pressurisation (Day 5277.36).*

The behaviour seen can be explained by drainage of the bentonite. Pressurisation of the canister resulted in it mechanically expanding ~50 µm in diameter. The addition of relatively warm gas will also have resulted in thermal expansion. The mechanical loading of the buffer was at such a rate that the bentonite could not drain and therefore started to react as an undrained medium. This raised pore pressure as the pore network contracted. Radial stress increased as a result of the mechanical deformation of the expanding canister and the swelling of the bentonite in response to an increased pore pressure. The raising of pore pressure will have initiated hydraulic flow, and therefore pore pressure then decayed as fluid was expelled from the bentonite buffer into the surrounding wall rock. The canister was deflated at a rapid rate in order to fix a leak. Again, this occurred at a rate greater than the hydraulic properties of the buffer and therefore the clay went into suction as the pore network expanded as a result of mechanical heave as the canister contracted and the buffer volume increased. Re-loading occurred at a relatively rapid rate as well, increasing radial stress and pore pressure in the same way as before. However, as the system had drained and then went into suction, the increase in stress was not as dramatic.

The response to mechanical loading is likely to be rate dependent. A rapid increase in pressure greater than the drainage properties of the buffer resulted in an increase in pore pressure and stress. As seen in the pressure ramp, which was conducted much slower than the initial pressurisation, the rate of pressurisation would have needed to be slow in order for there to be no change in stress or pore pressure. The mechanical loading of the canister during pressurisation and the relief of pressure during venting of the canister needs to be considered in Performance Assessment models.

14.2.2 Canister pressure

As the previous section has shown the boundary conditions were profoundly changed by the pressurisation of the canister, Figure 14-11 shows the pressure of the canister. It shows that after the initial pressurisation described above, a two-stage gas injection test was conducted by increasing the amount of gas in the canister. Unlike in previous gas injection tests, the volume of gas remained fairly constant. Pressure was increased to 7083 kPa and then held constant. As the initial pressurisation caused significant disturbance to the pore pressure and stress within the system, it was expected that the pressure ramp would also have an impact. The results of this will be discussed in the following section.

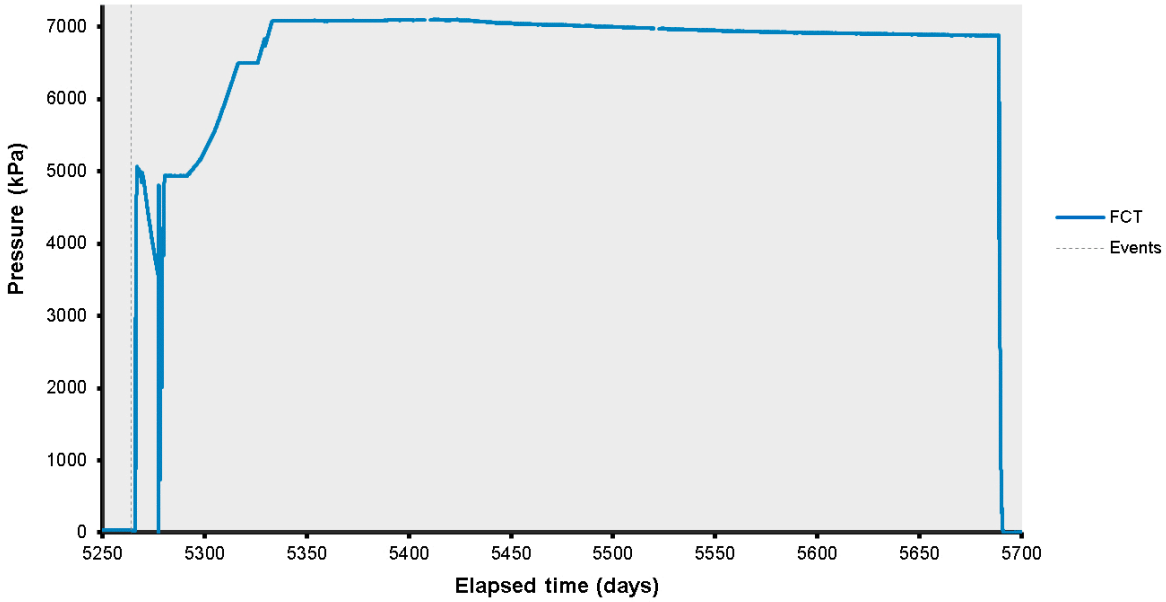

Figure 14-11. *Pressure of the canister during the Full Canister Test.*

14.2.3 Boundary conditions

Figure 14-12 shows the pore fluid pressure of the filter mats. As artificial hydration had stopped at Day 3751, all four filter mats recorded natural pore pressure. As can be seen, FB903 was unintentionally vented during the site visit at Day 5264, reducing the pressure in the filter mat from 690 to 221 kPa. Over the following 80 days the pressure in the filter mat recovered. Considerable heterogeneity existed in the pressure in the filter mats. At FR902 the pressure was low and only around 140 kPa at the start of the period and slowly increased to reach 255 kPa by the end of the stage. The other filter mat on the rock wall (FR901) had the largest pressure of all of the filter mats. At the start of the stage it had a pressure of 1 620 kPa and slowly decayed throughout the Full Canister Test to reaching 1 590 kPa by the end of the stage. Neither rock wall filter mat showed any annual variation and only FR901 showed any variation related to the pressurisation of the canister. The filter mats within the bentonite showed similar responses, with FB903 recording approximately 240 kPa more than FB904. Both filter mats within the bentonite showed considerable annual variation with an amplitude of around 285 kPa.

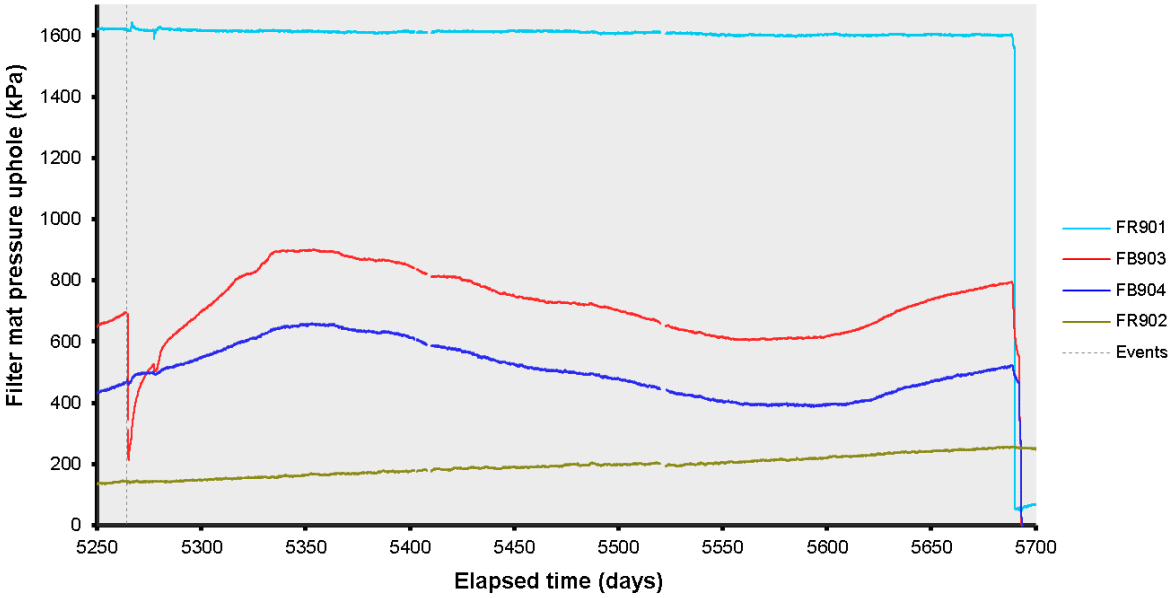

Figure 14-12. *Evolution of water pressure in the filter mats located on the borehole wall and within the bentonite blocks.*

Figure 14-13 shows the pore pressure within the bentonite buffer (UB), recorded at six locations. Figure 14-13a show the results were dominated by pressurisation of filter UB902 during previous gas injection testing. Figure 14-13b shows that all sensors showed considerable annual variation. This was most pronounced in filter UB926 towards the top of the deposition hole. As well as the variation on a yearly time-scale, a higher frequency response was seen with a period of around 40 days. Taking annual variation into account, pore pressure within the bentonite decreased during the period. The response of UB901 and UB902, situated below the canister, was dominated by changes in pore pressure as a result of the canister being pressurised. All other filters showed a response to this, except for UB923. The results of Figure 14-13a are dominated by a second episode of re-pressurisation of UB901 starting at Day 5410, this will be discussed in more detail in Section 14.3.

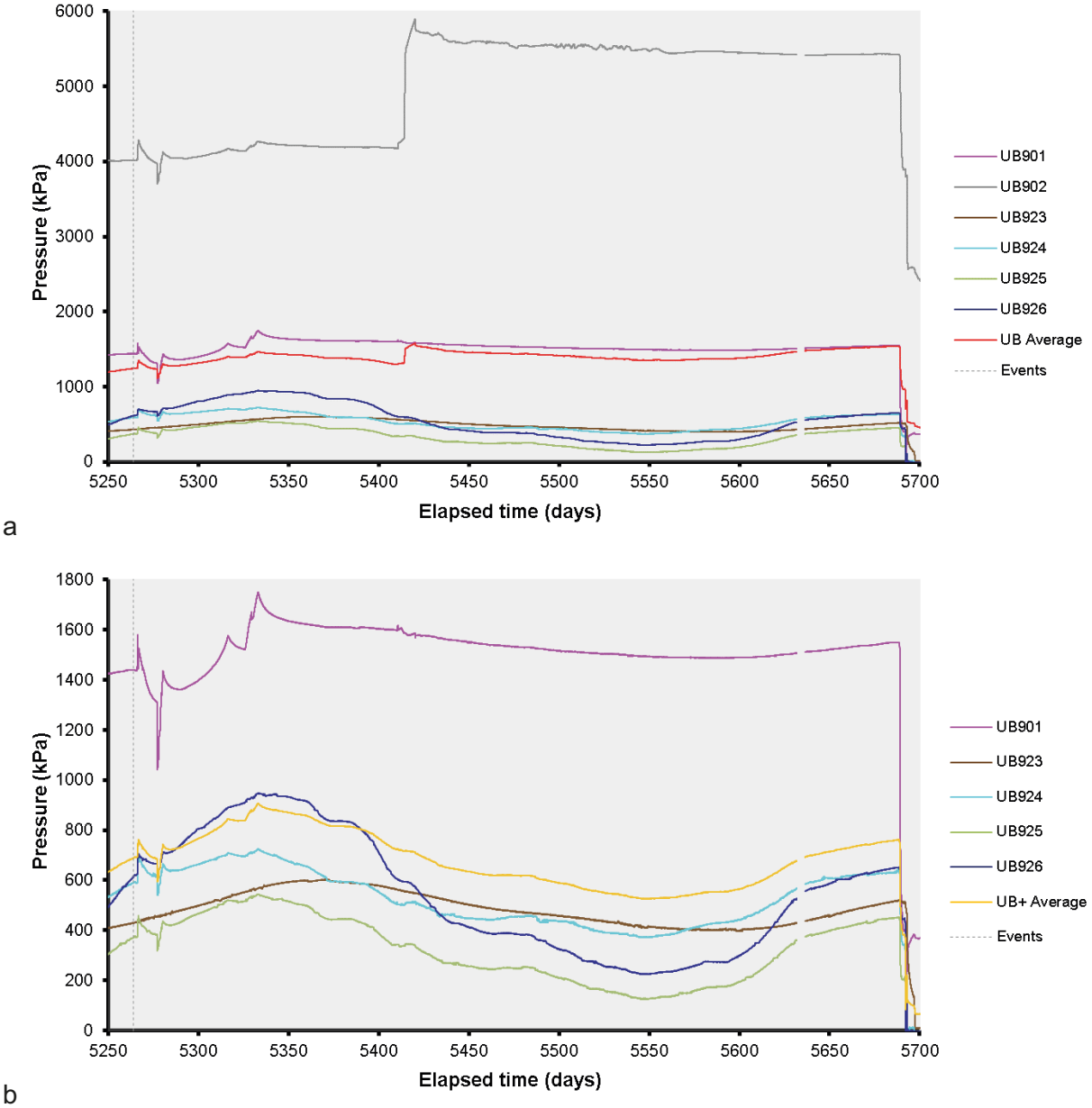

Figure 14-13. *Variation in porewater pressure within the bentonite at the 6 monitoring points: a) all six sensors; b) detail of five sensors.*

Pore pressure was also monitored at the canister filters as these were not used for artificial hydration of the system. Figure 14-14a shows that the data during this period were dominated by the hydraulic test at the start of the period in FL903, the raised pressure in filter FL901, and the raised pressure in FU909. The latter of these simply decayed during the reporting period, from a starting pressure of 4 650 to 2 800 kPa at the end. Filter FL901 was re-pressurised by the Full Canister Test at Day 5420; this will be discussed in more detail in Section 14.3. Figure 14-14b shows the details of the remaining filters, most of which were recording equilibrated pore pressure. Filter FL904 showed the lowest pressure, with a pressure of 100 kPa at the start of the period, increasing to 155 kPa by the end. After the two-stage hydraulic test, filter FL903 quickly recovered to a pressure of 1 750 kPa, slowly decaying to the end of the period. Filters FL902 and FU910 showed a slow, gradual increase in pressure during the period. The four filters of most interest were FM905 to FM908, which all showed a considerable response to the pressurisation of the canister. This showed that the centre of the canister was where the mechanical deformation was greatest as a result of pressurisation, Filters FL902, FU910, and FU911 showed minor pressure responses as a result of the initial filling of the canister. Following the increases in pressure seen at the mid-plane filters, the four FM90x filters decayed for the remainder of the period. This shows the increase in pressure was as a result of mechanical loading of the pore network, raising pore pressure and initiating hydraulic flow. This flow drained the system, reducing the pore pressure.

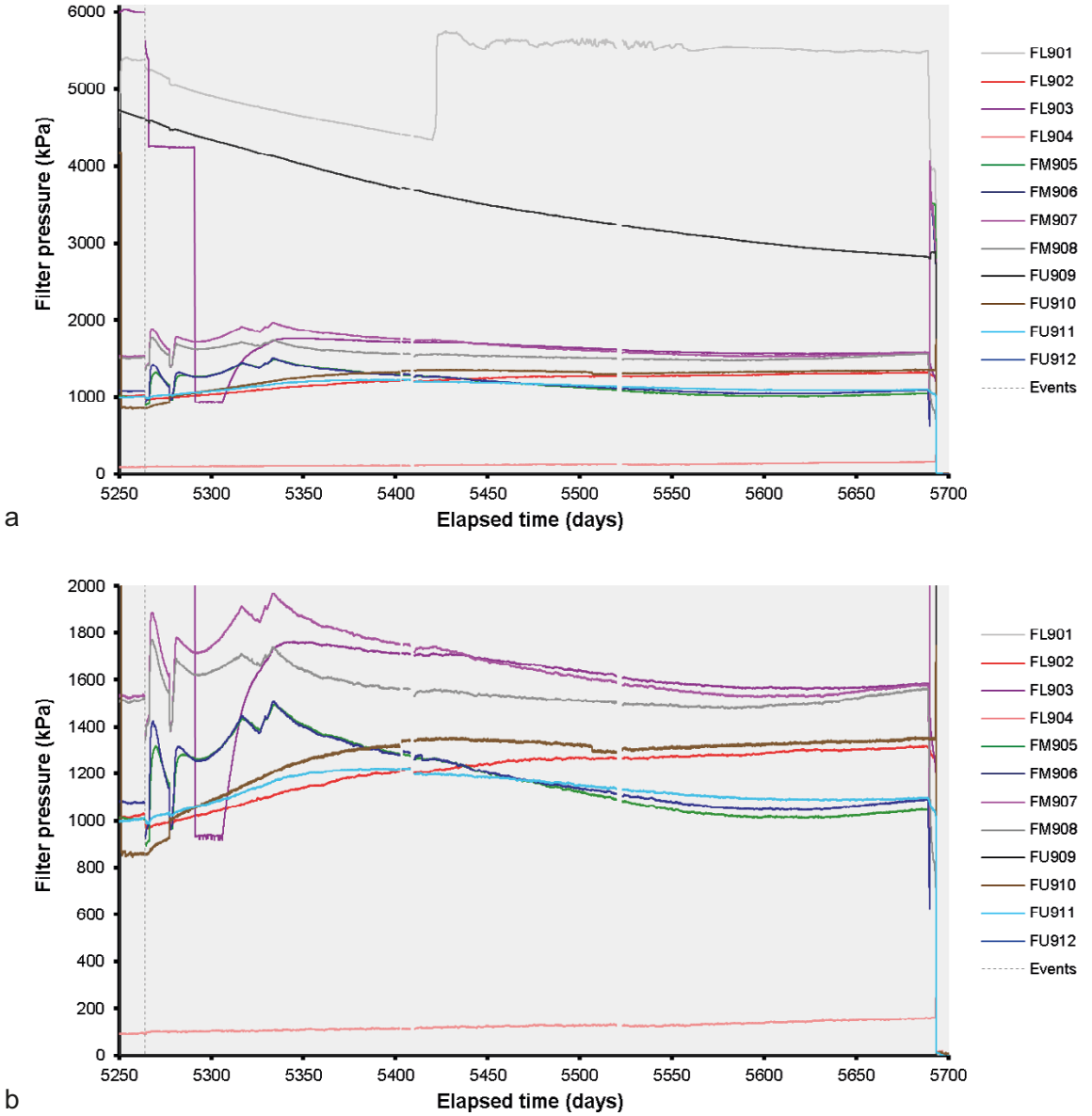

Figure 14-14. *Filter pressures on the canister surface. a) complete range of filter pressures dominated by the activities in filter FL903 and high pressures in FL901 and FU909; b) detail of the pore pressures in the canister filters.*

Figure 14-15 shows the variation of pore water pressure at the rock wall. As can be seen, pressure was heterogeneous within the deposition hole, with ~1 600 kPa variation prior to the pressurisation of the canister. Once the canister was filled with gas, this variation increased to ~2 350 kPa. The response up to around Day 5350 was dominated by the gas pressure in the canister. However, once gas pressure was held constant at Day 5333.07, pore pressure in several locations remained constant, whereas in others it reduced. There were features associated with gas movement around Day 5415 and these will be discussed in Section 14.3. Generally, most of the sensors showed annual variation during the remainder of the period. By the end of the test period, pore pressure ranged from 655 to 2 435 kPa, a range of 1 780 kPa. Figure 14-16 shows the distribution of pore pressure on the rock wall at the start and end of the test period. As seen, the distribution of stress remained unaltered, with a high in pore pressure at a height of 175 cm and at 270° along the length of the canister. Low pressure was seen at the top and bottom of the sensor array.

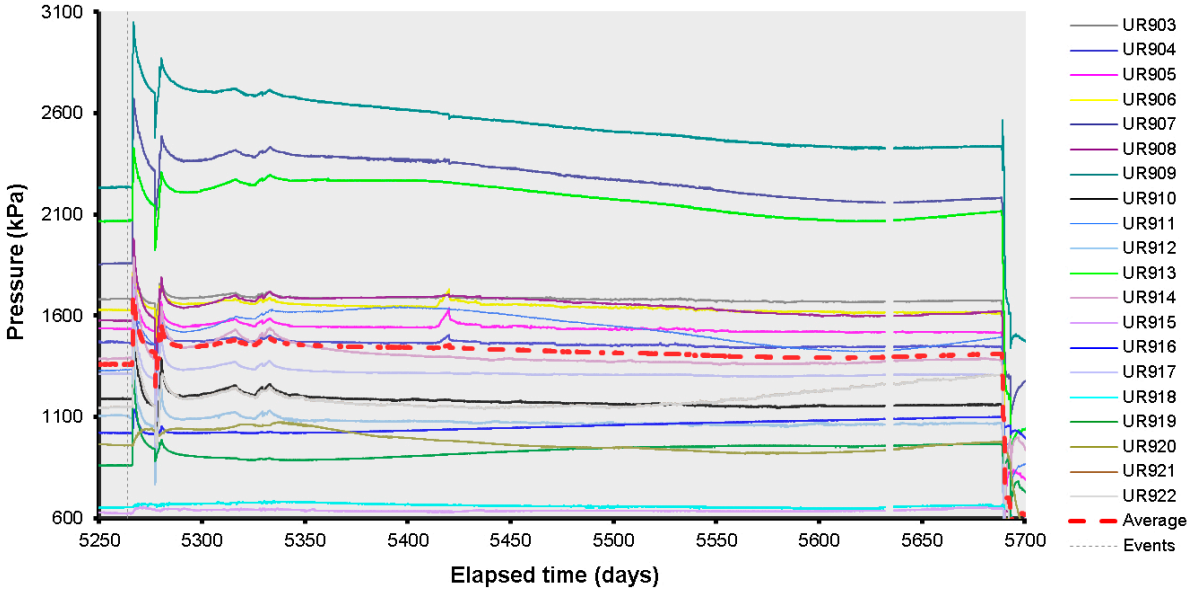

Figure 14-15. *Variation in porewater pressure with time measured at the rock face.*

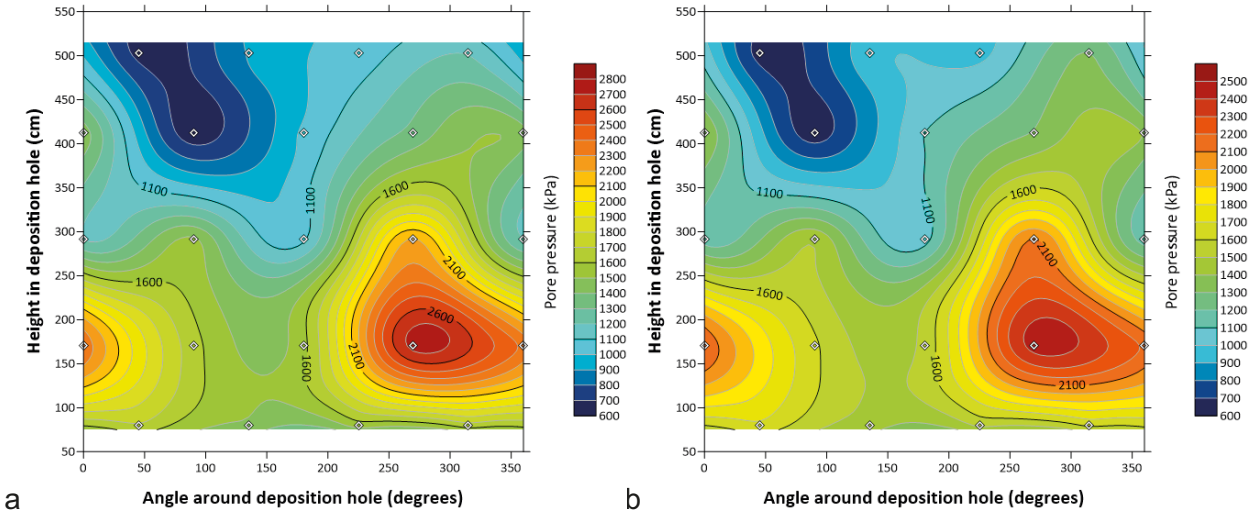

Figure 14-16. *Distribution of porewater pressure at the rock face. a) Day 5290.00, b) Day 5680.00.*

Radial stress measured at the rock wall is shown in Figure 14-17a for all locations and Figure 14-17b in detail for all sensors excluding PR921. The data were dominated by the gas pressure in the canister. There were secondary features around the time of gas entry (Day 5415) and these will be discussed in Section 14.3. At the start of the reporting period the radial stress ranged from 4 510 to 6 210 kPa, a range of 1 700 kPa. Following the disturbance in stress during pressurisation and at the end of the period the range was 4 620 to 6 290 kPa, a total range of 1 670 kPa. Figure 14-18 shows the distribution of radial stress at the rock wall at the start and end of the test period. As seen, the distribution of stress remained unaltered, with a high in stress at a height of 150 cm and at 315° along the length of the canister. Low stress was seen at the top and bottom of the sensor array.

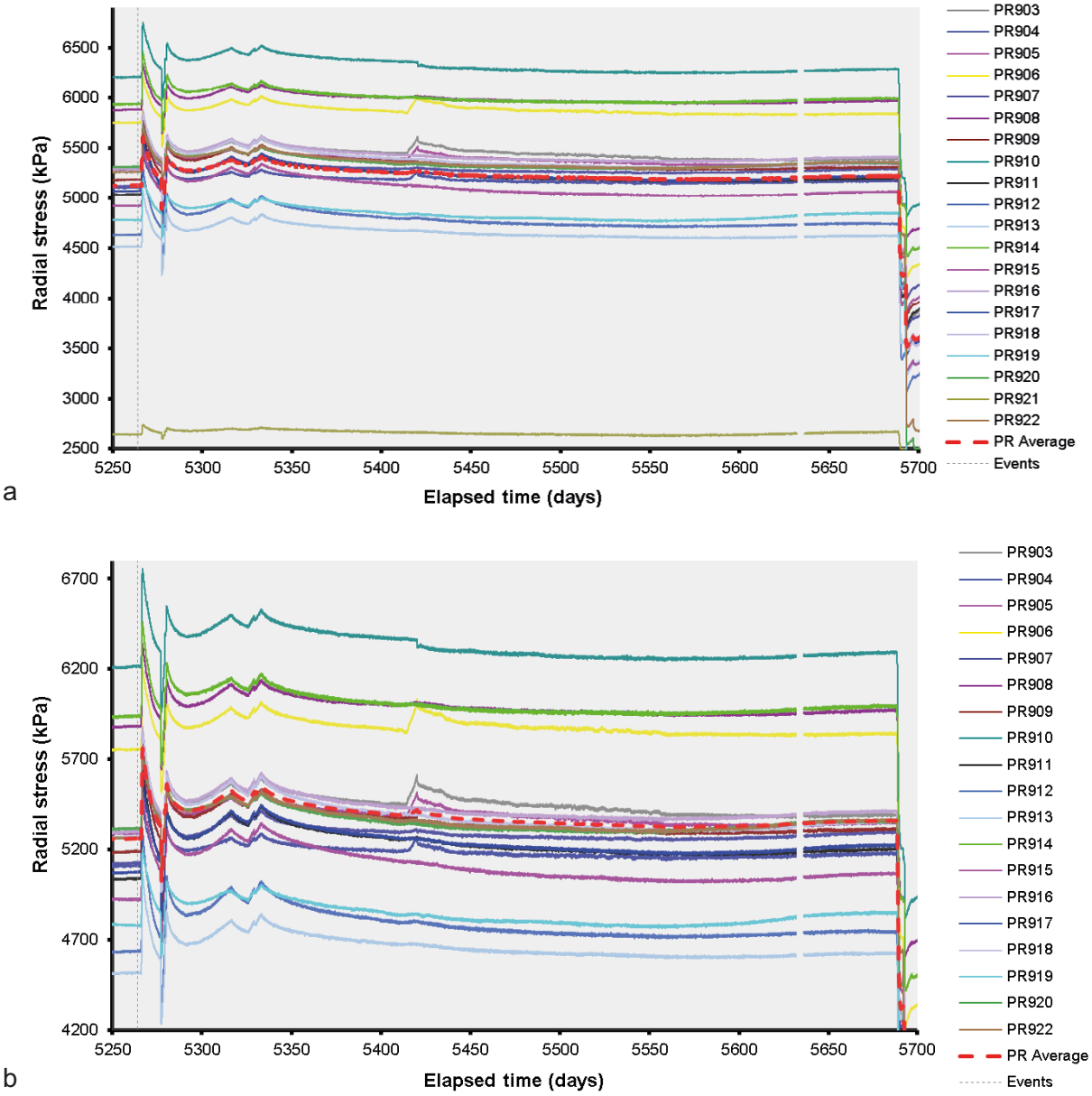

Figure 14-17. *Variation in radial stress at the rock wall with time. a) radial stress for all locations; b) radial stress for all locations excluding PR921.*

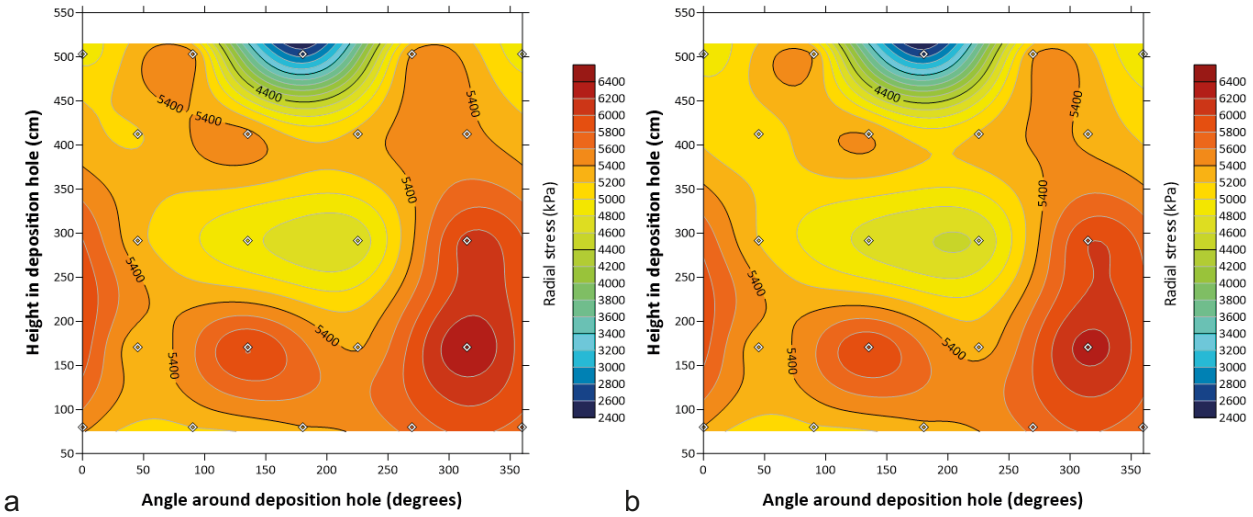

Figure 14-18. *Distribution of radial stress at the deposition hole wall. a) Day 5290.00, b) Day 5680.00.*

Axial stress within the bentonite is shown in Figure 14-19 and was complex. Prior to canister pressurisation there was considerable spread of ~1 200 kPa within the deposition hole. All sensors were perturbed by the pressurisation of the canister, especially PB901 below the canister which showed considerable change during the gas pressure ramp. Sensor PB902 below the canister also showed the movement of gas around Day 5410, this will be discussed in Section 14.3. All sensors showed annual variation, with a higher frequency feature of ~40 d superimposed at some locations. Generally, the period shows the disturbances of canister pressurisation and gas movement superimposed on an annually varying signal.

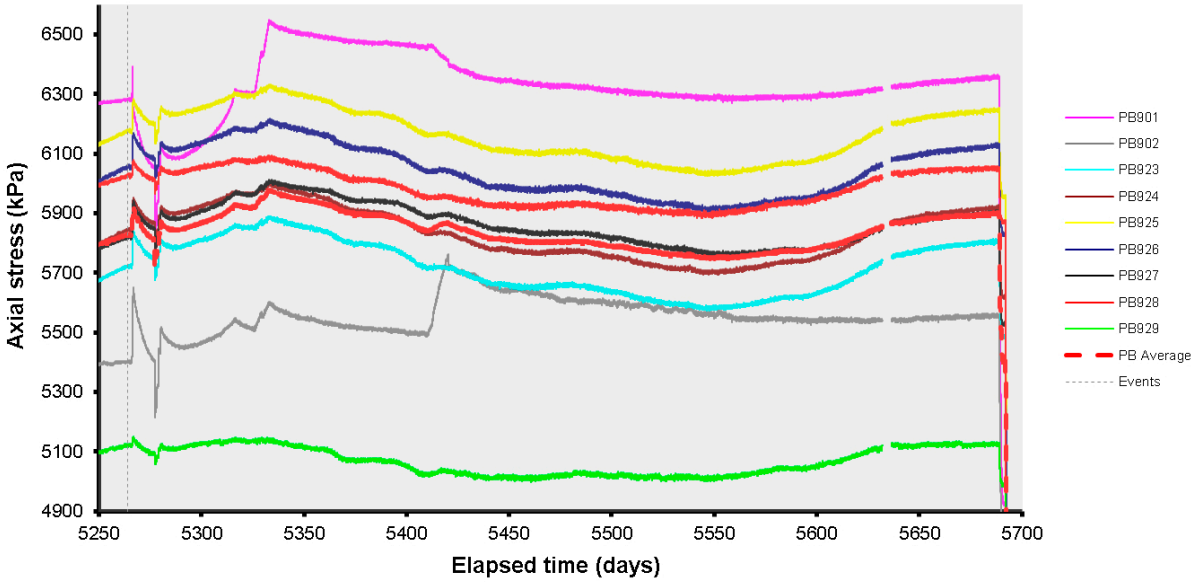

Figure 14-19. *Development of axial stress measured at 9 locations within the buffer.*

The general form of annually varying stress within the buffer was mirrored by the axial force on the lid, including the superimposed higher-frequency oscillation (Figure 14-20). However, the variation caused by the pressurisation was greatly reduced, with a disturbance of ~10 kPa as opposed to ~100 kPa within the buffer. This suggests that the response was attenuated by the compressible buffer and the rigid concrete plug.

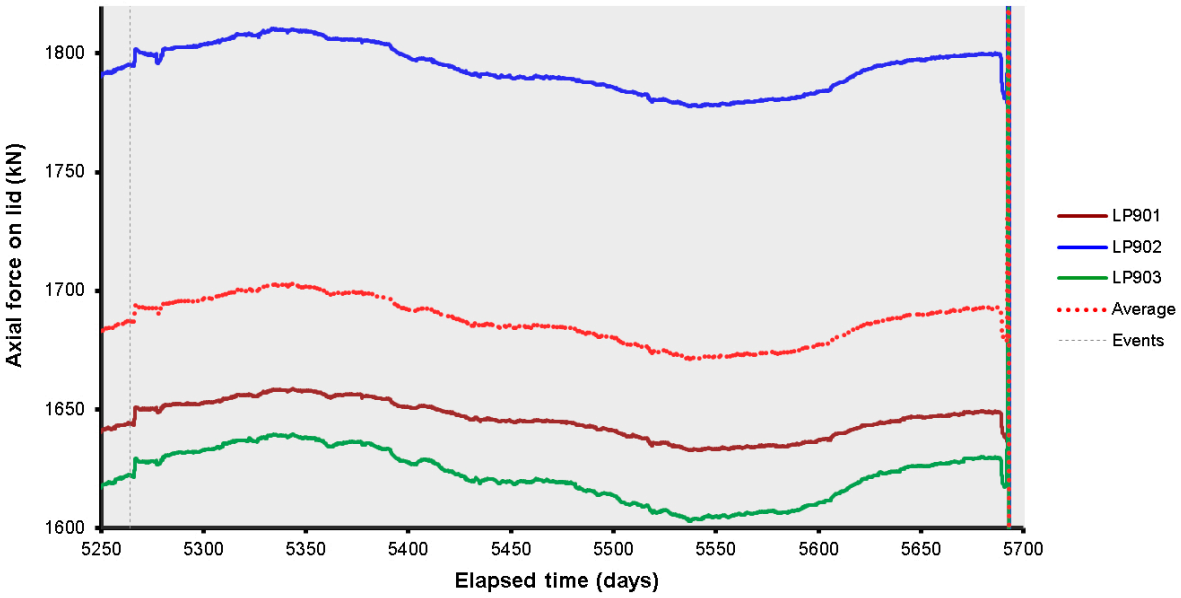

Figure 14-20. *Axial force acting on the steel lid measured by 3 Glötzl load cells attached to separate rock anchors.*

As stated previously, there was concern that the LVDTs measuring the movement of the lid were faulty and therefore the data are presented only to show disturbances that might have resulted from the movement of gas. As shown in Figure 14-21, all that can be noted was the annual variation similar to that described for other sensor types and no obvious features associated with the pressurisation of the canister or the movement of gas following gas entry.

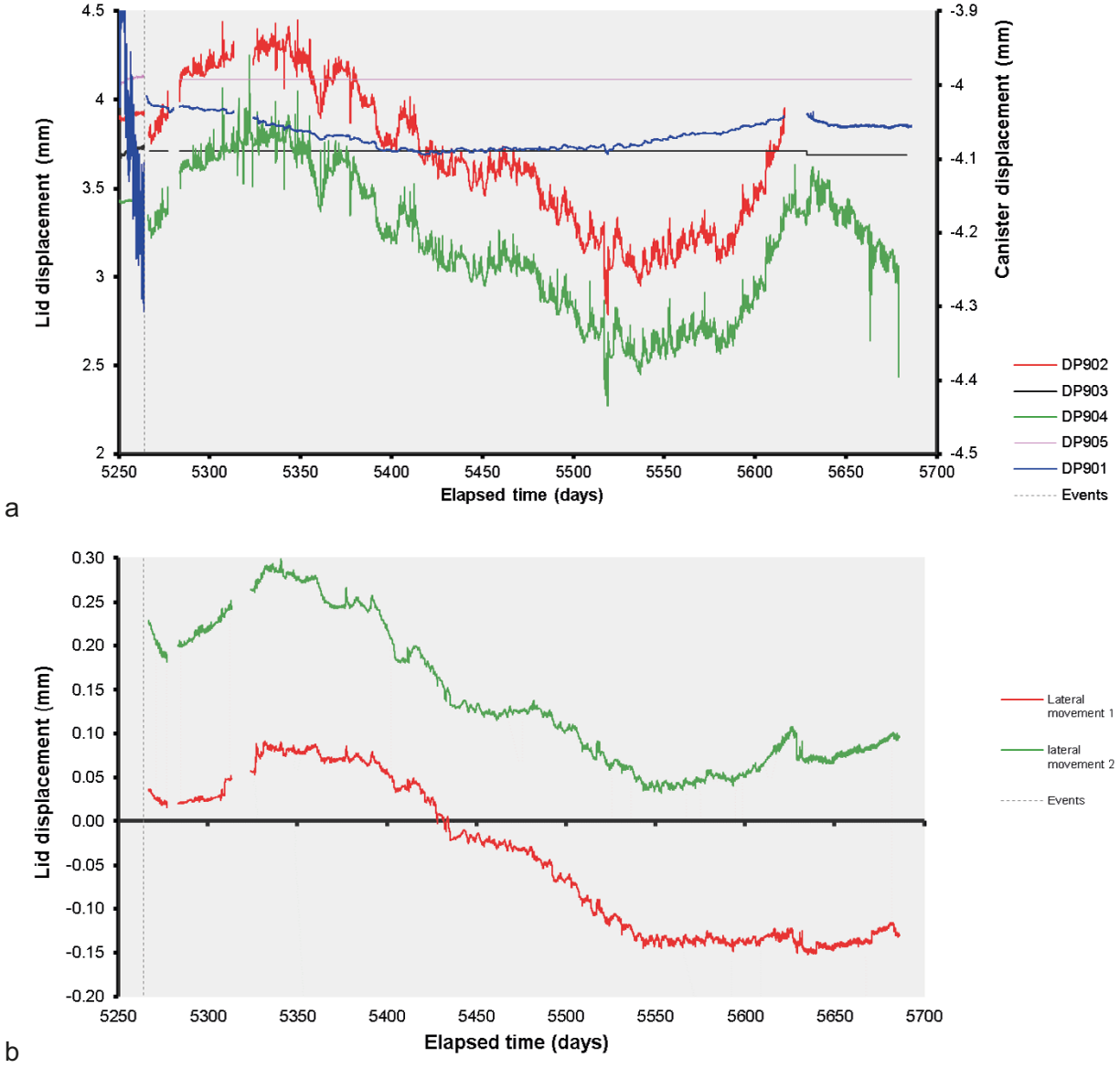

Figure 14-21. *Linear displacement of the steel lid and copper canister (a) and lateral movement of the lid (b). Movements of the lid are measured relative to both the gallery floor and ceiling. Movements of the canister are measured relative to the steel lid.*

Pore pressure away from the deposition hole within the pressure relief hole is shown in Figure 14-22. A small reduction in pressure over the period was seen of less than 50 kPa. As seen, interval PRH2–4 was affectively at atmospheric pressure, this interval was closest to the gallery. A small response was seen as a result of canister pressurisation at the start of the period in most of the intervals. Interval PRH1–5 did not show any response during canister pressurisation but did show a reduction at Day 5315.82 of approximately 50 kPa.

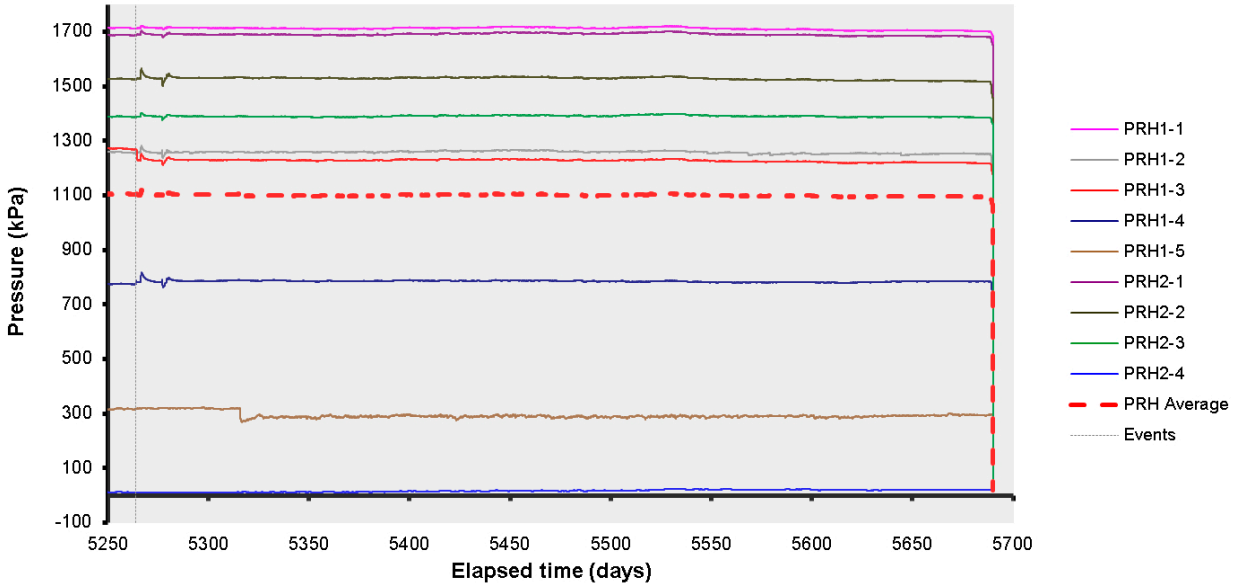

Figure 14-22. *Porewater pressures measured in the packered sections of the pressure relief boreholes.*

Temperature was monitored within the Lasgit laboratory, office, the HRL, and the canister. Figure 14-23a shows that the air conditioning unit within the laboratory was problematic at times during the period. This was most notable during two failures at Day 5402.23 and Day 5407.81. The air conditioning unit was fixed and then delivered a relatively stable temperature. As the syringe pumps were not in operation, these events will not have much of an effect on the data. Generally, temperature was relatively stable during the period.

Figure 14-23b shows the temperature of the canister and shows that pumping relatively warm gas into the canister raised temperature by ~0.75 °C. It then took around 7 days for the temperature to return to the previous level. **Note:** the thermocouple was severed during the emergency lab visit to find the canister leak.

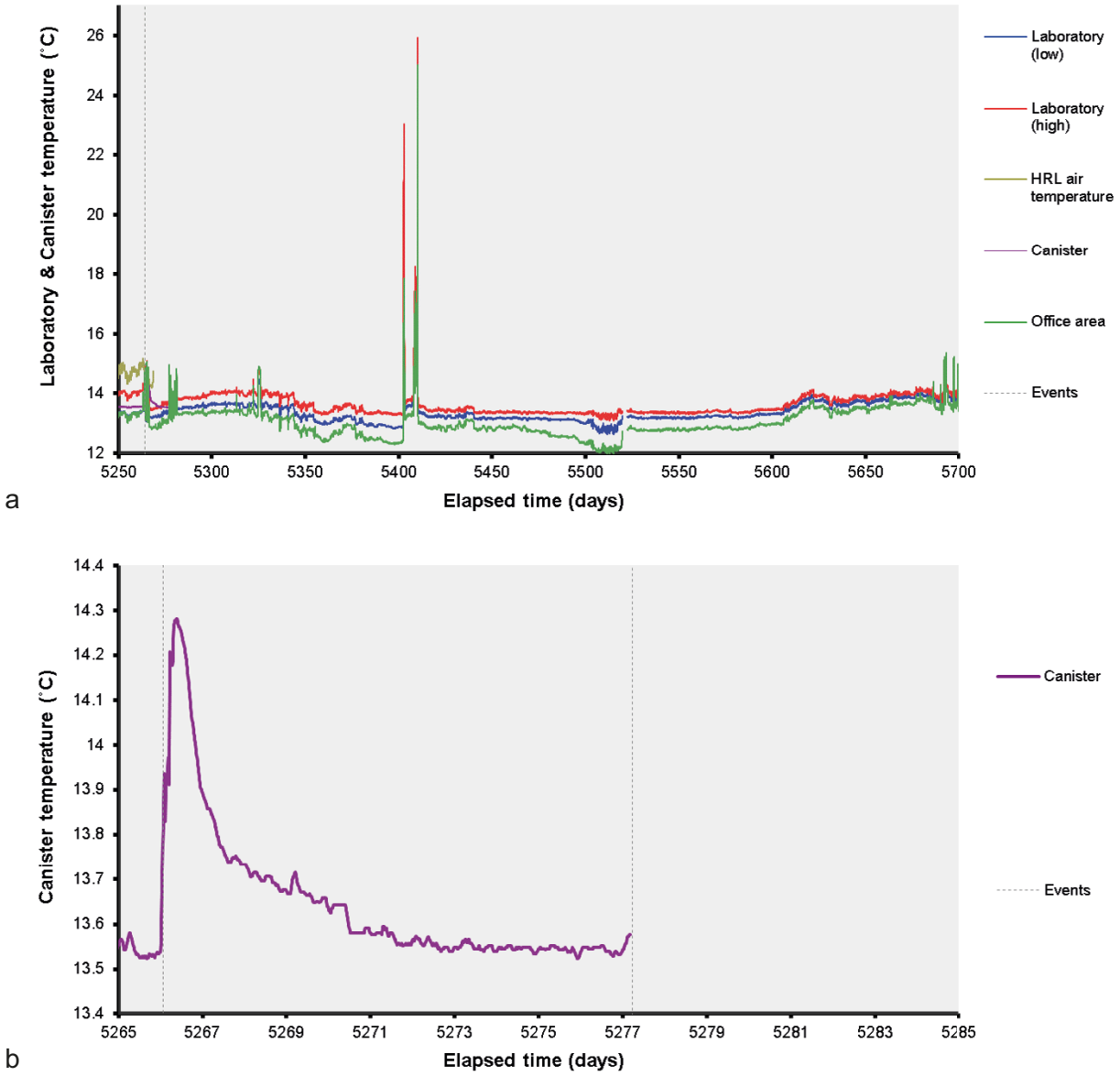

Figure 14-23. *Temperatures recorded in the Lasgit laboratory, office, canister, and HRL.*

Figure 14-24 shows average stresses, pore pressure, and forces observed during the Full Canister Test. Most sensor types were disturbed by the pressurisation of the canister as a result of mechanical and thermal loading. Stresses and pressures were generally constant throughout the period following the disturbance, with annual variation observed.

The Full Canister Test had a more complex set of boundary conditions than the previous gas injection tests. This was because pressurising the canister disturbed the stress field through mechanical and, to a lesser degree, thermal loading. This raised pore pressure and the pore network contracted and started the buffer to drain. This was a slow process and it took some time for the perturbations to subside because of the drainage characteristics of the bentonite. This meant that the stress and pressure fields were constantly evolving during the gas injection test and this needs to be considered when interpreting results.

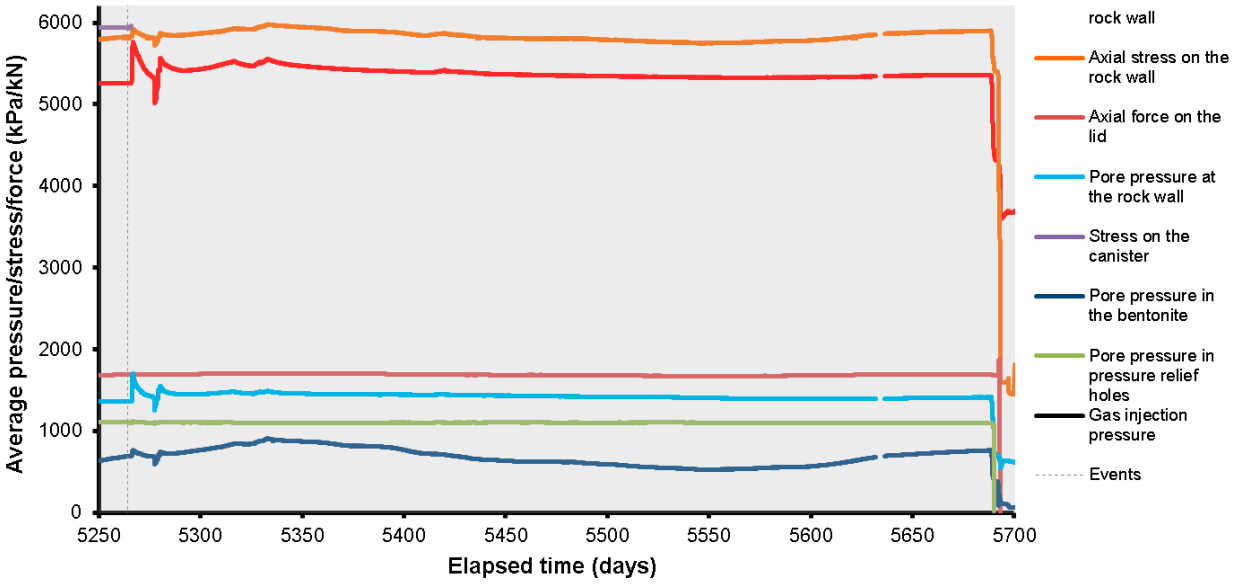

Figure 14-24. *Average pressures, stress, and force observed during the reporting period.*

14.3 Full Canister Test

The final gas injection test of Lasgit used the whole canister under pressure to see whether the volume of gas would have any impact on the gas migration behaviour. Previous gas injection tests showed a decrease in pressure as pathways formed. As these pathways were, volumetrically, of a small proportion of the gas volume in the interface vessel, it resulted in a reduction in pressure. If the same volume of pathways formed in the Full Canister Test there would be no instantaneous pressure reduction as the added volume taken up by the pathways would be insignificant compared with the volume of the canister. The question to be addressed was whether this would change the dynamics of gas migration.

The Full Canister Test was conducted as a two-stage gas ramp, as shown in Figure 14-25. However, the means for increasing pressure was different compared with previous gas injection tests. Previously, a fixed amount of gas was compressed within an interface vessel, with water pumped into the bottom of the vessel at a constant rate in order to reduce the volume of the gas and thus increase pressure. In the Full Canister Test, the volume of gas was constant, with more gas added from the two interface vessels by pumping water into the base of the vessels. Therefore, the volume of the canister varied by 10 litres while gas was being added. This meant that the calculation performed in previous tests had to be modified in order to determine predicted pressure and to identify when gas entry had occurred. For each of the 55 refills of the interface vessel, the starting pressure, end pressure, and volume of water pumped into the vessels was recorded so that the amount of gas added to the canister could be determined. Figure 14-25 shows the predicted pressure and shows a very good correlation with the observed pressure. The first seven refills were performed over 24-hour periods using one syringe pump. The next ten refills were conducted over 18 hours, also using a single syringe pump. It was then decided to switch to reciprocating pumps and to refill on a 12-hour basis for the remaining 38 refills. The first gas ramp started on Day 5291 (29th July 2019) and raised the pressure from 4 934 to 6 499 kPa in 25 days (Day 5316, 23rd August 2019). Pressure was held constant for around 10 days, when a second gas ramp was started on Day 5326 (2nd September, 2019), which lasted for nearly 7 days and took pressure from 6 550 to 7 085 kPa.

As stated in section 5, early in the test history a significant volume of water was unintentionally pumped into the canister. The exact volume was unknown, but it was not sufficient to fill the available void space of the canister. Water entering the canister had been anticipated at the outset of the experiment and the valve in the base of the canister had a snorkel so that water could pool in the base of the canister and not all of it would need to be expelled before gas could enter the buffer during the Full Canister Test. However, this snorkel was limited and was estimated to be around 300 – 400 mm in height. It was uncertain whether the water level was above the snorkel or not. A second potential issue was whether the air actuated FCT valve was still working. This valve had sat submerged in water for around 14 years and it had not been operated. Fortunately, the valve had been set to be open, so as long as the air supply was active the valve was open throughout the test history. There was no way of testing that the valve worked and its operational status was unknown. In all previous tests the gas entry pressure was approximately equal to the local stress state. The FCT valve was very close to stress sensor PC901 and this meant an estimate of local stress could be made. However, the canister stress sensors had to be severed in order to achieve a gas tight canister and stress had to be estimated from when the sensor had been active. At Day 5266.13 stress at PC901 was 7 063 kPa and this gave an estimate of what gas entry pressure would be. Therefore, there was a limit to how high canister pressure should be raised. If pressure was raised too high and water was in contact with the bentonite then there was a risk of hydrofracturing the buffer, something that was not of interest. Gas pressure was therefore held when it reached the estimate of local stress, and when at 7 085 kPa the pressure was held at this value by stopping the addition of gas to the canister.

Figure 14-25 also shows that an issue was experienced during the second gas ramp. During refill 47, a valve was unintentionally left open and gas was able to vent through the refill system, lowering the canister pressure as gas leaked from the system. Fortunately, only a small amount of gas was lost and the pressure was still able to be raised to the target value. Figure 14-26 shows the difference between the predicted gas pressure and the recorded pressure. As shown, a very close correlation was seen, up until the leak at refill 47. The volume of gas added during each refill was known accurately, meaning the start pressure, end pressure, and change of volume was known. From this, the volume of the canister could be determined, assuming there was no loss of gas from the system. This gave a canister volume of 1 313 litres.

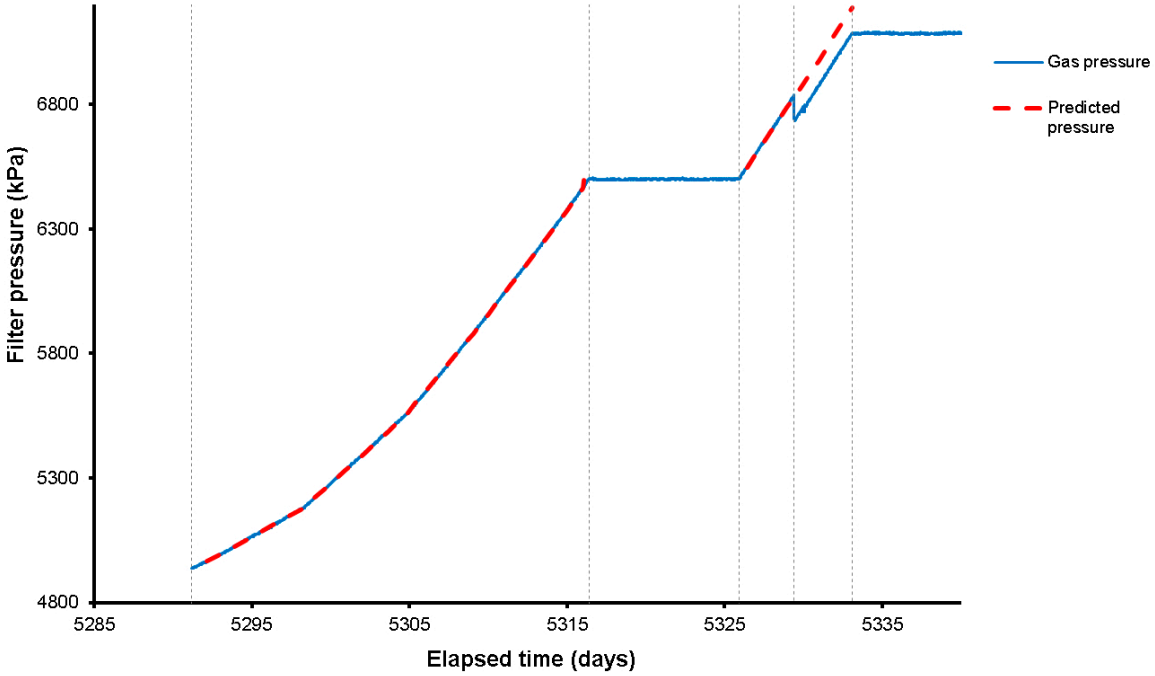

Figure 14-25. *Recorded and predicted gas pressure during the Full Canister Test.*

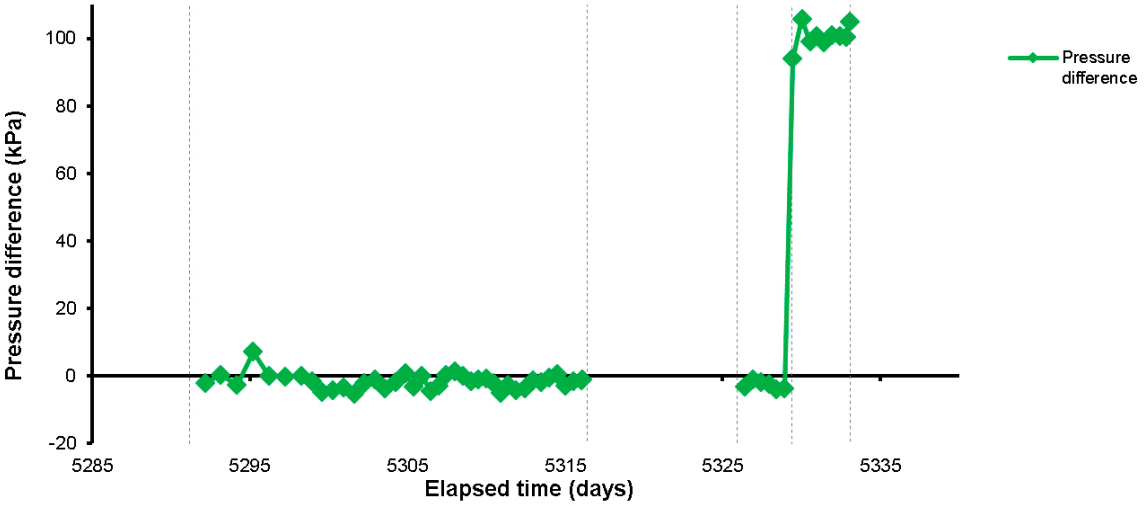

Figure 14-26. *Difference between recorded and predicted pressure during the Full Canister Test. This was used to estimate the volume of the canister.*

Figure 14-27a shows the time when gas pressure was held at ~6 500 kPa. It shows that the system was gas tight and that there was minimal loss of gas from the system through solution and/or diffusion. Figure 14-27b shows the final pressure hold. Again, this shows a gas tight system, with no loss of pressure. However, at Day 5390 the pressure in the canister went up. This event does not correspond with the temperature issues experienced in the laboratory and its cause remains unknown. Following the pressure increase the pressure remained fairly constant until gas entry occurred.

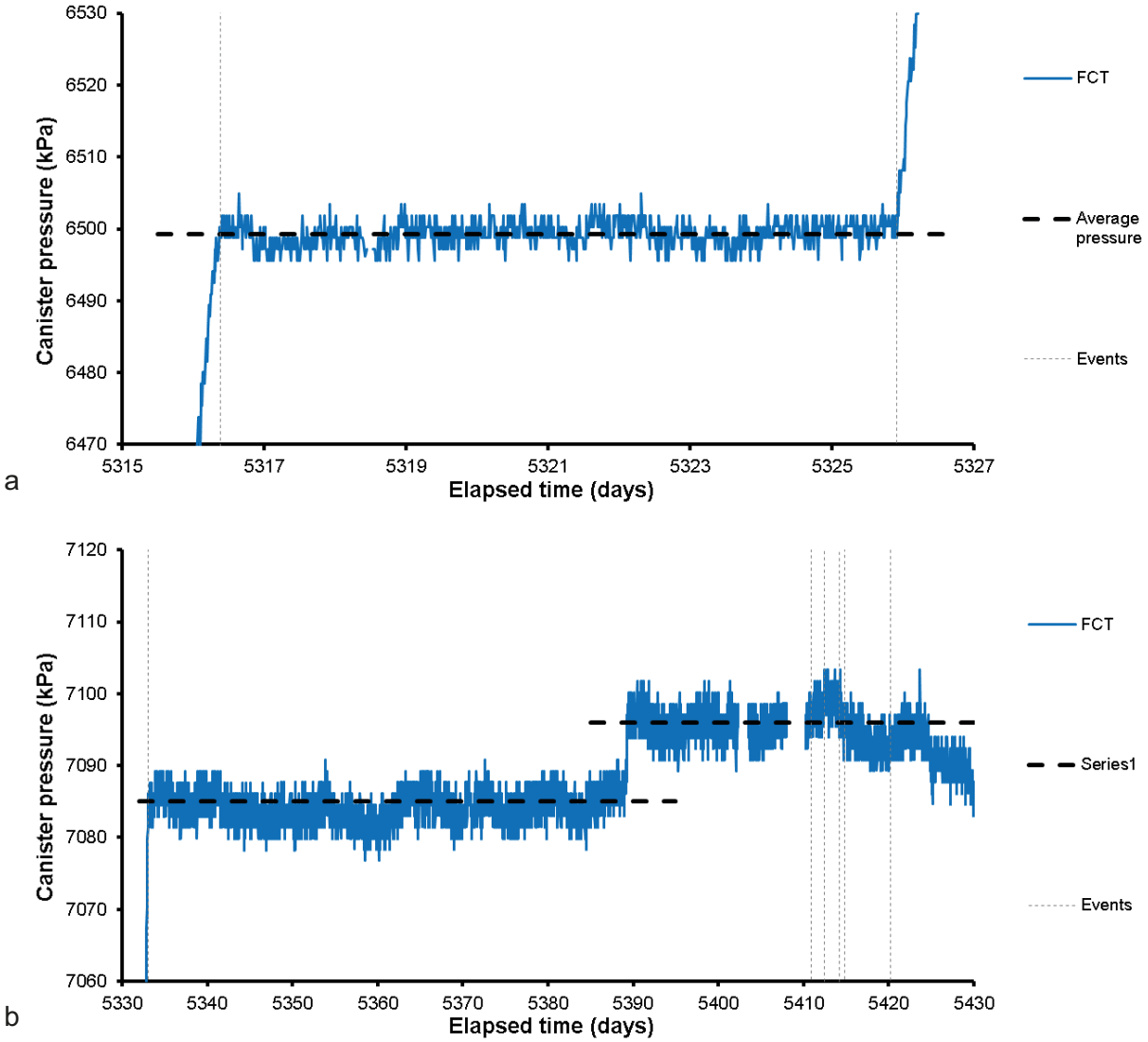

Figure 14-27. *Canister pressure during periods when pressure was held constant in the Full Canister Test. a) Initial hold; b) final pressure hold.*

Figure 14-28 shows the canister pressure for the remainder of the period. A series of event lines are shown starting from Day 5410. These correspond with variations in pressure and correlate with the start of pressure decay within the canister. From Day 5420 onwards the pressure reduced in the canister from 7 100 kPa to a final pressure of 6 878 kPa at Day 5688.92, a loss of 22 kPa. Figure 14-29 shows a crude estimate of the volume of gas pathways. As the volume of the canister was static, the reduction in pressure could be converted to a change in volume (i.e., pathway volume) assuming no loss of gas. This was a crude calculation as it assumed no loss of pressure along the pathway but gave an estimate of the minimum volume that the pathways would be occupying. Figure 14-29b shows that the increase in pressure seen during the pressure hold represents a reduction in canister volume of around 2 litres, which is unexplained as the canister volume was fixed. Figure 14-29a shows that the reduction in canister pressure would occur if there was a total of 41.5 litres of pathway. This volume of pathway is highly unlikely to have formed within the buffer, or for the gas to have found a sink of this size, as stresses and pore pressure within the system would have increased significantly if this was the case. Therefore, gas had escaped the system. This may have started at the point where the slope changed around Day 5440.

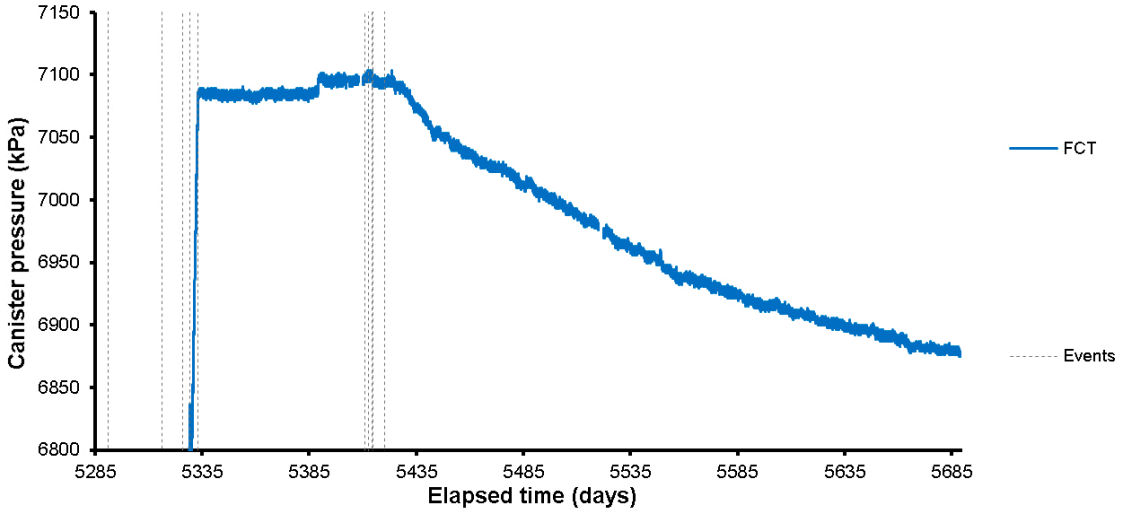

Figure 14-28. *Pressure of the canister during the Full Canister Test.*

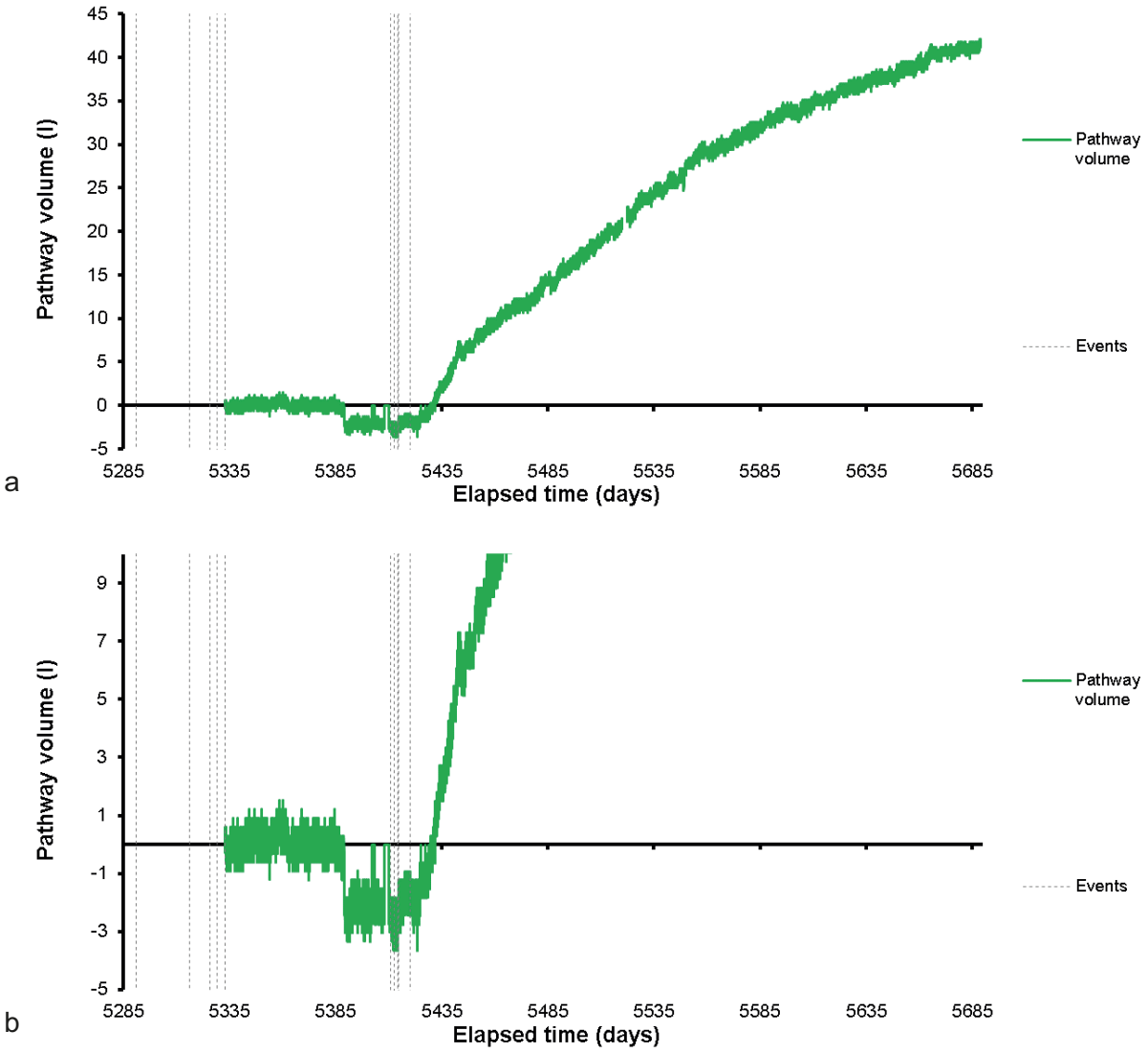

Figure 14-29. *Estimate of the volume of pathways during the Full Canister Test. a) Results for complete test history; b) detail around the time of gas entry.*

Figure 14-30a and Figure 14-31a show the pore water response at the deposition hole wall around the time of gas entry. As shown, the majority of sensors towards the bottom of the sensor array showed a response. Location UR905 showed the first response at Day 5410.86, with a minor peak in pore pressure. This was followed at Day 5412.49 by a slow increase in pressure of UR906, with UR905 increasing again a short time after, as did UR904. At Day 5420.25 pore pressure in UR903–UR906 and UR908 peaked, and then instantaneously reduced. In order of pressure increase, UR905, UR906, UR904, UR903, and UR908 increased by 99.2, 91.1, 43.6, 27.9, and 10.9 kPa respectively at the peak in pressure. This was followed by a rapid reduction of 59.3, 48.5, 26.3, 26.7, and 13.4 kPa respectively. UR910 showed slightly different behaviour in that there was no pressure increase but it showed a decrease of 23.3 kPa. Following the reduction in pressure after the peak, three further events occurred. The first occurred at Day 5428.31 with a reduction in pressure at UR908 and a disturbance in UR906 and UR903. The second occurred at Day 5396.15 when pressure reductions occurred in UR904–UR906 and UR908. The final pressure event saw a pressure step in UR904 at Day 5439.80. Many other small events could be seen. The multiple events seen in the pore pressure data showed that the gas was moving within the deposition hole.

Radial stress at the deposition hole wall is shown in Figure 14-30b and Figure 14-31b. As shown, radial stress was still recovering from the pressurisation of the canister. As with pore pressure, radial stress started to increase around Day 5414.21. At Day 5420.25 pore pressure in PR903–UR906 peaked, and then instantaneously reduced. In order of stress increase, PR906, PR903, PR905, and PR904 increased

by 195, 168, 118, and 84 kPa respectively at the peak in pressure. This was followed by a rapid reduction of 49, 54, 34, and 39 kPa respectively. The reduction in stress post-peak was not as dramatic as seen in the pore pressure results. PR910 showed slightly different behaviour in that there was no pressure increase but showed a decrease of 39 kPa. Little other stress changes occurred for the rest of the Full Canister Test. However, the event identified at Day 5436.35 for pore pressure corresponded with the start of slow pressure decrease in PR903–PR906. There was correlation between observed changes in pressure and stress at similar locations, demonstrating the coupling between the two.

Figure 14-30c shows axial stress within the bentonite below the canister, note that no response to gas entry was seen in the sensors above the canister. The first identified event line is shown at Day 5410.86. This corresponded with the start of pressure increase in PB902 and a small positive step in PB901. The rate of change of stress change at PB902 increased at Day 5412.49, while PB901 peaked and started to decrease. At Day 5420.25, when UR and PR sensors peaked, PB902 also peaked, while PB901 decreased. Stress at UB902 had increased by 262 kPa and after peaking reduced by 36 kPa initially. Some of the events identified for the UR sensors corresponded with changes in PB902. As gas continued to drain through the buffer, several pressure responses were seen in PB902, suggesting that gas pathways were still developing.

Pore pressure within the bentonite below the canister is shown in Figure 14-30d, note that no response to gas entry was seen in the UB sensors above the canister. At Day 5410.86, a small pressure spike of around 24 kPa was seen in UB901, while UB902 instantaneously increased by 68 kPa. This was followed by a stepped increase in UB902 until Day 5412.49, when the rate of pressure change increased, until Day 5414.21, when UB902 rapidly increased by around 1 000 kPa. The rate of change of pressure increase reduced at Day 5414.86, starting a further pressure increase of 440 kPa over 6.04 days. The pressure in UB902 peaked at Day 5420.25, a time when peaks were seen in UR, PR, and PB sensors. Pressure then instantaneously reduced by around 120 kPa, followed by a slow decay in pressure. Many further features are seen in UB902 that do not correspond with features in other sensor types.

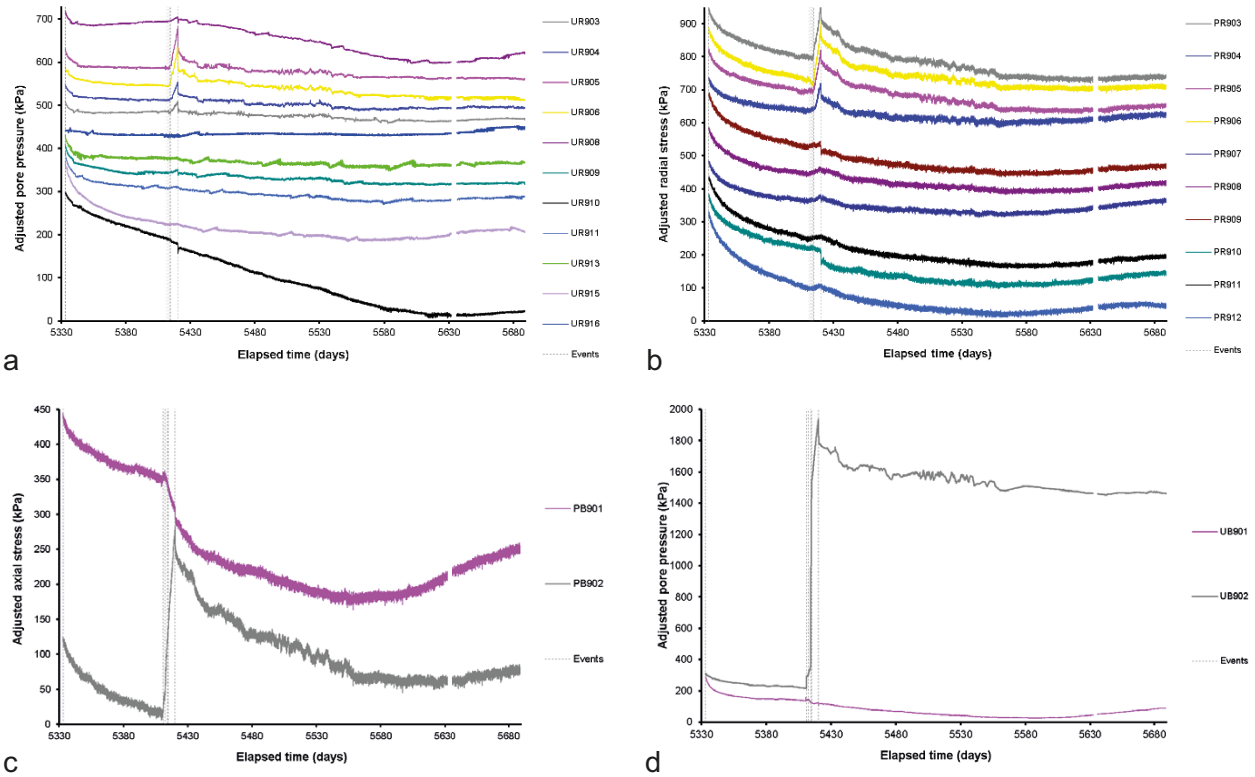

Figure 14-30. *Example of sensor response around the time of gas entry during the Full Canister Test. All parameters have been transposed about the y-axis to emphasise the detail observed. a) Pore pressure at the deposition wall; b) radial stress on the deposition wall; c) stress within the bentonite; d) pore pressure within the bentonite.*

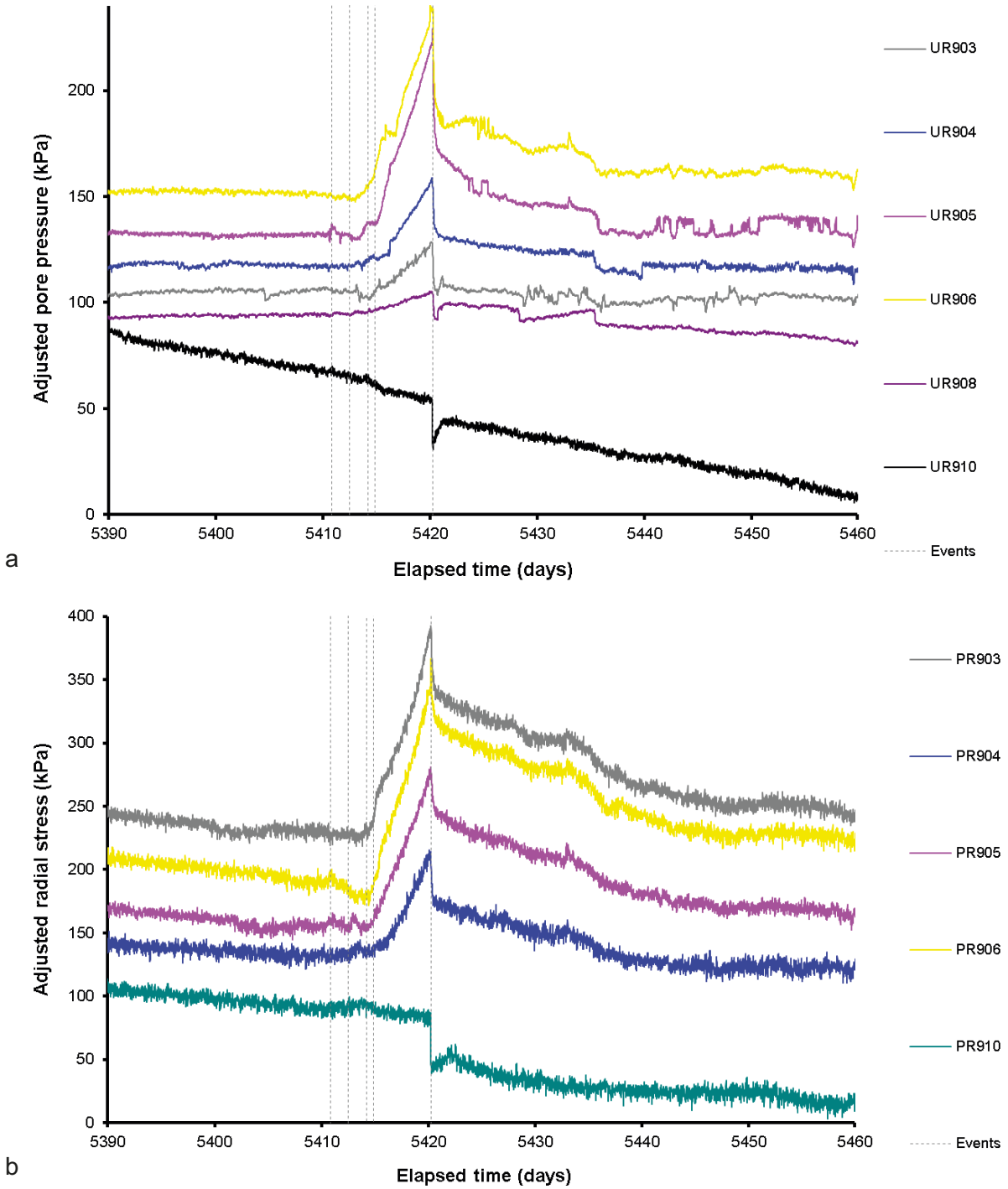

Figure 14-31. *Detail of radial stress and pore fluid pressure at the rock wall around the time of gas entry. a) Pore pressure at the deposition wall; b) Radial stress on the deposition wall.*

The distribution of radial stress on the deposition hole wall is shown in Figure 14-32. Stress prior to peak gas pressure is shown in Figure 14-32a at Day 5408.83. This shows that stress was greatest towards the bottom of the deposition hole in a band at around 150 cm height all around the canister. A band of high radial stress was also seen vertically, centred on 315°. A stress gradient was observed whereby the least stress was generally seen towards the top of the deposition hole, with stress increasing with depth.

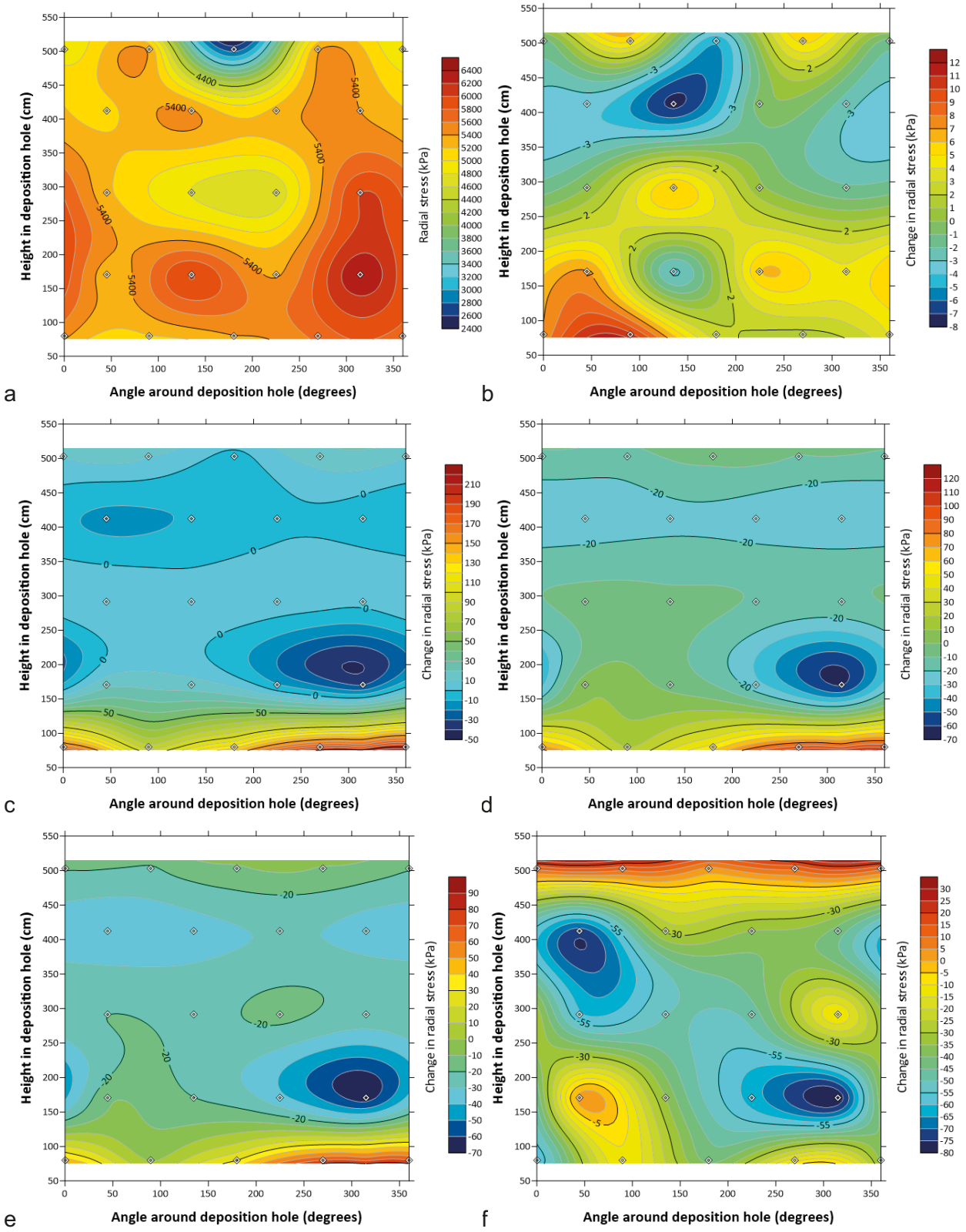

Figure 14-32. *Distribution of radial stress at the deposition hole wall at times around gas entry during the Full Canister Test. a) Day 5408.83; b) Day 5414.86; c) Day 5420.25; d) Day 5432.52; e) Day 5438.74; f) Day 5680.00.*

Figure 14-32b shows the change in radial stress from Day 5408.83 to Day 5414.86. This was at a time when UB902 was pressurised and an increase in radial stress was seen towards the bottom of the sensor array, with small increases at a height corresponding with the observed high in stress (150 cm height) and also a small increase in stress at the top of the deposition hole. At the time when sensors peaked at Day 5420.25 (Figure 14-32c) elevated radial stress was confined to the base of the sensor array and showed gas movement was occurring at the base of the canister. Figure 14-32d and Figure 14-32e show similar results at Day 5432.52 and Day 5438.74. This shows that as radial stress change dissipated, the distribution in stress change remained consistent, with raised stress in the base of the sensor array and a low stress region at around 200 cm height at an orientation of 315°. Figure 14-32f shows the change in stress relative to Day 5408.83 at Day 5680.00. This now shows that the raised stress in the base of the canister had been relieved and radial stress was elevated at the top of the sensor array.

Figure 14-33 shows the distribution of pore pressure at the deposition hole wall and how this varied during the Full Canister Test. Figure 14-33a shows the pore pressure distribution just prior to gas entry at Day 5408.83. This showed a general decrease in pore pressure down the deposition hole and a high in pore pressure at around 275° at a height of 175 cm. The first pore pressure response at Day 5414.86 (Figure 14-33b) showed only a slightly raised pore pressure at the base of the sensor array, with the magnitude of the identified high-pressure region reducing. When UR sensors peaked, at Day 5420.25, pore pressure at the base of the sensor array increased, showing that gas movement had occurred at the base of the canister. By Day 5432.52 (Figure 14-33d) the high-pressure region at the base of the filter array had subsided, with a new increased pressure forming at the top of the sensor array at an orientation of 135°. By Day 5438.74 (Figure 14-33e), the high stress region towards the top of the sensor array had increased and broadened, maybe suggesting that gas had migrated to the top of the canister. At the end of the stage at Day 5680.00 (Figure 14-33f), the increased stress at the base of the sensor array had dissipated, with raised pore pressure now seen at the top of the sensor array. This result suggests the movement of the gas around the canister and in the buffer.

Figure 14-34 shows sensor locations that record the direct movement of gas. As described previously, gas reached UB902 first (Figure 14-34b, Figure 14-35a). At Day 5410.86 UB902 instantaneously increased by 68 kPa. This was followed by a stepped increase in UB902 until Day 5412.49, when the rate of pressure change increased, until Day 5414.21, when UB902 again rapidly increased by ~1 000 kPa. The rate of change of pressure reduced at Day 5414.86, starting a further pressure increase of 440 kPa over 6.04 days. The pressure in UB902 peaked at Day 5420.25 and instantaneously reduced by around 120 kPa, followed by a slow decay in pressure. At this time (Day 5420.25) pressure at FL901 also started to increase, until at Day 5421.72 when the pressure increase accelerated, until the pressure in FL901 matched that in UB902, some 1 380 kPa below the pressure in the canister. This shows the decrease in pressure along the newly formed pathways. FL901 and UB902 approximately matched one another for the rest of the test and showed the same general reduction in pressure seen in the pressure of the canister. No other sensors showed evidence of direct gas movement. Figure 14-35b shows a schematic of the continued gas flow, showing gas reaching FL901 before finding a way out of the deposition hole.

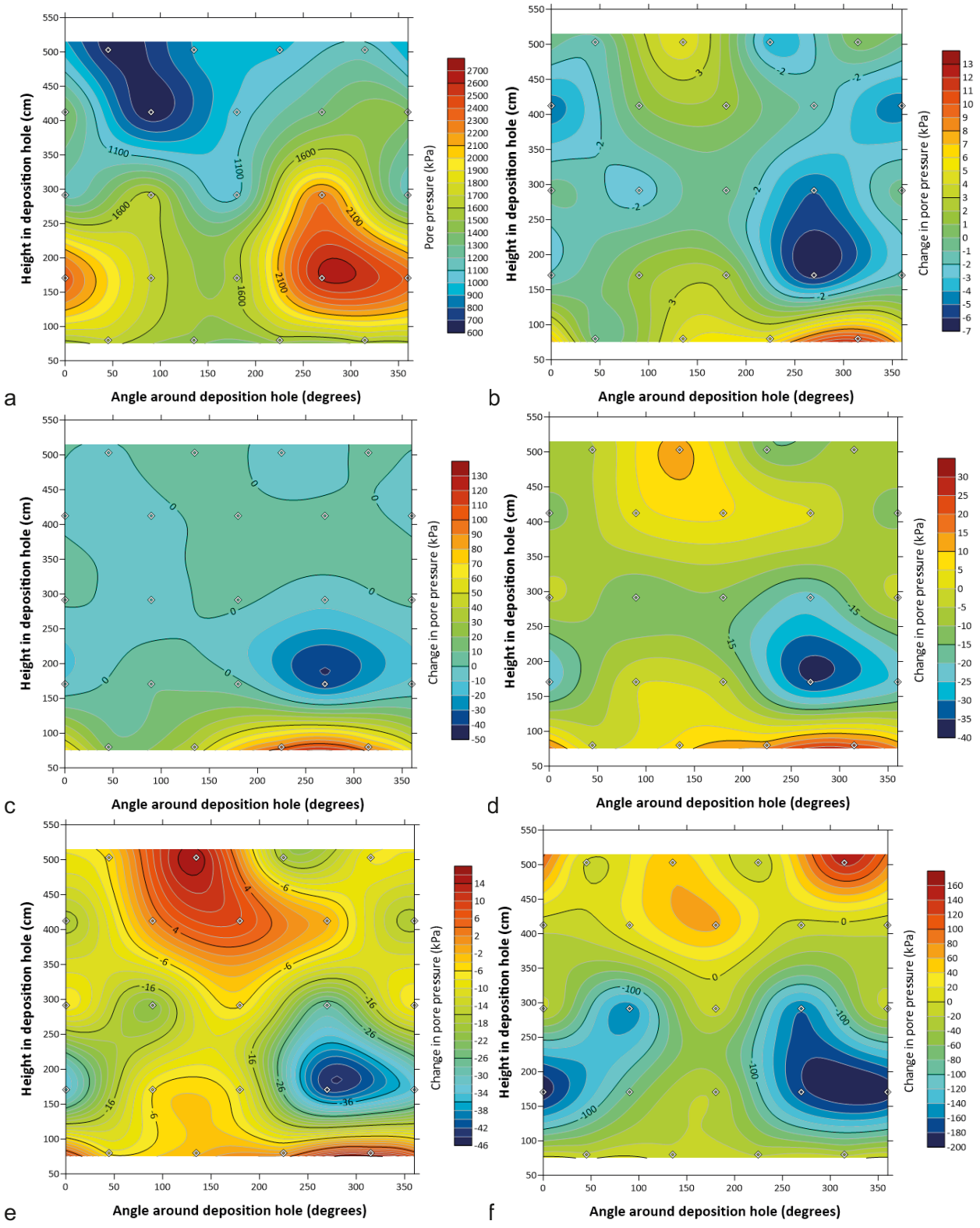

Figure 14-33. *Distribution of pore pressure at the deposition hole wall at times around gas entry during the Full Canister Test. a) Day 5408.83; b) Day 5414.86; c) Day 5420.25; d) Day 5432.52; e) Day 5438.74; f) Day 5680.00.*

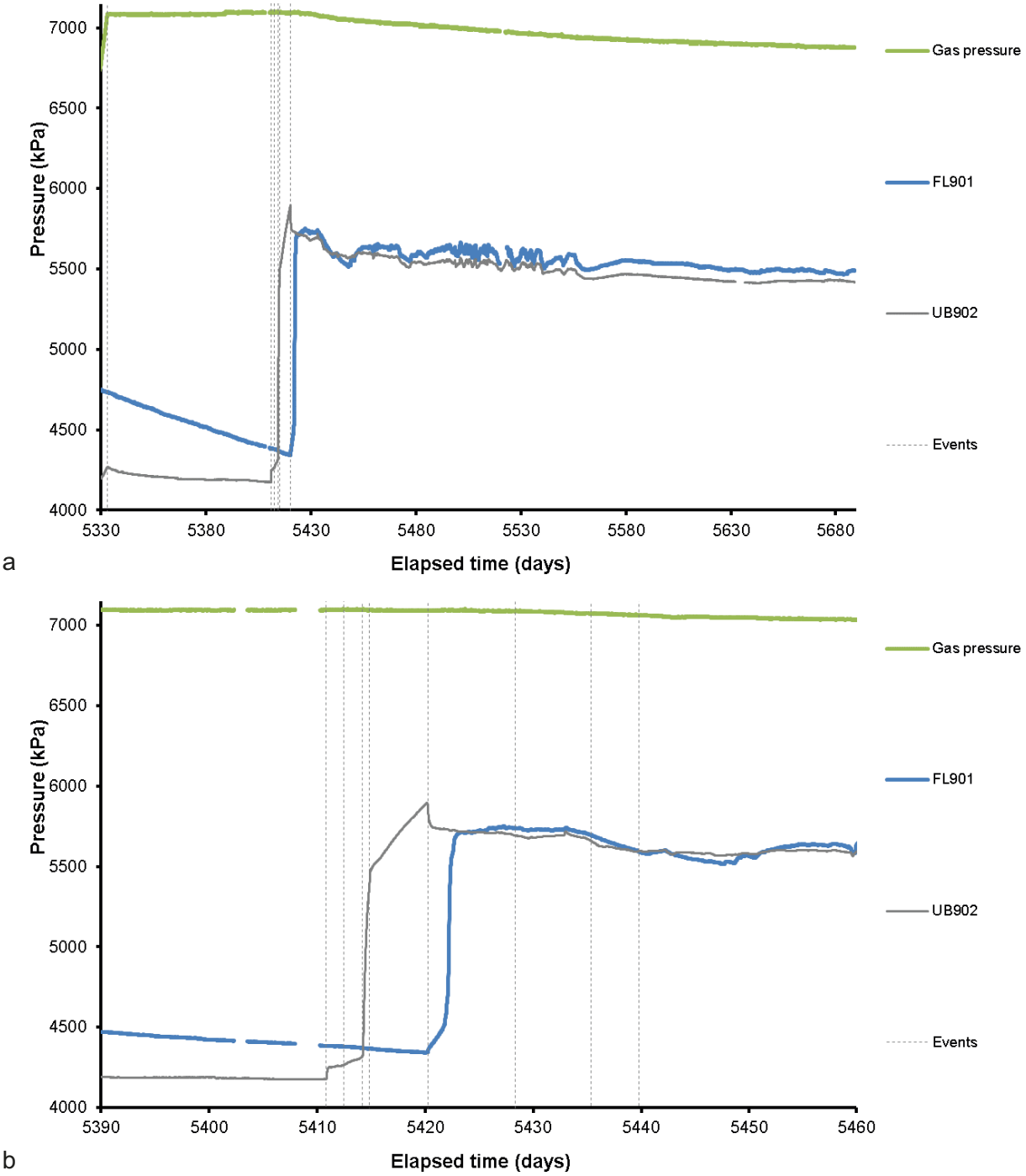

Figure 14-34. *Detail of sensors that showed evidence of gas pressurisation during the Full Canister Test. a) full test period; b) at the time of gas entry.*

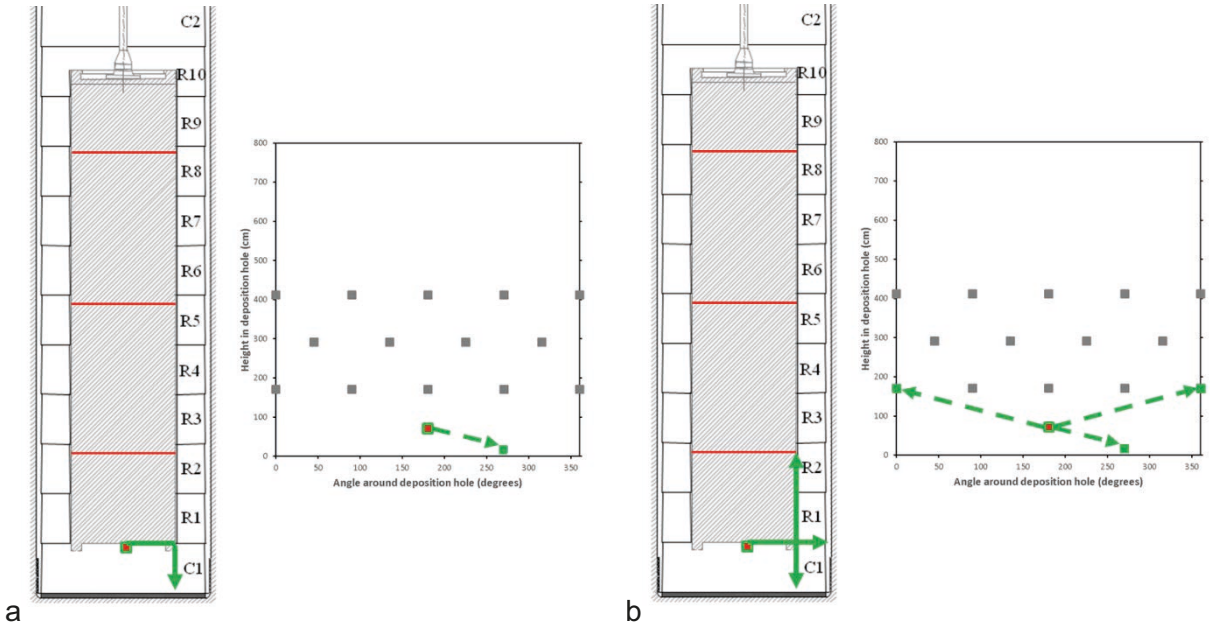

Figure 14-35. *Schematic of the direction of gas flow during the Full Canister Test. a) Gas movement to UB902; b) Gas movement to FL901.*

14.4 Summary of the Full Canister Test

The final gas injection test to be conducted was the Full Canister Test. This used the available void space of the canister to act as a large source of gas to see if the dynamics of gas transport changed. The system was modified to allow the careful filling of the fixed volume canister with gas. The canister was filled with nitrogen starting on Day 5266, this took 24 hours to bring the canister up to the nominal starting pressure of 5 000 kPa. Soon after filling the canister was seen to be leaking with no obvious cause at a rate of around 10 kPa per hour. An emergency field visit identified the source as the lines carrying the stress sensors on the canister surface. In order to seal these, it was necessary to vent the canister to 750 kPa. The canister was then slowly re-filled to 5 000 kPa ensuring no leakage. The initial test history therefore had the canister pressurised, slowly depressurised, rapidly depressurised, and then re-pressurised in steps. This had a profound influence on the stress and pore pressure of the system. Pressurisation of the canister resulted in it mechanically expanding less than 1 µm in diameter. The addition of relatively warm gas also resulted in thermal expansion. The mechanical loading of the buffer was at such a rate that the bentonite could not drain and therefore started to act as an undrained medium. This raised pore pressure as the pore network contracted. Radial stress increased as a result of the mechanical deformation of the expanding canister and the swelling of the bentonite in response to an increased pore pressure. The raising of pore pressure initiated hydraulic flow, and therefore pore pressure decayed as fluid was expelled from the buffer into the surrounding wall rock. The canister was deflated rapidly in order to fix the leak. Again, this occurred at a rate greater than buffer could react (controlled by the hydraulic properties of the buffer) and therefore the clay went into suction as the pore network expanded as a result of mechanical heave as the canister contracted and the buffer volume increased. Re-loading occurred at a relatively rapid rate, increasing radial stress and pore pressure in the same way as before. However, as the system had drained and then went into suction, the increase in stress was not as dramatic. The pressurisation of the canister greatly perturbed the stress and pore pressure field and meant that the Full Canister Test was not conducted under steady boundary conditions.

The Full Canister Test was conducted as a two-stage gas ramp. The first gas ramp started on Day 5291 and raised the pressure from 4 934 to 6 499 kPa in 25 days. The first seven refills were performed over 24-hour periods using one syringe pump, the next ten refills were conducted over 18 hours, then it was decided to switch to reciprocating pumps and to refill on a 12-hour cycle for the remaining refills. Pressure was held constant for around 10 days, when a second gas ramp was started on Day 5326, which lasted for nearly 7 days and took pressure from 6 550 kPa to 7 085 kPa. The local stress field had been determined to be 7 063 kPa at PC901 on Day 5266.13. Pressure was not raised so high that the clay

became gas- or hydro-fractured, therefore filling of the canister stopped at a pressure of 7 085 kPa. An issue occurred during the second gas ramp whereby a valve resulted in the leakage of gas from the system. The volume of gas added to the canister during each of the 55 refills was accurately known. From this, it was estimated that the available void space within the canister was 1 313 litres. Once the pressure in the canister had reached 7 085 kPa the canister was isolated and the system was given time for any remaining water to drain from the FCT valve and for gas to start entering the buffer.

1) Day 5410.86: The first evidence of gas movement was seen; UR905 showed a minor peak in pore pressure, PB902 started to increase, a small step in PB901 was seen, a small pressure spike of ~24 kPa was seen in UB901, while UB902 instantaneously increased by 68 kPa. This was followed by a stepped increase in UB902.

2) Day 5412.49: The rate of pressure change in UB902 and PB902 changed. Several pore pressure and radial stress sensors started to increase, while PB901 peaked and started to decrease.

3) Day 5414.21: Pressure at UB902 rapidly increased by ~1 000 kPa.

4) Day 5414.86: The rate of change of pressure at UB902 reduced, raising pressure a further 440 kPa over 6.04 days. The distribution of radial stress and pore pressure showed a raised pore pressure and radial stress at the base of the sensor array. A small increase in stress at the top of the sensor array was also seen.

5) Day 5420.25: The canister pressure started to decay from Day 5420.25 onwards, losing 22 kPa over the following 269 days. At Day 5420.25 pore pressure in UR903–UR906 and UR908 peaked after increasing between 11 and 99 kPa and after the peak, rapidly lost between 13 and 59 kPa. Radial stress at PR903–PR906 also peaked after increasing between 84 and 195 kPa, and after the peak rapidly lost between 34 and 49 kPa. UR910 and PR910 showed different behaviour in that they decreased 23 and 39 kPa respectively without the initial increase. At this time PB902 peaked and PB901 decreased, while UB902 decreased. Gas had reached FL901 and pressure had started to increase. The distribution of pore pressure and stress showed elevated radial stress and pore pressure confined to the base of the sensor array.

6) Day 5421.72: Pressure in FL901 increased until it matched the pressure in UB902, showing that the two were in direct contact.

7) Day 5428.31: Pressure in UR908 reduced, with UR903 and UR906 showing disturbance.

8) Day 5432.52: The distribution of stress and pore pressure showed an unchanged distribution in radial stress, but at a dissipated level. Stress was raised in the base of the sensor array and a low stress region at around 200 cm height at an orientation of 315°. High pore pressure at the base of the filter array was subsiding, with a new increased pressure forming at the top of the sensor array at an orientation of 135°.

9) Day 5396.15: Pressure reduced in UR904–UR906 and UR908. This time also corresponded with the start of slow pressure decrease in PR903–PR906.

10) Day 5680.00: By the end of the test period the distribution of radial stress and pore pressure showed that the raised levels at the base of the canister had been relieved and radial stress was elevated at the top of the sensor array. This may indicate the movement of the gas around the canister and in the buffer.

Once gas had entered the buffer, a total of 22 kPa was lost in canister pressure. This could be accounted for if 41.5 litres of pathway had formed. This volume of pathway is highly unlikely to have formed within the buffer, or for the gas to have found a sink of that size within the confines of the deposition hole as stresses and pore pressure in the buffer would have greatly increased in order to accommodate the volume change. Therefore, gas had escaped the system. This may have happened when a change in slope of the gas pressure and estimate of pathway volume was identified at around Day 5440.
As predicted, the entry of gas into the buffer did not give the pressure decay seen in all previous gas injection tests. However, gas pressure remaining high did not alter the dynamics of pathway movement. The gas safely found its way to UB902 and FL901 before finding a way out of the system, most likely between bentonite blocks. The formed pathways may have exploited pre-existing pathways from previous gas injection tests.

Section C – Decommissioning

15 Decommissioning (Day 5689 – 5782+)

The final significant stage of the Lasgit experiment started on Day 5688.95 (30th August 2020) and data recording ended at Day 5782.12 (1st December 2020); a total duration of 93.17 days. As shown in Figure 15-1, only decommissioning occurred during this period. While not necessarily being a direct scenario of interest, it was decided to keep logging all sensors until either all of the sensors were exhumed or failed, or when all of the bentonite was extracted. This enabled the observation of how the system reacted when the pre-stressed retaining lid was removed, and how the stress and pore pressures reacted when bentonite rings and segments above were removed.

Note: The grey areas displayed in the graphs shows periods when artificial hydration was not occurring.

Figure 15-2 shows the pressure of the canister prior to the start of decommissioning. It was necessary to decommission Lasgit in a manner that staff at Äspö could safely excavate the experiment. As previously stated in Chapter 14, the canister was emptied in a similar way to filling. It was felt that directly venting nearly 7000 kPa would not be safe and that pressure should be reduced to ~4000 kPa before allowing continuous direct venting. During each emptying step, the interface vessel was filled will gas from the canister. Once full the interface vessel was isolated from the system and then drained of gas. This gas was at high pressure but was a smaller volume. A total of 55 steps were taken to lower pressure before the canister was allowed to drain directly through the drain of the interface vessel.

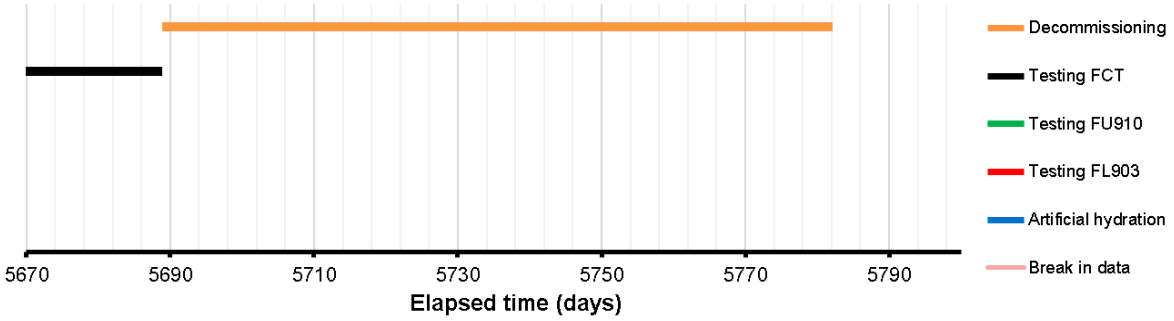

Figure 15-1. Test stages of the Lasgit experiment showing what was conducted during decommissioning.

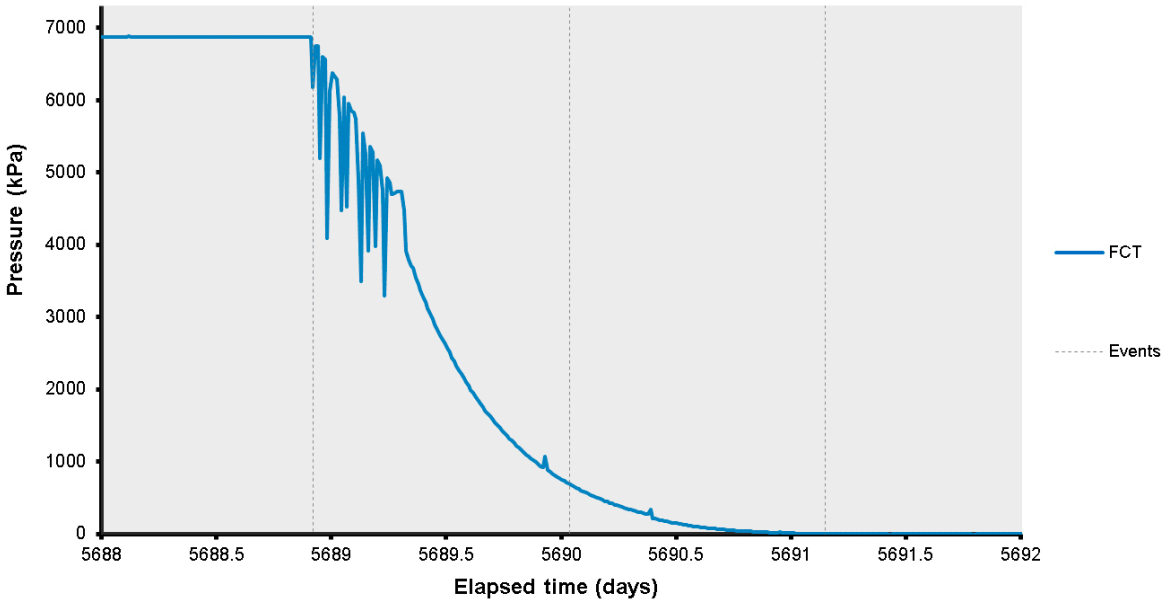

Figure 15-2. Pressure of the canister during safe venting of the system prior to decommissioning.

Drainage of canister pressure started at Day 5688.92 (30th August 2020). The interface vessels were used to lower the pressure of the canister until Day 5689.37 (0.45 days or 9 hours), after which the drain was left open to allow the canister to vent to atmosphere. Canister pressure slowly drained and reached atmospheric pressure at Day 5691.15, meaning it took 2.23 days to fully drain the canister. The pressure was safely vented without incident and the Lasgit experiment was handed from the experimental team to the decommissioning team, ready for exhumation, on 2nd September 2020.

This section of the report is split into three parts. The first section describes how the stresses and pore pressures responded during decommissioning. The second part outlines how the experiment was exhumed and describes the sampling of the bentonite. The third section describes the geotechnical results from the samples taken during decommissioning of the test.

15.1 Description of the field parameters during decommissioning

Pore pressure evolution away from the deposition hole within the pressure relief hole is shown in Figure 15-3. The first event line on the plot shows when depressurisation of the canister started. This shows that the pore pressure in the PRH intervals was disturbed and started to reduce, showing that the pressurised canister had an influence beyond the deposition hole. The second event line occurred at Day 5690.04 when the pressure in all PRH intervals was relieved in readiness for the decommissioning of the PRH packers and associated borehole instrumentation. This means that the system was undergoing two simultaneous events that will have greatly perturbed the boundary conditions; the depressurisation of the canister and the removal of the pressure relief holes.

The next event caused by human intervention was the removal of the anchors securing the canister lid and thus the relief of stress on the lid. Figure 15-4 shows the axial force on the steel lid. The depressurisation of the canister, starting at Day 5688.92 reduced the force on the lid but the reduction then stopped. In order to remove the anchors, it was necessary to increase the stress on each anchor in order to remove the retaining mechanism. Work started at Day 5691.98, with all anchors increased in force by Day 5692.38. Loading was relived on all anchors at Day 5693.02, meaning that the lid was no longer acting as a vertical support on the system. Over only four days, three significant events that would affect boundary conditions occurred, with the removal of the canister lid adding to the events created by depressurising the canister and removal of the pressure relief holes.

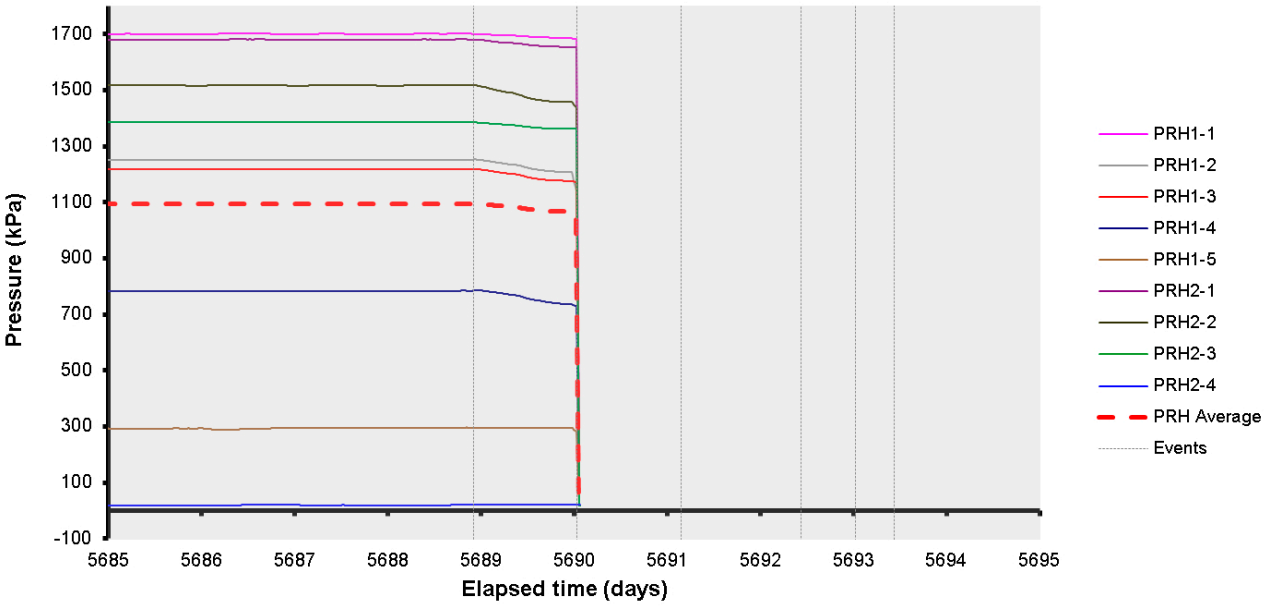

Figure 15-3. *Porewater pressures measured in the packered sections of the pressure relief boreholes. The system was decommissioned at Day 5690.04.*

Pore pressure was recorded at the canister filters, as shown in Figure 15-5. The depressurisation of the canister starting at Day 5688.92 had an influence on some of the canister filters, while appearing to have had no influence on others. Filter FL901 showed the largest pressure change, this filter was gas still pressurised from the Full Canister Test. Depressurising the canister reduced the gas pressure at FL901 by ~1 500 kPa from 5 493 to 3 954 kPa. Filters at the mid-plane of the canister also showed considerable reduction in pressure as the canister was de-pressurised, with FM905–908 all showing a similar rate of pressure reduction as FL901. The only other filter to show a response to the pressure in the canister was FL903. Filters FL902, FL904, and FU909–912 showed no significant influence from the canister pressure. This demonstrates that the inflation of the canister was mainly at its centre and not at the more rigid ends of the canister where the top and bottom were lids bolted to the main body of the canister.

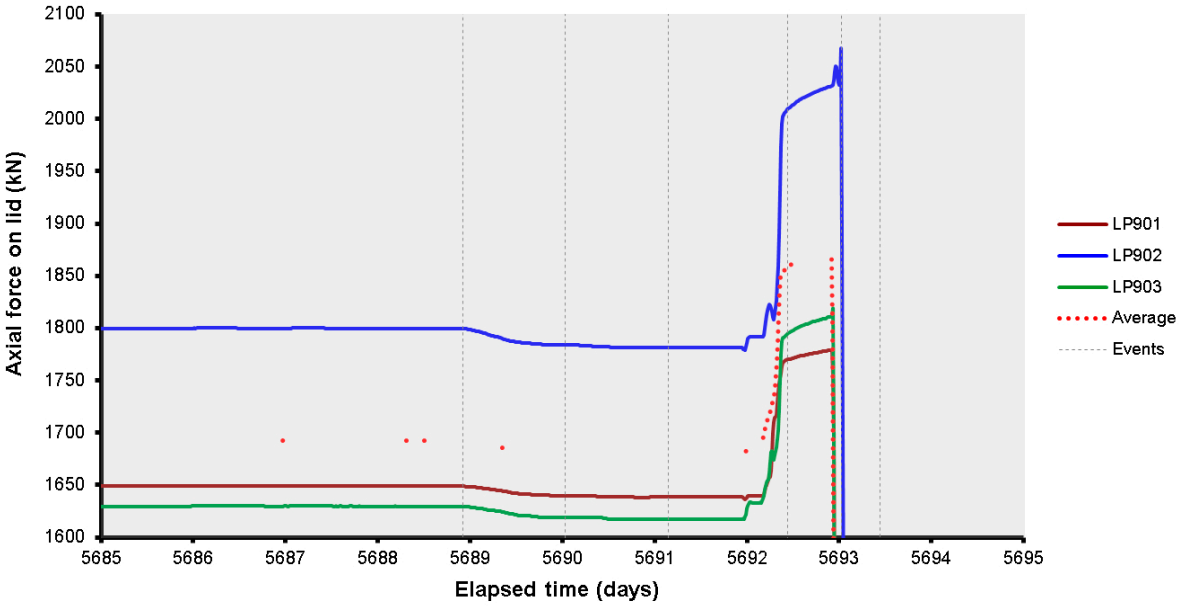

Figure 15-4. *Axial force acting on the steel lid measured by 3 Glötzl load cells attached to separate rock anchors. The load imposed by the retaining lid was removed at Day 5693.02.*

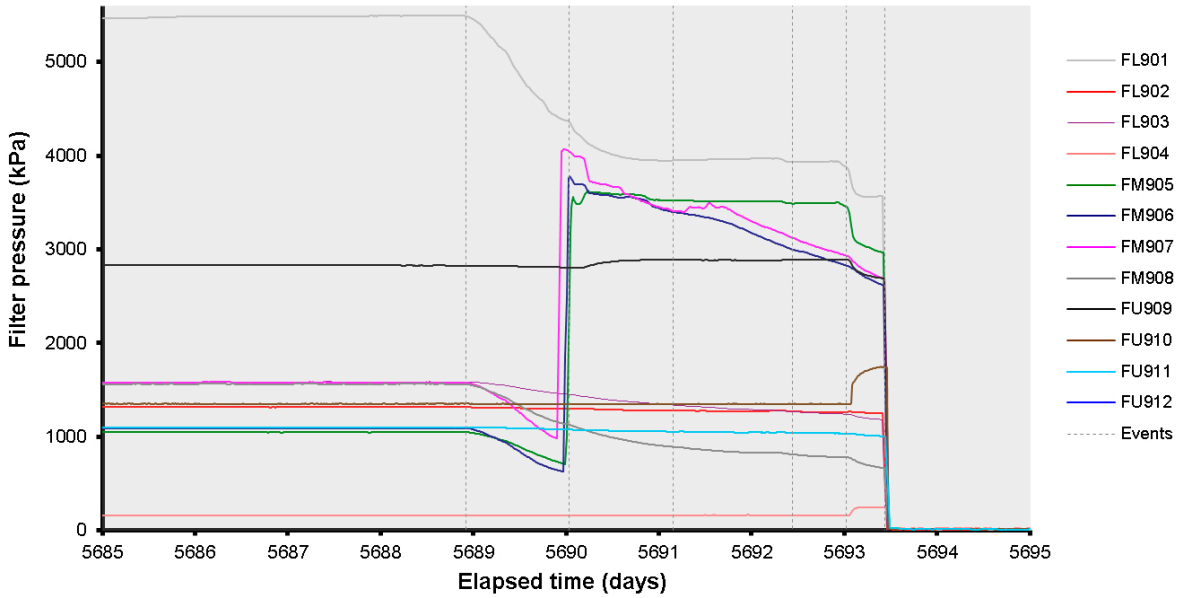

Figure 15-5. *Filter pressures on the canister surface. The filters were all depressurised at Day 5693.44.*

The removal of the pressure relief holes had a profound impact on filters FM905–907, all increasing by ~3 000 kPa when the PRH system was depressurised (Figure 15-5). The other filter to show a change was FU909, which only saw a minor pressure increase of ~90 kPa in a more gradual manner. Pressure in FM906 and FM907 started to decay after being pressurised, with FM907 showing chaotic response, possibly indicative of the presence of gas. The removal of the retaining lid at Day 5693.02 affected almost all canister filters. The largest reduction in pressure occurred at FM905, with a reduction of ~500 kPa. Filters FL901, FU909, and FM908 also showed noticeable pressure reductions at this time. However, filters FU910 and FL904 showed a pressure increase of 380 and 85 kPa respectively. All other filters showed minor decreases, or no change. For safety reasons, all canister filters were depressurised at Day 5693.44. It was felt to be unsafe to have potential pockets of high pressure within the buffer as it was excavated, especially if it was pressurised gas.

Figure 15-6 shows the pore fluid pressure of the filter mats. The depressurisation of the canister starting at Day 5688.92, reduced the pressure in most of the filter mats, with FR902 showing no change throughout the period. Filter mat FB903 showed the largest response to canister pressure, decreasing by over 250 kPa. Filter mat FB904 within the bentonite showed a lesser response reducing by < 60 kPa, while filter mat FR901 on the rock wall reduced by ~40 kPa. This latter filter mat was greatly perturbed by the decommissioning of the pressure relief holes, with pressure reducing from 1 560 to 54 kPa. This shows that the pressure relief holes played a significant role in maintaining pore pressure in the system. The event line shown at Day 5692.38 shows when all of the retaining anchors had increased load, which resulted in the filter mats within the bentonite losing pressure at a much faster rate than the response to canister de-pressurisation. It could be extrapolated that pressure in these two filter mats would have reached atmospheric pressure. However, the removal of the load on the retaining lid resulted in the filter mats within the bentonite rapidly losing all pressure. This event had a small influence on filter mat FR901. For the remainder of the period the pressure in the filter mats within the bentonite was effectively atmospheric pressure, while the filter mats at the rock wall both showed low pressure < 250 kPa. All four filter mats were drained to atmospheric pressure at Day 5706.99. The response of the filter mats during decommissioning shows that the engineered system of Lasgit played a vital role in maintaining consistent boundary conditions.

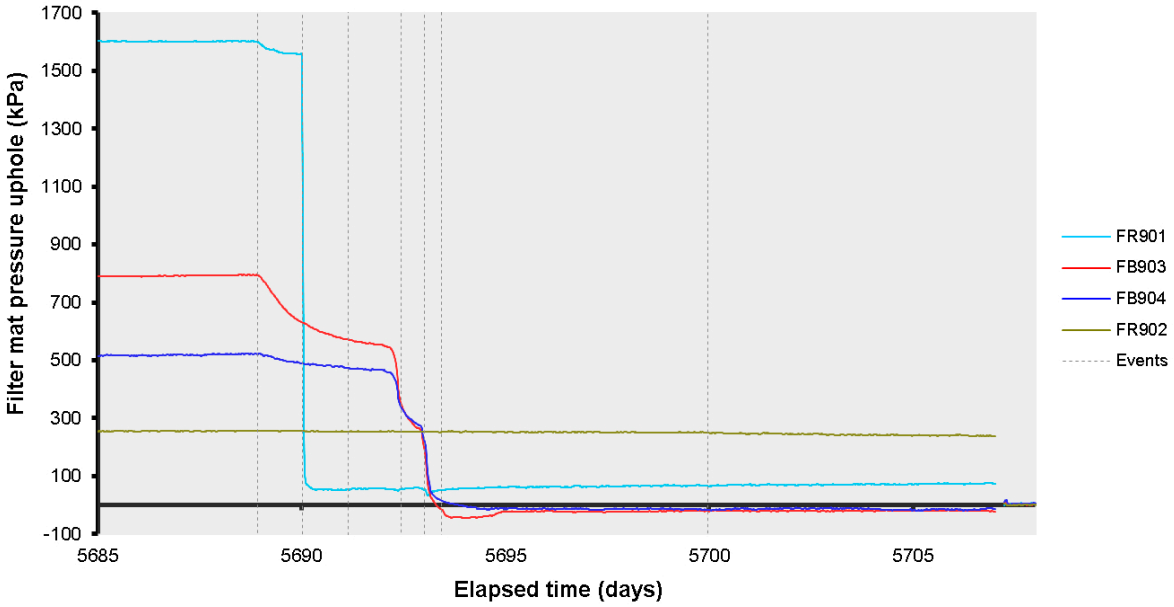

Figure 15-6. *Evolution of water pressure in the filter mats located on the borehole wall and within the bentonite blocks. The filter mats were opened to atmospheric pressure at Day 5706.99.*

Figure 15-7 shows the pore pressure within the bentonite buffer (UB), recorded at six locations. Figure 15-7a shows the detail of what happened during the initial steps of decommissioning. Almost all UB sensors showed a response to the depressurisation of the canister starting at Day 5688.92, the exception being UB923. The two sensors below the canister, UB901 and UB902, showed the greatest reduction from 1 550 to 402 kPa (1 150 kPa) and 5 420 to 3 890 kPa (1 530 kPa) respectively, Above the canister at UB924 to UB926 depressurisation of the canister resulted in a reduction of 295, 245, and 205 kPa respectively. Filter UB923 saw no change as a result of the canister pressure reducing. The increase of load on the canister lid had a large influence on pore pressure. The pore pressure at UB924–926 above the canister and UB901 below the canister all rapidly reduced to atmospheric pressure, while UB902 showed a small decrease and UB923 started to decay. The pressure at UB901 quickly recovered and increased to a pressure greater than before when the load was increased. The pressure at UB924 and UB926 also partially recovered. When the load was released and the lid was no longer under any load at Day 5692.38, the pressure in UB924 and UB926 rapidly reduced to atmospheric, UB901 reduced by over 200 kPa, UB902 reduced by over 1 200 kPa, and UB923 increased its rate of pressure decay. An unknown event occurred at Day 5697.19, when the pressure in UB923 rapidly decreased to atmospheric pressure, with disturbance in UB901 and UB902. This may have corresponded with failed attempts to lift the concrete plug.

The event line shown in Figure 15-7 at Day 5700.00 shows the time when the concrete plug was successfully lifted. By this time only the pore pressure sensors below the canister were registering any pore pressure. As seen, pore fluid pressure reduced on a near weekly basis as segments or rings were excavated. This would have reduced the weight of the overburden on these sensors and also relieved stress from the system. The pore pressure in UB901 increased at Day 5755.65, and subsequently had increases on a near weekly basis being superimposed on a decaying pore pressure. This is likely to be as a result of canister movement as it became more and more exposed along its length. Sensors UB902 and UB901 were lost at Day 5760.22 and 5782.09 respectively with both registering less than 350 kPa pore pressure.

Figure 15-8 shows the variation of pore water pressure at the rock wall. Figure 15-8a shows the detail during the initial decommissioning period. Almost all of the UR sensors showed a response when the canister was de-pressurised starting at Day 5688.92. This resulted in a loss of pressure of up to 700 kPa. The response at UR909 was complicated, an initial reduction in pressure was followed by an increase in pressure. This may indicate that a fracture network was activated by the reduction in mechanical loading. Most sensors were also significantly perturbed by the removal of the pressure relief hole at Day 5690.04. This resulted in most sensors losing more pressure and again shows that the PRH system was helping to control pore pressure within the deposition hole. Increasing load on the anchors attached to the retaining lid at Day 5692.38 also resulted in a minor reduction in pore pressure in many of the UR sensors. The removal of load at Day 5693.02 resulted in another loss of pore pressure in most sensors, with UR904 reducing to atmospheric pressure. Many of the sensor locations recovered pressure, either immediately following the loss of pressure in response to the removal of the anchors, or when the canister filters were depressurised at Day 5693.44. It should be noted that UR916, and UR918–UR920 behaved differently. At UR916 only small variations were seen, while UR918 and UR920 showed a slow and gradual loss of pressure. Sensor UR919 showed a complex history, with only a small decrease in pressure as a result of canister depressurisation and a much larger decrease in pressure as a result of load being relieved in the canister lid. The four sensors that behaved differently from the rest were towards the top of the sensor array.

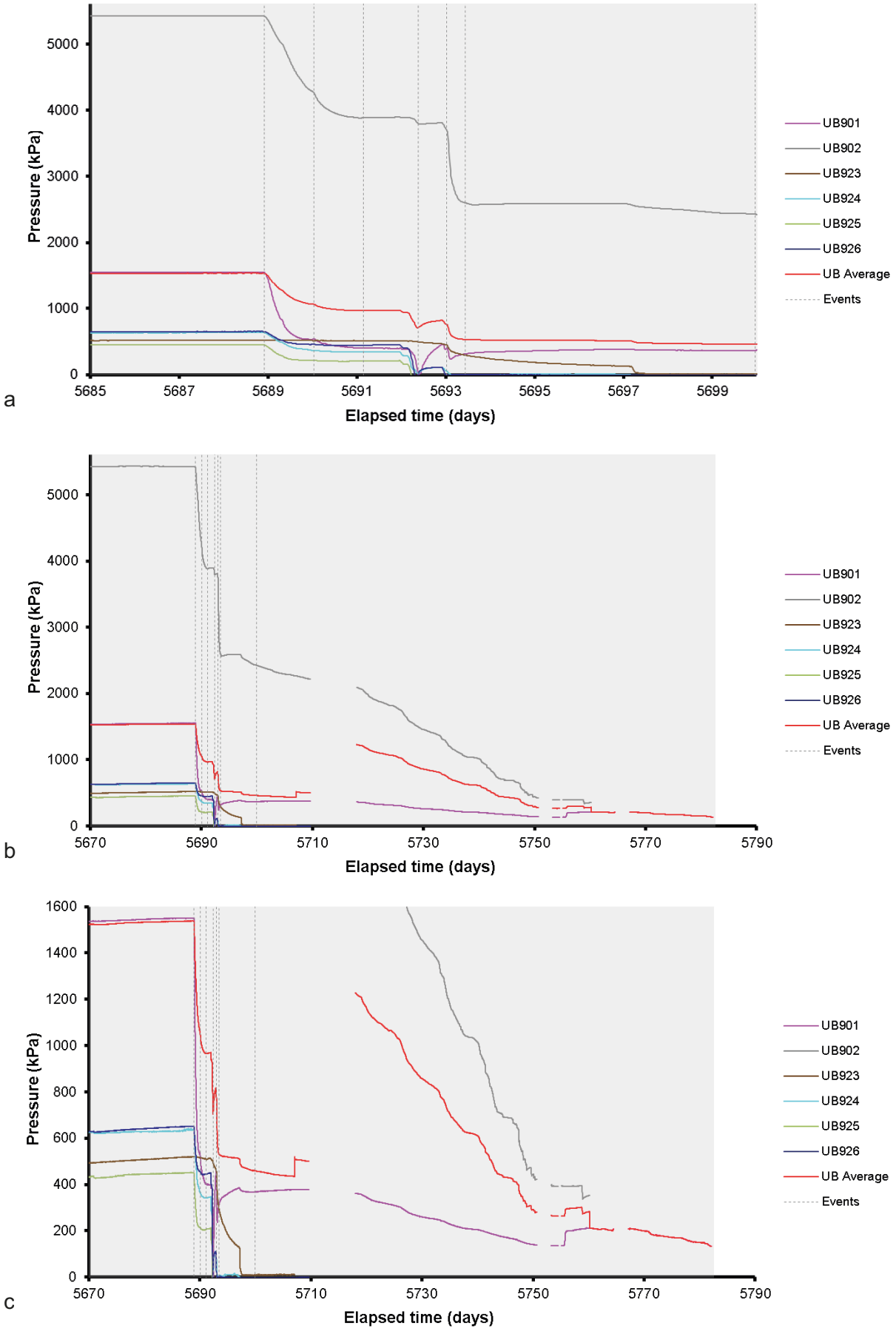

Figure 15-7. *Variation in porewater pressure within the bentonite at the 6 monitoring points: a) Initial decommissioning; b) Complete stage; c) Detail of complete stage.*

Figure 15-8b shows the pore pressure at the deposition hole wall for the complete decommissioning period. The majority of sensors showed a steady pressure decrease from the time of the concrete plug being removed at Day 5699.96. The exception was UR907, UR911, and UR913 which were still recovering in pressure from previous events. Data was lost between Day 5709.61 and Day 5717.94 as issues were experienced with the Geokon logger. By the time data was recorded again at Day 5717.94, all UR sensors were decaying. During the remaining time of the period a series of steps can be seen in most channels as the buffer continued to be excavated. Some of these steps showed considerable pressure reductions, with UR 918 reducing to atmospheric pressure at Day 5732.75. Sensor UR908 showed unusual behaviour at Day 5736.27 when pore pressure increased. This may have been the result of a fracture network in the rock wall becoming reactivated. As the period progressed, more and more sensors were lost as they were either exhumed or damaged, with the final sensors (UR903–904 and UR909) being the last sensors to log up until Day 5782.09.

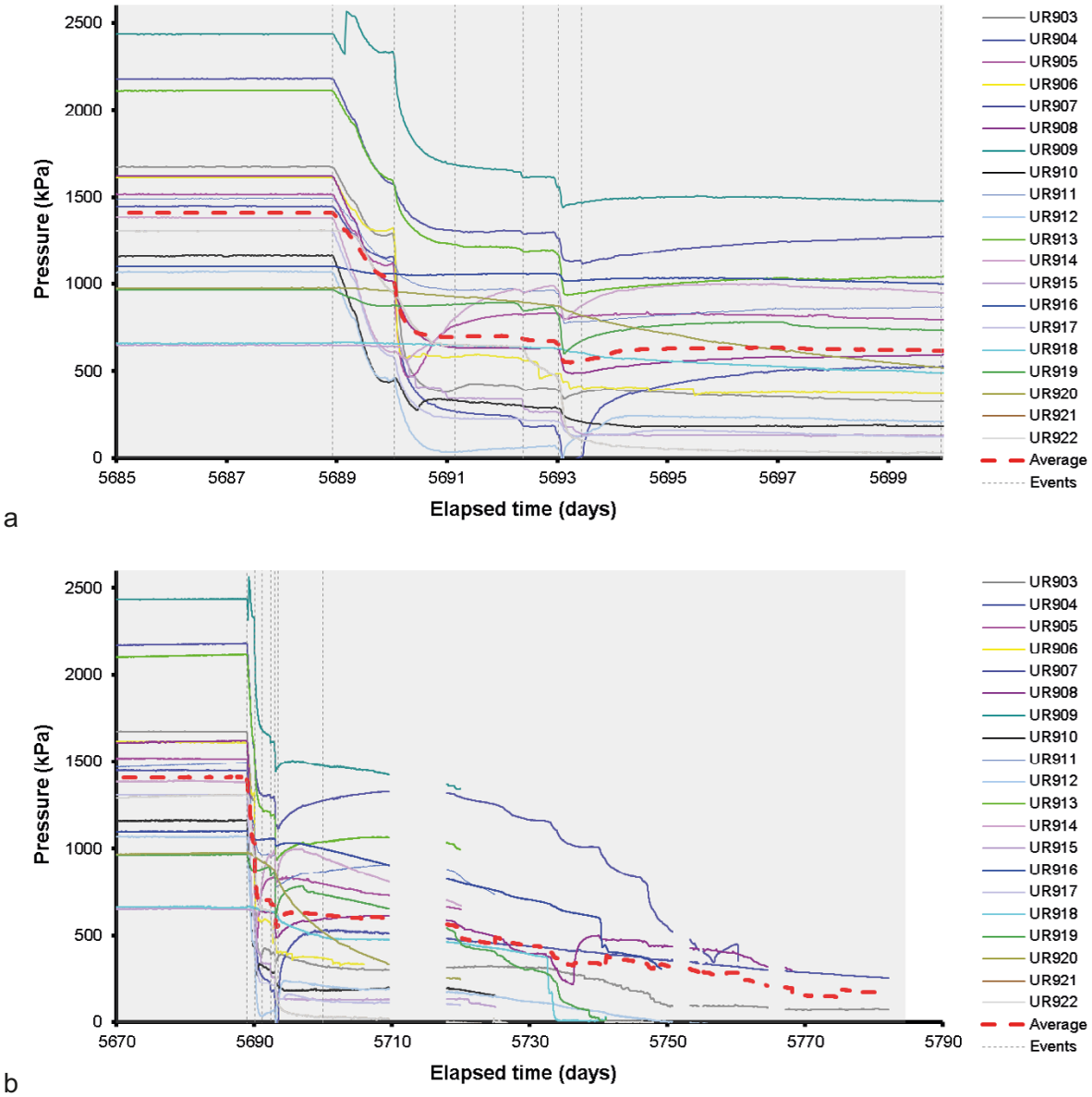

Figure 15-8. *Variation in porewater pressure with time measured at the rock face. a) Detail during initial decommissioning; b) Full decommissioning period.*

Figure 15-9 shows the distribution of pore water pressure at the deposition hole wall. At Day 5680.00, before decommissioning started (Figure 15-9a) the general distribution showed pore pressure increasing with depth in the deposition hole, although at the base of the sensor array there was reduced pore pressure. The general distribution seen throughout most of the decommissioning period was an elevated pressure at a height of around 150 cm and also at an orientation of 275°. The pore pressure distribution had significantly changed by Day 5700.00 (Figure 15-9b) when the concrete plug was lifted. The high-pressure zone at around 150 cm height and 270° still persisted, but a series of highs and lows formed higher in the deposition hole, with the low at 075° and above 400 cm height almost disappeared. By Day 5740.00 (Figure 15-9c) the number of highs and lows had changed with low pressure now observed at the top of the sensor array. This distribution may be the result of the limited number of sensors still recording. By Day 5770.00 (Figure 15-9d) there were only four sensors still recording and one of these was reading a negative pore pressure. Figure 15-9 shows that the exhumation of the system resulted in a complex distribution of stress that changed as more and more of the buffer was removed.

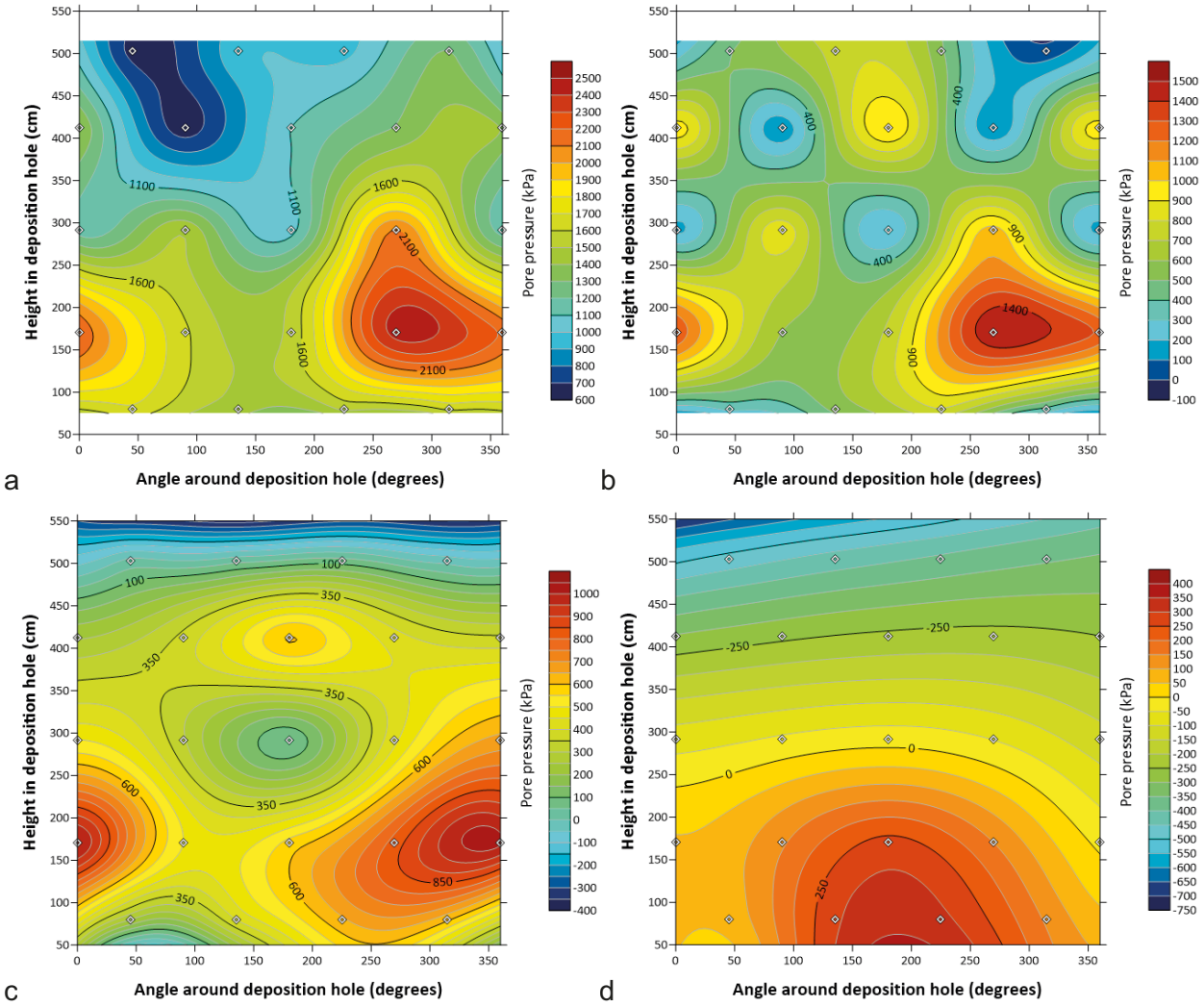

Figure 15-9. *Porewater pressure distribution at the rock face. a) Day 5680.00, b) Day 5700.00, c) Day 5740.00, d) Day 5770.00.*

Axial stress within the bentonite is shown in Figure 15-10. The initial decommissioning is shown in Figure 15-10a. All sensors showed a reduction in response to the depressurisation of the canister starting at Day 5688.92. The two sensors below the canister (PB901 and PB902) showed the greatest reduction in stress, with PB929 only showing a small response. The decommissioning of the pressure relief hole at Day 5690.04 reduced PB901 and PB902 further, resulting in a total decrease by the end of the depressurisation stage of 1 430 and 1 140 kPa respectively. In all other sensors pressure decreased by ~ 250–300 kPa. Axial stress greatly reduced when the stress on the retaining anchors was increased at Day 5692.38. The sensors above the canister were perturbed more than the two below the canister. Stress then further reduced when the force on the retaining lid was removed at Day 5693.02. By the time the concrete plug was lifted at Day 5699.96, only four sensors were still working or registering a meaningful reading; PB901 and PB902 below the canister and PB923 and PB924 above the canister. For the remainder of decommissioning, these all (with the exception of PB901) slowly reduced until the sensors were either exhumed or failed. Sensor PB901 in the base of the buffer lasted the longest. It showed the stepped reduction in stress seen in other sensors as each segment or ring of bentonite was removed. Pressure increased at Day 5761.11 by ~ 500 kPa. This may have been as a result of canister movement as bentonite rings were removed. Sensor PB901 was the final sensor to be still operational and failed at Day 5775.20.

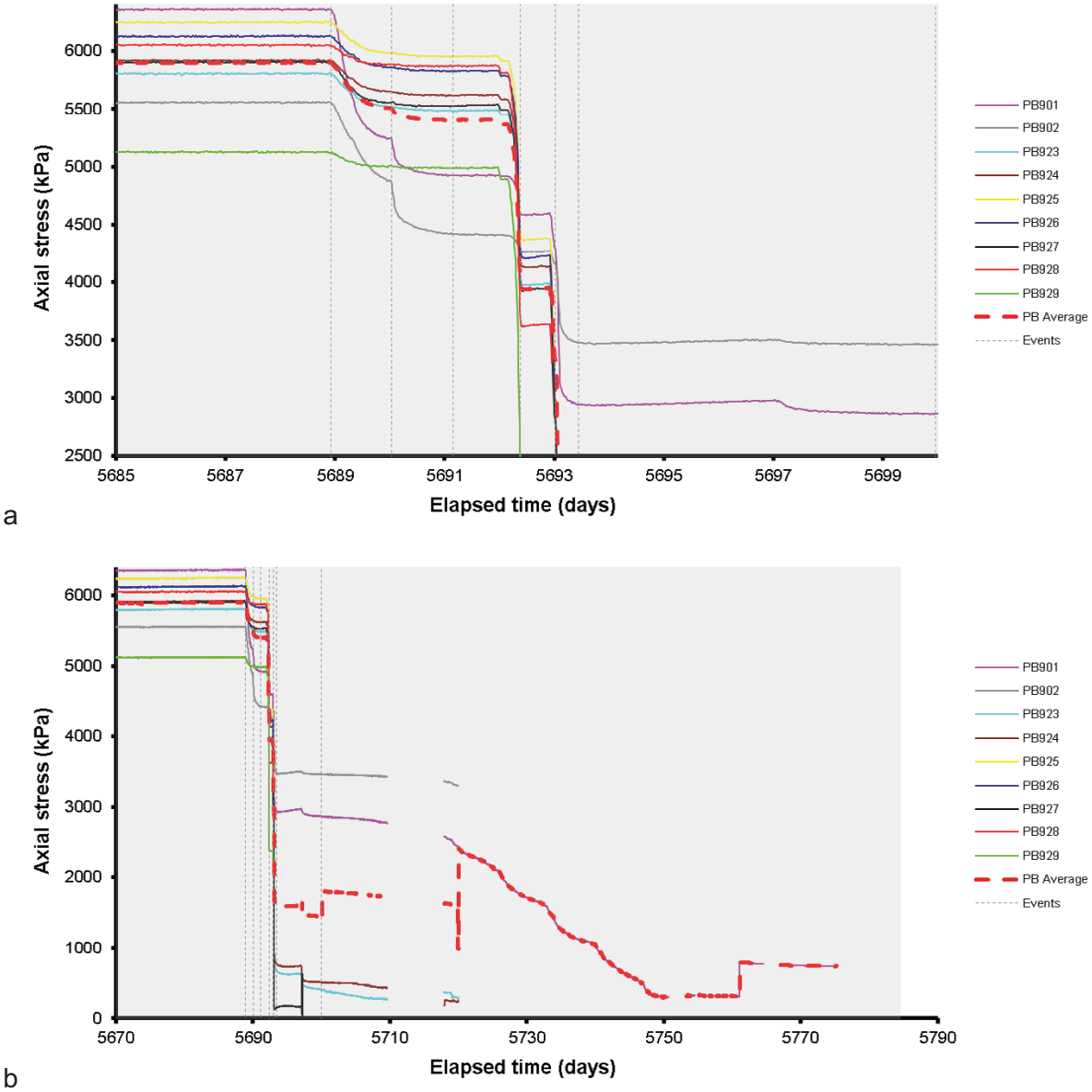

Figure 15-10. *Development of axial stress measured at 9 locations within the buffer. a) Detail during initial decommissioning; b) Result during complete stage.*

Radial stress measured at the rock wall is shown in Figure 15-11. Radial stress at the deposition hole wall started to decrease when depressurisation of the canister starting at Day 5688.92. When the pressure relief hole was decommissioned at Day 5690.04 a minor disturbance was recorded by most sensors, with some having an increased stress, while others decreased. By the end of the canister depressurisation the average reduction in axial stress was 993 kPa. Increasing the load on the retaining lid anchors resulted in a minor reduction in stress, with more stress relieved when the anchors were removed at Day 5693.02. Of special note are sensors UR921 and UR919. Throughout the test history, UR 921 had a reading much lower than all other PR sensors. When the retaining lid was removed the stress at PR919 reduced to match UR921. These two sensors were located on the same level of the deposition hole. This indicates that sensor UR921 may not have been faulty and was situated in an area where some form of feature meant that the sensor experienced reduced stress. Following the removal of the deposition hole lid at Day 5693.02 most of the PR sensor readings started to slowly show a recovery in stress. During the data drop-out between Day 5709.61 and Day 5717.94 this recovery must have peaked as all PR sensors showed a decrease afterwards. For the remainder of the test period radial stress reduced, with steps seen on an almost weekly basis as segments or rings of bentonite were removed. Sensors failed one by one, with the final PR sensor failing at Day 5782.14.

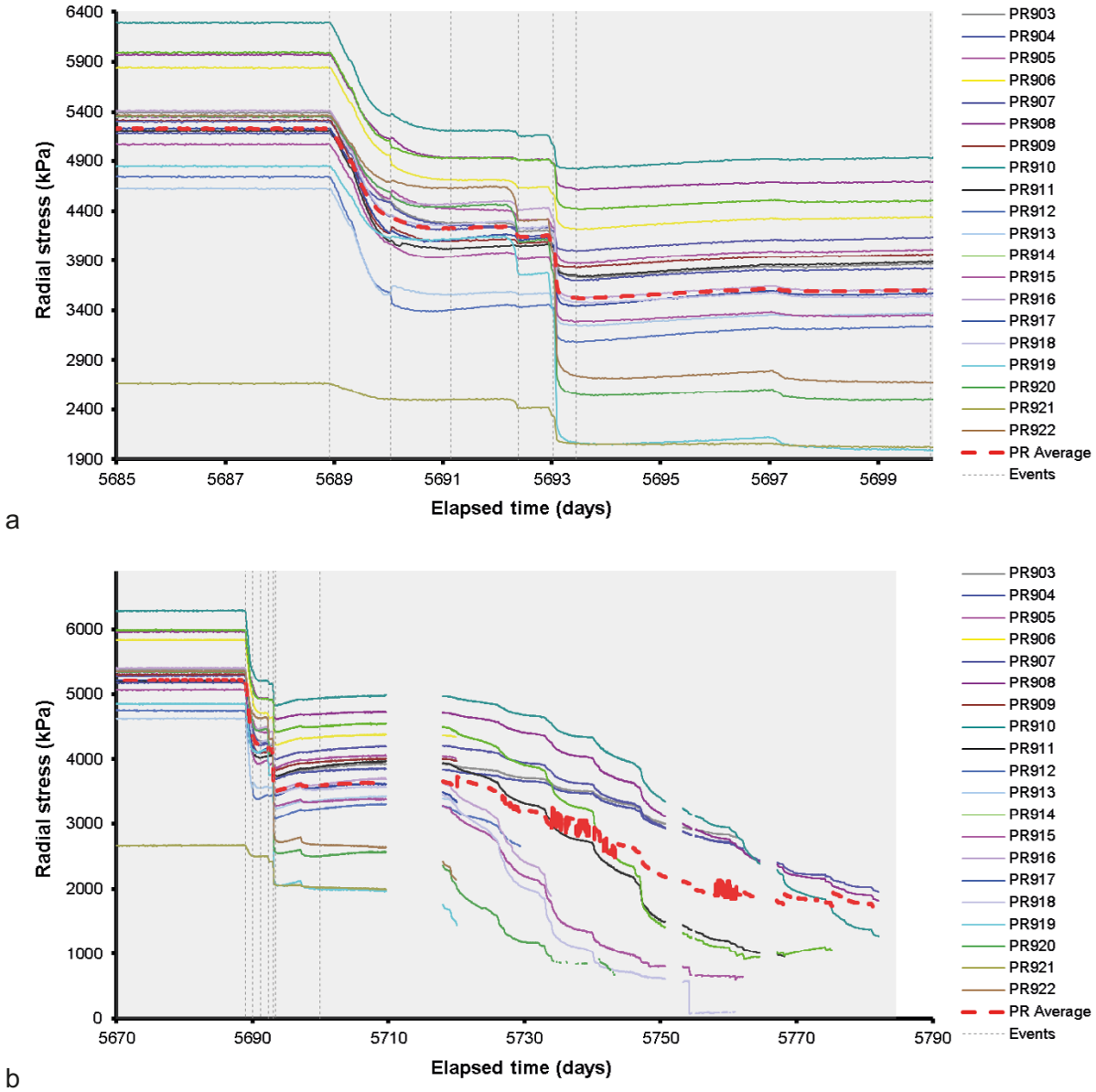

Figure 15-11. *Radial stress measured at the rock wall during decommissioning. a) Detail during initial decommissioning; b) Results for complete decommissioning history.*

Figure 15-12 shows the distribution of radial stress at the deposition hole wall during decommissioning. Before decommissioning started (Figure 15-12a; Day 5680.00), an increase in stress was seen at a height of ~150 cm and at an orientation of 315°. At Day 5700.00 (Figure 15-12b) at the time when the concrete plug was lifted the magnitude of the radial stress can be seen to have greatly reduced. The high stress at ~150 cm height prevailed, but the reduction of stress at the top of the sensor array meant that the high stress region at 315° was not as prominent. By Day 5740 (Figure 15-12c) most of the sensors at orientations of 90° and less had been lost as a shared cable run was damaged. However, the reduced number of sensors shows that the prevailing stress gradient was still apparent but decreasing. At Day 5770 (Figure 15-12d) when only a few sensors were still in operation the general stress gradient was still apparent in the data. However, interpolation of the data lead to an unrealistically low stress visualisation at the top of the sensor array.

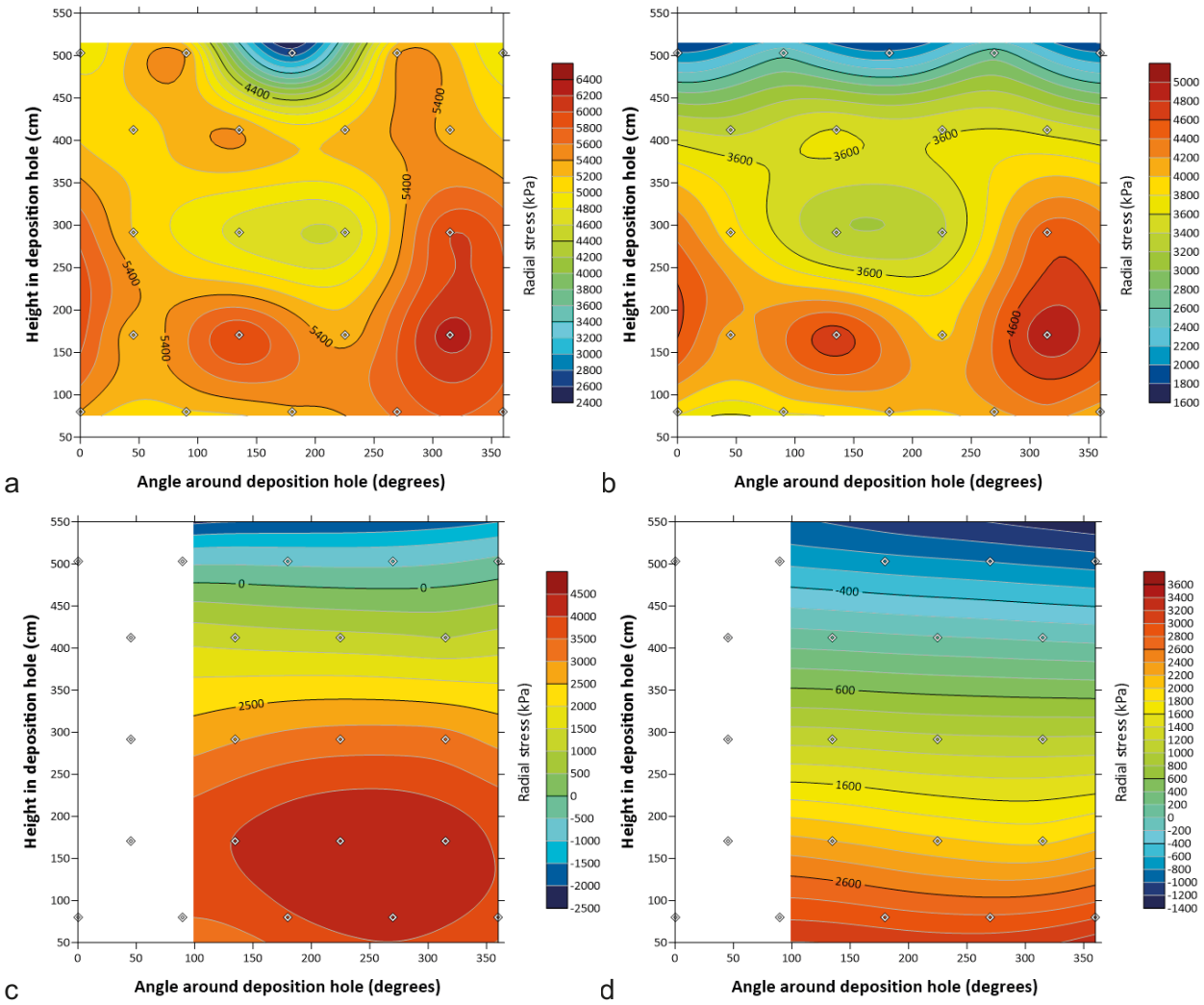

Figure 15-12. *Distribution of radial stress at the deposition hole wall during decommissioning. a) Day 5680.00, b) Day 5700.00, c) Day 5740.00, d) Day 5770.00. White space in c) and d) shows areas in which sensors had failed.*

Temperature was monitored within the Lasgit laboratory, office, the HRL, and the canister. Figure 15-13 shows that the air conditioning unit within the laboratory was problematic throughout the stage with several steps and a high of nearly 19 °C. However, as no pump operations were occurring during decommissioning the temperature will not have an influence on the data.

Figure 15-14 shows average stresses, pore pressure, and forces observed during decommissioning. Figure 15-14a shows that the initial steps of decommissioning had a profound influence on the boundary conditions. The reduction in canister pressure starting at Day 5688.92 had a big influence on pore pressure and stress seen within the bentonite and at the deposition hole wall. The removal of the pressure relief hole at Day 5690.04 had less of an impact. Increasing the stress on the retaining anchors at Day 5692.38 resulted in a decrease in pore pressure and stress, which was further reduced when the anchors were removed at Day 5693.02 when the retaining lid was removed. The rest of the period shows the slow decay of all parameters mostly in a stepped manner as individual segments or rings of bentonite were removed. The data becomes slightly confused as more and more sensors failed, often leading to an increase in the average. A complex stress and pore pressure evolution was observed as stress decreased whilst the buffer was removed. Although not a direct scenario of interest, it offers an insight into the strength and hydraulic properties of the buffer.

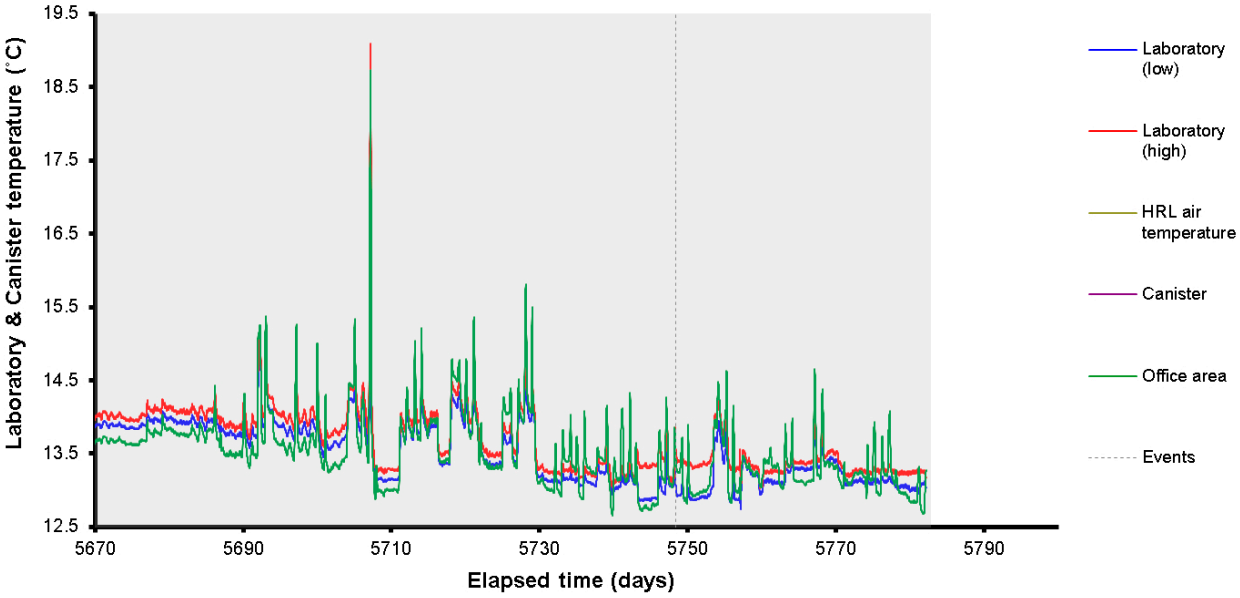

Figure 15-13. *Temperatures recorded in the Gas Laboratory, office, canister, and HRL.* ***Note:*** *the canister and HRL thermocouples were not working during decommissioning.*

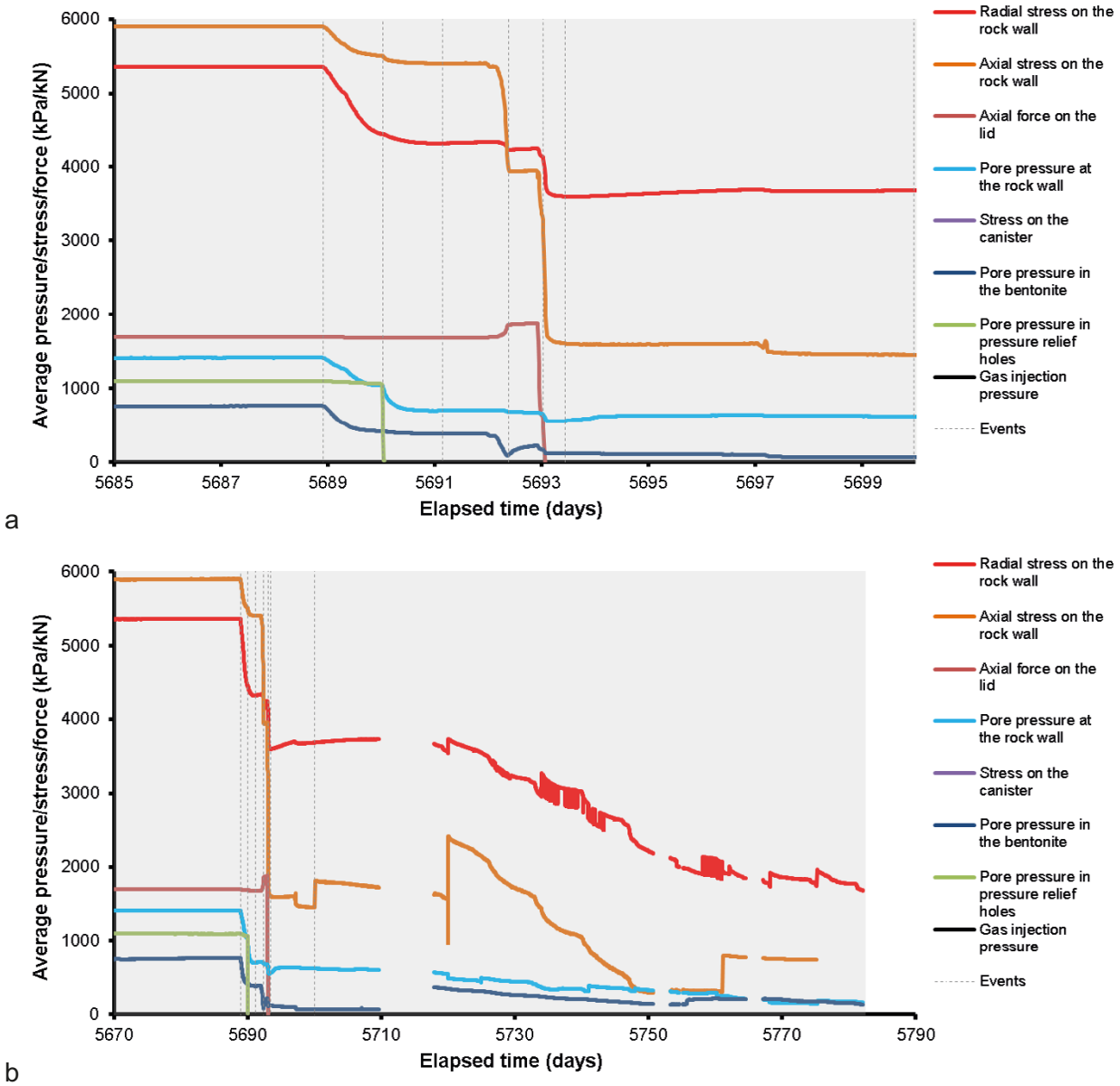

Figure 15-14. *Average pressures, stress, and force observed during the reporting period. a) Detail of initial decommissioning; b) Full decommissioning period.*

15.2 Sampling and dismantling of Lasgit

This section describes the practical steps taken for sampling and dismantling of the bentonite buffer in Lasgit. The main steps were:

- Relaxing the rock anchors.
- Lifting the steel lid and concrete plug.
- Sampling of the bentonite.
- Removal and disposal of the bentonite.
- Lifting the canister.

Dismantling of Lasgit began on Day 5691 (2nd September 2020), the original plan was to finish sampling and dismantling the experiment before the end of the calendar year (Day 5812). Although there were no major setbacks in the work it took longer than anticipated to remove all the bentonite. As a result, the work was completed by Day 5847 in February 2021.

Figure 15-15 shows the experimental setup as it was located in the underground part of Äspö Hard Rock Laboratory before dismantling and Figure 15-16 illustrates the installed components in the deposition hole.

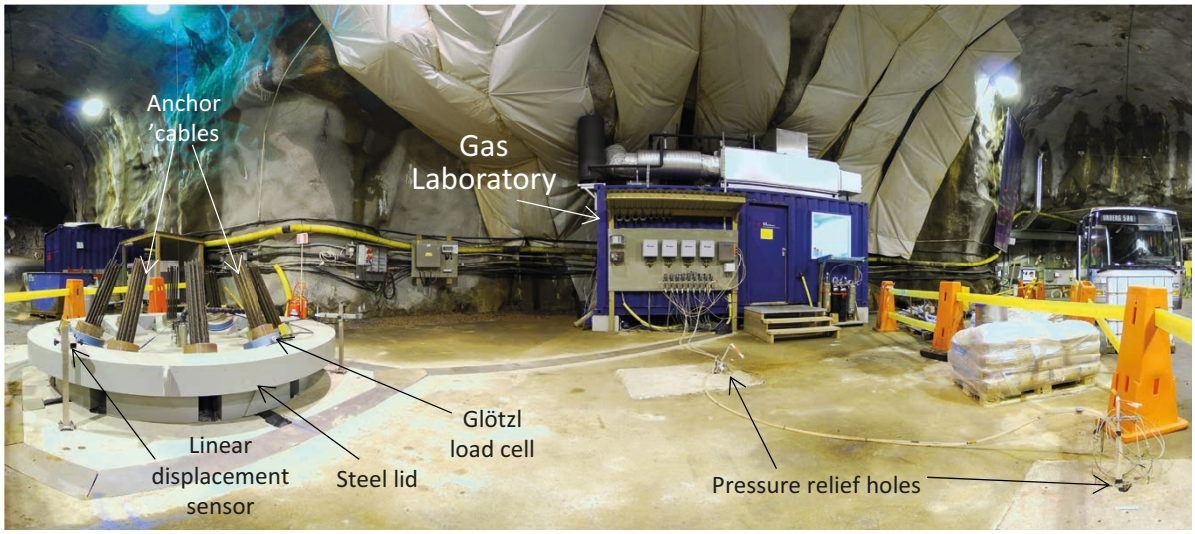

Figure 15-15. *Photograph showing the lid (coloured grey), the anchor cables, linear displacement sensors, and the Gas Laboratory.*

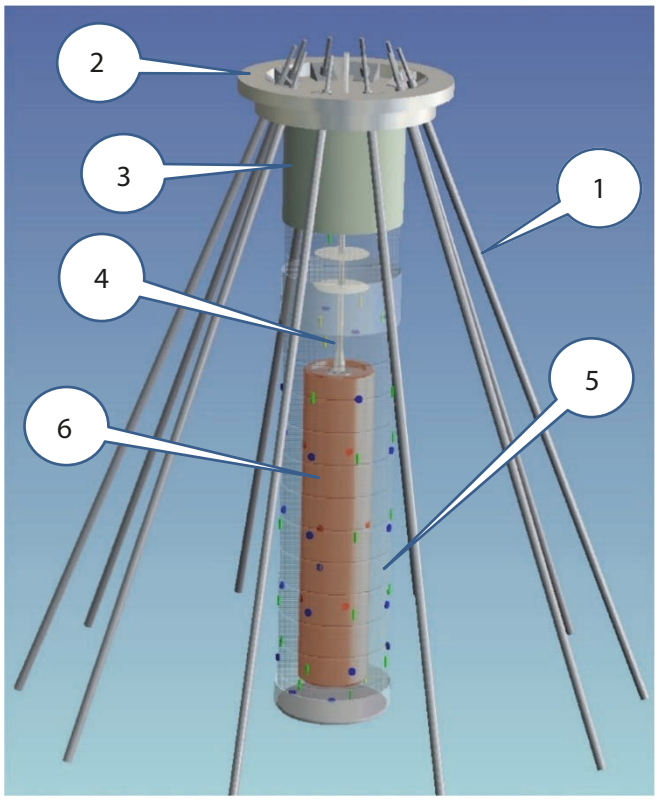

Figure 15-16. *Components of the Lasgit deposition hole. 1) Rock anchor cables; 2) Steel lid; 3) Concrete plug; 4) Central pipe for gas tubing and sensor cables (Monel pipe); 5) Bentonite buffer; 6) Copper canister.*

15.2.1 Dismantling of rock anchors, metal lid, and concrete plug removal

Dismantling of the Lasgit deposition hole began by disconnecting all gas lines and sensor cables that were connected between the canister and the gas laboratory. These were situated in channels between the laboratory and the lid and fed through the central Monel pipe to the canister. The next step was to loosen the rock anchor cables that held the steel lid in place during the experiment. To loosen the anchor cables, a specially adapted hydraulic tool was used, which can be seen in Figure 15-17a. This operation raised load on the canister lid for a short period of time. The removed anchor can be seen in Figure 15-17b.

Figure 15-17. *Removal of the anchor system. a) Loosening the anchor cable stop using a hydraulic tool; b) Anchor cable stop after removal.*

Once the rock anchor cables were loosened, first the steel cover and then the underlying concrete plug were removed with the help of a mobile crane. Figure 15-18 shows the lift of the concrete plug, the blue pillar swing crane to the right was used for lowering personnel down the hole using a safety harness and for lifting materials during sampling and removal of bentonite.

Figure 15-18. *Lift of the concrete plug using a crane.*

15.2.2 Sampling and dismantling of bentonite

It took approximately 5 months to sample and dismantle all of the bentonite. The work was mainly carried out by two workers, one who worked down in the deposition hole and one who took care of samples, disposal of material, handled lifting and so on. Working hours were Monday to Friday, 8 hours a day. Prior to weekends or planned interruptions in the dismantling, measures were taken to minimize the effect of the inflow of water from the surrounding rock mass, for example water-absorbing agents which were then removed when the work was resumed. On longer breaks such as Christmas and New Year, work was done on some holidays to prevent the bentonite from being exposed to water for longer periods of time.

The workflow was to sample and remove one block layer at a time. Figure 15-19 illustrates the test setup for Lasgit with the different block layers C1–C5 and R1–R10. Blocks denoted C were whole blocks and were situated above and below the canister. Blocks denoted R were annular in shape (rings) and were around the canister. Although it should be noted that R10 was a part ring and part complete block.

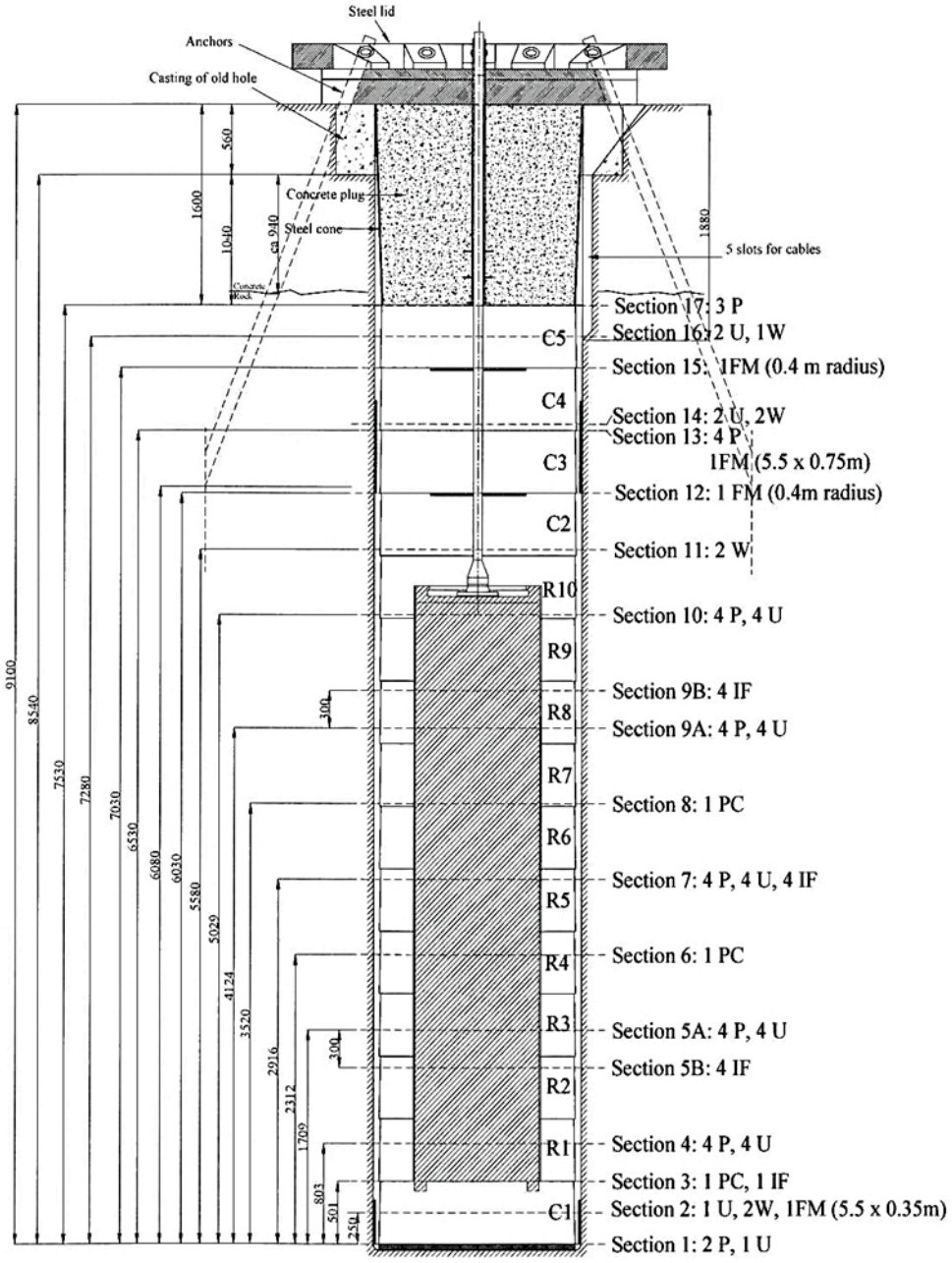

Figure 15-19. *Deposition hole with installed bentonite layers C1–C5 and R1–R10.*

The entire buffer stack was sampled by core drilling each block layer according to a predetermined pattern, the template used in the drilling is shown in Figure 15-21a. For complete blocks at angles of 0, 90, 180, and 270° samples were taken every 50 mm between 75 and 825 mm from the centre of the hole. An additional sample was taken at 850 mm within the pellets. In order to achieve a separation of 50 mm the cores were taken on alternate sides of the centre line (see Figure 15-21). At angles of 45, 135, 225, and 315° samples were taken at 100 mm separation between 575 and 850 mm from the centre of the hole. For ring blocks at angles of 0, 90, 180, and 270° samples were taken every 50 mm between 575 and 825 mm from the centre of the hole. An additional sample was taken at 850 mm within the pellets. At angles of 45, 135, 225, and 315° samples were taken at 100 mm separation between 575 and 850 mm from the centre of the hole. Cores were drilled through the full height of each block with a height of ~500 mm. Immediately after drilling, the cores were packaged in plastic and labelled with their unique position before being sent for analysis. From each core, two samples were sawn, both were analysed for water content and dry density at the Äspö Laboratory. Labelled cores and position of the samples on a core drill sample are shown in Figure 15-20.

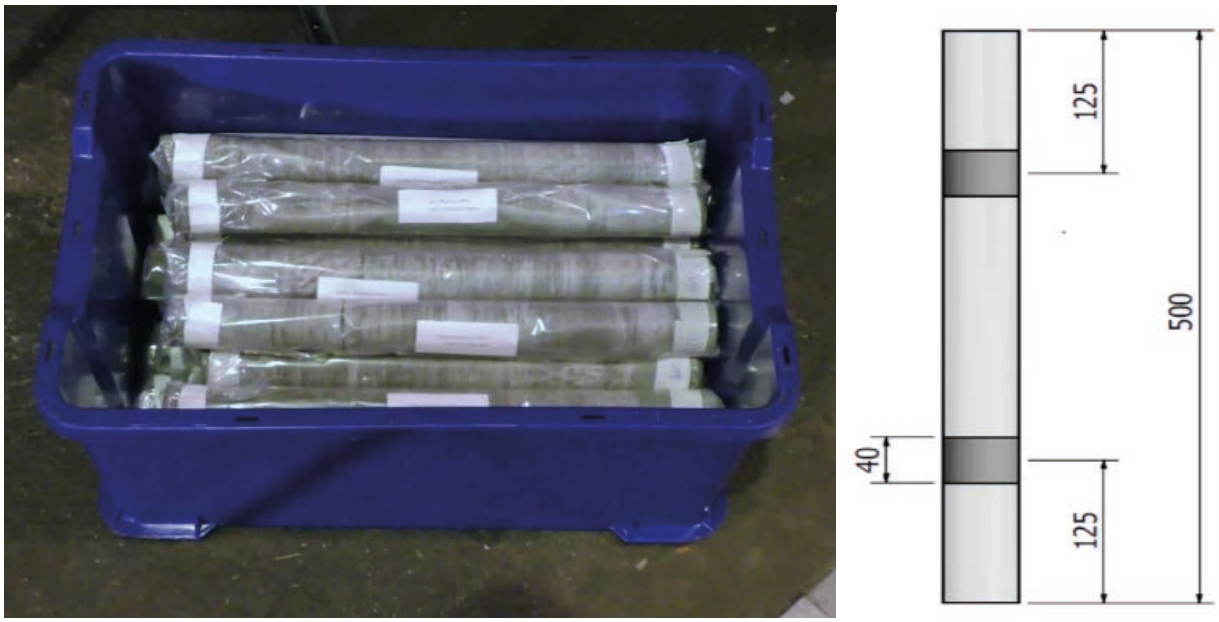

Figure 15-20. *Labelled cores and position for samples to be analysed.*

Figure 15-21. *Drilling template and sampling of bentonite by core drilling. a) Drill template for complete blocks; b) Sampling of a bentonite ring; c) Drilling of samples.*

When all cores had been drilled in the block layer, the remaining bentonite was removed and disposed of (Figure 15-22). The work of removing the bentonite was very time-consuming, as the bentonite had saturated and a swelling pressure had thus formed. This made it impossible to lift the canister before the surrounding bentonite had been removed. To remove ring R-blocks, personnel had to work in a gap between the rock and the canister that was no wider than 350 mm. Figure 15-23a shows how the canister was secured in order to allow staff to work safely without the risk of the canister moving, while Figure 15-23b shows how restricted the area was to work in. The saturated bentonite blocks were hard and difficult to remove, the best method was to use an electric chisel hammer to break it into small pieces (Figure 15-22a). To bring removed material to the surface, a specially adapted basket was used that fitted in the gap around the canister (Figure 15-22b).

Figure 15-22. *Removal of the buffer. a) Jack hammers were necessary to break the bentonite; b) Removed material was craned to the surface for disposal.*

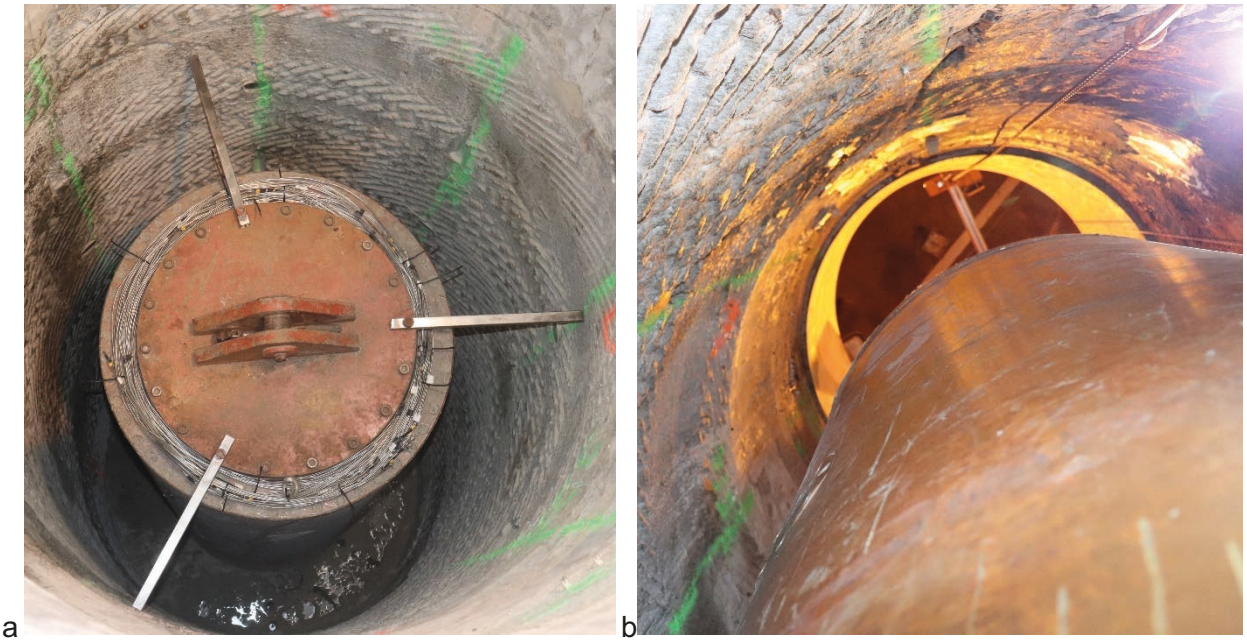

Figure 15-23. *Block removal from around the canister. a) The canister was secured to make sure it did not slip and endanger staff; b) A view from the bottom of the deposition hole to the surface showing the restricted working area.*

Photographs were taken to record features of interest during the removal of the buffer. Figure 15-24a shows an area of discolouration seen within the pellet zone of the deposition hole. Figure 15-24b shows a zone of material found within bentonite block C4. This has been assumed to have been an impurity that became incorporated within the block during manufacture. Figure 15-24c shows a photo of canister filter FM907. The surface of the canister showed many scrape marks formed during the removal of the buffer. However, it also shows patination of the canister surface that suggests localised channelling. Figure 15-24d shows the recovery of a sample around one of the injection filters. Before sampling was begun a list of sites of interest was made. This included the buffer surrounding a few of the injection filters to allow detailed geotechnical analysis. The buffer had swelled and filled the engineering void at the start of the experiment sufficiently to imprint the bentonite.

Figure 15-24. *Observations during buffer removal. See text for description.*

15.2.3 Removal of canister

After removing all of the bentonite around the canister, it was possible to lift the canister. Figure 15-25 and Figure 15-26 show the machine used in Lasgit to lift and remove the canister.

15.2.4 Sampling and dismantling the last bentonite layer, C1

After lifting the canister, all that remained was to sample and remove layer C1. Removing the canister took a few days and during this time some water flowed down and settled on layer C1 (Figure 15-27a). After the water had been pumped away, sampling proceeded (Figure 15-27b, Figure 15-27c). The fact that the block surface had been exposed to some water was not considered to affect the analysis of the bentonite since the samples that were analysed were situated some distance from the surface, see Figure 15-20. Figure 15-27d shows the deposition hole in mid-February 2021 after all bentonite had been removed.

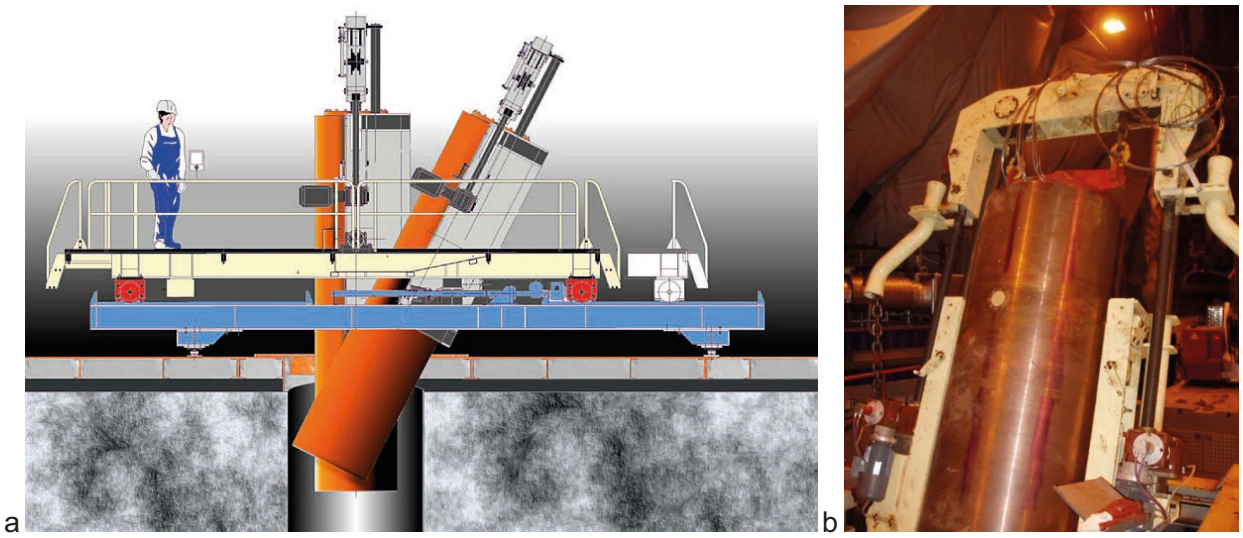

Figure 15-25. *Lifting of the canister. a) Concept for lifting the canister; b) Deposition machine in action.*

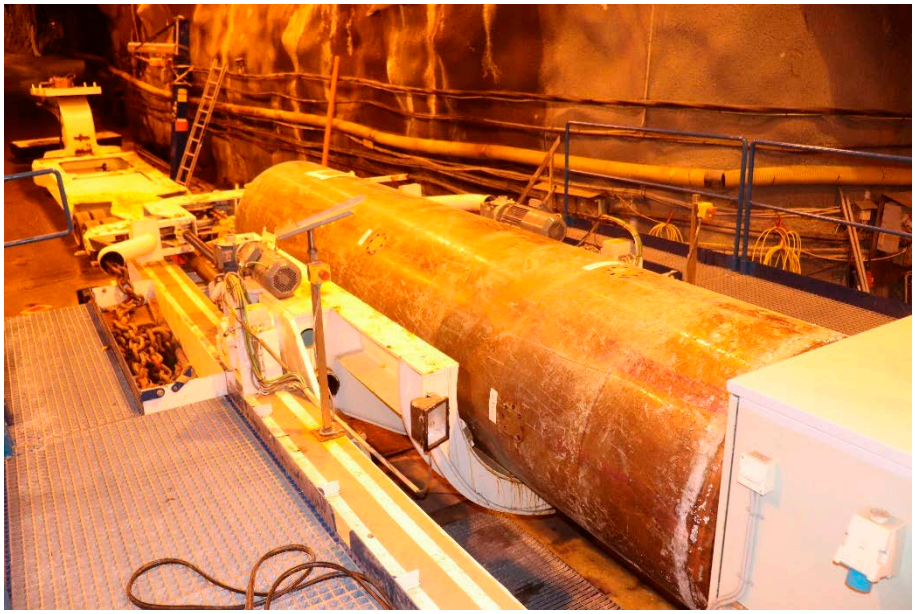

Figure 15-26. *The canister removed from the deposition hole.*

Following the removal of the buffer, all infrastructure of the experiment was removed. Channelling that had held pressure lines and/or cables was filled with concrete, the deposition hole was covered, and the Lasgit laboratory was removed. Figure 15-28 shows the Assembly Hall after the completion of decommissioning.

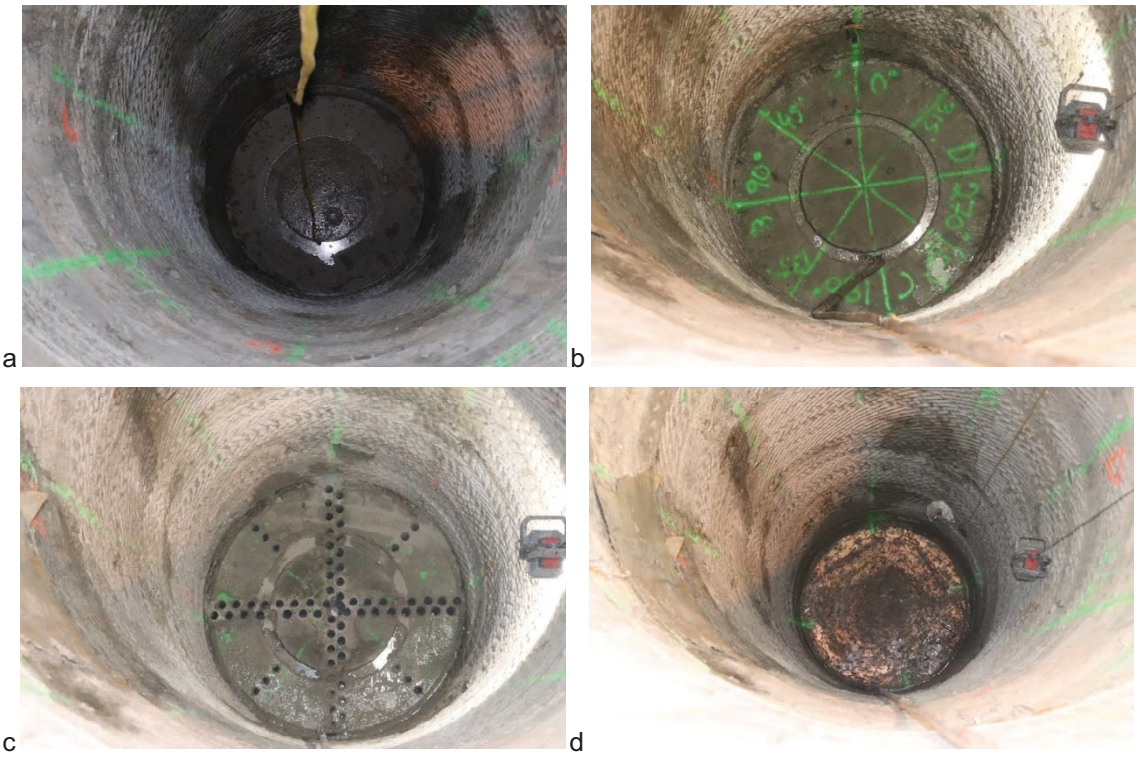

Figure 15-27. *Photos of sampling layer C1. a) Water had entered the hole during canister removal; b) Labelling in preparation of sampling; c) Samples were taken; d) All bentonite removed from the deposition hole.*

Figure 15-28. *The inevitable end. The Assembly Hall after the completion of decommissioning of Lasgit.*

15.3 Observations of the canister

The canister was brought to the surface at Äspö and carefully examined. In this section we only introduce features that may help to describe the movement of gas within Lasgit. Figure 15-29 shows the canister at the Äspö laboratory. It shows many features on the canister surface of interest.

Figure 15-29. *The Lasgit canister seen within the Äspö laboratory. White taped area cover the removed canister filter housings or stress sensor housings.*

A dark brown patination was seen in many places on the canister surface (Figure 15-30). These appear to show a pattern similar to those seen in fracture visualisation tests conducted at BGS (unpublished), with a dendritic pattern. These were seen on the bottom of the canister (Figure 15-30a) and on the side (Figure 15-30b). These features did not appear to be affected by the machining of the canister surface as they cross cut this raised pattern. The brown features were found to be superficial and could be scraped off using a scalpel. Other corrosion features were also seen with typical blue-green corrosion products, and black corrosion spots. These were also found to be superficial and easily removed. There was a greater accumulation of green corrosion products and bentonite on one side of the canister. The bottom of the canister was removed and showed considerable corrosion, confirming that the canister had water within it for most of the test history. When the lid was removed from the canister it was found to be uncorroded, demonstrating that the corrosion was not just from a humid atmosphere.

Figure 15-30. *Dark brown features were seen on the surface of the canister. a) Bottom of the canister; b) Side of the canister.*

15.4 Geotechnics of the buffer

All samples from the Lasgit buffer were analysed at the Äspö laboratory to determine geotechnical properties. A total of 1 800 samples were tested between the 21st September 2020 and 16th February 2021. By oven-drying the samples at 110 °C, each sample had water content (ratio of the weight of water to the weight of the solids in a sample), bulk density, and dry density determined. From these, simple calculations were made to determine void ratio and saturation (ratio of full saturation to measured saturation). These measures could be compared with the geotechnics determined for the individual bentonite blocks before emplacement. The following sections summarise the observations of the geotechnical properties of the buffer. Data can be considered along profiles at the same height, as profiles with depth, or as maps of distributed properties at the same level.

15.4.1 Horizontal profiles of geotechnical data through the buffer

Figure 15-31 shows a typical profile for the bottom segment (C1) of bentonite located in the base of the deposition hole below the canister. Only the data oriented 0/180° is shown. Figure 15-31a shows the measured water content. This shows that water content increased compared with that determined for the block prior to emplacement. Water content also increased towards the outside of the deposition hole, but also shows a region of lower water content roughly below where the canister would have been. This may have been as a result of compression when supporting the canister. Dry density (Figure 15-31b) shows the opposite to water content. Dry density has decreased compared with that for the block prior to emplacement. Saturation is shown in Figure 15-31c. The saturation state has been increased and averages close to unity, i.e. full saturation. However, at the edges of the deposition hole the buffer was over-saturated. It should be noted that the saturation calculation is very sensitive to small errors in measured values and can easily give estimates of over-saturation. The void ratio (Figure 15-31d) increased towards the margins of the deposition hole and had increased since manufacture of the blocks. It should be noted that the vales greatly increase/decrease close to the edge of the deposition hole, especially where the pellets were located.

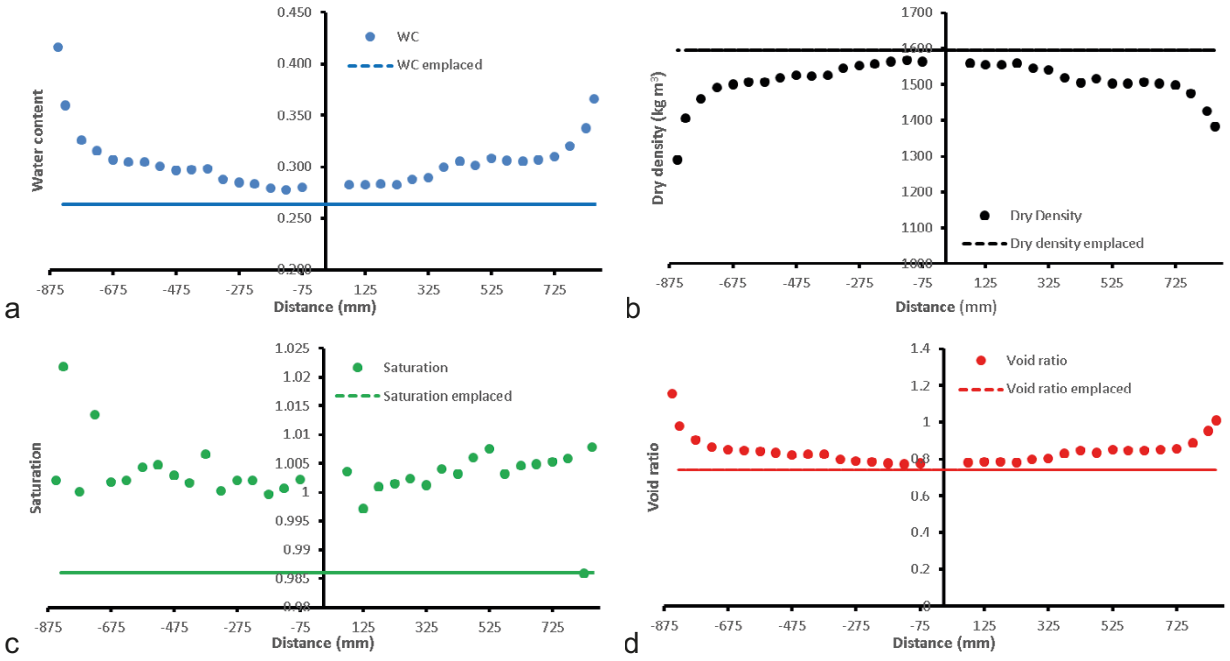

Figure 15-31. Profiles of geotechnical properties within the bottom bentonite segment (C1) oriented at 0/180°. a) Water content; b) Dry density; c) Saturation; d) Void ratio.

Figure 15-32 shows an example of geotechnical data at the level of one of the injection filter arrays (height 176.63 cm) on the canister surface, with the lower filter array shown. Similar results are seen to that for C1, with several differences. Water content (Figure 15-32a) of the bentonite ring had increased since emplacement and increased towards the outside of the deposition hole, especially within the pellets. In addition, water content also increased towards the inner buffer surface close to the canister. This may be as a result of swollen bentonite as it closed the engineered void, or may be as a result of artificial hydration through the canister filters. Dry density (Figure 15-32b) showed the opposite with a decrease since emplacement, with decreases more towards the outside of the deposition hole and towards the canister. Saturation of the bentonite had increased since emplacement (Figure 15-32c) and was close to unity, i.e., full saturation. Void ratio showed different behaviour (Figure 15-32d). Generally, void ratio had decreased since emplacement, with increases seen within the pellets.

The final example of profile data is given at a height of 627.7 cm, near to the level where many pore pressure (UB) and stress sensors (PB) were located in the buffer (Figure 15-33). Water content of the block had increased since emplacement (Figure 15-33a) with water content higher towards the outside of the buffer, especially within the pellets. However, water content had also increased on the inside of the block where the hole was located to allow the Monel pipe to feed through and allow pressure lines and cables to connect with the canister. This may be either as a result of swelling of the bentonite to fill the engineered void, or suggests that water was transported along the Monel pipe surface. Dry density shows the opposite general response (Figure 15-33b). Dry density had reduced since emplacement and reduced towards the outside of the deposition hole and the inside of the block where the Monel pipe was located. The saturation state of the block had been increased since emplacement (Figure 15-33c) and averaged around unity, showing it was fully saturated. On one side of the canister, saturation was increased towards the margins of the buffer. Void ratio increased within the block since emplacement (Figure 15-33d), with increases towards the outside of deposition hole and at the inside of the block where the Monel pipe was located. The data from this level was close to a filter mat within the buffer and did not show the variation seen in Figure 15-31 for the bottom bentonite segment. This suggests that the reduction/increase seen where the canister was located was not created by swelling pressure vertically within the deposition hole and was as a result of the weight of the canister.

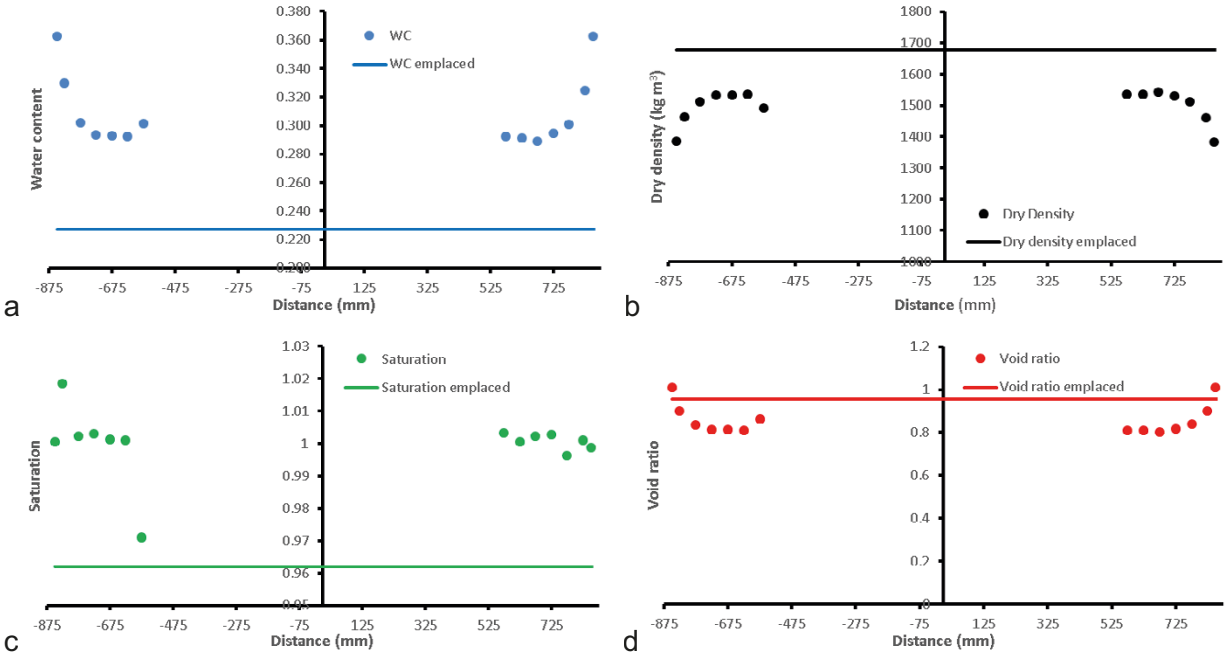

Figure 15-32. *Profiles of geotechnical properties at the level of the lower canister filter array oriented 90/270°. a) Water content; b) Dry density; c) Saturation; d) Void ratio.*

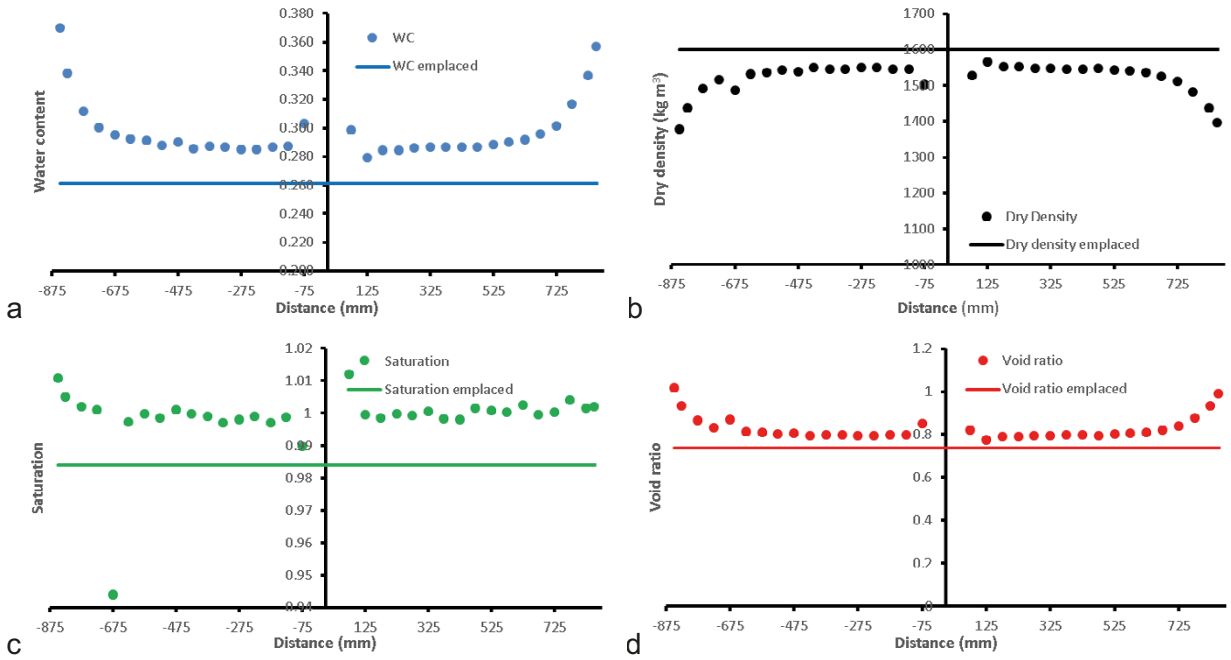

Figure 15-33. *Profiles of geotechnical properties at a height of 627.7 cm towards the top of the deposition hole. a) Water content; b) Dry density; c) Saturation; d) Void ratio.*

15.4.2 Vertical profiles of geotechnical data through the buffer

Geotechnical data can also be considered in a vertical context to see how properties change with depth. This is particularly interesting in Lasgit as a pore pressure and stress gradient was seen along the length of the deposition hole. Figure 15-34 shows how parameters varied with height in the 180° direction. The data are shown for a distance of 575 mm, which represents the data closest to the canister, with 180° being the orientation of the canister filter FL903. What can be seen in Figure 15-34 is the difference in geotechnical properties seen for segments (C) and rings (R) before the blocks were emplaced. Water content, void ratio, and saturation were lower in rings, while dry density was higher. Water content determined from decommissioning shows a relatively consistent water content along the length of the deposition hole. The differences seen before emplacement had disappeared. Water content did increase with depth. The data from along the length of the canister (50.1 to 533.1 cm height) was more varied, possibly as it would have included zones of increased hydration from the canister filters and because this region would have swelled to close the engineered gap.

Dry density showed similar results to water content (Figure 15-34b). The difference seen in the data before canister emplacement had gone, with a general decrease in dry density with depth. Similarly, results along the canisters length were quite dispersed. Saturation was generally close to unity along the complete length of the deposition hole (Figure 15-34c). In areas close to the canister filters the results showed over saturation. There was little change in saturation with depth. Void ratio increased with depth (Figure 15-34d) and like the other parameters was more chaotic along the length of the canister.

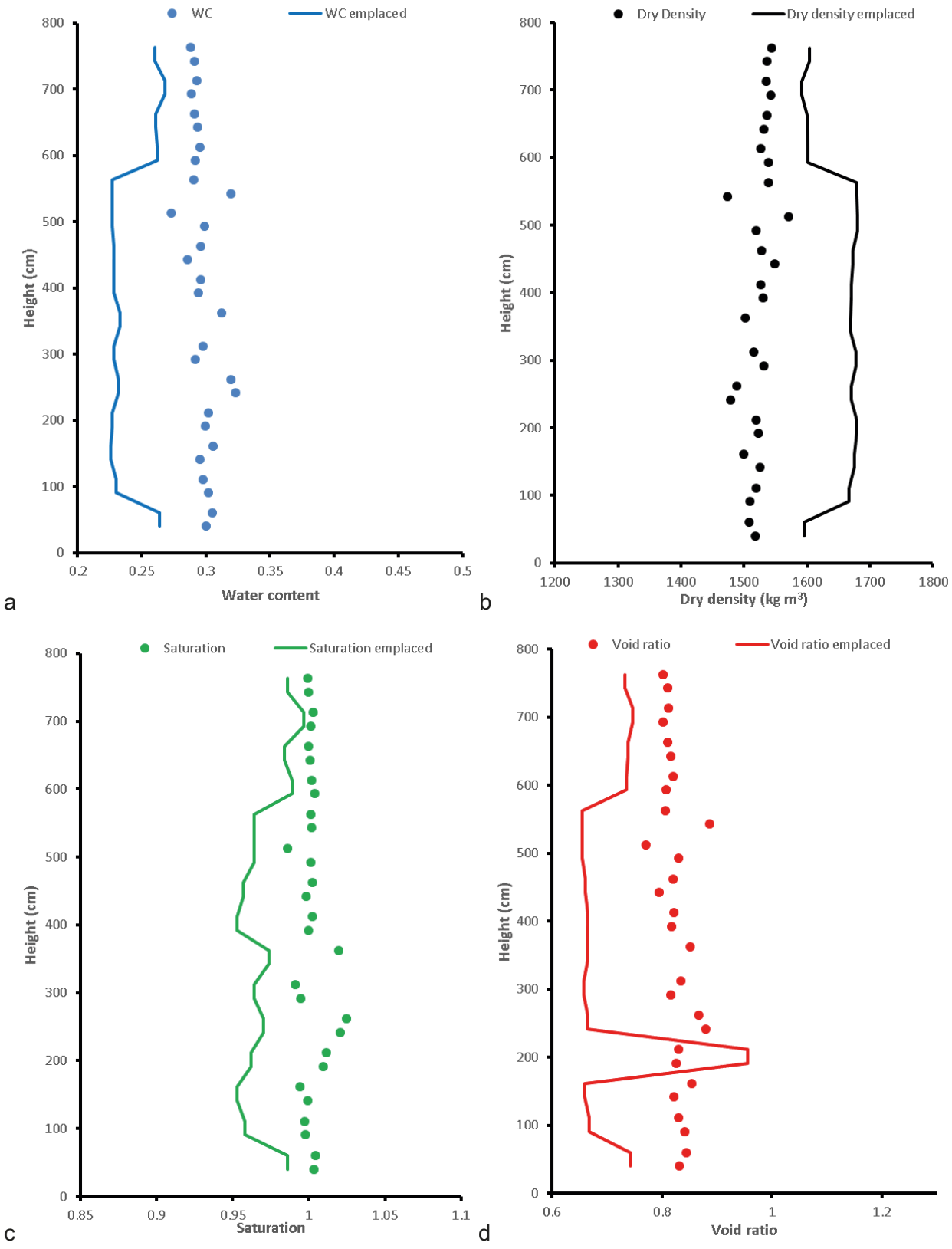

Figure 15-34. *Vertical profiles of geotechnical properties at an orientation of 180° at 575 mm from the centre of the hole. a) Water content; b) Dry density; c) Saturation; d) Void ratio.*

Figure 15-35 shows the geotechnical properties at an orientation of 180° at a distance of 725 mm, this being the mid-point of the bentonite rings. Water content (Figure 15-35a) generally showed a static value with depth, although it did increase at both the top and bottom of the buffer. The data from along the length where the canister would have been (50.1 to 533.1 cm height) this time was more consistent and shows that the data reported for a distance of 575 cm was showing variation close to the canister. The reduced water content seen before emplacement was no longer apparent, with water content increasing along the full length of the deposition hole. Dry density (Figure 15-35b) showed the inverse of water content. Dry density had decreased along the full length of the buffer and no longer showed a difference for the rings compared with bentonite segments. Dry density was fairly constant along the full length of the buffer, except at both the top and the bottom of the buffer where dry density decreased. Saturation along the full height of the buffer (Figure 15-35c) was relatively constant and very close to unity and full saturation. This shows that the buffer had been raised to full saturation. Void ratio (Figure 15-35d) showed a similar form to water content. Void ratio had been increased during the duration of Lasgit giving a relatively constant value along the full height of the buffer. However, void ratio did increase towards the top and bottom of the buffer.

Figure 15-36 shows the geotechnical properties at an orientation of 180° at a distance of 850 mm, this being the outer edge of the bentonite rings within the pellet region. Water content (Figure 15-36a) in this region was increased much more than in the previous two examples. Water content also increased significantly with depth, although it was also raised towards the top of the buffer. This corresponds with the fracture network and the zones that were identified as conductive, it also corresponds with the two filter mats used for artificial hydration. Dry density (Figure 15-36b) showed the opposite, with a much lower dry density than shown in the previous two examples with dry density increased towards the bottom and top of the buffer. Despite a much-increased water content, saturation (Figure 15-36c) was relatively consistent along the full height of the buffer, approximately equal to unity. This shows that the pellet zone was fully saturated. Void ratio (Figure 15-36d) showed a similar trend to water content and was greatly increased from the starting value. Void ration increased towards the bottom and the top of the deposition hole.

Figure 15-37 compares the data across the full width of the buffer in the 180° direction for 75, 325, 575, 725, and 850 mm distance from the centre. For water content (Figure 15-37a) there doesn't appear to be much variation in the pattern of results, except for the results seen in the pellet region. However, subtle difference can be seen. Below the canister, water content is lowest at the centre of the segment, whereas above the canister it is higher than at 325 mm. This suggests at both of these areas water is moving from the outside of the buffer inwards, with the Monel pipe assisting hydration above the canister. Similar can be seen in dry density (Figure 15-37b), with the highest dry density in the centre of the buffer. Little variation in dry density is seen, except in the pellet region. Saturation (Figure 15-37c) shows little variation with distance from the centre of the buffer, with the whole buffer in the direction of 180° close to full saturation. Void ratio data (Figure 15-37d) are more complicated, but similar to water content. At the base of the buffer void ratio clearly increase from the centre of the buffer to the outside. Similar can be seen above the canister, although the data close to the Monel pipe shows elevated void ratio.

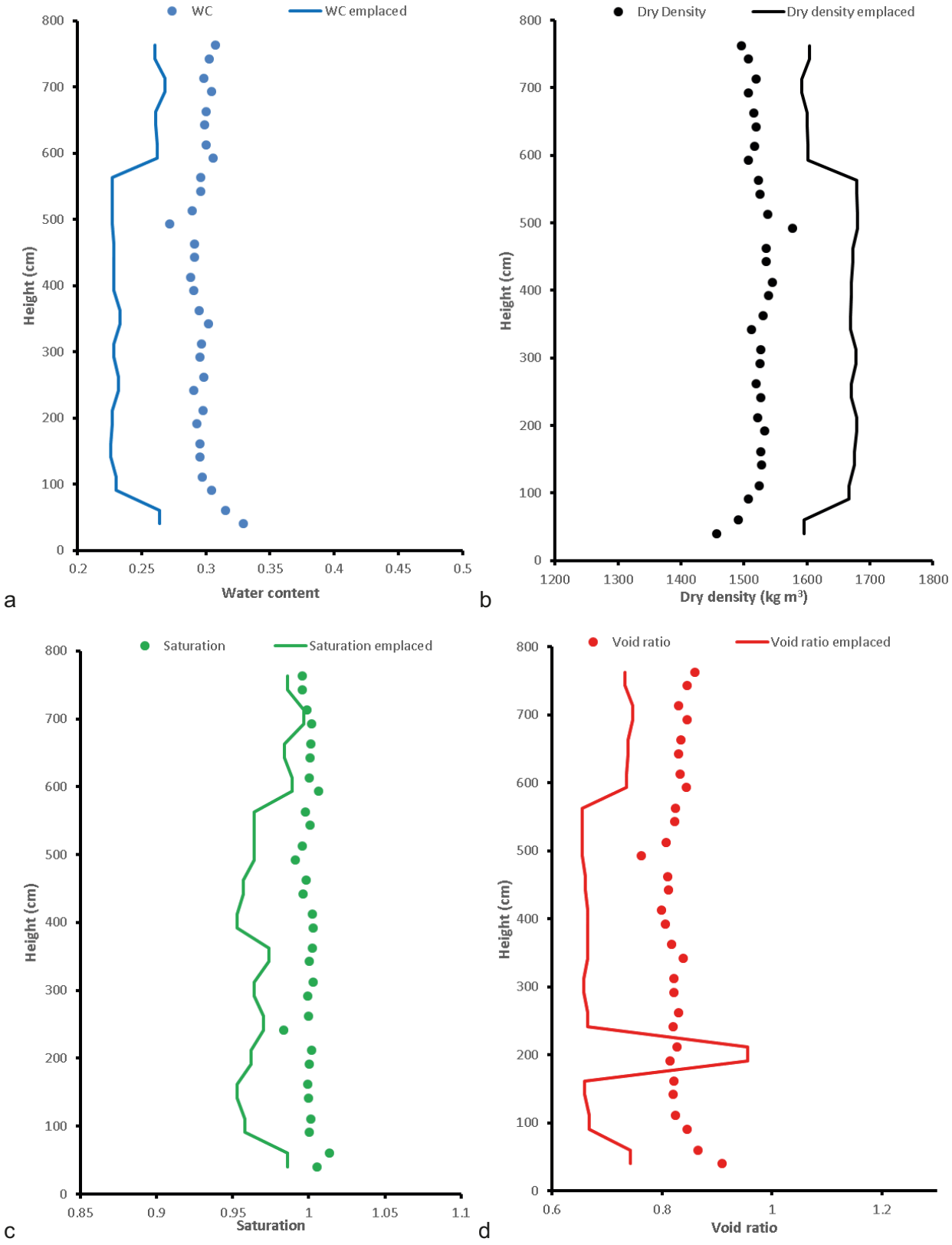

Figure 15-35. *Vertical profiles of geotechnical properties at an orientation of 180° at 725 mm from the centre of the hole. a) Water content; b) Dry density; c) Saturation; d) Void ratio.*

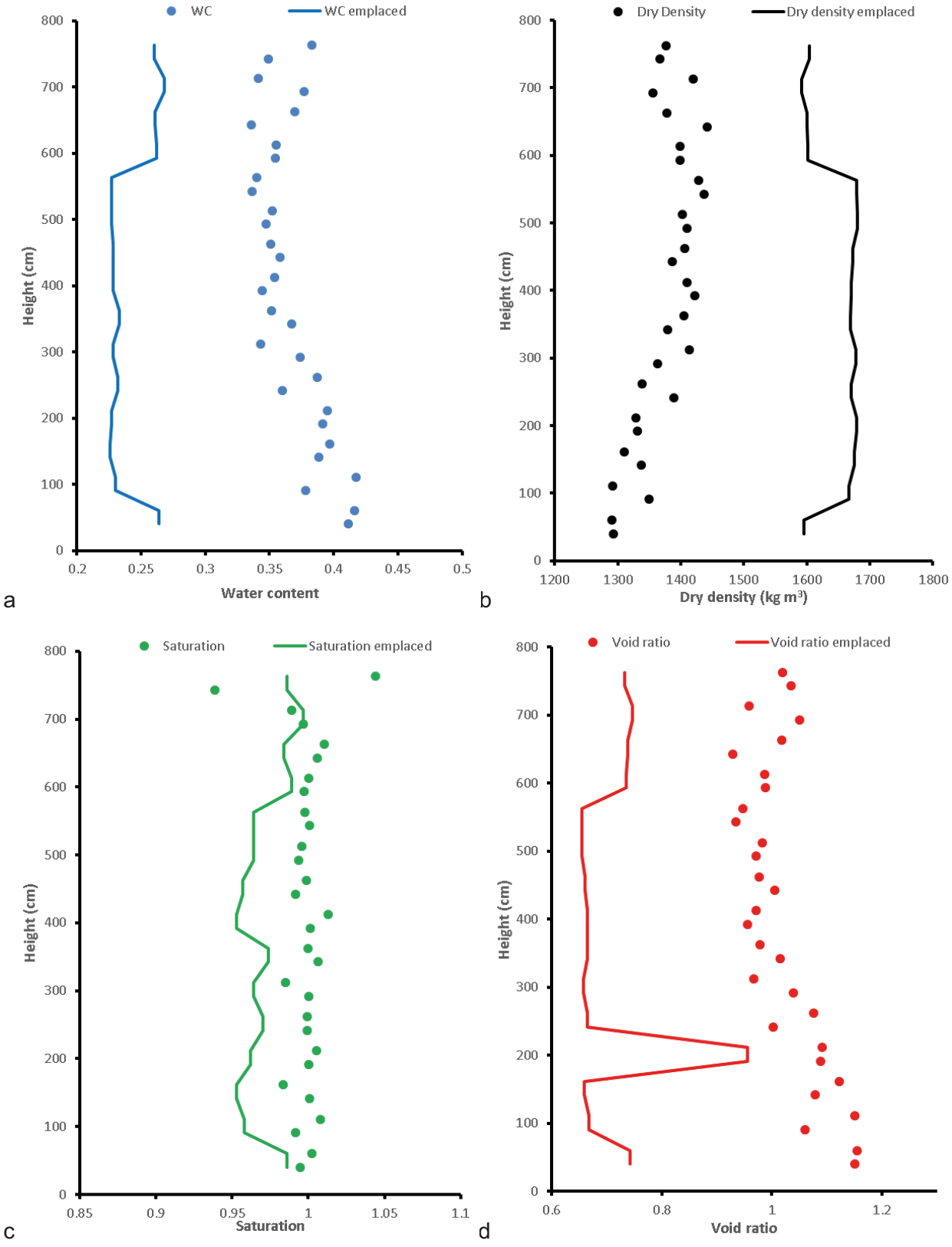

Figure 15-36. *Vertical profiles of geotechnical properties at an orientation of 180° at 850 mm from the centre of the hole. a) Water content; b) Dry density; c) Saturation; d) Void ratio.*

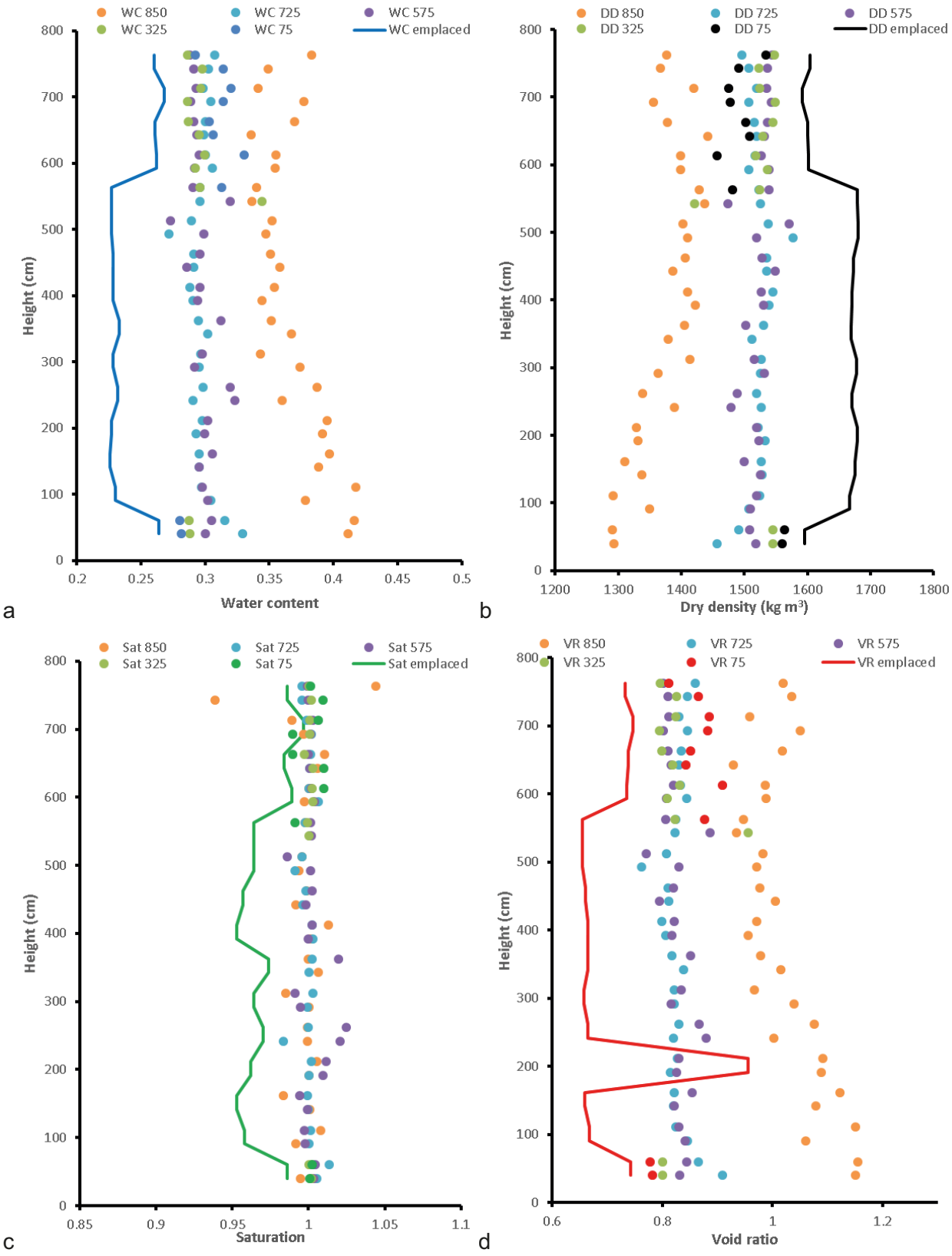

Figure 15-37. *Vertical profiles of geotechnical properties at different distances from the centre of the hole at an orientation of 180°. a) Water content; b) Dry density; c) Saturation; d) Void ratio.*

15.4.3 Distribution of geotechnical properties in plan

The distribution of geotechnical properties can also be considered in plan to look for zones of variation. It is important though to consider effects of interpolation. The distribution of data points show a high spread of data in two orthogonal directions, with a lesser spread of data at 45°. This distribution is not well suited to many interpolation algorithms, with the previously used minimum curvature prone to artefacts. All gridding methods in Surfer v22 were considered, with the radial basis function appearing most appropriate for the distribution of data points. This still resulted in artefacts that need considering when interpreting the results.

Figure 15-38 shows the results for the bottom of the deposition hole at a height of 35 cm. This shows that the highest water content (Figure 15-38a) was on the outside of the buffer, with the lowest clearly in the centre. The converse is seen in dry density (Figure 15-38b) where the highest dry density is seen in the centre, simply decreasing towards the outside of the buffer. Saturation (Figure 15-38c) is relatively constant and close to unity for the entire area, apart from a low region in the 90° direction. Void ratio (Figure 15-38d) was largest at the centre of the segment and increased towards the outside of the buffer. In all four plots, a simple circular variation can be seen, with some localised anomalies.

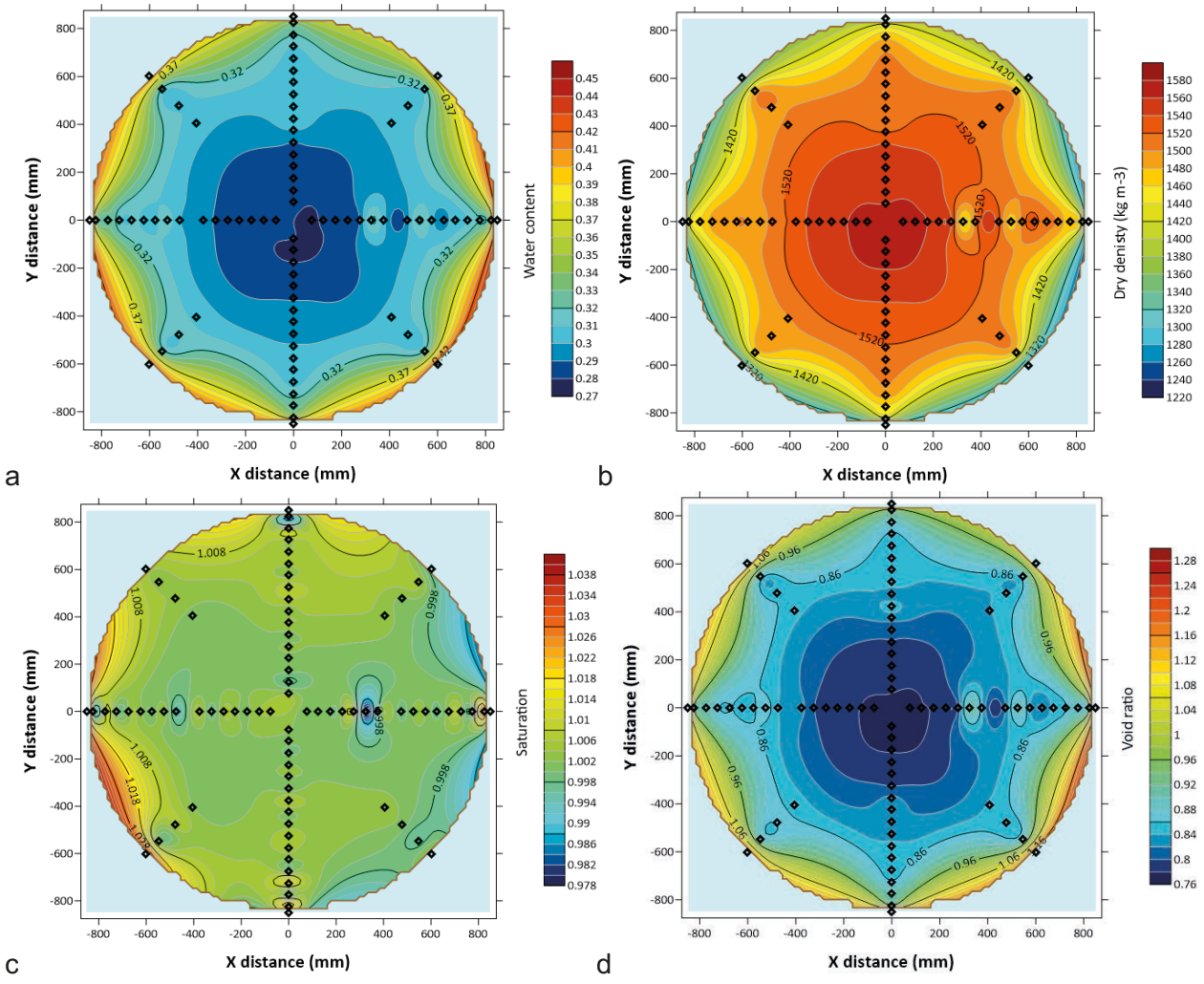

Figure 15-38. *Distribution of geotechnical properties at a height of 35 cm from the bottom of the deposition hole. a) Water content; b) Dry density; c) Saturation; d) Void ratio.*

Figure 15-39 shows the distribution of geotechnical properties at a height equivalent to the lower canister filter array, including FL903. Water content (Figure 15-39a) generally increased towards the outside of the deposition hole. However, at FL903 (180°) water content also increased towards the canister. This is not the case for all eight sampling directions, but is for most, with the lowest water content generally midway between the canister and the deposition hole wall. The inverse is seen in dry density (Figure 15-39b) with a general decrease towards the deposition hole wall, with the highest dry density midway between the canister and the wall. Saturation is generally close to unity for the entire area, but does show an area of lower saturation at 270° where FL902 was located and a slight over-saturation at 180° where FL903 was located. Void ratio (Figure 15-39 d) generally increased towards the deposition hole wall, with a low approximately halfway between the canister and the wall. In detail, a gradient of water content, dry density, and void ratio can be seen from 45° to 225°, showing that the buffer was not fully equilibrated and this may be reflected in the distribution of radial stress seen.

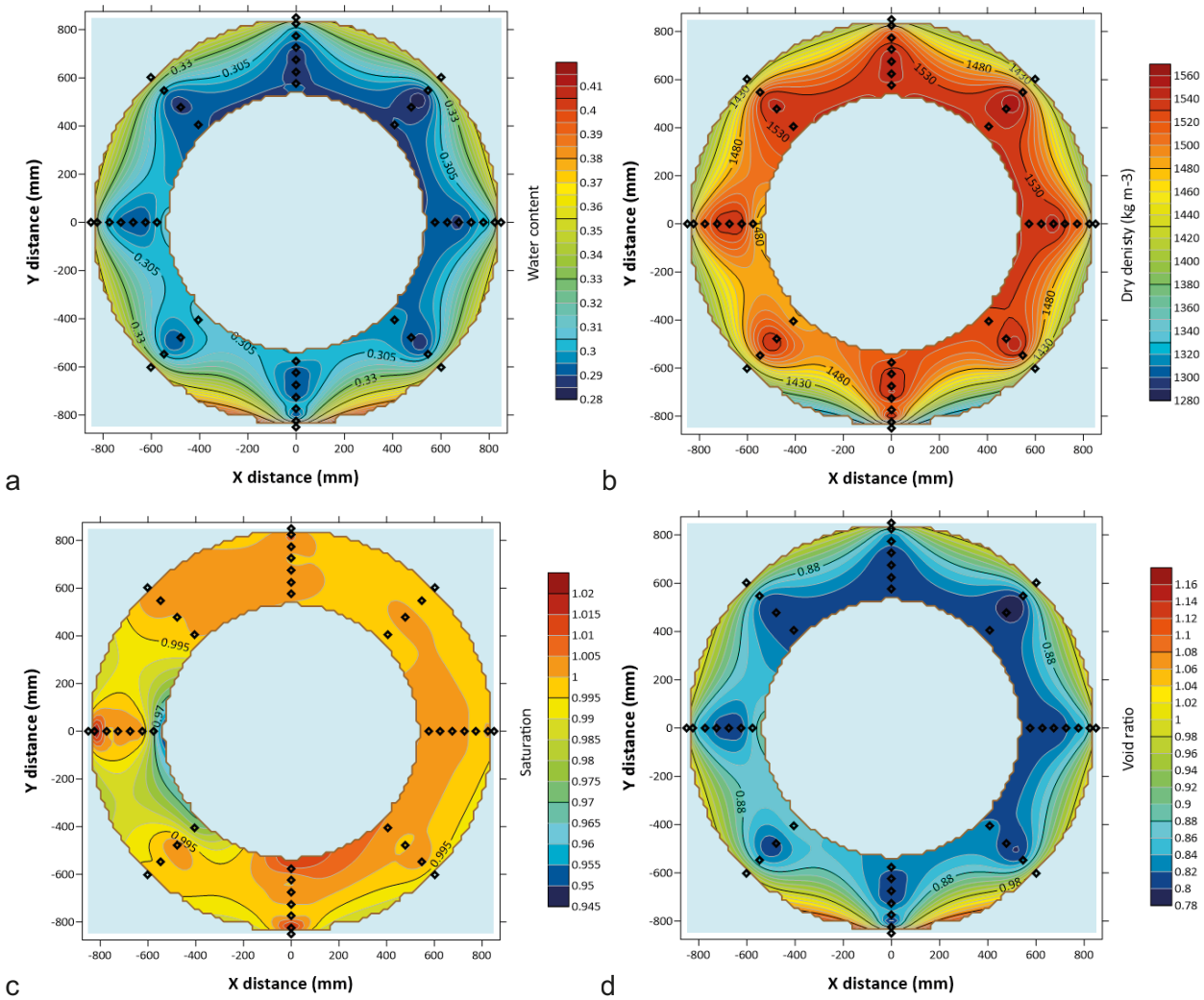

Figure 15-39. *Distribution of geotechnical properties at a height of 176 cm from the bottom of the deposition hole. a) Water content; b) Dry density; c) Saturation; d) Void ratio.*

Figure 15-40 shows the distribution of geotechnical properties at a height of 627 close to the height of stress (PB) and pore pressure (UB) sensors above the canister. Water content (Figure 15-40a) shows an offset circular pattern with water content increasing towards the outside of the deposition hole. However, the minimum water content occurs non-centrally. Dry density (Figure 15-40b) decreased from the centre of the hole towards the outside. The Monel pipe created an anomaly at the centre. Saturation (Figure 15-40c) was relatively constant throughout the segment and was close to unity. There were localised anomalies in places. Void ratio (Figure 15-40d) increased from the centre of the hole, although it was also raised as a result of the Monel pipe.

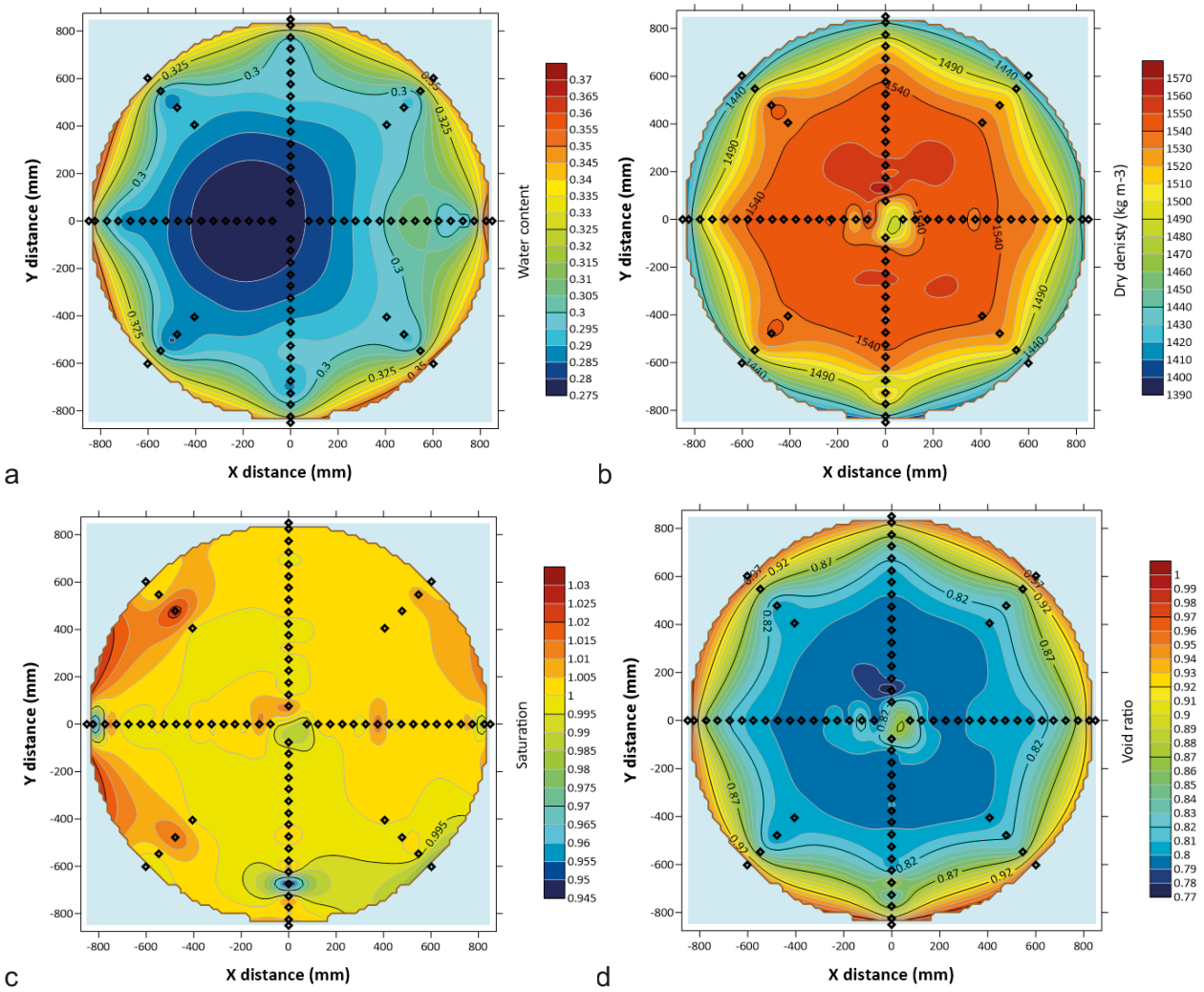

Figure 15-40. *Distribution of geotechnical properties at a height of 627 cm from the bottom of the deposition hole. a) Water content; b) Dry density; c) Saturation; d) Void ratio.*

A total of 1 800 samples gave a good description of the geotechnical properties of the buffer. The results show that the properties had greatly modified since the manufacture of the bentonite blocks. Pre-installation there was a significant difference between the properties of the full segments and the annular bentonite rings. By the end of the Lasgit, these differences were no longer apparent, as the buffer had modified to give a smooth variation in geotechnical properties with depth. In general, the data presented shows that the buffer was close to full saturation, with some zones of over-saturation (saturation > 1), which may result from the way the geotechnical properties are calculated. The average saturation for all samples within the bentonite blocks was 0.999. The buffer itself was relatively homogenous, with increases in water content and void ratio, and decreases in dry density, towards the outside of the buffer, especially where pellets were located. More variation was seen within the pellets, with water content and void ratio increasing towards the bottom of the hole and towards the concrete plug at the top of the buffer. In the zone closest to the canister, greater variation was seen in results. This was probably as a result of the buffer swelling to fill the engineered gap. This may also have been as a result of artificial hydration from the canister filters. The data also showed that the Monel pipe had an influence on geotechnical properties, with an increased water content and decreased dry density. The distribution of properties showed that as well as variation from centre to outside, a variation existed around the hole from 45 to 225°. The geotechnical properties show that the bulk of the pre-compacted bentonite blocks were homogenous, with the outsides of the blocks varying. This was as a result of the use of pellets and/or the swelling of the blocks to fill engineering voids. It is likely that gas would have exploited these zones if the properties meant that the movement of gas was easier. Dry density within the whole deposition hole reduced from emplacement values. This was as a result of swelling to fill the engineered gap and the pellet zone. This may have been greater than exected as a small amount of clay was flushed from the hole early in the test history, although compared with the total volume of clay this mass loss would have been minor.

Section D – Interpretation and discussion

16 Complete test history

In previous chapters individual test stages have been presented. In this section, the data as a whole from Day 0 to Day 5782 are discussed to highlight the evolution of the buffer over a 15-year period. Two significant influences play a part on the test data achieved; 1) Artificial hydration, and 2) Annual variation of temperature. Both of these influences were experimental artefacts that could not be controlled or isolated. In real-world scenarios they are largely irrelevant, but need to be understood in order to fully describe how the KBS-3 system would behave in their absence. However, both influences do offer insight into how the system behaves in response to changing influx of water or in response to temperature changes related to climate variations.

The primary interest of the Lasgit experiment was how gas behaved in a KBS-3 system in the event of a canister breach. The experiment was designed to answer this question and to speed buffer hydration to achieve a more realistic set of boundary conditions. A secondary interest of the experiment was the evolution of the buffer over the life of the experiment. This was investigated to see how saturation state affected gas entry and migration, but also offered information on buffer evolution and homogenisation. Figure 16-1 shows the full test history with four tests conducted in canister filter FL903, two in FU910, and the full canister test.

Note: The grey areas displayed in the graphs in this chapter show periods when artificial hydration was not occurring.

Figure 16-2 shows the gas test history for the 6 gas injection tests. It clearly shows that a significant proportion of the total time was taken up with either gas injection testing or associated two-step hydraulic tests before and after gas injection. By comparing Figure 16-1 and Figure 16-2 it can be noted that the first four gas injection tests were conducted when artificial hydration was occuring, while the last two tests were conducted after artificial hydration had stopped.

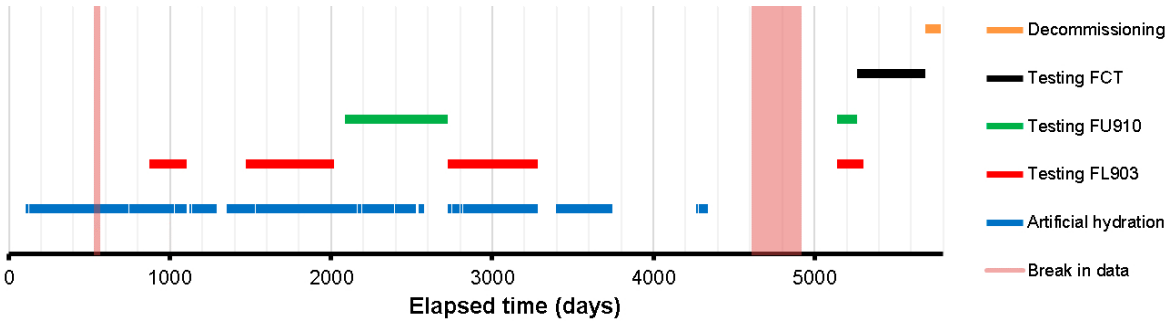

Figure 16-1. *Test stages of the complete Lasgit test history.*

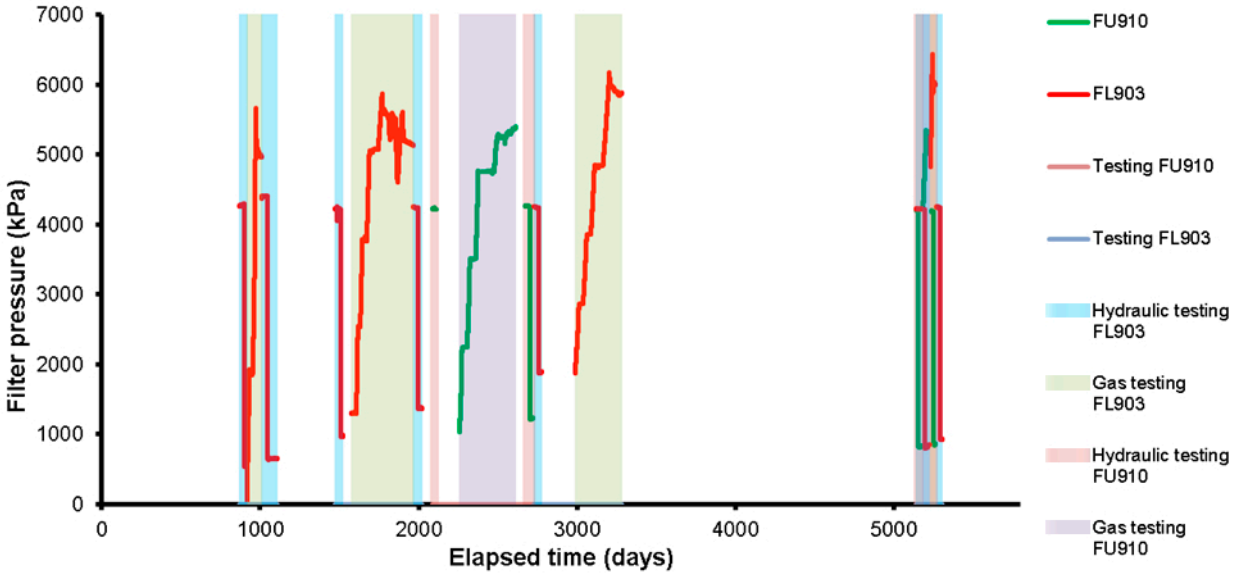

Figure 16-2. *Gas test history for the complete Lasgit test.*

16.1 Artificial hydration history

The Lasgit system was equipped with four filter mats; two of these were at the edge of the buffer between the bentonite and the rock wall, while two of them were located between bentonite blocks above the canister. The canister also had 12 filters that were used for artificial hydration during periods when they weren't being used for gas testing. The intention was to artificially hydrate the buffer throughout the test history to raise the saturation state of the buffer much quicker than would be achieved by natural hydration alone. However, many events, as described in previous sections, meant that artificial hydration was not constant throughout the test. Artificial hydration was also paused in some filters/mats during gas injection testing. As stated in discussion of the individual tests, during periods when no artificial hydration occurred, pore pressure and stress significantly reduced. This showed that the artificial hydration process was a vital control on the total stress within the deposition hole. Therefore, an understanding on the impact of pausing/stopping artificial hydrating is vital to understand the behaviour of the system. Figure 16-3 shows when the system was artificially hydrated (white) and when it was not (grey). Generally, the timeline can be split into two periods; Day 0 to Day 3745 when artificial hydration occurred and Day 3745 to Day 5782 when the system was only naturally hydrated. This became necessary as the aging equipment failed more often and it was deemed better to have a consistent system condition than intermittent hydration. Periods without hydration resulted in a dynamic boundary condition and when hydration was re-established the boundary condition was again dynamic. This caused issues and complicated interpretation of the test data.

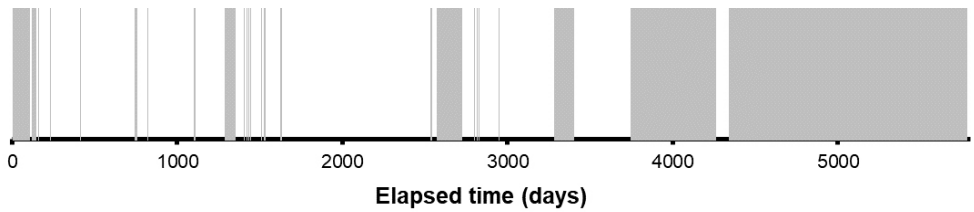

Figure 16-3. *Hydration history of the complete Lasgit test. White areas represent when artificial hydration was occurring, grey areas represent time when artificial hydration was paused.*

Figure 16-4 shows the cumulative volume of water pumped into the system as part of artificial hydration. **Note:** This also includes small volumes of water during two-stage hydraulic tests in individual filters. Artificial hydration of the clay began on Day 106 (18th May 2005). Figure 16-5 shows the volumetric flow into the artificial hydration system. This shows that early in the hydration process flow was greater than 2.5×10^{-9} m^3 s^{-1} and by Day 2500 had reached a relatively stable value of 1.3×10^{-10} m^3 s^{-1}. Flow approximated this until the end of artificial hydration at Day 3745 and suggests that steady flow had been achieved. It should be noted that the data is complicated by different filter mats and canister filters being active at different times during the different tests, but the general relationship of decaying flow to a plateau is evident.

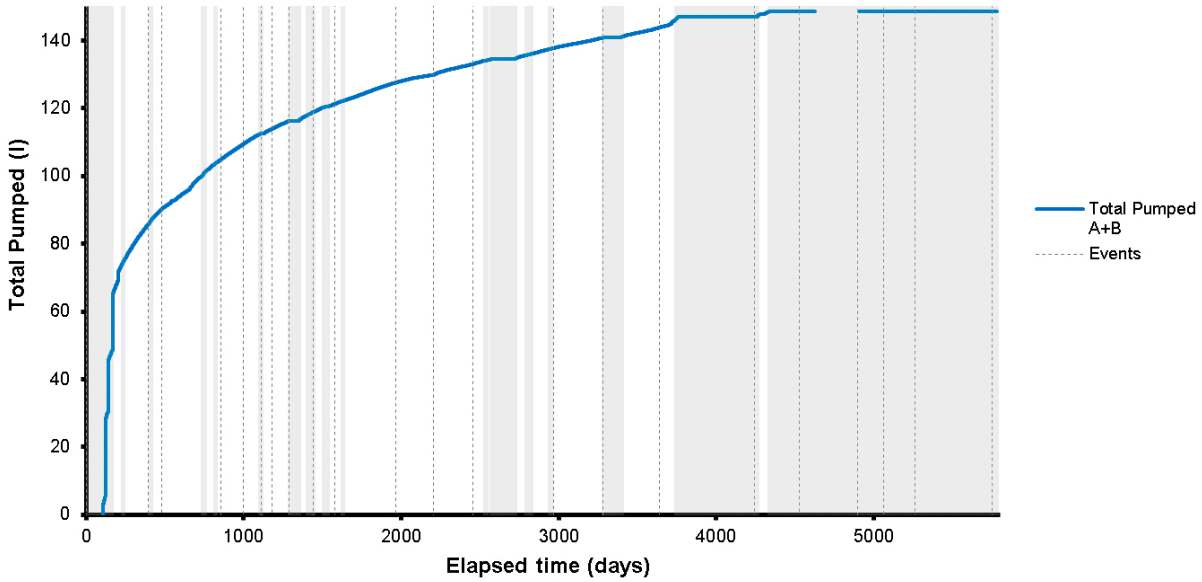

Figure 16-4. *Total volume of water injected during the complete test history of Lasgit.*

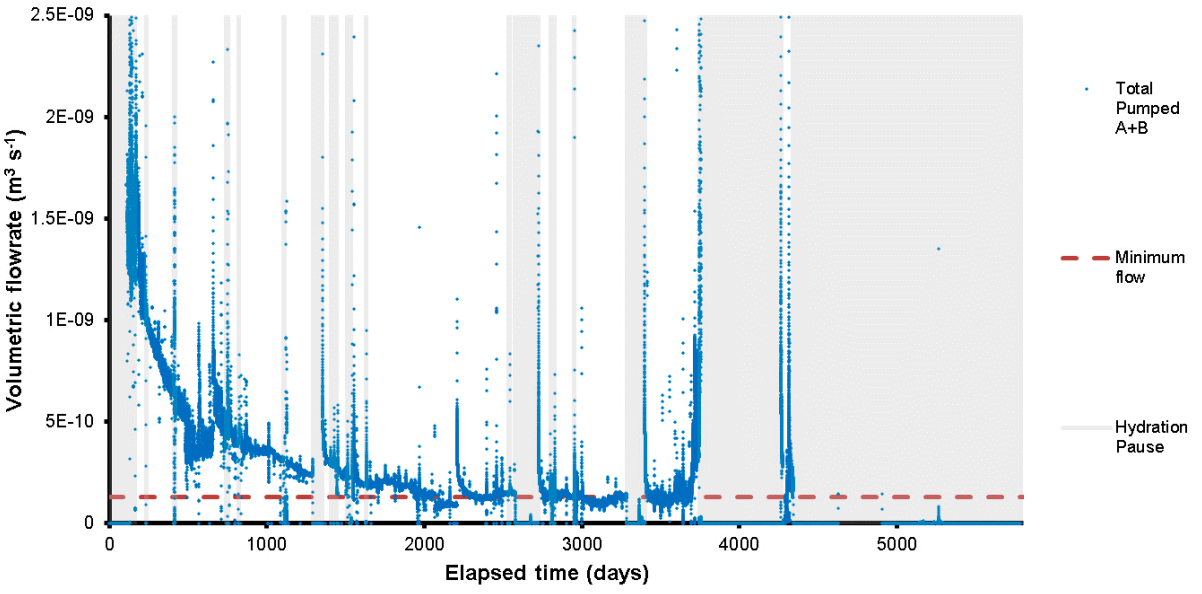

Figure 16-5. *Volumetric flow rate into the artificial hydration systems. Flowrate generally decreased into the buffer with time reaching a plateau around Day 2500.*

16.2 Temperature history

When dealing with short intervals of data that are often less than a year in duration, the impact of annual variations in temperature within the data are not always apparent. However, when considering Lasgit for the full 15-year duration it is clear that annual variations occurred in certain parameters. This was most apparent in temperature records but was seen in most parameter types.

Figure 16-6 shows the temperature variation in the gas laboratory and the office. Generally, the air-conditioning unit did not perform as well as expected and required regular maintenance and eventual replacement. At times, the temperature results also showed annual variation. Such variation could have impacted on the flow data recorded within the gas laboratory but this was not apparent in any of the gas injection testing periods. However, the spikes seen in the temperature data did impact flow data.

It was noted early in the Lasgit test that the temperature in the Hard Rock Laboratory was not stable and was varying by around 5 °C on an annual basis (Figure 16-7). This was not surprising as it was not necessary to keep the tunnels of the HRL at constant temperature or humidity. As a result, the air that was pumped into the tunnel varied in temperature, depending on the temperature at the surface. The HRL temperature variation ranged from approximately 10 °C to just above 16 °C in the first few years of the test. It can be seen that the winter of 2006/07 was not as cold as previous winters, with 2005/06 having a very short cold snap. In contrast, the summers were more consistent in both their maximum temperature and their duration. However, from around Day 2500 onwards the temperature in the HRL became more erratic and appears less controlled. In general, the temperature in the HRL was well controlled up until Day 2500 with only minor differences in temperature that related to differences in the weather conditions at the surface with a relatively constant average temperature. Post Day 2500, the average was no longer static as the lower temperature of the cyclicity increased as a number of mild winters were experienced. Figure 16-7 also shows the temperature recorded inside the copper canister of Lasgit, several metres depth in the system. This also showed clear cyclic response, that both lagged the HRL temperature and was attenuated compared with the HRL temperature. It also showed stable average temperature prior to Day 2500, with an increasing average after this time. This showed that the two temperatures were related and that the canister was likely to be influenced by the temperature in the HRL.

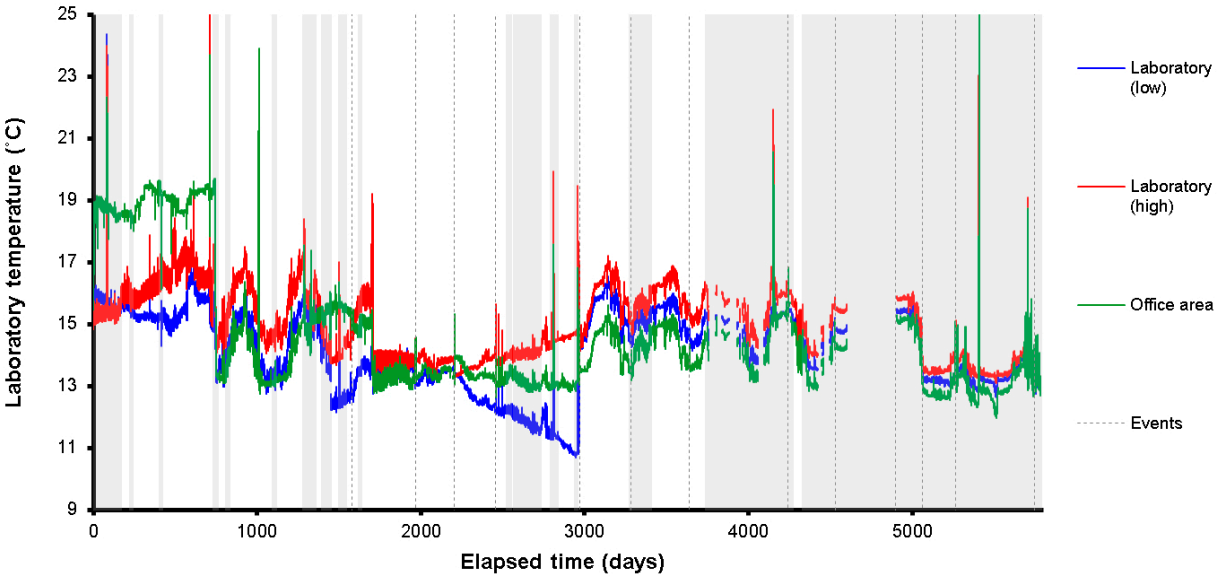

Figure 16-6. *Temperatures recorded in the Gas Laboratory and office.*

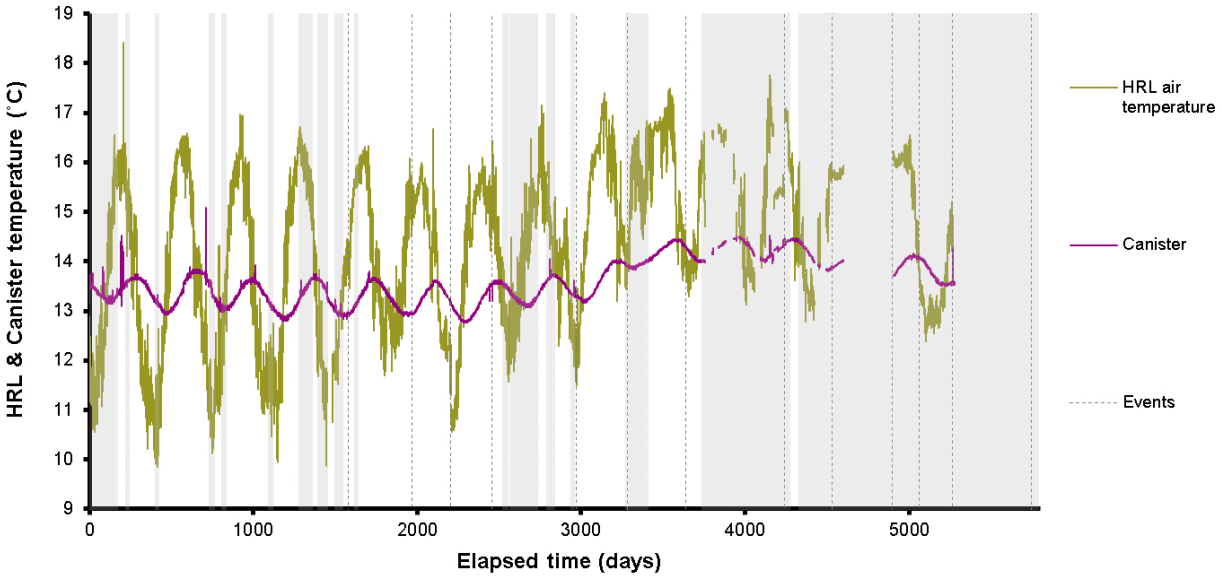

Figure 16-7. *Temperatures recorded in the canister, and HRL.*

Figure 16-8 attempts to illustrate the annual variation in a quantitative manner. The data presented in Figure 16-8a for each channel was averaged over a period of around 17 days (~1 600 data records) in order to produce a clean dataset without high frequency variations. From this data, the maximum and minimum points were determined, as shown as symbols in Figure 16-8a. This allowed the attenuation and time shift to be determined, assuming that the HRL temperature was the driving force of the annual variation and occurred prior to the other oscillating parameters. Figure 16-8b shows a comparison of the HRL and canister temperatures. It can be clearly seen that the amplitude in the variation decreased and that the maxima and minima of the two datasets had a clear time offset. This offset is shown in Figure 16-8c. The data up to Day 2700 were considered to be consistent, with changes occurring after this. For both maximum and minimum data points a delay of 81.7 days was seen. After Day 2700 the delay becomes more varied, but still averaged around 80 days.

To illustrate that the data are seasonal, Figure 16-9 shows the Julian day that the minimum occurred in the HRL and canister temperatures. The HRL temperature varied depending on the temperature at the surface and represents the variation in the severity of winter in the Äspö area. On average, the minimum occurred on Julian day 53 (February 22nd). The minimum in canister temperature was much more consistent and occurred on Julian day 131 (May 11th). This shows that the higher frequency variation in temperature was attenuated by depth. However, it is clear that the variation was annual and was associated with the temperature of the HRL, which in itself was associated with the surface temperature.

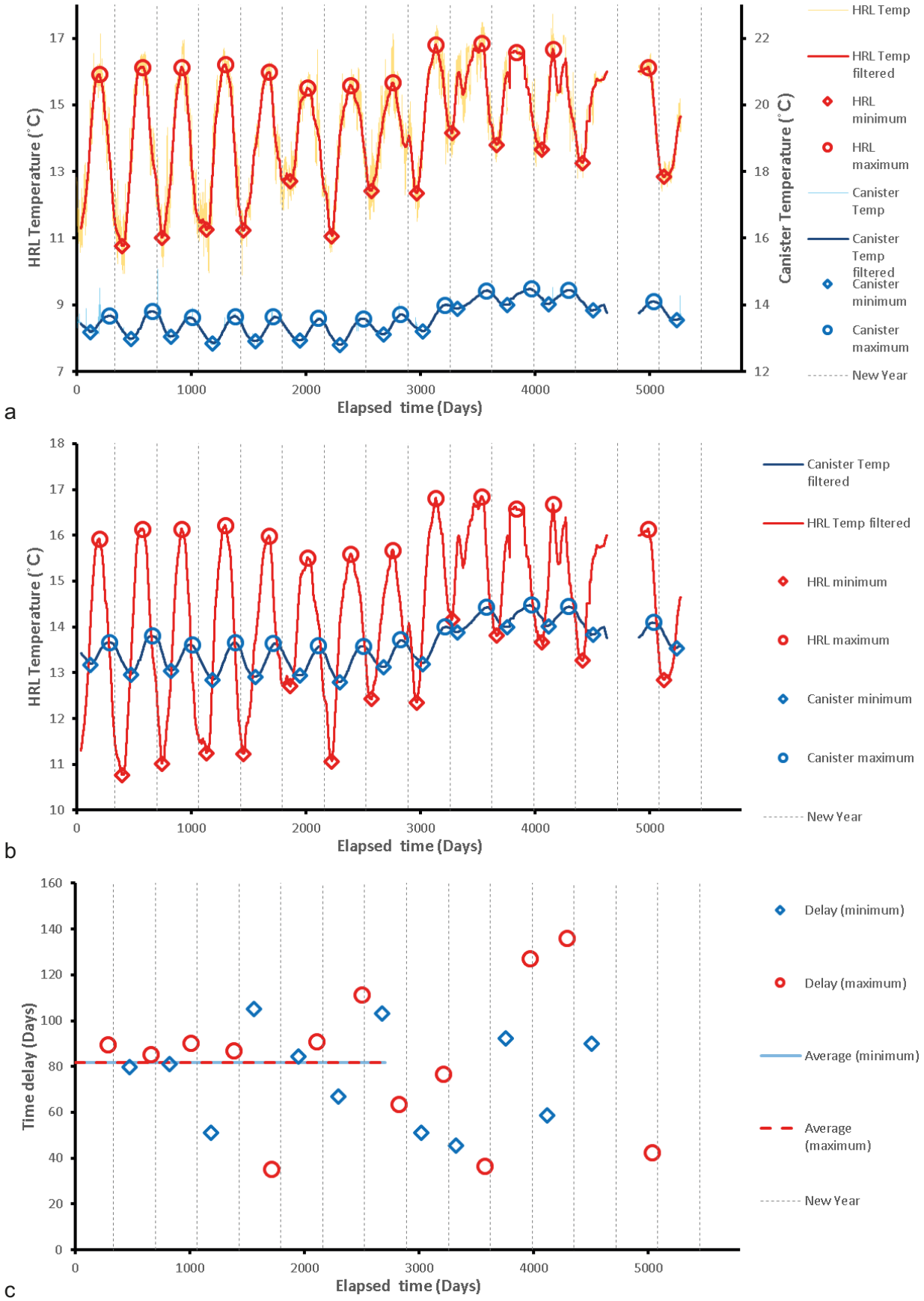

Figure 16-8. *Temperature cyclicity seen in HRL temperature and canister temperature. a) Filtering and identification of maximum and minimum points; b) Comparison of HRL and canister temperature showing attenuation and time shift of canister temperature; c) Time delay of maximum and minimum data points of canister temperature.*

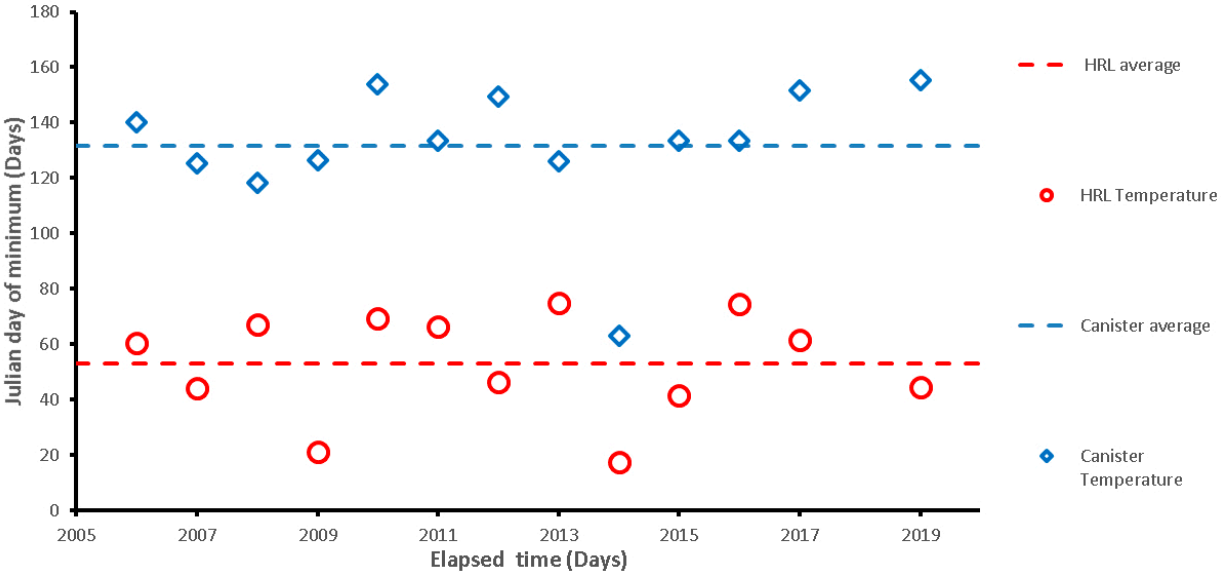

Figure 16-9. *The Julian day of the minimum in HRL and canister temperatures.*

Within the deposition hole, every pore pressure sensor at the deposition hole wall (UR) within the bentonite (UB); the stress sensors at the deposition hole wall (PR); and within the bentonite (PB) have an associated thermocouple. This means that there were 55 thermocouples in addition to the canister temperature within Lasgit. All of these channels were processed in the manner described above to identify the time and magnitude of each channel at the maximum and minimum during annual cyclicity. Each location of the thermocouples was accurately known, meaning that variation with height in the deposition hole and distribution could be examined. Figure 16-10 shows the delay of the sinusoidal data plotted against height in the deposition hole. This clearly shows that the time shift increased with depth from the tunnel floor (Figure 16-10a). At the base of the deposition hole the delay was ~130 days, whereas the sensor closest to the surface at a height of 751 cm had a delay of just 29 days. This clearly shows that the delay was attenuated with depth and shows that the temperature variation derived from the HRL temperature fluctuation. Figure 16-10b shows the data in more detail and separates data from different sensor types. This is most significant for UB and PB sensors as all UR and PR sensors occur at a radius of 875 mm on the outside of the deposition hole, whereas all UB and PB sensors occur within the buffer. This data is most informative at a height of 18.2 cm for UB902 and PB902. These show a shorter time delay and may suggest that temperature fluctuations were emanating from within the deposition hole and not from outside. It may mean that the canister conducted heat through the Monel pipe, meaning that a shorter delay was experienced. It is likely that the temperature fluctuation was a combination both the canister and the surrounding rock mass variations. Figure 16-10c shows the data for the delay in minimum and maximum data points. This suggests that there was a difference between the lag experienced at the temperature minimum compared with the temperature maximum.

Figure 16-11 shows the differences between the minimum and maximum temperatures compared with the HRL temperature. The plot shows how the amplitude of oscillation changes with depth in the deposition hole, this being the difference between the maximum and minimum data points. The data clearly shows that the amplitude of the oscillation was attenuated with depth from the canister lid. The HRL temperature had an average amplitude of 4.4 °C (2.8–5.3 °C) for the first 2 700 days of the test. Closest to the lid at a height of 751 cm the amplitude of oscillation was 3.1 °C, whilst at the bottom of the deposition hole it was less than 1 °C. This clearly shows that the temperature effect was attenuated with distance from the HRL tunnel.

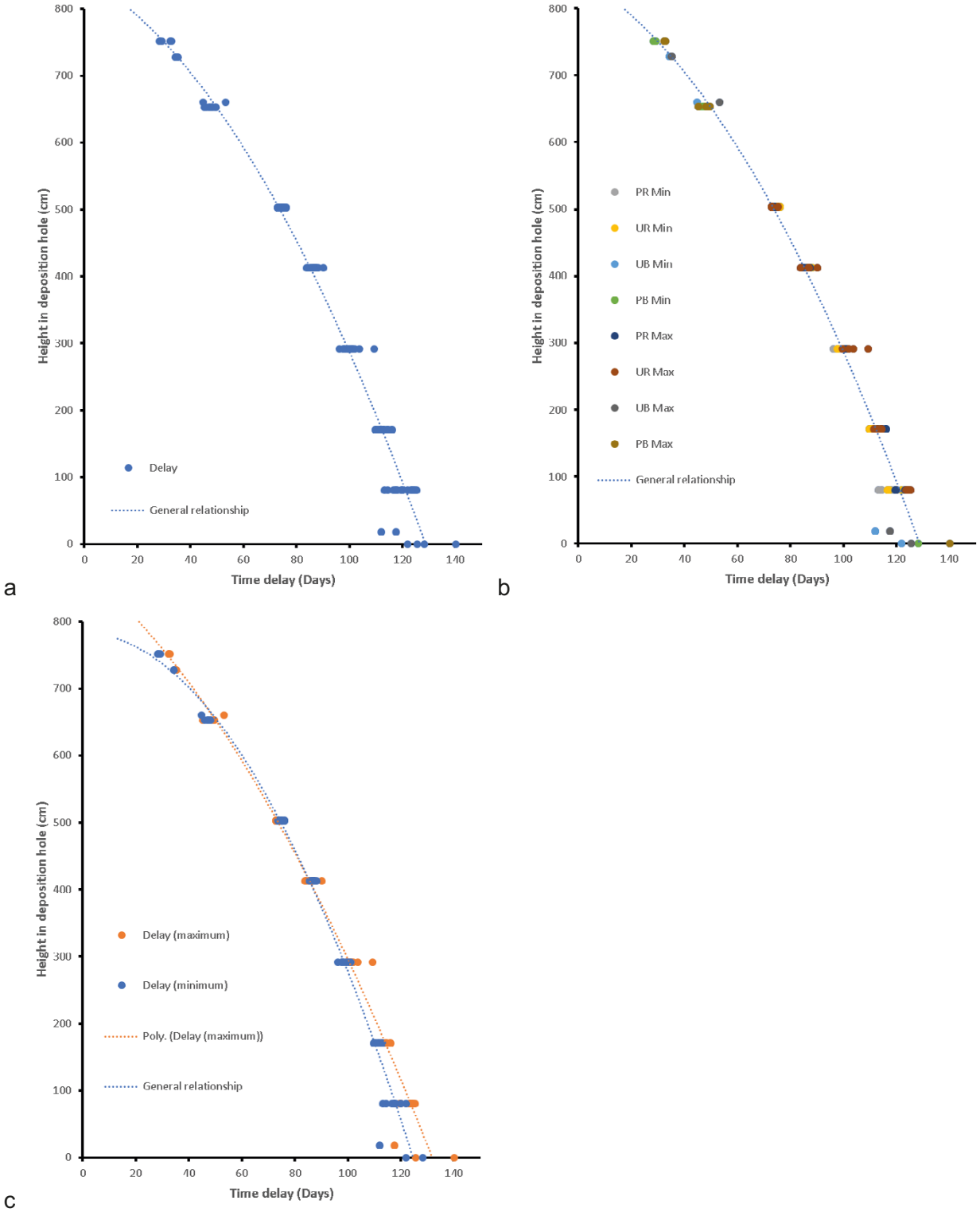

Figure 16-10. *Time delay in cyclic response for all temperature recordings in Lasgit. a) All data; b) All data plotted per sensor type; c) All data plotted for maximum and minimum data.*

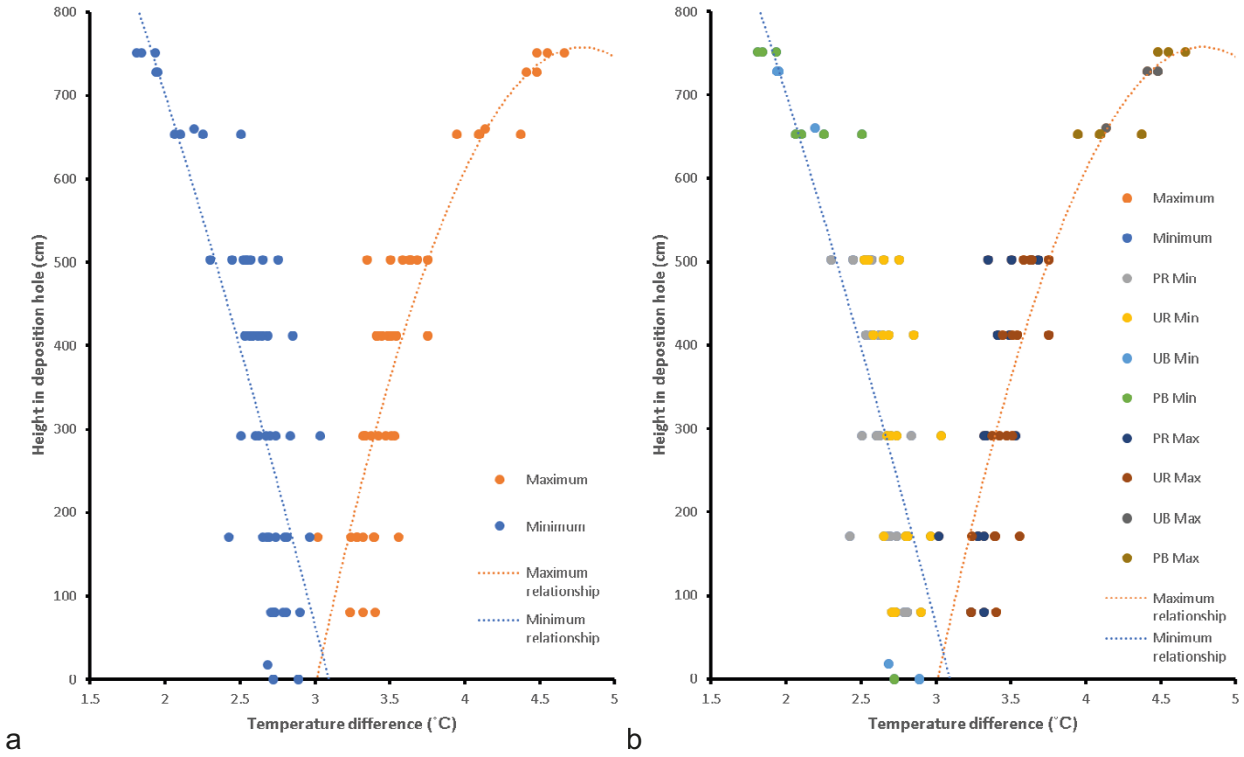

Figure 16-11. *Attenuation of temperature data with depth. a) All data for maximum and minimum; b) All data plotted per sensor type.*

Figure 16-12 shows the distribution of time delay for the minimum and maximum of temperature variation within the deposition hole at 55 locations. This clearly shows the result reported in Figure 16-10 with temperature delay increasing with distance from the HRL. This is clearly seen for both minimum (Figure 16-12a) and maximum temperature (Figure 16-12b). However, it also shows that there were subtle differences around the deposition hole wall. This is most clear at a height of around 90 cm, but is apparent at most heights. The subtle variations around the deposition hole wall and with height may have been because of different flow properties as a result of the fractured deposition hole wall. Flowing water will transfer heat better than non-flowing areas and this was especially evident in the conductive region at the base of the deposition hole.

Figure 16-13 shows the temperature difference between the minimum and maximum data points compared with the HRL temperature. This confirms the observations of Figure 16-11 with the amplitude of oscillation decreasing away from the canister lid. However, it clearly shows variation around the deposition hole wall as well.

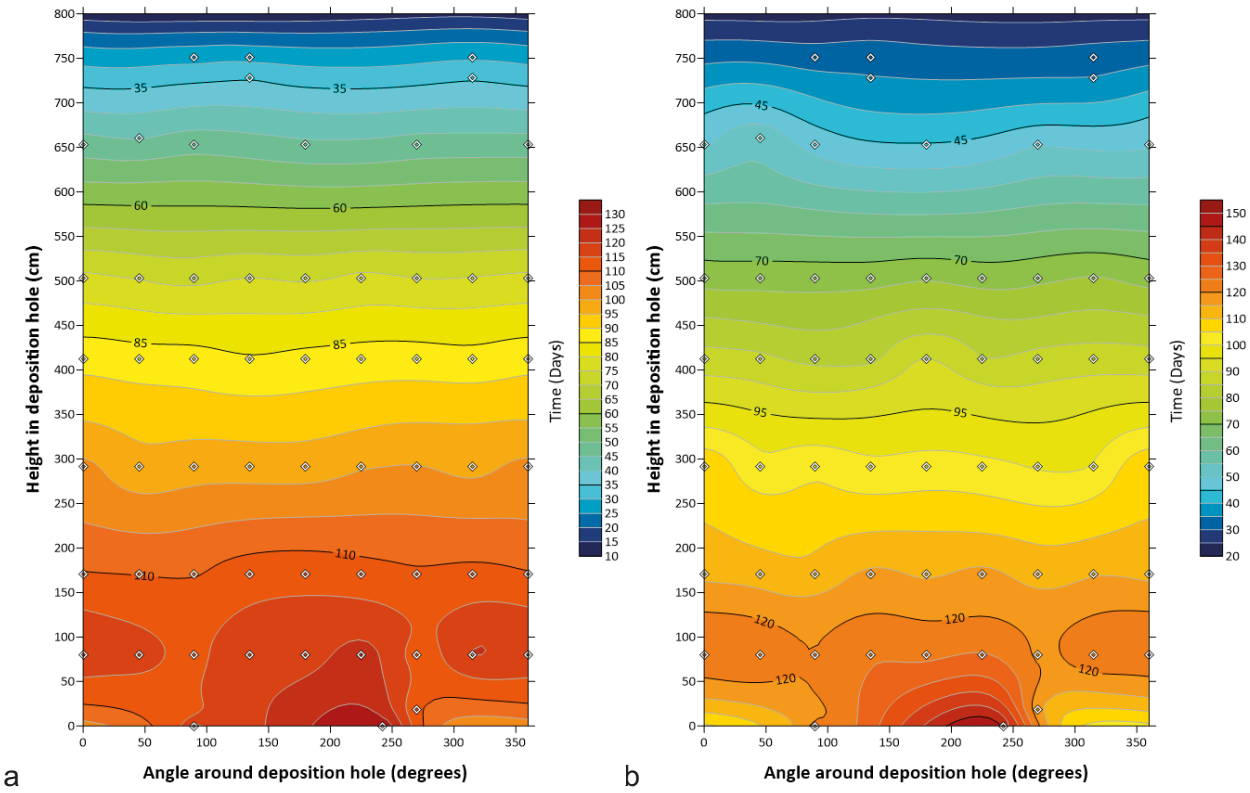

Figure 16-12. *Delay in minimum and maximum temperatures within the deposition hole compared with HRL temperature. a) Minimum temperature; b) Maximum temperature.*

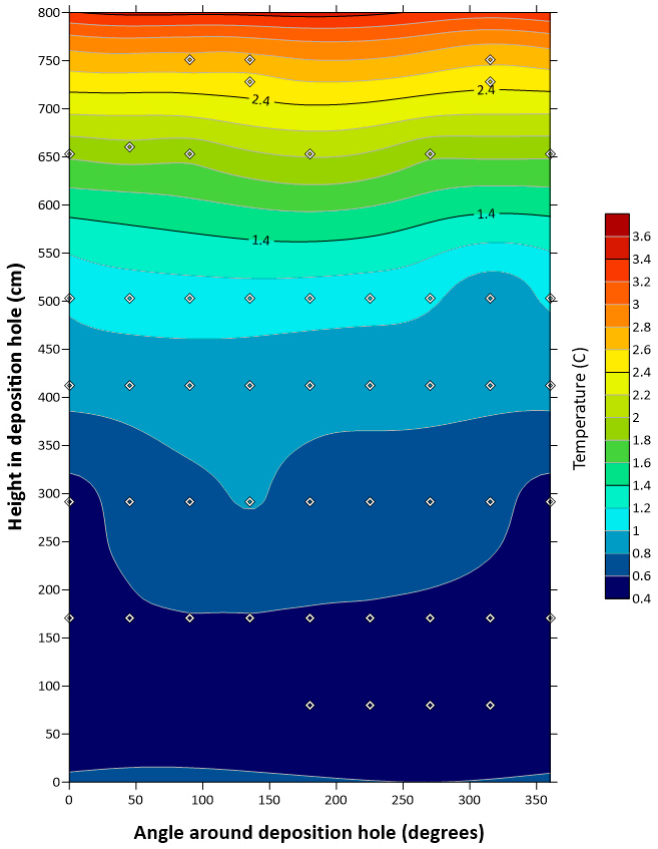

Figure 16-13. *Amplitude of temperature difference within the deposition hole.*

16.3 Pore pressure

The following sections describe the temporal evolution of porewater pressure in the Lasgit system, reflecting the complex interaction between artificial and natural sources and their cumulative role in the hydration of the buffer clay.

16.3.1 Canister filters (FL9xx, FM9xx, FU9xx)

Figure 16-14 shows the canister filter pressure throughout the entire duration of the Lasgit experiment. As can be seen, there was minimal long-term observation of annual variation within this data and no other conclusions can be drawn in addition to those stated for each individual test period. This was to be expected since the canister filters were controlled and should not have been influenced by seasonal variations. However, towards the end of the test history many of the canister filters were shut-in and measured natural pore pressure and these showed annual oscillation, e.g. around Day 5000. Figure 16-14b shows the average for the lower-, mid-, and upper-array of canister filters. Figure 16-14c shows the range of the lower-, mid-, and upper-array of canister filters. This shows that at times there was a considerable range of pressure at the different levels.

16.3.2 Filter mats (FR9xx, FB9xx)

The filter mats were also largely controlled during the full test history and mainly show the pressure of artificial hydration (Figure 16-15). However, filter mat FR901 was not used for artificial hydration and none of the filter mats were used after Day 4340 and after this time annual variation can be seen in FB903 and FB904. All four filter mats showed low pore pressure at the end of the test, especially the filters within the bentonite that were considerably lower than 1 000 kPa. Filter mat FR901 was in direct communication with the pressure relief holes and showed a decline in pressure through the test history. However, at around Day 2590 the pressure in FR901 increased at the same time as the other filter mats were shut in and their pressure decayed. Figure 16-15 highlights why artificial hydration was stopped with many periods of unstable pressure as a result of stopping hydration. Pore pressure in the mats quickly dropped when artificial hydration was paused, which affected many of the other sensor types. Figure 16-15 shows that many of these shut-in events occurred for a number of different reasons. Natural hydration offered a more stable boundary condition once the flow into the buffer had stabilised and the buffer appeared to be in hydraulic equilibrium.

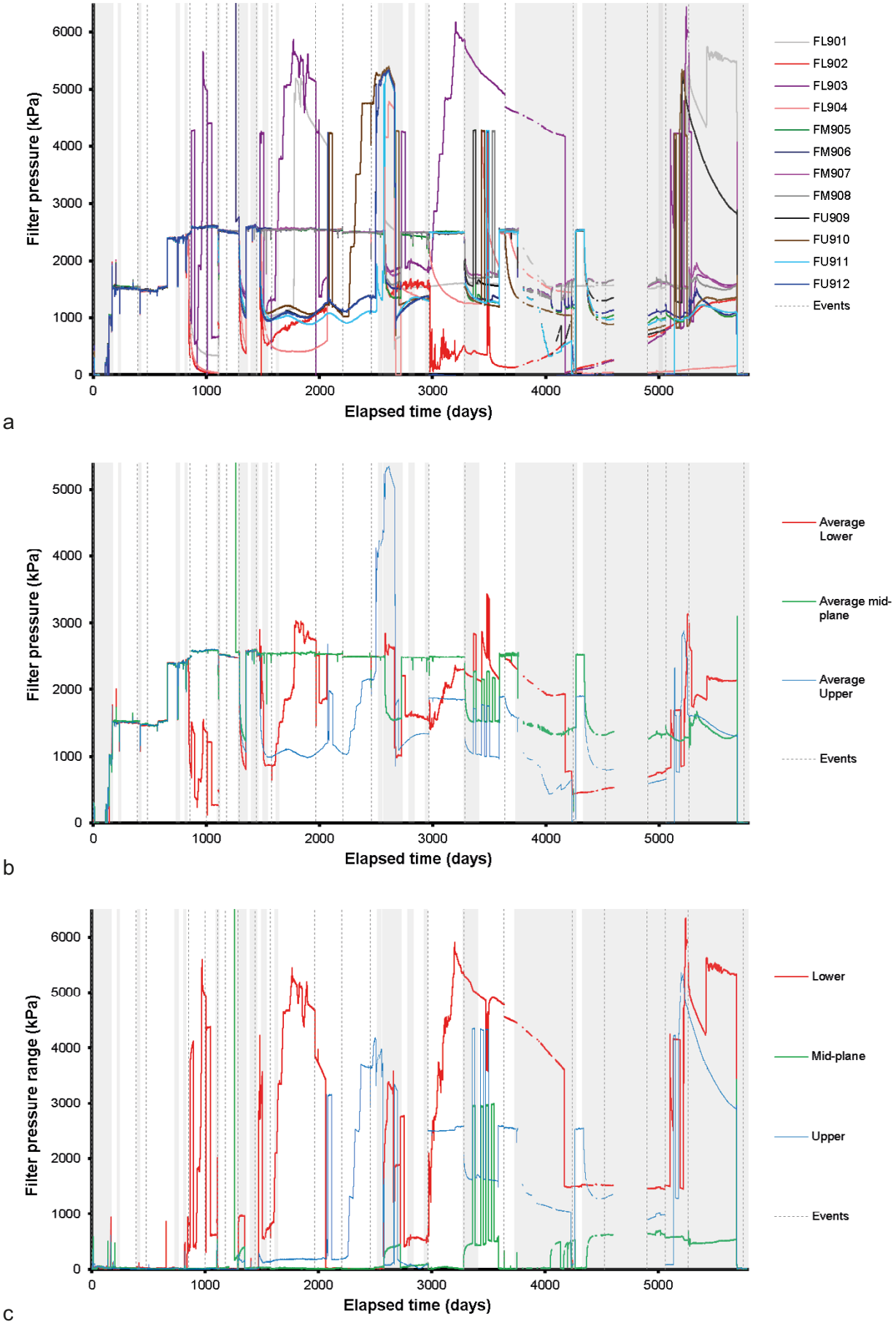

Figure 16-14. *Evolution of water pressure within the canister filters. a) All filters; b) Average for different heights on the canister; c) Pressure range for different heights on the canister.*

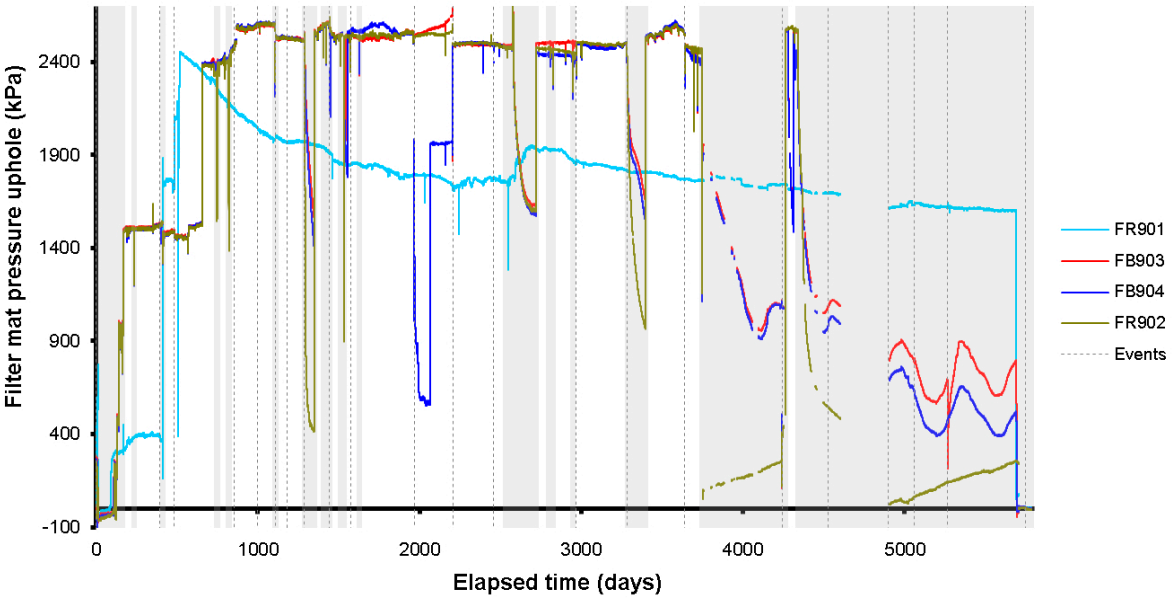

Figure 16-15. *Evolution of water pressure in the filter mats located on the borehole wall and within the bentonite blocks.*

16.3.3 Pore pressure within the bentonite (UB9xx)

Porewater pressure within the bentonite was measured at 6 discrete locations, as shown in Figure 16-16. The data were dominated by the pressurisation of UB902 (Figure 16-16a), therefore are presented excluding UB902 for clarity (Figure 16-16b). Different behaviour was seen below the canister (UB90x) than above the canister (UB92x). Below the canister, UB901 and UB902 increased to around 700–750 kPa in the first 1 000–2 000 days of the test and then both showed a pressure loss of around 300 kPa over the following 500 days. UB902 showed this behaviour around 500 days before UB901. The reason for the increase and then decrease in pressure is not known. However, throughout this period, cyclic annual variation is apparent. UB902 was pressurised by gas at Day 1785. Once UB901 had decayed by 300 kPa, reaching a minimum of 450 kPa around Day 2670. Following this, UB901 increased for the rest of the test. Pore pressure had increased to about 1 500 kPa displaying annual variation throughout. Even though UB902 was gas pressurised, it still showed dynamic behaviour. Pressure increased to 4 700 kPa, before decaying to 3 400 kPa at around Day 2590. Following this, pressure recovered to approximately 4 000 kPa at Day 5260, before being perturbed by the inflation of the canister and being pressurised for a second time by the Full Canister Test. Annual variation was apparent throughout the pressure increase period. It should be noted that the UB90x sensors below the canister showed no influence of artificial hydration, most likely because the filter mat in the base of the deposition hole was not used for artificial hydration.

Above the canister, the UB92x sensors all showed similar behaviour, which was subtly different to those below the canister (Figure 16-16). Sensor UB926 showed similar behaviour to the UB90x sensors in increasing to 370 kPa in the first 1 000 days of testing, before decaying to 150 kPa around Day 1980. From this time onward, all UB92x sensors above the canister significantly increased in pressure, with significant annual variation clearly seen. This variation was as large as 500 kPa in UB926. It appears that pore pressure increase took ~2 000 days to start increasing. However, routine artificial hydration was paused at Day 3745 and this resulted in all UB92x sensors showing a decrease in pressure, reaching modest pressure by the end of the test. This shows that above the canister the pore pressure was dependent on artificial hydration, whereas below the canister it was not. Throughout the Lasgit test annual variations were seen with considerable amplitude. It is uncertain how long pore pressure in the buffer would have taken to naturally reach the pore pressure of the surrounding rock mass. As pressure had started to increase in the base of the deposition hole without the help of artificial hydration, it is suspected that pore pressure would have increased on the scale of 10s of years.

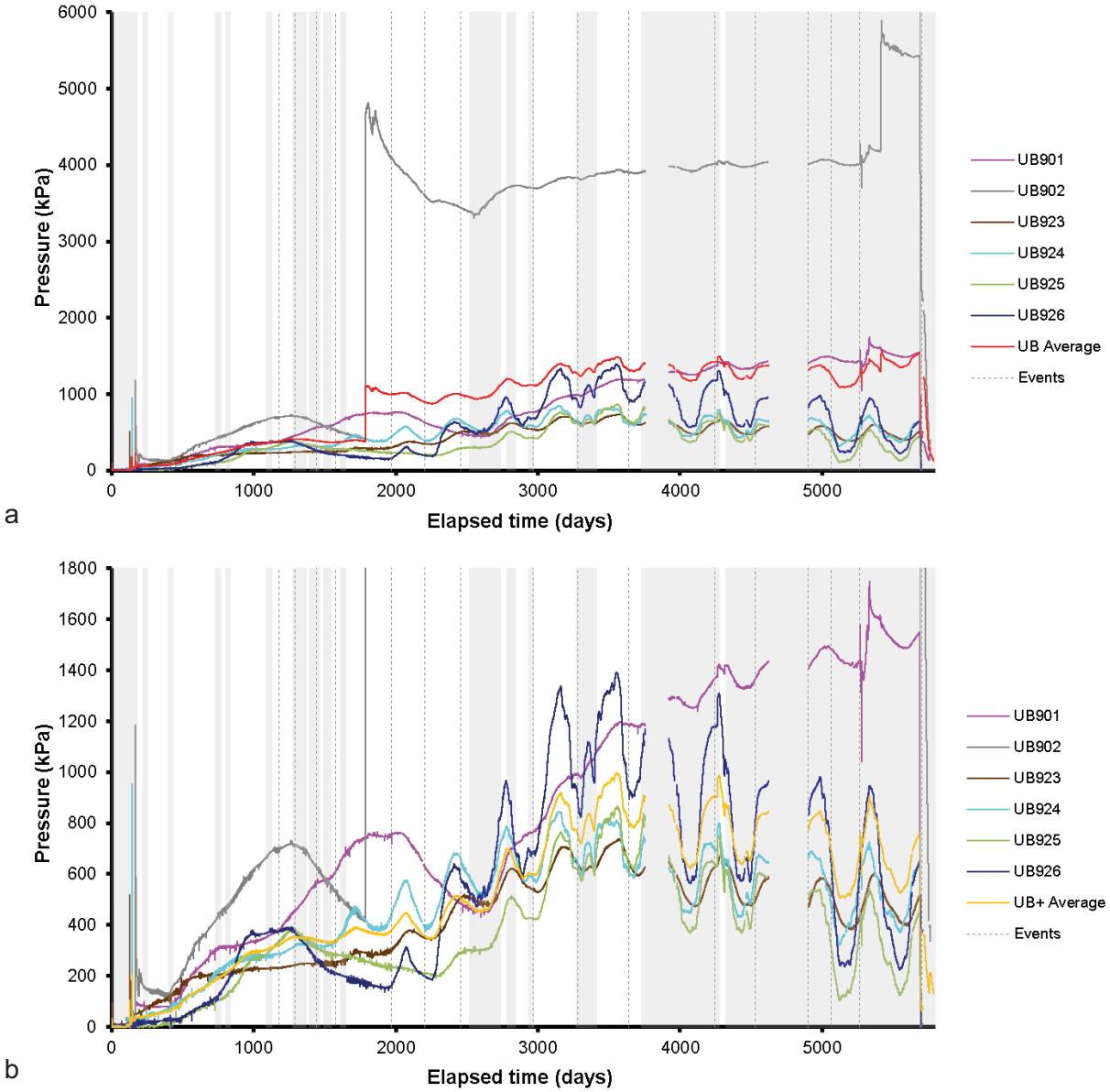

Figure 16-16. *Porewater pressure within the bentonite at the 6 monitoring points for the complete testing history of Lasgit. a) Data for all 6 sensors; b) Detail of all sensors except UB902.*

Figure 16-17 shows the average (Figure 16-17a) and range (Figure 16-17b) of the UB9xx sensors for given levels within the deposition hole. The average data for level UB1 was dominated by the pressurisation of UB902 and does not show much. The averages for UB14 and UB16 have averages that were similar, with UB16 showing higher amplitude annual variation. This level was closest to the canister lid. The range of the data shows greater variation in UB16 compared with UB14. Little variation was seen in UB14 with a maximum range of ~200 kPa, compared with ~600 kPa at UB16. The range appears not to be influenced by the end of artificial hydration, whereas UB16 reduced in range when artificial hydration stopped.

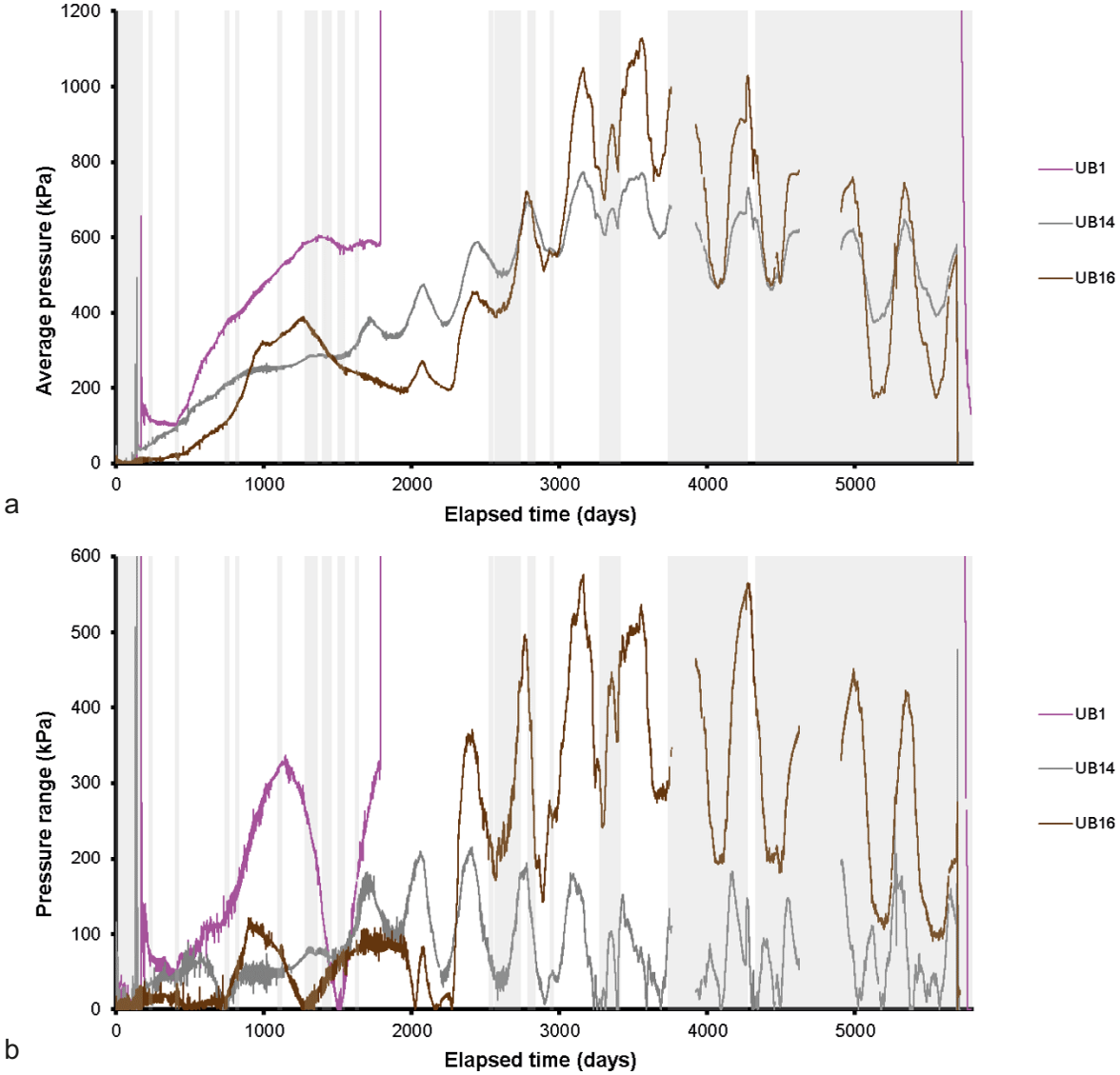

Figure 16-17. *Average and range of porewater pressure within the bentonite for the complete testing history of Lasgit. a) Average for each level; b) Range for each level.*

16.3.4 Pore pressure at the deposition hole wall (UR9xx)

Porewater pressure was measured at 20 locations on the deposition hole surface and the data are shown in Figure 16-18. After pressure increased at Day 480 a considerable amount of variation was seen in the magnitude of pore pressure. A difference of over 1 000 kPa was seen between the locations of highest and least pore pressure, after which pore pressure generally decreased in the deposition hole. The exceptions were UR907 and UR909 which showed pressure increases, as described previously. This increased the pressure at these locations through a number of breakout events. Most locations showed annual variation, with some locations showing greater variation than others. Figure 16-18b shows the UR data averaged for the five different levels that the sensors were located. This generally shows that pore pressure increased from the top of the deposition hole to the bottom. The exception was UR4 towards the bottom of the deposition hole, which showed a lower pore pressure than level UR5. The average data clearly show that pore pressure decreased after pore pressure was established at the rock wall. However, around Day 2550 pore pressure increased over a 300-day period. This was around the time when UR909 increased in pressure during Gas Injection Test 3.

Figure 16-18c shows the variation of the UR sensors. The average for all the data shows that the range increased from ~1 200 to ~2 000 kPa when artificial hydration was stopped. Following this, the total range in the data decreased to ~1 600 kPa when the canister was pressurised. This shows that artificial hydration influenced the pore pressure at the deposition hole wall. The range in the data increased for all levels until artificial hydration was stopped, following which the ranges decreased. Figure 16-18b shows that the annual variation was greatest at the canister centre and was least at the top and bottom of the sensor array. This suggests that the source of the variation of pore pressure may have been related to deformation of the canister in response to changes of temperature. The canister was likely to expand most at its centre as each end of the canister was more rigid.

All levels showed annual variation (Figure 16-18a, b). There was little much variation in the amplitude with depth, except for UR4, which saw limited annual variation. Close inspection of the data in Figure 16-19 shows that the oscillations of UR920 and UR915 were offset by approximately 20 days from that of UR912 and UR914. These latter pair of sensors (UR912 and UR914) were positioned on the same level (section 7) but were separated by 180° (i.e. 90° and 270° respectively). Sensors UR915 and UR920 were situated higher in the hole (section 9 and 10 respectively) and were situated at 0° and 135° respectively. This suggests that the thermally induced pulse in pressure propagated vertically down the hole, demonstrated by the fact that the variation in pressure of UR920 predated the increase in canister temperature (Figure 16-19).

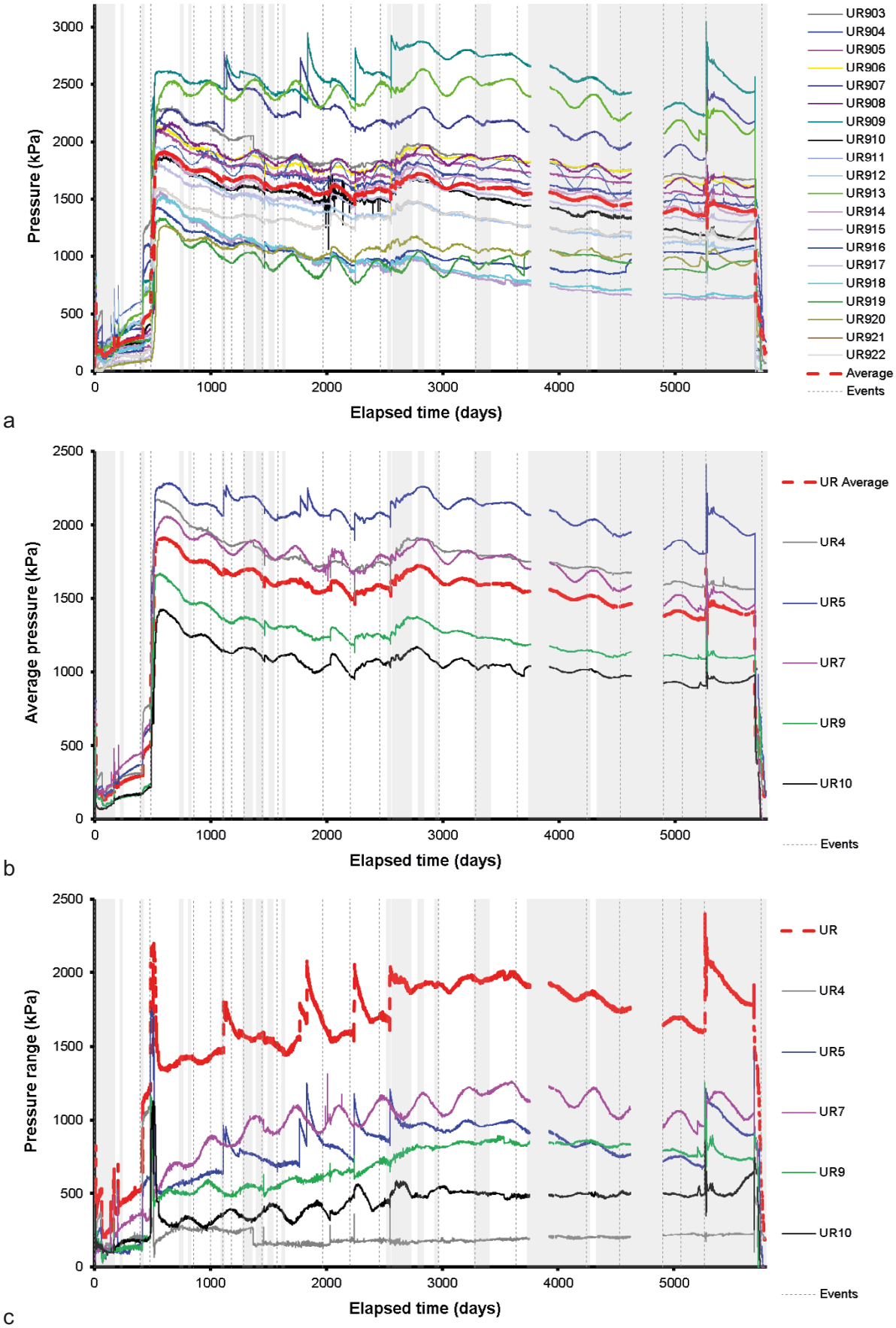

Figure 16-18. *Variation in porewater pressure measured at the rock face with time. a) Pore pressure; b) Average pore pressure for each level; c) Range of data for each level.*

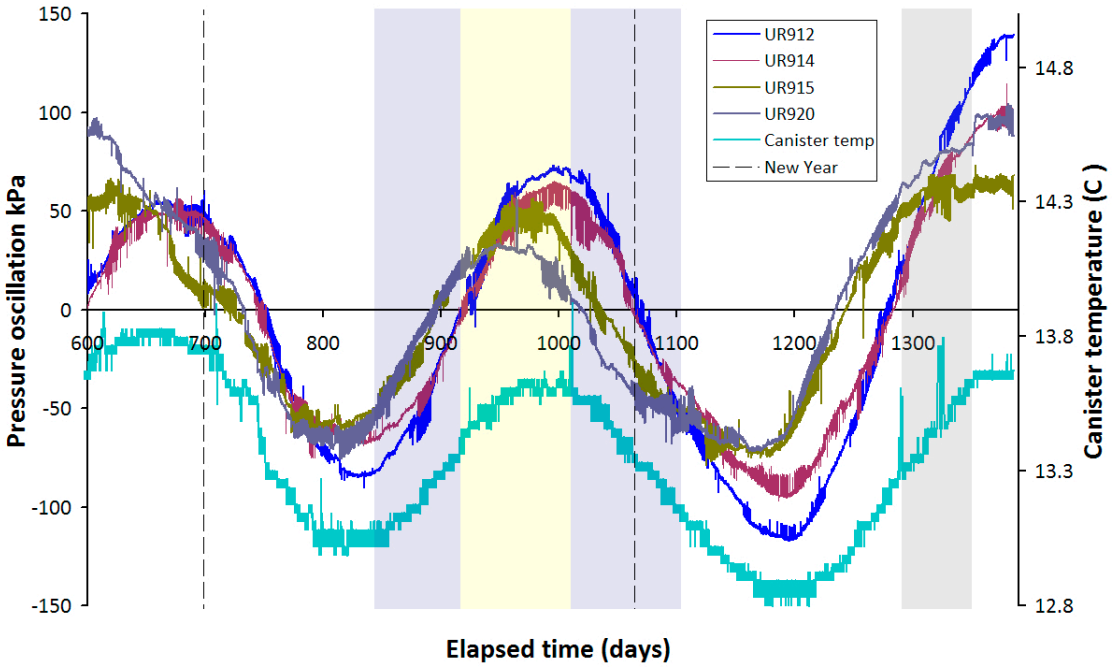

Figure 16-19. *Annual variation in porewater pressure measured at the rock face for four sensors with long term variation removed. It can be seen that UR912 and UR914 have no lag (these devices were positioned at the same level). When viewed in total the system displays lag can be explained as a thermal pulse propagating down the deposition hole.*

Figure 16-20 shows the distribution of pore pressure at the deposition hole at seven times during the Lasgit test. The general distribution of pore water pressure developed early in the test. At Day 50 (Figure 16-20a) the greatest pressure was in the bottom of the sensor array. By Day 500 (Figure 16-20b), a high-pressure region had developed at a height of ~150 cm at 275°. This further developed by Day 1500 (Figure 16-20c), but the general distribution seen from then onwards did not significantly change (Figure 16-20c–g), even though the magnitude of the pore pressure decreased. This shows that the heterogeneous pore pressure developed early in the test history and persisted throughout the remainder of the Lasgit test.

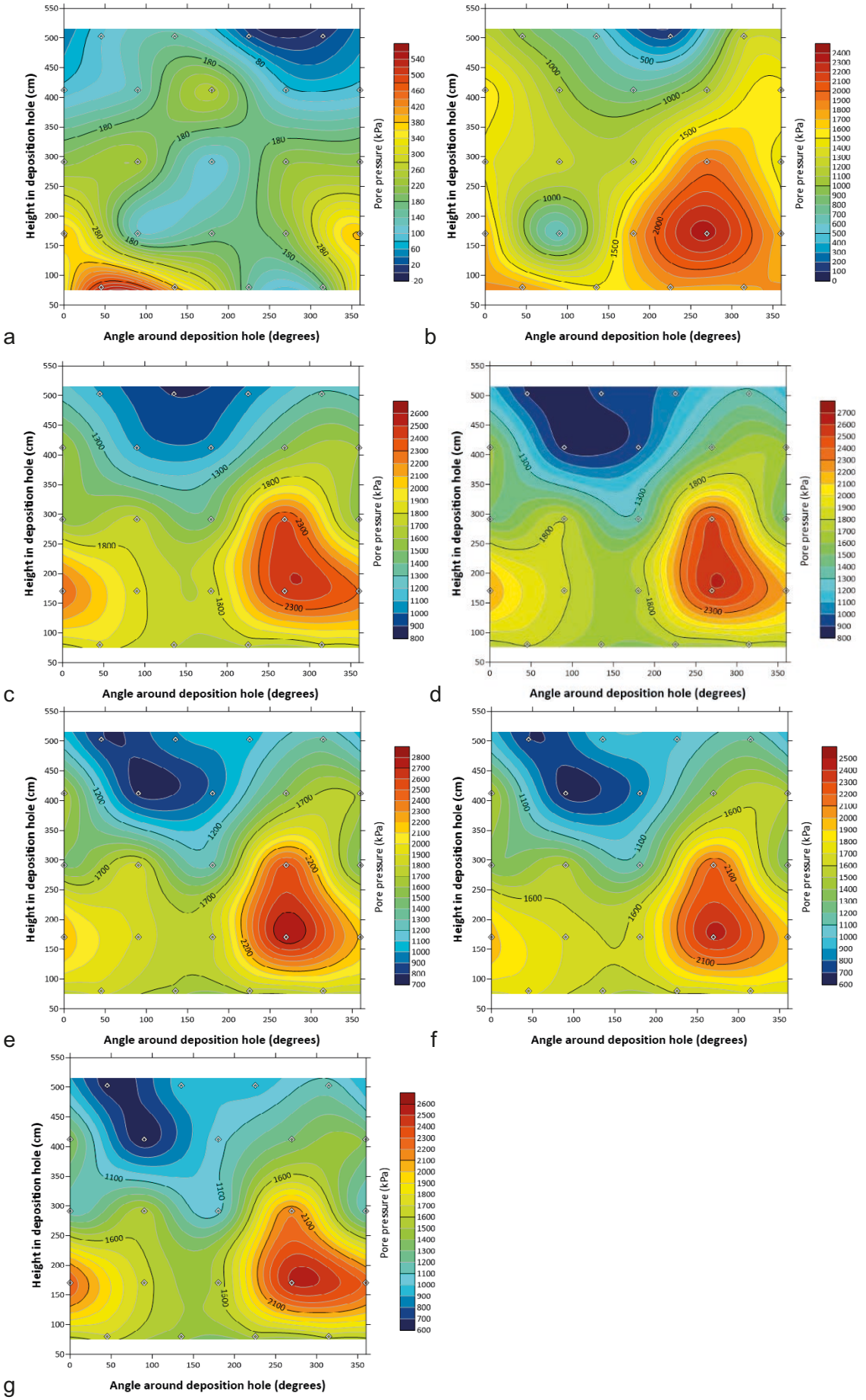

Figure 16-20. *Distribution of pore water pressure at the deposition hole wall. a) Day 50; b) Day 500; c) Day 1500; d) Day 2500; e) Day 3500; f) Day 4500; g) Day 5500.*

16.3.5 Pore pressure in the pressure relief holes (PRHx–x)

Pressure data from the individual packered sections of the two pressure relief boreholes are shown in Figure 16-21. After pore pressure was raised around Day 500, pore pressure in all intervals decreased. These appear to have neared asymptote by Day 2000 but then pressure increased at Day 2550 for around 300 days, as seen in the pore pressure measurements at the deposition hole wall. Following this increase in pressure, all intervals showed a decrease in pore pressure. Some intervals appeared to be close to asymptote by the end of the test.

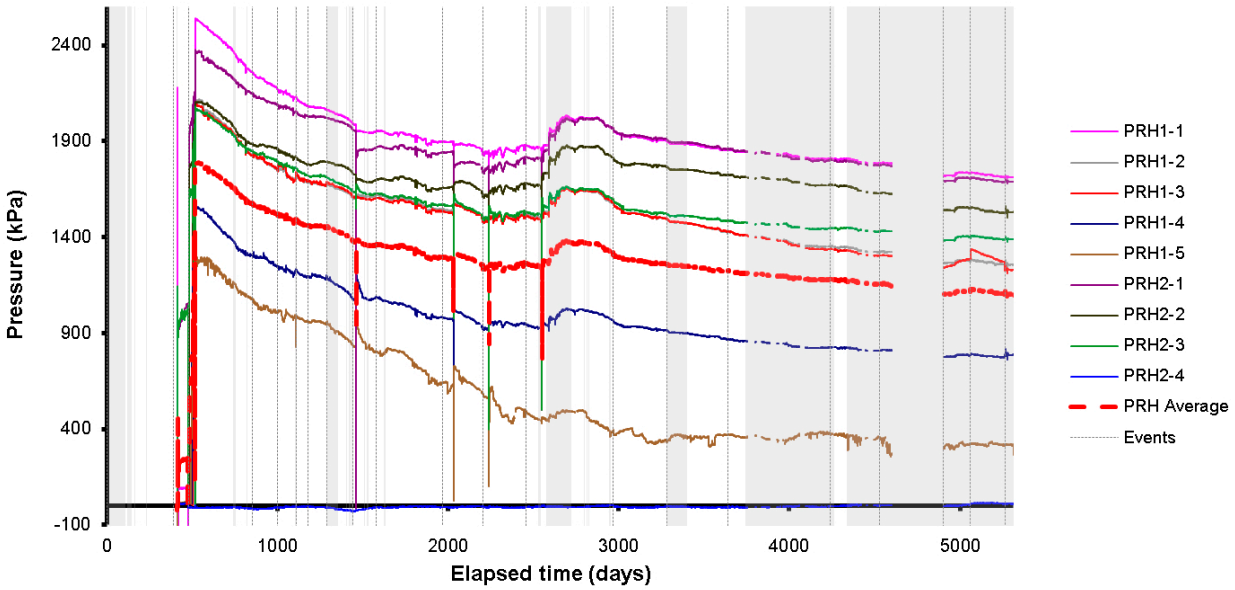

Figure 16-21. *Porewater pressures measured in the packered sections of the pressure relief boreholes.*

Figure 16-18a and Figure 16-21 both show long term decay in porewater pressures at the deposition hole wall and in the pressure relief boreholes. This was of concern and could have been symptomatic of a problem with the Lasgit experiment. However, close inspection of pore pressure data from other locations in the Äspö HRL also exhibited a long-term decay in porewater pressure that predated Lasgit, particularly between depths of 420 to 450 m. Figure 16-22 shows pore pressure data from borehole KA3105A located close to the Lasgit deposition hole. This clearly shows the slow time-dependent decay of pore pressure and a general declining trend within the HRL between the 420 to 450 m depth. This decline was related to draw-down of pressure as a result of pumping of water from the HRL tunnels. As pore pressure decreased, swelling pressure in the bentonite buffer also decreased. Therefore, this boundary condition variation is complicated, as the hydration state of the buffer increased, while pore pressure decreased. During deposition in a KBS-3 system, this reducing boundary condition is unlikely, with pore pressure remaining constant shortly after the deposition tunnels are back-filled.

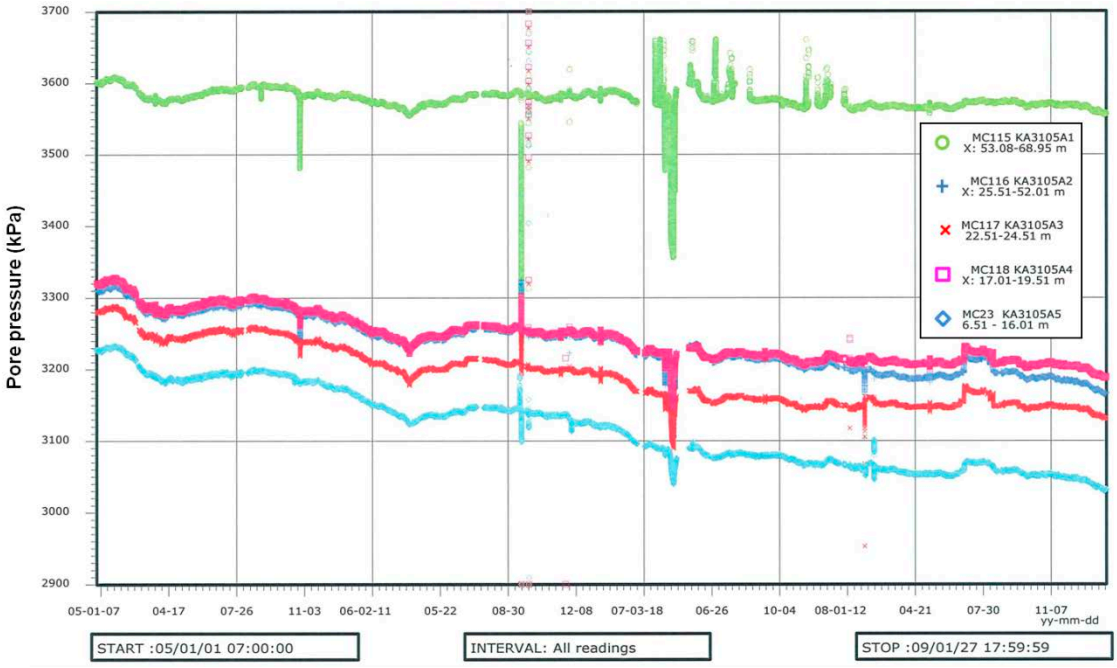

Figure 16-22. *Porewater pressures measured in nearby borehole KA3105A.*

16.4 Stress

Stress of the Lasgit system was measured at 32 locations within the deposition hole. Sensors mounted on the canister, rock wall, and within the clay were used to determine both the axial and radial components of stress and the distribution of values throughout the deposition hole.

16.4.1 Radial stress at the deposition hole wall (PR9xx)

Data from radial stress sensors PR903 to PR922 are plotted in Figure 16-23. Stress increased rapidly in the first 500 days of the Lasgit test and once pore pressure was established increased further (Figure 16-23a) with considerable heterogeneity being apparent. However, there was little difference between the average for each level (Figure 16-23b). This suggests that the heterogeneity was within each level. The total range of the data was almost 1 500 kPa at Day 500, with most of this coming from the PR7 level, at the mid-height of the canister (Figure 16-23c). Stress continued to evolve and between Day 1500 and Day 3000 increased at a near linear rate. By which time, the ranges in stress at the PR4, PR5, and PR10 levels, at the top and bottom of the sensor array, were steady and relatively constant. Around Day 1750, range recorded by PR7 started to decrease, suggesting that this level was becoming more homogeneous in terms of stress distribution. The radial stress data was affected by the halting of artificial hydration starting at Day 2533, Day 3284, and Day 3745. Some locations reached plateau as a result of pausing the artificial hydration and a clear change in slope for the average stresses can be seen around Day 3000. The pause at Day 3284 resulted in the range and average of PR4 reducing. The end of hydration at Day 3745 resulted in a second change in slope of average stress and resulted in the range of radial stress decreasing. The radial stress data was clearly sensitive to the (artificial) hydration state. The stress data had not reached a plateau by the time that artificial hydration ended. Once hydration ceased, the data did appear to reach near plateau. However, continued artificial hydration may have resulted in higher radial stresses forming in the deposition hole. The data prior to Day 2533 suggests that radial stress may have continued to a higher value. It is difficult to predict from the data at what magnitude of stress the data would have levelled but it could have been substantially greater than the 5 200 kPa average stress seen prior to pressurisation of the canister. This may have been 7 000 – 8 000 kPa if artificial hydration was continued for sufficient time. Thus, it should be noted that the end of artificial hydration resulted in the plateau of stress, at a level less than the system would have achieved if artificial hydration had continued.

The distribution of radial stress within the deposition hole is shown in Figure 16-24. The general distribution of stress was established early in the test. By Day 50 (Figure 16-24a), increased stress had established at an orientation of ~ 315° and at the bottom of the sensor array. At Day 500, the high stress region along the full length at 315° had established, with raised stress low in the sensor array. Sensor PR921, centrally at the top of the sensor array, showed a localised low. Comparing Figure 16-24a and Figure 16-24b suggests that PR912 was within a low stress region but for some reason stress increased in the centre of the plot, although PR921 remained isolated at a low stress. Between Day 1500 (Figure 16-24c) and Day 5500 (Figure 16-24g) there was very little change in the distribution of stress. The high pressure at 315° predominated, as did a high stress region at ~ 150 cm height. There was not much difference between the distribution in stress at Day 500 and Day 5500, demonstrating that the heterogeneity in stress formed early on in the Lasgit test and was persistent. There was no noticeable change in stress distribution when artificial hydration was paused or stopped.

All sensors showed annual variation of varying magnitude (Figure 16-23a). These oscillations were most obvious in PR914, PR915, PR919 and PR920, which are shown in Figure 16-25 following the removal of the swelling stress component. The annual transients were less well defined than those previously described but did have a period of one year. As seen, PR915 closely correlated with the HRL temperature, whereas PR914 had a lag of ~ 30 days. The correlation of PR915 with HRL temperature was unexpected as it occurred in section 9 of the deposition hole, approximately halfway up the deposition hole. This was a considerable distance from the expected influence of the environmental conditions in the gallery. It is possible that the influence in these parameters was actually a considerable lag of 50 – 100 days from the temperature observed at the canister. It was noted that a negative correlation was seen between radial stress and canister temperature, i.e. radial stress had a negative oscillation when temperature was highest. This may relate to thermal contraction of the bentonite as the temperature increased.

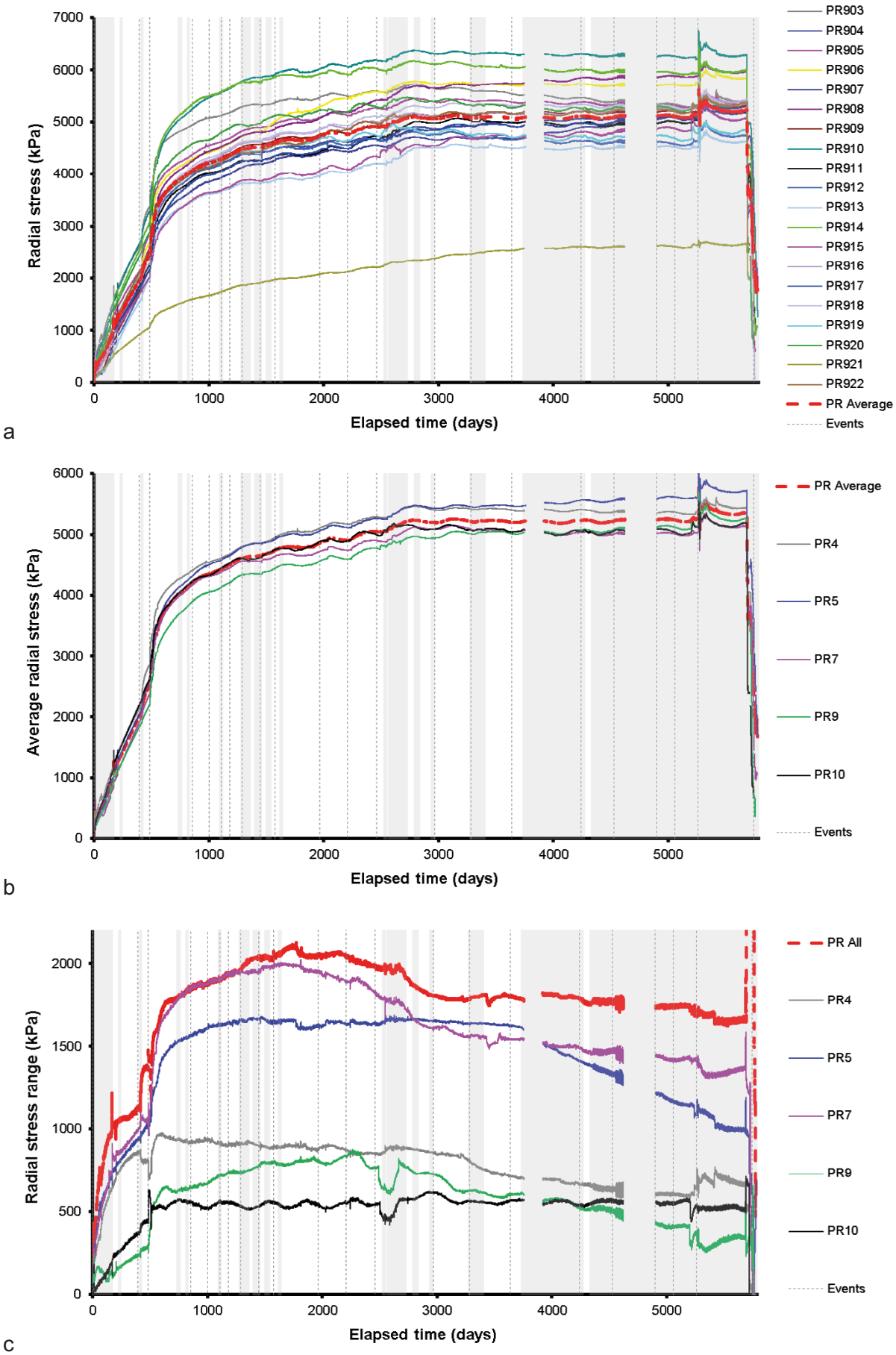

Figure 16-23. *Variation in radial stress at the deposition hole wall. a) Radial stress; b) Average stress for each interval; c) Range of data for each interval.* ***Note:*** *b and c do not include PR921.*

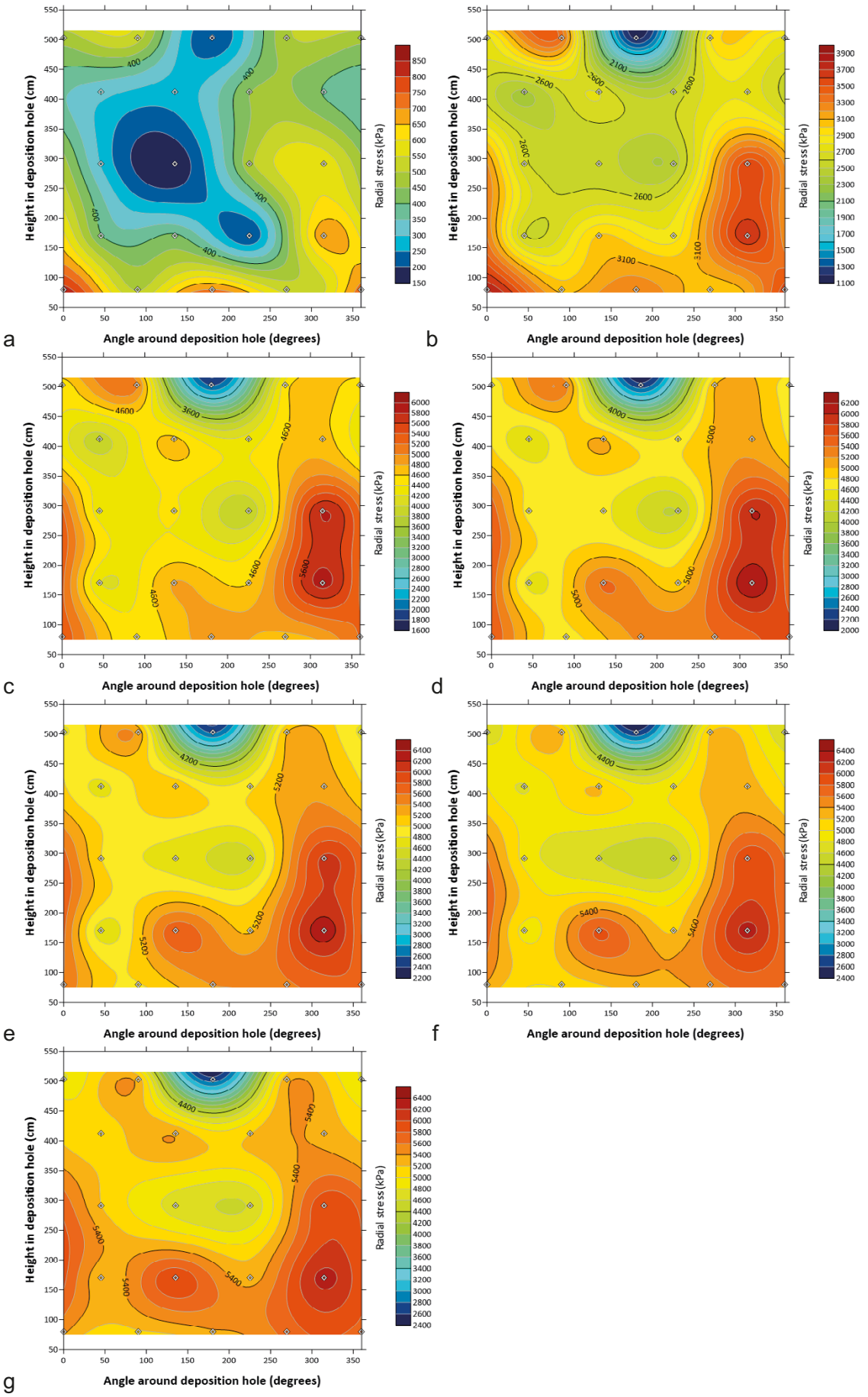

Figure 16-24. *Distribution of radial stress at the deposition hole wall. a) Day 50; b) Day 500; c) Day 1500; d) Day 2500; e) Day 3500; f) Day 4500; g) Day 5500.*

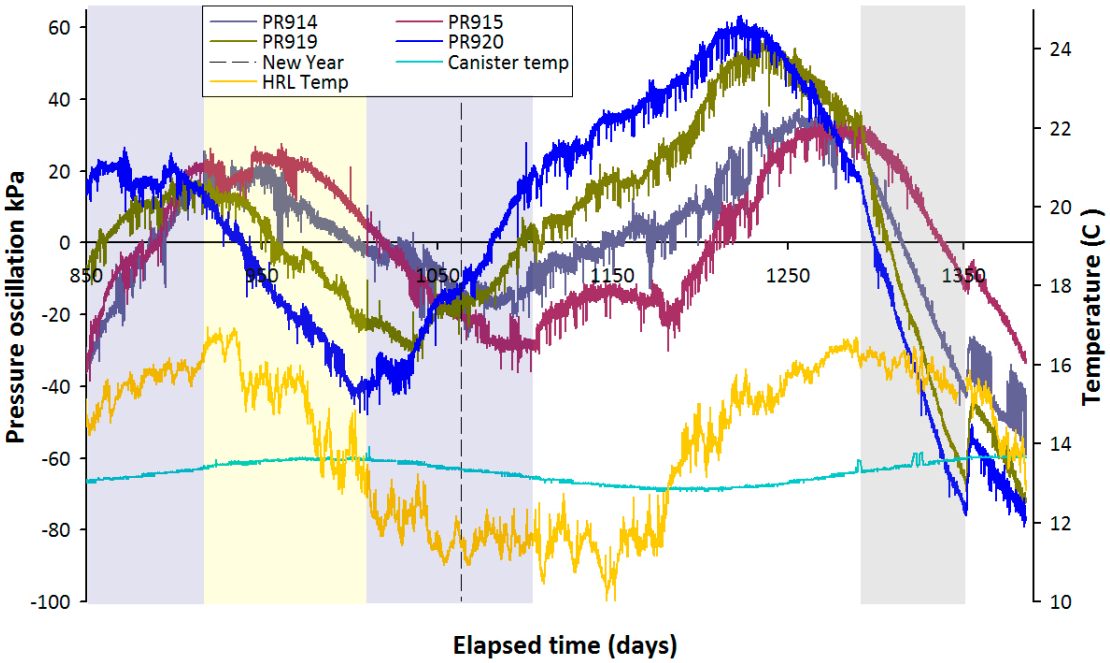

Figure 16-25. *Variation in radial stress with time after the removal of increasing stress component compared with HRL and canister temperature.*

16.4.2 Axial stress in the buffer (PB9xx)

Figure 16-26 shows axial stress within the bentonite. At most sensor locations stress increased relatively quickly and by Day 1000 were close to their maximum level. The exception to this was PB901 (Figure 16-26a), which took much longer to increase in stress and continued to increase in stress all through the Lasgit experiment. At PB929, the data reached a plateau by Day 1000, whereas other locations (e.g. PB927 and PB928) took longer to reach a plateau but still achieved a clear plateau before Day 2000. This is reflected in the average for PB17 (Figure 16-26b), which reached a plateau around Day 1500. This shows that stress had attained equilibrium at the top of the bentonite buffer quite early in the Lasgit test. The result of the sensors above the canister on level PB13 showed a gradual increase in stress. This increase was halted by the pauses in artificial hydration starting at Days 2533, 3284, and 3745. This shows that this level had not achieved equilibrium and was still being hydrated by the filter mats. In the base of the deposition hole at level PB1, stress was slower to increase and was still increasing when artificial hydration was finally stopped at Day 3745. This reflects the distance between level PB1 and the artificial hydration mats, which were all above the canister. Each level generally showed small amounts of heterogeneity, as shown in Figure 16-26c. At level PB13 the range of stress by Day 1000 had plateaued at about 450 kPa. The range at level PB17 took 1 500 days to reach a maximum of around 1 500 kPa and for the rest of the Lasgit test reduced. In the base of the deposition hole at PB1 the range by Day 1500 was almost zero and increased for the rest of the Lasgit test as PB901 continued to increase. By the time the canister was pressurised the total range of axial stress was around 1 200 kPa.

The range of the data (Figure 16-26c) was affected by the ending of artificial hydration and shows that hydration controlled axial stress. However, several locations had reached a plateau early in the test and it is unlikely that axial stress would have increased significantly above the canister, although it may have got substantially higher at PB901.

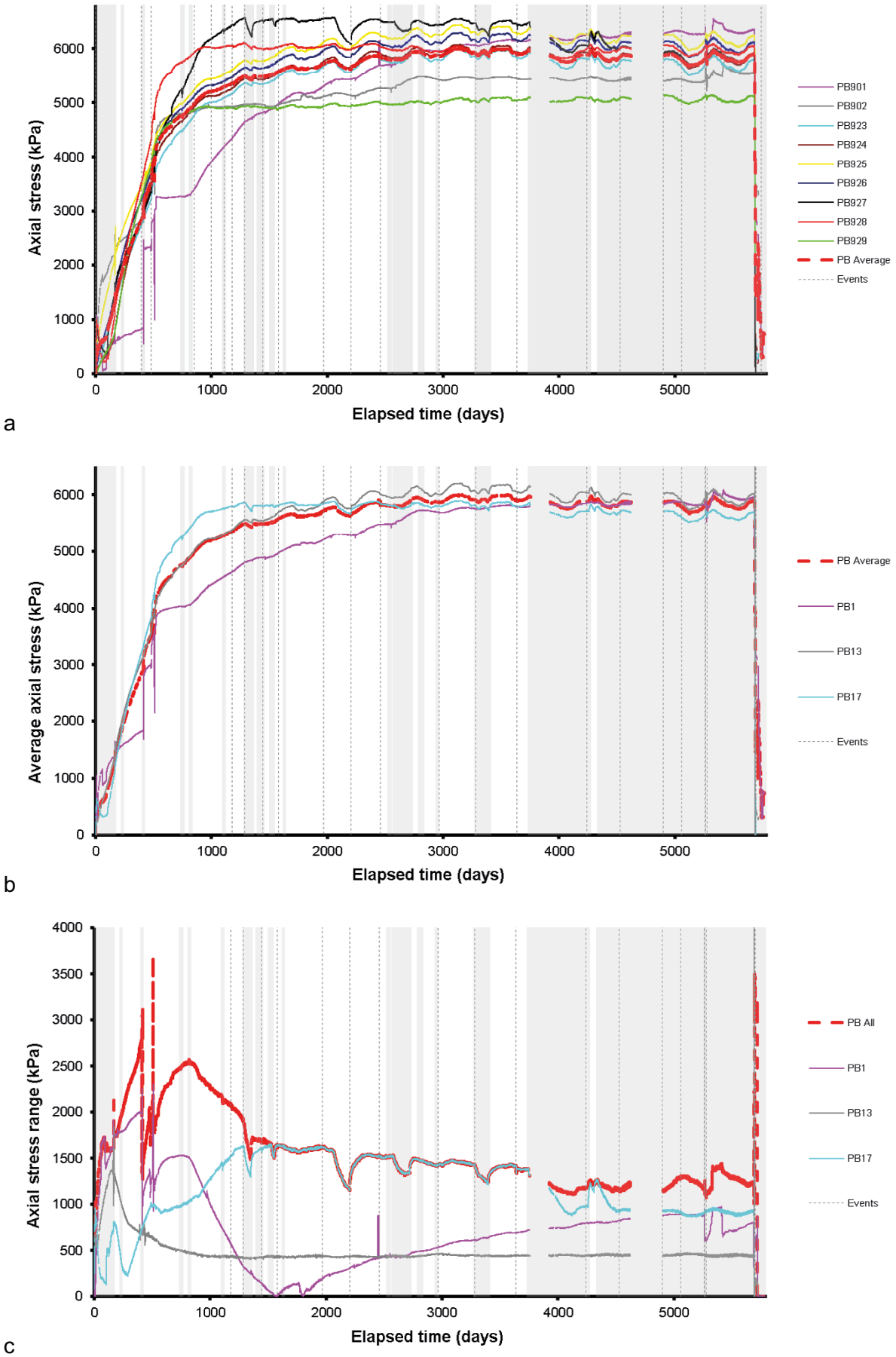

Figure 16-26. *Development of axial stress measured at 12 locations within the buffer. a) Axial stress; b) Average stress for each interval; c) Range of data for each interval.*

16.4.3 Axial and radial stress on the canister surface (PC90x)

Axial (PC901) and radial stress (PC902, PC903) around the canister are shown in Figure 16-27. Stress greatly increased around Day 500 when pore pressure was established in the system (Figure 16-27a). This had a greater impact on the radial stress measurements than the axial direction. The radial stress results followed that seen in the radial stress at the deposition hole, which not surprising as the two types of sensors were positioned on either side of the annular bentonite block. From Day 1000 to ~Day 2500 the radial stress increased but was perturbed by the pauses in artificial hydration starting at Days 2533, 3284, and 3745. This changed the slope of radial stress increase and suggests that artificial hydration was dictating radial stress. Axial stress had a different response. It took longer for stress to increase and did not show the steep increase at Day 500 as a result of pore pressure increase. Stress increased much slower and became the highest stress on the canister. This was not unexpected as the filter mats above the canister were likely to create a much greater axial stress than radial stress. The result of PC901 was similar to that seen in PB901.

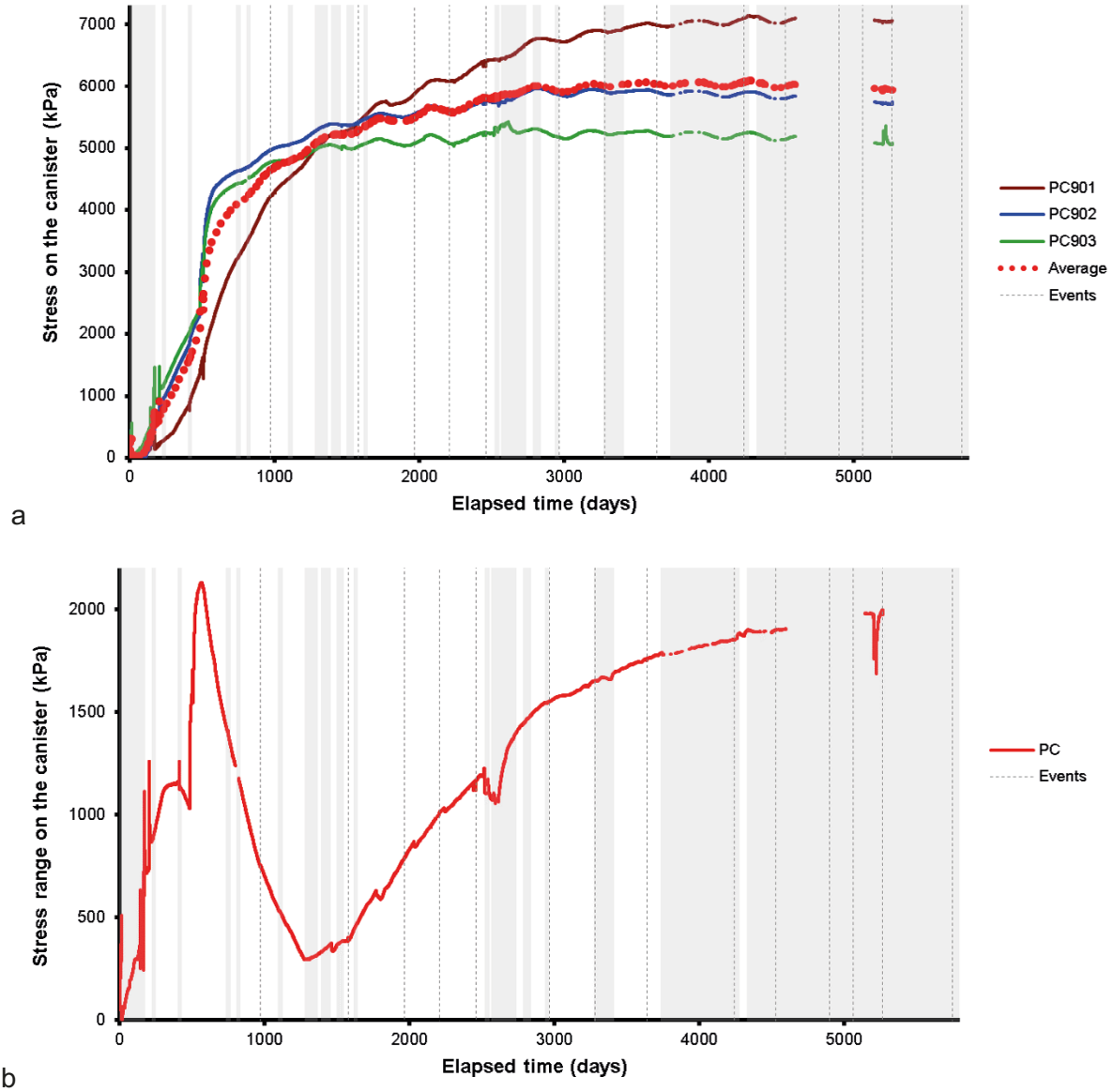

Figure 16-27. *Development of axial and radial stress on the side and base of the canister.*

The range of stress on the canister is shown in Figure 16-27b. This shows that by the time of the canister being pressurised, the range of stress on the canister was 1 900 kPa and was increasing. The canister stress data (Figure 16-27a) showed annual variation from around Day 600 onwards. The removal of a simple linear trend showed oscillations with a period of approximately 1 year, as shown in Figure 16-28 . The stress oscillations appear to correlate with canister temperature. It should be noted that axial stress lagged radial stresses as the sensor was located on the base of the canister and was further evidence of the propagation of a thermal pulse down the deposition hole.

16.4.4 Net pressure

The distribution of radial stress (Figure 16-26) shows that high radial stresses were concentrated along the part of the deposition hole wall at about 300° and that stress varied mainly with angular position rather than with depth. To examine this in more detail the data were divided into 16 angular strips and the stress values averaged over depth. This gave a set of pressures that can be represented as vectors in the horizontal plane as shown in Figure 16-29. Since these pressures act upon equal area segments of the hole wall they can be summed to give a net horizontal force acting on the hole. The data from PR903 to PR922 have been used to generate this net force vector throughout the entire history of the experiment. Its magnitude as a function of time is plotted in Figure 16-30 and its locus in the horizontal plane is shown in Figure 16-31.

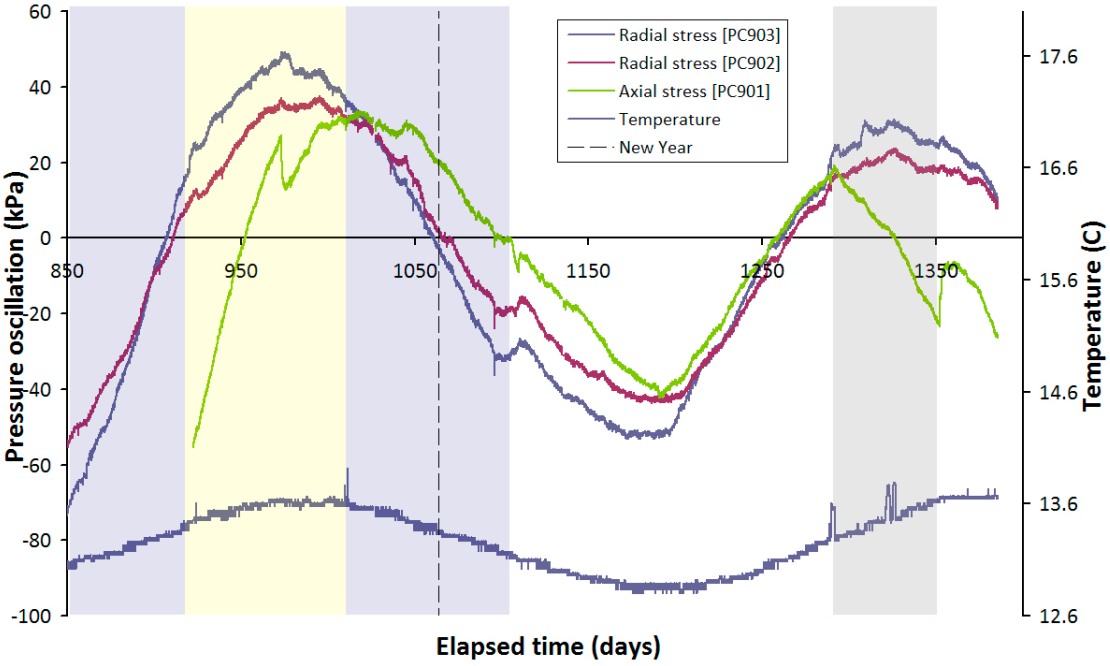

Figure 16-28. *Pressure oscillation observed in axial and radial pressure on the side and base of canister.*

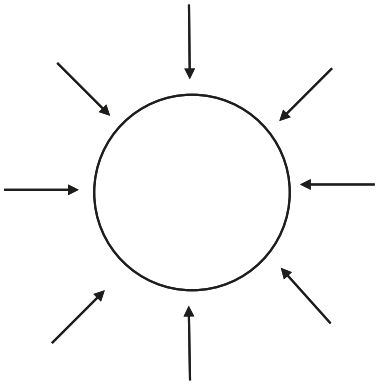

Figure 16-29. *Depth averaged radial stresses represented as vectors in the horizontal plane.*

It can be seen in Figure 16-30 that the magnitude of the net pressure reached a well-defined plateau by the time that packers were installed into the pressure relief holes. During installation of the packers there were significant changes in net stress, which afterwards, increased more rapidly. This levelled off once again by around Day 1000 and remained constant for some time. Net pressure reduced to zero as the system approached an equilibrium state. This end point in the evolution of the system may be impossible to attain (certainly within the life-span of the Lasgit experiment), given the variability in composition of the bentonite blocks; their position in relation to the side-wall of the hole; the dependence of the system on the availability of water; and importantly their inherent shear strength. Net pressure remained at ~3 000 kPa until the first of the artificial hydration pauses at Day 2533, following which net-pressure reduced. This suggests that the system was becoming more homogeneous but may also reflect that stresses were relaxing as a result of stopping artificial hydration.

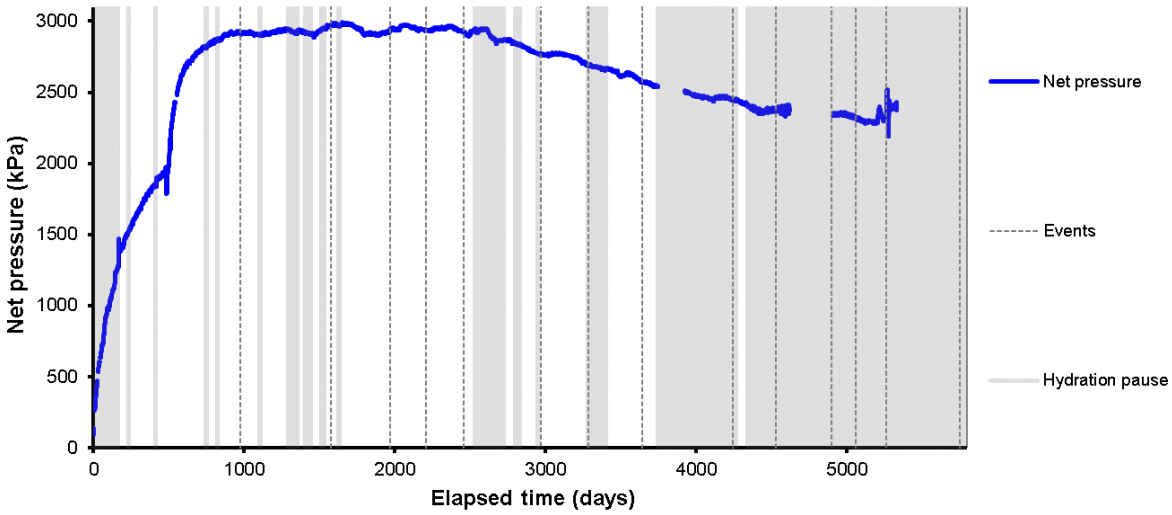

Figure 16-30. *Variation of magnitude of net pressure with time.*

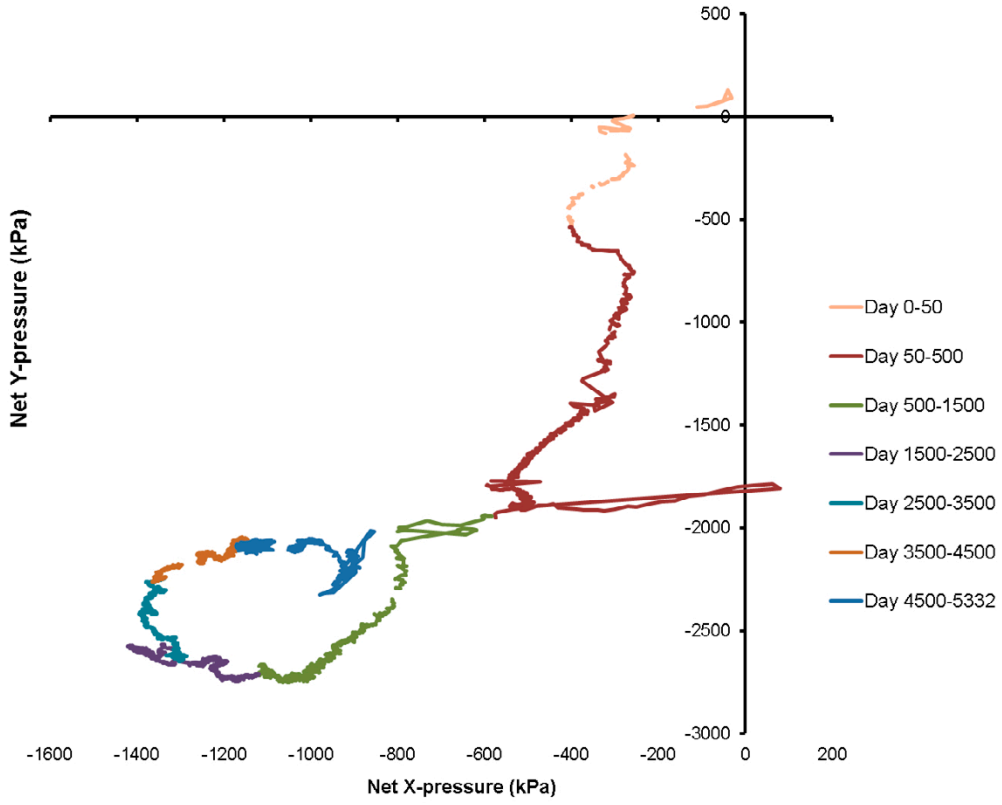

Figure 16-31. *Variation of net pressure direction with time.*

The locus plot in Figure 16-31 shows a fairly erratic path during the first 50 days of hydration which then settled to an almost linear path between Day 200 and Day 400. The packer installation caused a further period of erratic change in the net pressure locus but thereafter, the path returned to the previous gradient observed from Day 200 to Day 400, until Day 940. The locus then changed direction with little change in net Y-pressure, while net X-pressure slowly became more negative. Over the following 4400 days the locus evolved to follow a circular pattern. This may have, in part, been as a consequence of artificial hydration stopping. There is clearly no indication of a return to the origin as one would expect for a true equilibrium condition.

16.5 Suction

Figure 16-32 shows the suction pressures recorded at the seven psychrometers WB901 to WB907 embedded at locations within the bentonite buffer. Suction decreased with time, confirming ongoing hydration of the clay. However, the rate of hydration slowed. Greatest progress in hydrating the clay was made near to the filter mats above the canister, whilst the least progress had occurred just below the canister. There was no data for WB903 which was found to be defective following closure of the hole. While a number of psychrometers appeared to be levelling (e.g. WB906), close inspection of the data revealed a steady downward trend, indicating that most, if not all of the clay, remained in some degree of suction by the time the data recording stopped.

It was anticipated that when the bentonite was fully saturated, the psychrometer values would plateau at a finite (positive) suction, reflecting the natural salinity of the Äspö groundwater/salinity of the water in the buffer. However, the system was unlikely to be in hydraulic equilibrium at the time shown in Figure 16-32 as the development of porewater pressure lagged well behind the saturation of the clay. Ideally, in relation to gas testing, the clay should be in a state of hydraulic equilibrium, else the suction would introduce an unknown variable in the interpretation of the results. Unfortunately, the logging of the psychrometers stopped early as they were recorded from a nearby experiment that finished. This means that the suction state of the buffer when later gas testing occurred was unknown. No annual variation was noted in the data, as expected.

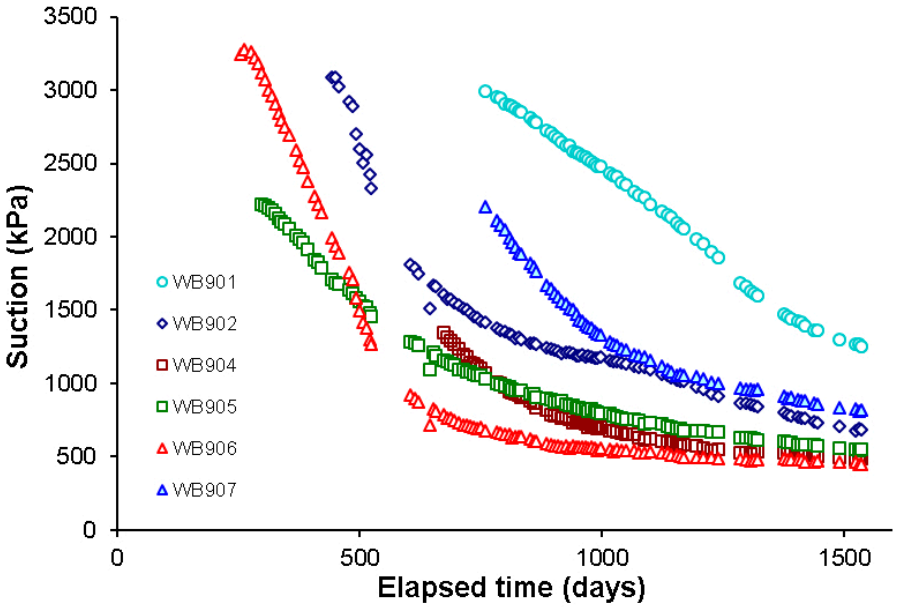

Figure 16-32. *Suction pressures recorded at sensors WB901 to WB907 for the entire test.*

16.6 Axial force and lid movement

16.6.1 Axial force on the lid (LP90x)

Figure 16-33a shows a plot of the axial force measured by the Glötzl load cells measured at the retaining lid. The pre-stressed lid remained at a constant stress until around Day 500 when the pore pressure in the system increased, and as a result, radial stress in the system increased. At the start of the experiment the average load on the lid was ~1 200 kPa and over the next 2 000 days increased to ~1 700 kPa, as swelling pressure in the system increased. The slope of this force increase was perturbed by the three pauses in artificial hydration that started at Days 2533, 3284, and 3745. This was most apparent when artificial hydration was stopped at Day 3745 and for the remainder of the test the force on the lid slowly decreased by ~100 kPa. This shows that the force was created by the artificial hydration of the buffer. The data very clearly have a cyclicity, with a period of one year. It should be noted that the Glötzl load cells were not well temperature compensated and this result will be the combination of real changes in load as a result of temperature cyclicity within the HRL, and the limited temperature compensation of the load cells. Figure 16-33b shows the range in the data for the three load cells. This shows that the pre-stressing of the canister caused a small variation in loading. As swelling pressure increased in the deposition hole and the lid moved, the variation slowly decreased (Figure 16-33b). Annual variation is seen in the range of the data, which suggests a real heterogeneity in stress within the system as all three load cells were exposed to the same thermal variation in the HRL.

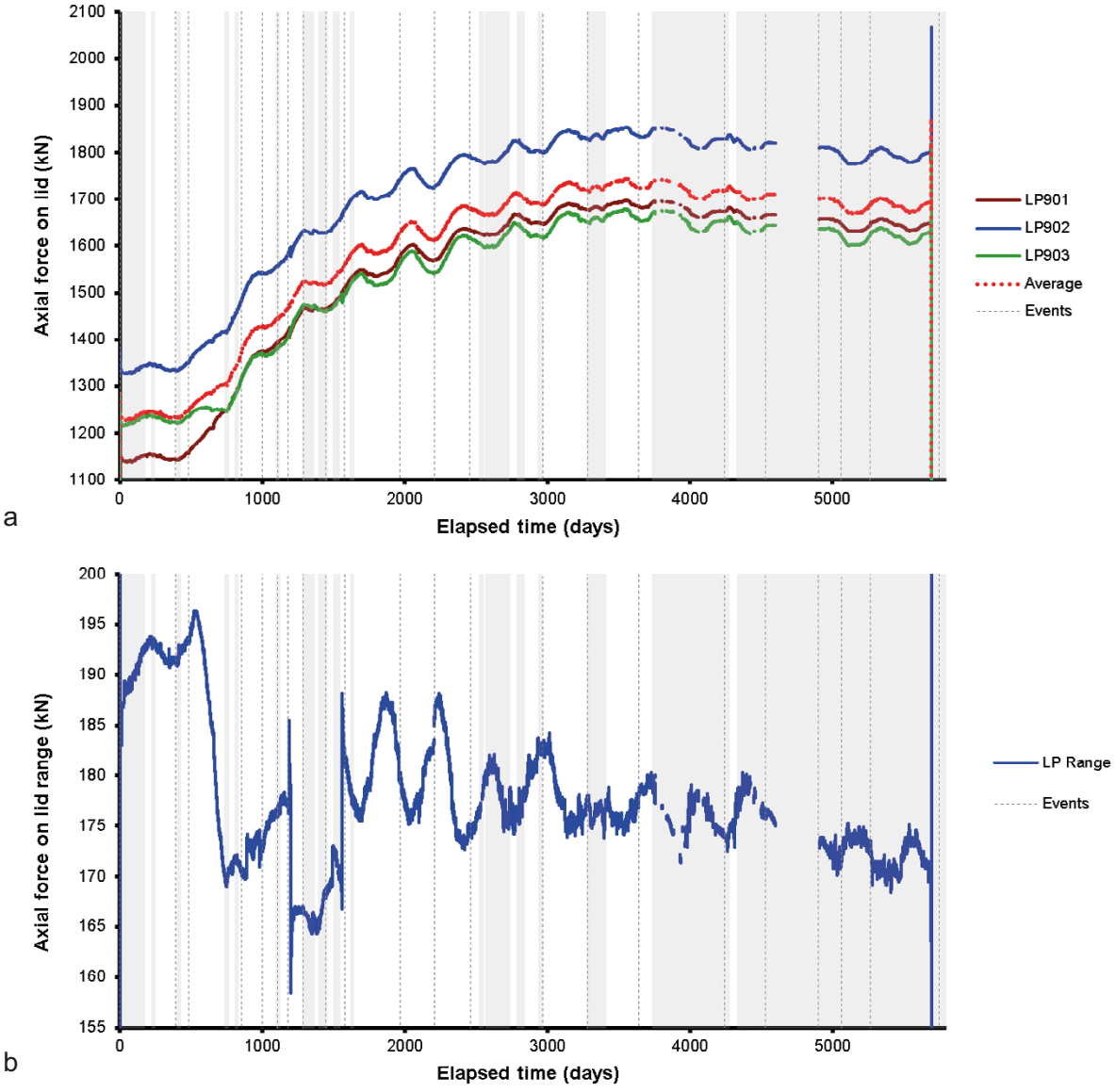

Figure 16-33. *Axial force acting on the steel lid measured by 3 load cells attached to separate rock anchors.*

16.6.2 Lid movement (DP90x)

The displacement of the lid was measured by seven sensors to monitor the vertical movement (3 sensors), lateral movement (2 sensors), lid movement in relation to the HRL Assembly Hall roof, and the movement of the canister in relation to the lid (Figure 16-34a). The movement of the lid relative to the gallery floor was recorded by DP902 to DP904. This showed a similar response to the force on the lid (LP90x). The pre-stressed lid showed limited movement until around Day 500 when the pore pressure started to increase and the stresses in the system increased. This resulted in the lid lifting as stresses developed. The rate of displacement change was influenced by the pausing of artificial hydration starting at Day 2533, Day 3284, and Day 3745. This was most apparent at Day 3745 when the lid movement started to decrease, showing that the lid moved downwards as stresses in the system relaxed as hydration stopped. It is uncertain how much the displacement would have been if the system had reached equilibrium. A vertical displacement of ~4 mm may at first appear large but as the movement will have been as a result of swelling of the bentonite buffer, it actually represents a vertical strain of only 0.053 % (increase of 4 mm of a bentonite buffer of 7 530 mm height). This compares with radial strains that will have been of the order of 3 % as the 290 mm diameter bentonite rings and 50 mm pellet infill swelled and filled the 10 mm engineering void between the annular bentonite ring and the canister. The vertical displacement data showed considerable annual cyclicity. As with the force on the lid, this will have been a mix of actual cyclicity in the movement and thermal expansion of the metal supports of the sensors. However, it is clear that the lid had an annual component of movement. Figure 16-34a also shows that the replacement LVDTs installed at Day 5264 were faulty as it highly unlikely that annual cyclicity increased at this time. It also shows that the LVDTs that were replaced were faulty from Day 4900 onwards.

Figure 16-34b shows the lateral movement of the canister. This data shows considerable annual variation, which was likely to be a combination of thermal expansion of the brackets holding the LVDTs and real movement. Taking the annual variation into account, the lid did move laterally, but only on the order of less than 0.2 µm. The replacement LVDTs at Day 5264 similarly show that the sensors were faulty.

Data from sensors DP901 and DP905 are plotted in Figure 16-34a. These show the position of the Monel pipe on the canister with respect to the lid (DP901) and the position of the lid with respect to the gallery roof. From all displacement measurements it is possible to calculate the relative position of the canister with reference to the gallery floor and gallery roof, as shown in Figure 16-35. This shows that early in the test history the canister had a complex movement and initially moved 0.5 mm down, before rebounding nearly to where it first started. The canister then moved downwards to reach ~2 mm below where it started at around Day 400, when pore pressure was established in the system. This resulted in the canister rebounding by ~1 mm. This early history shows that the canister moved under its weight and the pre-stress of the lid. Swelling below the canister through natural hydration caused the canister to rise, before swelling of the much greater thickness of bentonite above the canister resulted in the canister moving downwards. The establishment of pore pressure all around the deposition hole resulted in the bentonite segment below the canister swelling and the canister moved upwards as a result. This rapid movement ended by around Day 800 and from then on, the canister slowly moved upwards. This movement ended when artificial hydration was stopped at Day 3745.

Figure 16-34 clearly shows that from approximately Day 440 to Day 1400 displacement of the lid had propagated upwards in a linear manner. The removal of this linear trend is shown in Figure 16-36, which reveals a strong annual cyclicity. It can also be seen that as HRL temperature increased there was an acceleration of lid displacement rate. However, it is interesting to note that this correlation is not perfect and at times there was an offset between displacement and temperature.

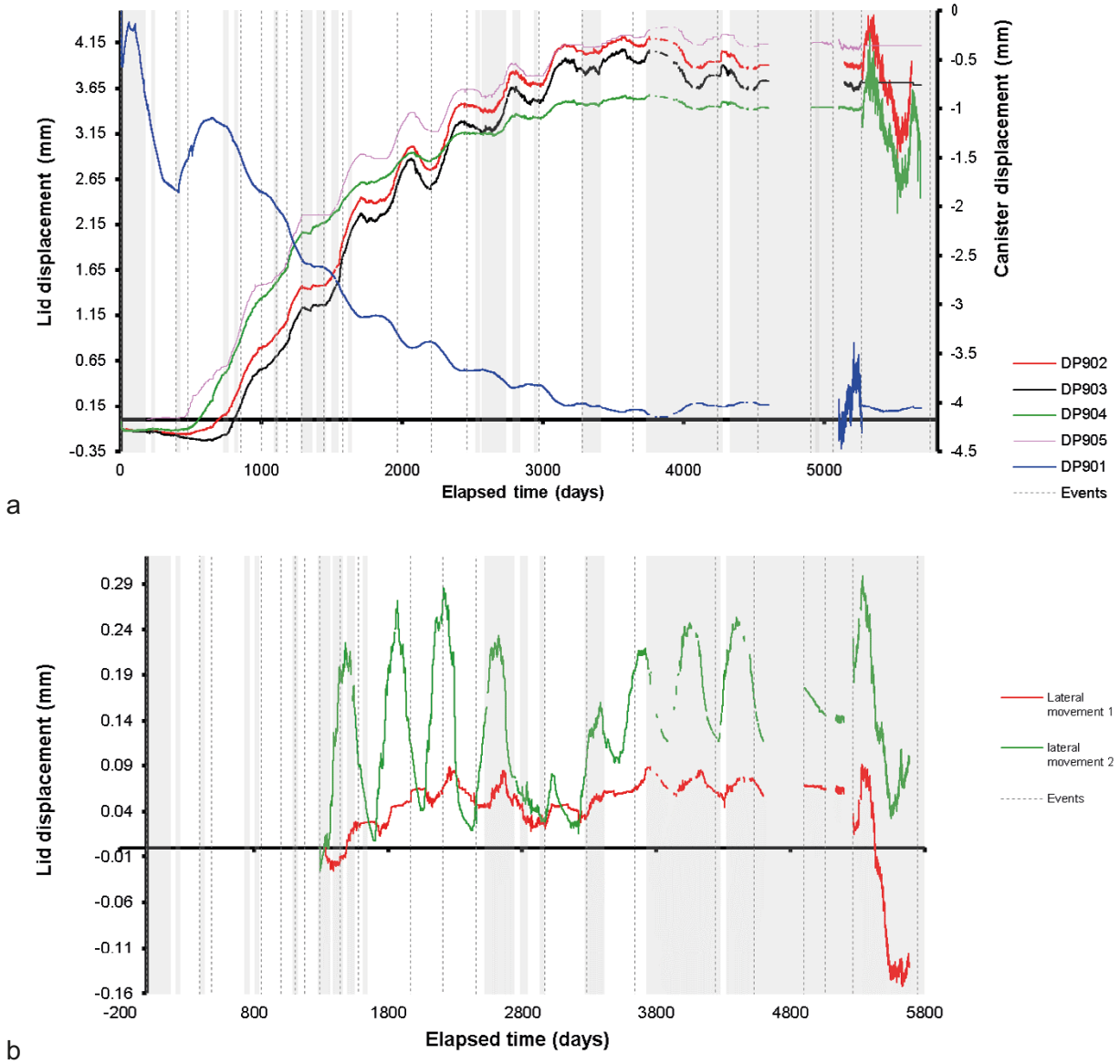

Figure 16-34. *Linear displacement of the steel lid and copper canister. Movements of the lid are measured relative to both the gallery floor and ceiling. Movements of the canister are measured relative to the steel lid. a) Vertical movement; b) Horizontal movement.*

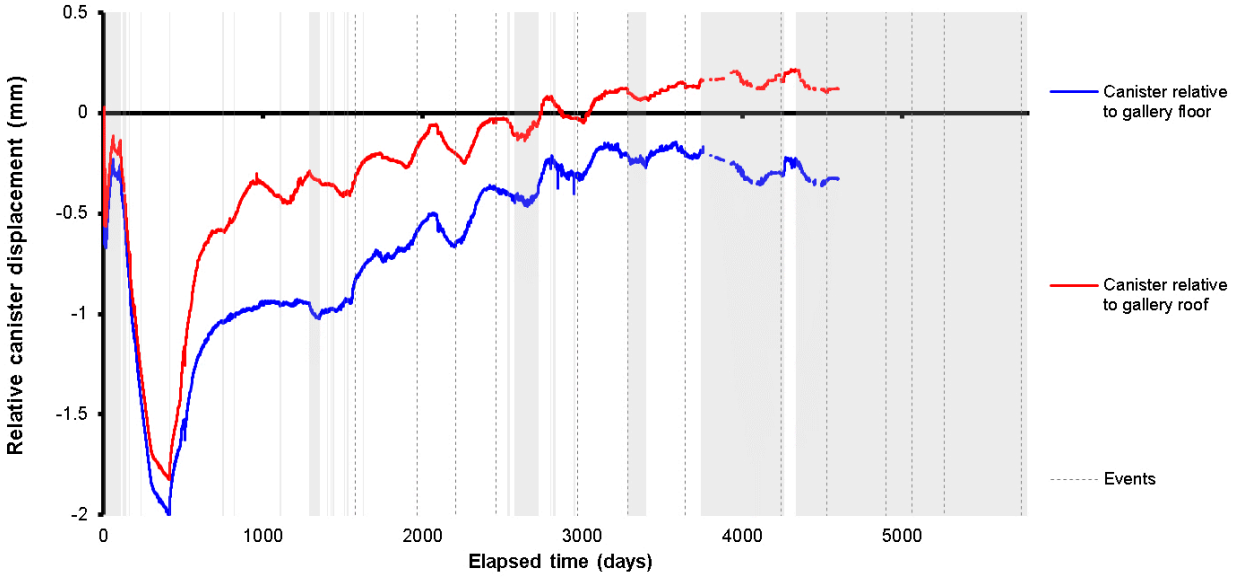

Figure 16-35. *Relative position of the canister with respect to the gallery floor and roof.*

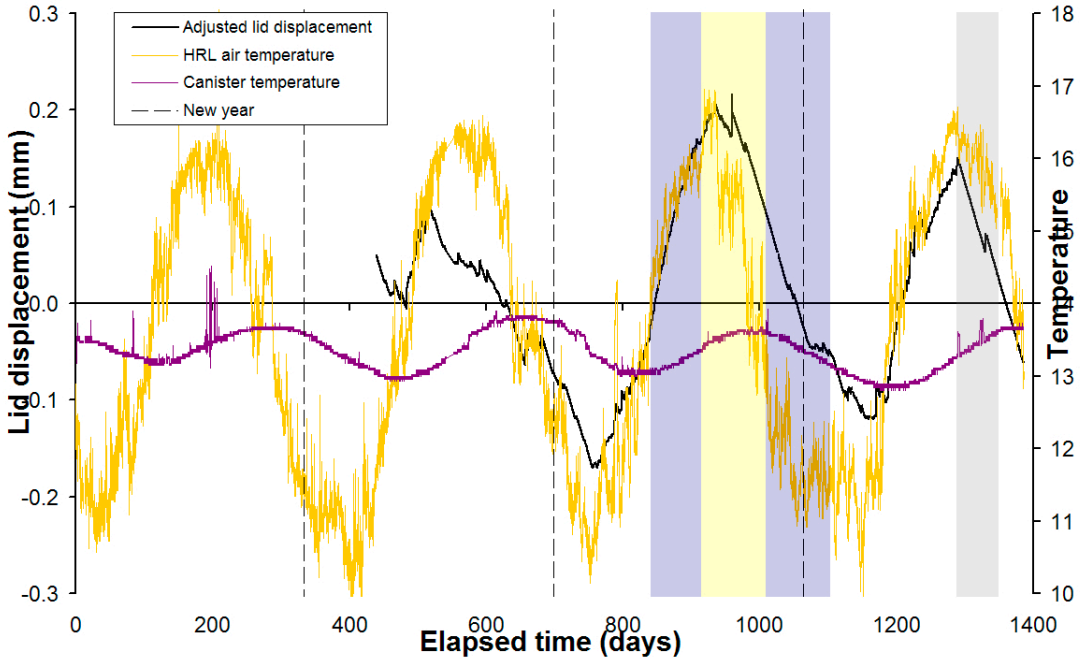

Figure 16-36. *Adjusted lid to gallery roof displacement data from DP905 plotted against temperature. The removal of the linear trend seen in DP905 in Figure 16-34 from Day 400 to Day 1400 demonstrates that the annual variation was primarily related to HRL temperature.* ***Note:*** *New Year is January 1st.*

Annual cyclicity was also seen in the stick-slip behaviour of lid movement. Figure 16-37 shows the change in lid position for DP905, filtered to only show movements above 0.002 mm, which occur during stick-slip behaviour. The main conclusion from this data is that stick-slip occurred predominantly during the period of minimum canister temperature and increasing HRL temperature. The cause of the stick slip is uncertain, but could be linked to the thermal characteristics of the various system components and their interaction. It may also represent friction between the concrete plug and the concrete lining at the top of the deposition hole.

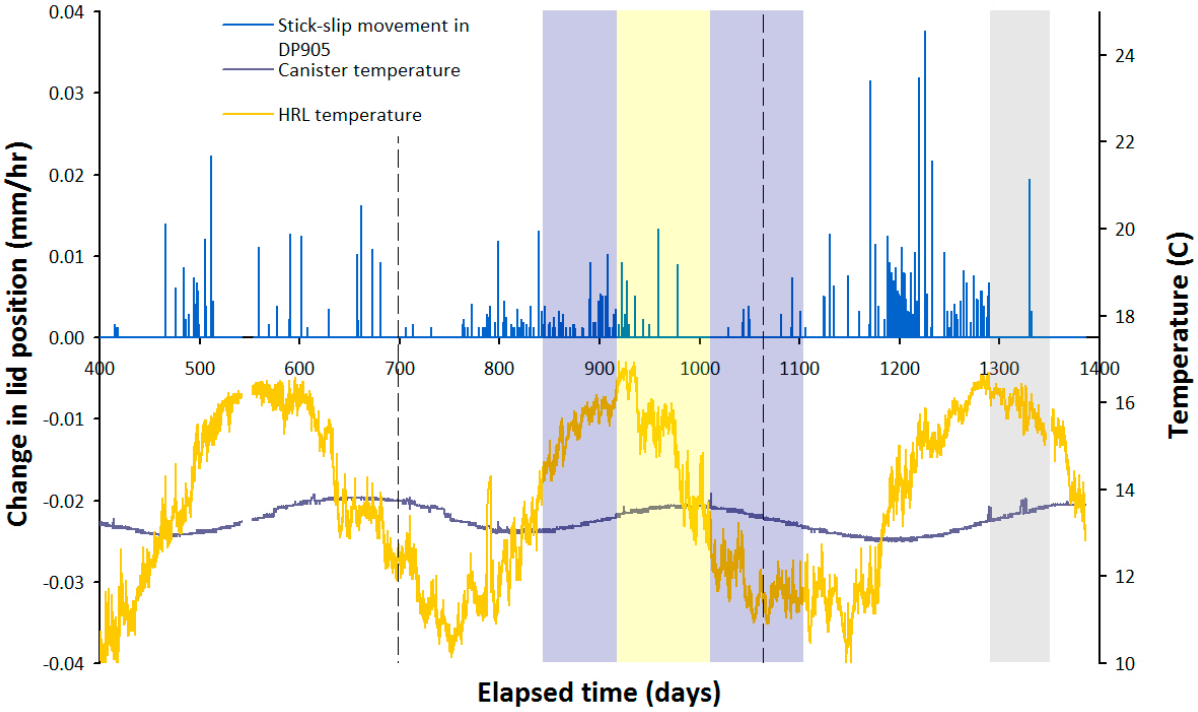

Figure 16-37. *Stick-slip movement of DP905 plotted against temperature. Individual stick-slip events can be seen to have occurred most frequently when HRL temperature was increasing.*

16.7 Average of each sensor type

Figure 16-38 shows the average of each sensor type. Figure 16-38a shows the stress and force averages in the deposition hole. This shows that stresses generally increased in a similar manner. The establishment of pore pressure (Figure 16-38b) increased all of the stresses and forces in the system in a similar manner. The average data show that the system settled by Day 1500 with all sensor types continuing to increase. All of the sensor types were affected by the pausing of artificial hydration starting at Days 2533, 3284, and 3745. The ending of artificial hydration at Day 3745 resulted in all sensor types either reaching a plateau or decreasing. The radial stress on the rock wall and stress on the canister plateaued, whereas the axial stress in the bentonite and axial force on the lid decreased. This shows that artificial hydration had a greater impact on the system in an axial direction than it did on the radial direction. The sensor array for radial stresses were situated away from the filter mats and were in areas where natural hydration had a greater influence on the system. The average stress and force data clearly show that artificial hydration played a key role on the stresses in the system. It is unclear what the stresses would have achieved if artificial hydration had been continued, or what the stresses would have been if the system was only hydrated in a natural manner over a much longer time. However, it is clear that the high swelling pressures encountered in the laboratory for high dry density bentonite would not have occurred in a full-scale KBS-3 setup.

Figure 16-38b shows the average pore pressures in Lasgit and this shows that the system had yet to reach hydraulic equilibrium by the end of the experiment. Pore pressure was established around Day 500, increasing the pore pressure in the pressure relief holes and at the deposition hole wall to ~2 000 kPa. From this time onwards, both of these sensor types decreased. This corresponded with the general decrease in pore pressure seen in the HRL as a result of drawdown of the tunnel and pumping of water from the Äspö HRL tunnels. Pore pressure in the system increased in both sensor types around Day 2550 over a 300-day period. The start of this increase corresponded with a pressure increase in UR909 and also with the pausing of artificial hydration. The actual cause of this behaviour is not certain but it likely derives from pore pressure variation in the surrounding rock mass. The pore pressure at the rock wall showed annual variation, whereas the pressure at the pressure relief holes did not. This confirms that the driving force for the annual feature derived within the deposition hole and not from the surrounding rock mass. Figure 16-38b also shows the average pore pressure within the bentonite. This showed that within the bentonite, the pore pressure took a longer to become established. By the end of artificial hydration at Day 3745 the pore pressure within the bentonite had not reached a magnitude comparable with the surrounding pore fluid. It is suggested that a further ~1 000 days may have been needed for average buffer pore pressure to be in equilibrium with the surrounding pore fluid pressure. When artificial hydration was stopped, the pore pressure within the buffer started to slowly decrease. This shows that the pore pressure was dictated by the artificial hydration. The pore pressure within the bentonite was strongly influenced by annual variation, with oscillations much greater in magnitude than seen at the rock wall. This feature was not dependent on artificial hydration as the same magnitude of oscillations were seen when artificial hydration was stopped.

Figure 16-38c shows the range of data for each sensor type. The range of data was generally greatest around Day 750 – 1500 and then the range tended to reduce. Comparing the data at the rock wall shows that up until when artificial hydration was stopped, the range in the axial stress in the bentonite and radial stress on the rock wall was reducing, while the range in pore pressures at the rock wall; pore pressure in the bentonite; and stress on the canister was increasing. This shows that stresses were homogenising, while pore pressures were not. The range (Figure 16-38c) and average (Figure 16-38a, b) of the data types shows that the system was not in equilibrium and was still developing, not only up to the ending artificial hydration at Day 3745 but also until the end of the test.

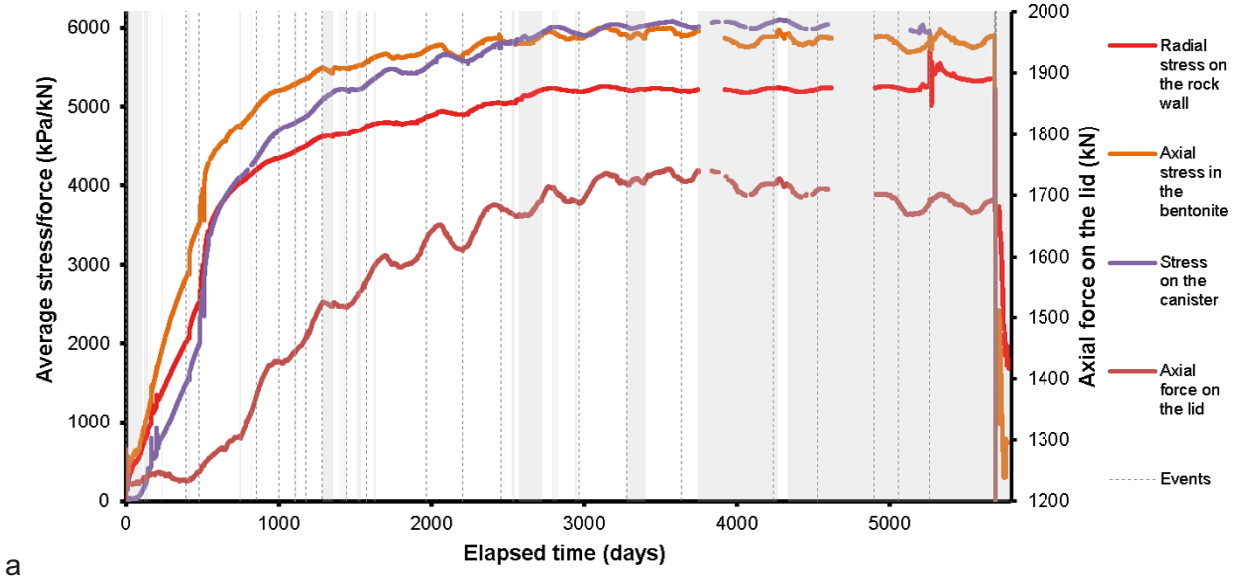

a

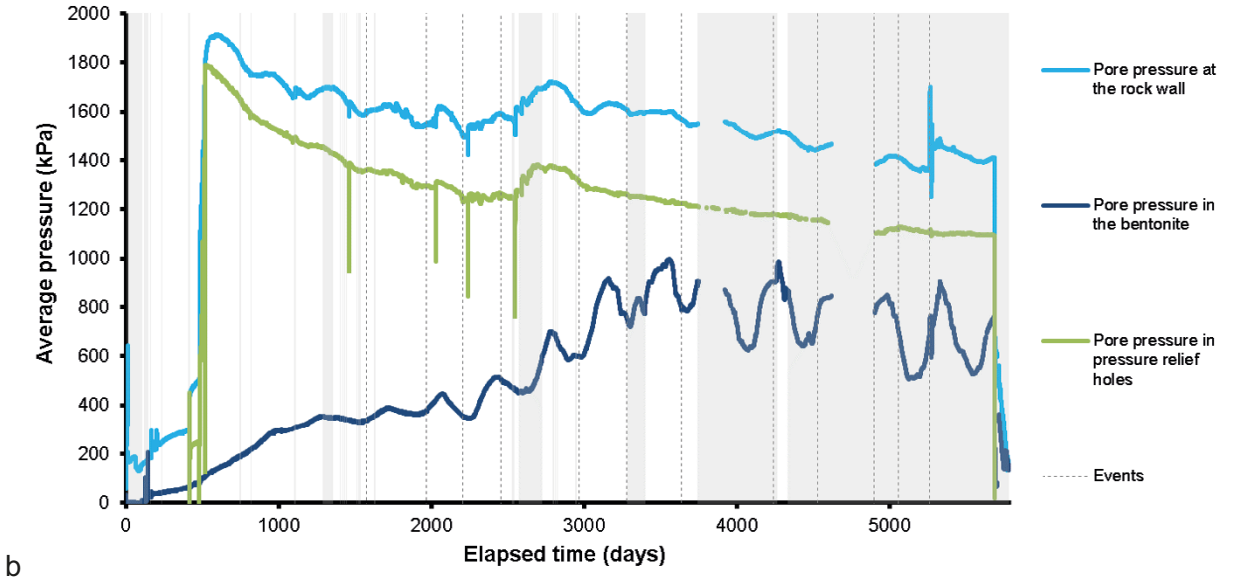

b

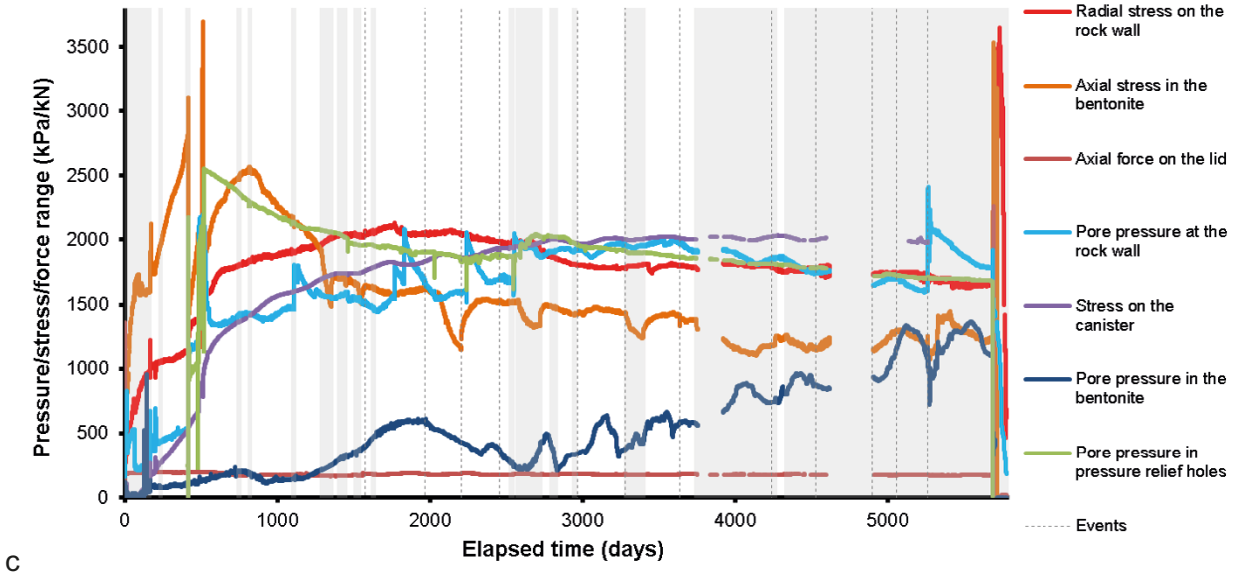

c

Figure 16-38. *Average of the stress and pore pressure sensor types for the complete Lasgit test history. a) Average of stress and force sensor types; b) Average of pore pressure sensor types; c) Range of each sensor type.*

16.8 Hydraulic testing

Many two-stage hydraulic tests were conducted during the course of the Lasgit experiment. The majority of these were in filters FL903 and FU910, with tests conducted before each gas injection test and after most. This allowed the hydraulic properties and specific storage to be examined as each test represented a snap-shot of the state of the buffer. Around Day 3500, most of the canister filters were tested. While these were a single snap shot of the hydraulic properties, it gave an indication of the variation in properties around the canister. The data were modelled using a simple 1-D model with flow assumed to be along a pipe of diameter equivalent to the filter diameter, with the pore pressure at the deposition hole wall used to define the boundary conditions.

Figure 16-39 shows the evolution of hydraulic properties for filters FL903 and FU910. For canister filter FL903, the hydraulic properties of the buffer reduced over the course of the test history (Figure 16-39a). At Day 870, hydraulic conductivity was 1.3×10^{-12} m s^{-1}, decreasing to 1.7×10^{-13} m s^{-1} at Day 5266. This represents a near order of magnitude reduction in conductivity over the 12-year period. However, it should be noted that the modelled data is quite variable. For most tests there was a fit for the high-pressure stage and the low-pressure stage, and the average, value but these also showed considerable spread. At the same time specific storage increased (Figure 16-39b), from 6.7×10^{-6} m^{-1} at Day 870 to 3.1×10^{-5} m^{-1} at Day 5266. For canister filter FU910, hydraulic conductivity also decreased from 1.7×10^{-12} m s^{-1} at Day 2086 to 7.8×10^{-13} m s^{-1} at Day 5235 (Figure 16-39c). This was considerably less of a reduction than seen at FL903. Over the same period specific storage increased from 2.1×10^{-6} m^{-1} to 8.8×10^{-6} m^{-1} (Figure 16-39d). These data show that the hydraulic properties of the buffer were continuing to evolve and reduce, at the injection filter locations, as the buffer matured. The system was far from attaining hydraulic equilibrium, even though the geotechnical data showed that the buffer was close to, or at, full saturation.

Figure 16-40 shows the hydraulic properties for seven two-step hydraulic tests conducted between Day 3360 and Day 3478. These are single snap shots of the properties of the buffer but show the heterogeneity around the canister. Filter FU911 showed the lowest hydraulic conductivity of 7.1×10^{-13} m s^{-1} with FU909 showing the highest conductivity of 4.2×10^{-12} m s^{-1} (Figure 16-40a). This shows a six-fold variation in hydraulic conductivity. Specific storage varied between a minimum of 6.3×10^{-6} m^{-1} for FM908 and a maximum of 1.1×10^{-5} m^{-1} for FM907 (Figure 16-40b). This shows limited variation. This snapshot of the buffer shows considerable variability around the canister and highlights that the zone surrounding the canister was variable in terms of the transport properties.

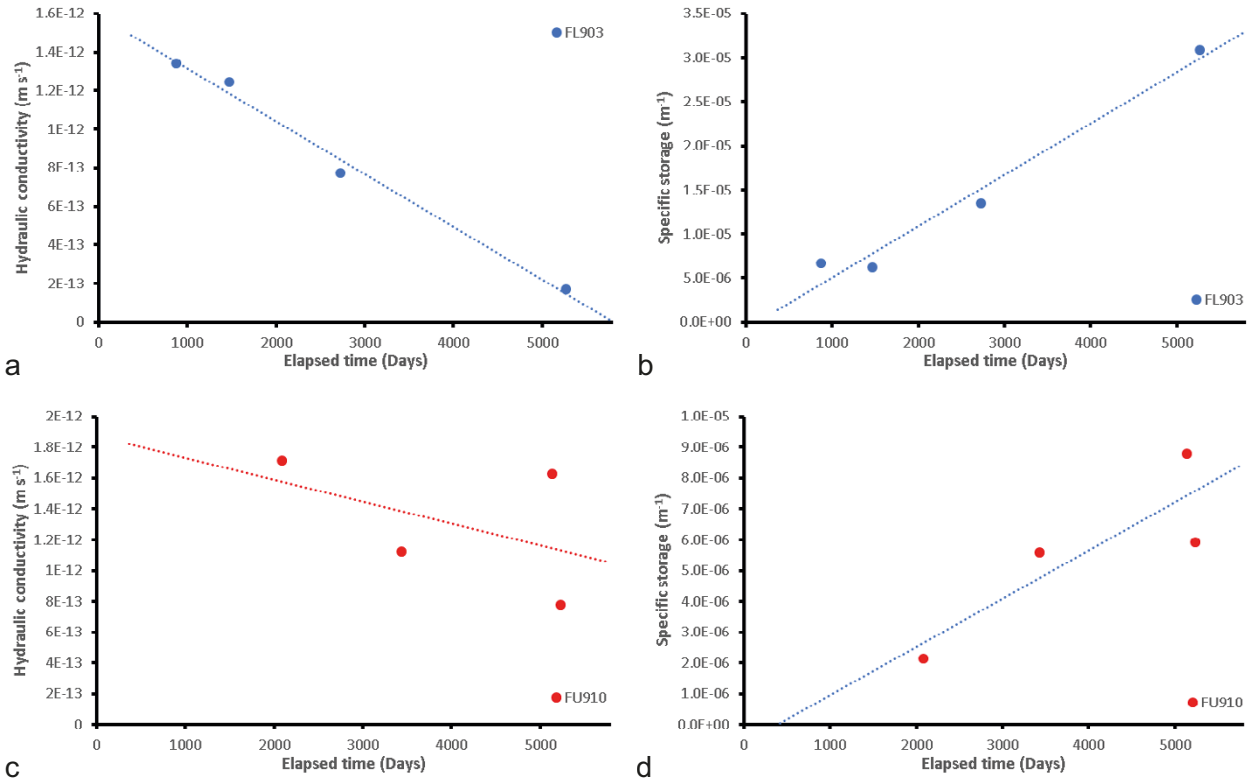

Figure 16-39. *Evolution of hydraulic properties at FL903 and FU910. a) Hydraulic conductivity of FL903; b) Specific storage of FL903; c) Hydraulic conductivity of FU910; d) Specific storage of FU910.*

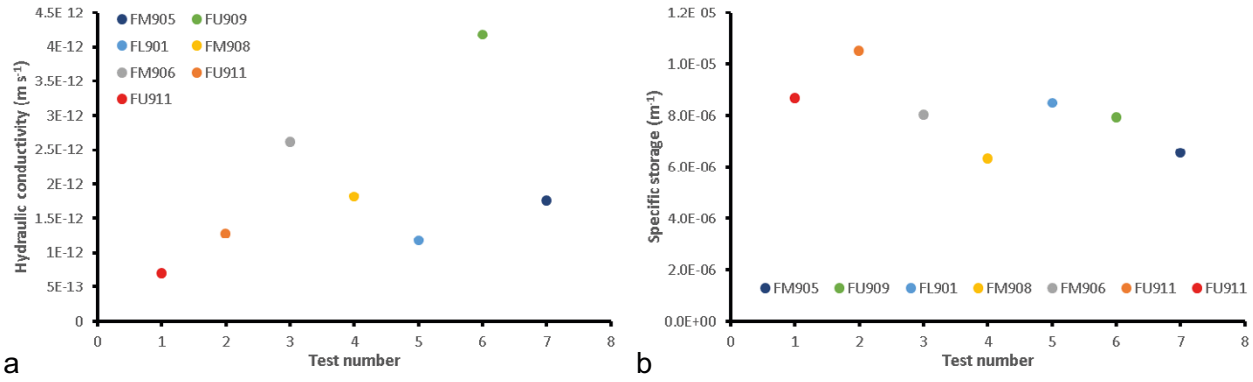

Figure 16-40. *Average of the stress and pore pressure sensor types for the complete Lasgit test history. a) Average of stress and force sensor types; b) Average of pore pressure sensor types; c) Range of each sensor type.*

16.9 Summary of the complete test history

This section outlines features of the boundary conditions of the Lasgit test over the full 5782-day period. These observations relate to the maturation of the buffer in response to both natural and artificial hydration. The main observations relate to annual variation, the effect of artificial hydration, pore pressure decay at the Äspö HRL, and maturation of the buffer. These observations can be split into two categories; 1) features of the test that are influenced by the experimental set-up that would not occur in a real KBS-3 disposal facility, and 2) natural influences on the system.

16.9.1 Comment on seasonal/annual variation

Once pore pressures and stresses had established early in the test, it was apparent that many of the system parameters displayed annual variation. These oscillations had a period of around one year. Annual variation was seen in the HRL temperature; canister temperature; pore pressure within the bentonite (UB); pore pressure at the wall rock (UR); radial stress (PR); the radial & axial stresses on the canister (PC); the force on the lid (LP); and the movement of the lid (DP) including stick-slip behaviour. It was important to determine whether these oscillations were natural or an artefact of the experimental setup and the way the test was conducted. Natural pore pressure in a fractured rock mass can vary as the water table varies over a year. This occurs when water recharge occurs at times of high rainfall and water levels drop in periods of dry weather. However, the pore pressure data from the pressure relief holes did not show the same annual variability, and if it was present in the data, the magnitude of the oscillations was small. This is not surprising as Äspö is close to the sea and therefore the water table will be very shallow and constant all year around. The pressure relief holes were hydraulically connected to the Lasgit experiment but represented a measure of hydraulic behaviour a small distance from the experiment. As the PRH data had an absence of strong annual variability it shows that the behaviour seen in the Lasgit experiment did not derive from natural fluctuations in pore pressure in response to water table changes. Temperature within the natural pore water can also cycle in response to temperature variations at the surface. However, this is unlikely to transfer to 420 m depth in such a rapid manner. The lag between pore water temperature and surface temperature would be expected to be much greater than seen. Therefore, it is unlikely that the annual variation was natural. However, natural variation of pore water pressure will occur in a closed KBS-3 disposal facility in response to climatic changes and variations in the water table.

As natural sources can be discounted as the primary driver for the annual variation fluctuations seen in the data, the source was investigated by looking at the temperature data within the deposition hole and the HRL. The greatest amplitude oscillation was observed in the HRL assembly tunnel where Lasgit was situated. Around 5 °C of temperature variation was seen. This was as a result of the air circulation system in the main tunnels not having good temperature nor humidity control and thus reflected the temperature at the surface. The minimum temperature of the oscillations was variable but was observed around Julian Day 53 (February 22nd). The variation reflected the natural variation in temperature at the surface at Äspö, with some minimums delayed by earlier mild winter weather. Examination of the canister temperature showed that the minimum temperature occurred in a more restricted time-frame generally around Julian Day 131 (May 11th). This showed a 78-day lag between the HRL temperature and canister temperature at depth. A total of 55 thermocouples were present within the bentonite as all pore pressure and stress sensors had a corresponding thermocouple for temperature compensation. This data clearly showed that the time lag between the HRL temperature and each sensor location increased with distance from the HRL tunnel. Towards the top of the deposition hole at a height of 751 cm the delay was just 29 days, whereas in the base of the deposition hole the delay was 130 days. The amplitude of the oscillations also showed a clear relationship with depth. In the bentonite above the canister at a height of 751 cm the amplitude was ~2.7 °C, whereas at the base of the deposition hole it was ~0.5 °C. This data clearly showed that temperature oscillations in the HRL were both attenuated, and time-lagged, with distance away from HRL tunnel. To be free of the temperature affect the deposition hole would have had to have been substantially deeper. However, the data suggests that the Monel pipe that connected the canister with the Lasgit laboratory was also a contributory factor in transferring heat from the main HRL tunnel to the canister and Lasgit system. This would not be part of a KBS-3 disposal hole and thus is an experimental artefact of the Lasgit setup. However, the transfer of heat to the system was not just from the Monel pipe, since the response at the deposition hole wall would be delayed further than was observed. This suggests that the pore fluid in the surrounding rock mass was also transporting heat into the system. In a real KBS-3 facility, the tunnel would be back-filled and this

temperature variation would not be present. However, the data show that the KBS-3 system is very capable at transferring heat and that any changes in temperature related to variations in climate would result in temperature variations in a deposition hole. The distribution in delay of temperature minima was a simple one with distance from the top of the deposition hole, but variation was seen around the deposition hole that may reflect variations in fluid flow within the fractured rock mass.

The variation in temperature would be largely irrelevant if oscillations were not seen in the stress and pore pressure data, since the phenomena could be discounted as an experimental artefact. However, the annual variation was seen in the stress and displacement data, in some cases strongly. Pore pressure within the bentonite buffer showed strong annual variation, probably because drainage distances were longer, with up to 600 kPa seen at level UB16 at the top of the buffer and close to the HRL tunnel. This was a huge variation given that the magnitude of the average pore pressure at this level was < 1 000 kPa. Less significant variation was seen in the pore pressure data at the deposition hole wall. In this dataset it was clear that the oscillation was similar at most heights in the deposition hole and that the oscillation was largely absent from the base of the hole because of all the fractures and more transmissive boundary condition. Differences in the time of the oscillation were seen with depth, meaning that the delay and attenuation in the signal seen in temperature was also reflected in the pore pressure response. Similar observations were seen in the radial stress data at the deposition hole wall, with a variation in delay with depth and attenuation of the oscillations. Axial stress within the buffer showed considerably higher amplitude oscillation above the canister than seen below, again showing attenuation with distance from the HRL tunnel.

Lasgit was influenced by the varying air temperature within the HRL tunnel. This resulted in oscillations in temperature, that were attenuated and delayed with distance from the tunnel. The result of this variation in temperature was oscillations on an annual basis of stress and pore pressure. Heat was transferred from the tunnel to the canister and also to the pore fluid in the surrounding rock mass. The different components of the KBS-3 system thermally expand at varying degrees, which may explain some of the changes in pore pressure and stress. However, thermal variation of the rock mass can alter pore pressure and this would in turn change stresses as the swelling response. It must be noted that the pressure relief holes saw little annual variation and therefore thermally induced pore pressure was unlikely. Therefore, the primary driving force for the features seen was the conduction of heat along the Monel pipe to the canister and thermal expansion of the canister. The thermal expansion of the rock anchors and retaining lid may also have had an influence, although this is less certain as the load cells used were not thermally compensated. The pressurisation of the canister at the start of the Full Canister Test showed that small mechanical deformation could significantly increase pore pressure and stress within the deposition hole. Heat was also transferred to the buffer and thermal expansion/contraction of the bentonite may also have been a contributory factor. While the actual disposal scenario will not likely have such a thermally induced annual variation, the data in Lasgit shows that considerable pore pressure and stress changes can be induced by small changes in temperature of the canister, driven by only a 5 °C variation in tunnel temperature. It should be noted that annual temperature cycling may be apparent in the early emplacement period when the disposal facility is still in operation.

16.9.2 Comment on artificial hydration

The aging infrastructure of Lasgit meant that certain key parts of the experimental set-up failed during the test. The decision was taken to end artificial hydration at Day 3745 and this impacted the data. At the outset of Lasgit, artificial hydration was vital in order to speed the hydration of the buffer and to get to a condition close to hydraulic equilibrium as a result of full saturation of the buffer. Modelling had shown that natural hydration alone would result in an experiment that took excessive time to get to full saturation. The filter mats in the system were in operation for most of the test history up to Day 3745, apart from two periods of prolonged failure of the equipment. This allowed the system to generate significant stresses and pore pressures, with the geotechnical data at the end of the experiment suggesting the buffer was close to full saturation. Pore pressure was still developing within the buffer itself and net pressure data shows that the system was not yet in stress or hydraulic equilibrium. This meant that the stress within the system was still increasing at the time of ending artificial hydration. As a result, many sensors either reached a plateau or decreased in magnitude. As a result, the data appeared to reach an equilibrium end-state, where-as that was not the case. In order to highlight this, all boundary condition graphs in this report show when artificial hydration was paused. It is uncertain what stress level the system would have attained had artificial hydration continued, or if only natural hydration had

been allowed. It is apparent that the pore pressure within the bentonite would have reached equilibrium within 10s of years but it is less clear what the ultimate radial stress condition would have been in the system and how long this would have taken. It is not expected that pore pressure and stress would reach high levels that would result in high gas pressures as expected swelling pressure was calculated to be 3 970 kPa. While the buffer was fully saturated, hydraulic disequilibrium was still apparent.

16.9.3 Comment on pore pressure decay at Äspö

Pore pressure measured within Lasgit at the deposition hole and within the pressure relief holes all showed a decrease in time once pore pressure had been established by around Day 500. This was of concern and could have resulted from leakage of the pressure relief hole packers. A stable pore pressure boundary condition was desired for the Lasgit experiment and failure of experimental equipment was not favourable, especially if this resulted in the long-term reduction of boundary conditions. As with temperature fluctuations, Lasgit was prone to influence from outside of the immediate experimental area. The Äspö HRL included many boreholes that have been monitored for much longer than the Lasgit experiment. Examination of data from these showed that the reduction in pore pressure occurred outside of Lasgit. This was as a result of drawdown of pressure as a result of pumping of water from the HRL tunnel network and was an on-going phenomenon. This meant that the surrounding rock mass had an evolving pore pressure that was outside of the control of the experiment. This boundary condition change would not occur in a backfilled disposal facility, once pore pressure had been re-established post-back fill and post-closure. Pore pressure will have an influence on stresses in the system since it controls total stress. The test history showed an increase in stress over the Lasgit test, yet pore pressure had decreased at the deposition hole wall. If pore pressure been more constant it is expected that stresses would have been greater, proportional to the pore pressure drop experienced (~300 kPa).

16.9.4 Comment on maturation of the buffer

Ideally, the KBS-3 system should mature to full saturation, with limited heterogeneity in the deposition hole in terms of stress and pore pressure. Net pressure should evolved to a small finite value, as should suction. The saturation of the bentonite should reach unity and not vary significantly within the deposition hole. This was not the case. It was impractical to run Lasgit for longer and the gradual failure of experimental components showed that the system was slowly failing. However, even within this, non-ideal, context clear conclusions can still be drawn.

The establishment of pore pressure around Day 500 increased all of the stresses and forces in the system in a similar manner. The average data showed that the system settled by Day 1500 with all sensor types continuing to record increase in pore pressure. All of the sensor types were affected by the pausing of artificial hydration starting at Days 2533, 3284, Day 3745. The ending of artificial hydration at Day 3745 resulted in all sensor readings either reaching a plateau or decreasing. The radial stress and stress on the canister plateaued, whereas the axial stress in the bentonite and axial force on the lid decreased. This shows that artificial hydration had more of an impact on the system in an axial direction than it did in the radial direction. For pore pressure, once pressure was established as a result of the pressure relief holes, pore pressure in the system decreased. The pore pressure in the bentonite itself took some time to increase but was still increasing at the time when artificial hydration was halted. As stresses and the pore pressure in the bentonite were continuing to increase, it shows that the system had yet to reach an equilibrium point and was still evolving. However, the distribution of both pore pressure and radial stress at the deposition hole wall showed that the heterogeneity in these parameters was “locked-in” early in the test history and were established as early as Day 500. The heterogeneity shown by the distribution did not alter, even though the magnitude of the parameters did. The system showed no sign of homogenising in either stress of pore pressure. It is unlikely that prolonged time much greater than the length of the Lasgit experiment would have changed this, with the locked-in heterogeneity persisting. It is likely to have derived from subtle variations in the thickness of the pellet region; difference in the fracture network around the canister; and how well the pellets and bentonite were saturated early in the test history. It was noted that pellets were flushed from the hole in the early test history and this have resulted in differential quantities in bentonite around the hole. However, no such variation was noted during the sampling of the buffer during decommissioning. Net pressure showed that the system was far from equilibrium. A finite net-pressure of ~3 000 kPa had formed and stabilised by Day 1000, but this reduced as a result of the ending of artificial hydration. The locus of net pressure progressed throughout the test history but still showed a heterogeneous system.

The final observations of buffer maturity come from the results of hydraulic testing and this can be compared with the geotechnical observations. Hydraulic conductivity of repeat testing at canister filters showed a reduction with time. At Day 870, hydraulic conductivity was 1.3×10^{-12} m s^{-1}, decreasing to 1.7×10^{-13} m s^{-1} at Day 5266. This represented a near order of magnitude reduction in conductivity over a 12-year period. For injection filter FU910 the reduction was not as great, but reduced from 1.7×10^{-12} m s^{-1} at Day 2086 to 7.8×10^{-13} m s^{-1} at Day 5235. Over the same period, specific storage increased at both locations. There is limited data and considerable scatter in the results but there does not appear to be a defined asymptote to the changes as the buffer continued to mature. Most of the canister filters were hydraulically tested around Day 3500. This showed a variable result with hydraulic conductivity between 7.1×10^{-13} m s^{-1} and 4.2×10^{-12} m s^{-1}. This showed that the transport properties close to the canister were varied over a 6-fold range. Considerable variation was seen in the geotechnical properties close to the canister and in the pellet region. This may reflect the hydraulic conductivity heterogeneity. However, the geotechnical data showed that the average saturation for the 1 522 samples in the buffer was 0.999, meaning that the buffer was nearly fully saturated. The geotechnical data also showed a distinct difference between the properties of segments and rings before emplacement, which at the end of the test had homogenised. Therefore, the bentonite buffer appeared to be in equilibrium, but was not in hydraulic or stress equilibrium and was continuing to mature.

17 Gas Injection Test observations

In previous sections each individual gas test was discussed. Some observations were made comparing the different tests but this was limited. In this section the observations from the gas tests are compared in combination with the observations of the boundary stresses and maturity of the buffer, the controls on gas migration are also discussed. Firstly, the four gas injection tests conducted in canister filter FL903 are compared (Gas Injection Tests 1, 2, 4, and 6). Secondly, the two gas injection tests conducted in canister filter FU910 are compared (Gas Injection Tests 3 and 5). Finally, all gas injection tests, including the Full Canister Test are compared to examine similarities and differences in gas transport behaviour at different locations on the canister surface.

17.1 Gas Injection Tests in canister filter FL903

Four tests were conducted in canister filter FL903 on the lower array of canister filters at a height of 1 709 mm in the deposition hole. The first test, Gas Injection Test 1 (GT1) was conducted between Day 917 and Day 1010; Gas Injection Test 2 (GT2) between Day 1577 and Day 1967; Gas Injection Test 4 (GT4) between Day 2988 and Day 3283; while the final test, Gas Injection Test 6 (GT6) was conducted between Day 5230 and Day 5263. This means there was 917 days between the start of Lasgit and GT1; 567 days between GT1 and GT2; 1 020 days between GT2 and GT4; and 1 947 days between GT4 and GT6. The main data relating to the tests conducted in filter FL903 are summarised in Table 17-1.

Table 17-1. Data relating to gas injection tests conducted in canister filter FL903.

	Test	Gas ramps	Start (Days)	End (Days)	Time gap (Days)	Peak pressure (kPa)	Time at peak (Days)	Gas entry pressure (kPa)
1	GT1	2	917.32	1 010.03	917.32	5 666	972.24	-
2	GT2	4	1 577.40	1 967.98	567.36	5 868	1 769.65	-
3	GT4	4	2 988.08	3 283.02	1 020.11	6 174	3 205.31	6 141
4	GT6	1	5 230.29	5 263.95	1 947.26	5 827	5 235.96	6 382

Figure 17-1 compares the gas pressure and flow data for all four tests conducted in FL903, with the gas pressure compared in more detail in Figure 17-2. Figure 17-1 shows that the gas flow into the system was different for all of the four tests. This potentially means that the results could have varied if the processes controlling gas entry were dependent on the rate of pressurisation. Variations in flow rate can derive from difference in the starting volume and if processes are also dependent on the volume of the gas, this could introduce a further variation to the data. However, the volumes of gas were not significantly different and the variation in pressurisation rate was only around 14.5 times faster in GT1 compared with GT2. For significant variation in behaviour it would be expected that orders of magnitude variation in flow rate would be required to observe different behaviour as gas fracturing has not be seen in the laboratory at similar pressurisation rates (Mechanism 4; Marschall et al. 2005). This must be the case, otherwise the rate employed during laboratory testing or during Lasgit would be un-representative since the pressure increase rate used in the tests conducted here were several orders of magnitude greater than that expected during gas generation in the canister.

Figure 17-1 shows difference in response for flow into the clay. In GT1, flow into the clay slowly increased during the final gas ramp. This suggests that gas started to enter the clay but could also represent the loss of gas through diffusion and solution. In the other gas injection tests, flow into the clay was generally low and only increased around the time of peak pressure. As GT1 was the first test that was conducted in FL903, the difference might be related to gas saturation of the clay around the injection filter. The buffer would have been unsaturated with respect to the gas, and the first test would have had more gas going into solution than in subsequent tests. GT1 showed a pre-cursor flow event, which was largely absent from the repeat tests. This suggests that gas started to enter the buffer at a lower pressure than peak pressure but that pathways soon became unstable and stopped propagating as gas pressure continued to increase at a rate similar to that seen before the pre-cursor flow event.

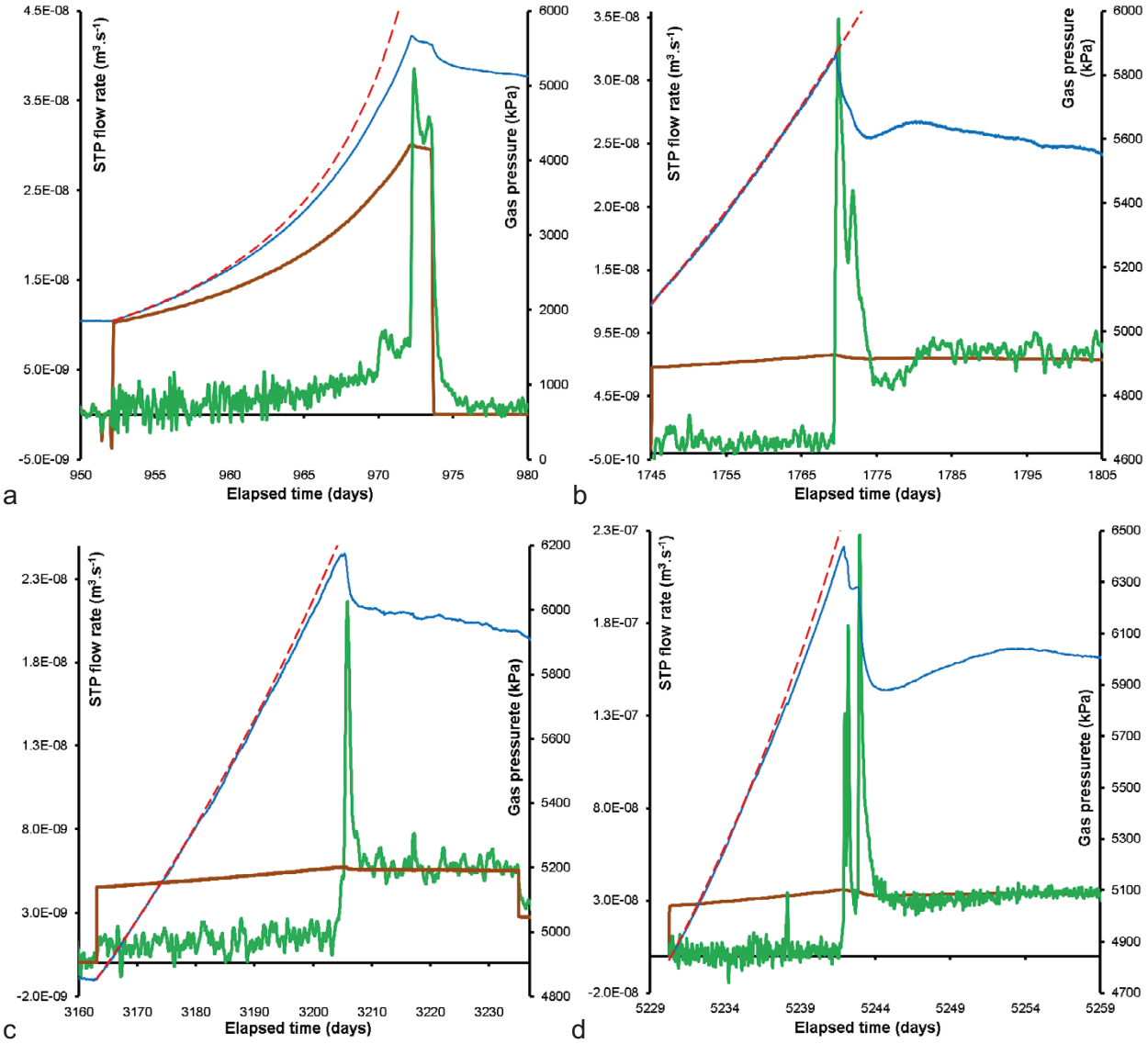

Figure 17-1. *Comparison of gas entry behaviour for the four tests conducted in canister filter FL903. a) Gas Injection Test 1; b) Gas Injection Test 2; Gas Injection Test 4; Gas Injection Test 6.*

At peak pressure, flow greatly increased and peaked. In GT1 two peaks were seen, a similar pattern was observed in GT2. However, GT4 only had a single peak in flow, while GT6 showed at least 3 peaks. In GT1 and GT2, the initial peak was the greatest flow into the buffer, whereas in GT6, the three peaks increased in magnitude for successive events. A peak in flow is created as new volume is generated, i.e., as pathways form. The effective volume occupied by the gas increases, resulting in a reduction in pressure. When a subsequent peak is observed it means that the effective volume occupied by the gas has increased again. This might be as a result of encountering a sink (void or porous region), the formation of a new pathway network or might mean that gas flowed along existing pathways out of the buffer. The peaks may also indicate that gas has intercepted a different type of buffer component, for example at the canister filter, gas can either enter the clay or move along the clay/canister interface. It is likely that these two types of buffer component will have different properties.

Early in the test, the bentonite rings swelled and closed the 10 mm engineered gap between the canister and buffer. This means that the bentonite in contact with the canister had swelled and will have had slightly different properties to that of deep within the buffer. This was observed in differences in geotechnical properties close to the canister compared to within the middle of the annular rings. Therefore, gas was more likely to move within this region at, or near, the canister/buffer interface. However, to exit the KBS-3 system, it had to either propagate through the buffer, or exploit an interface been individual rings. It was interpreted in GT1 that gas moved initially down the canister following

the prevailing stress gradient, before exiting the deposition hole through the interface between rings R1 and R2. The first peak seen in GT1 thus represents the formation of pathways and movement along the canister/buffer zone, while the second peak represents the pathways exploiting weaknesses between bentonite rings.

During decommissioning, it was noted that negligible self-healing had occurred between bentonite blocks and during excavation, clean surfaces were created when the buffer had been extracted. One interface was cored so that it could be tested in the laboratory but it was impossible to core the buffer interface without the two sides detaching. In Lasgit, it was expected that initial formation of pathways would require the greatest energy and that the propagation of pathways would be easier. GT6 suggests that the initial formation of pathways resulted in new pathway formation that encountered two weaknesses or sinks. It is likely that the second peak occurred as a pre-existing open pathway was intercepted, with the third peak because of intercepting an interface between two rings. This third peak in flow resulted in considerable loss of pressure suggesting that gas had exited the deposition hole.

GT2 and GT6 had similar characteristics, that match flow responses in the laboratory. Flow into the clay rapidly decreased as gas pressure loss slowed, with the flowrate into the clay becoming lower than the flowrate into the system, i.e., gas pressure increased. This over- and under-shooting of flow has been seen in laboratory-scale experiments (e.g., Harrington and Horseman 2003, Harrington et al. 2017). With time, flow into the clay matched flow into the system, meaning that steady-state flow was established. Test GT1 was not conducted for long enough to know whether it would have seen the same behaviour. However, GT4 just showed a single peak in flow, resulting in a loss of gas pressure followed by a stable reduction of gas pressure. This suggests that pathways formed in previous tests were re-activated with relative ease.

The qualitative gas flow behaviour shown in Figure 17-1 was similar for all four tests, apart from the differences that have been accounted for above. GT2 was conducted using neon as a tracer, instead of the usual helium. There was no significant difference for GT2 to suggest that the type of gas used had an influence on the gas transport behaviour.

Figure 17-2 compares the gas pressure result for all four tests conducted in FL903. The data have been normalised so that peak pressure occurred at a time of 0 days. The individual gas tests have then been transposed about the y-axis in order to compare the response in Figure 17-2a. This figure highlights the differences in pressurisation rate, as shown by the different slopes seen for the four tests up until the time of peak pressure. However, comparisons can still be made. After peak pressure, the gas pressure rapidly reduced and in three of the tests this occurred in two events, the exception being GT4 with just a single reduction event. In GT2 and GT6 gas pressure recovered after an initial drop in pressure. This could be explained by propagating pathway(s) reaching the outside of the deposition hole or that pathway propagation continued along new paths. The pressurised pathway would propagate until it reached the outside of the buffer, resulting in the loss of gas, the pressure in the conductive pathway reducing and the pathway contracting slightly. This results in less gas movement and the gas pressure increases until the pathway dilates sufficiently that gas flow is steady-state and the pressure reduces at a constant rate. Eventually, gas pressure will reduce to a point that the gas pathway is unstable and closes, resulting in an increase in gas pressure once more until with the pathway is re-opened or a new pathway is formed.

Figure 17-2b shows the pressure data corrected for pressurisation rate. Data were corrected so that all tests had the same slope of pressure increase up until peak gas pressure. To achieve this, time was adjusted by multiplying by 14.5, 1.08, and 5 for GT1, GT4, and GT6 respectively so that tests showed the same pressurisation rate as GT2. This shows that GT2, GT4, and GT6 progressed to a similar rate of pressure loss as shown by the black dashed line. This was the pressure loss of a pathway from FL903 to the surrounding wall rock in the deposition hole. Test GT1 has a similar slope, although the data is limited. This suggests that the processes governing flow along a conductive pathway were not pressurisation rate dependent. Comparing Figure 17-2a and Figure 17-2b shows an additional pressurisation-rate independent feature. Figure 17-2a shows that the pressure decrease and recovery in GT2 and GT6 both took about 10 days to create a secondary peak in pressure, irrespective of pressurisation rate. When the data were corrected for flow rate (Figure 17-2b), the features now had considerable different forms, with GT2 recovering in 10 days compared with 60 days in the corrected data for GT6. Figure 17-2b shows that GT1 did not see the same initial pressure decrease as the subsequent gas injection tests. This suggests that GT2, GT4, and GT6 exploited pathways formed by GT1 and that the buffer had not fully self-healed following the first gas test.

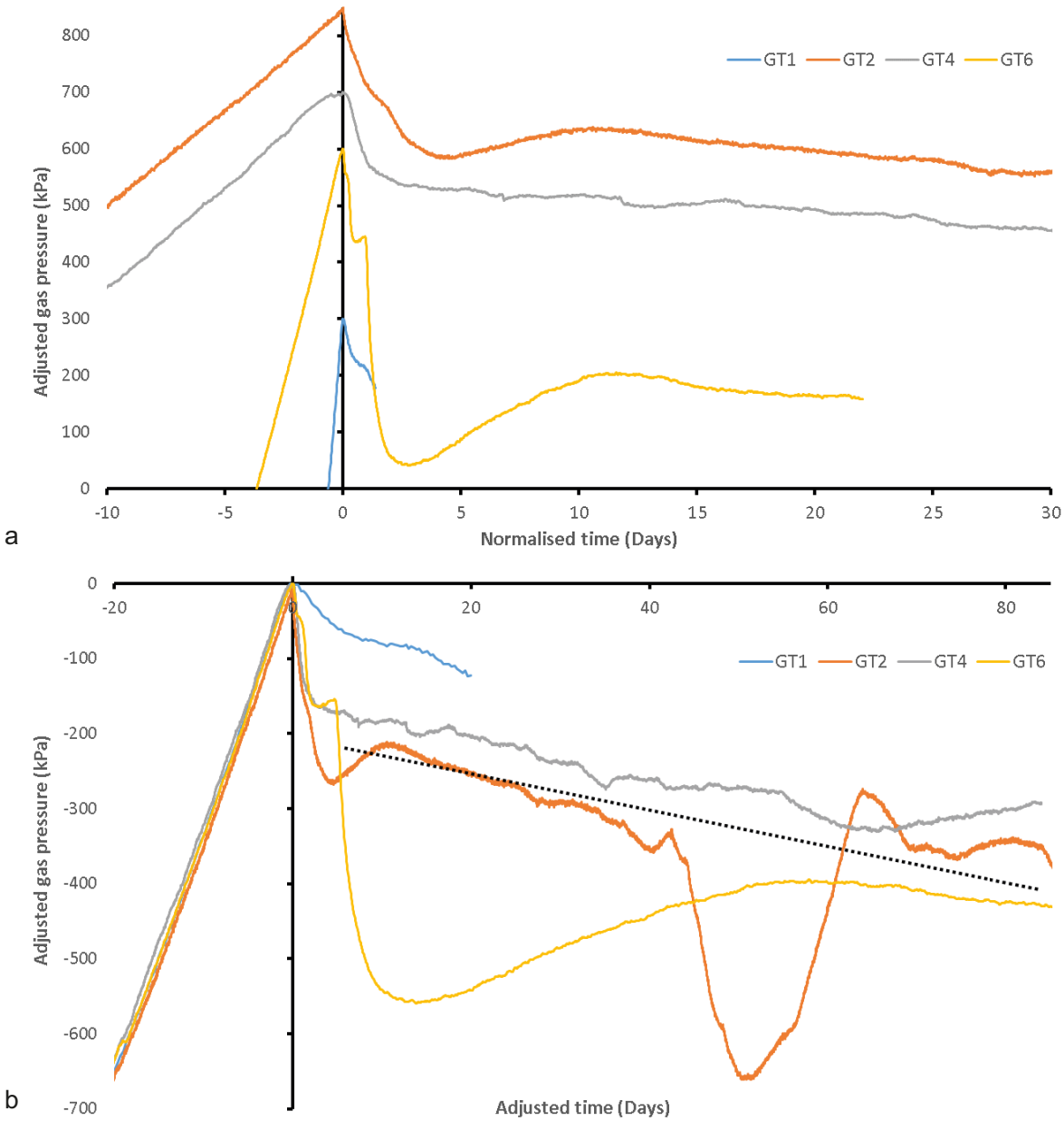

Figure 17-2. *Comparison of gas pressure for the four tests conducted in canister filter FL903. a) Gas pressure around peak pressure for all four tests; b) Gas pressure adjusted to correct for different pressurisation rates.*

Figure 17-3 compares the response seen in selected pore pressure (UR) sensors around the time of peak stress and gas entry. Test GT1 (Figure 17-3a) saw a distinctive form in UR906. Pressure started to increase, before a secondary feature resulted in a much greater pressure increase. This relatively quickly peaked and then decayed back to the starting pressure over several days. Several other sensors showed a single peak of similar form to the initial pressure rise seen in UR906, while UR909 saw a pressure decrease. During GT2 (Figure 17-3b), the form of UG905 was very similar, with a pressure increase similar to that seen in GT1. Sensor UR909 also decreased, as seen in GT1. However, the pressure increase at other locations was largely absent. This may suggest that GT1 showed virgin formation of pathways, with GT2 re-activating these pathways. Test GT4 showed a different response (Figure 17-3c). Small steps in pore pressure were seen in UR905, with UR908 showing the greatest increase in pore pressure. This suggests that GT4 showed different propagation response than GT1 and GT2 and that some new pathways formed. Test GT6 (Figure 17-3d) then showed similar response to GT1 and GT2, with some comparison to GT4. UR905 was again the dominant pore pressure response but as in GT4, UR908 also showed pressure increase. This suggests that features formed in GT1 and reactivated in GT2 were again reactivated but additional features formed in GT4 were also reactivated. The form of the response for GT6 is more similar to GT1 and may suggest that a degree of self-sealing had occurred.

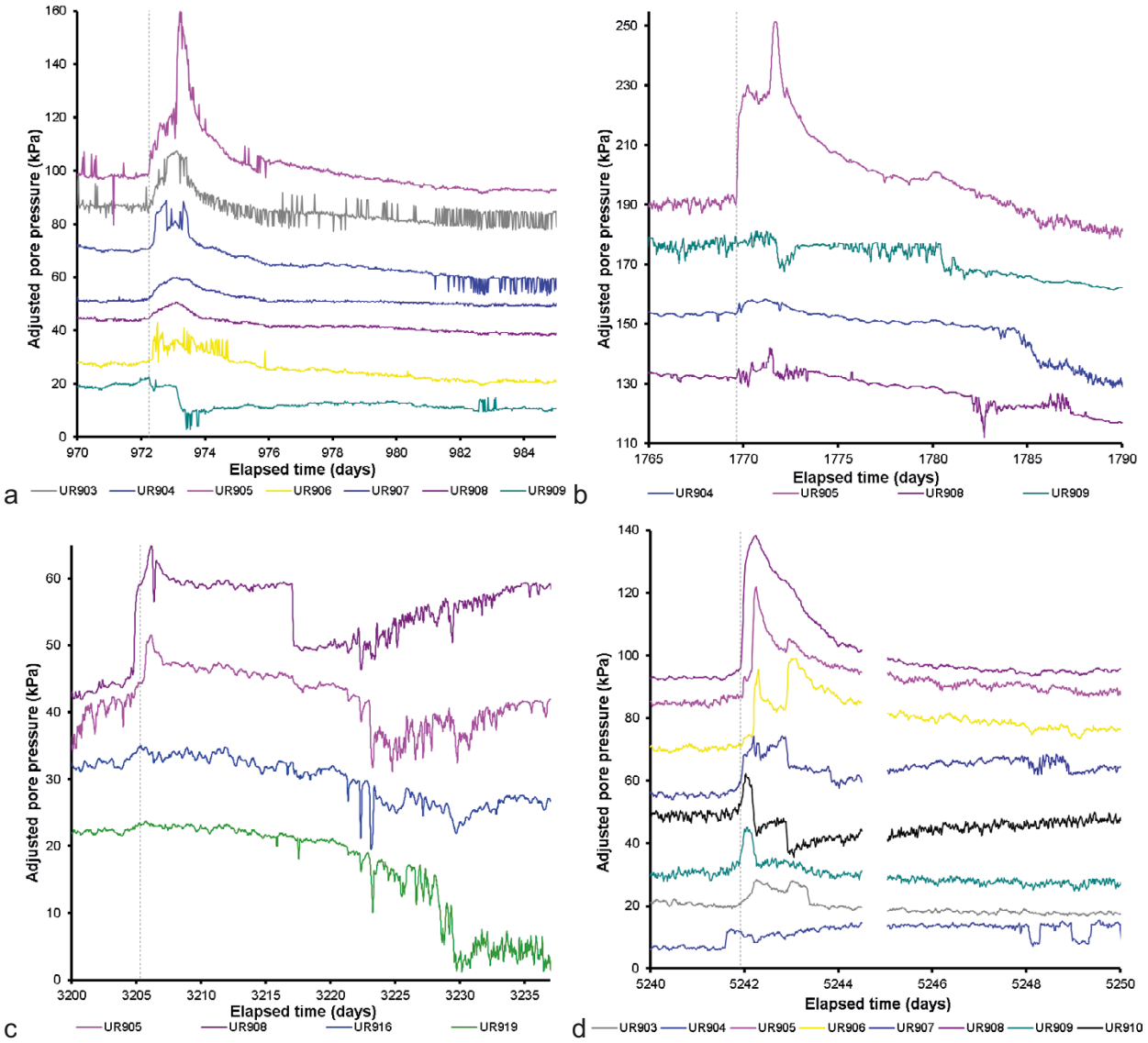

Figure 17-3. *Pore pressure observed in a selection of sensors close to FL903 around peak gas pressure. a) Gas Injection Test 1; b) Gas Injection Test 2; c) Gas Injection Test 4; d) Gas Injection Test 6. Each sensor has been adjusted about the y-axis for display purposes. Gas peak pressure is highlighted as a dashed event line.*

Figure 17-4 compares the response observed in selected radial stress (PR) sensors around the time of peak pressure and gas entry. In GT1, PR905 and PR906 showed the dominant response (Figure 17-4a). Stress increased over nearly a day, until peaking and then taking several days to decay. The response was seen in several locations, with PR909 showing a decrease in stress. Similarities were seen in GT2 (Figure 17-4b), with PR906 now being the dominant feature, with UR905 also showing considerable stress increase. However, the form of the result was subtly different, with a sharper peak and more rapid stress drop compared with the gradual reduction in stress seen in GT1. As with GT1, PR909 decreased in stress. As with pore pressure, radial stress showed a different form in GT4 compared with GT1 and GT2 (Figure 17-4c). Stress increases were considerably lower in magnitude with a more step-like response for PR906. Sensor PR907 showed a response and as with pore pressure, suggests that the direction of gas migration was different for this gas test. In the final gas test, GT6 (Figure 17-4d), the response was different to that seen in GT1 and GT2. For pore pressure, the responses of GT1, GT2, and GT6 were similar but for radial stress, GT6 differs from GT1 and GT2. This time, a stepped response in stress was seen, with little stress decay after the increase. Sensors PR905 and PR906 showed the dominant response as seen in GT1 and GT2 but with the additional response of PR904, as seen in GT4. For this test, PR909 showed a stress increase and peak, whereas in the other gas injection tests this location saw a stress reduction. This time, PR910 showed the stress reduction.

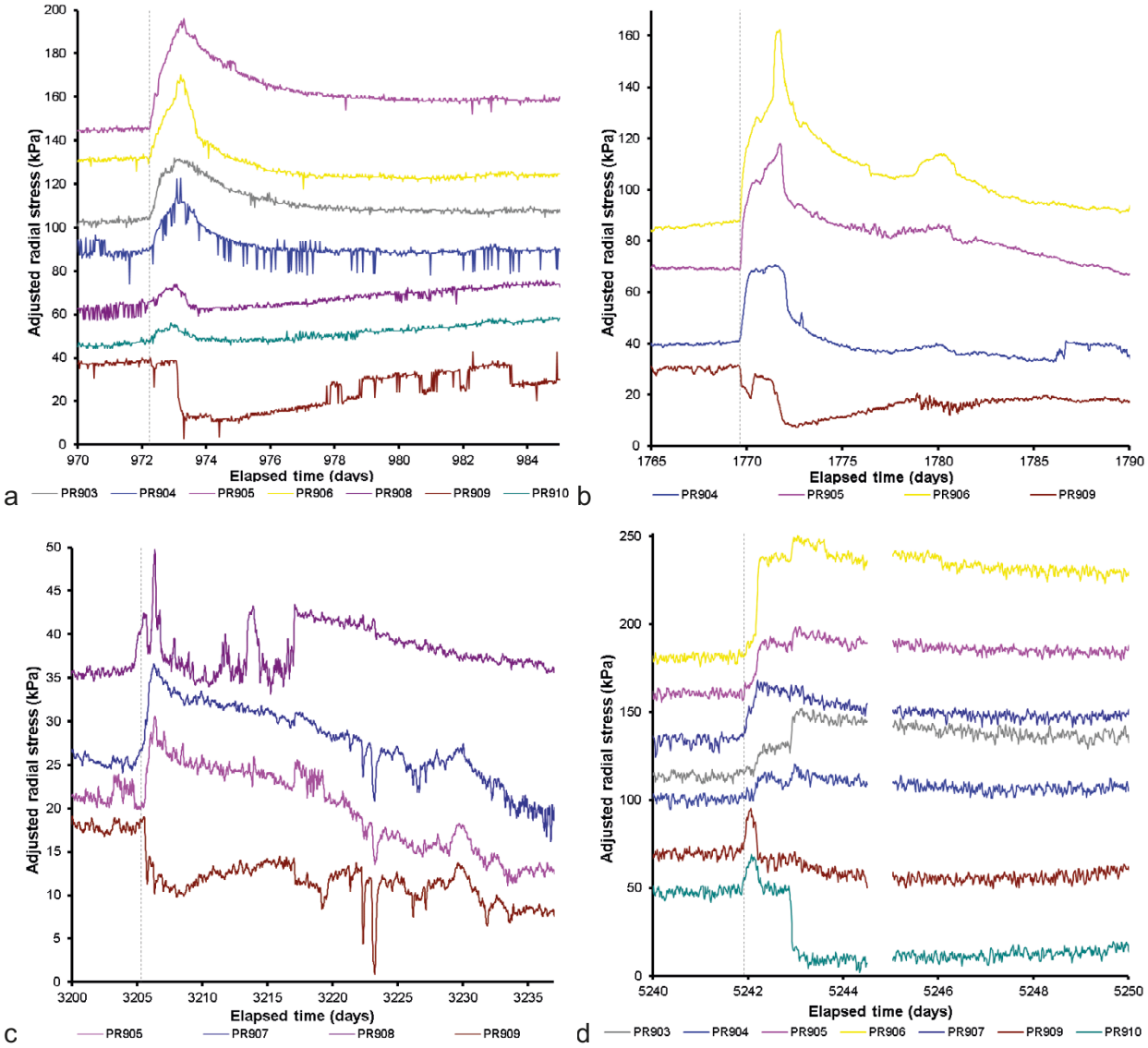

Figure 17-4. *Radial stresses observed in a selection of sensors close to FL903 around peak gas pressure. a) Gas Injection Test 1; b) Gas Injection Test 2; c) Gas Injection Test 4; d) Gas Injection Test 6. Each sensor has been adjusted about the y-axis for display purposes. Gas peak pressure is highlighted as a dashed event line.*

The pore pressure and radial stress responses (Figure 17-3, Figure 17-4) show that in GT1 new pathways formed in the buffer. Certain characteristics suggest that gas pathway propagation was in a similar direction, possibly re-opening pathways. However, GT4 showed a different response and that gas movement was in a different direction to GT1 and GT2 and not just through the re-establishment of pathways formed in the previous tests, i.e. pathways had self-sealed. The final gas injection test then showed gas propagation in the directions that match all three previous gas injection tests and may show that pathways formed in these tests were re-established.

Figure 17-5 shows additional features for GT2 and GT4 that are relevant to the comparison to tests. In GT2, flow was continued after gas entry for much longer than in GT1 (Figure 17-5a). This shows a series of over- and under-shoots of flow into the clay, with periods of pressure decay, recovery, and peak behaviour. As stated in GT2 earlier, the red area shown in Figure 17-5a occurred when a leak occurred as an air actuated valve failed to operate. It is possible that the pressure decay around Day 1810 may have been a similar event, but it is unlikely, it is probable that a prominent gas pathway had formed, resulting in a loss of gas pressure. The reducing pressure resulted in the pathway closing, either partially or completely, resulting in an increase gas pressure, before a secondary peak suggests the re-establishment of the pathway out of the buffer, or the formation of a new pathway within the buffer. Following the experimental artefact around Day 1865 and the re-establishment of gas pressure, the pressure started to rise, until another peak was encountered. It is worth noting that the gas peaks around Day 1832 and Day 1898 were of similar magnitude and the reductions in pressure at Day 1770 following peak stress, Day 1815, and Day 1900 all have similar slope. Therefore, the re-establishment of a gas pathway occurred at the same pressure, and the rate of pathway growth is similar. This shows that the physics driving gas pathway formation and propagation is repeatable.

Figure 17-5b shows the flow result for Gas Injection Test 4. This test had a single peak in flow and the system quickly established steady state flow, with gas pressure slowly reducing at a constant rate. Flowrate into the system was approximately halved, with flow into the clay quickly reducing to match flow into the system. This changed the slope of the pressure decay in filter FL903, becoming almost level. Flow into the system then reduced for a second time. So that flow into the clay again was almost the same as flow into the system. Again, the slope of the gas injection pressure changed and this time gas pressure started to increase. This suggests that the aperture of the conductive pathways was flow rate dependent. As flow was reduced, the pathways contracted sufficiently that the flow into the clay was less than the flow into the system. The degree of dilation of the pathways being flow rate dependent is a fundamental observation.

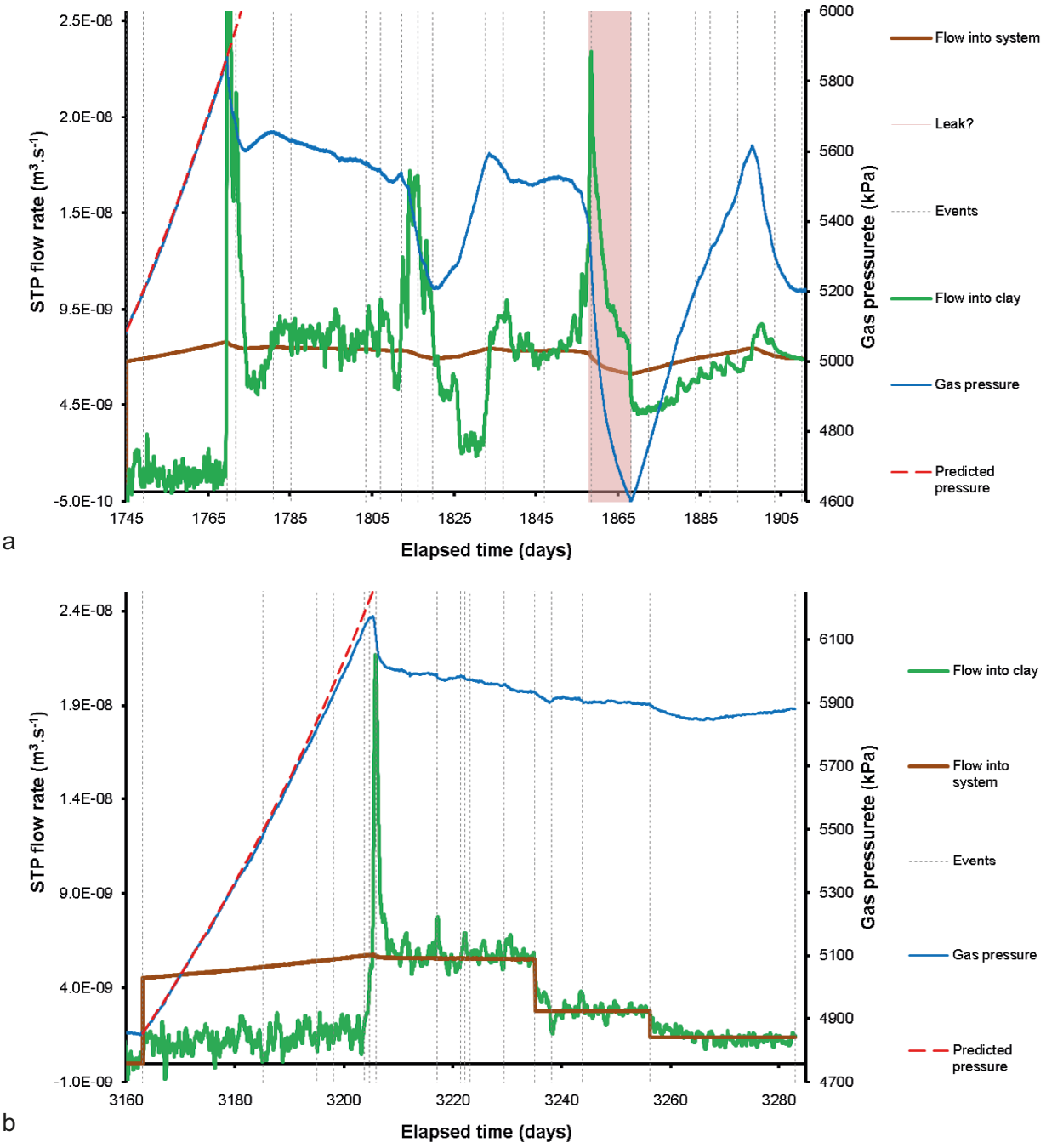

Figure 17-5. *Additional features of flow of gas into the system and the clay during. a) Gas Injection Test 2; b) Gas Injection Test 4.*

In GT1, it was interpreted that gas had moved down the outside of the canister following the prevailing stress gradient, before exiting the deposition hole, most likely along the interface between bentonite rings R1 and R2 and/or C1 and R1 (Figure 17-7a). Figure 17-6a,b and Figure 17-7 shows that gas directly migrated to two sensor locations within the deposition hole during GT2. Analysis of the data suggested that gas migrated around the canister and was first detected 180° around the canister to filter FL901. Figure 17-6b shows that gas movement to FL901 occurred through a series of events, raising pressure towards the gas injection pressure in at least 6 separate events. Gas also propagated downwards towards the bottom of the deposition hole and reached sensor UB902 in a single event. It is possible that gas was able to flow along cable runs in the bentonite in order to reach UB902. Figure 17-6a shows that the injection filter, FL901, and UB902 were all directly connected and that the drop in gas pressure along the pathway was relatively small. However, when pressure dropped, this connection was lost, and was only re-established around the time gas pressure peaked for a

second time. This suggests that the peak in pressure occurred when the pathway was re-opened. When pressure reduced because of leakage in the laboratory, connection was lost again but this time was not re-established by increases in pressure and another gas peak. This demonstrates the dynamic nature of the gas pathways and that multiple pathways existed. In time, gas migrated up the deposition hole towards the top of the canister. Gas sampling in the pressure relief holes showed that gas had escaped the deposition hole.

It is uncertain where gas migration occurred in Gas Injection Test 4. Gas pathways did not intercept any other sensor location in the system. The stress response at gas entry was small which suggests that the test exploited pre-existing flow-paths in the system that were still open, or easy to open. It is possible that the test exploited the gas pathway network created either during GT1 or GT2 from FL903, or more likely the network created by test GT3 in FU910, which had resulted in the migration of gas to filter FL904 on the same level of the canister as FL903. Figure 17-7c shows a possible interpretation of gas movement in GT4. Gas Injection Test 6 showed that gas quite rapidly directly reached canister filter FL901 (Figure 17-6c, Figure 17-7d). Migration was through a few discrete events but pressure quickly rose to match the gas injection pressure. Gas had therefore migrated 180° around the canister without intercepting either of the two injection filters in between (FL902 or FL904). Gas then moved towards the bottom of the canister. From here, the gas found a pathway out of the deposition hole, most likely along the interface between bentonite rings R1 and R2, or R1 and C1 at the level of the bottom of the canister.

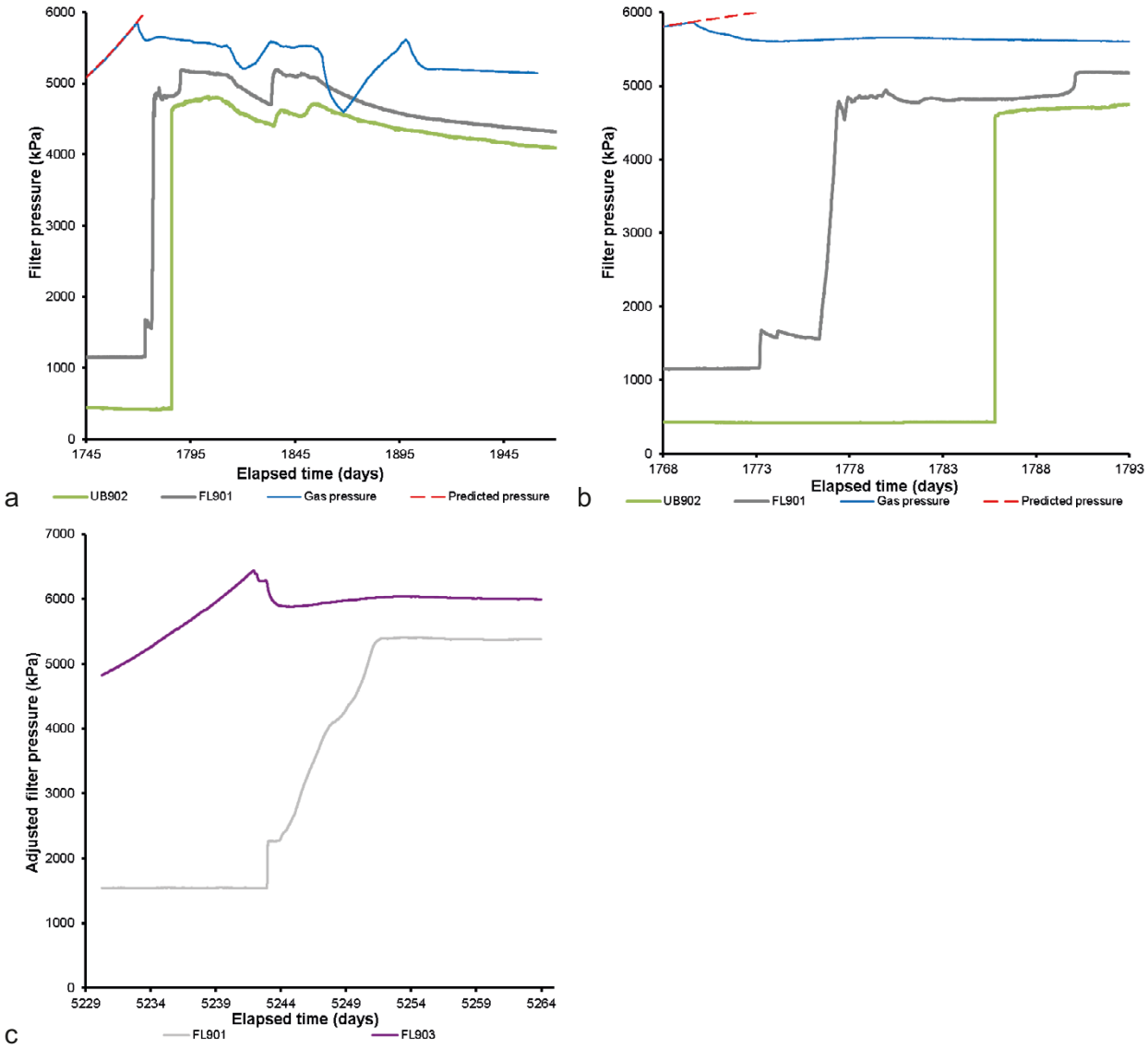

Figure 17-6. *Detail of sensors that showed evidence of gas pressurisation during Gas Injection Tests. a) Gas Injection Test 2; b) Detail of Gas Injection Test 2; c) Gas Injection Test 4.*

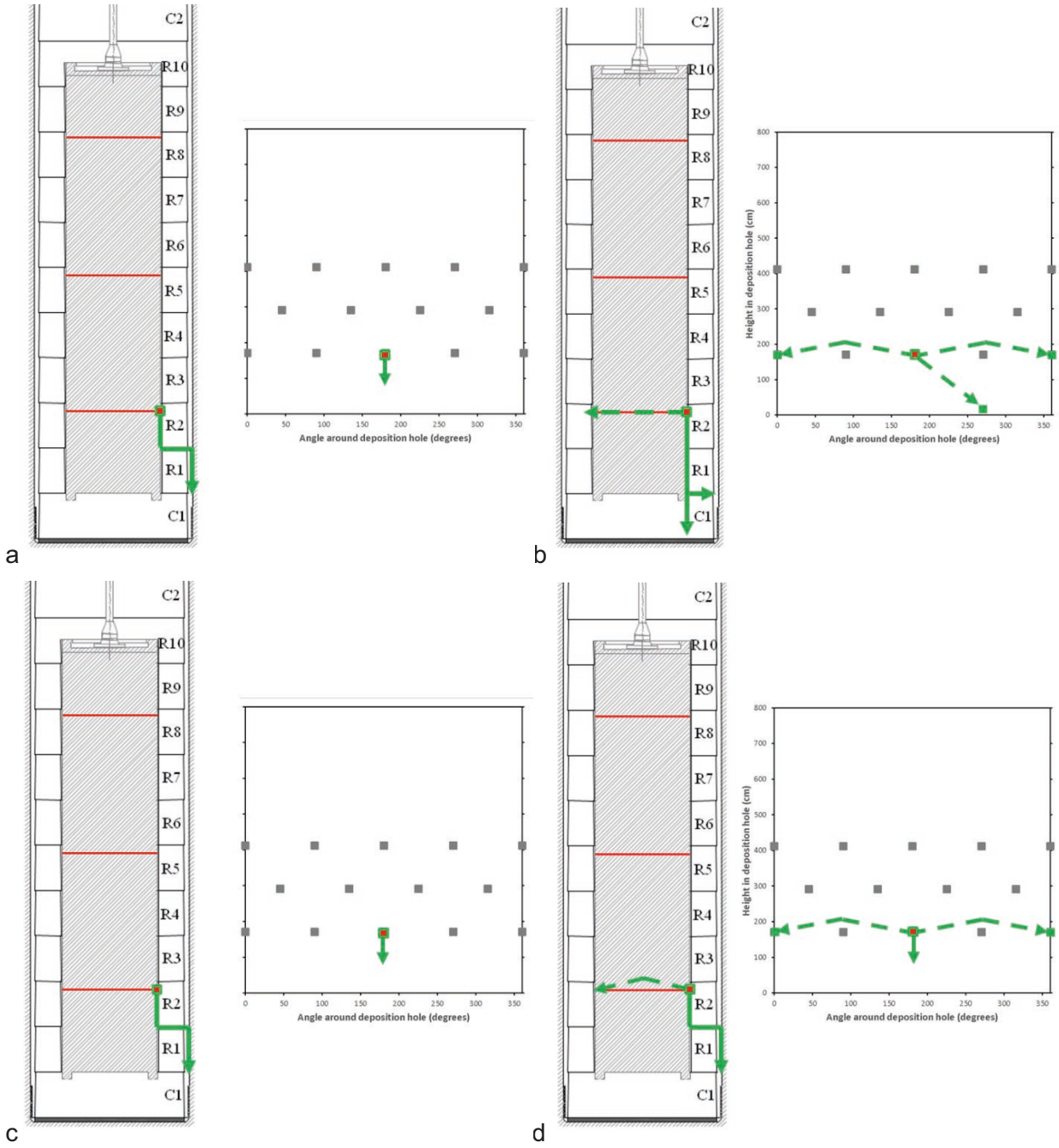

Figure 17-7. *Schematic of the direction of gas flow during gas testing in lower filter FL903. a) Flow in Gas Test 1; b) Flow in Gas Test 2; c) Flow in Gas Test 2; d) Flow in Gas Test 2.*

There is evidence that subsequent gas injection tests behaved similarly and that pathways may have re-activated. However, it is clear that the migration of gas was not identical between tests, with new pathways forming. The formed pathways self-sealed, at least partially.

17.1.1 Peak pressure evolution

One of the primary reasons for repeating the gas injection tests was to see if the gas transport properties changed with time, as the buffer matured. Conducting four gas injection tests in the same filter offered a good insight into the controls on the gas injection pressure. It has been shown that stress was considerably heterogeneous within the deposition hole. Considerable variation was seen at the deposition hole wall in the 20 sensors, as was axial and radial stress on the canister surface at just 3 locations. Unfortunately, stress was not measured at each canister filter and therefore local stress had to be estimated. The radial sensor array was positioned such that no sensor was directly opposite the injection filter, had testing occurred in the mid-plane canister filters then there would have been radial stress sensors opposite the injection filter. This meant that the closest sensors were 45° around the canister at PR908 and PR909 on the same level as the injector, at 45° at PR912 and PR913 on the next level above the injector, and directly below the injector at PR905. These five sensors are plotted in Figure 17-8 for each of the four gas injection tests. In addition, the radial stress at the deposition hole wall directly opposite FL903 was estimated from the interpolated data from all 20 PR sensors, this is also shown in Figure 17-8. Also shown is canister filter PC902, which was on the level above the injector but 135° around the canister surface. The heterogeneity seen in the canister stress data means that this estimate of stress at FL903 may be inaccurate.

Figure 17-8 shows that the interpolated radial stress opposite the injection filter was considerably lower than the peak gas pressure, a range of 750 to 1 365 kPa lower. The canister stress at PC902 was also seen to be lower than the gas injection pressure. Figure 17-9 shows a collation of the results of Figure 17-8. Gas peak pressure increased through the history of the full test. The data is shown with a logarithmic best-fit, which describes the increase in peak pressure well. Figure 17-9 shows the interpolated estimate of radial stress. This also increased through the lasgit test and is also shown with a logarithmic fit. However, the fit to the data is not as good. Also shown in Figure 17-9 is the value of radial stress at the surface of the canister at PC902. This was shown to increase with time and is also shown with a logarithmic fit. As with interpolated radial stress, the fit is also poor. The reason for this was the end of artificial hydration which resulted in radial stress levelling and the stress at PC902 reducing. It is apparent that the ending of hydration greatly impacted the local stresses in the system. However, no such affect is seen in the gas peak pressure. Figure 17-9 shows the results for interpolated radial stress and for PC901 for only the first three tests prior to the ending of artificial hydration. This shows a good logarithmic fit. However, the form of the slope was much steeper for both radial stress and PC901 than for the gas peak pressure. These observations suggest that gas peak pressure was independent of the increase of stress within the system. Figure 17-10 shows the relationship between gas peak pressure and radial stress on the canister at PC902. The dotted line shows when stress and gas pressure are equal, therefore the plot shows that pressure peaked when greater than the local radial stress by up to 600 kPa.

Hydraulic conductivity determined from the two-stage constant head tests showed that the hydraulic properties reduced in filter FL903 over the whole lasgit test. This data was also independent of artificial hydration. Figure 17-11 shows the relationship between hydraulic conductivity and the peak gas pressure. This shows that peak pressure increased in FL903 as the hydraulic conductivity reduced. This is not surprising as the buffer matured in response to hydration and increasing stress on the system.

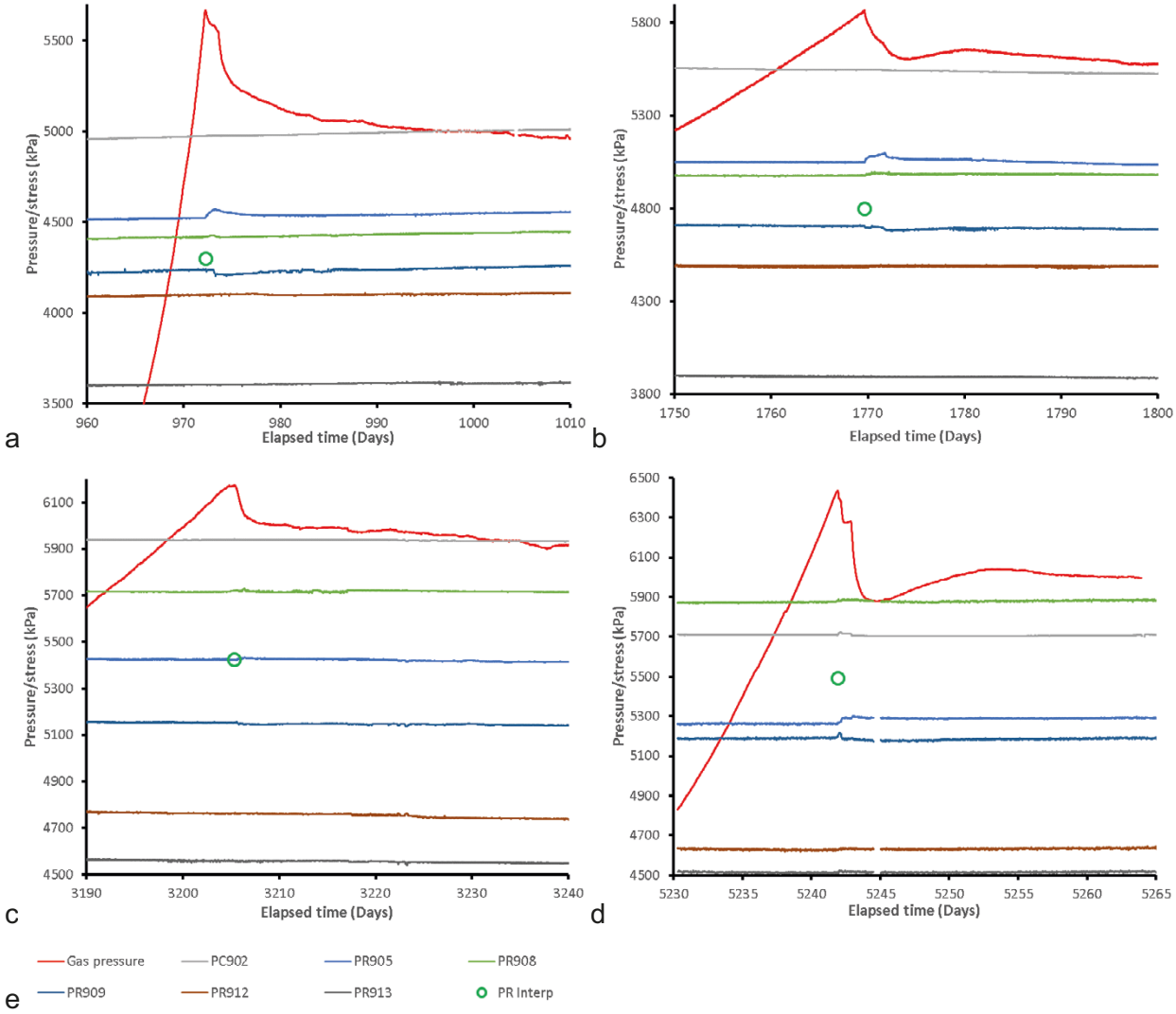

Figure 17-8. *Gas Peak pressure and local stress. a) Gas Injection Test 1; b) Gas Injection Test 2; c) Gas Injection Test 4; d) Gas Injection Test 6; e) Legend.*

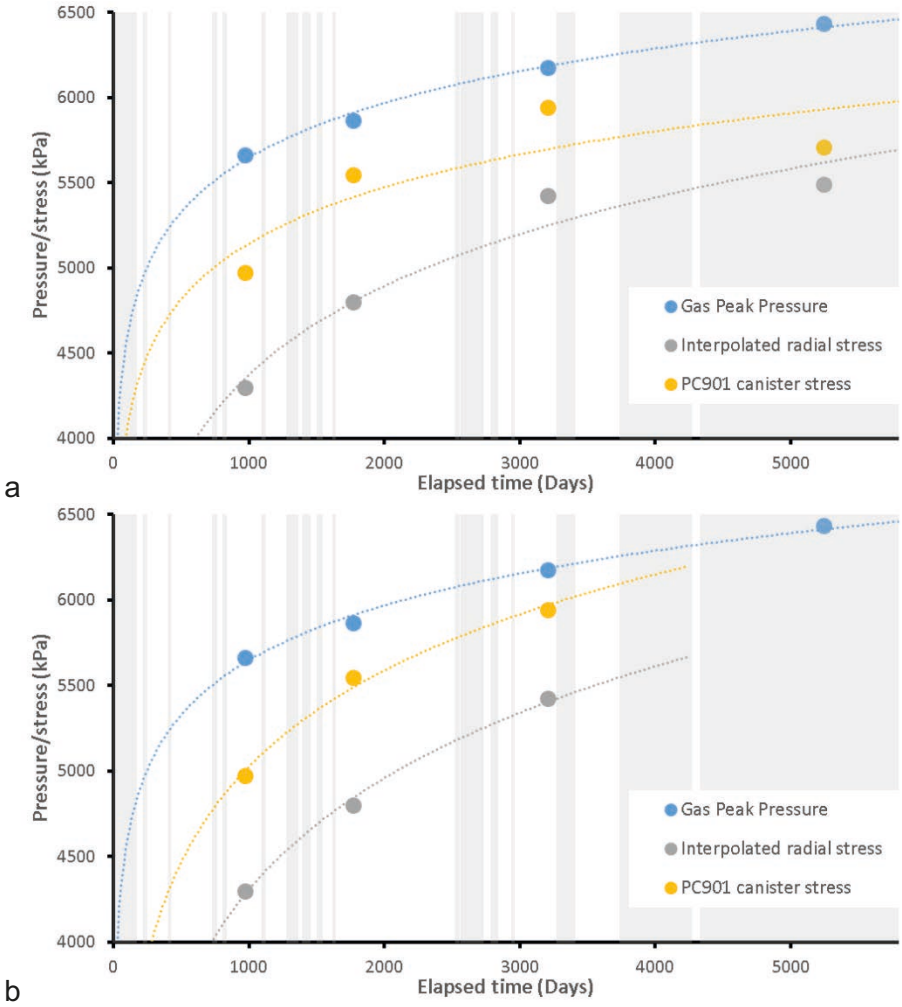

Figure 17-9. *Increase in peak pressure, interpolated radial stress, and canister stress for the four gas injection tests in FL903. a) All test results; b) Estimated stress only up until the end of artificial hydration.*

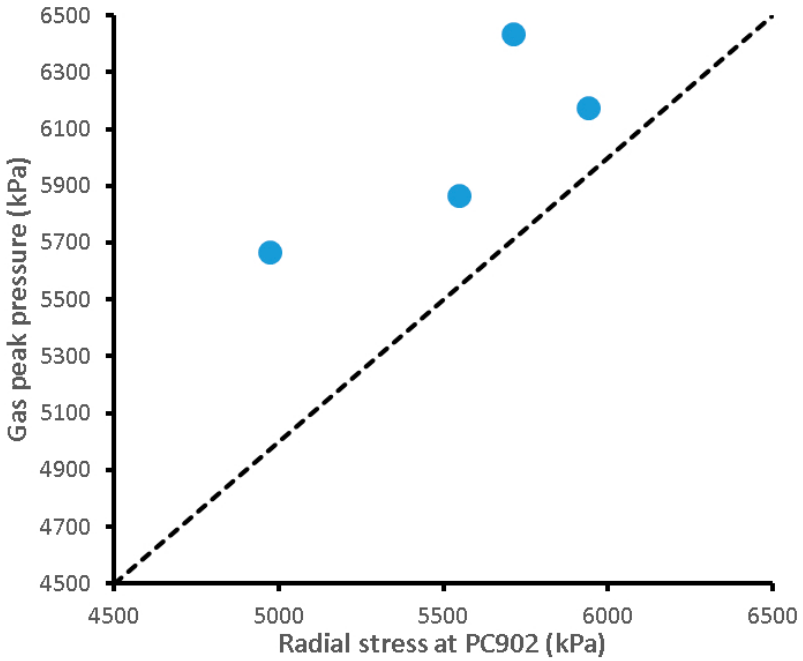

Figure 17-10. *The relationship between gas peak pressure and radial stress on the canister. The dotted line shows when radial stress is equal to gas peak pressure.*

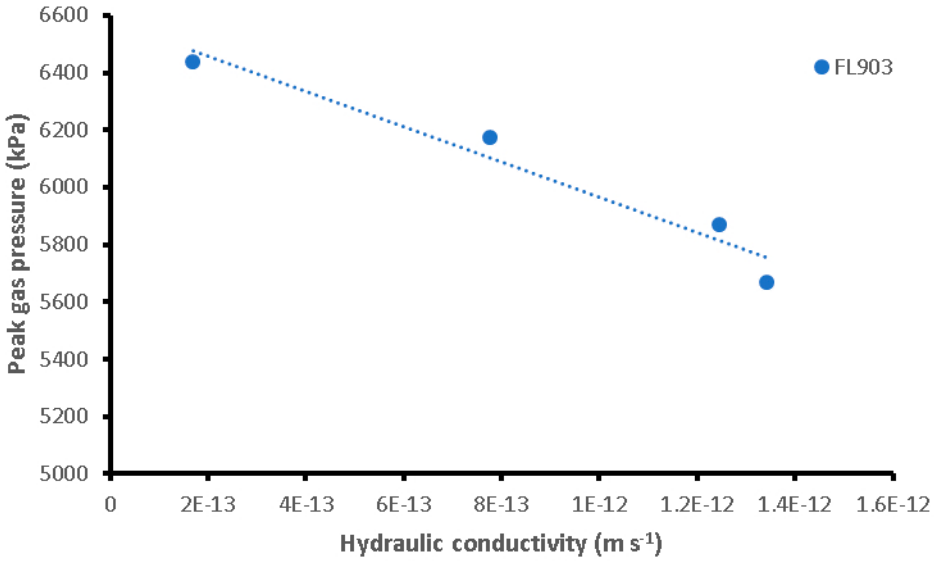

Figure 17-11. *Relationship between hydraulic conductivity and peak gas pressure.*

17.2 Gas Injection Tests in canister filter FU910

Two tests were conducted in canister filter FU910 on the upper array of canister filters at a height of 4 124 mm in the deposition hole. The first test, Gas Injection Test 3 (GT3) was conducted between Day 2257 and Day 5183, Gas Injection Test 5 (GT5) was conducted between Day 5183 and Day 5220. This means there was 2 490 days between the start of Lasgit and GT3, and 2 568 days between the end of GT3 and the start of GT5. The main data relating to the tests conducted in filter FL903 are summarised in Table 17-2.

Table 17-2. Data relating to gas injection tests conducted in canister filter FU910.

	Test	Gas ramps	Start (Days)	End (Days)	Time gap (Days)	Peak pressure (kPa)	Time at peak (Days)	Gas entry pressure (kPa)
1	GT3	4	2257.23	2614.46	2257.23	5192	2490.37	-
2	GT5	1	5183.27	5220.47	2568.82	5347	5202.57	4919

Figure 17-12 compares the gas pressure and flow data for the two tests conducted in FU910 (GT3 and 5), with the gas pressure compared in more detail in Figure 17-13. Figure 17-12 shows that the gas flow into the system was different for the two tests. This potentially means that the results could have been affected if the processes controlling gas entry were dependent on the rate of pressurisation. Variations in flow rate can derive from differences in the starting volume and if processes were dependent on the volume of the gas, this could introduce a further variation to the data. However, the volumes of gas were not significantly different and the variation in pressurisation rate was only around two times faster in GT5 compared with GT3. For significant variation in behaviour it would be expected that many orders of magnitude variation in flow rate would result in different behaviour. This must be the case, otherwise the rate employed during laboratory testing or during Lasgit would be un-representative as the pressure increase rate was several orders of magnitude greater than that expected during gas generation in the canister.

Figure 17-12 shows the difference in the flow into the and the clay response. In GT3, flow into the clay was low, up until the sudden increase in flow at around peak pressure. There were no pre-cursor flows and a single peak in flow was formed, reducing gas pressure rapidly. The peak in flow was short lived and flow into the clay quickly reduced to below that of flow into the system and as a result gas pressure started to rise again. Similar behaviour was seen in GT5. There was no pre-cursor flow and a rapid increase in flow with a single short-lived spike. However, in GT5 flow into the clay did not reduce below the flowrate into the system for some time so gas pressure slowly increased. In both cases, gas entry saw a rapid propagation of pathways, lowering gas pressure. These pathways either became unstable or the gas flow encountered a baffle in the system, resulting in an increase in gas pressure. In both tests, gas pressure had a secondary peak, which this time was broader compared with the instantaneous pressure drop seen at initial peak pressure. In both tests pressure increased above, or very close to, the initial peak pressure. This contrasts with what was seen in FL903, with peak pressure being followed by reducing gas pressure. At FU910, this suggests that continued propagation of pathways was more difficult higher in the canister or that an easy route out of the system was not achieved. In both tests, during the initial recovery of gas pressure there was a change of slope, suggesting that pathway propagation increased. This change in slope was more obvious in GT5 but is present in GT3 as well. In both tests, this event also corresponded with a short-lived spike in flow, although in GT3 there was a break in data recording that may have masked the feature. The qualitative gas flow behaviour shown in Figure 17-12 shows a similar behaviour and form for both gas pressure and flow, with short lived spike in flow resulting in steady-state movement of gas as flow into the clay matches flow into the system.

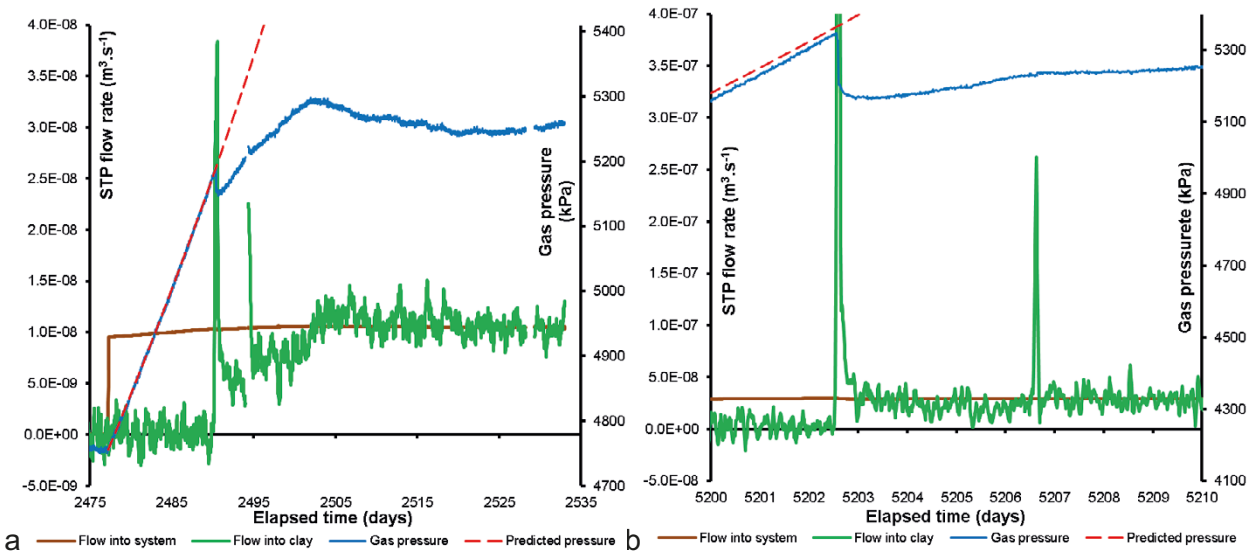

Figure 17-12. *Comparison of gas entry behaviour for the two tests conducted in canister filter FU910. a) Gas Injection Test 3; b) Gas Injection Test 5.*

Figure 17-13 compares the gas pressure result for the two tests conducted in FU910. The data were normalised so that peak pressure occurred at a time of 0 days. The individual gas tests have then been transposed along the y-axis in order to compare the response in Figure 17-13a. This figure highlights the differences in pressurisation rate, as shown by the different slopes seen up until the time of peak pressure, although the difference is not excessive. At peak pressure, the gas pressure rapidly reduced. In GT3 a reduction of ~40 kPa was seen, with GT5 reducing ~180 kPa. This suggests that GT5 re-activated existing pathways in the system quite easily. In GT3 pressure recovered to create a secondary, broad, peak, while in GT5 a second instantaneous pressure drop was seen at a gas pressure similar to the initial peak gas pressure. This behaviour suggests that gas pathways were continuing to grow and that gas had not been able to exit the deposition hole, at least until the secondary peaks occurred. Correcting the data for differences in flow rate into the system (Figure 17-13b) shows that the pressure recovery had a similar slope. In GT3 this resulted in a secondary peak, but in GT5 at a similar adjusted time there was a change in slope. This suggests slight differences between the propagation of pathways in the two tests. The rapid loss of more pressure in GT5 suggests that the repeat test exploited features formed during GT3 and that the buffer had not fully self-healed following the first gas test.

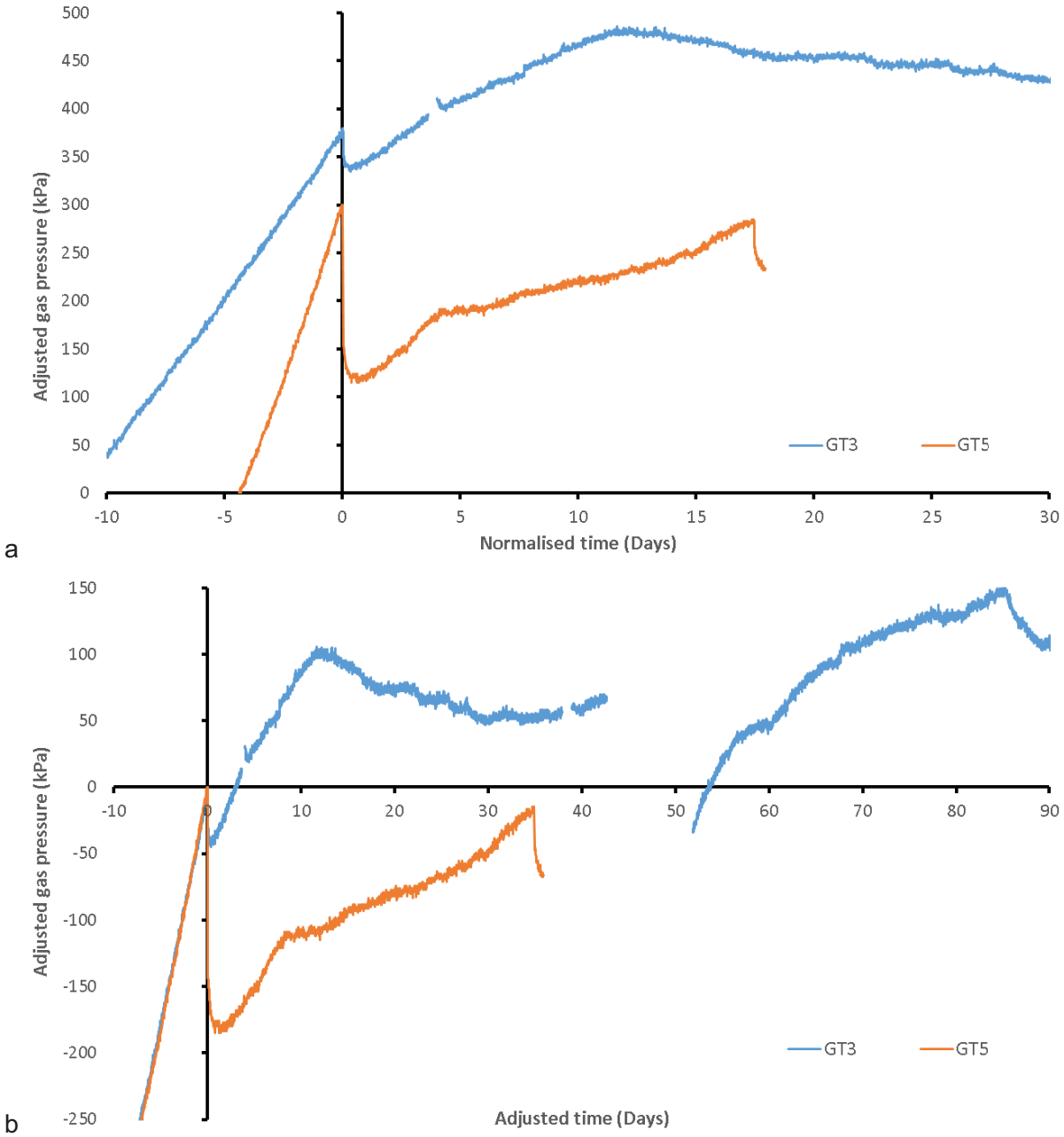

Figure 17-13. *Comparison of gas pressure for the two tests conducted in canister filter FU910. a) Gas pressure around peak pressure for both tests; b) Gas pressure adjusted to correct for different pressurisation rates.*

Figure 17-14 compares the response observed in selected pore pressure (UR) sensors around the time of peak stress and gas entry. For test GT3 (Figure 17-14a) peak pressure occurred at Day 2490.37. Note that UR916 was situated opposite the injection filter on the outer edge of the bentonite buffer. This sensor saw little variation at the time of peak pressure but was considerably noisy. Instantaneous pressure increases were seen in UR915 and UR921, suggesting that initial gas movement was in the general direction of these sensors, along the canister surface. It is noted that few pore pressure sensors registered a change at peak gas pressure, which is surprising given the instantaneous drop in gas pressure. For test GT5 (Figure 17-14b) peak pressure occurred at Day 5202.57. Again, FU916 directly opposite the injection filter recorded only a minor pressure reduction. Pore pressure greatly increased in at least five locations, but with varying form. Three sensors showed an instantaneous pressure increase followed by a slow pressure decay, one sensor showed a pressure increase in a series of steps, and one sensor showed a gradual slow pressure increase. It is clear that the form of the response of pore pressure in tests GT3 and GT5 was very different. However, GT5 was similar to that seen in most of the tests conducted in filter FL903.

Figure 17-15 compares the response seen in selected radial stress (PR) sensors at the time of peak gas pressure. No radial stress sensors were located opposite the injection filter. Sensors PR915 and PR916 were situated at the same level as FU910 but 45° around the canister in both directions. PR911 and PR912 were situated below PR915 and PR916 respectively, with PR921 situated above the injector at the same orientation. Peak pressure occurred in GT3 at Day 2490.37 (Figure 17-15a). At this time, PR915 and PR917 increased in stress, with PR919 increasing around five days later. This suggests that gas moved in this general direction along the canister surface. Radial stress increased at PR911 some 100 days later. This suggests that gas movement was transient throughout this test. For GT5 (Figure 17-15b), gas peak pressure occurred at Day 5202.57 and this was accompanied by an increase in almost all PR sensors. A stepped response was seen, with some sensors showing a delayed response. As with pore pressure, the radial stress data suggest the slow formation of pathways in GT3, which were reactivated in GT5. In sensor PR917 the form of the response was similar between tests, with PR915 also superficially being similar, although the response was more complex in GT3 and the amplitude of variation in GT5 was significantly greater. In both tests, PR919 saw a delayed increase of stress as gas moved.

The pore pressure and radial stress responses (Figure 17-14, Figure 17-15) show that GT3 saw the slow formation of virgin pathways in the buffer. Certain features of GT5 suggest that gas pathway propagation was in a similar direction, probably re-opening pathways extant from the earlier gas injection test. This suggests that pathways had not fully self-sealed and were easily reactivated, but near the injection filter the system had self-sealed, probably as a result of the two-step hydraulic tests conducted.

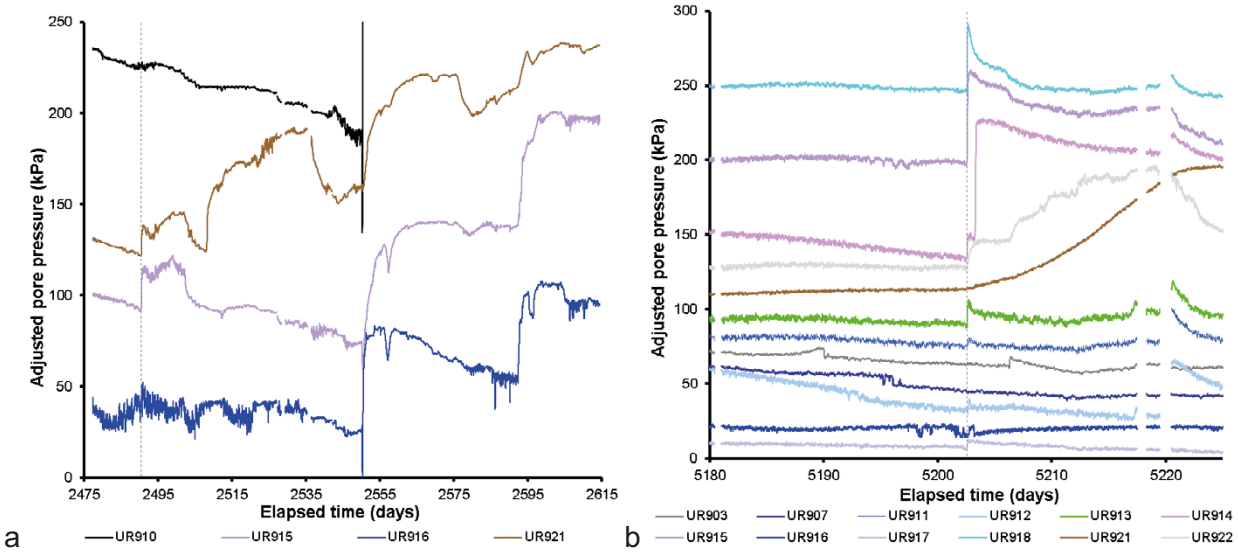

Figure 17-14. *Pore pressure observed in a selection of sensors close to FU910 around peak gas pressure. a) Gas Injection Test 3; b) Gas Injection Test 5. Each sensor has been adjusted about the y-axis for display purposes. Gas peak pressure is highlighted as a dashed event line.*

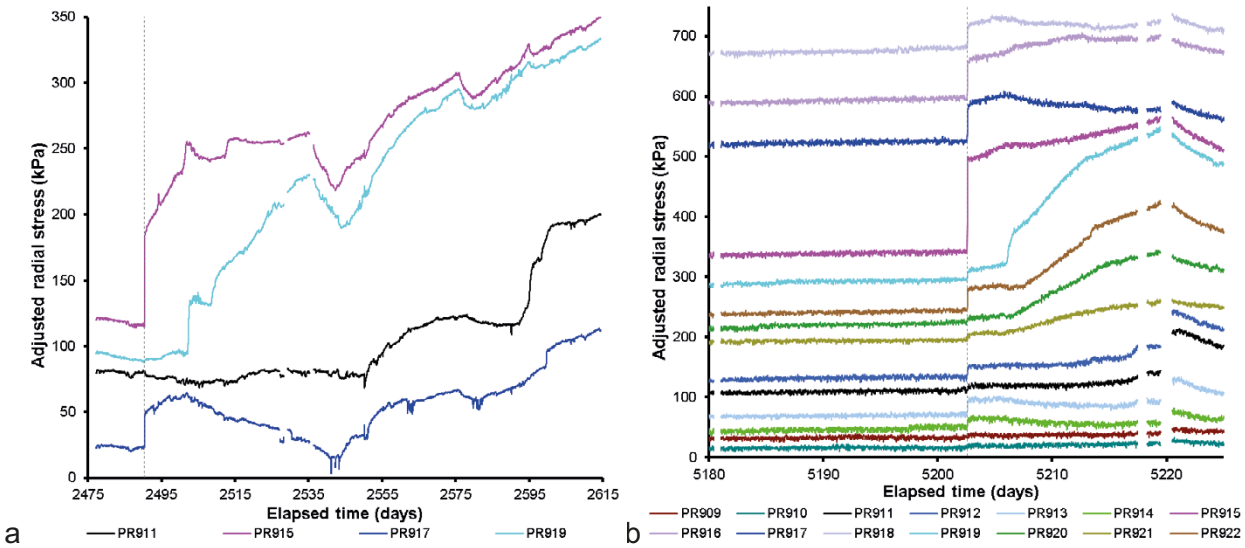

Figure 17-15. *Radial stresses observed in a selection of sensors close to FU910 around peak gas pressure. a) Gas Injection Test 3; b) Gas Injection Test 5. Each sensor has been adjusted about the y-axis for display purposes. Gas peak pressure is highlighted as a dashed event line.*

Figure 17-16 shows additional features for GT3 and GT5 that are relevant to the discussion. In GT3, flow was continued for considerable time after gas entry (Figure 17-16a). Generally, flow into the clay quickly equalled flow in the system and steady-state flow was established. By Day 2530, the pressure in FU910 had peaked twice, troughed twice, and was increasing for a third time. Shortly after, a system failure in the lab halted gas injection and when it was re-started gas pressure had reduced but it quickly recovered and by around Day 2555 was increasing at a rate similar to that seen at Day 2534 before the shut-in. A series of pressure decreases then occurred demonstrating that either new pathways were forming, or that gas venting from the deposition hole was episodic. When the test was halted, gas pressure was at its highest and was continuing to increase. It was approximately 200 kPa higher than the initial peak pressure event. The data suggest that pathway formation continued.

Figure 17-16b shows the flow result for Gas Injection Test 5. This test had a single peak in flow and showed the system quickly established near steady-state flow, with gas pressure slowly increasing at a constant rate. Flow into the clay was only marginally lower than the flow into the system, resulting in a slow increase in pressure. When gas pressure approached that of the peak pressure, a second peak was seen with instantaneous pressure loss. The slope of this linear pressure increase was similar to that seen in GT3 when the data were corrected for differences in flow rate (Figure 17-13b). This suggests that the physics governing the increasing pressure was repeatable and scaled with flow rate.

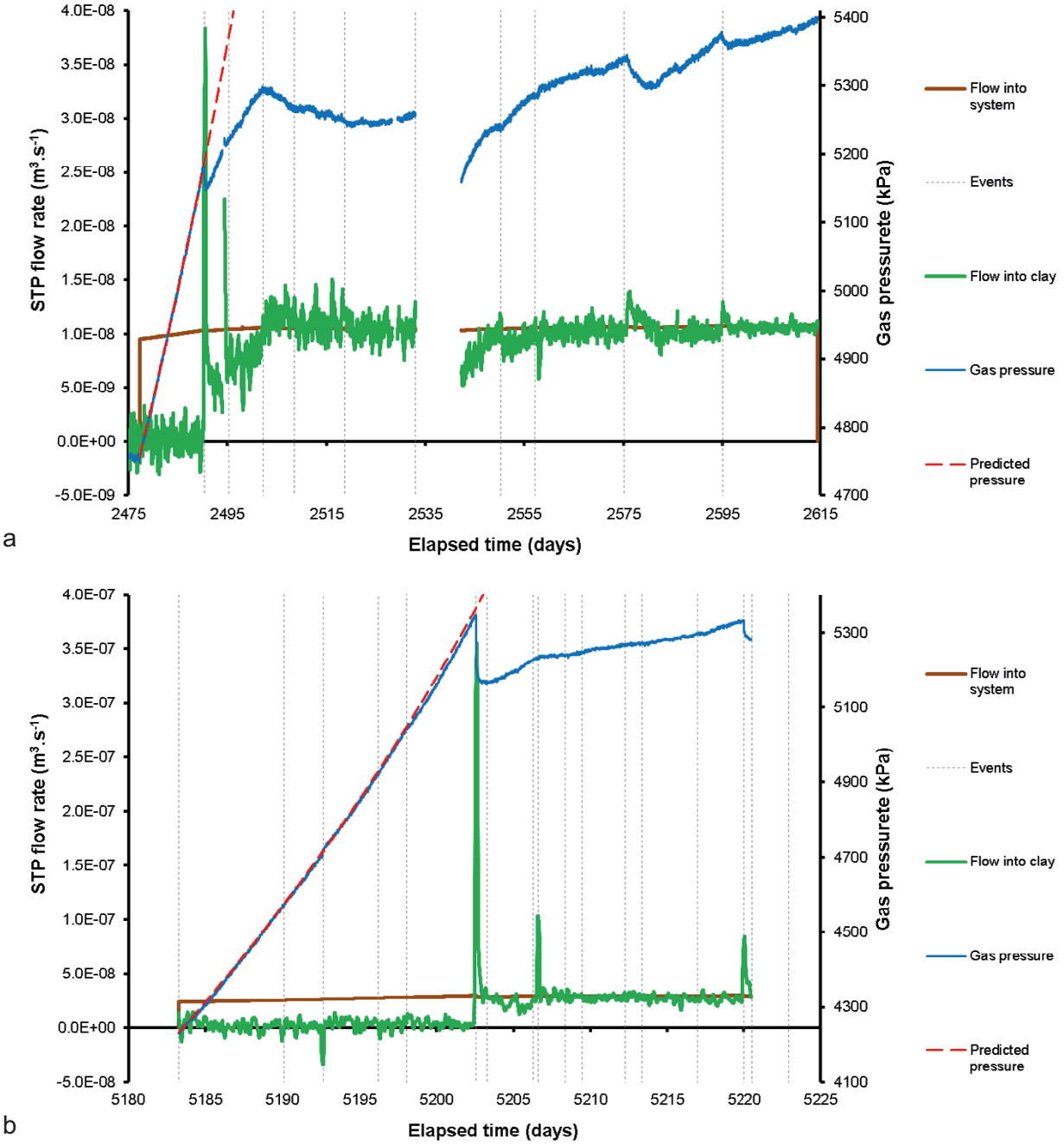

Figure 17-16. *Additional features of flow of gas into the system and the clay during gas injection testing. a) Gas Injection Test 3; b) Gas Injection Test 5.*

In both gas injection tests, pathways were seen to directly propagate to other sensors within the deposition hole, as shown in Figure 17-17 and Figure 17-18. In GT3 (Figure 17-17a, b, Figure 17-18a), gas first moved to FU909/FU912 in a series of pressure events. Following GT3, it was found that FU909 and FU912 were wrongly connected within the Lasgit laboratory, meaning that filter FU912 was not connected to the laboratory and therefore FU909 had been the pressurised filter. This was corrected before GT5. Gas then arrived at FU911, again in a series of pressure increases, albeit over a longer period of time. Next, gas reached PC903, and finally reached FL904 towards the bottom of the canister. Figure 17-17d shows the location of these sensors on the canister surface. For GT5 (Figure 17-17c, Figure 17-18b), at peak gas pressure, pressure at FU909 and PC903 increased instantaneously. This confirms that pathways created during GT3 were re-opened at peak pressure during GT5 and shows that limited sealing of the existing pathway network occurred in the ~2 500 days between the two tests. Gas did not reach FU911 or FL904, showing that at least some of the pathway network was not reactivated and may have even self-sealed. It should be noted that both FU911 and FL904 were hydraulically tested between the two gas injection tests and this may have aided self-sealing. However, FU909 was also hydraulically tested and this was not self-sealed. It is not certain whether gas managed to escape the deposition hole as pathways were still forming or developing in GT3.

There is evidence that subsequent gas injection tests behaved similarly and that pathways were re-activated. However, it is clear that the migration of gas was not identical between tests, with new pathways forming or at least some existing pathways not reactivating. The formed pathways self-sealed, at least partially.

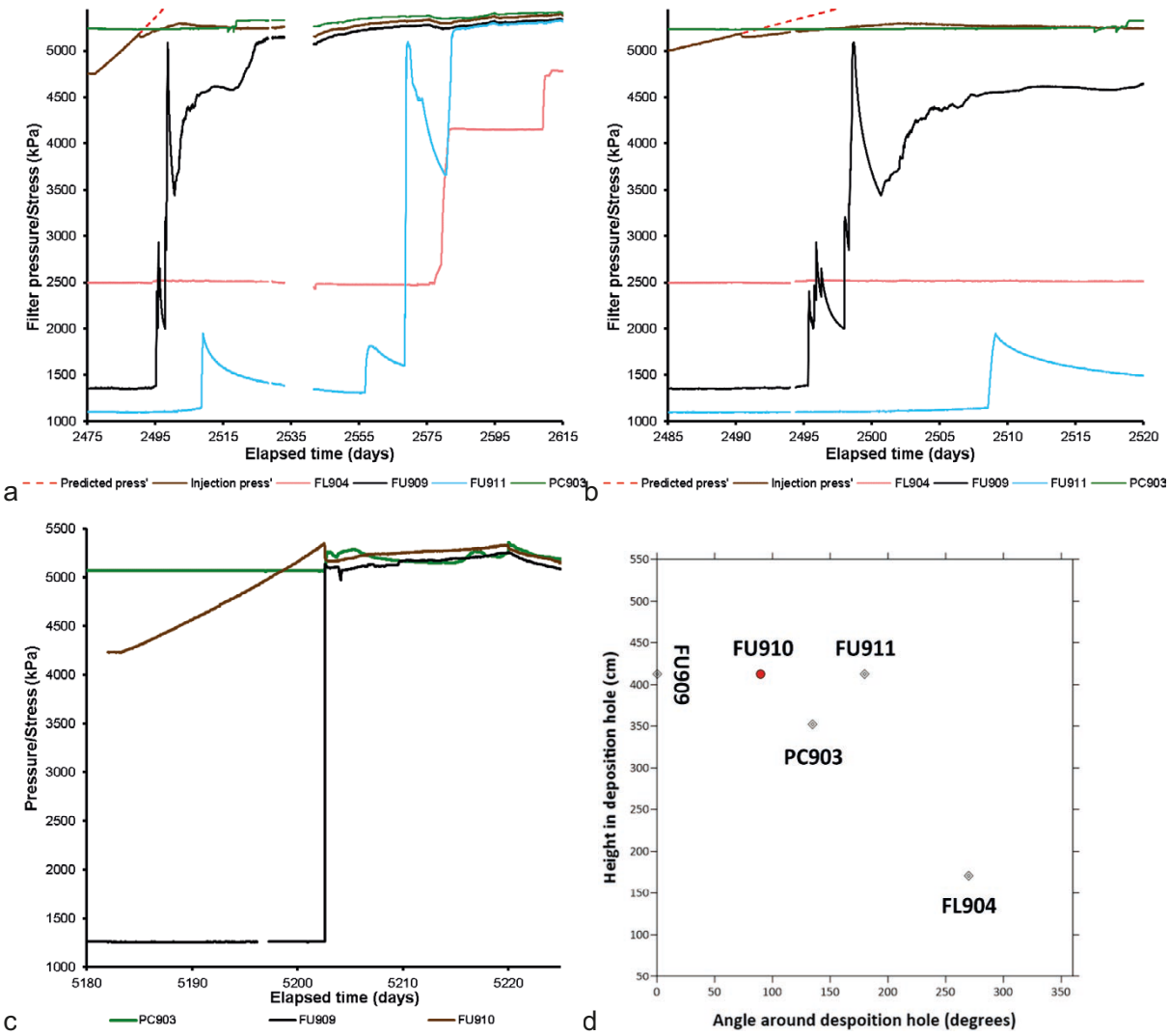

Figure 17-17. *Detail of sensors that showed evidence of gas pressurisation during Gas Injection Tests in FU910. a) Gas Injection Test 3; b) Detail of Gas Injection Test 3; c) Gas Injection Test 5; d) Location of sensors in the deposition hole.*

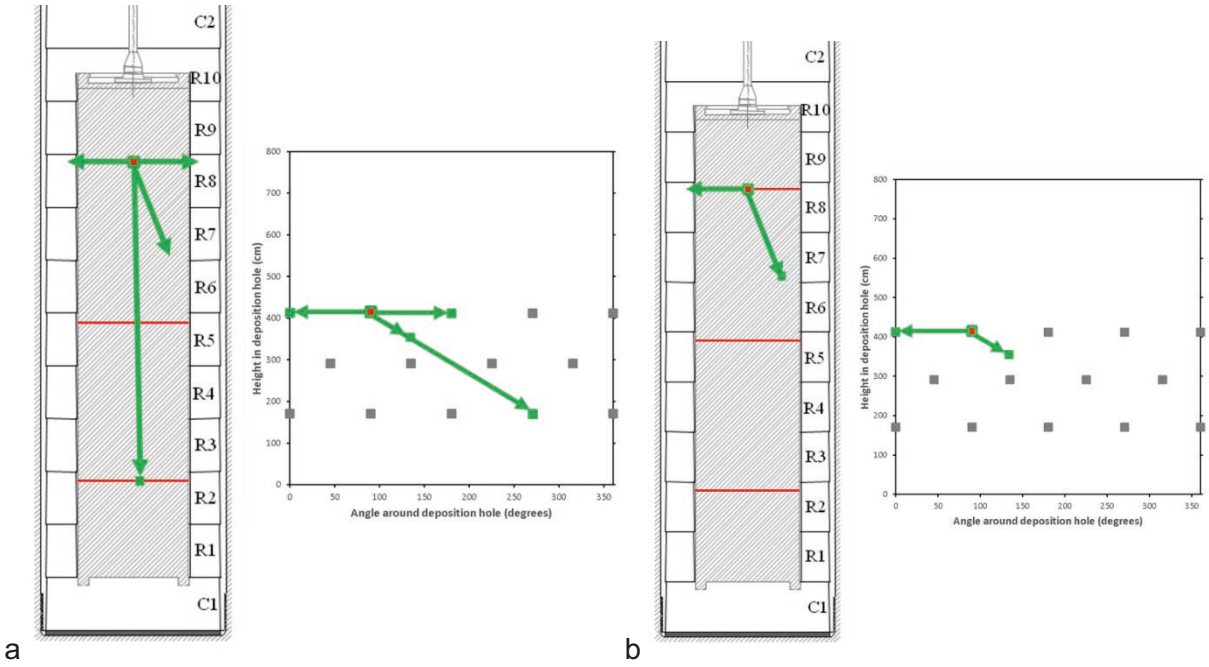

Figure 17-18. *Schematic of the direction of gas flow during gas testing in upper filter FU910. a) Flow in Gas Test 3; b) Flow in Gas Test 5.*

17.2.1 Peak pressure evolution

One of the primary reasons for repeating the gas injection tests was to see if the gas transport properties had changed with time as the buffer matured. However, as only two gas injection tests were conducted in the same filter this offers limited insight into the controls of the gas injection pressure. It has been shown that stress was considerably heterogeneous within the deposition hole. Considerable variation was seen at the deposition hole wall in the 20 PR9xx sensors, as was axial and radial stress on the canister surface (PC90x) at just 3 locations. Unfortunately, stress was not measured at each canister filter and therefore local stress had to be estimated. The radial sensor array was positioned such that no sensor was directly opposite the injection filter. This meant that the closest sensors were 45° around the canister at PR915 and PR916 on the same level as the injector, at 45° at PR911 and PR912 on the next level below the injector, and directly above the injector at PR921. These five sensors are plotted in Figure 17-19 for each of the two gas injection tests. In addition, the radial stress at the deposition hole wall directly opposite FU910 was estimated from the interpolated data from all 20 PR9xx sensors, this is also shown in Figure 17-19. Also shown is canister filter PC903, which was on the level below the injector but 45° around the canister surface. The heterogeneity seen in the canister stress data means that this estimate of stress at FU910 may be inaccurate.

Figure 17-19 shows that the interpolated radial stress opposite the injection filter was considerably lower than the peak gas pressure, i.e. between 235 and 460 kPa lower. The canister stress at PC903 was seen to be approximately equal to the gas peak pressure in GT3 and was 280 kPa below peak pressure in GT5. Figure 17-20 shows the collation of the results of Figure 17-19. Gas peak pressure increased throughout the whole Lasgit test. The data is shown with a logarithmic best-fit, only because this fitted the data for FL903 well. Figure 17-20 shows the interpolated estimate of radial stress. This also increased throughout the Lasgit test and is also shown with a logarithmic fit. The increase in interpolated radial stress was greater than that seen in the gas peak pressure. Also shown in Figure 17-20 is the value of radial stress at the surface of the canister at PC903. This was seen to decrease between the two tests since artificial hydration was stopped. It was expected that gas entry would occur at, or near, the local stress and that PC903 was relatively local to the injection filter. Figure 17-20 shows that gas peak pressure was close to the canister stress and this is confirmed in Figure 17-21 with gas peak pressure occurring close to the dashed line, which represents the condition when gas pressure is equal to local stress. However, the condition at peak gas pressure for GT5 showed gas entry at a pressure 280 kPa above the local stress. For stress to be the control on gas peak pressure, it would be expected that it would have reduced between tests since canister stress had reduced as a result of ending artificial hydration.

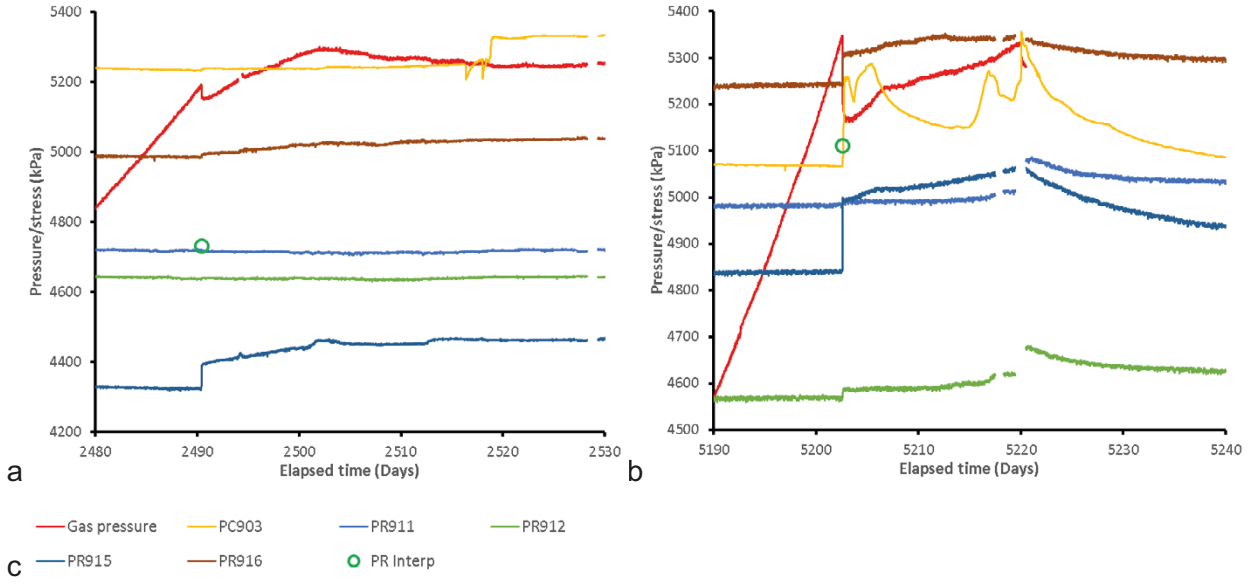

Figure 17-19. *Gas peak pressure and local stress. a) Gas Injection Test 3; b) Gas Injection Test 5; c) Legend.*

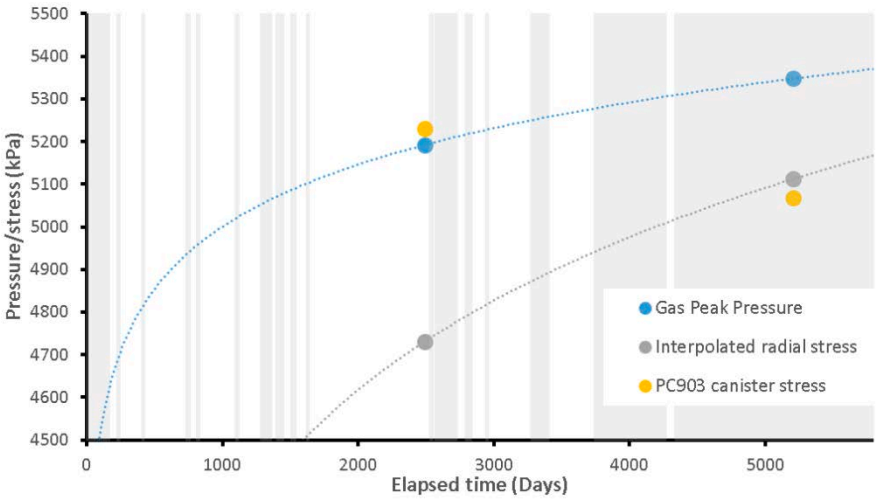

Figure 17-20. *Increase in peak pressure, interpolated radial stress, and canister stress for the two gas injection tests in FU910.*

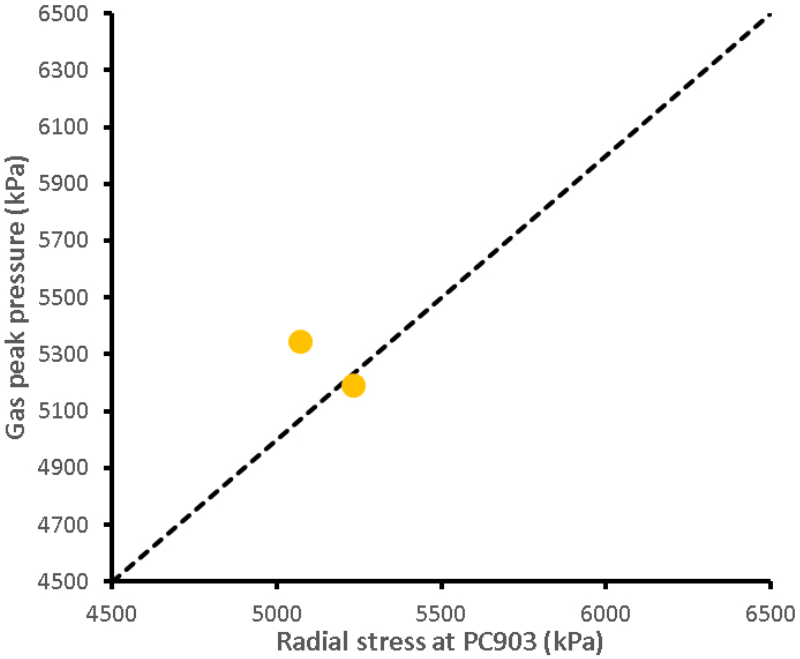

Figure 17-21. *The relationship between gas peak pressure and radial stress on the canister. The dotted line shows when radial stress is equal to gas peak pressure.*

Hydraulic conductivity determined from the two-stage constant head tests showed that the hydraulic properties reduced in the bentonite surrounding filter FU910 over the full test. This data was also independent of artificial hydration for FL903 and was likely to be similar for FU910. Figure 17-22 shows the relationship between hydraulic conductivity and the peak gas pressure. Figure 17-22 suggests that peak pressure increased in FU910 as the hydraulic conductivity reduced.

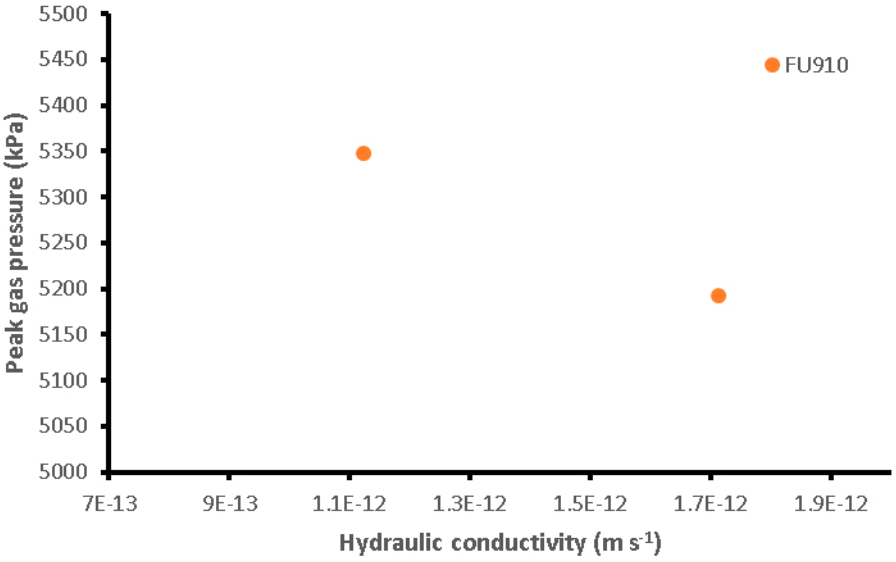

Figure 17-22. *Relationship between hydraulic conductivity and peak gas pressure.*

17.3 The Full Canister Test

The Full Canister Test reached gas entry in a different manner than for the six gas injection tests. Gas pressure was held constant at a magnitude a little higher than gas entry was expected while what in the canister slowly drained through the FCT filter. Had the gas ramp been increased it was likely that the buffer would have been hydrofractured by the water in the filter, something that was of no interest to Lasgit. All previous tests had gas entry at a pressure close to the local stress. The Full Canister Test filter (FCT) was located close to the axial stress sensor on the bottom of the canister, PC901. This meant that gas entry was expected ~7 000 kPa. When pressure reached 7 100 kPa, it was kept constant to allow the FCT filter to drain of water and to wait until gas entry occurred. It was estimated that 7 100 kPa was sufficient for gas entry to occur, but would not high enough that the bentonite would be gas fractured.

Figure 17-23 shows the radial stress and pore pressure results for the FCT test for selected sensors. It should be noted that the sensor array was optimised for testing in the canister filters and that the coverage at the base of the canister was limited. However, gas entry was observed. The form of the pore pressure (Figure 17-23a) profile was different from that seen in all the other gas injection tests. Pore pressure increased and then when it peaked, quickly dropped. This is almost the opposite behaviour to that seen in the previous tests where pore pressure tended to rise instantaneously and take time to decay. However, the general form has similarities to that seen at FL903. The rapid decrease in pore pressure suggests that gas moved into the buffer and relieved the loading of the deposition hole wall. Radial stress had a similar form to pore pressure (Figure 17-23b), which had similarities to that seen in GT2. This may mean that the FCT test exploited pathways formed in previous gas injection tests and simply re-activated extant pathways. The data may also suggest that the buffer was "inflated" by the gas and that the reduction in pore pressure and stress was this "balloon" being deflated as a pathway reached the outside of the deposition hole and gas could exit the system.

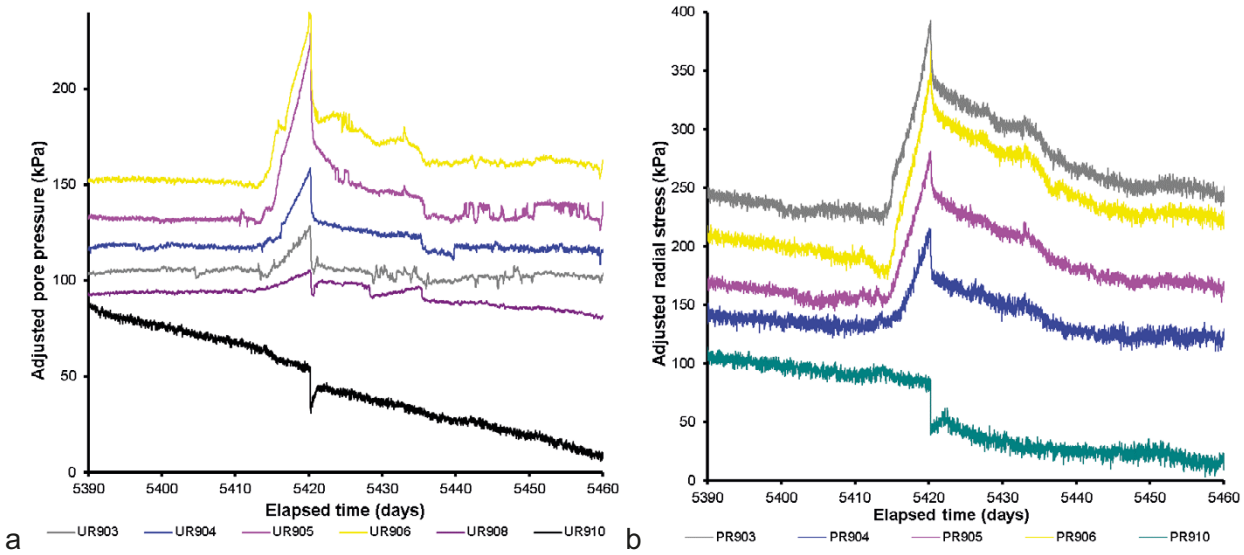

Figure 17-23. *Detail of radial stress and pore fluid pressure at the rock wall around the time of gas entry. a) Pore pressure at the deposition wall; b) Radial stress on the deposition wall.*

Figure 17-24 shows that gas migrated within the KBS-3 system and directly intercepted the canister filter FL901 and pore pressure sensor UB902 within the bentonite, near to the FCT filter. The gas took at least two pressure events to fully pressurise UB902. Once both sensors registered pressurisation they had similar pore pressure, and both decayed for the remainder of the test period at a similar rate to that of the FCT gas pressure. This pressure decay showed chaotic response, before eventually resulting in a slow and steady reduction in pressure. Both FL901 and UB902 were clearly in direct, open communication with one another. However, the pressures recorded at UB902 and FL901 were considerably lower than the canister pressure which suggests that the connection between the canister and sensors was not complete. The slow pressure decay of the canister pressure at FL901, and UB902 is thought to have occurred as gas exited the deposition hole. It should be noted that FL901 was pressurised in both GT2 and GT4 and UB902 was pressurised in GT2 when testing from canister filter FL903. It is probable that the FCT test exploited pre-existing features in the clay from this earlier testing. It is evident that the significantly larger volume of gas used in the FCT had not altered the gas propagation behaviour, except that an initial gas pressure reduction was not seen in the FCT test as gas entered the bentonite buffer.

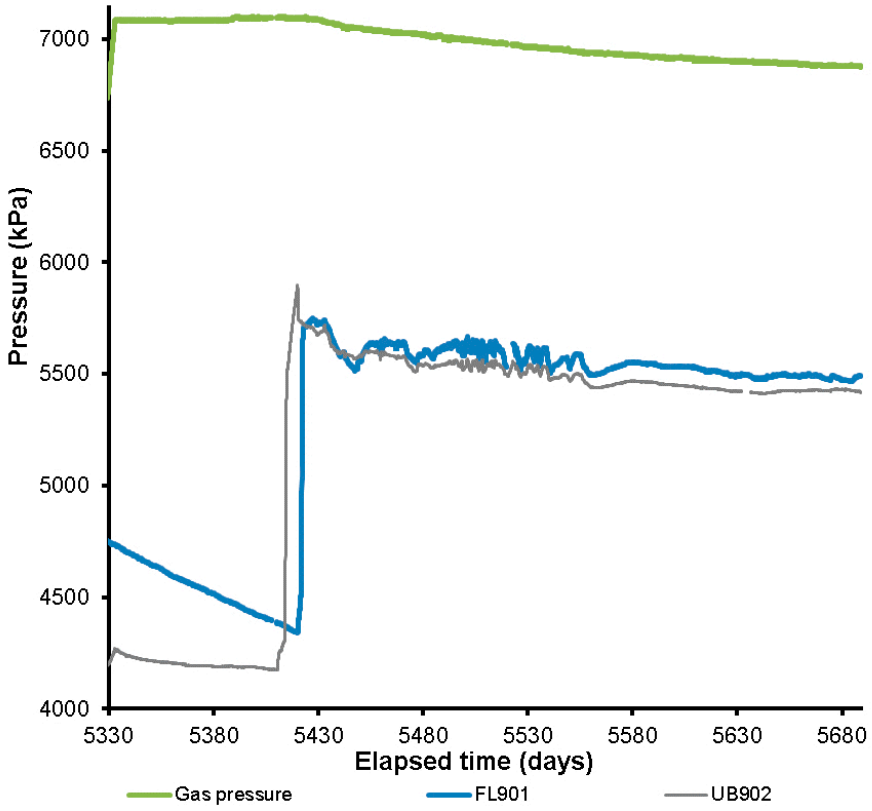

Figure 17-24. *Detail of sensors that showed evidence of gas pressurisation during the Full Canister Test.*

17.4 Conceptual model of gas movement

The following concenptual model of gas movement has been devised from all observations from all gas injection tests. It is clear that the interface between the canister and buffer played an integral role in gas movement. In several gas injection tests the gas reached isolated points within the deposition hole (various sensors/filters). In GT2 gas moved 180° around the canister surface from filter FL903 to FL901 whilst no pressure change was observed in filters FL902 or FL904. This demonstrated that the entire interface was not conductive. It is possible that gas entered the buffer. However, it is unprobable that whilst migrating in the buffer that it managed to intercept FL901 on the opposite side of the canister. Therefore, it is likely that localised gas pathways formed that moved around the canister surface intercepting a limited number of sensors. In test GT3, the gas injection stage was prolonged. This showed that movement occurred on multiple pathways. A single pathway could not have seen the pressurisation of sensors over a series of pressure increase events. Therefore, multiple pathways were forming at the same time, even once a predominant pathway had formed allowing gas to exit the deposition hole. Test GT3 also showed behaviour of episodic flow. Many sensors increased to the gas injection pressure through a series of pressure increases. This shows that the pathways that formed were not continuously open, and that gas movement was like the propagation of bubbles. This may suggest that pathways became unstable as they grew, i.e., as they lengthen there was sufficient energy to keep the pathway open. Therefore, pathways were not simple tensile fractures in the bentonite.

Figure 17-25 shows a general model to describe gas movement. At the start of the experiment there was a nominal 10 mm gap between the canister and the bentonite rings (Figure 17-25a). Water started to hydrate the buffer and pellets from the outside of the deposition hole resulting in swelling and the slow closure of the engineered gap. Water was also carefully introduced from the canister filters to aid swelling of the buffer (Figure 17-25b). This resulted in the formation of a zone close to the canister that filled the engineered gap that was of variable density (Figure 17-25c). In general, this zone was relatively homogenous as shown by the geotechnical results, but a clear zone of different properties was formed close to the canister. The radial stress at the deposition hole wall was seen to be heterogeneous and this may derive from variations in the properties of the pellet zone, which will have resulted in variations in the properties of the canister/buffer interface. This is shown schematically in Figure 17-25c. As gas injection occurred, gas entered the low-density interface zone resulting in mechanical opening of pathways seen as increases in radial stress (Figure 17-25d). As shown in Figure 17-25d, the gas pathway propagated as far as it could, reaching a zone of higher density that it could not pass. This may explain the pre-cursor flow event seen in GT1. More gas pathways formed (Figure 17-25e) or the single formed pathway increased in size. This continued until sufficient energy was available to overcome the obstruction identified in Figure 17-25d and the pathway started to grow (Figure 17-25e). This resulted in the formation of a dominant pathway (Figure 17-25f) which ultimately found a way out of the buffer. Figure 17-25 shows the concept for a single pathway. All evidence suggests that multiple localised pathways formed coincidently. Therefore, the feature that stops one pathway continuing may result in other pathways forming as more gas entered the system. However, GT3 shows that pathways that demonstrated episodic flow re-opened with time.

In mosts test it was evident that gas had found a way out of the deposition hole, most notably GT2 when the injection of neon was detected in the pressure-relief holes. The conceptual model for gas movement suggests that the interface between the canister and buffer was exploited. It would be difficult for gas to leave the low-density interface zone and enter the higher-density buffer to propagate to the deposition hole wall. Therefore, it was interpreted that gas probably moved along the interface between two blocks/rings in the deposition hole. During decommissioning, this interface was seen to be still prominent with limited self healing. Axial stress in the deposition hole was seen to be high as shown by the PB9xx sensors. The interfaces would have been mechanically closed by the stress field, but the interface was likely to have properties favourable to gas movement compared with the internal body of each bentonite block/ring. Movement along the interface was likely to be similar to the conceptual model introduced in Figure 17-25.

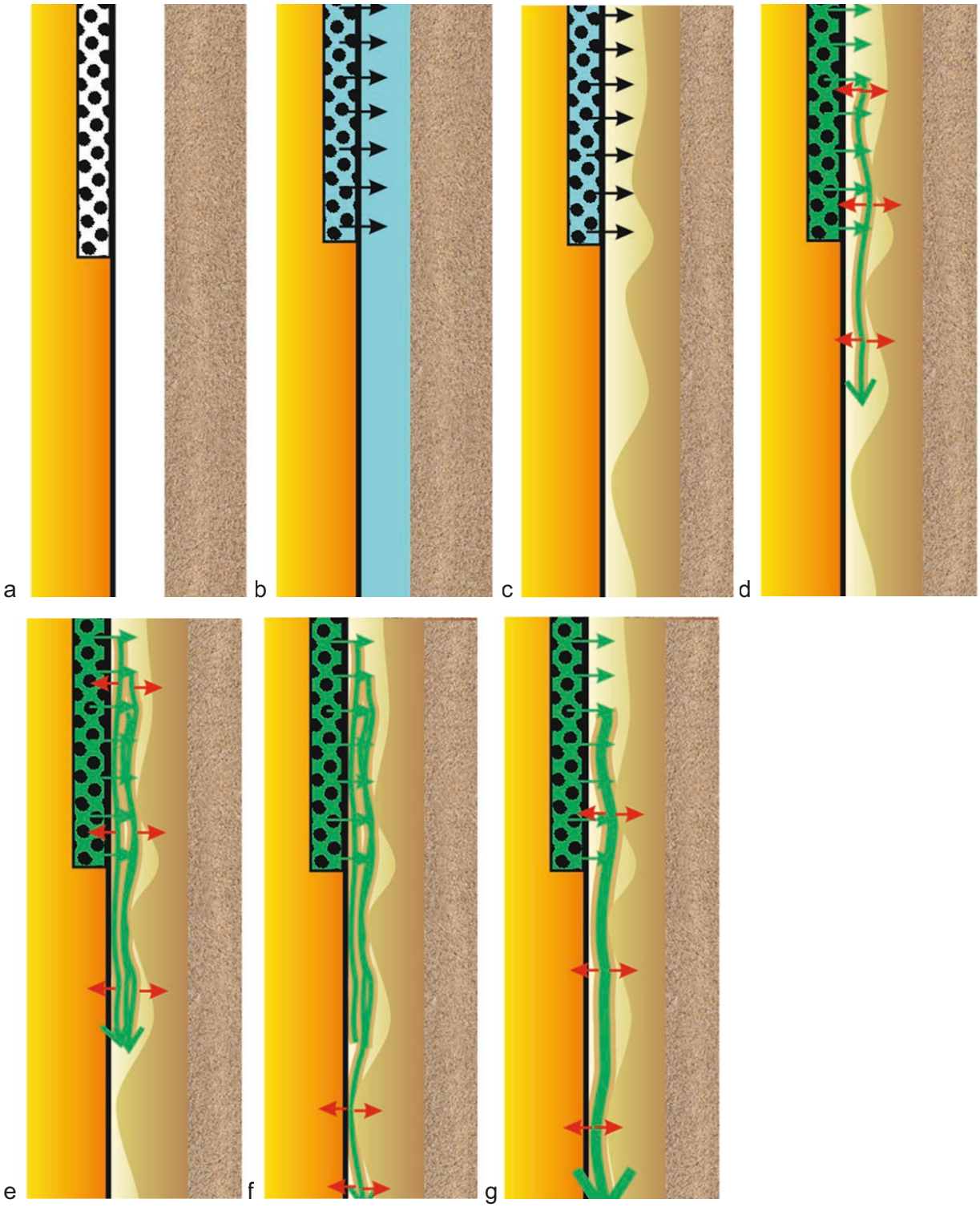

Figure 17-25. *Conceptual model of gas flow. See text for full description.*

17.5 Comparing all gas injection tests

Gas injection tests were conducted from canister filters FL903, FU910, and the FCT filter. In all seven tests, gas injection occurred around the peak pressure and it appeared that gas found a pathway out of the deposition hole. This resulted in the careful venting of pressurised gas in a controlled manner that had little to no long-term effect on the physical properties of the buffer. Repeat gas testing suggested that pathways were extant for prolonged periods and were sometimes re-activated by subsequent tests in the same filter. Moreover, testing in filters may have intercepted pathways created in previous tests at other filters.

Figure 17-26 shows gas peak pressure for the six gas injection tests. Peak pressure increased for tests conducted in filter FL903 as described by a logarithmic fit. Peak pressure at FU910 was at a lower pressure and is also shown with a logarithmic fit, for consistency with FL903. Neither filter showed an influence from artificial hydration ending, even though stress had reduced in the system as a result of this. It appears that gas peak pressure was independent of this boundary condition. Previously, it had been suggested that stress was the primary controller of gas peak pressure. Figure 17-27 shows the relationship between gas peak pressure and stress for the seven tests in Lasgit and for laboratory tests (Graham et al. 2016). The dashed line in Figure 17-27 represents unity, when stress on the canister would be equal to the gas peak pressure. It can be seen that one test in FU910 and the FCT were close to this condition. However, the majority of tests in FL903 occurred at a pressure up to 600 kPa above local stress. This may be as a result in inaccurate estimates of stress at the filter but may represent a need for a slight excess pressure to cause peak conditions. It should be noted that gas peak pressure was not significantly above local stress, as had been seen in a limited number of laboratory-scale experiments (Figure 17-27b). Therefore, stress was the primary control on gas migration but hysteresis in the system meant that a reducing stress field had not altered the gas peak pressure.

Figure 17-28 shows the relationship between hydraulic conductivity determined from two-stage constant head tests with peak gas pressure. All the data suggest that peak gas pressure scales with hydraulic conductivity and as the buffer matured, the peak pressure increased as hydraulic conductivity reduced. This isn't surprising as both hydraulic and gas properties will be dependent on the pore network of the buffer, and as the buffer matured, porosity would reduce and water and gas flow would become more difficult. The progress of hydraulic properties appears independent of, or at most affected only very slightly by the ending of artificial hydration. It is suggested that hydraulic conductivity evolution was a secondary control on gas peak flow, although this is a proxy for the maturity of the buffer. This control was partly dependent on the stress field.

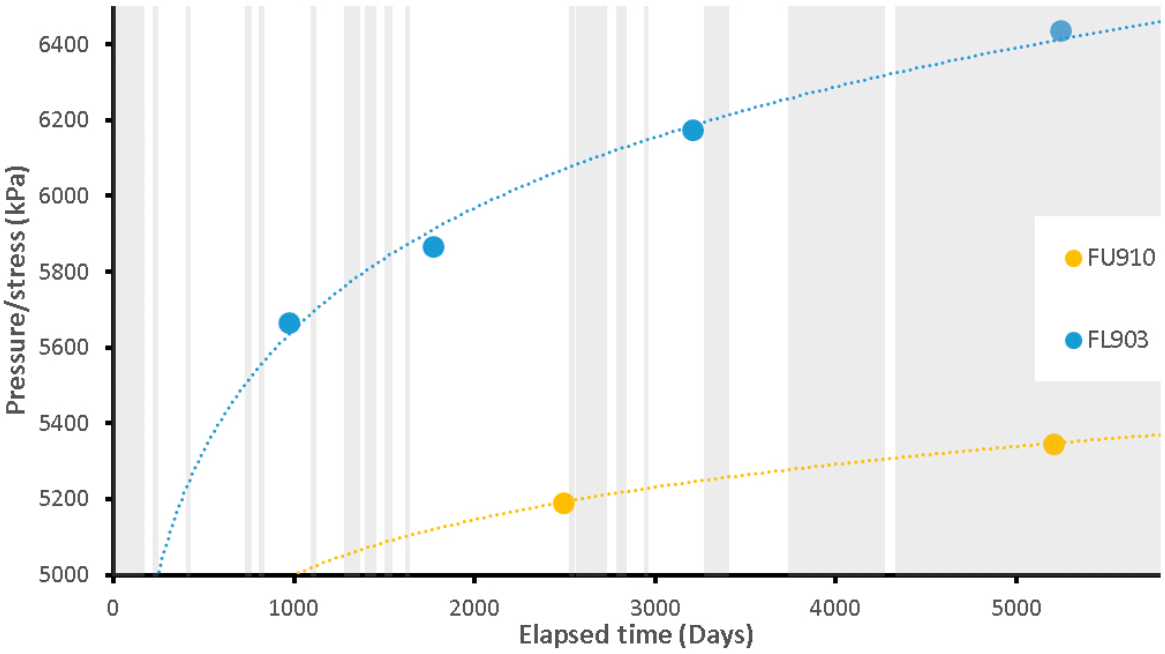

Figure 17-26. *Gas peak pressure evolution with time for six gas injection tests in Lasgit.*

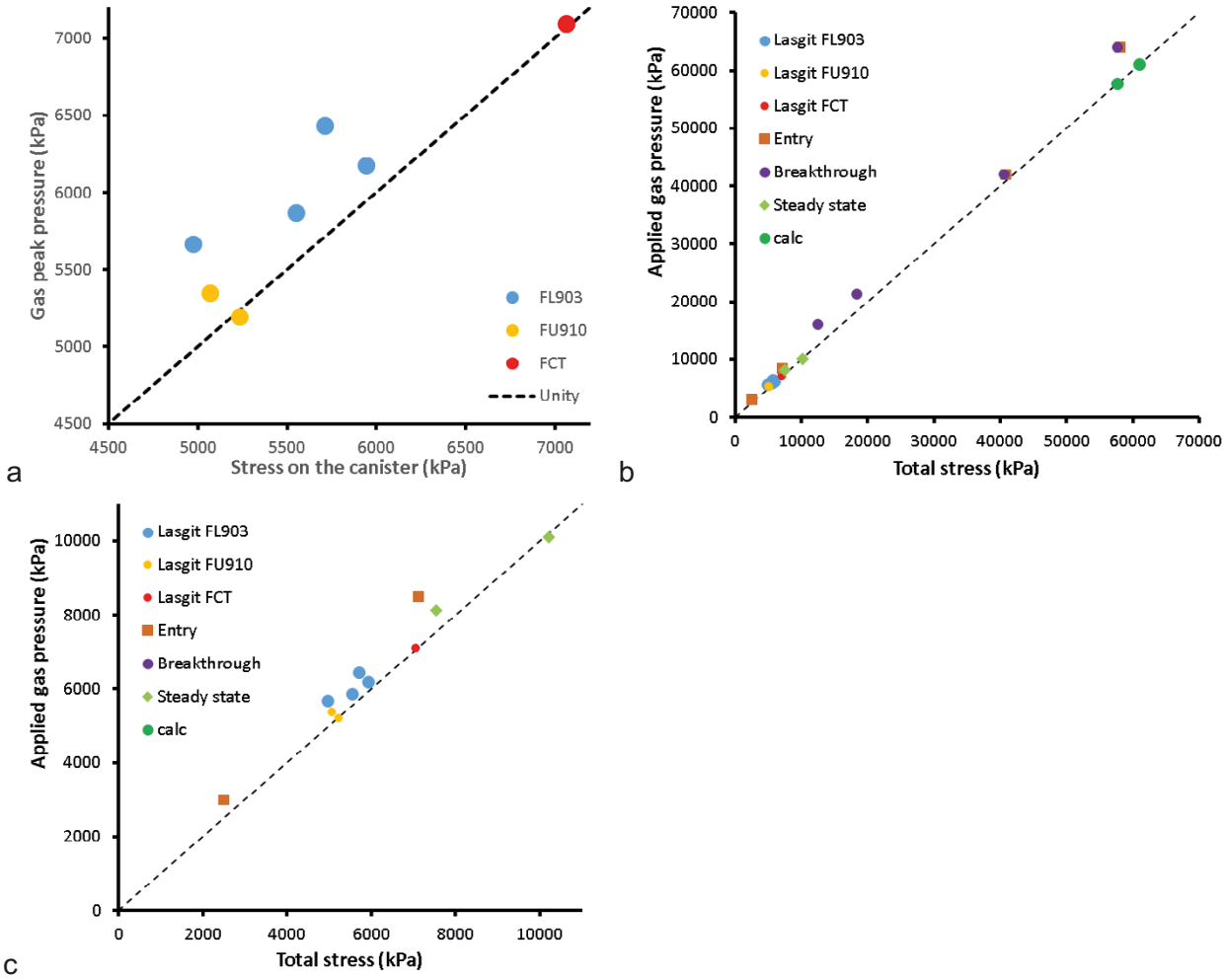

Figure 17-27. *The relationship between gas peak pressure and radial stress on the canister for all gas injection tests in Lasgit. a) Data from Lasgit; b) Compilation of data from tests in bentonite; c) Detail of data compilation.*

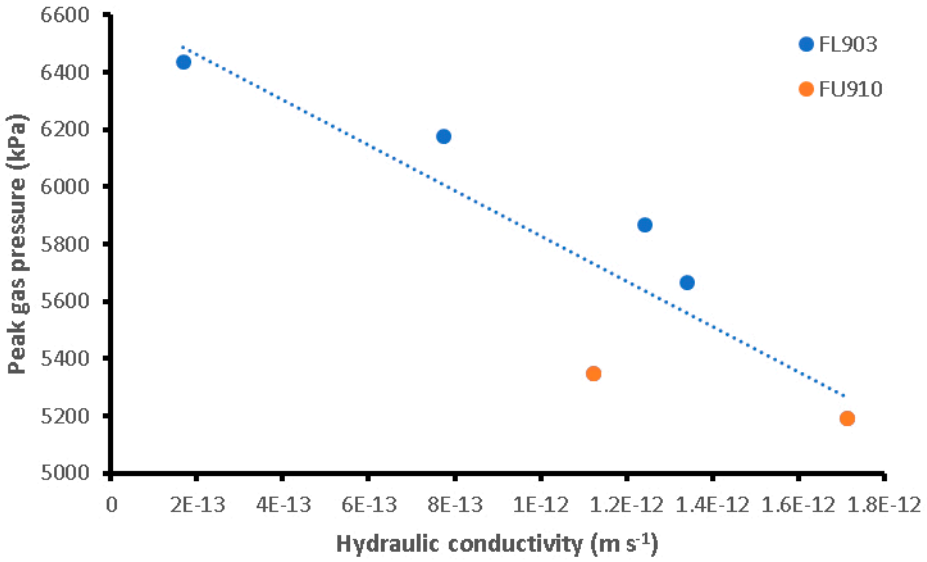

Figure 17-28. *The relationship between gas peak pressure and hydraulic conductivity six gas injection tests in Lasgit.*

17.6 Summary of gas injection testing

All four tests conducted in canister filter FL903 showed a similar pressure response at peak gas pressure, which was different to that seen in FU910. At FL903 pressure rapidly reduced at peak pressure, with generally two events occurring during the initial pressure reduction. Pressure recovered to a single slope of pressure reduction when the data were corrected for differences in injection flow rate. In tests conducted at FU910, the initial pressure reduction at peak gas pressure was followed by a recovery in pressure and a secondary peak either at a similar or higher pressure to the initial peak. The pressure reduction in the first test was smaller than observed in subsequent tests at both filter and this was related to the difference between formation of new pathways and the re-opening of existing pathways in repeat tests.

In the first test conducted at FL903, a pre-cursor flow event was observed, followed by a spike in flow. Most tests in FL903 saw one or more spikes in flow, showing that pathway formation was progressing in stages. After the short-lived spike in flow, the flow into the clay decreased to be lower than the flow into the system and pressure started to increase. This continued until a secondary peak in pressure was seen and the flow into the clay was then marginally greater than flow into the system and pressure slowly decreased. A similar flow response was seen at FU910. However, the initial peak in flow was greater and the flow into the clay reduced to be less than flow into the system for much longer, resulting in an increasing pore pressure. No pre-cursor flow events were seen at this filter.

Extended testing gave useful insights into gas flow. In GT2 a series of pressure reductions and recovery were seen. This suggests that flow paths were developing with time. The pressure reduction occurred as a conductive feature(s) allowed gas pressure to reduce, probably due to gas leaving the deposition hole. This pathway partially closed as gas pressure reduced and as a result, the conductivity of the pathway also reduced and gas pressure increased until the pathway was re-opened and pressure reduced once more. The results from GT4 confirm this. Gas flow into the system was reduced in two steps, once stable flow had been established, each approximately halving the flow of the previous step. On the third step, pressure started to increase, suggesting that the force required to keep pathways open was flow-rate dependent. As flow was reduced, the pathway partially closed, decreasing conductivity and thus increasing pressure. In GT3 and GT5, prolonged gas injection resulted in a series of peaks in gas pressure. This behaviour is similar to that seen in ‘fault valve behaviour’ or episodic flow, where the conductivity of a feature gets reactivated at a given pressure, allowing fluid to flow and pressure to decrease. In the two tests conducted at FU910, this may mean that the pathway connecting the gas to the wall rock was acting as a valve and that the pathways were unstable.

The primary control of gas peak pressure was local stress. This was difficult to determine in filters FL903 and FU910 with a high degree of certainty. However, estimates of the local stress show that gas peak pressure occurred at, or a little above, local stress. The maximum difference between the local stress and peak pressure was ~600 kPa. A secondary control on gas peak pressure was the maturity of the buffer, which in itself was linked to the development of stress. The ending of artificial hydration resulted in stresses in the system being reduced, yet gas peak pressure continued to increase. The buffer continued to mature even though stress had reduced. This was confirmed in the hydraulic conductivity data that showed continued reduction independent of whether or not artificial hydration was occurring. The results from Lasgit show that gas peak pressure was related to the modelled hydraulic conductivity determined from two-stage constant head tests.

The movement of gas was inferred from the array of pore pressure and radial stress sensors at the rock wall, and from the direct movement of gas to sensors during the test. In the first test in FL903 (GT1), the data indicate that the gas moved downwards along the outside of the canister and then along the interface between two bentonite blocks. In test GT2, the gas moved 180° around the canister, before migrating to the base of the canister and later finding a way from the deposition hole, most likely between bentonite blocks. This may have exploited the same features formed in GT1. In GT4, gas also moved to FL901 and it is likely that this test re-activated features formed in GT2.

In the first test conducted in FU910 (GT3), considerable movement was seen. The gas first moved 90° around the canister to FU909, before intercepting FU911, the filter 90° the other way around the canister. Gas then moved downwards, intercepting a stress sensor (PC903), before reaching FL904, the filter on the lower array of the canister filters. In GT5, this repeat test immediately reached FU909 and PC903. This showed re-activation of some of the pathways formed in GT3, but not the re-activation

of all. In the Full Canister Test, gas reached UB902 and FL901, pathways that had been established in previous tests using FL903. Therefore, there was evidence that subsequent gas injection tests behaved similarly and that pathways may have re-activated. However, it is clear that the migration of gas was not identical between tests, with new pathways forming. The formed pathways then, at least partially self-sealed.

18 Gas migration in safety assessment

18.1 Questions relating to the treatment of Gas in Safety Asessment

The bentonite buffer is an important barrier in the KBS-3 system. The key purpose of the buffer is to serve as a diffusional barrier between the canister and the groundwater in the surrounding rock. It is important to ensure that the core safety functions of the barrier components/systems are not disrupted by the interaction between gas and the buffer. However, gas build-up from corrosion of the iron insert could potentially affect the buffer performance in five ways:

1. Permanent pathways in the buffer could form at gas break-through. This could potentially lead to a loss of the diffusional barrier.
2. If the buffer does not let the gas through, gas pressure build-up could lead to mechanical damage of the other barriers. The main concern is damage to the near field rock.
3. The gas could de-water the buffer and alter its thermal conductivity.
4. A gas phase could push water containing radionuclides through the buffer, along gas-generated pathways.
5. If there is an interaction between the gas phase and the clay, clay particles could potentially be attached to the gas and be transported away.
6. Some radionuclides may be transported in a gaseous phase.

The process of gas transport within the buffer is only considered for the case of deposition holes containing a defective canister. Under these circumstances, results of model and experimental studies of gas build-up and transport are considered in an integrated assessment of the internal evolution of a damaged canister, including corrosion of the cast iron insert and water transport within the canister. The coupling between gas pressure, total stress and porewater pressure within the deposition hole and near field are considered.

The global rate of corrosion of the insert will determine if the hydrogen gas produced could escape by diffusion or if a separate gas phase would be formed. Therefore, the corrosion rate determines the rate of gas pressurisation. If gas advection (through pathway dilatancy) evolves as the dominant transport mechanism, gas pressures may be transferred to the near-field rock and tunnel backfill. It is assumed that the buffer will open and let the gas through at a pre-determined gas pressure. Neglecting the possible impact of gas-induced consolidation, this maximum pressure is considered to be dependent on the swelling pressure of the buffer and the prevailing groundwater pressure. However, while the swelling pressure (at constant volume) is a key parameter and should be approximately equal to the minimum pressure at which gas becomes mobile in the buffer, the maximum gas pressure is strongly associated with the ease at which gas can exit from the deposition hole. This is controlled by the number, location and geometry of the available sinks. If the gas fails to find a sink, the pressure will continue to rise which could lead to damage of repository systems. Laboratory measurements by Harrington and Horseman (2003) showed it was possible to create large gas pressures within buffer material, if gas was unable to find a suitable sink. Peak gas pressure is also influenced by the hydrostatic pressure (p_w) and therefore the effect of a glacial overburden, leading to increased hydrostatic pressure, needs special consideration (Graham et al. 2016). However, the latter was beyond the scope of Lasgit.

A remaining uncertainty in the understanding of gas transport in the buffer material therefore concerns the number, size and spatial arrangement of the gas-bearing features and the volume (stress/strain) behaviour of the clay during gas flow. One remaining uncertainty is the break-through pressure, i.e. the pressure at which the buffer opens and lets the gas through. This, in part, determines the maximum pressure that can be created within the near field of the repository. Another uncertainty is the closure pressure, the pressure at which the pathways in the bentonite close and whether or not a ‘memory’ of these features remains within the clay. Though laboratory experiments indicate that only a minimal volume of water is displaced during gas flow, the degree to which this applies at the field scale remains uncertain (Horseman et al. 1999, Harrington and Horseman 2003, Graham et al. 2012, Harrington et al. 2017). In addition, potential de-watering of the clay may affect the performance of the buffer.

The evolution of the gas pressure and the transport of gas in bentonite in the Preliminary Safety Analysis Report (PSAR) is still based entirely on values obtained from laboratory-scale experimental results. The complexity of the flow processes and the uncertainties regarding the interpretation of the experiments make predictive modelling difficult at this stage (see above). The paucity of laboratory data available for further model development and calibration (both conceptual and numerical) is an ongoing barrier to the quantitative forecasting of gas behaviour in performance assessment.

18.2 Background

If a canister used for the encapsulation of radioactive waste (Figure 18-1) should become defective such that groundwater could penetrate through the copper shell, the cast iron insert will corrode, resulting in the formation of hydrogen gas. If more hydrogen is produced than can be dissolved in the water present in the canister and surrounding buffer, a separate gas phase will form.

Gas which is trapped in or by the buffer can escape by two principal mechanisms:

- If the production rate is low or the gas quantity small, the gas may be dissolved in the porewater and be removed by diffusion.
- If the production rate is higher or the gas quantity is larger than can be removed via dissolution and diffusive processes, a separate gas phase will form, the pressure will rise and a flow path is expected to be formed through deformation of the buffer at a critical pressure.

Figure 18-1. *The KBS-3 disposal concept. Fuel rod assemblies are held within an iron insert, inside a copper canister. Surrounding this is pre-compacted bentonite rings isolating the canister from the crystalline wall rock.*

Before the buffer is saturated, only water is expected to be able to enter a damaged canister via vapour-phase diffusion. Hydrogen production from corrosion will therefore be limited, and if sufficiently small, the gas that will be formed may be able to migrate from the buffer via diffusive transport (Wikramaratna et al. 1993). The resistance to gas transport, in terms of the gas pressures necessary to allow migration in an unsaturated buffer is considerably lower than in a saturated one (Graham et al. 2002, Villar et al. 2012). Canister damage at this early (unsaturated) stage is thus unlikely and the interaction with gas at high buffer saturation states is a more probable scenario. This was the governing rationale for performing Lasgit under ambient temperature conditions and with the buffer in a fully saturated state. Under these conditions, the thermodynamic equilibrium condition is summarised as:

$$\sigma = \sigma_{eff} + p_w = \Pi + p_w$$

where σ is the total stress, σ_{eff} the conventional (Terzaghi) effective stress, p_w the hydrostatic pressure (often referred to as porewater pressure) and Π is the swelling pressure. In clay such as bentonite, which contains a high proportion of swelling minerals, the effective stress and swelling pressure are directly proportional (Horseman et al. 1996).

Hydrogen gas formed by corrosion of the cast iron insert can dissolve in the porewater and migrate from the canister by diffusion and advection under the prevailing hydraulic gradient. The maximum transport capacity for different conditions has been estimated by Wikramaratna et al. (1993). The results of the calculations show that the diffusive transport capacity is considerably lower than the hydrogen gas production from corrosion, if it is assumed that the entire surface of the cast iron insert is accessible for corrosion and the water supply does not limit corrosion. Under such conditions it is probable that a gas phase will be formed inside the canister and that the gas must, therefore, escape as a discrete gas phase (advection).

The following account of the subsequent course of events is an interpretation of the results of theoretical and experimental studies (Horseman et al. 1999): At a critical pressure (the entry pressure), the buffer is expected to develop pathways that will allow the gas to migrate by advection. When the pressure reaches this value, a transport pathway is formed through the buffer and gas is released. After the pathway is formed, two different evolutions are possible:

1. If gas production is maintained, the pressure will fall to a steady-state pressure i.e. pressure remains at a constant value. When the production ceases, the pressure falls and, if the gas production is low enough, the transport pathway is expected to close. This takes place at a so-called “shut-in pressure”, which is related to the swelling pressure of the clay (Horseman et al. 1999). At pressures lower than the shut-in pressure, gas will again only migrate solely by diffusion.
2. If the gas production rate is small compared to the permeability of the initial flow path(s), as gas pressure declines, the permeability of the pathway(s) will decline. If gas production is unable to produce sufficient gas to maintain an adequate supply, then the aperture of the pathways will decrease (and may close). Under such conditions, variations in gas production rate may potentially result in episodic periods of gas migration along these pathway(s).

In an unsaturated or partially saturated bentonite there is a linear dependence between gas flow rate and pressure gradient, which indicates that two-phase flow would be the dominating transport mechanism (Villar et al. 2012). This may also be the case for saturated sand-bentonite mixtures if the sand content is sufficiently high. At a degree of saturation of ~ 80–90 % or higher the behaviour changes entirely (Graham et al. 2002, Villar et al. 2012, Sellin 2014). No advection of gas will take place in the bentonite unless the applied pressure is equal to or higher than the total stress. The only transport mechanism is the omnipresent diffusion of dissolved gas and the movement of dissolved gas by advection under the prevailing hydraulic gradient. If the gas pressure reaches a higher value than the total stress within the bentonite, a mechanical interaction will occur (Birgersson et al. 2008, Graham et al. 2012). This will lead to either:

1. Consolidation of the bentonite, and/or
2. Formation of dilatant pathways.

Consolidation can occur when the clay material is compressed by the formation of a gas phase. This occurs at gas pressures in excess of the initial local total stress and can result in the possible movement of water and densification of the clay. This increase in clay density as gas pressure increases results in a commensurate increase in the local swelling pressure, which evolves to match further increases in gas pressure. While the limit to the extent of localized consolidation remains unclear, at some critical pressure, dilatant pathways are formed, and the gas will become mobile. These pathways are characterized by: that a gas volume will be formed within the clay which is then compressed as the gas pressure rises. This increases the clay density closest to the gas volume and the local swelling pressure is increased to balance the gas pressure. While the limit to the extent of consolidation remains unclear, at some critical pressure, pathways are formed, and the gas will become mobile. These pathways are characterized by:

(i) a strong coupling between total stress (σ), Π_{sw} (swelling pressure) and pore pressure (p_w),

(ii) variable aperture and number distributions of pathways,

(iii) localised changes in σ, Π and p_w, and

(iv) unstable flow pathways that exhibit spatio-temporal evolution (Graham et al. 2012).

Outflow is localised during gas breakthrough and in previous experiments no measurable desaturation of the bentonite was observed (Horseman et al. 1999; Harrington and Horseman 1999, 2003, Graham et al. 2012, Harrington et al. 2019).

The energy that drives gas transport comes from compression of the gas inside the canister and is proportional to the available gas volume. If it is assumed that the volume is a cubic metre and the gas pressure drops from 12 to 9 MPa, 30 MJ of energy will be released when the transport pathway is formed. In the case of experiments performed in low density clays, under unconfined conditions, gas breakthrough has been shown to have the potential to be a violent process (Donohew et al. 2000). However, in a system with confined clay (such as the deposition holes in the SKB KBS-3 concept), the expectation is that gas will be released in a controlled manner, i.e. it will not entrain the buffer material along with it.

18.3 Information from Lasgit

The main objective of the Lasgit project was to derive further information on the uncertainty regarding up-scaling of laboratory-based gas migration tests in bentonite. The issues of interest were:

- The maximum (peak) gas pressure.
- The pressure transient response after gas breakthrough (self-sealing capacity).
- Hydraulic properties of the bentonite after gas breakthrough.
- Possible desaturation of the bentonite.
- Gas transport mechanisms.

All of these issues have been examined in this project and are presented in this report. An additional issue of potential concern would be the attachment of clay particles (colloids) to the gas phase and a subsequent loss of buffer material. This process has not been studied in Lasgit, since the mass of bentonite in the test is so large that it would be impossible to detect any loss of material. However, clay attachment to a gas phase is more likely to occur if the gas moves in the form of bubbles (Neretnieks and Ernstsson 1997). Clay transport with gas has however not been observed in any of the laboratory test preceding Lasgit (e.g. Harrington and Horseman 2003).

18.3.1 The maximum (peak) gas pressure

Background

With the assumption that the generated gas would be unable to escape by diffusion alone, a gas phase will form and a gas pressure will be generated. The magnitude of the pressure determines how much force will potentially be transmitted to the barrier components within the repository, including the surrounding rock. It will also determine the amount of energy stored and then released during gas breakthrough. The maximum pressure is therefore the most important parameter regarding the performance of the repository.

In the SR 97 safety assessment (SKB 1999) it was stated that gas would start to move through the buffer when the gas pressure exceeded the sum of the swelling pressure and the hydrostatic pressure. When the pressure reaches this value, a transport pathway is formed through the buffer and gas is released. The experimental results (e.g. Horseman et al. 1999, Harrington and Horseman 1997, 2003, Graham et al. 2012, Harrington et al. 2017, 2019) suggest a system of microfractures is formed due to rupturing of the clay. Gas pressure then falls and the gas production rate determines the further course of events. If the pressure falls to a sufficiently low value, the transport pathway(s) begin to close. This so-called "shut-in pressure" is dependent on the swelling pressure. At normal swelling pressure, ~5–6 MPa in the Lasgit experiment (assuming homogenization of the buffer), the shut-in pressure is equal to the sum of the swelling pressure and porewater pressure. Gas pressures can fall somewhat below this value if pathways are unable to spontaneously seal. After that, gas would once again migrate solely by diffusion, see Figure 18-2. If gas production continues long enough, a cycle is obtained with successive gas pulse releases and pressure build-ups (Graham et al. 2016). If, on the other hand, gas production is high enough to sustain a higher pressure, the gas transport pathway is expected to remain open.

Later laboratory tests e.g. Harrington and Horseman (2003) showed that the gas pressure could reach values substantially higher than the sum of the swelling pressure and the hydrostatic pressure. In the test MX-80-10, the gas pressure was in excess of 7 MPa greater than the total stress in the clay (Figure 18-3). The results showed that gas pressure under constant volume conditions could rise to exceed the total stress by a significant amount, depending on the ability of the gas to find a suitable sink.

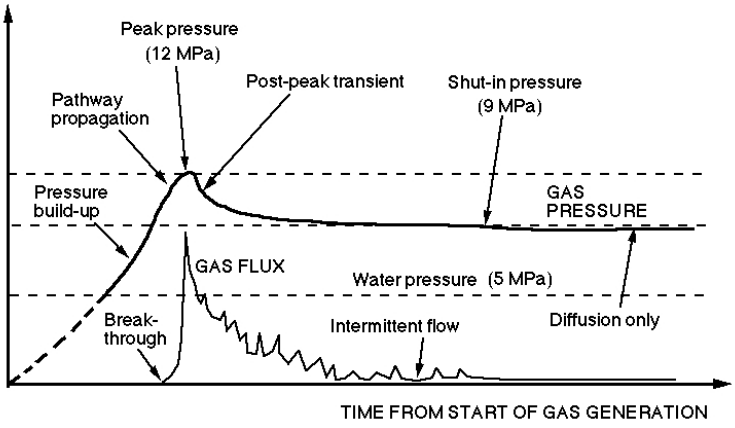

Figure 18-2. *Temporal course of gas transport through bentonite. The timescale in the figure is relative and dependent on the rate of pressure build-up (SKB 1999).*

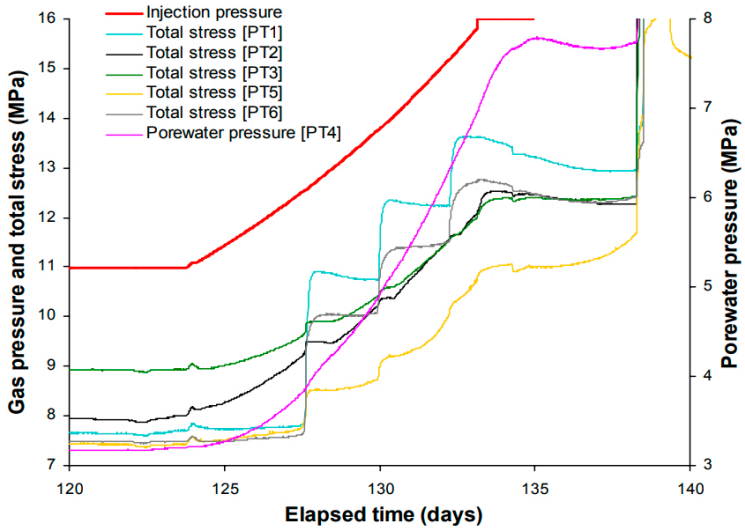

Figure 18-3. *Response of the total stress and porewater pressure sensors in MX-80-10 (Harrington and Horseman 2003).*

Birgersson and Karnland (2015) performed a number of pressure response tests with water and gas on relatively low-density bentonite samples. In some samples, states could be maintained where injection pressure exceeded the initial sample pressure without inducing gas breakthrough. In these states, sample pressures did respond to the applied gas pressure: in some cases, sample pressure equalled injection pressure, while in others injection pressure could exceed sample pressure quite considerably. This type of behaviour was interpreted as consolidation of the clay body (i.e. volume reduction by release of water). In one specific case, consolidation was also confirmed visually.

It is clear that gas pathways do not form at a gas pressure equal to the sum of the swelling pressure and hydrostatic pressure under all experimental conditions. The reason, or at least one reason, for this is local consolidation of the clay close to the entry point of the gas. This seems to occur under some experimental conditions but not at others and may relate to the pressurisation rate of the gas. As such, it is not clear when consolidation will occur, though it may also relate to sample size, sample density, sample heterogeneity, sample geometry, the shape of the clay/gas interface or a combination of these factors.

Observations

In total, seven gas injection tests were performed in the Lasgit experiment, with tests GT1, GT2, GT4 and GT6 performed near the base of the canister in filter FL903, and tests GT3 and GT5 undertaken in filter FU910 towards the top of the canister. The seventh FCT test was performed through a filter located in the base of the canister, just before the end of the Lasgit project. In the early tests (GT1 and GT2) performed whilst the buffer was in a poor state of maturity (i.e. the bentonite was in a state of porewater pressure and stress disequilibrium), small precursor gas flows into the bentonite were thought to have occurred, based on an assumption of the starting gas volume. However, when gas pressure was held constant, the rates of inflow massively reduced suggesting a hiatus in (or very limited) pathway growth. In all tests, injection led to the continued pressurisation of the gas and an increase in gas pressure. Data presented in Figure 18-4 and Figure 18-5 shows a systematic increase in peak gas pressures as the bentonite continued to mature and move towards hydraulic equilibrium. Similar to laboratory tests, peak gas pressure was always equal to, or, in most cases in excess of, local total stress.

Data presented in earlier chapters (e.g. Section 16.3) clearly shows the importance of porewater pressure (and the accessibility of groundwater) in the development of total stress in the deposition hole, and that even after nearly 6 000 days of testing, the buffer was still not in hydraulic equilibrium. As the behaviour of the bentonite in the Lasgit experiment mirrored that of previous laboratory experiments, it is reasonable to extrapolate the data in Figure 18-4 to the expected final swelling pressure of the clay. Under these circumstances, peak gas pressures would remain within manageable levels and would be unlikely to exceed 8–9 MPa. There is no evidence, based on the observations from the Lasgit experiment, that large gas pressures, similar to those sometimes observed in laboratory tests, occur under field conditions. Data suggests that the mechanisms governing advective gas flow are scale invariant and the sheer volume of bentonite and density variations caused by engineering voids, provides a compressibility within the system that is likely to moderate peak gas pressures and allow gas to find a suitable sink.

Homogenisation of the buffer, therefore, emerges as an important consideration in the treatment of gas in safety assessment. In Lasgit, gas pathways were shown to have developed in regions of lower dry density close to the canister surface and the walls of the deposition hole, and to have exploited interfaces between the pre-compacted bentonite blocks. These residual heterogeneities will have acted to lower peak gas pressures within the Lasgit experiment and allowed gas to more readily egress the deposition hole through one of many intersecting fractures. In a fully homogenised system it is conceivable that gas movement may be even more restricted and that peak gas pressure could increase marginally. That said, given the scale invariant nature of the processes controlling gas flow, it seems unlikely this would lead to substantially higher gas pressures as those observed in laboratory testing (assuming gas can find a suitable sink).

While peak gas pressures were seen to increase from one test to the next during the lifespan of Lasgit, within an individual test where two peaks were observed e.g. GT5, both values remained consistent. In contrast, in GT3 gas pressure exhibited a continuous upward trend, exceeding even the initial peak pressure associated with the onset of gas flow. Similar behaviour has been noted in laboratory tests, where successive steady state pressures (following a shut-in period) increased with each flow event. The cause of such behaviour is unclear but is thought to be linked to localised consolidation around flow paths making it harder for successive gas events to deform the clay. As it is generally considered gas will always take the "path of least resistance," subsequent flow events may have to access progressively more difficult and tortuous routes through the clay. The impact, if any, of such behaviour was not directly tested or observed during Lasgit.

Nevertheless, it must be acknowledged that the role of gas-induced consolidation of the buffer and its potential impact on peak gas pressure was not examined as part of the Lasgit project. It is conceivable that gas compression rates higher than the limit for diffusive transport but below the hydraulic drainage rate of the buffer, could result in consolidation and densification of the clay adjacent to the gas phase, ultimately leading to an increase in peak gas pressures. The impact of this coupled process therefore remains an uncertainty in the treatment of gas within safety assessment.

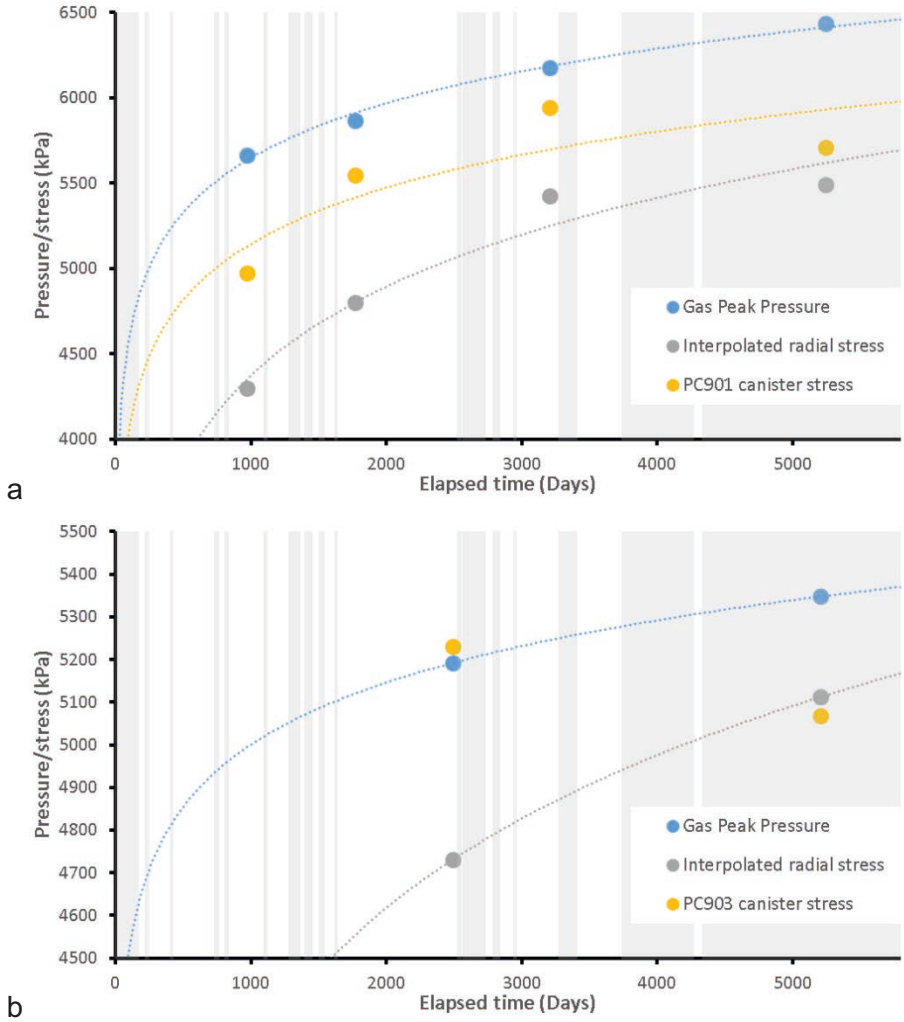

Figure 18-4. *Increase in peak pressure, interpolated radial stress, and canister stress for the (a) tests performed in filter FL903 and (b) the two tests in FU910 fitted with a logarithmic curve to be consistent with the data presented in (a).*

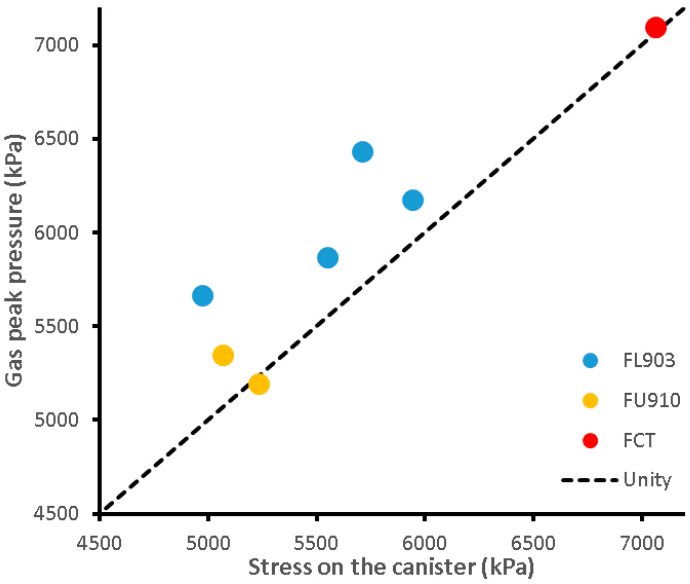

Figure 18-5. *The relationship between peak gas pressure and stress on the canister.*

Summary of the maximum (peak) gas pressure

The maximum recorded pressures in Gas Injection Tests 1–6 were always close in magnitude to the total stress. The peak gas pressure increased between each successive test (Table 18-1) but there were no indications of the substantially elevated gas pressures sometimes observed in small scale laboratory tests. This suggests that over pressurisation from the generation of gas due to corrosion of an iron insert will not occur in a KBS-3 repository. The maximum gas pressures are therefore expected to be in the same range as the sum of the swelling pressure of the bentonite and the hydrostatic pressure. Finally, the impact of gas-induced consolidation was not observed in Lasgit, though compression rates of the gas were high compared to those associated with corrosion. Whilst highly unlikely to lead to over-pressuring, this process remains unresolved in safety assessment.

Table 18-1. Summary of breakthrough pressures in Lasgit.

Gas test	Filter	Breakthrough pressure (kPa)
1	FL903	5660
2	FL903	5868
3	FU910	5192
4	FL903	6174
5	FU910	5347
6	FL903	6437
7	FCT	7100

18.3.2 The pressure transient response after gas breakthrough (self-sealing capacity)

Background

The time dependence of the pressure drop determines how fast the energy stored in the pressurised canister can be released. It is not clear if this has an impact on the performance of the repository. A fast energy release could potentially lead to damage to the bentonite barriers but it has never been confirmed that this is the case. However, the transient after breakthrough can be used for the interpretation of the gas transport mechanism and can give information about the self-sealing ability of the bentonite. Small scale experiments generally show a rather rapid early transient followed by a slower drop in pressure. A typical example of this is the MX-80-10 test conducted by Harrington and Horseman (2003) (Figure 18-6).

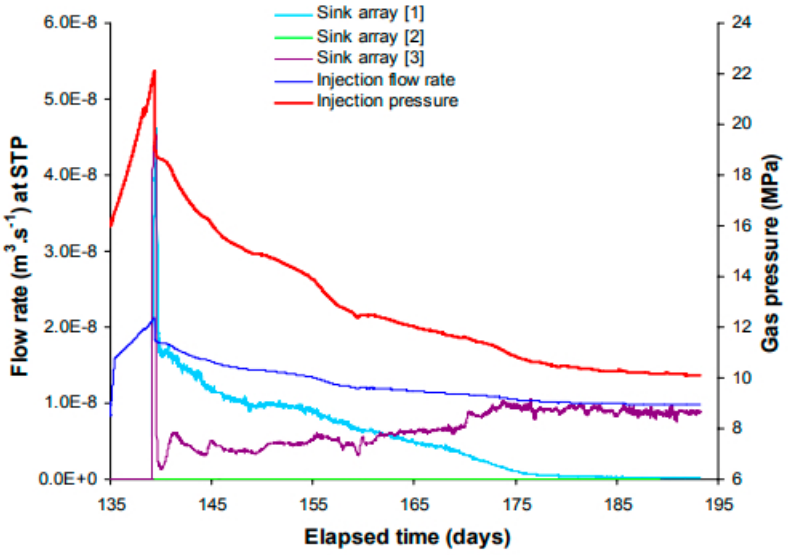

Figure 18-6. *Post-peak transient of the controlled flow-rate stage of laboratory test MX-80-10, showing the STP flow rates into the system and out of the sink array. Mass balance considerations confirm that the flow is predominantly gas. The pressure transient approaches an asymptote at the (near) steady-state condition, at which flow rate into and out of the specimen are approximately equal. The sharp drop in pressure immediately after the peak is suggestive of a breakdown in tensile strength (Harrington and Horseman 2003).*

In Figure 18-6 the relative flow to the different sinks changed during the negative transient. This was a clear indication that the gas pathway(s) changed temporally and spatially and that the flow took place in a number (> 1) of discrete pathways. Based on a detailed analysis of the total stress data, more recent data by Harrington et al. (2017) indicated the number of pathways can be > 100 at the laboratory scale. Data from the same authors also showed a qualitatively similar post-peak response to Figure 18-6 but with a small peak pressure. Clearly the size and rate of the post peak pressure transient will be linked to the ability of the gas to find a sink outside of the deposition hole.

Observations

As discussed in the previous section and earlier chapters (section 17) the size of the negative pressure transients were small compared to some previous laboratory studies. However, there was some variability between the tests. In some tests, GT1 and GT6, a relatively stable "steady state" was reached quite quickly after gas breakthrough. In GT2 the pressure after breakthrough was rather unstable, suggesting closing and opening of pathways. In gas tests GT3 and GT5 there was a second increase in gas pressure after breakthrough, suggesting that the pathways did not have sufficient transport capacity for the actual gas flow. The results from the FC, are not directly comparable to the other tests, since gas entry occurred after displacement of water from the canister at a gas pressure slightly higher than that expected for gas flow. In the FCT, the pressure reduced at a slow rate which appeared to be decreasing with time.

Data also indicated that pathway sealing following a gas injection event was only partially successful. Analysis of porewater and stress data showed repeat gas injections through the same filter, often many hundreds of days apart, utilise, at least in part, the same network of pathways as in the previous test. However, similar to the spatial and temporal evolution of pathways seen in Figure 18-6 and Figure 18-7, observations also indicated that new pathway(s) developed as gas pressures decayed. Data also showed that pathway sealing was locally enhanced through the injection of water between tests.

Summary of self-sealing capacity

Observations of the pressure gradient after breakthrough and peak gas pressure in Lasgit were generally consistent with the observations from laboratory studies. There was always an initial drop in pressure after breakthrough. If pumping/gas generation continued at a sufficient level, the gas pressure levelled off to a steady-state value. In laboratory experiments at shut-in there was a further pressure

decay down to a capillary threshold pressure. This behaviour was not examined in Lasgit due to the exponential nature of the pressure decay curve and the very long experimental duration this would have necessitated. However, there was nothing in the Lasgit data to suggest that a dissimilar response to that of laboratory tests might occur, given sufficient time. The rate of pressure drop in the FCT was much lower compared to the other tests, because of the much larger upstream gas volume. This clearly demonstrated that a slow energy release can be expected, even if the volume of gas is large. It also suggests that the number and volume of gas pathways was gas volume invariant and was more sensitive to gas pressure than gas volume. This is an important observation from the Lasgit experiment.

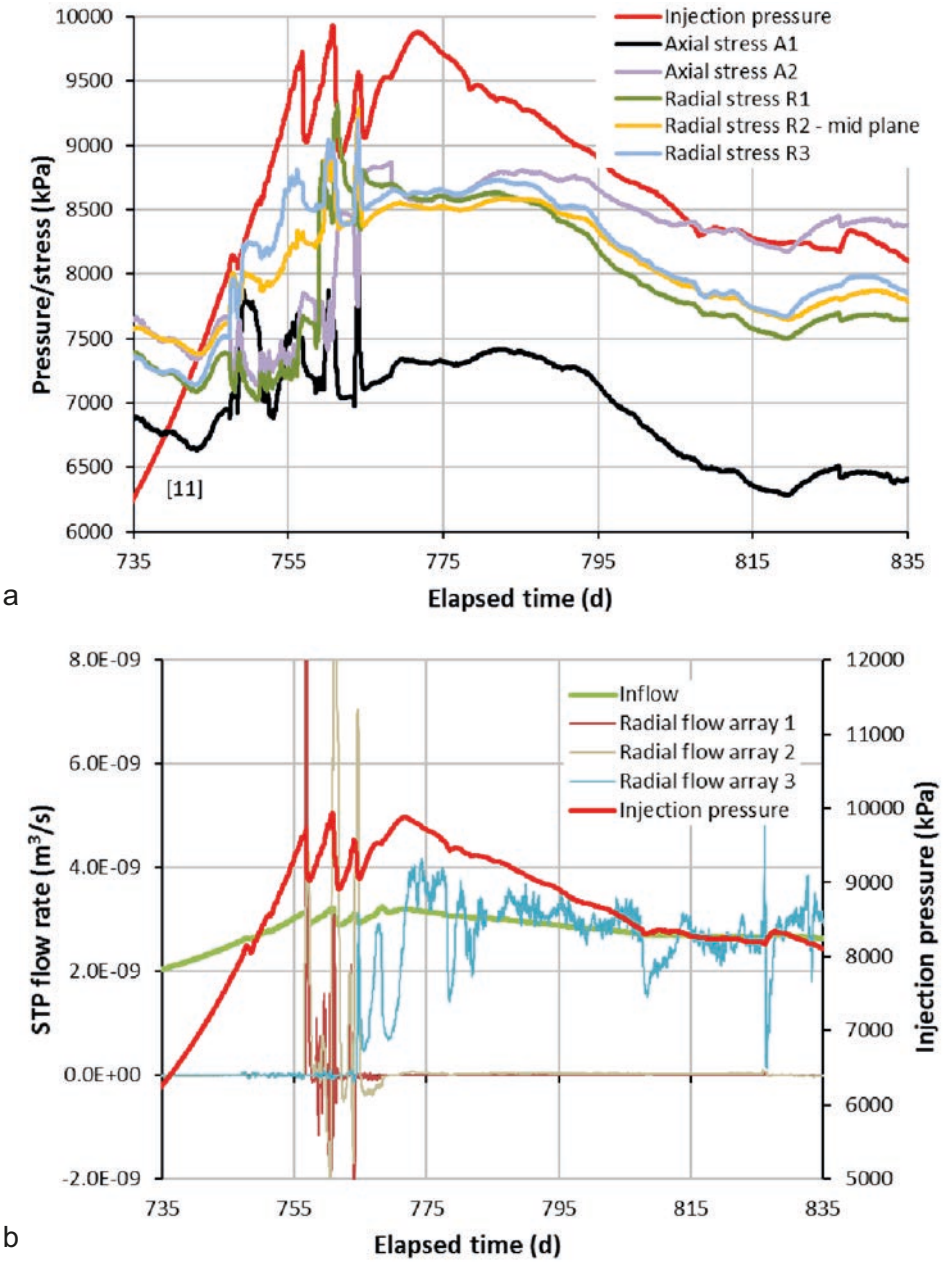

Figure 18-7. *Injection pressure, stress and out flow data from laboratory tests (Harrington et al. 2017). a) The evolution in stress behaviour from initial gas entry to steady state conditions. The peak in gas pressure (around Day 767.6) was followed by a protracted negative pressure transient leading to a quasi-steady state by around Day 825. During this period, the change in injection pressure was mirrored by the total stress, which exhibited none of the chaotic patterns observed with earlier breakthrough events. The reduction in the variability of stress from Day 768 onwards was accompanied by the development of 'stable' outflow conditions (b) with flux localised to one drainage array.*

It was also clear that, within the Lasgit experiment when water was not directly injected into the network of pathways, gas pathway closure was a very slow process. Accessibility of water, the hydration state of the buffer and the volume of gas stored within the pathways emerged as key factors controlling pathway self-sealing. In part, these relate to the homogenisation state of the buffer. As gas generation is most likely to post-date the main thermal stage of the repository, it is expected that the bentonite will be in a good state of homogenisation (including hydraulic equilibrium). Under these conditions, it is expected that pathway sealing will be more efficient once gas migration has ceased. This is dependent on the rate of gas production and pressurisation, the impact of which has been discussed earlier in this chapter.

18.3.3 Hydraulic properties of the bentonite after gas breakthrough

Background

A key uncertainty regarding gas transfer through bentonite relates to the likelihood that hydraulic properties will be restored once gas generation ceases or reduces to levels where diffusion of dissolved gas is the dominating transport mechanism. Previous laboratory experiments by Harrington and Horseman (2003) suggest that the permeability of the bentonite before and after gas testing remains very similar, with only differences in the specific storage term due to the presence of residual gas thought to be trapped within the network of previously conductive gas pathways. This is intuitive, since the bentonite has a high swelling capacity and will have access to water.

Observations

To examine the effect, if any, on the hydraulic properties of the buffer following gas injection, multiple hydraulic tests were performed in filters used for gas testing. An example of the hydraulic data before and after gas testing is shown in Figure 18-8. A visual inspection of the data clearly indicates that little, if any, significant change in hydraulic permeability had occurred following injection of gas. The slight offset in the red line is indicative of a small change in hydraulic storage, similar to that inferred in laboratory scale testing. Based on the data available, gas pathway formation appeared to have had no significant effect on the hydraulic performance of the buffer after gas injection had ceased.

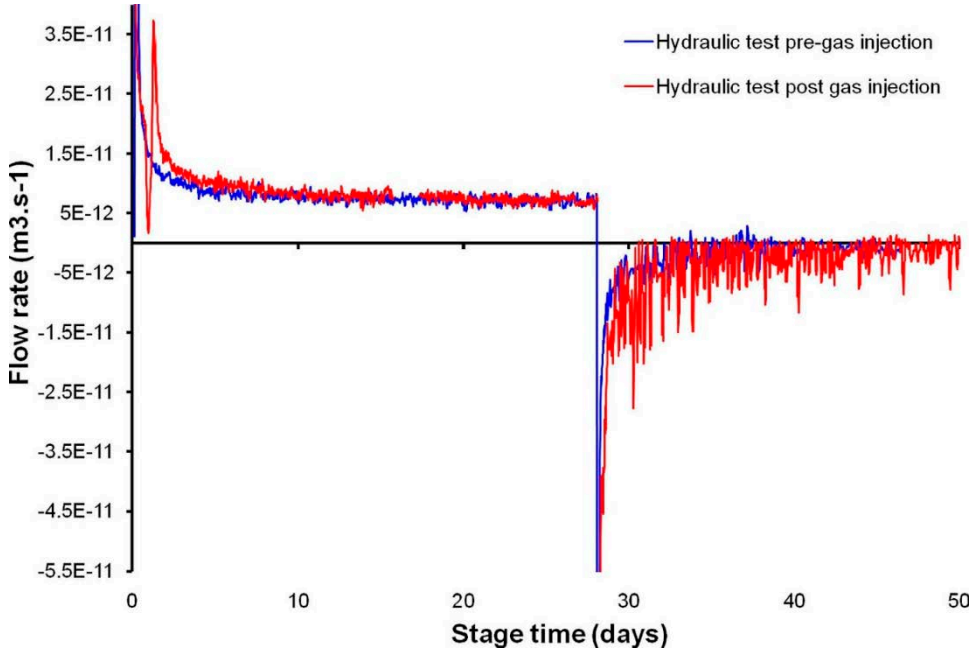

Figure 18-8. *In flow rate for hydraulic tests performed before and after gas injection in Lasgit.*

In Figure 16-39, the hydraulic conductivity of the buffer adjacent to the gas injection filters is plotted as a function of time. Even though four gas injection tests were performed in filter FL903 and two gas injection tests in filter FU910, the intrinsic permeability showed a negative trend with time, i.e. decreasing as the buffer matured. There was no sign within this data of any significant impact of gas on the hydraulic properties of the buffer. Estimates of specific storage, Figure 16-39b, d also showed no obvious impact of gas testing, instead exhibiting a general trend of increasing storage coefficient commensurate with a slow and progressive expansion of the buffer as it hydrated and matured.

Summary of hydraulic properties of the bentonite after gas breakthrough

From the post-gas hydraulic tests performed in Lasgit, it is clear that gas transport through the bentonite had no significant effect on the hydraulic properties of the buffer. As long as water is present the diffusional properties of the barrier will be maintained even after a gas breakthrough event. The data suggest that as the efficiency of self-sealing appears to be strongly linked to the availability of water, residual gas is likely to be trapped within the buffer following the cessation of gas flow. Data from Lasgit suggests that, in the absence of water and on the timescales of the experiment, these pathways remain, at least partially open and can be accessed by subsequent gas flow events. However, it is likely that on the timescales of interest to a repository, removal of residual gas will occur through dissolution and diffusion of gas, and the integrity of the buffer restored. Where access to water is restricted and gas generation rates are high, as are the number of pathways within the clay, the diffusional properties of the buffer may be compromised for an indeterminant period of time. However, given the localised nature of the gas flow pathways, the total fraction of the clay volume containing residual gas is expected to be small in relation to the bulk of the clay where diffusional properties would be expected to dominate.

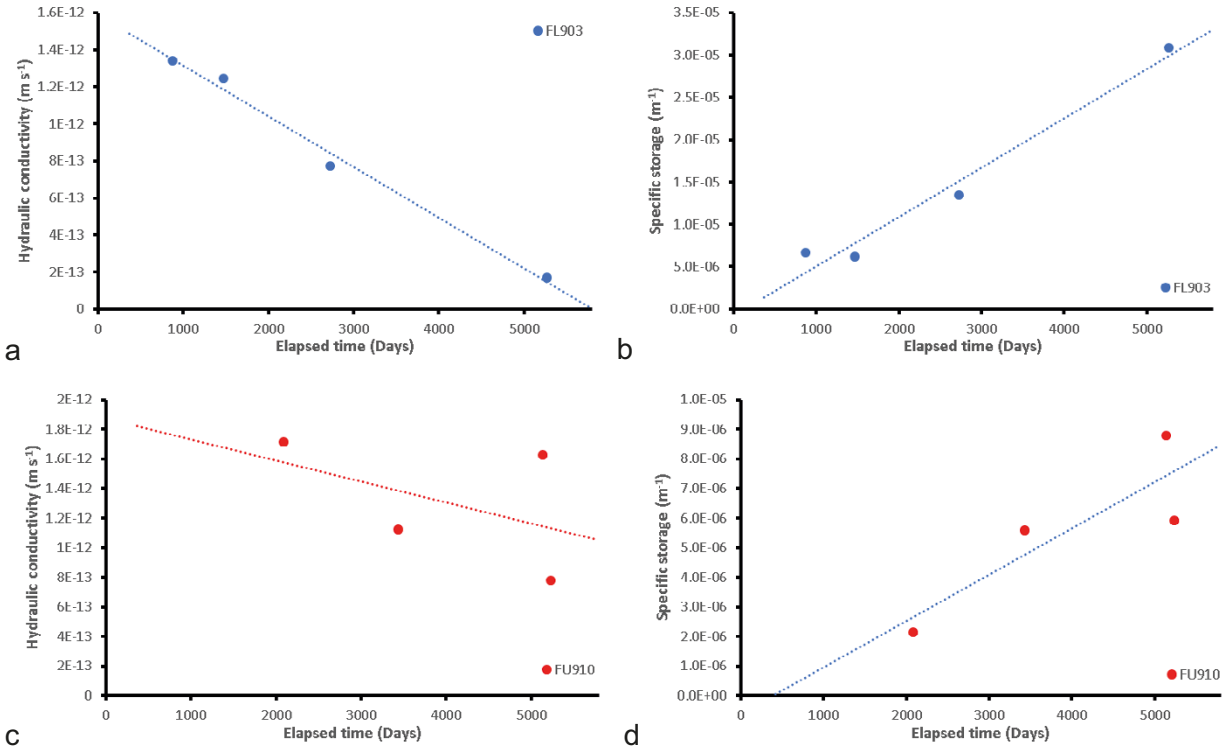

Figure 18-9. *Evolution of hydraulic properties at FL903 and FU910. a) Hydraulic conductivity of FL903; b) Specific storage of FL903; c) Hydraulic conductivity of FU910; d) Specific storage of FU910.*

18.3.4 Possible desaturation of the bentonite

Background

One potential effect of gas migration through bentonite is the possibility for gas to push interstitial water out of the bentonite and for the clay to become at least partially desaturated. However, this behaviour is not expected to occur as the water in the bentonite is tightly bound to the mineral surfaces. It is also questionable whether desaturation would have any negative impact on the barrier; while the thermal conductivity of the buffer would decrease, gas migration is not expected to occur during the period of elevated temperature. Apart from that, a desaturated buffer would limit the transport of dissolved species from the canister to the rock. In laboratory scale experiments (Harrington and Horseman 2003, Harrington et al. 2017) the degree of water saturation was shown to increase during testing, as a result of the initial uptake of water during the hydration phase of experimentation.

Observations

The overall conclusion from all gas injection tests in Lasgit is that gas travels in a finite number of pathways of limited size. During decommissioning, extensive geotechnical measurements were made throughout the buffer. At no time was any evidence of desaturation observed in the test data. The buffer was not in hydraulic equilibrium as the (water) saturation of the clay increased in all locations. The increasing pressures between the tests performed in the same filters (Table 18-1), indicate that the buffer continued to mature during the Lasgit experiment and gas pathways were partially resealed. No evidence for any detrimental impacts on the hydraulic properties, including the presence of residual gas saturations between tests, was observed in Lasgit. This confirms that observations made in the laboratory are valid regardless of the increased scale of testing.

Summary of possible desaturation of the bentonite

No evidence for desaturation of the buffer was observed and the presence of residual gas trapped within the buffer did not result in measurable signs of dewatering.

18.3.5 Gas transport mechanisms

Background

Gas transport in low permeability materials is controlled by the hydraulic and mechanical properties of the material, as well the gas pressurisation rate and the hydromechanical state of the buffer (i.e. water saturation, porewater pressure, stress state etc.). According to Marschall et al. (2005) the transport of gas can potentially occur according to the following mechanisms:

1. Diffusive transport of gas;
2. Visco-capillary two-phase flow;
3. Dilatancy-controlled gas flow;
4. Gas transport along macroscopic tensile fractures (hydro and gas-fracturing).

Advective transport of dissolved gas is unlikely to occur in a bentonite buffer because of the very low hydraulic gradients within a repository. As such, in the absence of gas advection (mechanisms 2 and 3), the diffusive transport of gas (mechanism 1) will be the dominant process and will continue to be so, as long at the rate of gas production is sufficiently low. When the gas production rates exceed the rate at which gas is transported away by dissolution-diffusion, a gas phase will form and mechanisms 2 and 3 will become dominant.

In the context of long-term performance, the mechanism itself may not be that important. The key factor is the consequences of gas transport for key safety functions, as discussed in the previous sections of this chapter. Knowledge of the mechanism is nevertheless valuable, since it may aid the upscaling of experimental understanding, and provide a greater understanding on the consequences for repository performance.

Observations

Diffusive transport of dissolved gas was difficult to evaluate in the Lasgit test. However, this was not intended to be a key area of study in Lasgit.

Data from Lasgit (Figure 17-12) and laboratory scale observations (Figure 18-6 and Figure 18-7) show visco-capillary two-phase flow (mechanism 2, above) is an unlikely transport mechanism at relevant saturations, as no gas movement was observed through the bentonite at gas pressures below the total stress in the system and no desaturation of the bentonite was observed. In addition, the coupling between gas pressure, total stress, and porewater pressure explored in detail in previous chapters further supports dilatancy-controlled gas flow (mechanism 3) as the primary transport mechanism.

Laboratory-scale experiments by Harrington and Horseman (2003) showed that gas flow may change pathway(s) in a negative pressure gradient (Figure 18-10). The observation of dominant gas outflow moving between different available sink locations was interpreted as a clear demonstration of the existence of multiple flow pathways. Similar observations can be seen in Figure 18-6 and Figure 18-7, as flow pathways developed during the onset of gas flow.

While it was impossible to directly measure outflow in the Lasgit experiment, the data from the numerous pore pressure and stress sensors, in what was a highly instrumented deposition hole (and buffer), were used to track the movement of gas within the system. The data shows the complex temporal and spatial development of pathways, as gas intersected specific sensors, e.g. Figure 18-11 from the GT2. These paths were often tortuous and always developed following the onset of gas flow i.e. were not fixed in time and space. The Lasgit data suggests similar behaviour to that seen in the laboratory-scale experiments was also observed in this study. In GT2, gas reached filter FL901 more than ten days before it reached sensor UB902 (Figure 18-11), suggesting a relatively slow growing pathway network. It seems likely that this was caused by multiple transport paths. In the FORGE project (Norris 2015, Sellin 2014), it was found that gas moved preferentially along interfaces. This is confirmed by the results from GT2, where gas was detected in another filter on the canister surface. However, gas was not seen in all filters on the canister surface, which suggests that gas may have migrated through the body of the bentonite before the entire interface between the bentonite and the canister was filled with gas.

The pressure decay in the FCT indicated sudden changes in pressure at certain times (Figure 18-12). This could be interpreted as closure or reduction in the size of pathways. The slow pressure decay in the FCT also suggests that the gas was transported in pathways of more limited size to those observed in GT1 through 6, even when the buffer was exposed to a large volume of gas. This contradicts, at least to some extent, the mechanism of rapid macroscopic tensile fracturing (mechanism 4).

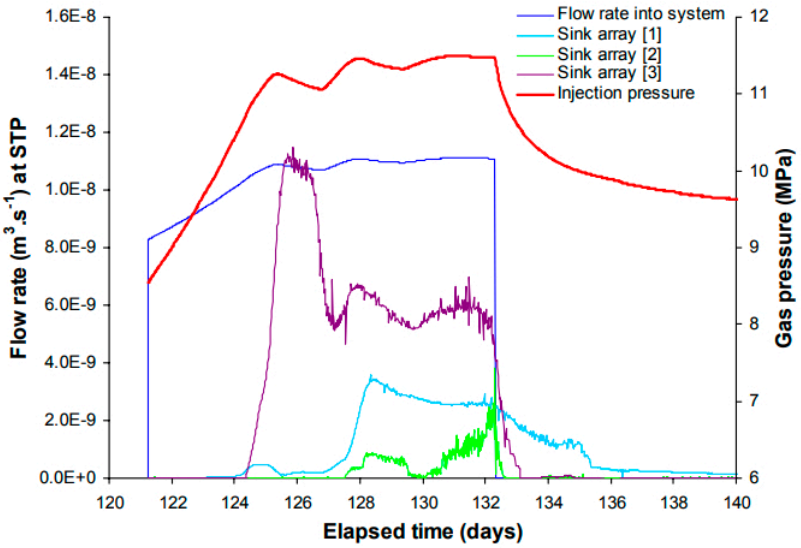

Figure 18-10. *Gas injection pressure versus time for the second breakthrough and shut-in stages of laboratory-scale test MX-80-8, showing flow rates into the system and out of the sink filter arrays. Mass balance considerations show that the flows are predominantly gas (Harrington and Horseman 2003).*

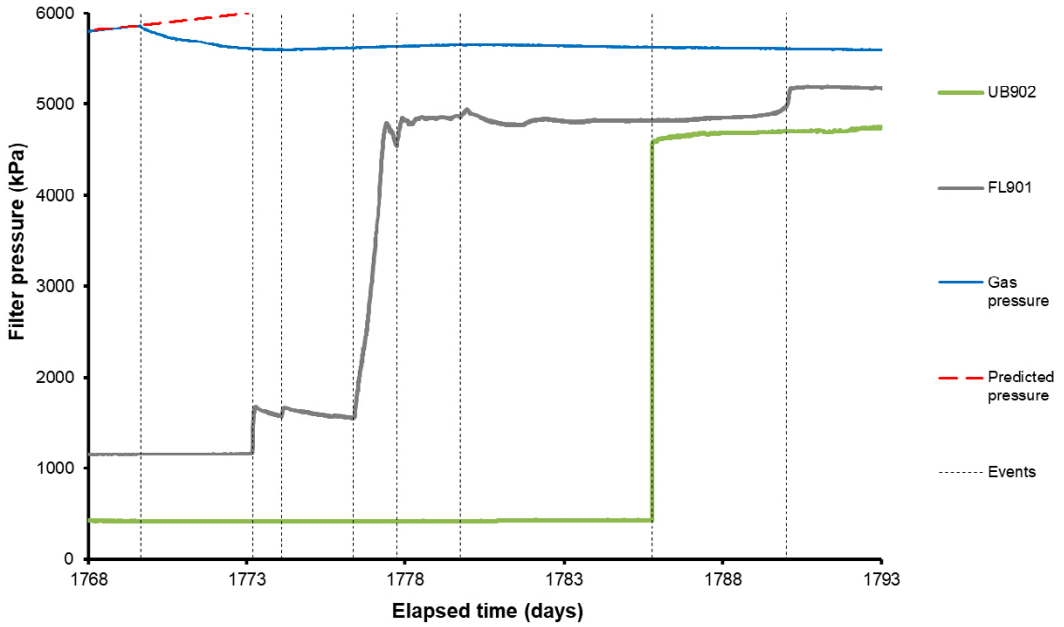

Figure 18-11. *Detail of sensors that show evidence of gas pressurisation during Gas Injection Test 2.*

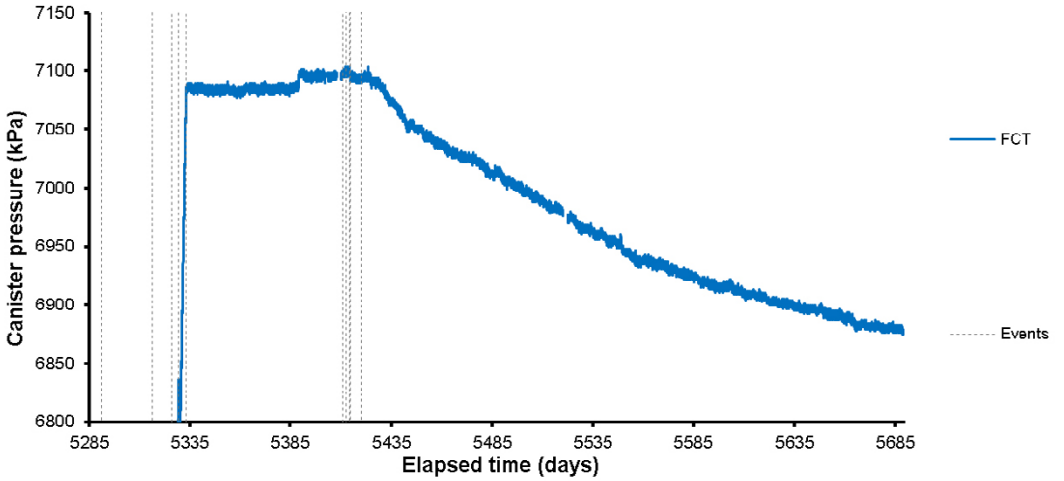

Figure 18-12. *Canister pressure during the Full Canister Test.*

It is clear from the data that interfaces (e.g. between the canister, individual blocks and the rock wall) strongly influenced the conditions and processes observed to control gas flow. Recent work from the EU BEACON project (e.g. Harrington et al. 2020, Daniels et al. 2021, Villar et al. 2021, Graham et al. 2014) suggest homogenization of the buffer may take many years, and that some degree of persistent density (and therefore parameter) variation may exist over repository time scales. The complete homogenization of the buffer would likely result in higher gas pressures than those observed within the lifespan of the Lasgit experiment. However, in contrast, it should also be acknowledged that a buffer with persistent heterogeneities, in particular exhibiting variations in density, may act to help moderate peak gas pressures, as gas would intuitively exploit these features, which represent pathways of least resistance and the foci for gas flow. As the final homogenization state of the buffer within a repository system is unclear (Bernachy-Barbe et al. 2022), the full impact of heterogeneity on gas pressure and the associated transport processes remains unclear.

Summary of gas transport mechanisms

Taken in their totality, the observations from Lasgit seem to support the idea that gas is mainly transported through dilatant pathways (mechanism 3) in a saturated buffer bentonite. The presence of emplacement and long-lived persistent heterogeneities within the bentonite are likely to impact both gas pressure and the size, position and number of gas pathways. However, the impact of this observation is unclear at the present time and remains an open question.

18.4 Summary of how Lasgit can be used in safety assessment

In summary, all observations from Lasgit support and give argument to the handling of gas transport through compact buffer bentonite in the manner presented at the beginning of this section:

1. In all tests, regardless of initial gas volume, the movement of gas occurred at a pressure very close to the local total stress.
2. While not specifically tested, no signs of localised consolidation of the bentonite were observed.
3. The measured peak gas pressures should not lead to any mechanical damage to the buffer or to other barrier components in the repository.
4. Peak gas pressure is linked to the hydraulic permeability of the buffer and the ease at which gas can exit a deposition hole.
5. Gas is transported through a limited number of dilatant pathways. The pathways are expected to be small, in relation to the total volume of the buffer, and temporally variable.
6. No desaturation, of the bentonite buffer, as a result of gas transport was observed.
7. Over the timescale of the project, pathway closure was only partially successful in the absence of injected water.
8. The gas pathways are expected to slowly close at a finite “shut-in” pressure.
9. Gas migration through a bentonite will notis highly unlikely to alter the favourable hydro-mechanical properties of the barrier.
10. The impact of emplaced and long-lived persistent heterogeneities within the bentonite on gas pressure remains unclear.

The results from GT1 through GT6 and the FCT show gas transport processes are scale invariant and insensitive to the initial upstream gas volume. This may have been expected but had never been tested, beyond laboratory scales, prior to Lasgit. The role of water and the maturity (i.e. state of homogenisation of the buffer) have been shown to strongly impact gas flow in the buffer. While the Lasgit system was not in hydraulic equilibrium, given the similarities in behaviour between individual tests and those performed in the laboratory, it is reasonable to assume that while peak gas pressures would increase, and any change would be relatively small, linked to increases in swelling and porewater pressure. The absence of high peak gas pressures (Figure 18-5) such as those sometimes observed during laboratory testing (Figure 18-6) is an important outcome from Lasgit. While gas-induced consolidation may not have been directly observed, the similarities in gas migration behaviour at both scales indicate that it can be further investigated in the laboratory.

The main objectives for the Lasgit experiment (Section 18.3) were fully achieved during this 17-year project, allowing the upscaling of laboratory-derived process understanding to the field scale. The findings provide fundamental information that addresses key questions relating to the treatment of gas in safety assessment (Section 18.1) and the resulting implications for the evolution of the buffer in the event of a deposition hole containing a defective canister.

Section E – Conclusions

19 Summary

In this chapter we summarise all observations of the experiment before making concluding statements in the next chapter. Lasgit was a full-scale demonstration experiment conducted at a depth of 420 m at the Äspö Hard Rock Laboratory. The experiment started following the closure of the deposition hole on 1st February 2005 and logged data for a total of 5 782 days, finally being decommissioned by mid-February 2021.

19.1 Observations of buffer hydration

At the outset of Lasgit, artificial hydration was vital to speed the hydration of the buffer and to get to a condition close to hydraulic equilibrium as a result of full saturation of the buffer. This allowed the system to generate significant stresses and pore pressures, with the geotechnical data at the end of the experiment suggesting the buffer was close to full saturation. The decision was taken to end artificial hydration at Day 3745 and this impacted the data. The filter mats in the system were in operation for most of the test history up to Day 3745, apart from two periods of prolonged time. Pore pressure was still developing within the buffer itself and net pressure data shows that the system was not yet in stress or hydraulic equilibrium. This meant that the stress within the system was still increasing at the time of ending artificial hydration. As a result of ending artificial hydration, many sensors either reached a plateau or decreased in magnitude. Data appeared to reach an equilibrium end-state, where-as that was not the case. It is uncertain what stress level the system would have attained had artificial hydration continued, or if only natural hydration had been allowed. It is apparent that the pore pressure within the bentonite would have reached equilibrium within 10s of years but it is less clear what the ultimate radial stress condition would have been in the system and how long this would have taken. While the buffer was fully saturated, hydraulic disequilibrium was still apparent.

Pore pressure measured within Lasgit at the deposition hole wall and within the pressure relief holes all showed a decrease in time once pore pressure had been established by around Day 500. As with temperature fluctuations, Lasgit was prone to influence from outside of the immediate experimental area. The Äspö HRL included many boreholes that have been monitored for much longer than the Lasgit experiment. Examination of data from these showed that the reduction in pore pressure occurred outside of Lasgit. This was as a result of drawdown of pressure as a result of pumping of water from the HRL tunnel network and was an on-going phenomenon. This meant that the surrounding rock mass had an evolving pore pressure that was outside of the control of the experiment. The test history showed an increase in stress over the Lasgit test, yet pore pressure had decreased at the deposition hole wall. If pore pressure had been more constant it is expected that stresses would have been greater, proportional to the pore pressure drop experienced (~300 kPa).

The KBS-3 system should mature to full saturation, with limited heterogeneity in the deposition hole in terms of stress and pore pressure. Net pressure should evolve to a small finite value, as should suction. The saturation of the bentonite should reach unity and not vary significantly within the deposition hole. This was not the case. The establishment of pore pressure around Day 500 increased all of the stresses and forces in the system in a similar manner. The average data showed that the system settled by Day 1500 with all sensor types continuing to record increase in pore pressure. All of the sensor types were affected by the pausing of artificial hydration starting at Days 2533, 3284, and 3745. The ending of artificial hydration at Day 3745 resulted in all sensor readings either reaching a plateau or decreasing. The radial stress and stress on the canister plateaued, whereas the axial stress in the bentonite and axial force on the lid decreased. This shows that artificial hydration had more of an impact on the system in an axial direction than it did in the radial direction. For pore pressure, once pressure was established as a result of the pressure relief holes, pore pressure in the system decreased. The pore pressure in the bentonite itself took some time to increase but was still increasing at the time when artificial hydration was halted. As stresses and the pore pressure in the bentonite were continuing to increase, it shows that the system had yet to reach an equilibrium point and was still evolving. The distribution of both pore pressure and radial stress at the deposition hole wall showed that the heterogeneity in these parameters was “locked-in” early in the test history and were established as early as Day 500. The heterogeneity shown by the distribution did not alter, even

though the magnitude of the parameters did. The system showed no sign of homogenising in either stress of pore pressure. It is unlikely that prolonged time much greater than the length of the Lasgit experiment would have changed this, with the locked-in heterogeneity persisting. It is likely to have derived from subtle variations in the thickness of the pellet region; difference in the fracture network around the canister; and how well the pellets and bentonite were saturated early in the test history. Net pressure showed that the system was far from equilibrium. A finite net-pressure of ~3 000 kPa had formed and stabilised by Day 1000, but this reduced as a result of the ending of artificial hydration. The locus of net pressure progressed throughout the test history but still showed a heterogeneous system.

Hydraulic conductivity of repeat testing at canister filters showed a reduction with time. At Day 870, hydraulic conductivity was 1.3×10^{-12} m s^{-1} in FL903, decreasing to 1.7×10^{-13} m s^{-1} at Day 5266. This represented a near order of magnitude reduction in conductivity over a 12-year period. Over the same period, specific storage increased. Most of the canister filters were hydraulically tested around Day 3500. This showed a variable result with hydraulic conductivity between 7.1×10^{-13} m s^{-1} and 4.2×10^{-12} m s^{-1}. This showed that the transport properties close to the canister were varied over a 6-fold range. Considerable variation was seen in the geotechnical properties close to the canister and in the pellet region. This may reflect the hydraulic conductivity heterogeneity. However, the geotechnical data showed that the average saturation for the 1 522 samples in the buffer was 0.999, meaning that the buffer was nearly fully saturated. The geotechnical data also showed a distinct difference between the properties of segments and rings before emplacement, which at the end of the test had homogenised. Therefore, the bentonite buffer appeared to be in equilibrium, but was not in hydraulic or stress equilibrium and was continuing to mature.

Lasgit was influenced by the varying air temperature within the HRL tunnel. This resulted in oscillations in temperature, that were attenuated and delayed with distance from the tunnel (i.e depth in the deposition hole). The result of this variation in temperature was oscillations on an annual basis of stress and pore pressure. Heat was transferred from the tunnel to the canister and also to the pore fluid in the surrounding rock mass. The different components of the KBS-3 system thermally expand at varying degrees, which may explain some of the changes in pore pressure and stress. The primary driving force for the features seen was the conduction of heat along the Monel pipe to the canister and thermal expansion of the canister. The pressurisation of the canister at the start of the Full Canister Test showed that small mechanical deformation could significantly increase pore pressure and stress within the deposition hole. Heat was also transferred to the buffer and thermal expansion/contraction of the bentonite may also have been a contributory factor. While the actual disposal scenario will not likely have such a thermally induced annual variation, the data in Lasgit shows that considerable pore pressure and stress changes can be induced by small changes in temperature of the canister, driven by only a 5 °C variation in tunnel temperature. Therefore, the mechanical deformation of the canister has to be considered in modelling of the KBS-3 system.

19.2 Observations of gas injection

All four tests conducted in canister filter FL903 showed a similar pressure response at peak gas pressure, which was different to that seen in FU910. At FL903 pressure rapidly reduced at peak pressure, with generally two events occurring during the initial pressure reduction. Pressure recovered to a single slope of pressure reduction when the data were corrected for differences in injection flow rate. In tests conducted at FU910, the initial pressure reduction at peak gas pressure was followed by a recovery in pressure and a secondary peak either at a similar or higher pressure to the initial peak. The pressure reduction in the first test was smaller than observed in subsequent tests at both filters and this was related to the difference between formation of new pathways and the re-opening of existing pathways in repeat tests.

In the first test conducted at FL903, a pre-cursor flow event was observed, followed by a spike in flow. Most tests in FL903 saw one or more spikes in flow, showing that pathway formation was progressing in stages. After the short-lived spike in flow, the flow into the clay decreased to be lower than the flow into the system and pressure started to increase. This continued until a secondary peak in pressure was seen and the flow into the clay was then marginally greater than flow into the system and pressure slowly decreased. A similar flow response was seen at FU910. However, the initial peak in flow was greater and the flow into the clay reduced to be less than flow into the system for much longer, resulting in an increasing pore pressure. No pre-cursor flow events were seen at this filter.

Extended testing gave useful insights into gas flow. In GT2 a series of pressure reductions and recovery were seen. This suggests that flow paths were developing with time. The pressure reduction occurred as a conductive feature(s) allowed gas pressure to reduce, probably due to gas leaving the deposition hole. This pathway partially closed as gas pressure reduced and as a result, the conductivity of the pathway also reduced and gas pressure increased until the pathway was re-opened and pressure reduced once more. The results from GT4 confirm this. Gas flow into the system was reduced in two steps, once stable flow had been established, each approximately halving the flow of the previous step. On the third step, pressure started to increase, suggesting that the force required to keep pathways open was flow-rate dependent. As flow was reduced, the pathway partially closed, decreasing conductivity and thus increasing pressure. In GT3 and GT5, prolonged gas injection resulted in a series of peaks in gas pressure. This behaviour is similar to that seen in 'fault valve behaviour' or episodic flow, where the conductivity of a feature gets reactivated at a given pressure, allowing fluid to flow and pressure to decrease. In the two tests conducted at FU910, this may mean that the pathway connecting the gas to the wall rock was acting as a valve and that the pathways were unstable.

The primary control of gas peak pressure was local stress. This was difficult to determine in filters FL903 and FU910 with a high degree of certainty. However, estimates of the local stress show that gas peak pressure occurred at, or a little above, local stress. The maximum difference between the local stress and peak pressure was ~600 kPa. A secondary control on gas peak pressure was the maturity of the buffer, which in itself was linked to the development of stress. The ending of artificial hydration resulted in stresses in the system being reduced, yet gas peak pressure continued to increase. The buffer continued to mature even though stress had reduced. This was confirmed in the hydraulic conductivity data that showed continued reduction independent of whether or not artificial hydration was occurring. The results from Lasgit show that gas peak pressure was related to the hydraulic conductivity.

The movement of gas was inferred from the array of pore pressure and radial stress sensors at the rock wall, and from the direct movement of gas to sensors during the test. In the first test in FL903 (GT1), the data indicated that the gas moved downwards along the outside of the canister and then along the interface between two bentonite blocks. In test GT2, the gas moved 180° around the canister, before migrating to the base of the canister and later finding a way from the deposition hole, most likely between bentonite blocks. This may have exploited the same features formed in GT1. In GT4, gas also moved to FL901 and it is likely that this test re-activated features formed in GT2.

In the first test conducted in FU910 (GT3), considerable movement was seen. The gas first moved 90° around the canister to FU909, before intercepting FU911, the filter 90° the other way around the canister. Gas then moved downwards, intercepting a stress sensor (PC903), before reaching FL904, a filter on the lower array of the canister filters. In GT5, this repeat test immediately reached FU909 and PC903. This showed re-activation of some of the pathways formed in GT3, but not the re-activation of all. In the Full Canister Test, gas reached UB902 and FL901, pathways that had been established in previous tests using FL903. Therefore, there was evidence that subsequent gas injection tests behaved similarly and that pathways may have re-activated. However, it is clear that the migration of gas was not identical between tests, with new pathways forming. The formed pathways then, at least partially self-sealed.

20 Conclusions

The main objectives for the Lasgit experiment were fully achieved during this 17-year project, allowing the upscaling of laboratory-derived process understanding to the field scale. The findings provide fundamental information that addresses key questions relating to the treatment of gas in safety assessment and the resulting implications for the evolution of the buffer in the event of a deposition hole containing a defective canister. The main conclusions were:

1. In all tests, regardless of initial gas volume, the movement of gas occurred at a pressure very close to the local total stress.
2. No signs of localised consolidation of the bentonite were observed.
3. The measured peak gas pressures should not lead to any mechanical damage to the buffer or to other barrier components in the repository.
4. Peak gas pressure is linked to the hydraulic permeability of the buffer and the ease at which gas can exit a deposition hole.
5. Gas is transported through a limited number of dilatant pathways. The pathways are expected to be small, in relation to the total volume of the buffer, and temporally variable.
6. No desaturation of the bentonite buffer as a result of gas transport was observed.
7. Over the timescale of the project, pathway closure was only partially successful in the absence of injected water.
8. The gas pathways are expected to slowly close at a finite “shut-in” pressure.
9. Gas migration through a bentonite will notis highly unlikely to alter the favourable hydromechanical properties of the barrier.
10. The impact of emplaced and long-lived persistent heterogeneities within the bentonite on gas pressure remains unclear.

The results from GT1 through GT6 and the FCT show gas transport processes are scale invariant when compared with laboratory experiments and insensitive to the initial upstream gas volume. This may have been expected but had never been tested, beyond laboratory scales, prior to Lasgit. The role of water and the maturity (i.e. state of pore-pressure, hydraulic conductivity, and stress homogenisation of the buffer in the time-frame of the experiment) have been shown to strongly impact gas flow in the buffer. Given the similarities in behaviour between individual tests and those performed in the laboratory, it is reasonable to assume that while peak gas pressures would increase as the buffer continued to mature and reach a state of hydraulic equilibrium, any change would be relatively small, linked to increases in swelling and porewater pressure. The absence of high peak gas pressures such as those sometimes observed during laboratory testing is an important outcome from Lasgit. While gas-induced consolidation may not have been directly observed, the similarities in gas migration behaviour at both scales indicate that it can be further investigated in the laboratory.

References

SKB's (Svensk Kärnbränslehantering AB) publications can be found at www.skb.com/publications.

Bennett D, 2014. Exploratory data analysis of the Large Scale Gas Injection Test (Lasgit). PhD thesis. Cardiff University, UK.

Bennett D P, Cuss R J, Vardon P J, Harrington J F, Philp R N, Thomas H R, 2012. Data analysis toolkit for long-term, large-scale experiments. Mineralogical Magazine 76, 3355–3364.

Bennett D P, Cuss R J, Vardon P J, Harrington J F, Thomas H R, 2014. Phenomena exposure from the large scale gas injection test (Lasgit) dataset using a bespoke data analysis toolkit. In Norris A, Bruni J, Cathelineau M, Delage P, Fairhurst C, Gaucher E C, Hohn E H, Kalinichev A, Lalieux P, Sellin P (eds). Clays in natural and engineered barriers for radioactive waste confinement. London: Geological Society of London. (Geological Society Special Publications 400), 497–505.

Bennett D P, Cuss R J, Vardon P J, Harrington J F, Sedighi M, Thomas H R, 2015. Exploratory data analysis of the Large Scale Gas Injection Test (Lasgit) dataset, focusing on 'second-order' events around macro-scale gas flows. In Shaw R P (ed). Gas generation and migration in deep geological radioactive waste repositories. London: Geological Society of London. (Geological Society Special Publication 415), 225–239.

Bernachy-Barbe F, Bosch J A, Campos G, Carbonell B, Daniels K A, Ferrari A, Graham C C, Guillot W, Gutiérrez-Álvarez C, Harrington J F, Iglesias R J, Kataja M, Kröhn K-P, Michael Kröhn, Mašín D, Najser J, Pingel L J, Real E, Schäfer T, Svoboda J, Sun H, Tanttu J, Villar M V, Wieczorek K, 2022. Experimental work on bentonite evolution in the frame of BEACON – final report of WP4. BEACON Deliverable Report D4.3.

Birgersson M, Karnland O, 2015. Flow and pressure repsonse in compacted bentonite due to external fluid pressure. SKB TR-14-28, Svensk Kärnbränslehantering AB.

Birgersson M, Åkesson M, Hökmark H, 2008. Gas intrusion in saturated bentonite – A thermodynamic approach. Physics and Chemistry of the Earth, Parts A/B/C 33, S248–S251.

Cuss R J, Harrington J F, Noy D J, 2008. Large scale gas injection test (Lasgit) performed at the Äspö Hard Rock Laboratory: Summary report 2008. Report CR/08/173, British Geological Survey.

Cuss R J, Harrington J F, Noy D J, Wikman A, Sellin P, 2011. Large scale gas injection test (Lasgit): Results from two gas injection tests. Physics and Chemistry of the Earth, Parts A/B/C 36, 1729–1742.

Cuss R J, Harrington J F, Noy D J, Graham C C, 2012. Final report of FORGE WP3.1.1: The large scale gas injection test (Lasgit) performed at the Äspö Hard Rock Laboratory. Report CR/12/141, British Geological Survey.

Cuss R J, Harrington J F, Noy D J, Graham C C, Sellin P, 2014. Evidence of localised gas propagation pathways in a field-scale bentonite engineered barrier system; results from three gas injection tests in the Large scale gas injection test (Lasgit). Applied Clay Science 102, 81–92.

Daniels K A, Harrington J F, Sellin P, Norris S, 2021. Closing repository void spaces using bentonite: does heat make a difference? Applied Clay Science 210, 106124. doi:10.1016/j.clay.2021.106124

Donohew A T, Horseman S T, Harrington J F, 2000. Gas entry into unconfined clay pastes between the liquid and plastic limits. In Cotter-Howells J D, Campbell L S, Valsami-Jones E, Batchelder M (eds). Environmental mineralogy: microbial interactions, anthropogenic influences, contaminated land and waste management. London: Mineralogical Society. (Mineralogical Society special publication 9), 369–394.

Graham C C, Harrington J F, Cuss R J, Sellin P, 2012. Gas migration experiments in bentonite: implications for numerical modelling. Mineralogical Magazine 76, 3279–3292.

Graham C C, Harrington J F, Cuss R J, 2014. Gas migration in bentonite – fundamental issues. In Sellin P (ed). Experiments and modelling on the behaviour of EBS. FORGE Report D3.38, Chapter 10.

Graham C C, Harrington J F, Sellin P, 2016. Gas migration in pre-compacted bentonite under elevated pore-water pressure conditions. Applied Clay Science 132, 353–365.

Graham J, Halayko K G, Hume H, Kirkham T, Gray M, Oscarson D, 2002. A capillarity-advective model for gas break-through in clays. Engineering Geology 64, 273–286.

Hardenby C, 2004. Äspö Hard Rock Laboratory. Large scale gas injection test. The LASGIT hole DA3147G01. Hydrogeology. SKB IPR-04-52, Svensk Kärnbränslehantering AB.

Hardenby C, Lundin J, 2003. Äspö Hard Rock Laboratory. TBM assembly hall. Geological mapping of the assembly hall and deposition hole. SKB IPR-03-28, Svensk Kärnbränslehantering AB.

Harrington J F, Horseman S T, 1999. Gas transport properties of clays and mudrocks. In Aplin A C, Fleet A J, Macquaker J H S (eds). Muds and mudstones: physical and fluid flow properties. Bath: Geological Society of London. (Geological Society Special Publication 158), 107–124.

Harrington J F, Horseman S T, 2003. Gas migration in KBS-3 buffer bentonite. Sensitivity of test parameters to experimental boundary conditions. SKB TR-03-02, Svensk Kärbränslehantering AB.

Harrington J F, Birchall D J, Noy D J, Cuss R J, 2007. Large scale gas injection test (Lasgit) performed at the Äspö Hard Rock Laboratory: Summary report 2007. Report CR/07/211, British Geological Survey.

Harrington J F, Graham C C, Cuss R J, Norris S, 2017. Gas network development in a precompacted bentonite experiment: Evidence of generation and evolution. Applied Clay Science 147, 80–89.

Harrington J F, Graham C C, Cuss R J, Norris S, 2019. Gas network development in compact bentonite: key controls on the stability of flow pathways. Geofluids, 3815095. doi:10.1155/2019/3815095

Harrington J F, Daniels K A, Wiseall A C, Sellin P, 2020. Bentonite homogenisation during the closure of void spaces. International Journal of Rock Mechanics and Mining Sciences 136, 104535. doi:10.1016/j.ijrmms.2020.104535

Horseman S T, Higgo J J W, Alexander J, Harrington J F, 1996. Water, gas and solute movement in argillaceous media. Report CC-96/1 to OECD/NEA Working Group on Measurement and Physical Understanding of Groundwater Flow through Argillaceous Media. Paris: Nuclear Energy Agency, OECD.

Horseman S T, Harrington J F, Sellin P, 1997. Gas migration in MX-80 buffer bentonite. In Gray W J, Triay I R (eds). Scientific basis for nuclear waste management XX, Boston, 2–6 December 1996. Warrendale, PA: Materials Research Society. (Materials Research Society Symposium Proceedings 465), 1003–1010.

Horseman S T, Harrington J F, Sellin P, 1999. Gas migration in clay barriers. In Pusch R, Yong R N (eds). Microstructural modelling of natural and artificially prepared clay soils with special emphasis on the use of clays for waste isolation (1999 Special Edition). Engineering Geology 54, 139–149.

Horseman S T, Harrington J F, Sellin P, 2004. Water and gas flow in MX-80 bentonite buffer clay. In Oversb V M, Werme L O (eds). Scientific basis for nuclear waste management XXVII, Kalmar, Sweden, 15–19 June 1993. Warrendale, PA: Materials Research Society. (Materials Research Society Symposium Proceedings 807), 715–720.

Hume H B, 1999. Gas breakthrough in compacted Avonlea bentonite. MSc thesis. Department of Soil Science, University of Manitoba, Canada.

Marschall P, Horseman S, Gimmi T, 2005. Characterisation of gas transport properties of the Opalinus Clay, a potential host rock formation for radioactive waste disposal. Oil & Gas Science and Technology 60, 121–139.

Neretnieks I, Ernstsson M-L, 1997. A note on radionuclide transport by gas bubbles. In Gray W J, Triay I R (eds). Scientific basis for nuclear waste management XX, Boston, Massachusetts, USA, 2–6 December 1996. Warrendale, PA: Materials Research Society. (Materials Research Society Symposium Proceedings 465), 855–862.

Norris S, 2015. EC FORGE project: Updated consideration of gas generation and migration in the safety case. In Shaw R P (ed). Gas generation and migration in deep geological radioactive waste repositories. Bath: Geological Society of London. (Geological Society Special Publication 415), 241–258.

Nowak T, Köster H, Flentje R, Sanchez-Herrero S, Lege C, 2007. Äspö Hard Rock Laboratory. LASGIT Large Scale Gas Injection Test. Hydraulic tests with surface packer system. SKB IPR-07-14, Svensk Kärnbränslehantering AB.

Pusch R, Ranhagen L, Nilsson K, 1985. Gas migration through MX-80 bentonite. Nagra Technical Report NTB 85-36, Nagra, Switzerland.

Pusch R, Hökmark H, Börgesson L, 1987. Outline of models of water and gas flow through smectite clay buffers. SKB TR 87-10, Svensk Kärnbränslehantering AB.

Sellin P (ed), 2014. Experiments and modelling on the behaviour of EBS. FORGE Report D3.38.

SKB, 1999. SR 97 – Processes in the repository evolution. Background report to SR 97. SKB TR-99-07, Svensk Kärnbränslehantering AB.

SKB, 2009. Design premises for a KBS-3V repository based on results from the safety assessment SR-Can and some subsequent analyses. SKB TR-09-22, Svensk Kärnbränslehantering AB.

Tanai K, Kanno T, Gallé C, 1997. Experimental study of gas permeabilities and breakthrough pressures in clays. In Gray W J, Triay I R (eds). Scientific basis for nuclear waste management XX, Boston, 2–6 December 1996. Warrendale, PA: Materials Research Society. (Materials Research Society Symposium Proceedings 465), 1003–1010.

Villar M V, Martín P L, Romero F J, Barcala J M, Gutiérrez-Rodrigo V, Skoczylas F, Davy C A, Agostini F, Burlion N, 2012. Gas transport through bentonite: influence of dry density, water content and boundary conditions. Propiétés de transfert des géomatériaux – Transfert 2012, 379–389.

Villar M V, Iglesias R J, Gutiérrez-Álvarez C, Carbonell B, 2021. Pellets/block bentonite barriers: Laboratory study of their evolution upon hydration. Engineering Geology 292, 106272. doi:10.1016/j.enggeo.2021.106272

Wendel E, Gordon A, Börjesson E, Wärnheim A, Johansson J, Svensson D, Bergendal E, 2022. Analysis of corrosion products on filter housings in the Lasgit field experiment. SKB TR-22-01, Svensk Kärnbränslehantering AB.

Wikramaratna R S, Goodfield M, Rodwell W R, Nash P J, Agg P J, 1993. A preliminary assessment of gas migration from the copper/steel canister. SKB TR 93-31, Svensk Kärnbränslehantering AB.

Xu T, Sonnenthal E, Spycher N, Pruess K, 2004. TOUGHREACT User's guide: a simulation program for non-isothermal multiphase reactive geochemical transport in variably saturated geologic media. LBNL-55460, Lawrence Berkeley National Laboratory. doi:10.2172/834237

Appendix

Calibration data

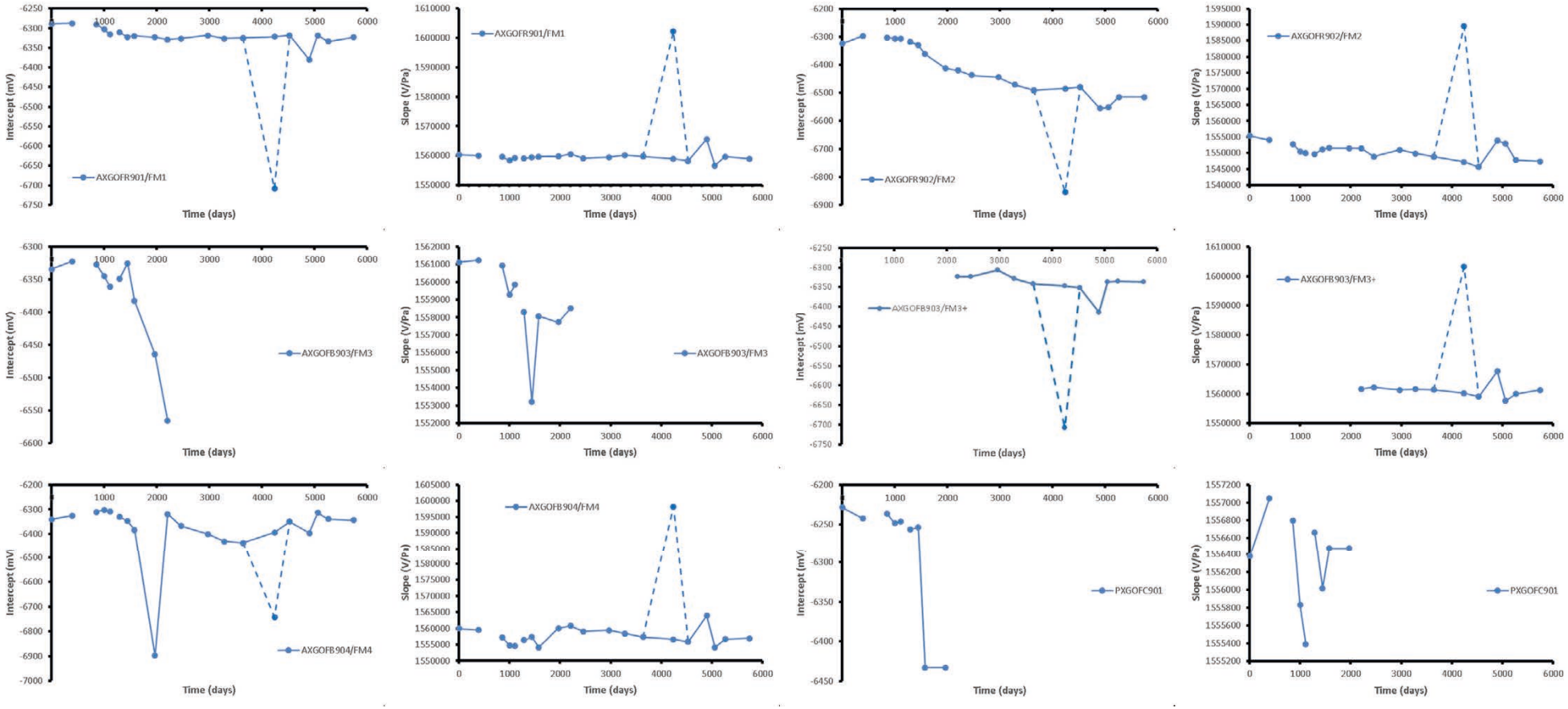

Figure A-1. Calibration data.

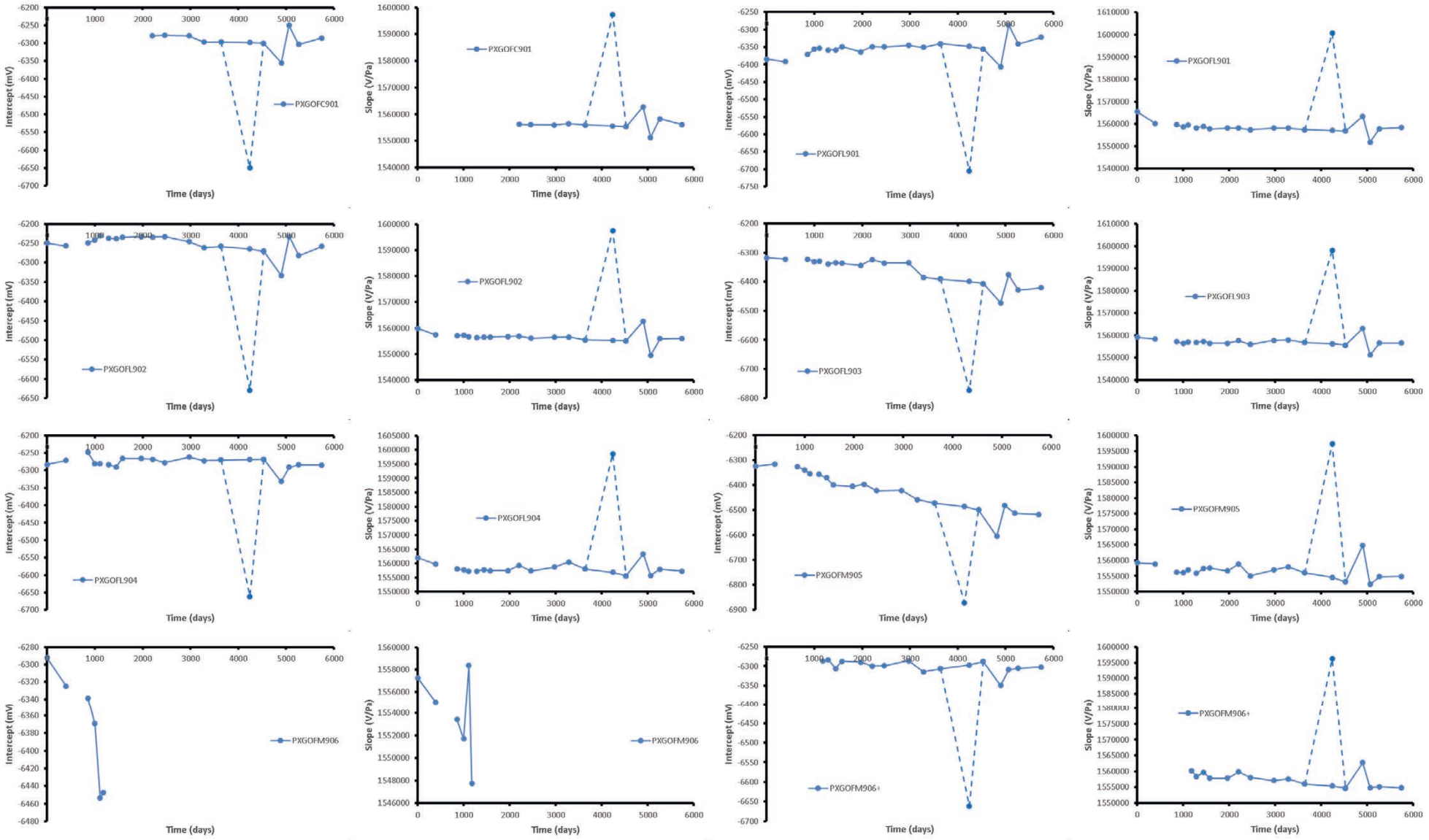

Figure A-2. *Calibration data.*

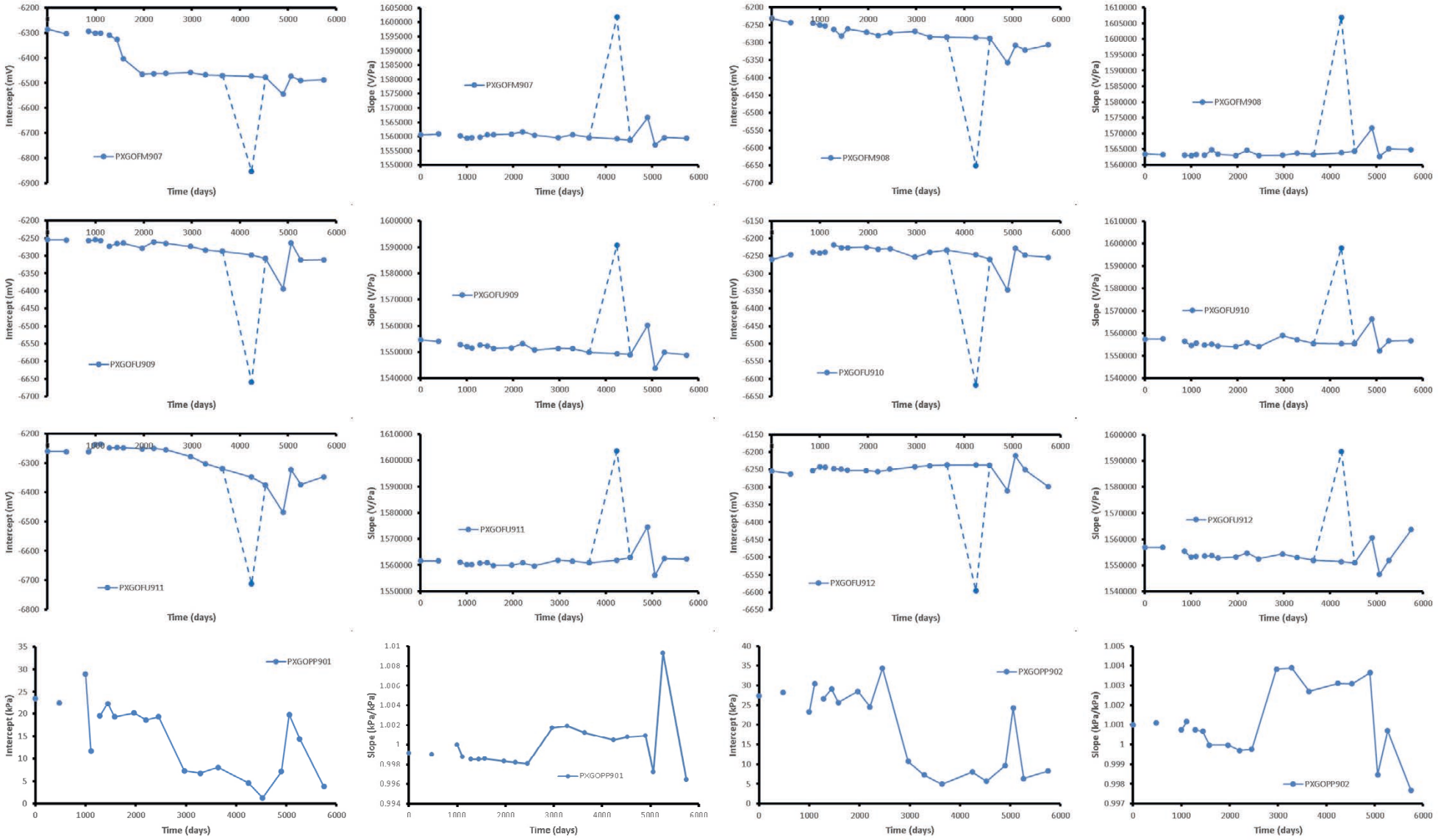

Figure A-3. *Calibration data.*

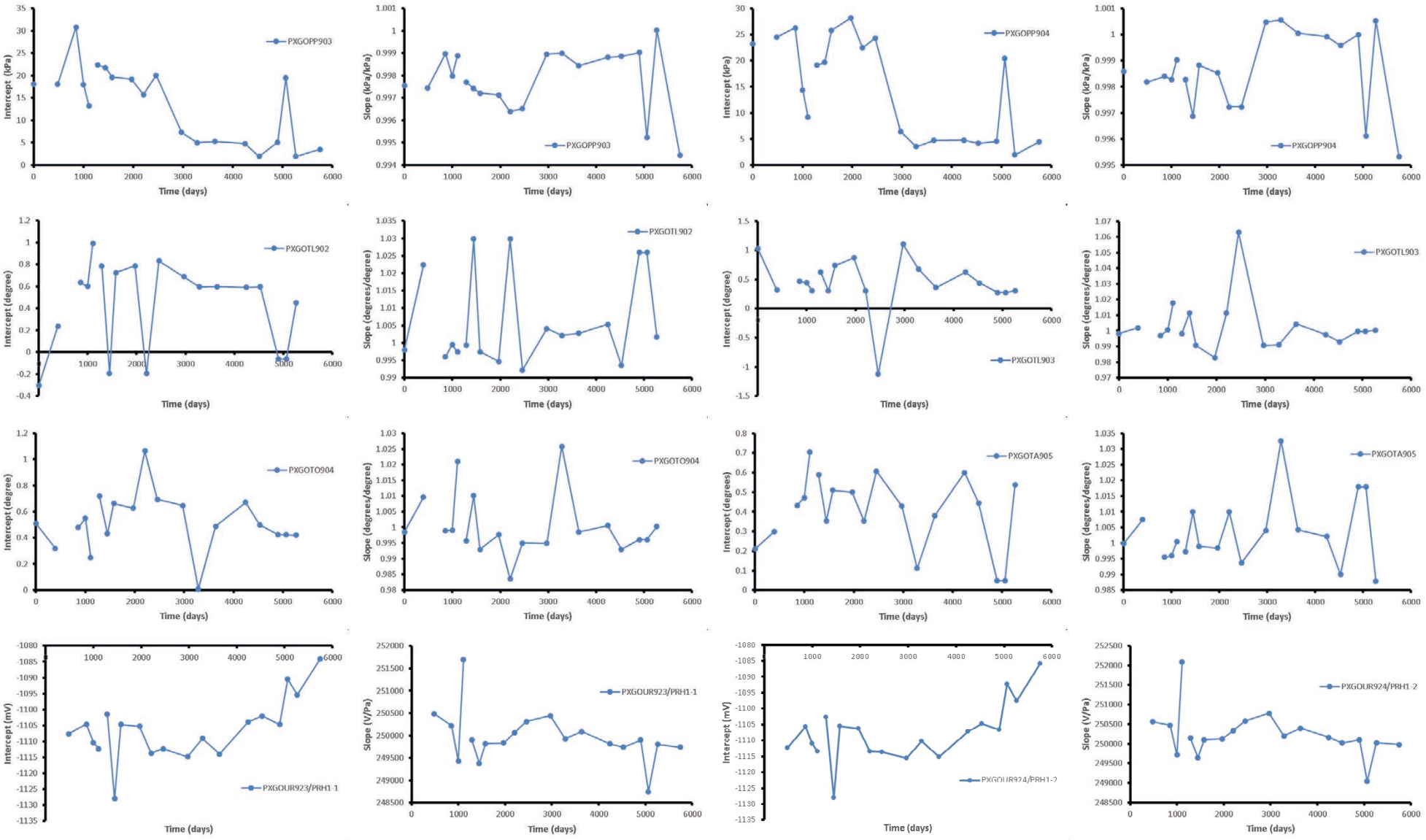

Figure A-4. *Calibration data.*

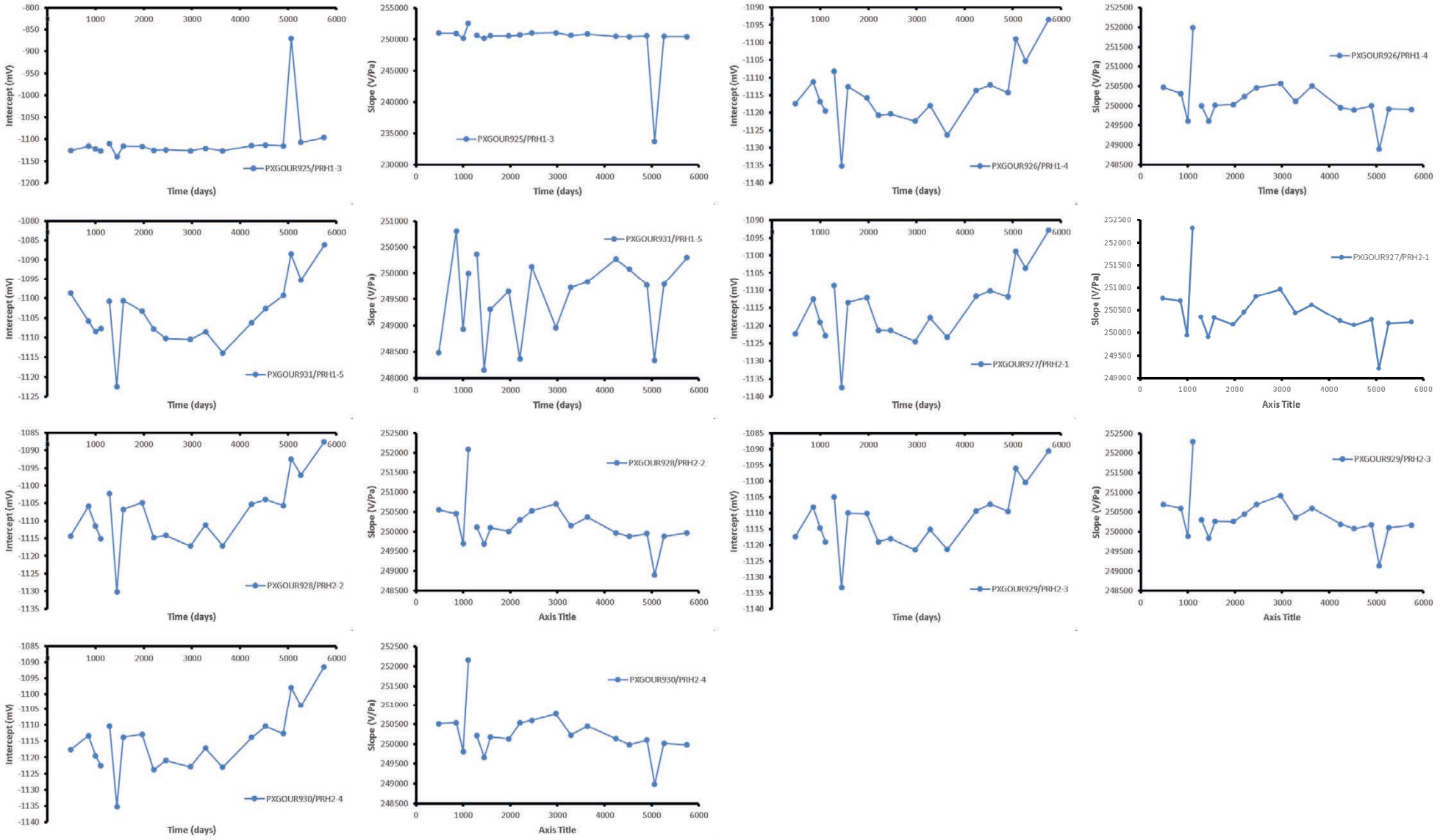

Figure A-5. *Calibration data.*

Table A-1. Calibration data. Data highlighted in red have been discounted as erroneous.

Date	Time (days)	FM1		FM2		FM3		FM3+		FM4		FC901	
		Intercept	Slope	Intercept	Slope	Intercept	Slope	Intercept	Slope	Intercept	Slope	Intercept	Slope
01/02/2005	0	−6288.58	1560230	−6324.29	1555338.0	−6334.41	1561121.0			−6339.81	1559947.0	−6228.40	1556380.0
01/03/2006	393	−6287.61	1560027.5	−6297.61	1554027.6	−6322.17	1561236.4			−6324.79	1559484.3	−6242.53	1557050.5
05/06/2007	854	−6289.89	1559508.7	−6302.75	1552816.4	−6327.58	1560941.1			−6310.73	1557288.7	−6236.40	1556800.1
15/02/2008	1 000	−6302.99	1558398.0	−6307.31	1550460.8	−6344.88	1559280.8			−6301.16	1554796.6	−6248.71	1555830.6
15/02/2008	1 109	−6315.61	1559210.9	−6306.17	1549956.0	−6360.73	1559845.4			−6307.75	1554525.1	−6246.70	1555388.3
12/08/2008	1 288	−6310.60	1559132.1	−6317.67	1549654.7	−6349.04	1558295.2			−6329.76	1556373.6	−6256.53	1556662.9
15/01/2009	1 444	−6322.36	1559398.4	−6329.75	1551191.0	−6325.36	1553216.7			−6347.85	1557336.0	−6253.94	1556016.3
28/05/2009	1 577	−6319.91	1559673.1	−6362.41	1551544.4	−6382.44	1558073.2			−6383.34	1554169.0	−6432.79	1556482.2
22/06/2010	1 967	−6322.81	1559684.7	−6413.19	1551482.0	−6464.24	1557718.5			−6897.43	1560034.5	−6432.79	1556482.2
16/02/2011	2 206	−6328.86	1560536.0	−6419.98	1551479.1	−6565.41	1558495.1	−6324.05	1561646.6	−6318.51	1560808.7		
26/10/2011	2 458	−6325.99	1559091.9	−6436.92	1548892.9			−6323.70	1562183.5	−6367.58	1559075.6		
20/03/2013	2 969	−6318.44	1559486.4	−6444.39	1550954.9			−6307.23	1561353.8	−6400.89	1559383.1		
28/01/2014	3 283	−6326.29	1560148.0	−6471.29	1549836.6			−6328.35	1561599.6	−6430.11	1558434.0		
20/01/2015	3 640	−6325.23	1559729.0	−6490.44	1548846.2			−6340.94	1561391.3	−6437.30	1557327.1		
13/09/2016	**4 242**	**−6707.95**	**1602254.3**	**−6853.55**	**1589510.1**			**−6707.83**	**1603159.1**	**−6741.53**	**1598203.6**		
13/09/2016	4 242	−6321.72	1558952.8	−6484.92	1547231.6			−6346.67	1560214.3	−6393.58	1556589.1		
27/06/2017	4 529	−6318.21	1558176.5	−6479.40	1545617.0			−6352.40	1559037.3	−6349.85	1555851.2		
03/07/2018	4 900	−6379.91	1565572.0	−6555.57	1553834.7			−6413.60	1567696.6	−6396.63	1563946.0		
11/12/2018	5 061	−6318.46	1556621.4	−6551.40	1552945.5			−6337.08	1557611.0	−6313.64	1554130.8		
02/07/2019	5 264	−6333.86	1559672.8	−6514.74	1547756.5			−6334.37	1559998.1	−6339.69	1556665.0		
28/10/2020	5 748	−6322.97	1558959.1	−6515.28	1547398.4			−6335.87	1561278.6	−6343.55	1556929.4		

Table A-2. Calibration data. Data highlighted in red have been discounted as erroneous.

Date	Time (days)	FC901+		PXG0FL901		PXG0FL902		PXG0FL903		PXG0FL904		PXG0FM905	
		Intercept	Slope	Intercept	Slope	Intercept	Slope	Intercept	Slope	Intercept	Slope	Intercept	Slope
01/02/2005	0			−6384.26	1565456.0	−6249.66	1559850.0	−6317.69	1559173.0	−6283.33	1562015.0	−6323.43	1559265.0
01/03/2006	393			−6392.14	1560136.8	−6256.99	1557444.3	−6322.21	1558399.8	−6271.72	1559695.0	−6315.38	1558863.3
05/06/2007	854			−6371.59	1559584.5	−6249.44	1557016.6	−6322.55	1557195.7	−6247.99	1558133.9	−6324.81	1556238.7
15/02/2008	1 000			−6356.55	1558615.4	−6242.09	1557335.8	−6330.64	1556324.6	−6280.72	1557712.9	−6339.09	1556022.1
15/02/2008	1 109			−6353.63	1559497.6	−6230.94	1556642.5	−6329.75	1556942.2	−6281.29	1557237.4	−6354.19	1556965.3
12/08/2008	1 288			−6358.57	1558208.1	−6236.67	1556334.2	−6338.69	1556837.0	−6283.78	1557300.5	−6356.63	1555859.8
15/01/2009	1 444			−6358.44	1558916.7	−6238.58	1556524.5	−6334.15	1557298.4	−6290.14	1557813.3	−6369.85	1557511.0
28/05/2009	1 577			−6348.56	1557713.9	−6235.01	1556594.0	−6336.59	1556443.4	−6266.38	1557438.3	−6399.17	1557547.3
22/06/2010	1 967			−6363.68	1558100.5	−6233.15	1556735.9	−6343.57	1556429.8	−6266.04	1557401.6	−6405.13	1556619.8
16/02/2011	2 206	−6279.24	1556169.3	−6348.85	1558130.8	−6234.49	1556944.1	−6324.02	1557661.7	−6268.41	1559276.1	−6396.31	1558909.8
26/10/2011	2 458	−6277.95	1555994.7	−6349.16	1557353.6	−6233.11	1556077.6	−6335.75	1555876.7	−6277.86	1557334.1	−6422.37	1555035.3
20/03/2013	2 969	−6279.17	1555930.7	−6345.53	1558121.6	−6245.99	1556434.7	−6334.65	1557700.4	−6261.98	1558710.6	−6421.30	1556948.8
28/01/2014	3 283	−6297.01	1556463.0	−6351.07	1558073.1	−6261.26	1556594.9	−6385.01	1557998.5	−6272.12	1560488.3	−6457.87	1557922.9
20/01/2015	3 640	−6296.74	1555898.4	−6340.40	1557327.7	−6258.26	1555484.7	−6391.00	1556818.8	−6270.15	1558053.0	−6472.00	1556064.6
13/09/2016	**4 242**	**−6649.39**	**1597312.0**	**−6705.76**	**1600715.1**	**−6629.10**	**1597509.4**	**−6773.72**	**1598185.0**	**−6661.80**	**1598637.7**	**−6871.52**	**1597427.9**
13/09/2016	4 242	−6298.36	1555605.4	−6347.96	1557059.6	−6264.51	1555298.2	−6398.90	1556179.5	−6269.02	1556838.0	−6485.60	1554608.4
27/06/2017	4 529	−6299.97	1555312.4	−6355.52	1556791.6	−6270.77	1555111.7	−6406.81	1555540.1	−6267.90	1555623.0	−6499.21	1553152.3
03/07/2018	4 900	−6355.40	1562783.4	−6406.75	1563376.6	−6333.56	1562639.0	−6472.52	1563069.1	−6331.81	1563366.8	−6604.54	1564902.6
11/12/2018	5 061	−6249.89	1551299.1	−6286.85	1551782.6	−6233.03	1549506.1	−6375.61	1551185.8	−6291.10	1555790.4	−6481.76	1552356.5
02/07/2019	5 264	−6303.75	1558224.1	−6341.21	1557782.3	−6282.20	1555952.8	−6428.97	1556595.0	−6284.30	1557938.4	−6512.68	1554780.7
28/10/2020	5 748	−6285.60	1556150.6	−6322.00	1558292.1	−6258.42	1555996.1	−6420.58	1556514.0	−6284.59	1557310.0	−6517.28	1554897.5

Table A-3. Calibration data. Data highlighted in red have been discounted as erroneous.

Date	Time (days)	PXG0FM906		PXG0FM906+		PXG0FM907		PXG0FM908		PXG0FU909		PXG0FU910	
		Intercept	Slope	Intercept	Slope	Intercept	Slope	Intercept	Slope	Intercept	Slope	Intercept	Slope
01/02/2005	0	−6292.30	1557265.0			−6285.75	1560590.0	−6231.10	1563436.0	−6254.13	1554648.0	−6260.53	1557431.0
01/03/2006	393	−6324.94	1555037.0			−6303.65	1560913.9	−6243.13	1563210.2	−6254.93	1554075.9	−6246.11	1557466.0
05/06/2007	854	−6338.62	1553415.0			−6294.34	1560204.8	−6244.71	1563153.1	−6256.75	1552747.2	−6239.20	1556423.7
15/02/2008	1 000	−6369.21	1551690.2			−6302.22	1559366.1	−6250.09	1562957.6	−6254.18	1552110.6	−6242.19	1554577.4
15/02/2008	1 109	−6453.47	1558378.1			−6302.44	1559612.8	−6252.75	1563340.0	−6255.88	1551567.2	−6239.64	1555635.0
25/04/2008	1 180	−6447.38	1547747.6	−6286.17	1560215.8								
12/08/2008	1 288			−6283.82	1558387.4	−6309.46	1559786.1	−6262.12	1563105.0	−6272.96	1552710.8	−6218.43	1554838.5
15/01/2009	1 444			−6305.78	1559699.4	−6326.85	1560528.5	−6281.94	1564767.7	−6264.95	1552332.9	−6226.49	1555132.5
28/05/2009	1 577			−6287.23	1557846.8	−6402.82	1560652.2	−6260.91	1563420.4	−6263.47	1551425.3	−6226.48	1554406.4
22/06/2010	1 967			−6289.65	1557827.7	−6464.81	1560780.9	−6270.02	1563041.9	−6278.32	1551578.9	−6225.29	1554074.2
16/02/2011	2 206			−6299.56	1559788.8	−6463.33	1561656.1	−6279.91	1564643.8	−6260.49	1553243.2	−6230.95	1555796.9
26/10/2011	2 458			−6299.01	1558084.6	−6462.19	1560451.8	−6272.39	1562995.3	−6264.57	1550698.5	−6229.28	1554084.1
20/03/2013	2 969			−6286.15	1557042.4	−6458.49	1559542.0	−6267.90	1563080.6	−6273.01	1551367.2	−6253.14	1559011.2
28/01/2014	3 283			−6314.62	1557632.7	−6468.05	1560612.6	−6283.73	1563717.3	−6283.41	1551278.2	−6239.38	1557162.0
20/01/2015	3 640			−6306.78	1555999.7	−6470.80	1559653.7	−6284.30	1563340.7	−6286.97	1549852.4	−6233.73	1555435.2
13/09/2016	**4 242**			**−6661.58**	**1596233.4**	**−6852.00**	**1601805.0**	**−6650.52**	**1606903.2**	**−6659.06**	**1590769.3**	**−6617.60**	**1598052.9**
13/09/2016	4 242			−6297.37	1555337.4	−6473.98	1559199.8	−6286.22	1563877.9	−6297.32	1549403.3	−6246.63	1555373.6
27/06/2017	4 529			−6287.97	1554675.2	−6477.16	1558745.9	−6288.15	1564415.1	−6307.66	1548954.2	−6259.53	1555311.9
03/07/2018	4 900			−6349.58	1562720.0	−6544.76	1566629.3	−6357.81	1571716.4	−6393.40	1560204.7	−6347.04	1566313.5
11/12/2018	5 061			−6308.74	1554868.8	−6473.90	1557082.1	−6308.13	1562701.0	−6263.04	1543740.1	−6228.19	1552254.1
02/07/2019	5 264			−6305.22	1555181.7	−6490.80	1559638.5	−6320.75	1565120.4	−6312.01	1549815.4	−6247.70	1556693.5
28/10/2020	5 748			−6302.44	1554784.9	−6488.01	1559422.7	−6306.94	1564821.0	−6310.88	1548834.9	−6254.20	1556715.0

Table A-4. Calibration data. Data highlighted in red have been discounted as erroneous.

Date	Time (days)	PXG0FU911		PXG0FU912		PP901		PP902		PP903		PP904	
		Intercept	Slope	Intercept	Slope	Intercept	Slope	Intercept	Slope	Intercept	Slope	Intercept	Slope
01/02/2005	0	−6260.12	1561648.0	−6254.20	1556861.0	23.53	0.9991	27.34	1.0010	18.08	0.9975	23.17	0.9986
01/03/2006	393	−6261.03	1561629.6	−6262.36	1556827.5								
28/05/2006	481					22.48	0.9990	28.17	1.0011	18.05	0.9974	24.51	0.9982
05/06/2007	854	−6261.65	1561163.0	−6252.81	1555480.5					30.78	0.9990	26.26	0.9984
15/02/2008	1000	−6237.10	1560118.2	−6241.91	1553168.2	28.99	1.0000	23.24	1.0008	18.02	0.9980	14.40	0.9983
15/02/2008	1109	−6234.51	1560156.3	−6243.70	1553362.0	11.70	0.9988	30.36	1.0012	13.29	0.9989	9.22	0.9990
12/08/2008	1288	−6247.99	1560810.5	−6247.25	1553580.2	19.48	0.9985	26.63	1.0007	22.37	0.9977	19.12	0.9983
15/01/2009	1444	−6247.08	1560825.5	−6248.90	1553754.2	22.33	0.9985	29.07	1.0007	21.75	0.9974	19.66	0.9969
28/05/2009	1577	−6248.29	1559825.5	−6251.78	1552833.2	19.30	0.9985	25.64	1.0000	19.61	0.9972	25.81	0.9988
22/06/2010	1967	−6251.70	1559941.9	−6252.27	1553244.0	20.14	0.9983	28.51	1.0000	19.16	0.9971	28.14	0.9985
16/02/2011	2206	−6249.82	1560913.8	−6255.78	1554726.1	18.60	0.9982	24.59	0.9997	15.73	0.9964	22.43	0.9972
26/10/2011	2458	−6254.97	1559664.0	−6249.11	1552576.7	19.28	0.9981	34.36	0.9998	20.06	0.9965	24.31	0.9972
20/03/2013	2969	−6277.82	1561870.1	−6242.54	1554427.5	7.29	1.0017	10.71	1.0038	7.31	0.9990	6.44	1.0005
28/01/2014	3283	−6302.42	1561488.4	−6238.80	1553133.7	6.74	1.0019	7.30	1.0039	4.98	0.9990	3.55	1.0006
20/01/2015	3640	−6320.12	1560915.4	−6236.70	1551943.8	8.06	1.0012	4.99	1.0027	5.28	0.9984	4.74	1.0001
13/09/2016	**4242**	**−6712.90**	**1603579.3**	**−6595.16**	**1593509.0**								
13/09/2016	4242	−6347.81	1561907.3	−6237.05	1551457.7	4.60	1.0004	8.02	1.0031	4.81	0.9988	4.81	0.9999
27/06/2017	4529	−6375.51	1562899.3	−6237.40	1550971.7	1.29	1.0008	5.68	1.0031	1.95	0.9989	4.21	0.9996
03/07/2018	4900	−6468.40	1574568.1	−6310.58	1560511.8	7.13	1.0009	9.67	1.0036	5.10	0.9990	4.59	1.0000
11/12/2018	5061	−6323.39	1556110.5	−6210.55	1546598.3	19.76	0.9972	24.28	0.9985	19.46	0.9952	20.46	0.9961
02/07/2019	5264	−6373.41	1562530.4	−6250.39	1551941.7	14.36	1.0093	6.37	1.0007	1.96	1.0000	1.96	1.0005
28/10/2020	5748	−6346.94	1562380.3	−6298.93	1563654.6	3.79	0.9964	8.28	0.9977	3.48	0.9944	4.48	0.9953

Table A-5. Calibration data. Data highlighted in red have been discounted as erroneous.

Date	Time (days)	TL902		TL903		TO904		TA905		PRH1-1		PRH1-2	
		Intercept	Slope	Intercept	Slope	Intercept	Slope	Intercept	Slope	Intercept	Slope	Intercept	Slope
01/02/2005	0	−0.31	0.9980	1.03	0.9983	0.51	0.9985	0.21	0.9999				
01/03/2006	393	0.24	1.0224	0.32	1.0020	0.32	1.0096	0.30	1.0075				
28/05/2006	481									−1107.63	250486.05	−1112.25	250561.57
05/06/2007	854	0.63	0.9960	0.47	0.9970	0.48	0.9990	0.43	0.9955	−1104.61	250216.75	−1105.78	250470.21
15/02/2008	1000	0.60	0.9995	0.44	1.0005	0.55	0.9990	0.47	0.9960	−1110.42	249432.17	−1111.08	249715.85
15/02/2008	1109	0.99	0.9974	0.31	1.0177	0.25	1.0210	0.71	1.0004	−1112.35	251695.42	−1113.38	252092.86
12/08/2008	1288	0.79	0.9993	0.62	0.9980	0.72	0.9958	0.59	0.9973	−1101.53	249903.82	−1102.72	250146.32
15/01/2009	1444	−0.20	1.0299	0.30	1.0114	0.43	1.0101	0.35	1.0099	−1128.03	249379.13	−1128.01	249646.72
28/05/2009	1577	0.73	0.9975	0.74	0.9907	0.66	0.9930	0.51	0.9990	−1104.74	249818.90	−1105.46	250102.50
22/06/2010	1967	0.79	0.9947	0.87	0.9828	0.63	0.9976	0.50	0.9985	−1105.35	249833.56	−1106.32	250127.43
16/02/2011	2206	−0.20	1.0299	0.30	1.0114	1.06	0.9835	0.35	1.0099	−1113.71	250068.12	−1113.36	250336.45
26/10/2011	2458	0.83	0.9922	−1.13	1.0628	0.70	0.9950	0.61	0.9937	−1112.38	250313.12	−1113.63	250579.92
20/03/2013	2969	0.69	1.0041	1.10	0.9907	0.65	0.9949	0.43	1.0041	−1114.87	250444.19	−1115.59	250774.50
28/01/2014	3283	0.59	1.0021	0.68	0.9910	0.01	1.0258	0.11	1.0326	−1109.10	249929.18	−1110.16	250199.43
20/01/2015	3640	0.60	1.0027	0.36	1.0043	0.49	0.9985	0.38	1.0043	−1113.98	250091.09	−1115.19	250394.97
13/09/2016	4242	0.59	1.0053	0.63	0.9976	0.67	1.0006	0.60	1.0021	−1103.86	249813.23	−1107.25	250161.45
27/06/2017	4529	0.60	0.9935	0.44	0.9930	0.50	0.9930	0.45	0.9900	−1102.10	249740.85	−1104.72	250018.65
03/07/2018	4900	−0.06	1.0260	0.27	0.9996	0.42	0.9961	0.05	1.0180	−1104.73	249901.37	−1106.66	250099.18
11/12/2018	5061	−0.06	1.0260	0.27	0.9996	0.42	0.9961	0.05	1.0180	−1090.47	248744.09	−1092.21	249036.90
02/07/2019	5264	0.45	1.0017	0.31	1.0004	0.42	1.0003	0.54	0.9879	−1095.38	249802.41	−1097.65	250028.00
28/10/2020	5748	−0.31	0.9980	1.03	0.9983	0.51	0.9985	0.21	0.9999	−1084.02	249738.32	−1085.91	249981.52

Table A-6. Calibration data. Data highlighted in red have been discounted as erroneous.

Date	Time (days)	PRH1-3		PRH1-4		PRH2-1		PRH2-2		PRH2-3		PRH2-4	
		Intercept	Slope	Intercept	Slope	Intercept	Slope	Intercept	Slope	Intercept	Slope	Intercept	Slope
28/05/2006	481	−1126.14	250990.55	−1117.48	250465.27	−1122.32	250759.92	−1114.32	250549.03	−1117.38	250689.76	−1117.61	250506.59
05/06/2007	854	−1115.89	250937.75	−1111.22	250313.12	−1112.56	250714.47	−1105.87	250450.67	−1108.09	250601.50	−1113.30	250532.80
15/02/2008	1 000	−1122.13	250146.90	−1116.90	249605.38	−1119.06	249947.49	−1111.52	249693.03	−1114.65	249882.65	−1119.51	249807.68
15/02/2008	1 109	−1126.64	252542.93	−1119.51	251990.43	−1122.93	252325.12	−1115.08	252087.11	−1118.96	252286.80	−1122.58	252158.00
12/08/2008	1 288	−1110.66	250591.68	−1108.18	250002.26	−1108.76	250348.44	−1102.32	250113.63	−1104.90	250305.64	−1110.27	250215.12
15/01/2009	1 444	−1140.37	250161.36	−1135.14	249603.41	−1137.46	249901.01	−1130.16	249674.97	−1133.29	249837.51	−1135.28	249662.52
28/05/2009	1 577	−1116.25	250531.00	−1112.57	250013.60	−1113.50	250330.20	−1106.79	250092.30	−1110.00	250268.10	−1113.77	250177.30
22/06/2010	1 967	−1116.35	250527.44	−1115.81	250031.50	−1112.13	250184.48	−1104.83	250004.41	−1110.16	250259.05	−1112.86	250126.71
16/02/2011	2 206	−1125.40	250700.99	−1120.73	250235.48	−1121.33	250456.59	−1114.72	250289.18	−1119.02	250453.47	−1123.85	250528.86
26/10/2011	2 458	−1124.00	251005.08	−1120.33	250458.96	−1121.37	250798.58	−1114.13	250524.06	−1117.94	250694.65	−1120.93	250596.63
20/03/2013	2 969	−1126.71	251036.52	−1122.43	250560.60	−1124.50	250965.50	−1117.18	250704.25	−1121.53	250918.48	−1122.88	250762.61
28/01/2014	3 283	−1121.03	250625.45	−1117.96	250108.58	−1117.84	250436.13	−1111.16	250143.22	−1115.14	250359.20	−1117.17	250226.99
20/01/2015	3 640	−1126.49	250828.20	−1126.41	250509.55	−1123.34	250621.30	−1117.11	250366.69	−1121.32	250598.69	−1123.07	250445.20
13/09/2016	4 242	−1114.68	250470.51	−1113.69	249950.76	−1111.74	250270.80	−1105.23	249963.61	−1109.33	250197.08	−1113.84	250133.58
27/06/2017	4 529	−1113.36	250400.40	−1112.10	249896.37	−1110.16	250168.68	−1103.97	249873.22	−1107.16	250077.29	−1110.40	249979.83
03/07/2018	4 900	−1115.44	250518.28	−1114.28	250000.32	−1111.94	250289.10	−1105.69	249948.59	−1109.45	250177.69	−1112.67	250095.43
11/12/2018	5 061	−870.66	233763.24	−1099.03	248890.70	−1098.87	249207.62	−1092.50	248899.23	−1096.09	249135.29	−1097.92	248987.19
02/07/2019	5 264	−1107.29	250445.99	−1105.29	249920.97	−1103.57	250217.68	−1097.03	249877.28	−1100.46	250100.56	−1103.71	250015.58
28/10/2020	5 748	−1096.43	250410.19	−1093.47	249906.92	−1092.80	250234.46	−1087.58	249965.10	−1090.59	250169.58	−1091.40	249972.91

Table A-7. Calibration data. Data highlighted in red have been discounted as erroneous.

Date	Time (days)	PRH1-5	
		Intercept	Slope
28/05/2006	481	−1098.70	248487.67
05/06/2007	854	−1105.91	250807.70
15/02/2008	1 000	−1108.49	248928.59
15/02/2008	1109	−1107.68	249993.82
12/08/2008	1 288	−1100.77	250365.95
15/01/2009	1444	−1122.38	248158.03
28/05/2009	1577	−1100.63	249301.90
22/06/2010	1967	−1103.30	249649.36
16/02/2011	2206	−1107.88	248369.12
26/10/2011	2458	−1110.19	250124.90
20/03/2013	2969	−1110.44	248959.82
28/01/2014	3283	−1108.53	249718.45
20/01/2015	3640	−1113.86	249835.74
13/09/2016	4242	−1106.17	250270.84
27/06/2017	4529	−1102.68	250077.67
03/07/2018	4900	−1099.33	249771.44
11/12/2018	5061	−1088.58	248343.38
02/07/2019	5264	−1095.30	249788.70
28/10/2020	5748	−1086.22	250300.20

Arkitektkopia AB, Bromma, 2022

SKB is responsible for managing spent nuclear fuel and radioactive waste produced by the Swedish nuclear power plants such that man and the environment are protected in the near and distant future.

skb.se